Defense Meteorological Satellite Program
Special Sensor Microwave Imager Sounder (F-16)
Calibration/Validation Final Report

The First Conical Scanning Passive Microwave Surface and Atmospheric Sounding Imager

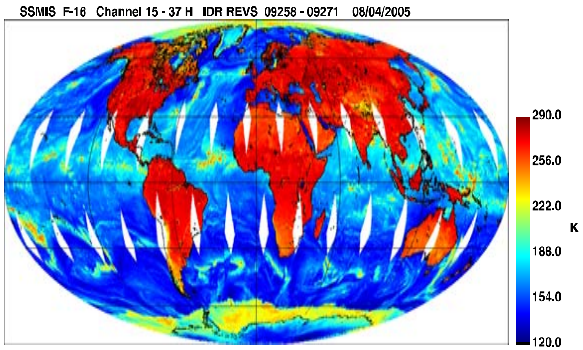

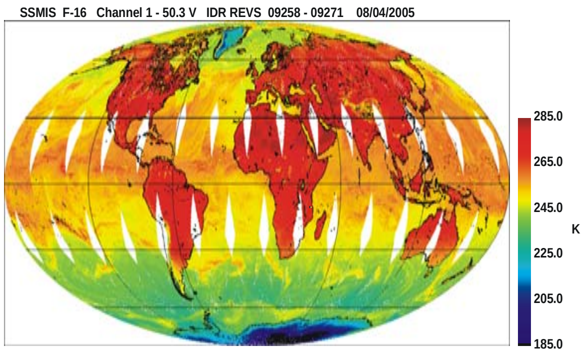

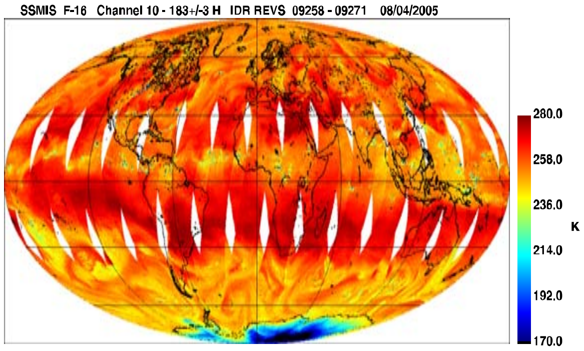

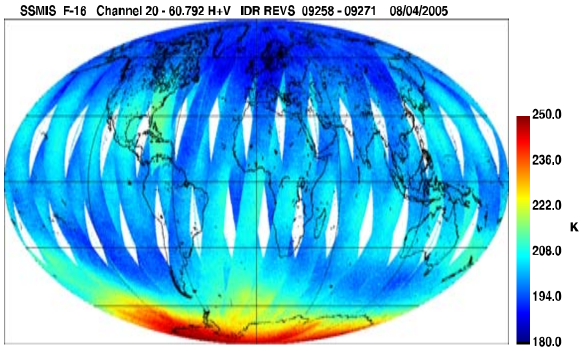

Prepared by

SSMIS Cal/Val Team

30 November 2005

Volume I

Table of Contents

Acknowledgement

- The SSMIS Cal/Val team wishes to thank Col. Wagner, Director of the Defense Meteorological Satellite Program (DMSP) and Mr. Thomas Piwowar (Navy, PMW-180) for their strong support and encouragement in the performance of the SSMIS Cal/Val program. In addition thanks are due Air Force Col. Randy Odle (former Director of DMSP), Ms. Smith (Deputy Director), Mr. Weeks (former Deputy Director) and Capt. Chambers (Program manager of SSMIS) for their enthusiasm and support. Also, special thanks are due Cdr. Gottshall and Mr. Godin and Mr. Berkowitz (associated with Navy PMW-180) for their strong and steady support. The team thanks Mr. Bruce Thomas of the Air Force Weather Agency (AFWA) and Drs. Haferman and Tesmer of the Fleet Numerical Oceanography and Meteorology (FNMOC) for providing SSMIS data products and supporting cal/val data. The team also thanks Drs. M. Werner and M. Meshishnek (Aerospace) for their support. Finally the team wishes to thank Dr. Shapiro (UCAR) and Dr. Parrish (NOAA AOC), Dr. McDermid (JPL), Professor Collins (U. Alaska), Drs. Hazen, Post, Westwater, Fairall and Wolf (NOAA ETL) and Drs. Bougeault, Hollingsworth, McNally, Kelly, Hennessey and Burridge (ECMWF) and ECMWF operations for providing exceptionally high quality validation data without which this cal/val effort would have been severely limited.

SSMIS Cal/Val Team

- **Naval Research Laboratory**

  Gene Poe, Enzo Uliana, Beverly Gardiner, Steve Swadley, Justin Bobak, Troy vonRentzell, Dave Dowgiallo, Norman McGlothlin, Glen Martner, Marla Helveston and Karen St. Germain

- **Aerospace Corporation**

  Donald Boucher, David Kunkee, John Wessel, Ye Hong,

  Bruce Thomas, Al Fote, Mike Plonski, Arlene Kishi and Robert Farley

- **NASA Goddard Space Flight Center**

  James Wang, Paul Racette and Jeff Piepmeier

- **Northrop Grumman Electronic Systems**

  George Vana, David Schultz, Daniel Shalit, Dana Kerola, Mike Heasily and Alex Stogryn

Foreword

- The joint Air Force and Navy DMSP program has a rich heritage of flying new, state-of-the art remote sensing instruments to provide the best global weather intelligence to the military users at Air Force Weather Agency (AFWA) and Fleet Numerical Oceanography and Meteorology Center (FNMOC). DMSP has had a string of successes flying new capability microwave sensors. The Special Sensor Microwave Temperature (SSM/T) was developed in the 1970’s as an “all-weather” cross-track scanning microwave temperature profiler and still serves the users today. The Special Sensor Microwave Imager (SSM/I) followed in the 1980’s with a revolutionary conically scanning imager to measure surface parameters such as ocean surface wind speed, sea-ice concentration, land surface temperature, soil moisture and atmospheric parameters such as rain fall rate, cloud liquid water and integrated water vapor. Soon to follow the SSM/I was the SSM/T-2 microwave water vapor profiler with a cross-track scan geometry tied to the SSM/T. This instrument pushed mm-wave technology into very high frequencies (150-183 GHz). All three of these instruments are still flying today and provide an excellent source of independent collaborative data to verify the newest instrument program for DMSP, the Special Sensor Microwave Imager/Sounder (SSMIS).

Foreword (Cont'd)

- **The SSMIS instrument first began back in the June time frame of 1989 with a kick-off meeting at Aerojet, Azusa, now Northrop-Grumman Electronic Systems (NGES). The SSMIS was considered to be a major step foreword for the user communities in that this sensor combined the functionality of the heritage DMSP sounders (SSM/T and SSM/T-2) and imager (SSM/I) into a single integrated conically scanning instrument with additional channels to profile the mesosphere. For the first time atmospheric soundings are derived by an instrument with a constant viewing geometry in lieu of the more traditional cross-track, dwell and step-stare geometry such as the heritage DMSP and NOAA AMSU sensors. Additional benefits of the conical scan are constant pixel resolution across the swath, constant polarization and common fields of view of the surface and atmosphere for both sounding and imaging channels.**
- **The development process was not an easy one, as many components in the very complex system resisted passing rigorous tests resulting in a protracted development cycle. Many lessons learned were captured along the way and are being applied to future sensor developments, specifically, the NPOESS Conical Microwave Imager Sounder (CMIS).**

Foreward (Cont'd)

- To facilitate the transition of the SSMIS data products to the users, the DMSP in conjunction with Navy PMW-180 decided to conduct a comprehensive end-to-end calibration/validation (Cal/Val) of the first SSMIS. The Naval Research Laboratory was selected to lead the technical efforts with support from remote sensing scientists and data analysts of the Aerospace Corporation resident within AFWA and DMSP program office. Patterned after the joint Air Force/Navy sponsored SSM/I Cal/Val, the first SSMIS Cal/Val was tasked to verify and quantify the instrument performance in terms of its Sensor Data Record (radiometric calibration, geo-location, scan-uniformity, noise level and stability) and validate the Environmental Data Record (EDR) performance (lower-air temperature and humidity, upper-air temperature and SSM/I type parameters). If necessary correction coefficients or modifications to Ground Data Processing Software resident at AFWA and FNMOC would be made to bring the SDRs and EDRs within specification. Additionally, the results of the Cal/Val would be used to determine if hardware modifications are necessary to bring subsequent SSMIS instruments within sensor specification.

Foreward (Cont'd)

- **The F-16 SSMIS was launched 18 October 2003 from Vandenburg Air Force Base, CA, aboard the last Titan 2 vehicle. After successfully passing early-orbit testing the SSMIS was subjected to an intensive Cal/Val program. This report documents the major results of this Cal/Val effort and the long series of software and hardware modifications resulting from the cal/val findings. Many lessons learned from F-16 Cal/Val will be applied to subsequent SSMIS instruments, hopefully shortening the cal/val period and expediting the release of SSMIS data products. It is with great pleasure that the Cal/Val team presents this document for the first SSMIS sensor.**

F16 SSMIS Calibration/Validation Final Report

Section 1.0 Introduction and Summary

Donald Boucher and Gene Poe

THE AEROSPACE CORPORATION

Outline

Part 1

- Important historical perspective
- Atmosphere/Ocean Overview
- What the users will do with SSMIS data
- EDR performance quick-look

Part 2

- SSMIS instrument basics
- Role and importance of Calibration/Validation (Cal/Val)
- Cal/Val approach
- Team organization
- Instrument and algorithm issues
- The way ahead

Important Historical Perspective

- **SSMIS EDR requirements were generated in late 1989**
- **Users at that time required "products" such as vertical temperature and water vapor profiles, ocean surface wind speeds, the EDR's**
- **The SSM/T-1 was flying, along with the SSM/I, and performance for these instruments were proven**
- **The SSM/T-2 had yet to fly, so the government had no experience with how this water vapor profiler would perform, let alone the SSMIS with nearly identical frequencies**
- **The SSM/T-2 Cal/Val concluded that there was insufficient accuracy in the balloon measurements to validate the products, hence Aerospace built our ground-based LIDAR which the team has used very successfully for SSMIS**
- **NWP users will soon require SDR's which are the calibrated and earth located SSMIS brightness temperatures, with less interest in EDR products**

Atmosphere/Ocean Overview

- **A brief look at the atmospheric temperature and water vapor structure**
- **A quick look at the ocean parameters**
- **A summary of who the DoD users are, and how they will use SSMIS data**

Atmospheric Temperature:Classical Regimes and SSMIS "Sampling"

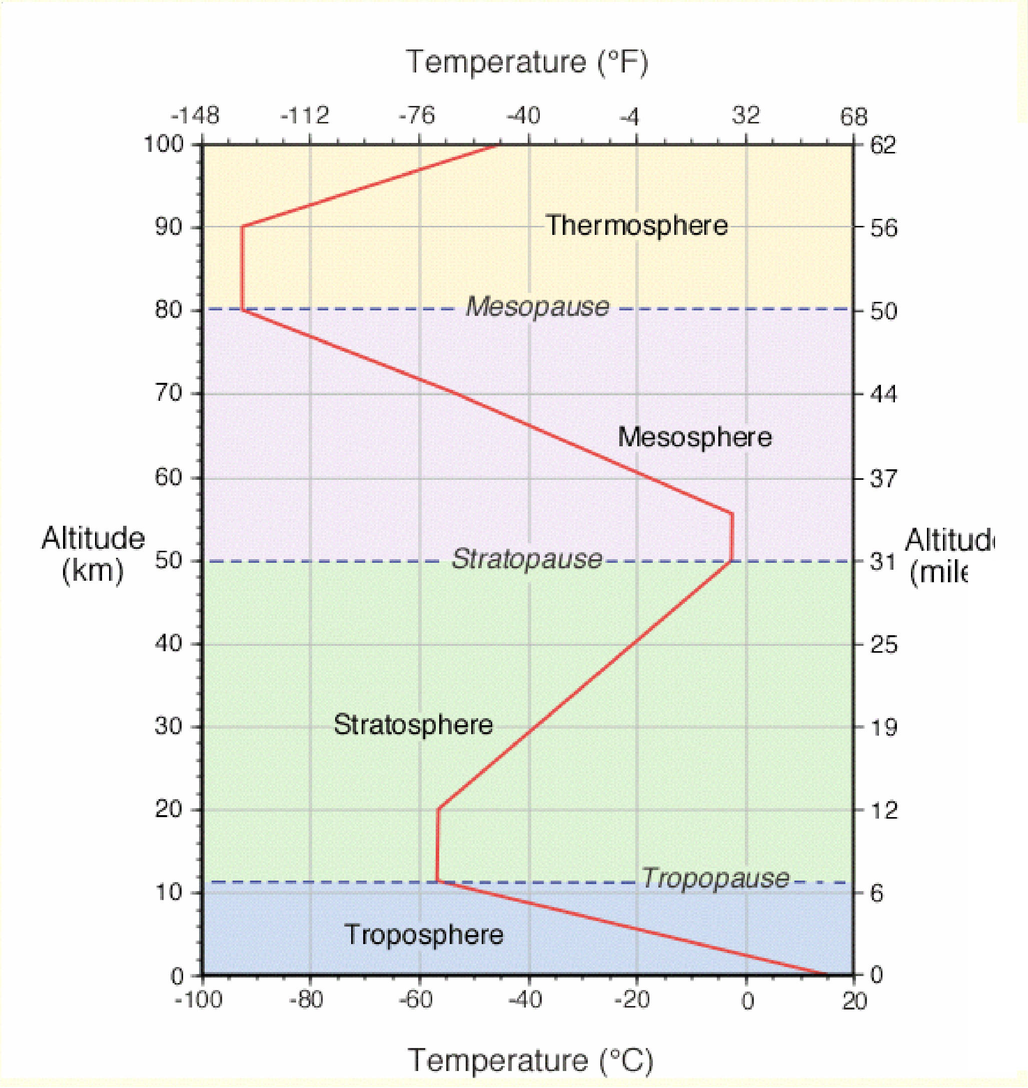

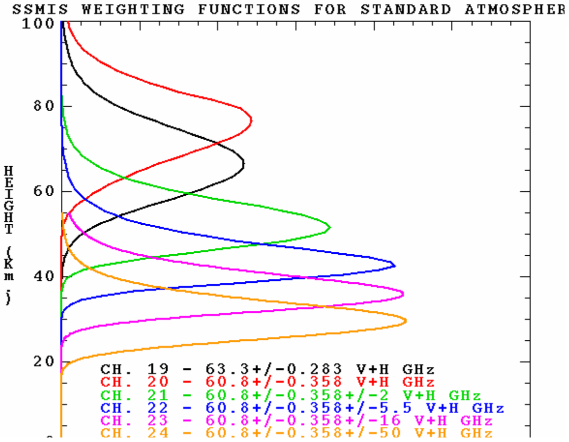

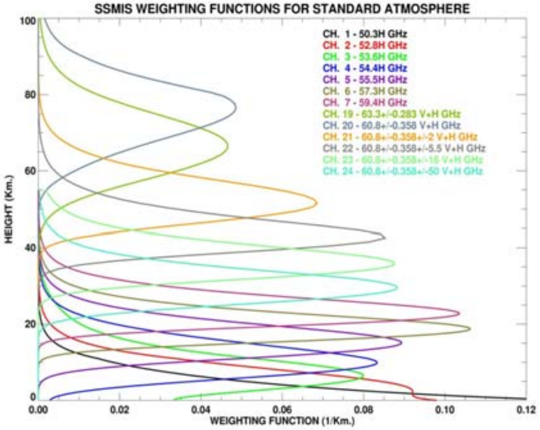

Atmospheric Water Vapor: A Typical Sounding over Boulder CO

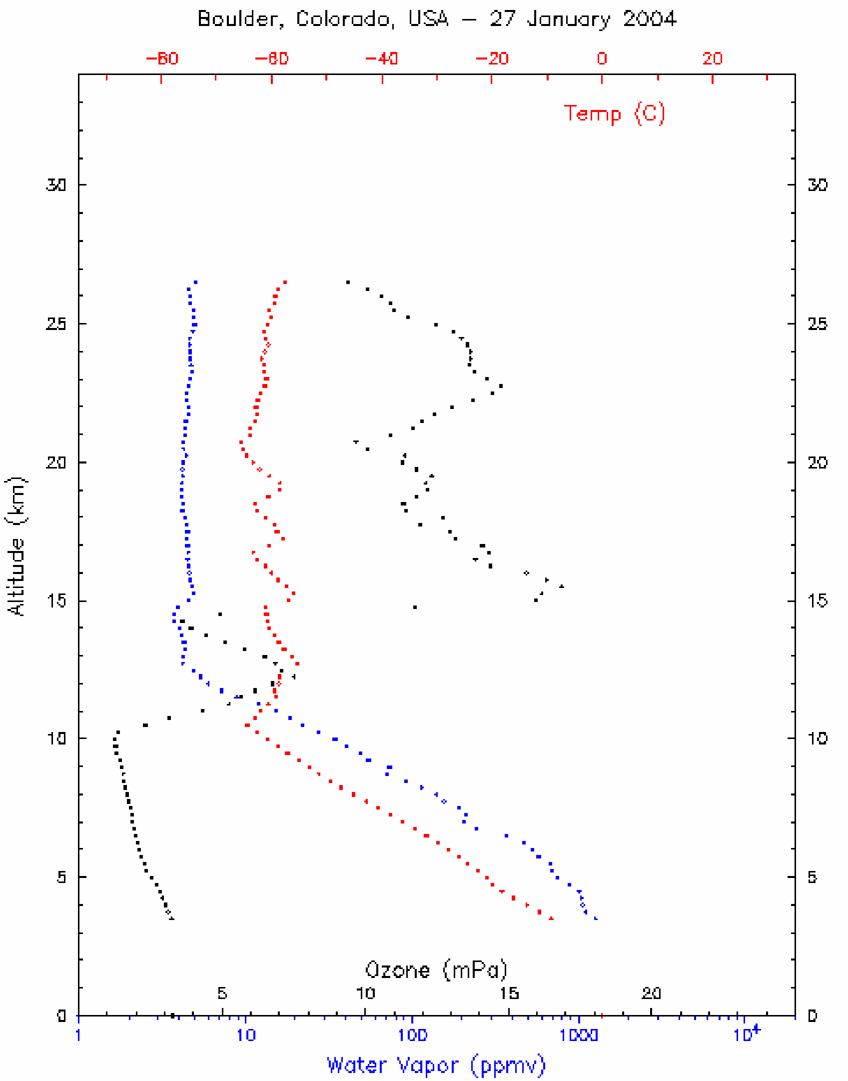

(Generated courtesy of NOAA/CMDL)

Typical Ocean EDR's Derived from the SSMIS (SSM/I Example Data)

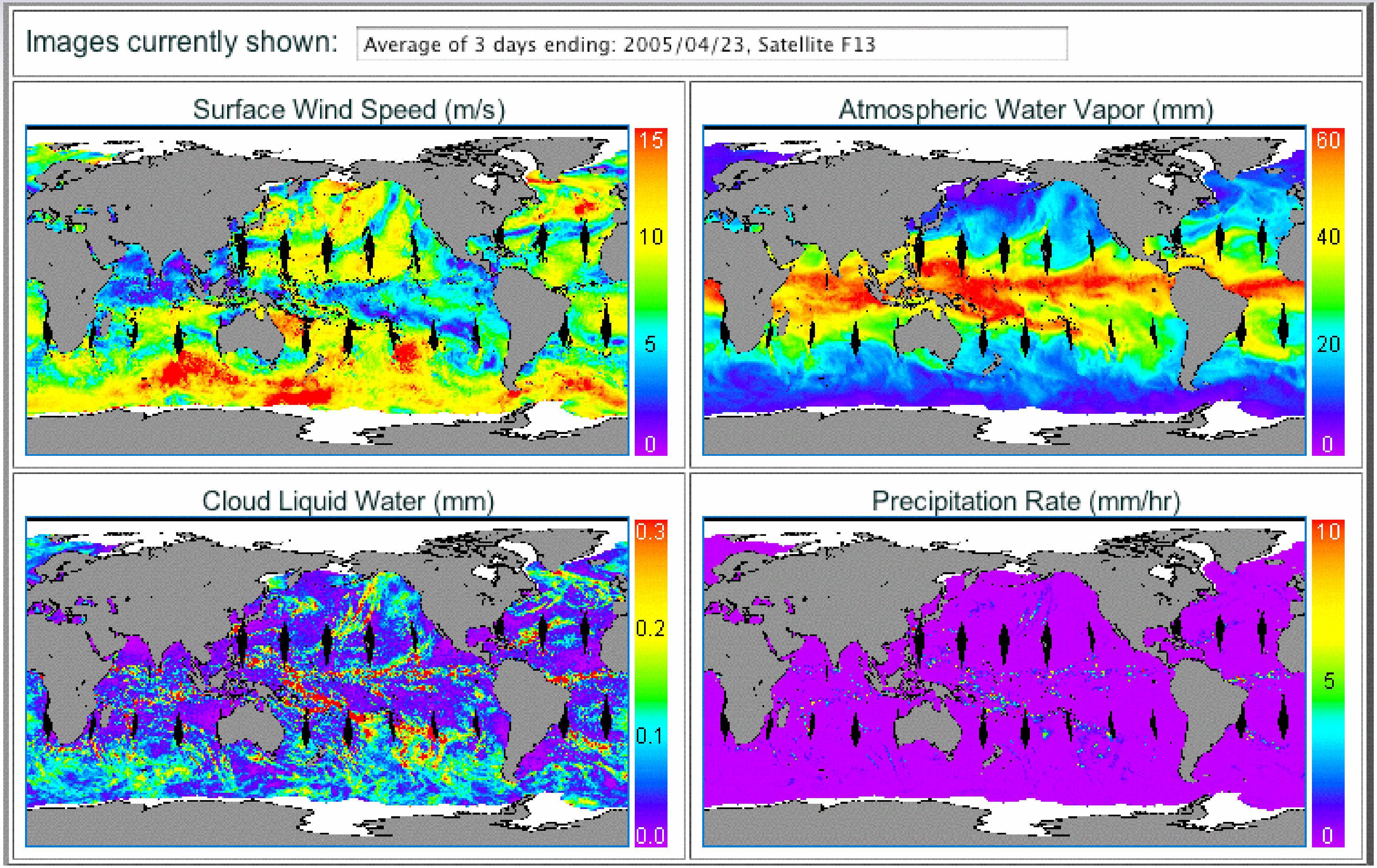

Images currently shown: Average of 3 days ending: 2005/04/23, Satellite F13

How Do The Users Use SSMIS Data?

- AFWA/FNMOC (and tactical world) use SSMIS data products (EDR’s) to be merged with other data such as balloon measurements to generate a global specification of the atmosphere. This is the EDR user.
- Numerical Weather Prediction users will require highly accurate SDR’s
- The SSMIS Cal/Val team has faced many SDR challenges along the way, which will be discussed later in the report.
- Now, how did the EDR’s perform?

EDR Performance Quick-look

- **Green means we meet the PIDS specification**
- **Yellow means we currently do not meet specification, but with addition work, we will meet the specification**
    - **E.g. Team is working on backing out results from warm load sun glint and main reflector emissivity to improve performance**
- **Red means we are not, and will not meet specification**

EDR Performance Quick-look:
Imaging EDR's (heritage SSM/I)

Ocean Winds	**Rain Parameters**	**Cloud Parameters**
Soil Moisture	**Sea Ice Parameters**	**Water Vapor**
Surface Type	**Snow Parameters**	**Land Surface Temperature**

SSMIS EDR Performance Quick-look: Soundings (Heritage SSM/T-1 & SSM/T-2)

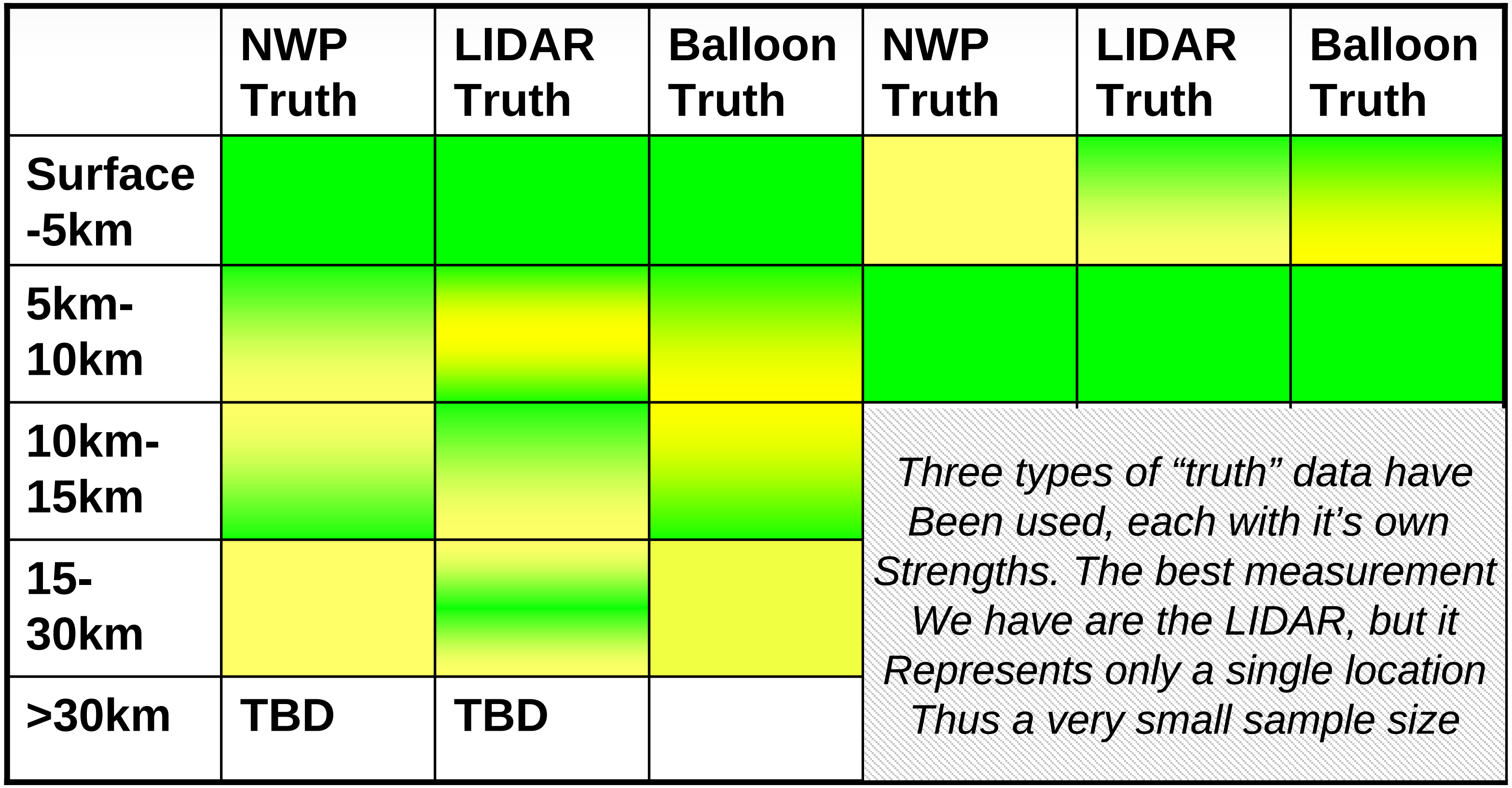

	Temperature			Water Vapor		
	NWP Truth	**LIDAR Truth**	**Balloon Truth**	**NWP Truth**	**LIDAR Truth**	**Balloon Truth**
Surface -5km	🟩	🟩	🟩	🟨	🟩🟨	🟩🟨
5km-10km	🟩🟨	🟩🟨🟩	🟩🟨	🟩	🟩	🟩
10km-15km	🟨🟩	🟩🟨	🟨🟩			
15-30km	🟨	🟨🟩🟨	🟨			
>30km	**TBD**	**TBD**				

Three types of "truth" data have Been used, each with it's own Strengths. The best measurement We have are the LIDAR, but it Represents only a single location Thus a very small sample size

SSMIS Products Are Ready For Operational Users

- **DMSP has released* TDRs, SRDs and EDRs to the users**
- ***With the Cal/Val team's caveats**
- **Final Cal/Val report will help non DoD users with the data products**

SSMIS Instrument Basics

- **Instrument characteristics**
- **Instrument specifications**
- **Let’s get a feel for how this all works on the spacecraft, examples of Digital Graphics System (Aerospace Spacecraft/Payload Simulator)**

SSMIS Key Instrument Characteristics

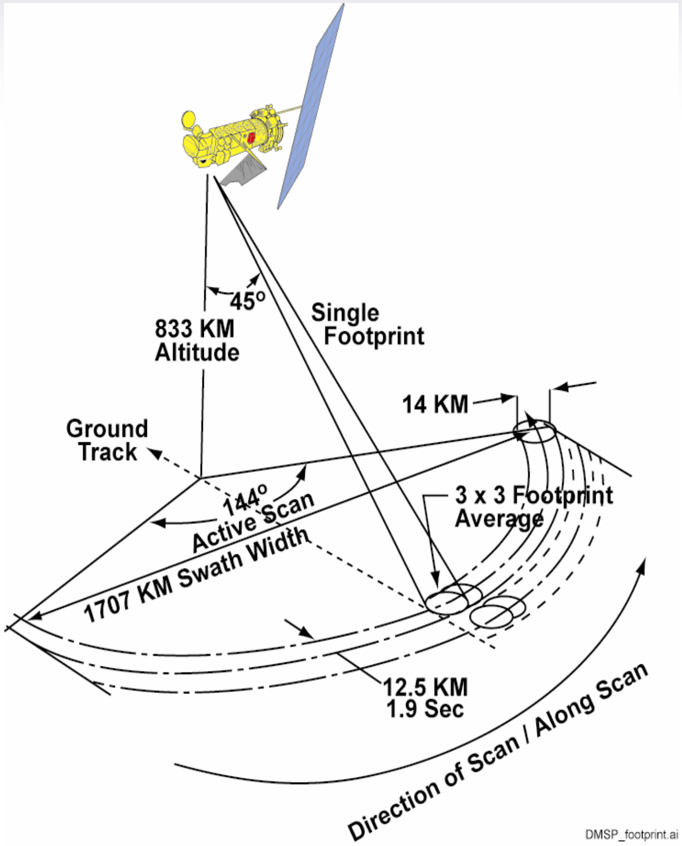

- 24 Channels (19-183 GHz)
- Conical Scan Geometry
- Mesospheric Sounding
- Improved Sounding HCS
- Swath Width 1700 km
- Scan Rate 31.6 rpm
- Calibration Accuracy
  - Better than 1K
  - Warm and Cold Targets each Scan

SSMIS Sensor Characteristics

Channel	Center Freq.(GHz)	Passband (MHz)	Freq. Stab.(MHz)	Pol	NEDT (Max)(K)	Sampling Interval(km)
1	50.3	400	10	H	0.4	37.5
2	52.8	400	10	H	0.4	37.5
3	53.596	400	10	H	0.4	37.5
4	54.4	400	10	H	0.4	37.5
5	55.5	400	10	H	0.4	37.5
6	57.29	350	10	*	0.5	37.5
7	59.4	250	10	*	0.6	37.5
8	150	1500	200	H	0.88	37.5
9	183.31+/-6.6	1500	200	H	1.2	37.5
10	183.31+/-3	1000	200	H	1.0	37.5
11	183.31+/-1	500	200	H	1.25	37.5
12	19.35	400	75	H	0.7	25
13	19.35	400	75	V	0.7	25
14	22.235	400	75	V	0.7	25
15	37	1500	75	H	0.5	25
16	37	1500	75	V	0.5	25
17	91.655	3000	100	V	0.9	12.5
18	91.655	3000	100	H	0.9	12.5
19	63.283248 +/-0.285271	3	0.08	V + H	2.4	75
20	60.792668 +/-0.357892	3	0.08	V + H	2.4	75
21	60.792668 +/-0.357892 +/-0.002	6	0.08	V + H	1.8	75
22	60.792668 +/-0.357892 +/-0.006	12	0.12	V + H	1.0	75
23	60.792668 +/-0.357892 +/-0.016	32	0.34	V + H	0.6	75
24	60.792668 +/-0.357892 +/-0.050	120	0.84	V + H	0.7	37.5

Notes:

1. The sampling interval refers to the along scan direction and is based on nominal spacecraft altitude.
2. The radiometer integration time is 4.20msec for a single 12.5km sample interval.
3. * = These channels are not polarization dependent.

SSMIS Imaging EDR Requirements*

Parameter	Scene Spacing (km)	Accuracy	Quantization
Ocean Surface Wind Speed (m/s)	25	2.0**	1.0
Rain over Land And Ocean			
Flag	12.5		
Rate(mm/hr)	25	5.0***	1.0
Cloud Water(mm) (Droplets < 100micm)	25	0.10	0.05
Soil Moisture (%)****	25	10	5.0
Sea Ice			
Concentration (% area covered)	25	10	5.0
Age (FY/MY)	25		
Edge	25		
Water Vapor over Ocean (mm)	25	3 (tropics)	0.5
		2 (mid-lat)	0.5
		1 (polar)	0.5
Surface Type (Same categories as SSM/I)			
Snow			
Water Content (cm)	25	3 (goal)	0.5
Edge	25		
Land Surface Temperature (K)	25	2.5 (goal)	1.0
Cloud Amount over Ocean (%)	25		10

*Taken from Prime Item Development Specification (PIDS) 19 May 1997.

**Error calculation based on a normal wind speed distribution (0-20 m/s) over the entire globe.

***Goal on a regional basis.

****Goal. The Antecedent Precipitation Index (API) will be used as a basis for analysis. Accuracy will be verified from curves relating the API to soil moisture.

SSMIS Sounding EDR Requirements*

Parameter	Level(mb)	Accuracy	
		rms	bias
Temperature (K)	1000	8.0	<1.0
(15 Mandatory levels	850	6.0	<1.0
1000-10mb, 8 levels	700	2.5	<1.0
7-0.03mb)	500-10	2.0	<1.0
	7-1	5.0	
	0.4	5.5	
	0.2-0.03	8.0 (goal)	
Tropopause			
Temperature (K)		5.0 (1K goal)	
Pressure (mb)		20.0	
Thicknesses between all levels (22)			
Humidity			
Specific and	1000	1.5 g/kg or 20%	***
Relative	850	whichever is greater	
	700	over ocean surface	
	500	under clear conditions	
	400	and goals for other	
	300	surfaces	
Vapor Mass	Surface-1000**		
	1000-850		
	850-700		
	700-500		
	500-400		
	400-300		
	above 300		
	Total		

*Taken from Prime Item Development Specification (PIDS) 19 May 1997.

**If the 1000mb height falls below the surface, the initial layer shall be from the surface to 850 mb.

***The bias error shall not exceed that determined from an analysis of SSM/T-2 data.

Visualize SSMIS with DMSP Graphics System (DGS)

- DGS was built to support Cal/Val
- Invaluable analysis tool which helped uncover and characterize:
  - Sun intrusion into the warm load
  - Reflector emission
- See Section 2 Early Orbit Results and Sections 11 and 12 (Calibration Anomalies) for examples of DGS simulations

Role and Importance of Cal/Val

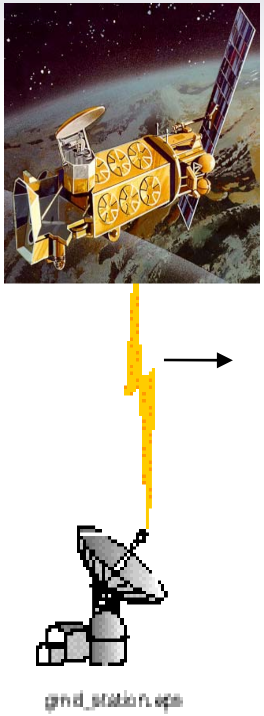

Calibration

- Absolute Accuracy
- Polarization Purity
- Geo-location Accuracy
- Instrument Stability
- Doppler Correction
- Antenna Pattern Correction

Validation

- Ocean Wind Speed
- Water Vapor
- Cloud Water
- Rain Rate
- Sea Ice
- Soil Moisture
- Snow water
- Land Temp
- Lower-Air Profiles
- Upper-Air Profiles

Ensures

Mission Success

- Meet Specification
- Operational production of synoptic maps and profiles of critical atmospheric, oceanographic, sea ice and land parameters
- Quality Control

Users

- NWP
- Real-time tactical
- Non-tactical
    - •JTWC
    - •NHC
    - •NIC
- Others

Importance of Cal/Val

First SSM/I: F8 in 1987

PRODUCT	SPECIFICATION	BEFORE CAL/VAL	AFTER CAL/VAL
Geolocation	7 km	>50 km	<7 km
Windspeed	2 m/s	>6 m/s	<1.9 m/s
Water Vapor	2 mm	>7 mm	< 2 mm
Cloud Water	0.1 mm	Failed	< .1 mm
Sea Ice Con.	12%	Failed	<10%
Rain Rate	5 mm/hr	>10 mm/hr	<2 mm/hr
Snow Water	3 cm	Failed	<2 cm
Soil Moist.	None		<2 mm
Land Temp.	None		<3 C

Cal/Val Approach

I Early Orbit Evaluation	Examine Overall Sensor Health, Stability, NEDT, FOV, Cal Samples, Beam Pointing
II Initial Assessment	Review Sensor and GDPS Products SSM/I (TDR,SDR, EDR) Limited Raob/Rocob/Lidar/NWP Geo-location Error Analysis (Preliminary) Radiative Transfer Modeling (Preliminary) SSM/T, SSM/T-2, AMSU (EDR) Limited APMIR and COSMIR Underflights
III System Calibration	APMIR and CoSMIR Underflights SSM/I (TDR,SDR) Radiative Transfer Modeling Geo-location Error Analysis
IV EDR Validation **Imaging** **Sounding**	EDR dependent. See Section 5.0 for Imaging EDRs and Sections 6.0 and 7.0 for Sounding. Example: For Ocean Wind Speed: Buoys (NDBC, TAO/TRITON, European) Example: For Cloud Liquid Water: Ship-mounted Up-looking NOAA ETL Radiometer Lidar (Aerospace, JPL and U. Alaska) Raob(WMO)/Rocobs (Special launches) Dropsondes(NOAA and USAF) NWP (NOGAPS,ECMWF,UKMO)
V Algorithm Improvements	As needed to meet SDR and EDR specifications

Team Organization/Schedule

- NRL: SDR validation and ocean parameter EDR validation, upper-air sounder partner, designer of aircraft under-flight experiments, (APMIR and CoSMIR) radiative transfer modeling
- Aerospace: processing and re-processing of data for the entire team via Omaha/El Segundo labs, SDR validation partner, LIDAR campaigns, balloon campaigns, sounder validation, DGS simulator provider, radiative transfer modeling
- NGES Azusa: hardware/software leads, partner in all activities
- NASA: ER-2 aircraft under-flight team

Team Organization

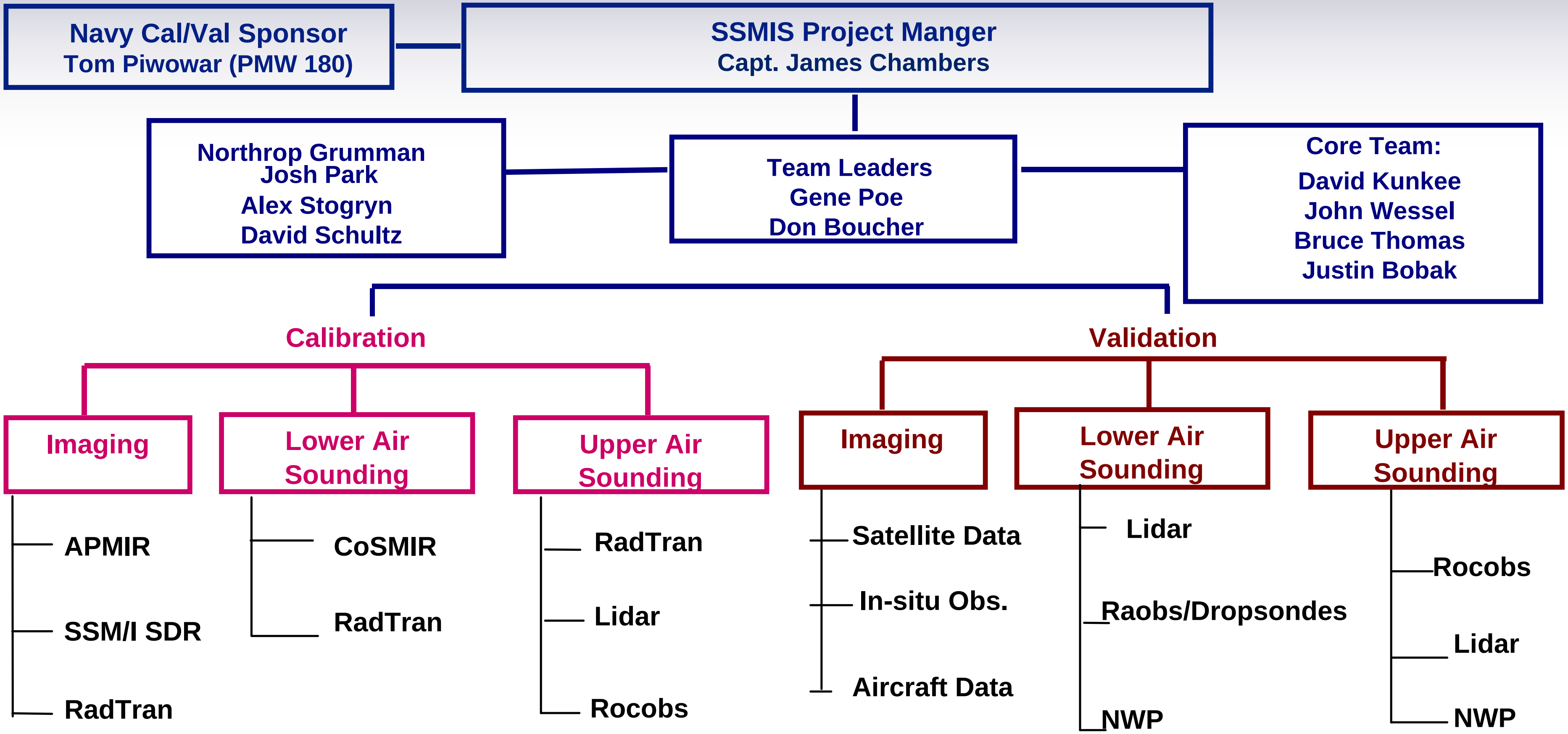

Navy Cal/Val Sponsor
Tom Piwowar (PMW 180)

SSMIS Project Manger
Capt. James Chambers

Northrop Grumman
Josh Park
Alex Stogryn
David Schultz

Team Leaders
Gene Poe
Don Boucher

Core Team:
David Kunkee
John Wessel
Bruce Thomas
Justin Bobak

Calibration

- Imaging
  - APMIR
  - SSM/I SDR
  - RadTran
- Lower Air Sounding
  - CoSMIR
  - RadTran
- Upper Air Sounding
  - RadTran
  - Lidar
  - Rocobs

Validation

- Imaging
  - Satellite Data
  - In-situ Obs.
  - Aircraft Data
- Lower Air Sounding
  - Lidar
  - Raobs/Dropsondes
  - NWP
- Upper Air Sounding
  - Rocobs
  - Lidar
  - NWP

Supporting Processing Centers:
Air Force Weather Agency
Fleet Numerical Meteorology and Oceanography Center

Supporting Team:
J. Wang, A. Fote, Ye Hong, M. Plonski
Enzo Uliana , Beverly Gardiner and Steve Swadley

Milestones/Schedule

(Healthy Sensor & Stable Ground Processing Software)

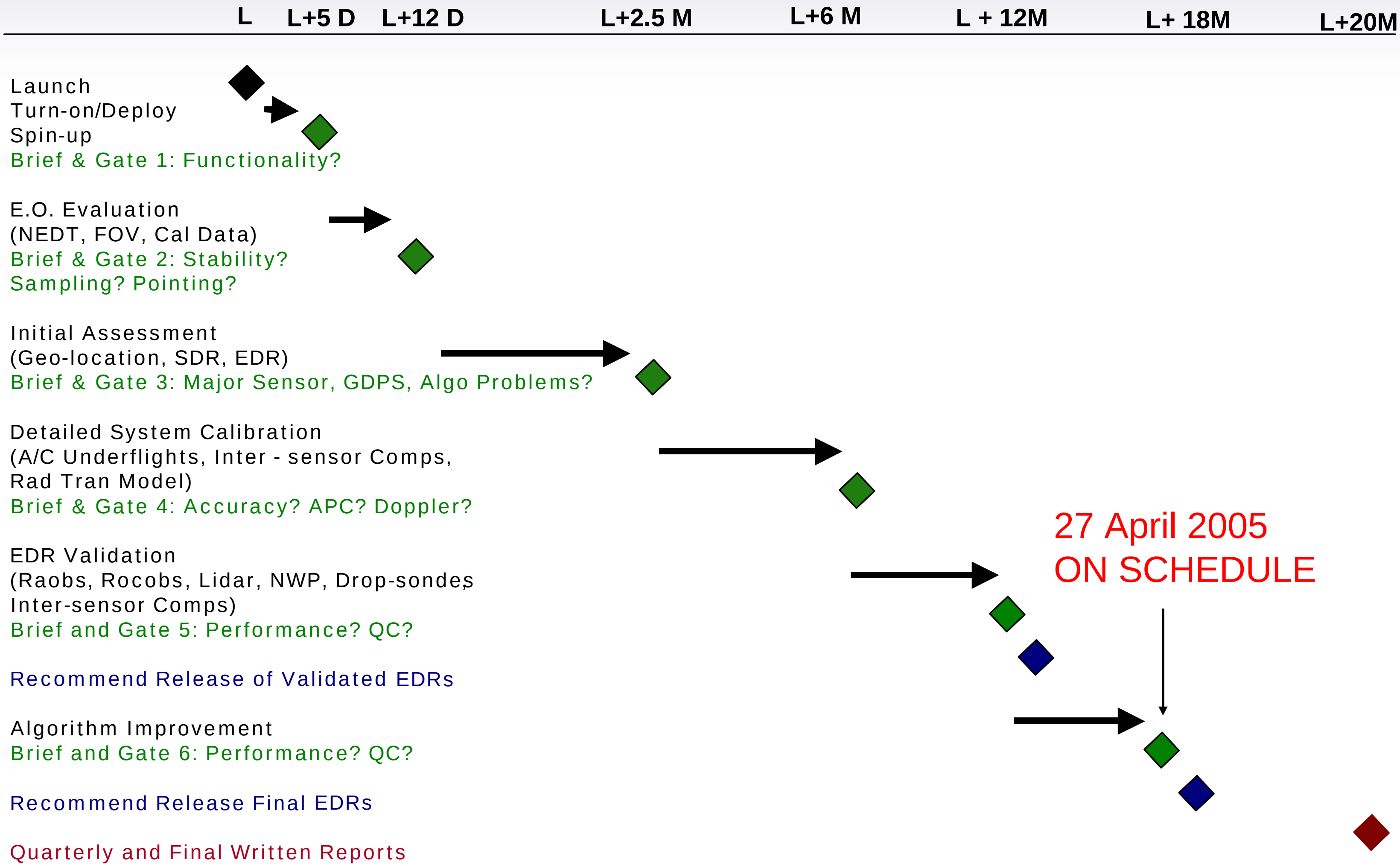

L L+5 D L+12 D L+2.5 M L+6 M L + 12M L+ 18M L+20M

Launch
Turn-on/Deploy
Spin-up
Brief & Gate 1: Functionality?

E.O. Evaluation
(NEDT, FOV, Cal Data)
Brief & Gate 2: Stability?
Sampling? Pointing?

Initial Assessment
(Geo-location, SDR, EDR)
Brief & Gate 3: Major Sensor, GDPS, Algo Problems?

Detailed System Calibration
(A/C Underflights, Inter - sensor Comps,
Rad Tran Model)
Brief & Gate 4: Accuracy? APC? Doppler?

EDR Validation
(Raobs, Rocobs, Lidar, NWP, Drop-sondes
Inter-sensor Comps)
Brief and Gate 5: Performance? QC?

Recommend Release of Validated EDRs

Algorithm Improvement
Brief and Gate 6: Performance? QC?

Recommend Release Final EDRs

Quarterly and Final Written Reports

27 April 2005
ON SCHEDULE

Instrument and Algorithm Issues

- Instrument issues the Team has worked
  - Spin-up anomaly: resolved
  - Channels 1-5 polarization: resolved with hardware change
  - Warm load sun glint: mitigated with fence and software modeling
  - Emissivity of the primary reflector: mitigation path defined, work underway
- Algorithm issues the Team has worked
  - Earth location and resampling routines developed and refined
  - Scan non-uniformity correction developed
  - Calibration routines refined
  - LAS temperature EDR algorithms developed to mitigate polarization issues
  - Algorithms designed to mitigate impact of sun glint into warm-load

SSMIS Instrument Issue: SDR Bias

- **Variable Bias Traced to High Main Reflector Emissivity**
- **Anomalous Gain Excursions Traced to Solar Impingement on Warm Load**

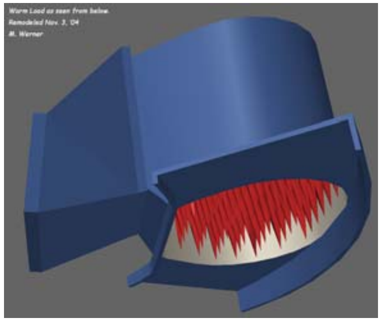

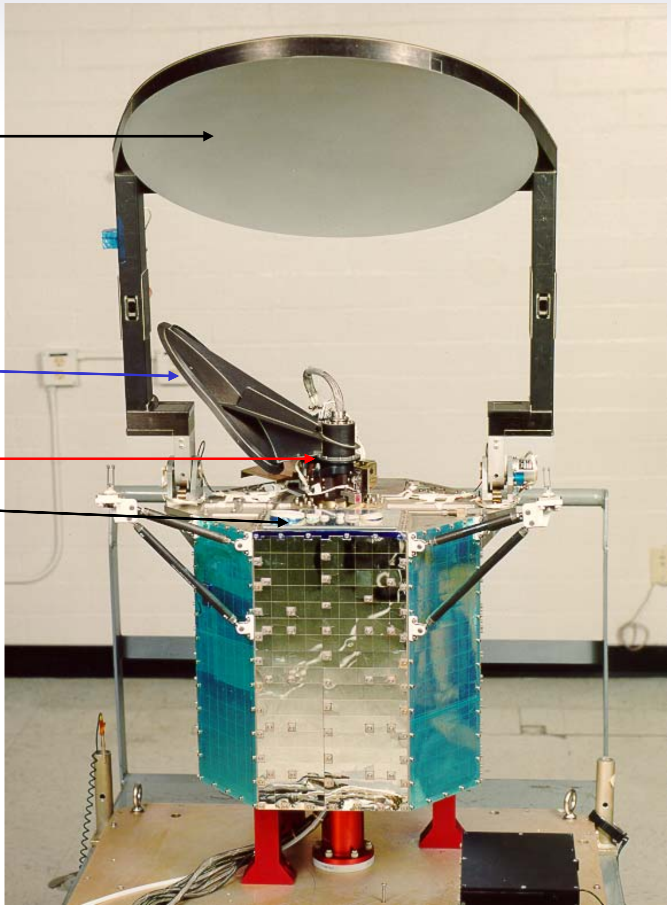

SSMIS Instrument Issue: SDR Bias

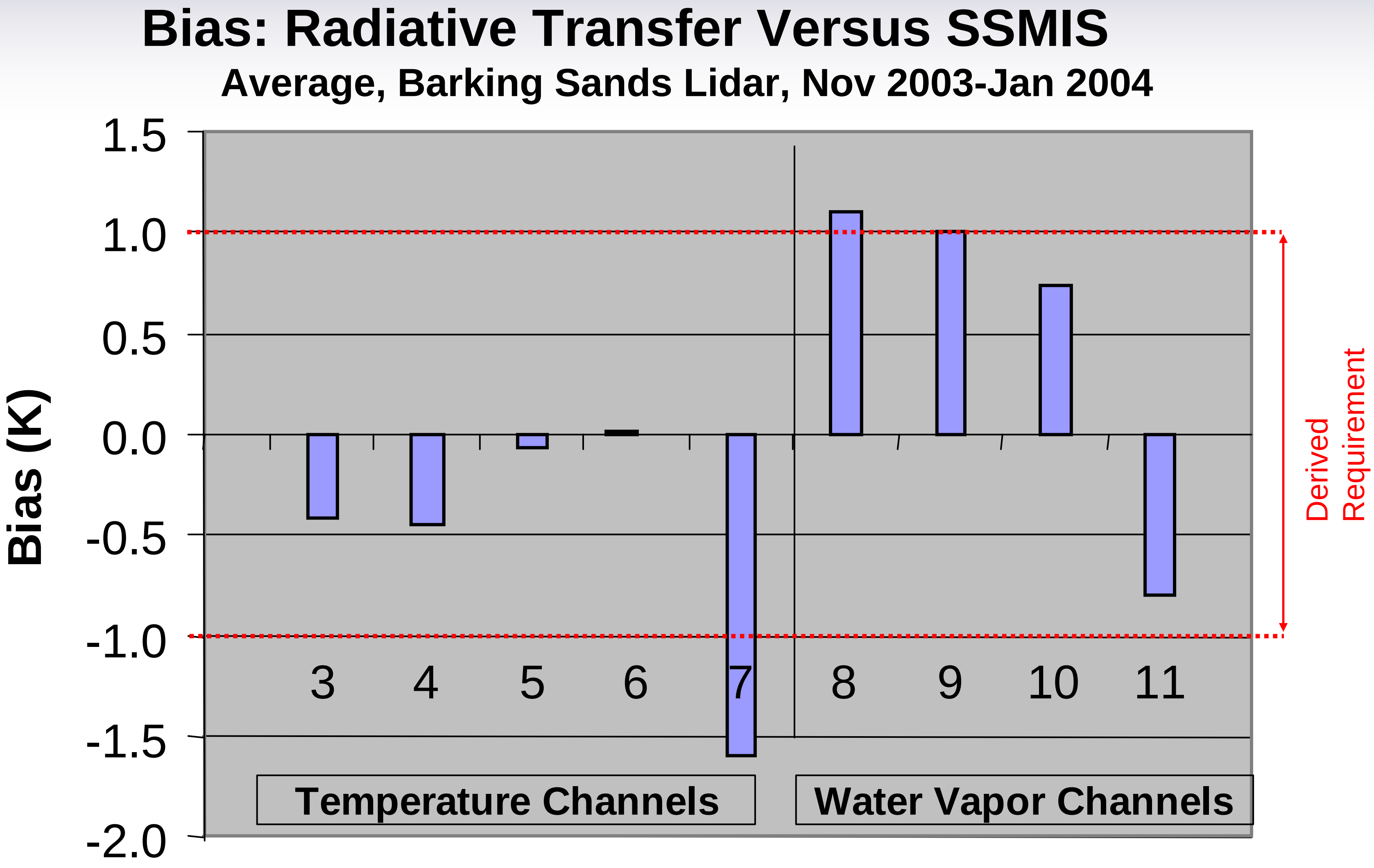

SSMIS Instrument Issue:
SDR Bias, Moisture Channels
Barking Sands Lidar Truth

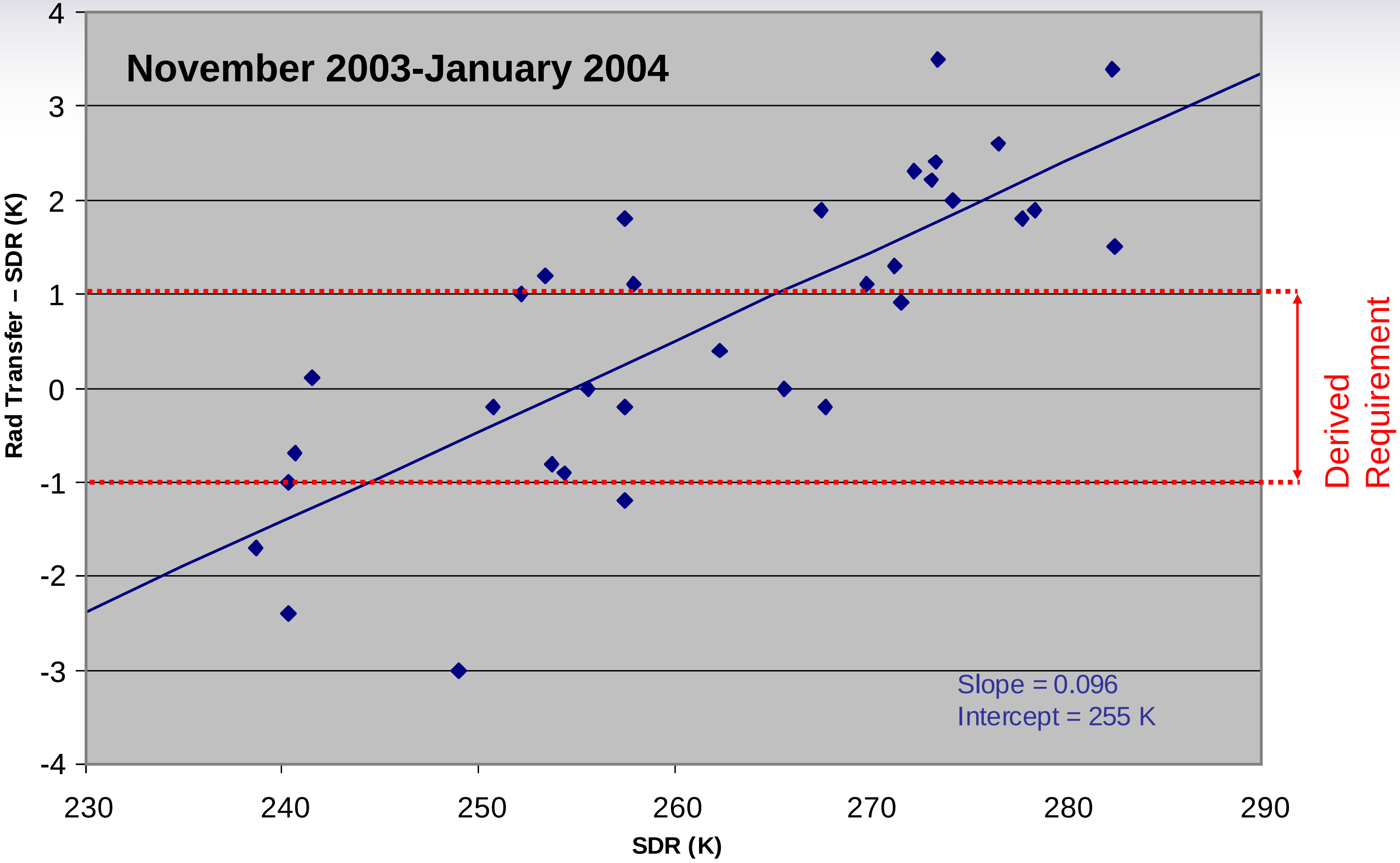

SSMIS Instrument Issue: SDR Bias

Bias: Radiative Transfer Versus SSMIS

Ch 3 ECMWF – SSMIS. 17 Mar 2004

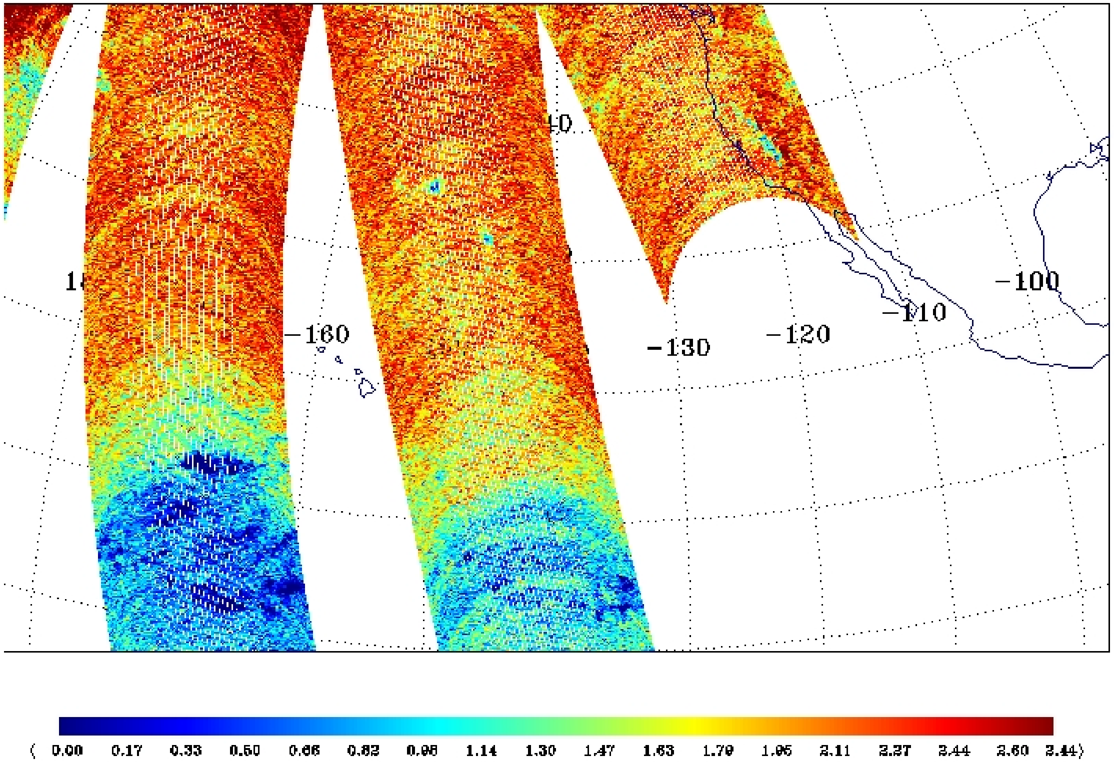

The Way Ahead

- Change hardware to H pol for Channels 1-5
- Remove bias in SDR’s
- Tune temperature and water vapor retrievals by running the SSMIS “off-line” code
- Implement algorithm to mitigate warm load solar bias
- Add solar fence to protect the warm load
- Correct for bias caused by main reflector emissivity
  - Characterize reflector and develop a thermal model
  - Move thermistor to back of main reflector
  - Anticipate a major new software release in the near future containing Cal/Val upgrades

Summary

- F16 SSMIS Cal/Val very successfully completed on schedule
- Resulting in numerous instrument modifications and algorithm updates
- The team is ready to support an aggressive cross-calibration activity with F16 vs F17 SSMIS
- The team will continue to work the upper air sounder EDR's
- Scientific publications will follow by team members
- Finally, all team members thank the DMSP SPO and Navy PMW 180 for their support and look forward to a successful future of the SSMIS program

F16 SSMIS Calibration/Validation Final Report

Section 2.0 Early Orbit Field of View Analysis

David Kunkee, Ye Hong, Michael Werner

AIR FORCE SPACE & MISSILE SYSTEMS CENTER

Defense Meteorological Satellite Program

THE AEROSPACE CORPORATION

DEPARTMENT OF THE NAVY NAVAL RESEARCH LABORATORY

Section 2.0 Early Orbit FOV Analysis

2.1 SSMIS Sensor Simulation and EO2 Data Collection Periods

During the calibration/validation period for SSMIS a detailed simulation tool was developed for visualization and anomaly resolution. Substantial detail was added to the SSMIS sensor graphic model contained in the DMSP Graphic Simulation or DGS. The more detailed simulation tool proved to be highly valuable in predicting and attributing SSMIS calibration anomalies and field-of-view intrusions inherent in the design that were brought to light by Early-Orbit (EO) data Analysis. The following charts show drawings of the SSMIS mounted on the F-16 spacecraft followed by a screen view of the DGS simulation. Details of the SSMIS sensor, showing the feedhorn layout on page 2-6 and 2-7 follow. A timing diagram of the SSMIS is shown on page 2-8. This chart has an extensive collection of information that was assembled to understand the sensor in operation and for interpreting the EO data. Recall that there are 4 EO modes, EO1, EO2A, EO2B, and EO2C. In any of these modes the sensor supplies raw counts without along-scan averaging or A/B integrator corrections allowing valuable insight regarding operation of the SSMIS sensor. In this section EO2 data from a collection period shown on page 2-9 are described. Although there was a second EO2 data collection period in early 2005, that EO data collection was for support of the Warm Load solar intrusion anomaly and will not be addressed in this section. The 2003 EO data analysis described in this section was fundamental to understanding the operation of the SSMIS sensor after spin-up.

Deployed SSMIS on F-16 Spacecraft

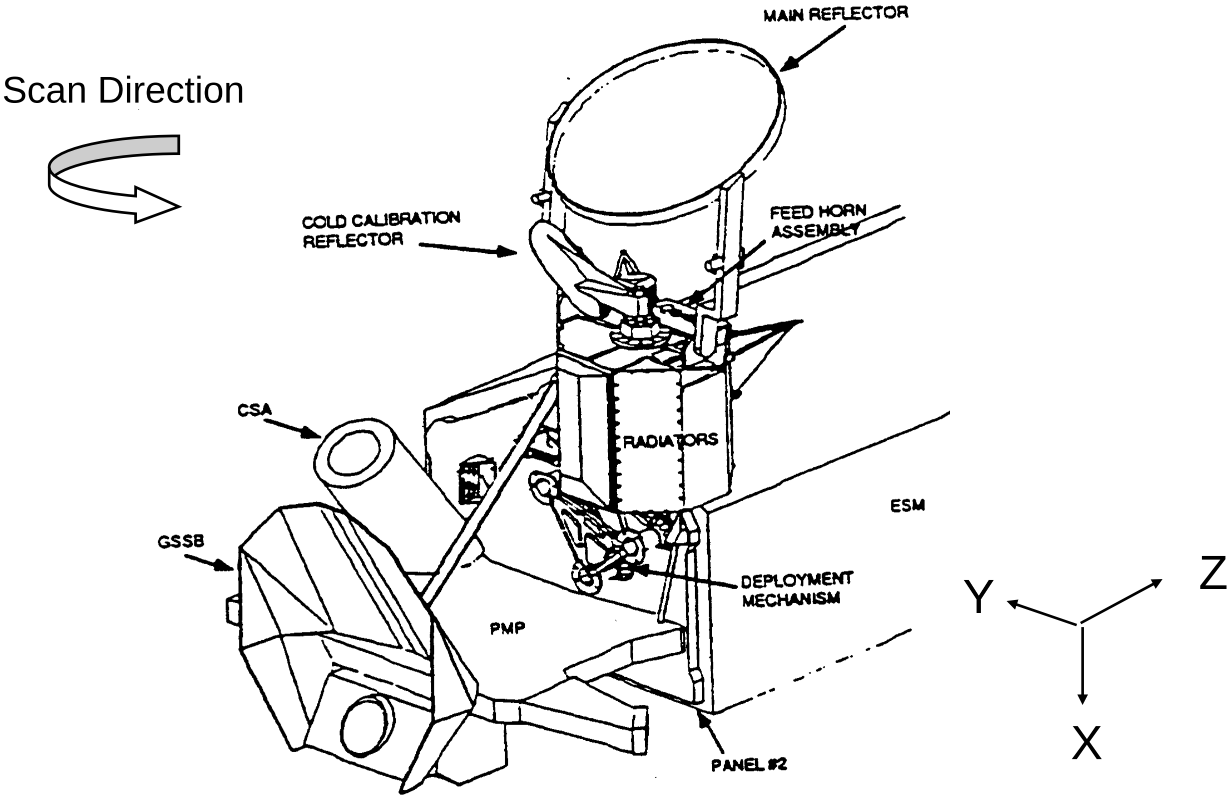

Simulation of Deployed SSMIS on F-16 Spacecraft

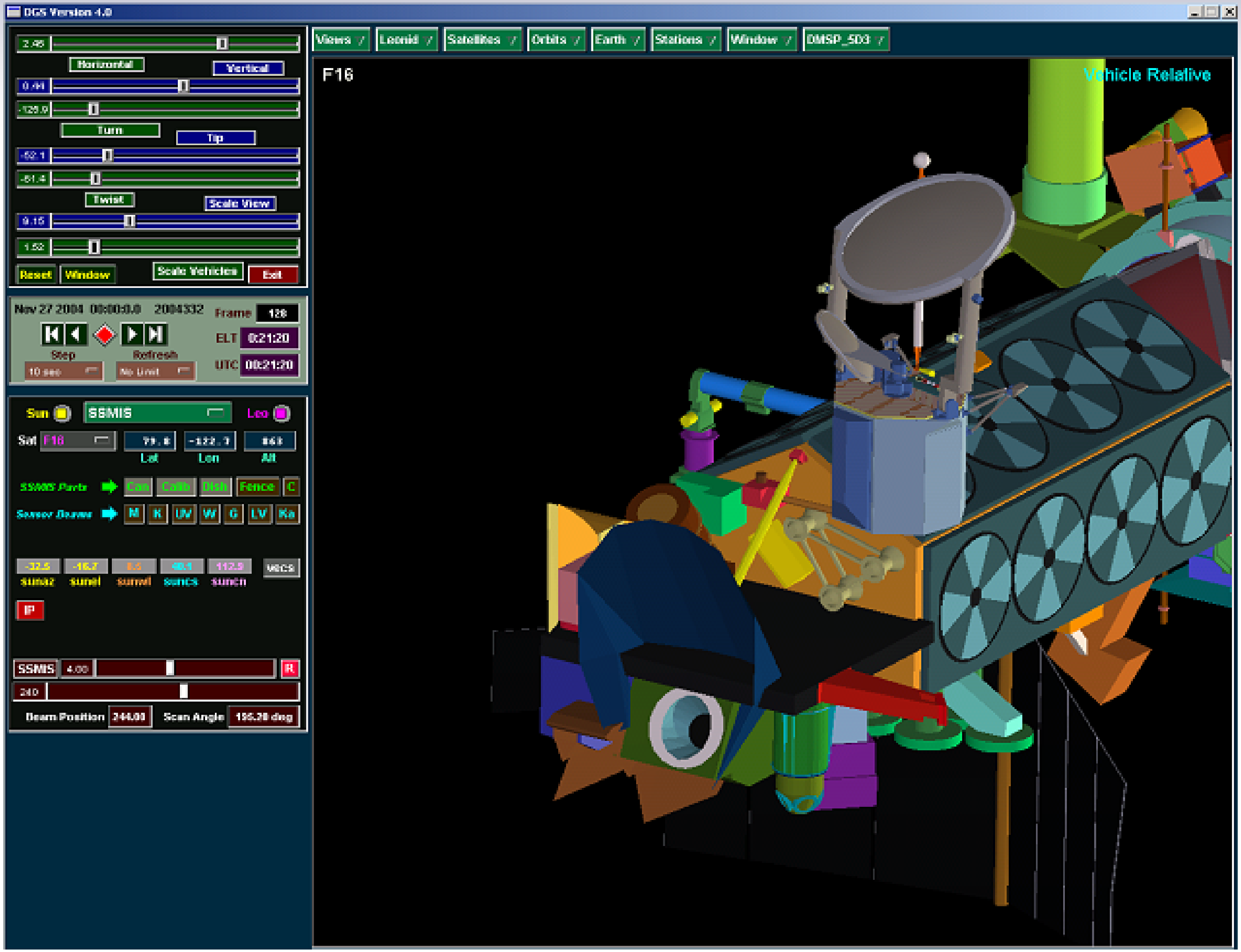

Nov 27 2004 00:00:0.0 2004332

Frame 128

ELT 0:21:20

UTC 00:21:20

Step 10 sec

Refresh No Limit

Sat F16

Beam Position 244.00

Scan Angle 195.28 deg

SSMIS Scan Diagram

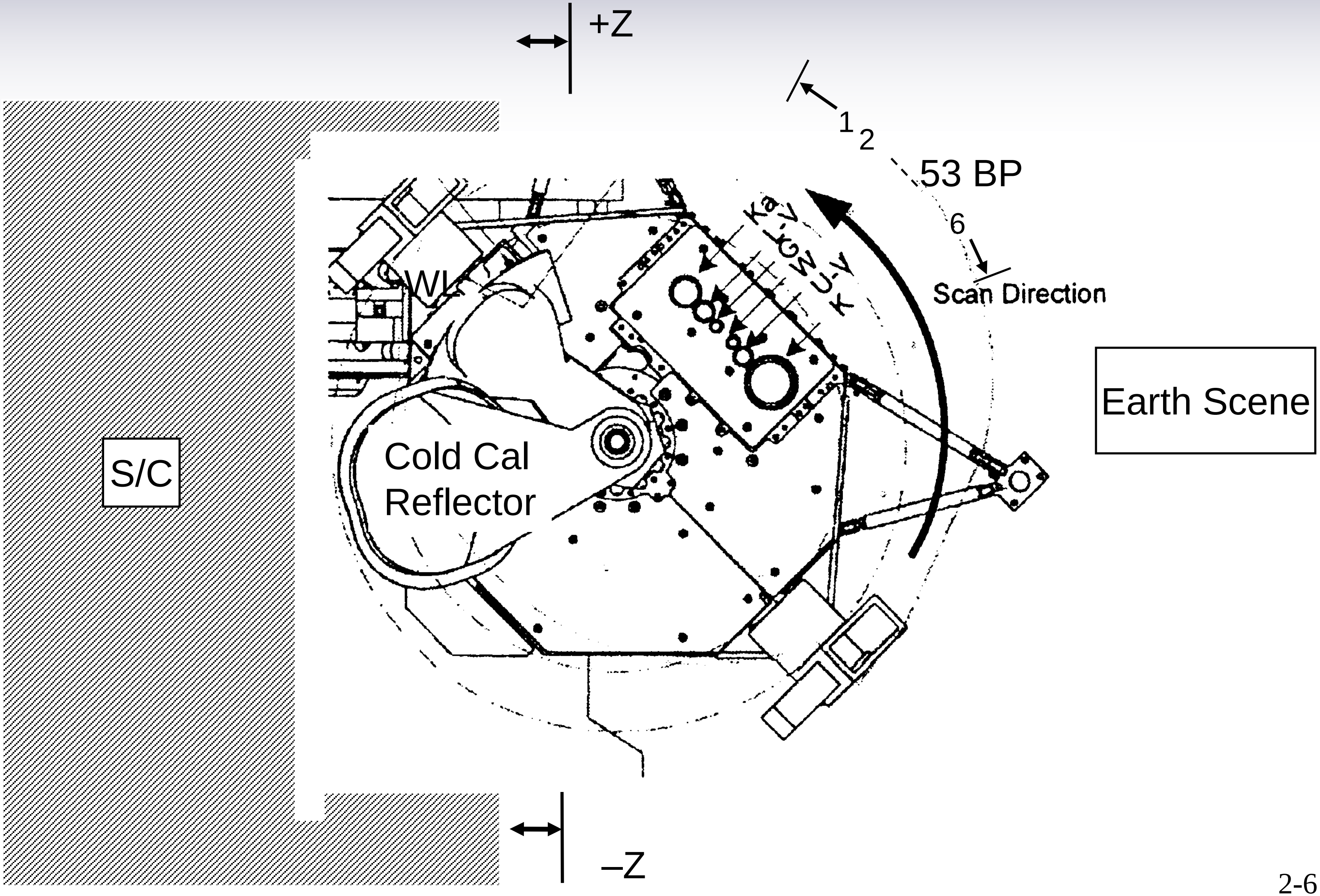

DGS Simulation of SSMIS and F-16 Spacecraft

Nov 27 2004 00:00:0.0 2004332

Frame 128

ELT 0:21:20

UTC 00:21:20

Step 10 sec

Refresh No Limit

SSMIS

Sat F16

Lat 79.8

Lon -122.7

Alt 863

-32.5	-16.7	8.5	40.1	112.9
sunaz	sunel	sunwl	suncs	suncn

SSMIS 4.00

200

Beam Position 204.00

Scan Angle 163.28 deg

SSMIS Scan Timing Diagram

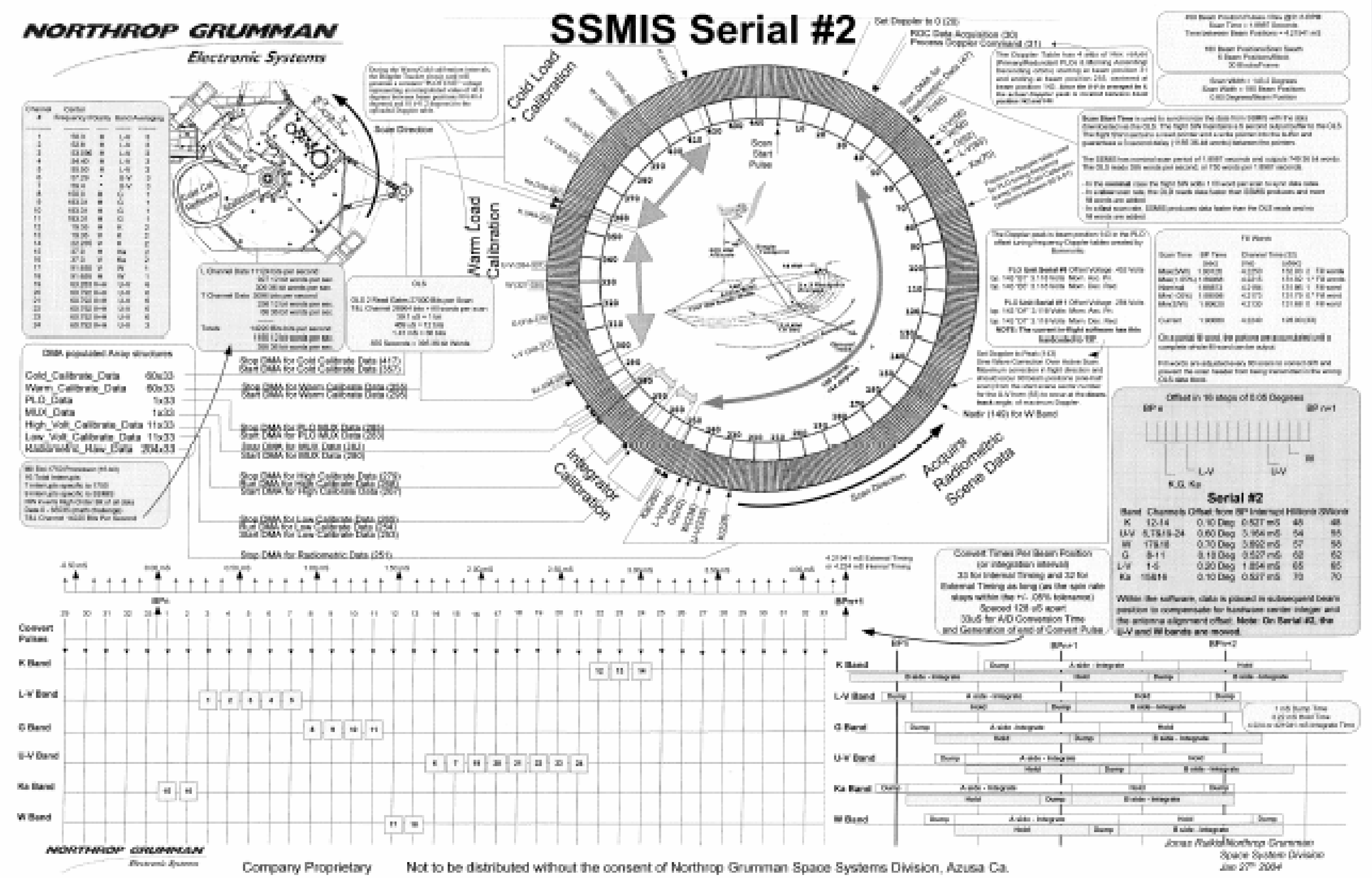

Early Orbit Mode 2 Data from S/N02 (2003)

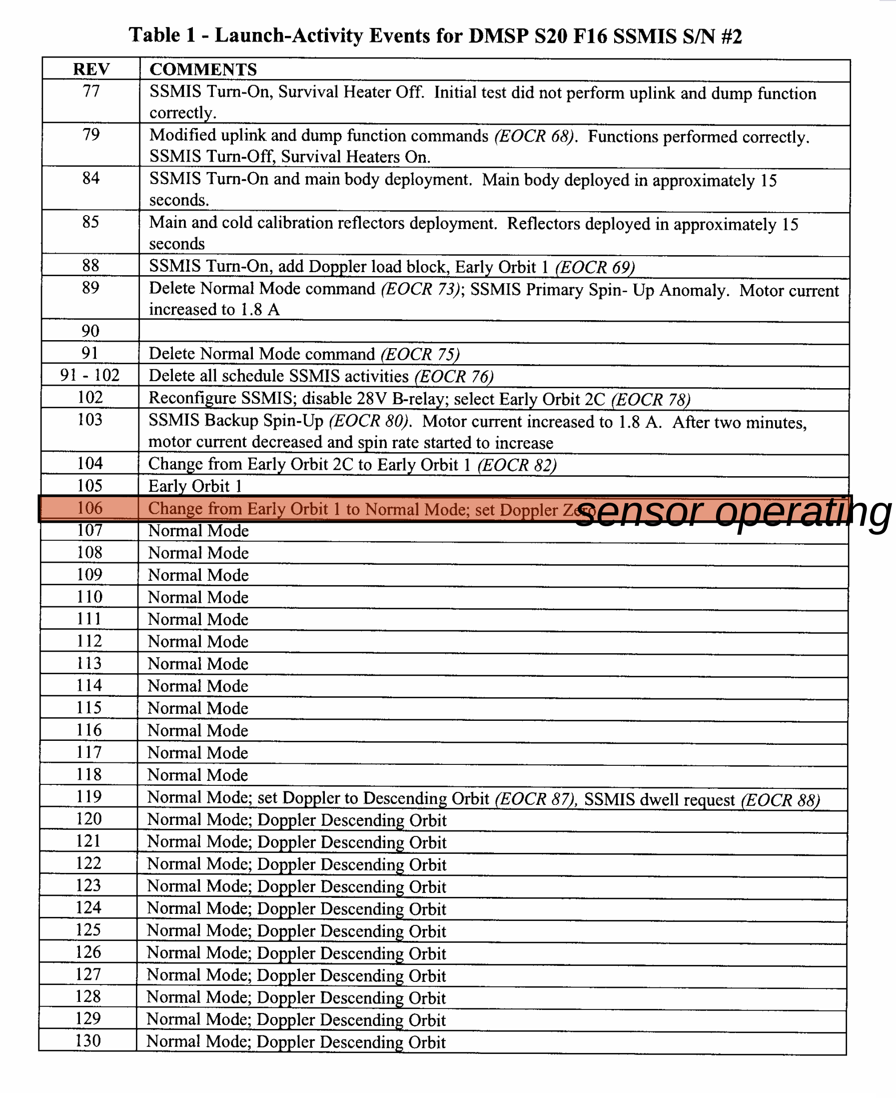

Table 1 - Launch-Activity Events for DMSP S20 F16 SSMIS S/N #2

REV	COMMENTS
77	SSMIS Turn-On, Survival Heater Off. Initial test did not perform uplink and dump function correctly.
79	Modified uplink and dump function commands *(EOCR 68)*. Functions performed correctly. SSMIS Turn-Off, Survival Heaters On.
84	SSMIS Turn-On and main body deployment. Main body deployed in approximately 15 seconds.
85	Main and cold calibration reflectors deployment. Reflectors deployed in approximately 15 seconds
88	SSMIS Turn-On, add Doppler load block, Early Orbit 1 *(EOCR 69)*
89	Delete Normal Mode command *(EOCR 73)*; SSMIS Primary Spin- Up Anomaly. Motor current increased to 1.8 A
90	
91	Delete Normal Mode command *(EOCR 75)*
91 - 102	Delete all schedule SSMIS activities *(EOCR 76)*
102	Reconfigure SSMIS; disable 28V B-relay; select Early Orbit 2C *(EOCR 78)*
103	SSMIS Backup Spin-Up *(EOCR 80)*. Motor current increased to 1.8 A. After two minutes, motor current decreased and spin rate started to increase
104	Change from Early Orbit 2C to Early Orbit 1 *(EOCR 82)*
105	Early Orbit 1
106	Change from Early Orbit 1 to Normal Mode; set Doppler Ze
107	Normal Mode
108	Normal Mode
109	Normal Mode
110	Normal Mode
111	Normal Mode
112	Normal Mode
113	Normal Mode
114	Normal Mode
115	Normal Mode
116	Normal Mode
117	Normal Mode
118	Normal Mode
119	Normal Mode; set Doppler to Descending Orbit *(EOCR 87)*, SSMIS dwell request *(EOCR 88)*
120	Normal Mode; Doppler Descending Orbit
121	Normal Mode; Doppler Descending Orbit
122	Normal Mode; Doppler Descending Orbit
123	Normal Mode; Doppler Descending Orbit
124	Normal Mode; Doppler Descending Orbit
125	Normal Mode; Doppler Descending Orbit
126	Normal Mode; Doppler Descending Orbit
127	Normal Mode; Doppler Descending Orbit
128	Normal Mode; Doppler Descending Orbit
129	Normal Mode; Doppler Descending Orbit
130	Normal Mode; Doppler Descending Orbit

sensor operating

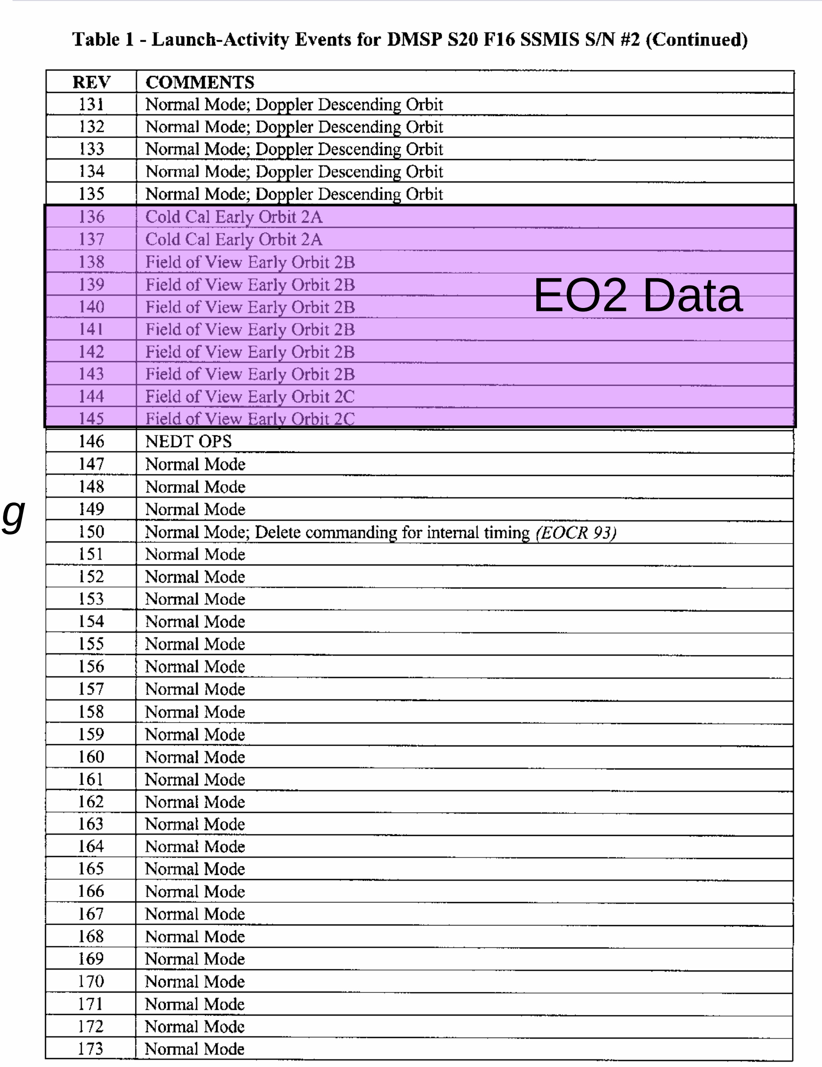

Table 1 - Launch-Activity Events for DMSP S20 F16 SSMIS S/N #2 (Continued)

REV	COMMENTS
131	Normal Mode; Doppler Descending Orbit
132	Normal Mode; Doppler Descending Orbit
133	Normal Mode; Doppler Descending Orbit
134	Normal Mode; Doppler Descending Orbit
135	Normal Mode; Doppler Descending Orbit
136	Cold Cal Early Orbit 2A
137	Cold Cal Early Orbit 2A
138	Field of View Early Orbit 2B
139	Field of View Early Orbit 2B
140	Field of View Early Orbit 2B
141	Field of View Early Orbit 2B
142	Field of View Early Orbit 2B
143	Field of View Early Orbit 2B
144	Field of View Early Orbit 2C
145	Field of View Early Orbit 2C
146	NEDT OPS
147	Normal Mode
148	Normal Mode
149	Normal Mode
150	Normal Mode; Delete commanding for internal timing *(EOCR 93)*
151	Normal Mode
152	Normal Mode
153	Normal Mode
154	Normal Mode
155	Normal Mode
156	Normal Mode
157	Normal Mode
158	Normal Mode
159	Normal Mode
160	Normal Mode
161	Normal Mode
162	Normal Mode
163	Normal Mode
164	Normal Mode
165	Normal Mode
166	Normal Mode
167	Normal Mode
168	Normal Mode
169	Normal Mode
170	Normal Mode
171	Normal Mode
172	Normal Mode
173	Normal Mode

EO2 Data

2.2 SSMIS Calibration Target Fields-of-View (FOV) Analysis

The first task was to verify the correct alignment of the hot and cold calibration target locations. Samples of the EO2 data for Channel 12 (19.35 GHz H-pol) the lowest channel frequency for SSMIS and Channel 8 150-GHz H-pol) high frequency channel are shown on pages 2-11 to 2-14. The timing diagram indicates that beam positions 351 – 354 and 414 – 417 are used for the Hot and Cold Calibration locations, respectively, for Channel 12 (K-band group) and that beam positions 317 – 320 and 380 – 383 are used for the Hot and Cold Calibration observations for Channel 8 (G-band group). Examples from the lowest and highest SSMIS channel frequency set were chosen to contrast the range of valid calibration target beam positions. Note the ‘sawtooth’ response between odd and even beam positions. The odd and even beam positions for each channel utilize separate integrator circuits in the SSMIS. This leads to slightly different radiometric ‘counts’ for the same scene brightness. The key result shown by pages 2-11 to 2-14 is the stable hot and cold calibration values over the correct range of beam positions for each channel. The calibration FOVs appeared to be correctly aligned and stable for all channels. In fact, in many cases it appeared that many more beam positions could be utilized for each calibration observation.

Channel 12 Warm Load Observations

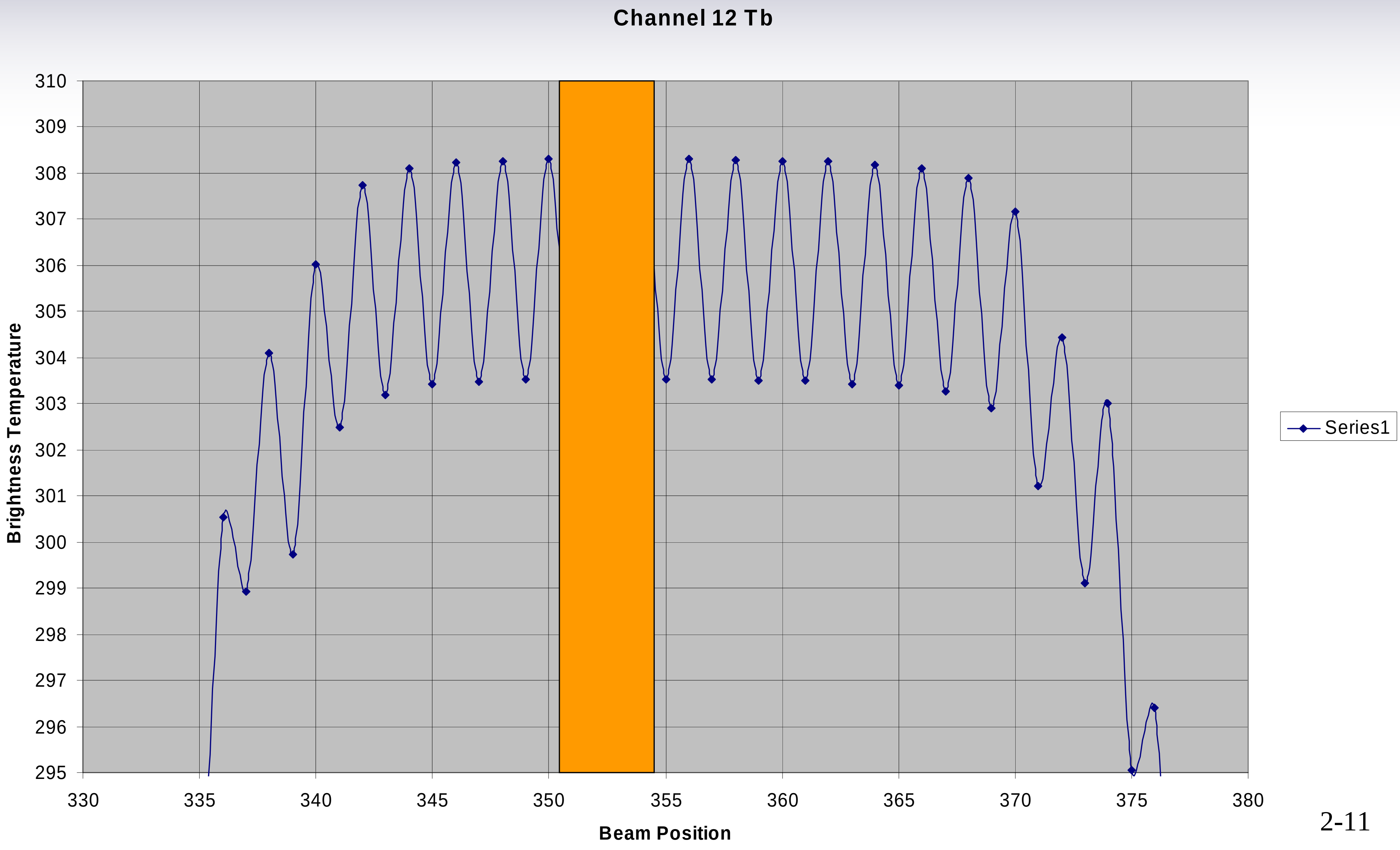

Channel 12 Cold Target Observations

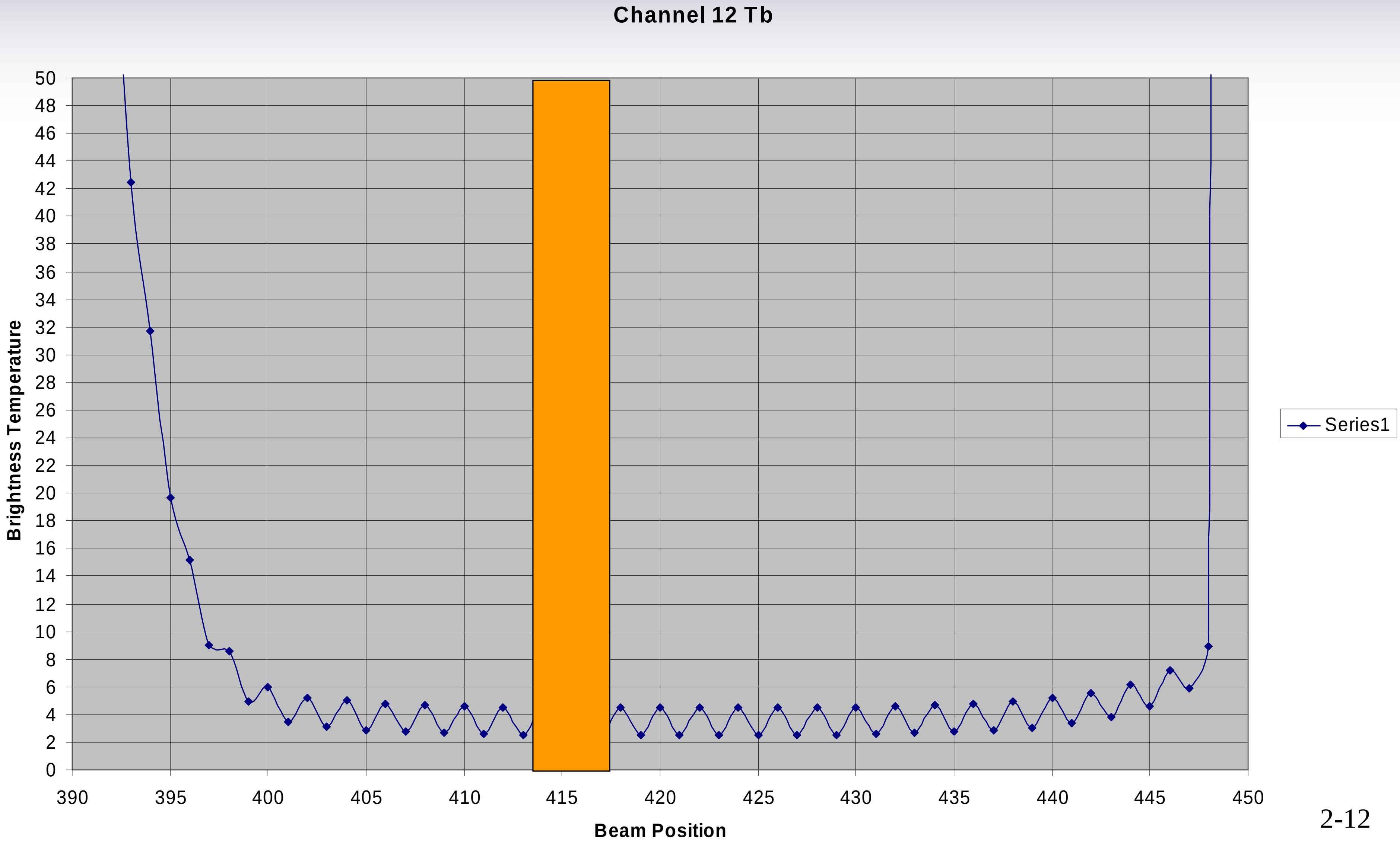

Channel 8 Warm Load Observations

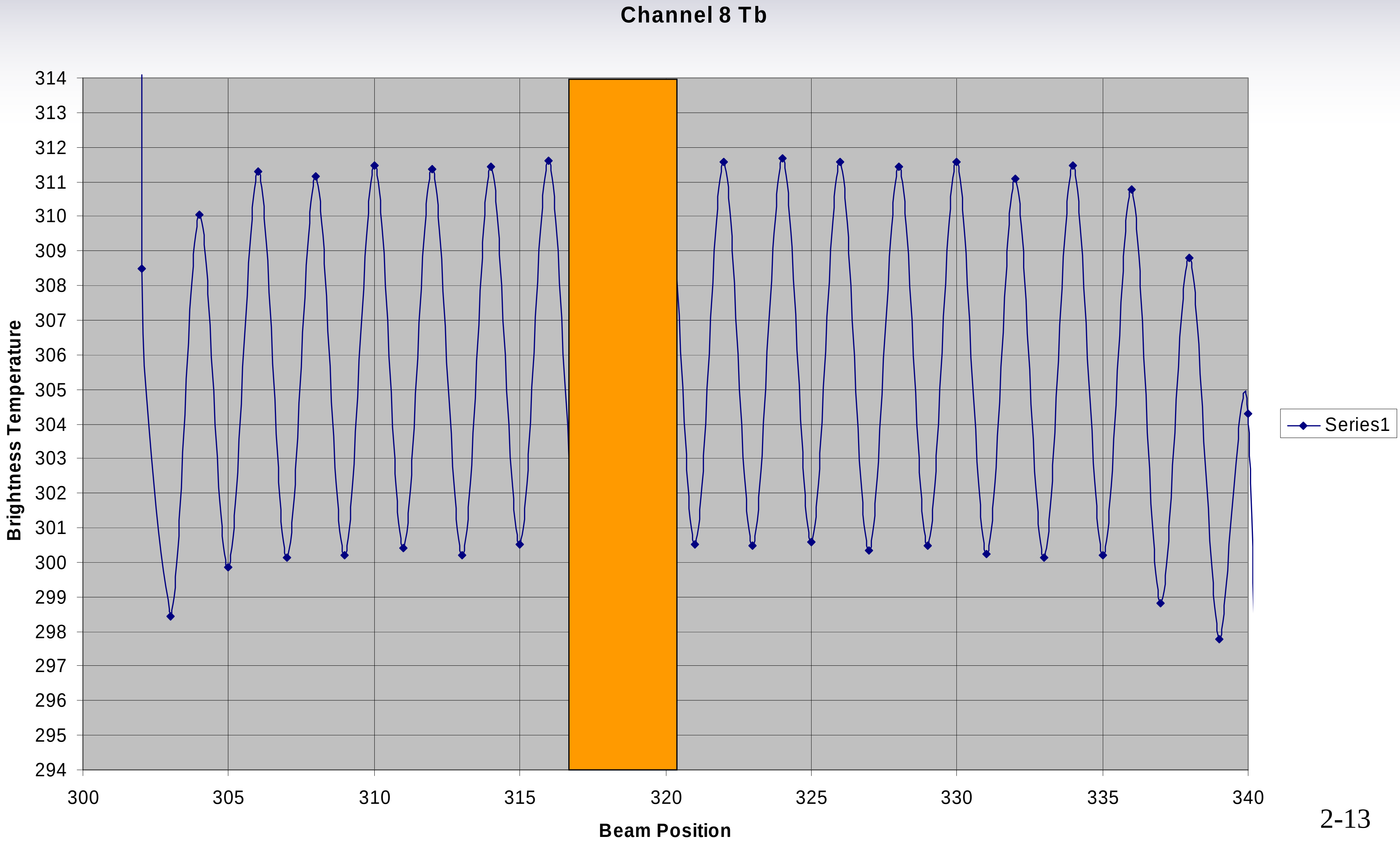

Channel 8 Cold Target Observations

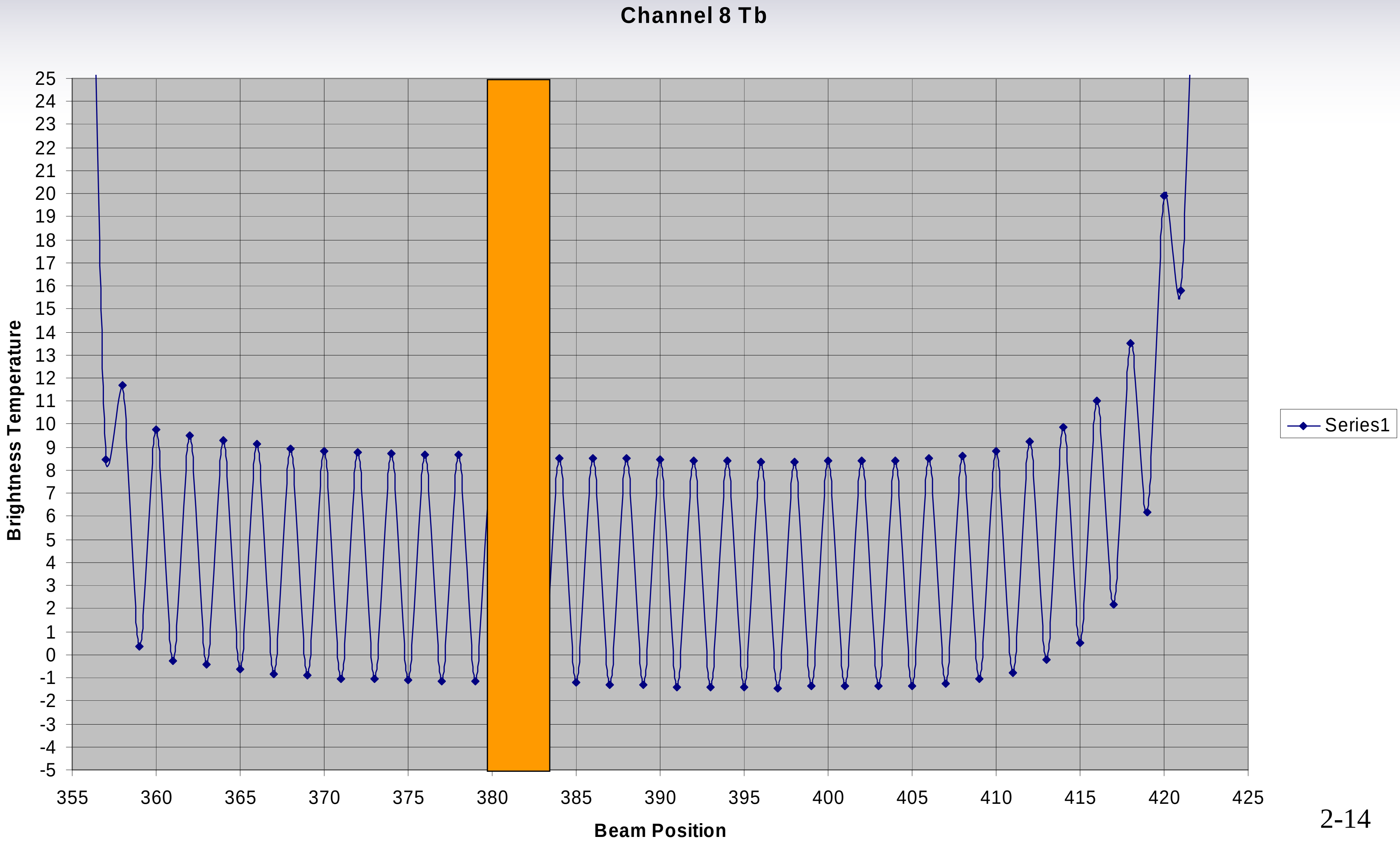

2.3 SSMIS Earth Scene FOV Analysis

The Earth Scene FOV was examined by scaling the radiometric ‘counts’ to a representative brightness temperature and viewing the data trends over the entire Earth scene FOV. Examples are again shown for Channel 12 and Channel 8, representing the lowest and highest frequency channel groups. Channel 15 is also included due to the location of this feedhorn at the opposite end of the Channel 12 feedhorn. Notice on page 2-16, the edge of the Earth scene FOV for Channel 12 is beam position 48 (see page 2-8), however, the radiometric counts, averaged over 2 orbits of EO2C data collection trends downward before reaching the edge of scan. This is an indicator of edge-of-scan bias caused by FOV intrusions at the beginning of scan for Channel 12. Left uncorrected, this bias could have significant impacts on the quality of SSMIS Environmental Data Records. The end-of-scan for Channel 12 shows no such ‘roll-off’. Likewise Channel 8 shows no indications of edge-of-scan bias at either end of its active scan range (indicated by the orange shaded bars). In contrast to Channel 12, Channel 15 data indicate a roll-off at the end-of-scan range shown on page 2-21, however, the beginning of scan (2-20) shows uniformity at the edge. Pages 2-22 to 2-27 show data from the entire 360° (450 BP) view of the sensor rotation. Page 2-28 summarizes these views in the order that the feedhorns pass into view of the calibration targets (K_A-Band first). The order is evident by the phase of the hot calibration beam position range which moves steadily later (beam positions with high T_B) in views 1 – 6. In contrast, page 2-29 shows the order of feedhorn views relative to the Earth scene. The K-band feed begins the Earth scene first at beam position 48.

Channel 12 Beginning of Scan

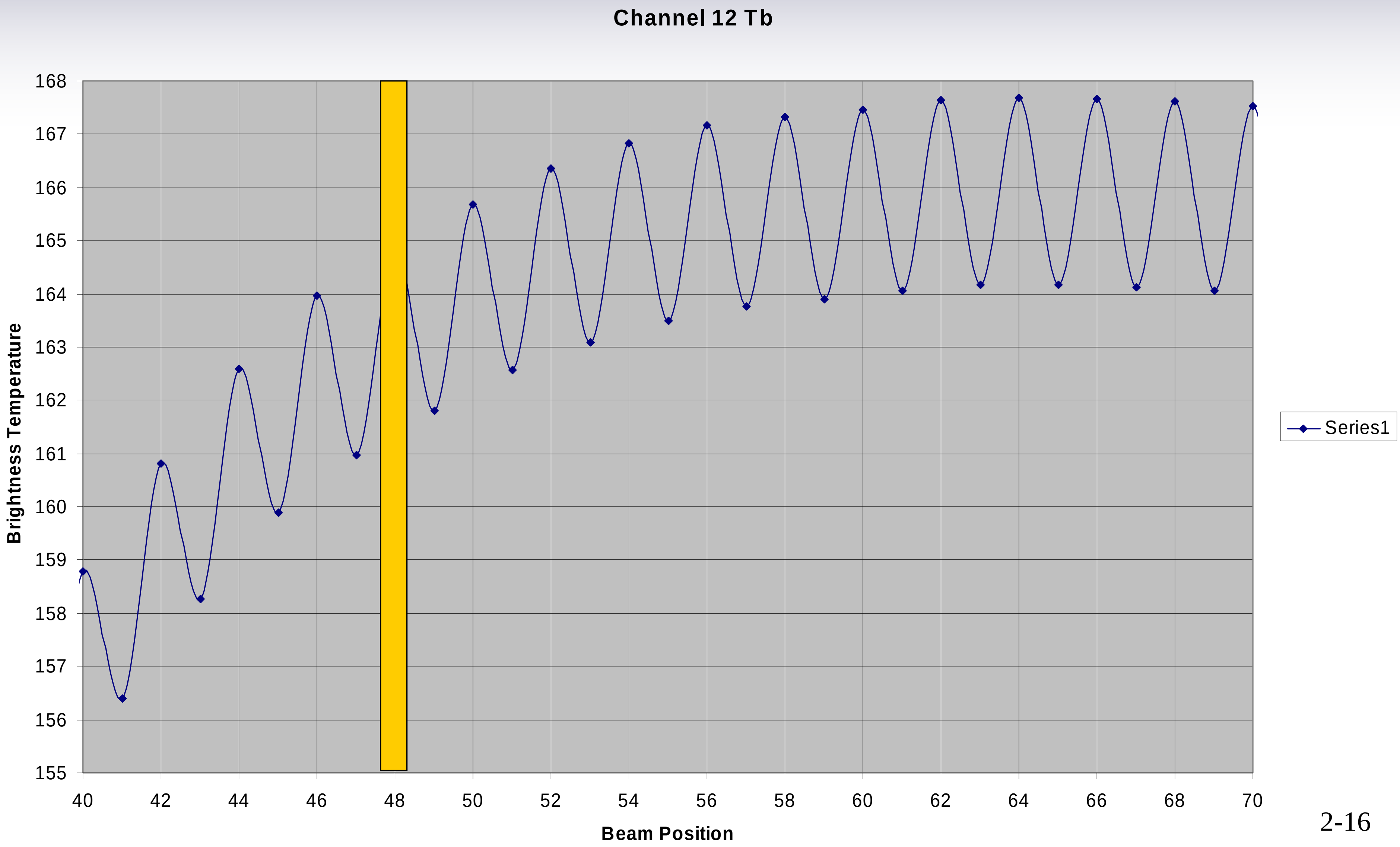

Channel 12 End of Scan

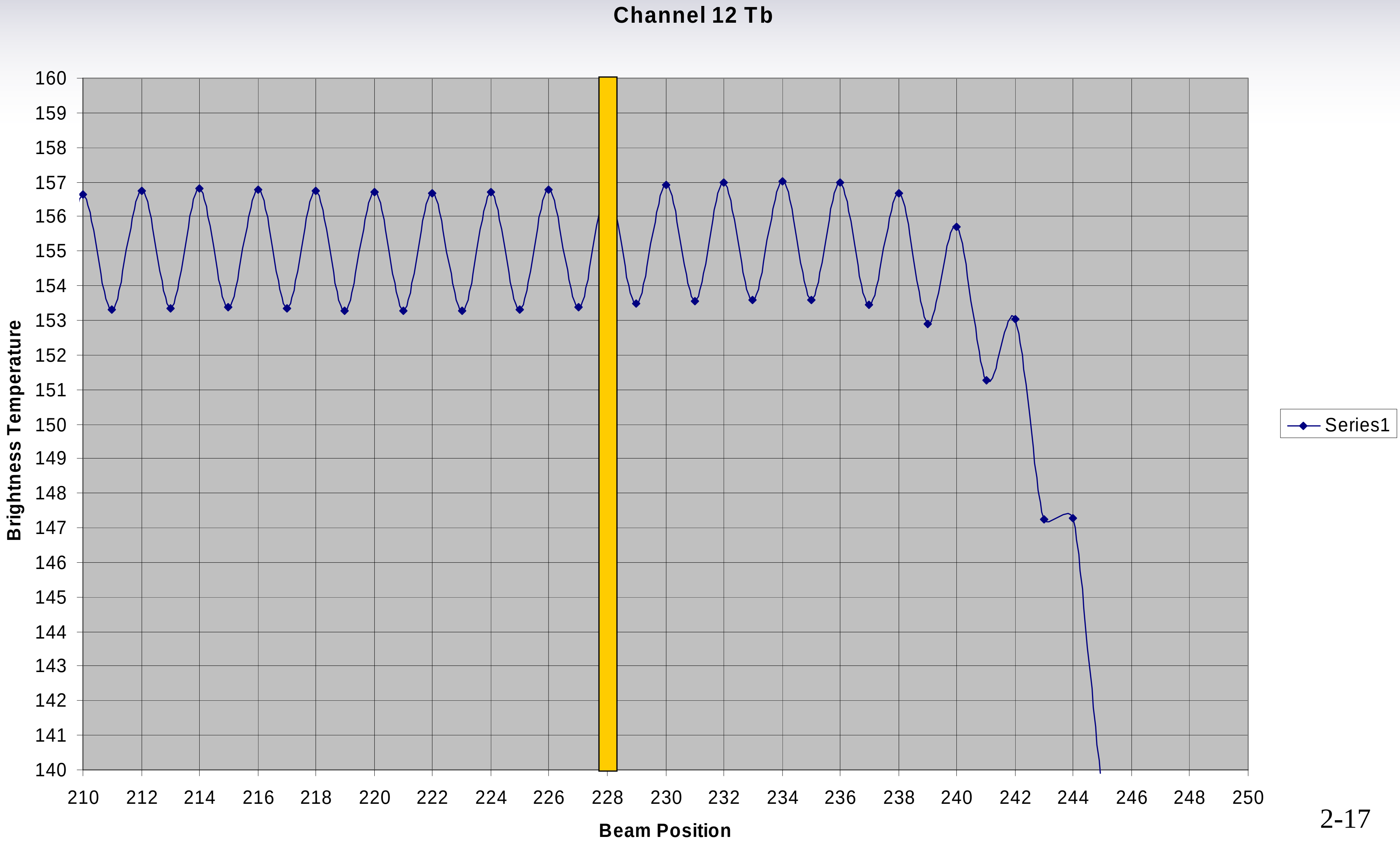

Channel 8 Beginning of Scan

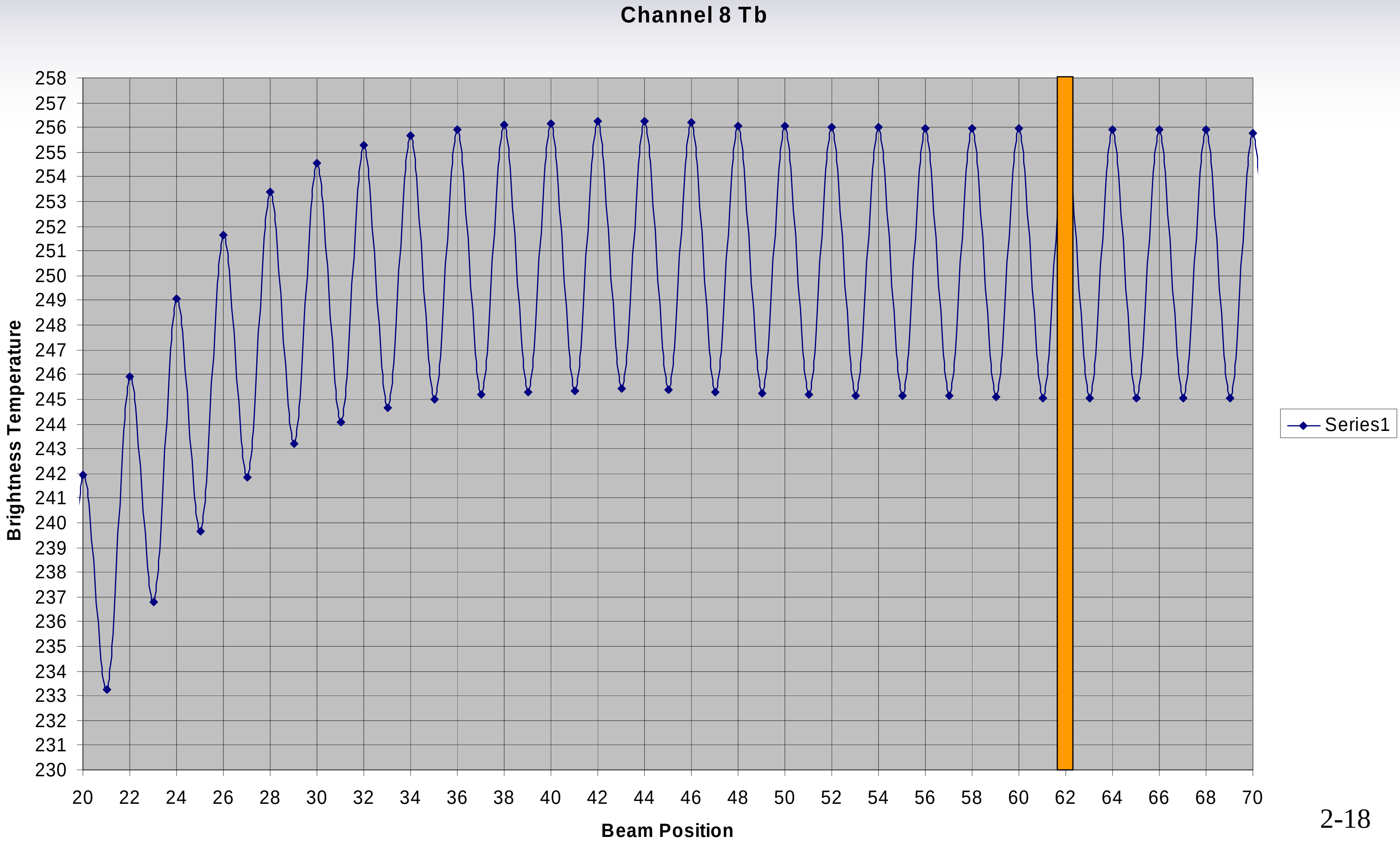

Channel 8 End of Scan

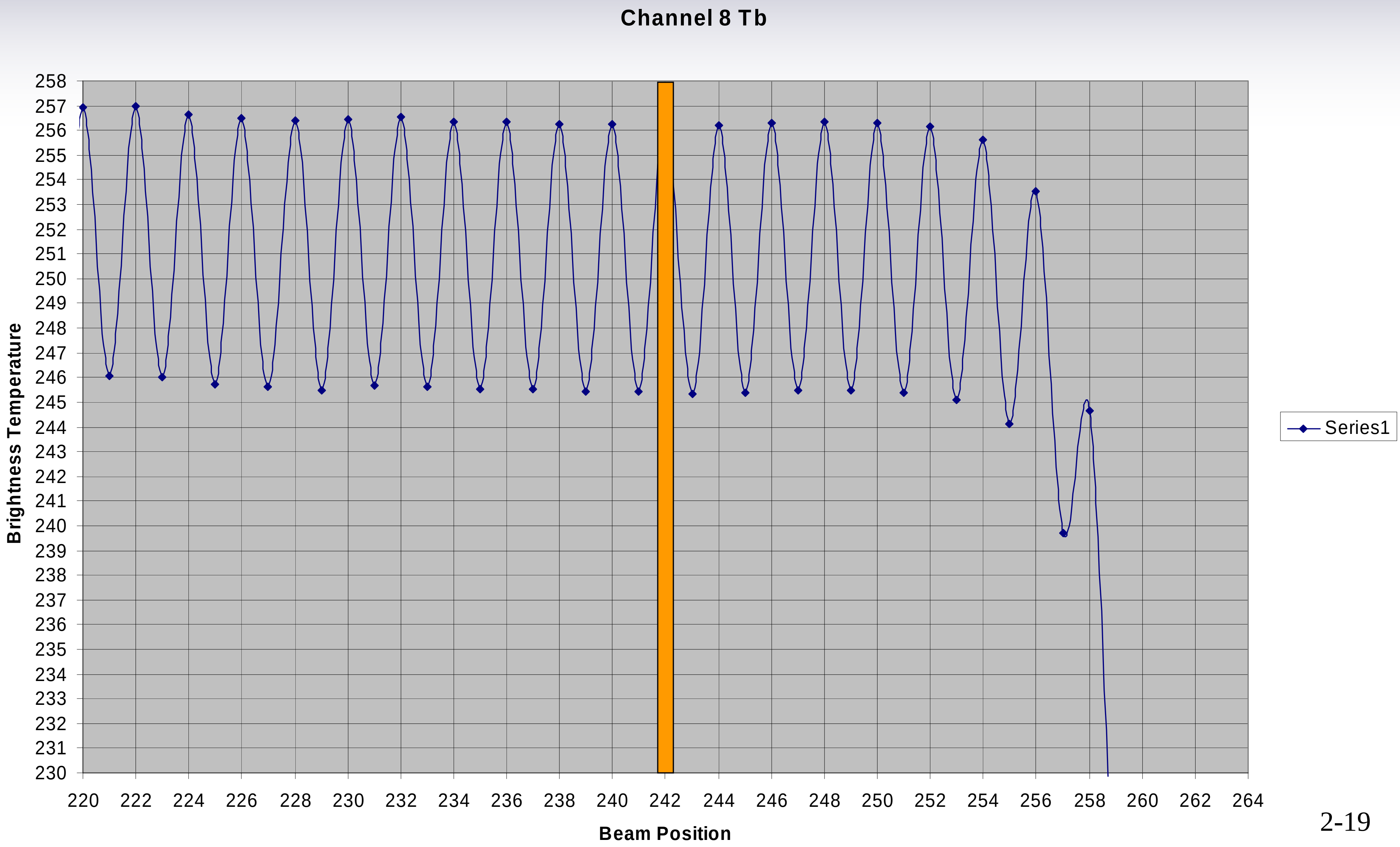

Channel 15 Beginning of Scan

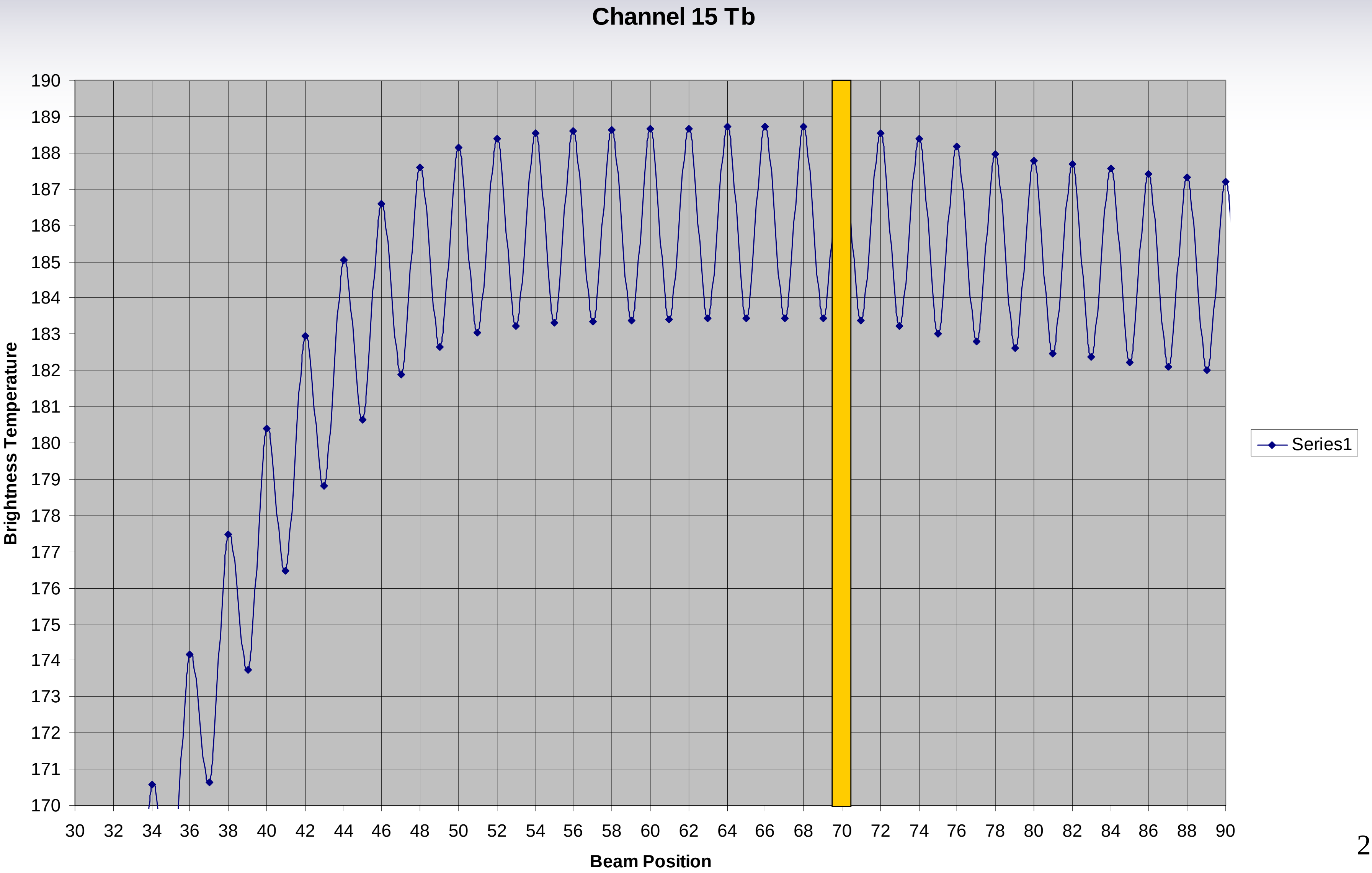

Channel 15 End of Scan

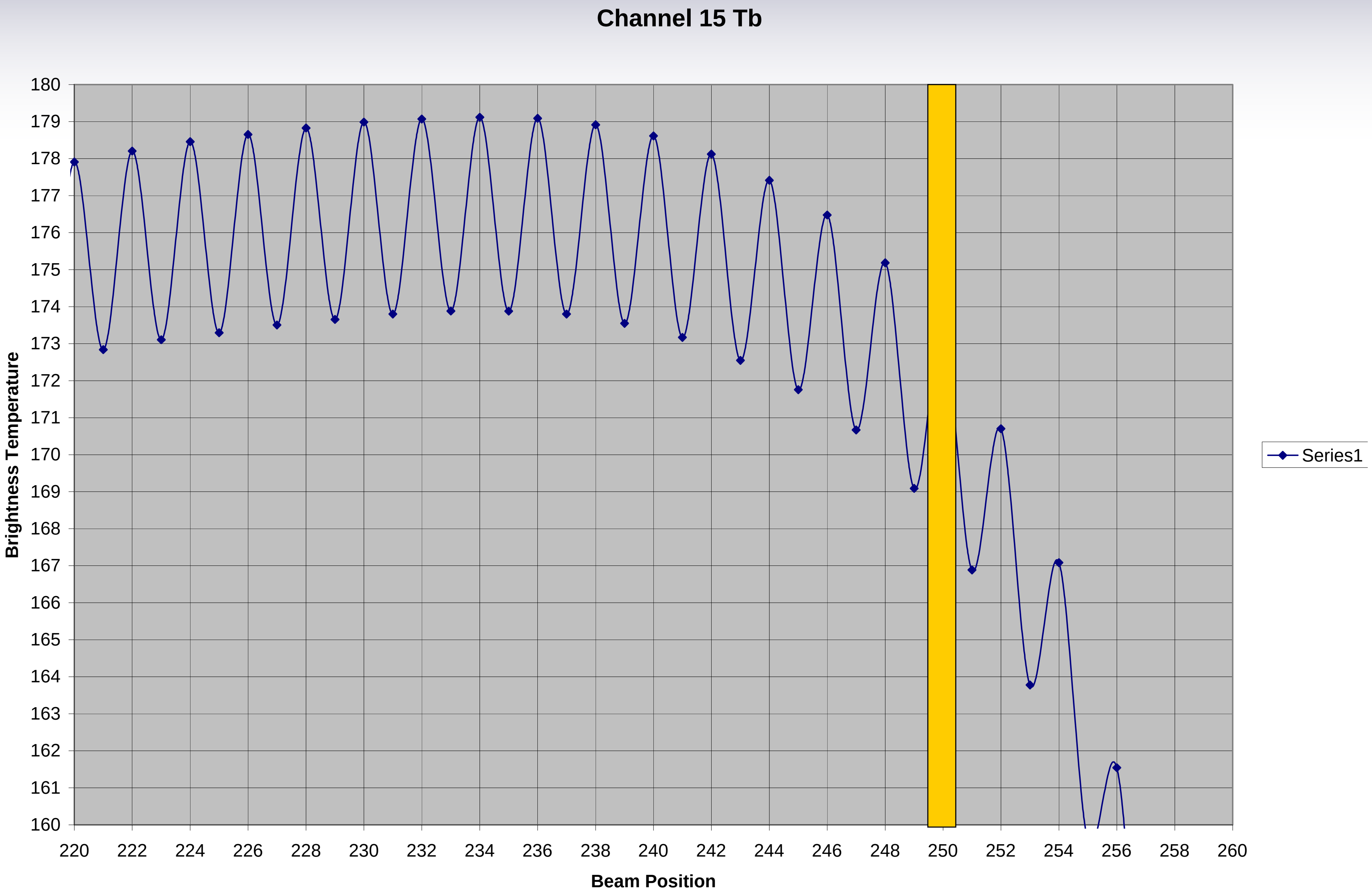

Channel 15 Full 360° Scan

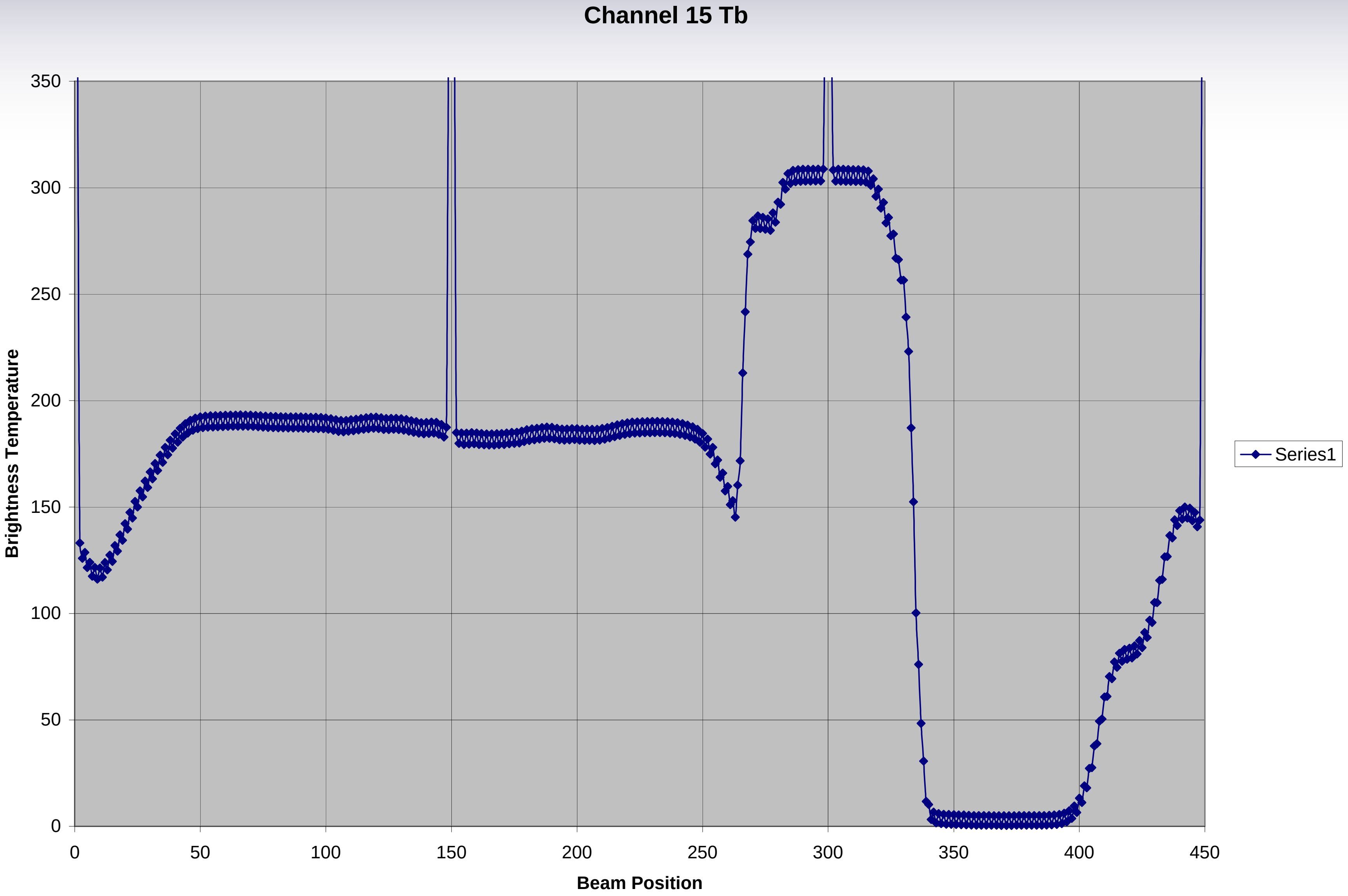

Channel 1 Full 360° Scan

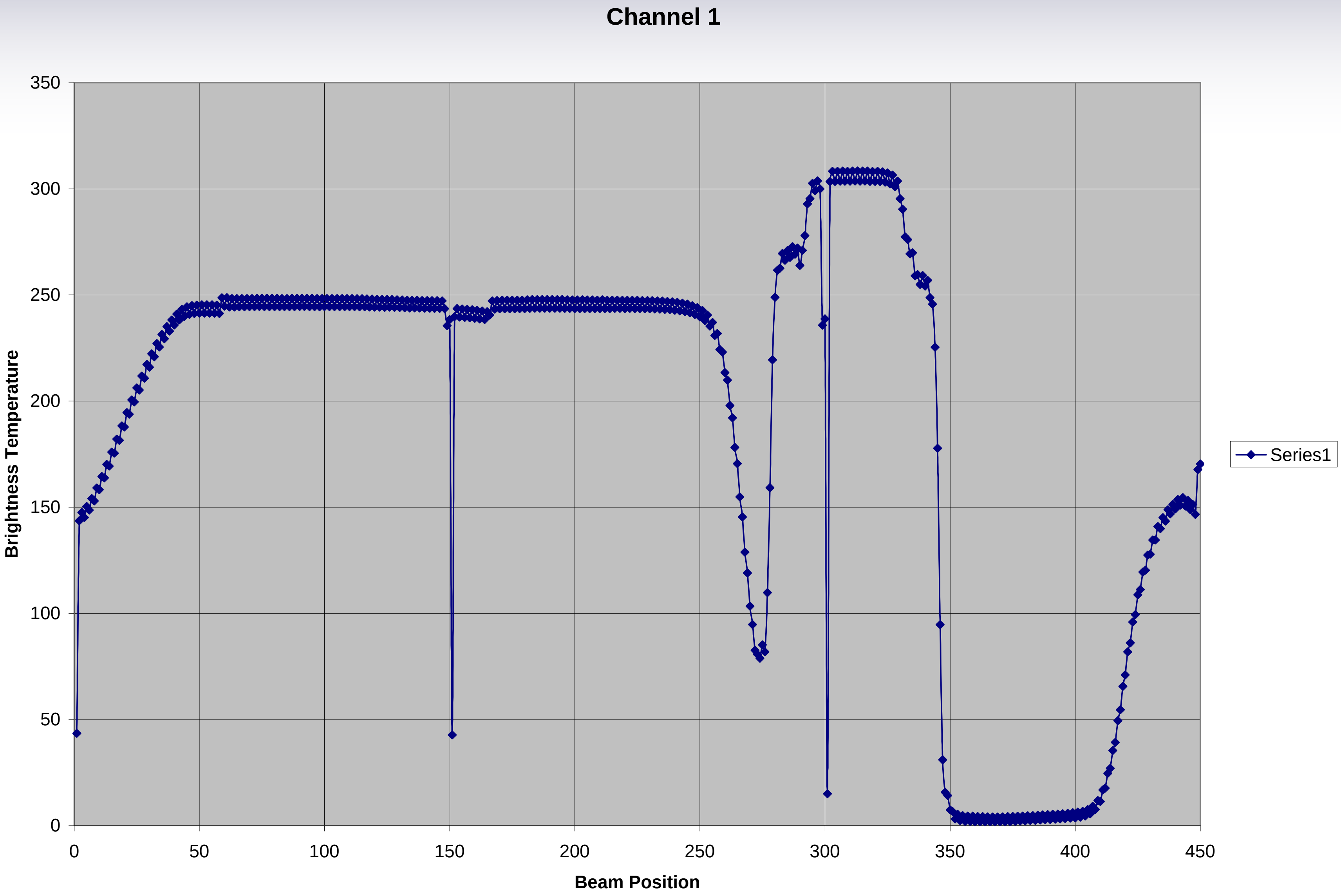

Channel 8 Full 360° Scan

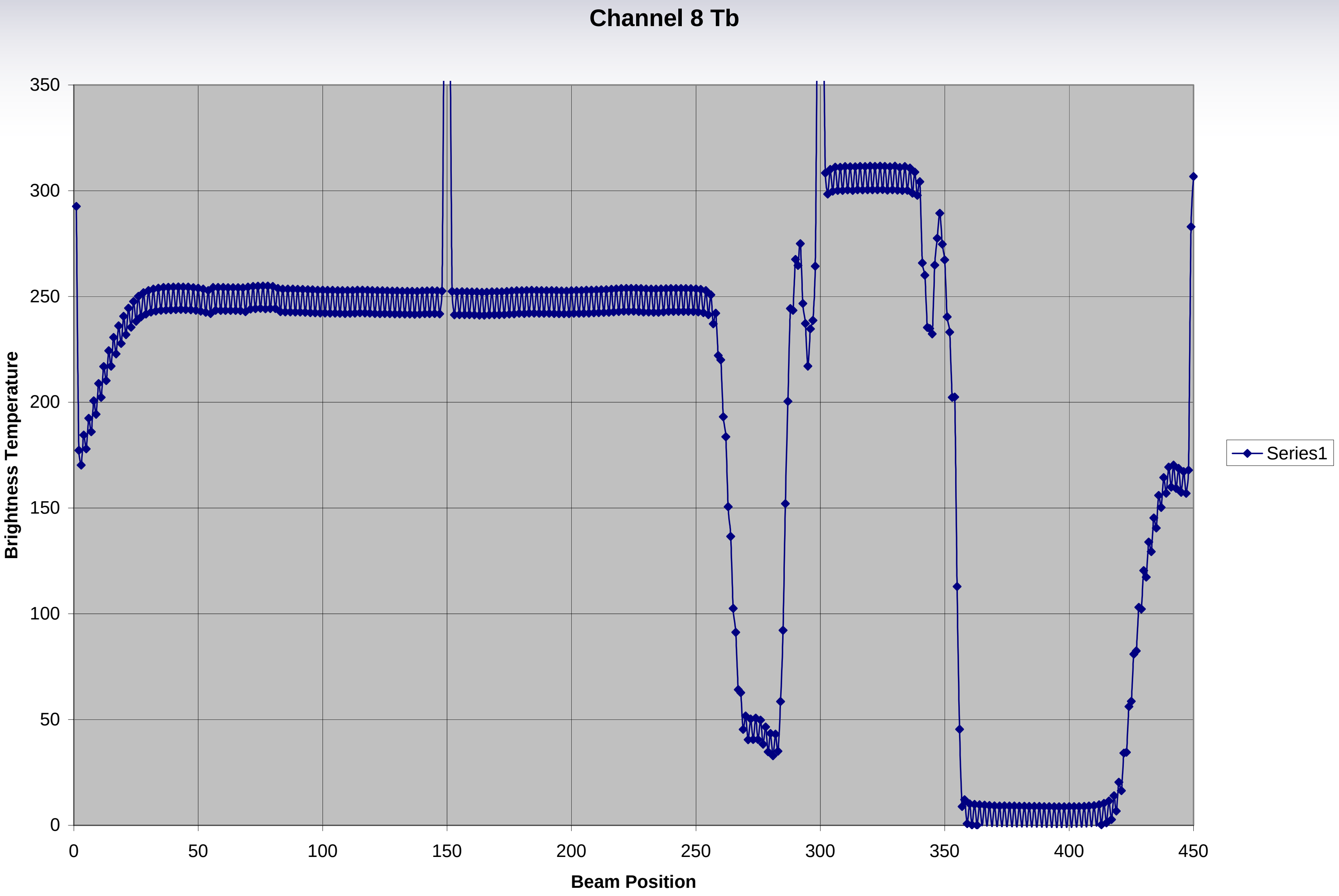

Channel 18 Full 360° Scan

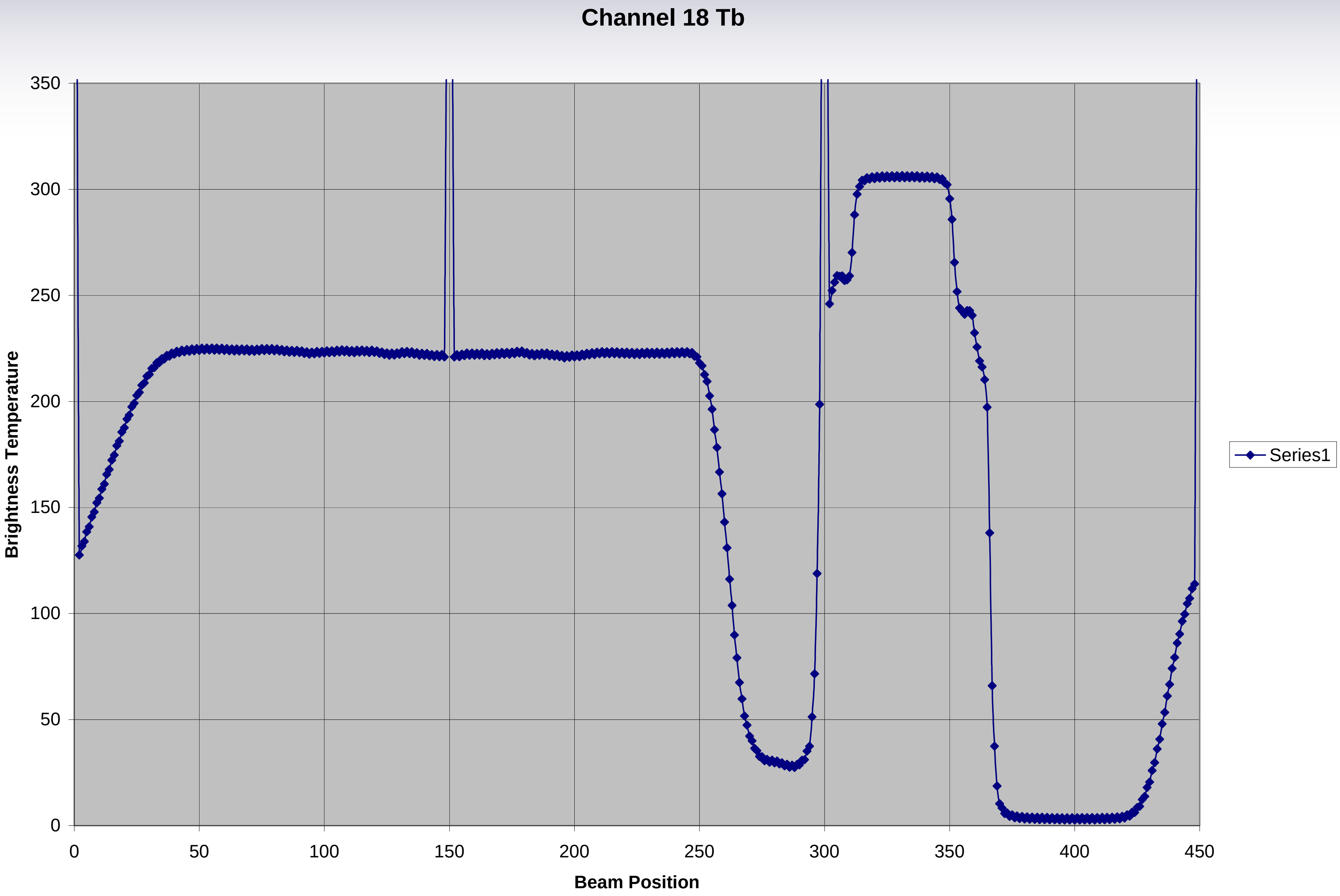

Channel 6 Full 360° Scan

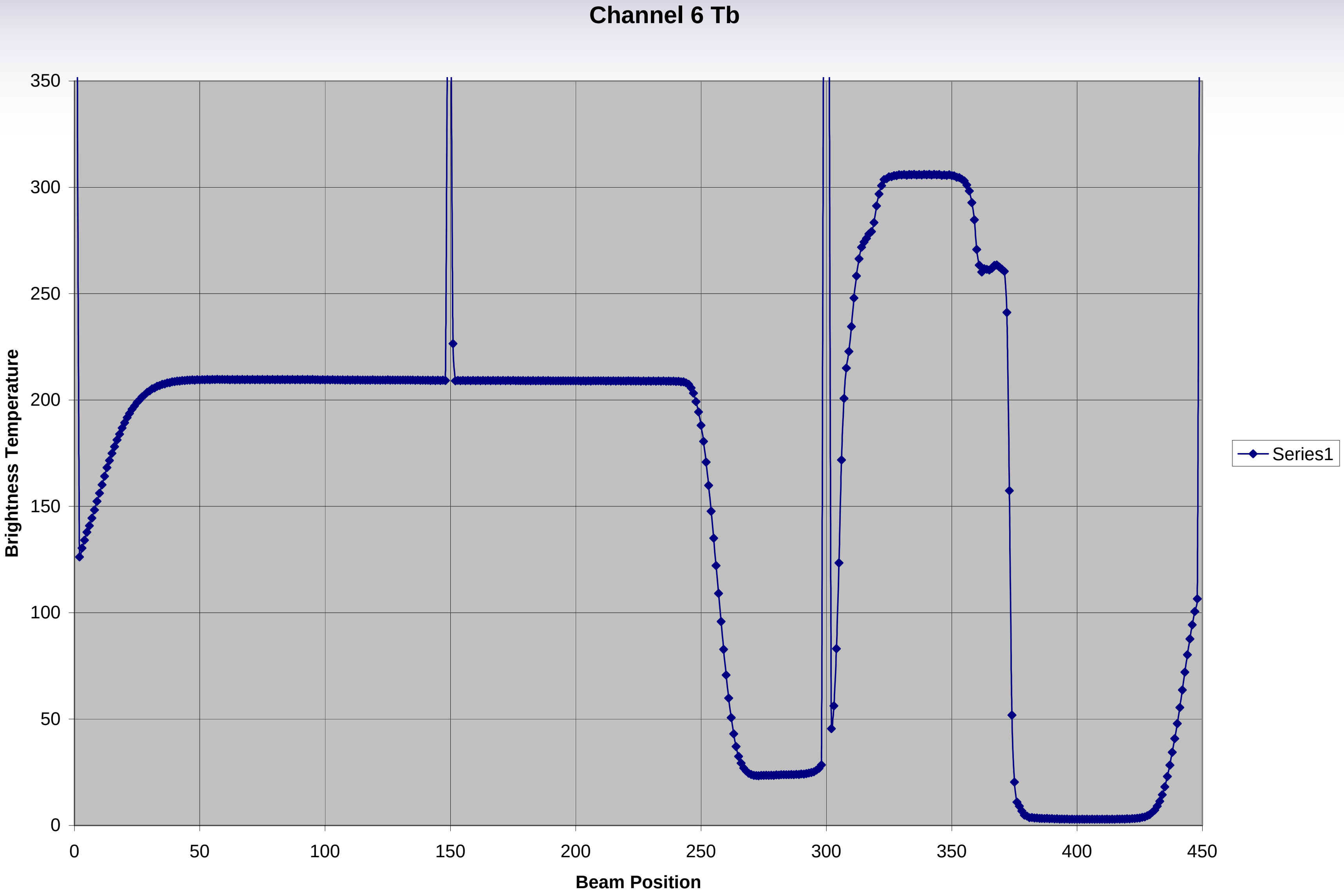

Channel 12 Full 360° Scan

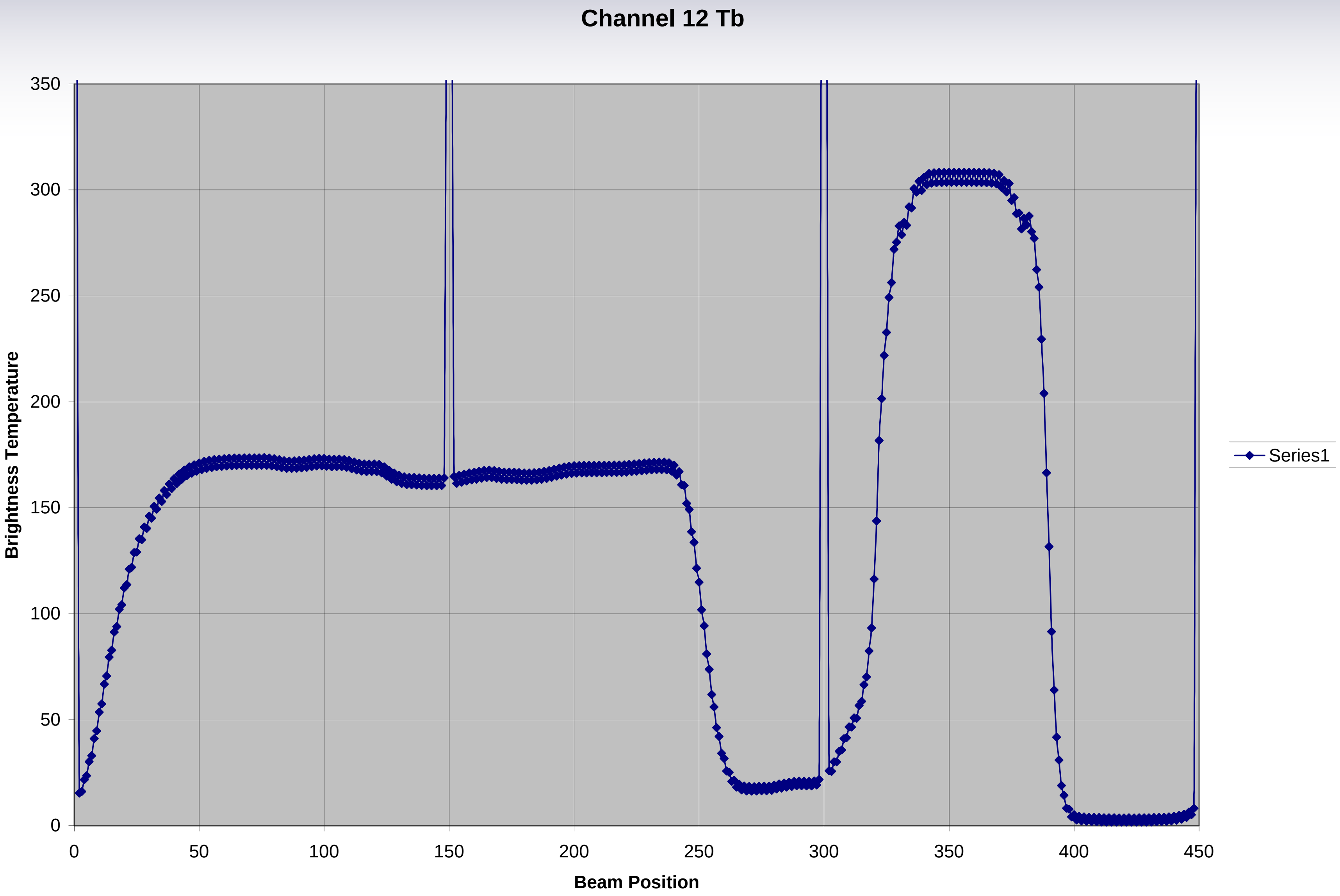

EO2B and EO2C 360º FOV (Sequence for Calibration)

K_A

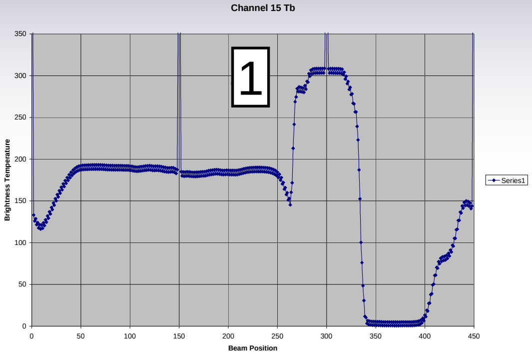

W

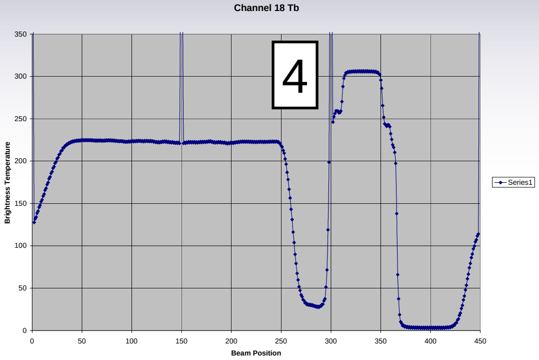

V_L

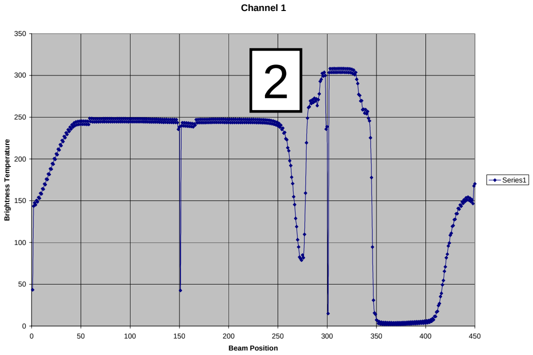

V_U

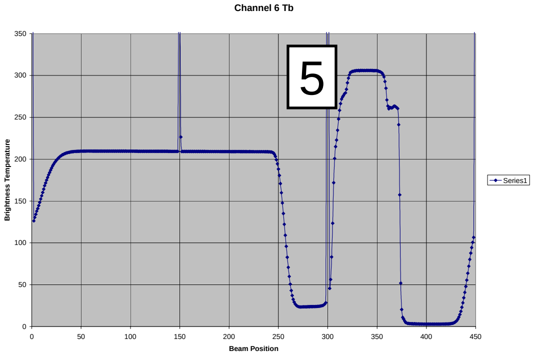

G

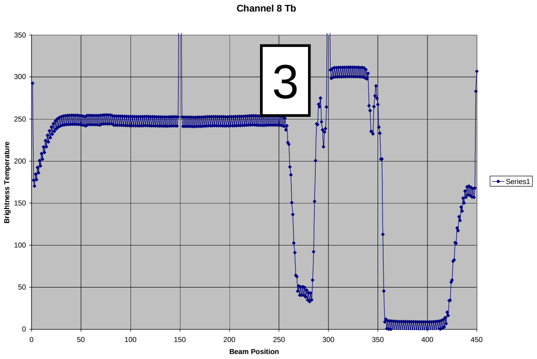

K

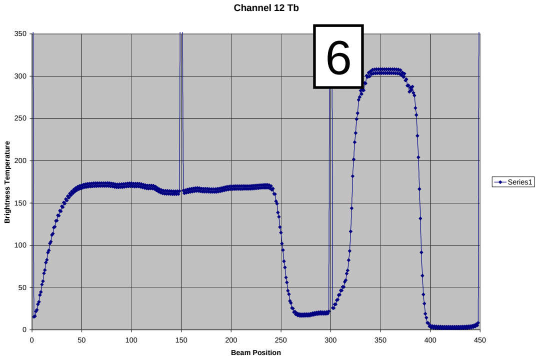

EO2B and EO2C 360º FOV (Sequence for Earth Scene)

K

Channel 12 Tb

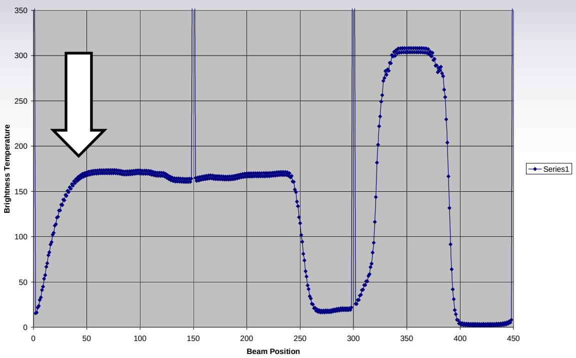

Channel 8 Tb

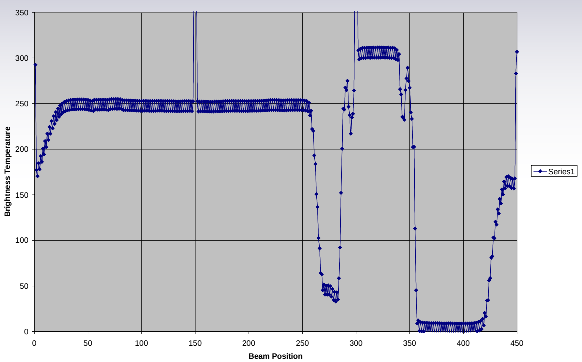

G

V_U

Channel 6 Tb

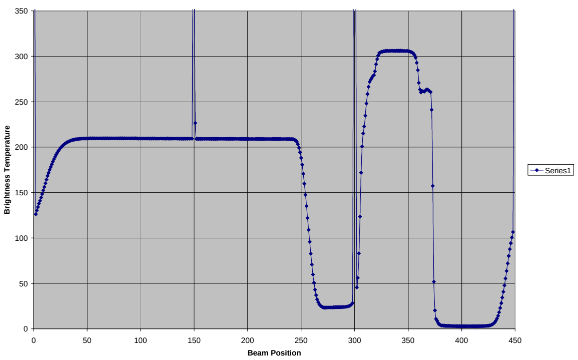

Channel 1

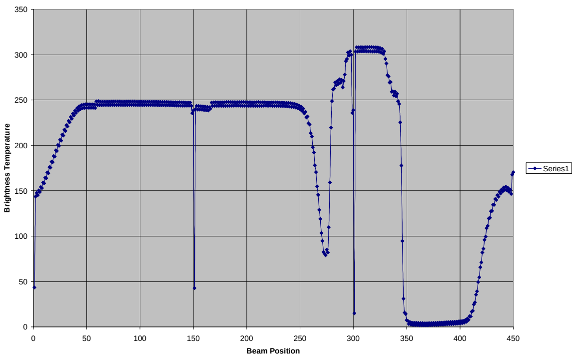

V_L

W

Channel 18 Tb

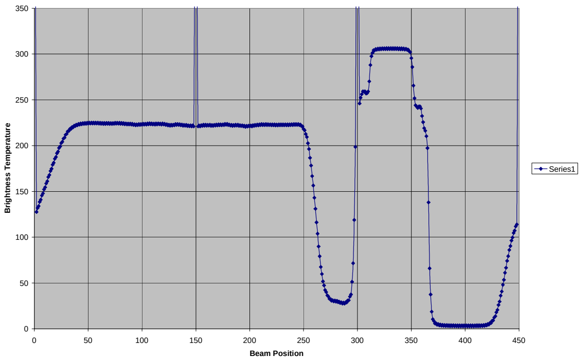

Channel 15 Tb

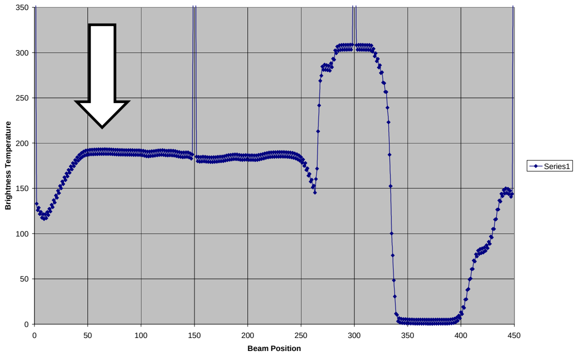

K_A

2.4 Explanation of Earth Scene FOV Intrusions

Page 2-31 shows graphically how the Earth scene FOV of Channel 12 leads the Channel 15 FOV. The Instantaneous Fields-of-View projected onto the Earth's surface are shown on page 2-32 showing 22 beam positions between Channel 12 (K-band) and Channel 15 (K_A-band). Page 2-33 summarizes the EO2B and EO2C data from the Earth Scene FOV of Channels 1, 6, 8, 12, 15, and 18. The Beam position of all channels have been co-aligned with Channel 12 over the Earth scene in this plot to align edge-of-scan for each channel on the same plot. Here the roll-off of Channel 12 at the beginning of scan (BOS) and Channels 1 and 15 at the end-of-scan (EOS) are clearly evident summarizing the findings of earlier pages 2-16 to 2-21 with other data from EO2B and EO2C. On pages 2-34 to 2-40 we consider the DGS simulation and representative ranges of Beam positions for Earth FOV for each feedhorn. Page 2-34, 35, and 36 show the 'secondary' beam (emanating from the main reflector) interference with the body of the F-16 spacecraft beginning at beam position 240 (near the end of the Earth scene FOV). This is the most likely explanation for the characteristic roll-off observed in the graph on page 2-33 in Channels 1 and 15 which are still active in their Earth Scene FOV at Beam Position 240 (see chart 2-9). Recall that BP have been adjusted for all channels except Channel 12 on page 2-33. Contributions to the characteristic roll-offs for Channel 12 (BOS) and Channel 15 (EOS) can be seen on pages 2-37 (BOS – Channel 12) and 2-38 (EOS – Channel 15) where the primary beam pattern shown by the purple cone intersects the Cold and Warm Calibration Targets respectively causing slight blockage of the earth Scene and leading to a roll-off in the averaged scene brightness due to the cold-space background. Chart 2-40 shows the SSMIS with the main reflector in place for reference (it has been removed on pages 2-37 to 2-39 to show the FOV intrusions. Page 2-41 summarizes the FOV intrusions for each SSMIS feedhorn. This table was created independent of the EO data analysis using only the DGS simulation tool to determine the FOV intrusions demonstrating consistency and utility of the tool.

SSMIS Scan Geometry

~BP 240

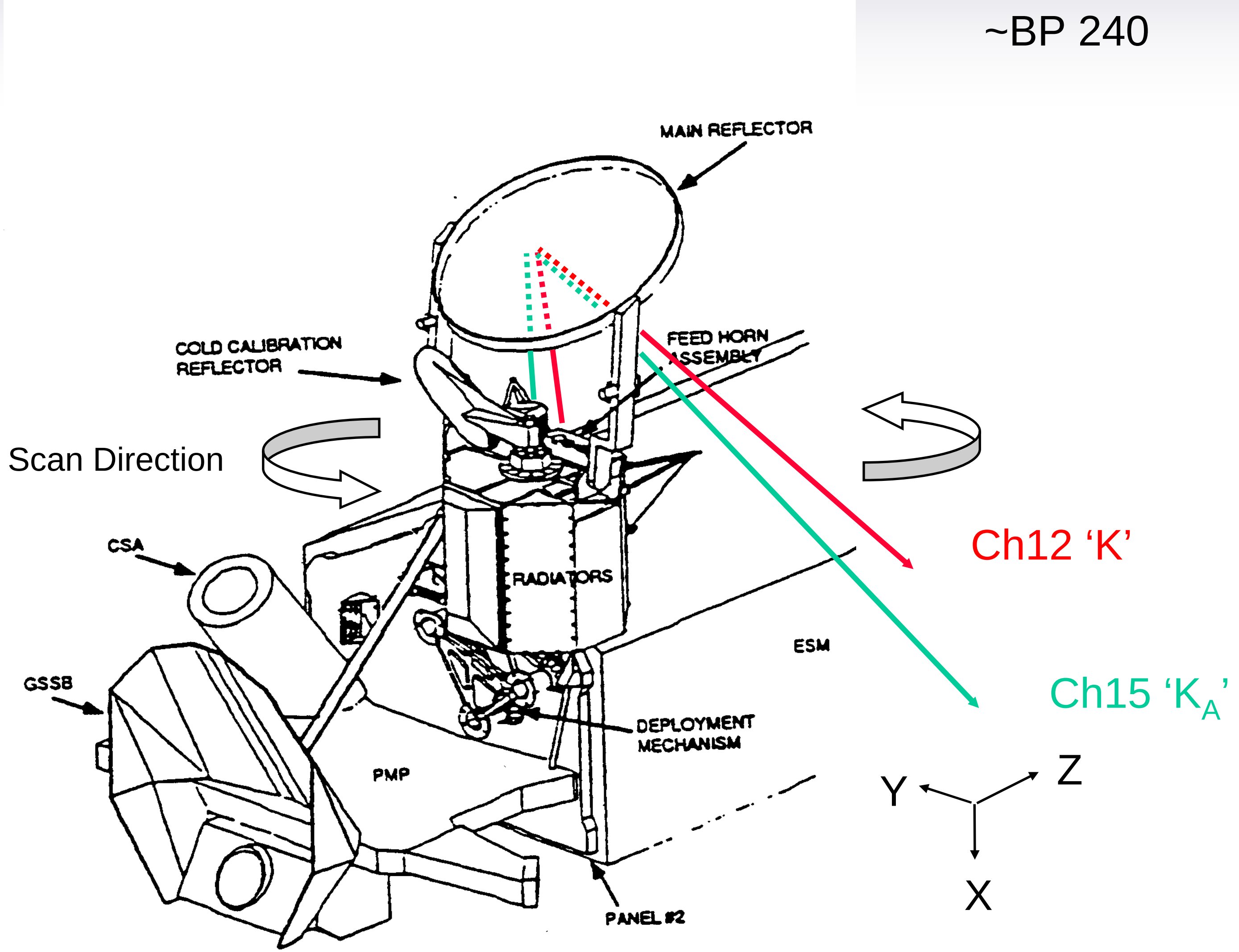

SSMIS and SSM/I 3dB IFOV Contours

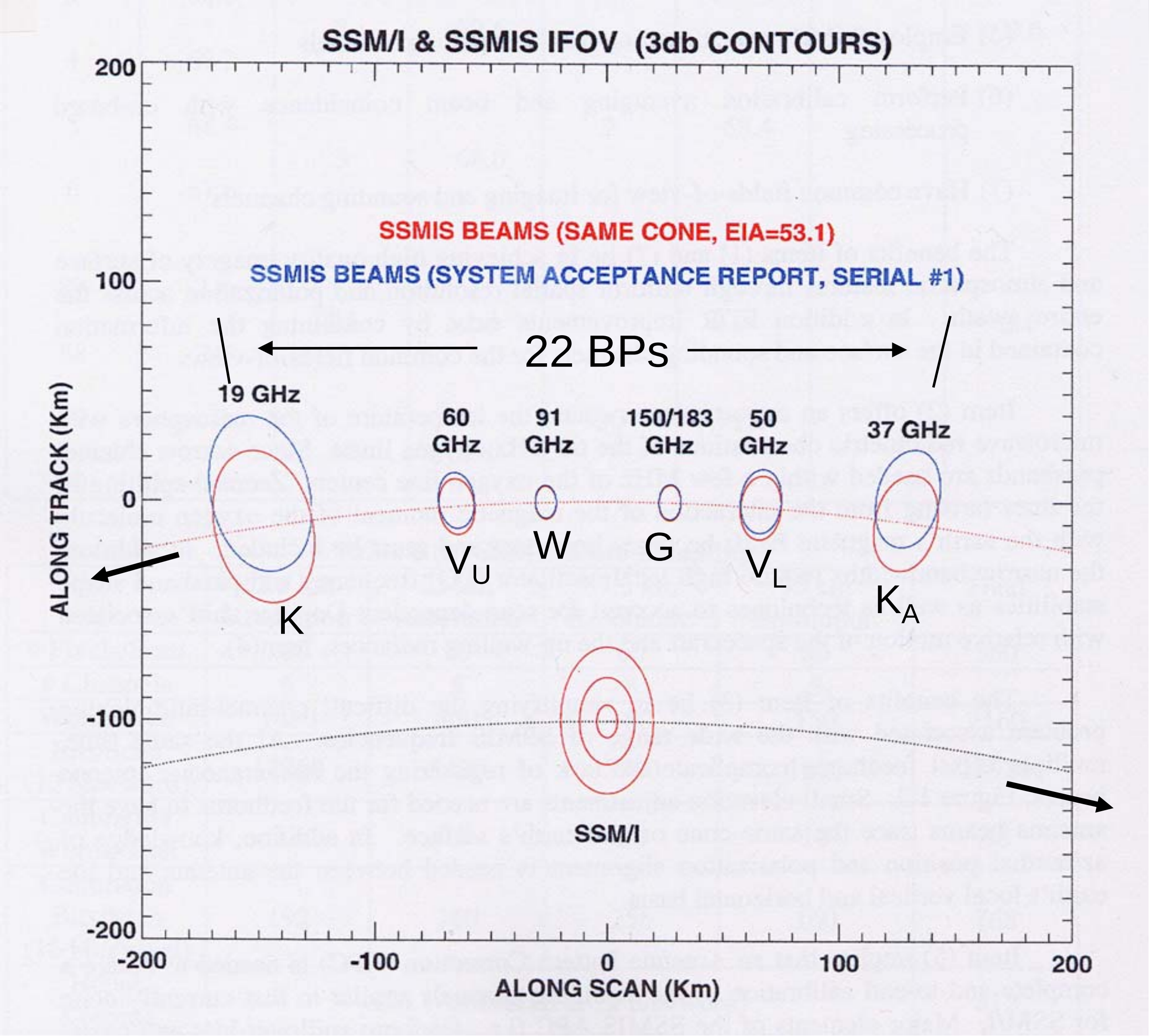

Earth Scene FOV and Edge Of Scan Effects

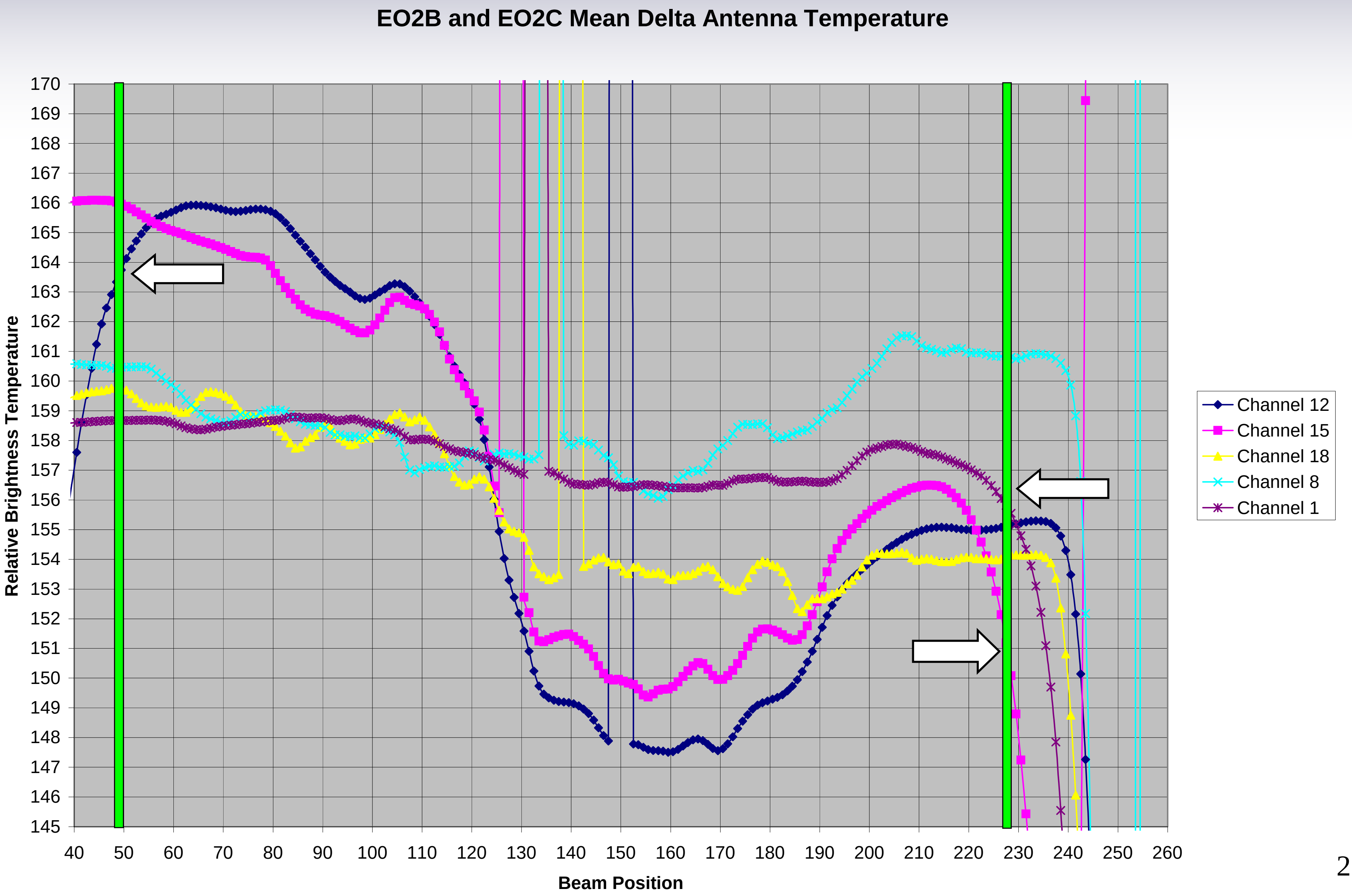

DGS Simulation: SSMIS Beam Position 240

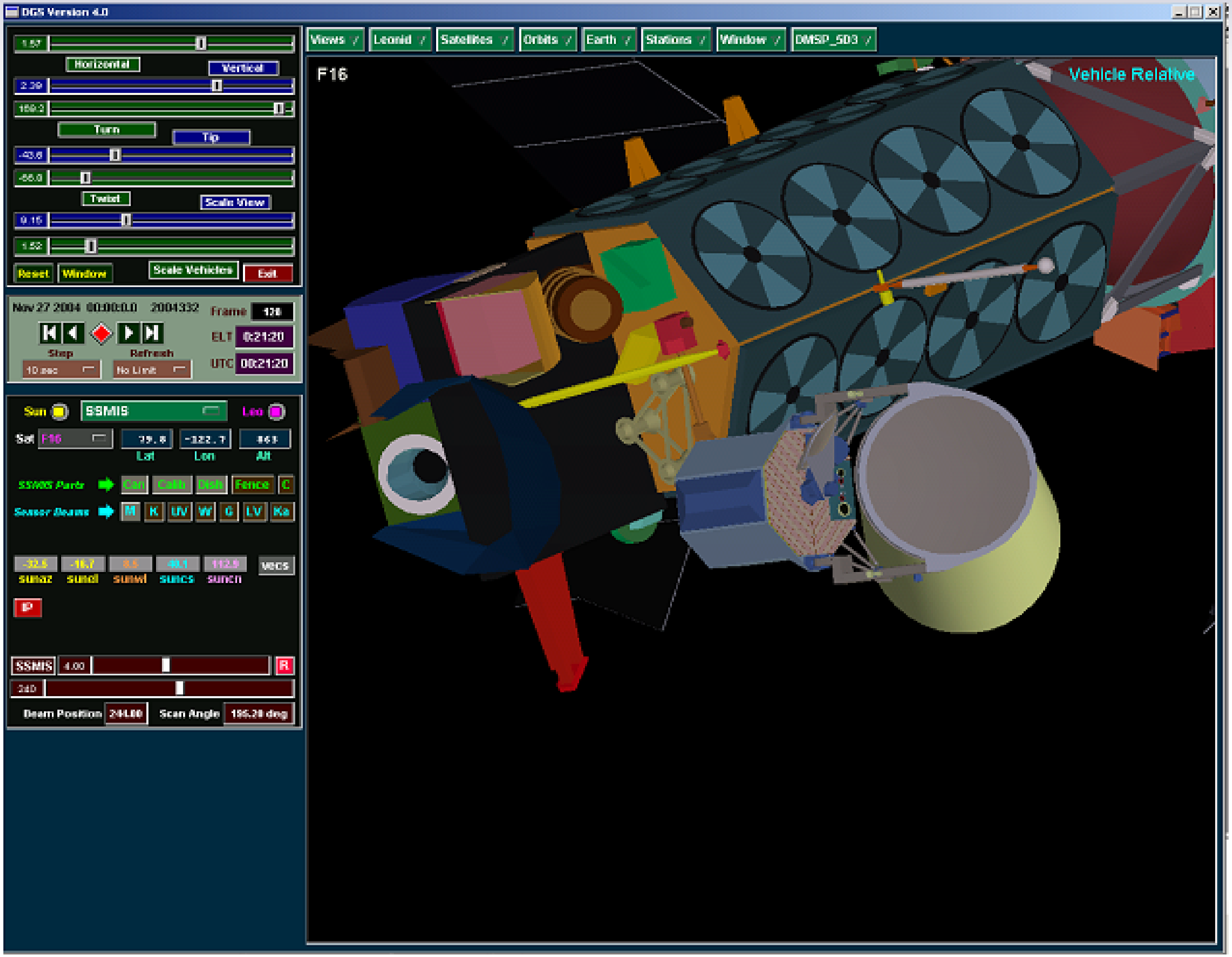

1.57
2.39
169.2
-43.6
-66.0
9.16
1.52

Nov 27 2004 00:00:0.0 2004332

Frame 120

ELT 0:21:20

UTC 00:21:20

Step: 10 sec

Refresh: No Limit

SSMIS

Sat F16

Lat 29.8 Lon -122.7 Alt 863

-32.5 sunaz
-16.7 sunel
8.5 sunwl
40.1 suncs
112.9 suncn

SSMIS 4.00

240

Beam Position 240.00

Scan Angle 195.28 deg

SSMIS BP 240: Main Beam Intrusion from S/C

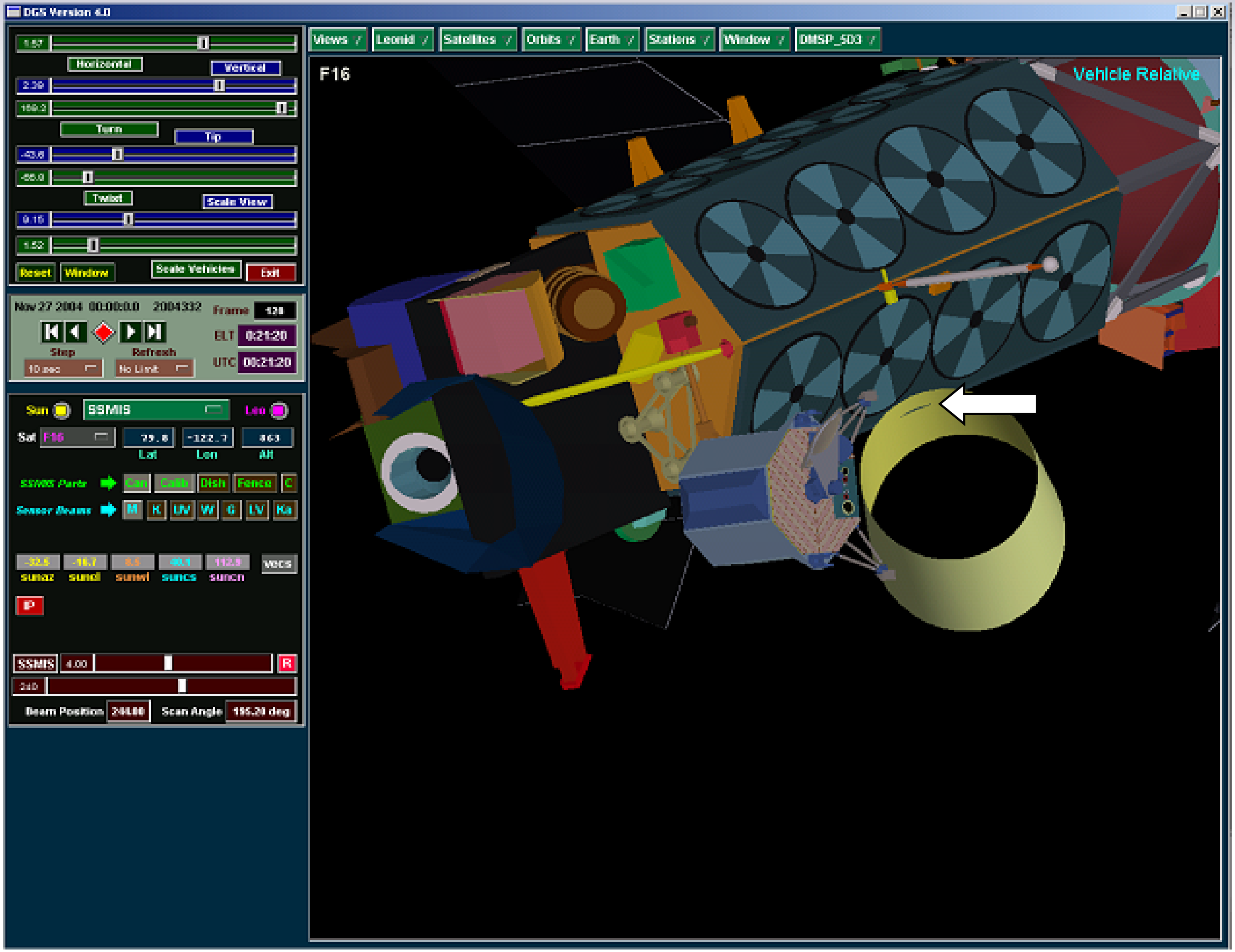

DGS Version 4.0

Nov 27 2004 00:00:0.0 2004332

Frame 120

ELT 0:21:20

UTC 00:21:20

Step 10 sec

Refresh No Limit

SSMIS

Sat F16

Lat 79.8

Lon -122.7

Alt 863

sunaz -32.5

sunel -16.7

sunwl 8.5

suncs 40.1

suncn 112.9

SSMIS 4.00

240

Beam Position 240.00

Scan Angle 195.20 deg

SSMIS BP 240: Main Beam Intrusion from S/C

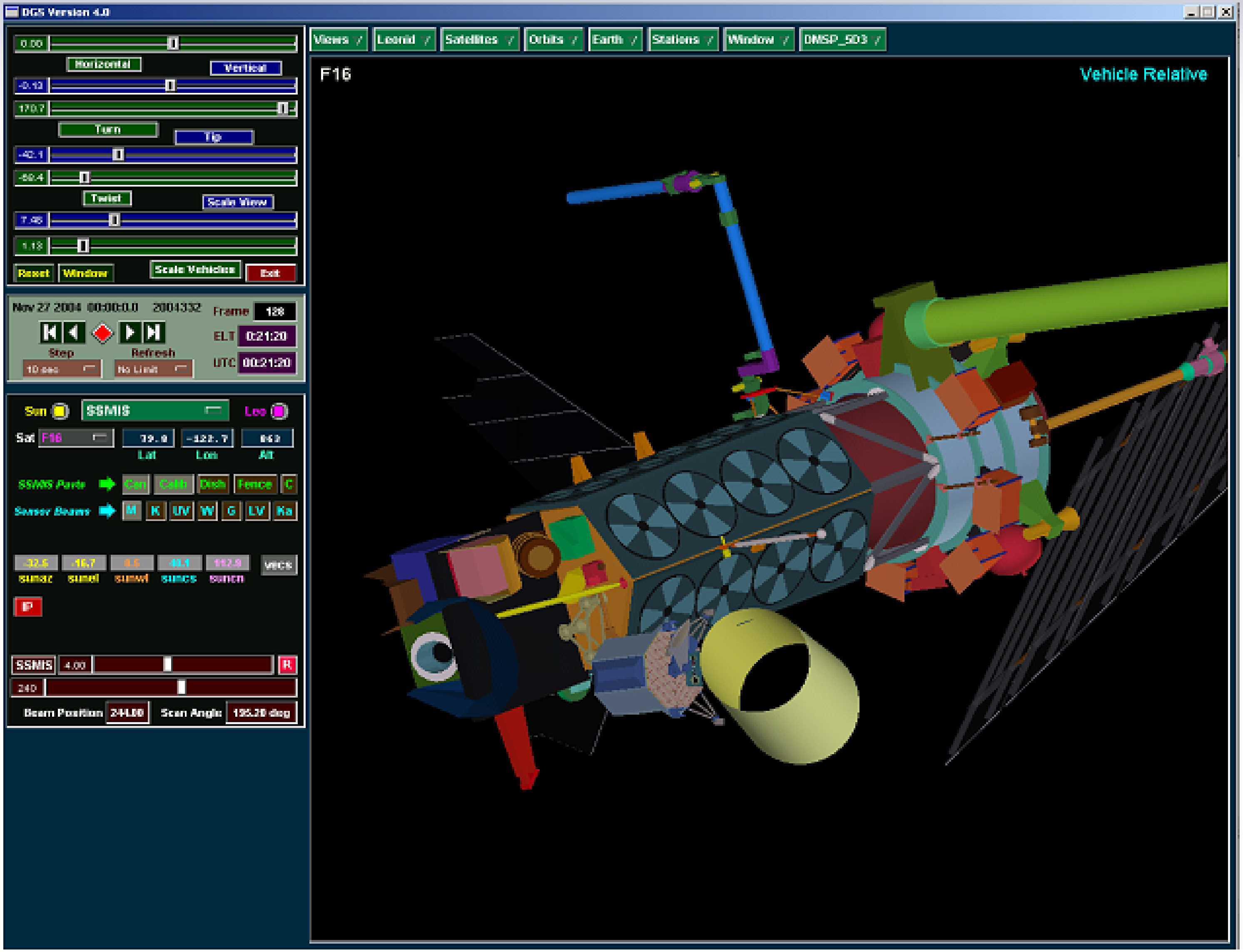

Nov 27 2004 00:00:0.0 2004332

Frame 128

ELT 0:21:20

UTC 00:21:20

Step 10 sec

Refresh No Limit

SSMIS

Sat F16

Lon -122.7

SSMIS 4.00

240

Beam Position 244.00

Scan Angle 195.20 deg

SSMIS BP 40: K-Band Feed Beam Intrusion from Cold Sky Reflector

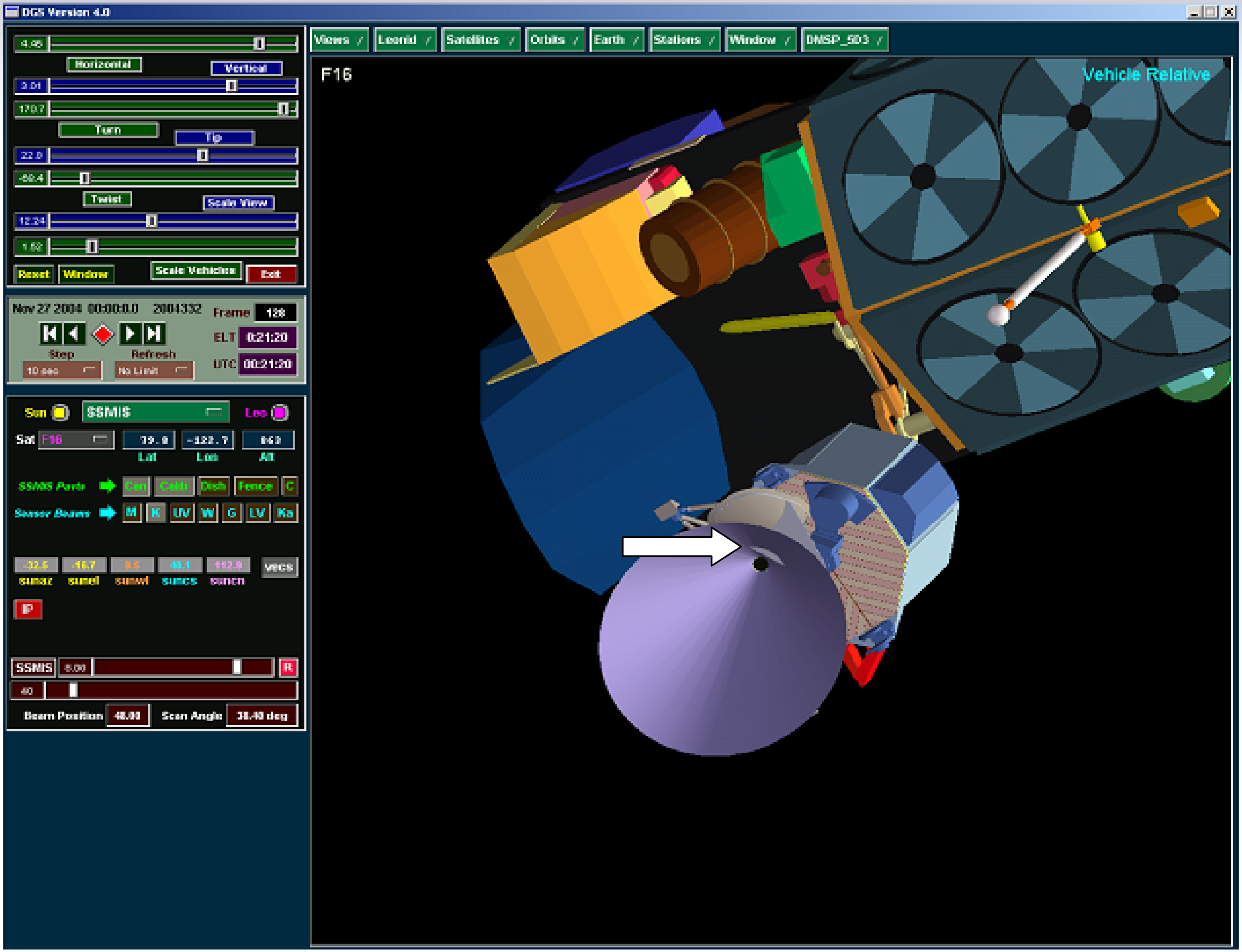

Nov 27 2004 00:00:0.0 2004332

Frame 128

ELT 0:21:20

UTC 00:21:20

Step 10 sec

Refresh No Limit

Sat F16

Beam Position 40.00

Scan Angle 38.40 deg

SSMIS BP 250: K_A-Band Feed Beam Intrusion from Warm Load Shroud

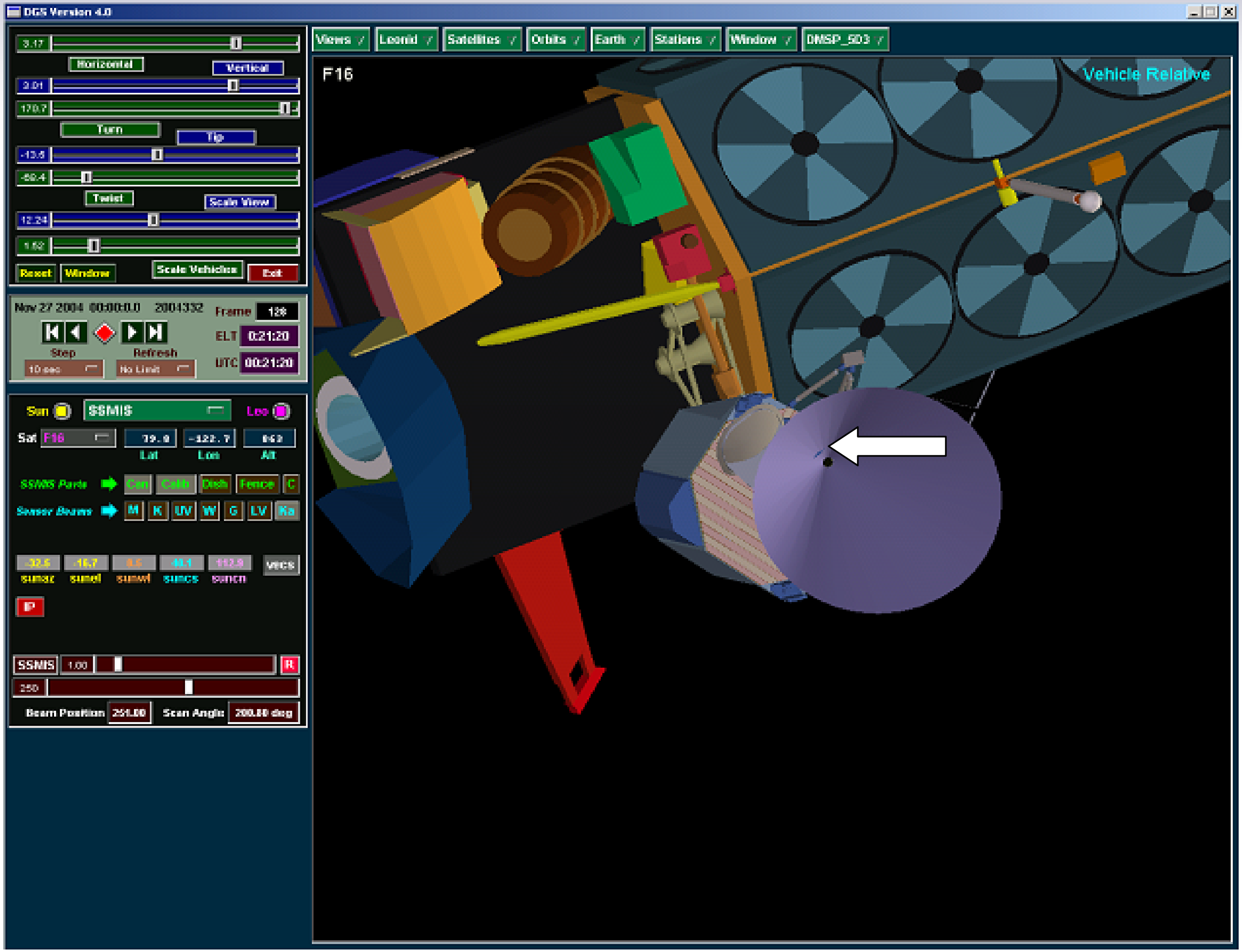

SSMIS BP 240: K_A-Band Feed Beam Intrusion from Warm Load Shroud

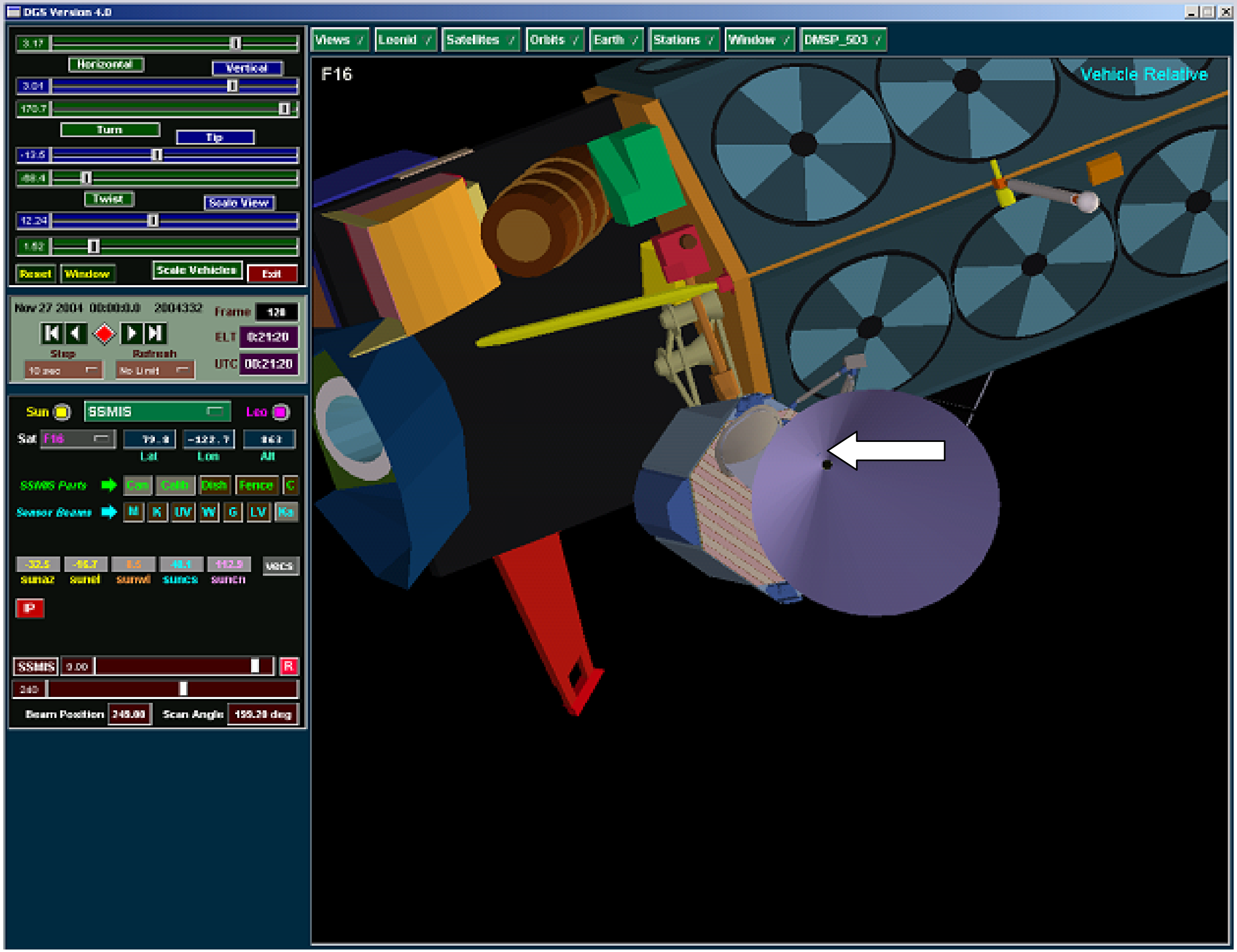

DGS Simulation: SSMIS BP 240 With Main Reflector

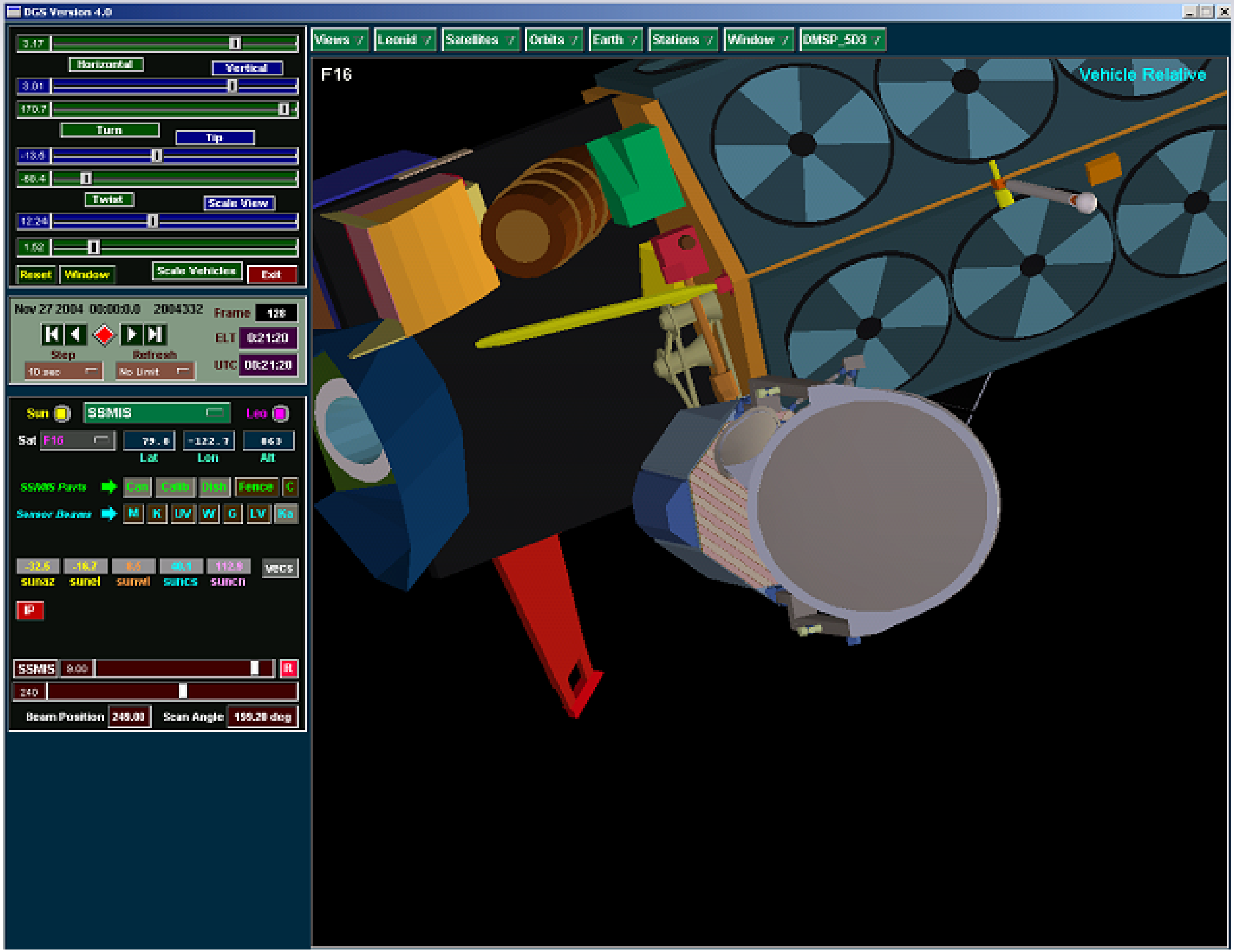

3.17

3.01

170.7

-13.6

-60.4

12.24

1.62

Nov 27 2004 00:00:0.0 2004332

Frame 128

ELT 0:21:20

UTC 00:21:20

Step 10 sec

Refresh No Limit

SSMIS

Sat F16

Lat 79.8

Lon -122.7

Alt 863

sunaz -32.5

sunel -16.7

sunwl 8.5

suncs 40.1

suncn 112.9

SSMIS 9.00

240

Beam Position 240.00

Scan Angle 159.20 deg

SSMIS Sensor FOV Obstruction Table

SSMIS Sensor FOV Obstruction Table

Mike Werner - Aerospace Corp. - March 3, 2005

Note: FOVs are modeled as truncated cones defined by the sensor aperture and reflecting surface of the main dish, or as a truncated cone emanating from the main dish with a 1.9 deg divergence angle.

Band	Scan	FOV Obstruction between Aperture & Main Reflector from Cold Sky Reflector	FOV Obstruction between Aperture & Main Reflector from Warm Load Shroud	FOV Obstruction between Main Reflector and Earth from Vehicle Body Parts
		(all numbers are in beam position units)		
Ka	70 - 250	< 8.5	**> 248.25**	**bp < 49 or bp > 243***
L-V	65 - 245	< 18.5	> 260.25	**bp < 49 or bp > 243***
G	62 - 242	< 25.0	> 270.25	bp < 49 or bp > 243*
W	58 - 238	< 34.0	> 280.75	bp < 49 or bp > 243*
U-V	55 - 235	< 44.0	> 286.50	bp < 49 or bp > 243*
K	48 - 228	**< 60.0**	> 298.00	bp < 49 or bp > 243*

* Assumes far field beam is identical for each feedhorn for simplification - corrected in later versions

2.5 Comparison of EO and Normal Mode Data Characteristics

To further establish the validity of the edge-of-scan bias estimates provide by EO data analysis, 3 month averaged Normal mode data was superimposed over the EO data trends as a function of beam position in order to evaluate consistency between the two data sets. For pages 2-43 to 2-48 the relative variation of Normal Mode data averaged over a three month period is overlaid on EO data. The yellow lines are adjusted for the relative values to match at the beginning of scan and the marine colored line represents averaged Normal mode data matched to the EO end-of-scan value to allow evaluation of the data trend at BOS and EOS. Note that variations of the Normal mode data for the window channels is greatly reduced for the Normal mode data due to the extensive three-month average compared to the relatively short, two orbit average allowed for the EO mode data. The key result is that the relatively large edge-of-scan roll-offs (typically greater than 1K) are represented consistently by the EO and Normal mode data. This agreement allowed a bias correction to be designed and applied to the Normal mode data with increased confidence that no spurious residual errors would be introduced into the operational data products by the correction and further, that the maximum amount of residual error would be removed from the data. Additional processing of EO mode data was applied for this stage of analysis: the EO mode data was calibrated each scan to duplicate, as close as possible, the normal mode data in an independent manner.

Channel 12 FOV

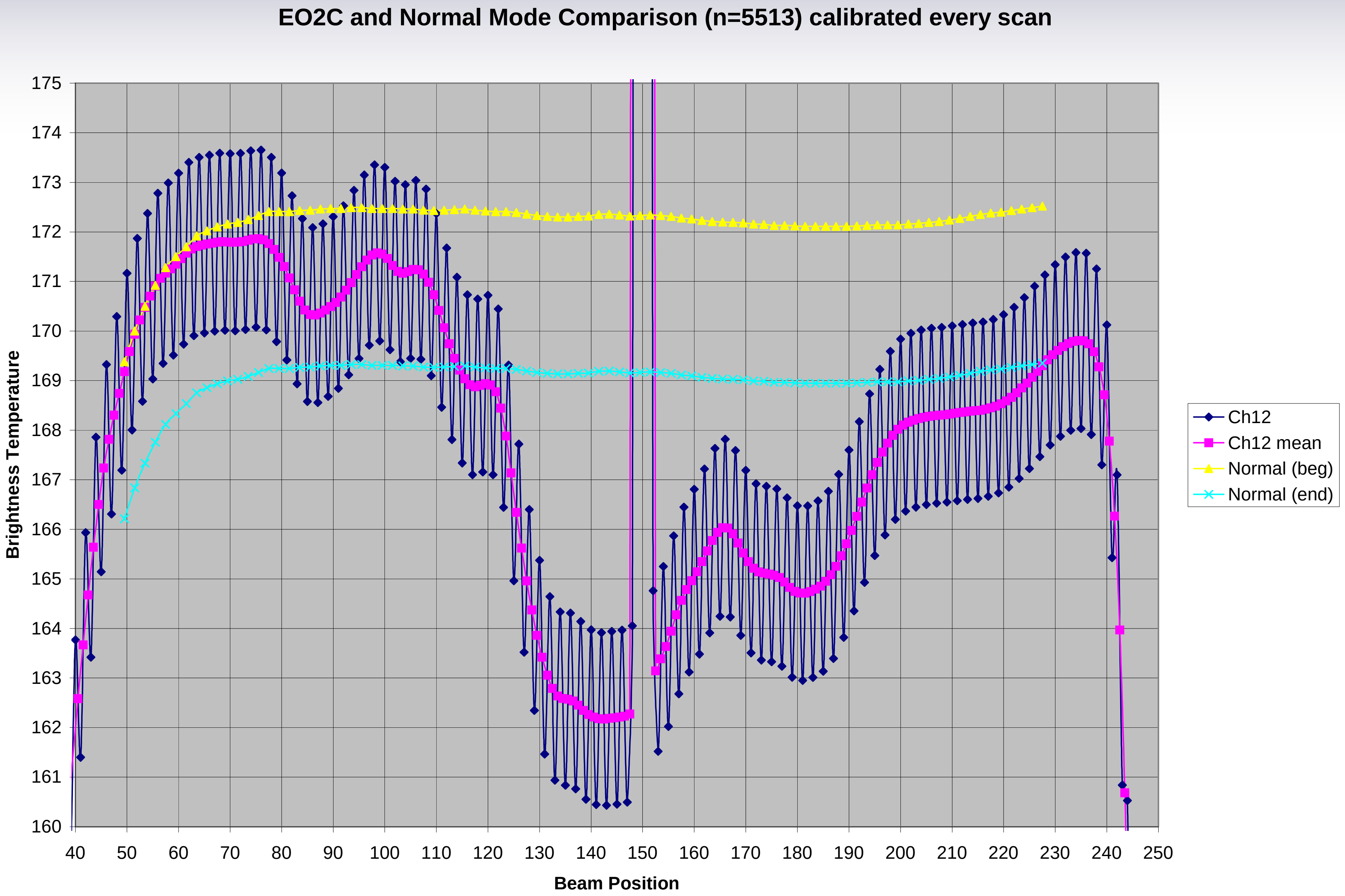

Channel 6 FOV

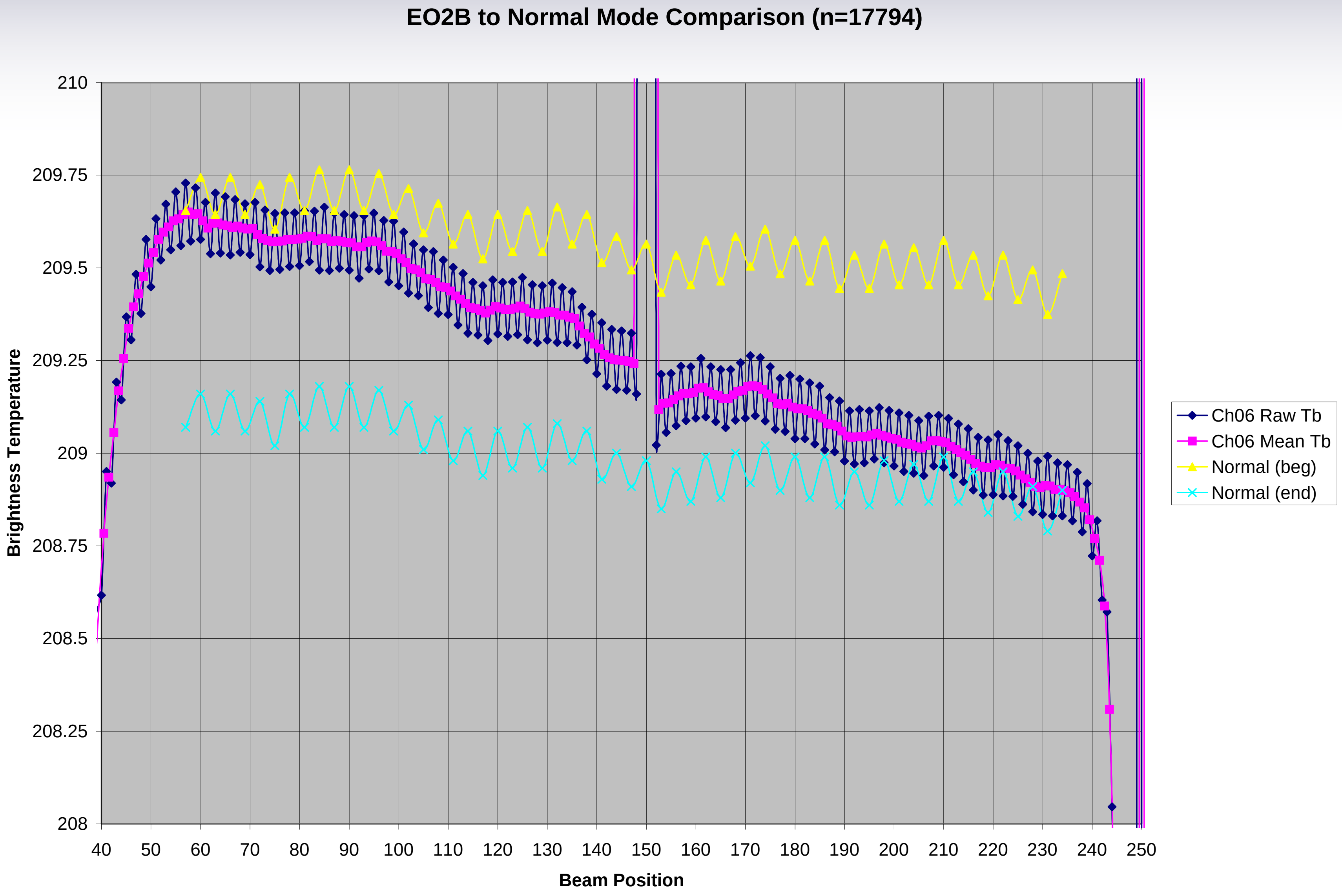

Channel 18 FOV

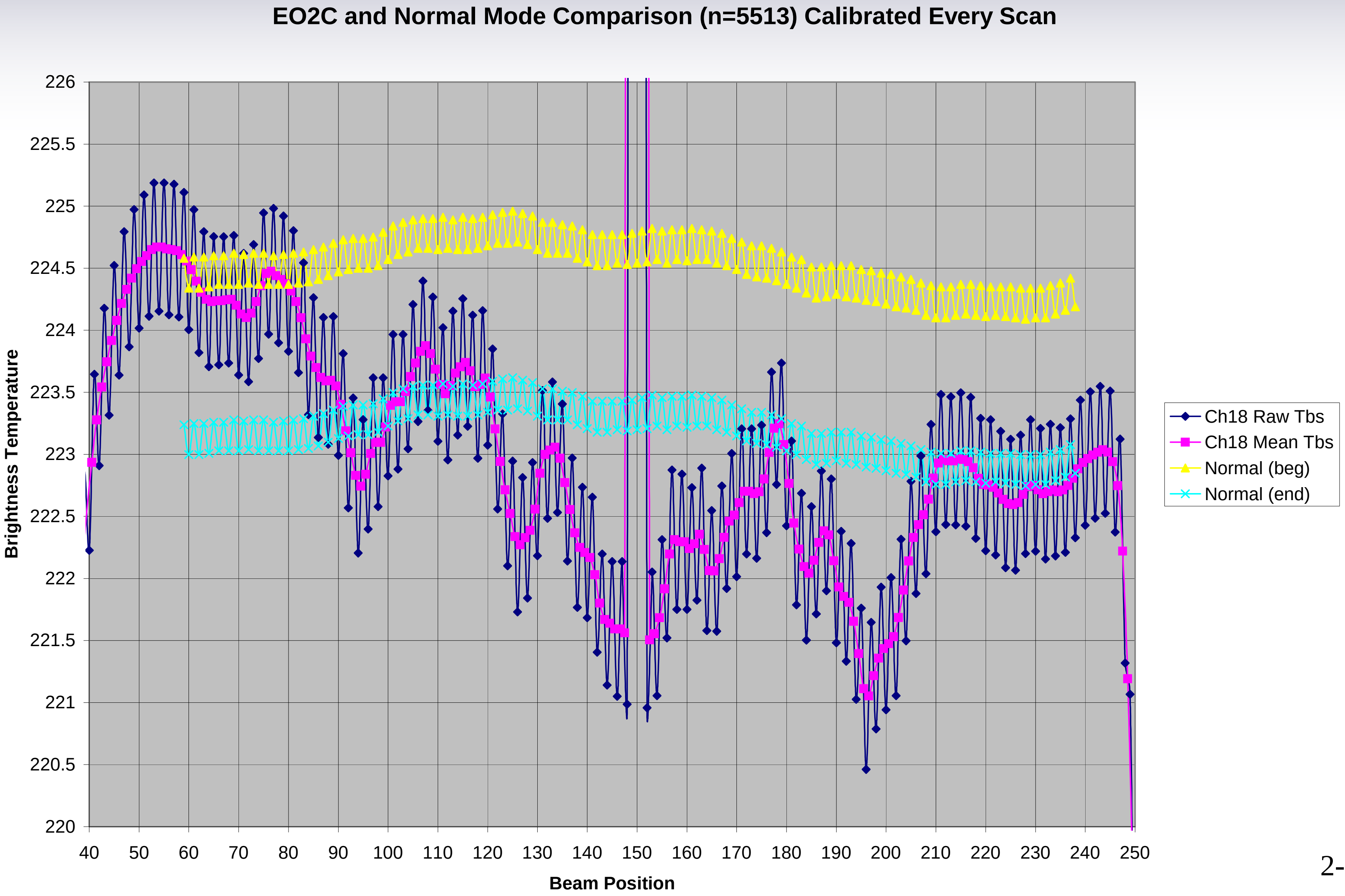

Channel 8 FOV

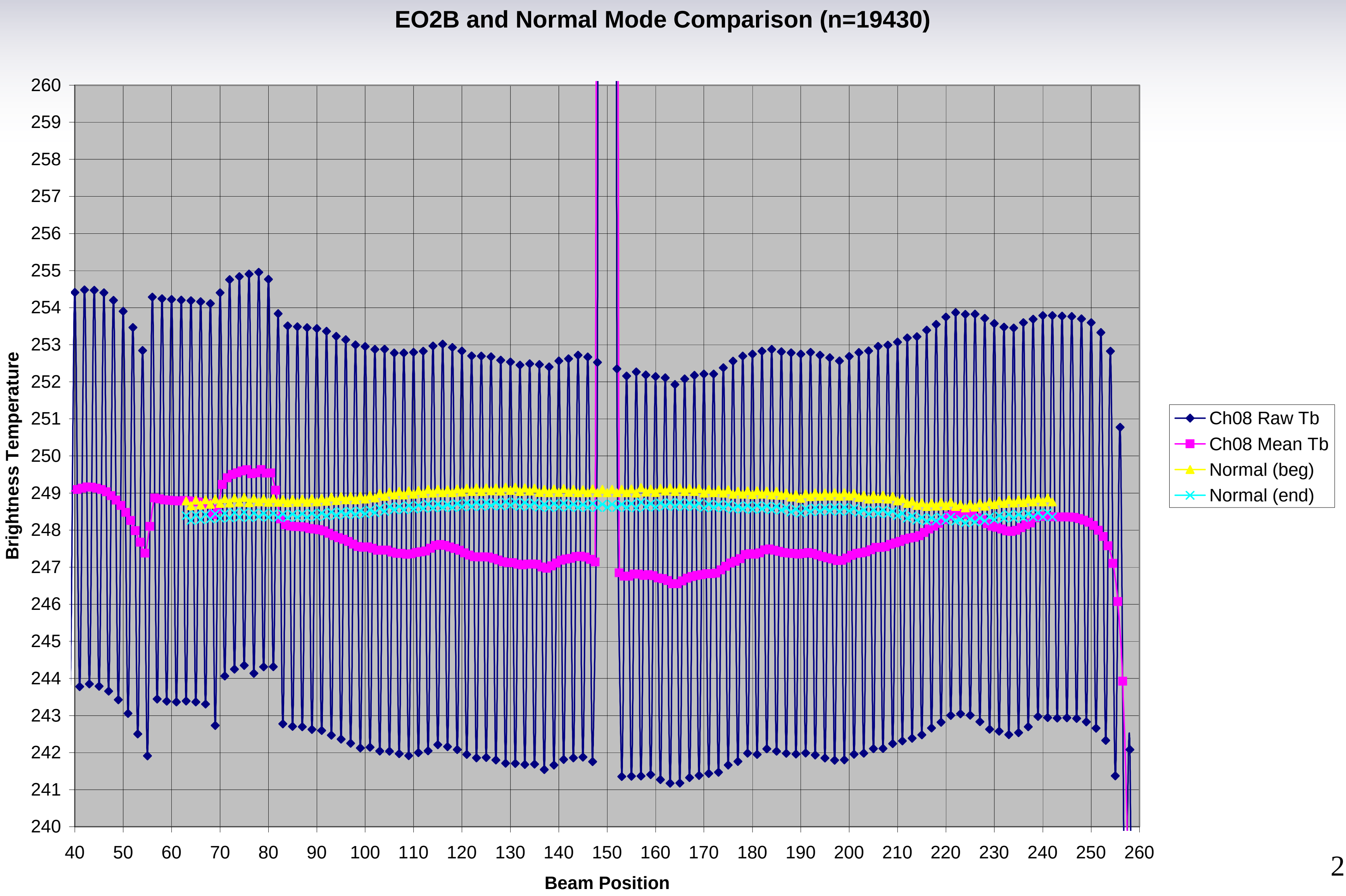

Channel 1 FOV

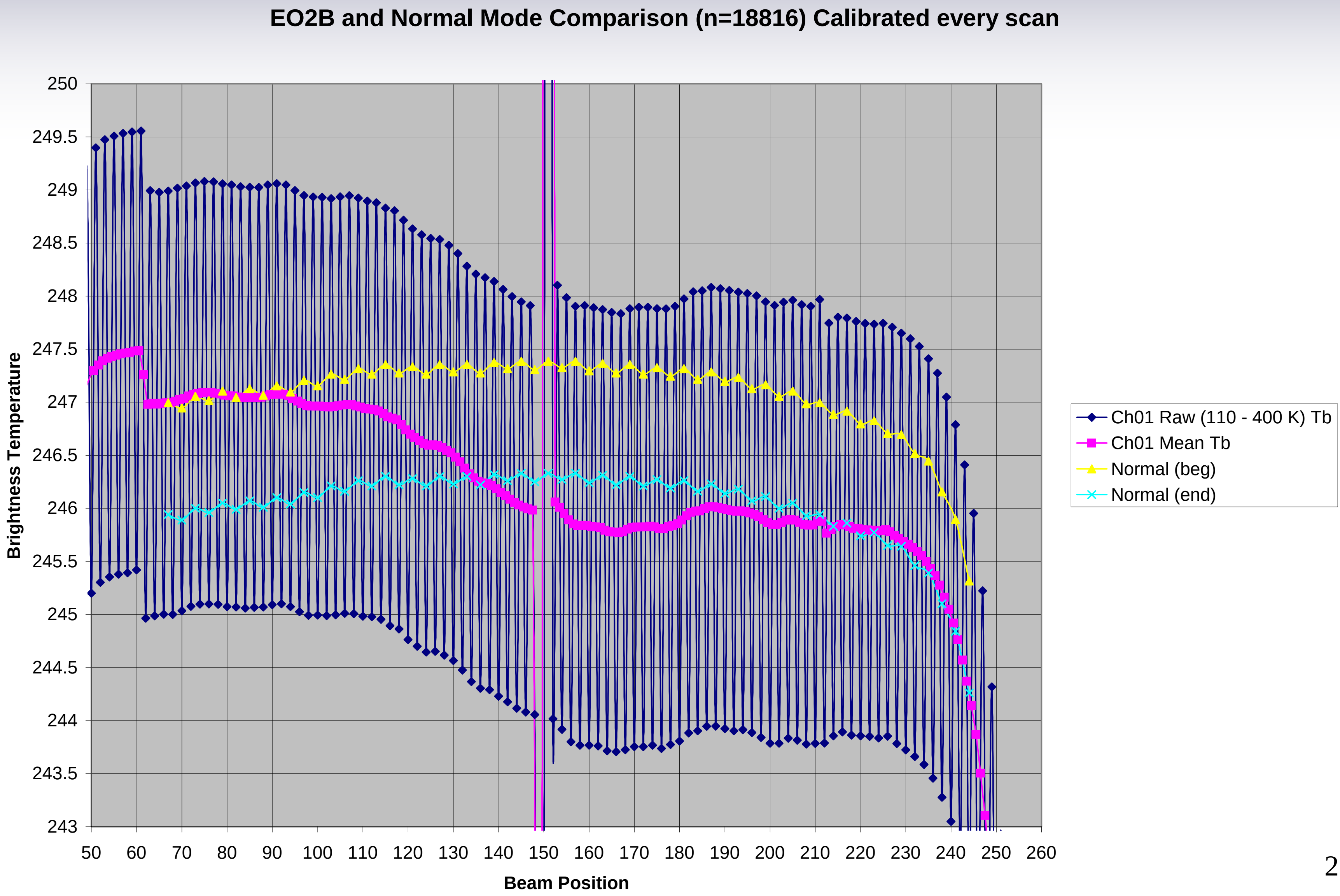

Channel 15 FOV

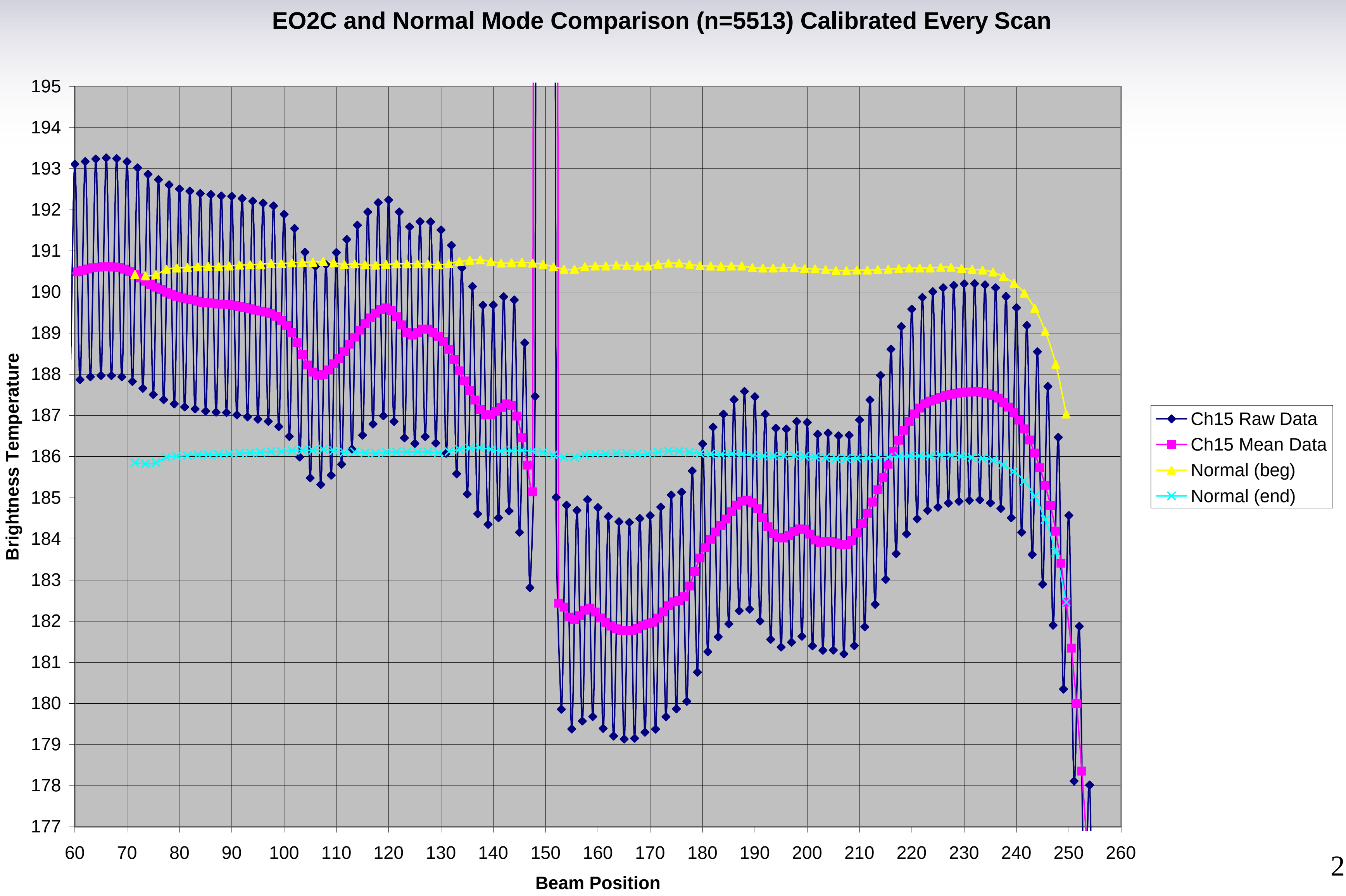

2.6 Consistency between EO2A, EO2B, and EO2C Earth scene FOV

It was important to establish consistency between EO2A and EO2B / C because all channels are not available using EO2B and EO2C data sets. All channels are available within the EO2A data sets, however, the 360° scan must be broken down into 48° (60 BP) continuous segments due to data rate and on-board processing constraints. This means that it takes 8 scans to assemble a full 360° view in EO2A mode. The data "chopping" sometimes results in additional level shifting at 60° intervals. However, the data trends at the BOS and EOS are still apparent and can be seen to be consistent between EO2A, EO2B and EO2C for the channels included in those data sets as seen on page 2-50. The top graph represents EO2A data for all channels represented in EO2B and EO2C except the UAS Channel 6. EO2A data has been "calibrated" to a brightness temperature based on mean EO2A data from beam positions representing the hot and cold calibration locations during the EO2A mode orbital period (rev 144 and 143). EO2B and EO2C raw count data also from Channels 1, 8, 12, 15, and 18 are shown on the bottom graph on a similar but not exact scale as the EO2A data. Of note is the Channel 12 upward trend at the BOS and Channel 15 roll-off at the EOS is similar in EO2A and EO2C. This comparison helps establish a link between EO2A and EO2B and EO2C allowing additional comparisons with data in EO2A from all SSMIS channels. This was important to evaluate data processing in the GPS that involves SSMIS channels that are not part of the EO2B or EO2C set.

Comparison of EO2A, EO2B, and EO2C Data

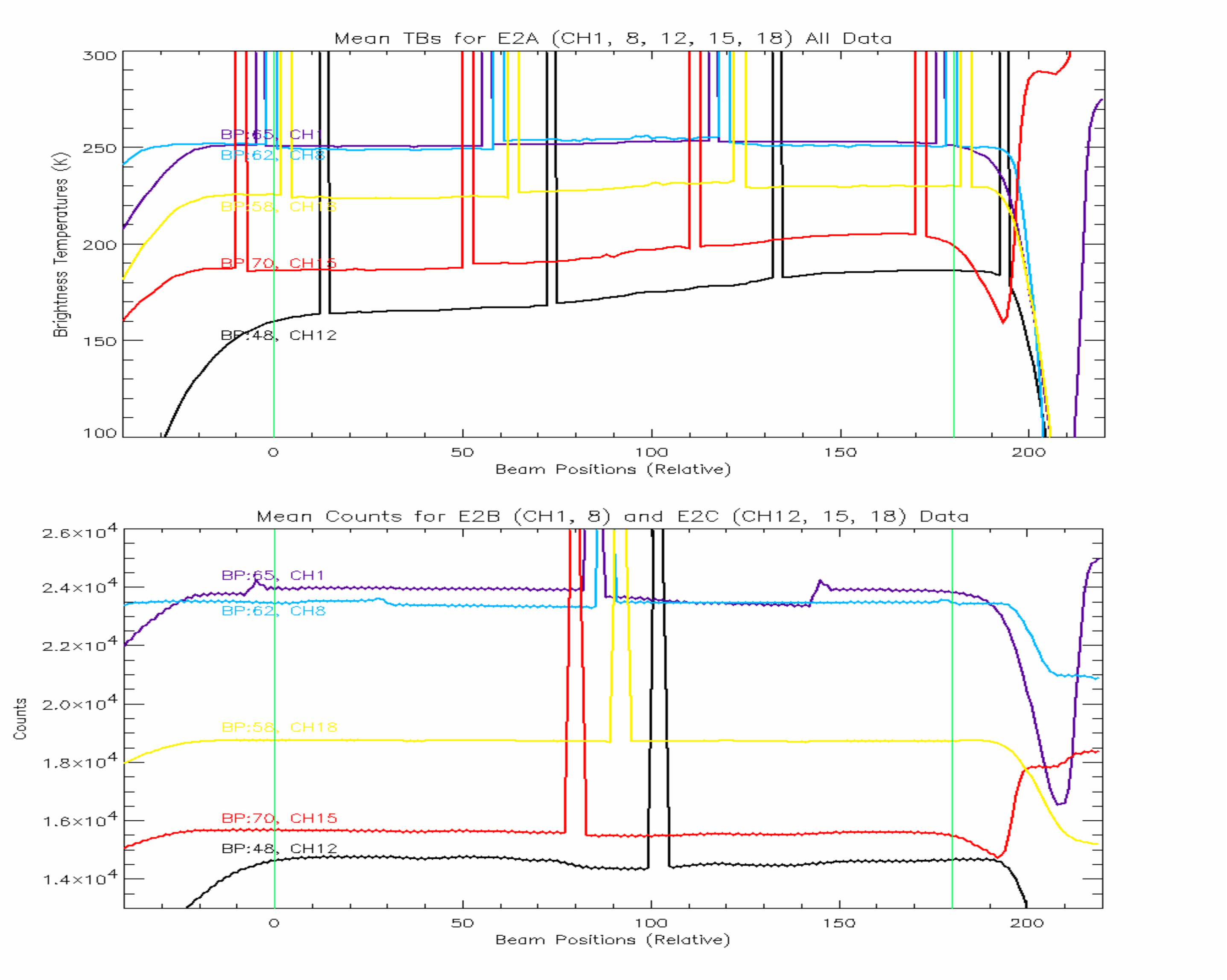

2.7 Early Orbit Data FOV Analysis Summary

Data collection from the SSMIS in Early Orbit (EO) modes EO2A, EO2B and EO2C were critical for correctly evaluating the sensor field of view for the calibration targets and earth scene. EO mode data offers the only opportunity to receive raw data counts over the full 360° rotation of the SSMIS. EO data are not spatially averaged or calibrated to remove A/B integrator bias thereby providing a unfettered look at the instrument raw counts and an additional basis for evaluation of proper sensor operation. For F-16, data collected in EO2B and EO2C mode proved to be extremely valuable for correctly determining the FOV intrusions of the Earth scene FOV and establishing the proper approach for correcting biases as a function of beam position over the scan. EO2A, EO2B and EO2C data also provided important insight for characterizing the warm load calibration anomalies caused by solar illumination of the tine structure. For more details regarding the warm load solar intrusion anomalies please see Section 11.

F16 SSMIS Calibration/Validation Final Report

Section 3.0 Instrument Performance

Beverly Gardiner, Enzo Uliana and Gene Poe

THE AEROSPACE CORPORATION

Section 3.0 Instrument Performance

3.1 Warm-Load NEDT Meets Specification

Channel	Orbit 518	Orbit 1718	Orbit 2918	Orbit 4399	Orbit 5728	Orbit 7994	Orbit 8500	Orbit 9500	Orbit 10200	Orbit 10538	T/V Recal	Spec.
1	0.21	0.19	0.21	0.18	0.20	0.22	0.19	0.21	0.24	0.20	0.19	0.40
2	0.21	0.21	0.18	0.18	0.20	0.24	0.20	0.19	0.24	0.20	0.19	0.40
3	0.21	0.19	0.19	0.19	0.21	0.24	0.19	0.20	0.21	0.20	0.19	0.40
4	0.22	0.20	0.19	0.19	0.21	0.20	0.21	0.19	0.20	0.22	0.20	0.40
5	0.25	0.22	0.22	0.20	0.24	0.22	0.23	0.21	0.24	0.20	0.22	0.40
6	0.28	0.28	0.27	0.27	0.28	0.28	0.29	0.28	0.27	0.25	0.28	0.50
7	0.34	0.32	0.30	0.33	0.33	0.32	0.32	0.34	0.34	0.34	0.32	0.60
8	0.52	0.52	0.47	0.49	0.54	0.45	0.51	0.52	0.49	0.54	0.40	0.88
9	0.66	0.67	0.69	0.69	0.69	0.59	0.65	0.70	0.63	0.71	0.59	1.20
10	0.60	0.64	0.60	0.61	0.63	0.66	0.65	0.65	0.63	0.63	0.54	1.00
11	0.83	0.86	0.88	0.91	0.85	0.86	0.87	0.88	0.90	0.93	0.74	1.25
12	0.38	0.31	0.37	0.37	0.34	0.35	0.35	0.35	0.37	0.37	0.32	0.70
13	0.49	0.47	0.46	0.48	0.47	0.46	0.48	0.49	0.51	0.45	0.42	0.70
14	0.40	0.36	0.45	0.38	0.39	0.40	0.40	0.40	0.39	0.40	0.37	0.70
15 *	0.40	0.32	0.37	0.37	0.35	0.99	2.96	1.46	1.26	0.37	0.28	0.50
16	0.32	0.27	0.28	0.29	0.27	0.29	0.29	0.27	0.28	0.31	0.22	0.50
17	0.21	0.21	0.21	0.20	0.20	0.19	0.20	0.21	0.21	0.21	0.16	0.30
18	0.28	0.28	0.31	0.27	0.31	0.49	0.57	0.44	0.43	0.46	0.25	0.30
19	1.49	1.34	1.28	1.37	1.33	1.36	1.38	1.24	1.43	1.33	1.42	2.38
20	1.35	1.21	1.40	1.28	1.30	1.30	1.29	1.33	1.20	1.43	1.43	2.38
21	1.01	0.94	1.03	0.93	0.98	1.13	0.98	0.93	1.16	1.02	1.05	1.75
22	0.66	0.64	0.69	0.72	0.67	0.72	0.70	0.63	0.66	0.71	0.75	1.00
23	0.44	0.42	0.40	0.36	0.39	0.47	0.42	0.43	0.48	0.40	0.43	0.60
24	0.23	0.24	0.23	0.22	0.21	0.33	0.23	0.22	0.34	0.21	0.23	0.35

- ***The computed NEDT for channel 15 contains anomalous intermittent orbital receiver gain changes starting Jan 05. These changes do not affect scene SDRs due to periodic warm and cold space calibration**

3.1 SSMIS NEDT
October 2003 – November 2005

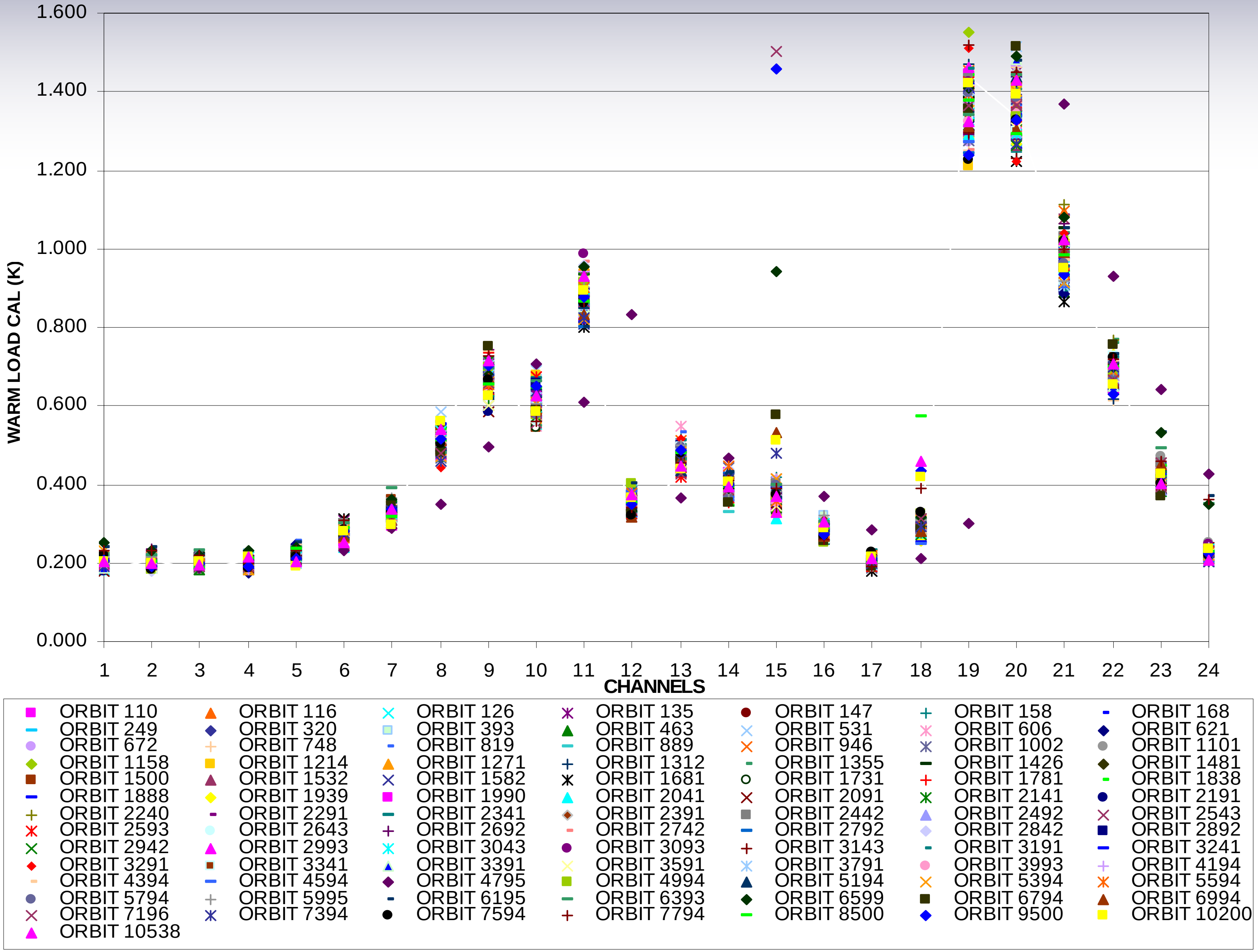

3.1 SSMIS NEDT
October 2003 - November 2005

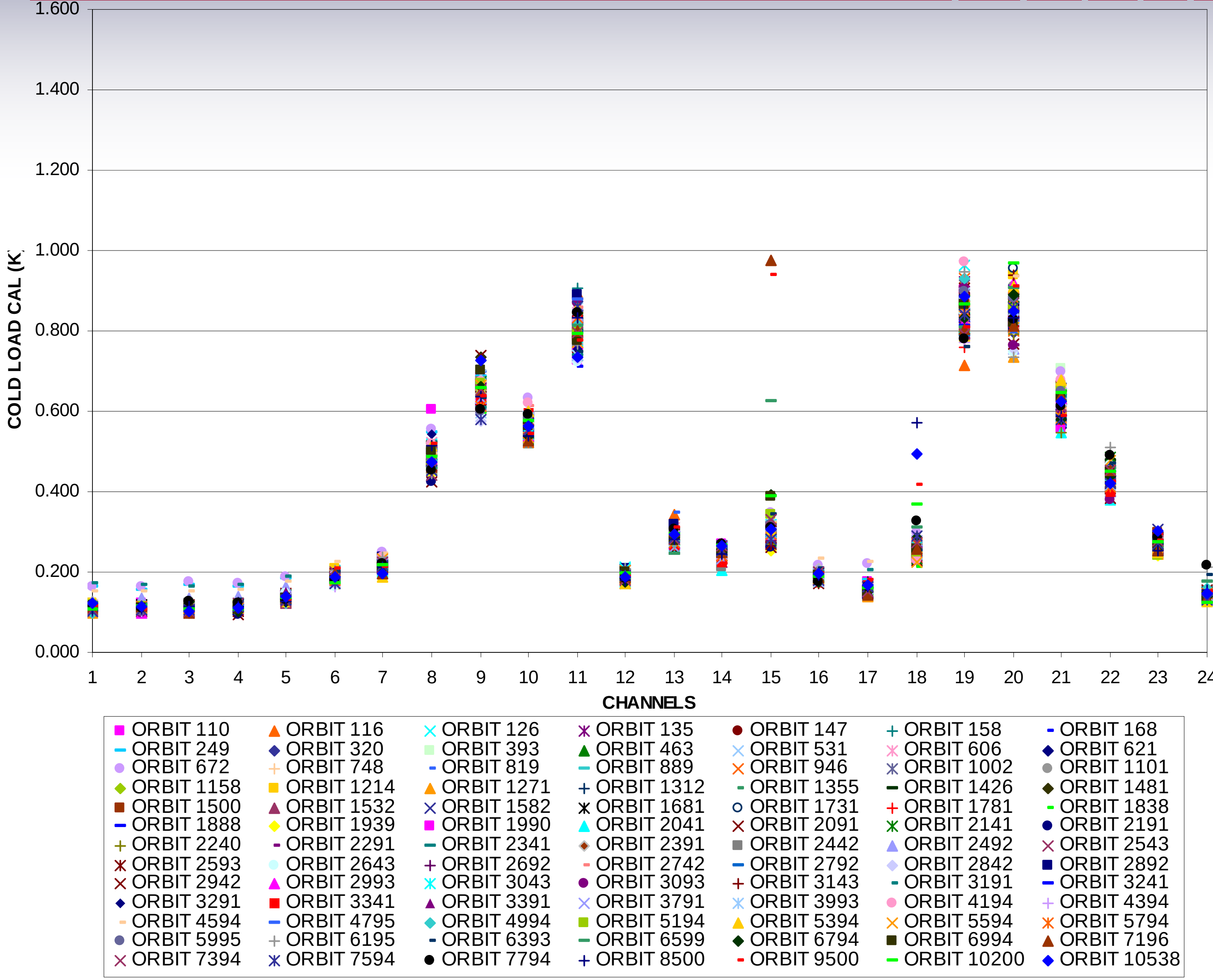

3.2 SSMIS Radiometer Gain Stability
October 2003 – November 2005

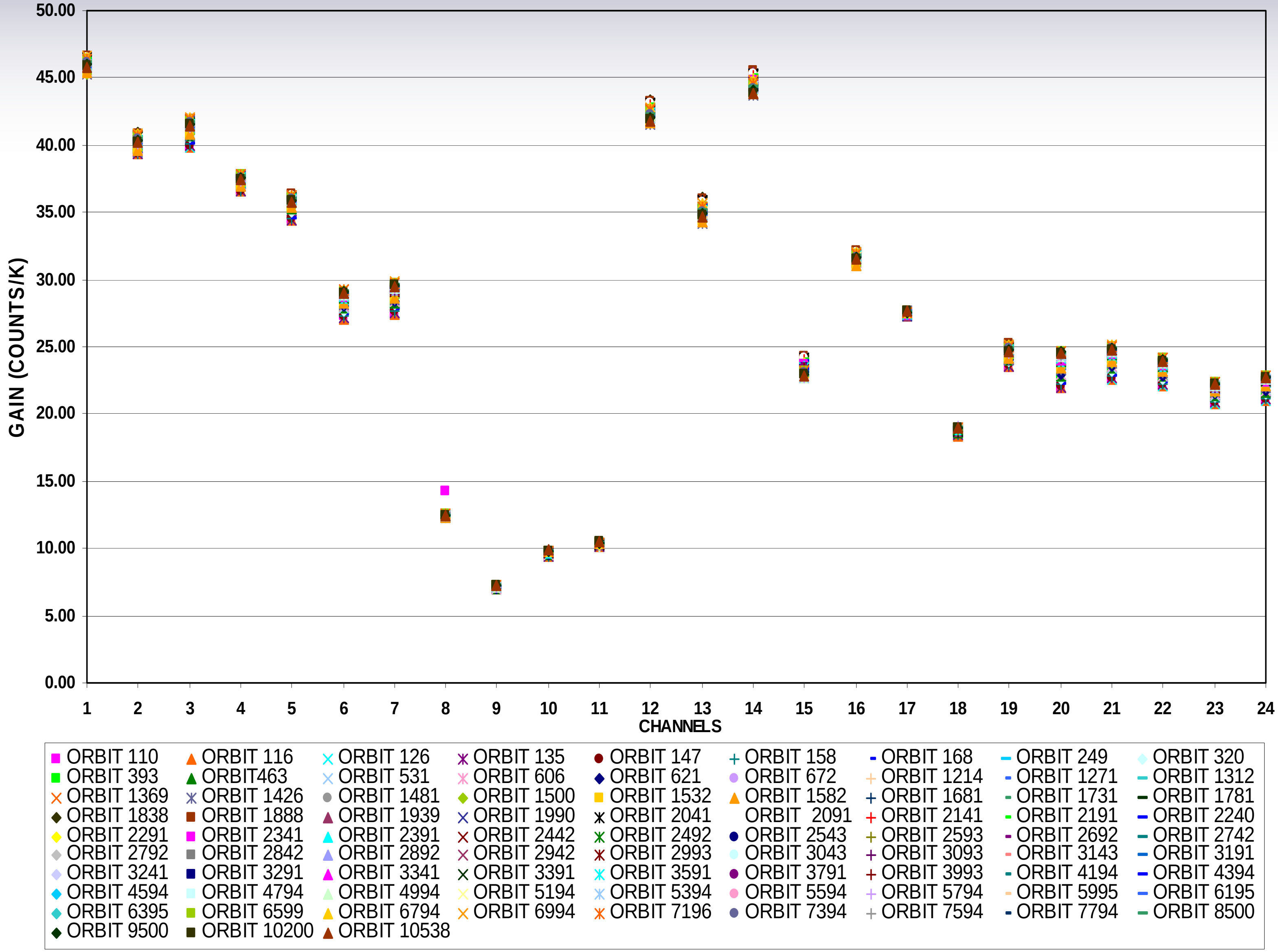

3.3 SSMIS Receiver/Warm-Load Temperatures (Orbital Average)
October 2003 – November 2005

[redacted]

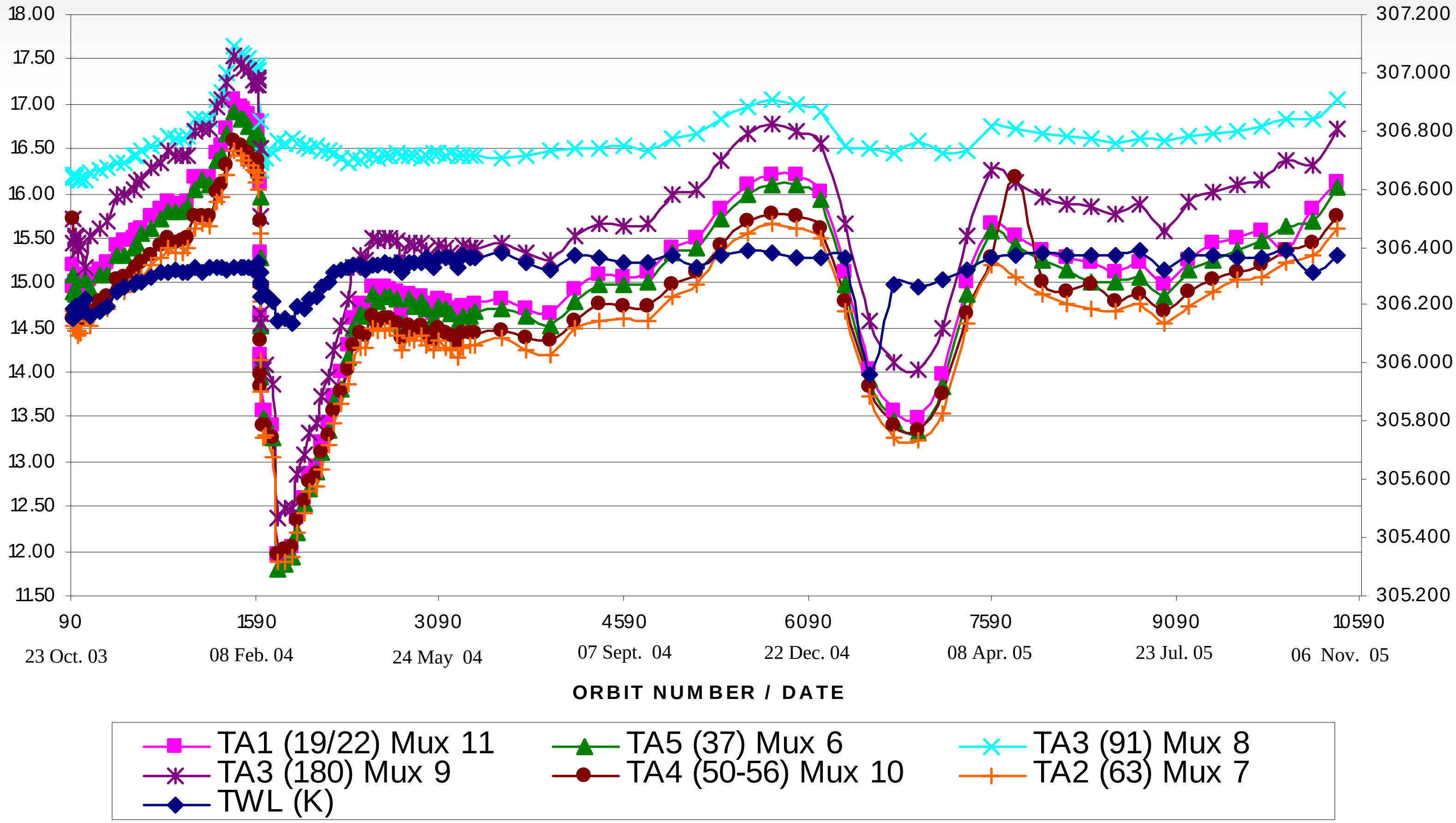

[redacted]

Note: Large drops in receiver temperature due to re-positioning of the Solar Array

3.3 F-16 Sun Angle and Time in Earth Shadow (November 03 – October 05)

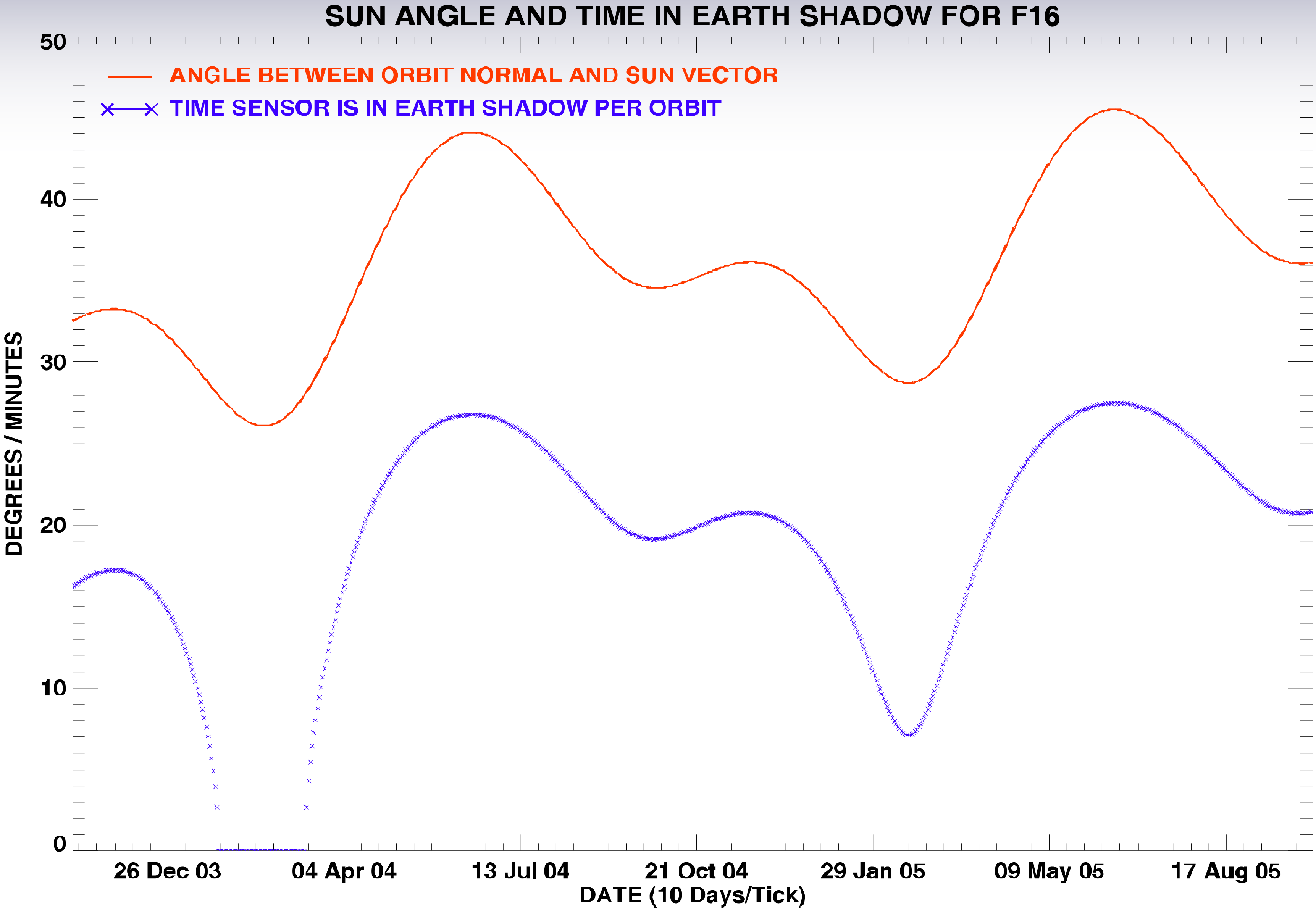

3.4 Orbital Variation
Warm Load Counts/Avg. Gain (Rev. 1718)

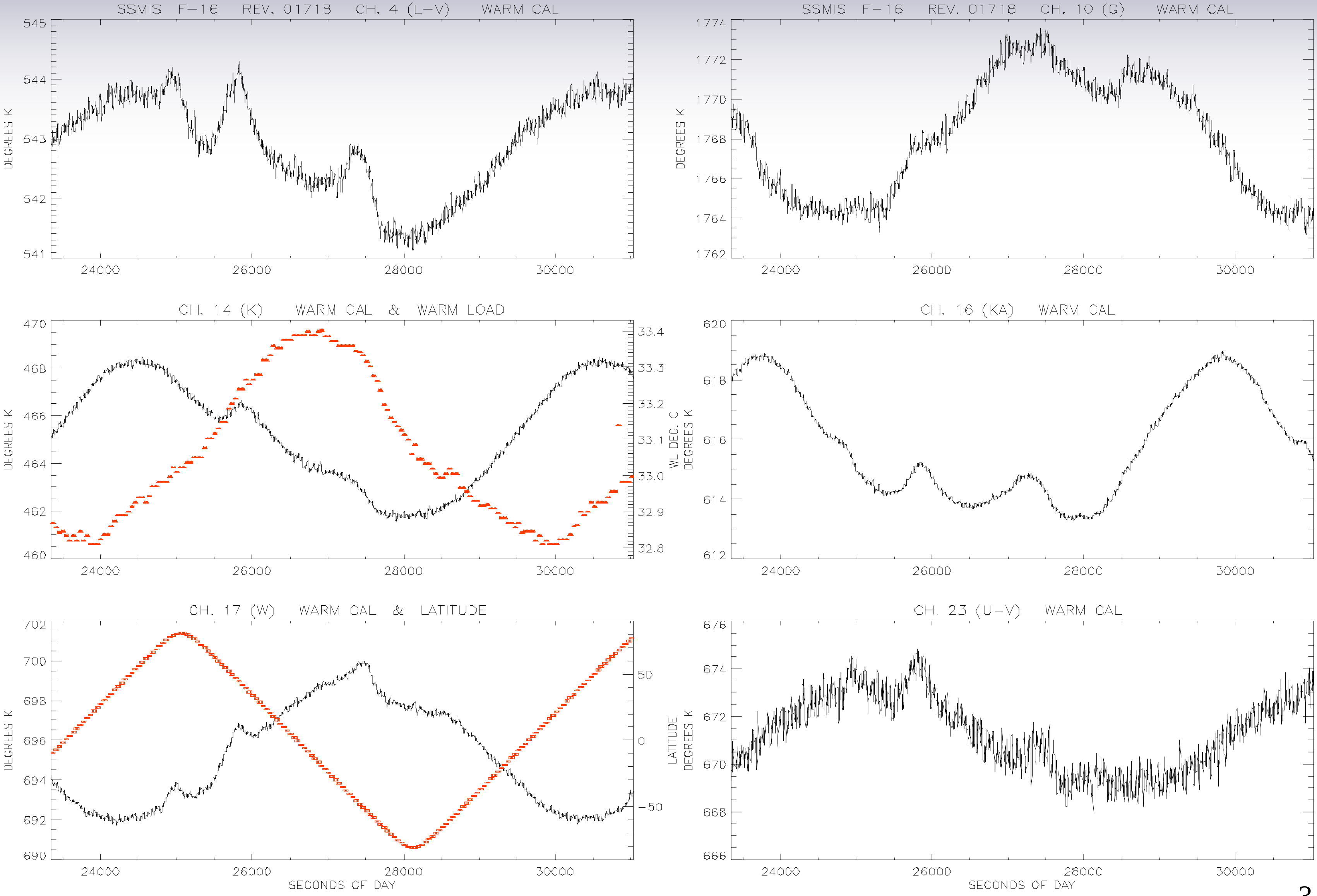

3.4 Orbital Variation
Cold Space Counts/Avg. Gain (Rev. 1718)

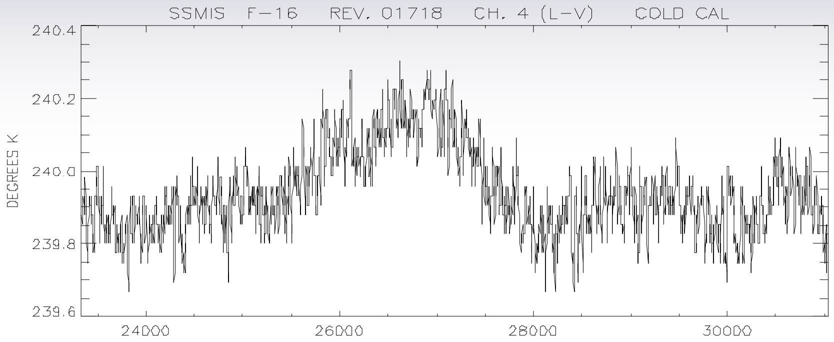

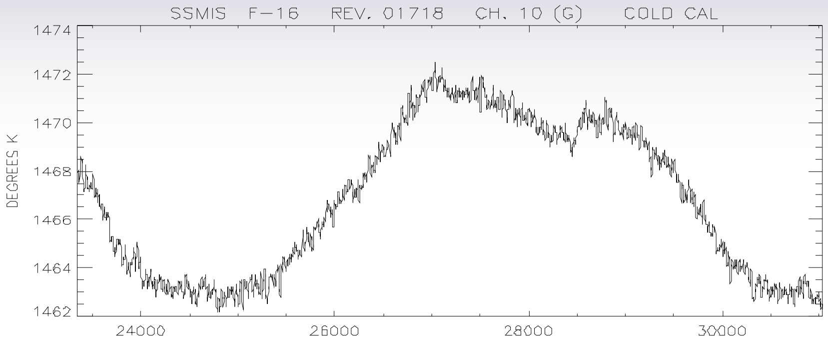

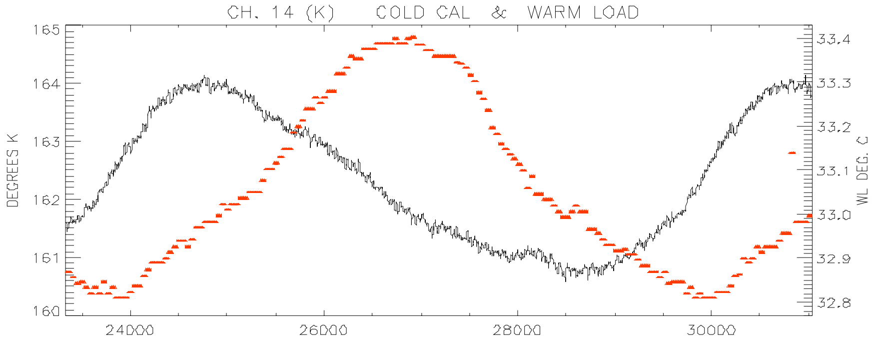

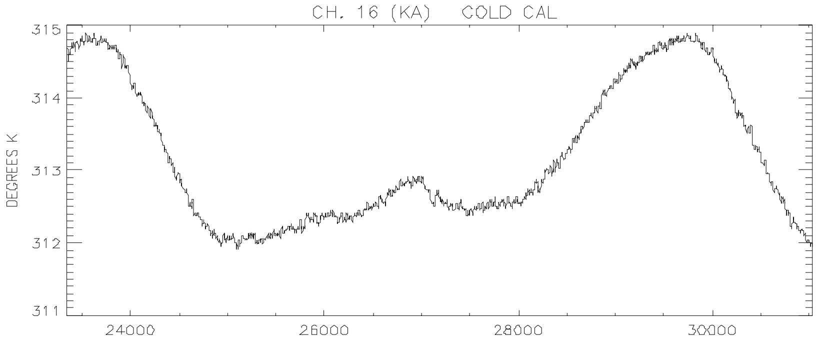

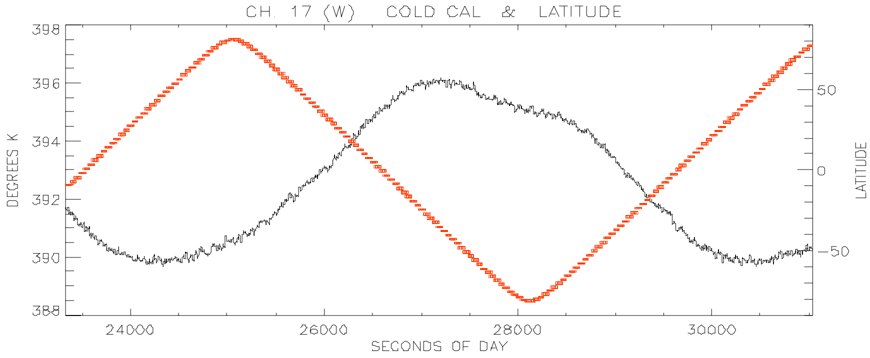

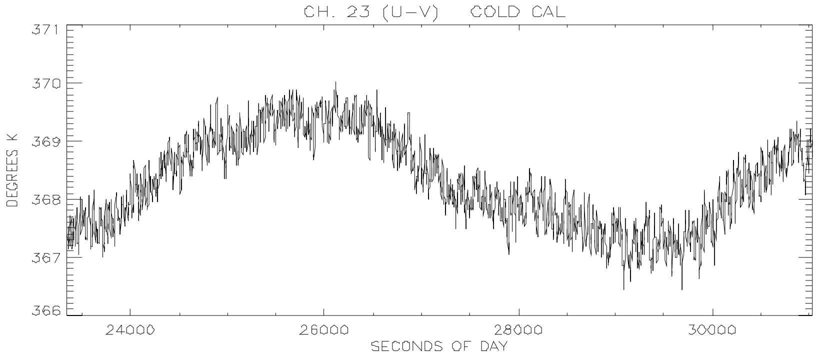

3.4 Orbital Variation
Radiometer Gain (Ct/K) (Rev. 1718)

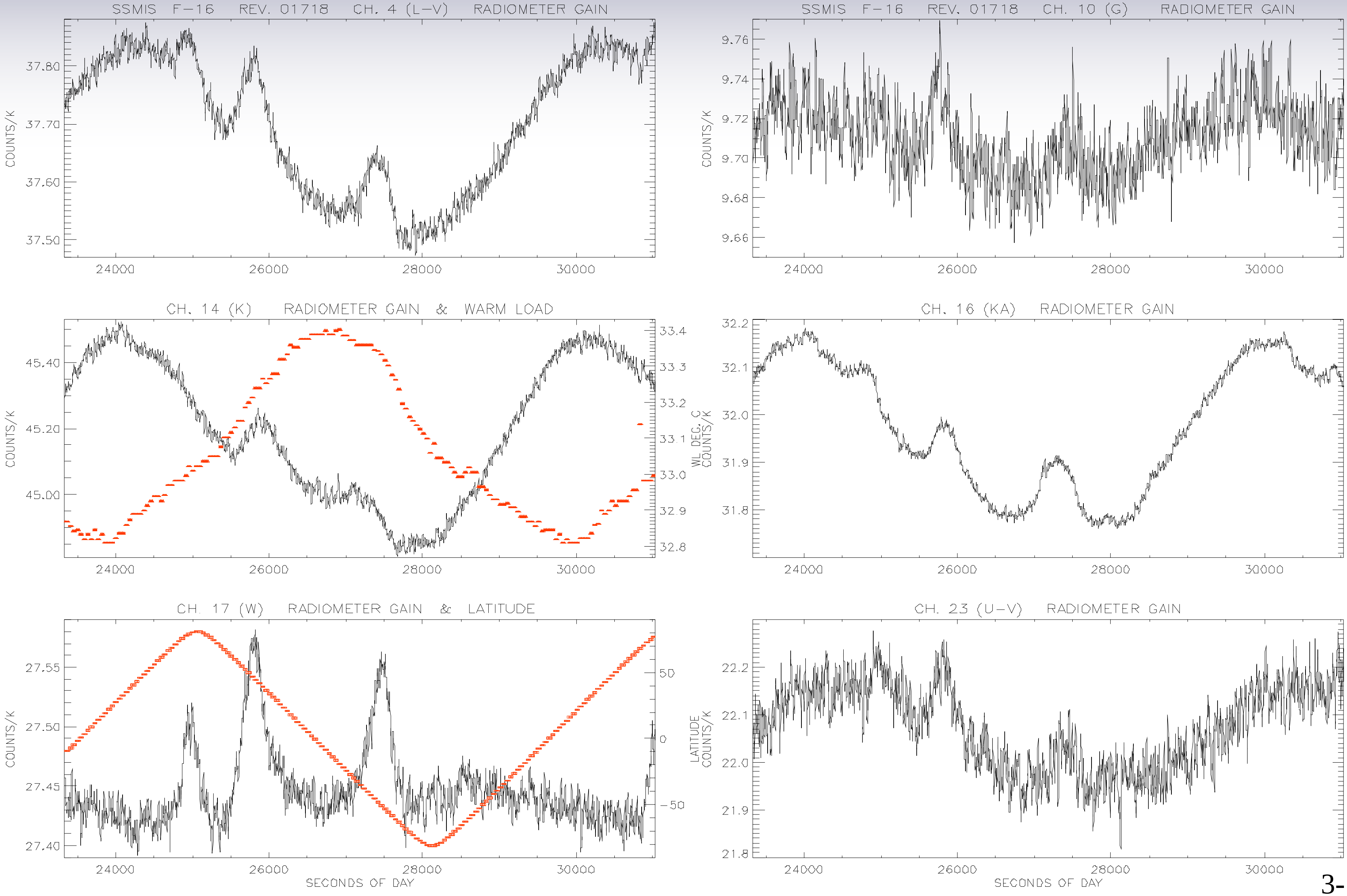

3.4 Orbital Variation
Receiver Plate Temperatures (Rev. 1718)

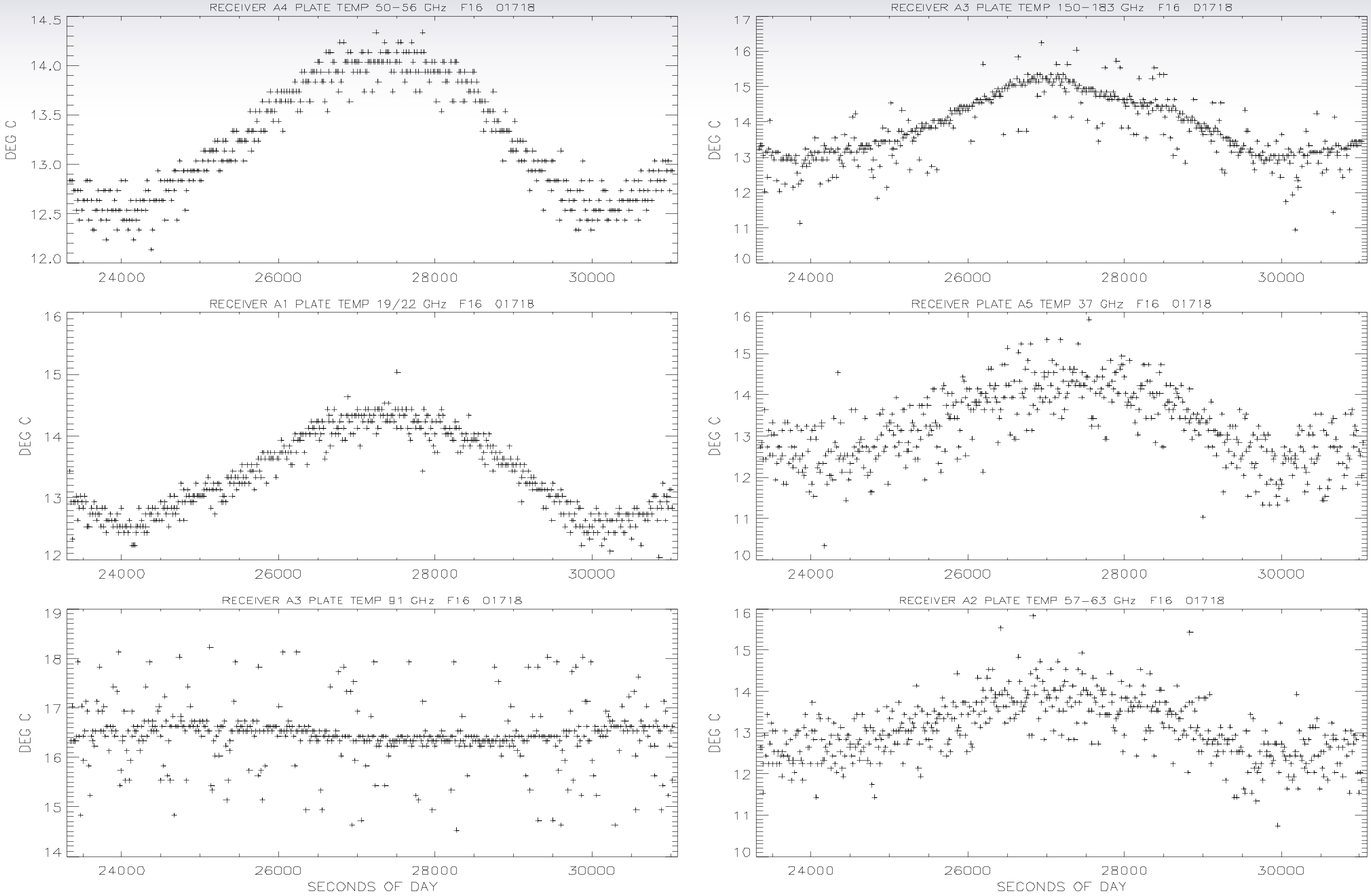

3.4 Orbital Variation
Arm/Rim Temp and Other Mux Parameters

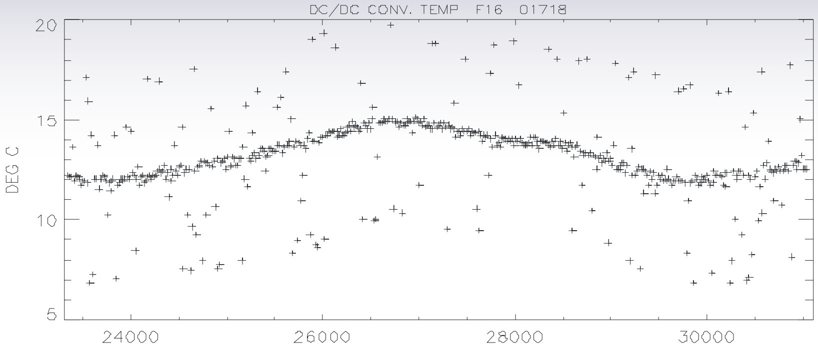
DC/DC CONV. TEMP F16 01718

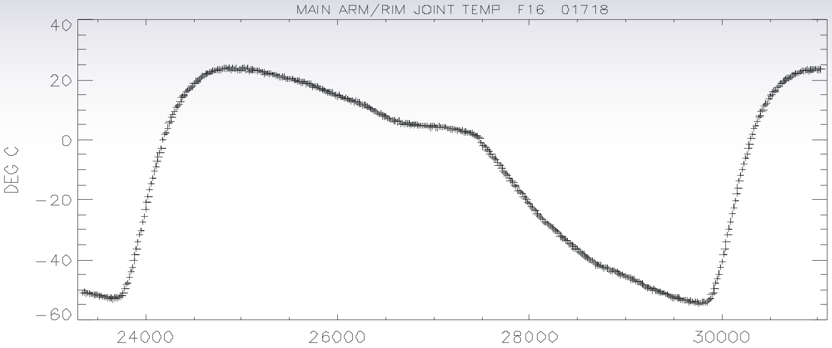
MAIN ARM/RIM JOINT TEMP F16 01718

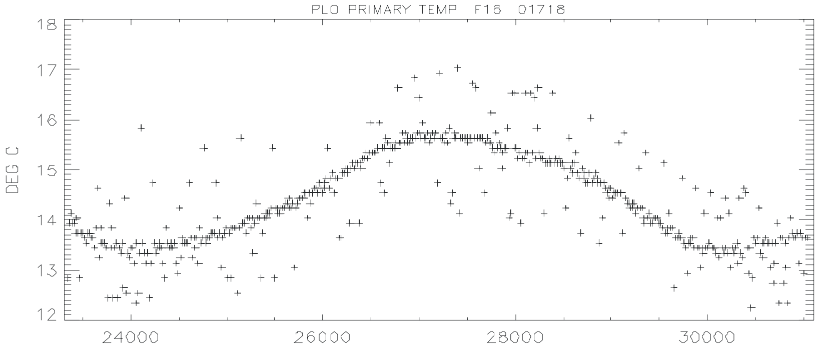
PLO PRIMARY TEMP F16 01718

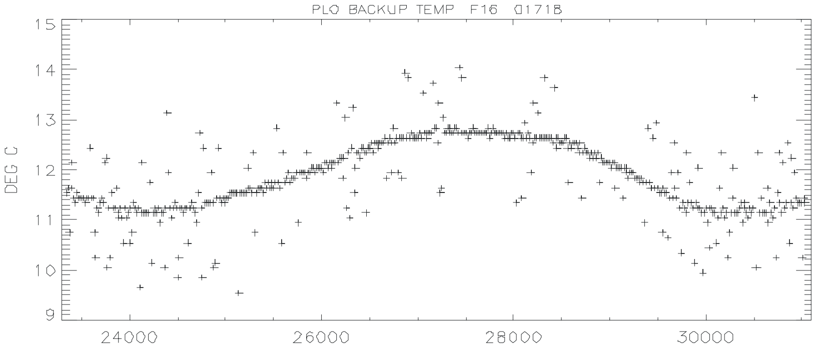
PLO BACKUP TEMP F16 01718

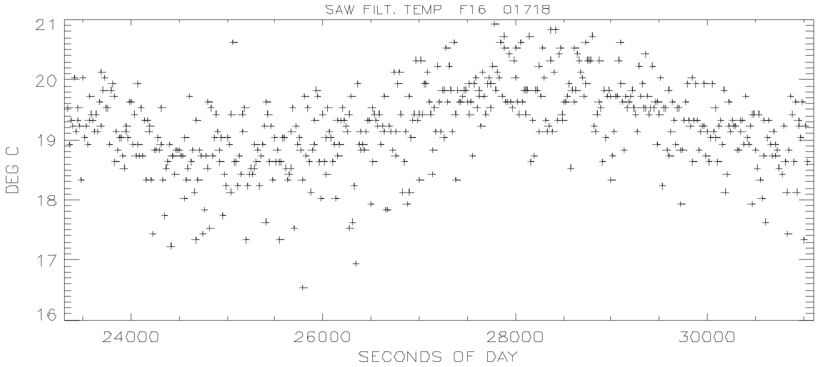
SAW FILT. TEMP F16 01718

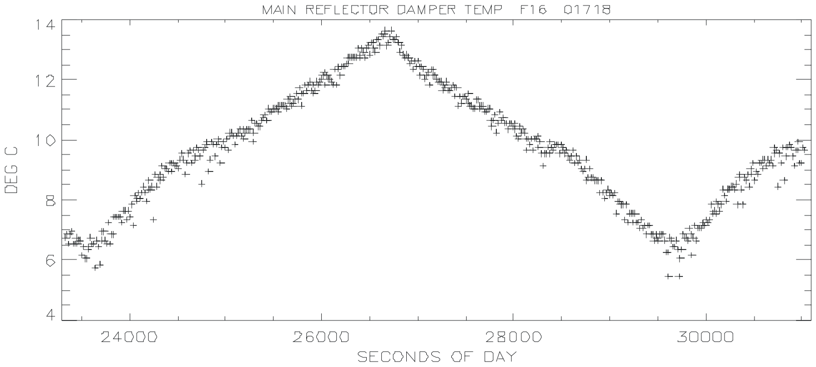
MAIN REFLECTOR DAMPER TEMP F16 01718

3.4 Ch. 15 Receiver Gain Anomaly (Post Jan 05) & CH. 16 Gain (Revs. 6385,6878

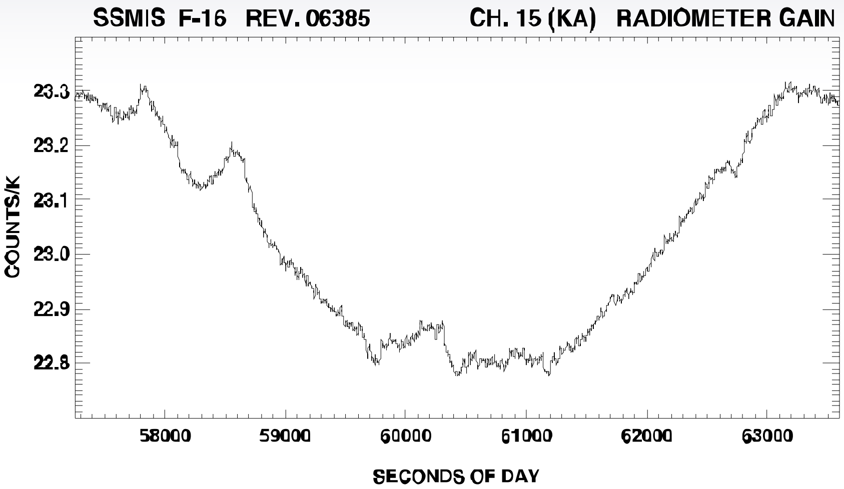

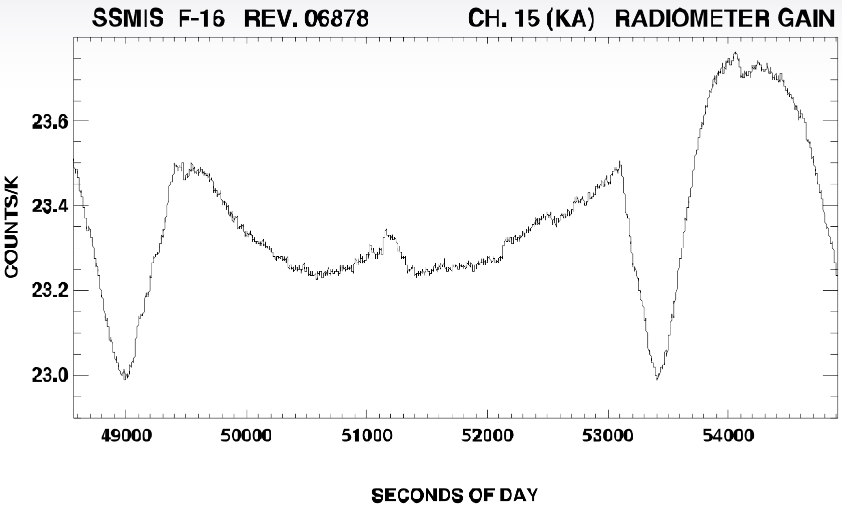

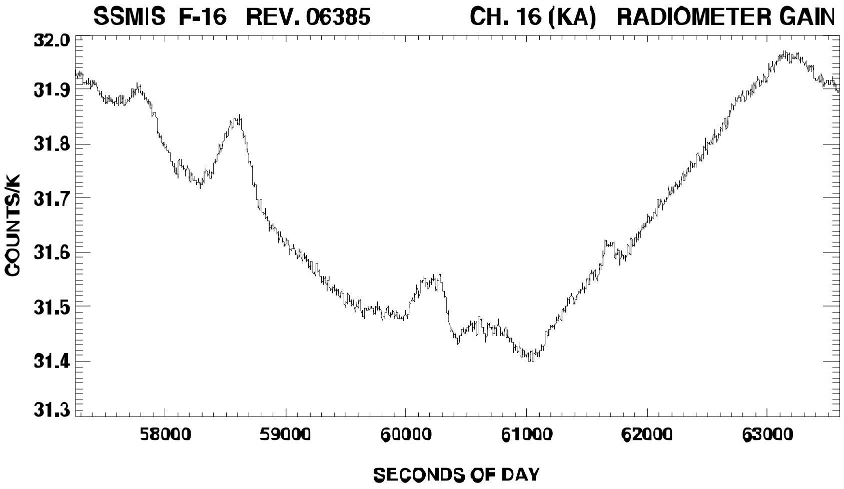

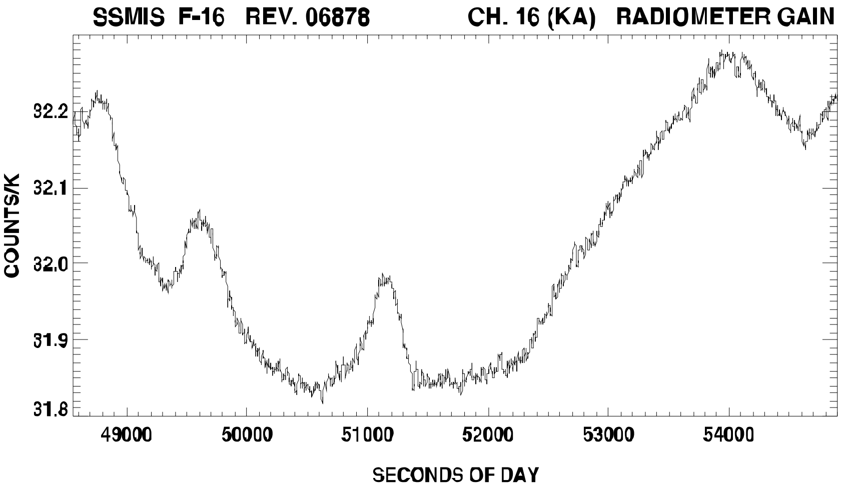

3.4 Ch. 15 Gain Anomaly & Ch. 16 Gain(Cont'd) Revs. 7273,7686

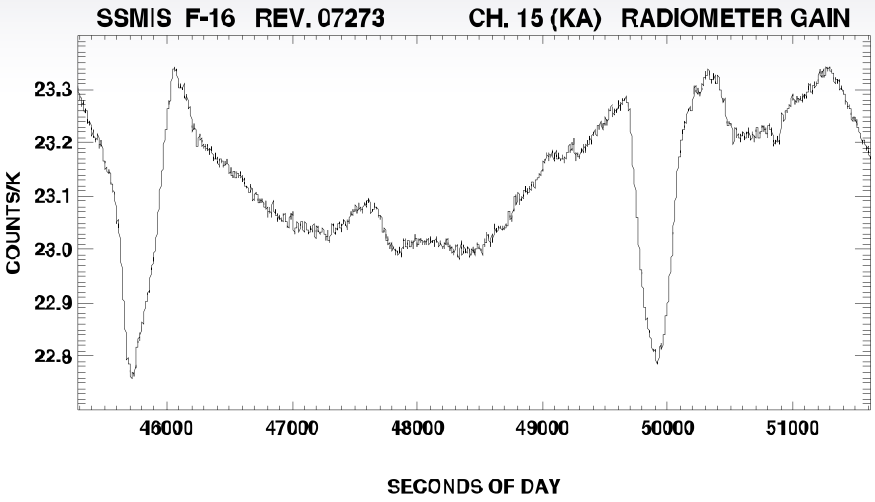

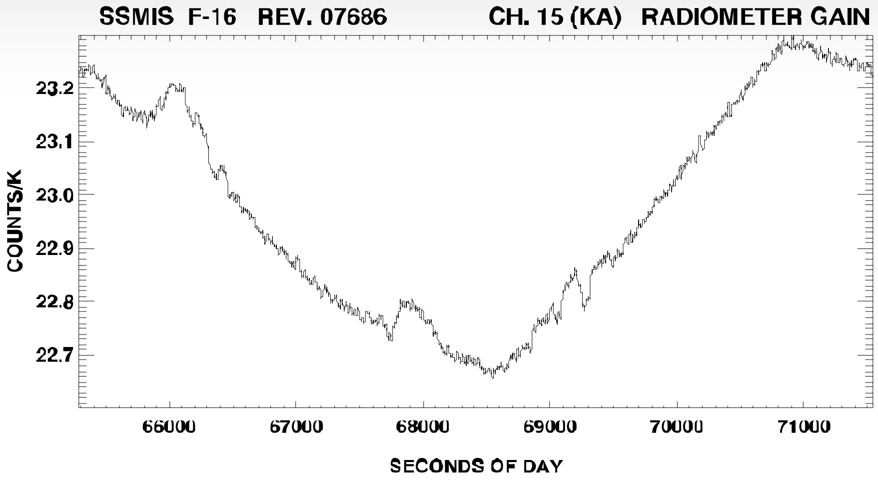

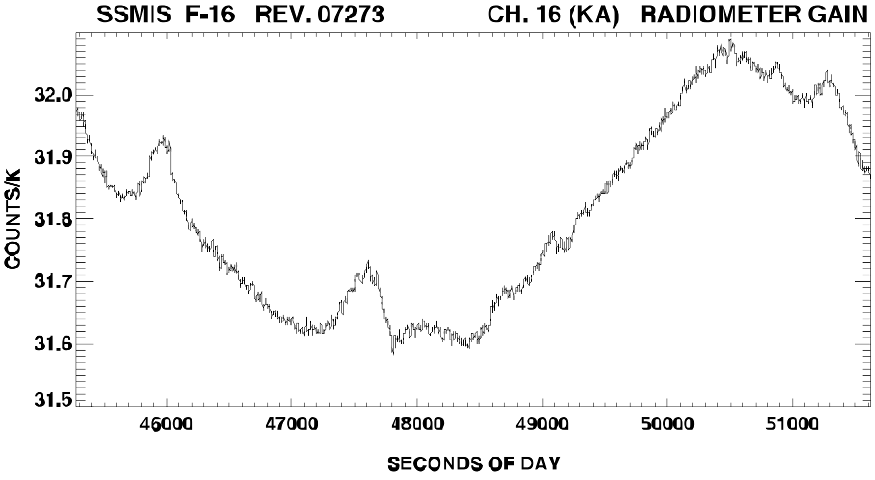

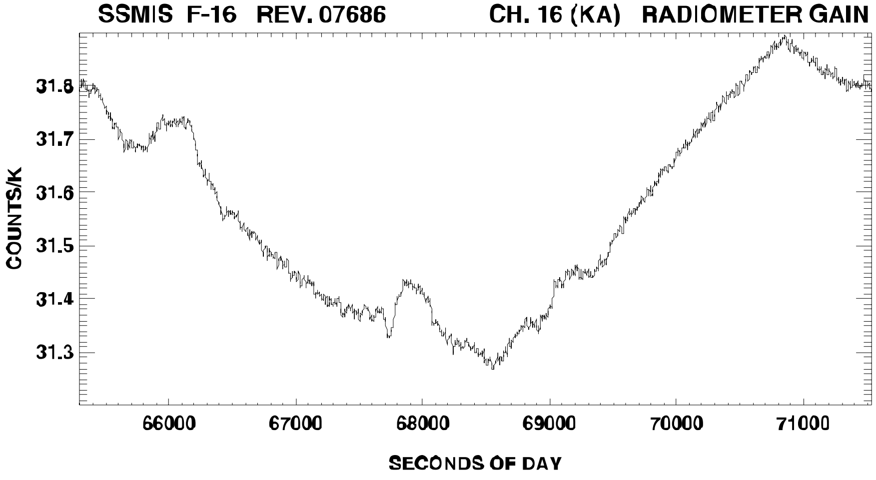

3.4 Ch. 15 Gain Anomaly & Ch. 16 Gain(Cont'd)
Revs. 8178,8575

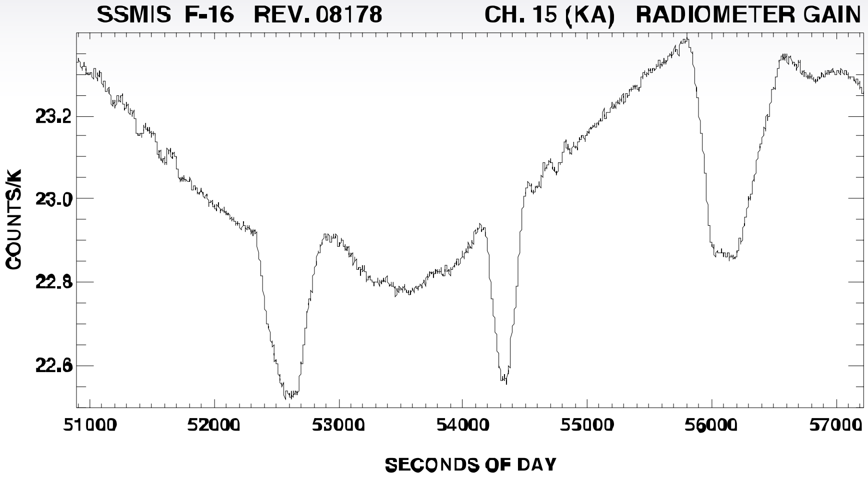

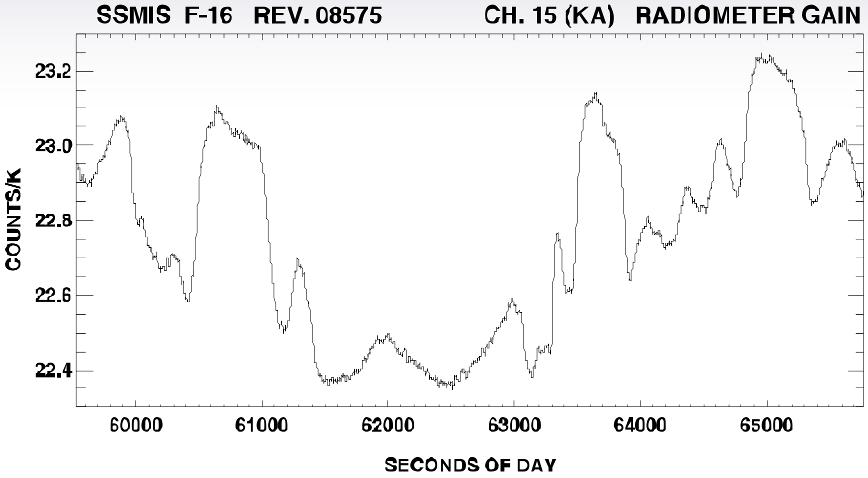

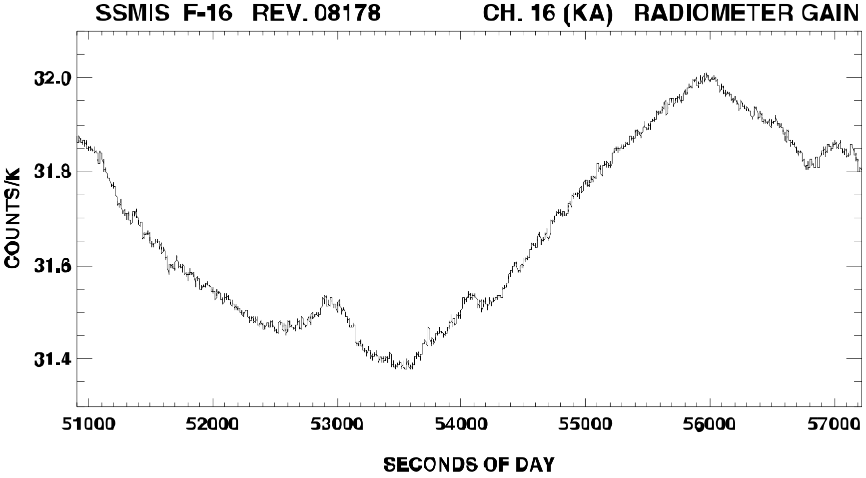

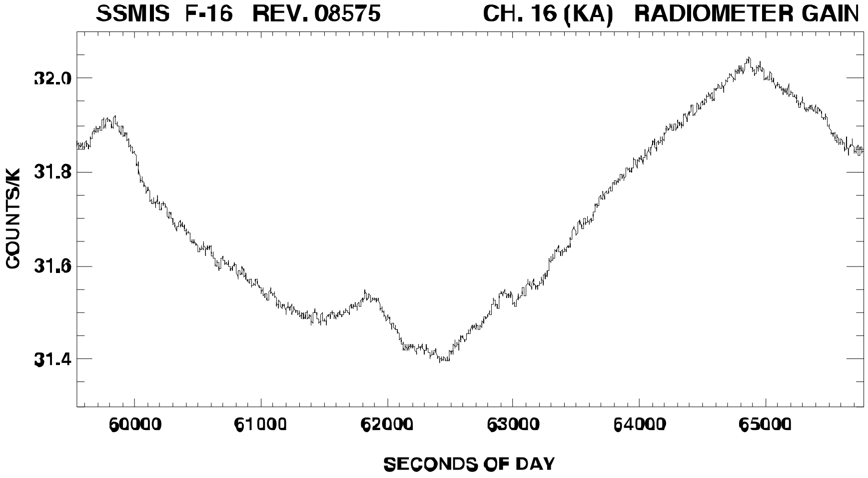

3.4 Ch. 15 Gain Anomaly & Ch. 16 Gain(Cont'd)
Revs. 8958,9565

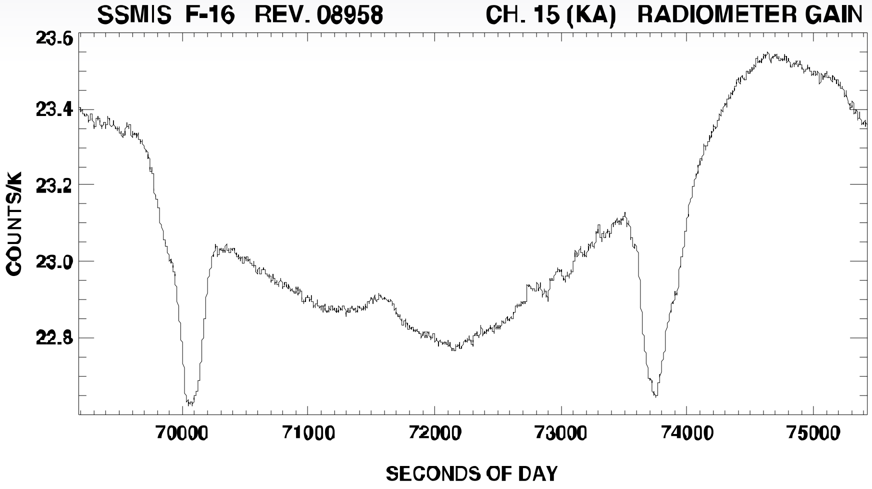

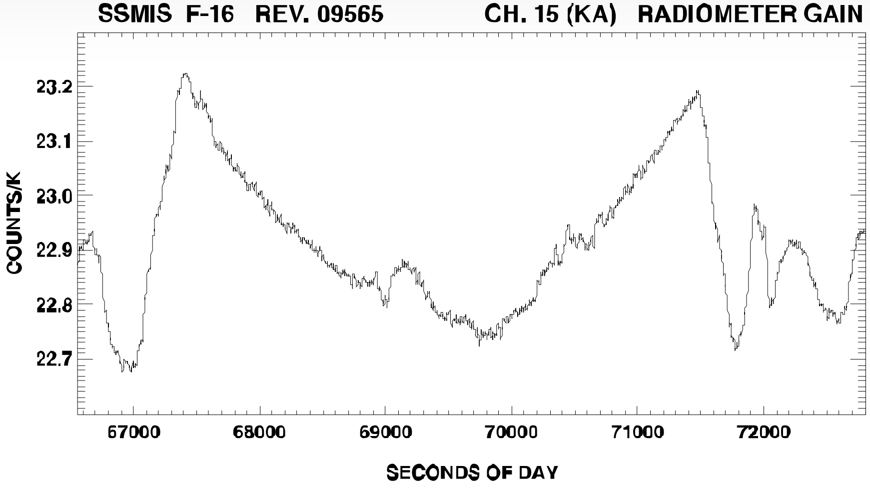

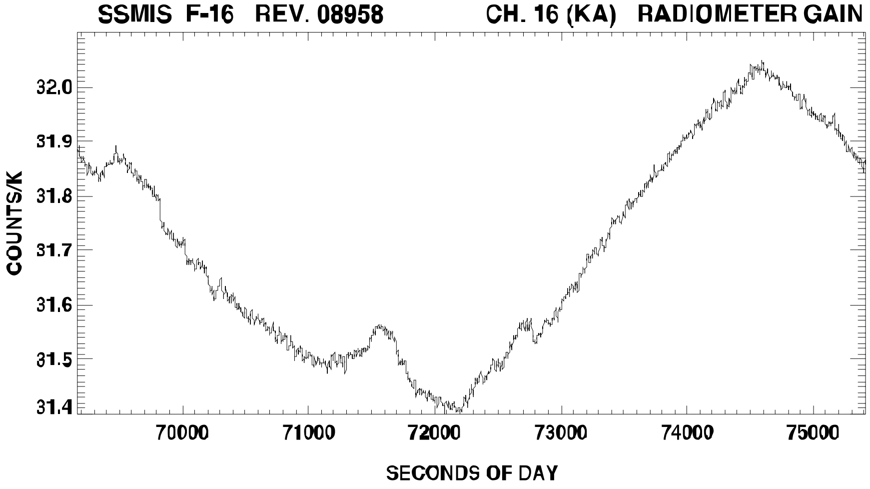

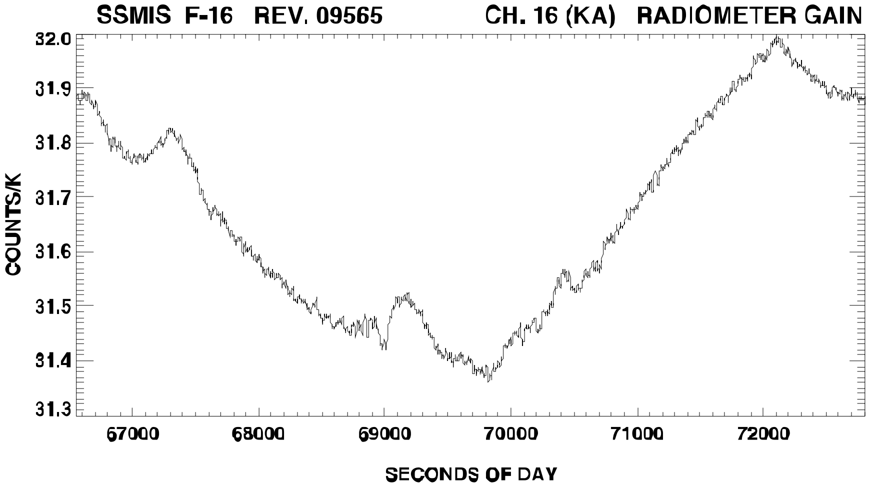

3.5 Radiometer Calibration Algorithm Summary

- **On-Board Flight Software Processing***
  - **Running average calibration data (8 scans/ 4 samples per scan)**
  - **Normalize scene counts**

$$C_R = \left(\frac{C_{SCENE} - C_{CS}}{C_{WL} - C_{CS}} \right) K$$

$$K = 16 \text{ Bit to12 Bit Scale Factor} (K = 3760)$$

  - **Align along-scan scene samples (0.8 degree grid)**
  - **Average along-scan scene data+:**

3 beams Chs.1-7,24	**(2.4 deg. grid starting at -70.8)**
1 beam Chs. 8-11,17-18	**(0.8 deg. Grid starting at -71.2)**
2 beams Chs. 12-16	**(1.6 deg. Grid starting at -71.6)**
6 beams Chs. 19-24	**(4.8 deg. Grid starting at –69.6)**

* **Normal mode only. See Section 2 for Early Orbit mode processing.**

\+ **No averaging of along-track samples (12.5 km grid).**

3.5 Radiometer Calibration Algorithm (Cont'd) Temperature Data Record (TDR)

- **GDPS TDR**
  - **Compute/average warm-load thermistor temperatures**
  - **Remove biases of warm-load/cold-space observations (Currently biases set to zero.)**
  - **Remove residual doppler compensation offsets: (Currently offsets set to zero.)**
  - **Convert scene count to Temperature Data Record (K) referenced at input to feed-horn:**

$$T_A = T_{COS} + \frac{\overline{T}_{WL} - T_{COS}}{K} C_R$$

3.5 Radiometer Calibration Algorithm (Cont'd) Sensor Data Record (SDR)

- **GDPS SDR**
  - **Symmetrize/Optimize averaging period of calibration data**

    (16 scans Chs. 1-7; 64 scans Chs. 19-24)
  - **Mitigate impact of solar intrusion into the warm-load data and moon into the cold-space data**
  - **Antenna Pattern Correction (APC):**

    Feed-horn spillover loss

    Cross-Polarization coupling

    Polarization rotation correction
  - **Scan Non-uniformity Correction: (See Section 4.0)**

    Correct for FOV intrusion at beginning and end of active scene sector.

    Correct for "saw-tooth" residual calibration differences between A and B A/D integrators.
  - **Map Channels 12-18 to F-14 SSM/I: See Section 8.0.**

Note: Mitigation of reflector emissions currently not done.

3.5 Optimize Averaging Period of Calibration Samples

- **Problem:**
  - **Noise in calibration samples degrades TDR accuracy (e.g., “Striping” in imagery of upper-air channels). Optimize length of averaging kernel (i.e., number of scans) that minimizes NEDT in resulting averaged calibration count without introducing significant gain drift errors:**

$$\mathbf{NEDT} = \mathbf{T}_{\mathbf{SYS}} \left[(\mathbf{B}\,\tau)^{-1} + \left(\frac{\Delta \mathbf{G}}{\mathbf{G}} \right)^{2} \right]^{\frac{1}{2}}$$

- **Approach:**
  - **Examine Allan variance of on-orbit (8-scan averaged) calibration samples as function of number of scans averaged**
- **Results:**

Channel	**Number of Scans**
1-7	**16**
19-24	**64**
8-18	**8 (no additional averaging)**

Note: **Significant reduction in “Striping” of upper air imagery**

3.5 Allan Variance Ch. 5-6 and Ch. 19-20

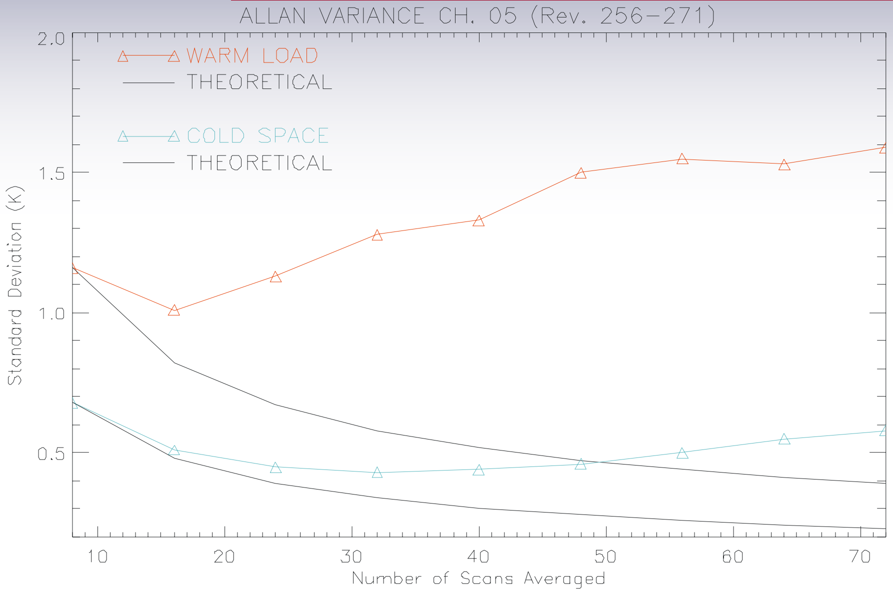

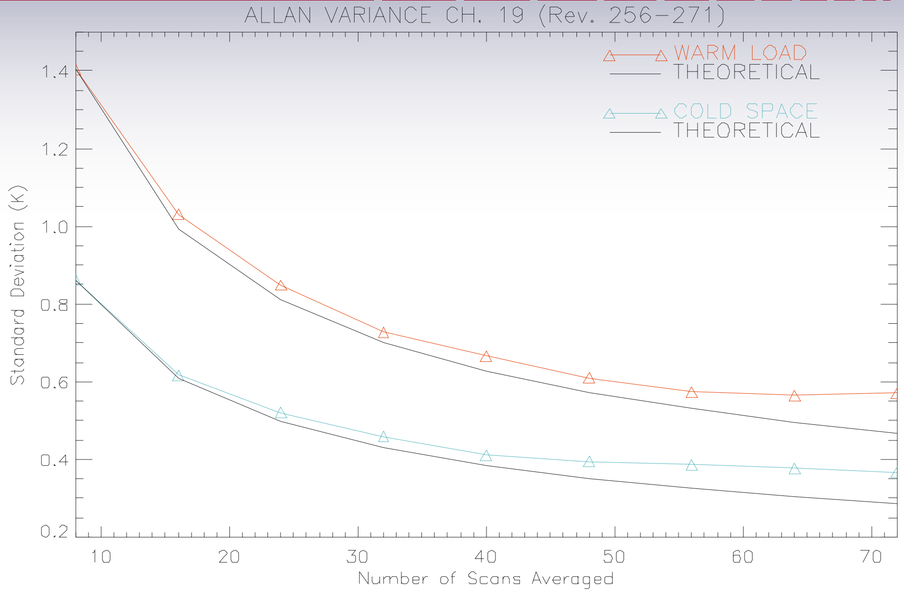

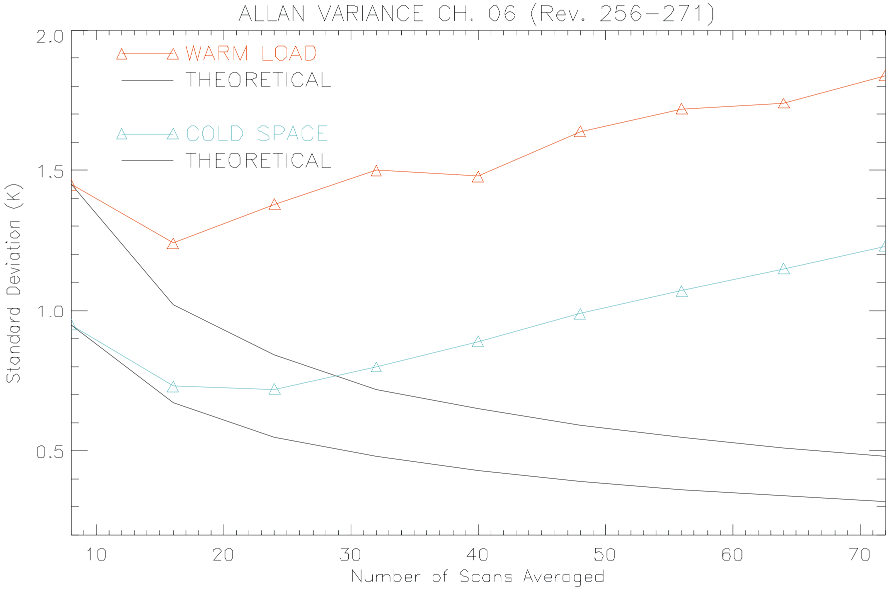

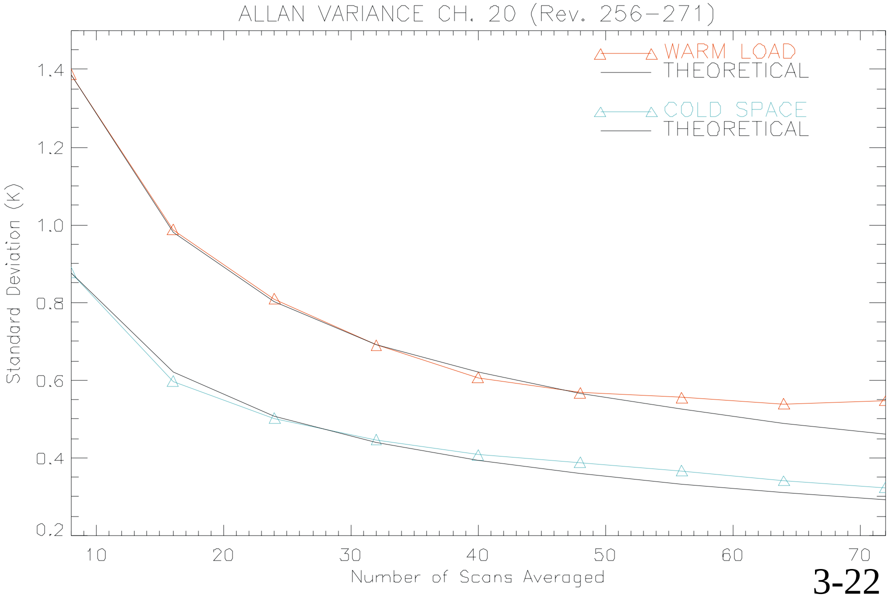

3.5 "Striping" Of Scene Imagery With 8-Scan Average of Calibration Data

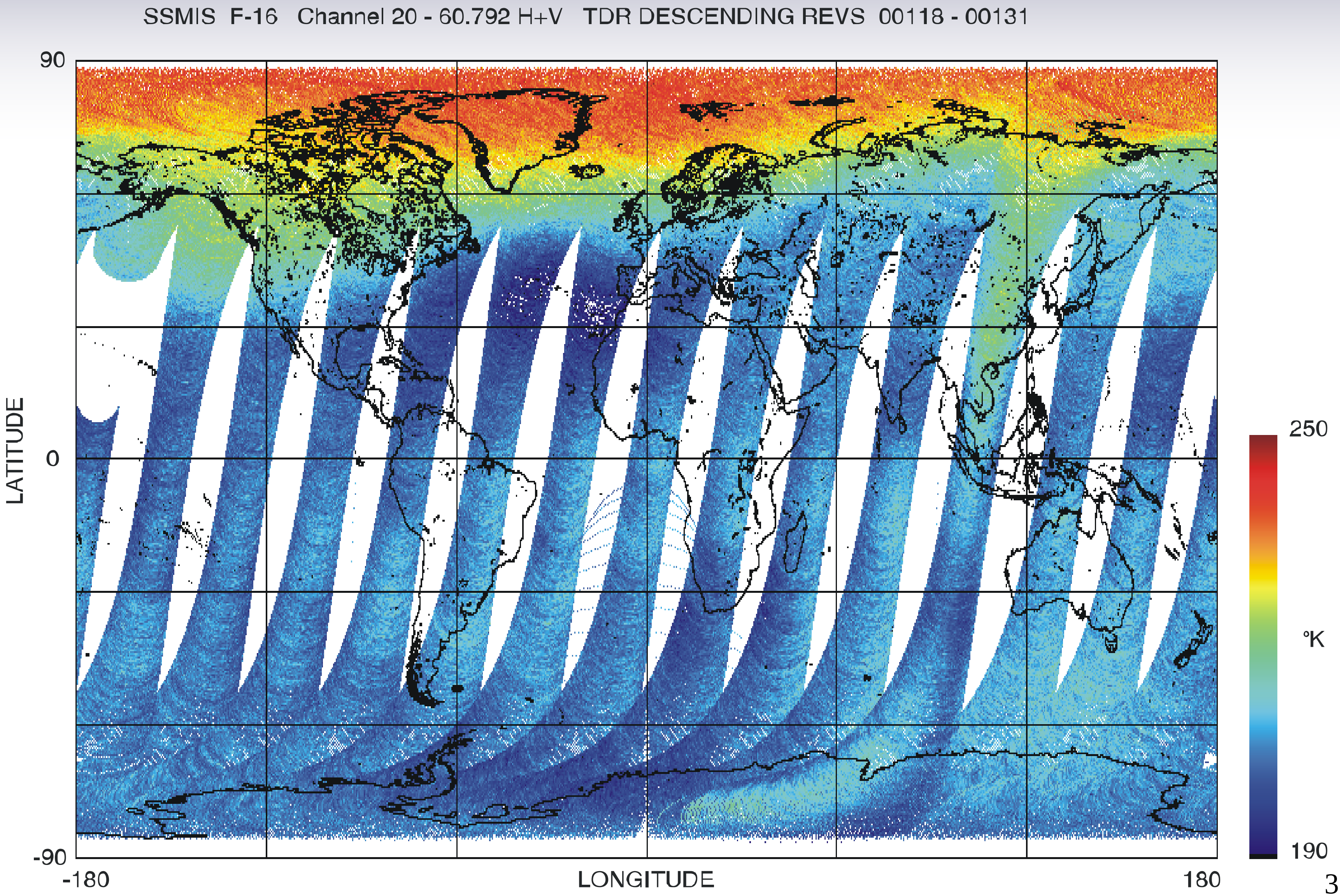

3.5 “Striping” Greatly Reduced With Optimized Algorithm

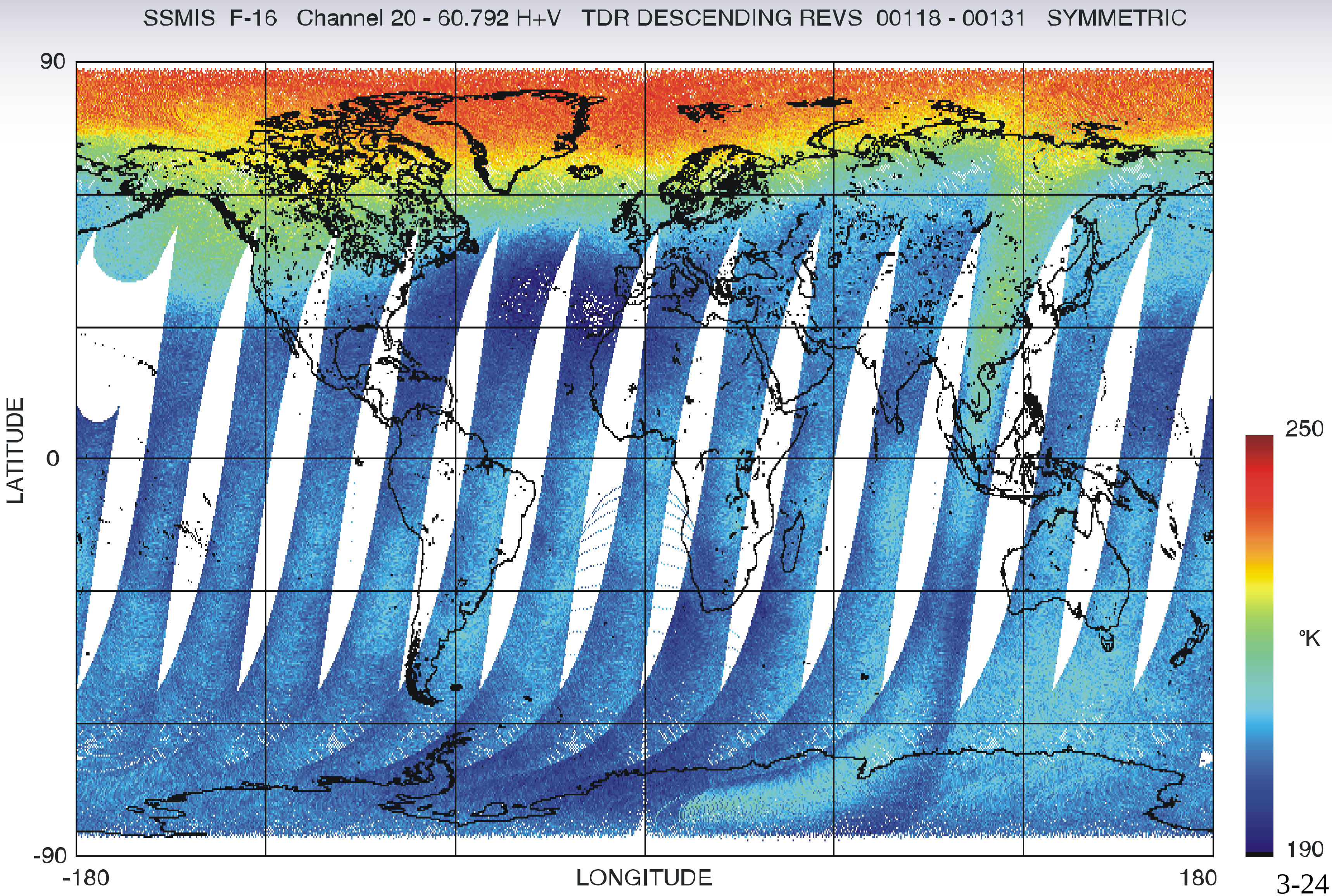

3.5 Algorithm to Filter Sun-glint from Warm-load Data

- Fourier Analyze Chs. 17-18 Orbital Gain Variation
  - Ch. 17-18 gains are relatively constant except during periods of solar intrusion into warm-load
- Identify Sun-Glint: Threshold Localized “Peaks” of Fourier Fit
- Create Time Intervals about “Peaks” for Interpolation and Exclude Contaminated Regions
- Linear Interpolate Gain in Segments from Edge Regions
- Assume Common Time Segments for all Channels
- Scale SDR with “uncontaminated” gain

3.5 Algorithm to Filter Sun-glint from Warm-load Data (Cont'd)

- **Subsequent Two Charts Present SSMIS Radiometer Gain and Warm-load Counts (All channels) of GDPS SDRP Version 5B for Revs. 1021-1023, 5 October 2005, With (red) and Without (blue) Sun-glint Corrections.**

GAIN REVS 10121-10123 2005/277

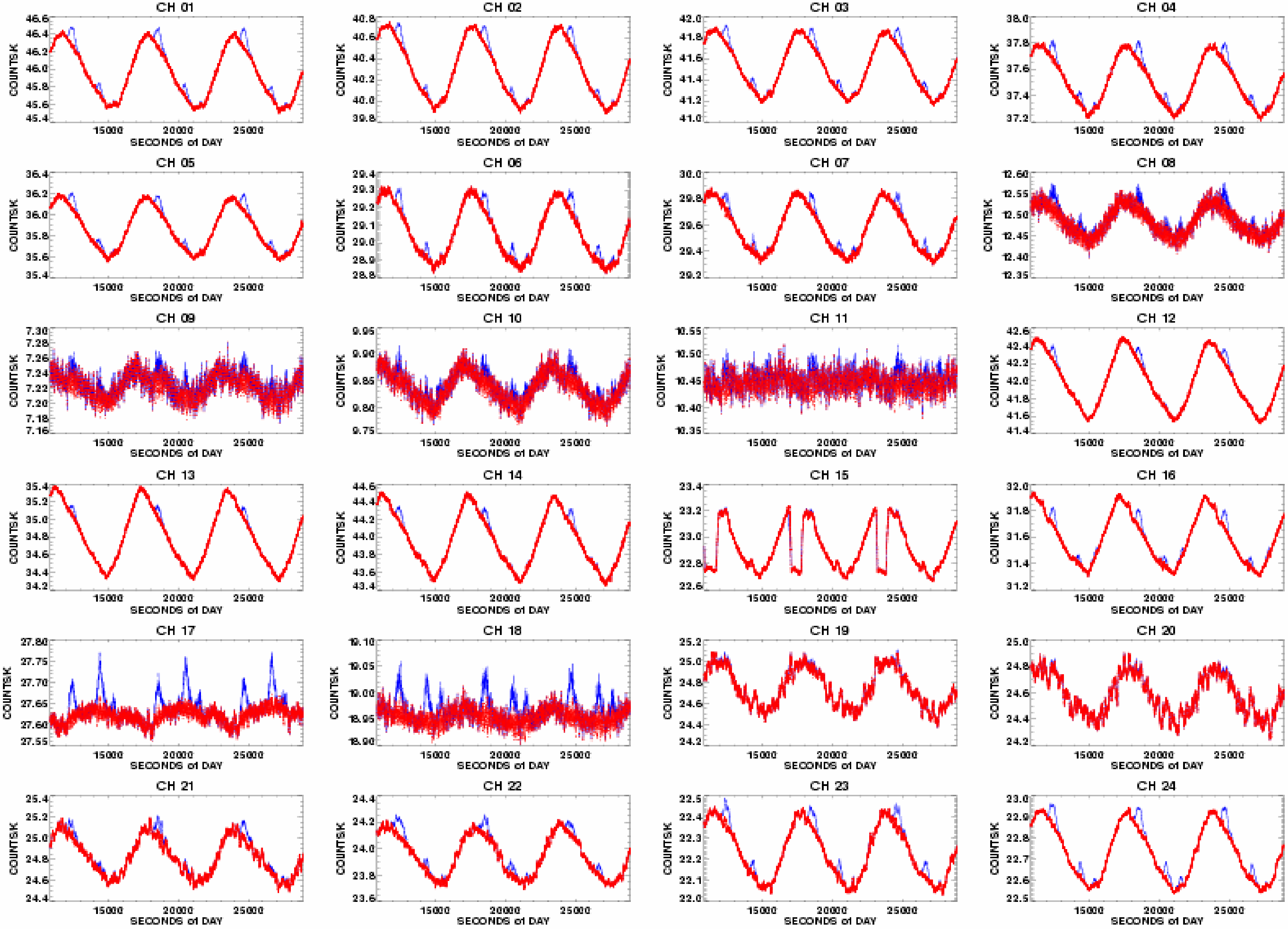

WARM CAL REVS 10121-10123 2005/277

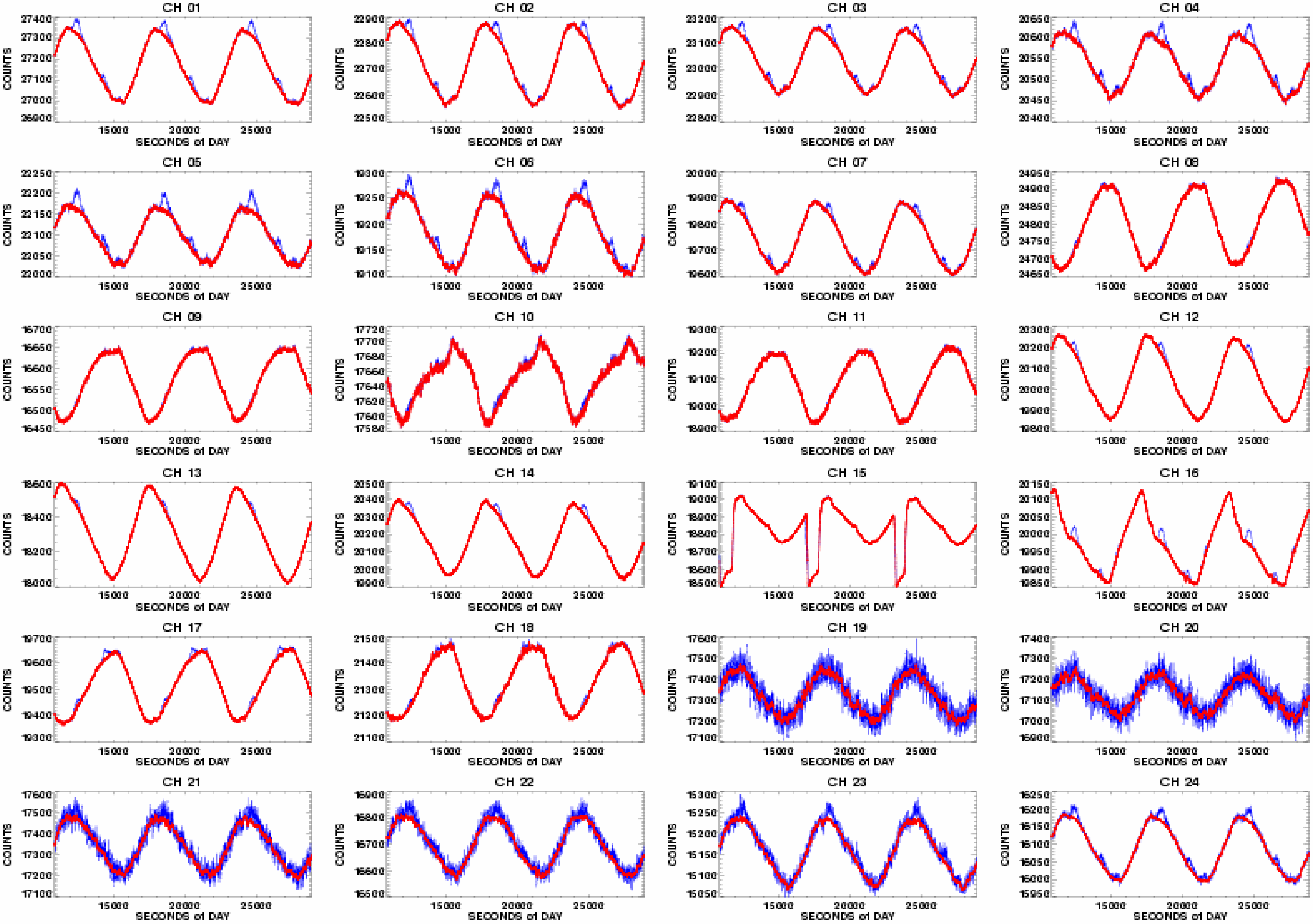

3.6 Sensor Doppler Compensation

- Significant doppler shift Chs. 19-24

$$\Delta\mu\,(\mathrm{MHz}) = \begin{cases} 1.055\cos\phi \\ 1.099\cos\phi \end{cases}$$

$\phi =$ Azimuth scan angle ($\phi = 0$ center of scene sector)

- On-board Local Oscillators (LO) synchronized to ϕ for compensation of doppler shift

- Negligible doppler shift due to earth rotation

$\left(\sim \pm 90\ \mathrm{kHz\ at\ Scan\ Edges}\right)$

- Small variation of shift about nominal orbit

(e.g., < 3 % Shift for 860 to 900 km altitude change)

3.6 Sensor Doppler Compensation (Cont'd)

- On-board LO doppler compensation set to zero during calibration measurements.

- Small receiver gain changes induced by LO shift documented in T/V laboratory tests (Not fully understood, potential artifact of T/V tests, not confirmed on-orbit data, possible future Early Orbit Mode test). Algorithm to address T/V test results Implemented in GDPS but currently coefficients are set to zero.

- Major impact on Ch. 19-21 TDR imagery without LO doppler compensation.

3.6 Receiver LO Compensation Removes Doppler Shift of Upper Air Channels (Ch. 19)

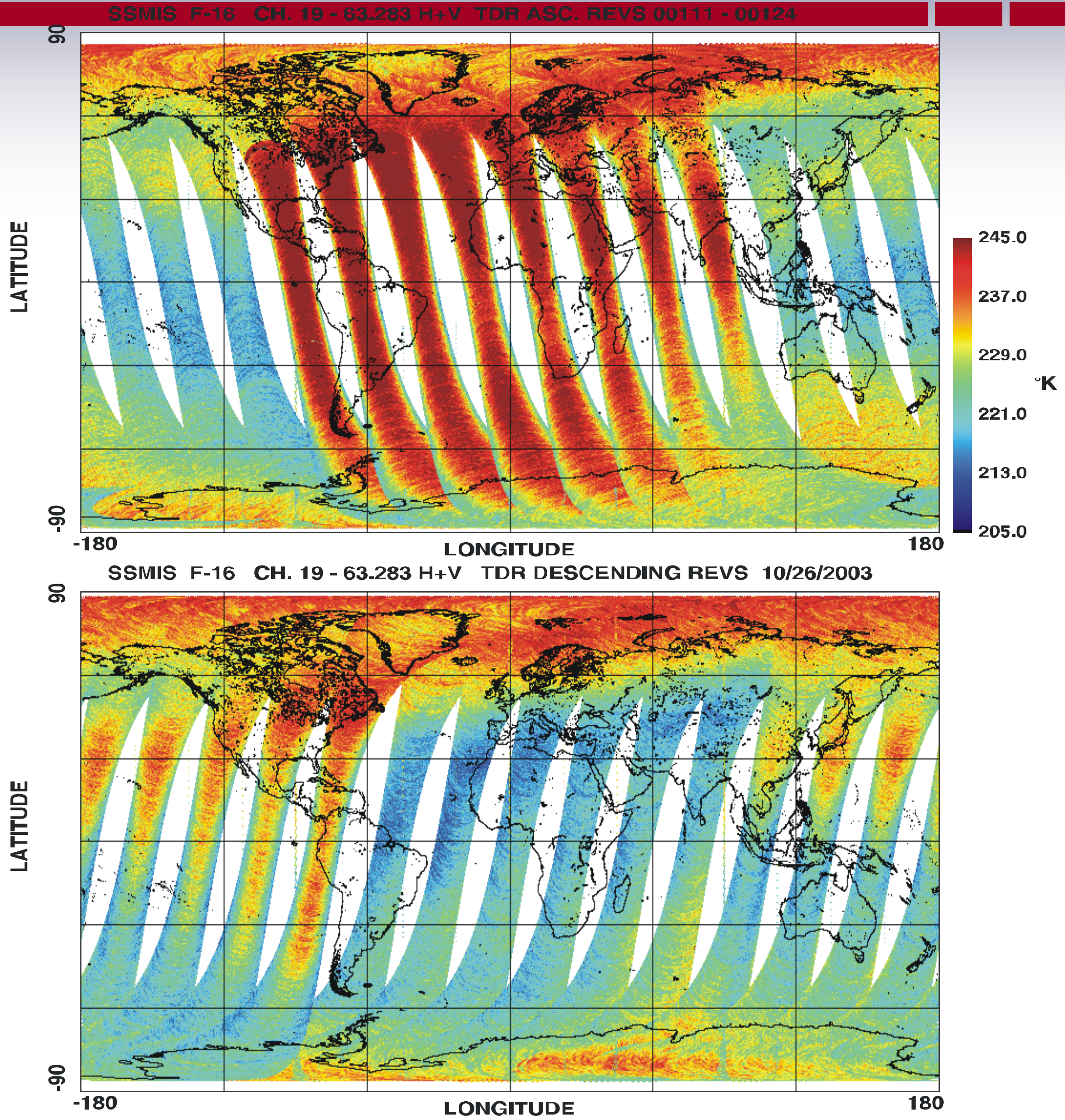

3.6 Receiver LO Compensation Removes Doppler Shift of Upper Air Channels (Ch. 20)

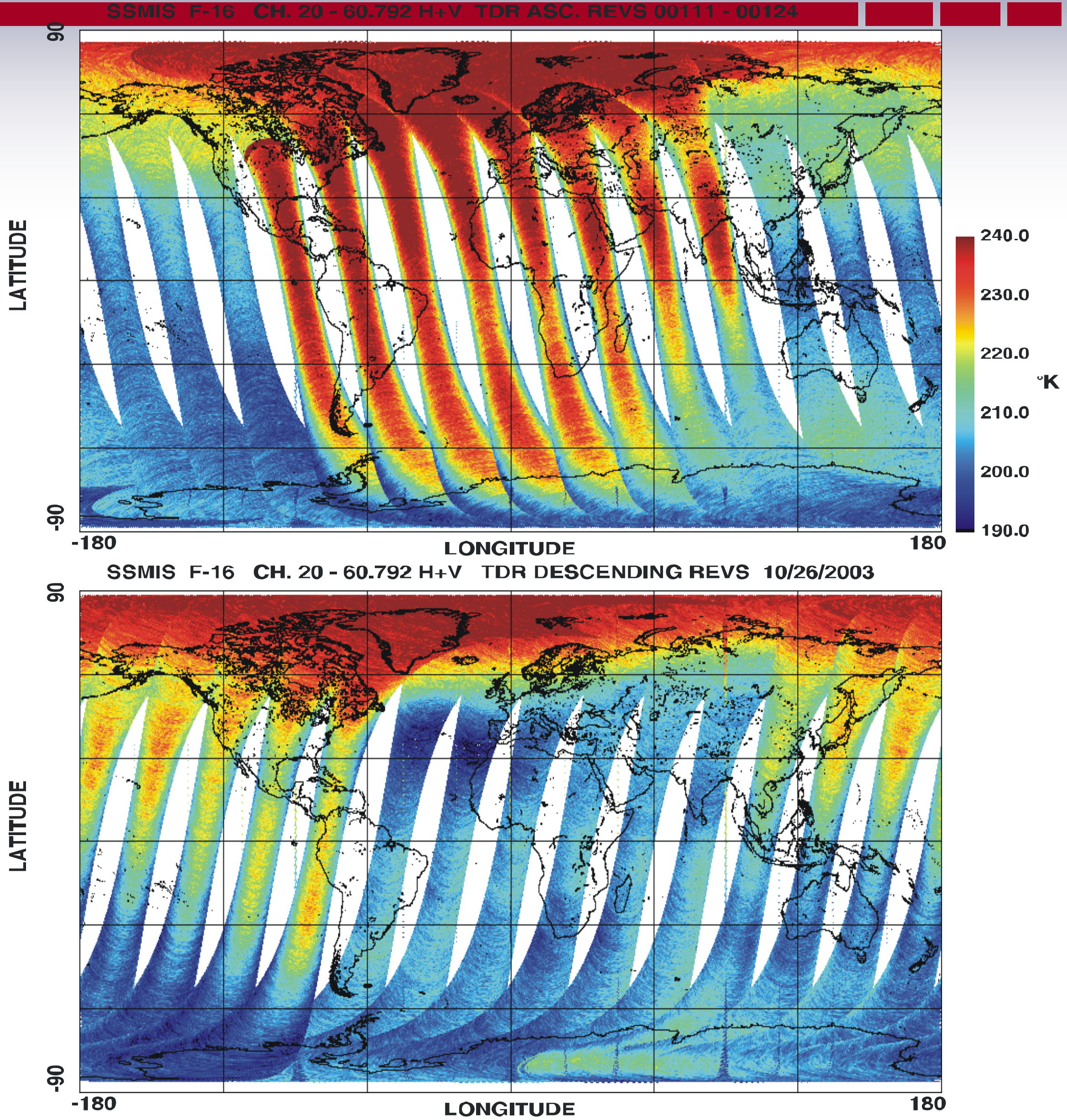

3.6 Optimized Calibration Algorithm Reduces "Striping" in Imagery of Upper Air Channels (Ch. 19)

SSMIS F-16 CH. 19 - 63.283 H+V TDR ASC. REVS 00111 - 00124 SYMMETRIC

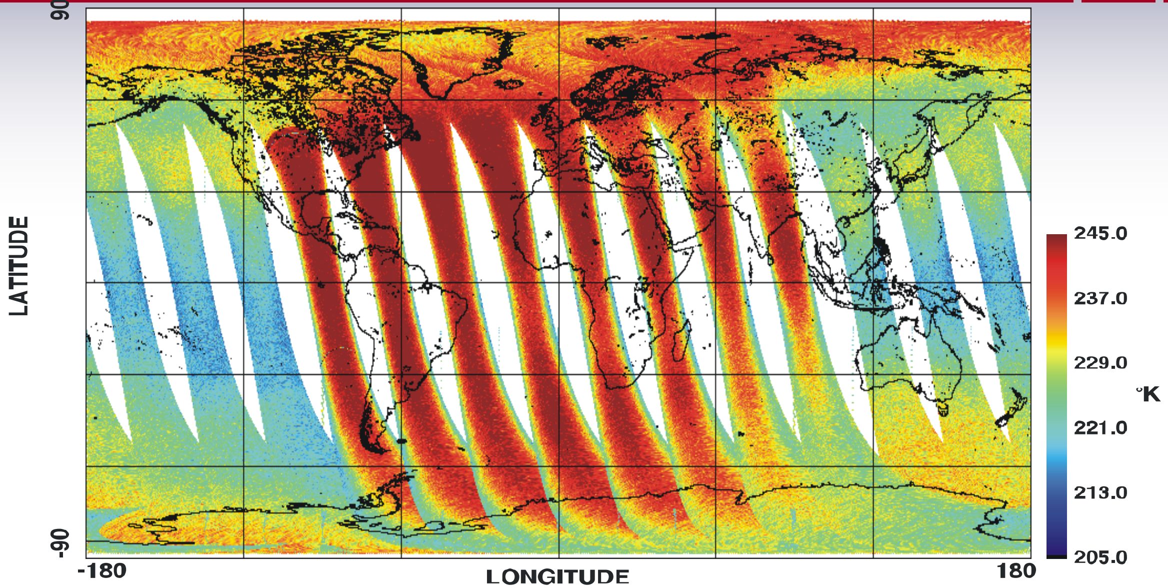

SSMIS F-16 CH. 19 - 63.283 H+V TDR DESCENDING REVS 10/26/2003

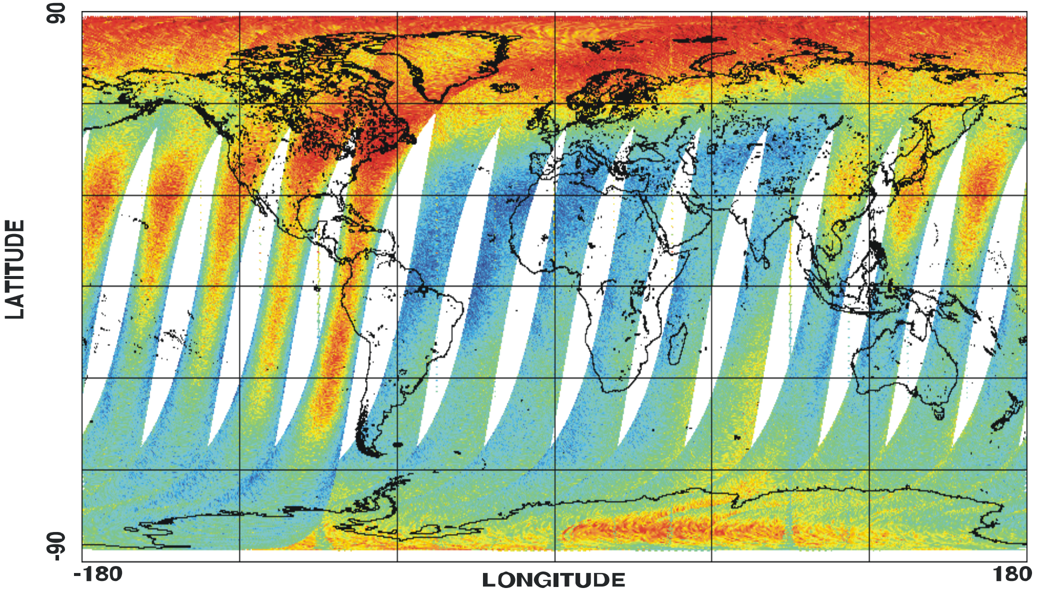

3.6 Optimized Calibration Algorithm Reduces "Striping" in Imagery of Upper Air Channels (Ch. 20)

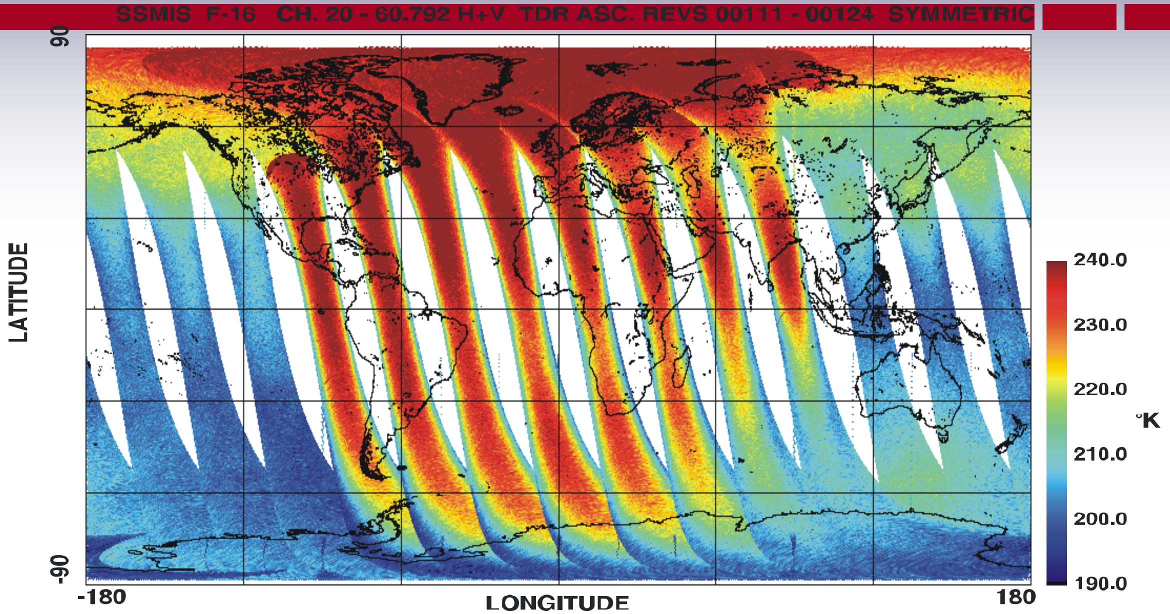

SSMIS F-16 CH. 20 - 60.792 H+V TDR ASC. REVS 00111 - 00124 SYMMETRIC

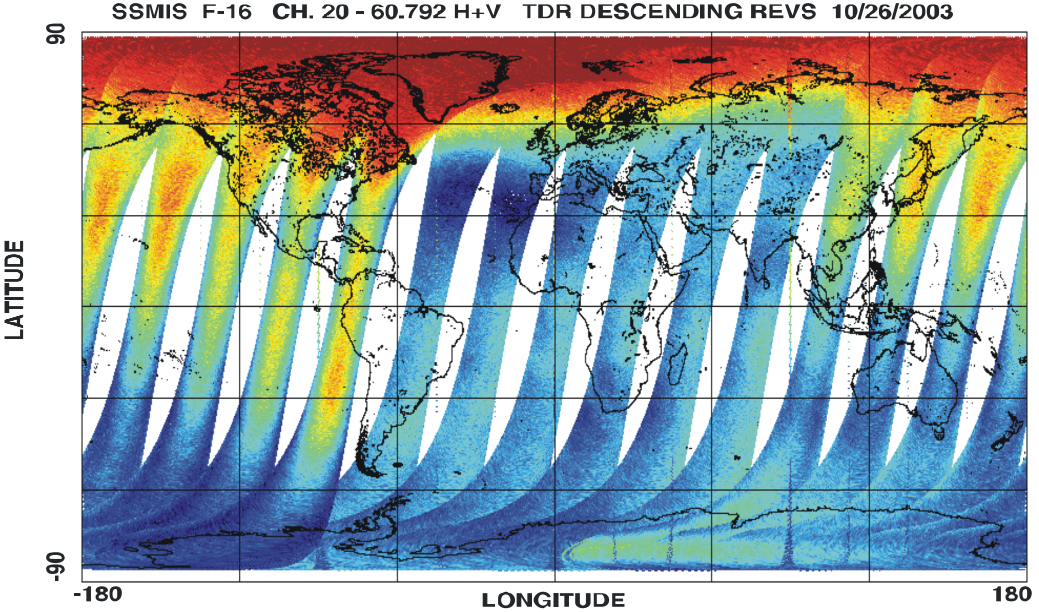

SSMIS F-16 CH. 20 - 60.792 H+V TDR DESCENDING REVS 10/26/2003

F16 SSMIS Calibration/Validation Final Report

Section 4.0 Geo-location/Resampling

Enzo Uliana, Gene Poe and Beverly Gardiner

4.0 Geo-location

4.1 Objectives

- Quantify and establish geo-location accuracy
- Derive pointing / time corrections to bring errors within specification
  - Parameters common to all channels
    - 1/2 cone angle offset
    - Pitch, roll, yaw offsets about spin axis
    - Scan start time offset
  - Individual beams
    - Beam azimuth / elevation offsets
- Determine repeatability / stability of performance
- Determine earth incidence angle (EIA)
- Develop re-sampling routines (if necessary) for common SDR grid

4.2 Approach

- Overlay world shoreline data base with SSMIS imagery
    - 15 Coastline Regions (See table)
    - Ascending and descending orbits
    - Along track and along scan variations
    - Scan start time offset
    - Global DMA shoreline data base
- Derive shoreline from SSMIS imagery with selected pointing and time offsets
- Successful approach for SSM/I and WINDSAT
- UAS channels performance inferred

4.2 Coast-lines Selected for Geo-location Analysis

Area	Location	Latitude	Longitude
1	Spain / North Africa	30 N - 50 N	15 W - 5 E
2	Gulf of California	20 N - 40 N	100 W - 120 W
3	Northern Australia / New Guinea	0 - 20 S	130 E - 150 E
4	Eastern Africa / Madagascar	10 S - 30 S	30 E - 50 E
5	South America	35 S – 55 S	55 W - 75 W
6	Korea / Japan	25 N - 45 N	125 E - 145 E
7	India	5 N –25 N	70 E – 90 E
8	Red Sea Area	15 N - 35 N	30 E - 50 E
9	Florida / Cuba	15 N - 35 N	70 W - 90 W
10	Black Sea / Caspian Sea	30 N - 50 N	35 E - 55 E
11	East Coast of Brazil	5 N - 15 S	35 W - 55 W
12	England / Ireland / Iceland	40 N - 60 N	15 W - 5 E
13	Gulf of Mexico / Yucatan	13 N - 33 N	83 W - 103 W
14	Persian Gulf	15 N - 35 N	50 E - 70 E
15	Somalia / Yemen (Horn of Africa)	0 - 20 N	40 E - 60 E

4.3 Major Results

- Offsets common to all channels:
  - -1.0 Deg. Yaw
  - -1.899 Sec. Time
- Individual beam offsets:
  - Channels 12-14 have a 0.4 deg. elevation and –0.3 deg. azimuth
  - Channels 17-18 & 8-11 have a -0.1 deg. elevation

4.3 Major Results (Cont'd.)

- **Different ½ cone angles: Chs. 12-14; Chs. 8-11,17-18; Chs. 1-7,15-16**
- **Stable geo-location error ≤6 km**
- **Resample channels 12 - 14 to 15 - 16 grid**
- **Independent review by Mr. Bill Purdy (NRL consultant for WINDSAT) confirms geo-location results**
- **Note:**

  TDR output file contains individual geo-located coordinates. Re-sampling done only in SDR file.

4.4 Representative Image Results

Ch. 18				
	Spain / N. Africa	**Ascending**	**Rev. 708**	**7 Dec.03**
	Somalia/Yemen	**Descending**	**Rev. 1787**	**17 Feb. 04**
	Northern Australia / New Guinea	**Descending**	**Rev. 3394**	**15 June 04**
Ch. 15				
	Gulf Of Mexico/Yucatan	**Ascending**	**Rev. 1786**	**17 Feb. 04**
	Black Sea / Caspian Sea	**Ascending**	**Rev. 2641**	**22 Apr. 04**
	Japan / Korea	**Descending**	**Rev. 3324**	**10 June 04**
Ch. 12				
	Spain/N.Africa	**Ascending**	**Rev. 1739**	**18 Feb. 04**
	Somalia / Yemen (Horn of Africa)	**Descending**	**Rev. 1787**	**17 Feb. 04**
	Eastern Africa / Madagascar	**Ascending**	**Rev. 2670**	**24 Apr. 04**
	India	**Ascending**	**Rev. 3318**	**9 June 04**
Ch. 1				
	Persian Gulf	**Ascending**	**Rev. 1751**	**19 Feb. 04**
	Eastern Africa / Madagascar	**Ascending**	**Rev. 2670**	**24 Apr.04**
	Northern Australia / New Guinea	**Descending**	**Rev. 3394**	**14 June 04**
Ch. 8				
	S. America	**Descending**	**Rev. 2653**	**24 Apr.04**
	S. America	**Ascending**	**Rev. 3282**	**7 June 04**

Geo-location Before and After Correction Ch. 18
Spain/N.Africa

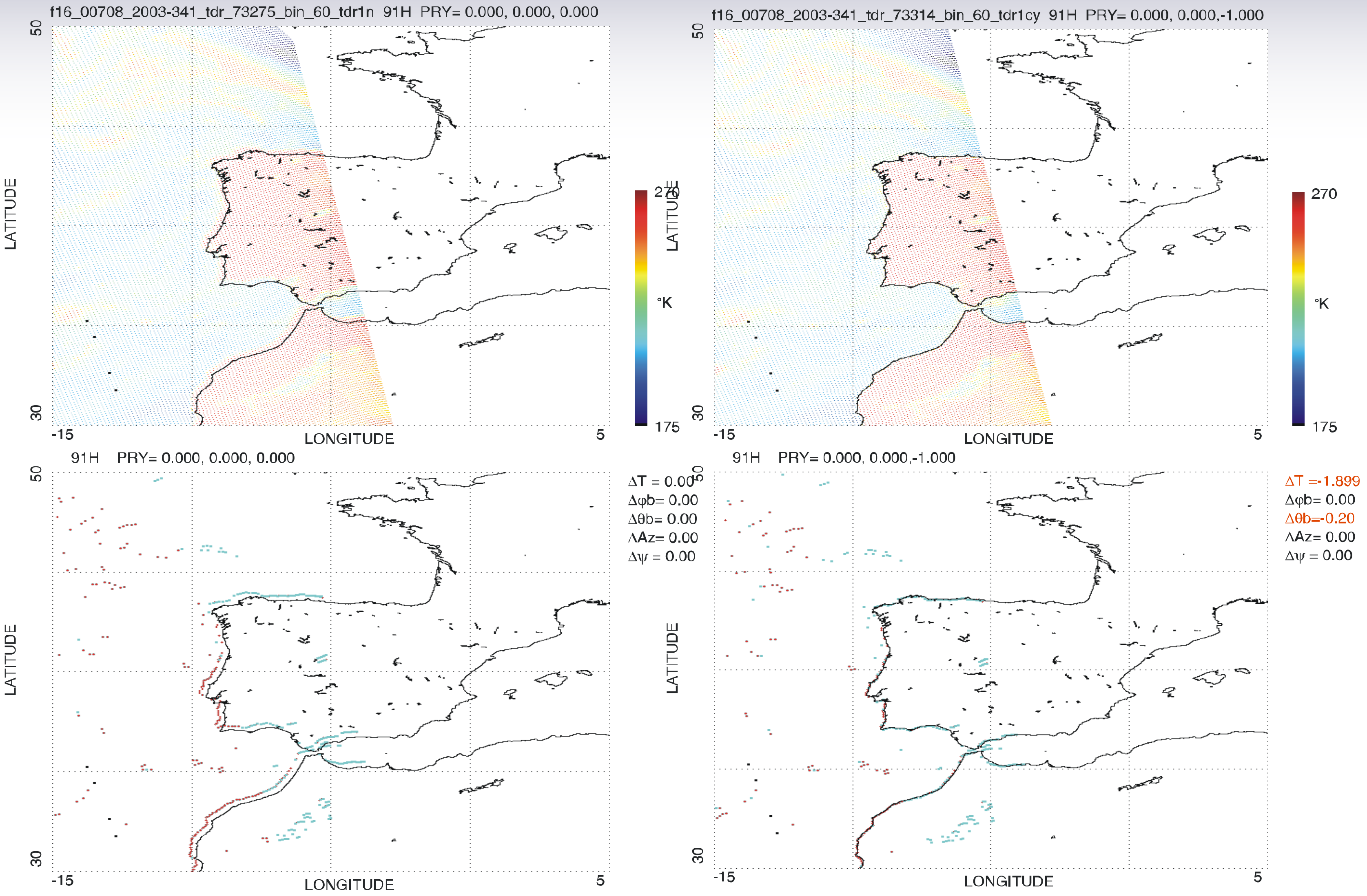

Geo-location Before and After Correction Ch. 18 Somalia/Yemen

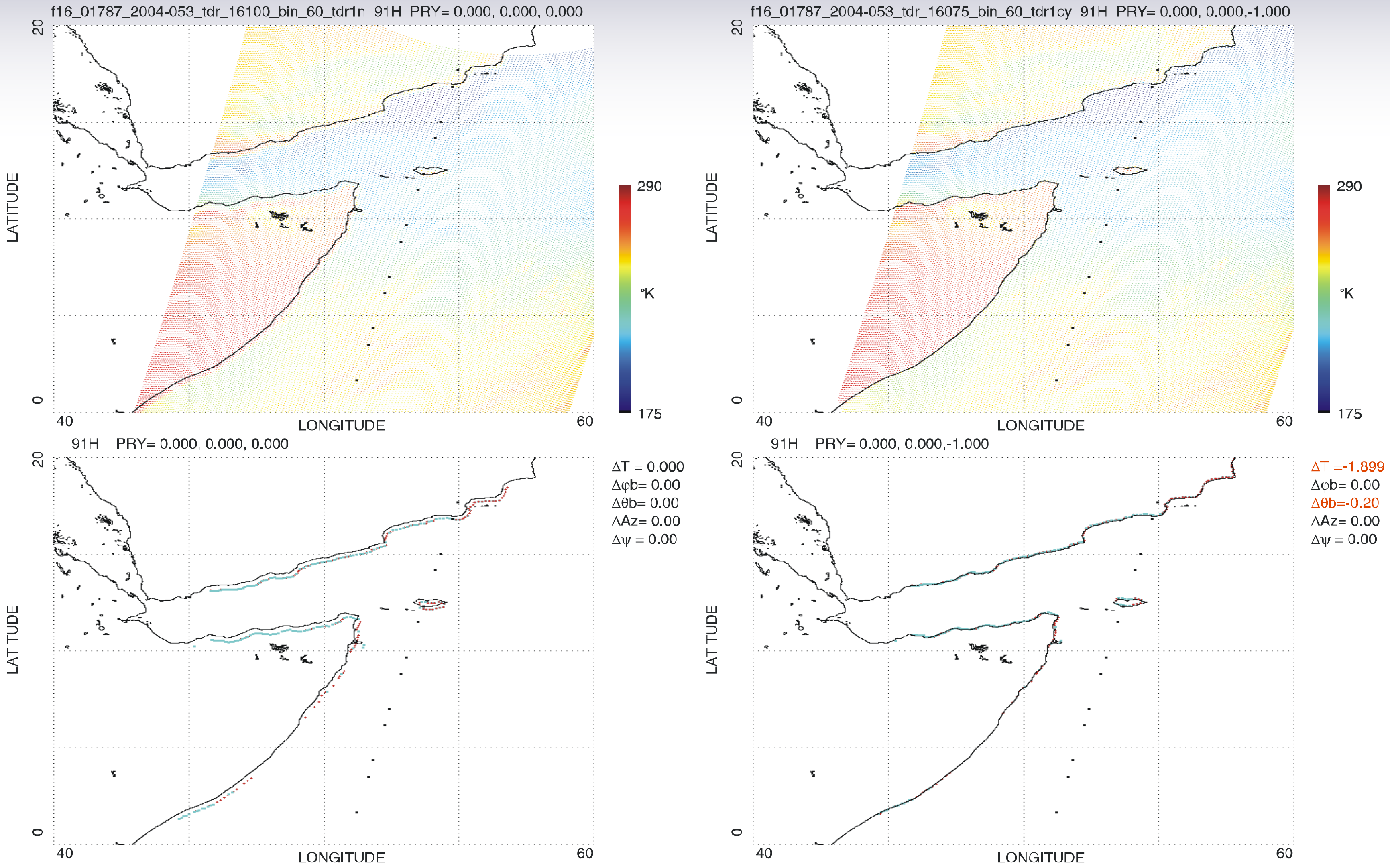

Geo-location Before and After Correction Ch. 18
Northern Australia / New Guinea

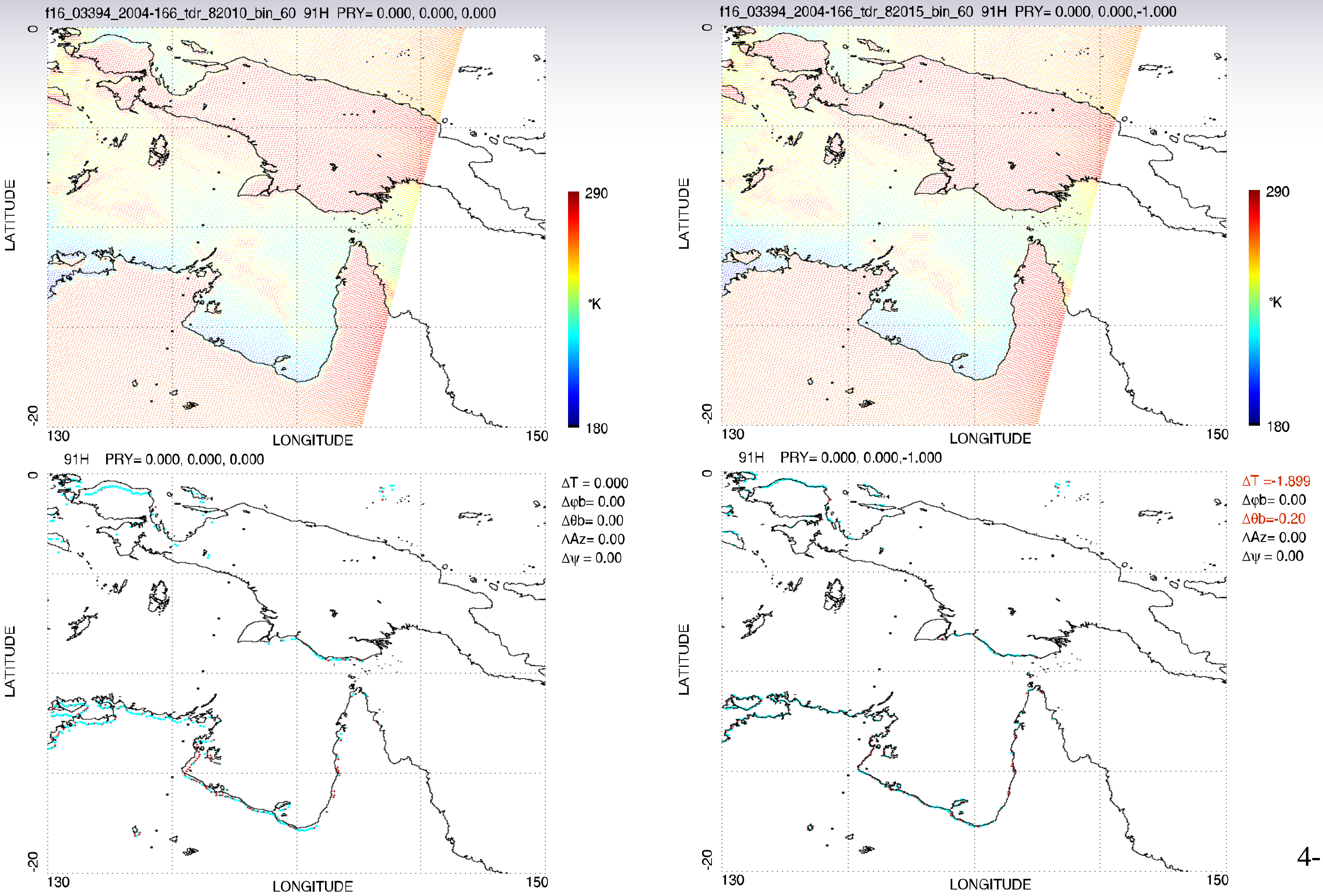

Geo-location Before and After Correction Ch. 15
Gulf Of Mexico/Yucatan

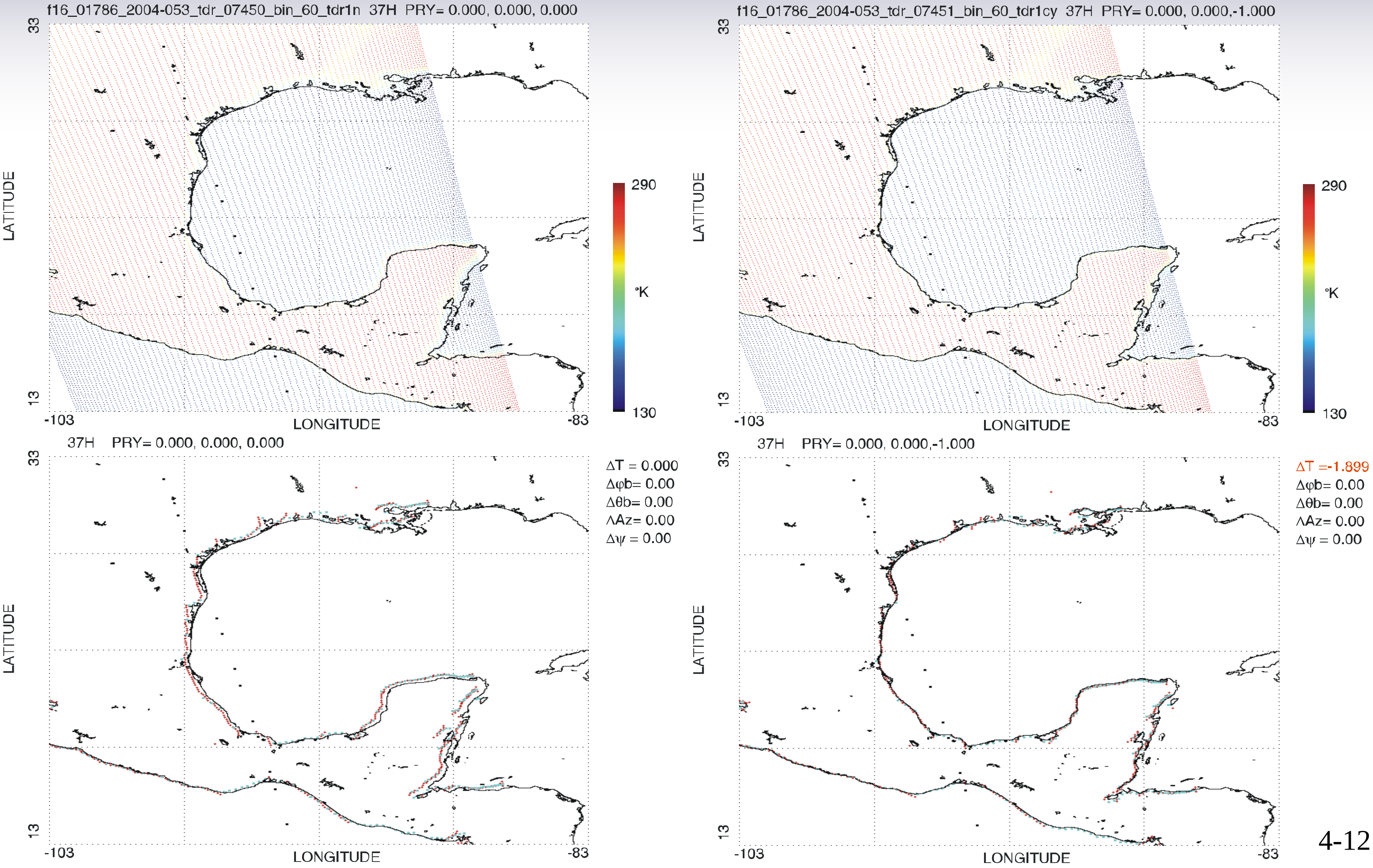

Geo-location Before and After Correction Ch. 15
Black Sea / Caspian Sea

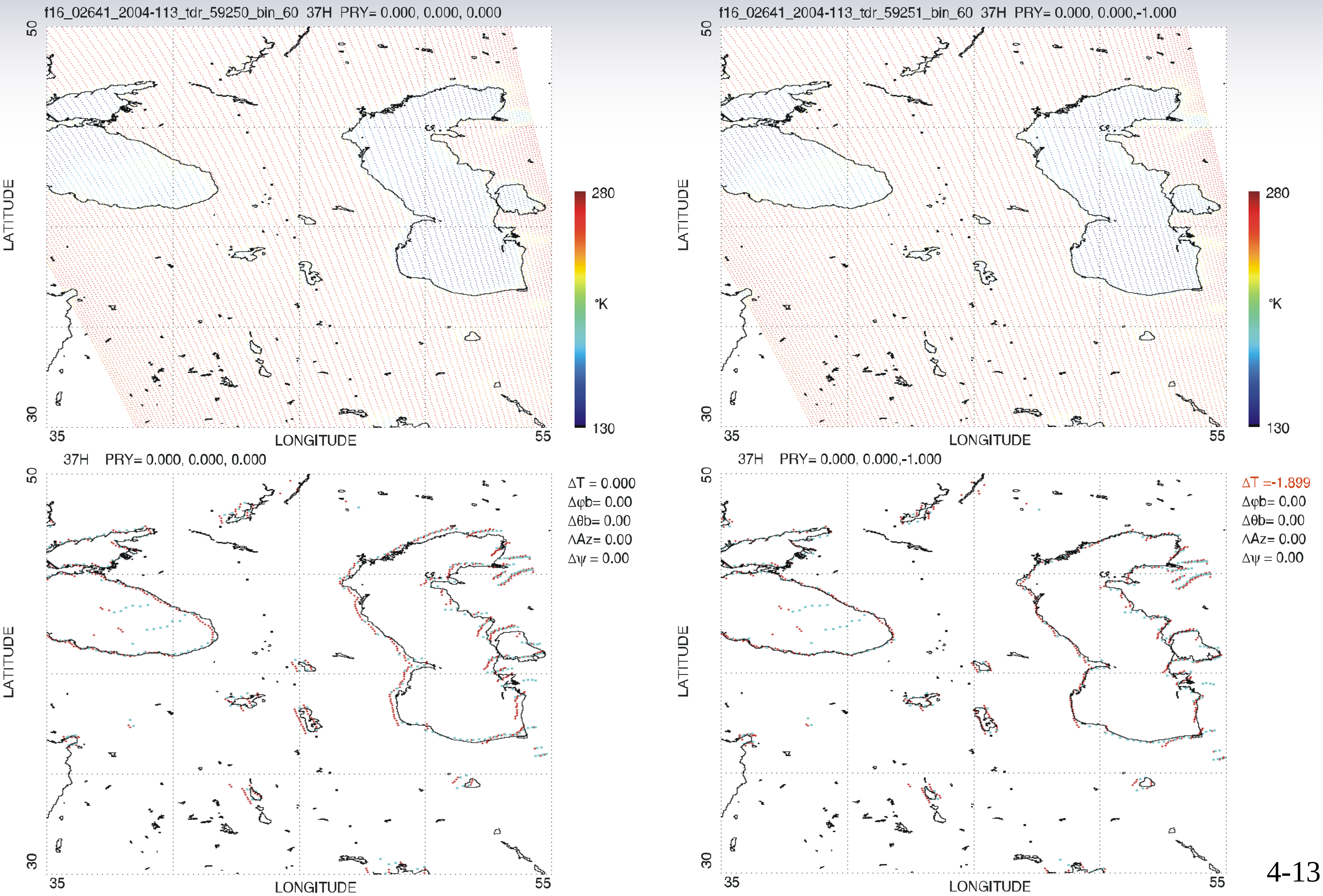

Geo-location Before and After Correction Ch. 15
Japan / Korea

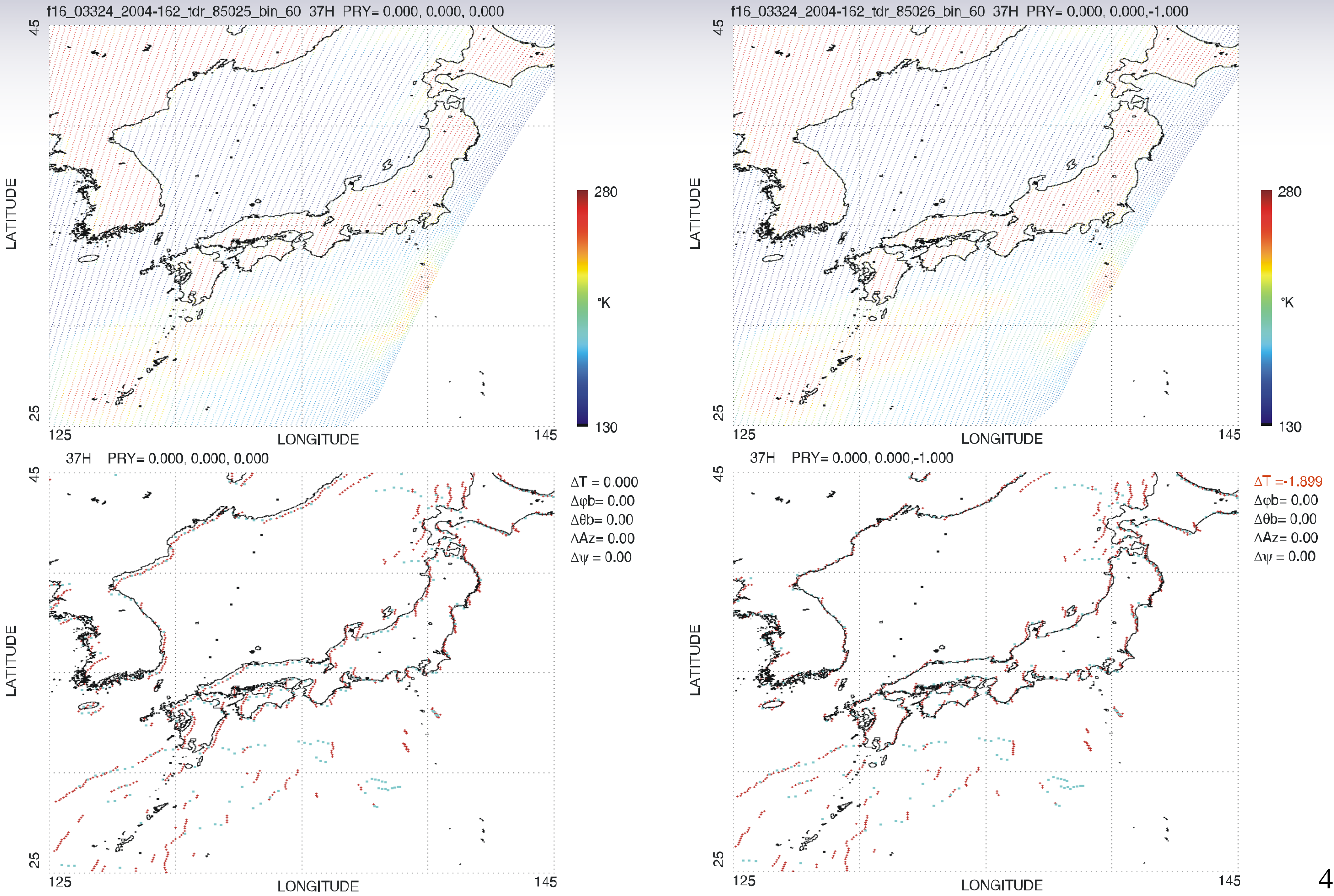

Geo-location Before and After Correction Ch. 12
Spain/N.Africa

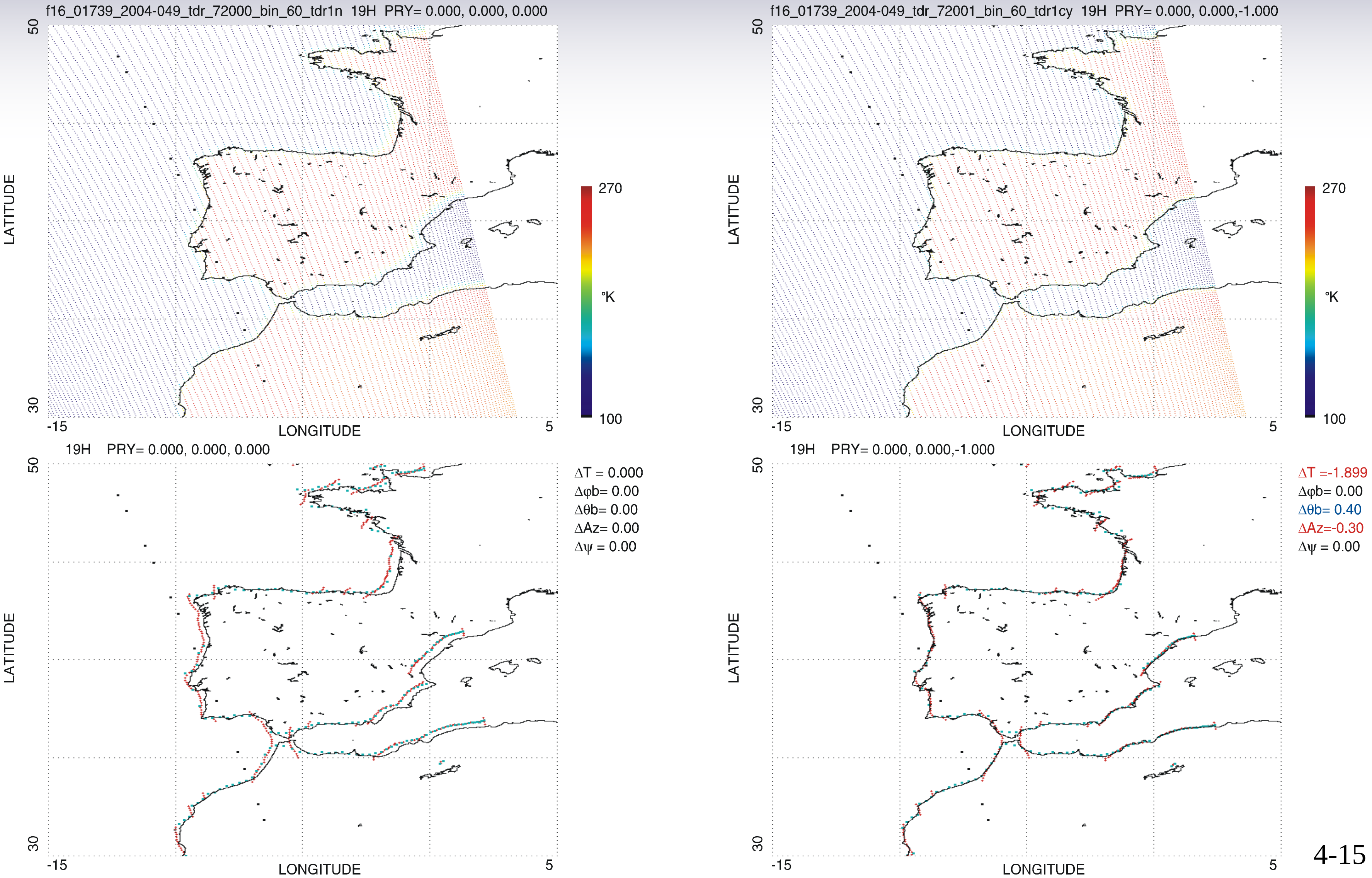

Geo-location Before and After Correction Ch. 12
Somalia / Yemen (Horn of Africa)

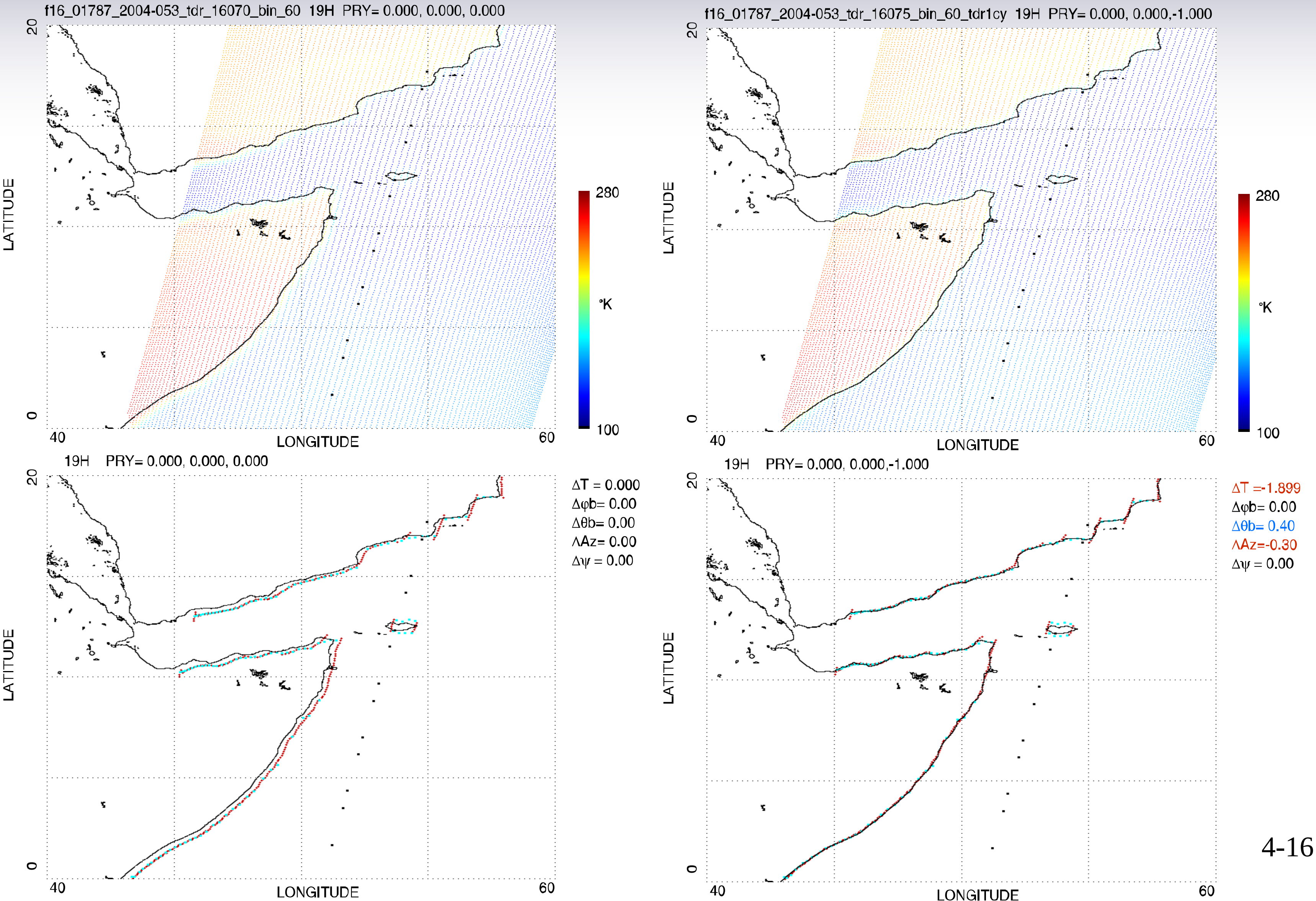

Geo-location Before and After Correction Ch. 12
Eastern Africa / Madagascar

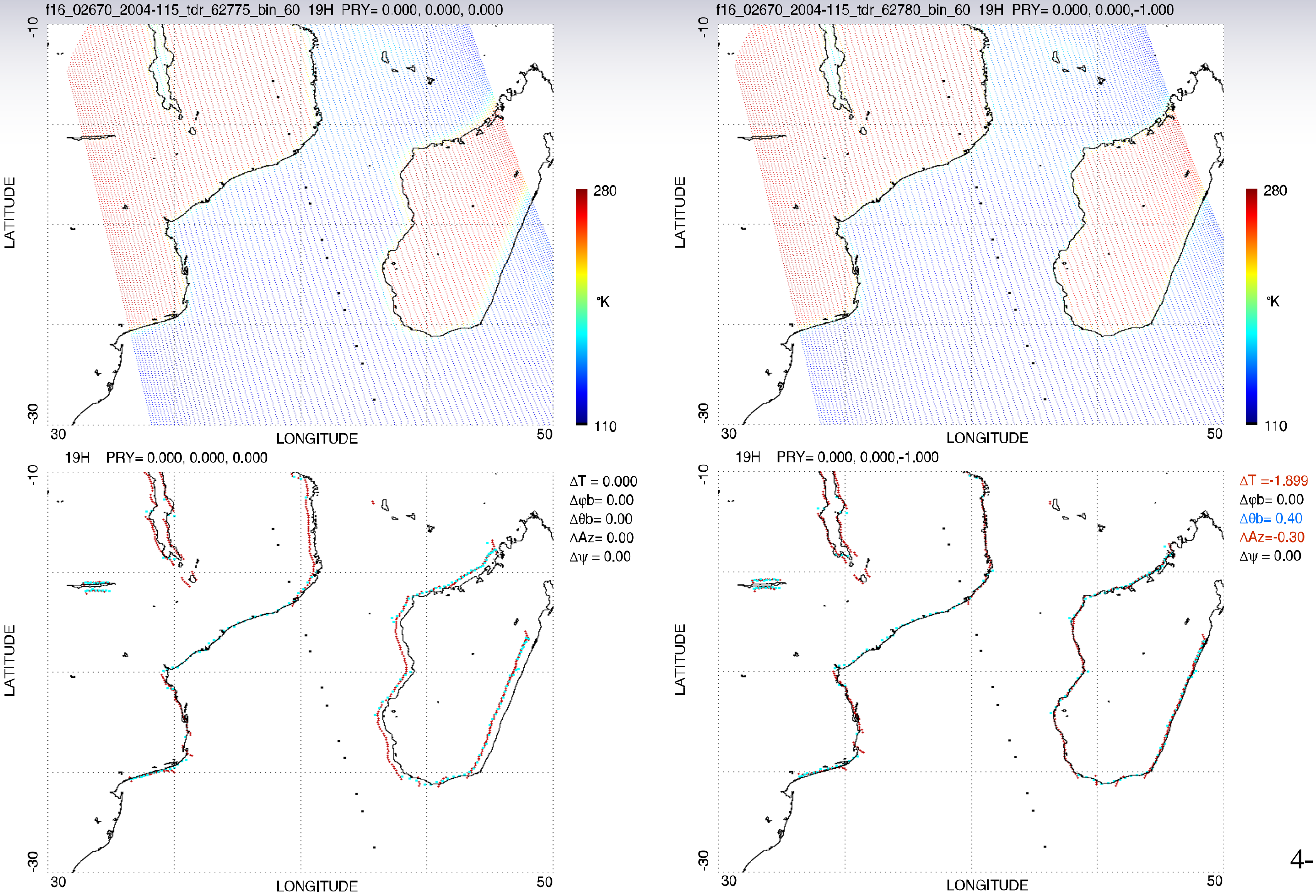

Geo-location Before and After Correction Ch. 12 India

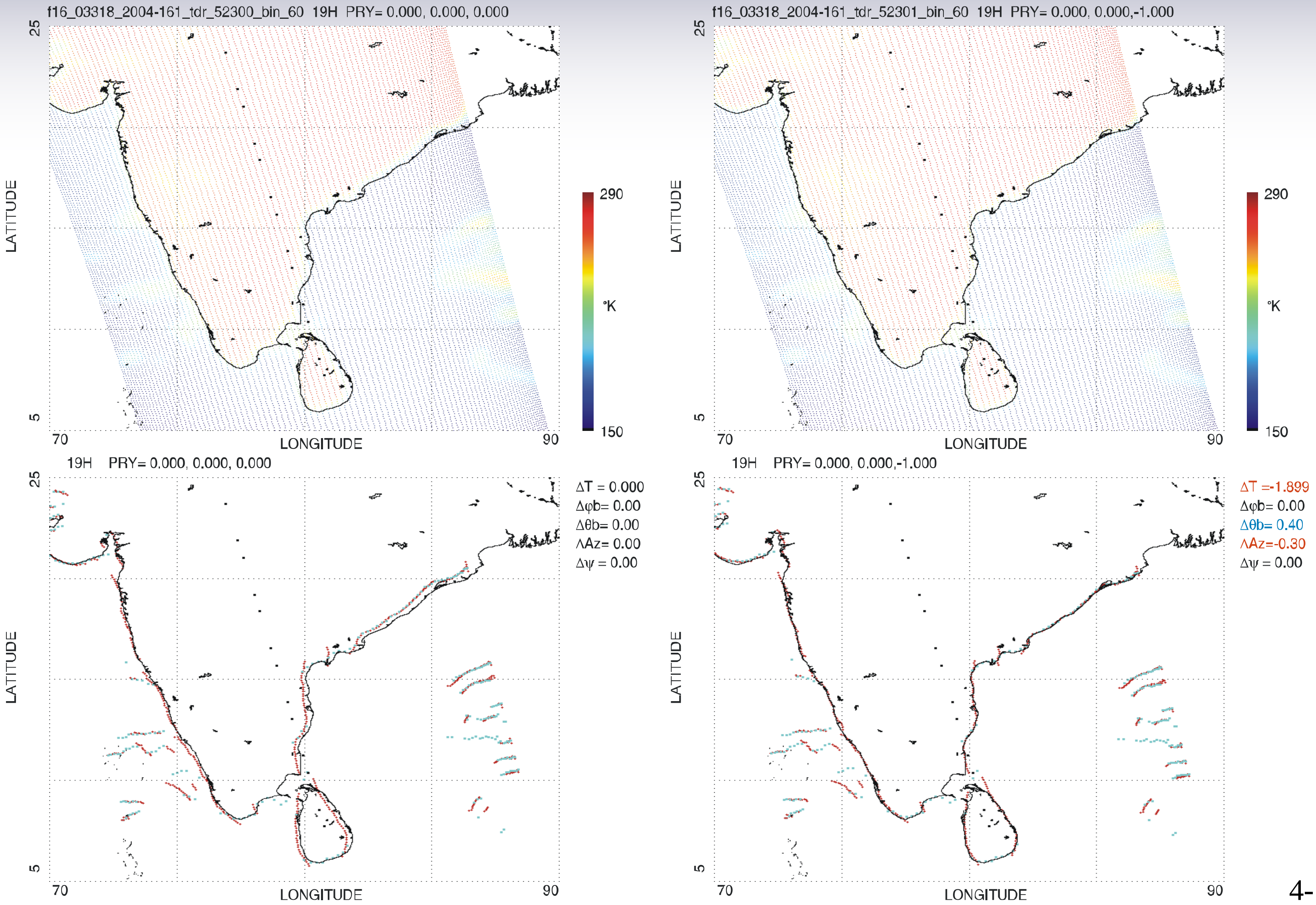

Geo-location Before and After Correction Ch. 1
Persian Gulf

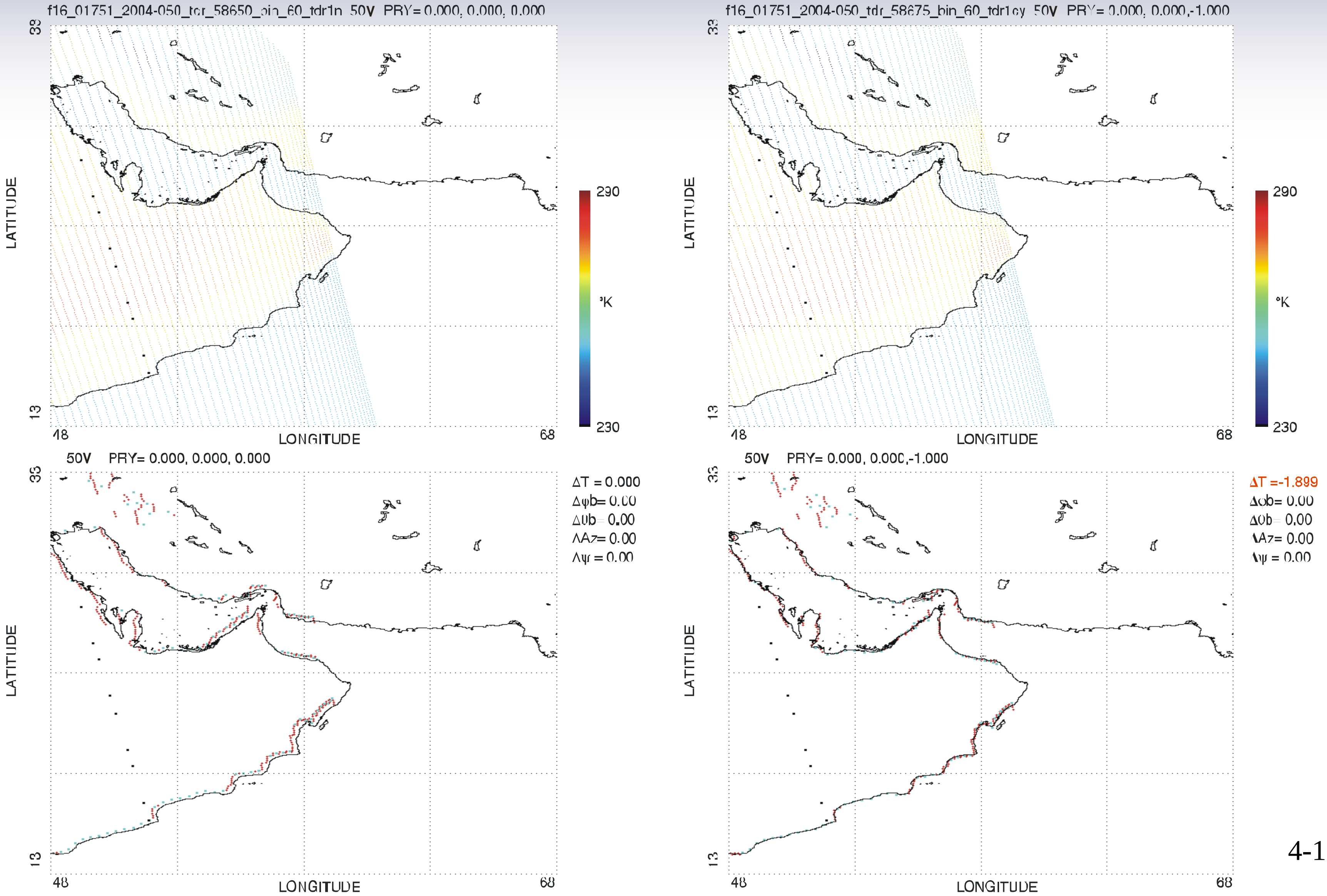

Geo-location Before and After Correction Ch. 1
Eastern Africa / Madagascar

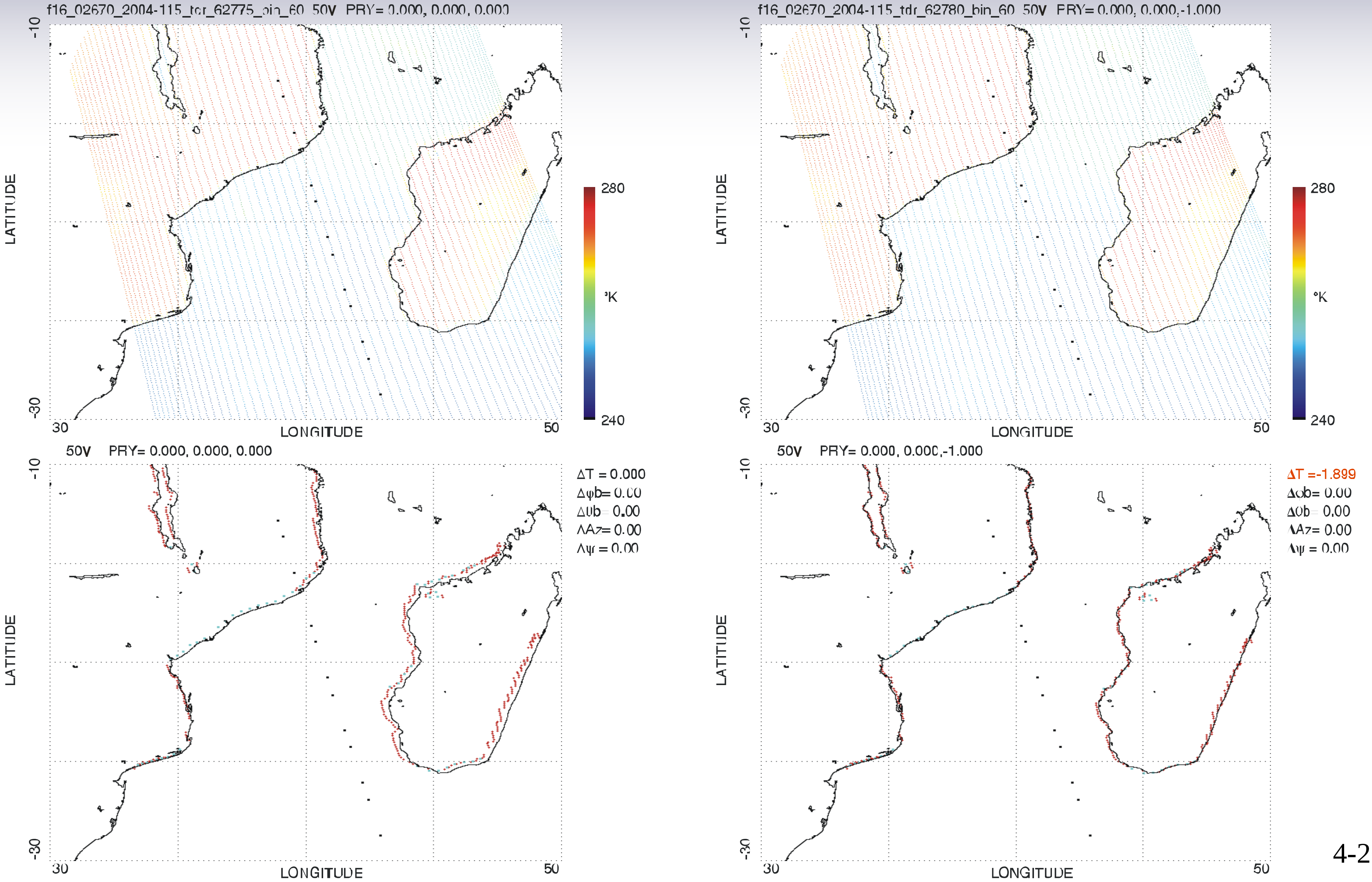

Geo-location Before and After Correction Ch. 1
Northern Australia / New Guinea

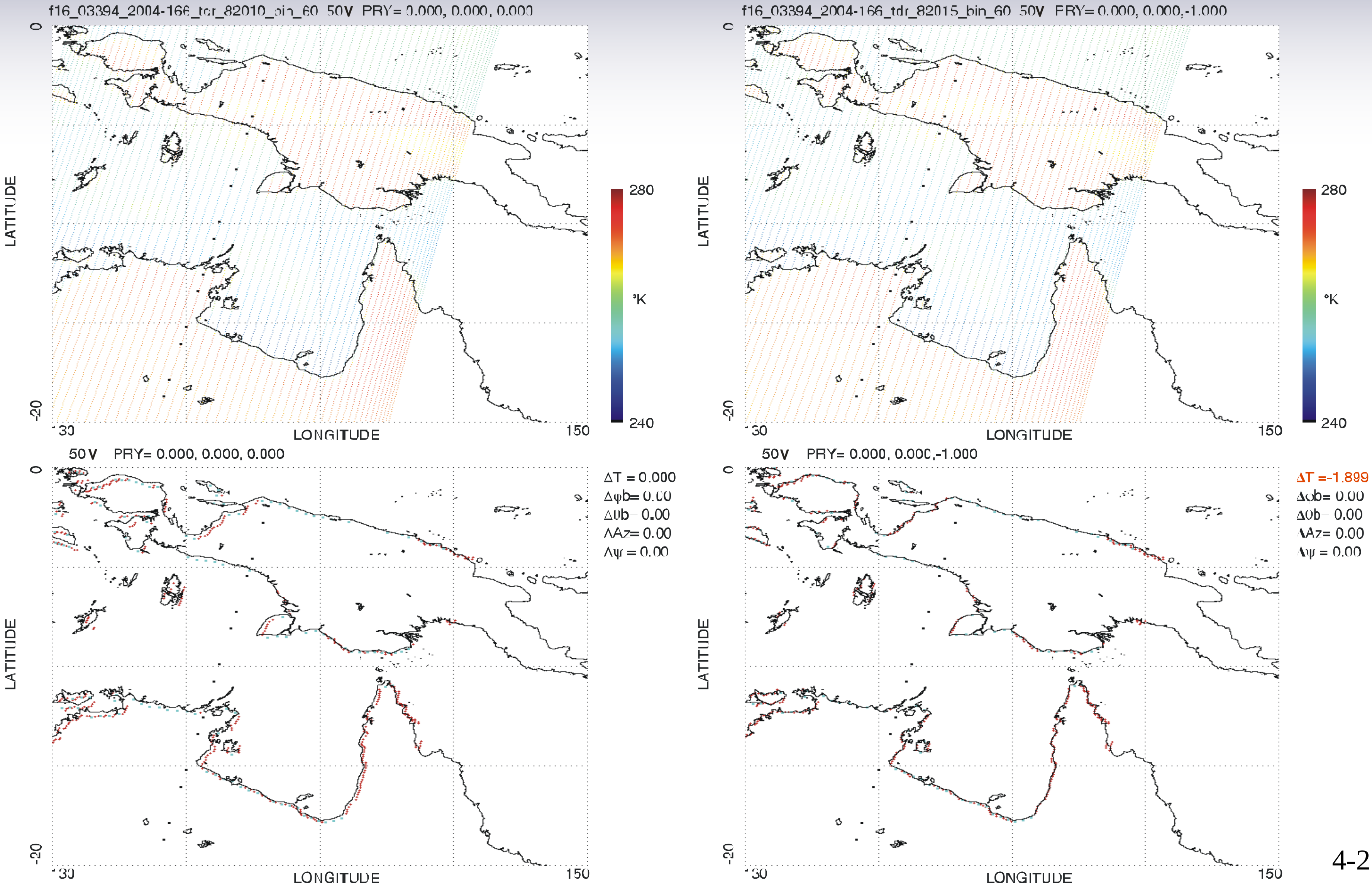

Geo-location Before and After Correction Ch. 8
South America

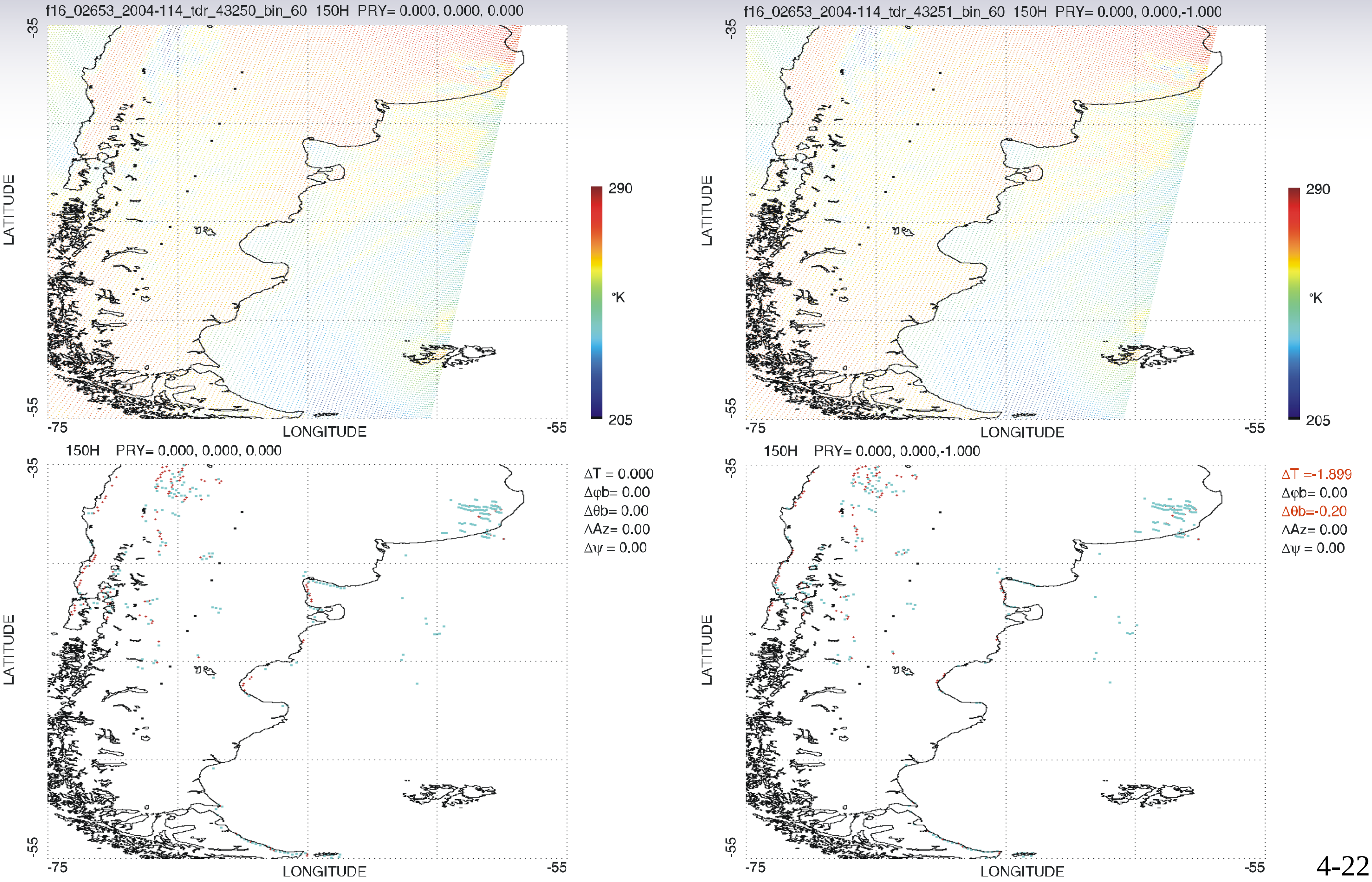

Geo-location Before and After Correction Ch. 8 South America

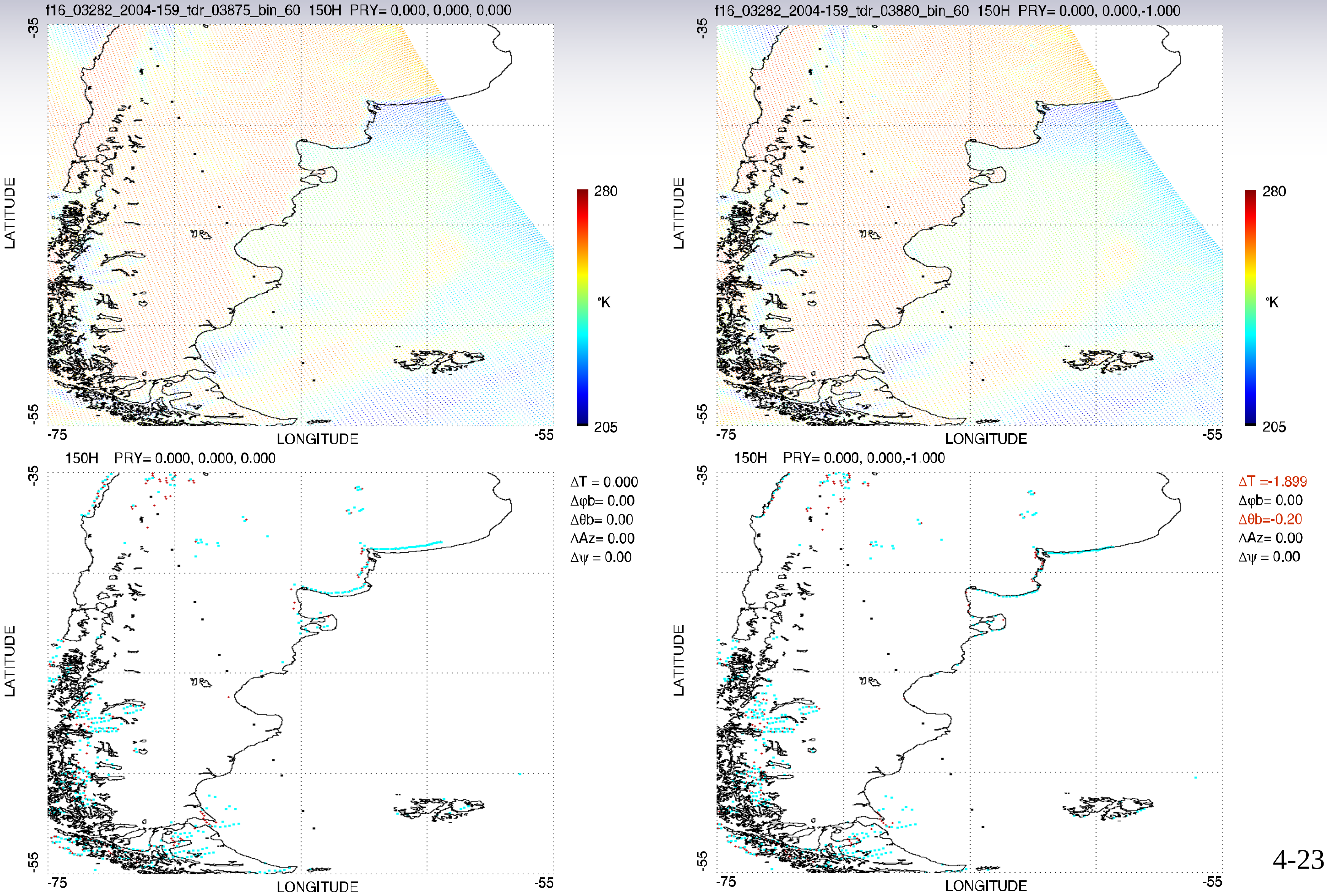

4.5 Long Term Performance

Excellent Long Term Geo-location Stability

4.5 SSMIS Ch. 18

2003 October 2004 October

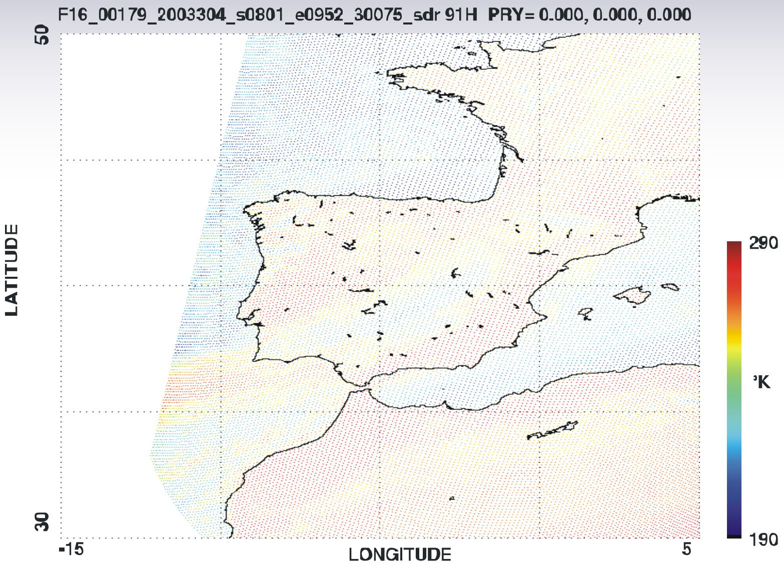

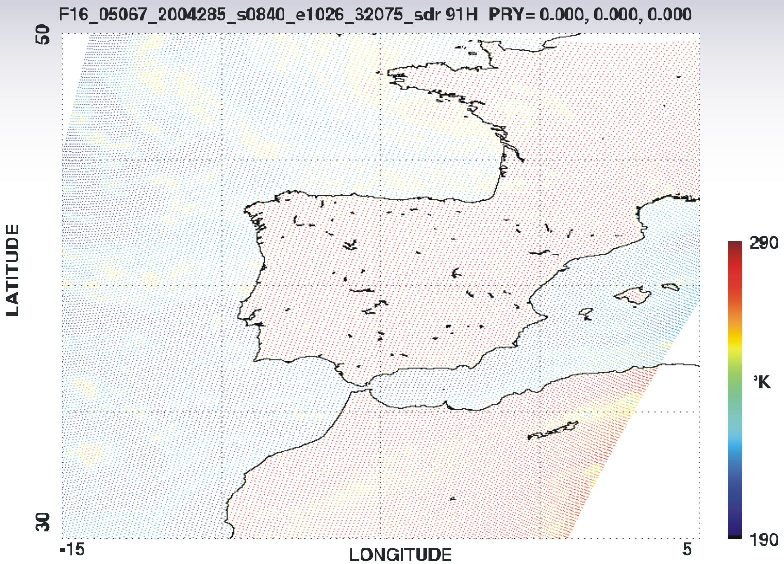

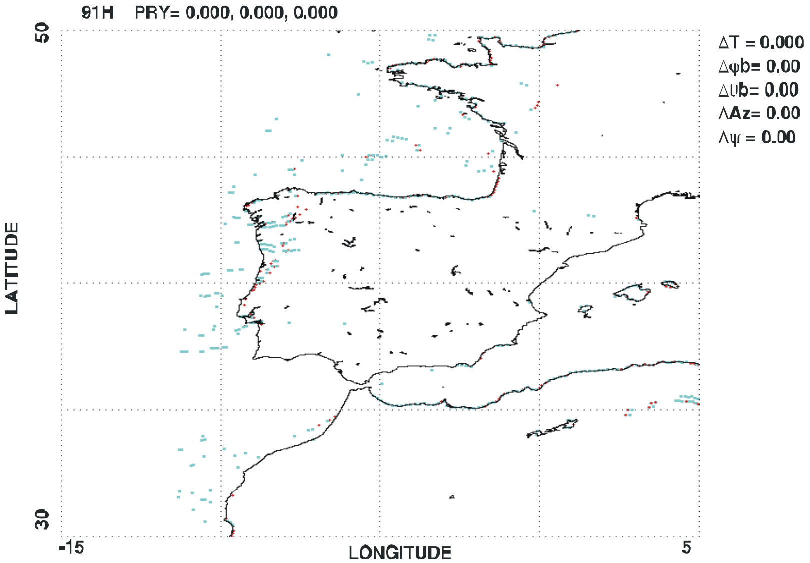

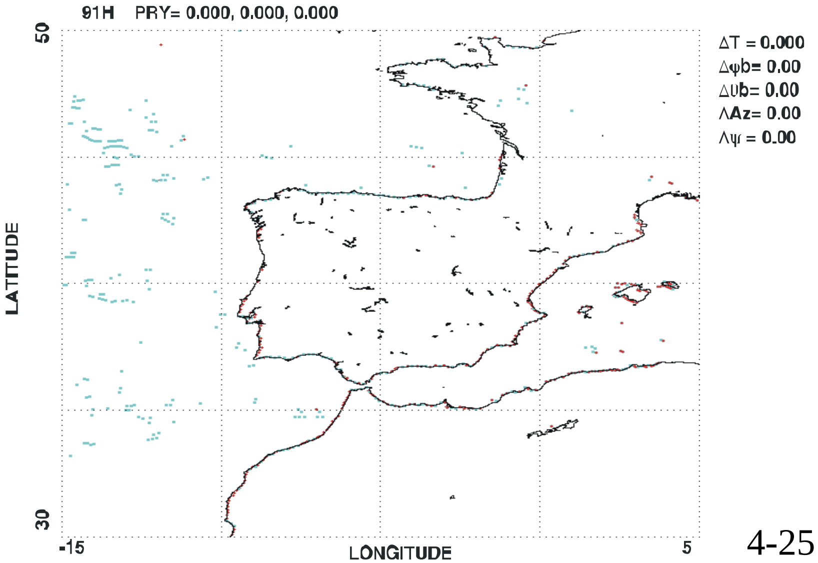

4.5 SSMIS Ch. 18

2003 October

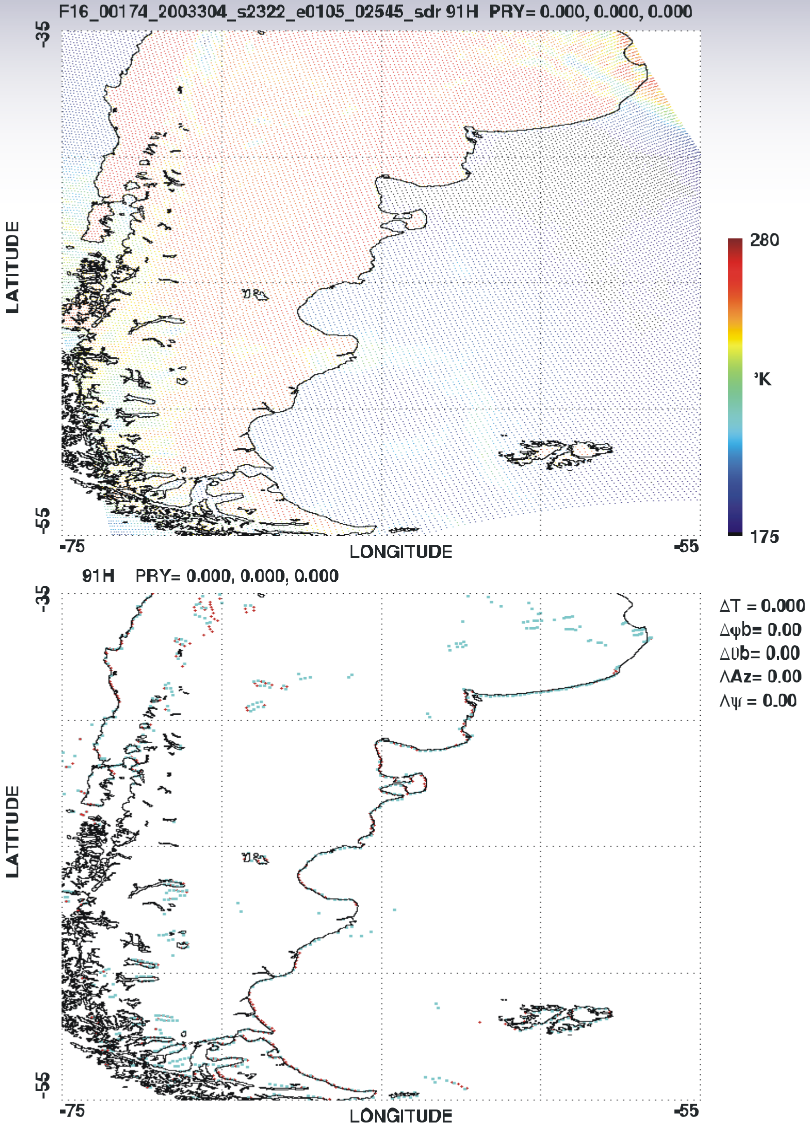

2004 October

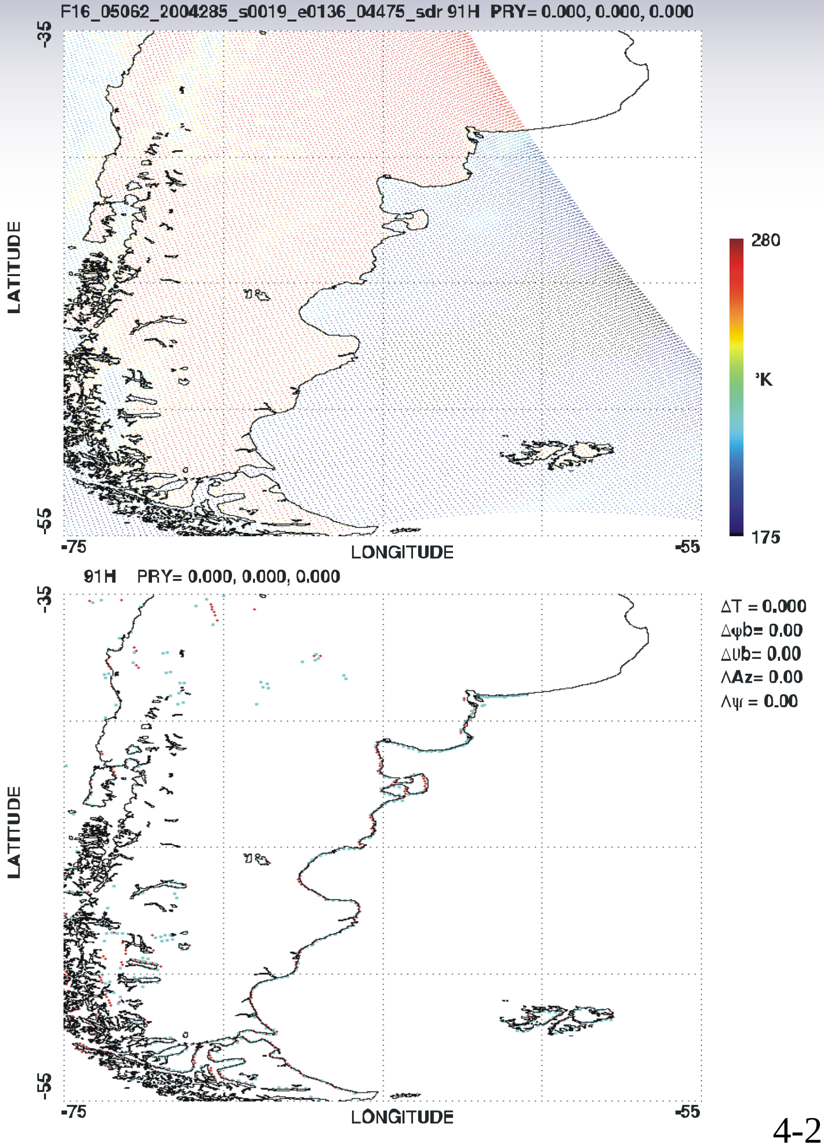

4.5 SSMIS Ch. 15

2004 October

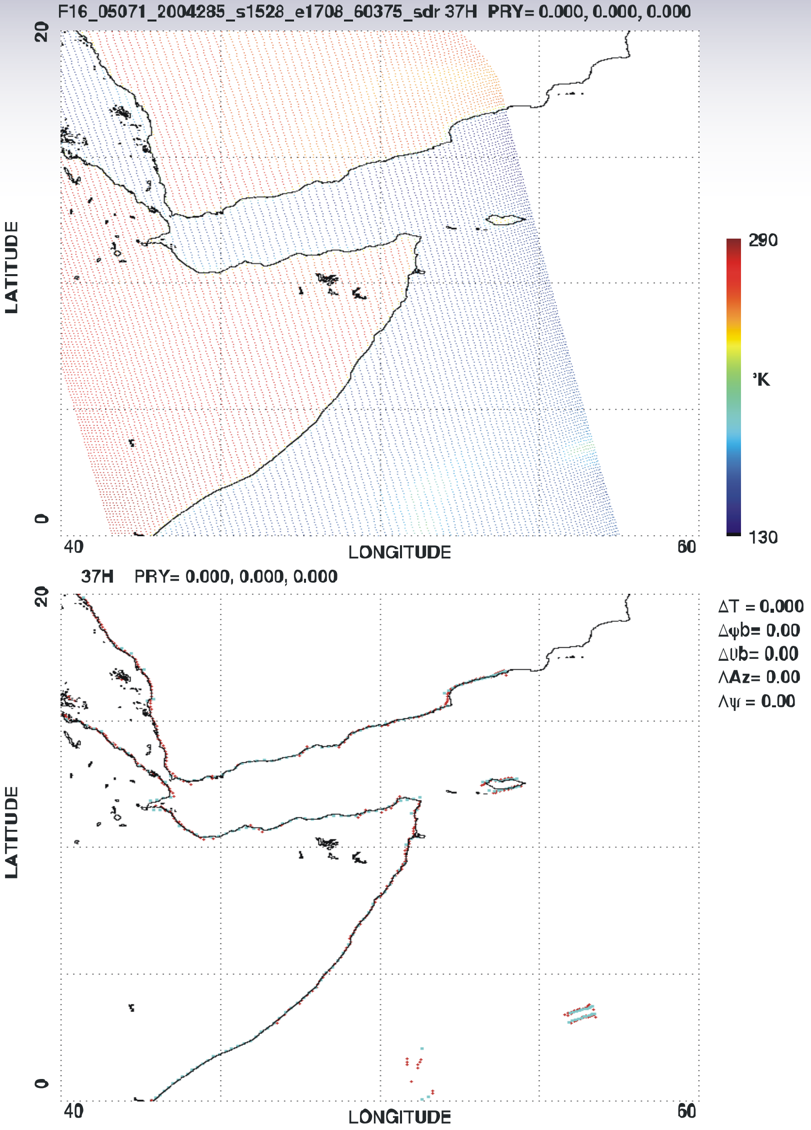

2005 October

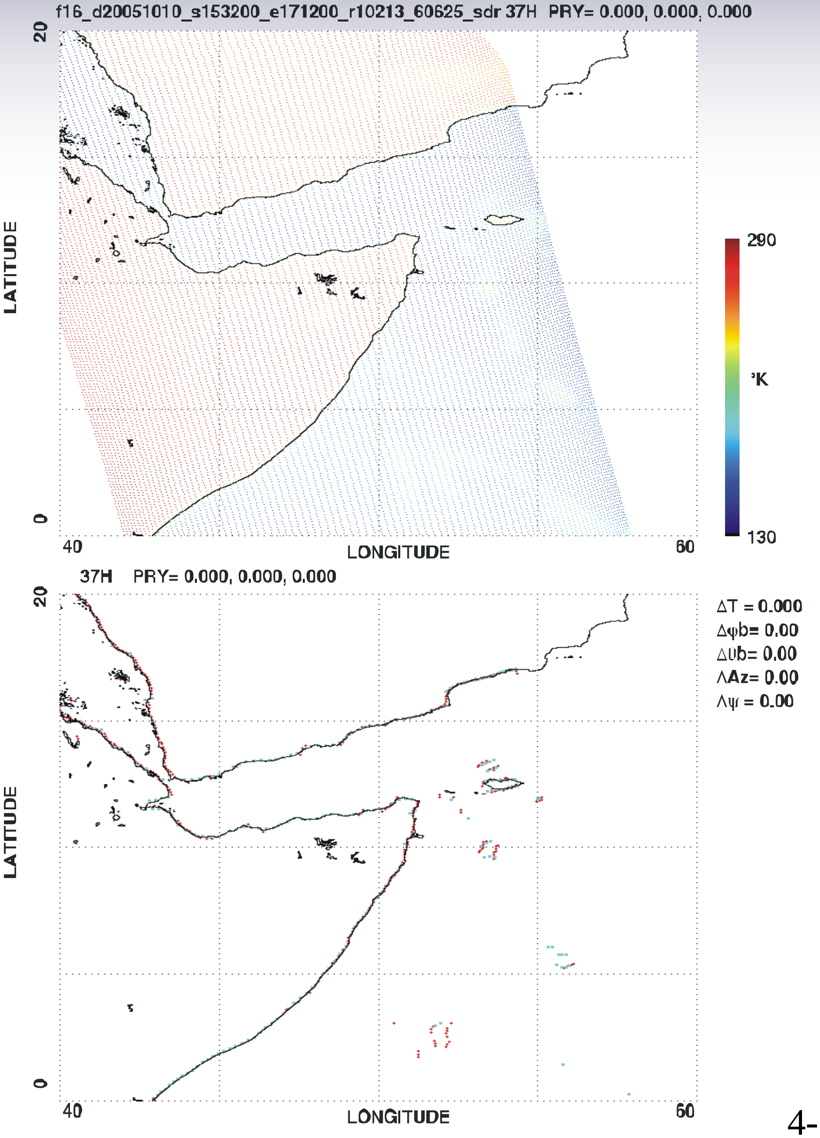

4.5 SSMIS Ch. 12

2004 October

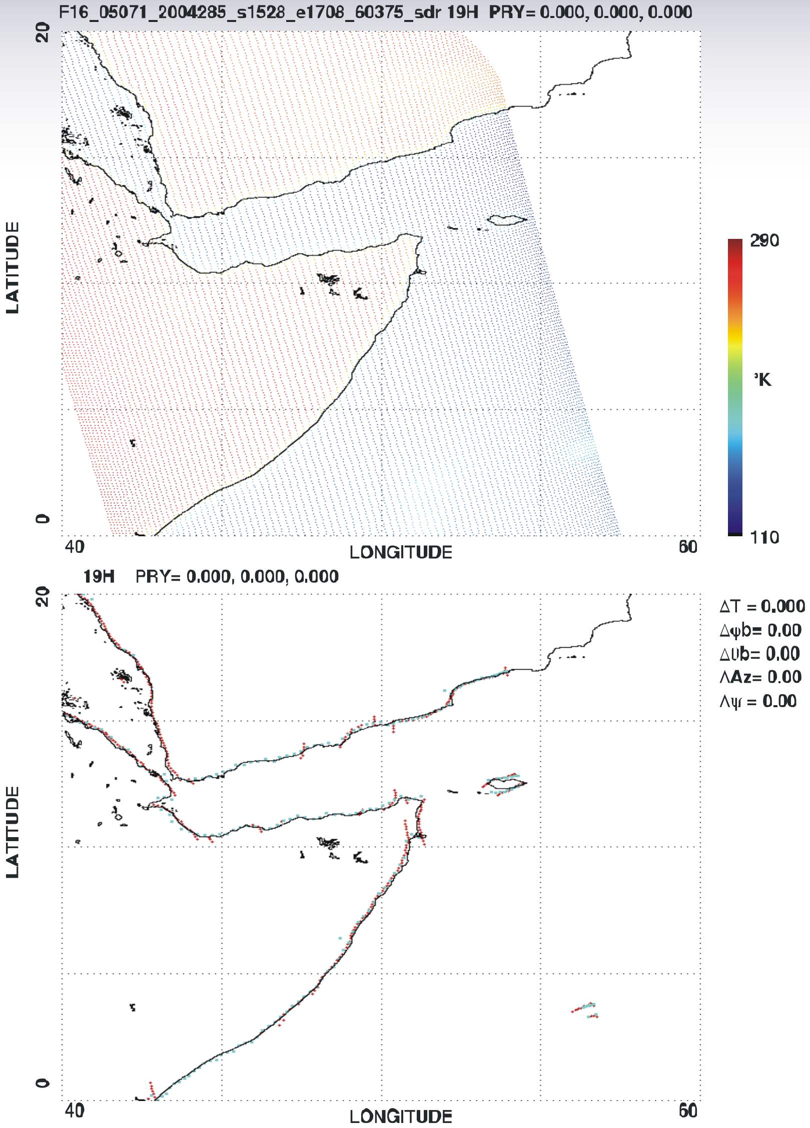

2005 October

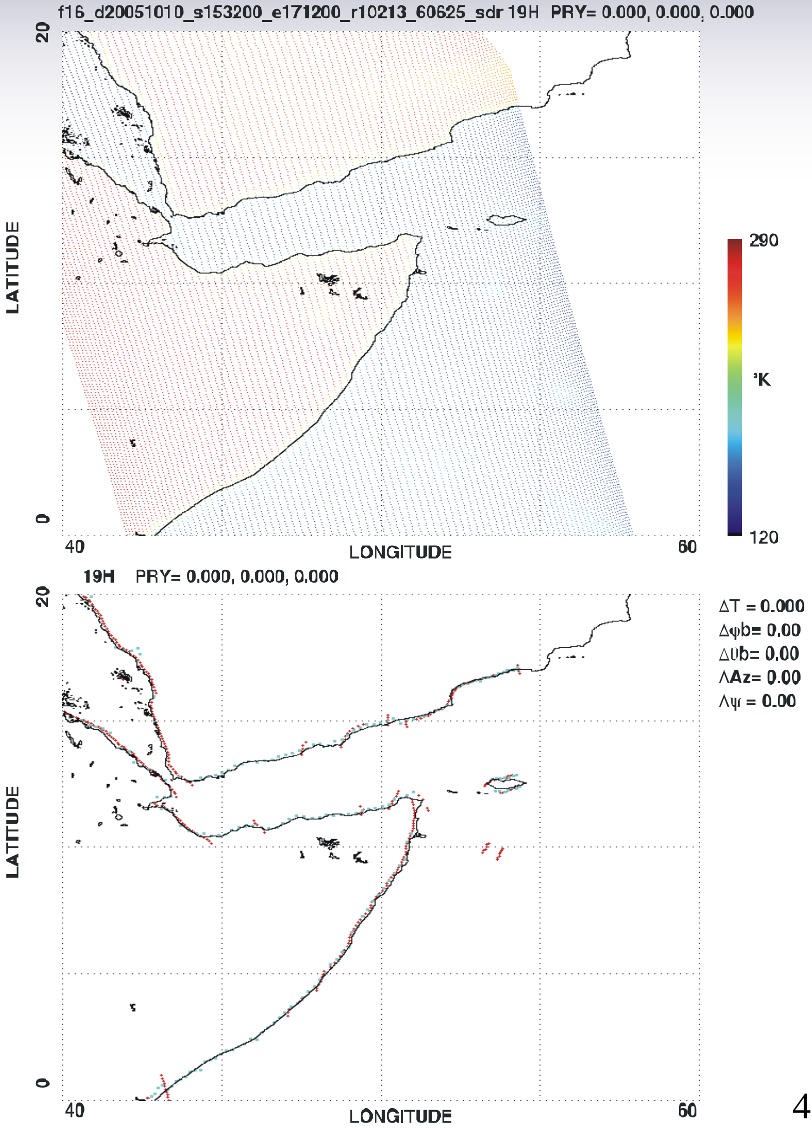

4.6 Re-sampling Chs 12-14 to Grid of Chs.15-16

- Backus – Gilbert Methodology
  - Size and spacing of interpolation kernel (3X3, 5X5, 7X7)
  - Trade off between noise, resolution, complexity and CPU
- Selection
  - 3 X 3 nearest neighbors on 25 km grid
  - Simple, fast, good interpolated main beam characteristics
  - No increase in pixel NEDT
- Results
  - Antenna beam comparisons (Ch. 12)
  - Imagery : Geo-located with Offsets and Re-sampled without Offsets

4.6 Ch. 12 Antenna Pattern Cuts for Pixel 45
(Center of Scan)

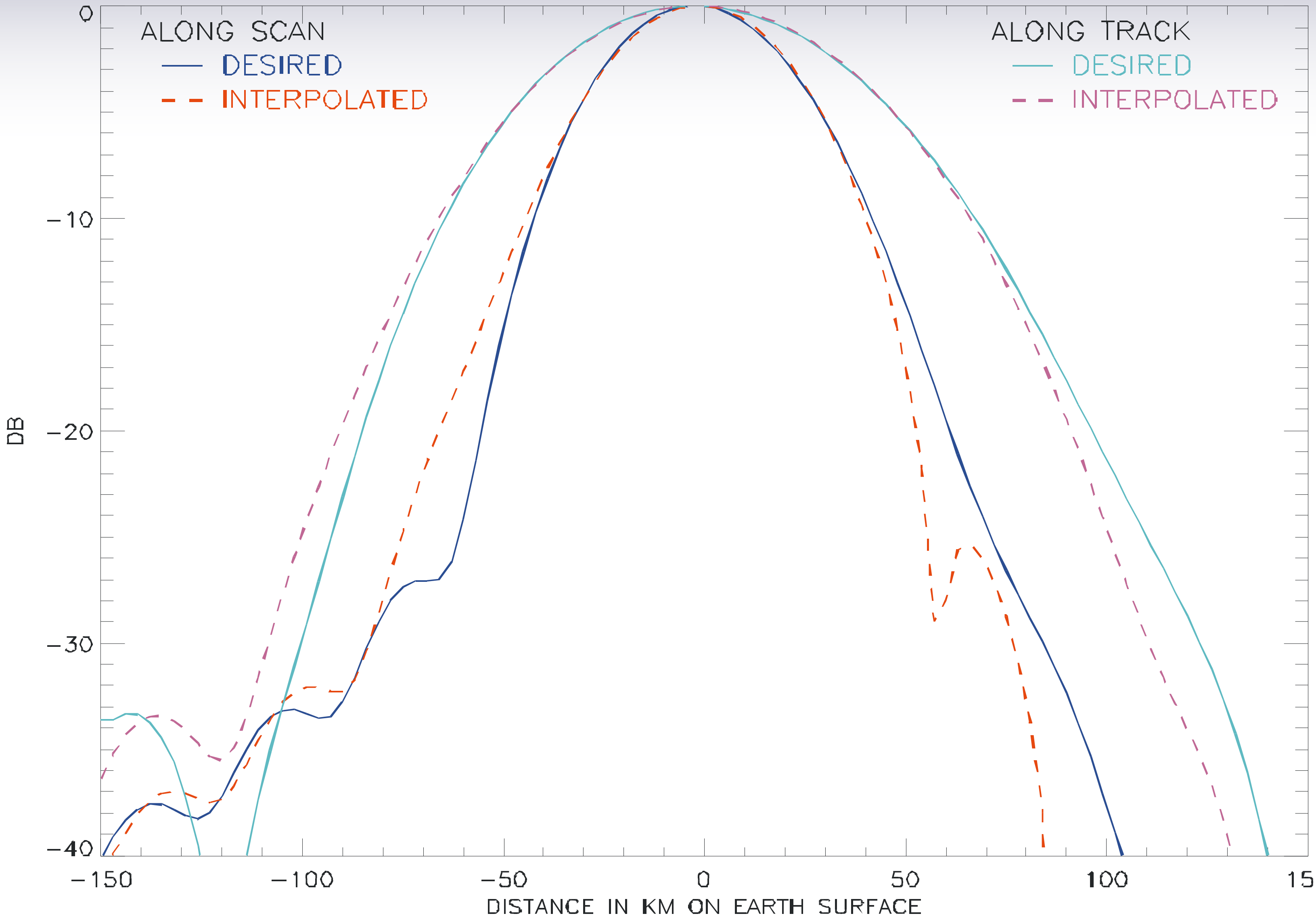

4.6 Ch. 12 Antenna Pattern Cuts for Pixel 85 (Near End of Scan)

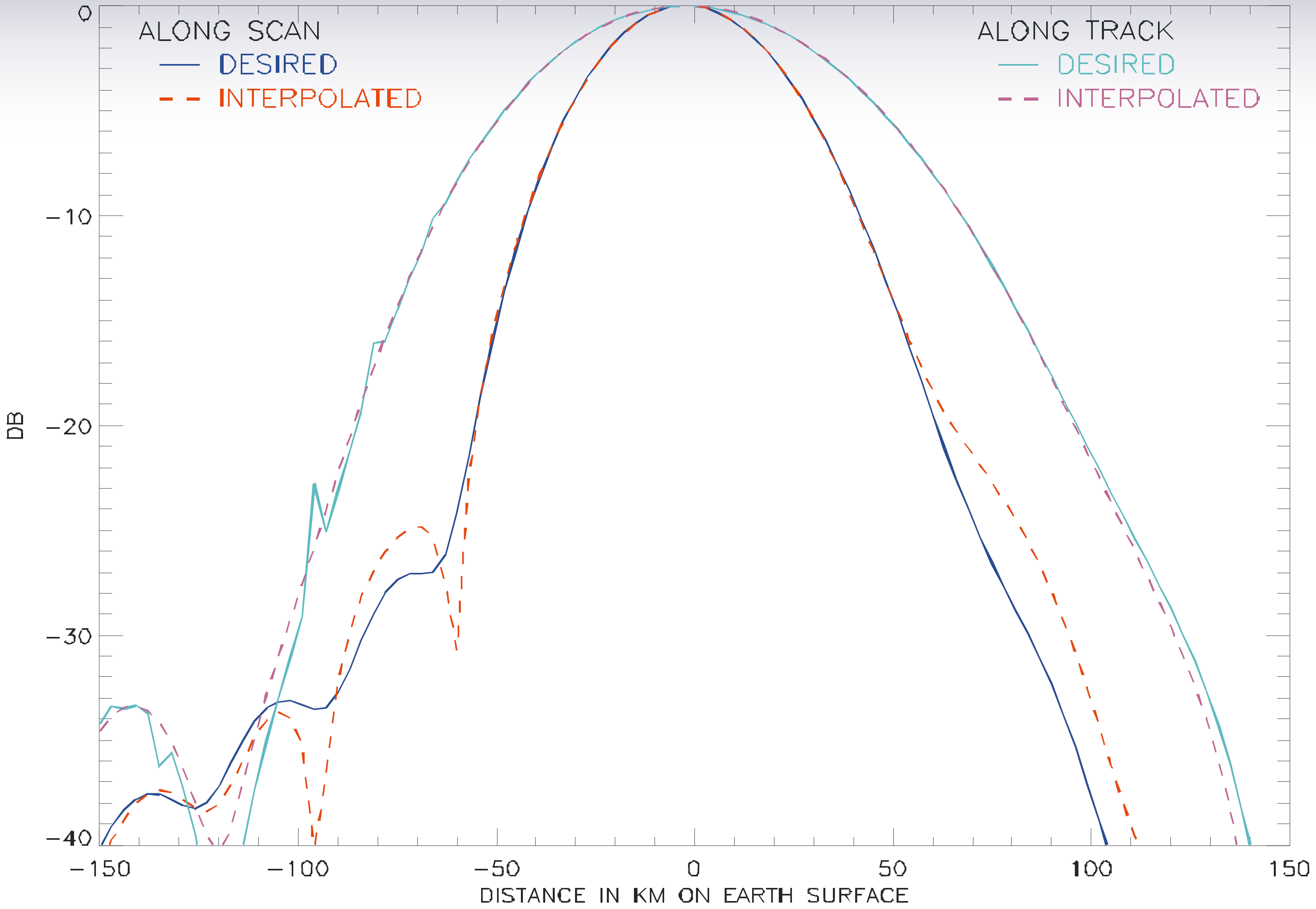

4.6 Before and After Re-sampling Ch.12

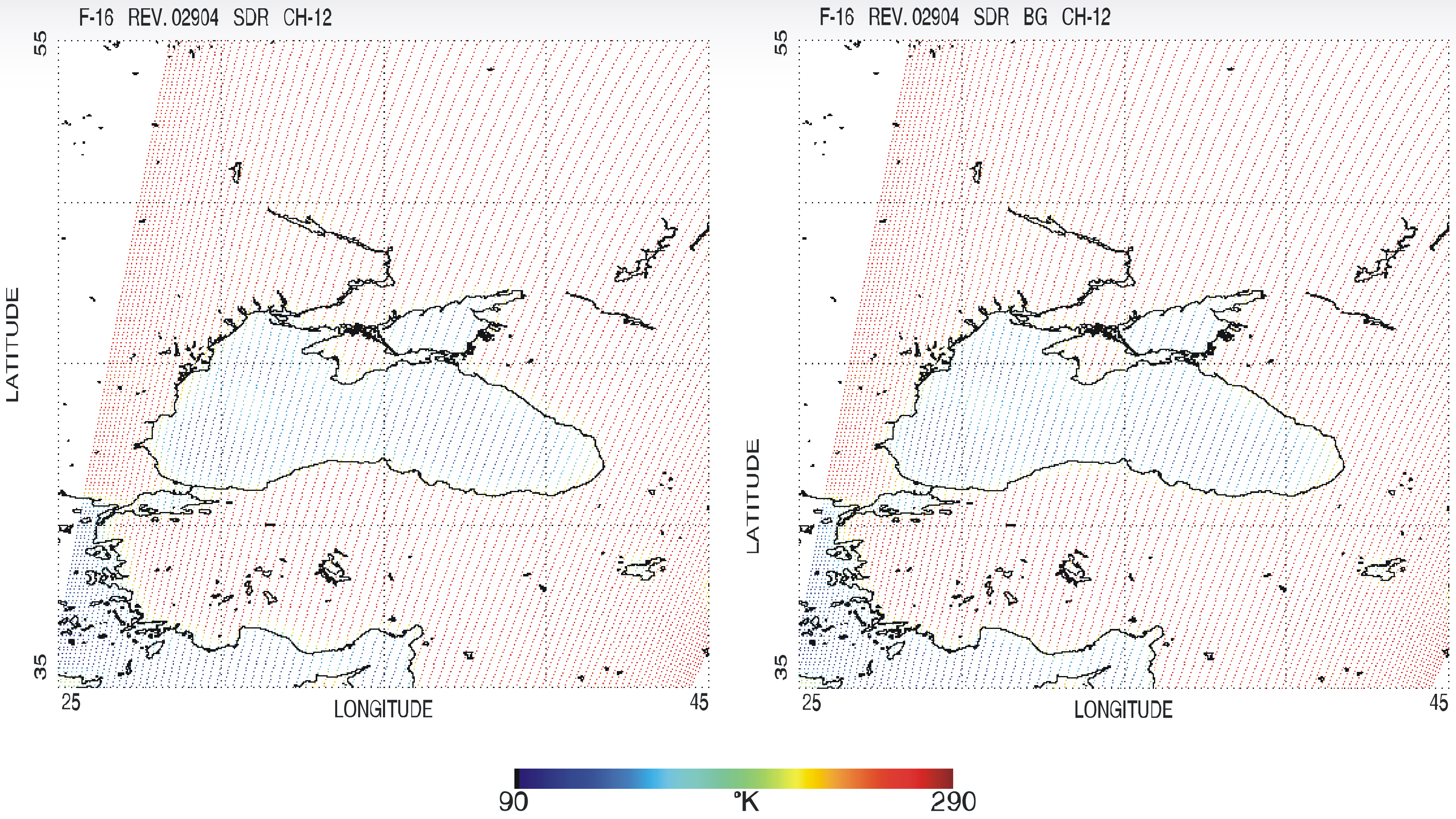

4.6 Before and After Re-sampling Ch.12

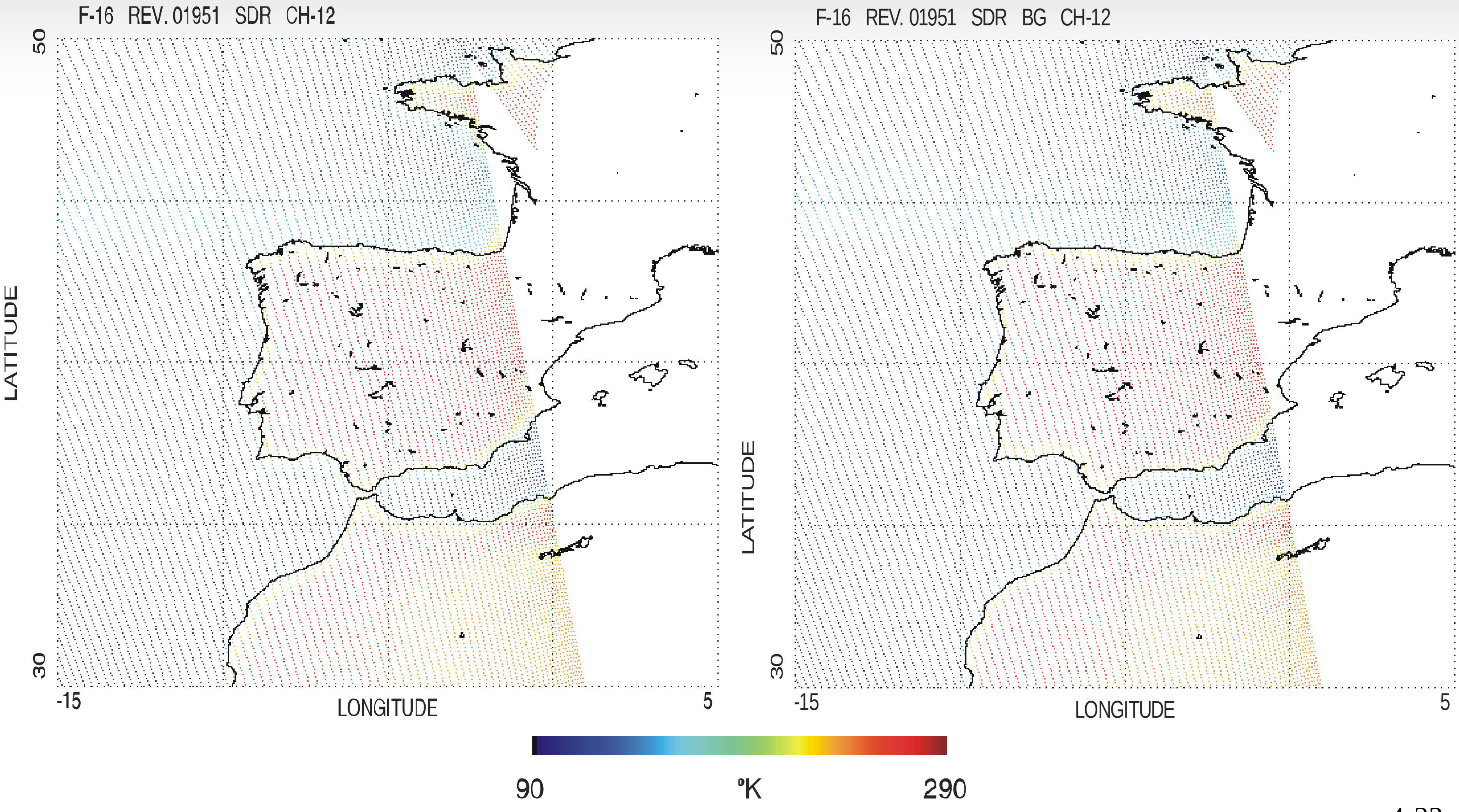

4.6 Before and After Re-sampling Ch.12

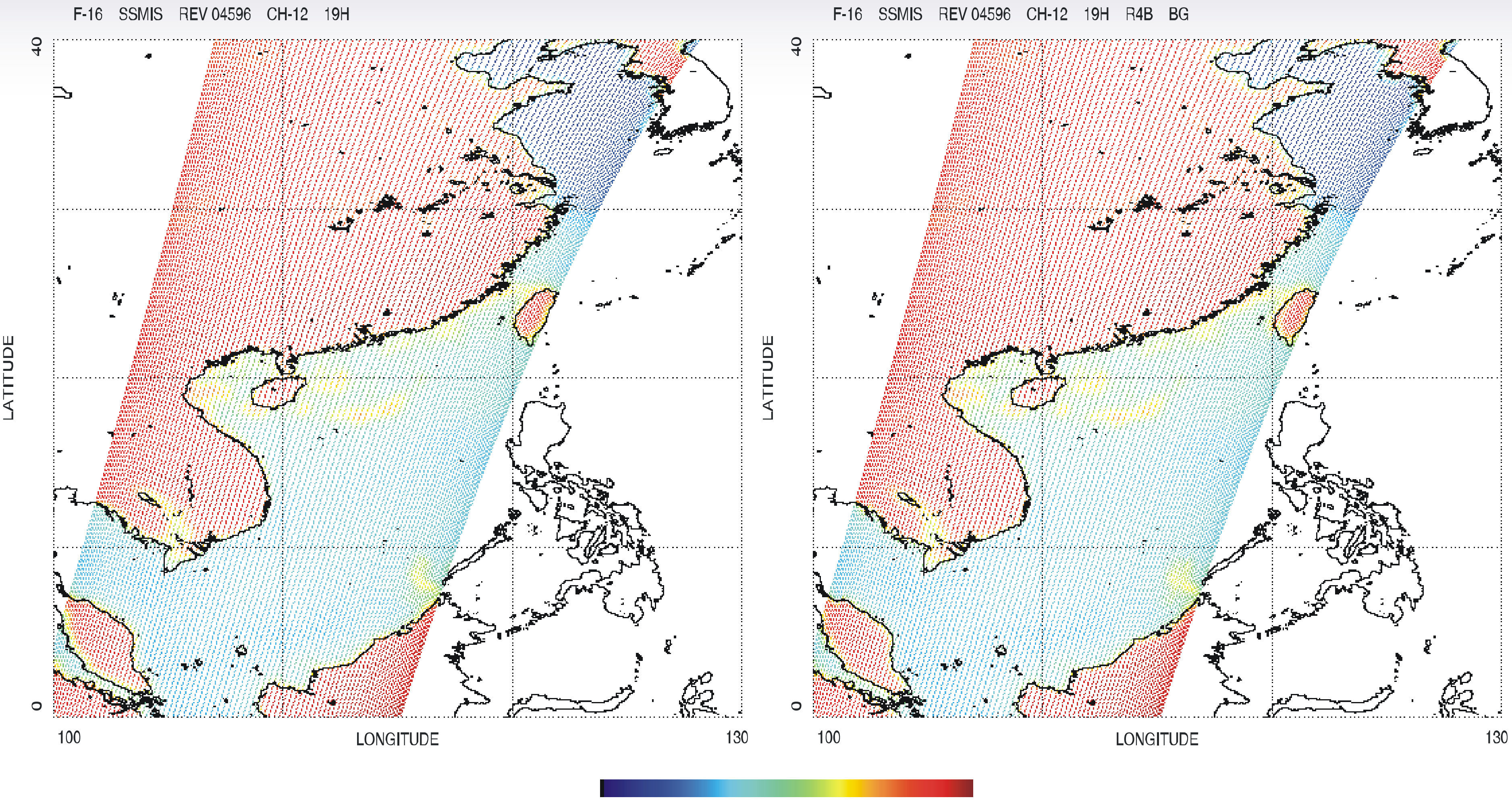

F16 SSMIS Calibration/Validation Final Report

Section 5.0 Scan /Sampling Non-Uniformity

Gene Poe, Enzo Uliana, Beverly Gardiner and David Kunkee

THE AEROSPACE CORPORATION

5.0 Scan / Sampling Non-Uniformity

5.1 Objectives

- Quantify potential Field-of-View (FOV) intrusions into active scene scan sector

  (SSM/I Instruments had FOV Intrusion at the end of scan due to Glare Suppression System–B)

- Determine uniformity of along-scan pixel to pixel sampling

- If needed, derive correction algorithm to remove or mitigate impact on SDR/EDR products and swath-width

5.2 Approach

- **Analyze ascending/descending monthly mean Ocean TDRs for fixed scene sample for channels sensing surface emissions. No surface restrictions for other channels (e.g. 19-24).**

- **Resolve source of scan non-uniformity**

- **Successful approach for SSM/I Instruments**

- **Coordinate with Early-Orbit analyses/results**

5.3 Observed Scan Non-Uniformity

(January – December 2004)

Chs. 12-14 (19v/h,22v)

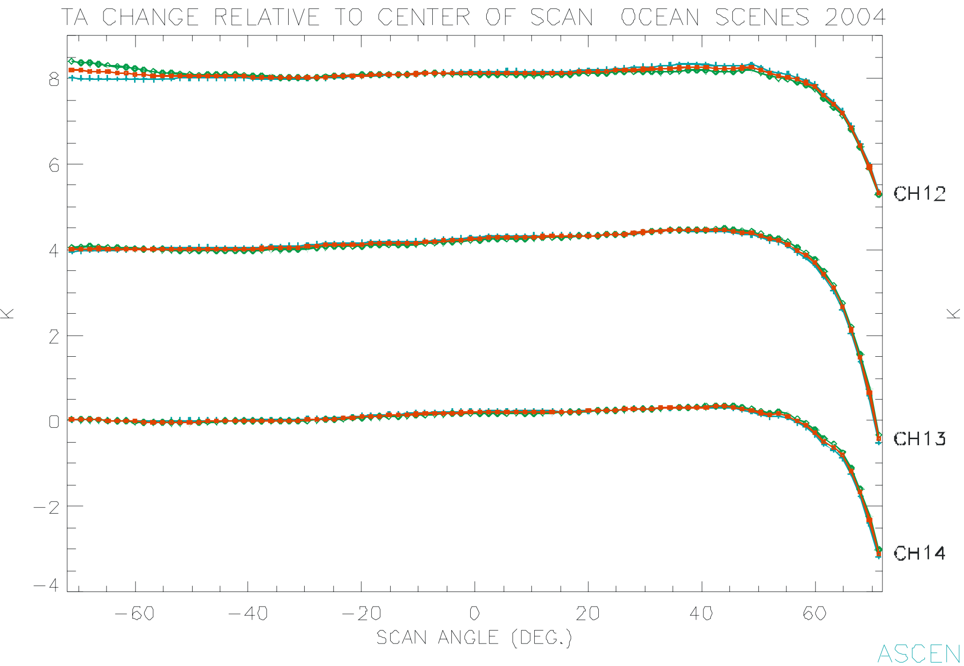

Chs. 1-5 (LAS)

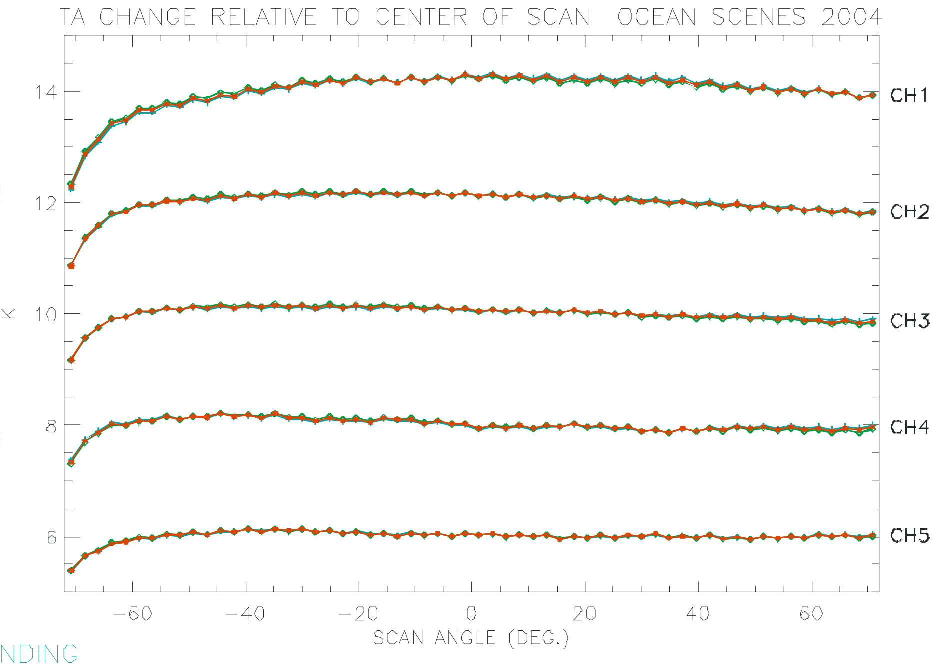

ASCENDING
DESCENDING
AVERAGE

Observed Scan-Non-uniformity

(January – December 2004)

Chs. 8-11 (150/183 GHz)

Chs. 17-18 (91v/h)

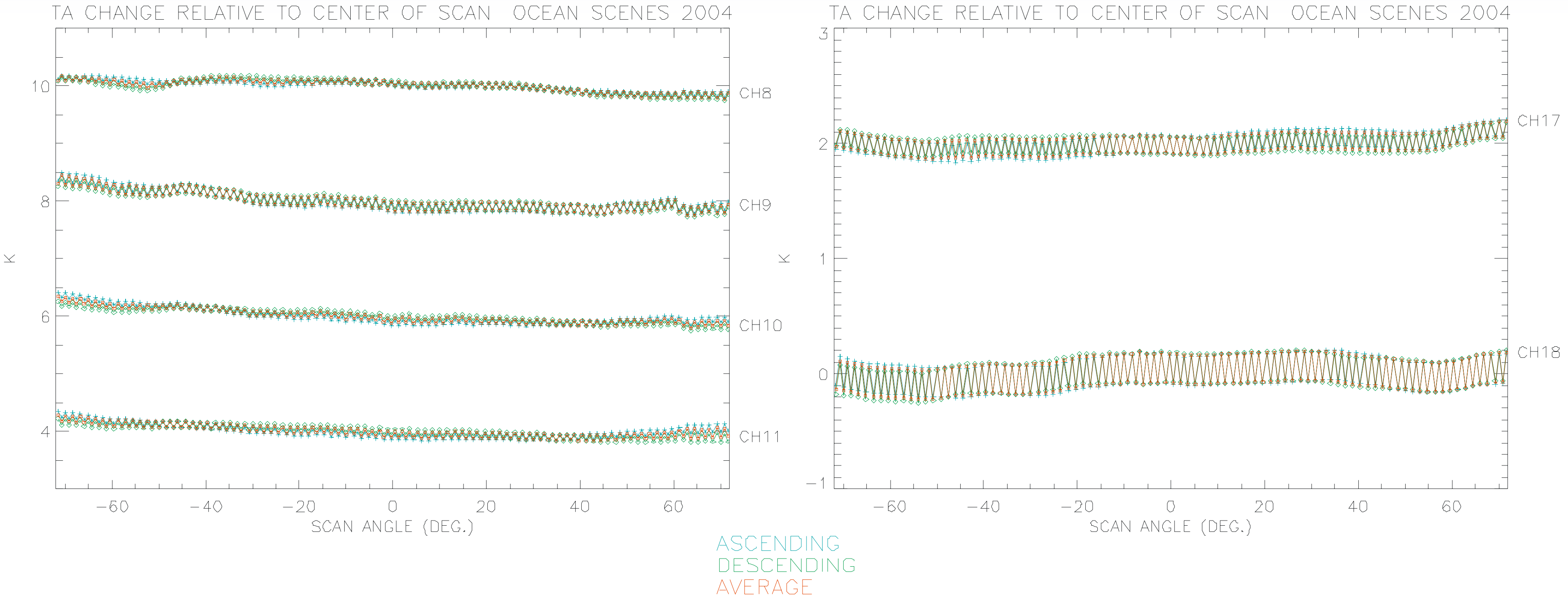

Observed Scan Non-Uniformity

(January – December 2004)

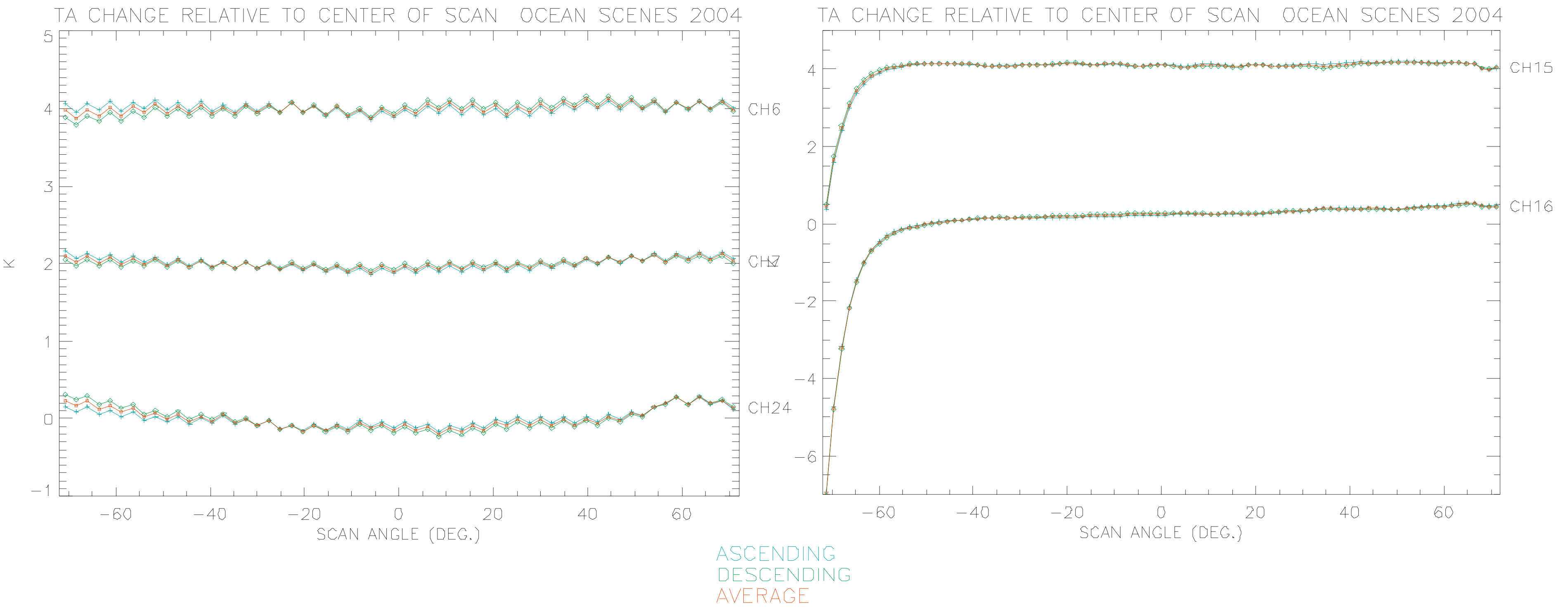

Chs. 6,7,24 (LAS)

Chs. 15-16 (37v,h)

Observed Scan Non-Uniformity

(January – December 2004)

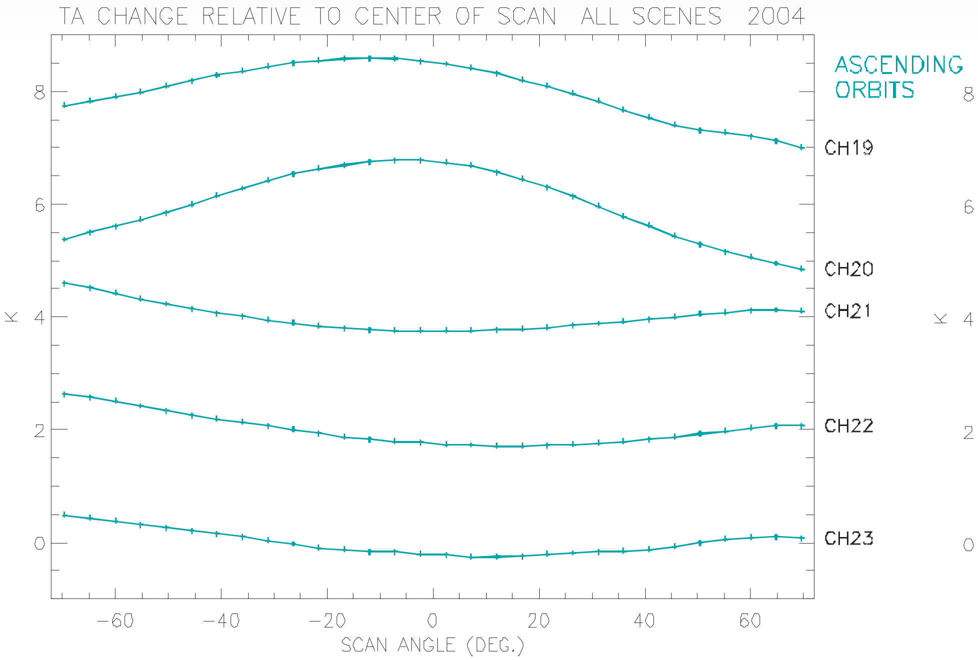

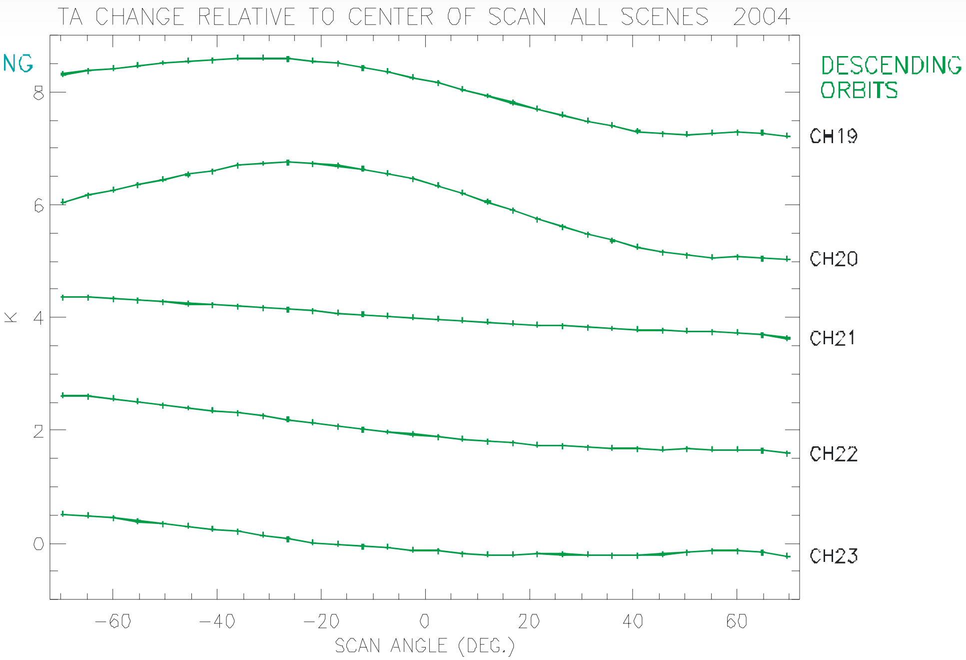

5.4 Major Results

- Chs. 12-14: Large repeatable monotonic increasing behavior at start of scan (3-5 K over 12 samples)
- Chs. 15-16: Large repeatable monotonic decreasing behavior at the end of scan (4-7 K over 12 samples)
- Chs. 6-7,24, 8-11,17-18:

  Small repeatable “saw-tooth” behavior across scan

  (0.5K P-P Ch.18)
- Chs. 1-5: Very small repeatable “saw-tooth” across scan and monotonic decreasing behavior at the end of scan
- Chs. 19-24: Scan behavior not repeatable nor understood. No correction implemented for Chs. 19-24.
- Consistent with Early Orbit results (See Section 2.0)

5.5 Sources of Non-Uniformities

- **Likely FOV intrusion Chs. 12-14 by Cold Space Reflector (CSR) at start of scene sector (Last of 6 Feed-horns to observe CSR).**

SSMIS Instantaneous FOV

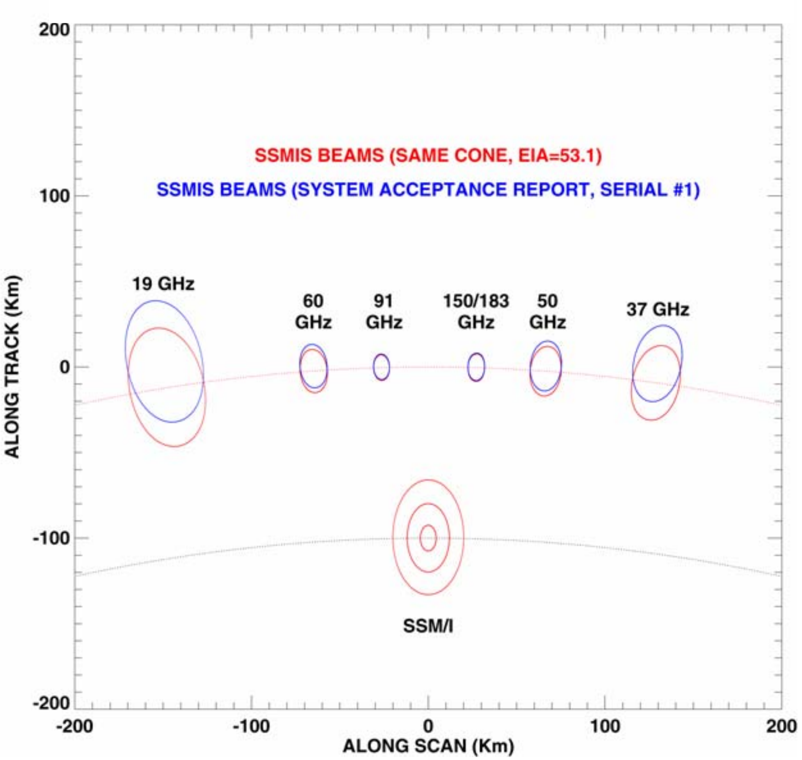

Sources Non-Uniformities (Cont'd.)

- Potential antenna near field interaction with Chs. 15–16

  (Feed-horn closest to S/C at the end of scene sector)

  Similar situation for Ch. 1-5 (2nd closest feed-horn at the end of scene sector)

- "Saw-tooth" behavior likely due to incomplete on-orbit calibration of A/B integrators by Flight Software (only observed for channels averaging odd numbers of samples)

- Very complex along-scan behavior of upper-air channels (Zeeman splitting and interaction of Earth magnetic field with propagation vector)-remains unresolved

5.6 Non-Uniformity Correction Algorithm (Channels 1-18 Only, All Surfaces)

- **To First Order**

$$T_A\left(\phi\right) = L\left(\phi\right) T_{Scene} + \left[1 - L\left(\phi\right)\right] T_X$$

where

ϕ = **Azimuth Scan Angle**

T_X = **Cosmic Background Brightness Temperature**

- **Since** $\left| 1 - L \right| << 1$

$$T_{Scene} \approx T_A \, \phi / L\left(\phi\right)$$

- **Approximate** $L\left(\phi\right) = \dfrac{\left\langle T_A\left(\phi\right) \right\rangle}{\left\langle T_A\left(\phi : \text{Center of Scan}\right)\right\rangle}$

< > = Ensemble Average of Scene (TDRs)

Defense Meteorological Satellite Program
Special Sensor Microwave Imager Sounder (F-16)
Calibration/Validation Final Report

The First Conical Scanning Passive Microwave Surface and Atmospheric Sounding Imager

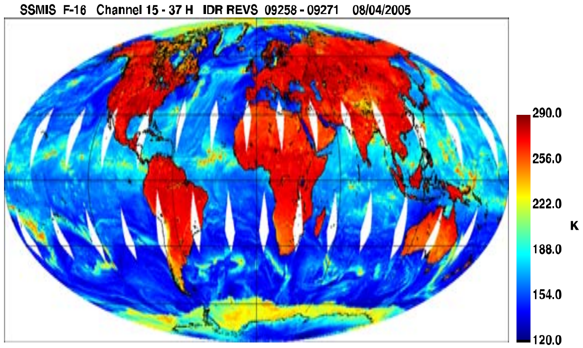
SSMIS F-16 Channel 15 - 37 H IDR REVS 09258 - 09271 08/04/2005

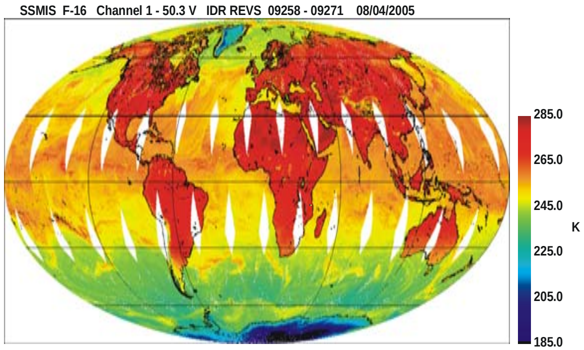
SSMIS F-16 Channel 1 - 50.3 V IDR REVS 09258 - 09271 08/04/2005

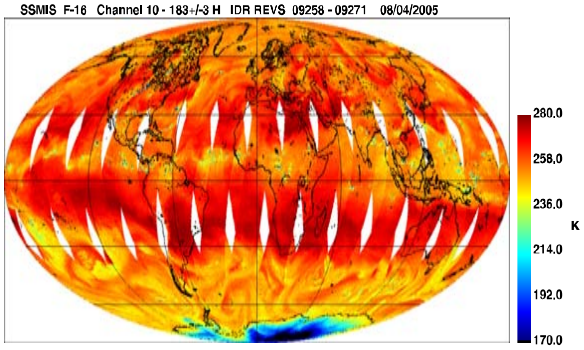
SSMIS F-16 Channel 10 - 183+/-3 H IDR REVS 09258 - 09271 08/04/2005

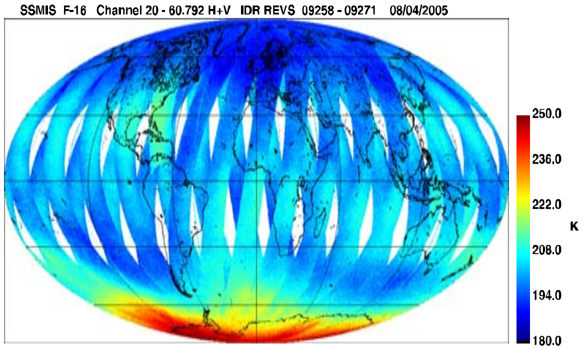
SSMIS F-16 Channel 20 - 60.792 H+V IDR REVS 09258 - 09271 08/04/2005

Prepared by

SSMIS Cal/Val Team

30 November 2005

Volume II

Table of Contents

F16 SSMIS Calibration/Validation Final Report

Section 6.0 APMIR Under-Flight Calibration

(Airborne Polarimetric Microwave Imaging Radiometer)

Justin Bobak, David Dowgiallo, Troy vonRentzell,

Norman McGlothlin, Steven Quinn, Louis Rose,

and Brian Hicks

THE AEROSPACE CORPORATION

APMIR

APMIR

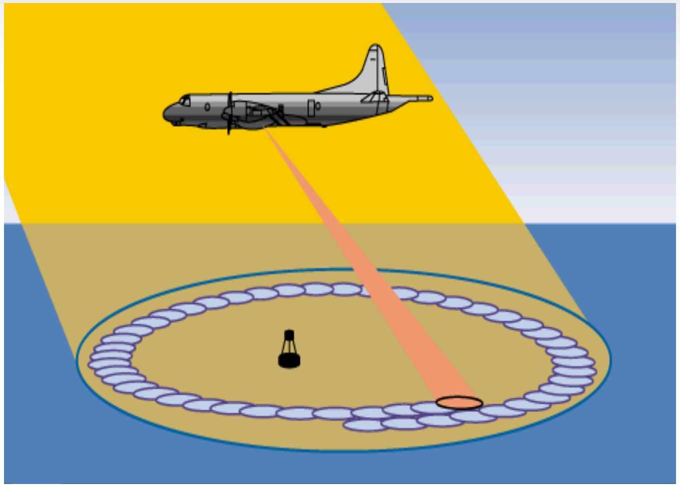

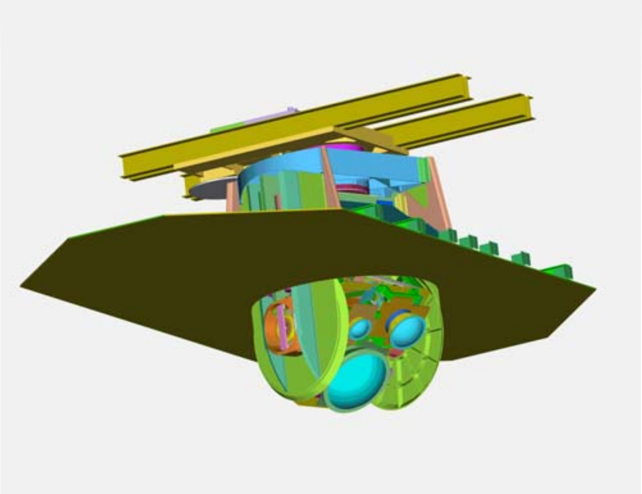

APMIR Sensor and support structure

A Tool to Assist in the Calibration of Space-borne Sensors

Channels tunable to match:

- SSMIS
- WindSat
- NPOESS CMIS
- AMSR

APMIR is a joint Air Force/Navy program

Spinning assembly:

- mimics space-borne sensor conical scan
- provides multiple azimuthal looks
- yields correlation between space-borne and airborne measurements by viewing concurrent scene

System Description

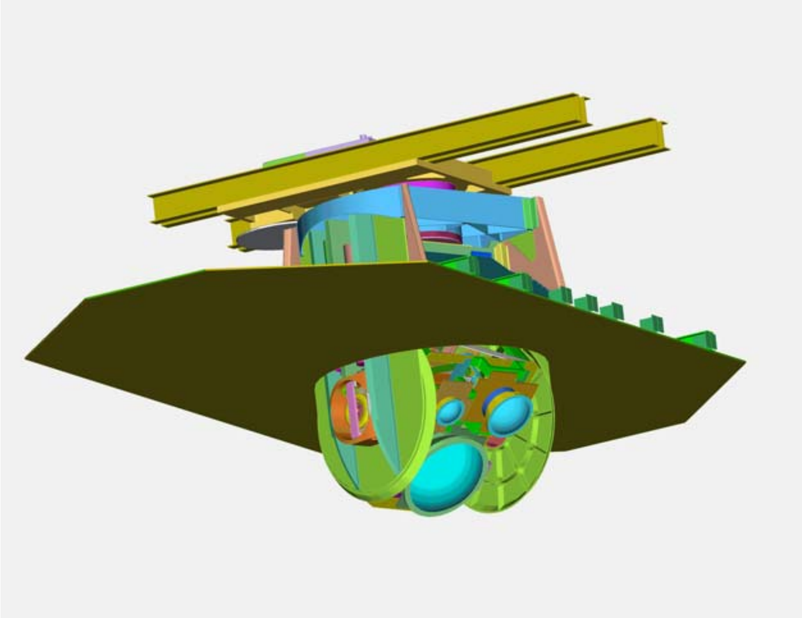

- Five radiometers
  - Match SSMIS (bands to 37.0 GHz) in frequency, bandwidth and polarization (6.8 and 10.7 for WindSat)
- Housing mounts in bomb bay of P3 aircraft with two external calibration targets
- Full azimuth and elevation motion
- GPS system for aircraft attitude and position

Radiometer Frequency Capabilities

Frequency (GHz)	**Polarization**	**Matching satellite radiometer**	**Notes**
6.6	T_V, T_H	None	Included feature
6.8	T_V, T_H	WindSat	
7.2	T_V, T_H	None	Included feature
10.7	T_V, T_H, T_3, T_4	WindSat	
18.7	T_V, T_H, T_3, T_4	WindSat	On APMIR, switchable with 19.35 GHz
19.35	T_V, T_H, T_3, T_4	SSMIS	SSMIS has T_V, T_H at 19.35; switchable on APMIR with 18.7 GHz
22.235	T_V, T_H	SSMIS	Switchable on APMIR with 23.8 GHz
23.8	T_V, T_H	WindSat	Switchable on APMIR with 22.235 GHz
37.0	T_V, T_H, T_3, T_4	SSMIS, WindSat	SSMIS has T_V, T_H at 37.0

Design Specification

Frequency (GHz)	Bandwidth (MHz)	NEDT (50mS) (K)	Beamwidth (degrees)
6.8, 6.6, 7.2	125	0.28	9.4
10.7	300	0.21	5.9
18.7, 19.35	750	0.21	6.8
23.8, 22.23	500	0.28	5.3
37.0	2000	0.14	6.0

- **Absolute radiometer accuracy, V and H channels better than 0.75 K**

External Calibration

- For scene viewing, sphere rotates in azimuth at 10 rpm

- Approx every 20-30 minutes, system performs an external calibration (hot target: 313K; ambient target: 250-270K)

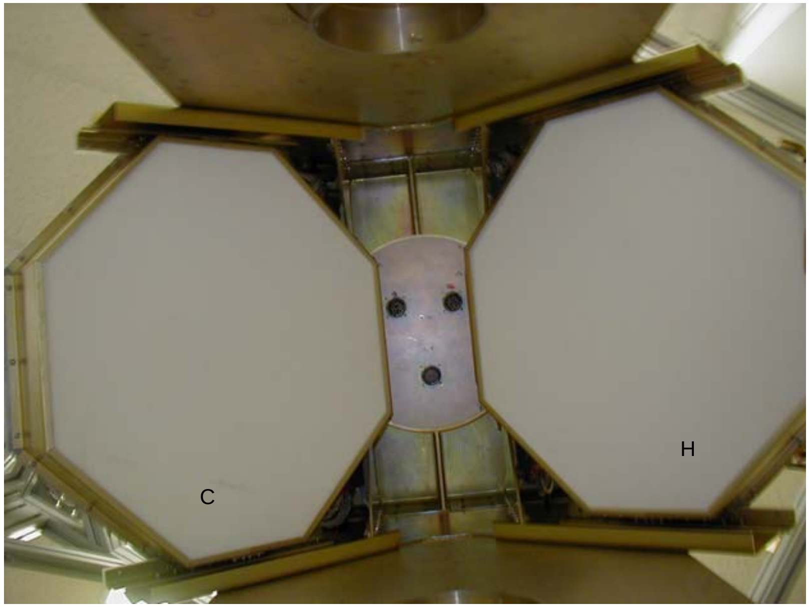

Flight Calibration Target (PRT placement)

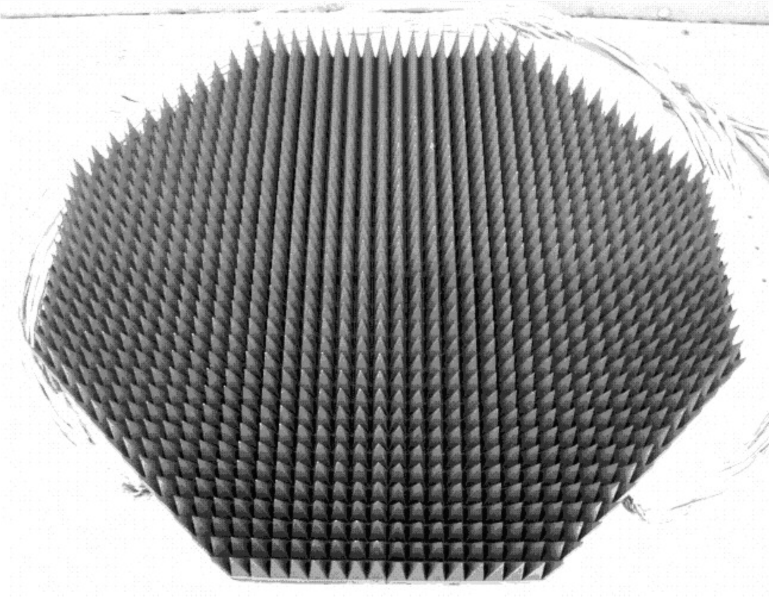

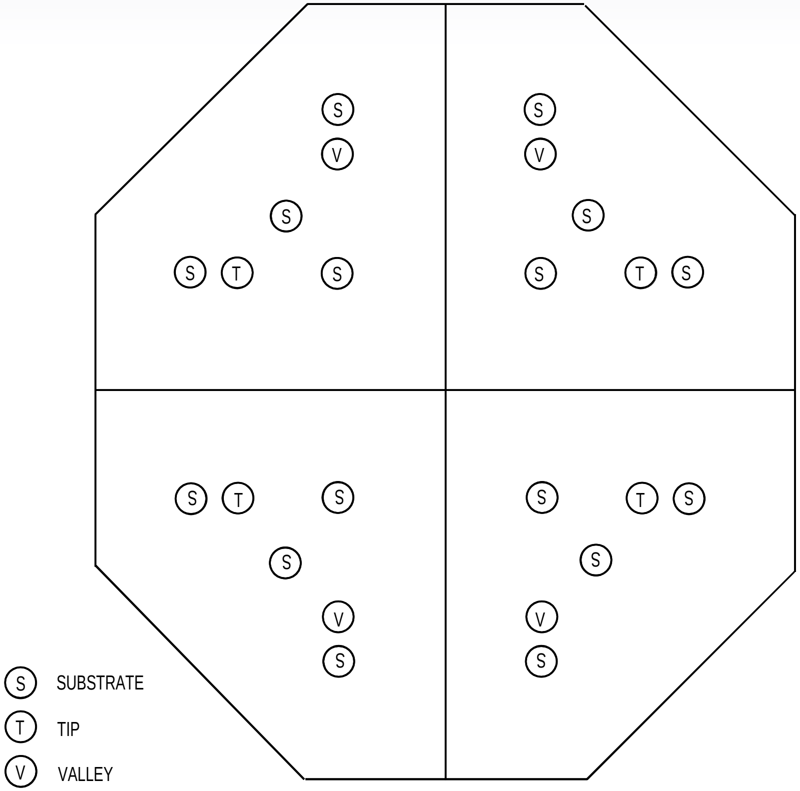

- 24 platinum resistance thermometers
- Accuracy better than 0.2K
- NIST Traceable prt calibration
- Hot load ~ 313K, Ambient load 250-270K, environment dependent

Temperature Stability

- **Radiometers and Power Module subjected to thermal chamber temperatures of -30°C to +35°C while operational**
- **Radiometers wrapped in thermal blankets to assist in temperature stabilization during flight**
- **In-flight temperature stability per station leg is typically ± 0.1°K**

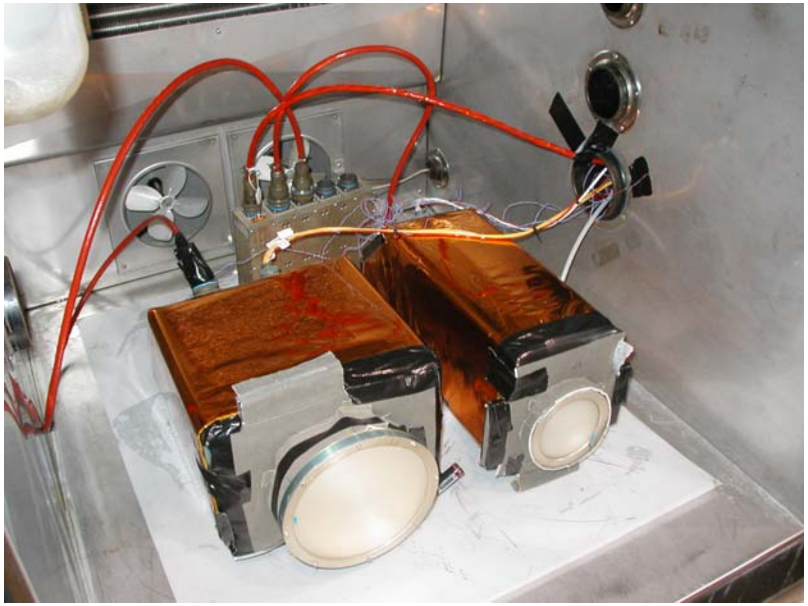

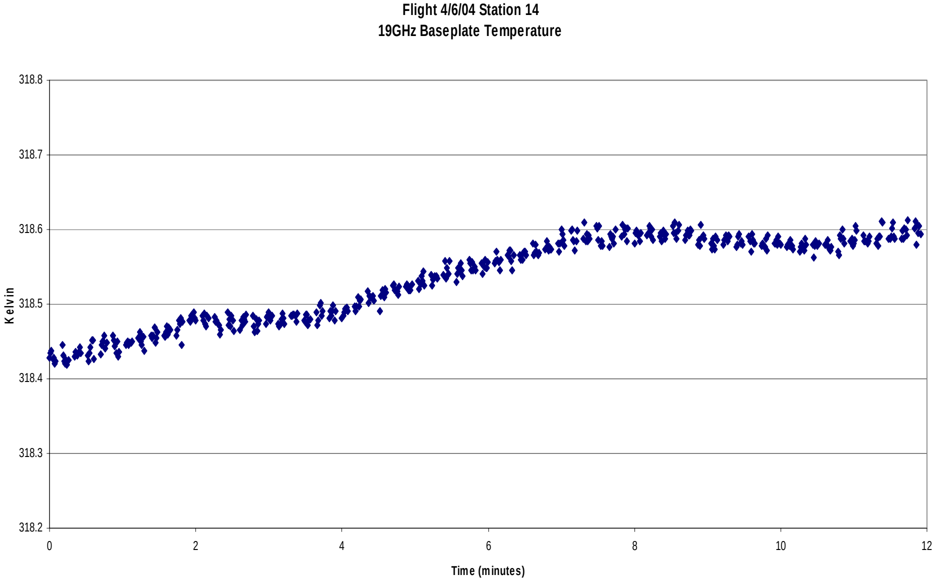

Radiometer Packaging

37 & 22/19 GHz Radiometers

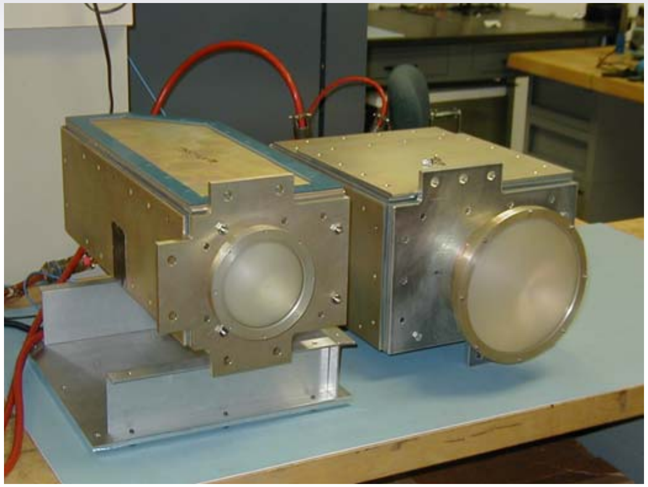

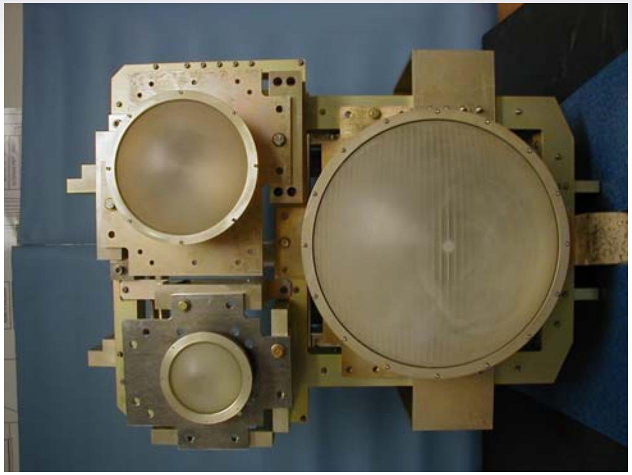

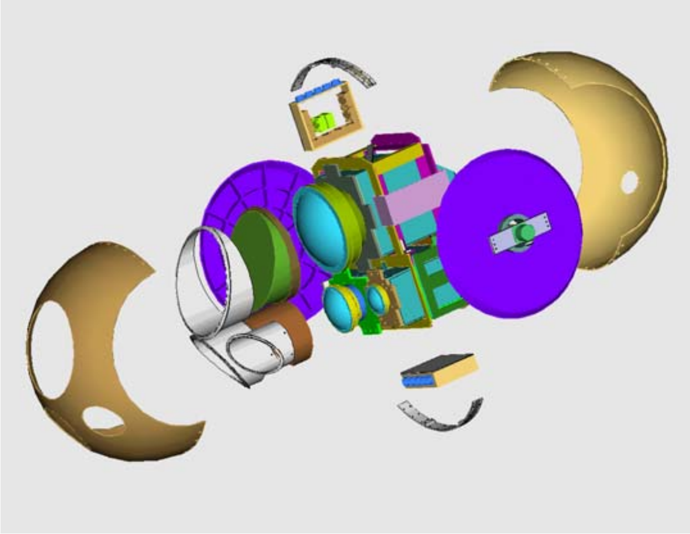

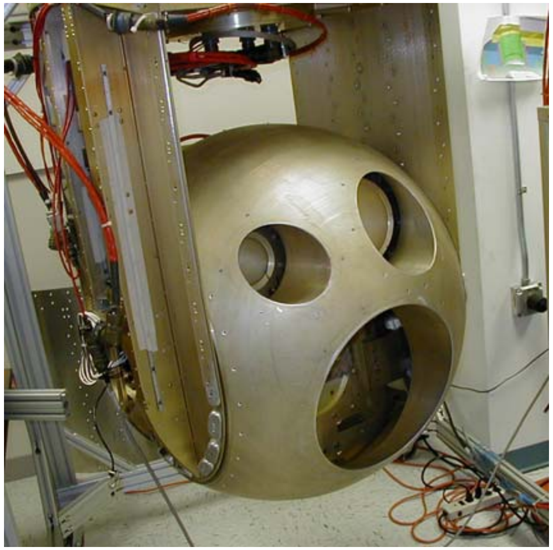

Antenna Characterization

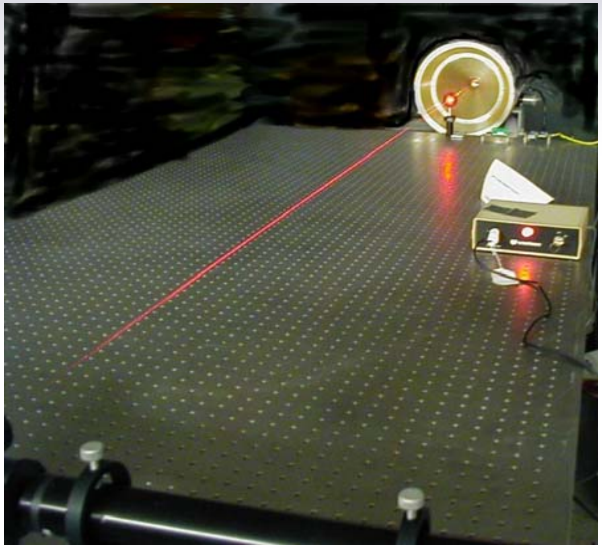

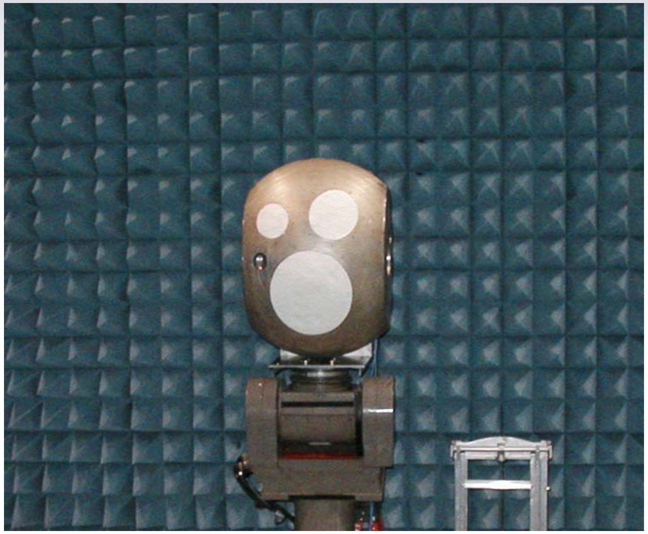

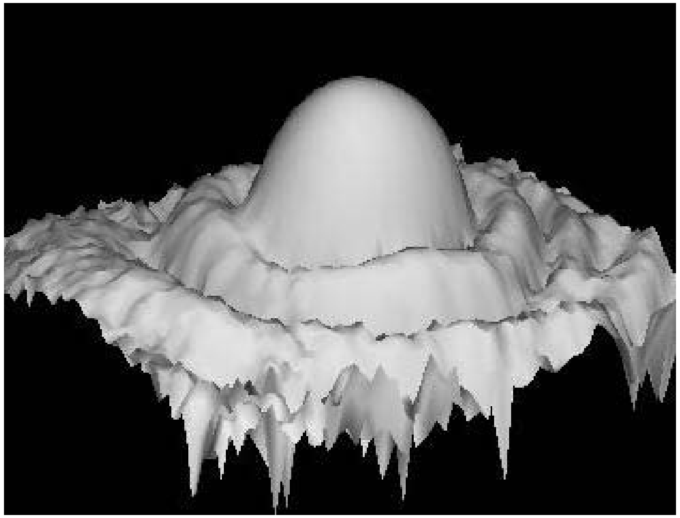

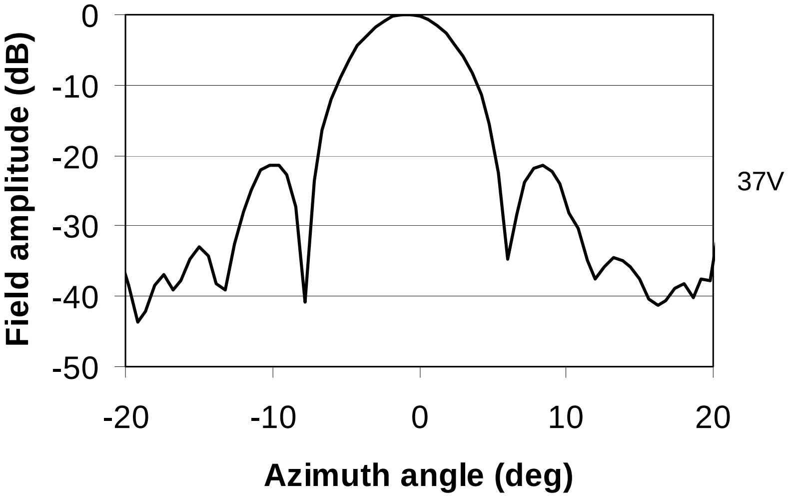

GPS

Attitude and Alignment

Antenna wing mount

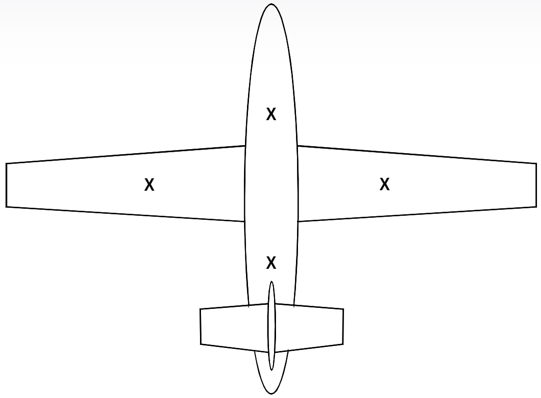

P-3 antenna positions

Tans Vector accuracy:

Pitch = 0.08 degrees

Roll = 0.08 degrees

Heading = 0.08 degrees

Position = 25 meters

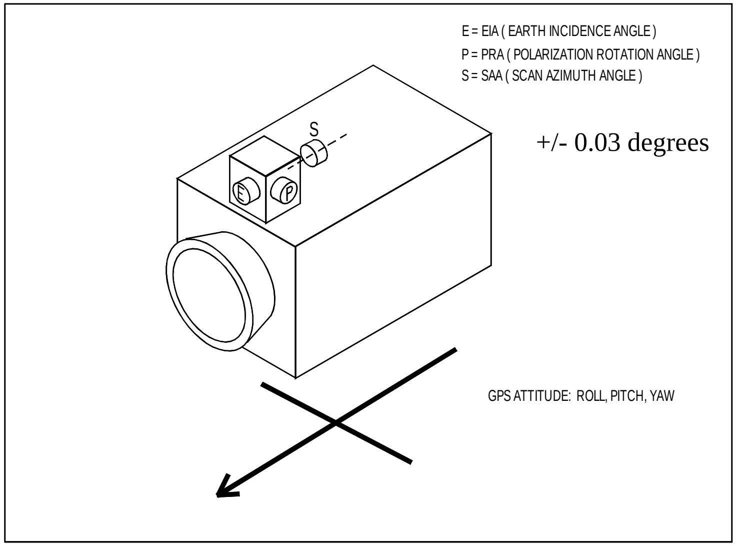

Test Flight 22H Norfolk, Virginia

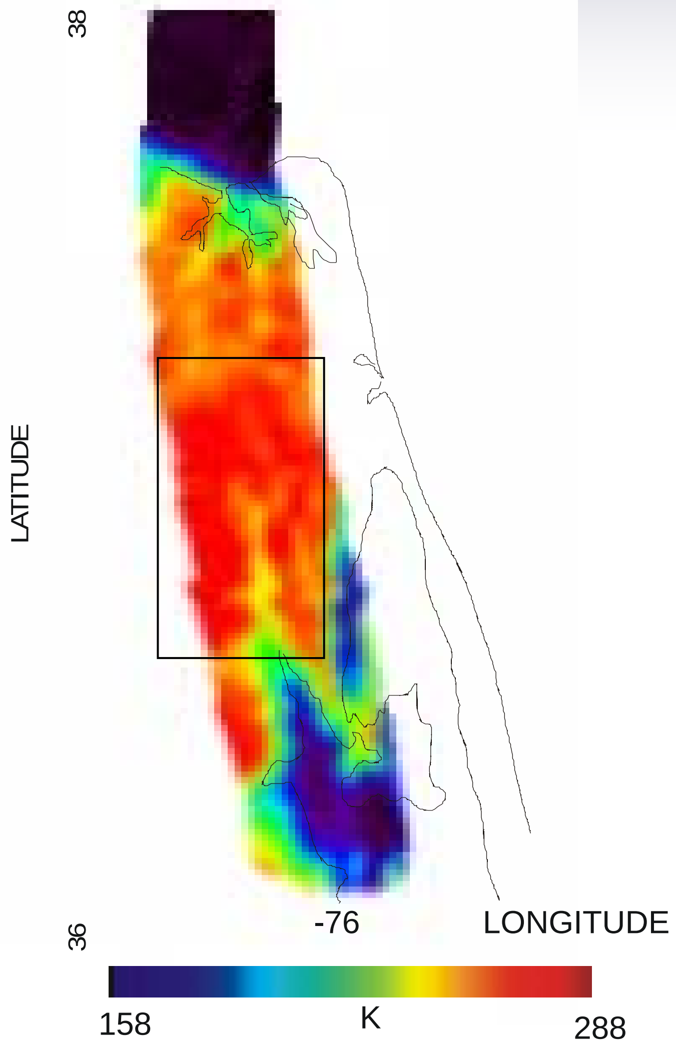

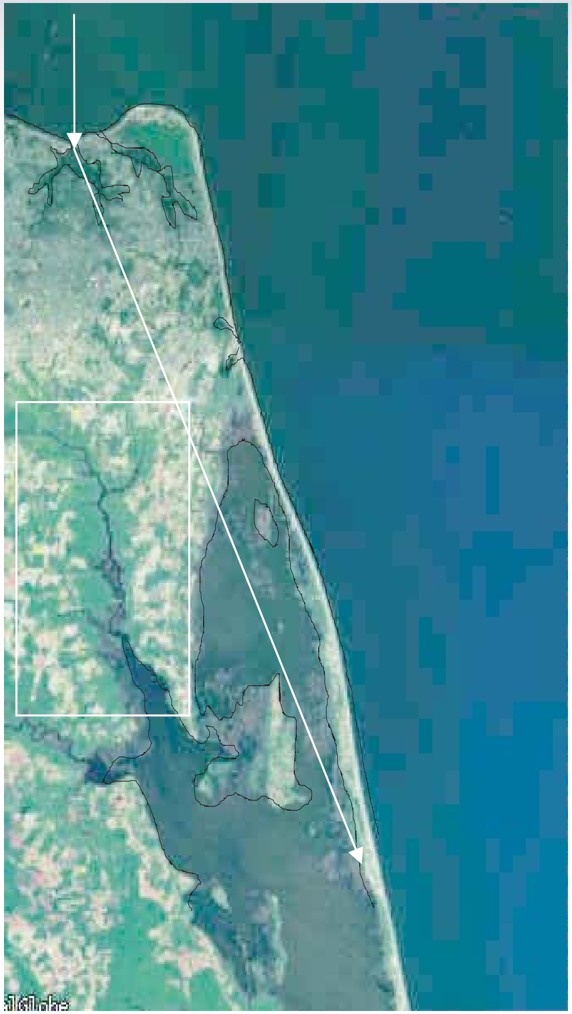

Virginia Beach

8.2 Under-Flight Campaigns

- 3/19/04 Cloudy (Buoy 41001)
- 3/23/04 Clear, scattered clouds (Buoys 44004/41002)
- 3/30/04 Cloudy (Buoys 41001/41002)
- 4/3/04 Cloudy (Buoys 41001/44004)
- 4/4/04 Cloudy, late clearing (Buoys 44004/44011)
- 4/5/04 Cloudy (Buoy 41002)
- 4/6/04 Clear, mild haze (Buoy 41002)


4/3/04 “Cloudy”

4/6/04 “Clear”

Flight Destination Buoys

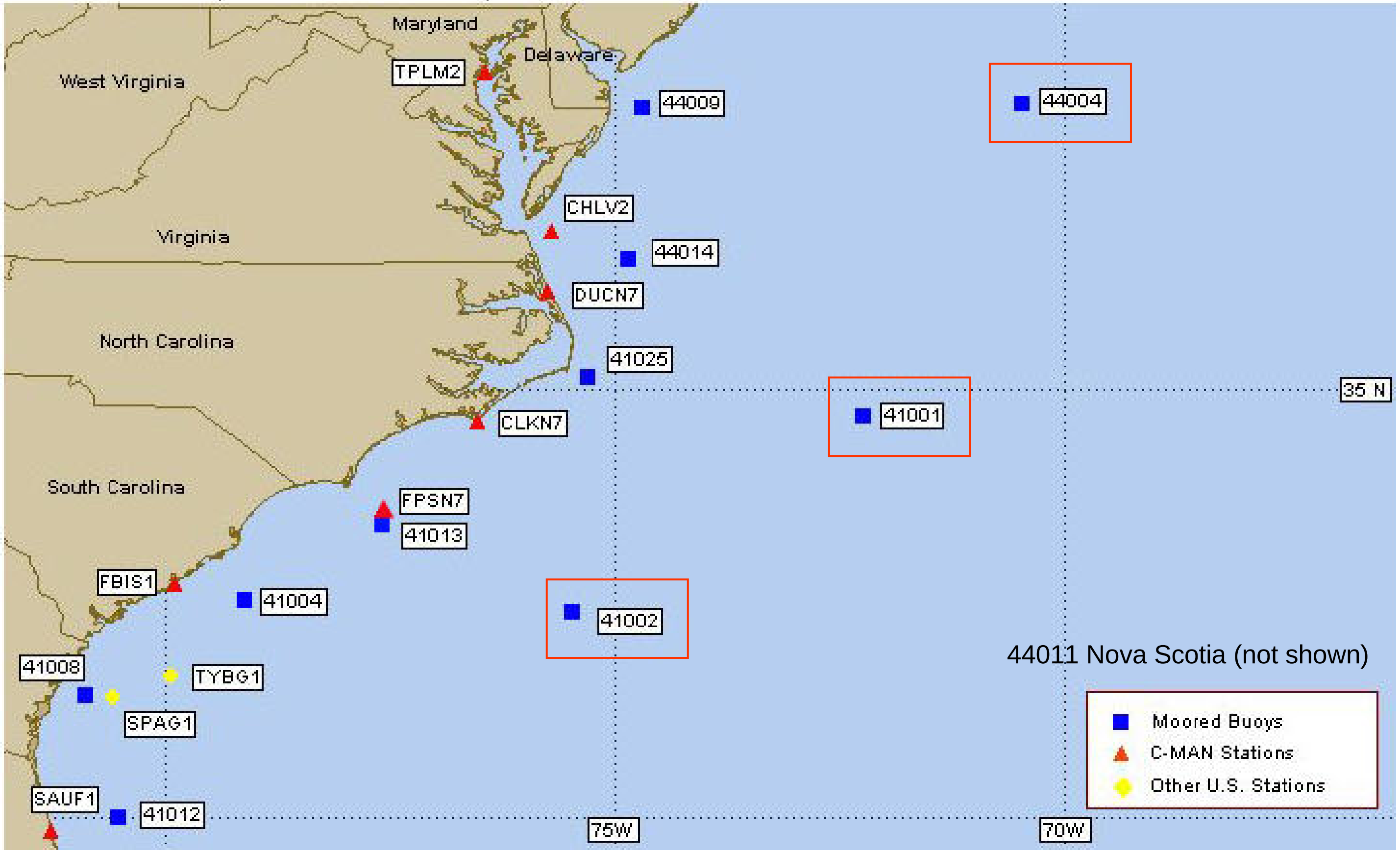

44011 Nova Scotia (not shown)

8.3 Under-Flight: 23 March 04

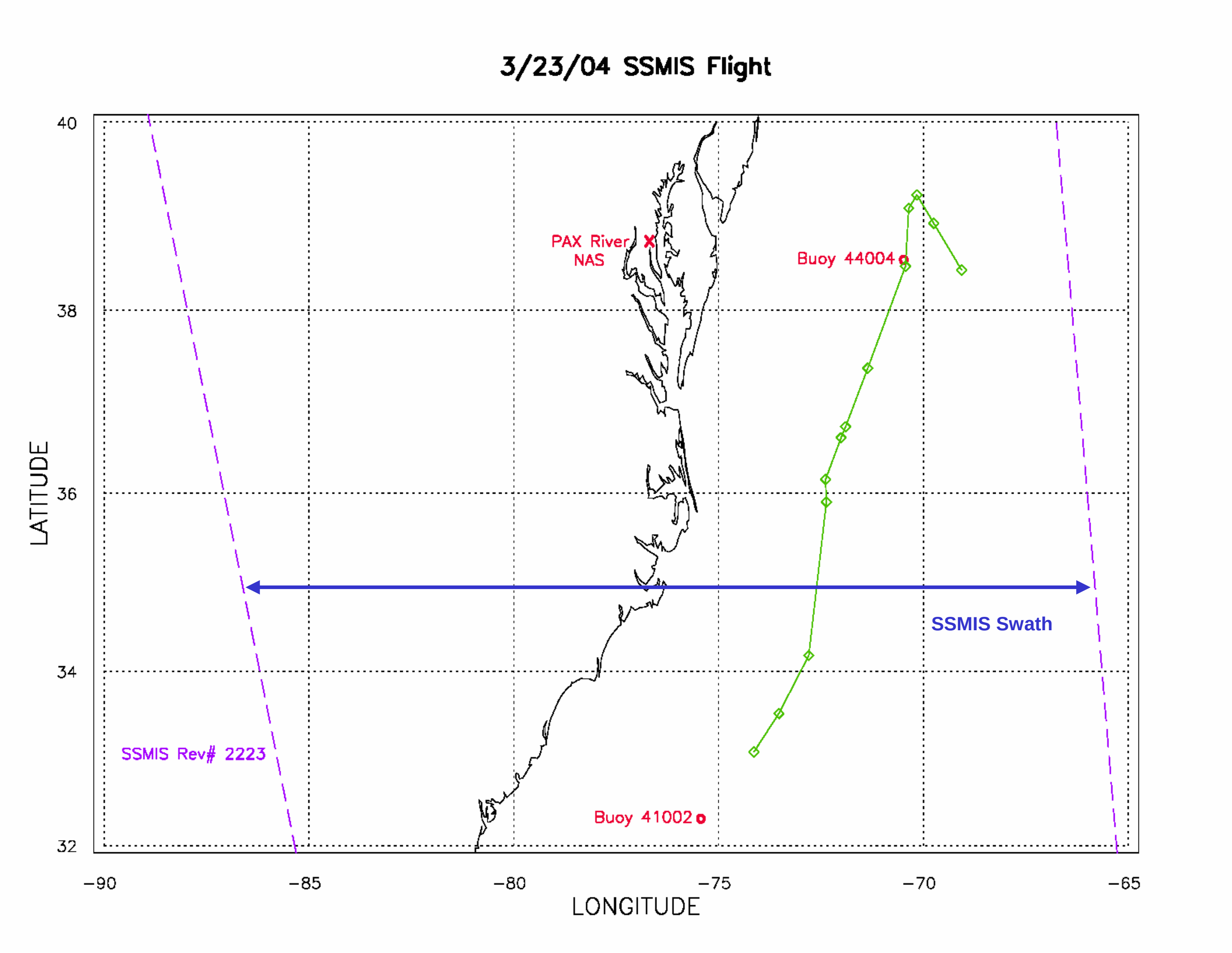

SSMIS Underflight 3/23/04
19V

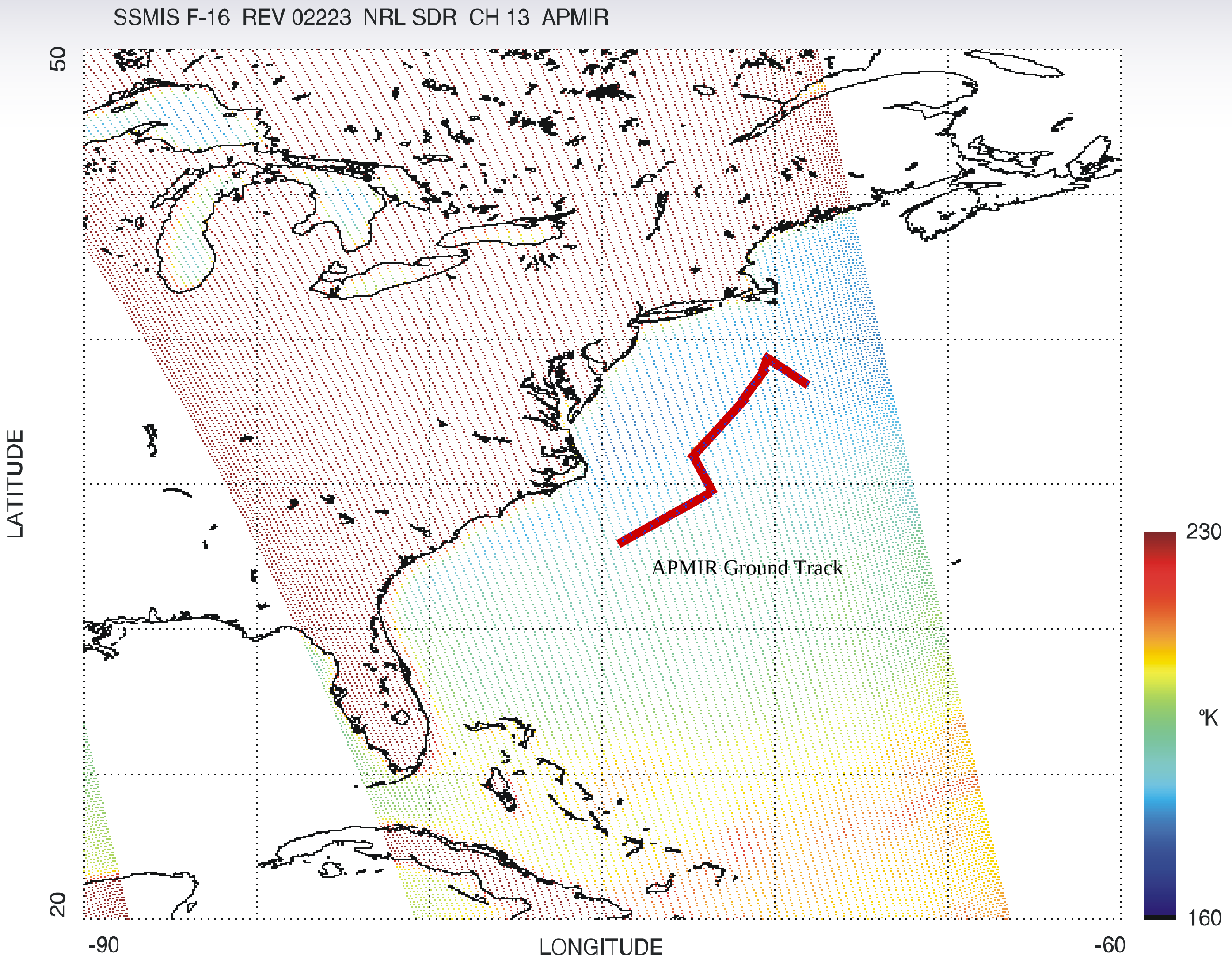

APMIR Flight 3/23/03

Station 1 flight video camera

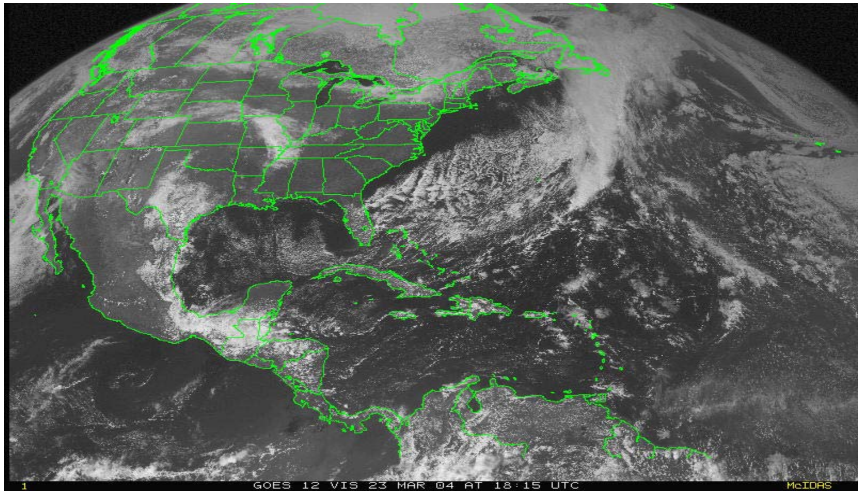

Visible Satellite Image (East Coast)

Table of Buoy 44004 Data
3/23/04

Environmental Parameter	Buoy Data
Surface air pressure (mbar)	1031.9
Surface air temperature (°C)	5.1*
Surface abs. humidity (g/m³)	4.0*
Sea surface temperature (°C)	14.3
Surface wind speed (m/s)	6.9

* These values were calculated from adjacent buoys since buoy 44004 was not recording air temperature or dew point temperature

Time Series Plot 37V FWD

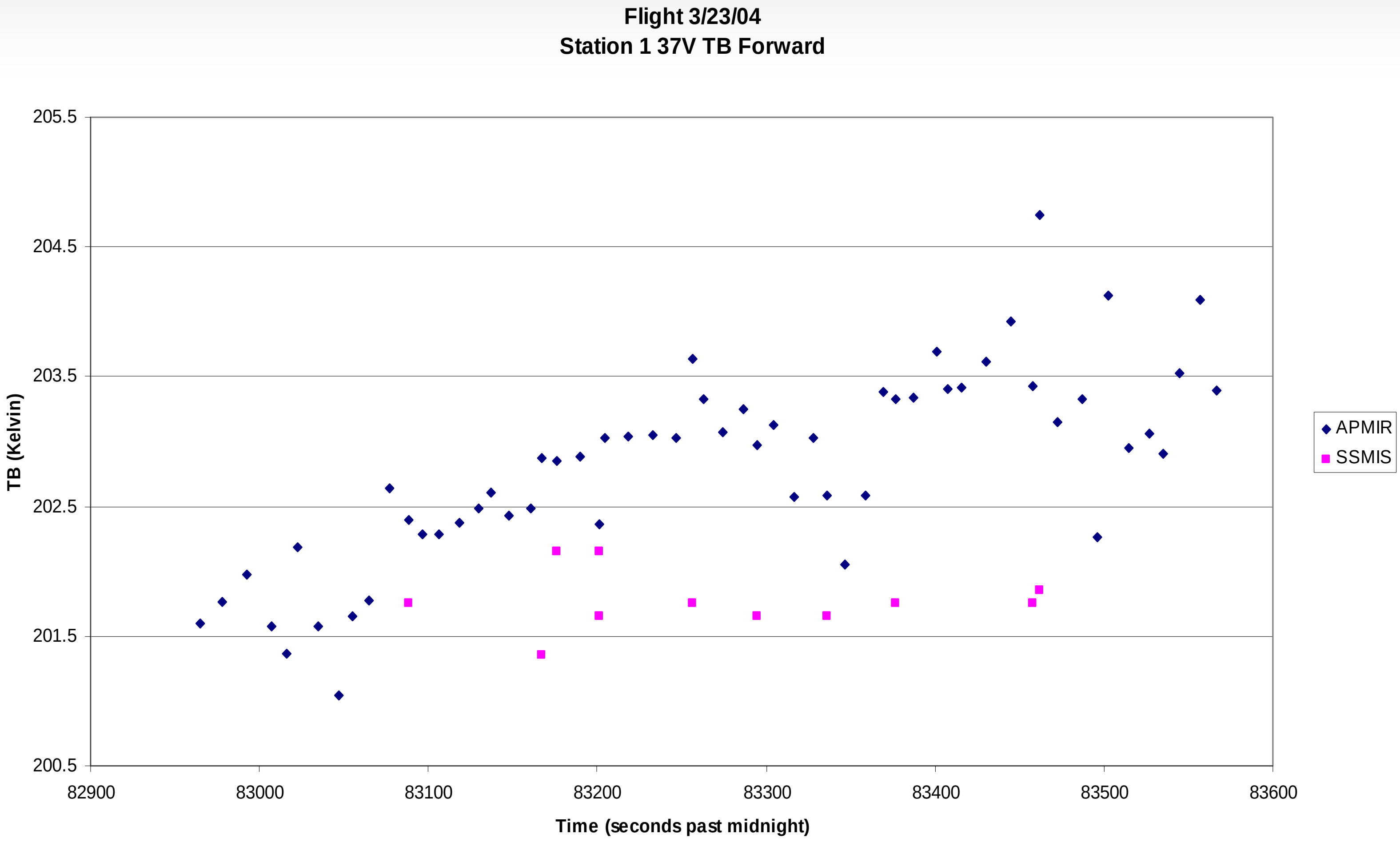

Time Series Plot 37H FWD

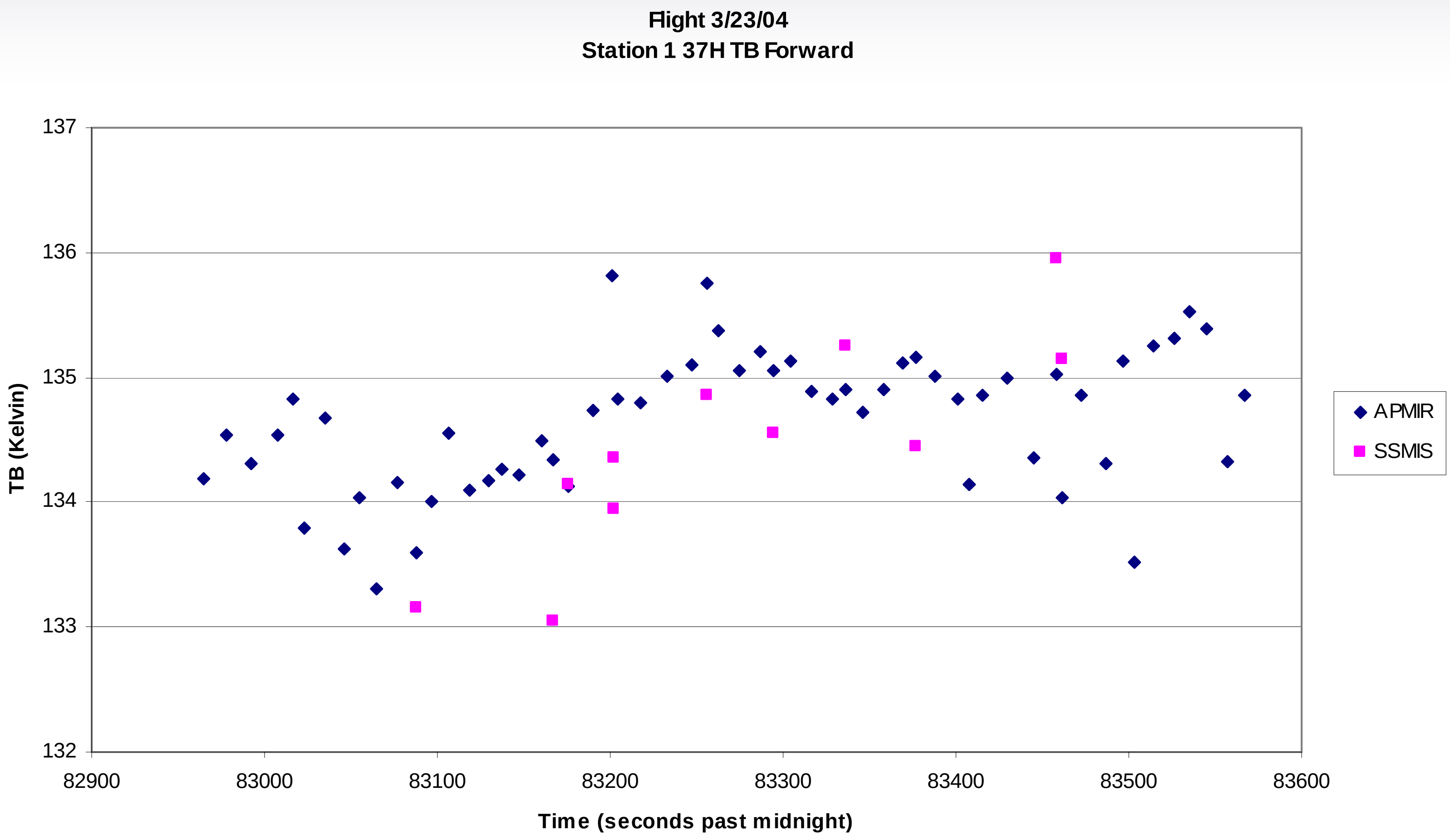

Time Series Plot 22V FWD

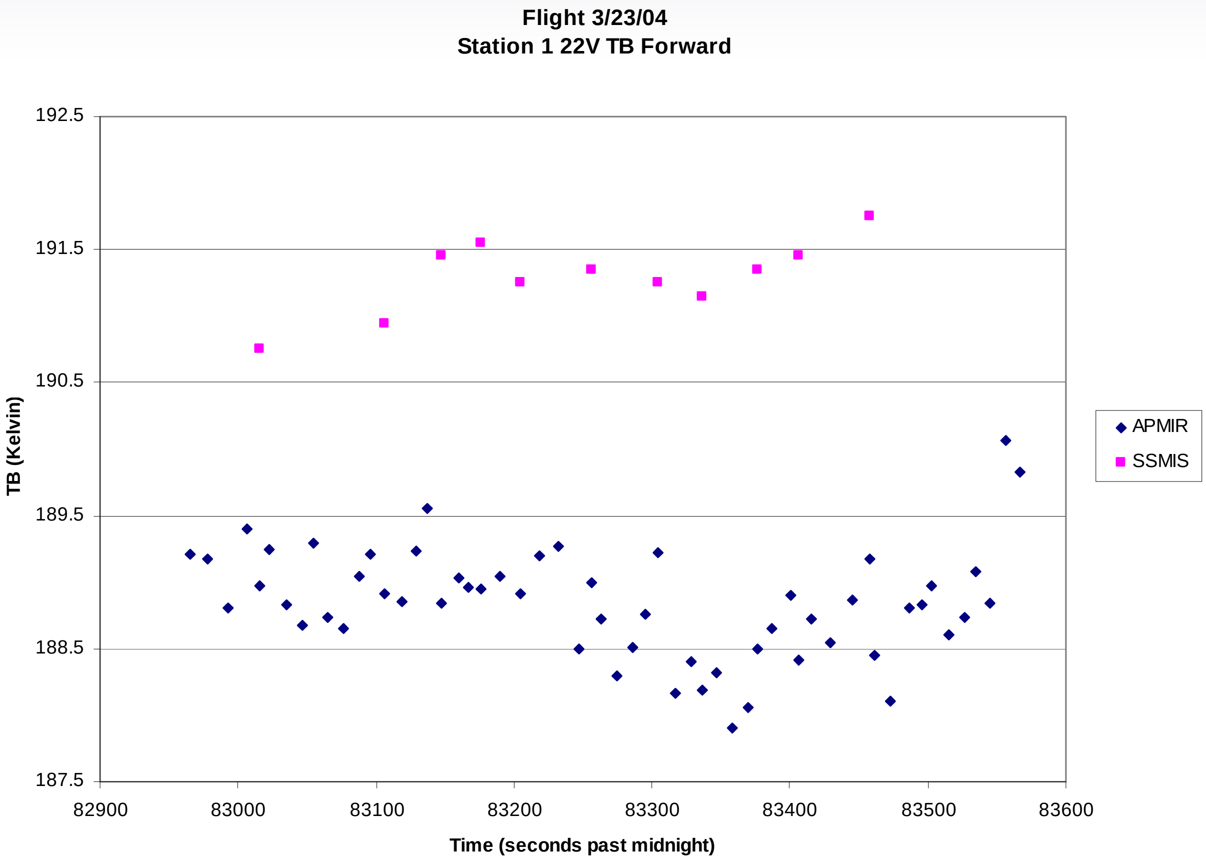

Time Series Plot 19V FWD

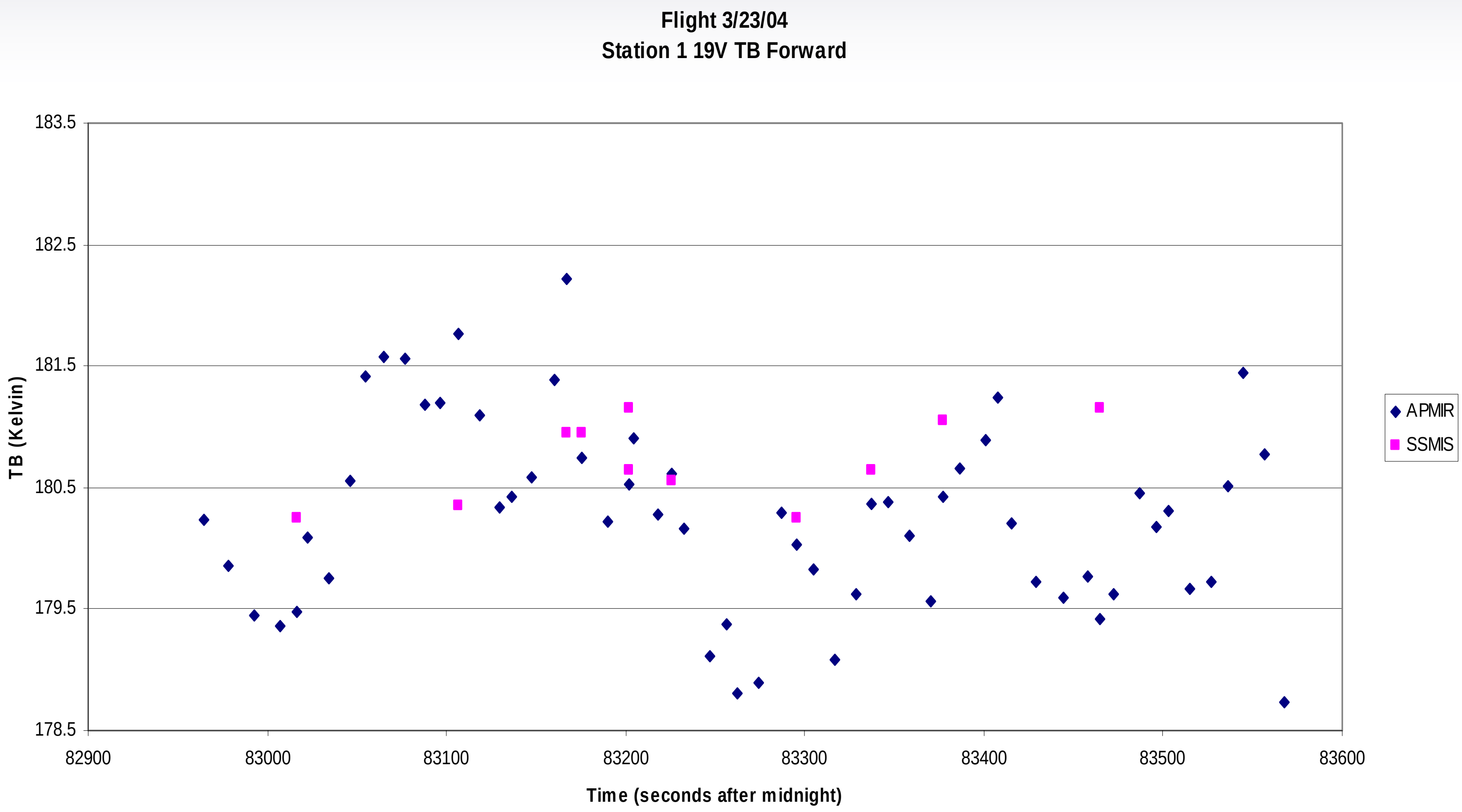

Time Series Plot 19H FWD

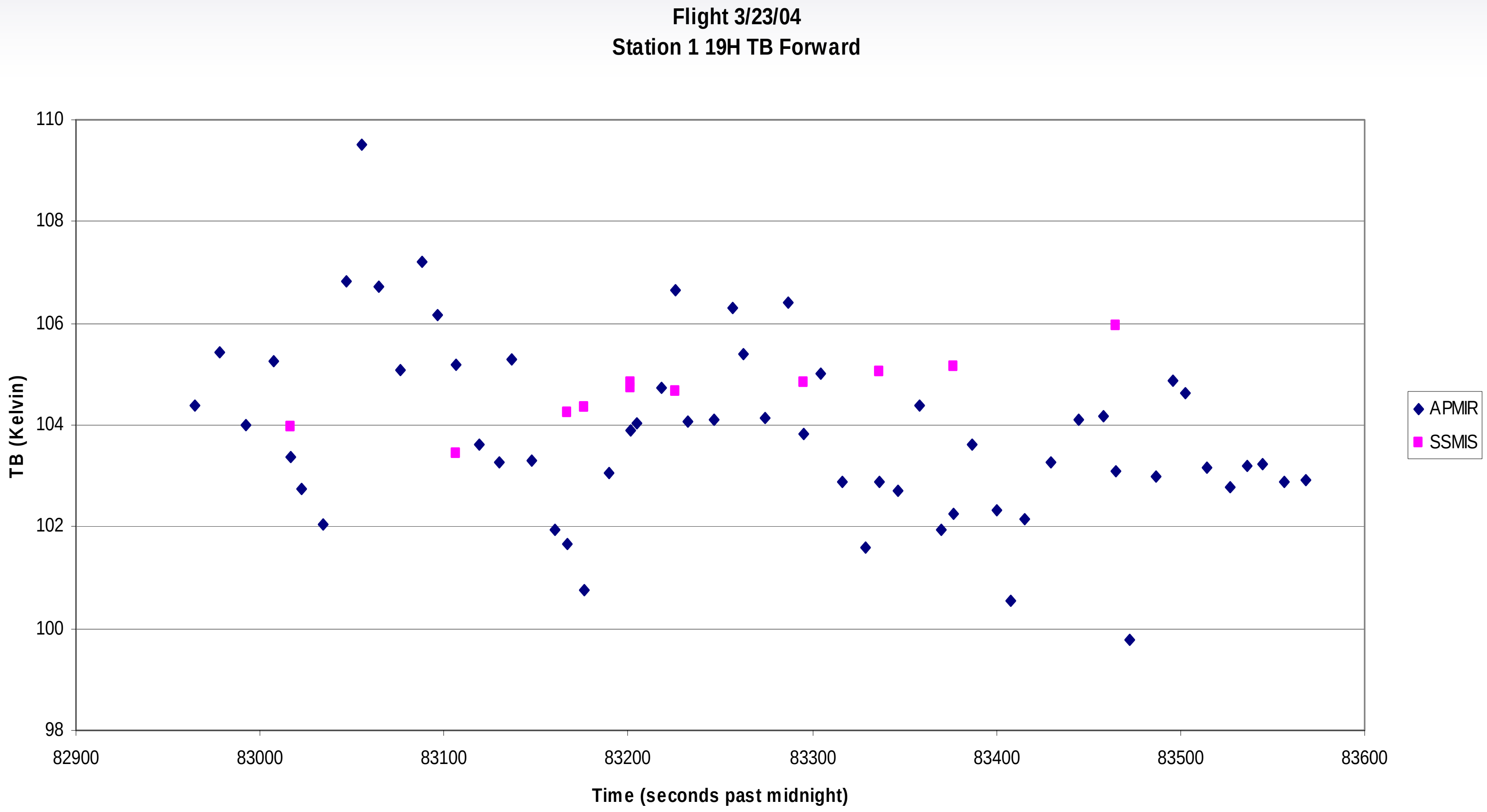

Cumulative Distribution Function 37GHz

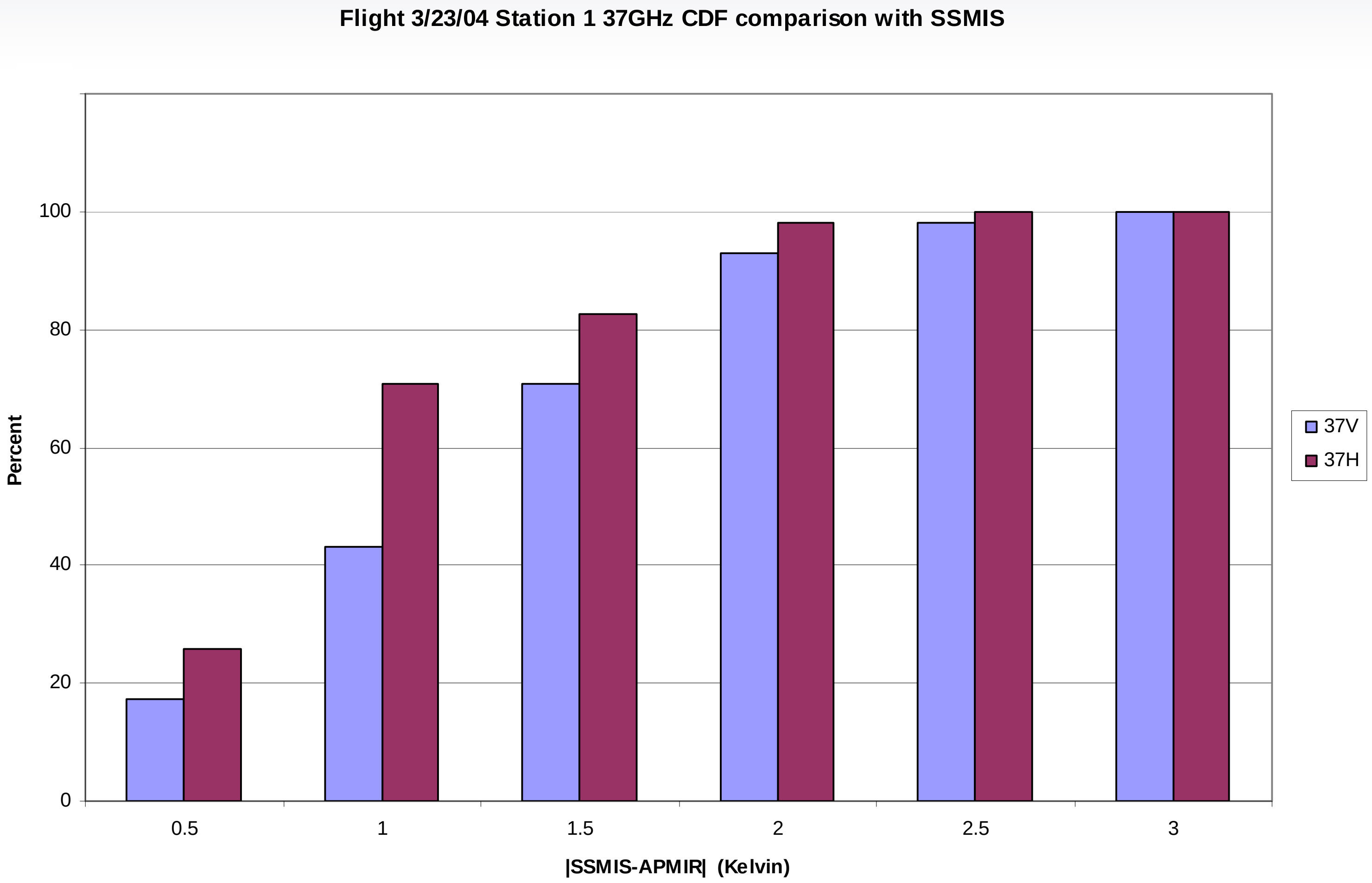

Cumulative Distribution Function 22GHz

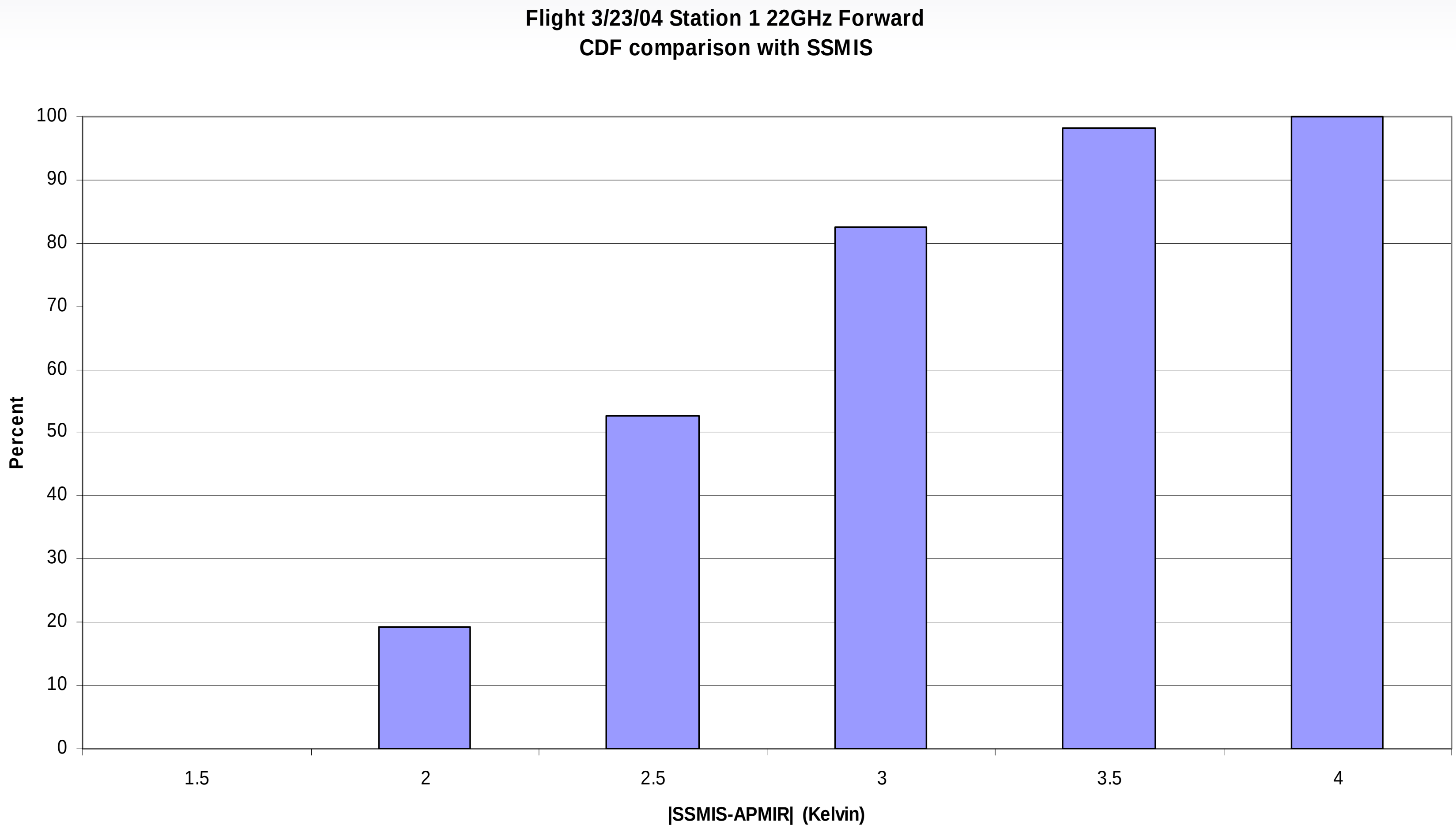

Cumulative Distribution Function 19GHz

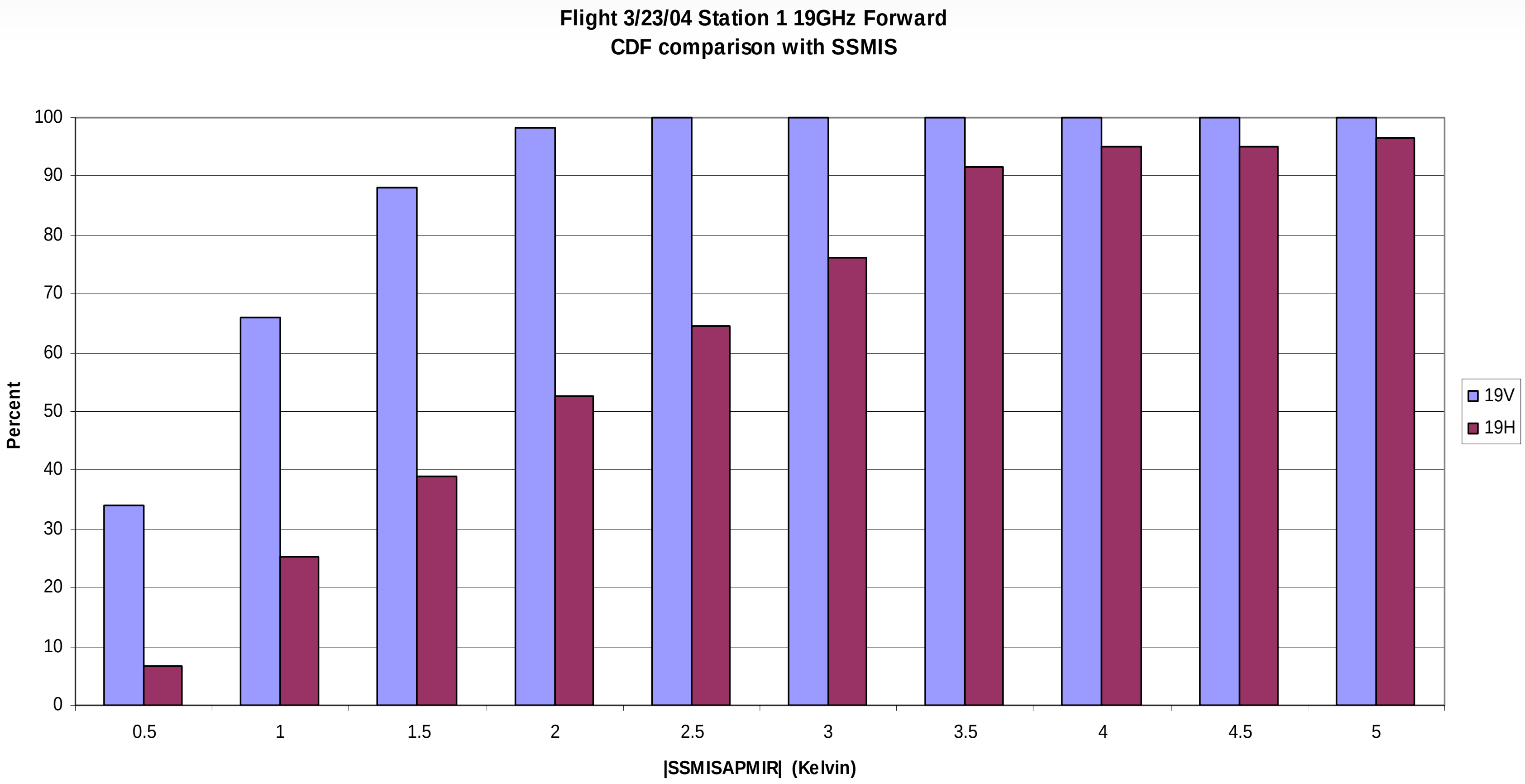

8.4 Under-Flight: April 04

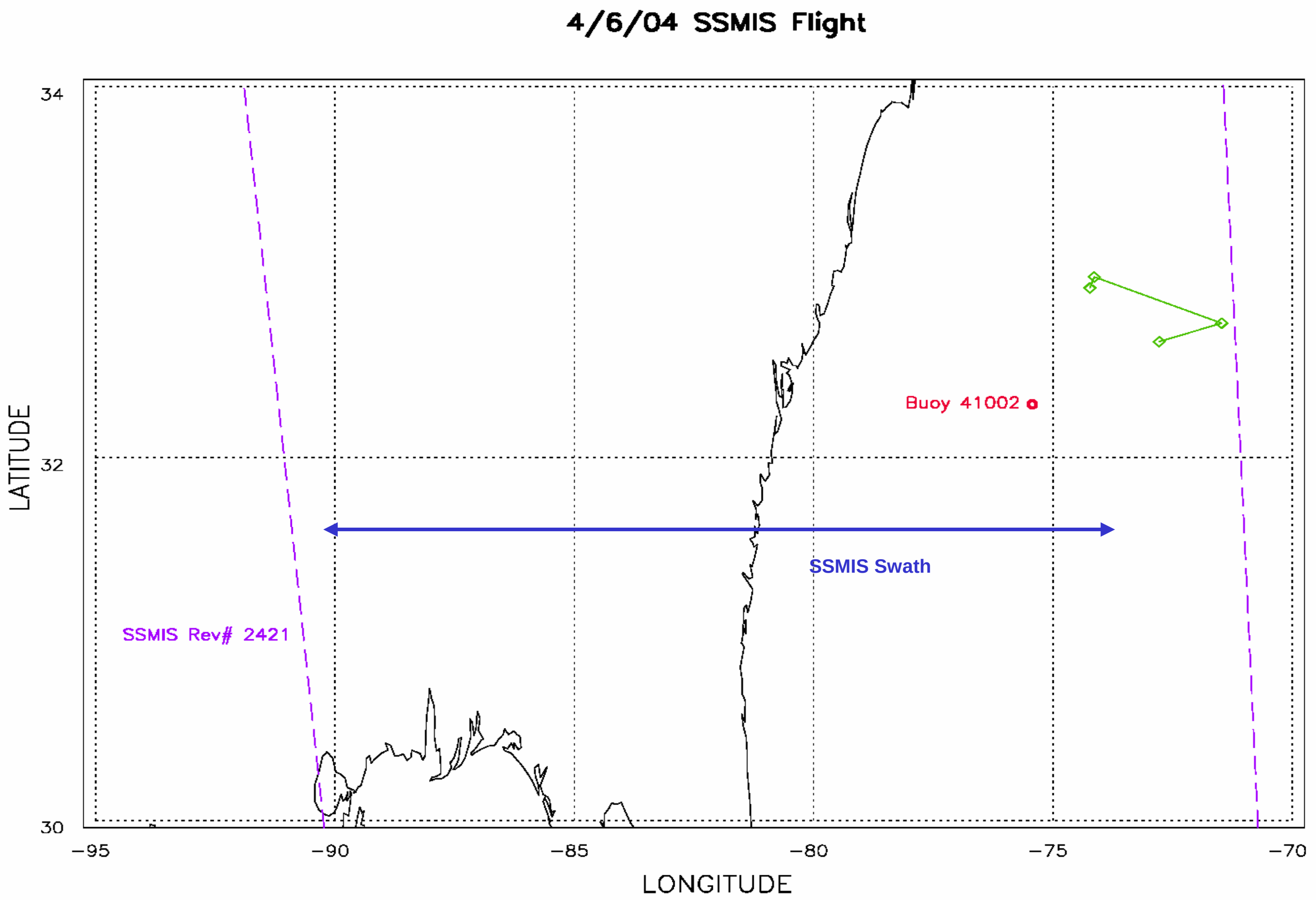

SSMIS Underflight 4/6/04
19V

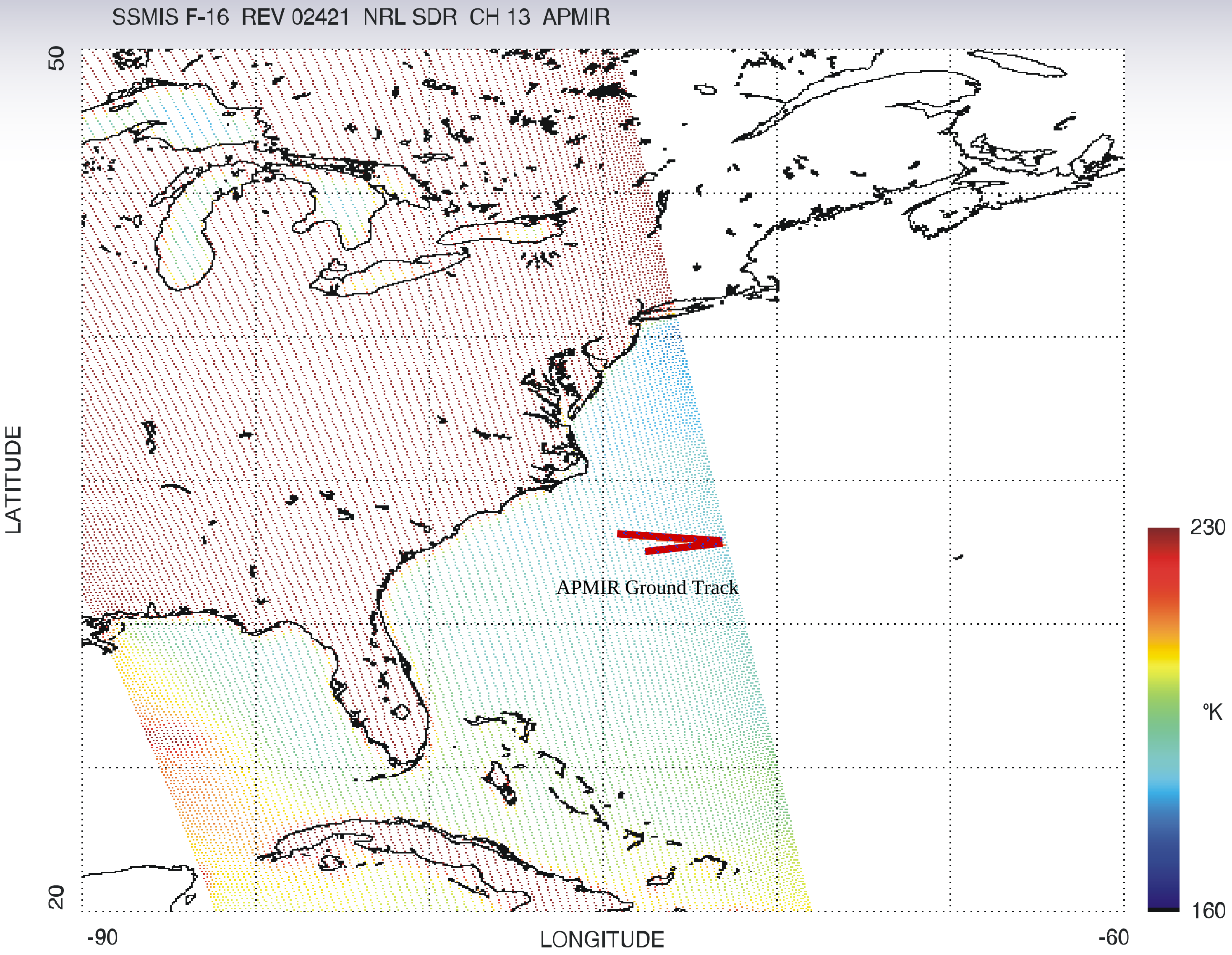

APMIR Flight 4/6/04

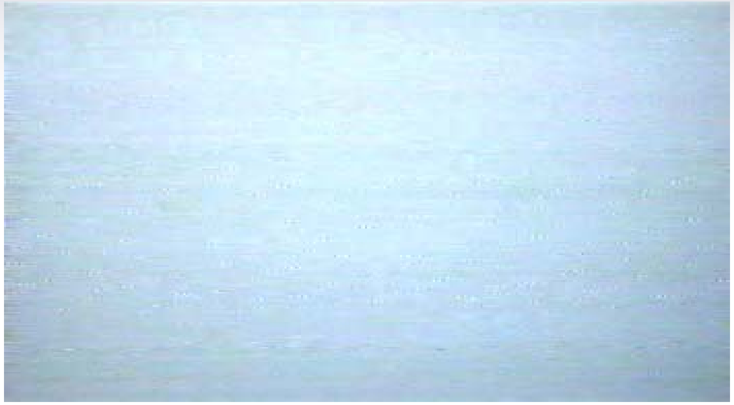

Station 10 flight video camera (Mild Haze)

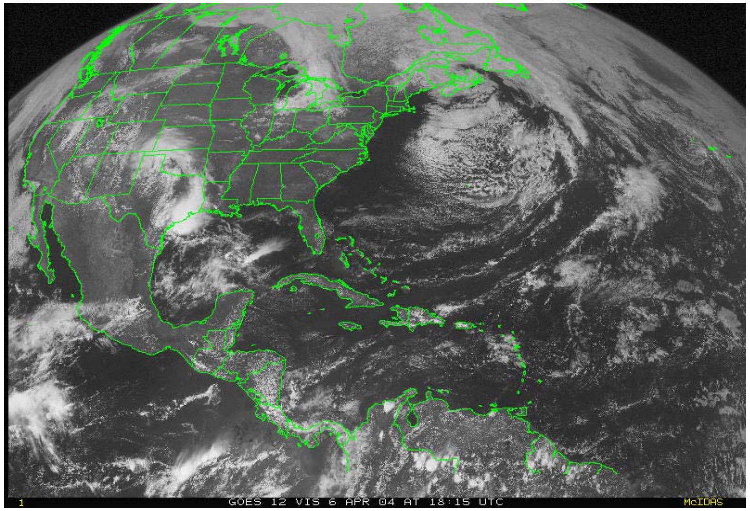

Visible Satellite Image (East Coast)

Surface Image 4/6/04

(Evening, no haze)

Table of Buoy 41002 Data
4/6/04

Environmental Parameter	Buoy Data
Surface air pressure (mbar)	1017.1
Surface air temperature (°C)	16.5
Surface abs. humidity (g/m³)	6.9
Sea surface temperature (°C)	23.7
Surface wind speed (m/s)	5.6

Time Series Plots 37GHz

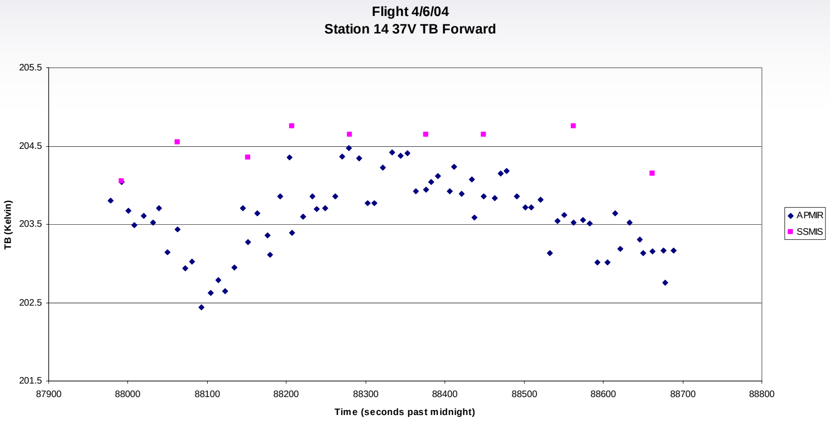

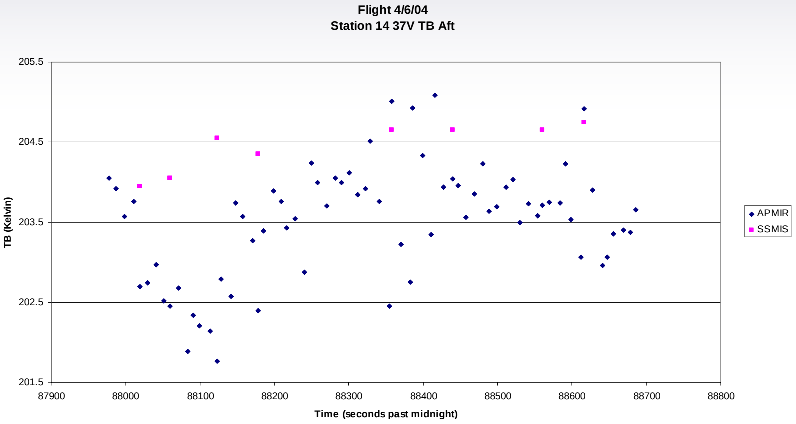

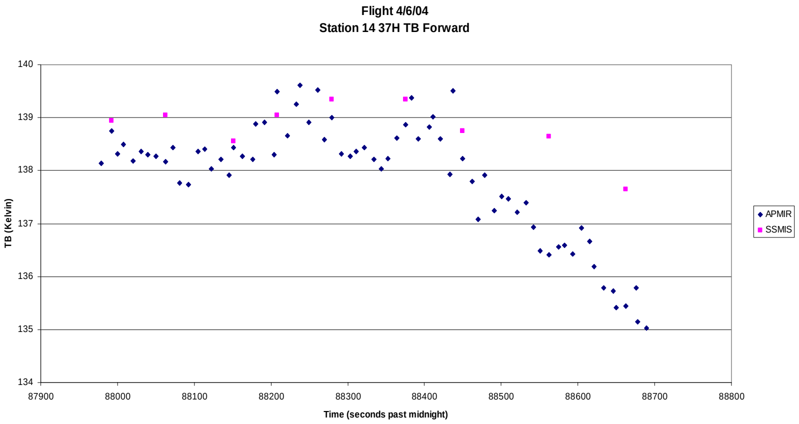

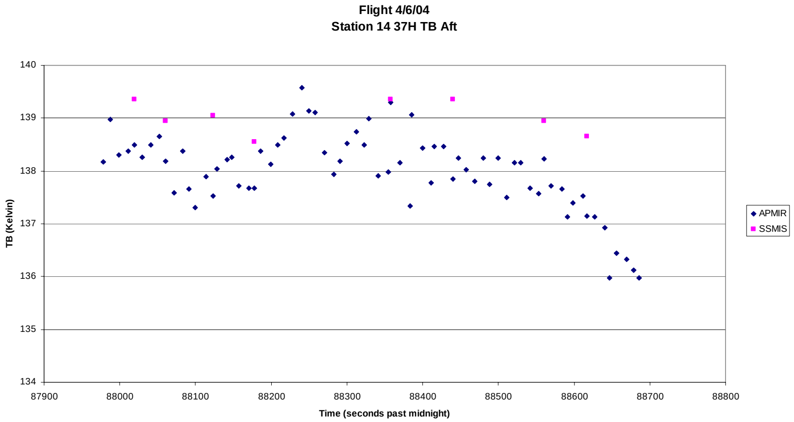

Time Series Plot 22GHz

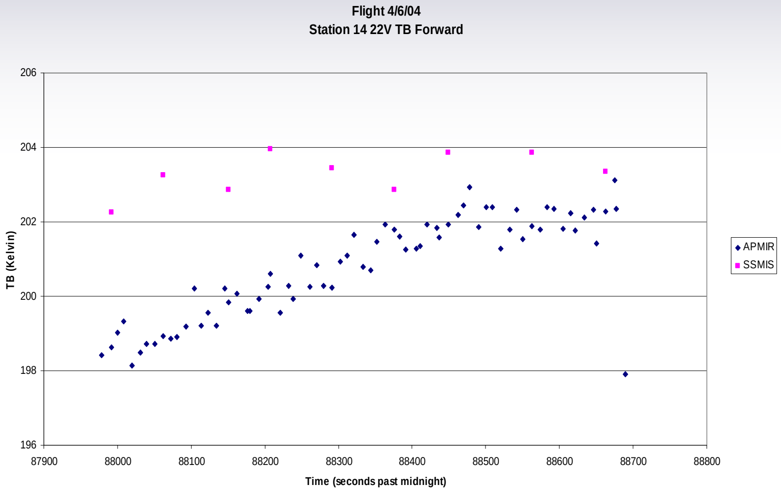

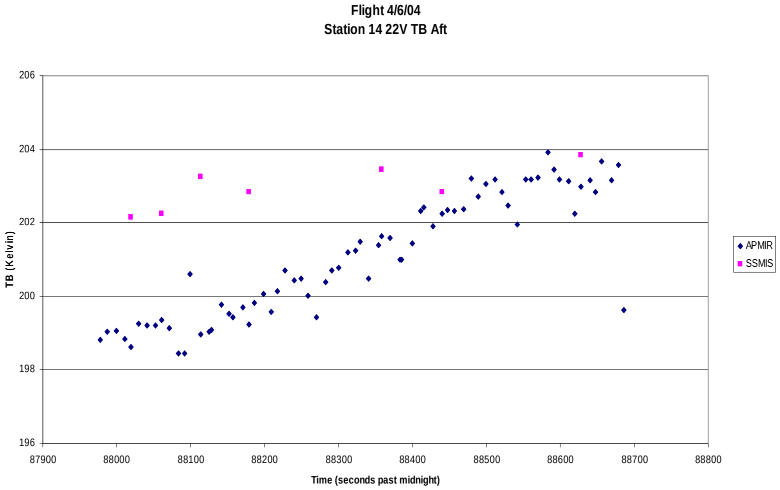

Time Series Plot   19GHz

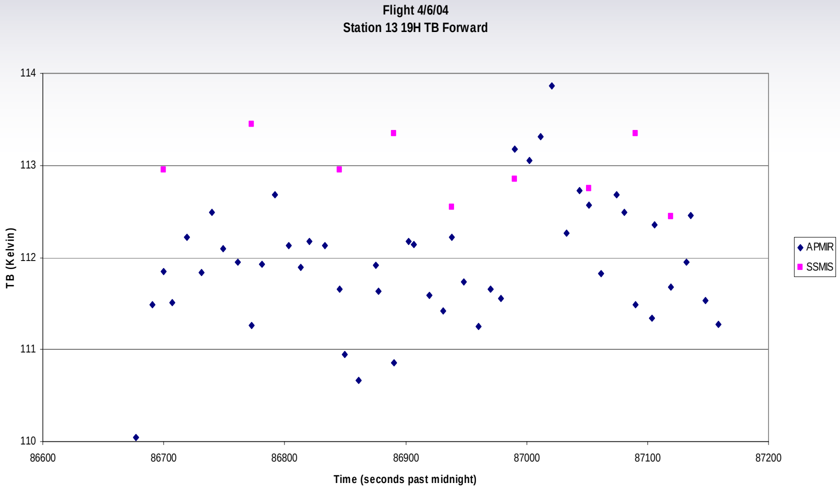
Flight 4/6/04
Station 13 19H TB Forward

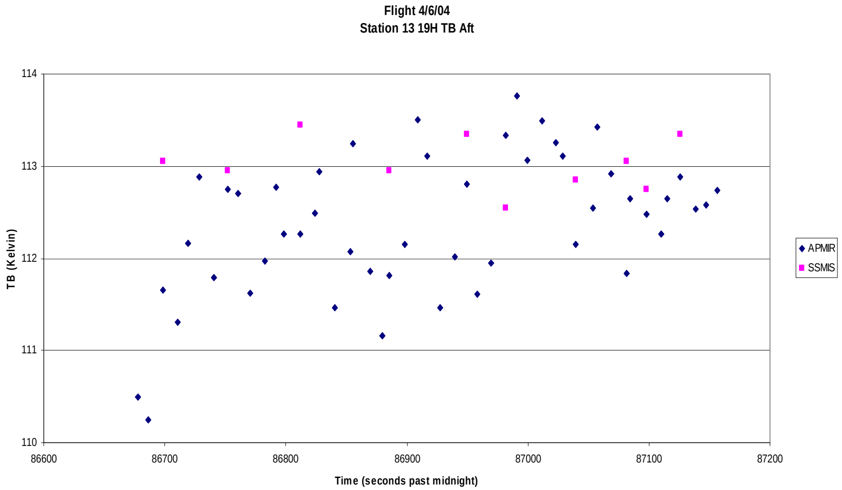
Flight 4/6/04
Station 13 19H TB Aft

8.5 Conclusions

- Excellent agreement between all SSMIS and APMIR channels
- Small bias exists on 22V
- Data trends in APMIR data match those in SSMIS data
- Over 60% of 19V and 37H data comparisons within 1 K
- No major calibration errors present in SSMIS

Acknowledgement

- Air Force (DMSP Program Office)
- Navy-SPAWAR (PMW 155)
- IPO/NPOESS

Special thanks to:

Dr. Stephen Mango

Mr. Ray Godin

Dr. Carrie Root

CDR Eric Gottshall

NRL Flight Support Detachment

F16 SSMIS Calibration/Validation Final Report

Section 7.0 CoSMIR Under-Flight Calibration

J. R. Wang, P. Racette, and J. Piepmeier

THE AEROSPACE CORPORATION

CoSMIR Under-Flights of SSMIS

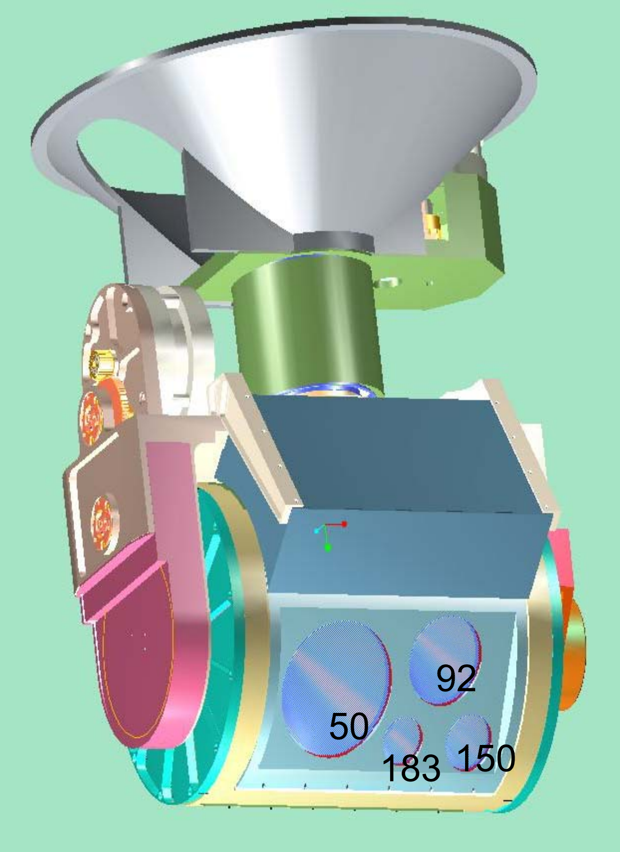

Outline

- CoSMIR Characteristics (Brief)

  - Channel Frequency and Polarization (slide #3)

  - Image Formation (slide #4)

- CoSMIR Calibration

  - Laboratory LN2 Test and Calibration

  - Fights over Lakes and Data Analysis

- CoSMIR Underflights of SSMIS and Inter-comparison

  - Scatter plots of T_b values from each flight

  - Comparison of T_b variations along the ER-2 flight path

- Calculations to Infer Measurements of 3 SSMIS 50 GHz Channels from the Corresponding CoSMIR Data

  - Comparison of calculated and measured T_b's at 50 GHz channels

  - Comparison of calculated and measured T_b's at 92 GHz channels

- Summary

CoSMIR Radiometer Overview

Center Frequency (GHz)	IF Bandwidth (MHz)	Noise Figure (dB)	Sensitivity 100 ms int. (K)
50.3 (H)	400	4.8 (SSB)	0.13
52.8 (H)	400	4.8 (SSB)	0.13
53.6 (H)	400	4.8 (SSB)	0.13
91.655 (V&H)	1000	6.5	0.10
150.0 (H)	1000	10.5	0.30
183.31±1 (H)	500	7.8	0.30
183.31±3 (H)	1000	7.8	0.21
183.31±6.6 (H)	1500	7.8	0.17

CoSMIR Image Formation

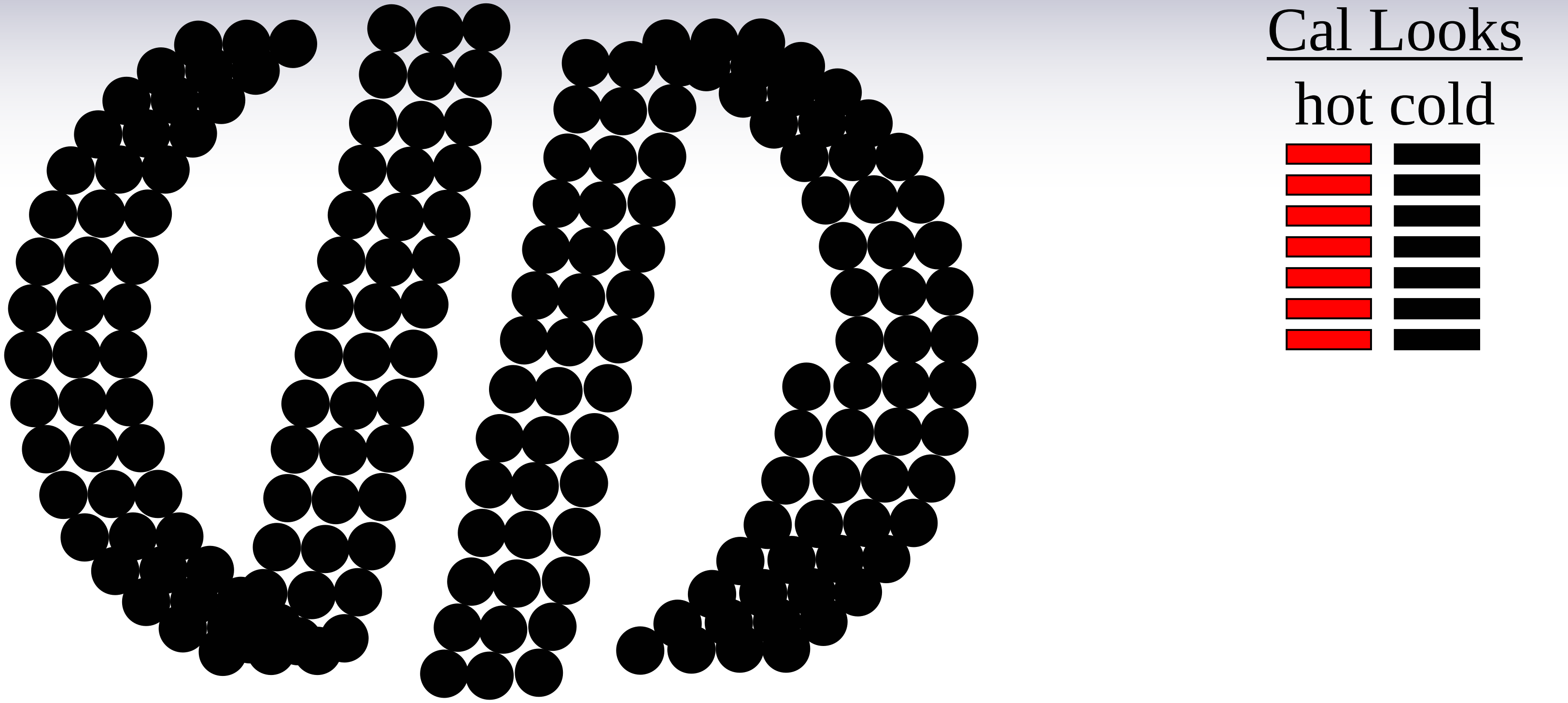

Cal Looks

hot cold

Frequency (GHz)	Surface Spot Size		Integration time per spot (s)		Sensitivity (K)	
	54 degrees	Nadir	Conical	Across Track	Conical	Across Track
50.3	5.0 km x 3.0 km	1.7 km	0.14	0.018	0.11	0.31
91.655	4.0 km x 2.4 km	0.9 km	0.11	0.014	0.10	0.28
150	4.0 km x 2.4 km	0.9 km	0.11	0.014	0.12	0.34
183.31+/- 3	4.0 km x 2.4 km	0.9 km	0.11	0.014	0.20	0.56

CoSMIR Calibration

- Laboratory LN2 Test and Analysis

  - Plots of raw counts from viewing the hot, cold, and LN2 targets at 1-sec intervals (slides #6-8).

  - Conversion to brightness temperature (slide #9).

- Flights over Lake Pyramid and Lake Tahoe

  - Lake Pyramid from flight on March 18, 2004 (slide #10).

  - Lake Tahoe from flights on March 24 and April 1 (slides #11-12).

  - Wind speed and surface temperature from Lake Tahoe during the times of flights (slides #13-14).

- Radiative Transfer Calculations with Tahoe Radiosondes and Comparison with Measurements (slide #15).

  - Calculations based on radiosondes from Lake Tahoe elevation of about 1.8 km, and from ECMQF modeled profiles.

  - Comparison.

- Brief Summary (slide #16)

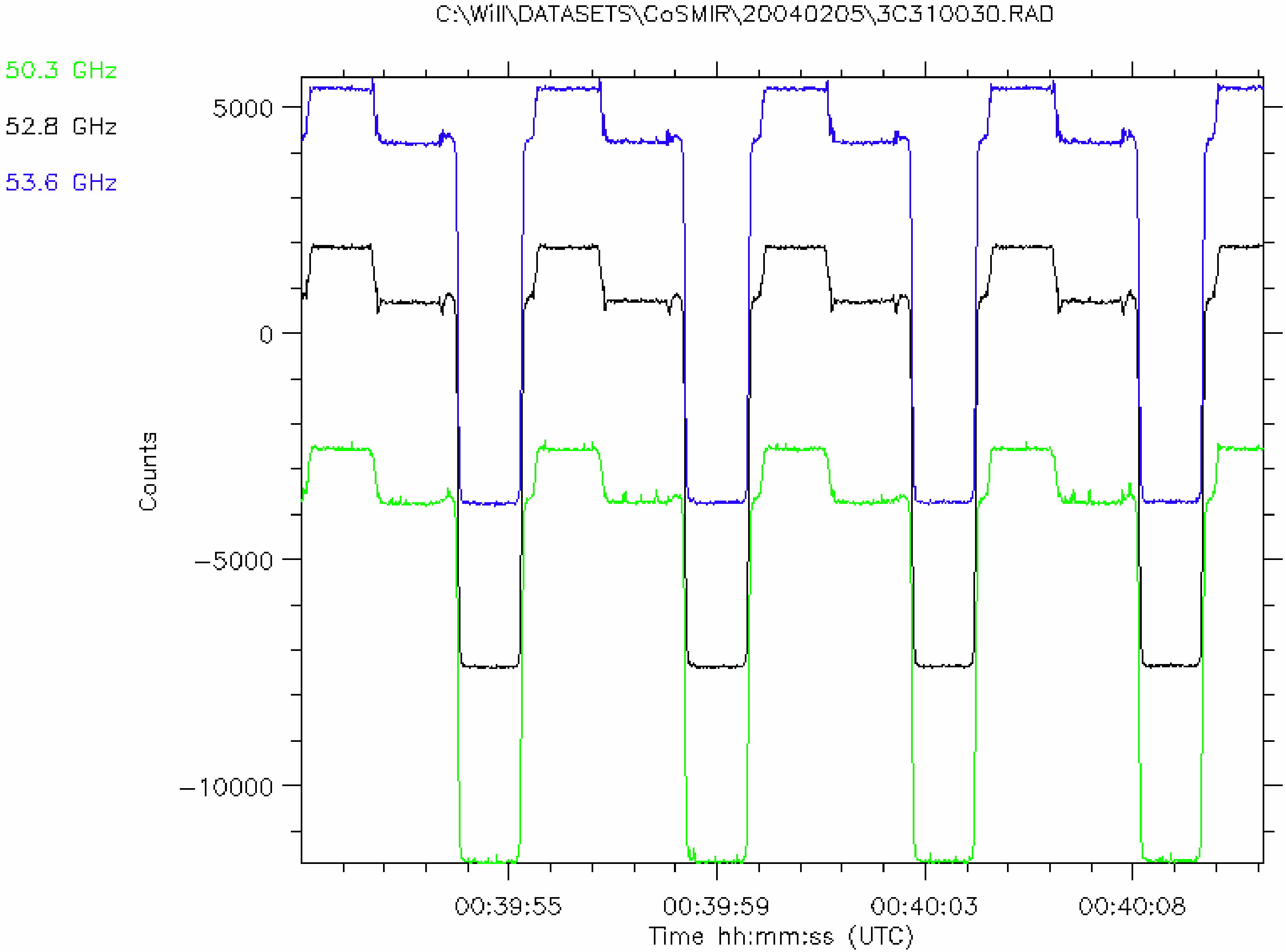
C:\Will\DATASETS\CoSMIR\20040205\3C310030.RAD
50.3 GHz
52.8 GHz
53.6 GHz
Counts
5000
0
−5000
−10000
00:39:55
00:39:59
00:40:03
00:40:08
Time hh:mm:ss (UTC)

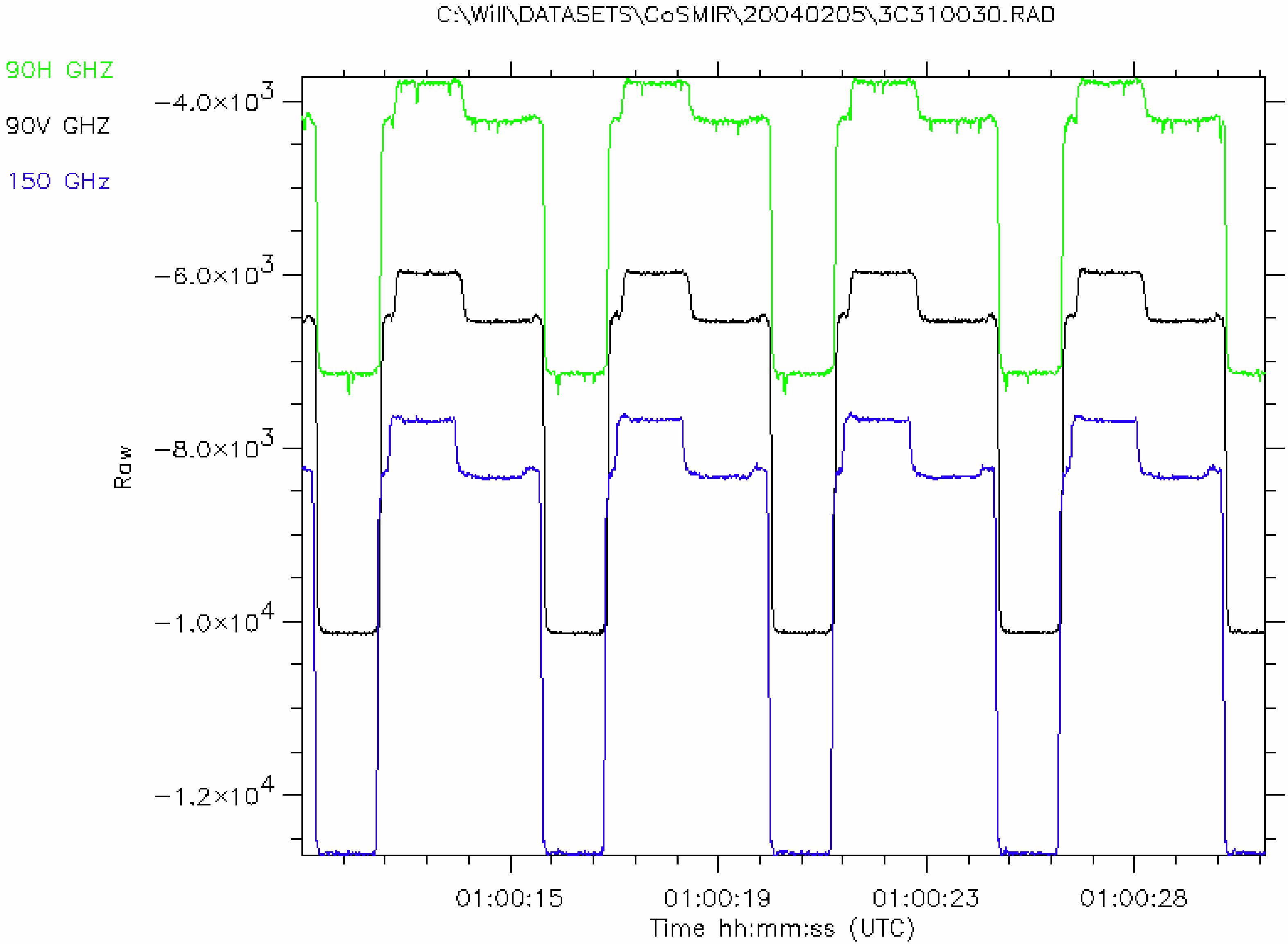
C:\Will\DATASETS\CoSMIR\20040205\3C310030.RAD
90H GHZ
90V GHZ
150 GHz
Raw
−4.0×10^3
−6.0×10^3
−8.0×10^3
−1.0×10^4
−1.2×10^4
01:00:15
01:00:19
01:00:23
01:00:28
Time hh:mm:ss (UTC)

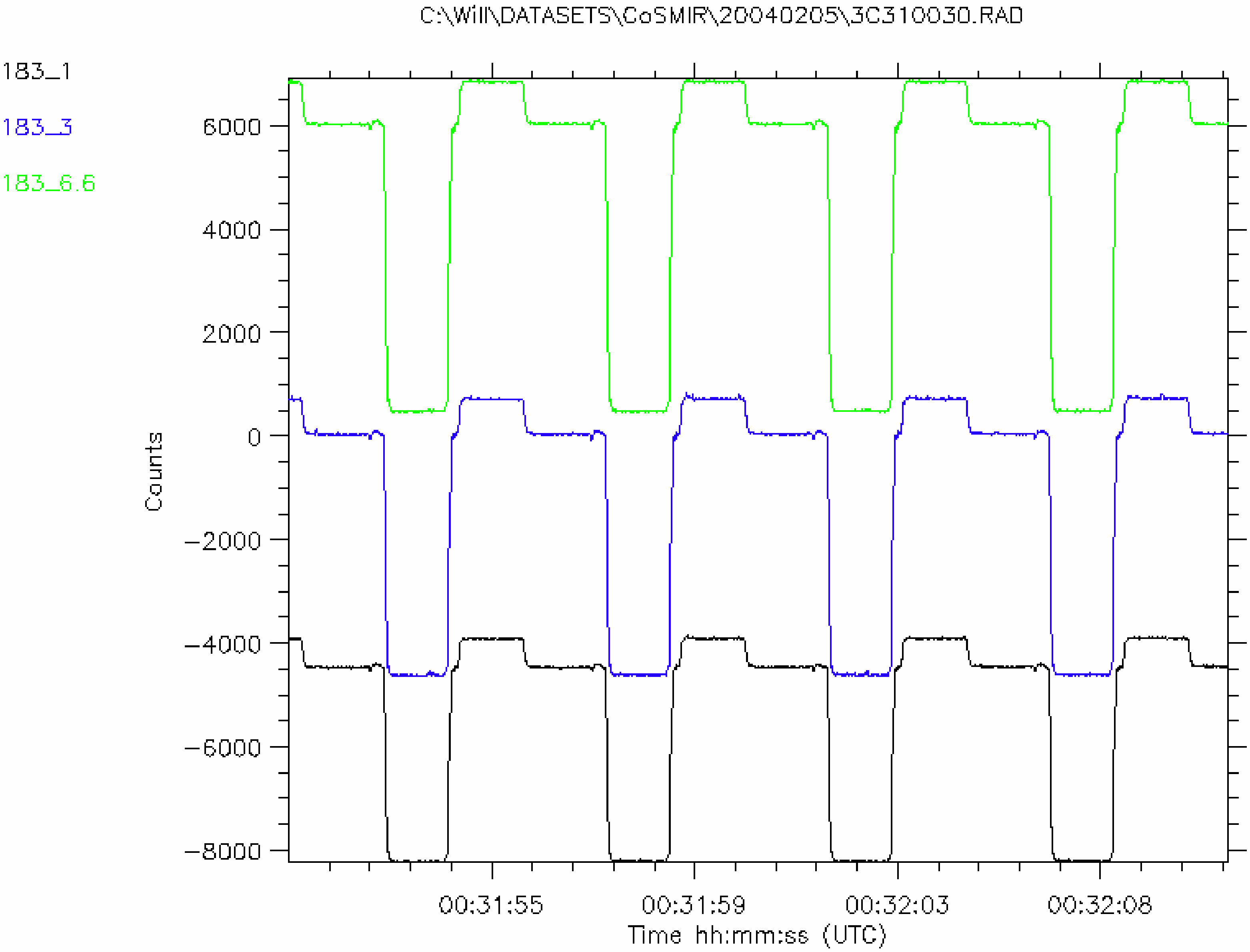
C:\Will\DATASETS\CoSMIR\20040205\3C310030.RAD
183_1
183_3
183_6.6
Counts
6000
4000
2000
0
−2000
−4000
−6000
−8000
00:31:55
00:31:59
00:32:03
00:32:08
Time hh:mm:ss (UTC)

The figure shows a sample result of CoSMIR LN2 calibration in the laboratory environment. The temperatures of the CoSMIR hot and cold calibration targets were maintained at 326 K and 295 K, respectively. The temperature of the LN2 target was monitored and maintained at 78.2±0.5 K. The data points are averages over 5 sec of data samples. The low data points for the 92H GHz channel are caused by noise spikes. Even with large extrapolation in the calibration from calibration target temperatures to LN2 temperature, the measured CoSMIR T_b's are quite close to LN2 temperature.

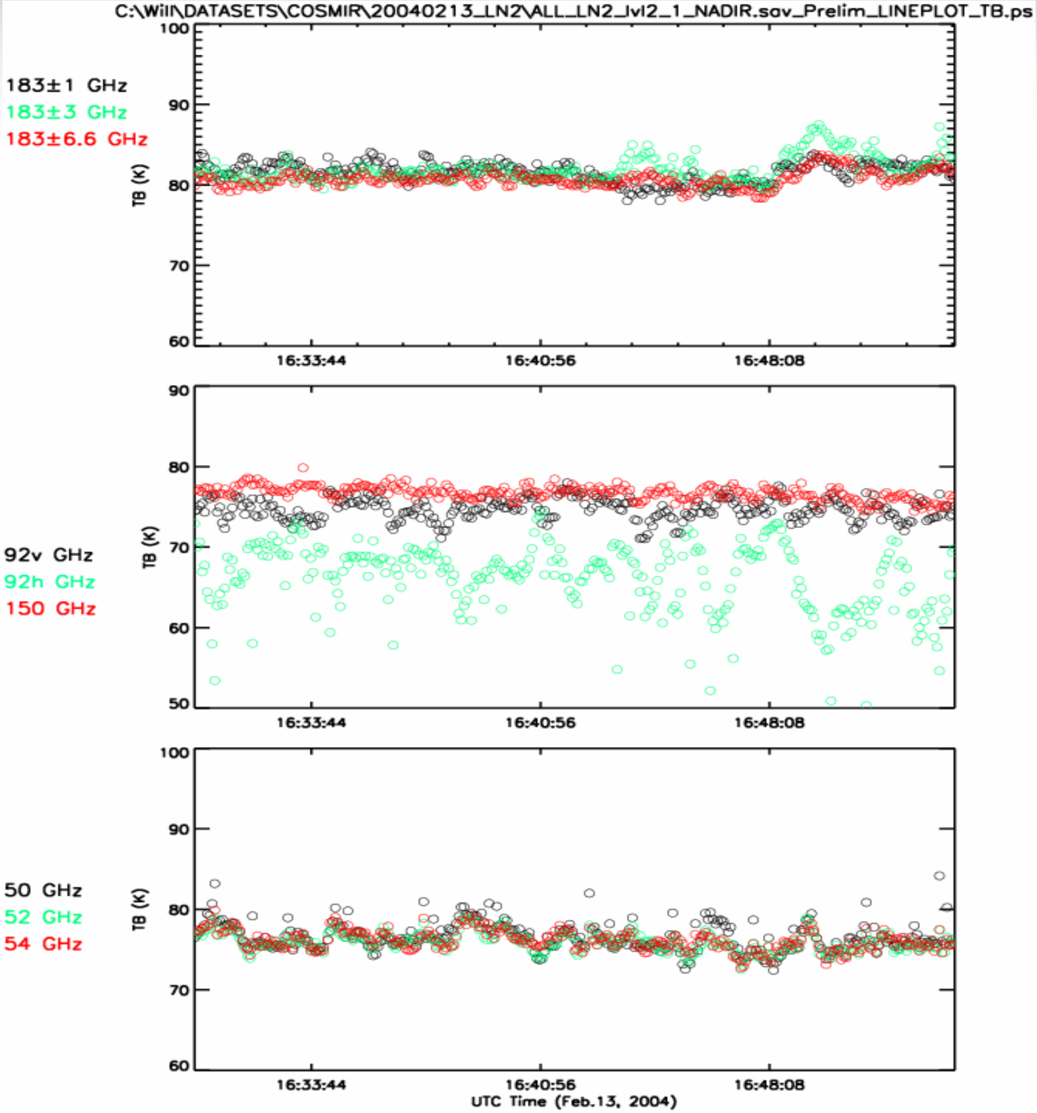

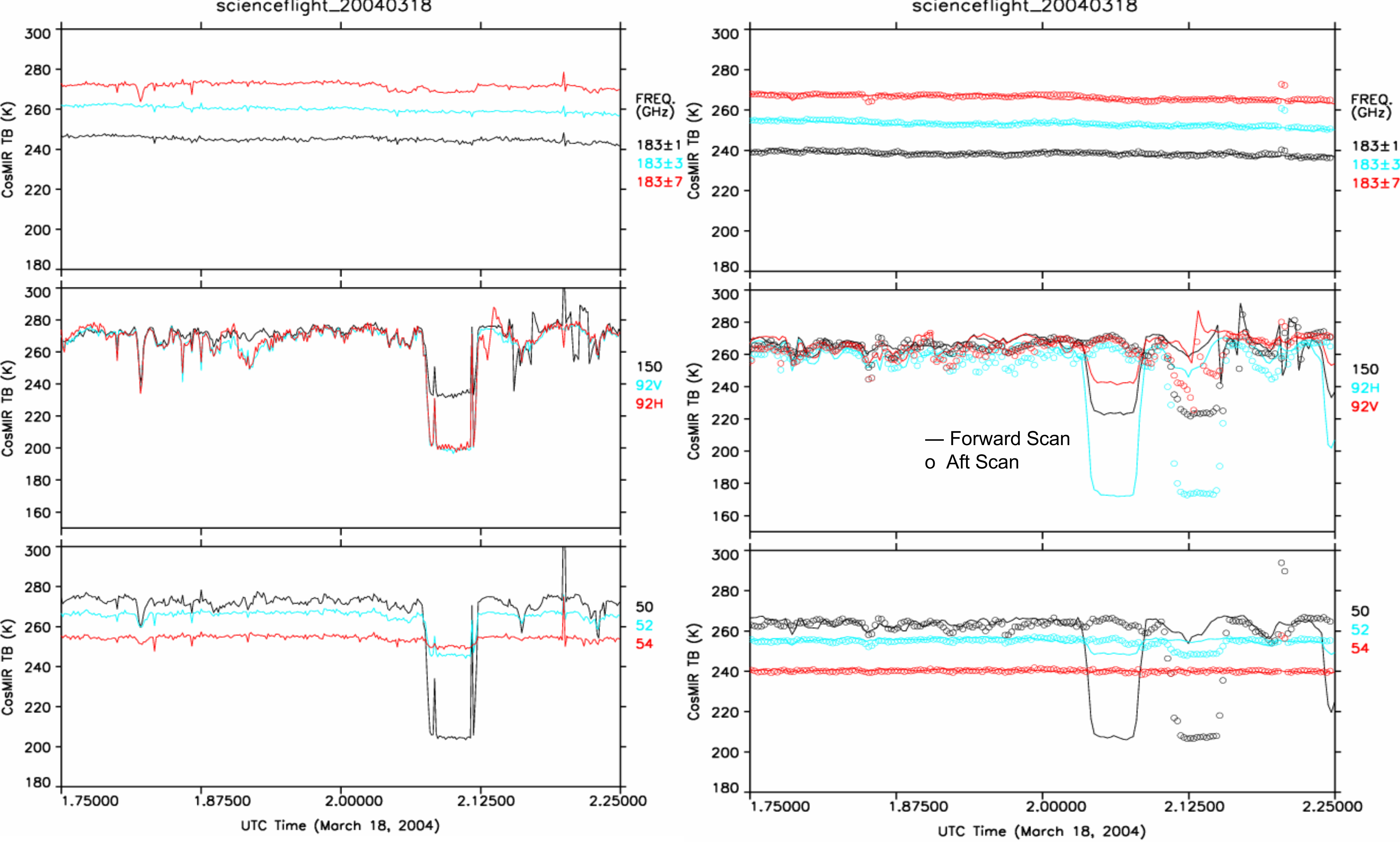

The variations of CoSMIR 9-channel T_b's across Lake Pyramid (Nevada). Data from both forward and aft scans are shown on the right plots, i.e., only the pixels at 0° and 180° azimuthal angles (e.g., along the flight path). The forward and aft Tb's at 92H, 50.3 and 52.8 GHz over the lake agree to within ±1 K; there is a noise spike at 92V channel in the aft scan. Plots on the left give nadir-viewing T_b variations.

Similar plots over Lake Tahoe from flight on 3/24/2004.

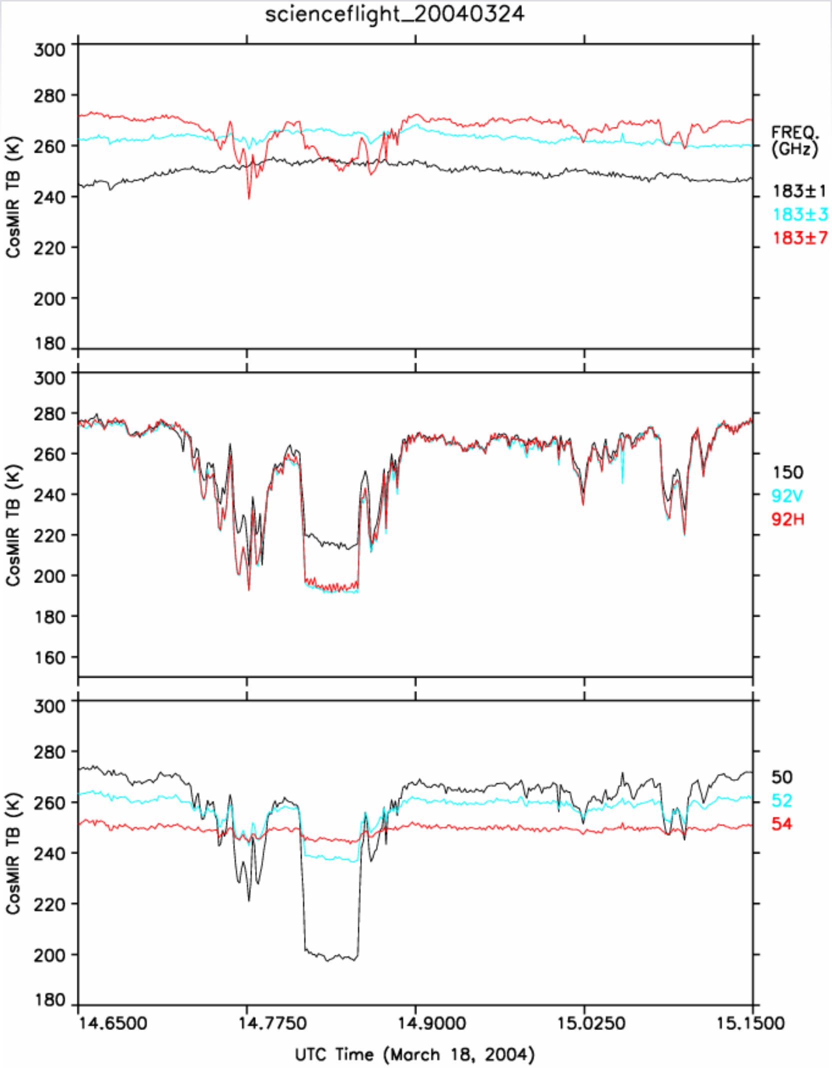

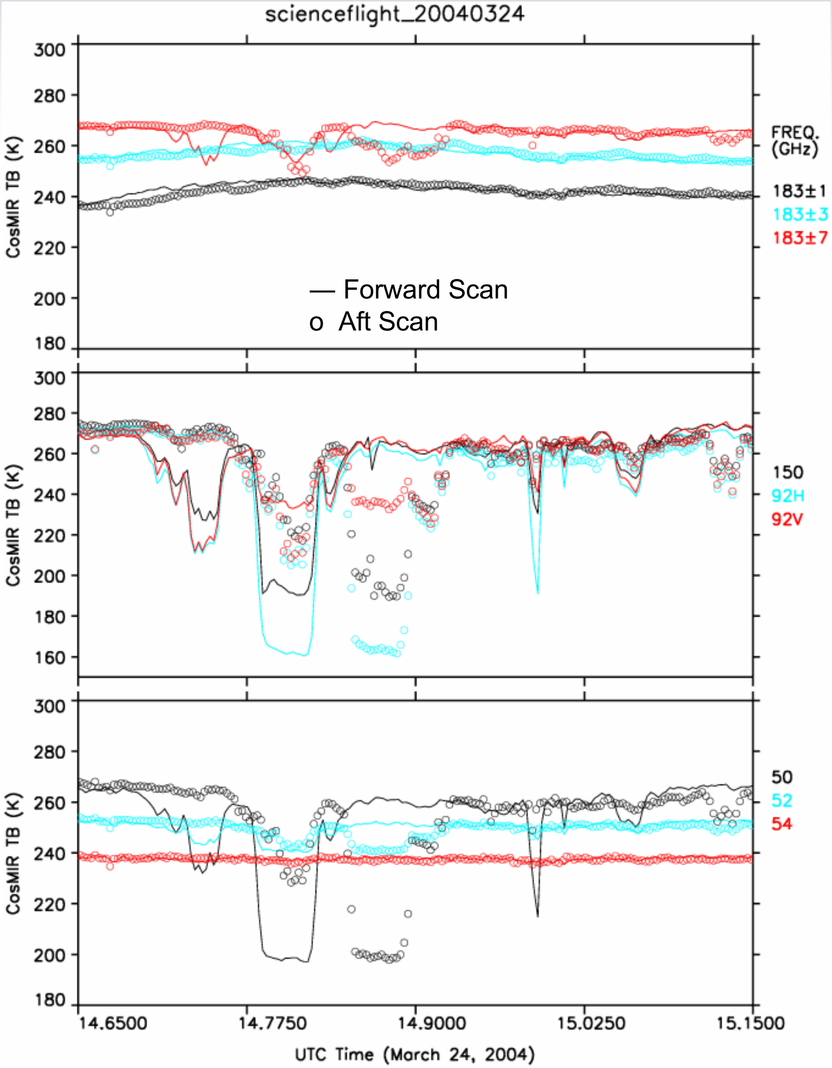

Similar plots over Lake Tahoe from flight on 4/1/2004

— Forward Scan
o Aft Scan

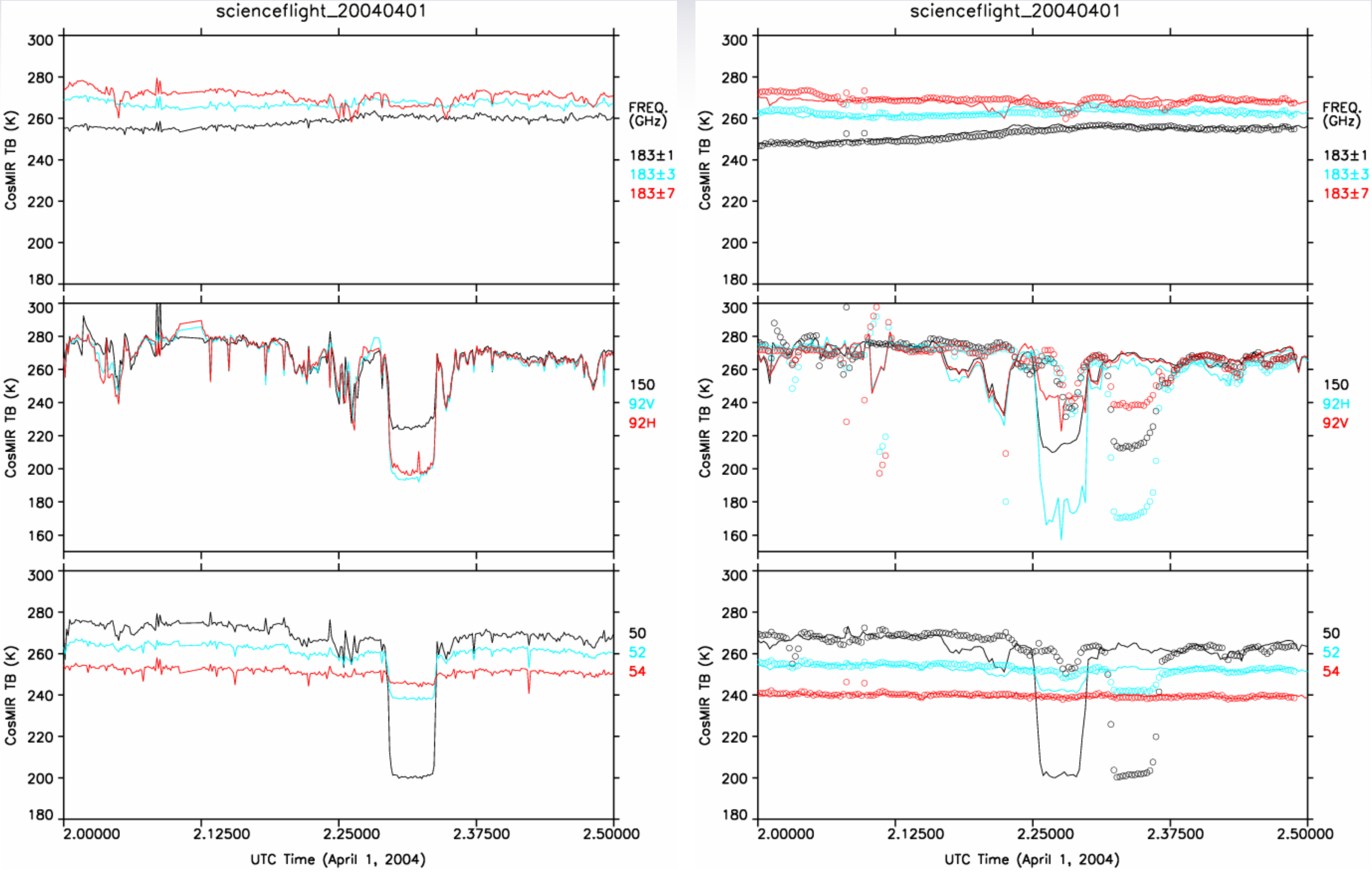

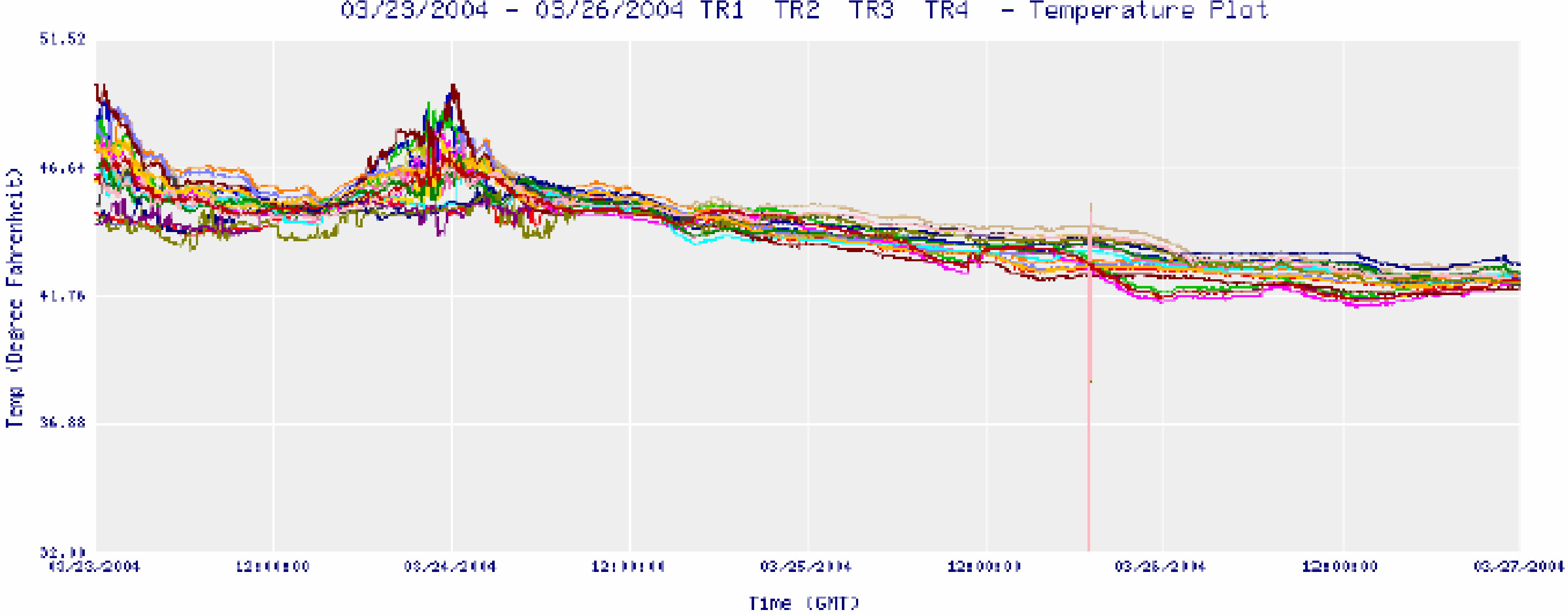
03/23/2004 - 03/26/2004 TR1 TR2 TR3 TR4 - Temperature Plot
Temp (Degree Fahrenheit)
51.52
46.64
41.76
36.88
32.00
03/23/2004
12:00:00
03/24/2004
12:00:00
03/25/2004
12:00:00
03/26/2004
12:00:00
03/27/2004
Time (GMT)

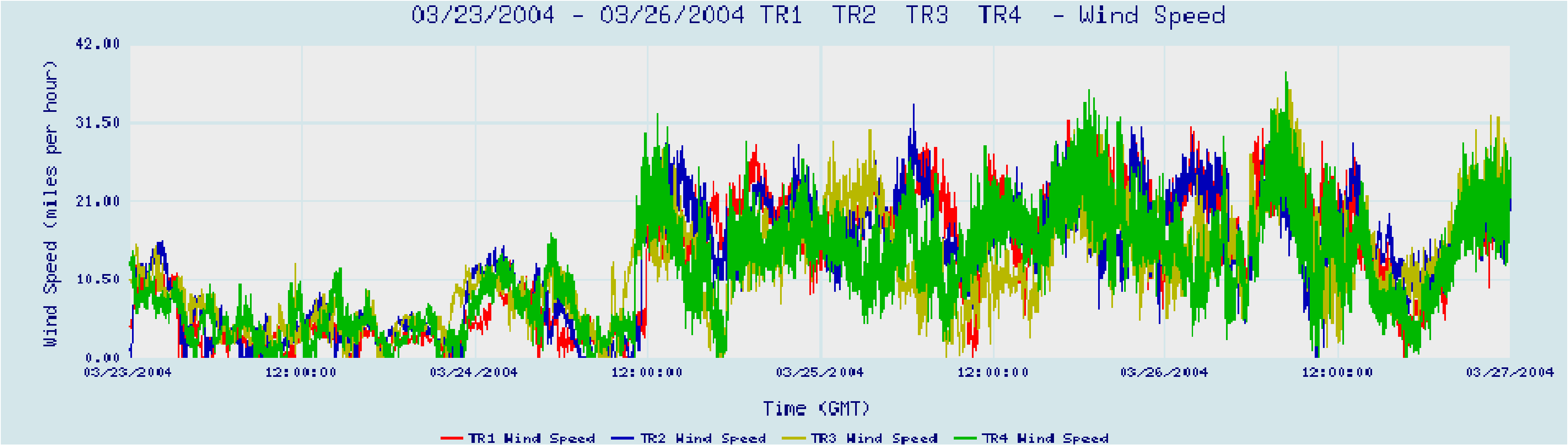
03/23/2004 - 03/26/2004 TR1 TR2 TR3 TR4 - Wind Speed
Wind Speed (miles per hour)
42.00
31.50
21.00
10.50
0.00
03/23/2004
12:00:00
03/24/2004
12:00:00
03/25/2004
12:00:00
03/26/2004
12:00:00
03/27/2004
Time (GMT)
TR1 Wind Speed
TR2 Wind Speed
TR3 Wind Speed
TR4 Wind Speed

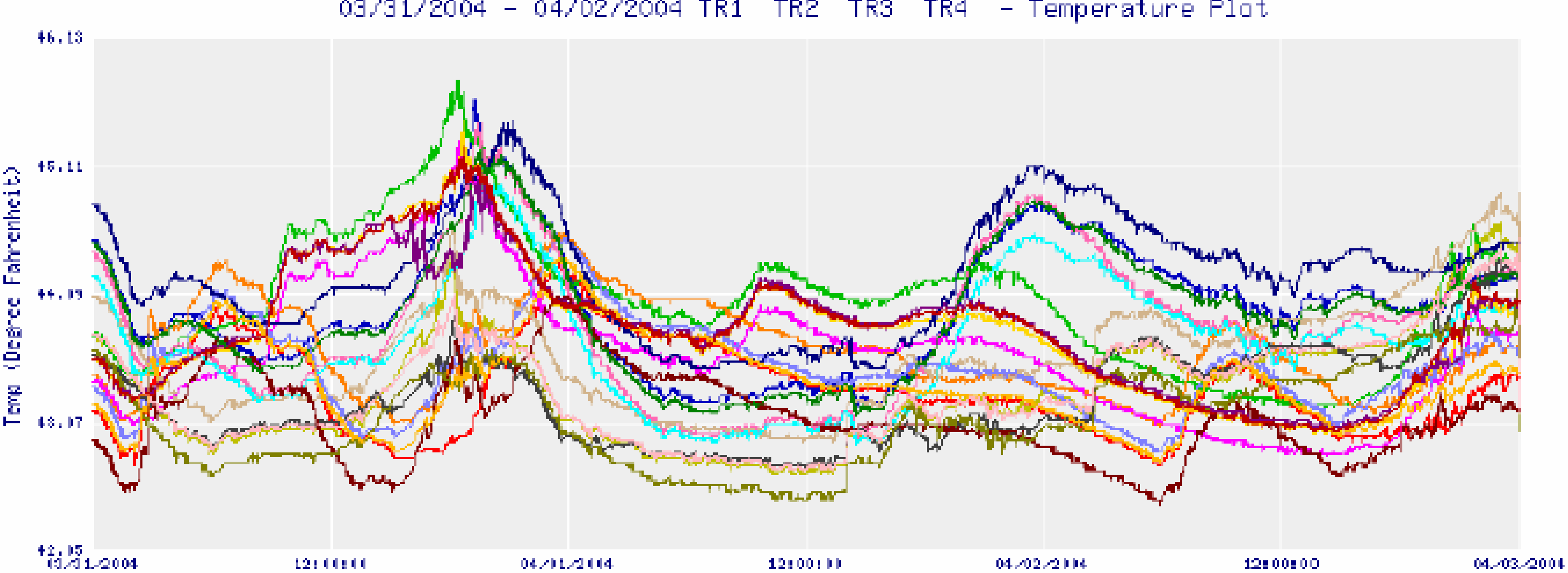
03/31/2004 - 04/02/2004 TR1 TR2 TR3 TR4 - Temperature Plot

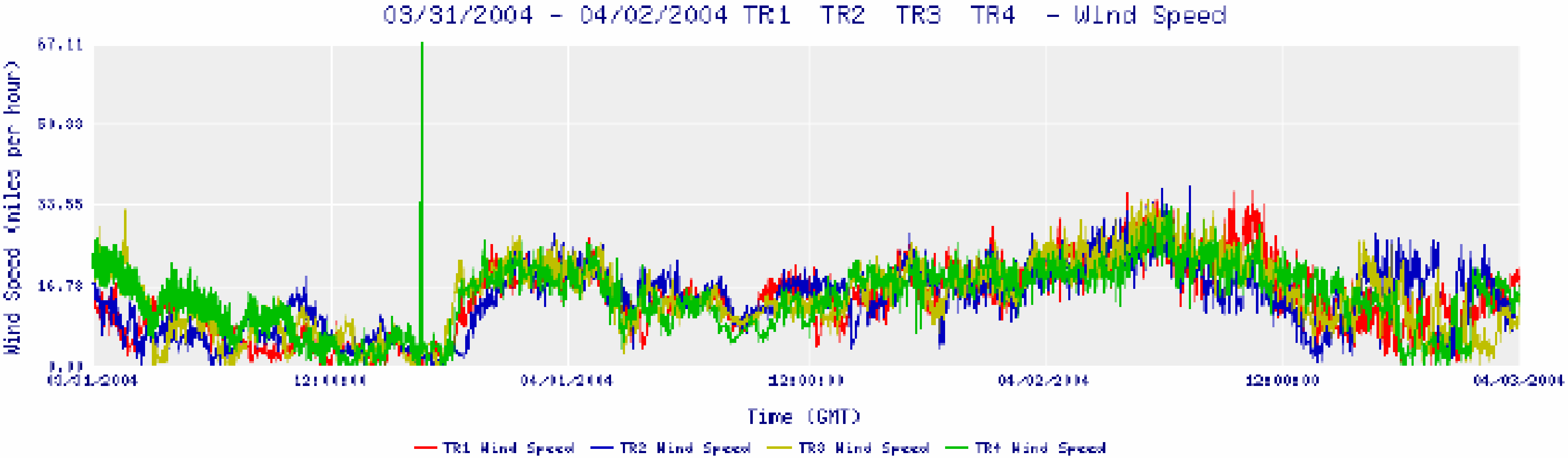
03/31/2004 - 04/02/2004 TR1 TR2 TR3 TR4 - Wind Speed

Incidence angle = 0 degree

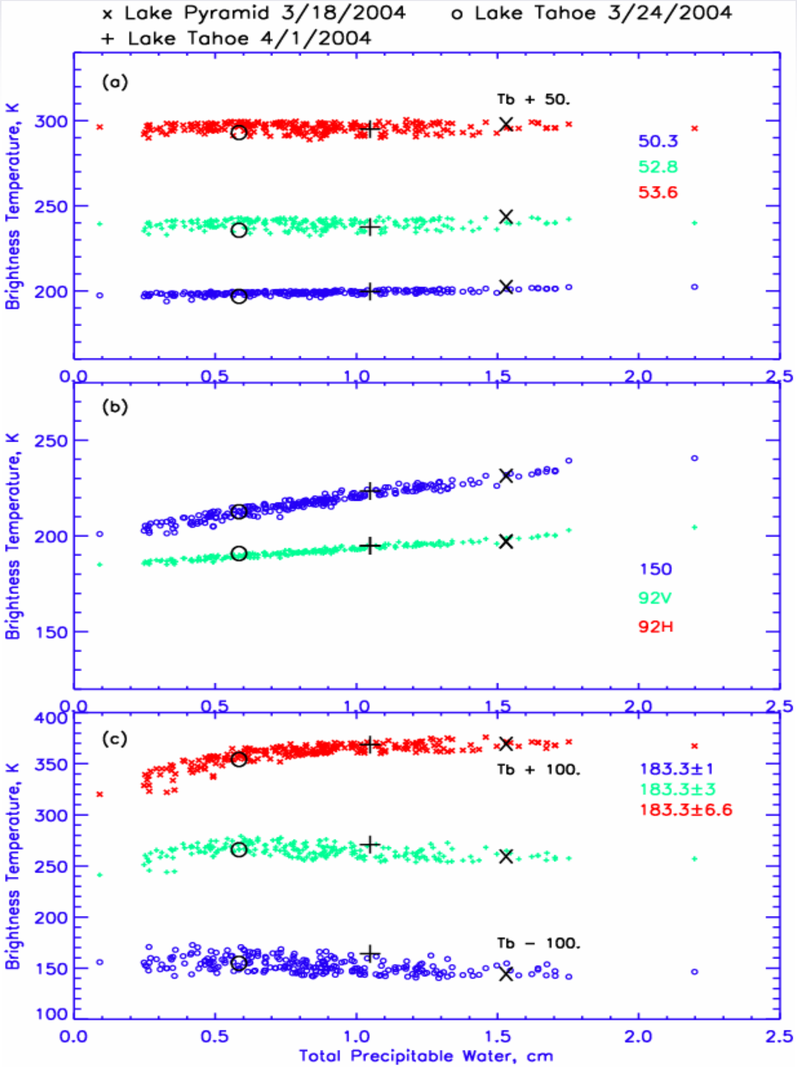

Incidence angle = 53.4 degrees

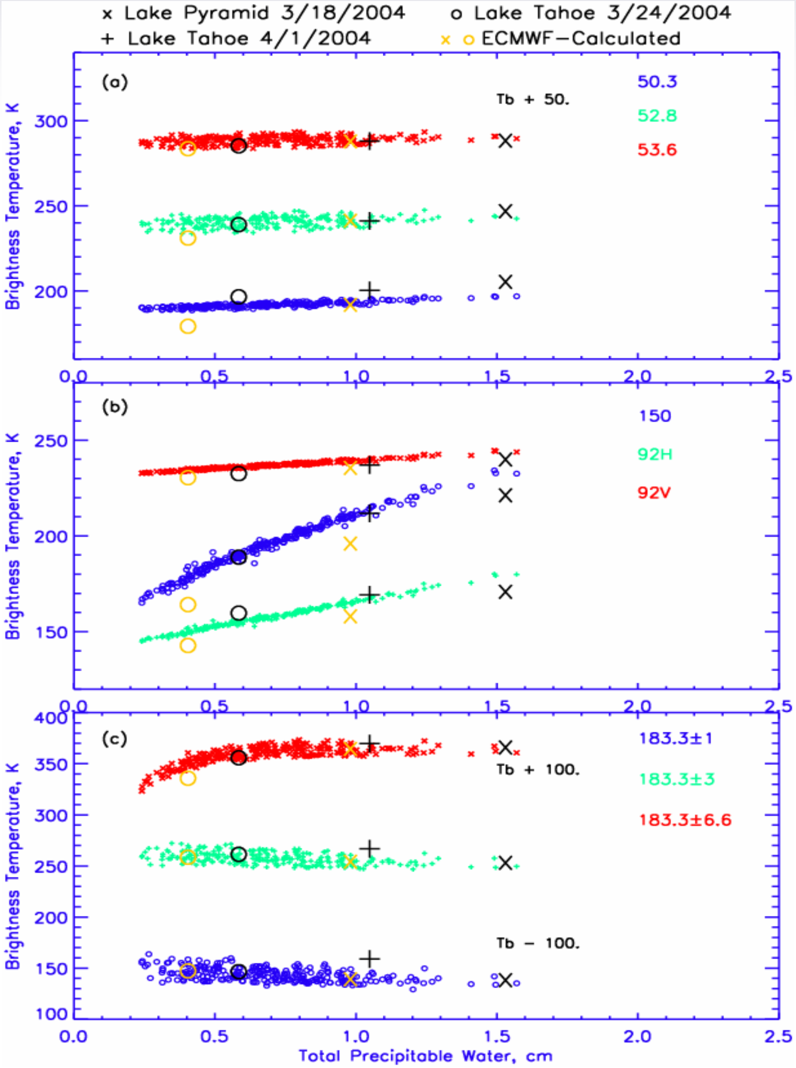

Brief Summary of CoSMIR Calibration

- LN2 Calibration in Laboratory

  - Conducted over 2 hours with LN2 target maintained at 78 K

  - Hot and cold calibration targets maintained at 327 and 295 K, respectively

  - Except the 92H GHz channel (about 8 K lower), the measured LN2 target brightness temperatures are within ± 4 K of 78 K.

- Flights over Lakes Pyramid (Nevada) and Tahoe

  - Hot and cold calibration targets are maintained at 327 K and about 257 K, respectively. The large separation gives a better calibration compared to the laboratory setting.

  - On leveled flights, the brightness temperatures from forward and aft scans agree to within 1 K.

  - Measured brightness temperatures over the lakes, from all 9 channels as a group, are in excellent agreement with calculated results. This suggests that CoSMIR in-flight calibration is very good.

CoSMIR Underflights of SSMIS and Inter-comparison

- CoSMIR flight patterns superimposed on the SSMIS 91.665H GHz brightness temperature maps (slides #18-23).
- A typical quick-look CoSMIR brightness temperature map (slide #24).
- Scatter plots of SSMIS and CoSMIR co-located brightness temperatures (slides #25-30).
- Comparisons of SSMIS and CoSMIR brightness temperatures along the ER-2 aircraft flight path (slides #31-36).
- Tables giving the comparison of average SSMIS and CoSMIR T_b values and their differences (slides #37-41).
- Plots summarizing the measured SSMIS and CoSMIR T_b differences (bias) from all six flights (slide#42).
- Brief summary (slide #43).

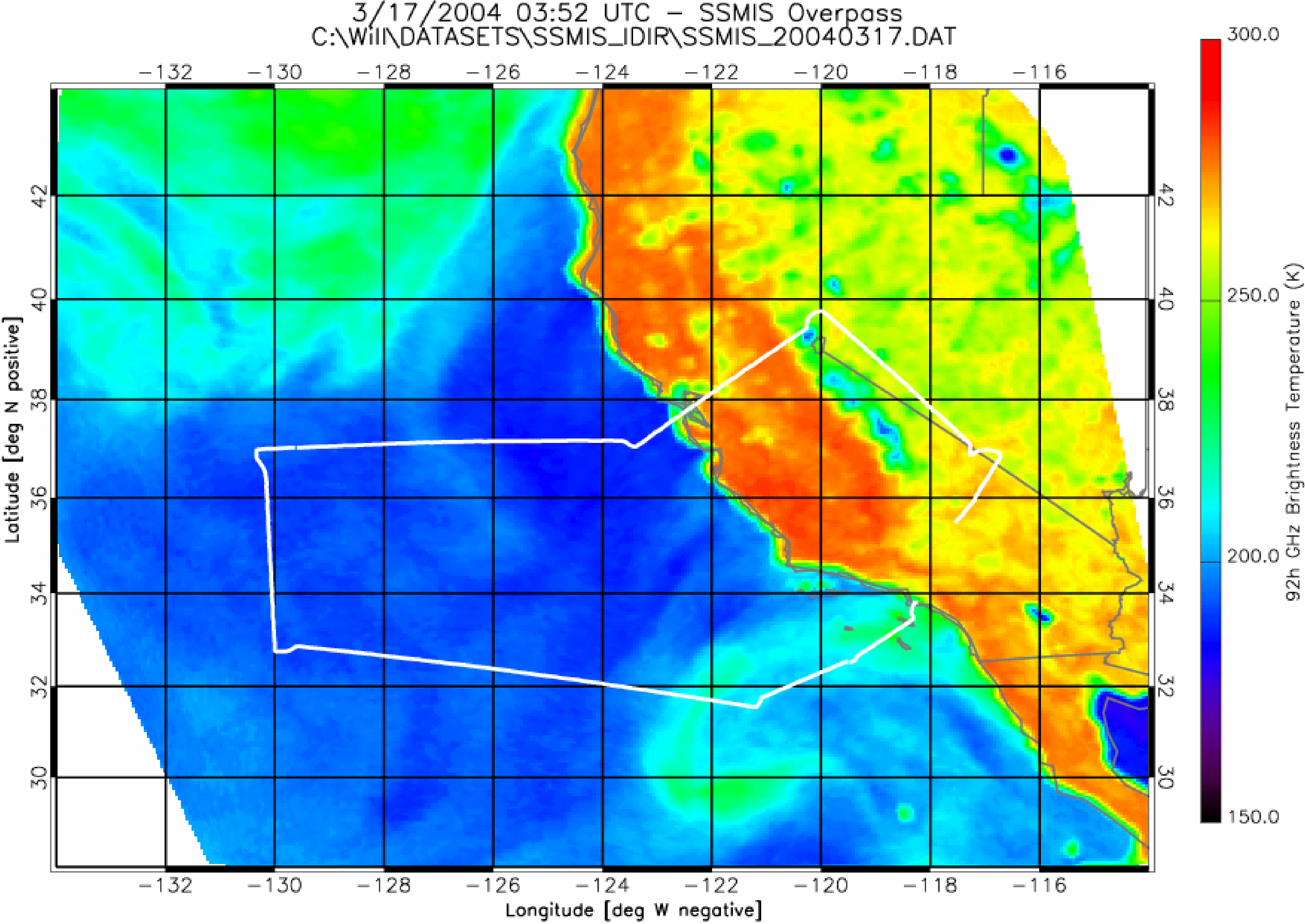
3/17/2004 03:52 UTC – SSMIS Overpass
C:\Will\DATASETS\SSMIS_IDIR\SSMIS_20040317.DAT
−132
−130
−128
−126
−124
−122
−120
−118
−116
42
40
38
36
34
32
30
Latitude [deg N positive]
Longitude [deg W negative]
300.0
250.0
200.0
150.0
92h GHz Brightness Temperature (K)

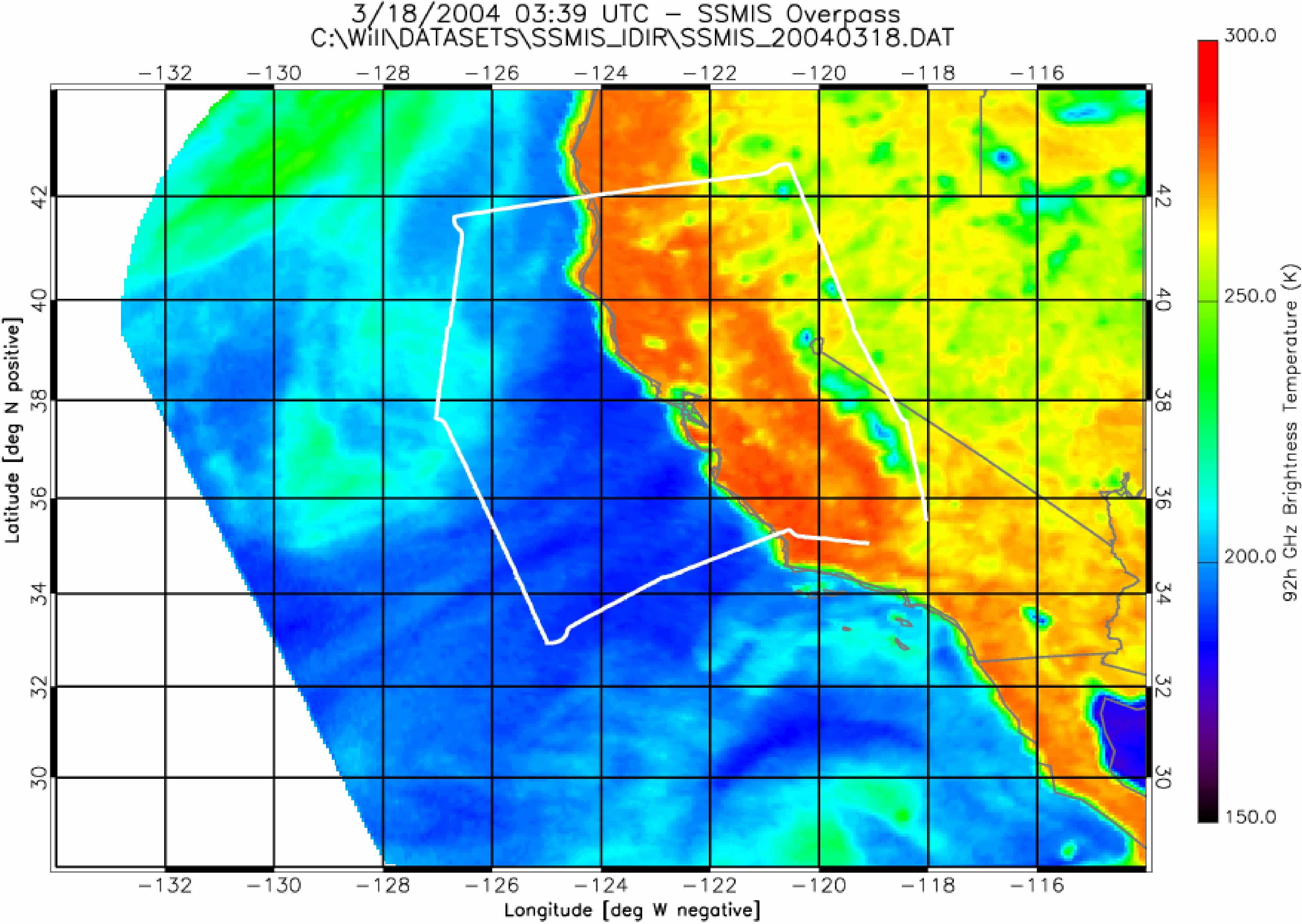
3/18/2004 03:39 UTC – SSMIS Overpass
C:\Will\DATASETS\SSMIS_IDIR\SSMIS_20040318.DAT
−132
−130
−128
−126
−124
−122
−120
−118
−116
42
40
38
36
34
32
30
Latitude [deg N positive]
Longitude [deg W negative]
300.0
250.0
200.0
150.0
92h GHz Brightness Temperature (K)

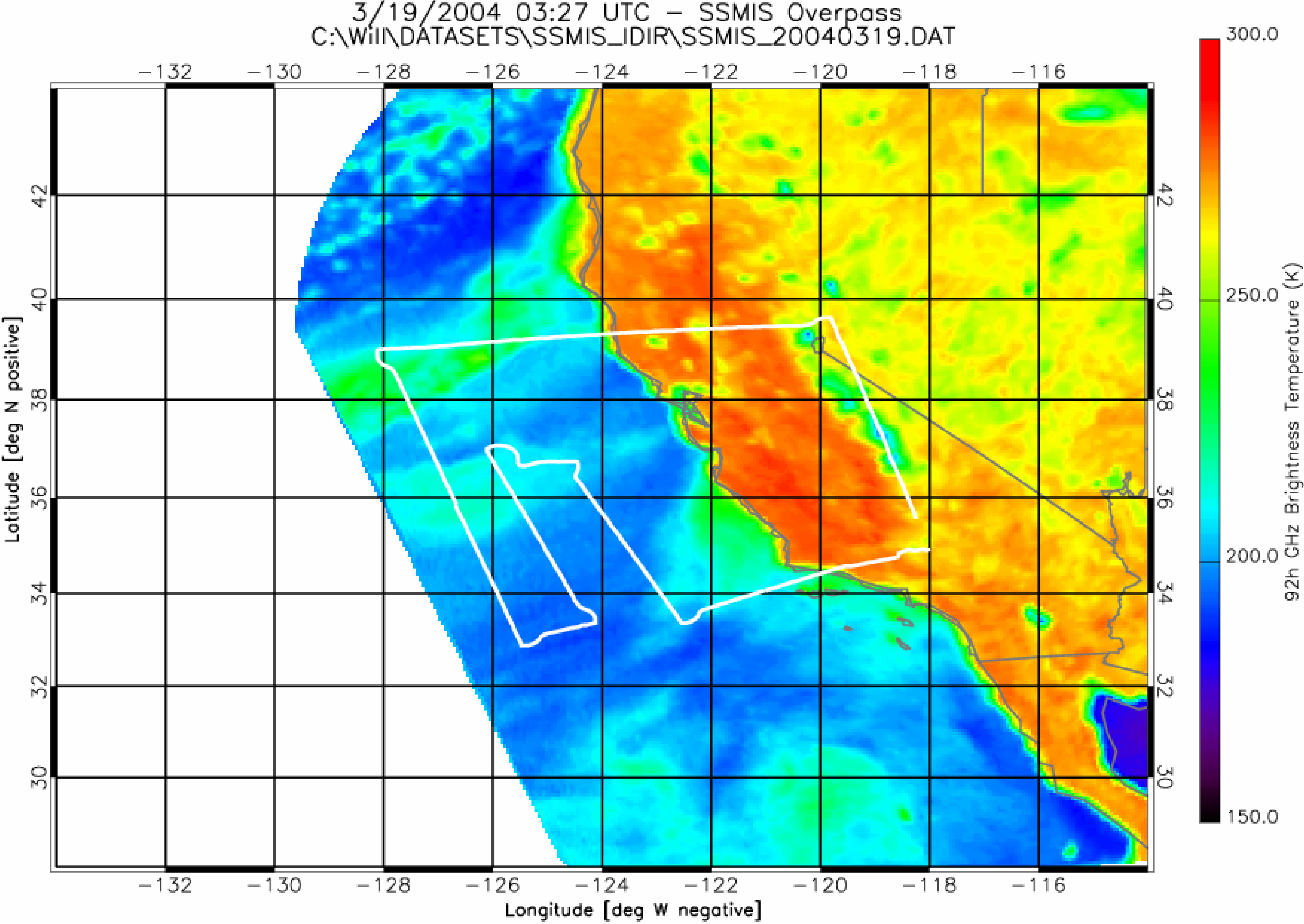
3/19/2004 03:27 UTC – SSMIS Overpass
C:\Will\DATASETS\SSMIS_IDIR\SSMIS_20040319.DAT
−132
−130
−128
−126
−124
−122
−120
−118
−116
42
40
38
36
34
32
30
Latitude [deg N positive]
Longitude [deg W negative]
300.0
250.0
200.0
150.0
92h GHz Brightness Temperature (K)

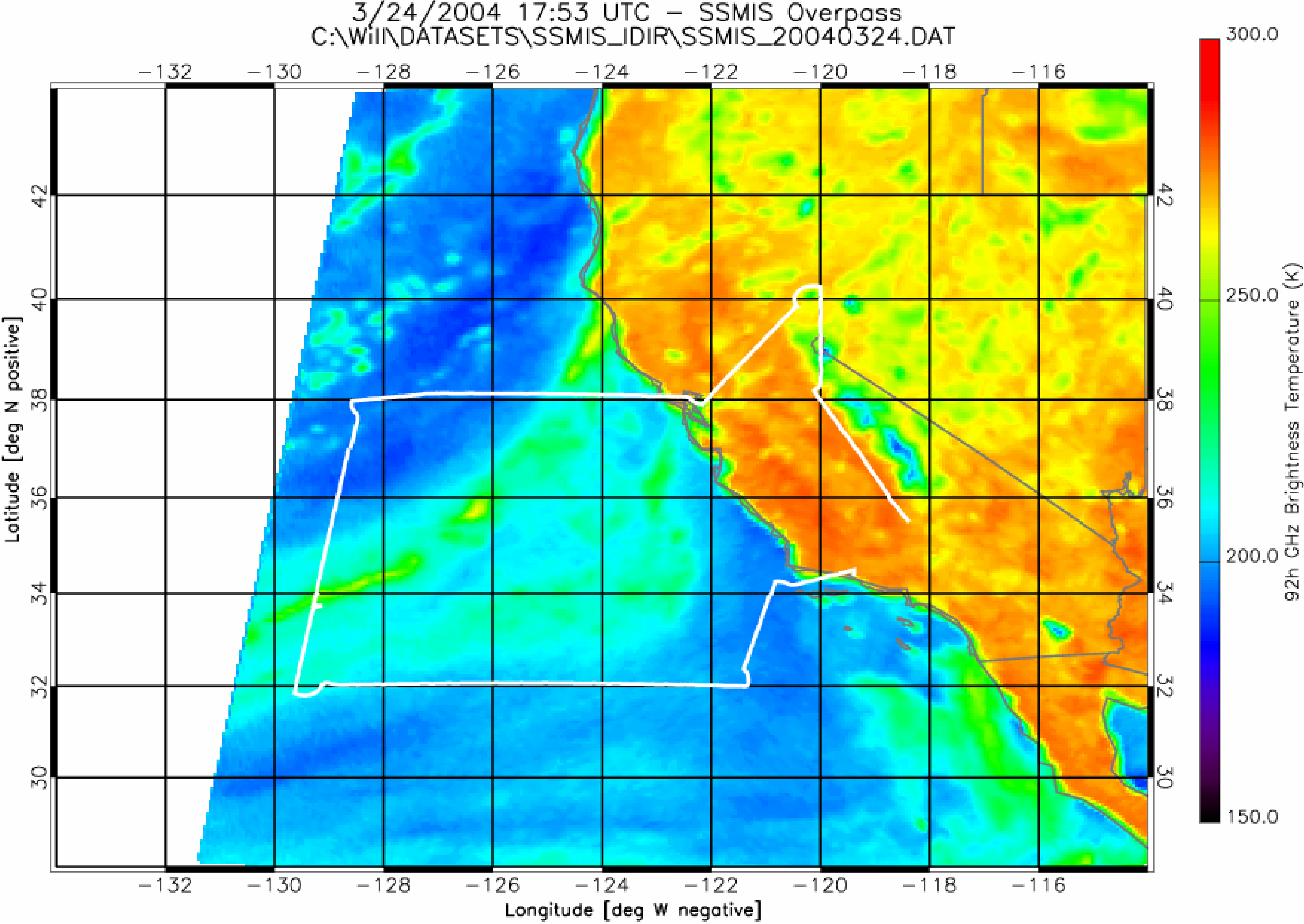
3/24/2004 17:53 UTC – SSMIS Overpass
C:\Will\DATASETS\SSMIS_IDIR\SSMIS_20040324.DAT
−132
−130
−128
−126
−124
−122
−120
−118
−116
42
40
38
36
34
32
30
Latitude [deg N positive]
Longitude [deg W negative]
300.0
250.0
200.0
150.0
92h GHz Brightness Temperature (K)

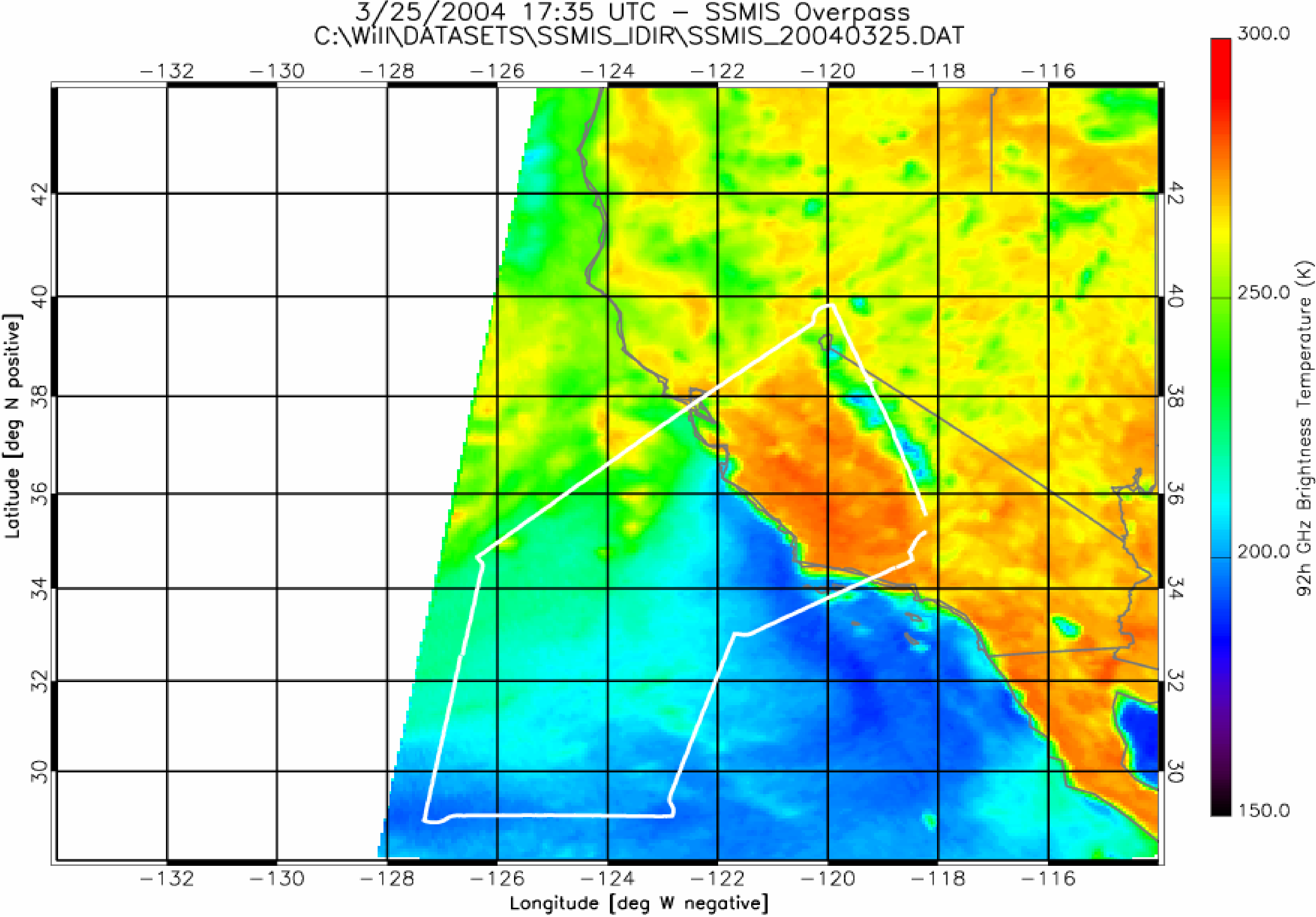
3/25/2004 17:35 UTC – SSMIS Overpass
C:\Will\DATASETS\SSMIS_IDIR\SSMIS_20040325.DAT
−132
−130
−128
−126
−124
−122
−120
−118
−116
42
40
38
36
34
32
30
Latitude [deg N positive]
Longitude [deg W negative]
300.0
250.0
200.0
150.0
92h GHz Brightness Temperature (K)

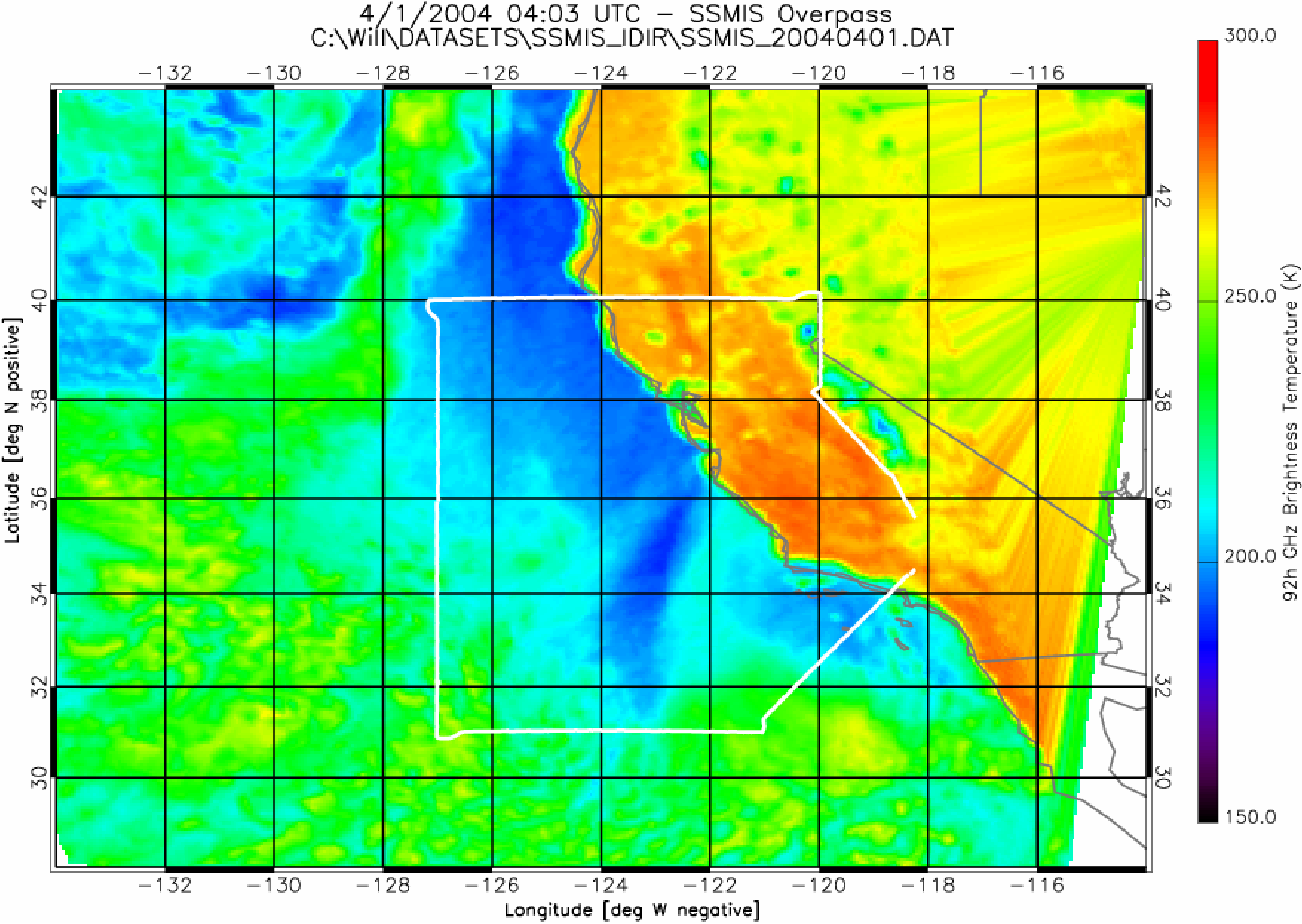
4/1/2004 04:03 UTC – SSMIS Overpass
C:\Will\DATASETS\SSMIS_IDIR\SSMIS_20040401.DAT
−132
−130
−128
−126
−124
−122
−120
−118
−116
42
40
38
36
34
32
30
Latitude [deg N positive]
Longitude [deg W negative]
300.0
250.0
200.0
150.0
92h GHz Brightness Temperature (K)

An example of CoSMIR 9-channel brightness temperature images (not geolocated, and the times are off). The middle portion of the images is the San Francisco Bay area. Some stripes in the images are noise, and the others (smoother ones) are times when the aircraft making turns.

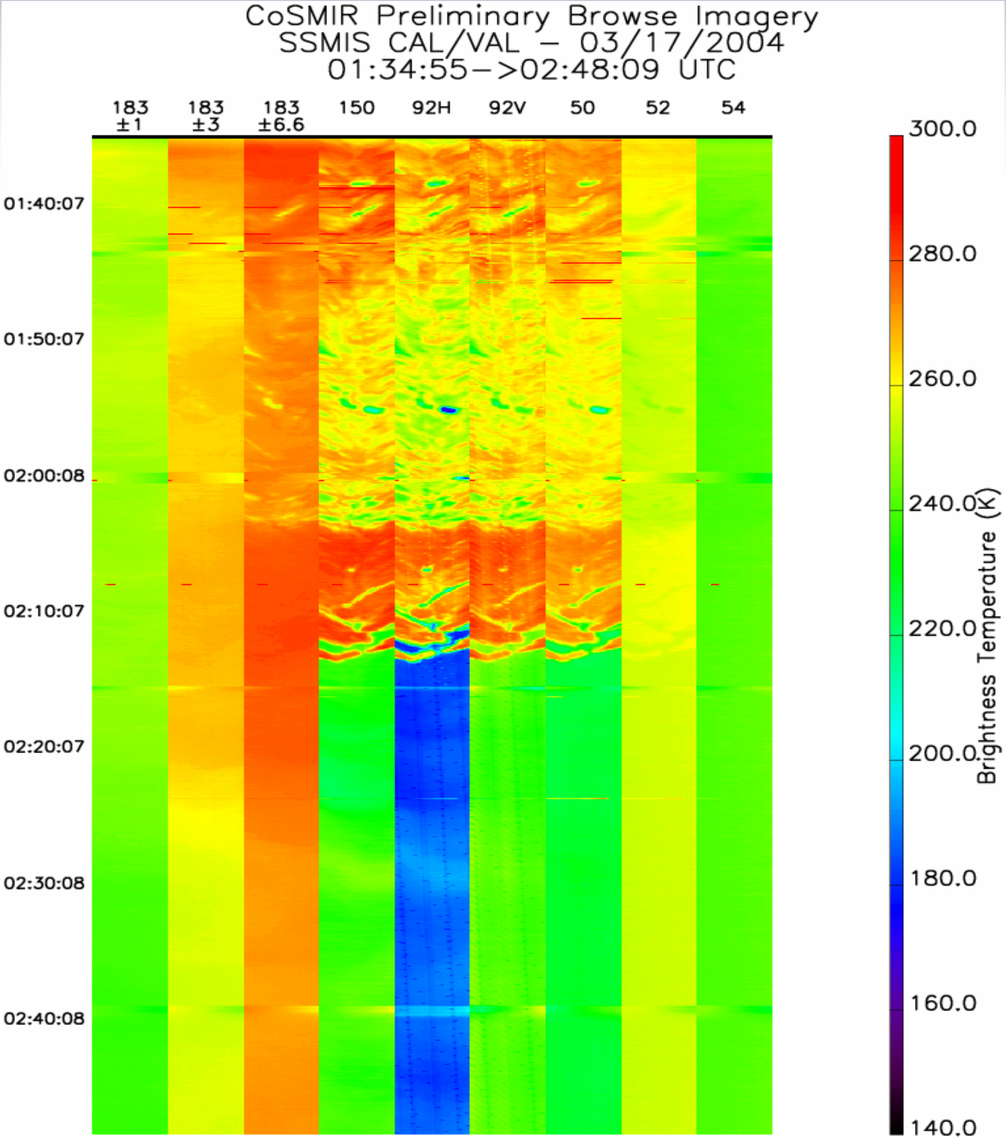

The figure shows a scatter plot of the CoSMIR (left-forward scans, right-aft scans) and SSMIS measured T_b's on 3/17/2004. The two groups of data points at 50.3 GHz in the top plot are over land (high T_b's) and ocean (low T_b's). Some of the outliers in the middle plot are caused by noise spikes of the CoSMIR (especially the 92H channel).

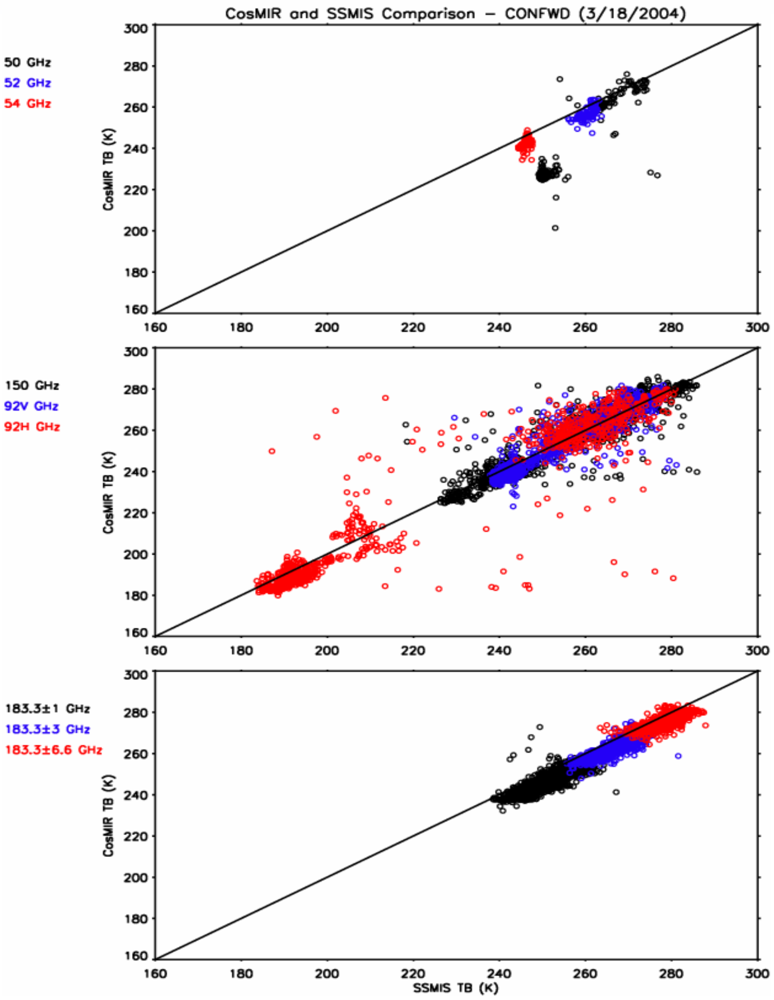

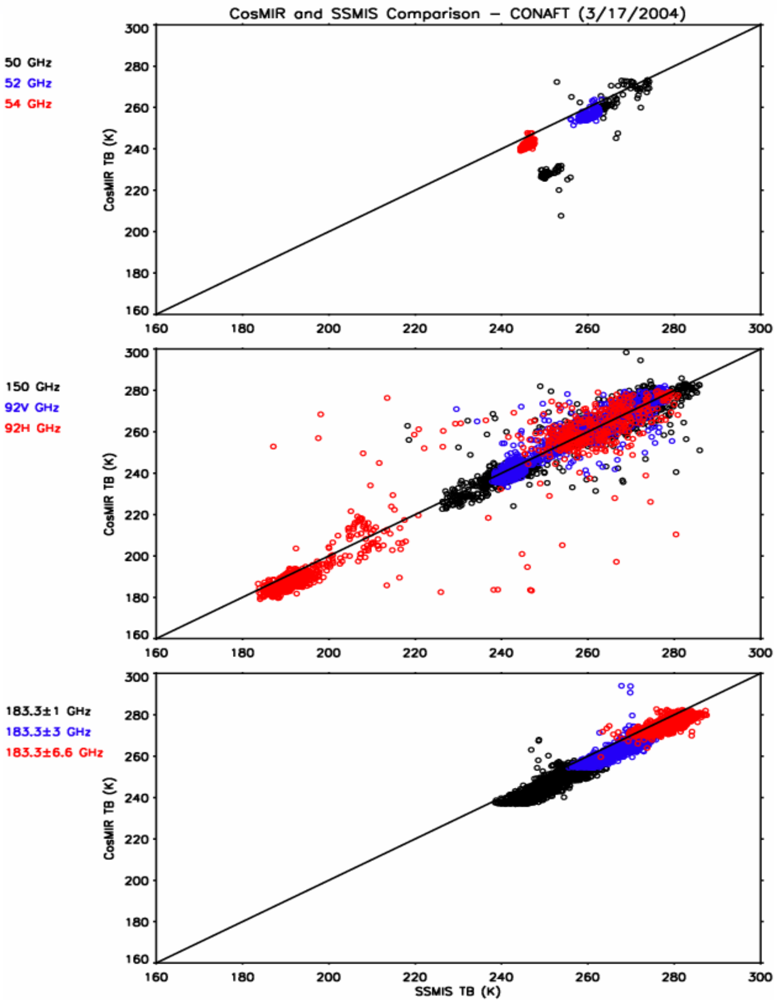

Scatter plot of CoSMIR and SSMIS T_b's from flight on 3/18/2004.

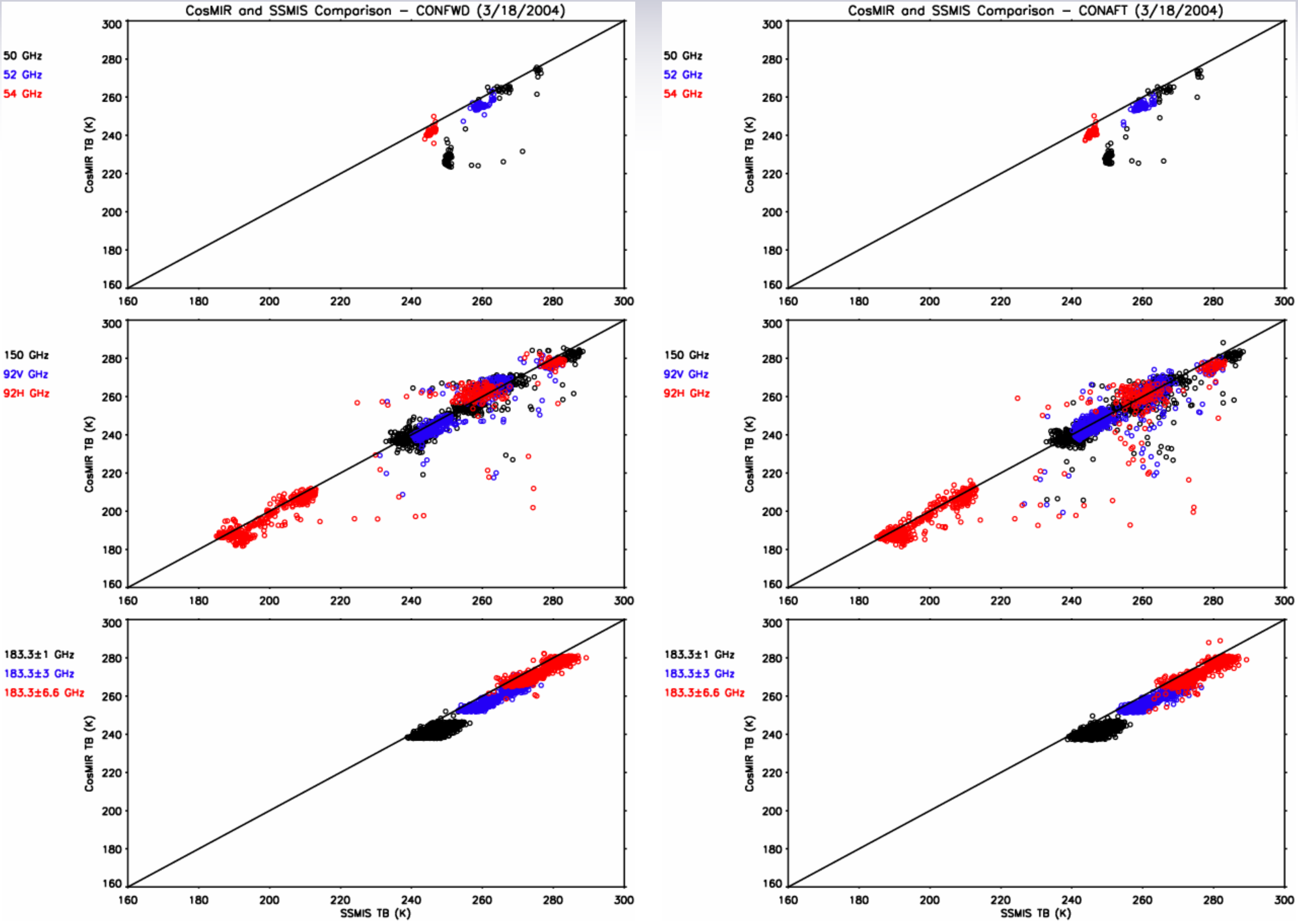

Similar plots from flight on 3/19/2004

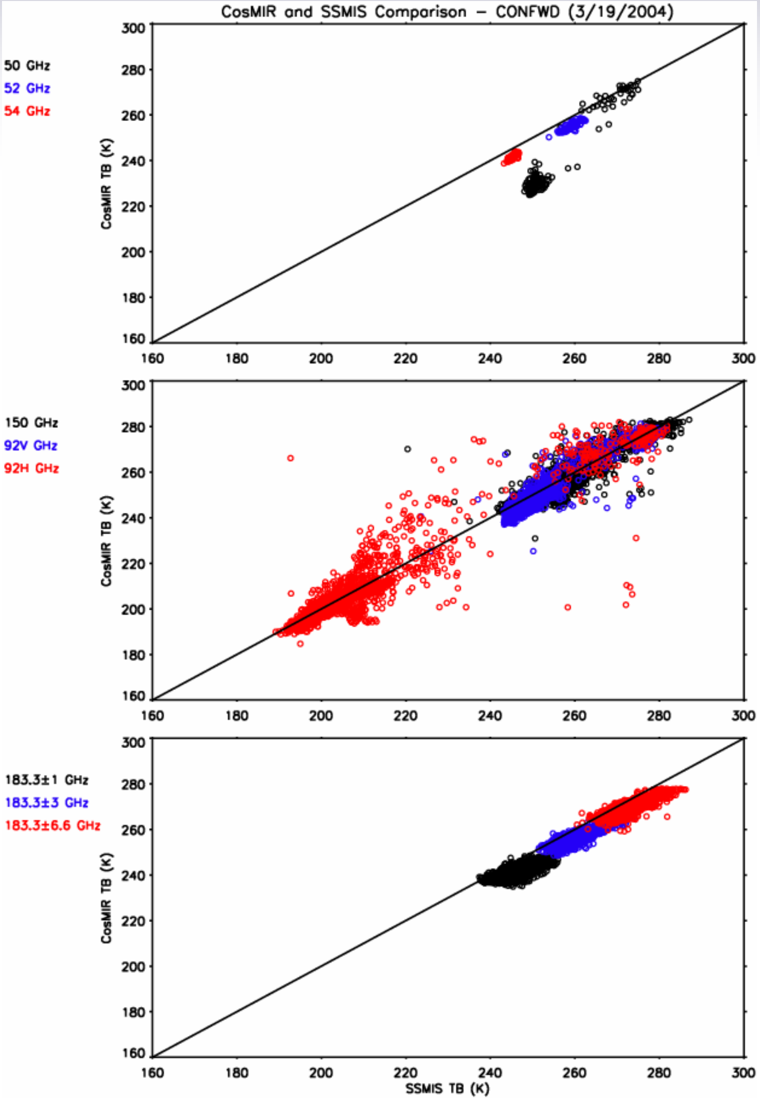

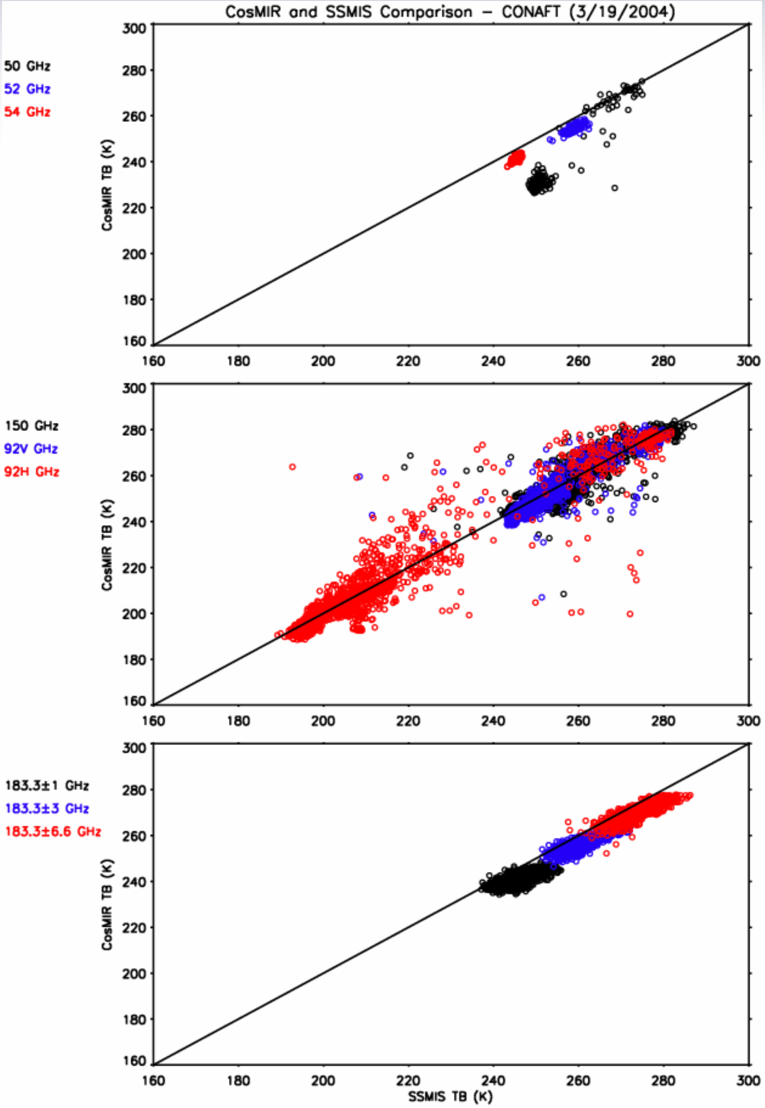

Similar plots of the CoSMIR and SSMIS T_b's from the flight on 3/24/2004 (descending pass)

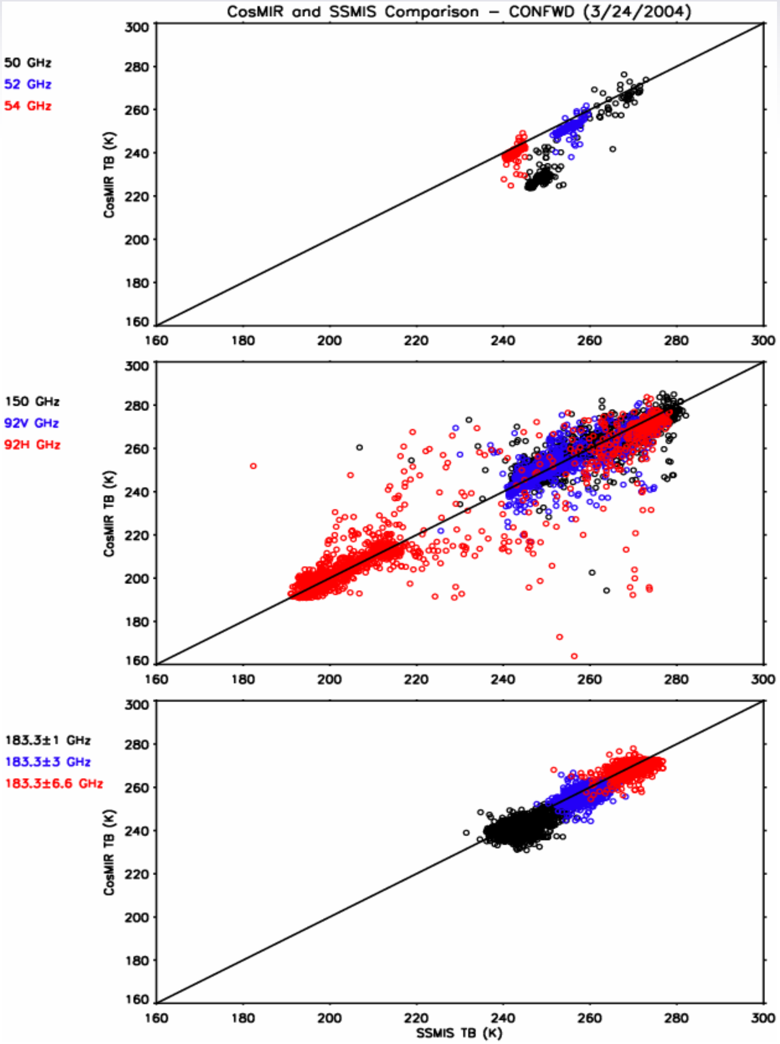
CosMIR and SSMIS Comparison – CONFWD (3/24/2004)

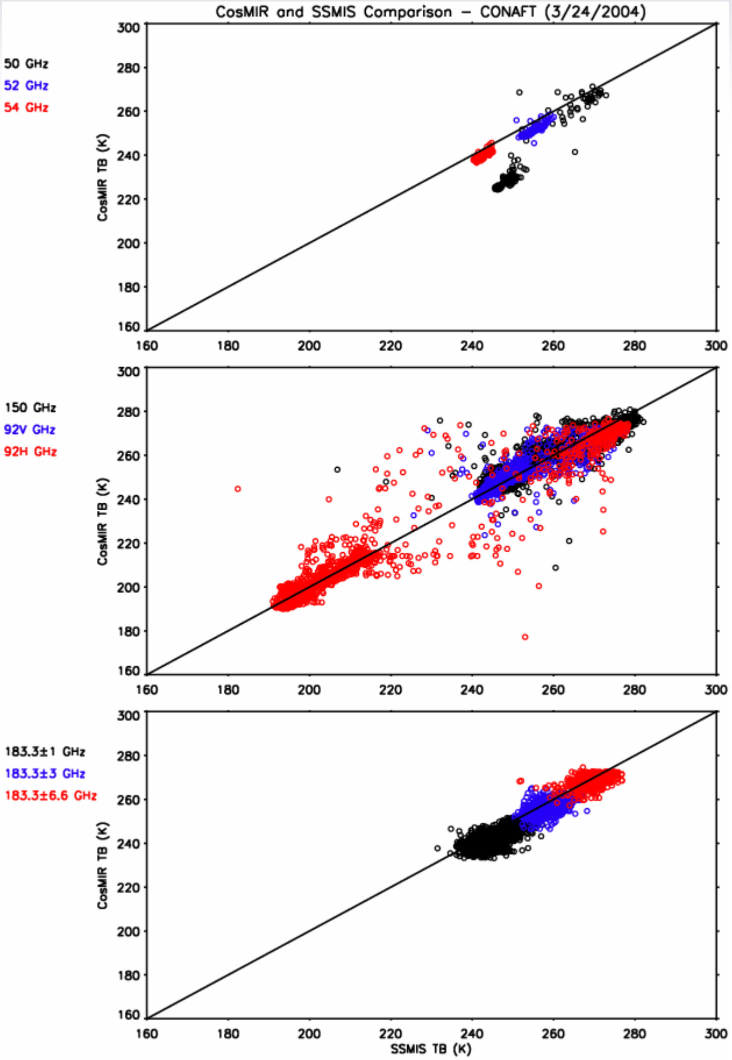
CosMIR and SSMIS Comparison – CONAFT (3/24/2004)

Similar plots of the CoSMIR and SSMIS T_b's from the flight on 3/25/2004 (descending pass).

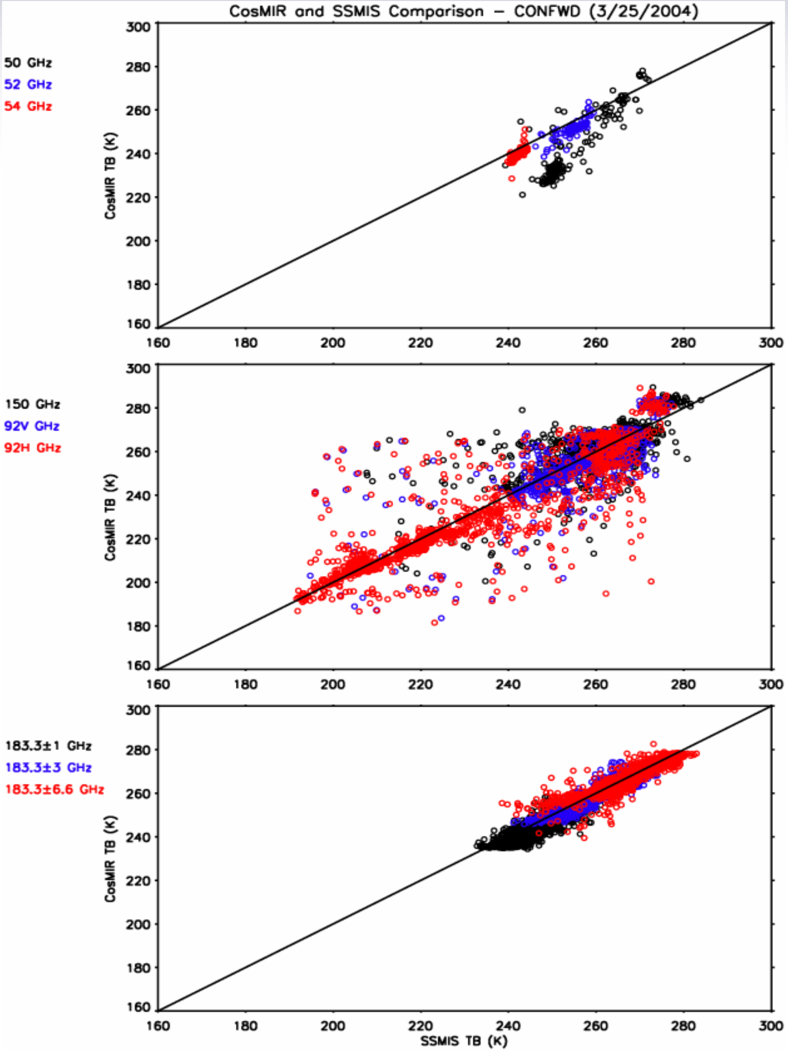

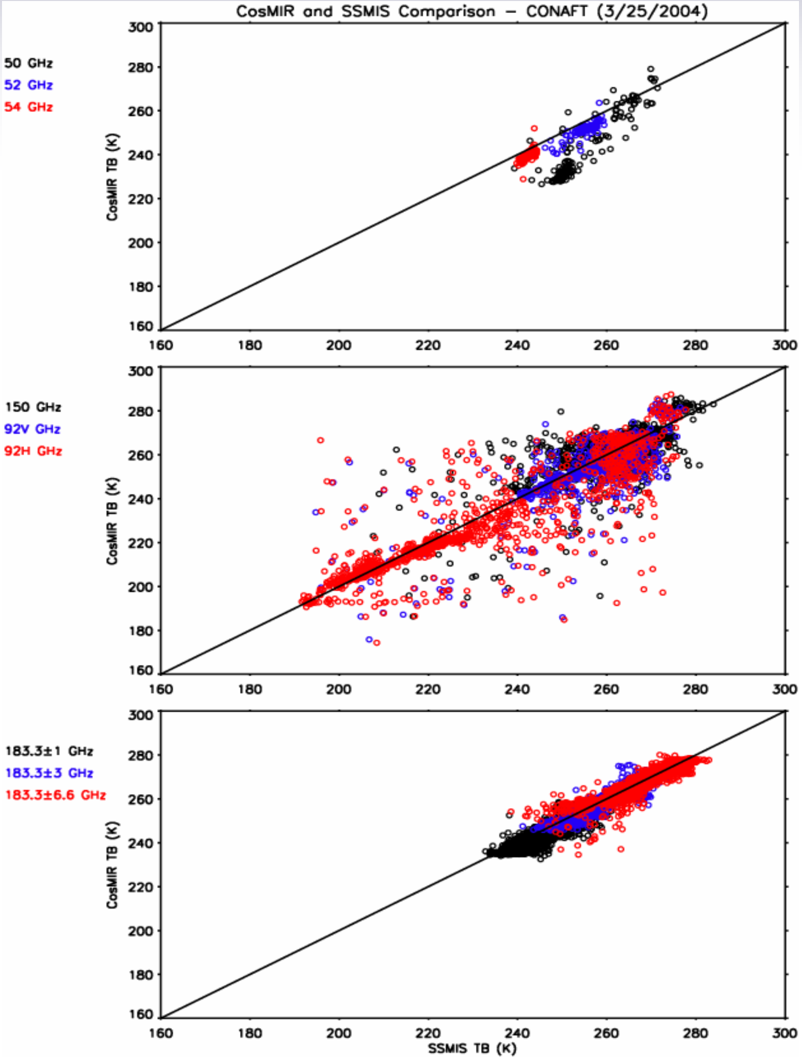

A scatter plot of the CoSMIR and SSMIS T_b's from the flight on 4/1/2004 (ascending pass).

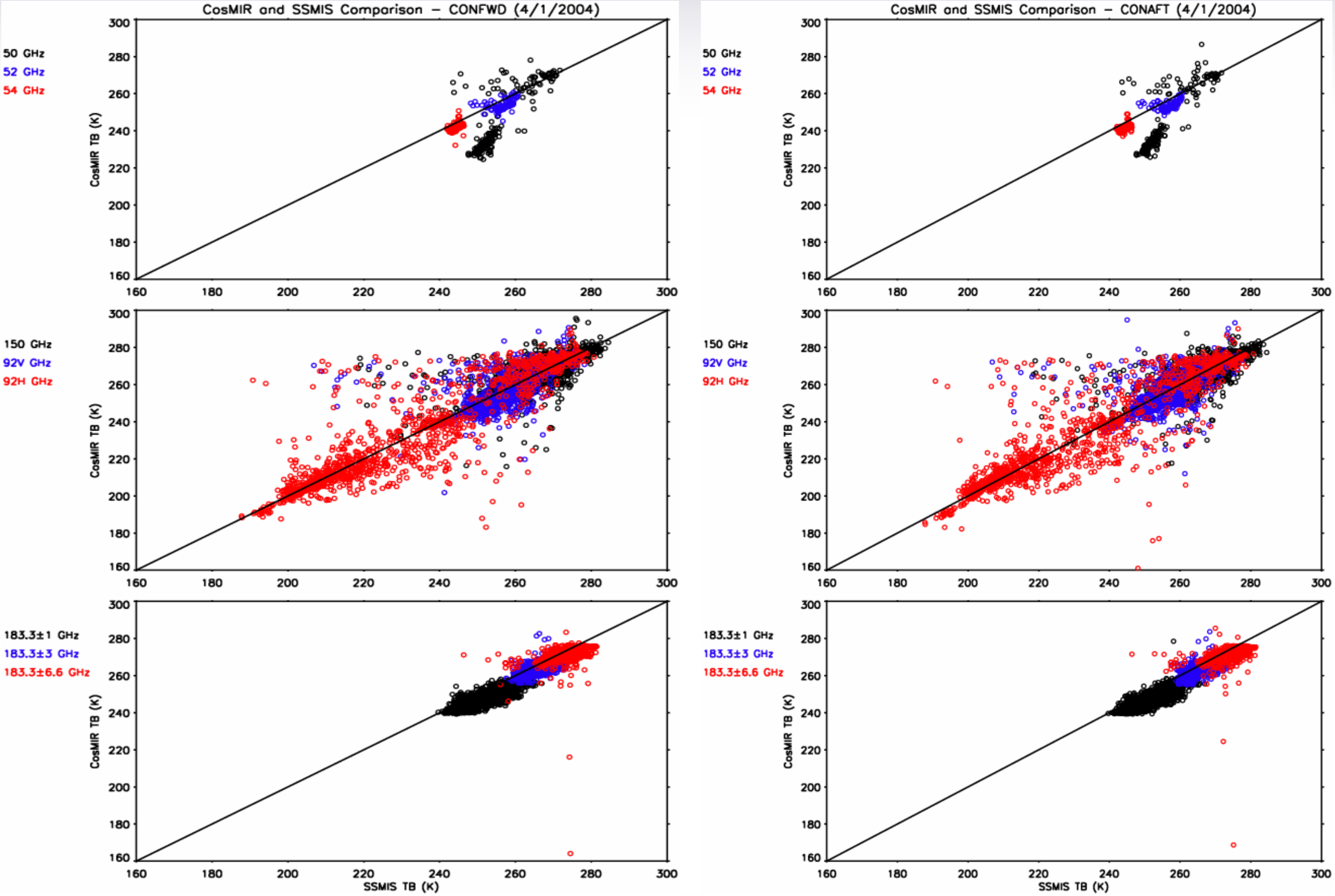

The T_b variations with time for 50.3 GHz (top), 92H GHz (middle), and 183±6.6 GHz (bottom) channels of the CoSMIR and SSMIS from flight on 3/17/2004: left plots forward scans along the flight path and right plots for aft scans. The SSMIS data points are only those coinciding with the CoSMIR. Notice the large differences between the CoSMIR and SSMIS 50.3 GHz T_b's over the ocean area.

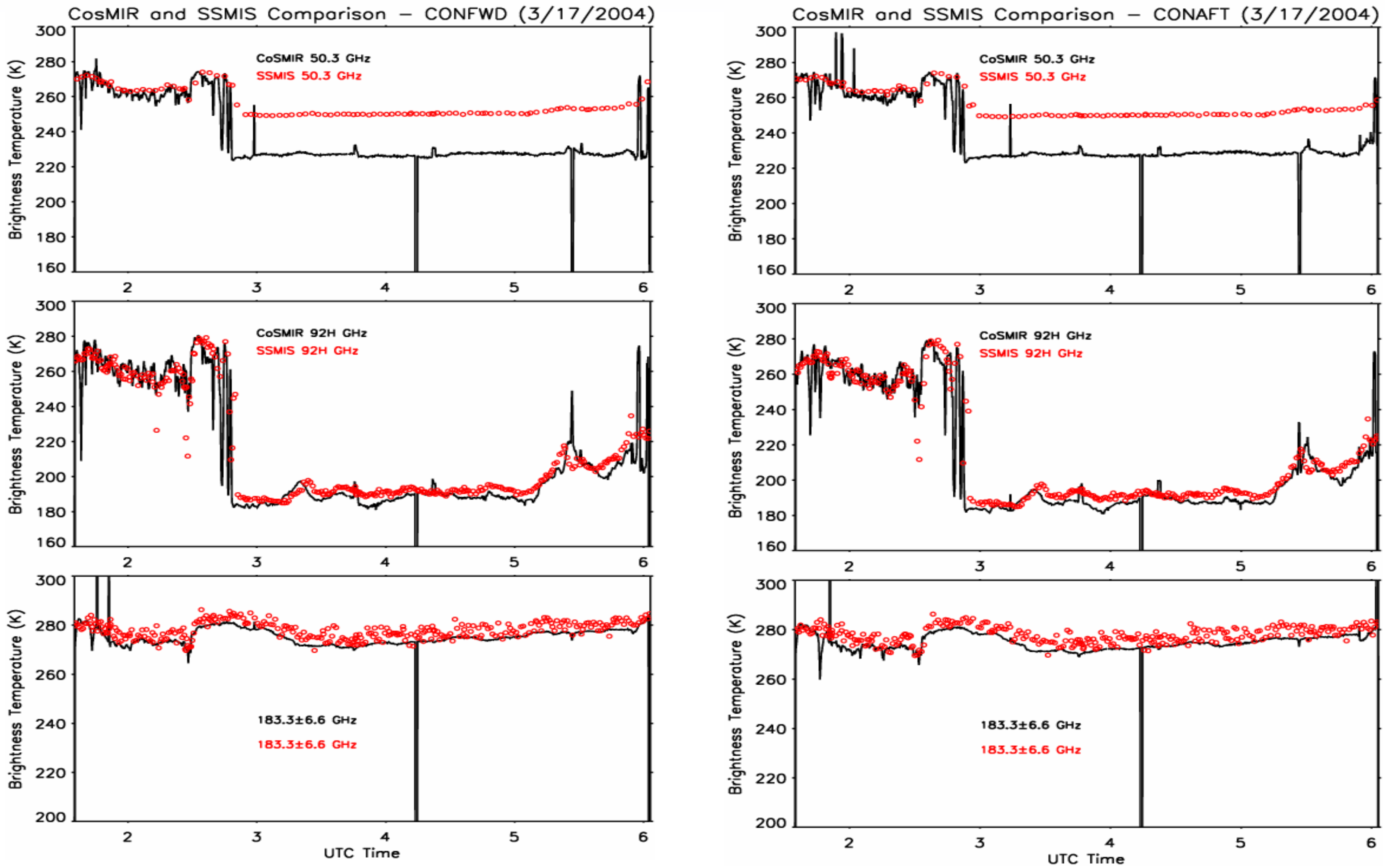

Similar plots as the previous slide,but from flight on 3/18/2004. These three channels are selected from their respective frequency groups for display because of their less opacity and thus likely to show more features. The low CoSMIR T_b valley around 0210 UTC is over Lake Pyramid.

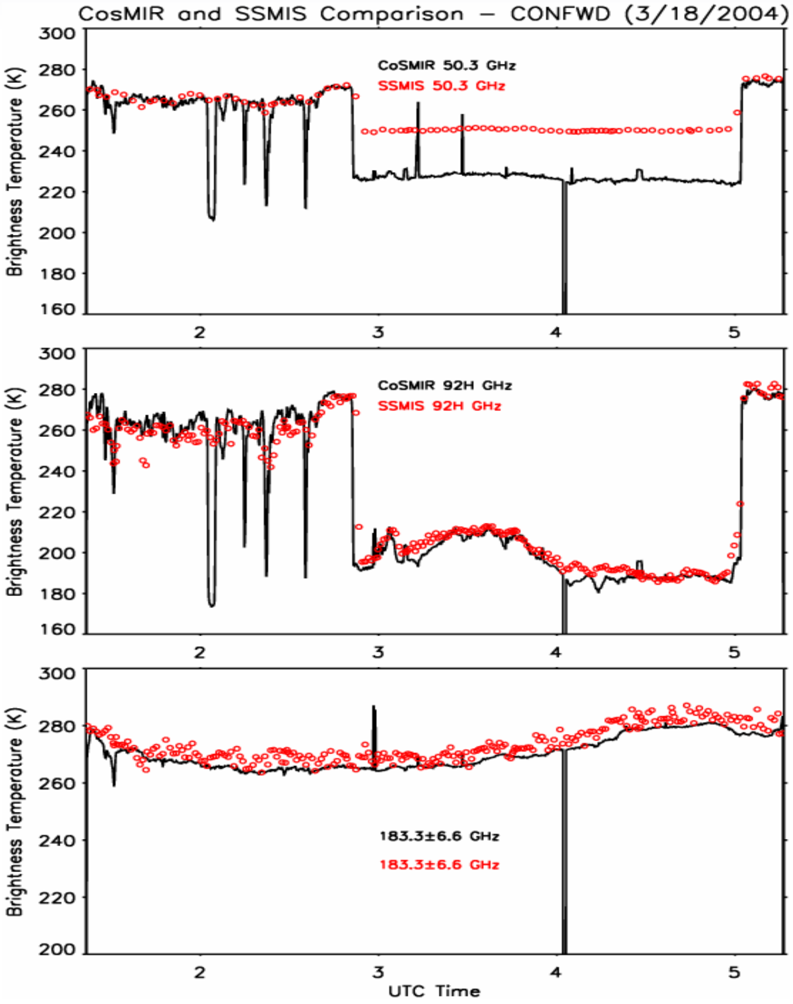

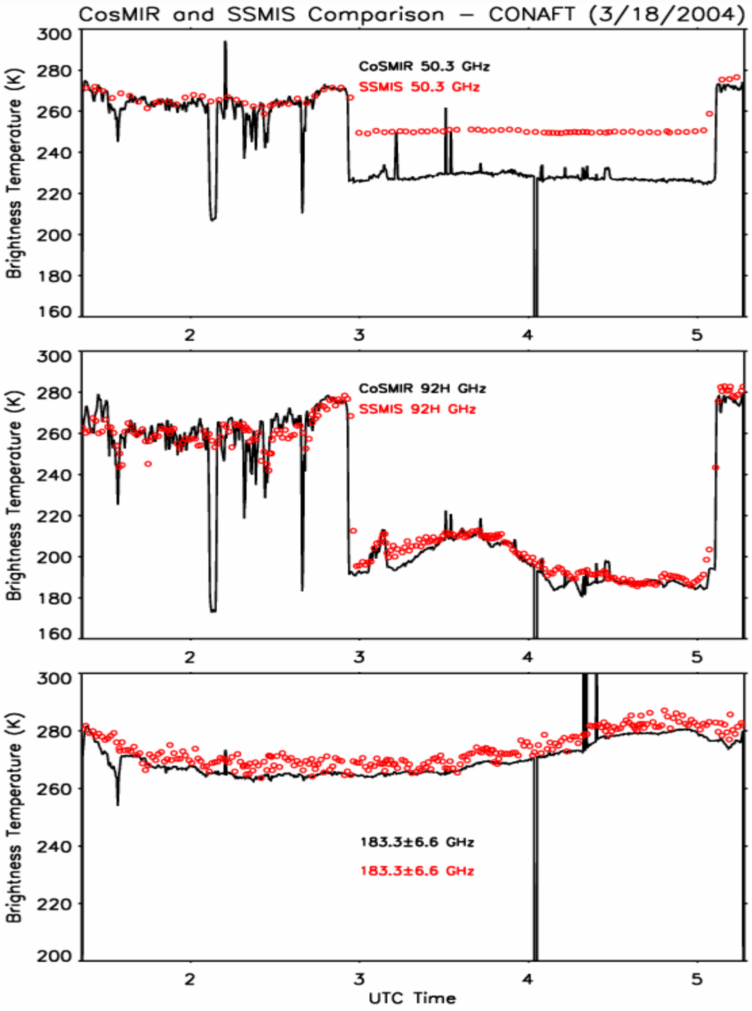

Similar plots for flight on 3/19/2004

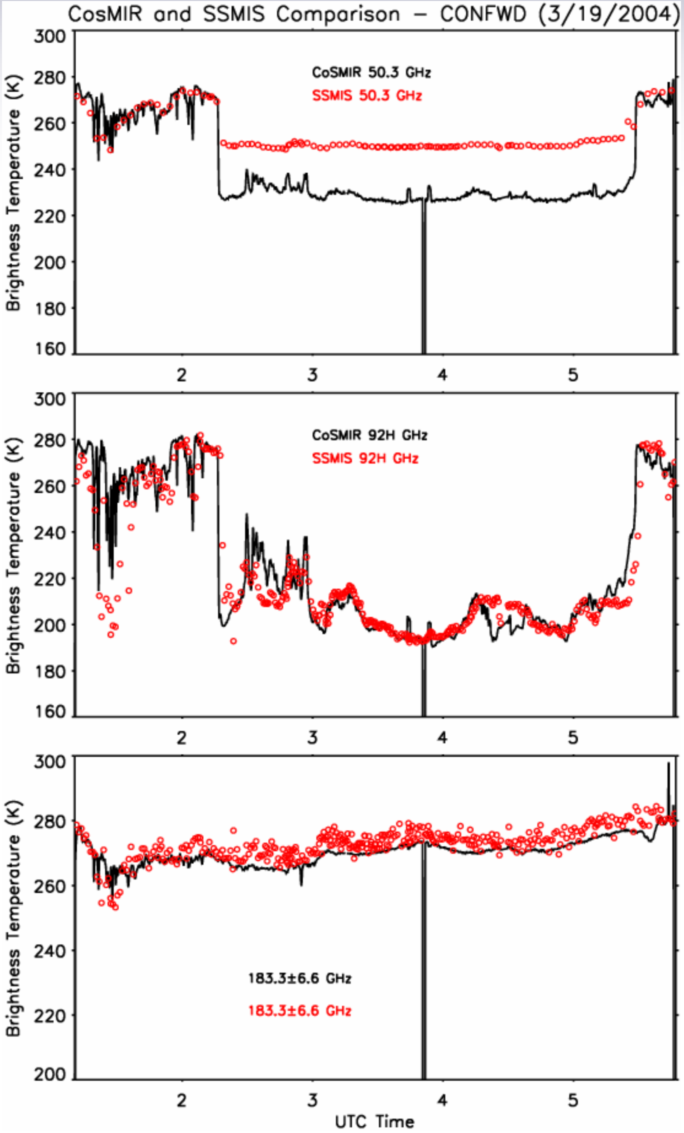

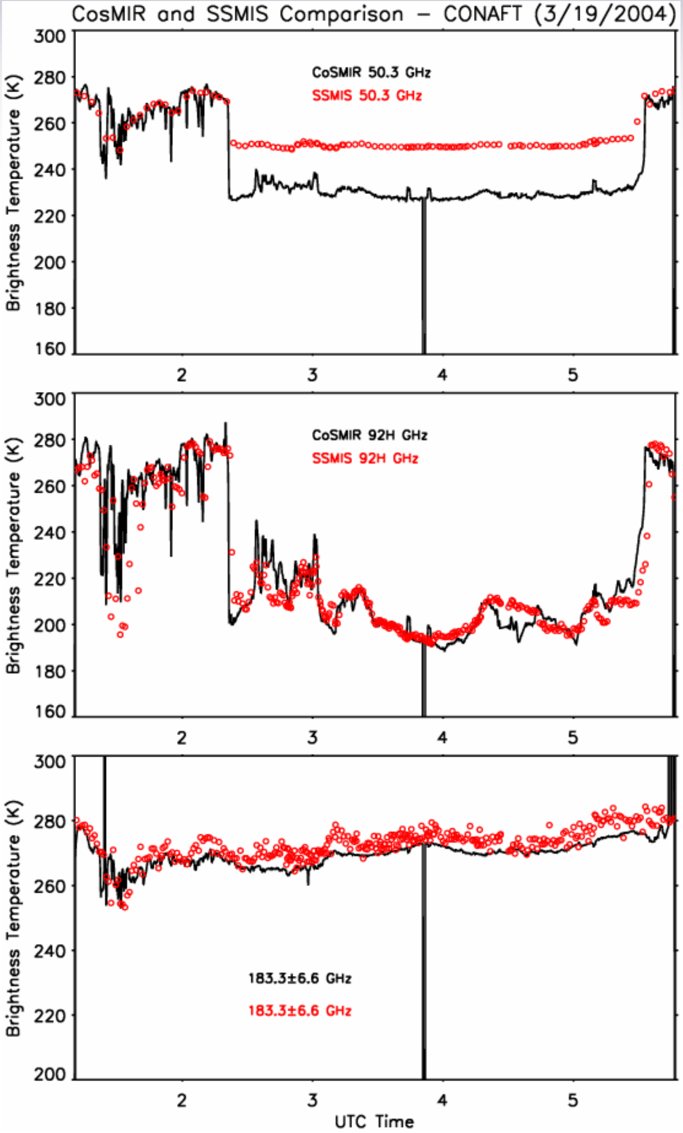

Similar plots for flight on 3/24/2004

Similar plots as the previous slide, but from the flight on 3/24/2004. Again, there are large differences between the CoSMIR and the SSMIS 50.3 GHz T_b's.

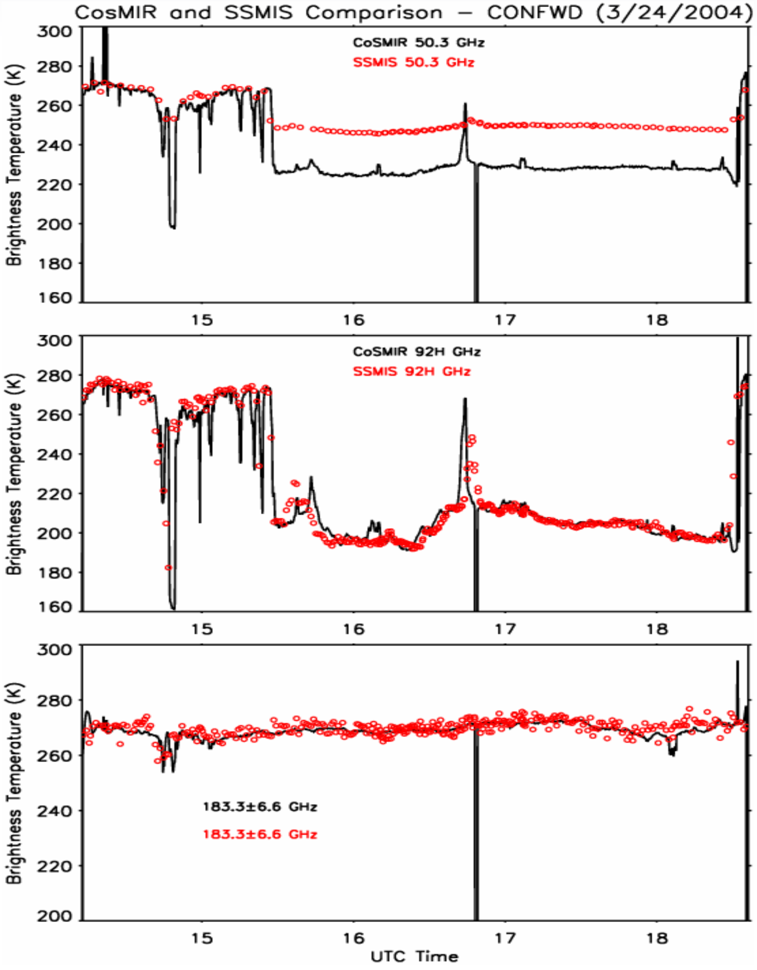

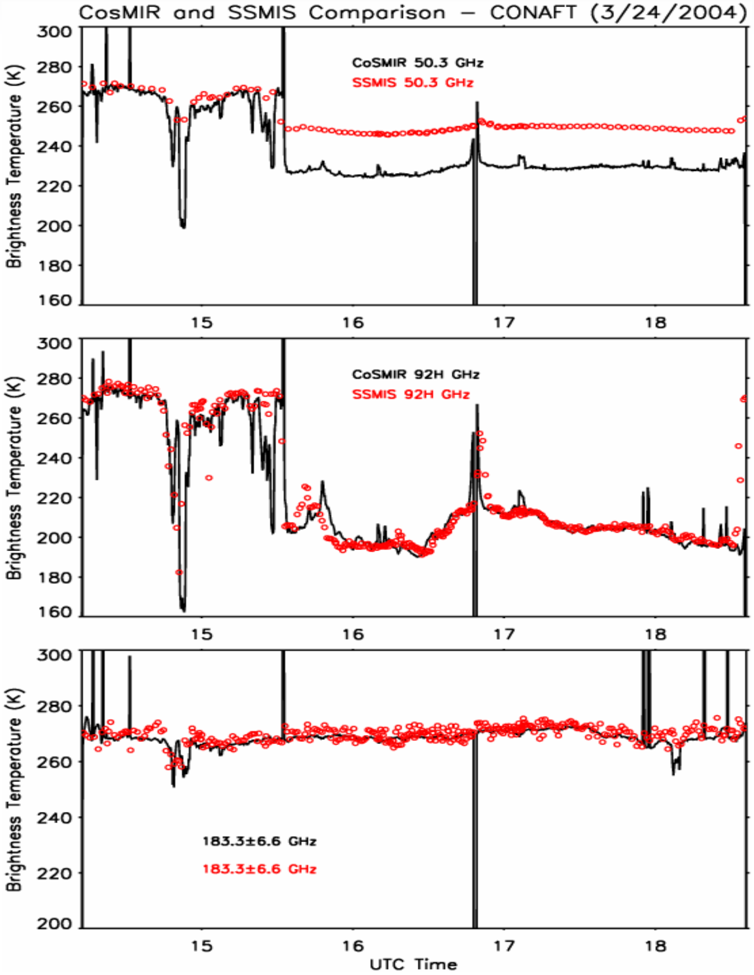

Similar plots for flight on 3/25/2004

Similar plots as the previous slide, but from flight on 3/25/2004. The same conclusion can be made as the previous slide.

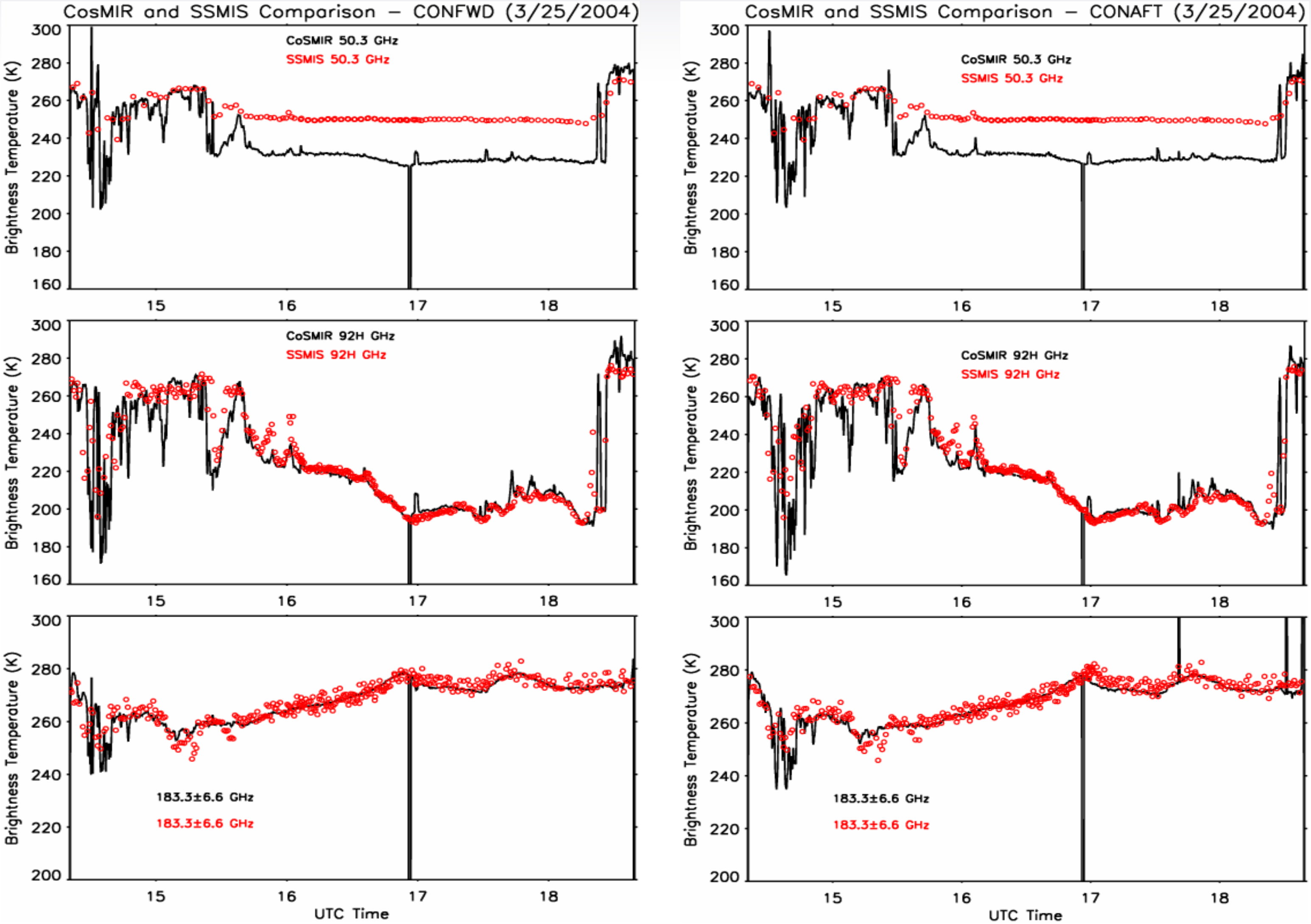

Similar plots as previous slide, but from flight on 4/1/2004

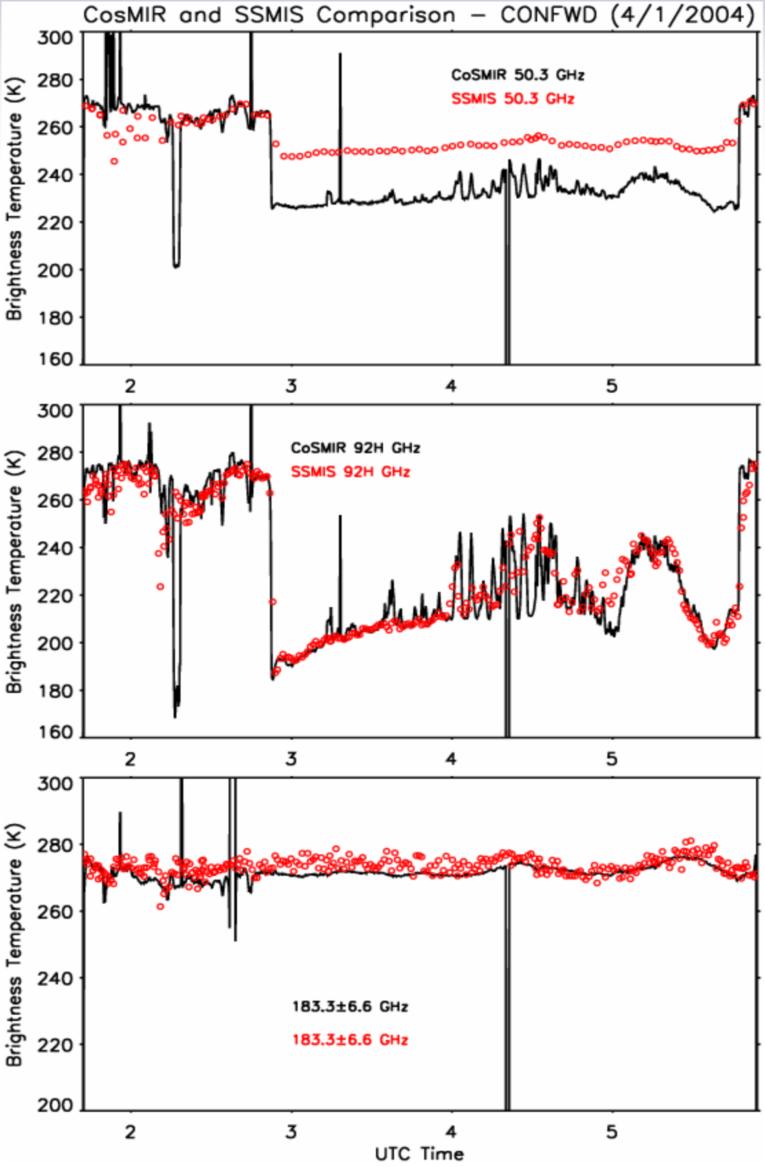
CosMIR and SSMIS Comparison – CONFWD (4/1/2004)

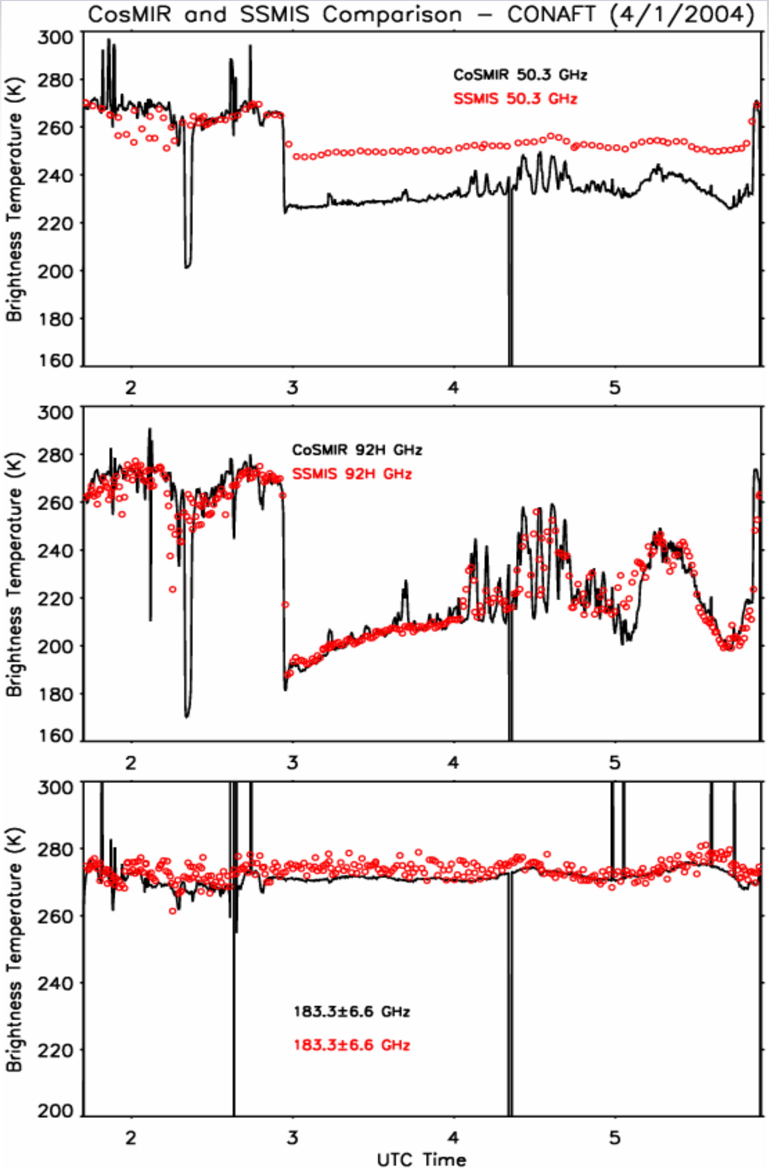
CosMIR and SSMIS Comparison – CONAFT (4/1/2004)

SSMIS and CoSMIR

Clean data from both SSMIS and CoSMIR over ocean from all the flights are selected. The differences in T_b's from coincident pixels are taken and averaged. The averages of the Tb differences include both directly forward and aft pixels. The following three tables (for different frequency groups) give the results.

Table 1. SSMIS-CoSMIR comparison for the 50 GHz channels

Date	**50.3 GHz**		**52.8 GHz**		**53.6 GHz**	
	Forward	**Aft**	**Forward**	**Aft**	**forward**	**Aft**
March 17, 2004	**23.84±3.75**	**22.84±2.36**	**4.85±1.03**	**5.05±0.75**	**3.81±0.79**	**4.27±0.90**
March 18, 2004	**22.86±2.98**	**21.83±1.90**	**4.57±0.59**	**5.01±0.62**	**3.41±0.78**	**4.21±0.79**
March 19, 2004	**21.15±2.26**	**20.45±2.04**	**4.45±0.36**	**4.71±0.70**	**3.45±0.42**	**3.85±0.73**
March 24, 2004	**20.51±2.13**	**20.1±1.96**	**3.57±0.39**	**3.90±0.53**	**2.04±0.56**	**2.47±0.69**
March 25, 2004	**19.14±1.93**	**18.73±1.89**	**3.54±0.45**	**3.87±0.66**	**2.12±0.49**	**2.57±0.63**
April 1, 2004	**19.00±2.71**	**18.32±2.66**	**4.51±0.42**	**4.78±0.49**	**2.83±0.50**	**3.19±0.65**

Table 2. SSMIS-CoSMIR comparison for the 92-150 GHz channels

Date	**92 H GHz**		**92 V GHz**		**150 GHz**	
	Forward	**Aft**	**Forward**	**Aft**	**Forward**	**Aft**
March 17, 2004	**3.24±3.02**	**3.43±3.04**	**2.37±2.26**	**0.89±2.51**	**1.70±3.02**	**1.442.68**
March 18, 2004	**2.26±2.57**	**1.70±2.60**	**2.33±1.73**	**0.58±2.51**	**1.71±2.90**	**0.95±2.84**
March 19, 2004	**0.99±3.65**	**1.06±3.51**	**2.88±2.66**	**2.35±2.09**	**1.19±3.20**	**0.86±2.91**
March 24, 2004	**-.17±2.82**	**-.14±3.10**	**-.30±2.25**	**-1.21±2.93**	**-.56±3.08**	**-1.02±3.22**
March 25, 2004	**0.87±3.00**	**0.90±2.81**	**2.11±1.88**	**1.80±1.77**	**0.00±2.33**	**-.11±2.27**
April 1, 2004	**0.92±3.98**	**0.24±4.23**	**2.71±2.79**	**2.13±2.90**	**1.30±3.08**	**0.89±3.27**

Table 3. SSMIS-CoSMIR comparison for the 183.3 GHz channels

Date	**183.3±1 GHz**		**183.3±3 GHz**		**183.3±6.6 GHz**	
	Forward	**Aft**	**Forward**	**Aft**	**Forward**	**Aft**
March 17, 2004	**5.25±2.38**	**5.53±2.40**	**3.94±1.75**	**4.27±1.78**	**3.19±1.92**	**3.43±1.94**
March 18, 2004	**5.01±2.43**	**5.44±2.41**	**4.27±1.89**	**4.57±2.01**	**3.42±2.01**	**3.60±2.08**
March 19, 2004	**5.12±2.25**	**5.29±2.26**	**4.11±1.81**	**4.28±1.78**	**3.44±2.08**	**3.57±2.04**
March 24, 2004	**2.89±3.01**	**3.31±3.10**	**1.49±2.31**	**1.90±2.33**	**0.55±2.22**	**0.93±2.20**
March 25, 2004	**2.20±2.78**	**2.09±2.70**	**0.86±1.88**	**0.85±1.86**	**0.27±1.95**	**0.29±1.96**
April 1, 2004	**4.29±2.83**	**4.46±2.66**	**2.45±2.32**	**2.56±2.24**	**1.99±2.06**	**1.99±2.13**

Average brightness temperatures of 50-54 GHz channels from SSMIS and CoSMIR over Ocean

Table 4. SSMIS and CoSMIR over Ocean

Date	Sensor	50.3 GHz		52.8 GHz		53.6 Ghz	
		Forward	Aft	Forward	Aft	Forward	Aft
03/17/04	SSMIS CoSMIR	251.1 227.0	250.5 227.6	260.4 255.6	260.3 255.3	246.5 242.6	246.4 242.2
03/18/04	SSMIS CoSMIR	250.5 227.7	250.2 228.4	259.6 255.1	259.6 254.6	245.9 242.5	245.9 241.7
03/19/04	SSMIS CoSMIR	250.1 228.9	250.1 229.6	258.6 254.1	258.6 253.9	245.4 242.0	245.4 241.6
03/24/04	SSMIS CoSMIR	248.6 228.1	248.6 228.4	255.2 251.7	255.1 251.2	242.5 240.5	242.4 240.0
03/25/04	SSMIS CoSMIR	250.1 231.0	250.2 231.4	256.0 252.5	256.0 252.1	243.0 240.8	242.9 240.4
04/01/04	SSMIS CoSMIR	251.7 232.7	251.7 233.4	257.8 253.3	257.8 253.0	245.3 242.5	245.3 242.1

Table 5. Average brightness temperatures of 92-150 GHz channels from SSMIS and CoSMIR over Ocean

Date	Sensor	92(H) GHz		92(V) GHz		150 Ghz	
		Forward	Aft	Forward	Aft	Forward	Aft
03/17/04	SSMIS CoSMIR	194.0 190.7	193.1 189.7	244.2 241.8	243.6 242.7	243.7 241.8	242.7 241.3
03/18/04	SSMIS CoSMIR	197.4 195.1	197.0 195.3	245.2 242.9	245.2 244.6	246.9 245.1	246.7 245.8
03/19/04	SSMIS CoSMIR	205.7 205.0	206.0 205.0	248.0 245.1	248.0 245.7	254.7 253.3	254.7 253.7
03/24/04	SSMIS CoSMIR	205.0 205.2	205.1 205.5	248.3 248.7	248.4 249.7	255.5 256.1	255.6 256.8
03/25/04	SSMIS CoSMIR	217.2 216.0	218.1 216.9	252.6 250.6	252.9 251.1	264.1 264.1	264.4 264.6
04/01/04	SSMIS CoSMIR	219.3 217.2	219.9 218.0	252.1 248.9	252.3 249.7	262.2 260.5	262.6 261.4

Table 4. Average brightness temperatures of 50-54 GHz channels from SSMIS and CoSMIR over Ocean

Date	Sensor	183.3±1 GHz		183.3±3 GHz		183.3±7 GHz	
		Forward	Aft	Forward	Aft	Forward	Aft
03/17/04	SSMIS CoSMIR	247.9 242.7	247.7 242.3	264.2 260.3	264.0 259.7	277.6 274.4	277.4 274.0
03/18/04	SSMIS CoSMIR	247.1 242.1	247.3 241.8	263.5 259.3	263.8 259.2	275.9 272.5	276.3 272.6
03/19/04	SSMIS CoSMIR	246.3 241.2	246.2 240.9	260.1 256.0	259.9 255.6	273.1 269.7	272.9 269.4
03/24/04	SSMIS CoSMIR	244.4 241.6	244.9 241.6	259.7 258.2	260.0 258.1	270.3 269.7	270.3 269.4
03/25/04	SSMIS CoSMIR	248.2 246.0	247.9 245.8	261.2 260.3	260.9 260.0	269.9 269.7	269.6 269.3
04/01/04	SSMIS CoSMIR	250.6 246.3	250.4 245.9	266.2 263.8	266.1 263.5	274.3 272.3	274.2 272.1

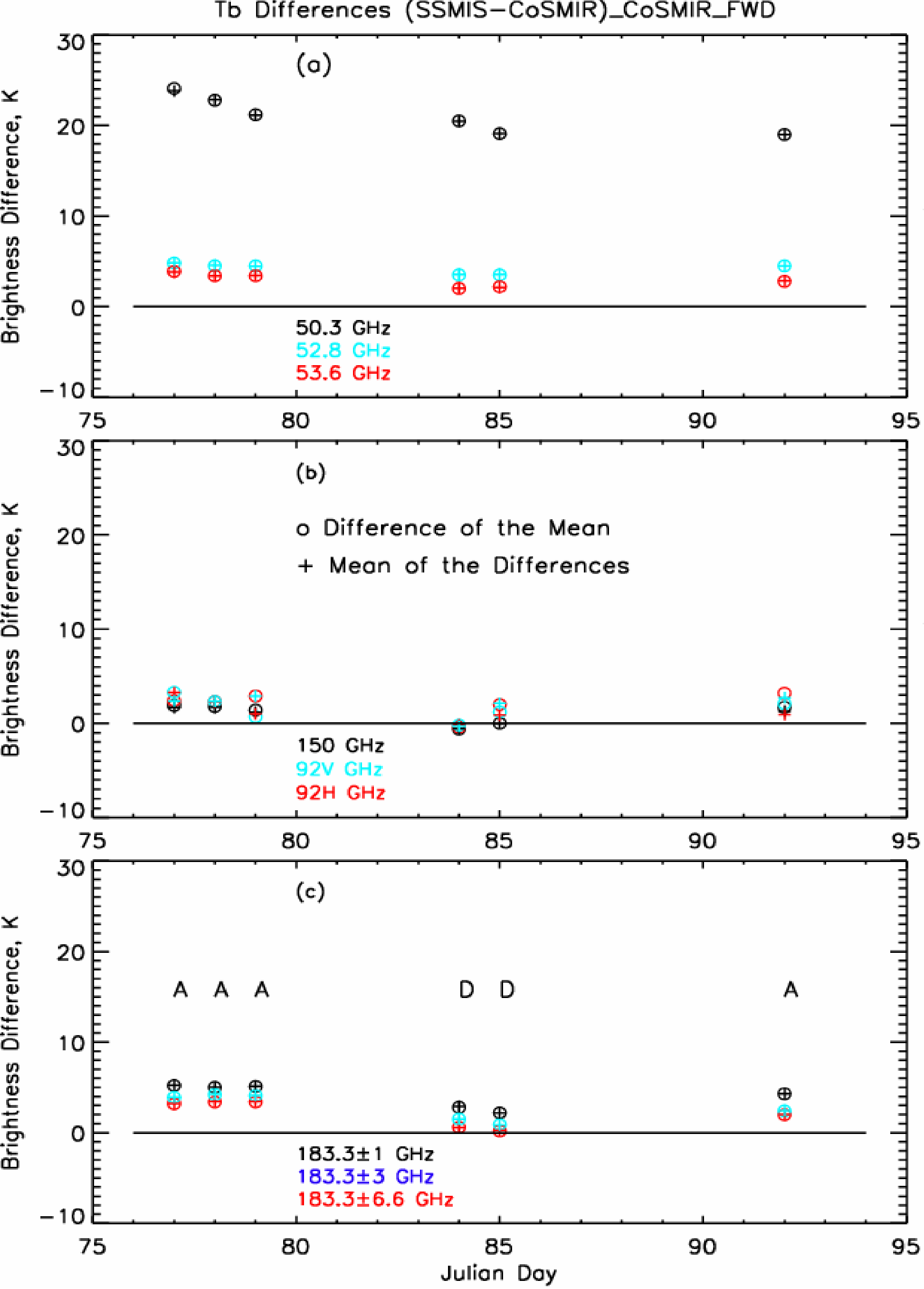
Tb Differences (SSMIS−CoSMIR)_CoSMIR_FWD
(a)
50.3 GHz
52.8 GHz
53.6 GHz
(b)
o Difference of the Mean
+ Mean of the Differences
150 GHz
92V GHz
92H GHz
(c)
A A A D D A
183.3±1 GHz
183.3±3 GHz
183.3±6.6 GHz
Brightness Difference, K
30
20
10
0
−10
75
80
85
90
95
Julian Day

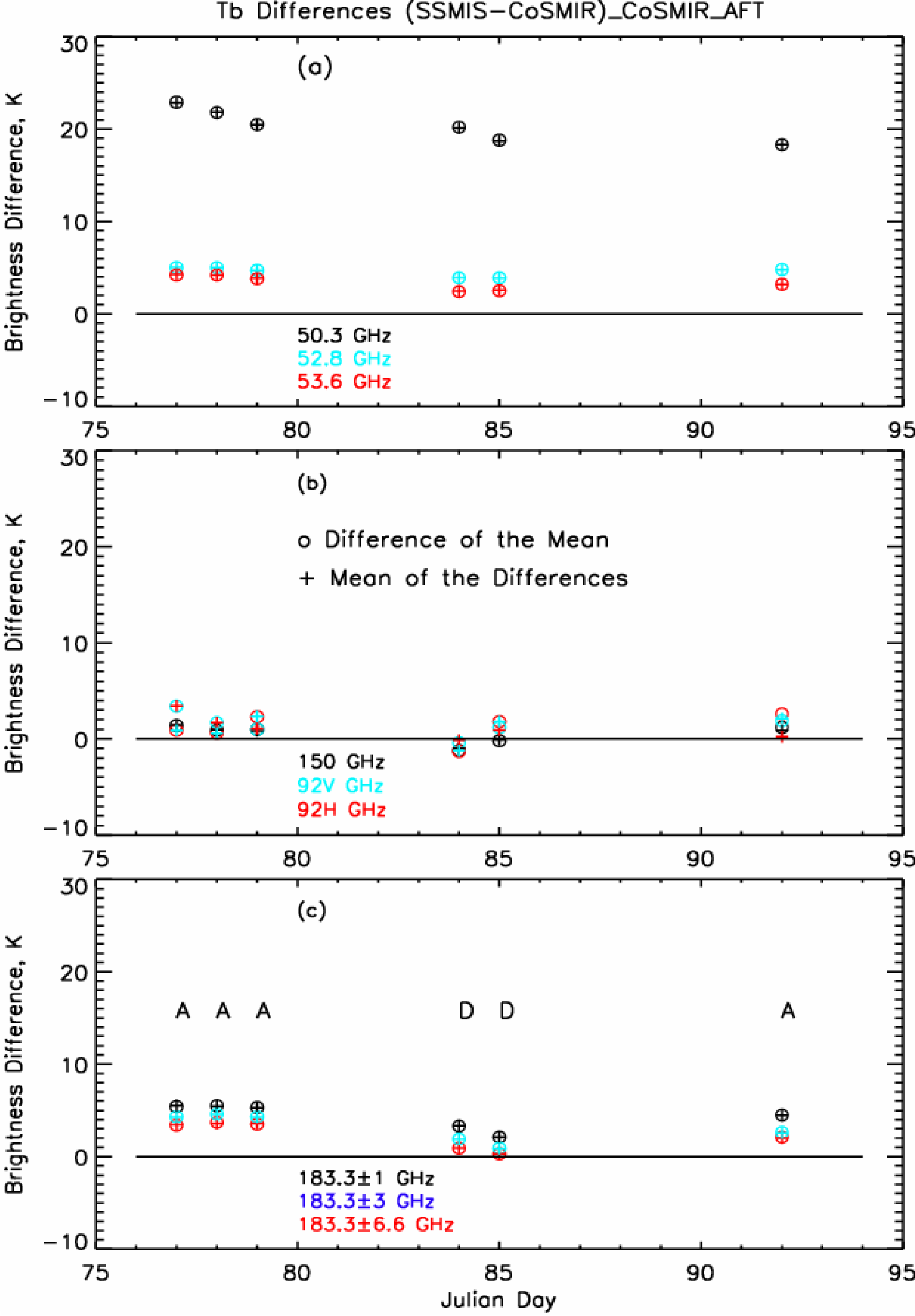
Tb Differences (SSMIS−CoSMIR)_CoSMIR_AFT
(a)
50.3 GHz
52.8 GHz
53.6 GHz
(b)
o Difference of the Mean
+ Mean of the Differences
150 GHz
92V GHz
92H GHz
(c)
A A A D D A
183.3±1 GHz
183.3±3 GHz
183.3±6.6 GHz
Brightness Difference, K
30
20
10
0
−10
75
80
85
90
95
Julian Day

Brief Summary of SSMIS-CoSMIR Inter-comparison

- T_b Variations of SSMIS and CoSMIR clearly track one another for all 9 channels over the ocean areas. Displacements of such variations are sometimes observed due to movements of weather patterns.
- Large T_b differences are observed at 50.3 GHz from all six flights, which points to a difference in polarization.
- There are definite T_b biases of different magnitudes on all channels; SSMIS T_b values are generally higher.
- These biases appear to differ between ascending and descending passes:

A - 03/17/04, ~0403 UTC

A - 03/18/04, ~0350 UTC

A - 03/19/04, ~0338 UTC

D - 03/24/04, ~1626 UTC

D - 03/25/04, ~1614 UTC

A - 04/01/04, ~0400 UTC

Reasons for these bias changes remain to be explored.

Calculations to Infer Brightness of the 3 SSMIS 50 Channels from the CoSMIR Data

- **Results of radiative transfer calculations over calm ocean surface, based on rawinsonde data from areas of CoSMIR flights (no island stations) and Key West (Florida), to form relationship between vertical and horizontal polarization (slides #45-46).**
- **Comparison of the calculated (from the CoSMIR-measured) and measured SSMIS T_b values at 50.3, 52.8, and 53.6 GHz (slides #47-52).**
- **Comparison of the T_{bv} values calculated from the CoSMIR-measured T_{bh}'s with those measured from the SSMIS and CoSMIR at 92 GHz channels (slides #53-58), to see if this approach works (both SSMIS and CoSMIR dual-polarized).**
- **Brief summary (slide #59)**

Results showing the calculated brightness temperature relation between vertical and horizontal polarization for the 50-54 GHz channels. Similar results for the 91.665 Ghz channels are given in the next slide. Rawinsonde data from the island stations near California coast could not be found; thus data from the Key West station in Florida were also used to extend the range of moisture. These derived relations were used to estimate vertically polarized brightness temperatures and compared with measurements from the SSMIS and CoSMIR.

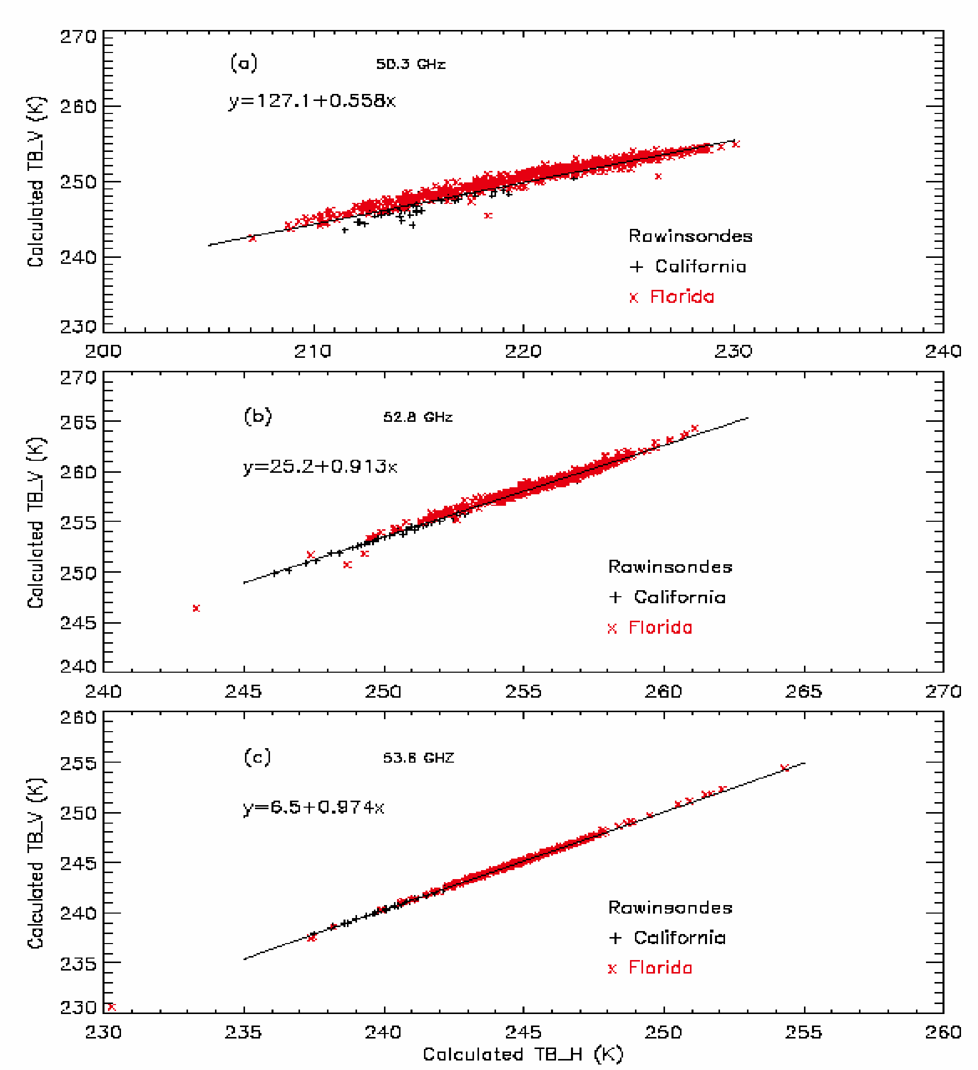

Calculated V and H Relation over Ocean Surface at 91.665 GHz

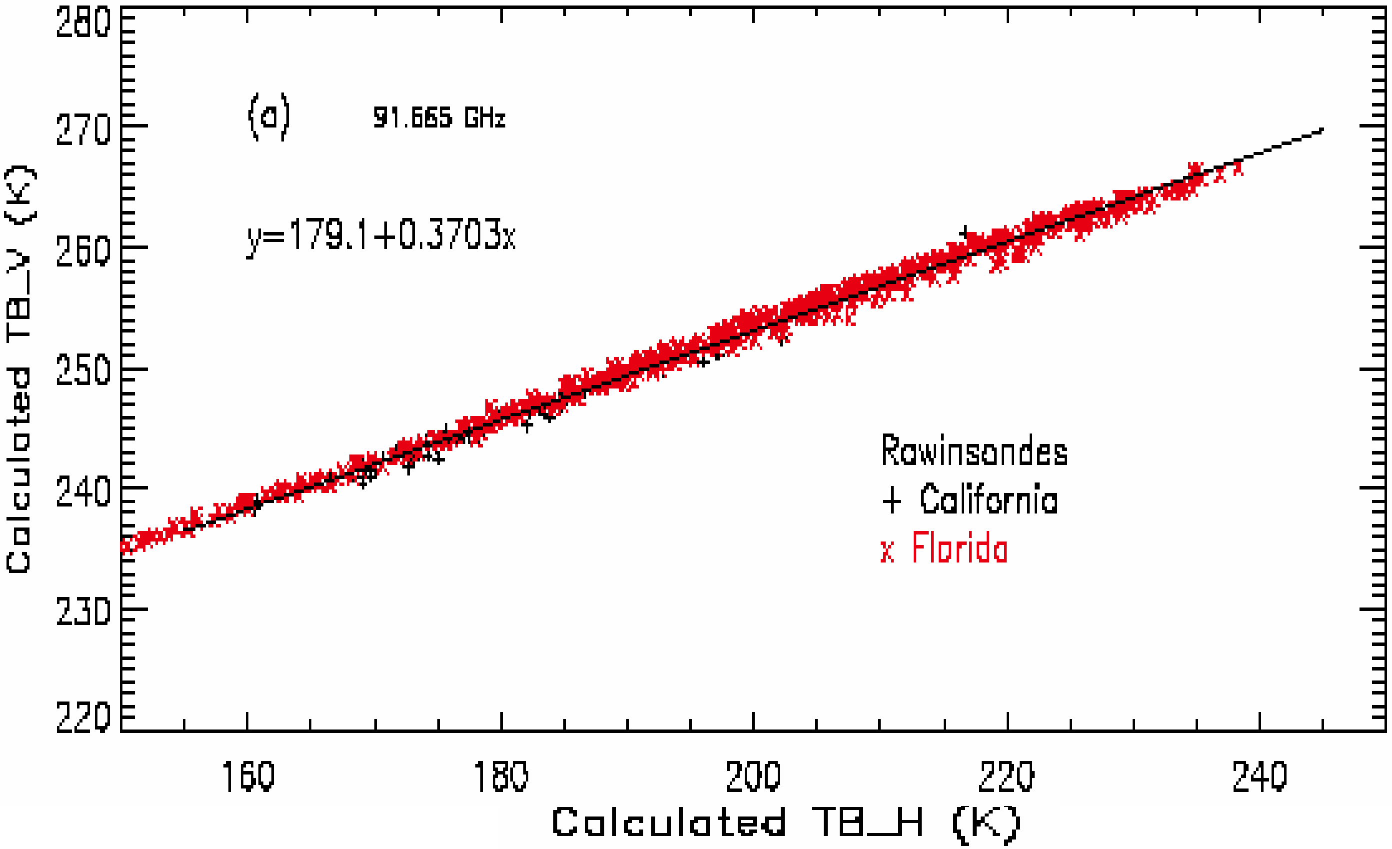

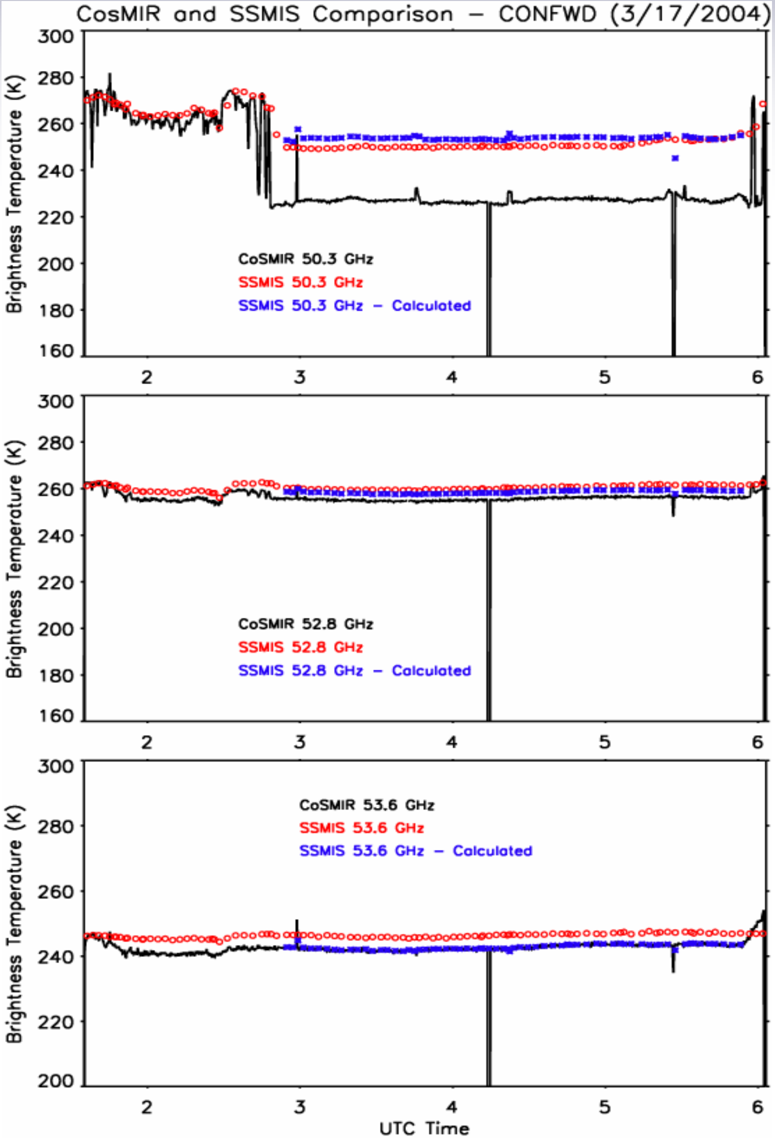
CosMIR and SSMIS Comparison – CONFWD (3/17/2004)
Brightness Temperature (K)
CoSMIR 50.3 GHz
SSMIS 50.3 GHz
SSMIS 50.3 GHz – Calculated
CoSMIR 52.8 GHz
SSMIS 52.8 GHz
SSMIS 52.8 GHz – Calculated
CoSMIR 53.6 GHz
SSMIS 53.6 GHz
SSMIS 53.6 GHz – Calculated
160
180
200
220
240
260
280
300
2
3
4
5
6
UTC Time

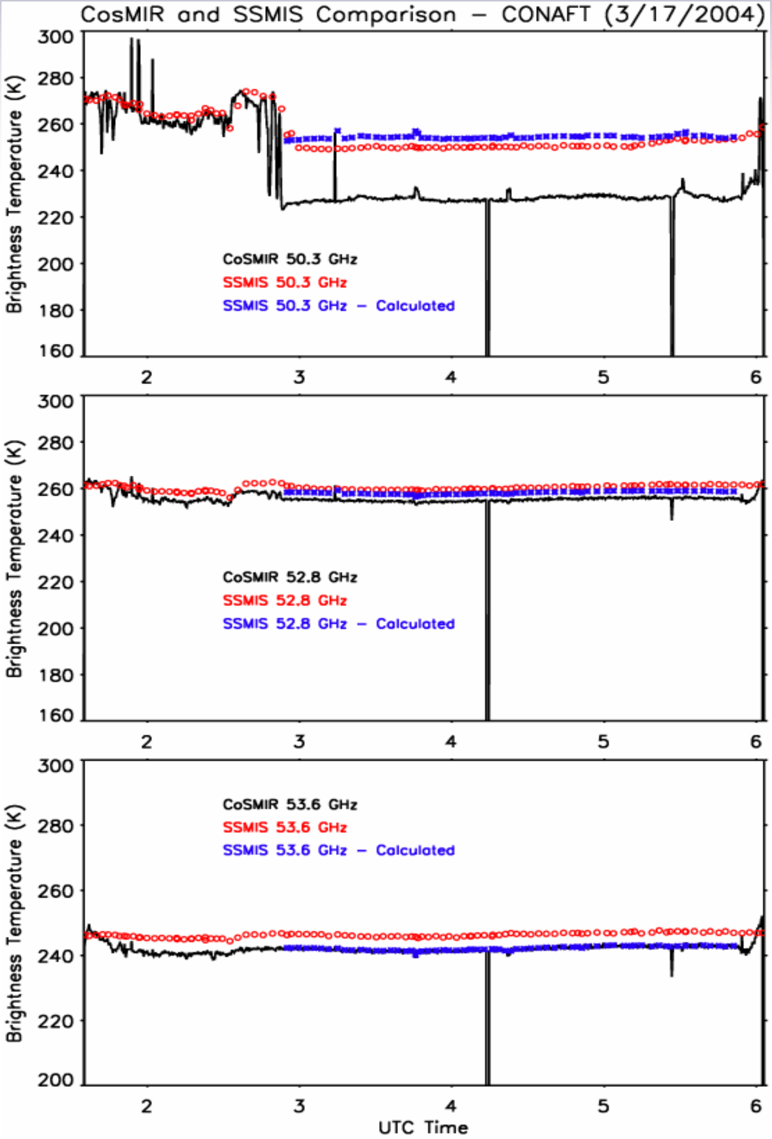
CosMIR and SSMIS Comparison – CONAFT (3/17/2004)
Brightness Temperature (K)
CoSMIR 50.3 GHz
SSMIS 50.3 GHz
SSMIS 50.3 GHz – Calculated
CoSMIR 52.8 GHz
SSMIS 52.8 GHz
SSMIS 52.8 GHz – Calculated
CoSMIR 53.6 GHz
SSMIS 53.6 GHz
SSMIS 53.6 GHz – Calculated
160
180
200
220
240
260
280
300
2
3
4
5
6
UTC Time

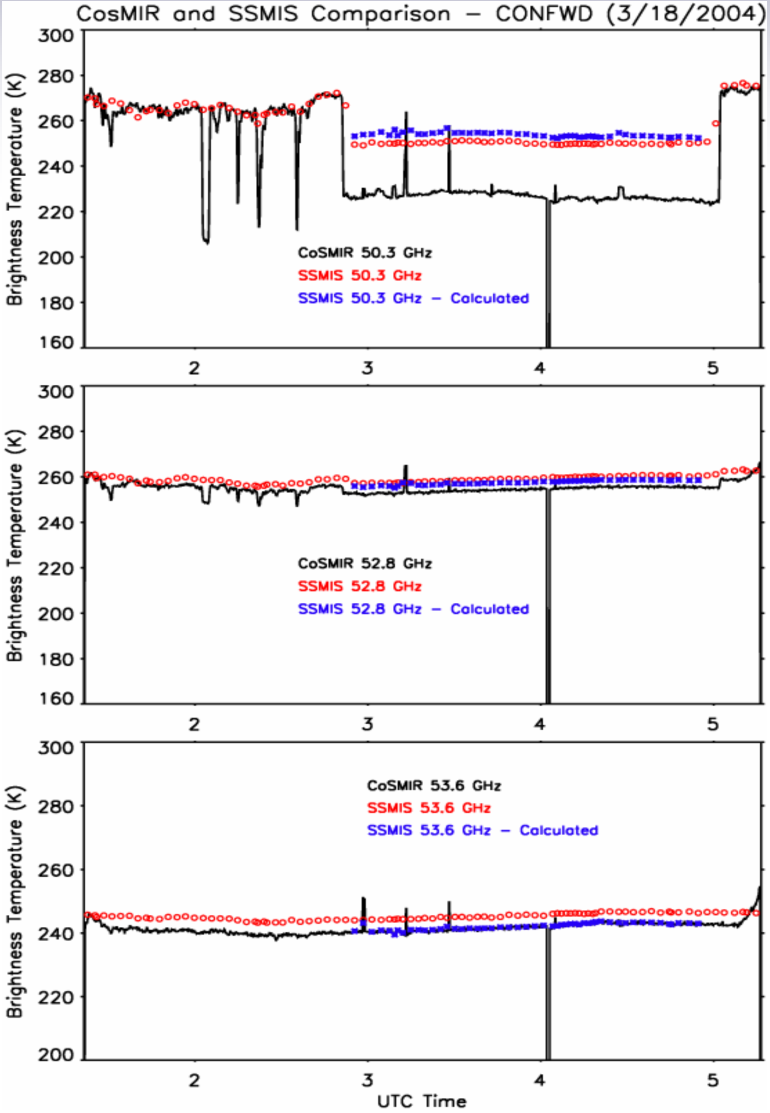
CosMIR and SSMIS Comparison – CONFWD (3/18/2004)
Brightness Temperature (K)
300
280
260
240
220
200
180
160
2
3
4
5
CoSMIR 50.3 GHz
SSMIS 50.3 GHz
SSMIS 50.3 GHz – Calculated
CoSMIR 52.8 GHz
SSMIS 52.8 GHz
SSMIS 52.8 GHz – Calculated
CoSMIR 53.6 GHz
SSMIS 53.6 GHz
SSMIS 53.6 GHz – Calculated
UTC Time

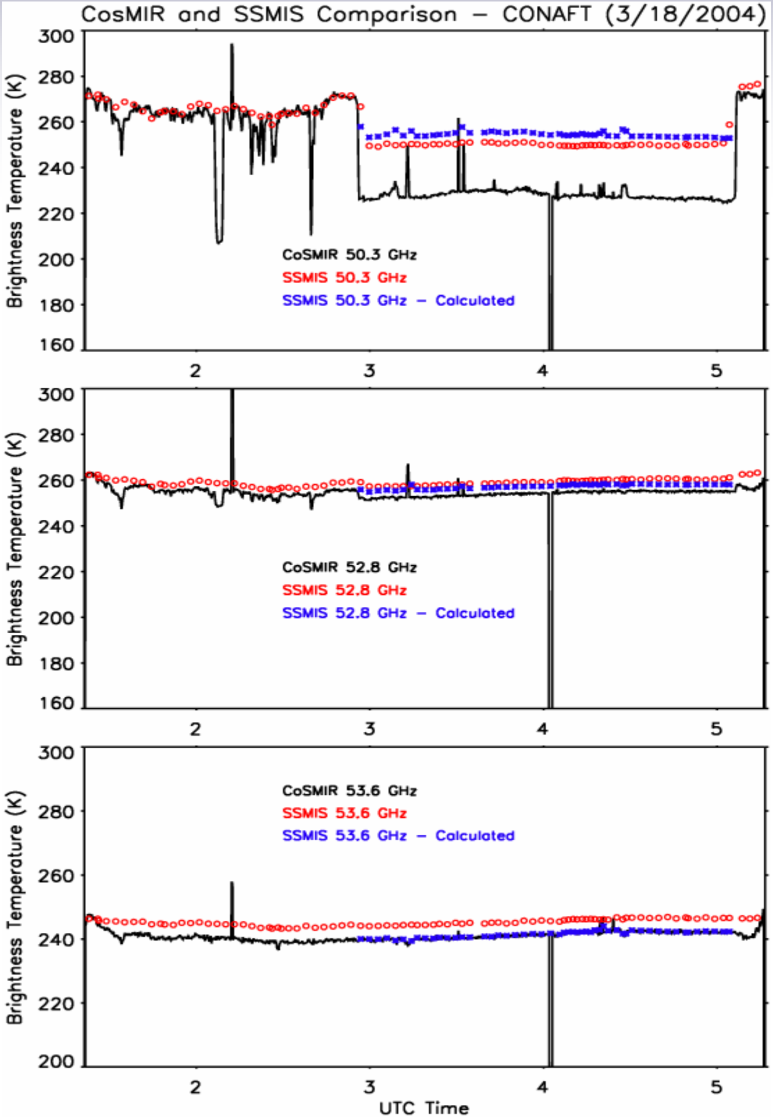
CosMIR and SSMIS Comparison – CONAFT (3/18/2004)
Brightness Temperature (K)
300
280
260
240
220
200
180
160
2
3
4
5
CoSMIR 50.3 GHz
SSMIS 50.3 GHz
SSMIS 50.3 GHz – Calculated
CoSMIR 52.8 GHz
SSMIS 52.8 GHz
SSMIS 52.8 GHz – Calculated
CoSMIR 53.6 GHz
SSMIS 53.6 GHz
SSMIS 53.6 GHz – Calculated
UTC Time

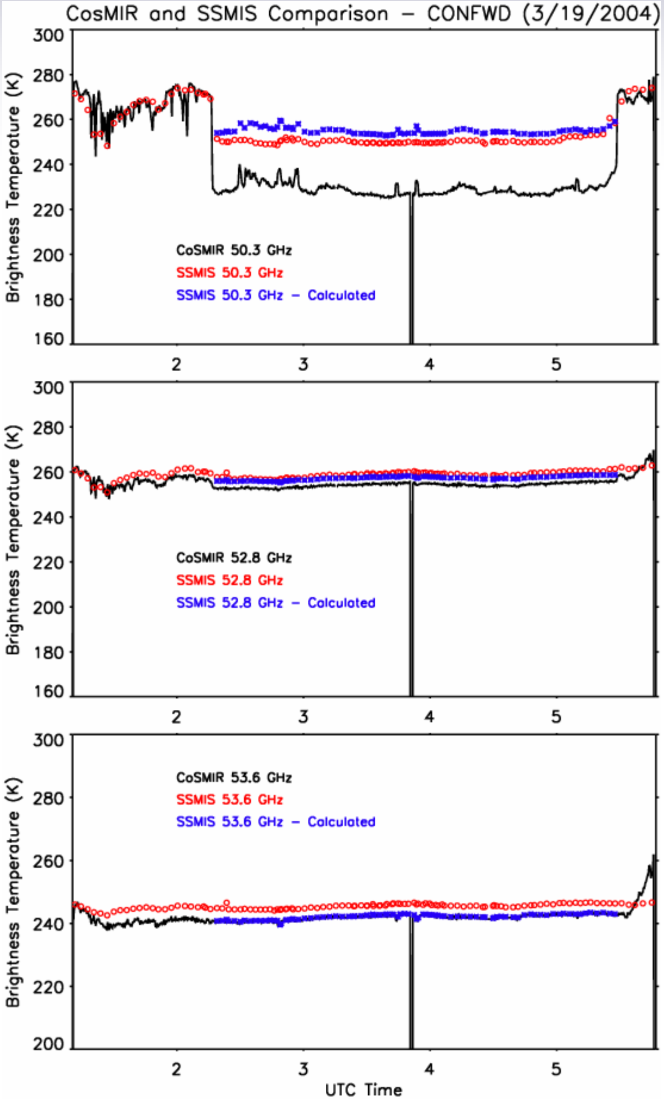
CosMIR and SSMIS Comparison – CONFWD (3/19/2004)
Brightness Temperature (K)
300
280
260
240
220
200
180
160
CoSMIR 50.3 GHz
SSMIS 50.3 GHz
SSMIS 50.3 GHz – Calculated
2
3
4
5
CoSMIR 52.8 GHz
SSMIS 52.8 GHz
SSMIS 52.8 GHz – Calculated
CoSMIR 53.6 GHz
SSMIS 53.6 GHz
SSMIS 53.6 GHz – Calculated
UTC Time

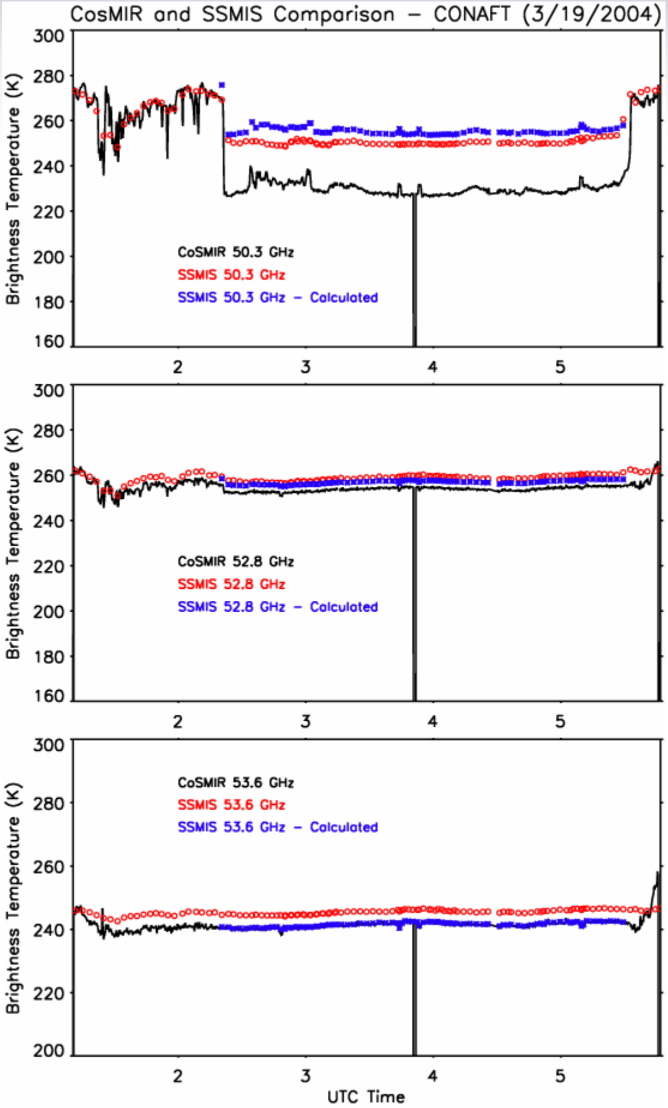
CosMIR and SSMIS Comparison – CONAFT (3/19/2004)
Brightness Temperature (K)
300
280
260
240
220
200
180
160
CoSMIR 50.3 GHz
SSMIS 50.3 GHz
SSMIS 50.3 GHz – Calculated
2
3
4
5
CoSMIR 52.8 GHz
SSMIS 52.8 GHz
SSMIS 52.8 GHz – Calculated
CoSMIR 53.6 GHz
SSMIS 53.6 GHz
SSMIS 53.6 GHz – Calculated
UTC Time

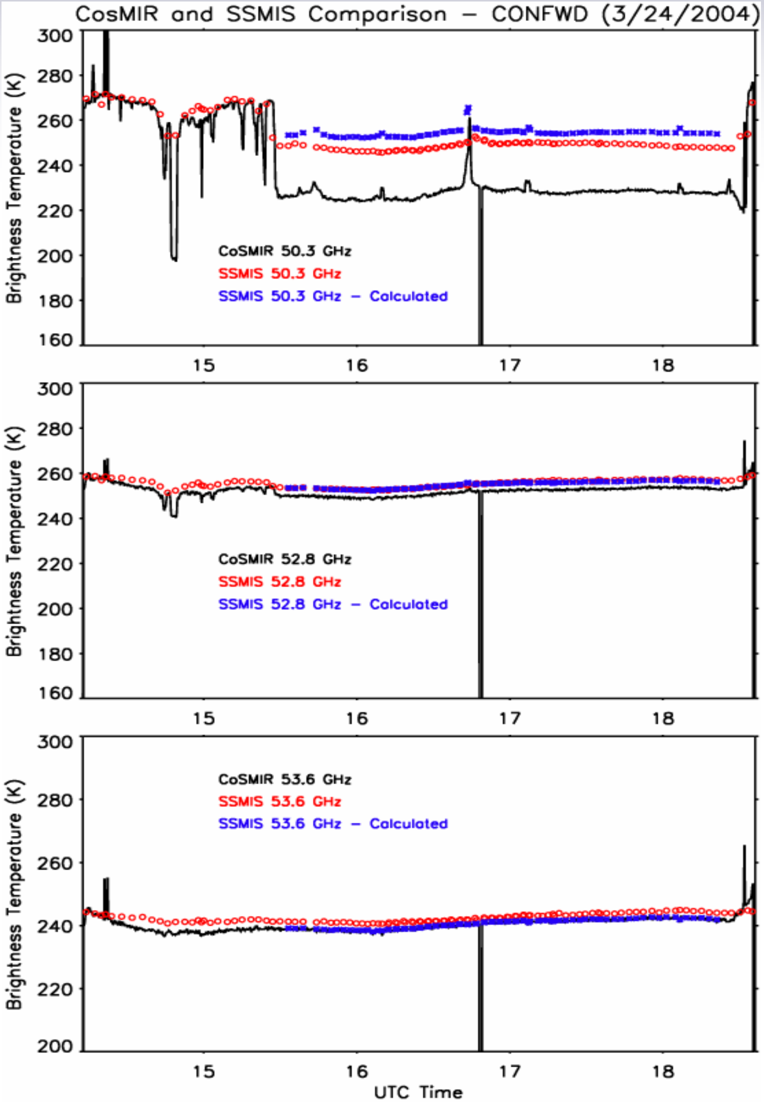
CosMIR and SSMIS Comparison – CONFWD (3/24/2004)
Brightness Temperature (K)
300
280
260
240
220
200
180
160
15
16
17
18
CoSMIR 50.3 GHz
SSMIS 50.3 GHz
SSMIS 50.3 GHz – Calculated
CoSMIR 52.8 GHz
SSMIS 52.8 GHz
SSMIS 52.8 GHz – Calculated
CoSMIR 53.6 GHz
SSMIS 53.6 GHz
SSMIS 53.6 GHz – Calculated
UTC Time

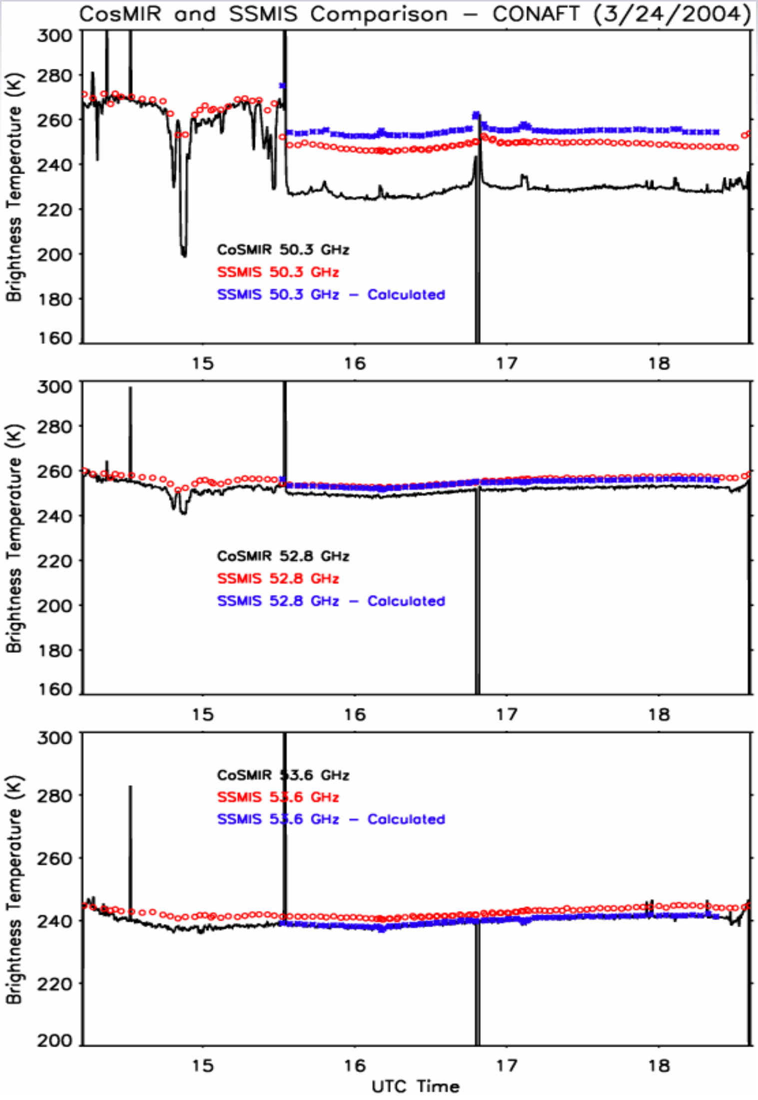
CosMIR and SSMIS Comparison – CONAFT (3/24/2004)
Brightness Temperature (K)
300
280
260
240
220
200
180
160
15
16
17
18
CoSMIR 50.3 GHz
SSMIS 50.3 GHz
SSMIS 50.3 GHz – Calculated
CoSMIR 52.8 GHz
SSMIS 52.8 GHz
SSMIS 52.8 GHz – Calculated
CoSMIR 53.6 GHz
SSMIS 53.6 GHz
SSMIS 53.6 GHz – Calculated
UTC Time

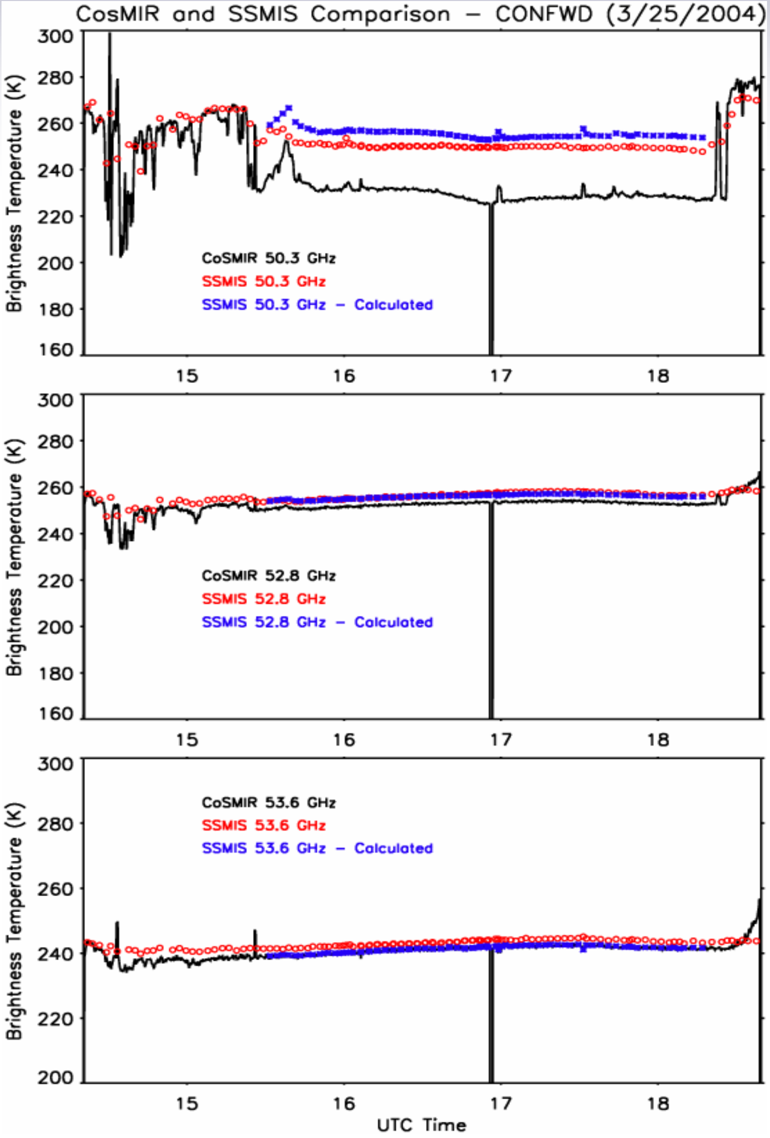
CosMIR and SSMIS Comparison – CONFWD (3/25/2004)

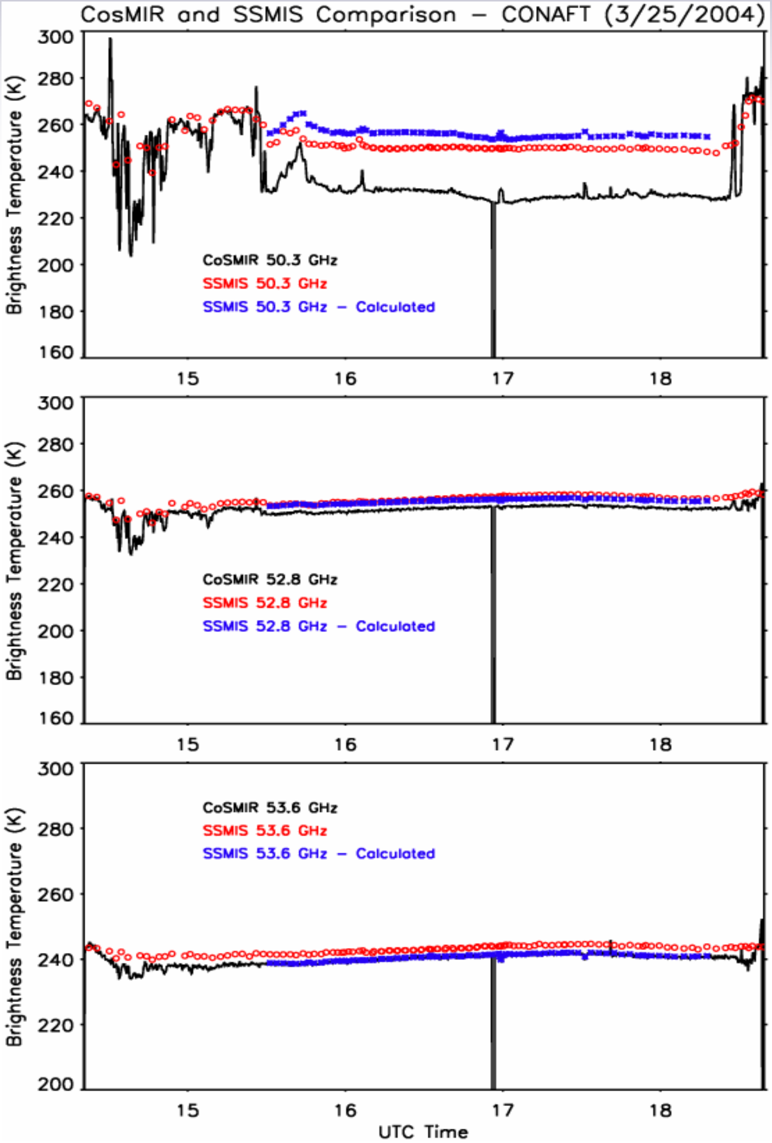
CosMIR and SSMIS Comparison – CONAFT (3/25/2004)

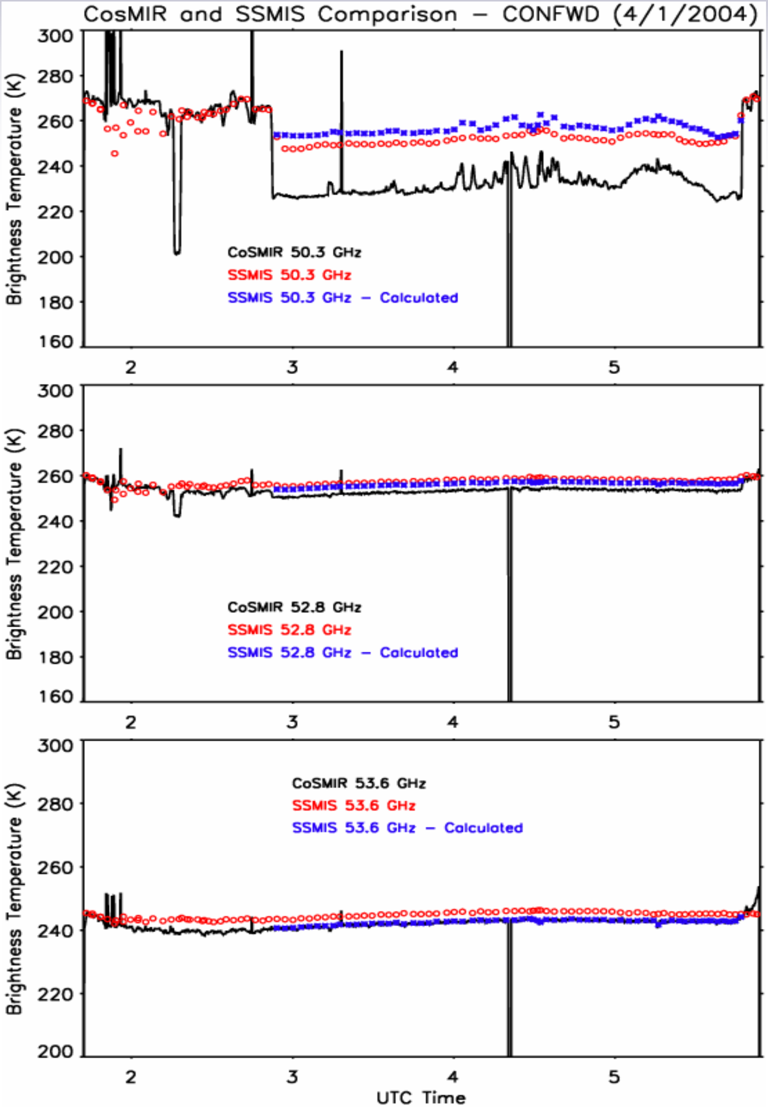
CosMIR and SSMIS Comparison – CONFWD (4/1/2004)
Brightness Temperature (K)
300
280
260
240
220
200
180
160
2
3
4
5
CoSMIR 50.3 GHz
SSMIS 50.3 GHz
SSMIS 50.3 GHz – Calculated
CoSMIR 52.8 GHz
SSMIS 52.8 GHz
SSMIS 52.8 GHz – Calculated
CoSMIR 53.6 GHz
SSMIS 53.6 GHz
SSMIS 53.6 GHz – Calculated
UTC Time

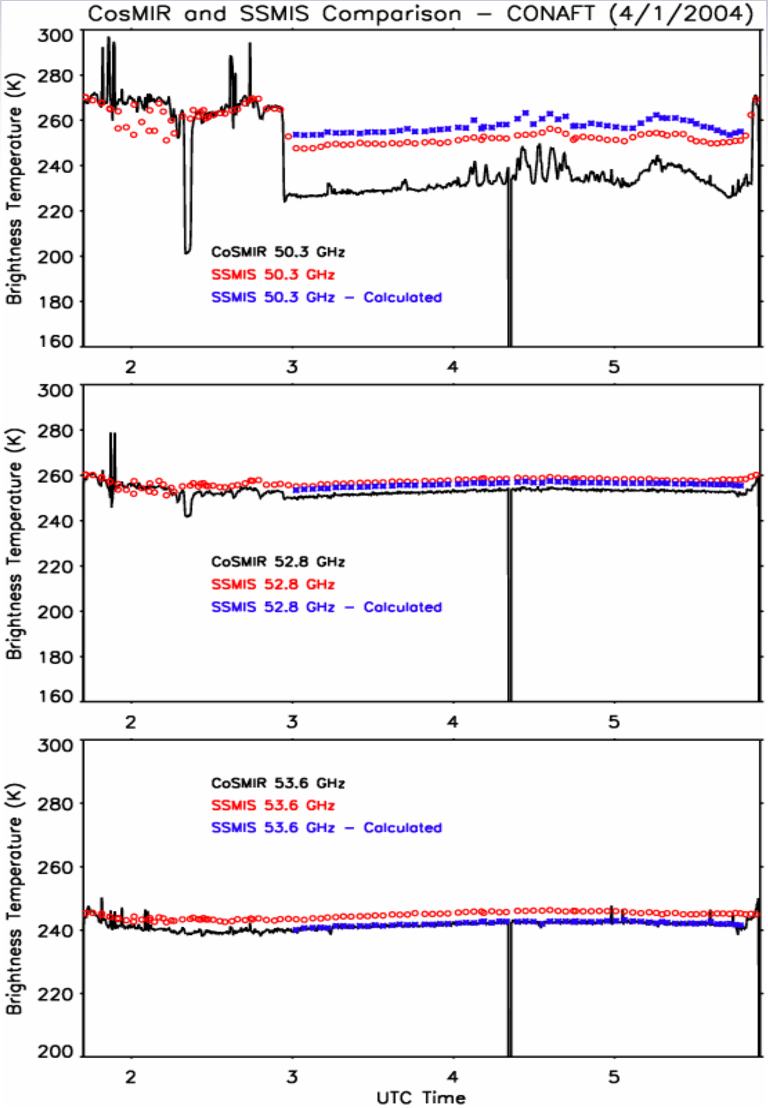
CosMIR and SSMIS Comparison – CONAFT (4/1/2004)
Brightness Temperature (K)
300
280
260
240
220
200
180
160
2
3
4
5
CoSMIR 50.3 GHz
SSMIS 50.3 GHz
SSMIS 50.3 GHz – Calculated
CoSMIR 52.8 GHz
SSMIS 52.8 GHz
SSMIS 52.8 GHz – Calculated
CoSMIR 53.6 GHz
SSMIS 53.6 GHz
SSMIS 53.6 GHz – Calculated
UTC Time

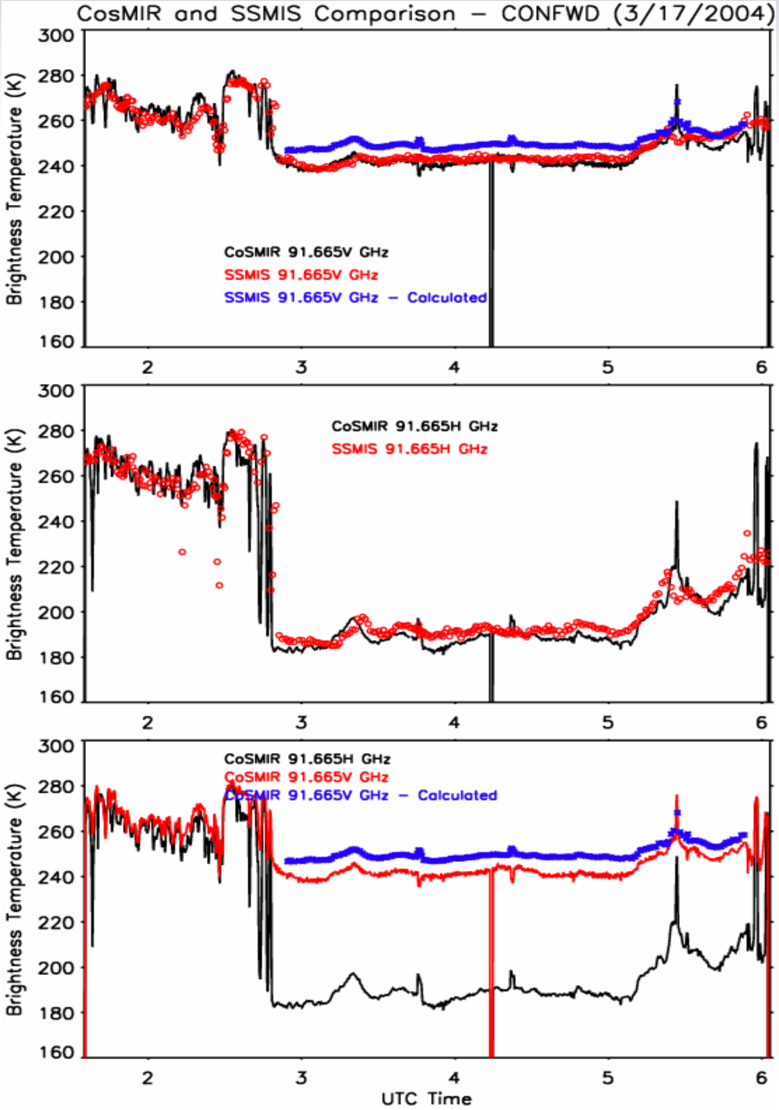

CosMIR and SSMIS Comparison – CONFWD (3/17/2004)
Brightness Temperature (K)
300
280
260
240
220
200
180
160
CoSMIR 91.665V GHz
SSMIS 91.665V GHz
SSMIS 91.665V GHz – Calculated
CoSMIR 91.665H GHz
SSMIS 91.665H GHz
CoSMIR 91.665H GHz
CoSMIR 91.665V GHz
CoSMIR 91.665V GHz – Calculated
2
3
4
5
6
UTC Time

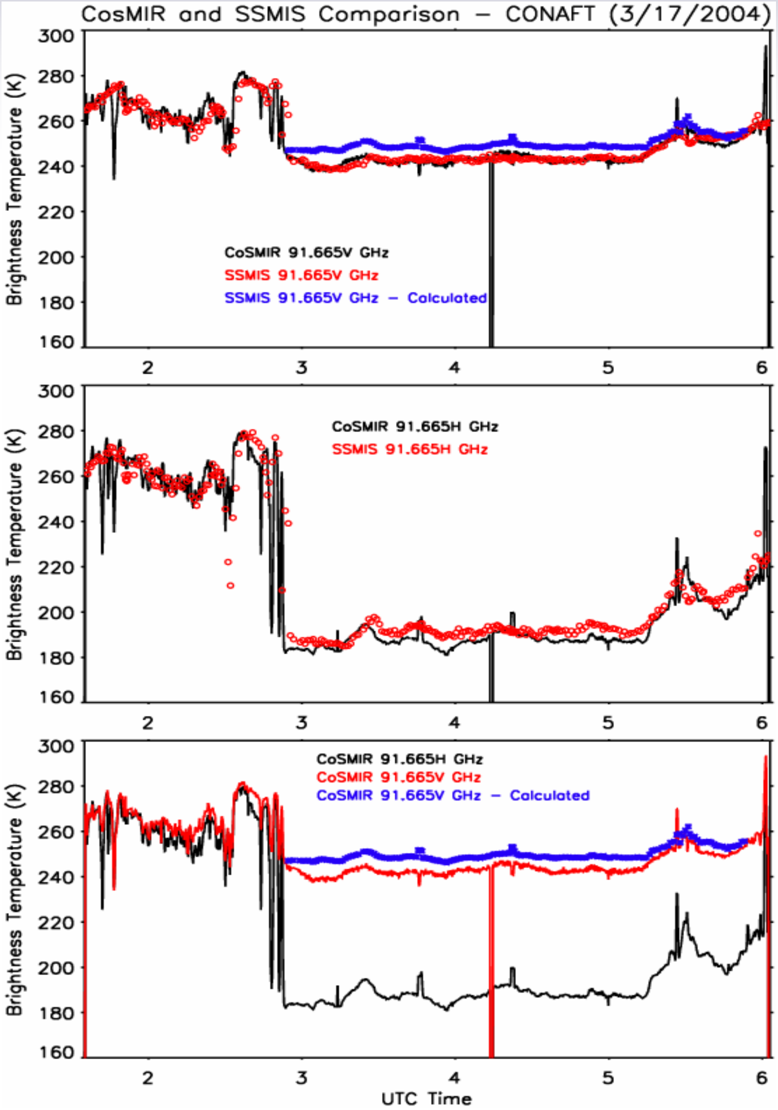

CosMIR and SSMIS Comparison – CONAFT (3/17/2004)
Brightness Temperature (K)
300
280
260
240
220
200
180
160
CoSMIR 91.665V GHz
SSMIS 91.665V GHz
SSMIS 91.665V GHz – Calculated
CoSMIR 91.665H GHz
SSMIS 91.665H GHz
CoSMIR 91.665H GHz
CoSMIR 91.665V GHz
CoSMIR 91.665V GHz – Calculated
2
3
4
5
6
UTC Time

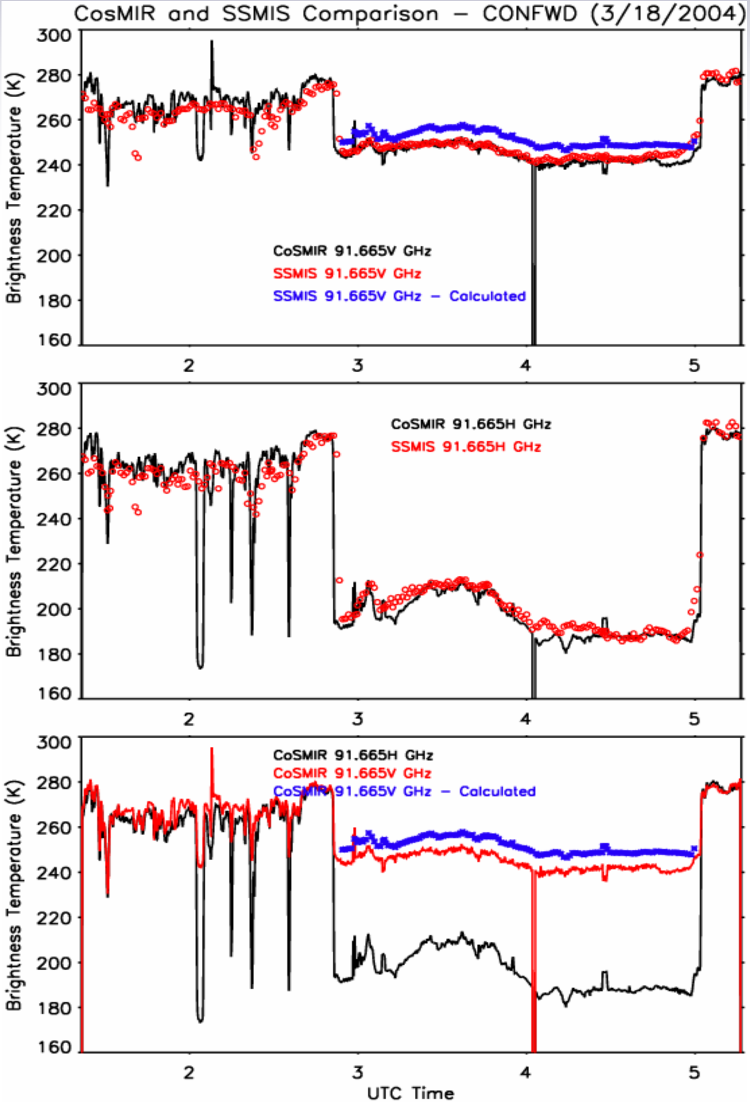
CosMIR and SSMIS Comparison – CONFWD (3/18/2004)

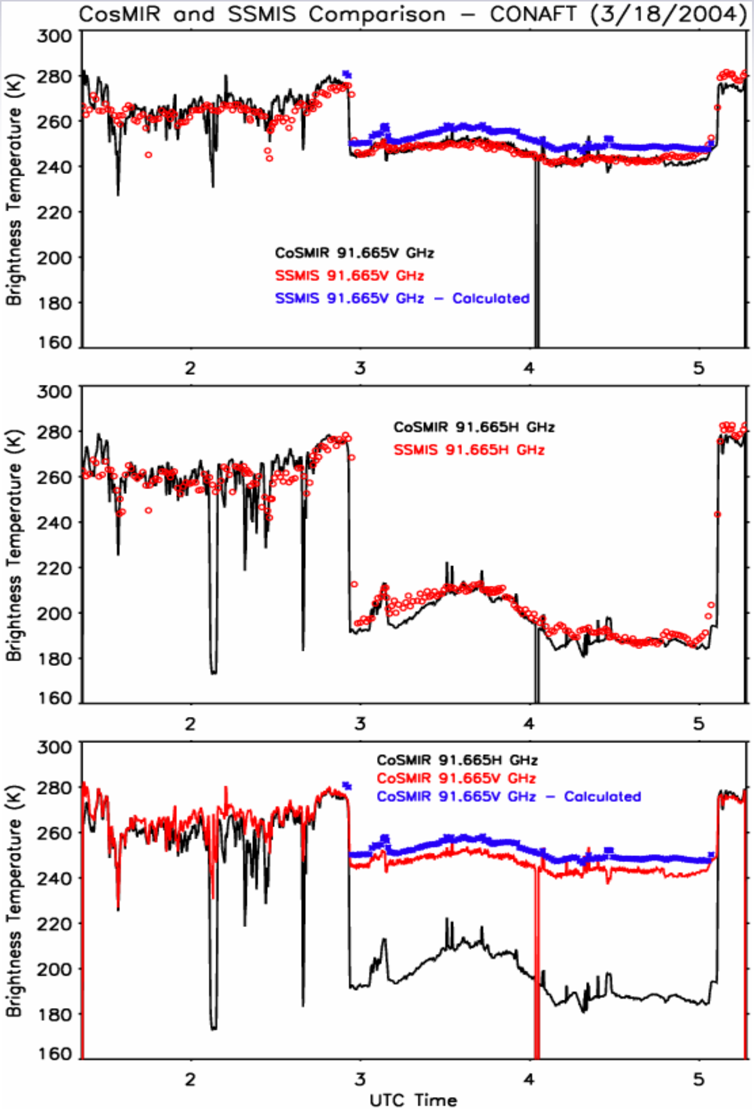
CosMIR and SSMIS Comparison – CONAFT (3/18/2004)

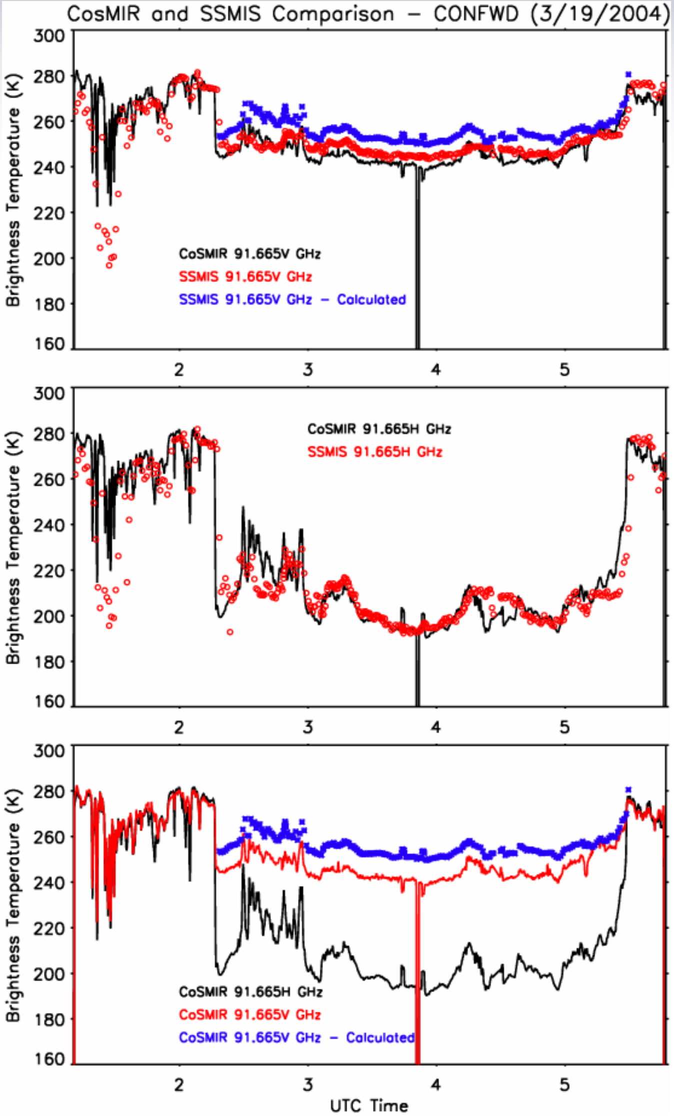
CosMIR and SSMIS Comparison – CONFWD (3/19/2004)
Brightness Temperature (K)
300
280
260
240
220
200
180
160
CoSMIR 91.665V GHz
SSMIS 91.665V GHz
SSMIS 91.665V GHz – Calculated
2
3
4
5
CoSMIR 91.665H GHz
SSMIS 91.665H GHz
CoSMIR 91.665H GHz
CoSMIR 91.665V GHz
CoSMIR 91.665V GHz – Calculated
UTC Time

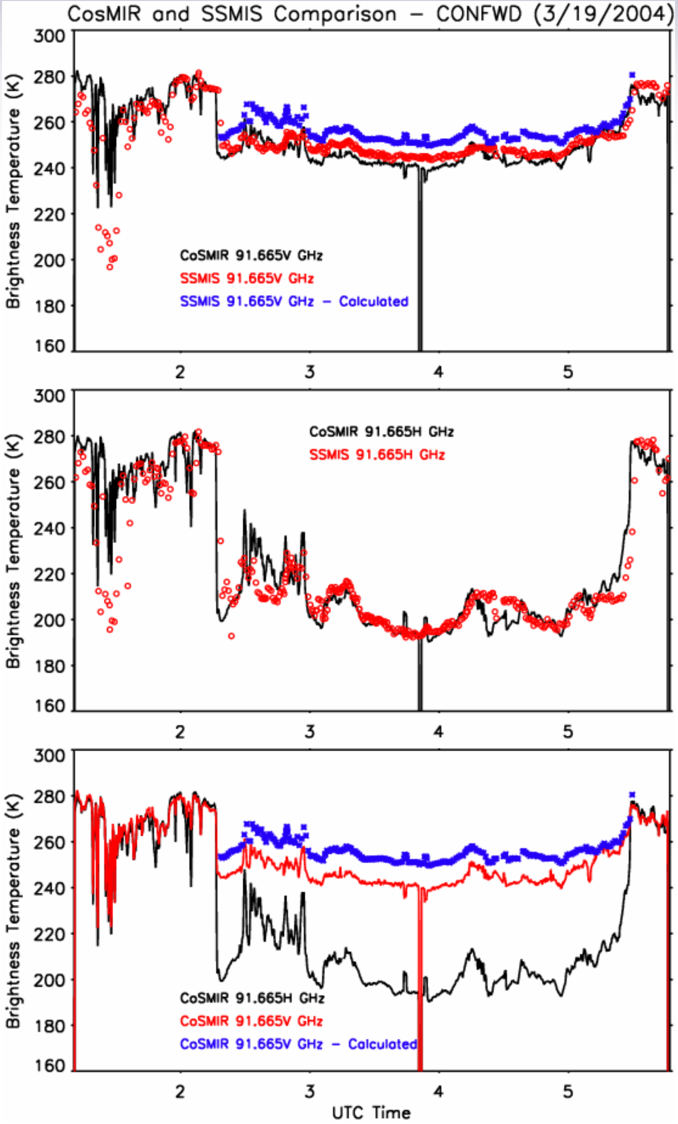
CosMIR and SSMIS Comparison – CONFWD (3/19/2004)
Brightness Temperature (K)
300
280
260
240
220
200
180
160
CoSMIR 91.665V GHz
SSMIS 91.665V GHz
SSMIS 91.665V GHz – Calculated
2
3
4
5
CoSMIR 91.665H GHz
SSMIS 91.665H GHz
CoSMIR 91.665H GHz
CoSMIR 91.665V GHz
CoSMIR 91.665V GHz – Calculated
UTC Time

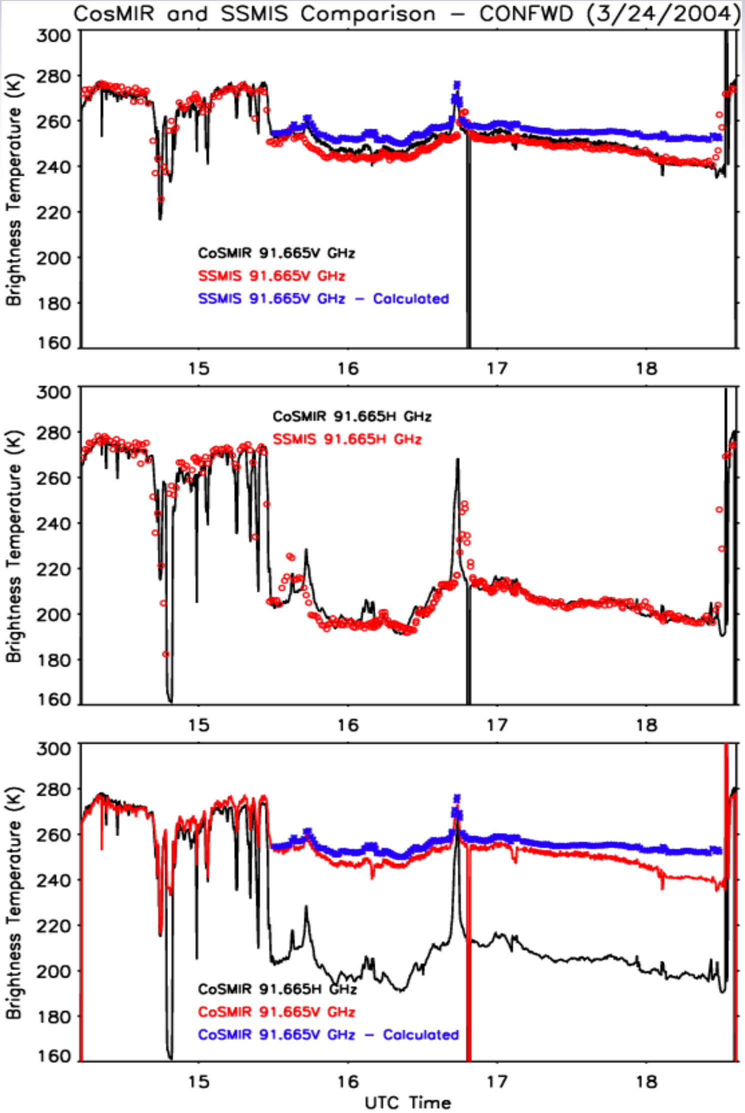

CosMIR and SSMIS Comparison – CONFWD (3/24/2004)

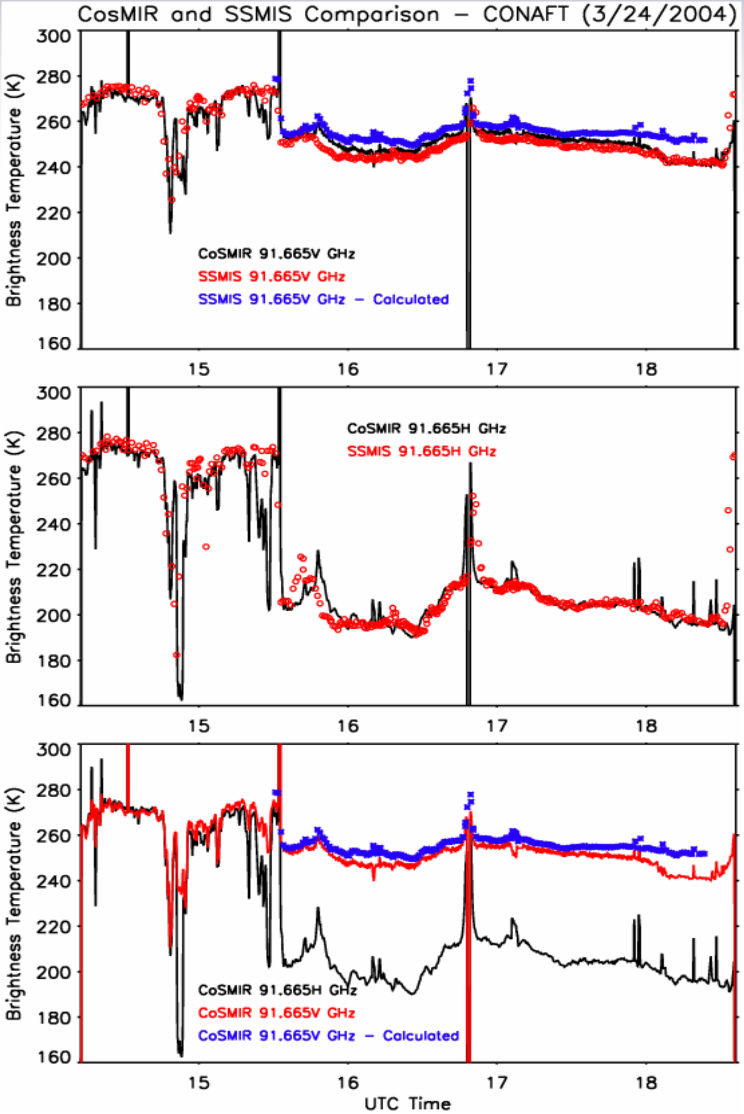

CosMIR and SSMIS Comparison – CONAFT (3/24/2004)

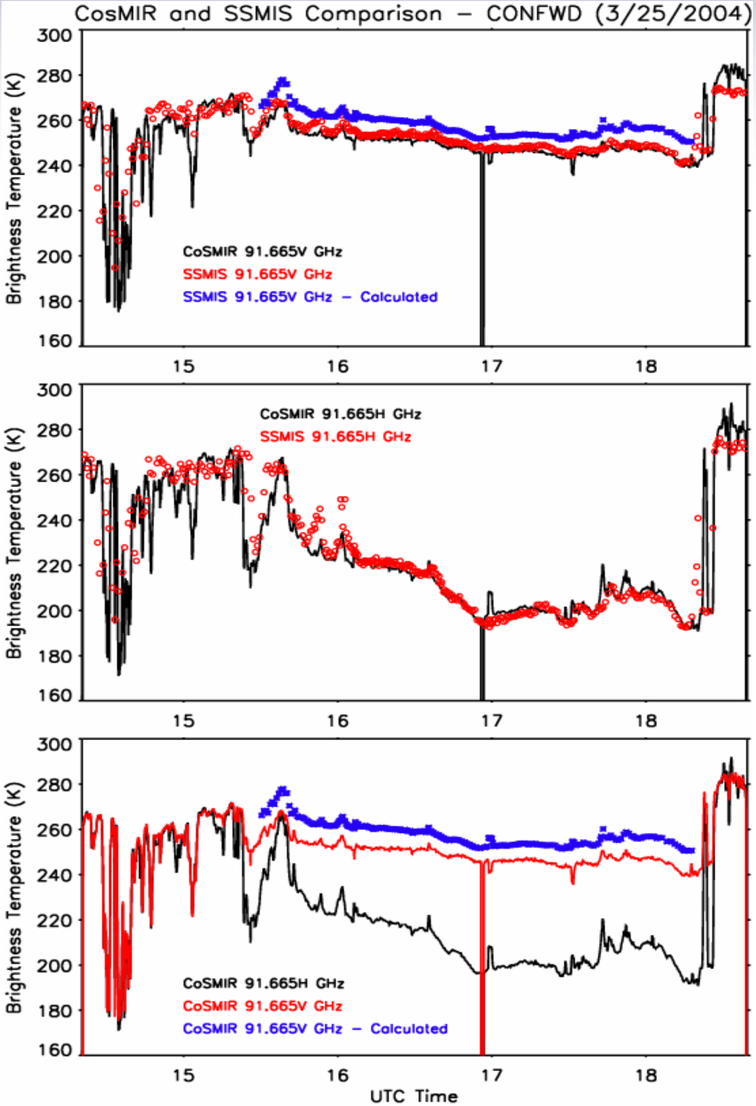

CosMIR and SSMIS Comparison – CONFWD (3/25/2004)

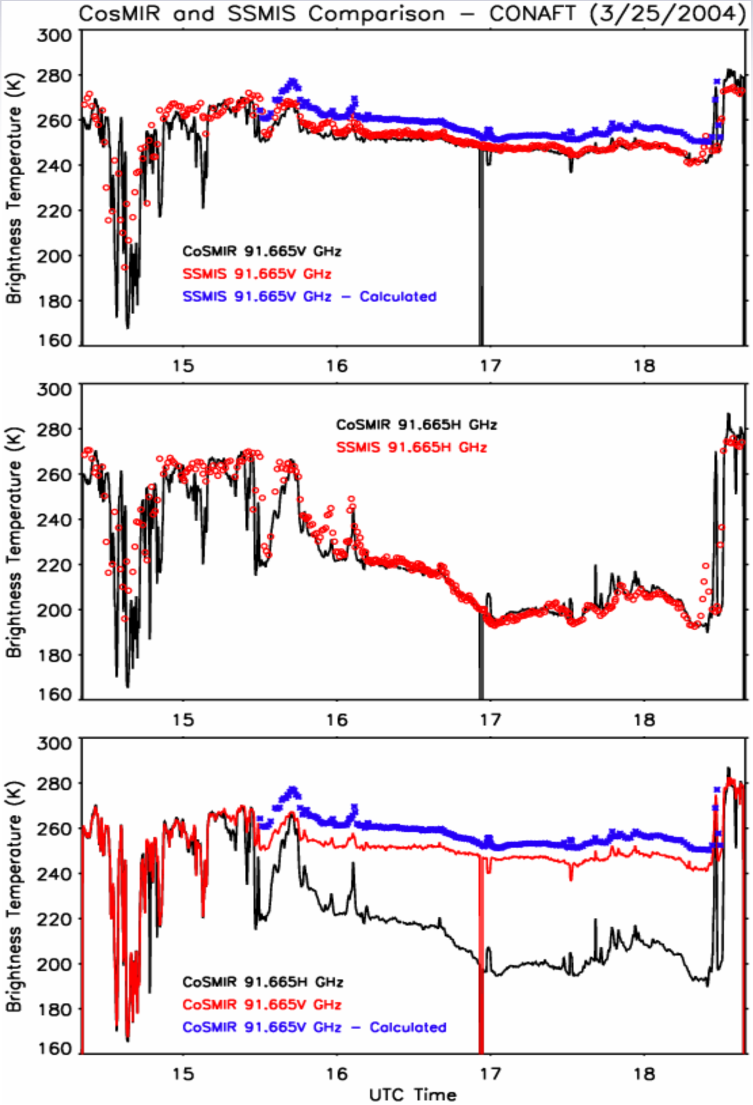

CosMIR and SSMIS Comparison – CONAFT (3/25/2004)

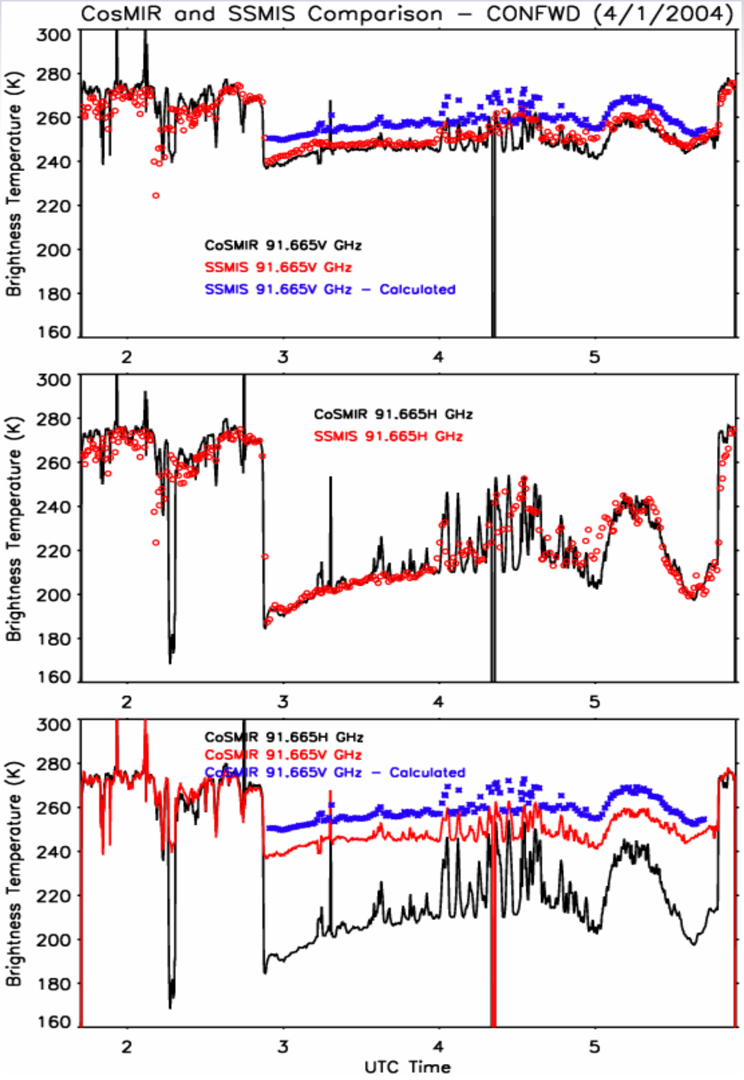
CosMIR and SSMIS Comparison – CONFWD (4/1/2004)
Brightness Temperature (K)
300
280
260
240
220
200
180
160
2
3
4
5
CoSMIR 91.665V GHz
SSMIS 91.665V GHz
SSMIS 91.665V GHz – Calculated
CoSMIR 91.665H GHz
SSMIS 91.665H GHz
CoSMIR 91.665H GHz
CoSMIR 91.665V GHz
CoSMIR 91.665V GHz – Calculated
UTC Time

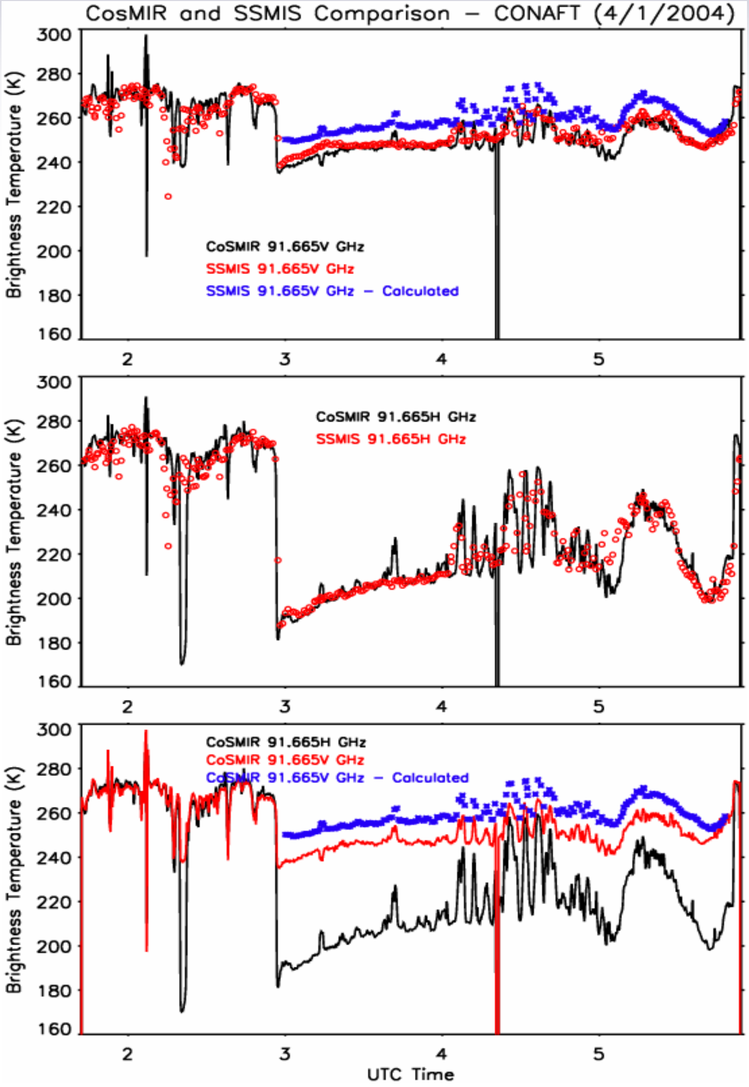
CosMIR and SSMIS Comparison – CONAFT (4/1/2004)
Brightness Temperature (K)
300
280
260
240
220
200
180
160
2
3
4
5
CoSMIR 91.665V GHz
SSMIS 91.665V GHz
SSMIS 91.665V GHz – Calculated
CoSMIR 91.665H GHz
SSMIS 91.665H GHz
CoSMIR 91.665H GHz
CoSMIR 91.665V GHz
CoSMIR 91.665V GHz – Calculated
UTC Time

Brief Summary of 50-54 GHz Brightness Calculations

- Relations between the vertically and horizontally T_b values at 50-54 GHz and 91.665 GHz over a calm ocean surface were derived from a vast set of rawinsonde data.
- The T_{bv} values at 50.3, 52.8 and 53.6 GHz were calculated from such relations from the CoSMIR T_{bh} measurements and compared with the corresponding SSMIS values. The calculated T_{bv} values were generally 5-10 K higher than those of SSMIS.
- The same procedure was applied to the 91.665 GHz channels of the SSMIS and CoSMIR. Again the calculated T_{bv} values were higher than those measured by both SSMIS and CoSMIR.
- Attempt to estimate the SSMIS 50-54 GHz T_b's from the CoSMIR measurements doesn't appear convincing because of many unknown factors (e.g., surface roughness).

Conclusions

- Based on laboratory test data and the in-flight data the lakes, the accuracy of the calibrated CoSMIR brightness temperatures (T_b) is very good. Thus, the data sets acquired from the under-flights are adequate for calibration/validation of the SSMIS.
- Comparison of the SSMIS and CoSMIR T_b values suggests that the 50 GHz channels of the SSMIS are vertically polarized. For the other channels between 91-183 GHz, the SSMIS measurements are generally higher.
- The positive biases of the SSMIS 50-183 GHz channels appear to depend slightly on the times of the overpasses.
- Attempts to estimate the T_b values of the SSMIS 50-54 GHz channels from the corresponding CoSMIR measurements are not plausible because of unknown environmental conditions.
- Calibration/validation efforts should be made at the same polarization – change the 50-54 GHz channels of the CoSMIR to vertical polarization and repeat the SSMIS under-flights.

Comparison of SSMIS – CoSMIR Brightness

Based on Under-Flights

Between 12/3/2004 – 3/14/2005

- **This flight sequence was made after the three 50 GHz channels of CoSMIR were modified from horizontal to vertical polarization.**
- **The SSMIS brightness temperatures were derived based on data prepared and coefficients supplied by Steve Swadley (coefficients supplied in December 2004).**
- **Four under-flights were completed, three of them for the ascending passes (12/3/2004, 3/9/2005, and 3/10/2005), and one for the descending pass (3/14/2005).**
- **The two flights on 12/3/2004 and 3/14/2005 are similar to the one conducted during March-April 2004, i.e., near the California coastal region.**
- **The two flights on 3/9/2005 and 3/10/2005 extends toward south to catch the anomaly described by Steve Swadley.**
- **The 50.3 GHz channel of CoSMIR became noisy during some parts of the flight on 3/102005. During the last flight on 3/14/2005, this noise problem became worse.**
- **The calibration at 91.655 GHz, V-pol., may be slightly off during this series of flights.**

Lake Calibration and Comparison from 12/2/2004 Flight

- **The flights on 12/3/2004 and 3/14/2005 passed over Lake Tahoe, which offers a good calibration target for CoSMIR measurements. Slide #3 below show a comparison of the measurements and calculations based on Rawinsondes from Reno, Nevada (between 12/1/2004 and March 2005). All except the V-pol. 91.655 GHz channel fit in nicely with calculations. The 91.655-V channel appears a little low at 53.4° incidence and high at nadir.**
- **CoSMIR lost about one hour of data towards the end of the flight on 12/3/2004. Slide #4 shows the flight track of available measurements.**
- **Slide #5 shows a comparison of T_b variations from 6 selected channels along the aircraft flight path. The comparison is made separately for CoSMIR's forward and aft scans.**
- **Slide #6 shows the scatter plots (separately for CoSMIR's forward and aft scans) of SSMIS and CoSMIR T_b values. The biases and rms values are calculated from the entire data set; thus observations over both land and ocean surfaces are included. A few data points with values of Tb differences greater than 10 K (more than 3 times standard deviation) are excluded in the calculations**

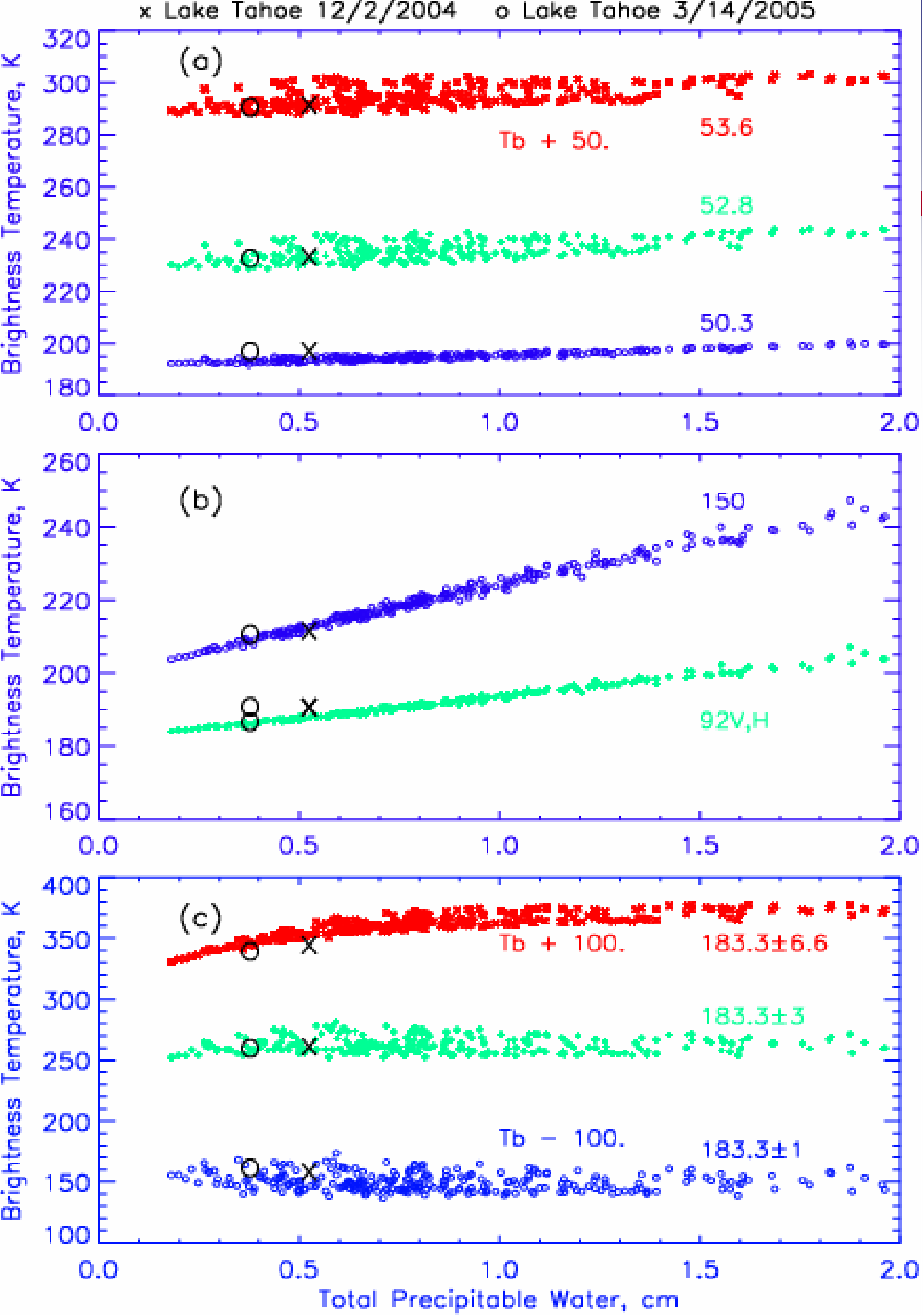
x Lake Tahoe 12/2/2004
o Lake Tahoe 3/14/2005
(a)
Tb + 50.
53.6
52.8
50.3
(b)
150
92V,H
(c)
Tb + 100.
183.3±6.6
183.3±3
Tb − 100.
183.3±1
Brightness Temperature, K
Total Precipitable Water, cm
320
300
280
260
240
220
200
180
160
400
350
250
150
100
0.0
0.5
1.0
1.5
2.0

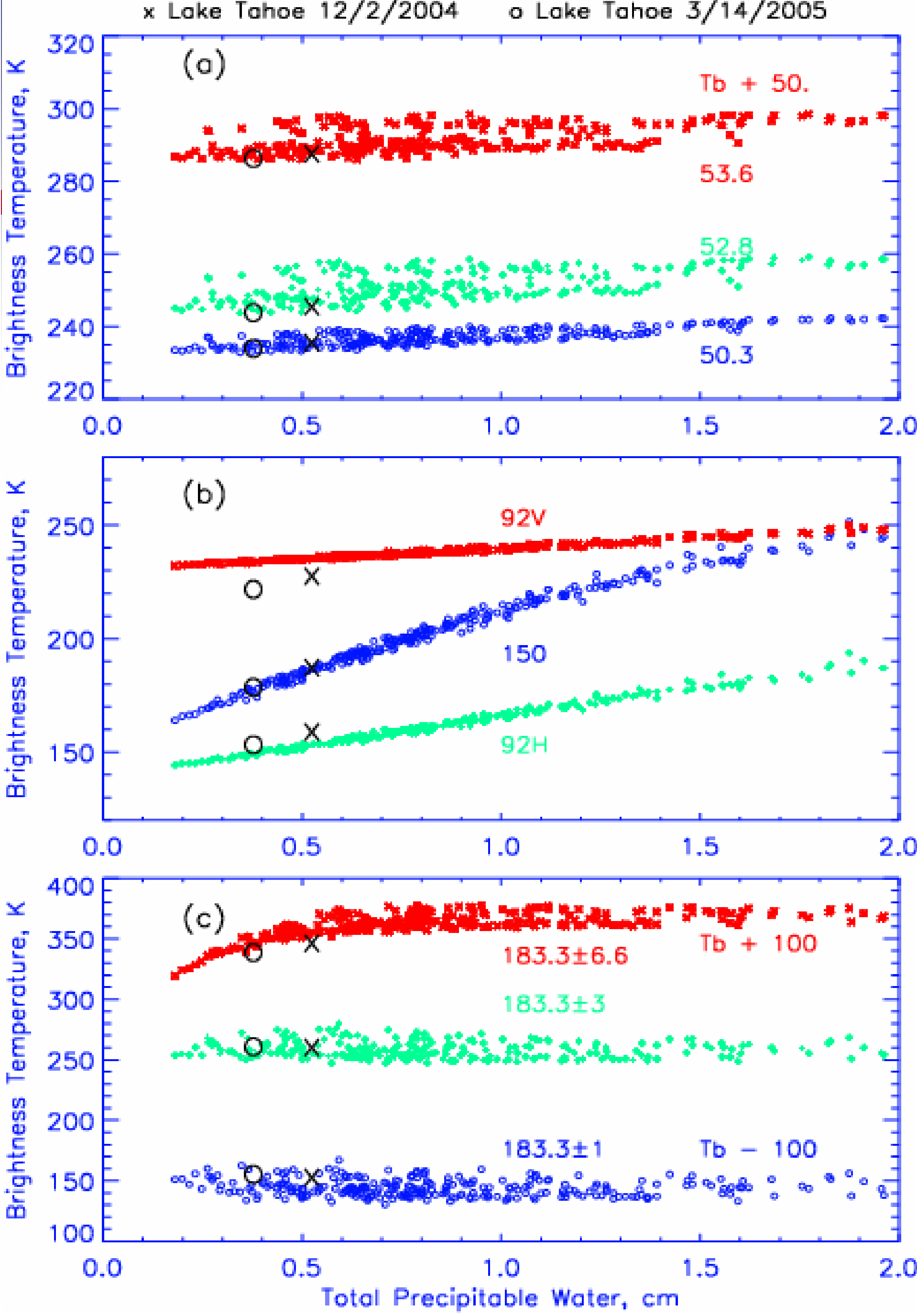
x Lake Tahoe 12/2/2004
o Lake Tahoe 3/14/2005
(a)
Tb + 50.
53.6
52.8
50.3
(b)
92V
150
92H
(c)
183.3±6.6
Tb + 100
183.3±3
183.3±1
Tb − 100
Brightness Temperature, K
Total Precipitable Water, cm
320
300
280
260
240
220
250
200
150
400
350
100
0.0
0.5
1.0
1.5
2.0

CoSMIR Flight Path

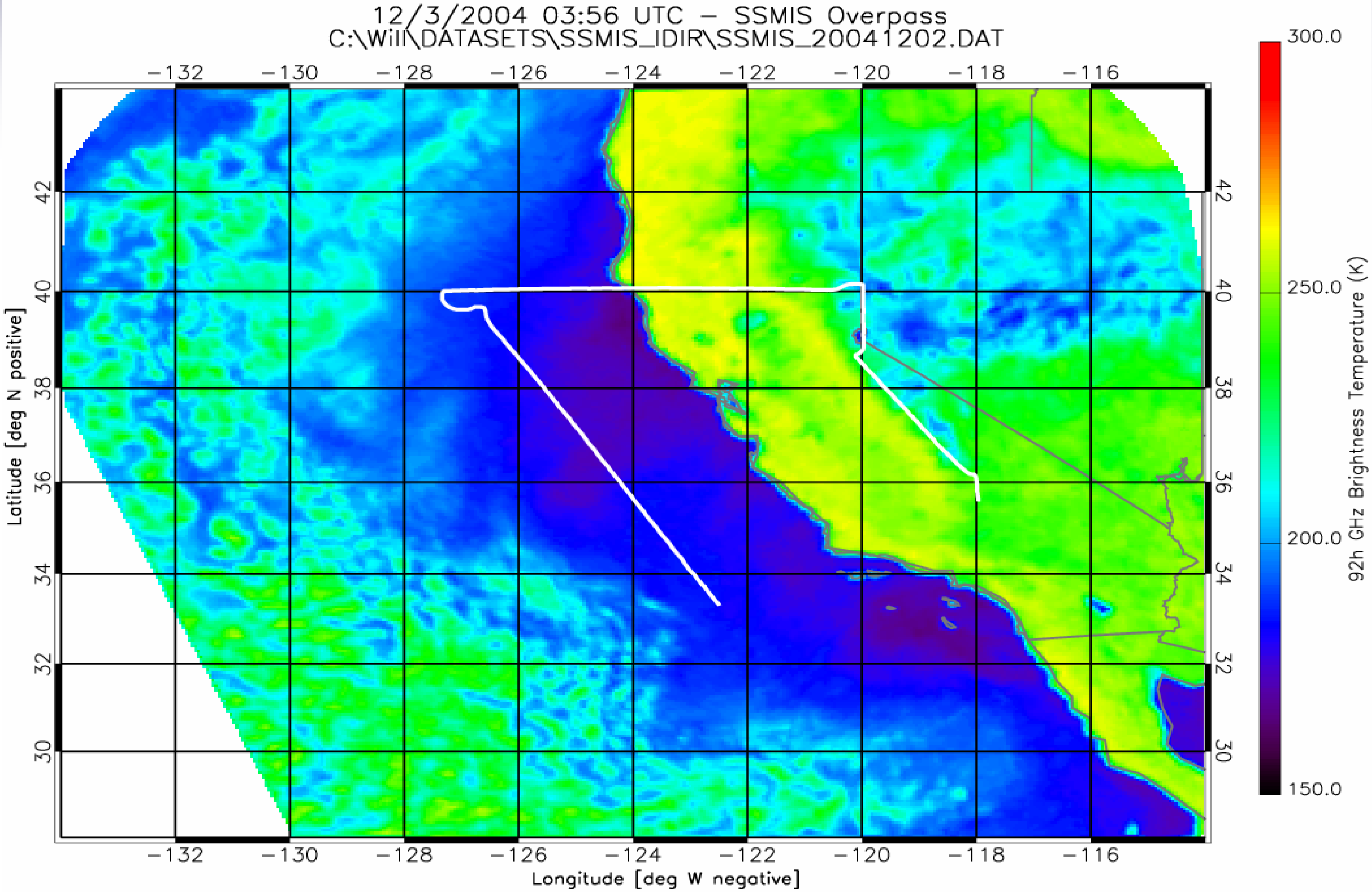

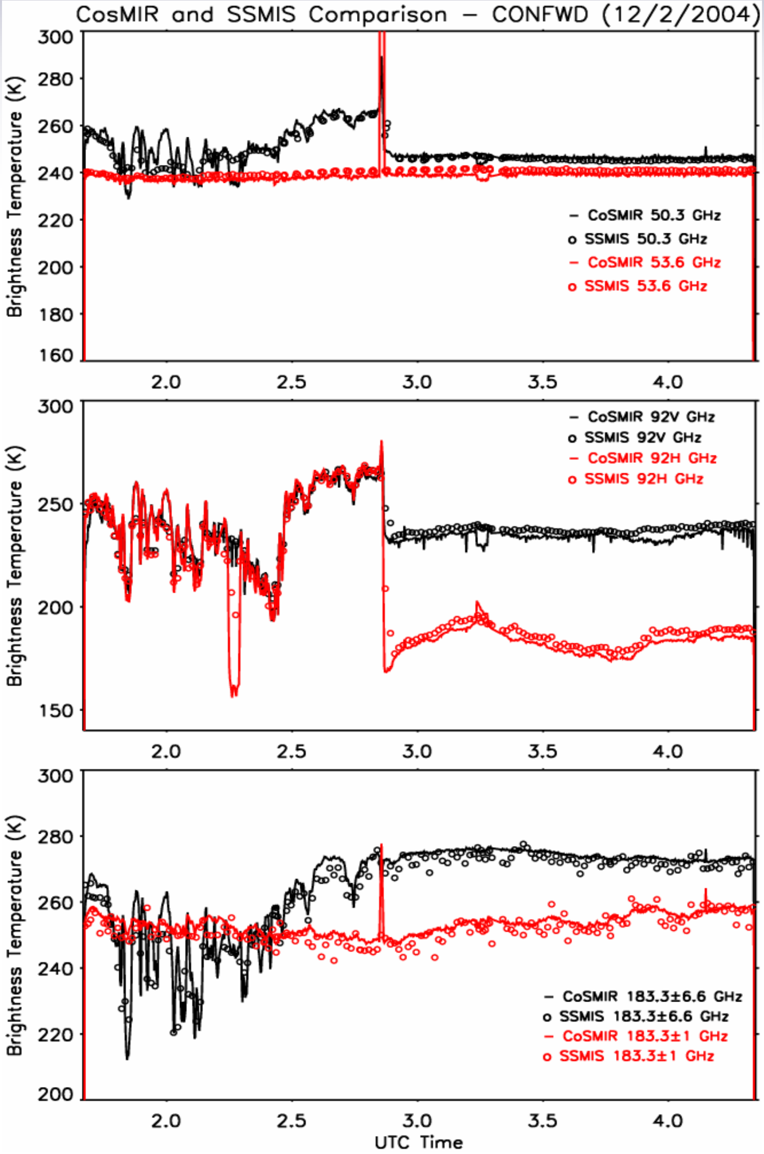

CosMIR and SSMIS Comparison – CONFWD (12/2/2004)

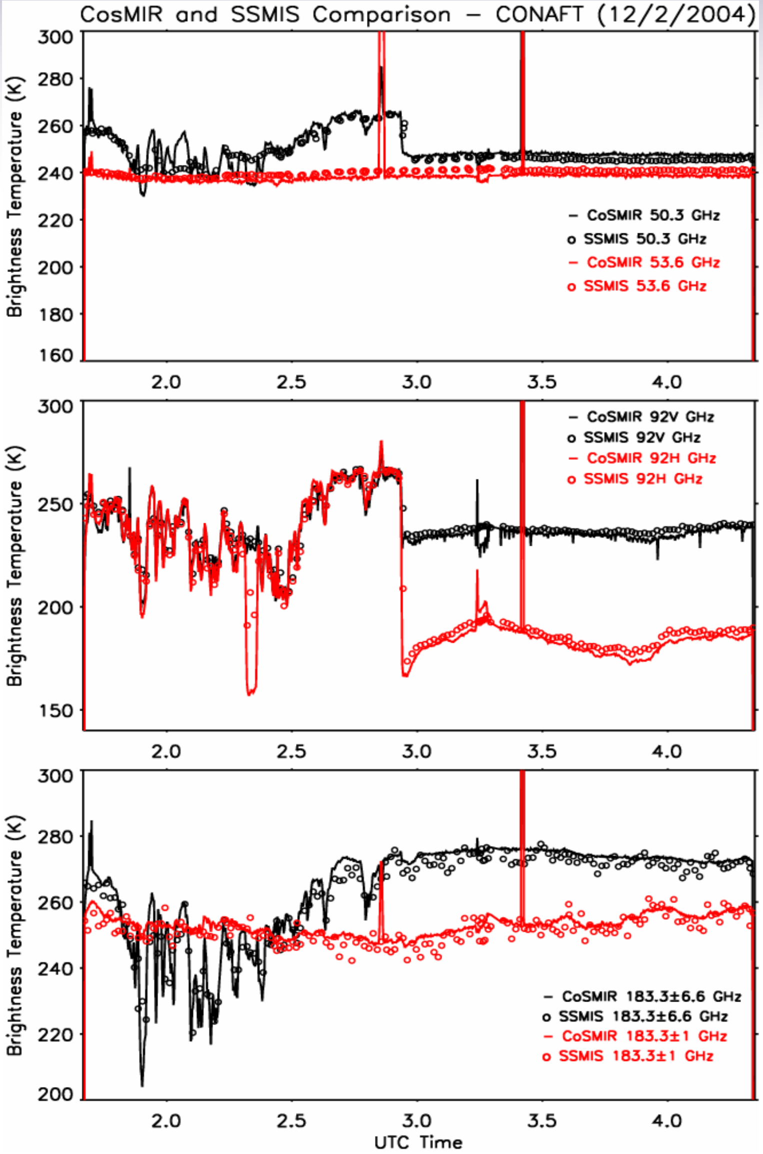

CosMIR and SSMIS Comparison – CONAFT (12/2/2004)

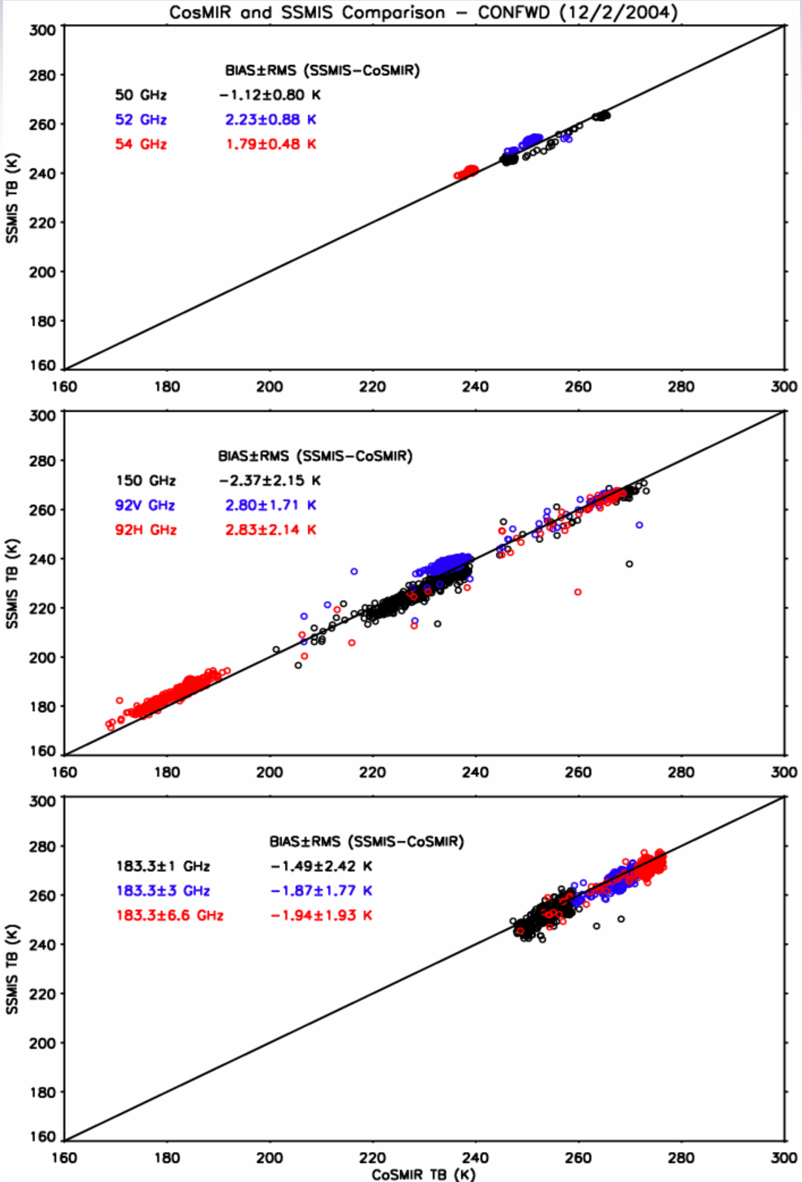
CosMIR and SSMIS Comparison – CONFWD (12/2/2004)
BIAS±RMS (SSMIS–CoSMIR)
50 GHz –1.12±0.80 K
52 GHz 2.23±0.88 K
54 GHz 1.79±0.48 K
BIAS±RMS (SSMIS–CoSMIR)
150 GHz –2.37±2.15 K
92V GHz 2.80±1.71 K
92H GHz 2.83±2.14 K
BIAS±RMS (SSMIS–CoSMIR)
183.3±1 GHz –1.49±2.42 K
183.3±3 GHz –1.87±1.77 K
183.3±6.6 GHz –1.94±1.93 K
SSMIS TB (K)
CoSMIR TB (K)
160
180
200
220
240
260
280
300

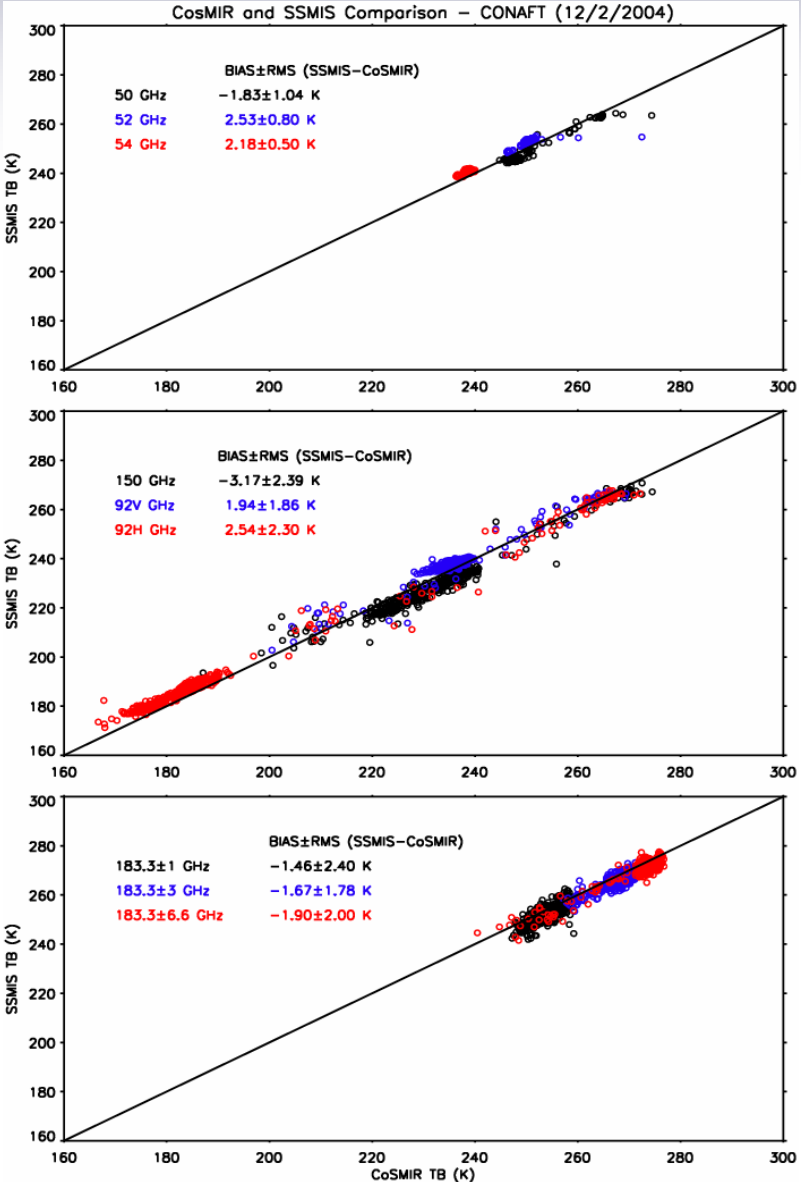
CosMIR and SSMIS Comparison – CONAFT (12/2/2004)
BIAS±RMS (SSMIS–CoSMIR)
50 GHz –1.83±1.04 K
52 GHz 2.53±0.80 K
54 GHz 2.18±0.50 K
BIAS±RMS (SSMIS–CoSMIR)
150 GHz –3.17±2.39 K
92V GHz 1.94±1.86 K
92H GHz 2.54±2.30 K
BIAS±RMS (SSMIS–CoSMIR)
183.3±1 GHz –1.46±2.40 K
183.3±3 GHz –1.67±1.78 K
183.3±6.6 GHz –1.90±2.00 K
SSMIS TB (K)
CoSMIR TB (K)
160
180
200
220
240
260
280
300

Comparison of SSMIS and CoSMIR from the 3/9/2005 Flight

- **Slide #8 gives the CoSMIR flight path overlaid on the brightness map of the SSMIS 91.655-H channel. Most of the region covered by the flight is cloudy.**
- **Slide #9 shows a comparison of T_b variations from 6 selected channels along the aircraft flight path. The comparison is made with CoSMIR data in the forward scans.**
- **Slide #10 shows a comparison of T_b variations from 6 selected channels along the aircraft flight path. The comparison is made with CoSMIR data in the aft scans.**
- **Slide #11 shows the scatter plots (again separately for CoSMIR's forward and aft scans) of SSMIS and CoSMIR T_b values. The biases and rms values are calculated from the entire data set; thus observations over both land and ocean surfaces are included.**
- **Slides #12 (50.3, 52.8 and 53.6 GHz), #13 (91.655 V&H, and 150 GHz), and #14 (three 183.3 GHz channels) show the variations of T_b differences with latitudes. The linear regressions cover the latitude ranges of 19°-32° and 19°-29° for the 50 and 183.3 GHz channels, respectively.**

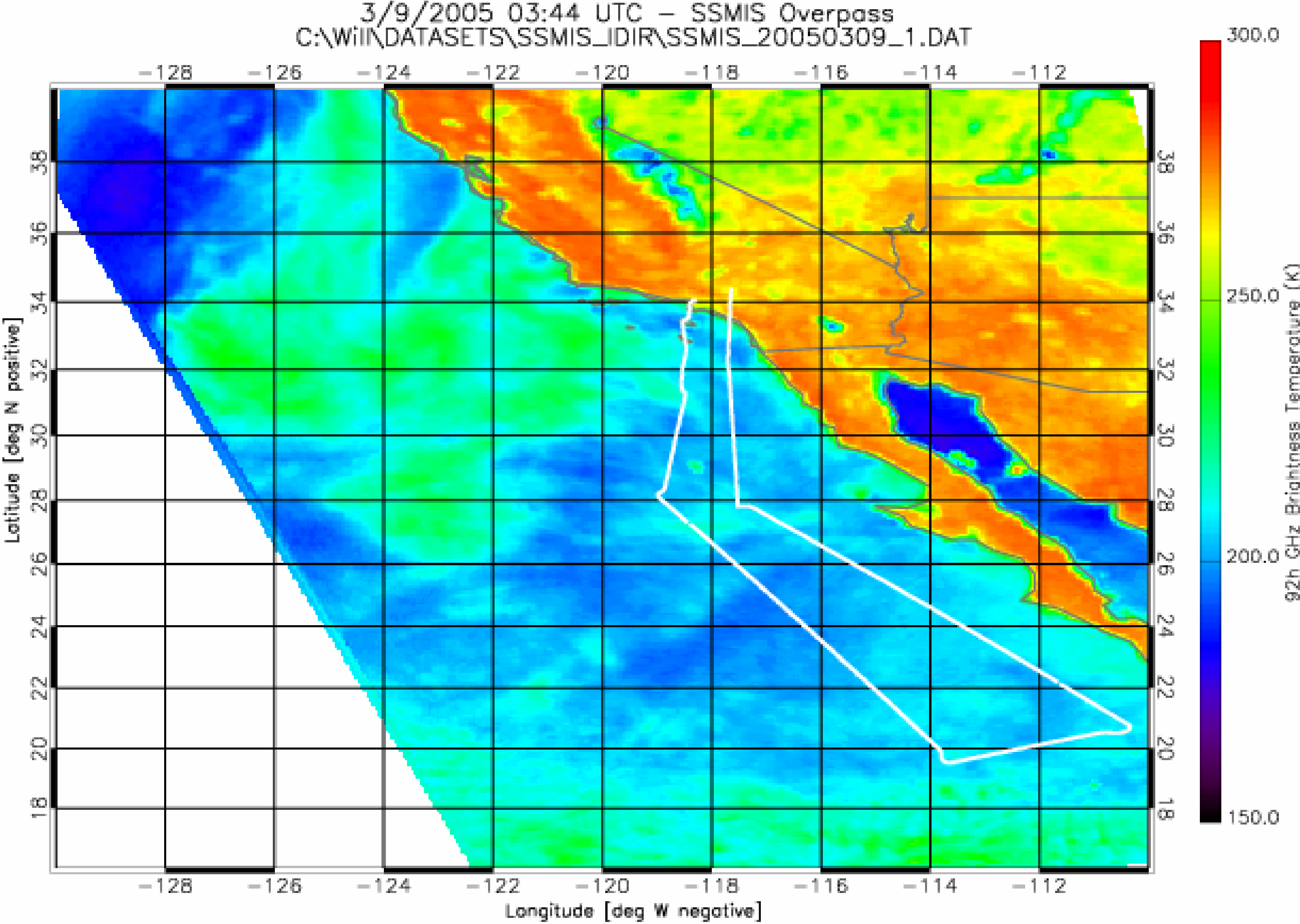
3/9/2005 03:44 UTC – SSMIS Overpass
C:\Will\DATASETS\SSMIS_IDIR\SSMIS_20050309_1.DAT
–128
–126
–124
–122
–120
–118
–116
–114
–112
38
36
34
32
30
28
26
24
22
20
18
Latitude [deg N positive]
Longitude [deg W negative]
300.0
250.0
200.0
150.0
92h GHz Brightness Temperature (K)

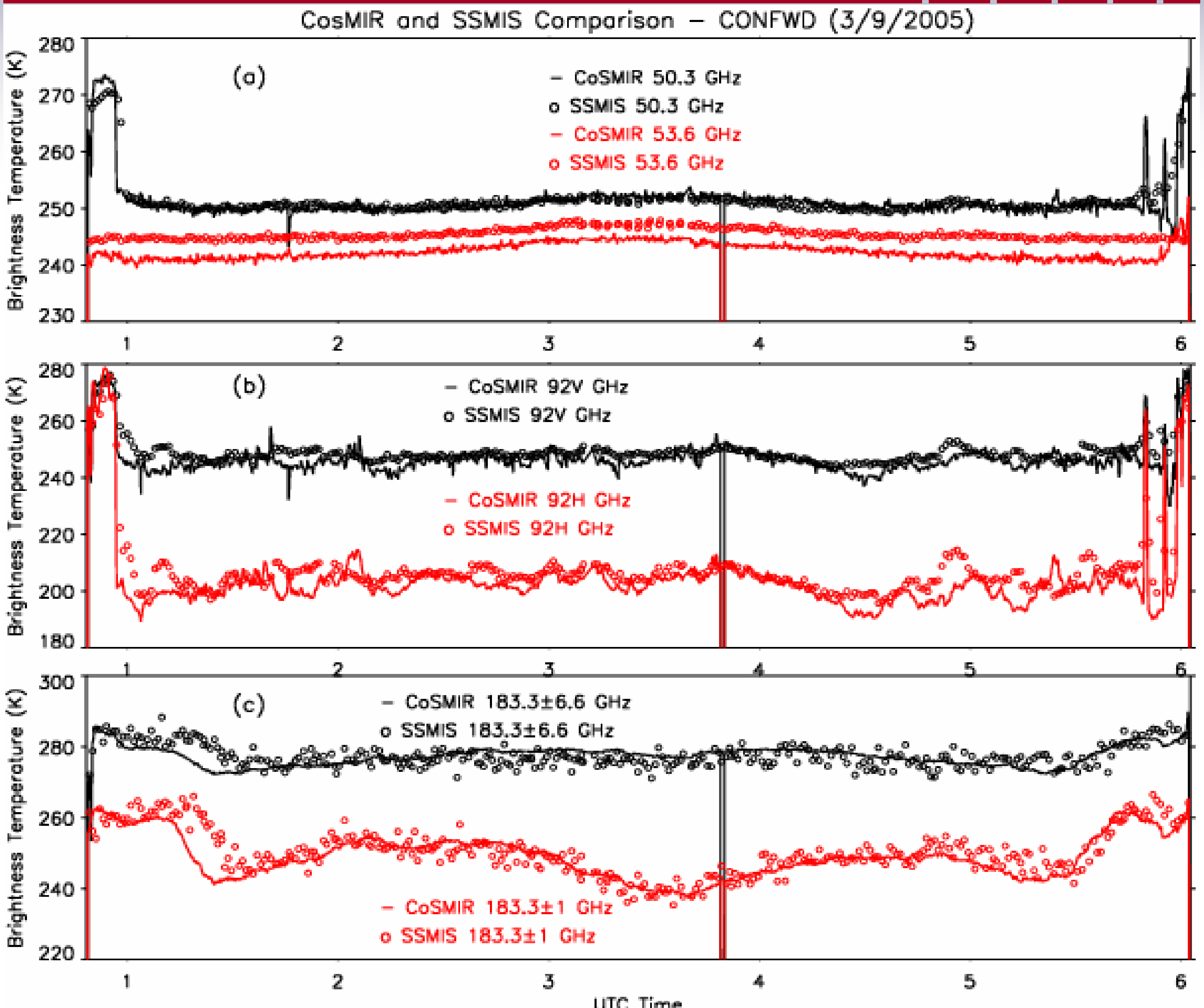
CoSMIR and SSMIS Comparison – CONFWD (3/9/2005)
(a)
– CoSMIR 50.3 GHz
o SSMIS 50.3 GHz
– CoSMIR 53.6 GHz
o SSMIS 53.6 GHz
Brightness Temperature (K)
280
270
260
250
240
230
1
2
3
4
5
6
(b)
– CoSMIR 92V GHz
o SSMIS 92V GHz
– CoSMIR 92H GHz
o SSMIS 92H GHz
Brightness Temperature (K)
280
260
240
220
200
180
(c)
– CoSMIR 183.3±6.6 GHz
o SSMIS 183.3±6.6 GHz
– CoSMIR 183.3±1 GHz
o SSMIS 183.3±1 GHz
Brightness Temperature (K)
300
280
260
240
220
UTC Time

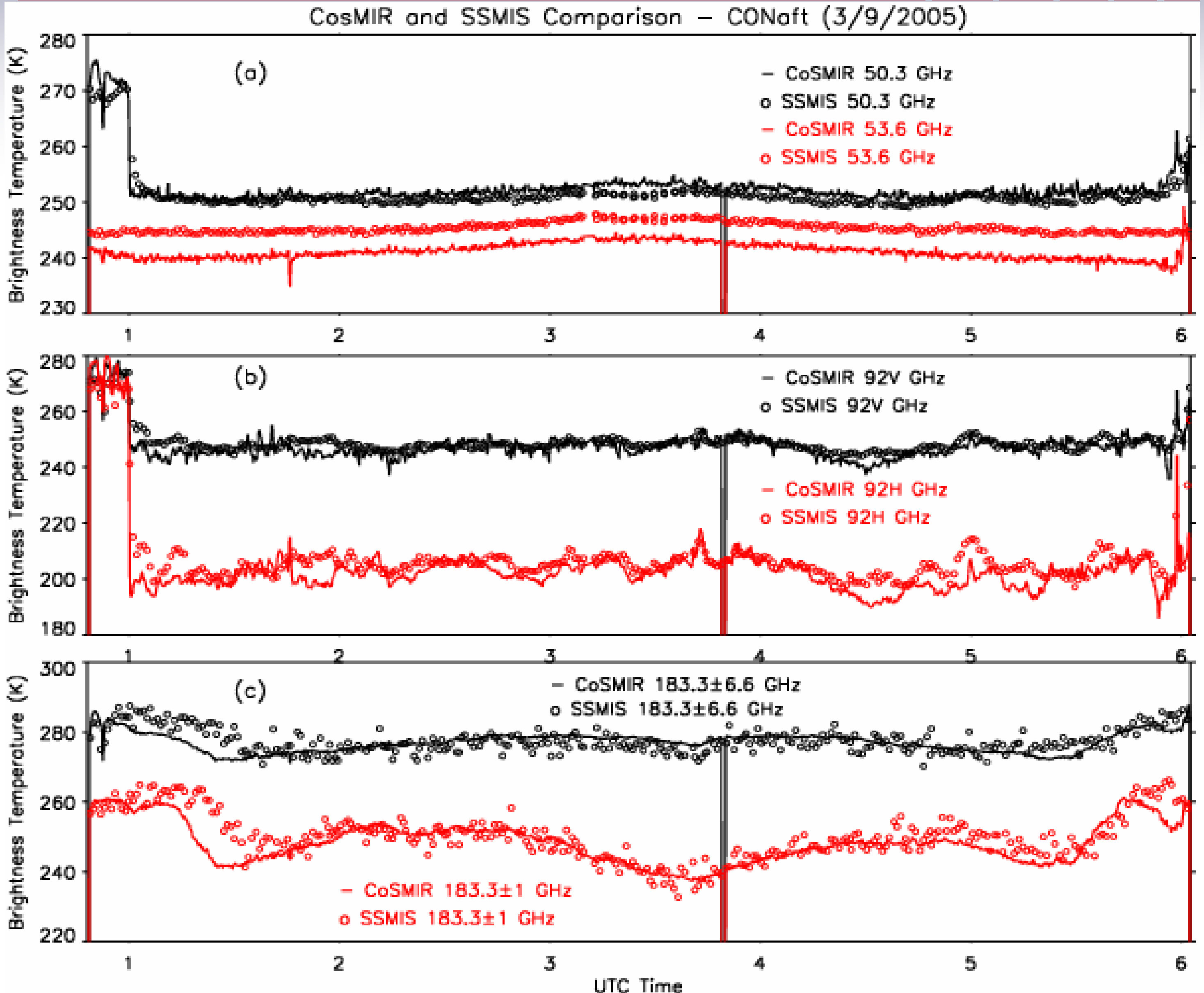
CosMIR and SSMIS Comparison – CONaft (3/9/2005)
(a)
– CoSMIR 50.3 GHz
o SSMIS 50.3 GHz
– CoSMIR 53.6 GHz
o SSMIS 53.6 GHz
(b)
– CoSMIR 92V GHz
o SSMIS 92V GHz
– CoSMIR 92H GHz
o SSMIS 92H GHz
(c)
– CoSMIR 183.3±6.6 GHz
o SSMIS 183.3±6.6 GHz
– CoSMIR 183.3±1 GHz
o SSMIS 183.3±1 GHz
Brightness Temperature (K)
280
270
260
250
240
230
260
220
200
180
300
1
2
3
4
5
6
UTC Time

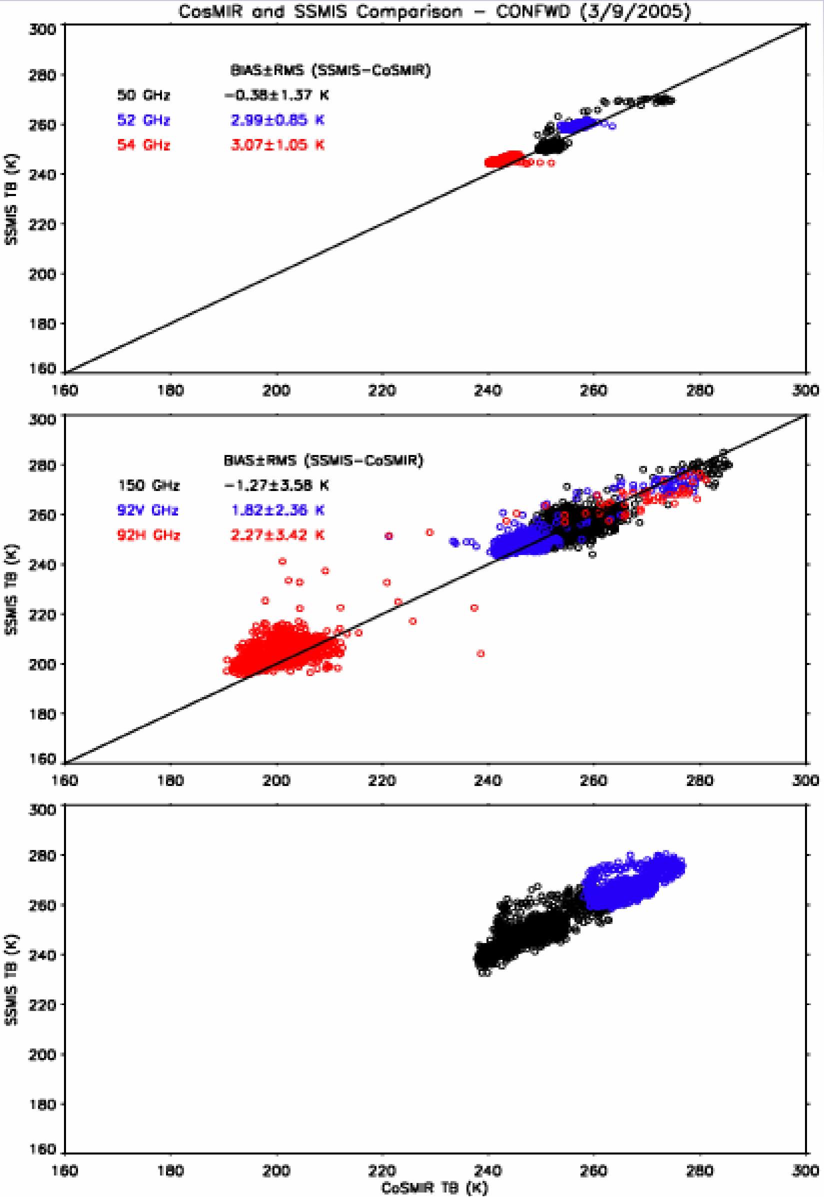

CosMIR and SSMIS Comparison – CONFWD (3/9/2005)

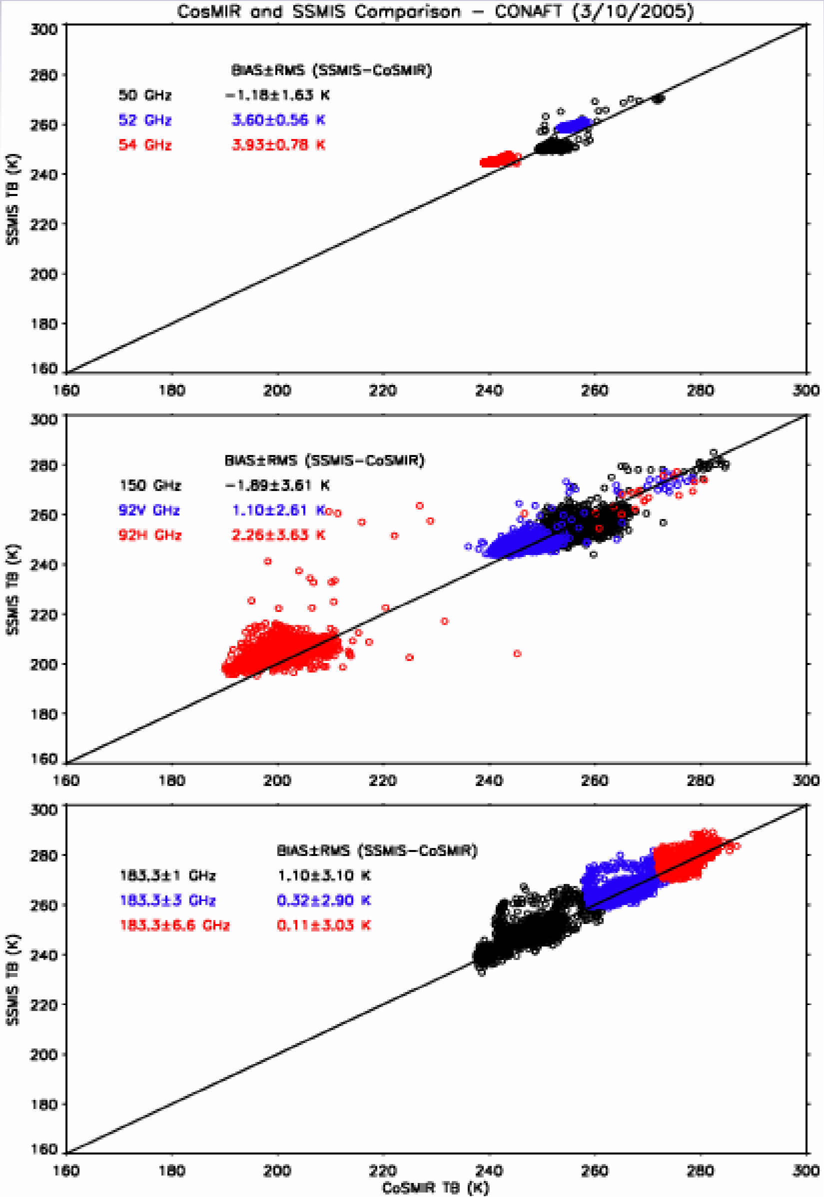

CosMIR and SSMIS Comparison – CONAFT (3/10/2005)

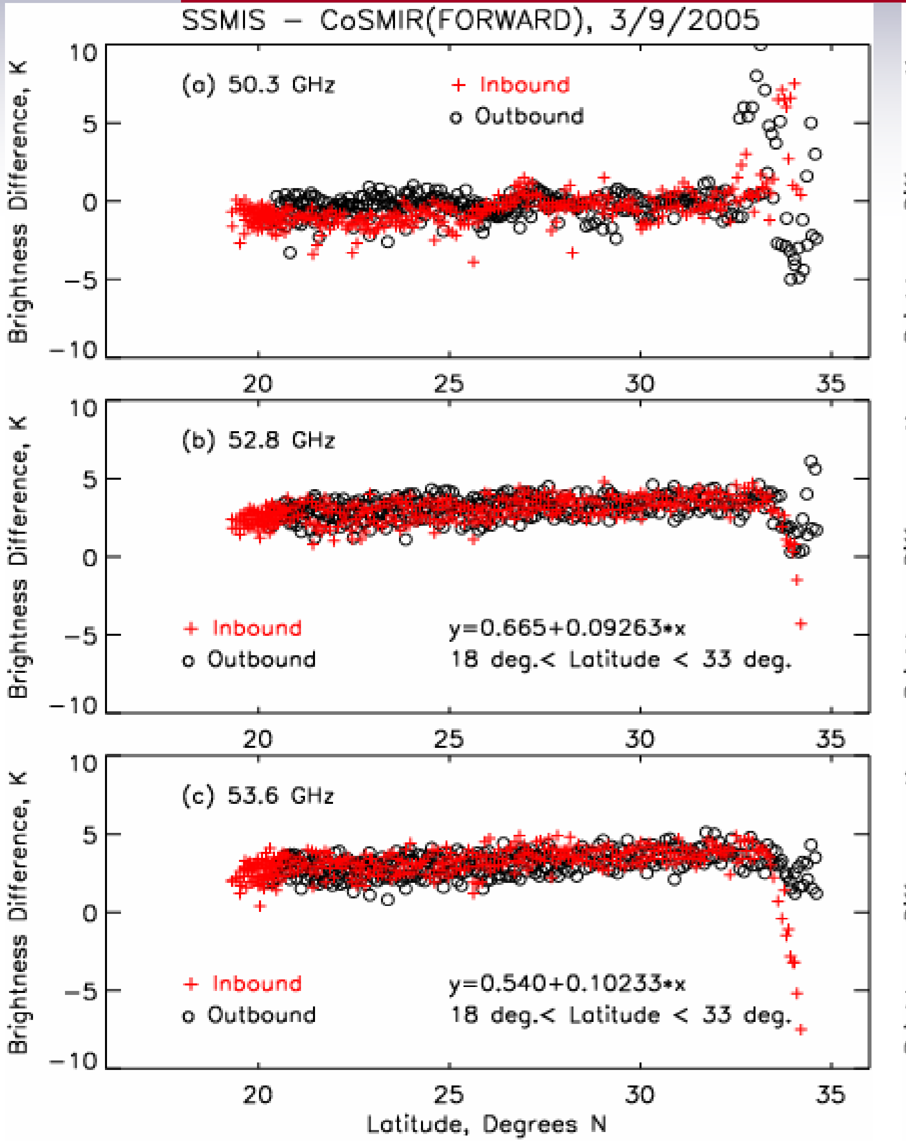
SSMIS – CoSMIR(FORWARD), 3/9/2005
(a) 50.3 GHz
+ Inbound
o Outbound
(b) 52.8 GHz
+ Inbound
o Outbound
y=0.665+0.09263*x
18 deg.< Latitude < 33 deg.
(c) 53.6 GHz
+ Inbound
o Outbound
y=0.540+0.10233*x
18 deg.< Latitude < 33 deg.
Brightness Difference, K
10
5
0
−5
−10
20
25
30
35
Latitude, Degrees N

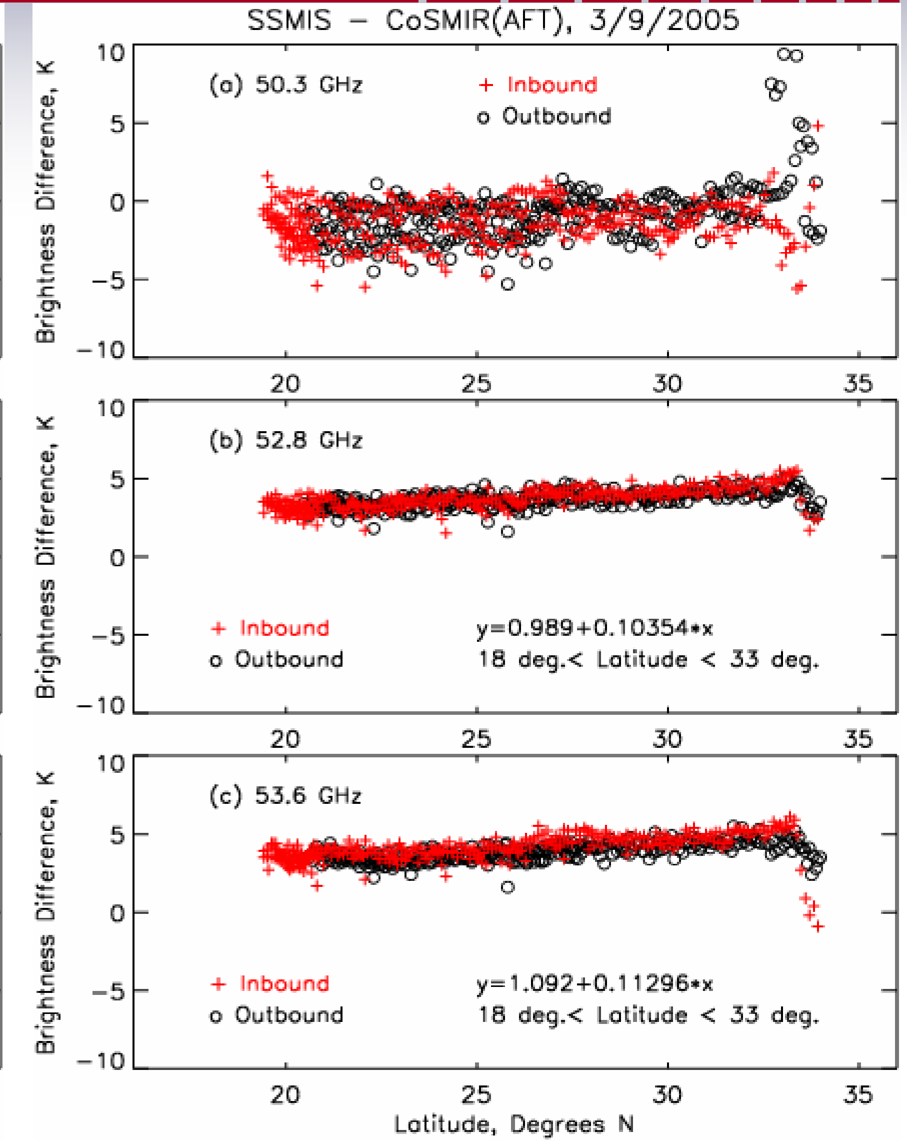
SSMIS – CoSMIR(AFT), 3/9/2005
(a) 50.3 GHz
+ Inbound
o Outbound
(b) 52.8 GHz
+ Inbound
o Outbound
y=0.989+0.10354*x
18 deg.< Latitude < 33 deg.
(c) 53.6 GHz
+ Inbound
o Outbound
y=1.092+0.11296*x
18 deg.< Latitude < 33 deg.
Brightness Difference, K
10
5
0
−5
−10
20
25
30
35
Latitude, Degrees N

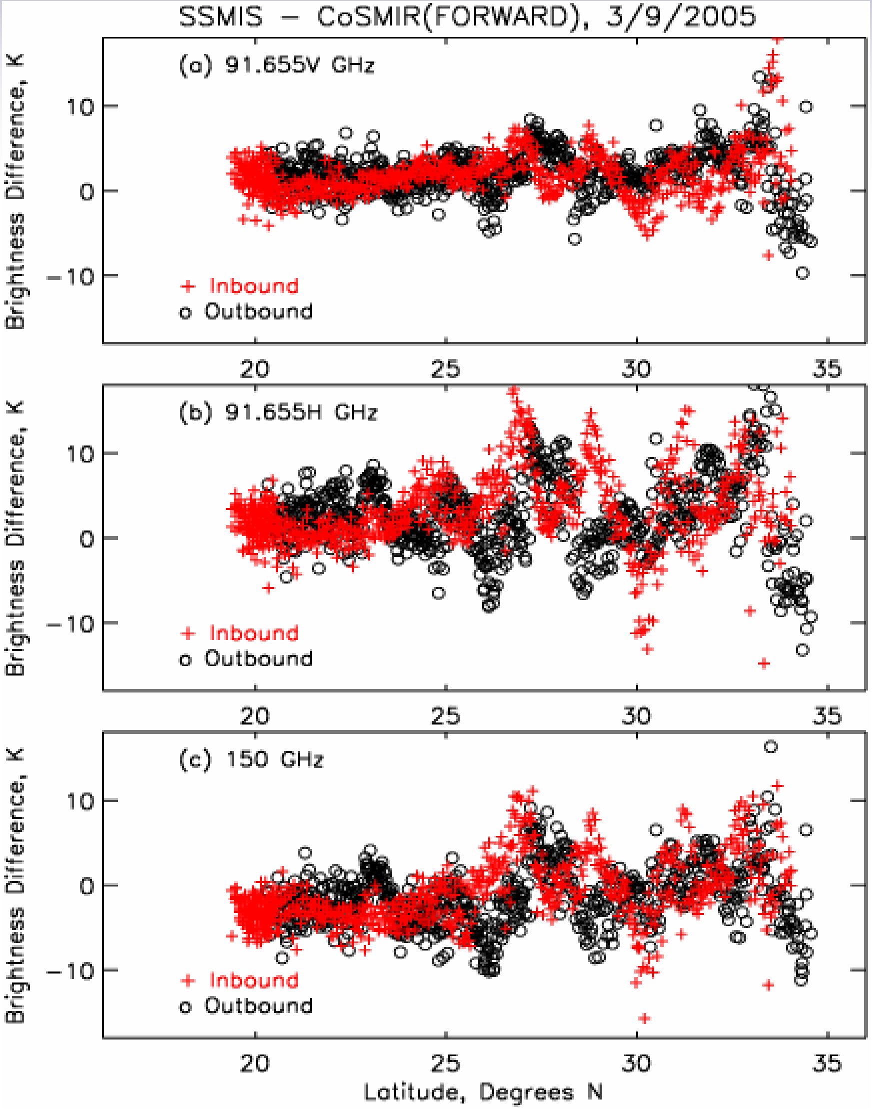
SSMIS − CoSMIR(FORWARD), 3/9/2005
(a) 91.655V GHz
(b) 91.655H GHz
(c) 150 GHz
+ Inbound
o Outbound
Brightness Difference, K
−10
0
10
20
25
30
35
Latitude, Degrees N

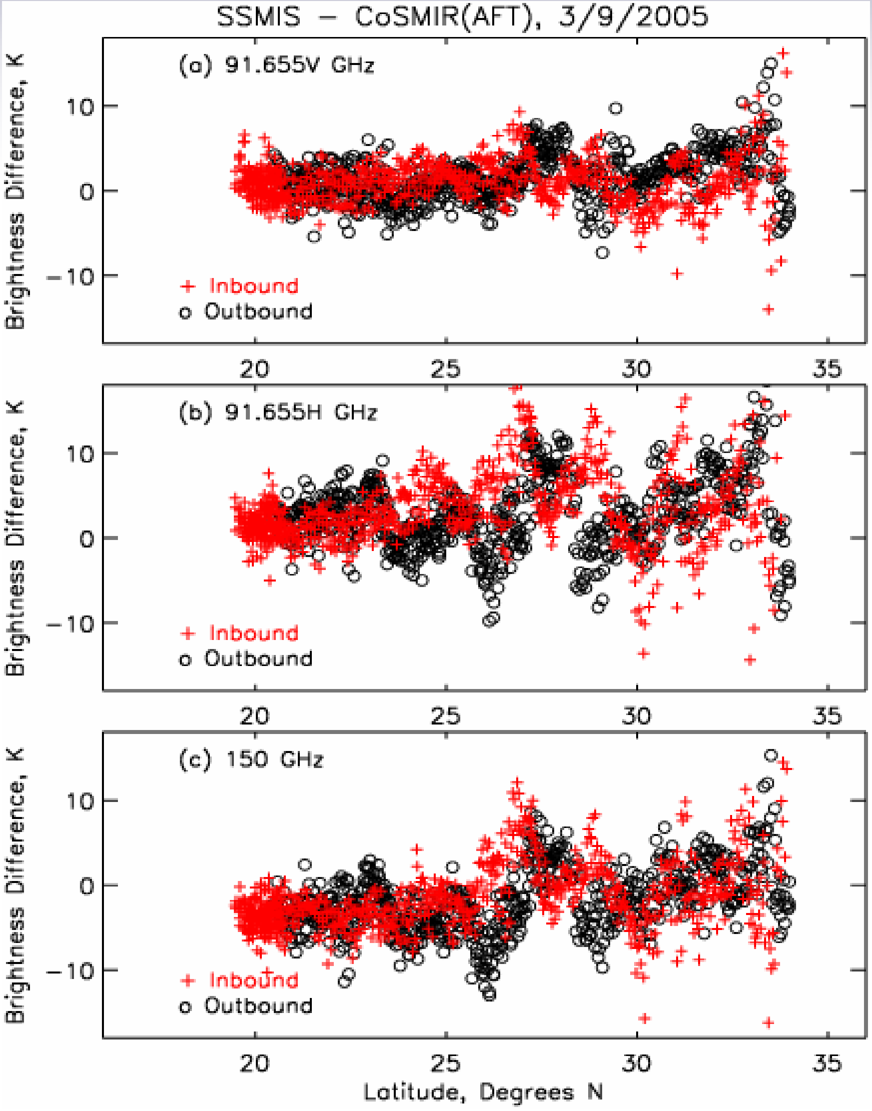
SSMIS − CoSMIR(AFT), 3/9/2005
(a) 91.655V GHz
(b) 91.655H GHz
(c) 150 GHz
+ Inbound
o Outbound
Brightness Difference, K
−10
0
10
20
25
30
35
Latitude, Degrees N

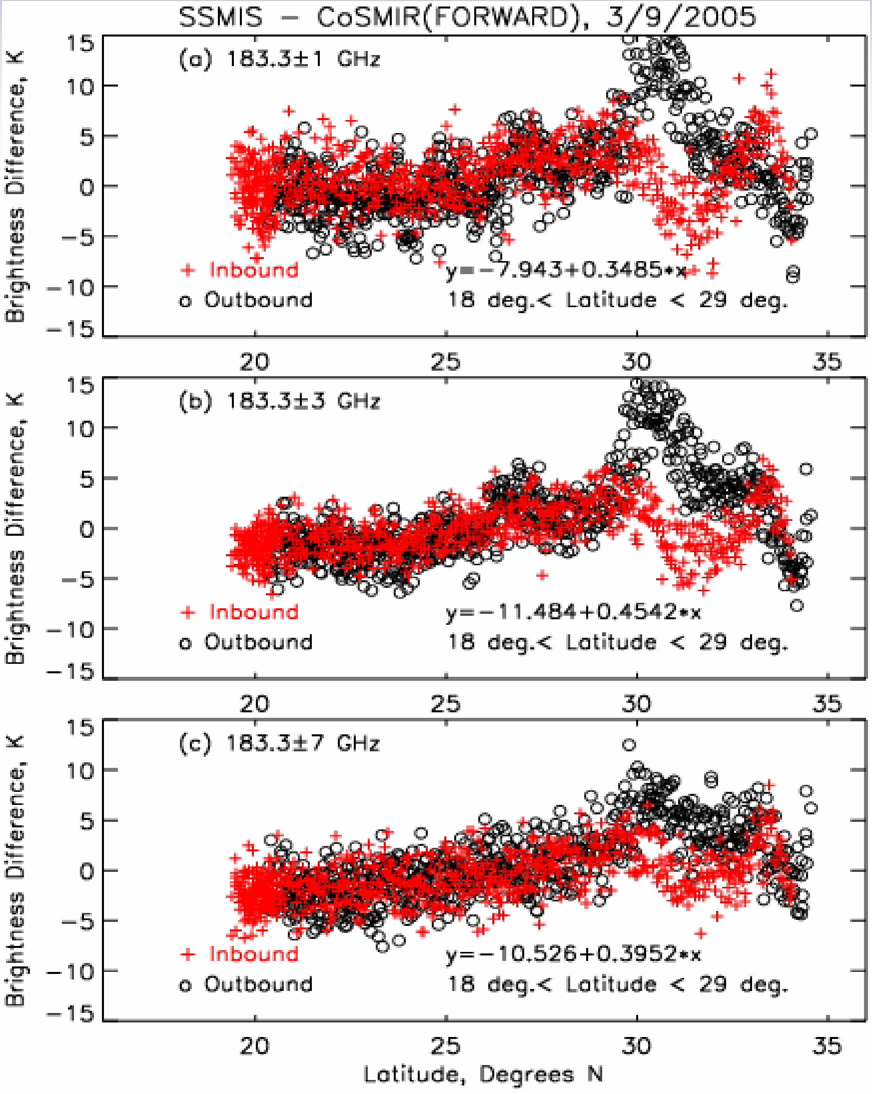

SSMIS – CoSMIR(FORWARD), 3/9/2005

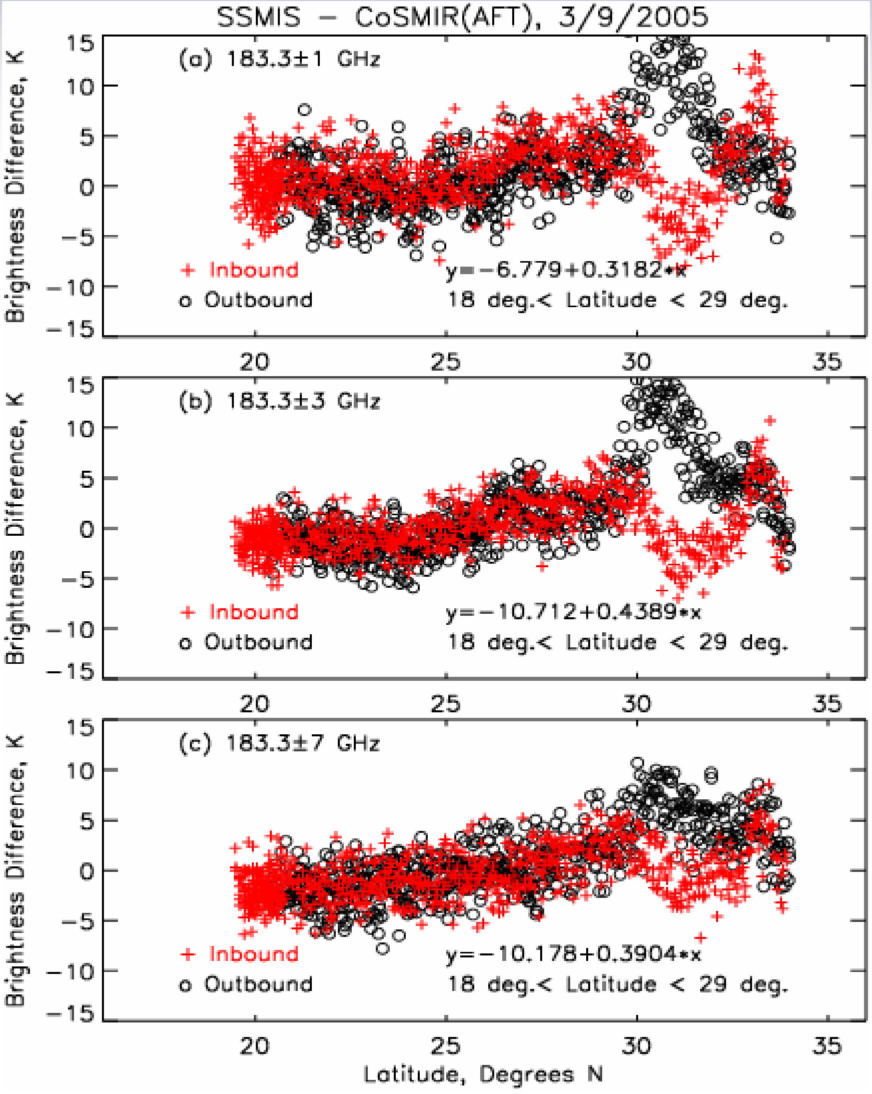

SSMIS – CoSMIR(AFT), 3/9/2005

Comparison of SSMIS and CoSMIR from the 3/10/2005 Flight

- **Slide #16 gives the CoSMIR flight path overlaid on the brightness map of the SSMIS 91.655-H channel. Again, most of the region covered by the flight is cloudy.**
- **Slide #17 shows a comparison of T_b variations from 6 selected channels along the aircraft flight path. The comparison is made with CoSMIR data in the forward scans.**
- **Slide #18 shows a comparison of T_b variations from 6 selected channels along the aircraft flight path. The comparison is made with CoSMIR data in the aft scans.**
- **Slide #19 shows the scatter plots (again separately for CoSMIR's forward and aft scans) of SSMIS and CoSMIR T_b values. The biases and rms values are calculated from the entire data set; thus observations over both land and ocean surfaces are included.**
- **Slides #20 (50.3, 52.8 and 53.6 GHz), #21 (91.655 V&H, and 150 GHz), and #22 (three 183.3 GHz channels) show the variations of T_b differences with latitudes. The linear regressions cover the latitude range of 18°-32° for both the 50 and 183.3 GHz channels.**
- **The 50.3 GHz channel is noisy during some parts of the flight.**

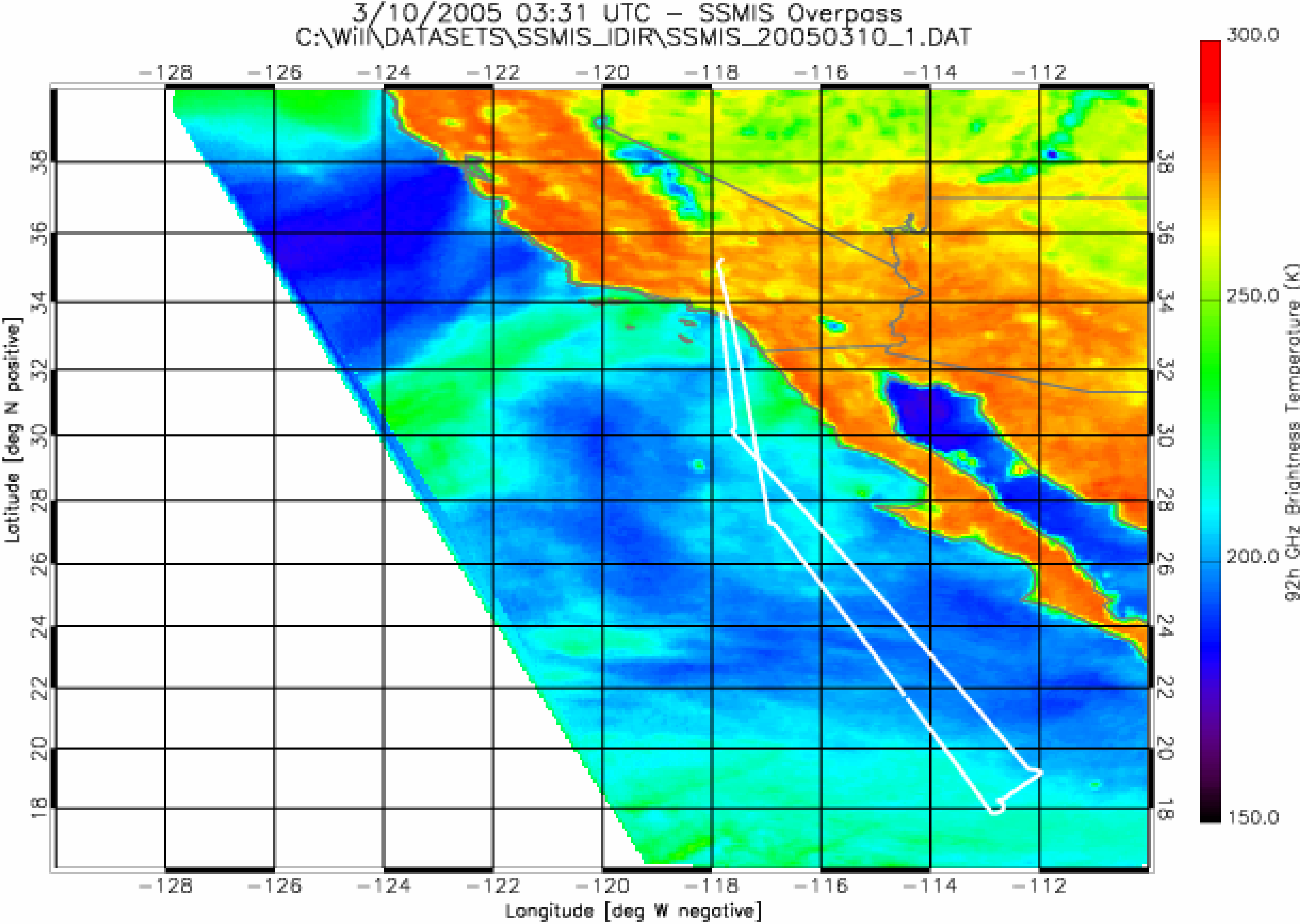
3/10/2005 03:31 UTC – SSMIS Overpass
C:\Will\DATASETS\SSMIS_IDIR\SSMIS_20050310_1.DAT
−128
−126
−124
−122
−120
−118
−116
−114
−112
38
36
34
32
30
28
26
24
22
20
18
Latitude [deg N positive]
Longitude [deg W negative]
300.0
250.0
200.0
150.0
92h GHz Brightness Temperature (K)

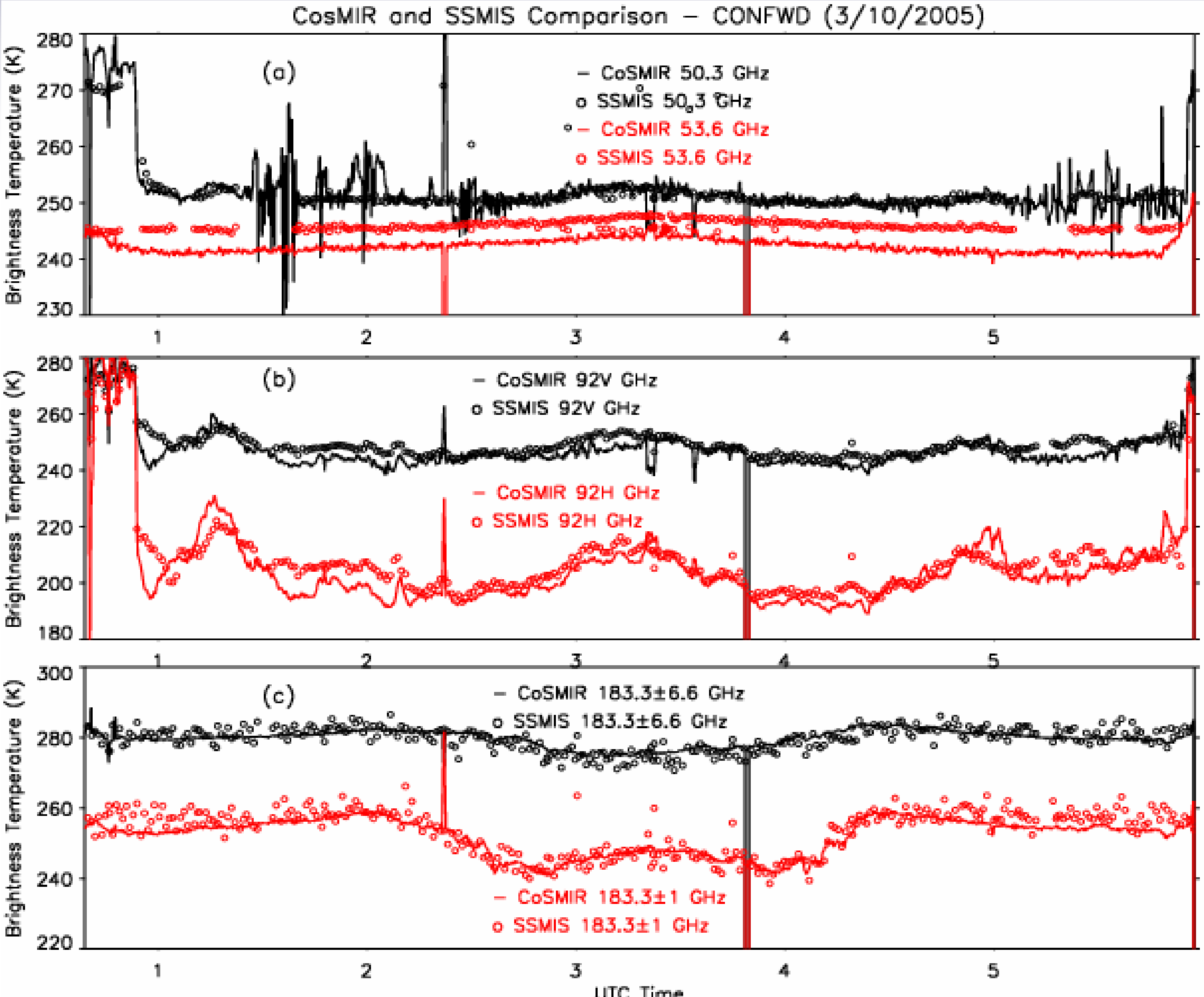

CosMIR and SSMIS Comparison – CONFWD (3/10/2005)

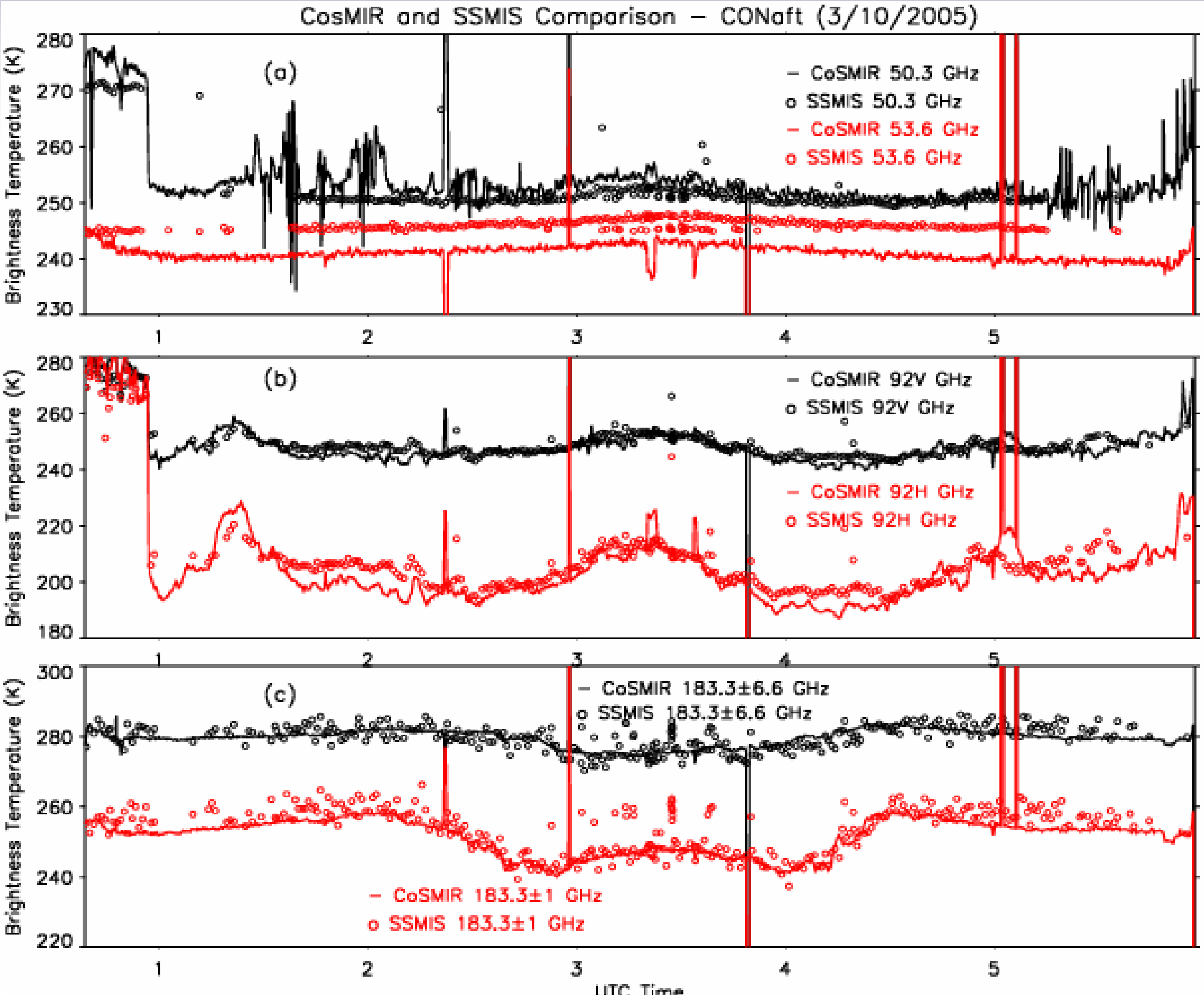
CosMIR and SSMIS Comparison – CONaft (3/10/2005)
(a)
– CoSMIR 50.3 GHz
o SSMIS 50.3 GHz
– CoSMIR 53.6 GHz
o SSMIS 53.6 GHz
Brightness Temperature (K)
280
270
260
250
240
230
1
2
3
4
5
(b)
– CoSMIR 92V GHz
o SSMIS 92V GHz
– CoSMIR 92H GHz
o SSMIS 92H GHz
Brightness Temperature (K)
280
260
240
220
200
180
(c)
– CoSMIR 183.3±6.6 GHz
o SSMIS 183.3±6.6 GHz
– CoSMIR 183.3±1 GHz
o SSMIS 183.3±1 GHz
Brightness Temperature (K)
300
280
260
240
220
1
2
3
4
5
UTC Time

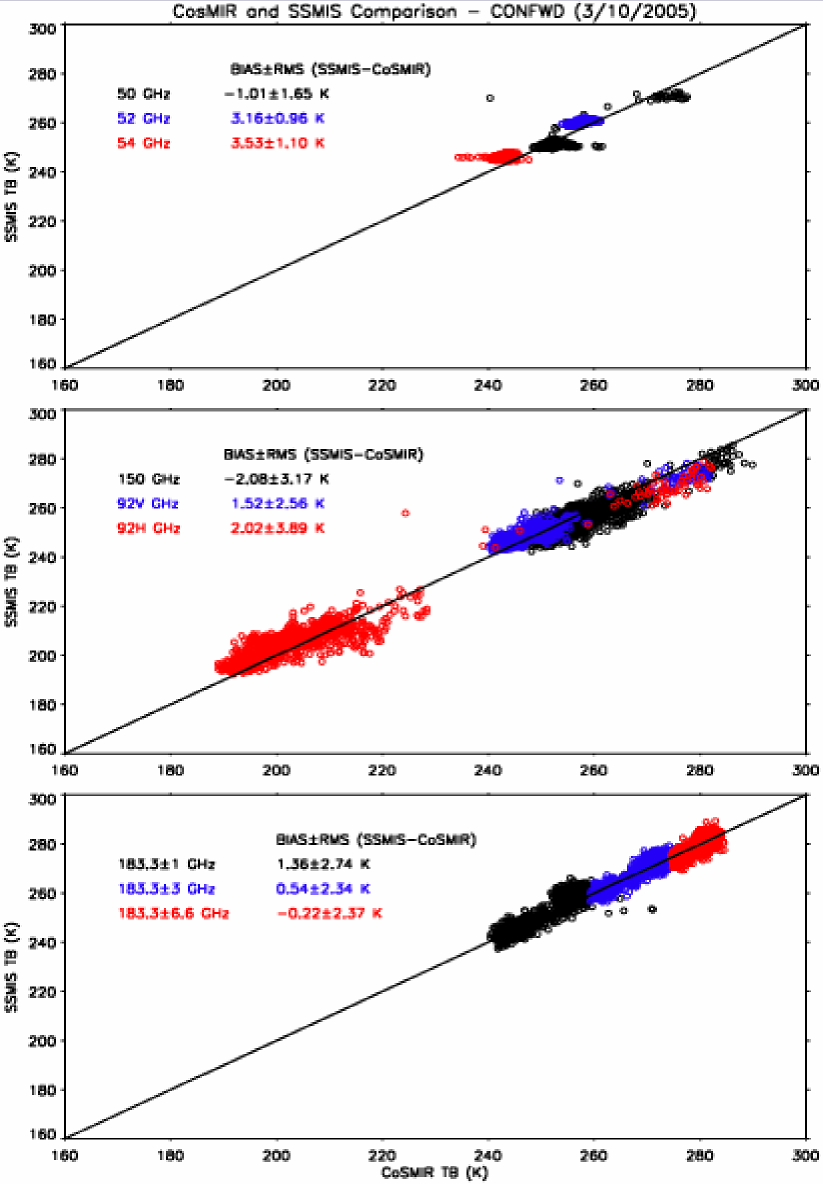

CosMIR and SSMIS Comparison – CONFWD (3/10/2005)

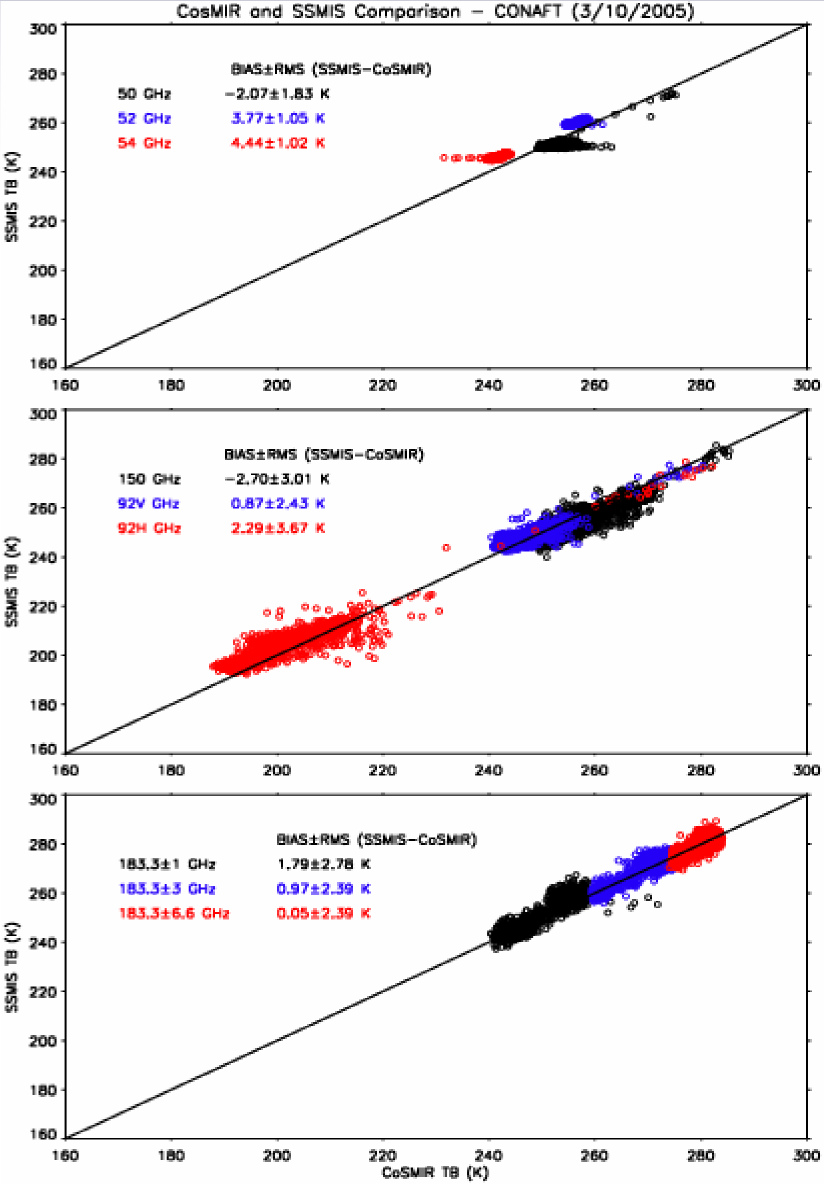

CosMIR and SSMIS Comparison – CONAFT (3/10/2005)

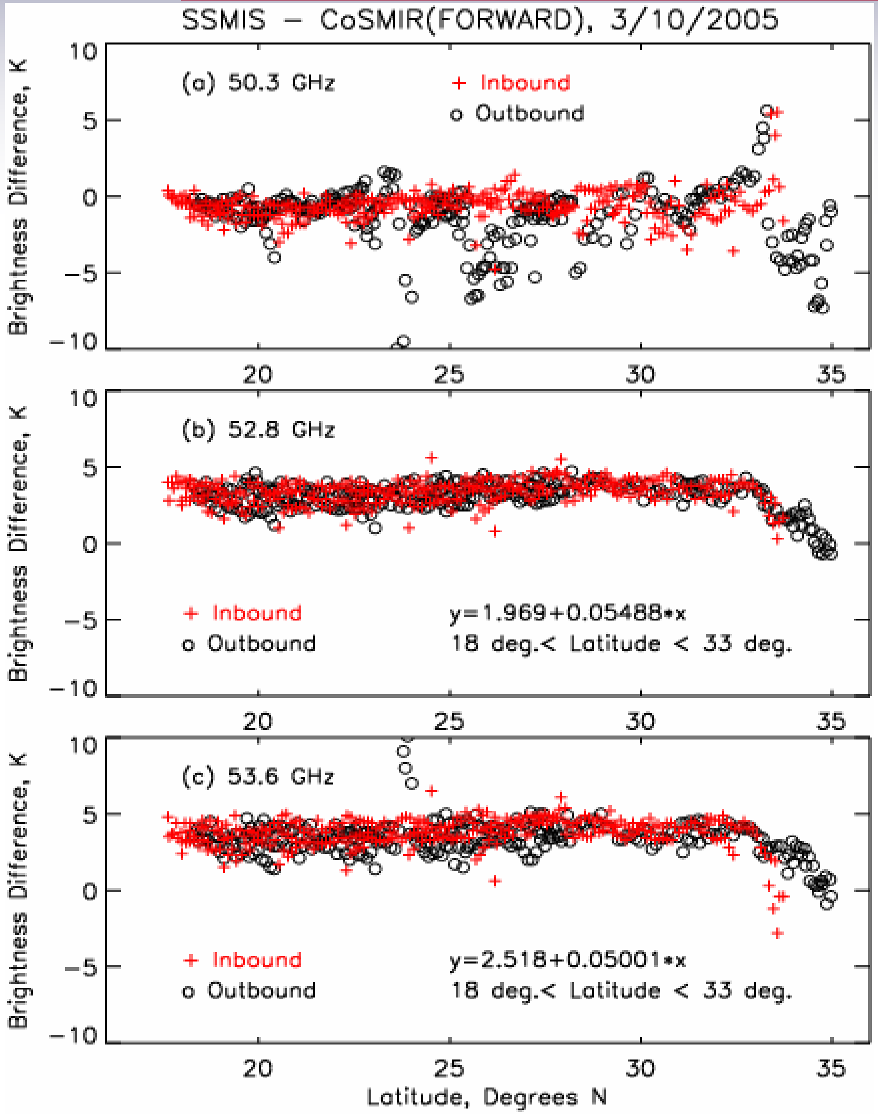

SSMIS – CoSMIR(FORWARD), 3/10/2005

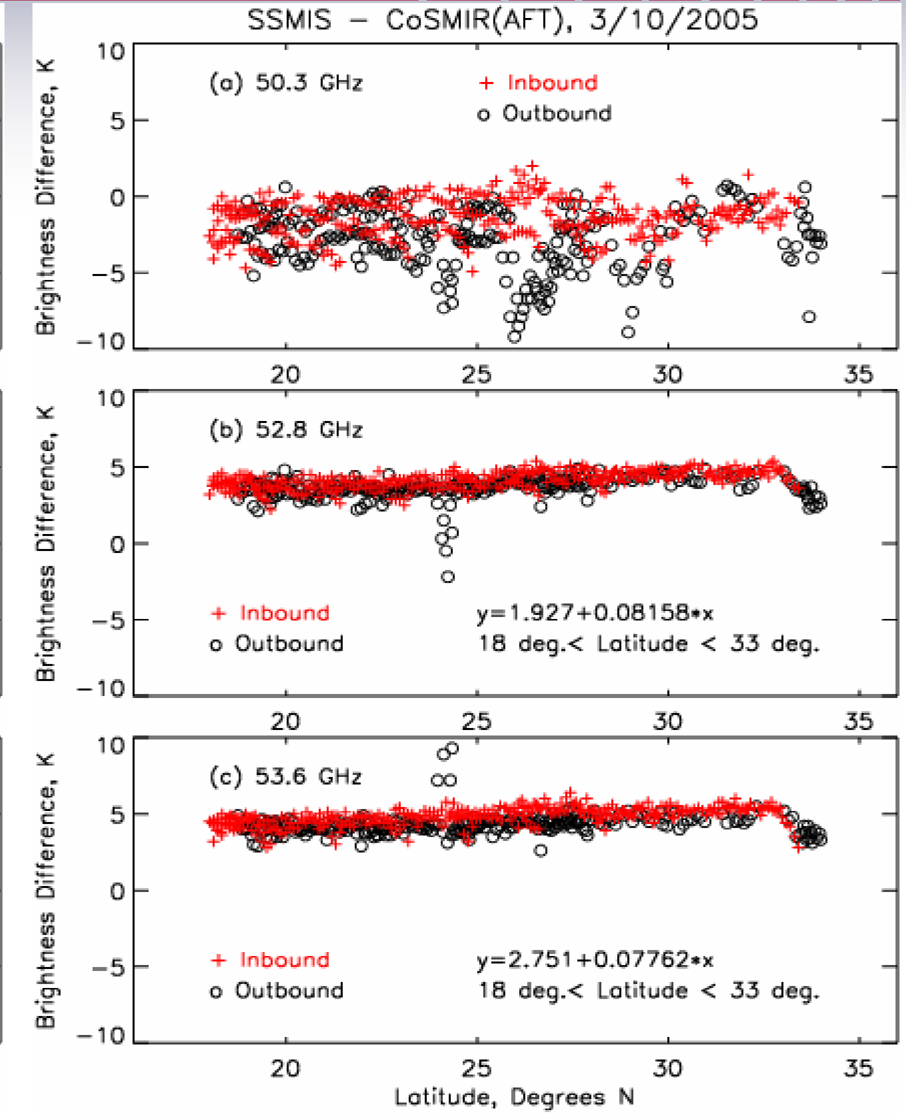

SSMIS – CoSMIR(AFT), 3/10/2005

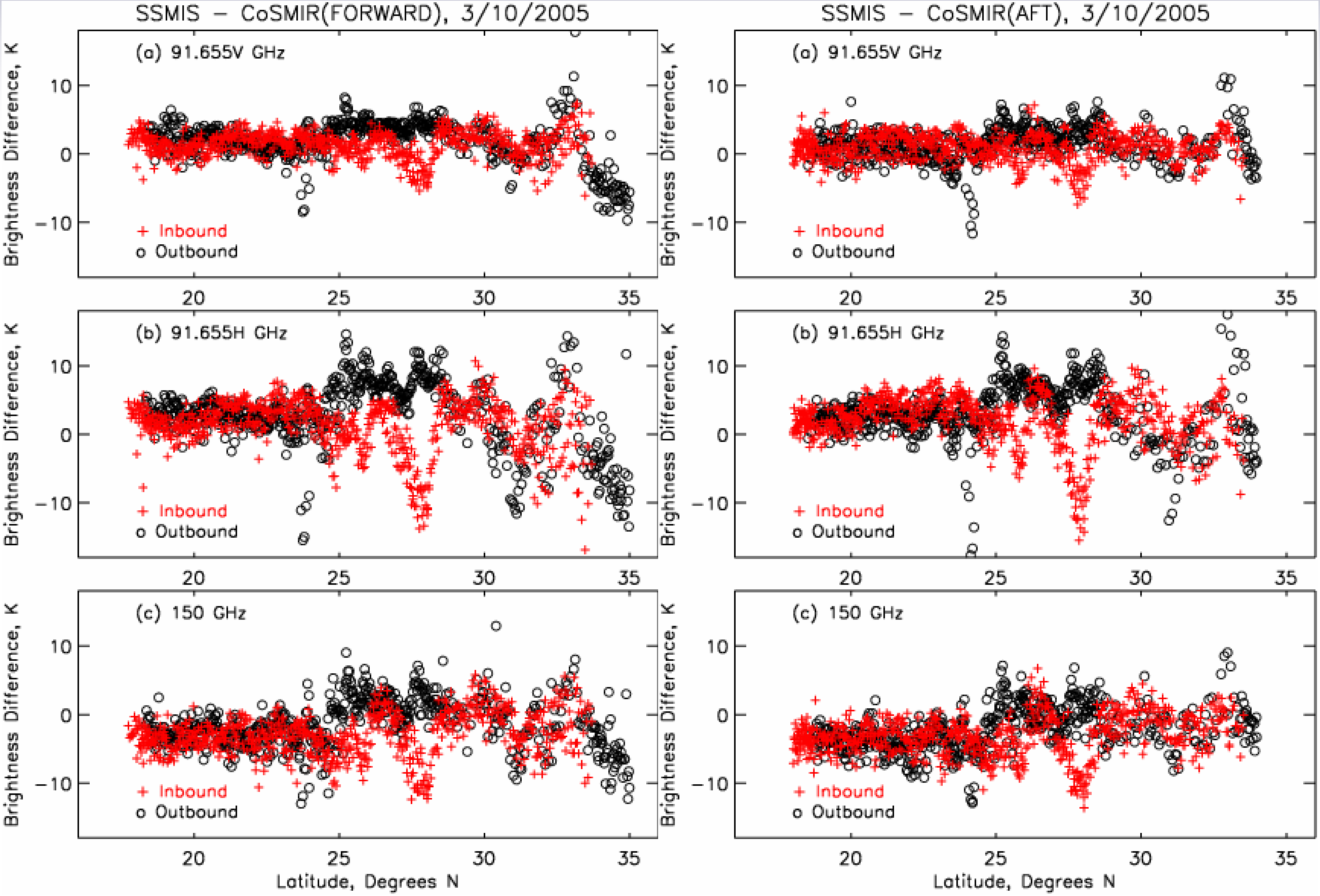
SSMIS – CoSMIR(FORWARD), 3/10/2005
SSMIS – CoSMIR(AFT), 3/10/2005
(a) 91.655V GHz
(b) 91.655H GHz
(c) 150 GHz
Brightness Difference, K
10
0
−10
20
25
30
35
+ Inbound
o Outbound
Latitude, Degrees N

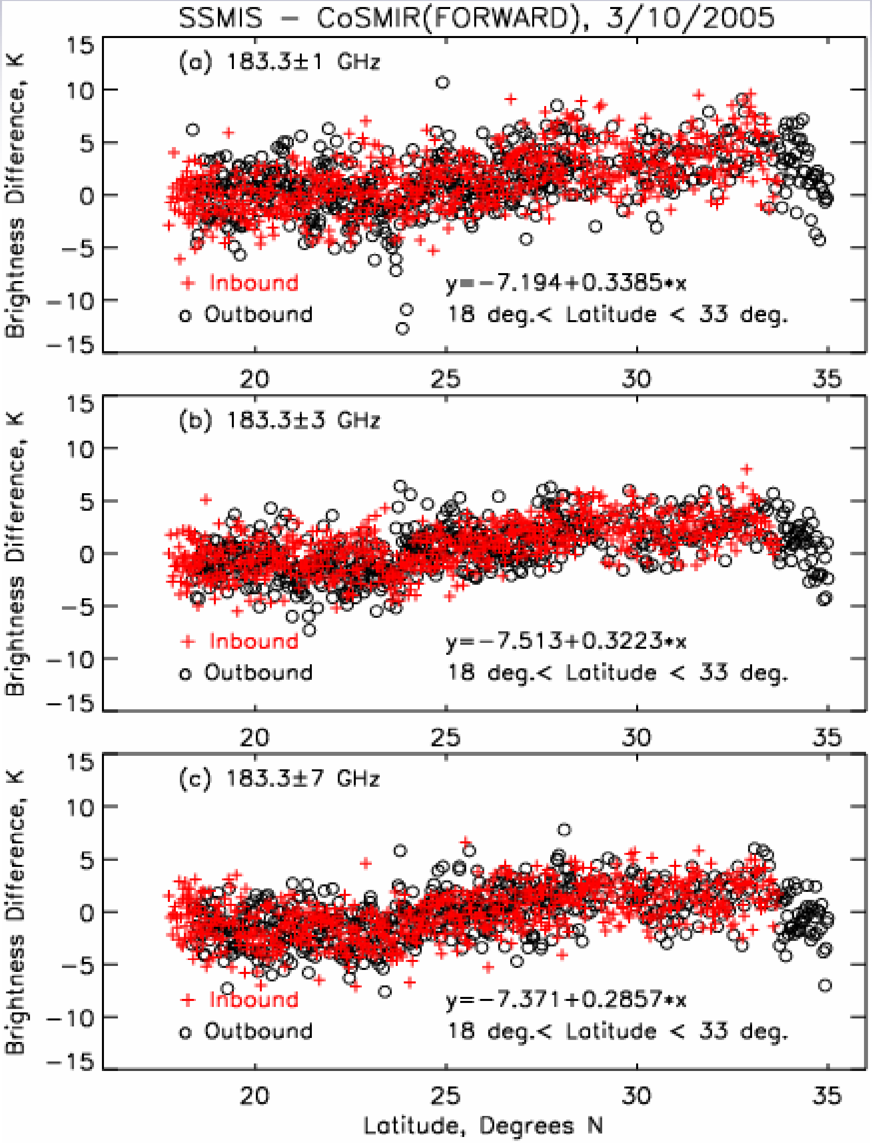
SSMIS – CoSMIR(FORWARD), 3/10/2005

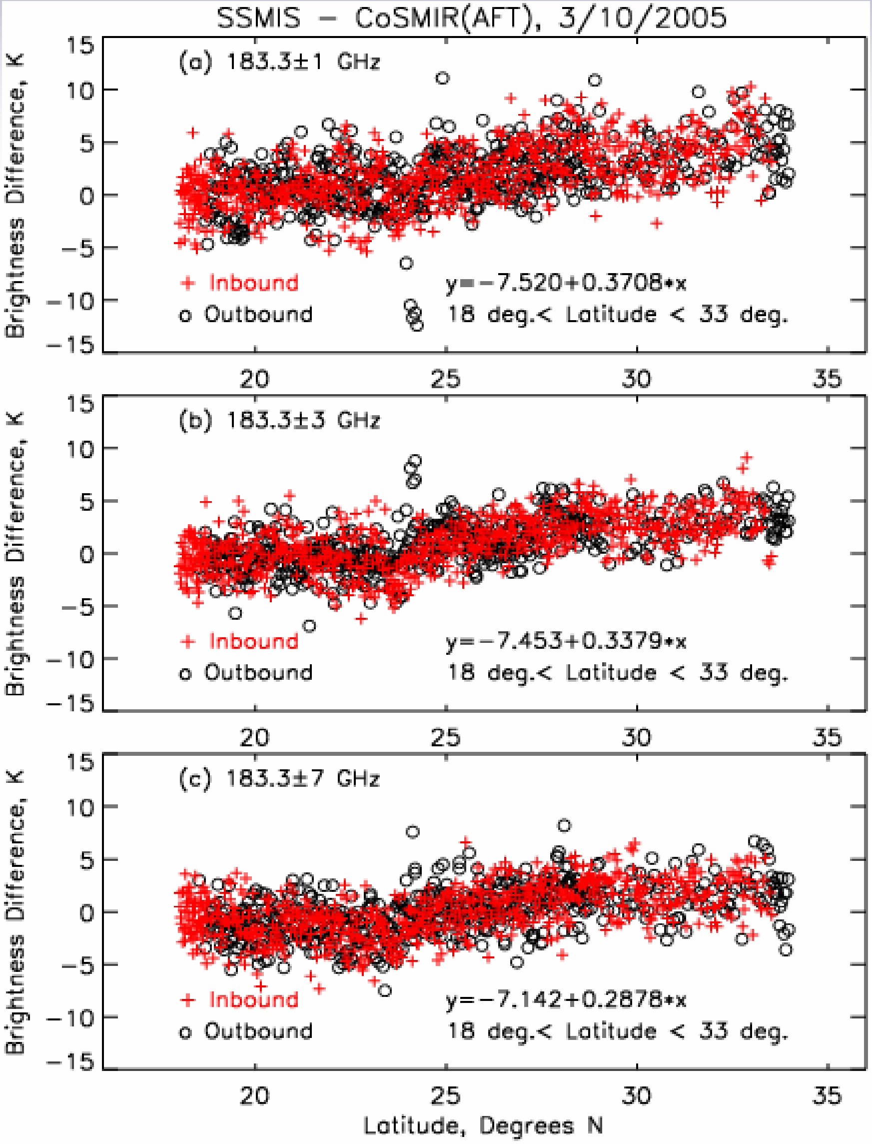
SSMIS – CoSMIR(AFT), 3/10/2005

Comparison of SSMIS and CoSMIR from the 3/14/2005 Flight

- **Slide #24 gives the CoSMIR flight path overlaid on the brightness map of the SSMIS 91.655-H channel. Most of the region covered by the flight is under clear sky.**
- **Slide #25 shows a comparison of T_b variations from 6 selected channels along the aircraft flight path. The comparison is made with CoSMIR data in the forward scans.**
- **Slide #26 shows a comparison of T_b variations from 6 selected channels along the aircraft flight path. The comparison is made with CoSMIR data in the aft scans.**
- **Slide #27 shows the scatter plots (separately for CoSMIR's forward and aft scans) of SSMIS and CoSMIR T_b values. The biases and rms values are calculated from the entire data set; thus observations over both land and ocean surfaces are included.**
- **CoSMIR data within ±15 minutes of the SSMIS passes are used to calculated the averages of T_b differences between the two sensors. The results are given by Tables 1 (CoSMIR forward scans) and 2 (CoSMIR aft scans) in slides #28 and #29. The CoSMIR's 50.3 GHz data during these periods from the 3/10/2005 and 3/14/2005 flights turned out to be not noisy.**

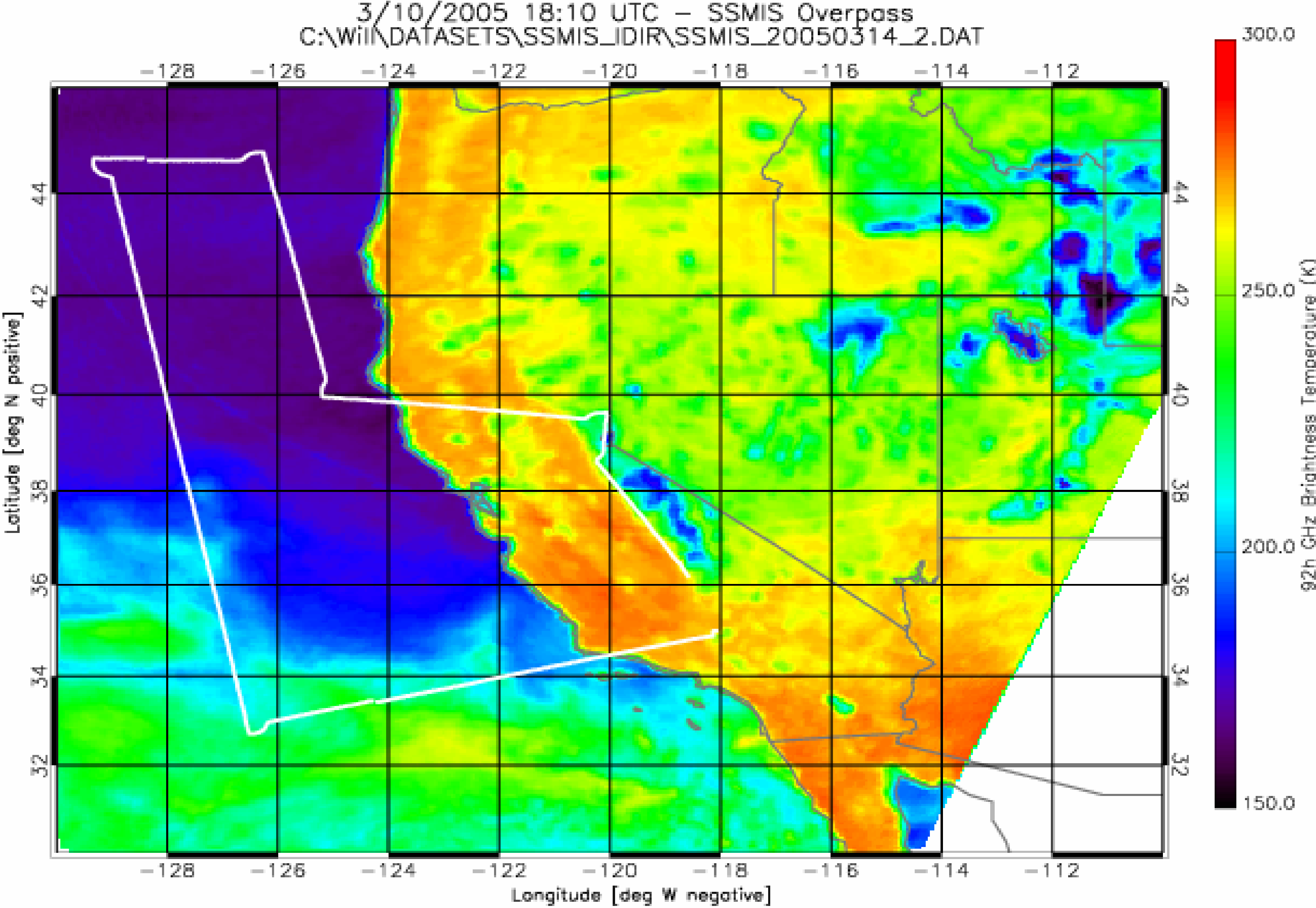
3/10/2005 18:10 UTC - SSMIS Overpass
C:\Will\DATASETS\SSMIS_IDIR\SSMIS_20050314_2.DAT
-128
-126
-124
-122
-120
-118
-116
-114
-112
44
42
40
38
36
34
32
Latitude [deg N positive]
Longitude [deg W negative]
300.0
250.0
200.0
150.0
92h GHz Brightness Temperature (K)

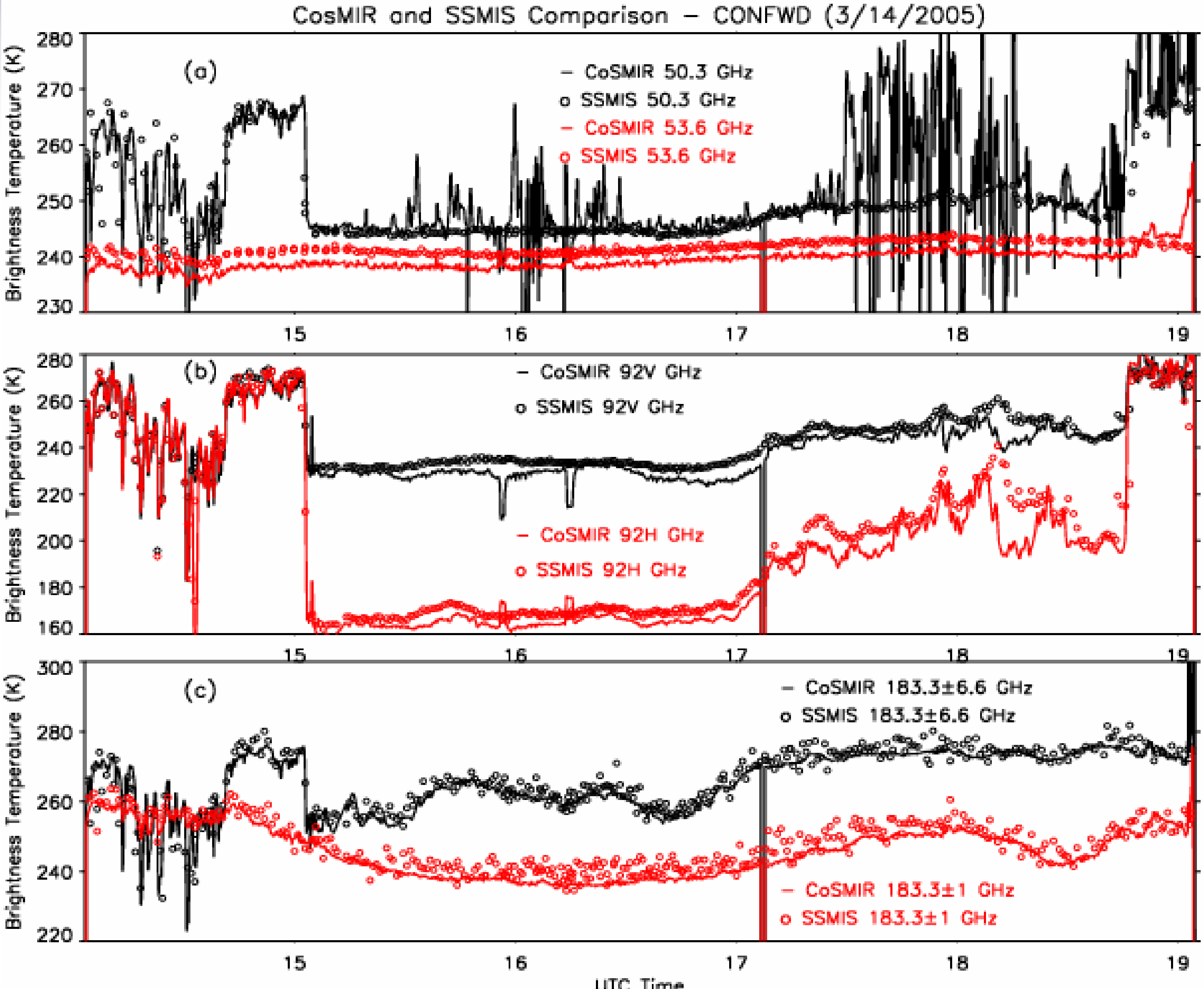
CosMIR and SSMIS Comparison – CONFWD (3/14/2005)
(a)
– CoSMIR 50.3 GHz
o SSMIS 50.3 GHz
– CoSMIR 53.6 GHz
o SSMIS 53.6 GHz
Brightness Temperature (K)
280
270
260
250
240
230
15
16
17
18
19
(b)
– CoSMIR 92V GHz
o SSMIS 92V GHz
– CoSMIR 92H GHz
o SSMIS 92H GHz
Brightness Temperature (K)
280
260
240
220
200
180
160
15
16
17
18
19
(c)
– CoSMIR 183.3±6.6 GHz
o SSMIS 183.3±6.6 GHz
– CoSMIR 183.3±1 GHz
o SSMIS 183.3±1 GHz
Brightness Temperature (K)
300
280
260
240
220
15
16
17
18
19
UTC Time

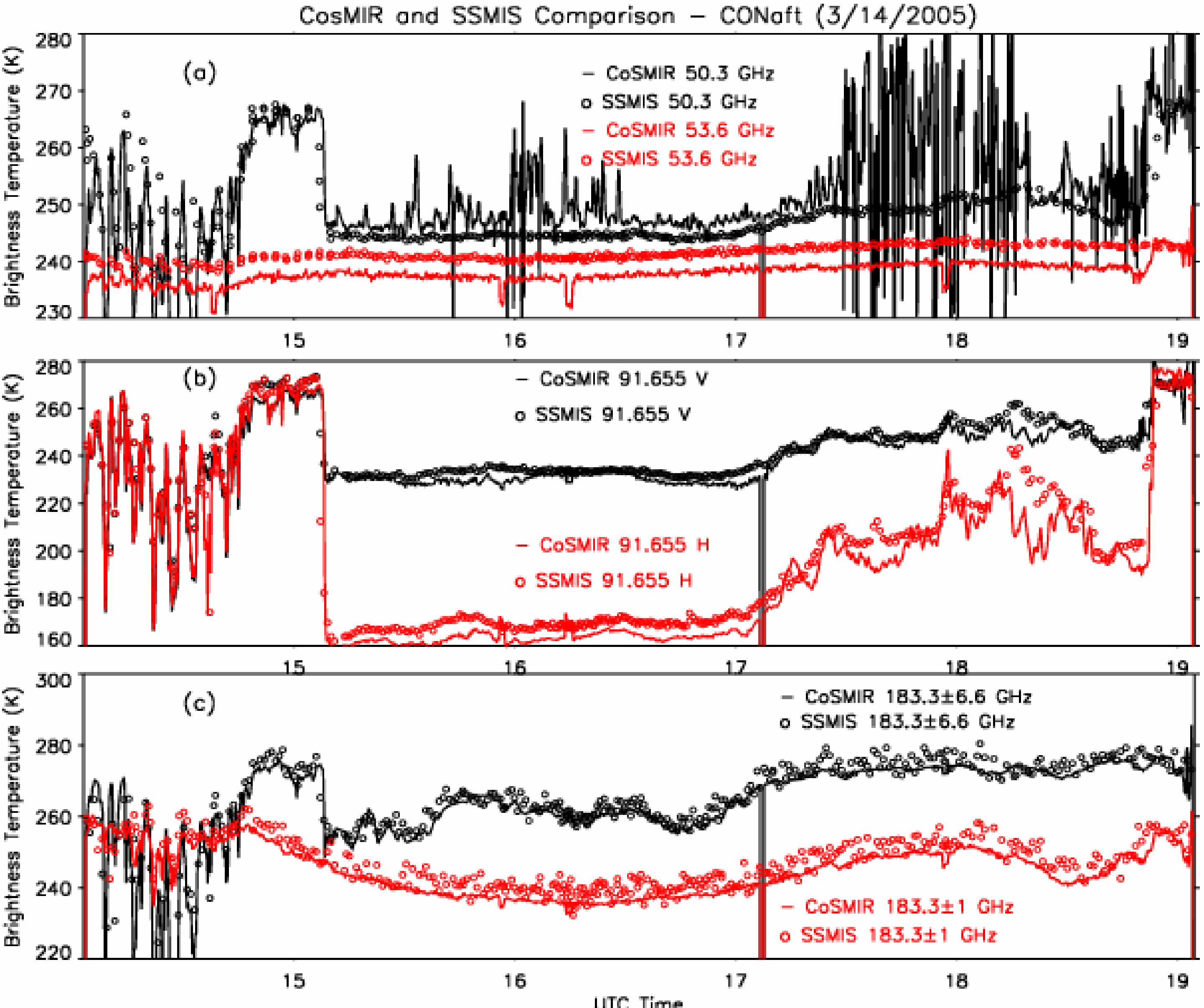
CosMIR and SSMIS Comparison – CONaft (3/14/2005)
(a)
– CoSMIR 50.3 GHz
o SSMIS 50.3 GHz
– CoSMIR 53.6 GHz
o SSMIS 53.6 GHz
Brightness Temperature (K)
280
270
260
250
240
230
15
16
17
18
19
(b)
– CoSMIR 91.655 V
o SSMIS 91.655 V
– CoSMIR 91.655 H
o SSMIS 91.655 H
Brightness Temperature (K)
280
260
240
220
200
180
160
(c)
– CoSMIR 183.3±6.6 GHz
o SSMIS 183.3±6.6 GHz
– CoSMIR 183.3±1 GHz
o SSMIS 183.3±1 GHz
Brightness Temperature (K)
300
280
260
240
220
UTC Time

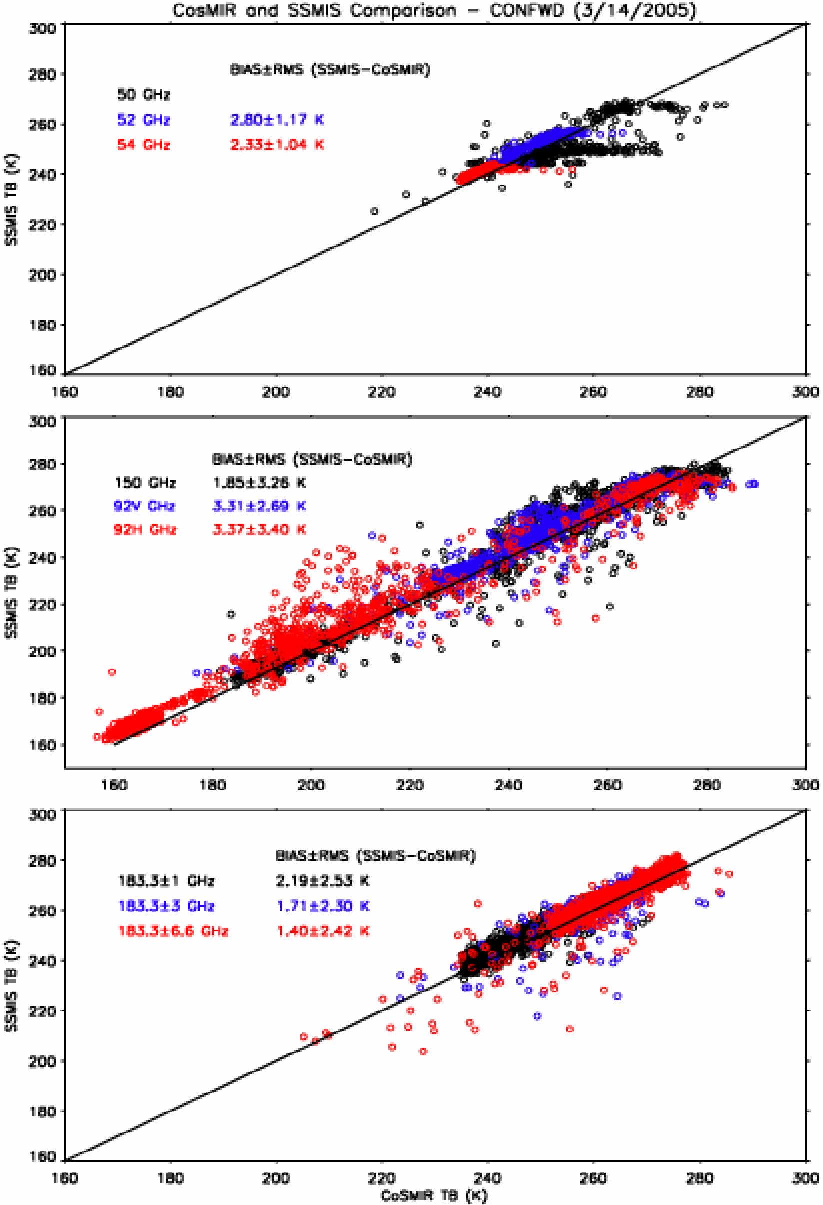
CosMIR and SSMIS Comparison – CONFWD (3/14/2005)

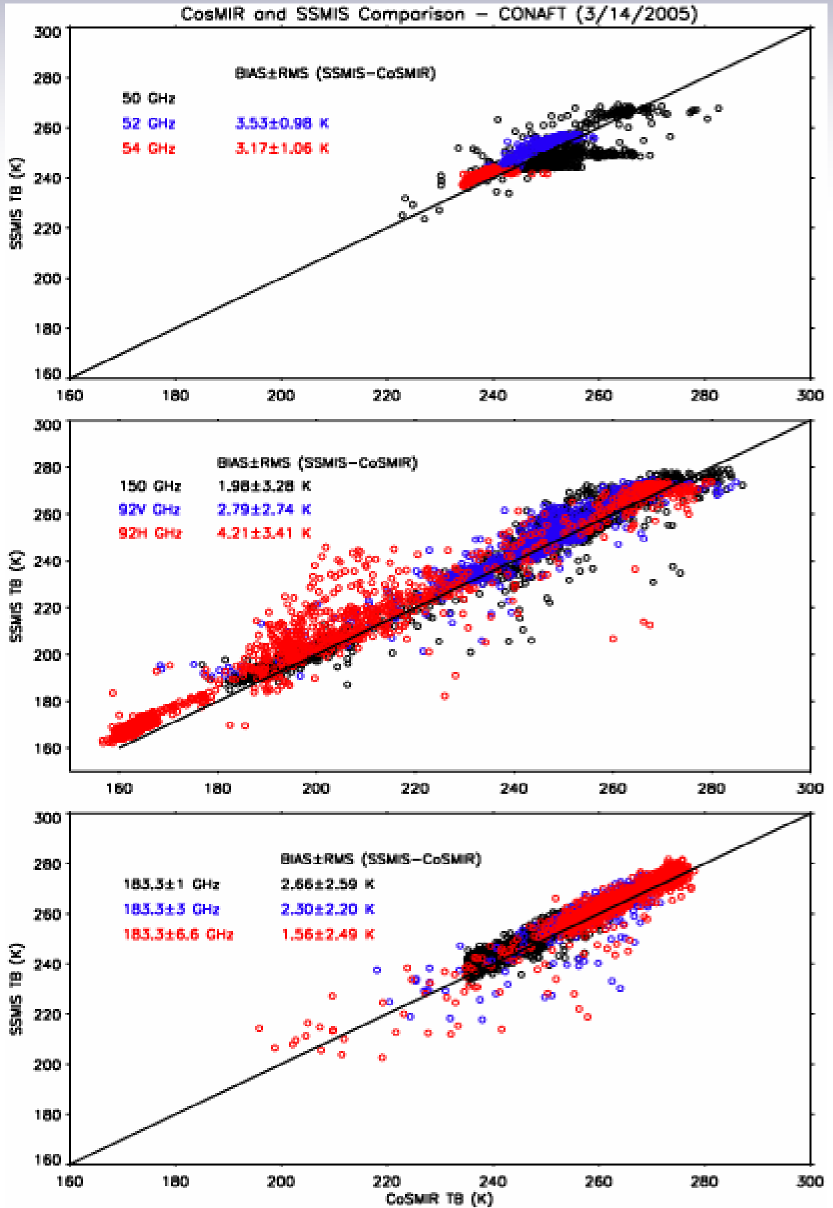
CosMIR and SSMIS Comparison – CONAFT (3/14/2005)

Table 1. Average Brightness Differences Between SSMIS and CoSMIR (forward scans within ±15 minutes of SSMIS pass)

Frequency GHz	SSMIS – CoSMIR, K			
	12/3/2004-A	3/9/2005-A	3/10/2005-A	3/14/2005-D
50.3	-1.27±0.42	-0.98±0.56	-0.42±1.21	-1.53±0.80
52.8	2.38±0.51	2.49±0.49	3.37±0.66	2.83±0.52
53.6	1.74±0.47	2.70±0.64	3.58±0.84	2.30±0.53
91.655V	3.31±1.20	1.15±1.78	2.01±1.76	3.84±1.71
91.655H	3.34±1.22	1.42±1.77	1.84±1.61	4.40±1.36
150	-2.81±1.68	-3.14±1.69	-1.84±2.75	2.09±2.23
183.3±1	-0.95±2.00	-0.11±2.27	0.21±2.02	1.77±1.74
183.3±3	-1.54±1.61	-1.57±1.48	0.55±2.46	2.37±1.87
183.3±6.6	-1.57±1.82	-2.17±1.77	0.18±2.22	1.98±1.93
Approximate Location	36.5°N 124.5°W	19.8°N 113.0°W	18.2°N 112.9°W	41.7°N 128.3°W

Table 2. Average Brightness Differences Between SSMIS and CoSMIR (Aft Scans within ±15 minutes of SSMIS pass)

Frequency GHz	**SSMIS – CoSMIR, K**			
	12/3/2004-A	**3/9/2005-A**	**3/10/2005-A**	**3/14/2005-D**
50.3	**-2.37±0.54**	**-1.59±1.24**	**-1.69±1.20**	**-2.53±1.17**
52.8	**2.64±0.42**	**3.07±0.39**	**4.19±0.59**	**3.40±0.36**
53.6	**2.20±0.53**	**3.51±0.46**	**4.70±0.61**	**3.10±0.38**
91.655V	**2.10±1.25**	**0.45±1.48**	**1.09±1.64**	**2.68±1.55**
91.655H	**3.43±1.08**	**1.57±1.71**	**2.16±2.30**	**5.75±1.22**
150	**-3.58±1.49**	**-3.68±1.79**	**-2.43±2.34**	**2.48±1.30**
183.3±1	**-1.10±2.10**	**0.10±1.95**	**0.49±2.09**	**1.95±1.38**
183.3±3	**-1.40±1.61**	**-1.14±1.38**	**0.97±2.48**	**2.92±1.68**
183.3±6.6	**-1.83±1.73**	**-2.02±1.79**	**0.35±2.27**	**1.79±1.84**
Approximate Location	**36.5°N 124.5°W**	**19.8°N 113.0°W**	**18.2°N 112.9°W**	**41.7°N 128.3°W**

Summary

- The calibration of the 91.655-V GHz channel of CoSMIR may be slightly off in this series of flights. The 50.3 GHz channel is noisy during portions of flights on 3/10/2005 and 3/14/2005 (data segments used to generate values in Tables 1 and 2 are alright).
- The variations of SSMIS and CoSMIR T_b values along the CoSMIR flight path generally track well for all nine channels, particularly for the opaque channels.
- The brightness differences (ΔT_b) between SSMIS and CoSMIR vary with latitude locations in a pattern consistent with the anomaly pointed out by Steve Swadley.
- Data from 3/9/2005 shows ΔT_b gradients of about 0.1 K per degree latitude at 52.8 and 53.6 GHz, and about 0.32-0.4 K per degree latitude for the 183.3 GHz channels.
- The 3/10/2005 data shows ΔT_b gradients of about 0.05-0.08 K per degree latitude at 52.8 and 53.6 GHz, and about 0.29-0.37 K per degree latitude for the 183.3 Ghz channels.
- The ΔTb gradients may be present also at the transparent channels of 150, 91.655, and 50.3 GHz, but are not obvious because of variations caused by surface features.
- Significant biases exist almost at all channels, based on four days of near coincident (within ±15 minutes) measurements between the two sensors.

Defense Meteorological Satellite Program
Special Sensor Microwave Imager Sounder (F-16)
Calibration/Validation Final Report

The First Conical Scanning Passive Microwave Surface and Atmospheric Sounding Imager

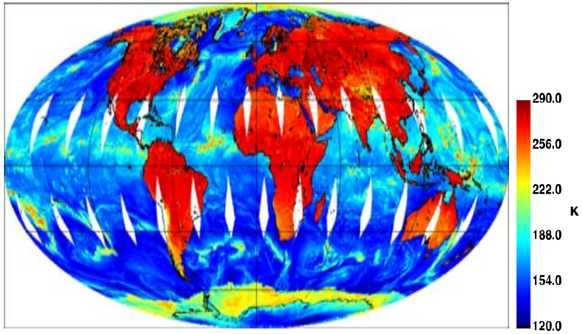
SSMIS F-16 Channel 15 - 37 H IDR REVS 09258 - 09271 08/04/2005

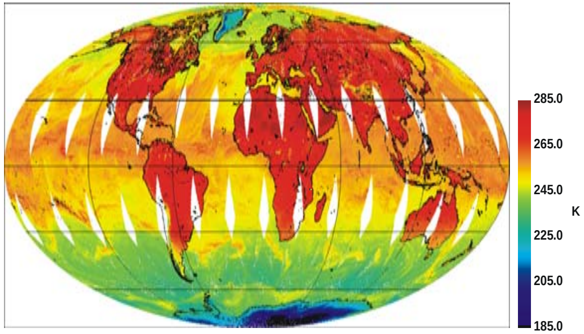
SSMIS F-16 Channel 1 - 50.3 V IDR REVS 09258 - 09271 08/04/2005

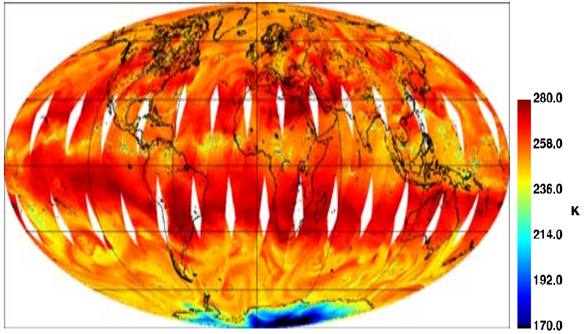
SSMIS F-16 Channel 10 - 183+/-3 H IDR REVS 09258 - 09271 08/04/2005

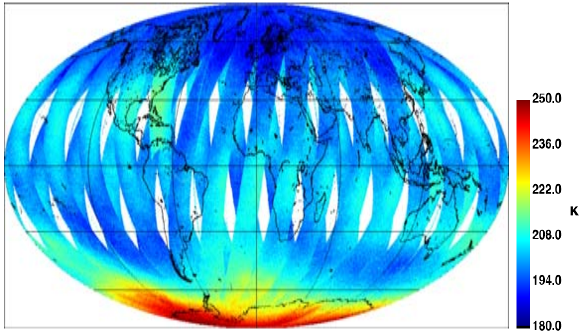
SSMIS F-16 Channel 20 - 60.792 H+V IDR REVS 09258 - 09271 08/04/2005

Prepared by

SSMIS Cal/Val Team

30 November 2005

Volume III

Table of Contents

F16 SSMIS Calibration/Validation Final Report

Section 8.0 Inter-Sensor Comparisons with F14 SSM/I

Gene A. Poe, Enzo Uliana,

Beverly Gardiner and Troy vonRentzell

THE AEROSPACE
CORPORATION

8.0 Inter-sensor Comparisons with F-14 SSM/I

8.1 Space/Time Coincidence with F-14 SSM/I

- **High Spatial/Temporal Coincidences:**

  (6 Nov 03; 14 Jan 04; 23 Mar 04)

- **Many Match-ups of all Surface Types/Atmospheres**

- **Nearly Same Slant Paths, Earth Incidence Angles and Pixel Compass Azimuths**

8.1 DMSP Operational Constellation

(Sun Synch -- Local Time Ascending Node)

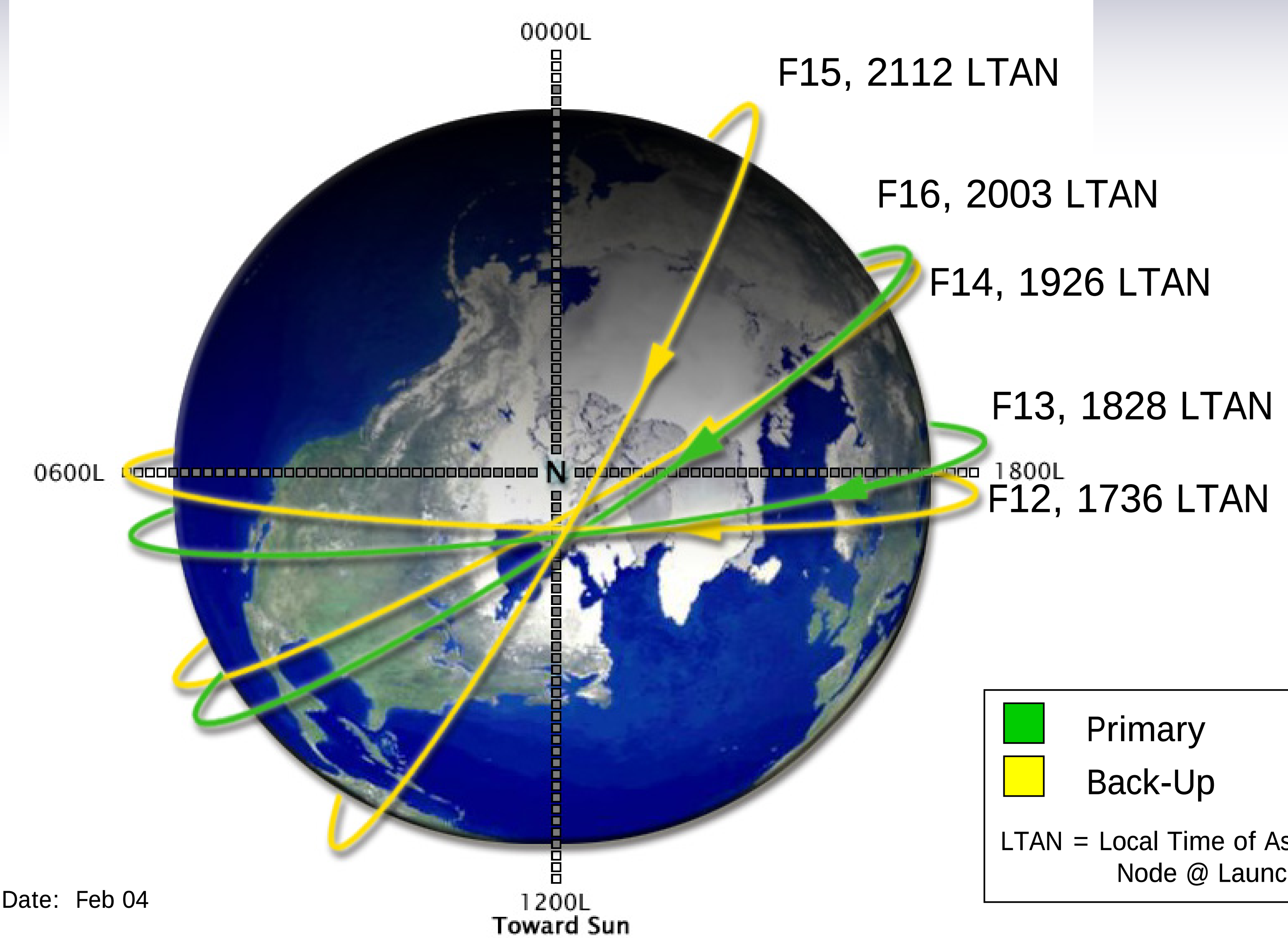

🟩 Primary

🟨 Back-Up

LTAN = Local Time of Ascending Node @ Launch

As of Date: Feb 04

8.1 SSM/I and SSMIS Scan Geometry

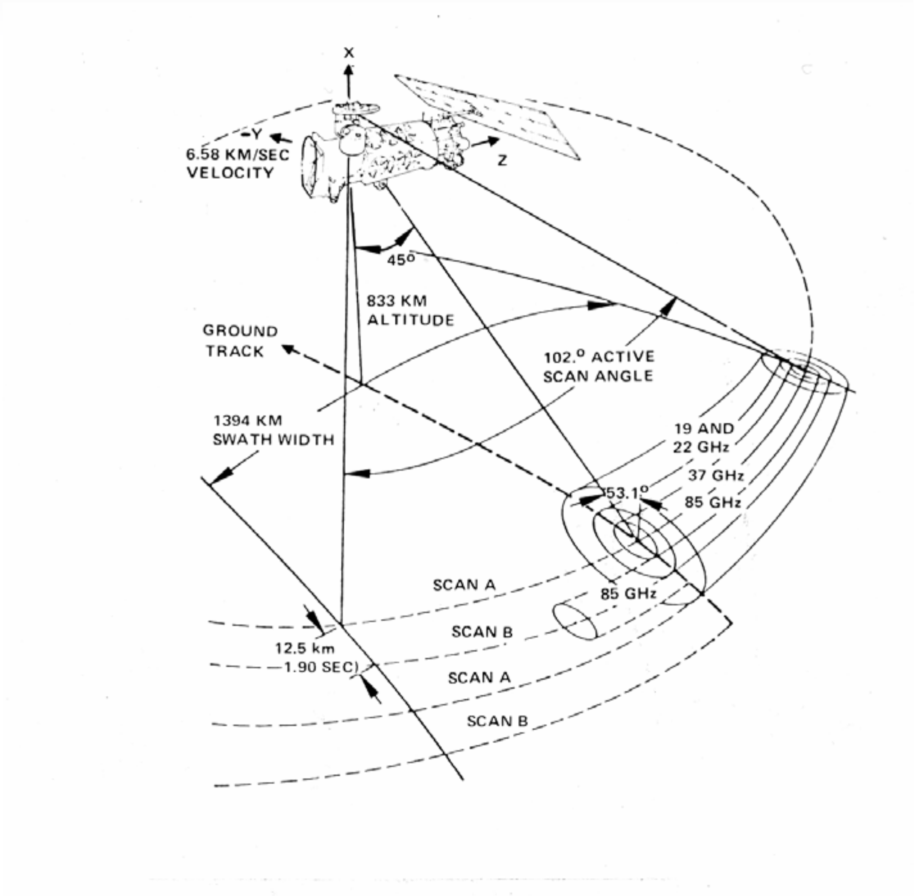

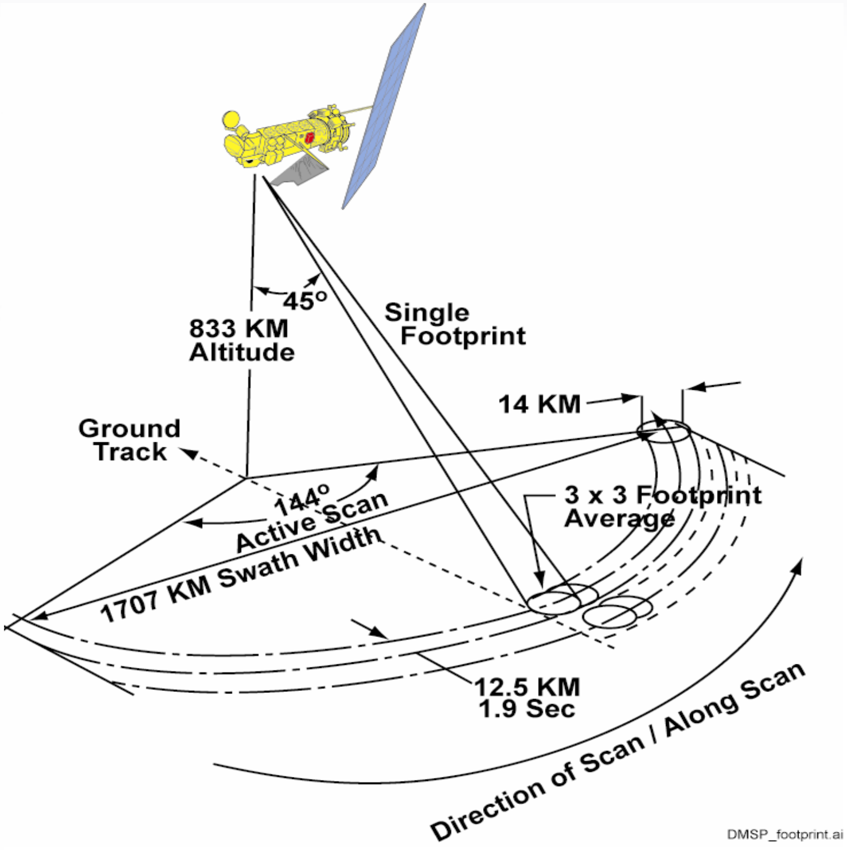

8.1 SSMIS & SSM/I Antenna Beams

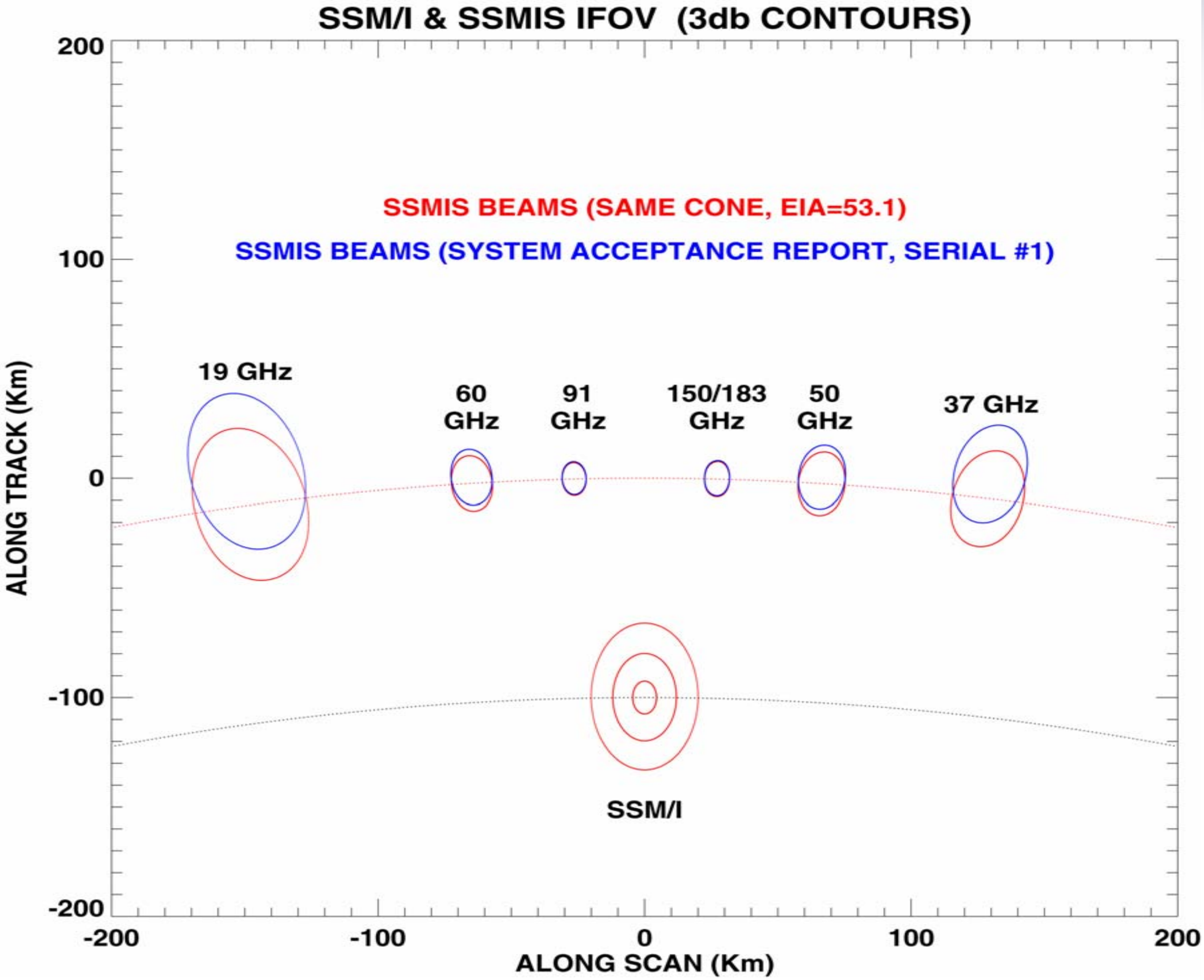

8.1 SSM/I – SSMIS Space /Time Coincidence

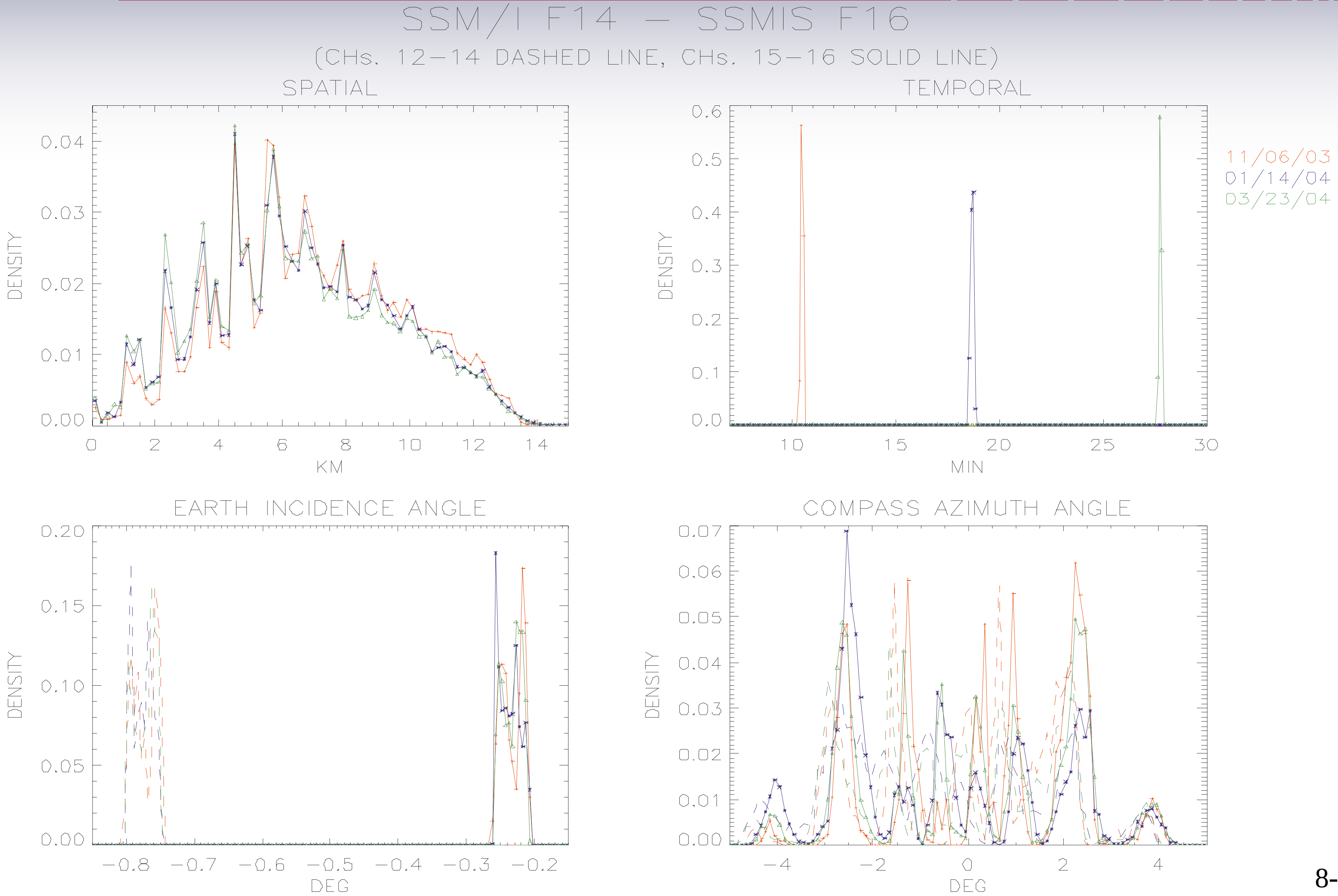

8.2 F-14 SSM/I and SSMIS Channel Characteristics

	Center Freq. (GHz)	Pol.	NEDT (1) (K)	Pol. Rot. (2) (Deg.)	Beam Width (Deg.)	Beam Efficiency (%)	Grid Sampling (3)		EIA (4) (Deg.)
							AT	AS (km)	
F-14 SSM/I	19.35	V	0.49	0.0	1.87	96.1	25.0	25.0	53.15
		H	0.48	0.0	1.88	96.5	25.0	25.0	53.15
	22.235	V	0.61	0.0	1.62	95.5	25.0	25.0	53.15
	37.0	V	0.31	0.0	1.05	91.4	25.0	25.0	53.15
		H	0.35	0.0	1.05	94.0	25.0	25.0	53.15
	85.5	V	0.54	0.0	0.42	93.2	12.5	12.5	53.15
		H	0.49	0.0	0.43	91.1	12.5	12.5	53.15
F-16 SSMIS	19.35	V	0.46	6.71	1.92	96.1	12.5	25.0	53.90
		H	0.35	6.71	1.94	96.0	12.5	25.0	53.90
	22.235	V	0.40	6.71	1.85	96.2	12.5	25.0	53.90
	37.0	V	0.29	- 5.61	1.20	95.9	12.5	25.0	53.36
		H	0.35	- 5.61	1.19	96.2	12.5	25.0	53.36
	91.655	V	0.21	1.19	0.40	94.4	12.5	12.5	53.10
		H	0.27	1.19	0.39	94.5	12.5	12.5	53.10

(1) Warm-Load temperature = 306.0 K. Integration time = 8.44 msec.

(2) Rotation of beam polarization relative to earth basis.

(3) AT = Along-Track, AS = Along-Scan

(4) Nominal Earth Incidence Angle (for 860 km altitude).

8.3 Cross-Calibration Mapping

- **F-16 SSMIS SDR → F-14 SSM/I**

$$T_p \xrightarrow{\quad f \quad} \hat{T}_p = f(T_p) = mT_p + b$$

- **SSMIS SDR: See Section 3.0**
- **SSM/I SDR:**
  - **Scan non-uniformity correction**
  - **Antenna Pattern Correction APC (Spillover/Xpol)**
  - **Solar intrusion into warm-load correction**
- **Mapping Addresses SDR Differences:**
  - **EIA (Primarily Chs. 12-14)**
  - **Antenna spillover/xpol**
  - **Channel Frequency (Primarily Chs. 17-18)**
  - **Warm-load and Cold Space Target Accuracies**
  - **Channel Bandwidths**

8.3 SSMIS Radiometer Gain (Without and With Correction for Solar Intrusion into Warm-load 11/6/03)

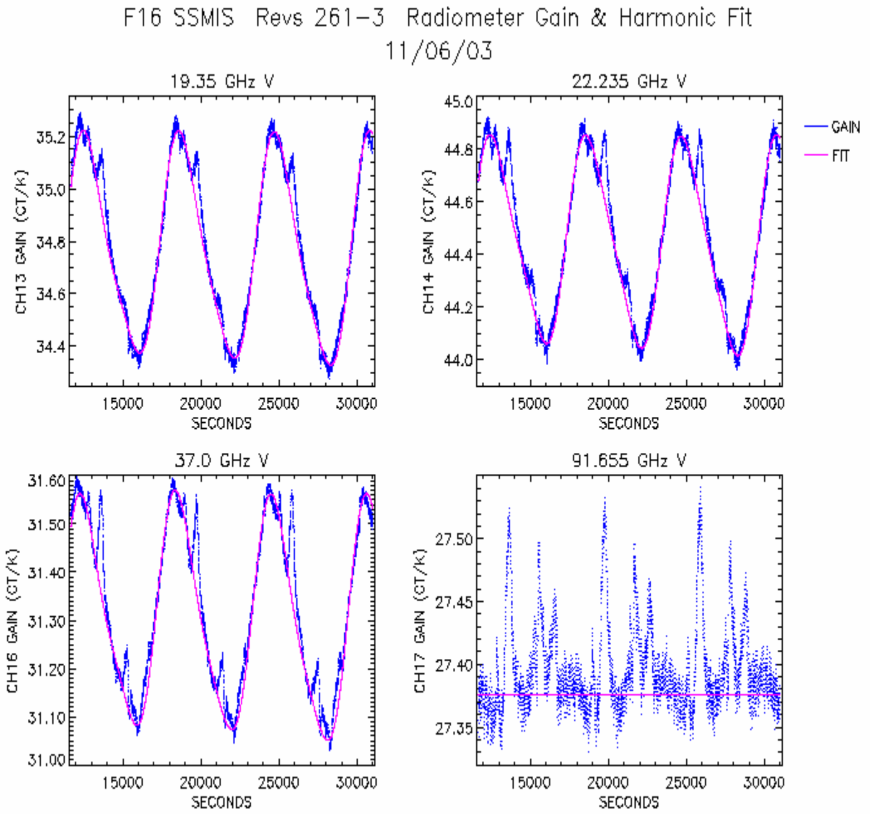

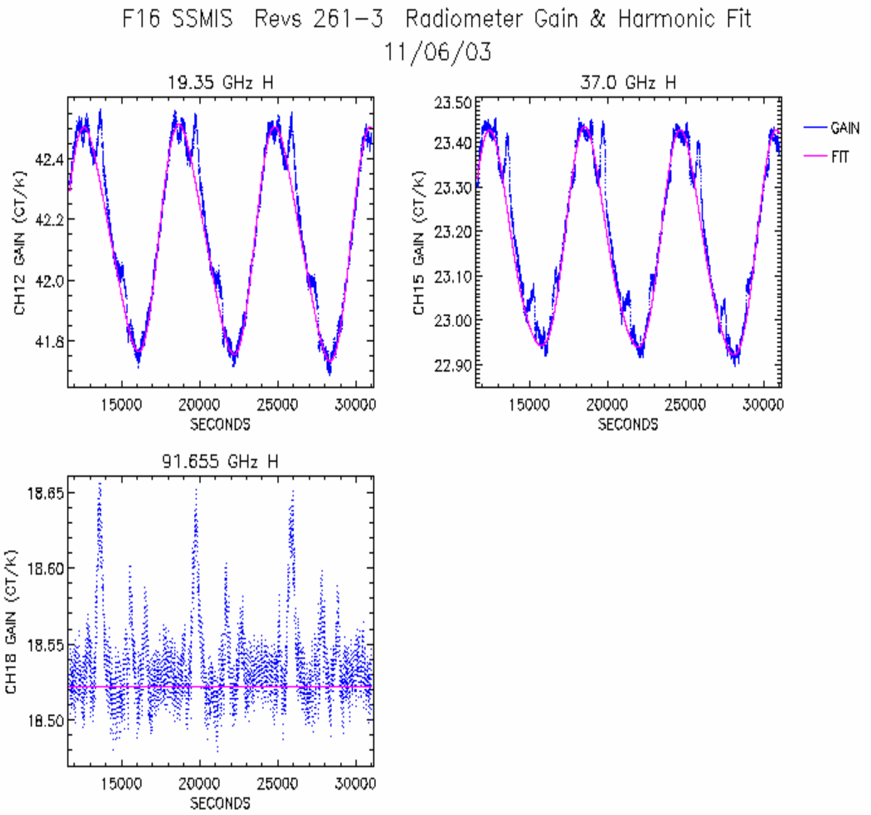

8.3 SSM/I Radiometer Gain (Without and With Correction for Solar Intrusion into Warm-load 11/6/03)

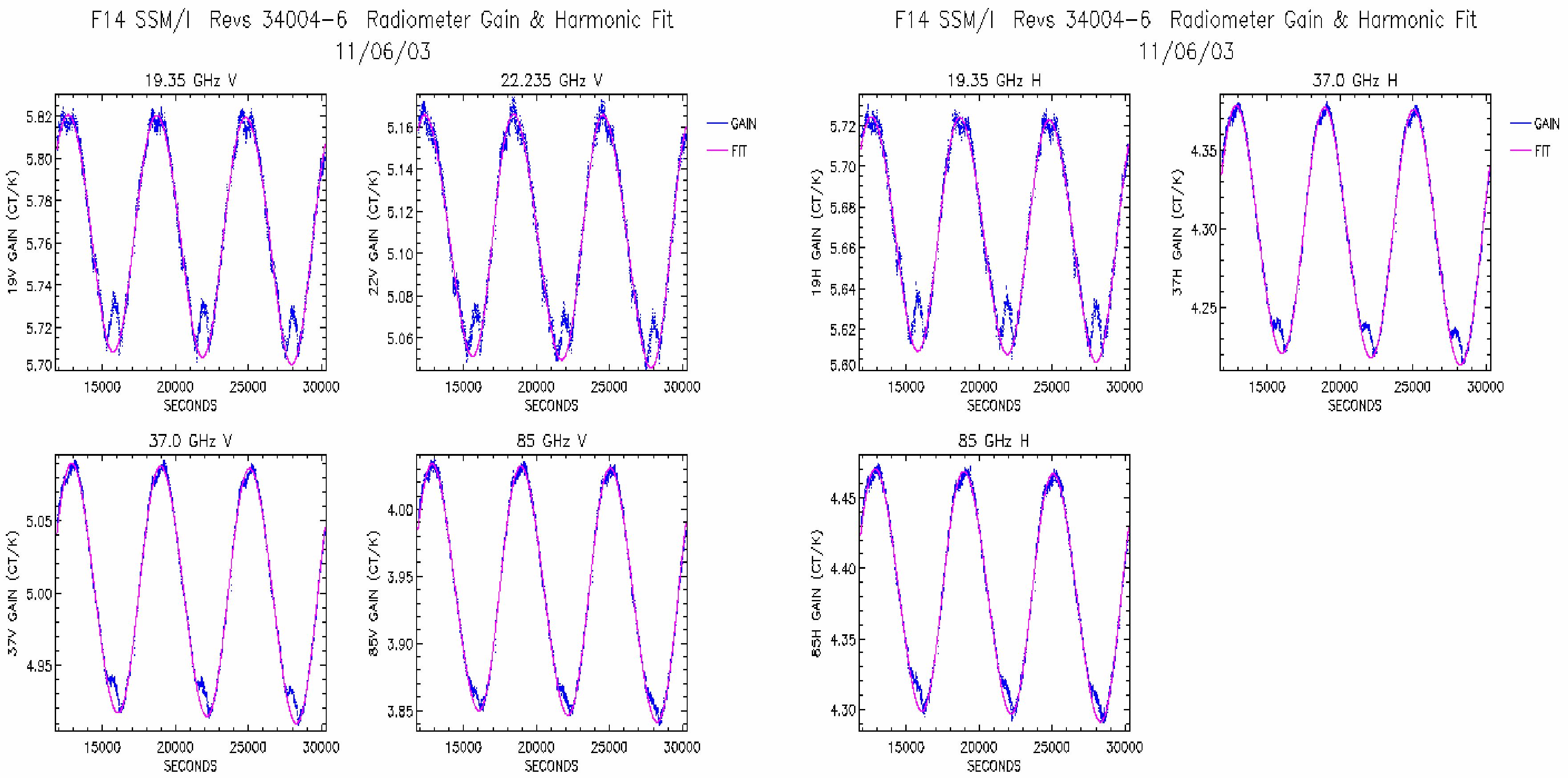
F14 SSM/I Revs 34004-6 Radiometer Gain & Harmonic Fit
11/06/03

F14 SSM/I Revs 34004-6 Radiometer Gain & Harmonic Fit
11/06/03

8.3 Cross-Calibration (Cont'd)

- Parameters b (offset) and m (slope) selected to minimize

$$\varepsilon^2(m,b) = \frac{1}{N}\sum_{k=1}^{N}\left[S_p(k) - b - mT_p(k)\right]^2$$

N= Number of match-ups of SSMIS and SSM/I

$S_p(k)$ = SSM/I SDR, channel p, match-up k

$T_p(k)$ = SSMIS with selected option, channel p, match-up k

- b and m depend on major surface types: ocean, land, sea ice under rain-free conditions (established by SSM/I rain flag)

- Match-up data

Development set: 6 November 03

Test sets : 14 January 04 , 23 March 04

8.4 Calibration Ocean Scenes

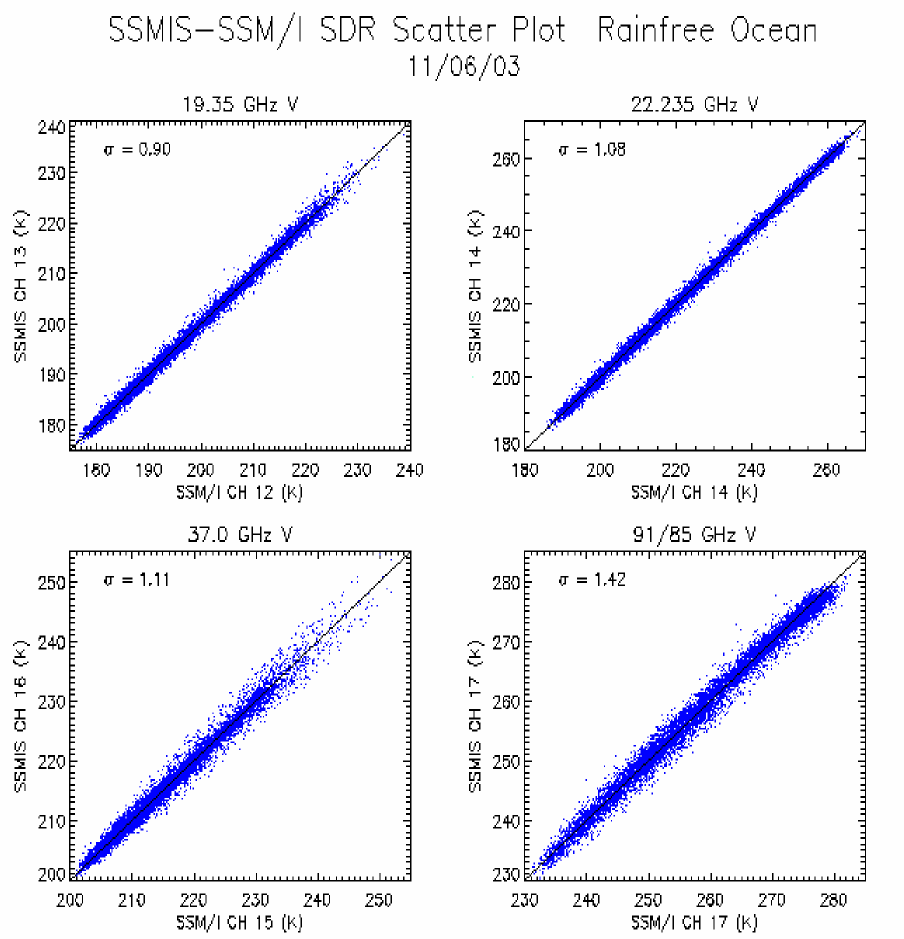

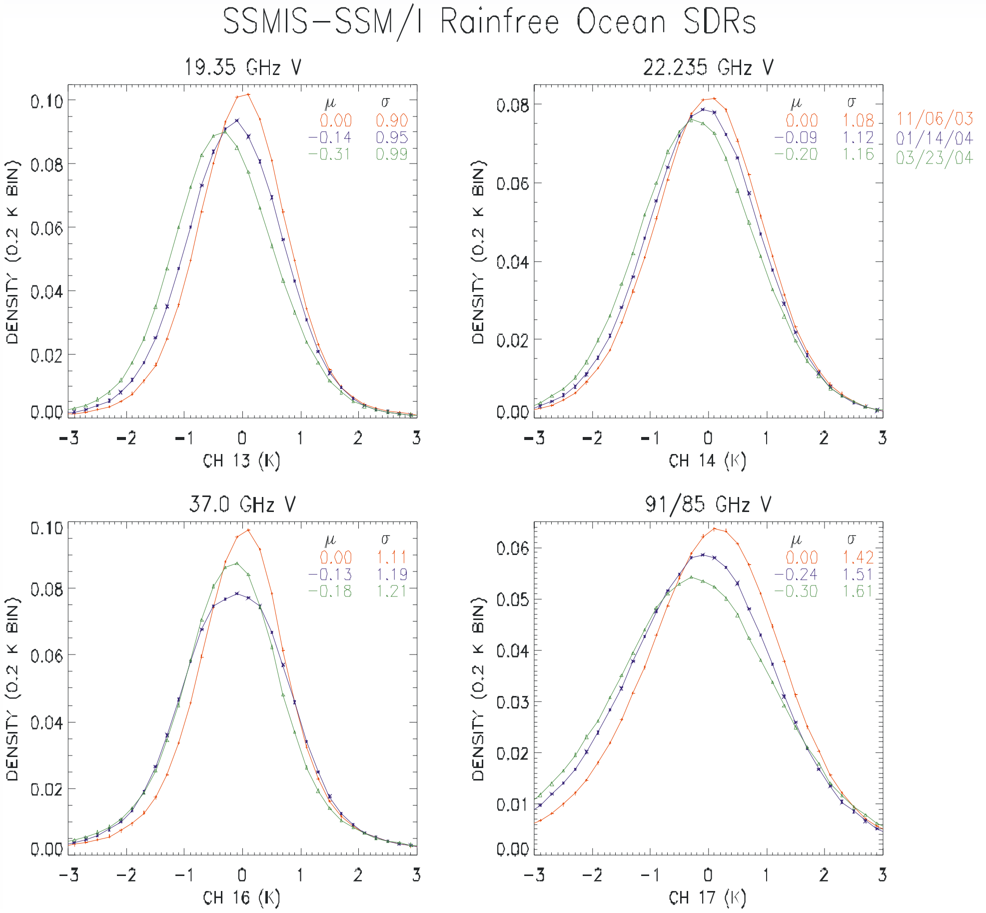

8.4 Calibration Ocean Scenes (Cont’d)

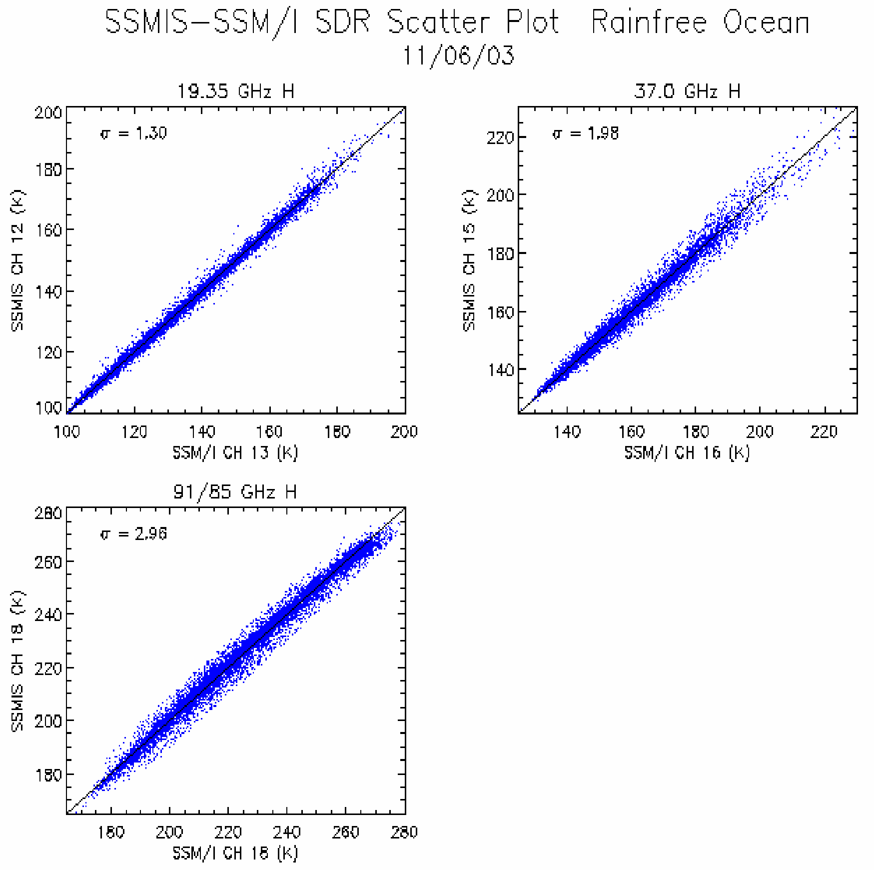

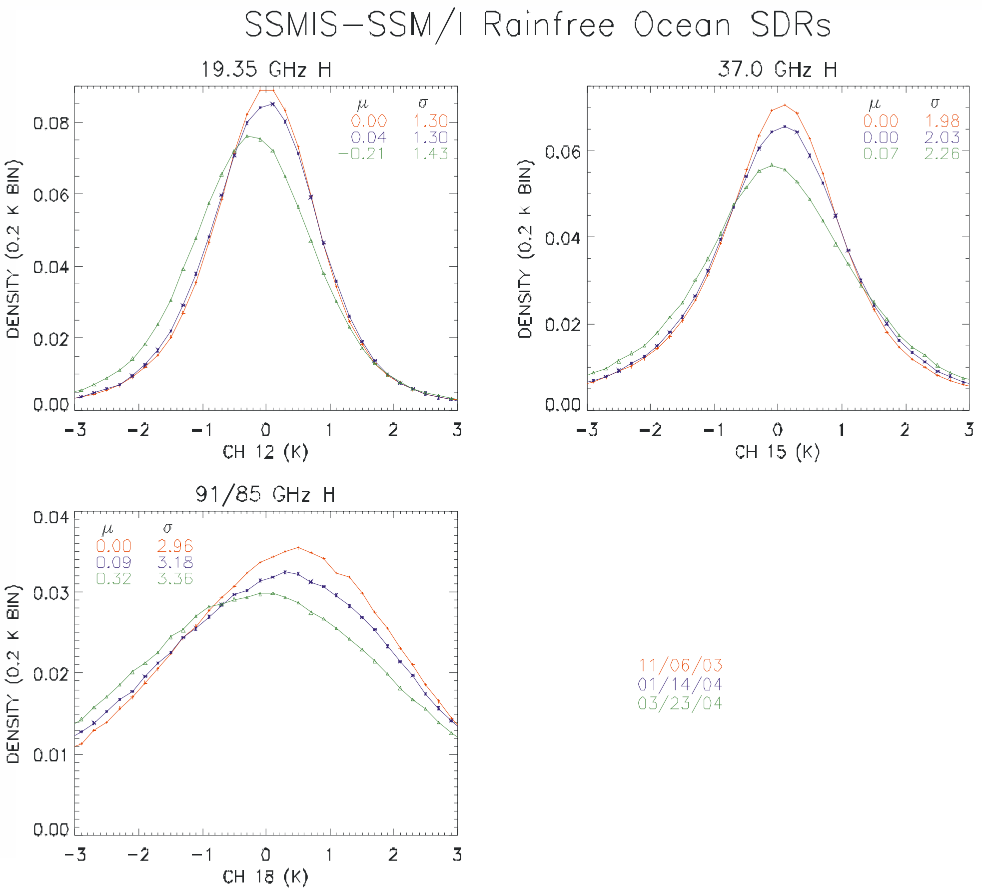

8.4 Calibration Ocean Scenes (Cont'd)

11/06/2003 Rain Free Ocean SDR Match-ups (N=609033)

Ch.	F14 Mean	F14 Standard Deviation	F14 – F16 Mean	F14 – F16 Standard Deviation	F14 Unexplained Variance (%)
12	134.6	19.0	0.0	1.30	0.47
13	198.5	12.6	0.0	0.90	0.51
14	225.0	21.4	0.0	1.08	0.25
15	159.1	15.8	0.0	1.98	1.56
16	216.4	9.0	0.0	1.11	1.52
17	258.8	12.9	0.0	1.42	1.19
18	228.4	24.9	0.0	2.96	1.42

01/14/2004 Rain Free Ocean SDR Match-ups (N=741163)

Ch.	F14 Mean	F14 Standard Deviation	F14 – F16 Mean	F14 – F16 Standard Deviation	F-14 Unexplained Variance (%)
12	134.2	18.2	0.04	1.30	0.51
13	198.4	12.2	0.14	0.95	0.61
14	224.7	21.0	0.09	1.12	0.28
15	158.7	15.1	0.00	2.03	1.81
16	216.3	8.7	0.13	1.19	1.85
17	258.8	13.0	0.24	1.51	1.35
18	228.2	24.4	0.09	3.18	1.69

03/23/2004 Rain Free Ocean SDR Match-ups (N=602231)

Ch.	F14 Mean	F14 Standard Deviation	F14 – F16 Mean	F14 – F16 Standard Deviation	F-14 Unexplained Variance (%)
12	137.1	19.5	0.21	1.43	0.54
13	200.2	12.8	0.31	0.99	0.60
14	228.2	21.9	0.20	1.16	0.28
15	160.2	15.8	0.07	2.25	2.05
16	217.4	9.1	0.18	1.21	1.80
17	260.5	13.5	0.30	1.61	1.52
18	231.3	25.2	0.32	3.36	1.77

8.5 Calibration Land Scenes

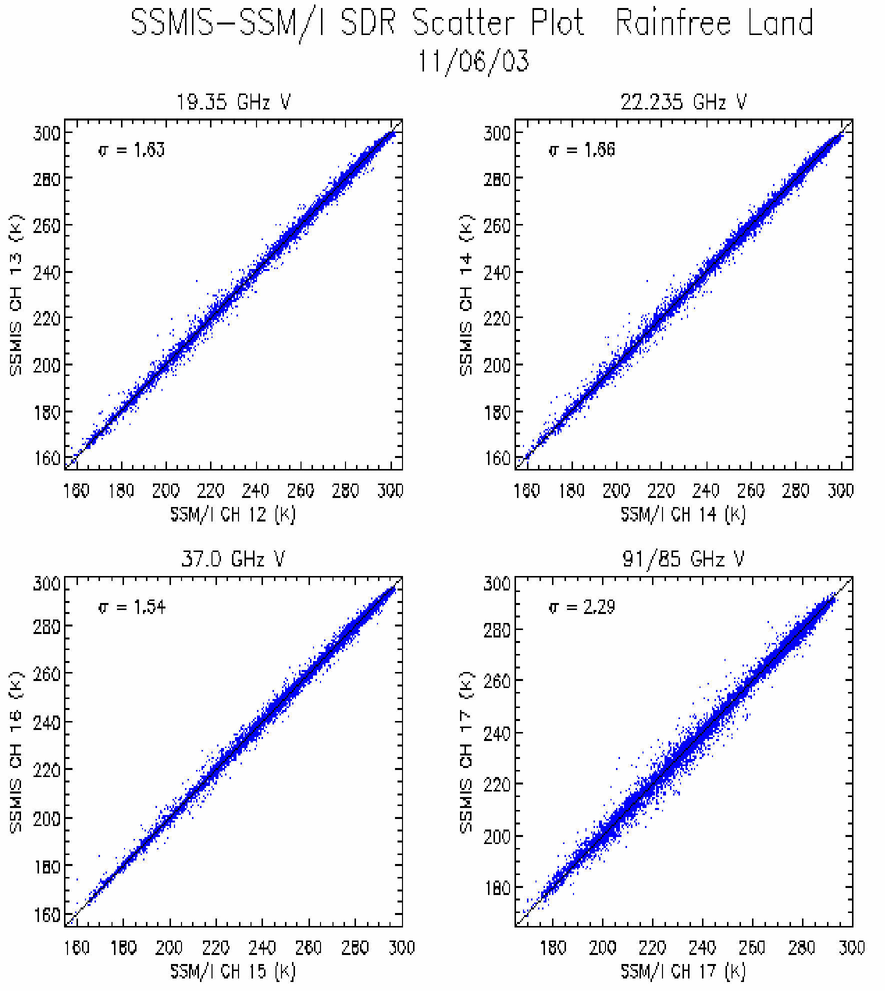

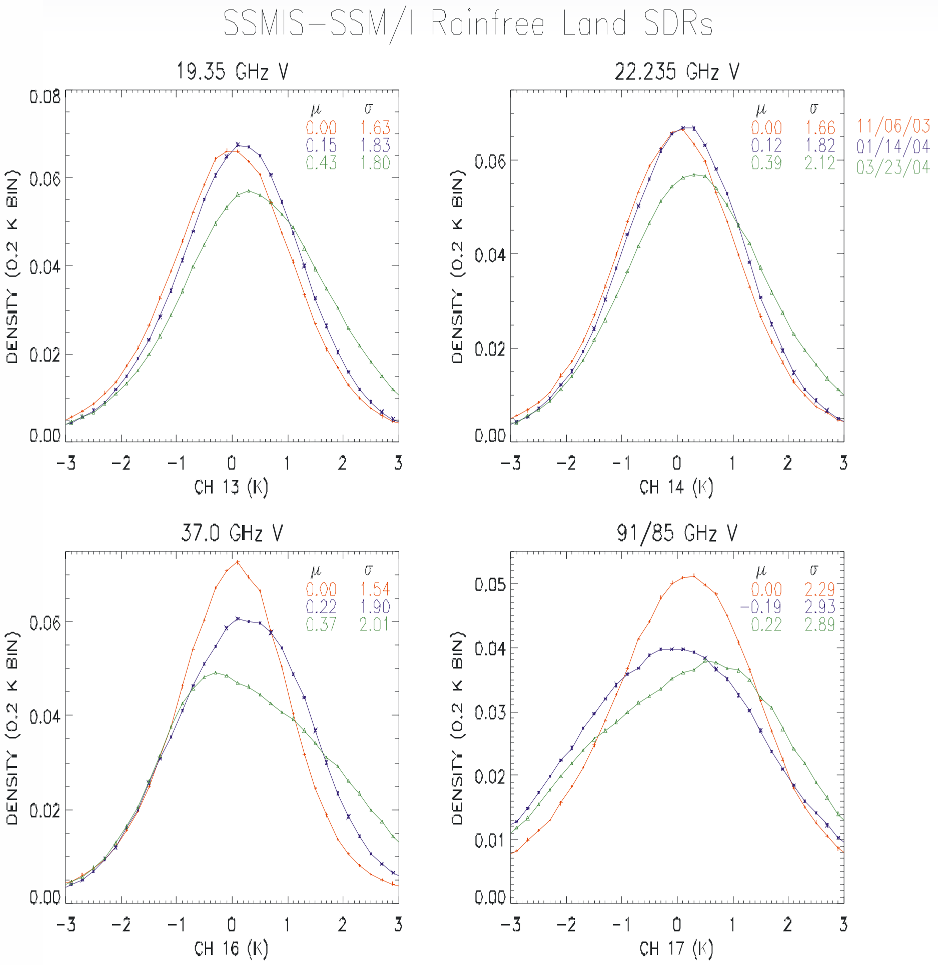

8.5 Calibration Land Scenes (Cont’d)

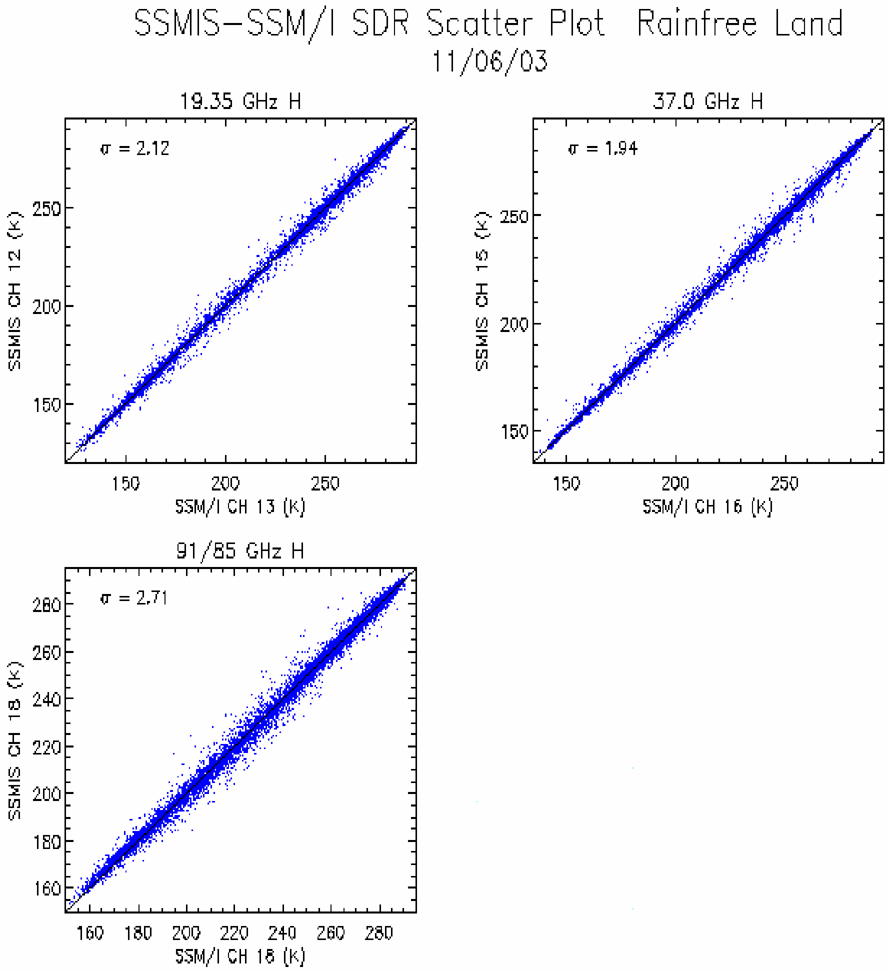

SSMIS–SSM/I SDR Scatter Plot Rainfree Land
11/06/03

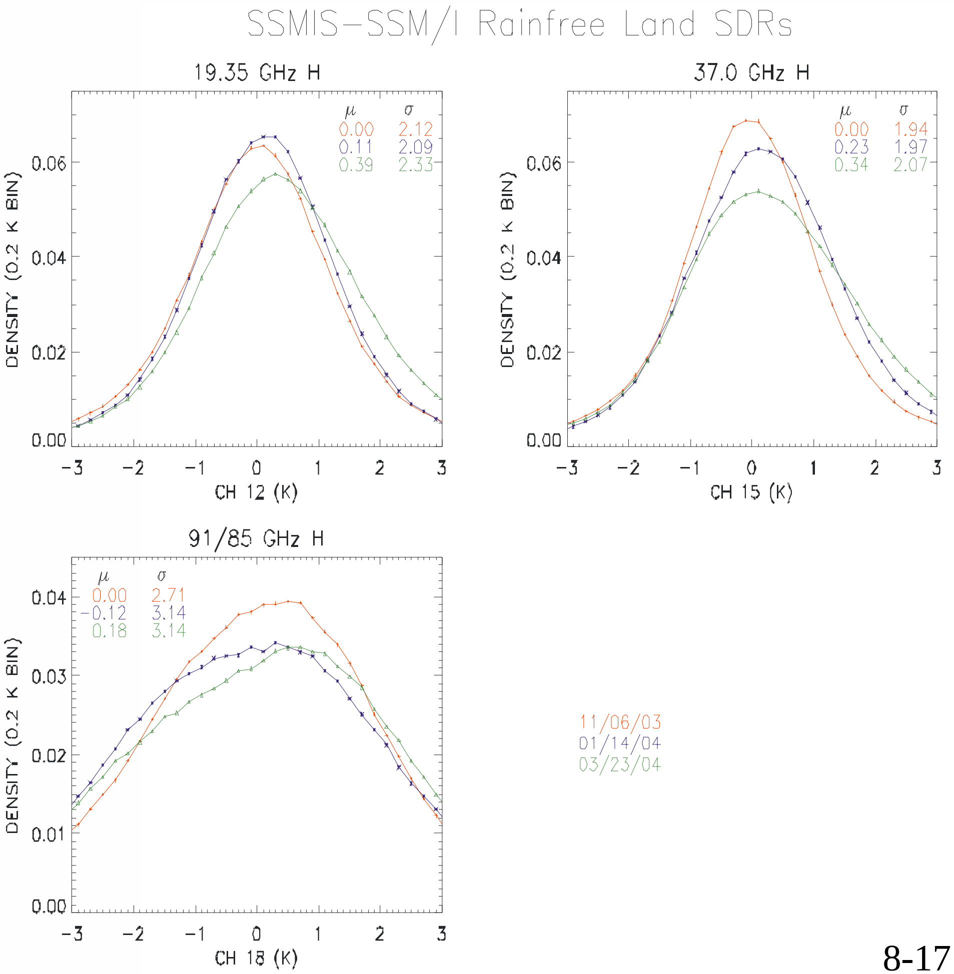

SSMIS–SSM/I Rainfree Land SDRs

8.5 Calibration Land Scenes (Cont'd)

11/06/2003 Rain Free Land SDR Match-ups (385979)

Ch.	F14 Mean	F14 Standard Deviation	F14 – F16 Mean	F14 – F16 Standard Deviation	F14 Unexplained Variance (%)
12	234.1	43.3	0.0	2.12	0.24
13	252.5	33.1	0.0	1.63	0.24
14	252.9	33.5	0.0	1.66	0.24
15	235.4	40.2	0.0	1.94	0.23
16	249.2	32.5	0.0	1.54	0.23
17	246.5	32.7	0.0	2.29	0.49
18	236.9	38.0	0.0	2.70	0.51

01/14/2004 Rain Free Land SDR Match-ups (460786)

Ch.	F14 Mean	F14 Standard Deviation	F14 – F16 Mean	F14 – F16 Standard Deviation	F-14 Unexplained Variance (%)
12	231.5	36.2	-0.11	2.09	0.33
13	249.7	28.1	-0.15	1.83	0.43
14	249.3	28.5	-0.12	1.82	0.41
15	227.2	35.7	-0.23	1.97	0.31
16	240.5	31.1	-0.22	1.90	0.37
17	233.3	36.4	0.19	2.93	0.65
18	224.7	39.1	0.12	3.15	0.64

03/23/2004 Rain Free Land SDR Match-ups (398325)

Ch.	F14 Mean	F14 Standard Deviation	F14 – F16 Mean	F14 – F16 Standard Deviation	F-14 Unexplained Variance (%)
12	231.8	40.7	-0.39	2.33	0.33
13	251.6	31.5	-0.43	1.80	0.33
14	250.9	32.5	-0.39	2.12	0.43
15	227.9	41.8	-0.34	2.07	0.25
16	242.6	35.6	-0.37	2.01	0.32
17	239.7	38.1	-0.22	2.89	0.58
18	229.4	43.1	-0.18	3.14	0.53

8.6 Calibration Sea Ice Scenes

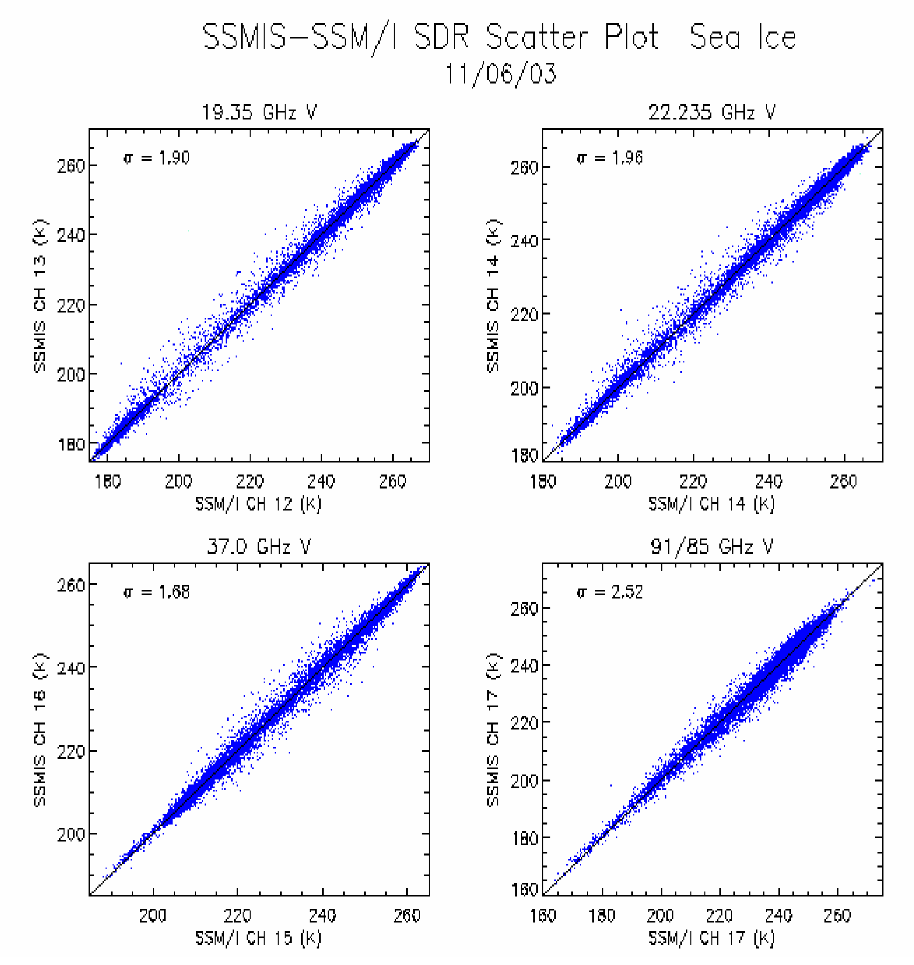

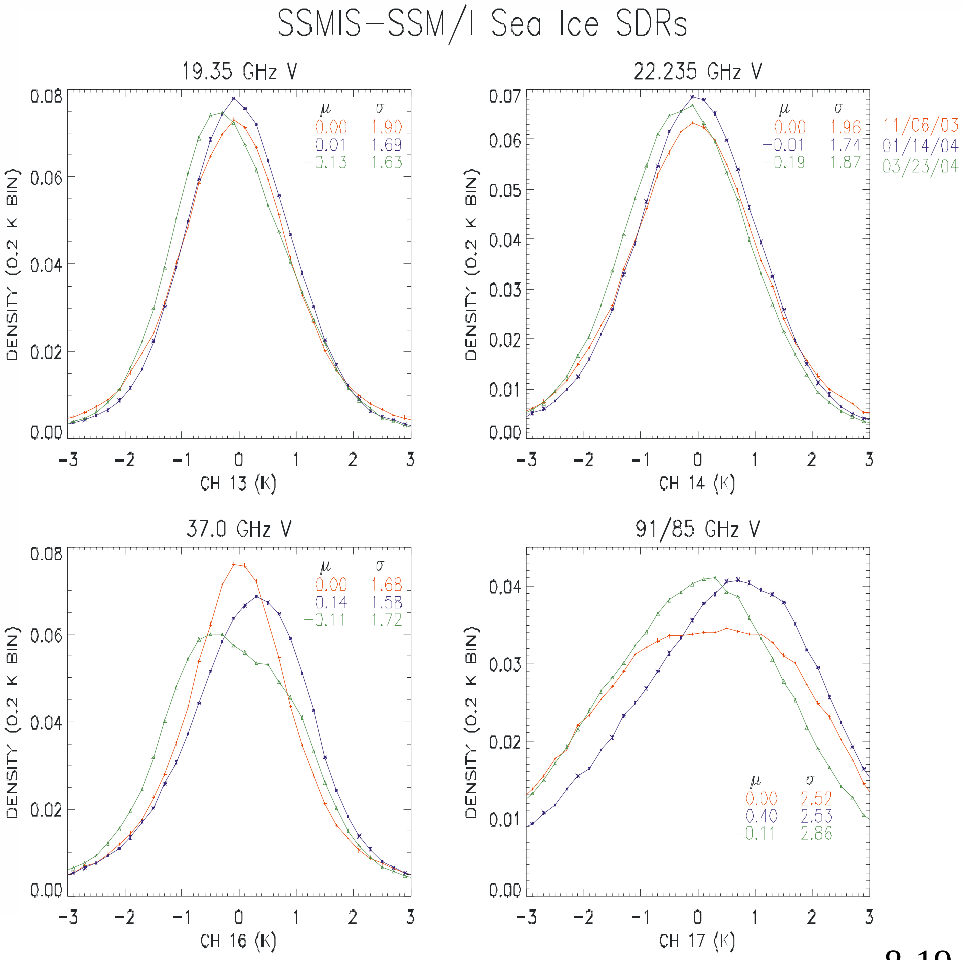

8.6 Calibration Sea Ice Scenes (Cont'd)

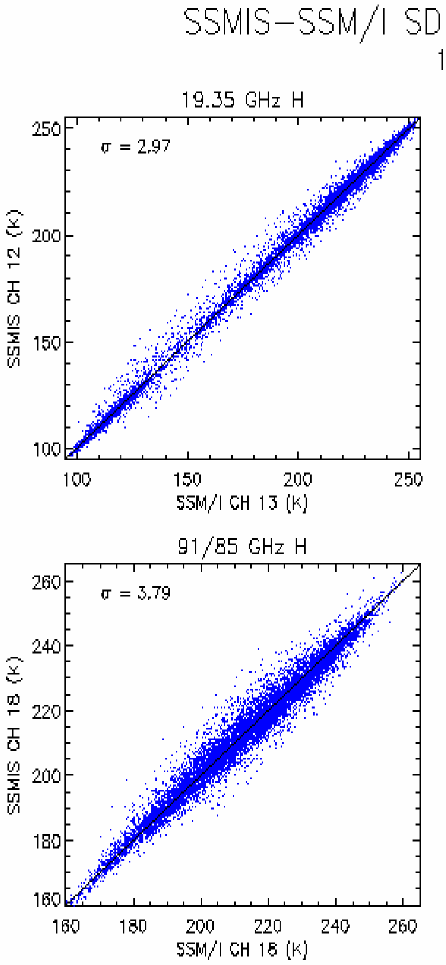

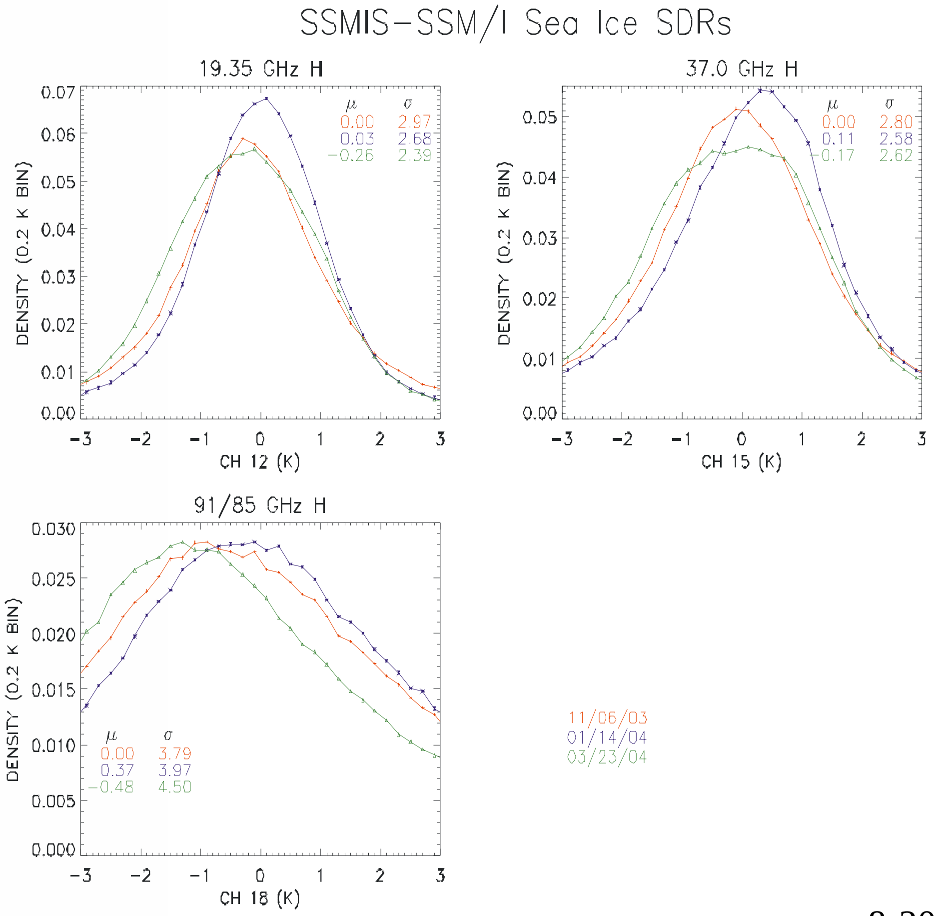

8.6 Calibration Sea Ice Scenes

111/06/2003 Sea Ice SDR Match-ups (175295)

Ch.	F14 Mean	F14 Standard Deviation	F14 – F16 Mean	Standard Deviation	F14 Unexplained Variance (%)
12	191.2	47.9	0.0	2.97	0.38
13	229.7	29.0	0.0	1.91	0.43
14	233.3	23.8	0.0	1.96	0.67
15	200.2	34.2	0.0	2.79	0.67
16	231.1	19.0	0.0	1.68	0.78
17	233.8	17.7	0.0	2.52	2.02
18	213.4	19.8	0.0	3.79	3.65

01/14/2004 Sea Ice SDR Match-ups (185862)

Ch.	F14 Mean	F14 Standard Deviation	F14 – F16 Mean	Standard Deviation	F-14 Unexplained Variance (%)
12	177.0	51.4	0.03	2.68	0.27
13	218.3	28.3	-0.01	1.69	0.36
14	223.1	22.0	0.01	1.74	0.62
15	187.6	33.3	-0.11	2.58	0.60
16	221.3	15.1	-0.14	1.58	1.09
17	226.0	18.9	-0.40	2.53	1.79
18	203.4	16.6	-0.37	3.97	5.69

03/23/2004 Sea Ice SDR Match-ups (116600)

Ch.	F14 Mean	F14 Standard Deviation	F14 – F16 Mean	Standard Deviation	F-14 Unexplained Variance (%)
12	171.4	53.6	0.26	2.39	0.20
13	215.9	30.2	0.13	1.63	0.29
14	220.7	24.6	0.19	1.87	0.58
15	184.2	35.8	0.17	2.62	0.54
16	220.7	17.3	0.11	1.72	0.99
17	228.3	19.7	0.11	2.86	2.11
18	202.8	19.8	0.48	4.50	5.19

8.7 SSMIS and F-14 SSM/I SDRs 19H/37H

(Ascending Passes 06 November 2003)

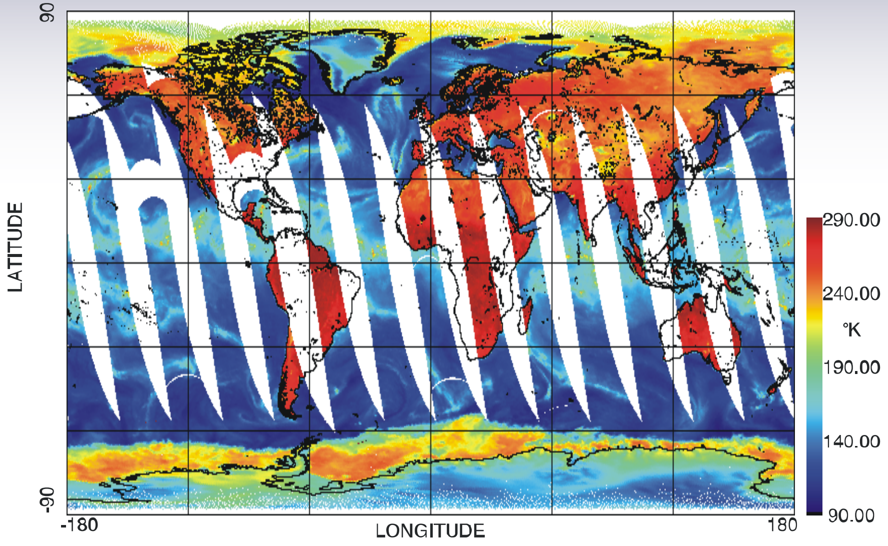
F-14 19H ASCENDING REVS 34002-34015

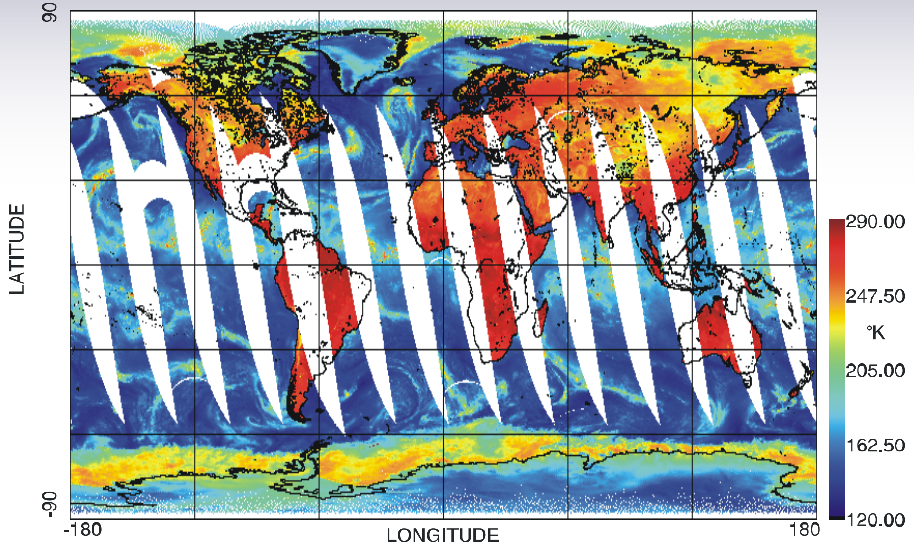
F-14 37H ASCENDING REVS 34002-34015

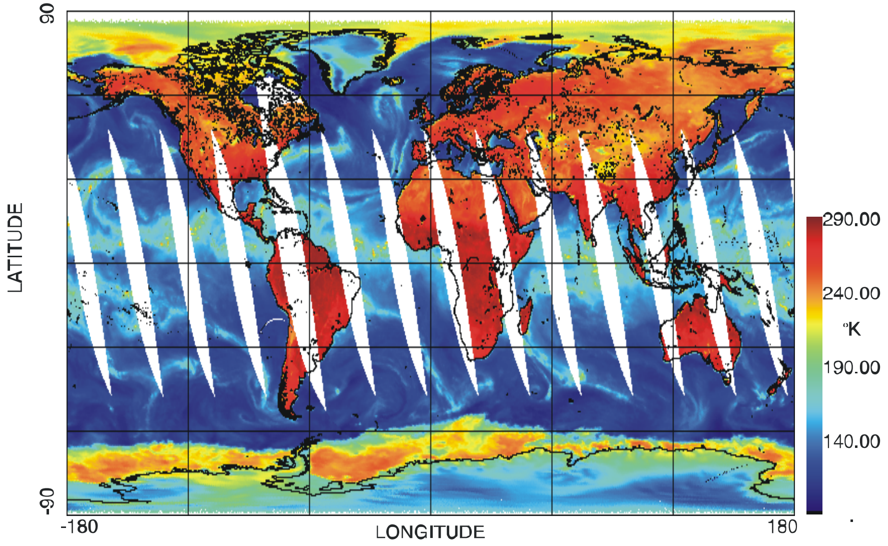
F-16 19H ASCENDING REVS 259-272

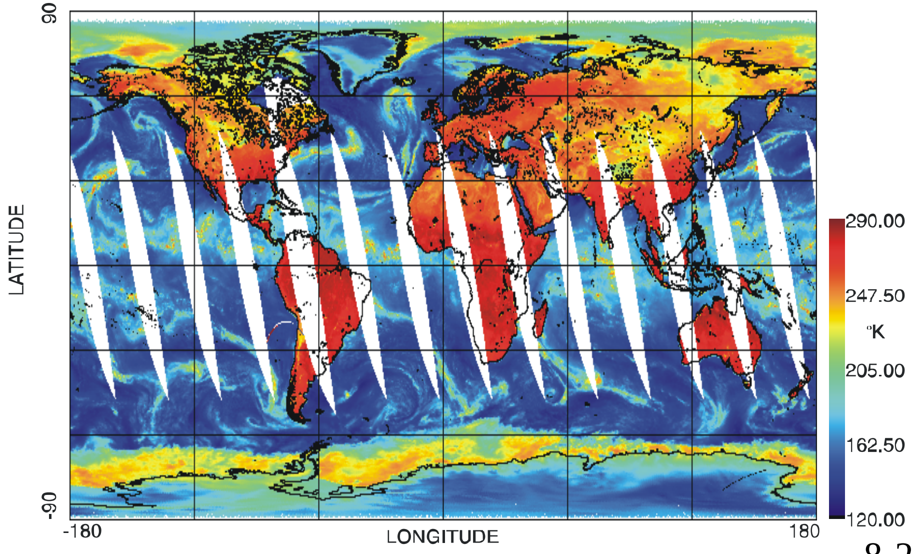
F-16 37H ASCENDING REVS 259-272

8.7 SSMIS and F-14 SSM/I SDRs 19H/37H

(Descending Passes 06 November 2003)

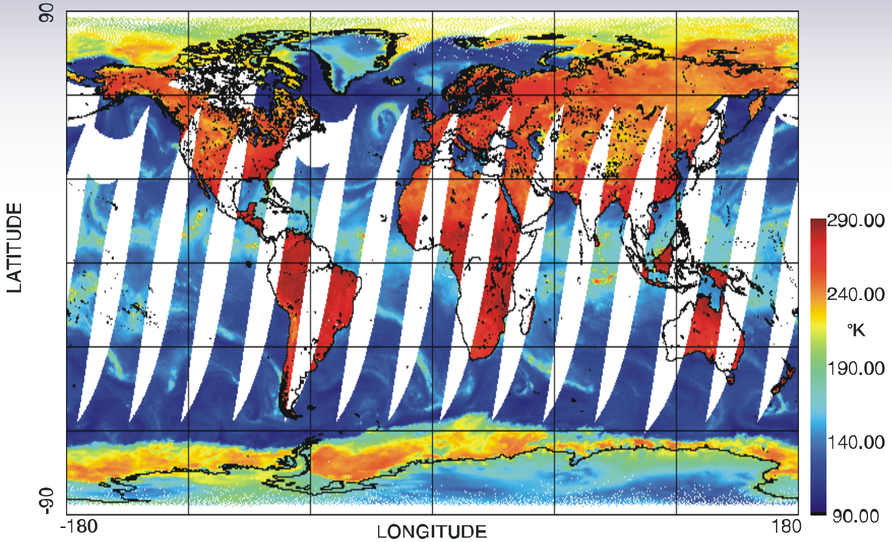
F-14 19H DESCENDING REVS 34002-34015

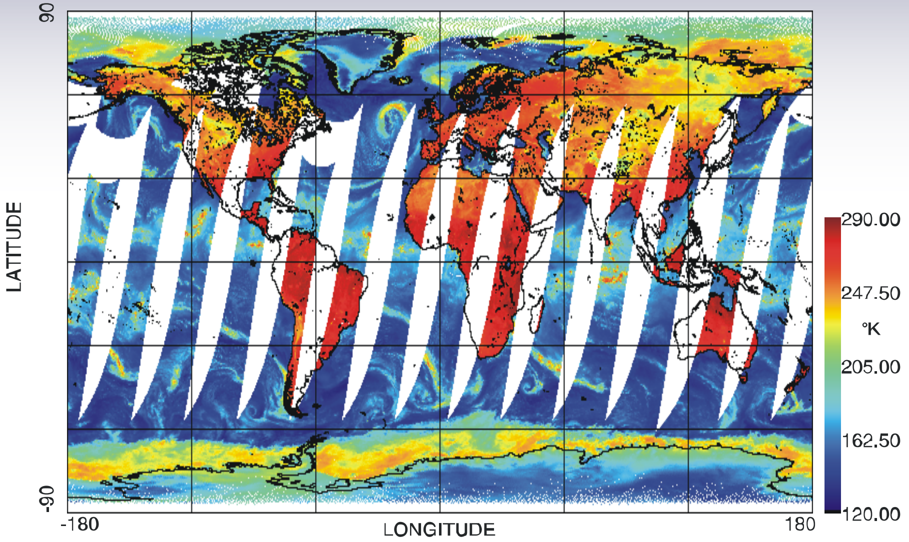
F-14 37H DESCENDING REVS 34002-34015

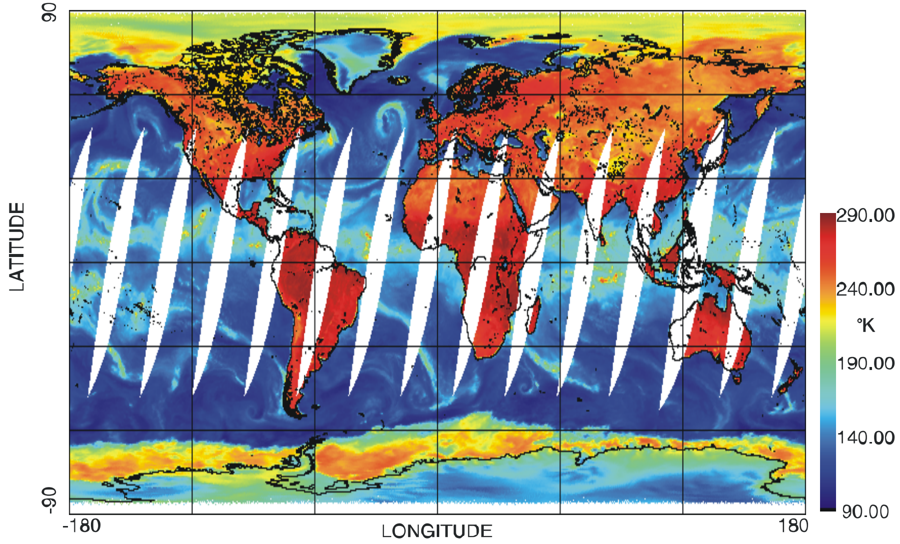
F-16 19H DESCENDING REVS 259-272

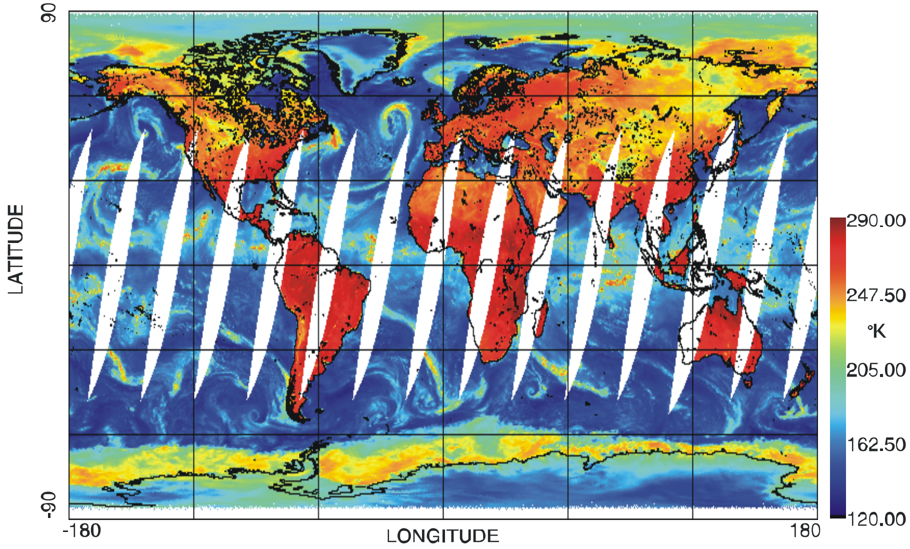
F-16 37H DESCENDING REVS 259-272

8.7 F-14 SSMI and SSMIS SDR 19V/37V

(Ascending Passes 06 November 2003)

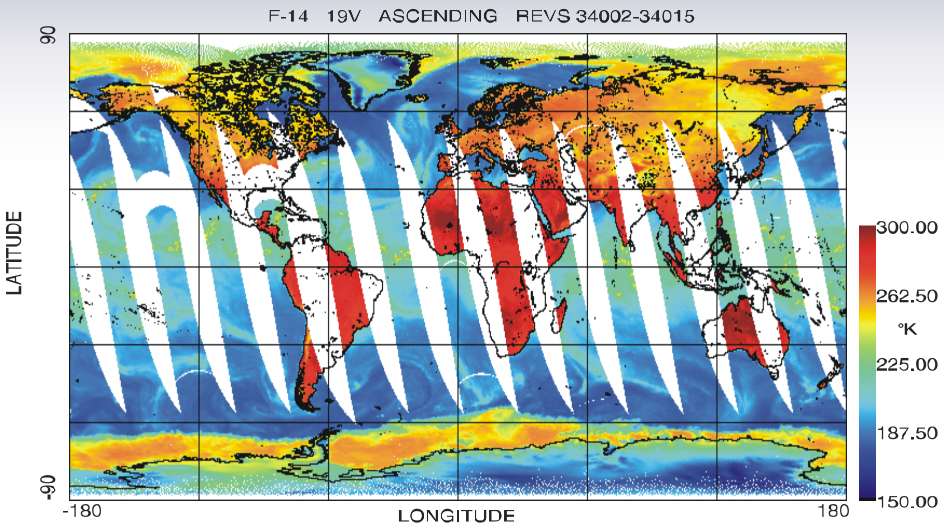
F-14 19V ASCENDING REVS 34002-34015

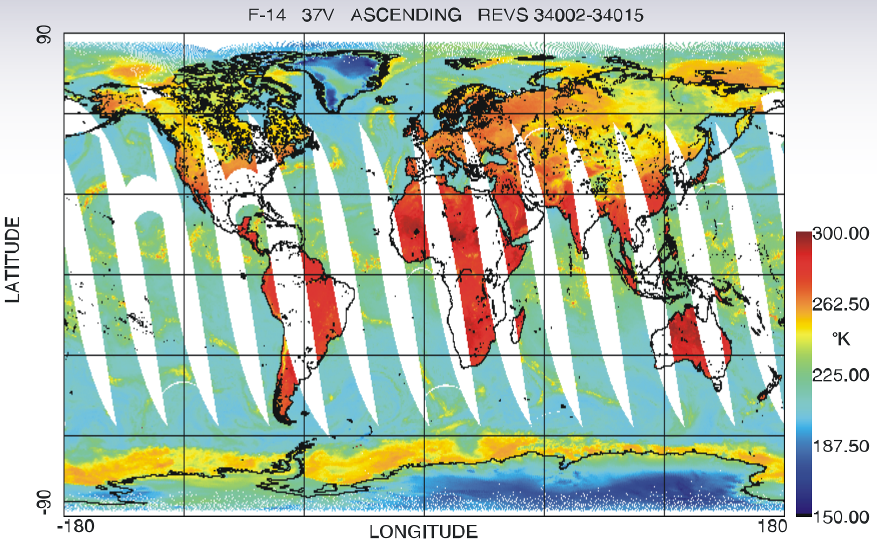
F-14 37V ASCENDING REVS 34002-34015

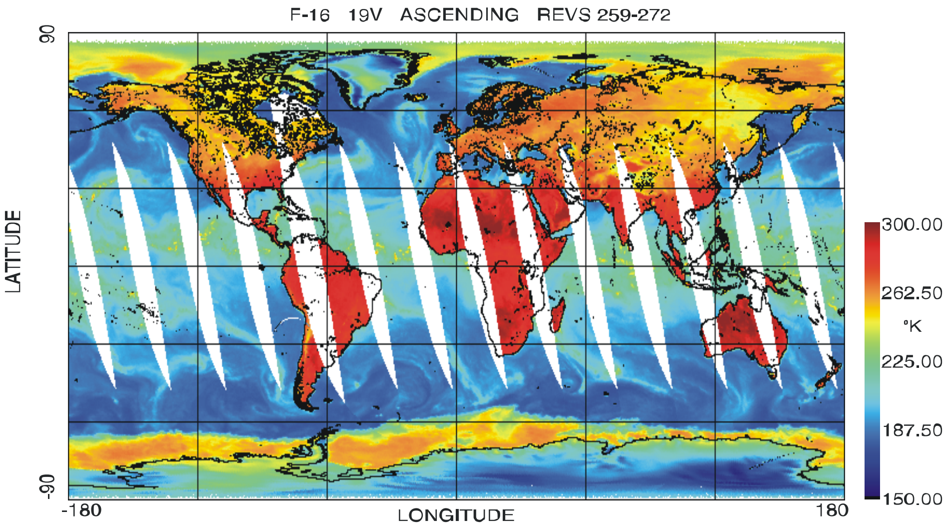
F-16 19V ASCENDING REVS 259-272

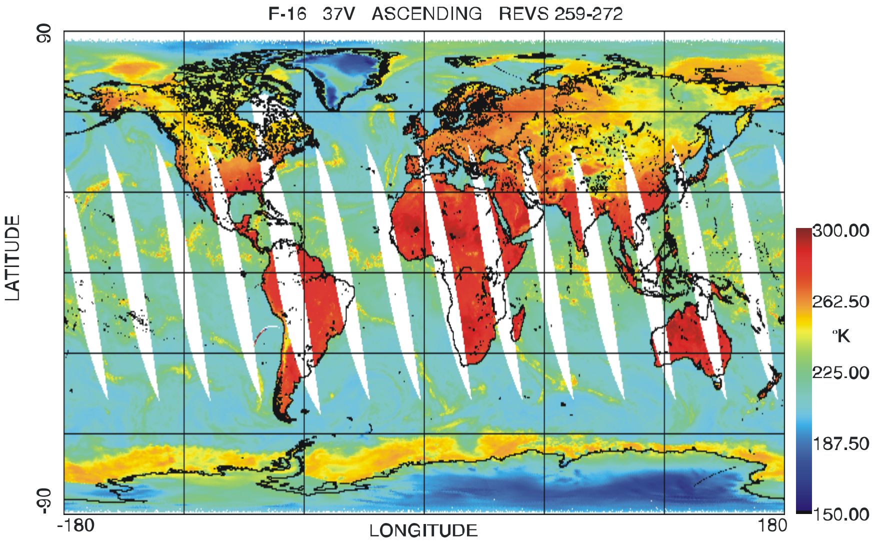
F-16 37V ASCENDING REVS 259-272

8.7 F-14 SSMI and SSMIS SDR 19V/37V

(Descending Passes 06 November 2003)

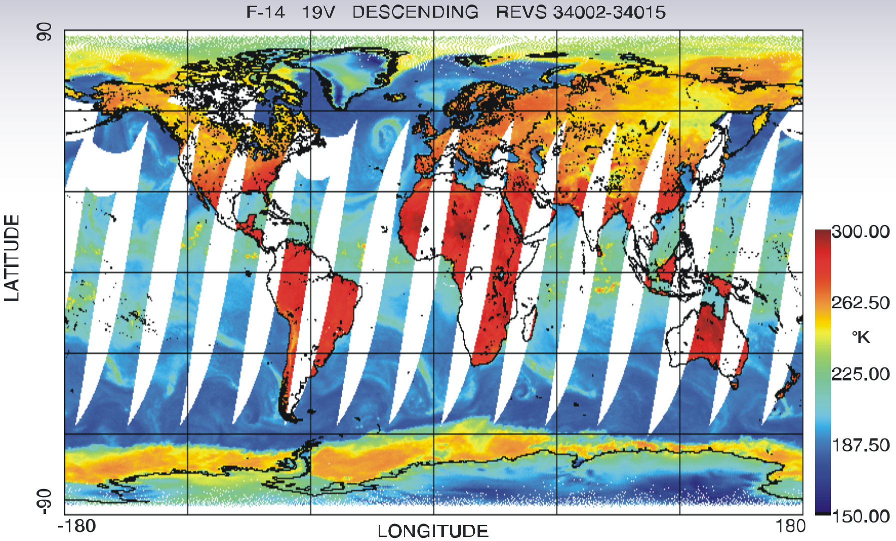

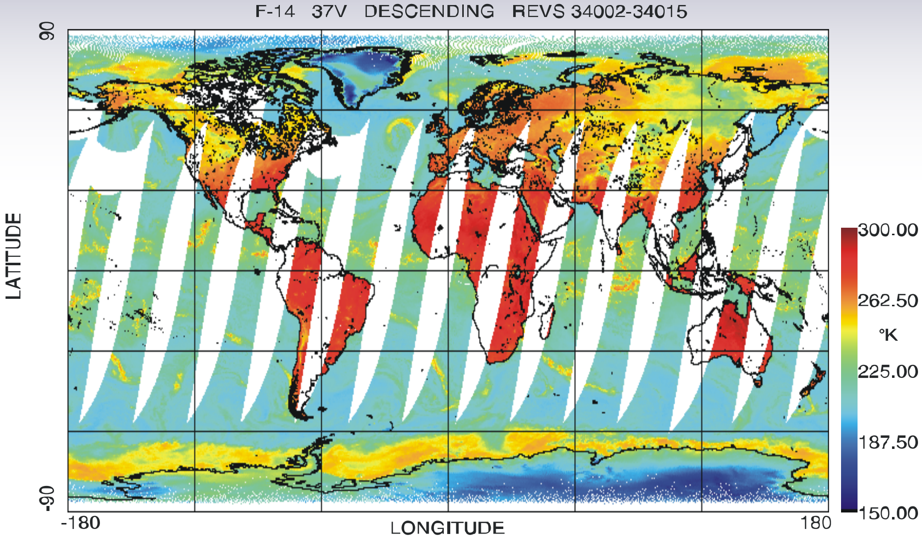

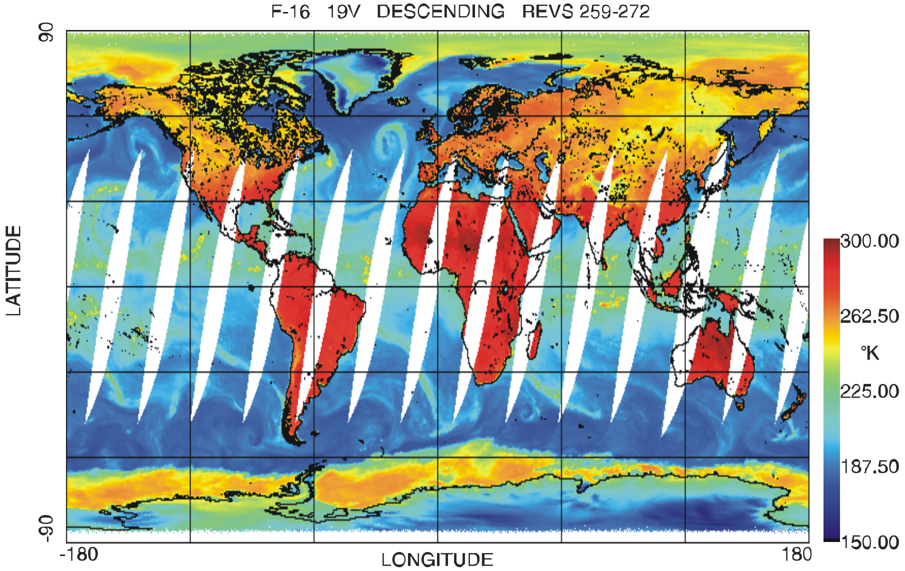

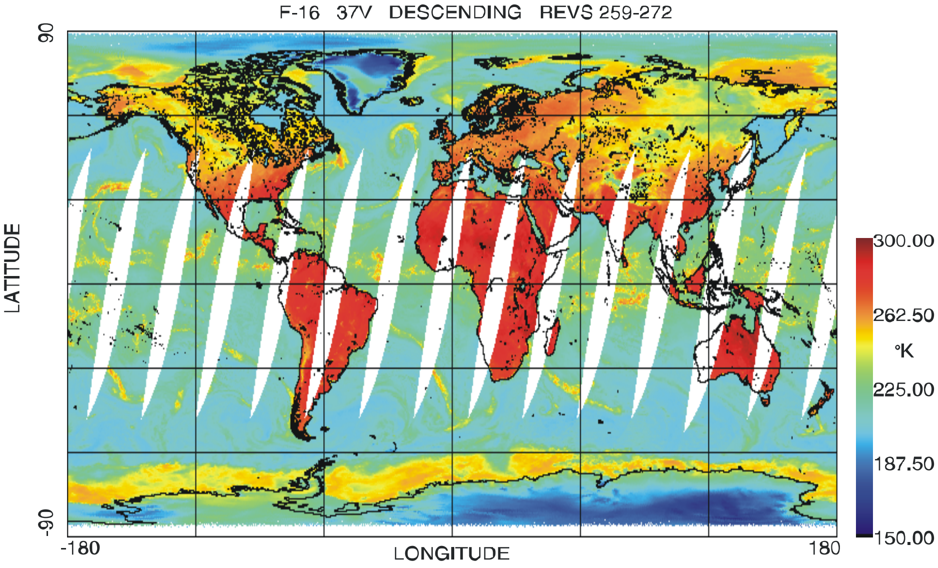

8.7 SSMIS and F-14 SSM/I SDRs 22v/85V/91V

(Ascending Passes 06 November 2003)

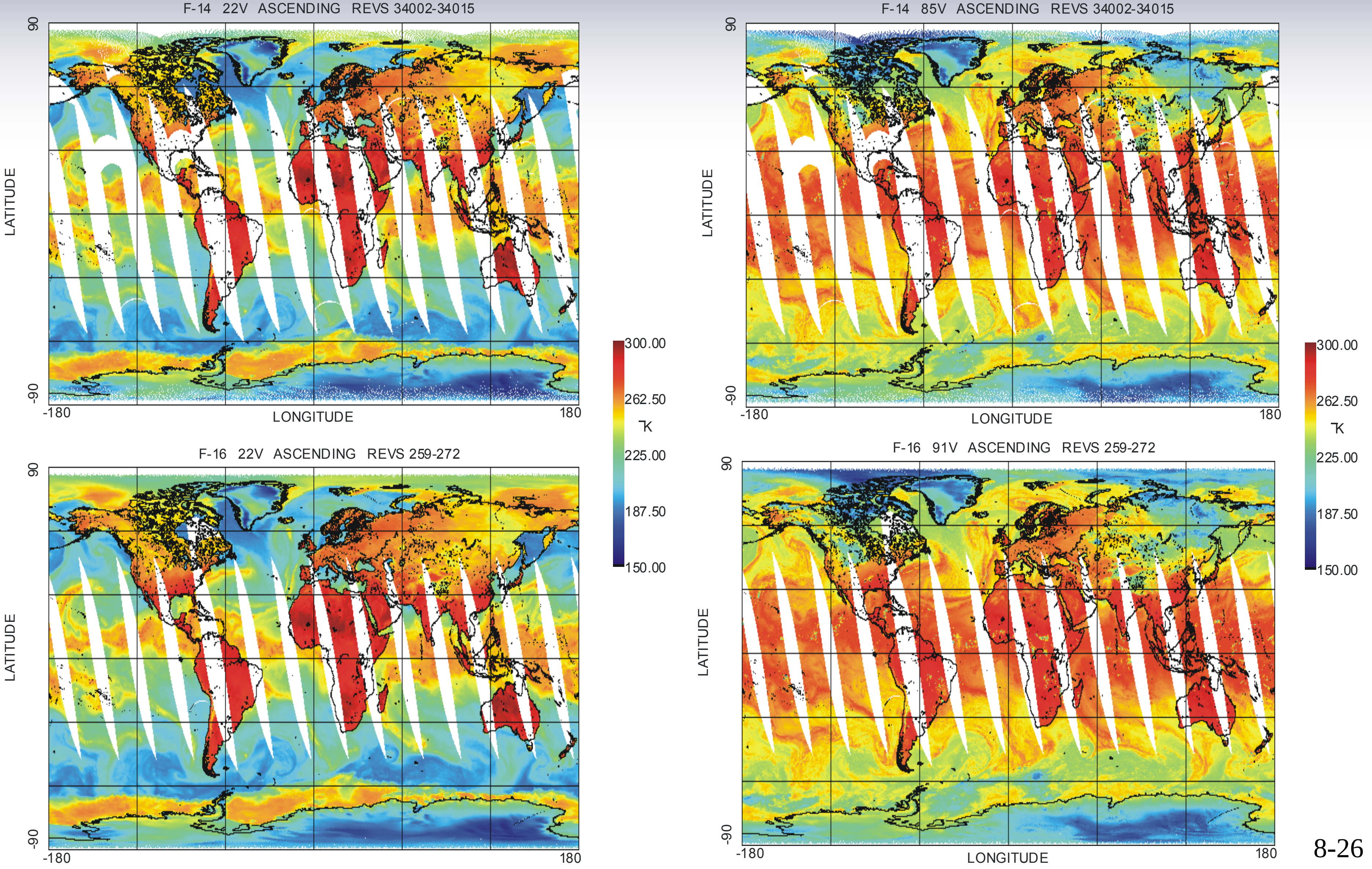

8.7 SSMIS and F-14 SSM/I SDRs 22V/85V/91V

(Descending Passes 06 November 2003)

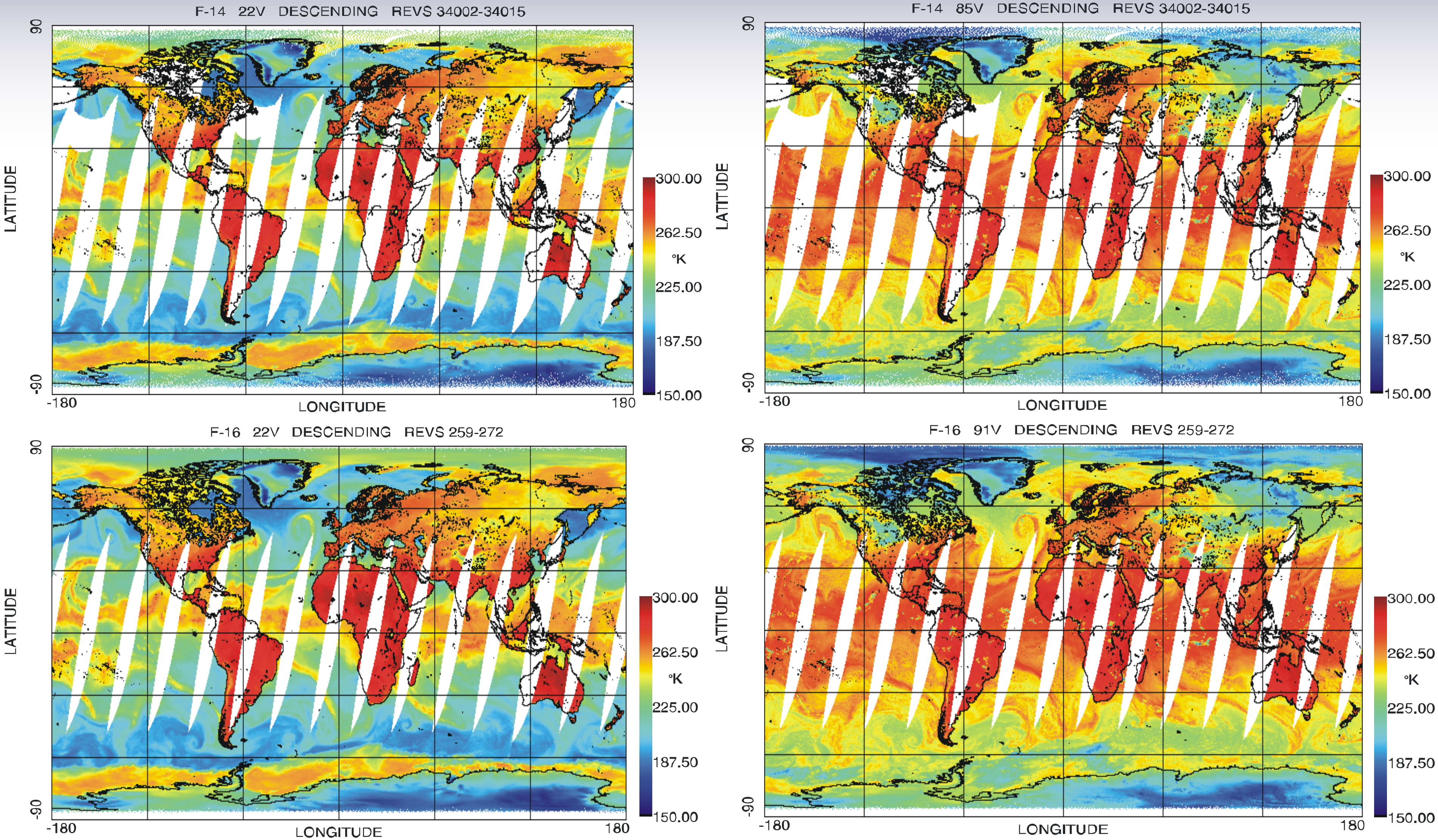

8.8 EDR Validation

- SSMIS EDRs based on Mapping to SSM/I

- EDR comparisons
  - Ocean Surface: wind speed, water vapor, cloud liquid water, rain flag and rainfall rate
  - Land Surface: surface type, surface temperature, soil moisture, snow water equivalent, snow edge, rain flag, rainfall rate
  - Sea Ice: concentration, age, edge
  - Coast/Near Coast: rain flag, rainfall rate

- Heritage SSM/I EDR algorithms employed for SSMIS

8.8 SSMIS – SSM/I Ocean, Land and Sea Ice EDR

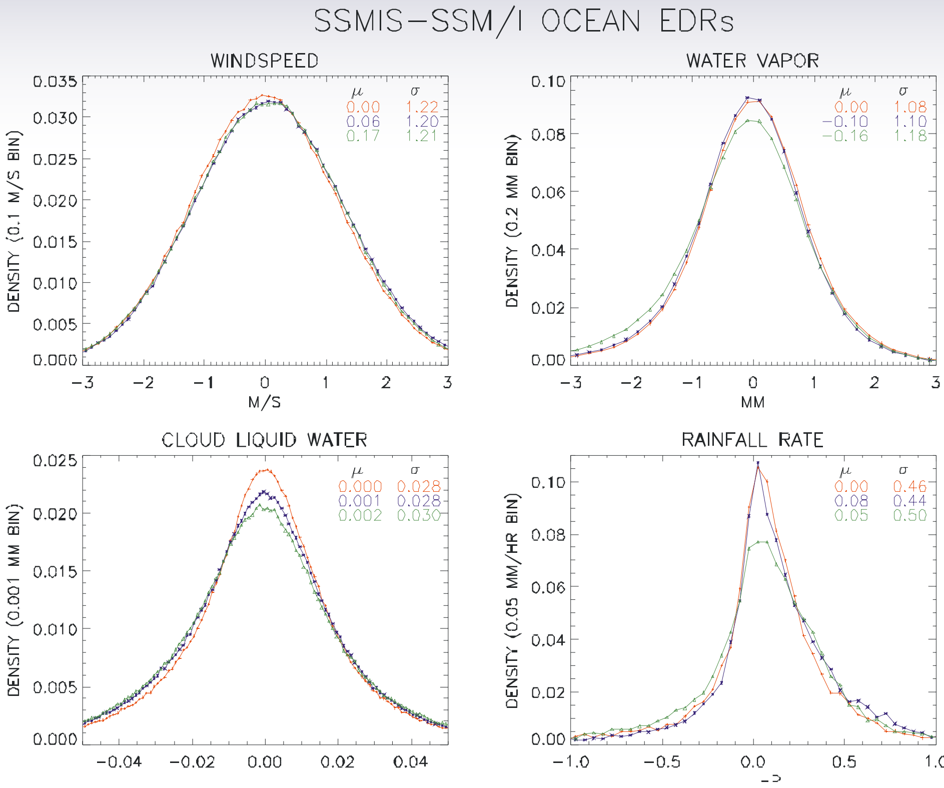

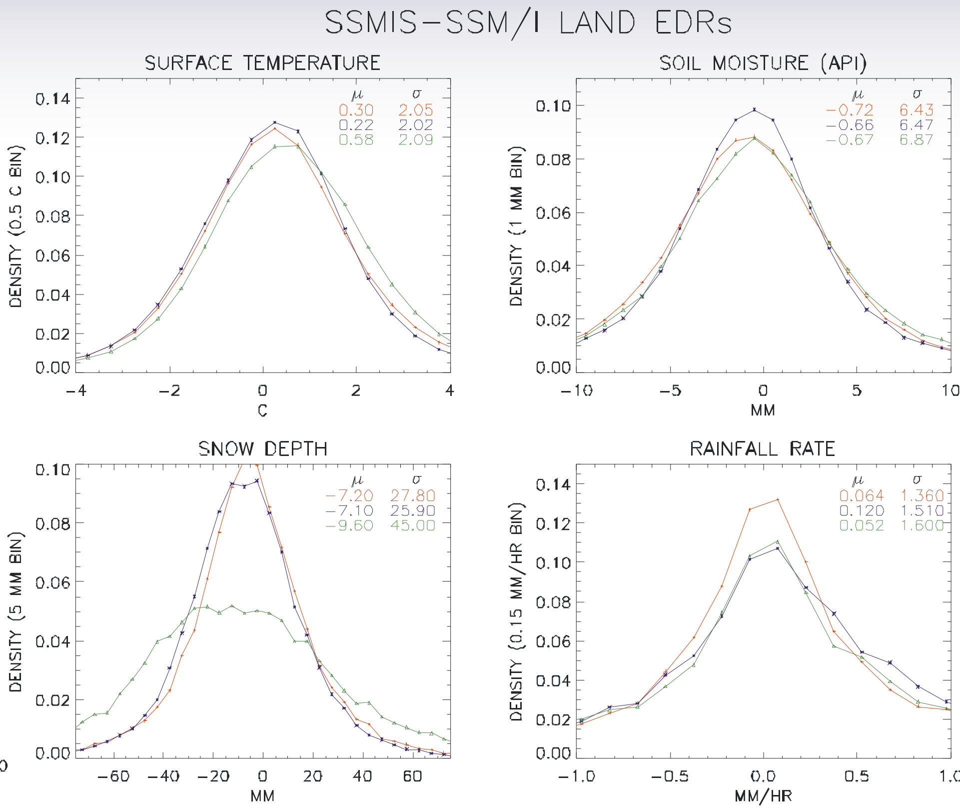

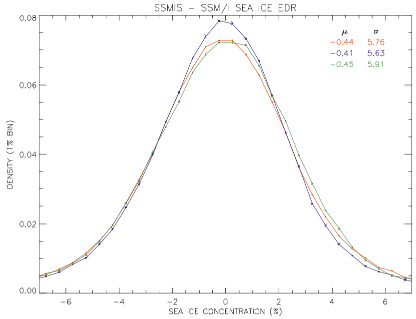

11/06/03
01/14/04
03/23/04

8.9 SSMIS – SSM/I Ocean Surface Wind Speed EDR (06 November 2003)

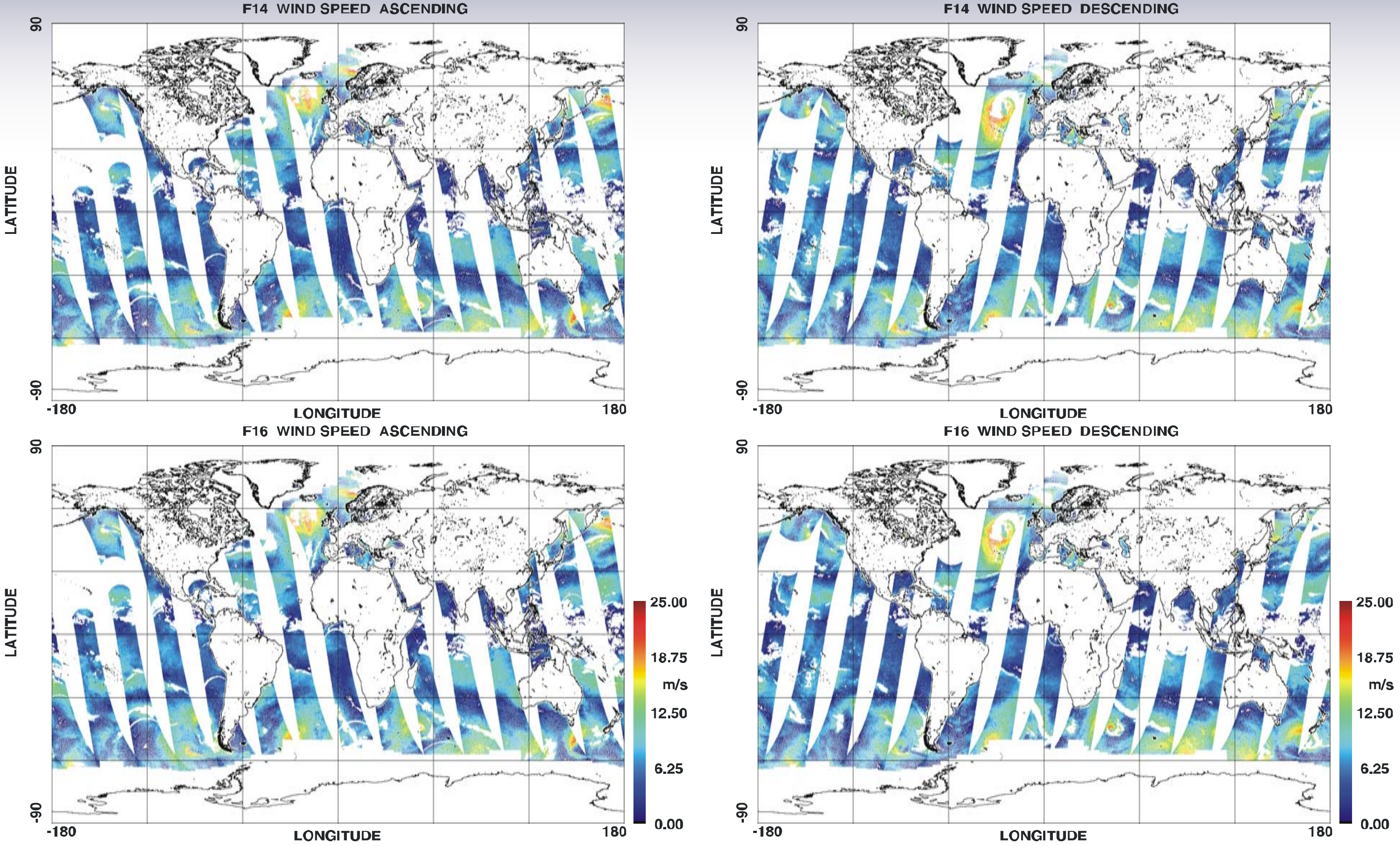

8.9 SSMIS – SSM/I Ocean Surface Wind Speed Difference (06 November 2003)

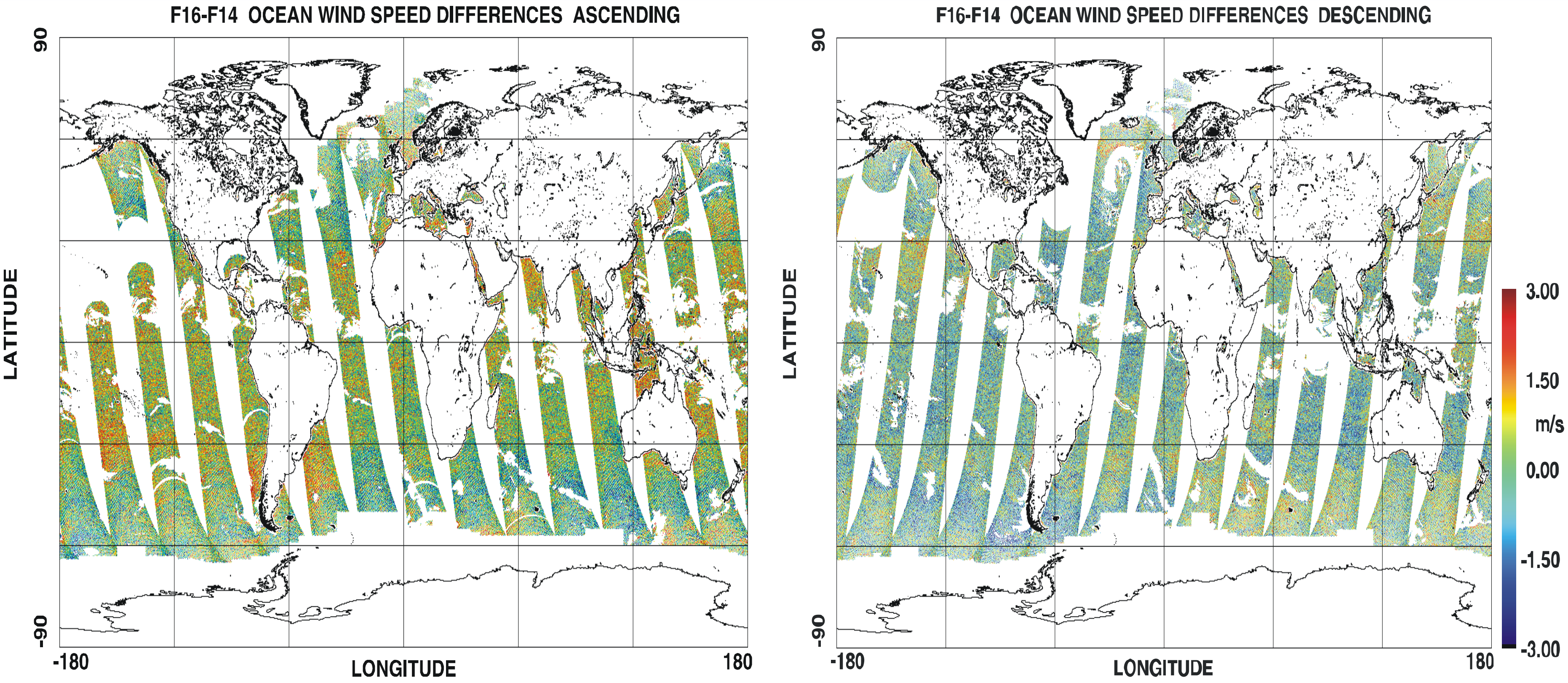
F16-F14 OCEAN WIND SPEED DIFFERENCES ASCENDING

F16-F14 OCEAN WIND SPEED DIFFERENCES DESCENDING

8.9 SSMIS – SSM/I Over Ocean Water Vapor EDR (06 November 2003)

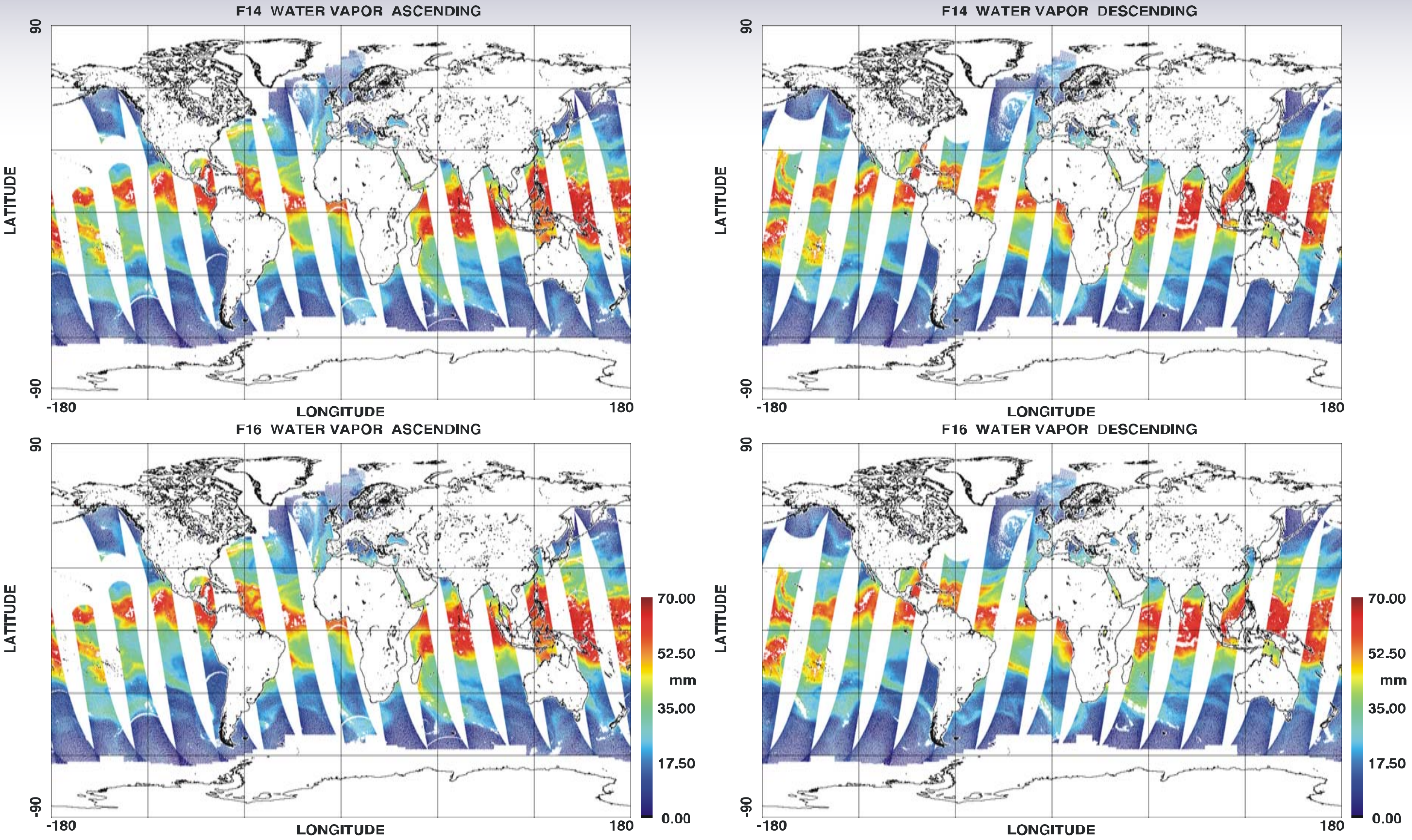

8.9 SSMIS – SSM/I Over Ocean Water Vapor Difference (06 November 2003)

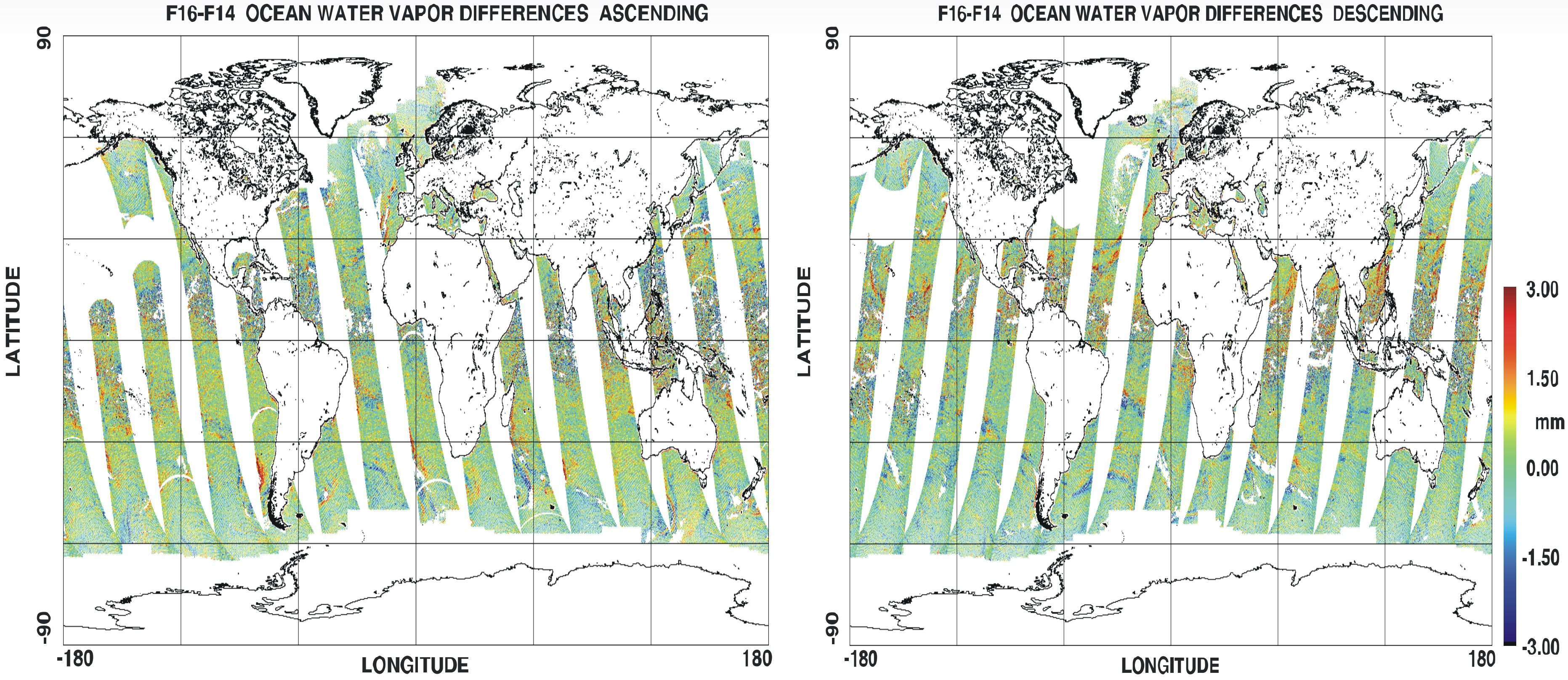
F16-F14 OCEAN WATER VAPOR DIFFERENCES ASCENDING

F16-F14 OCEAN WATER VAPOR DIFFERENCES DESCENDING

8.9 SSMIS – SSM/I Ocean Surface Wind Speed EDR (14 January 2004)

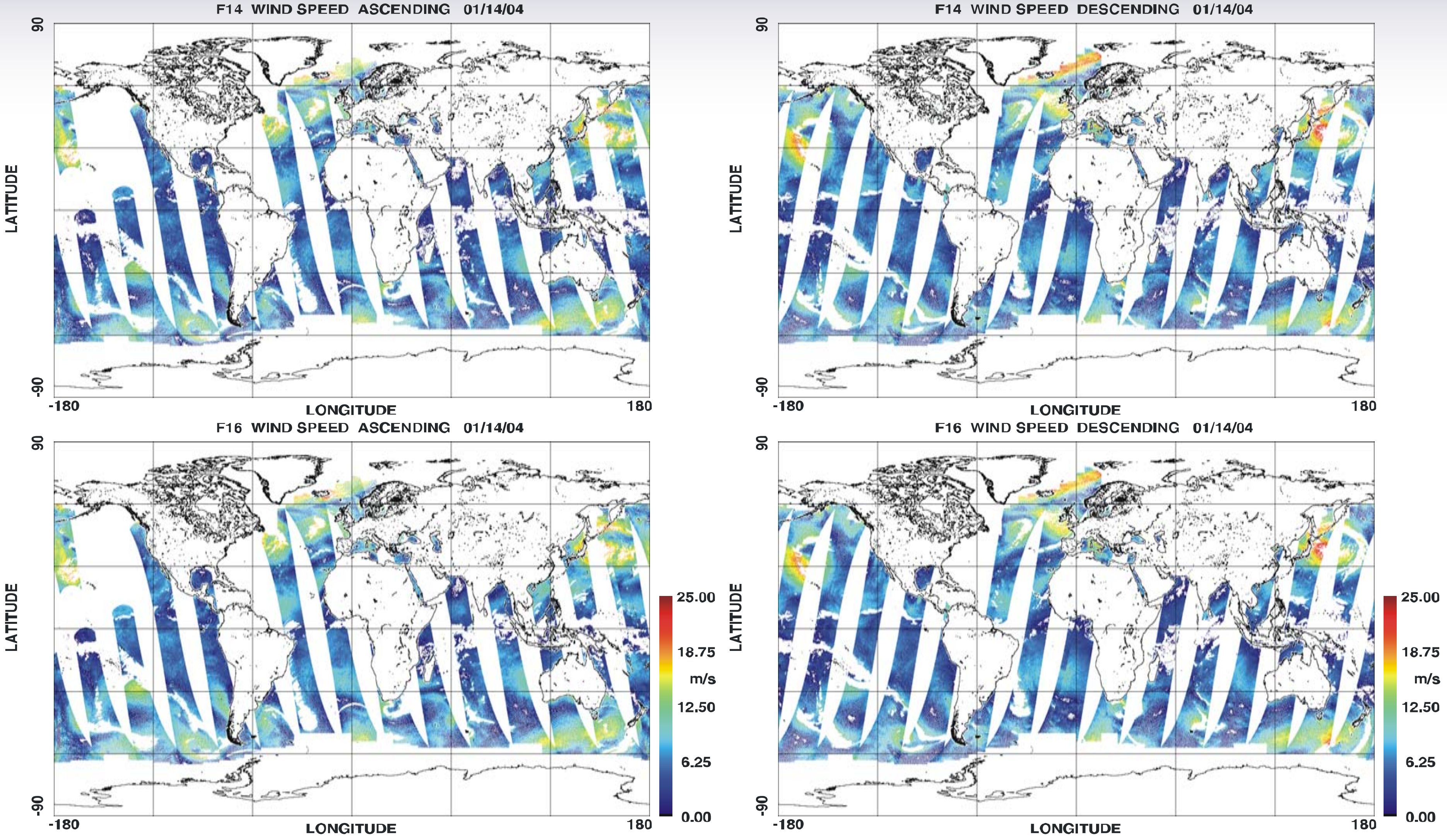

8.9 SSMIS – SSM/I Ocean Surface Wind Speed Difference (14 January 2004)

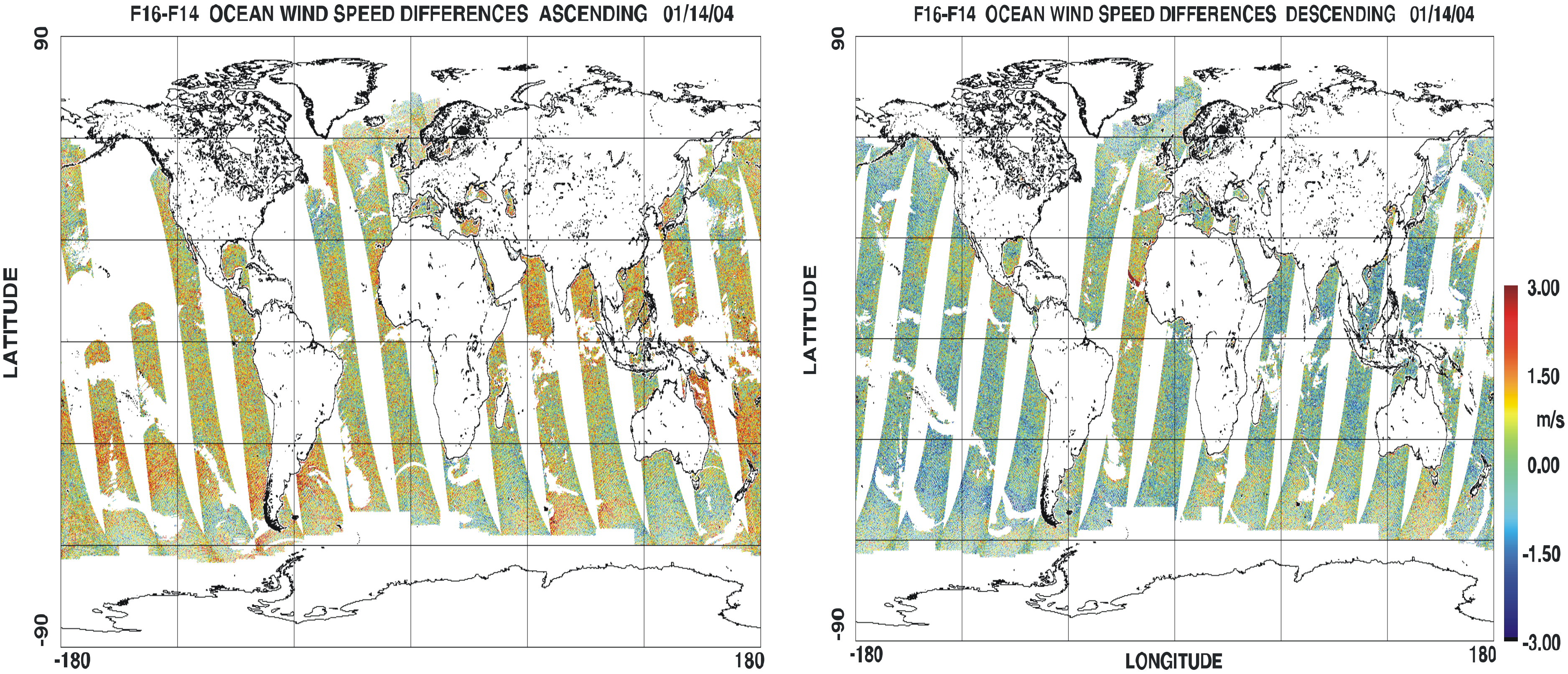

F16-F14 OCEAN WIND SPEED DIFFERENCES ASCENDING 01/14/04

F16-F14 OCEAN WIND SPEED DIFFERENCES DESCENDING 01/14/04

8.9 SSMIS – SSM/I Over Ocean Water Vapor EDR (14 January 2004)

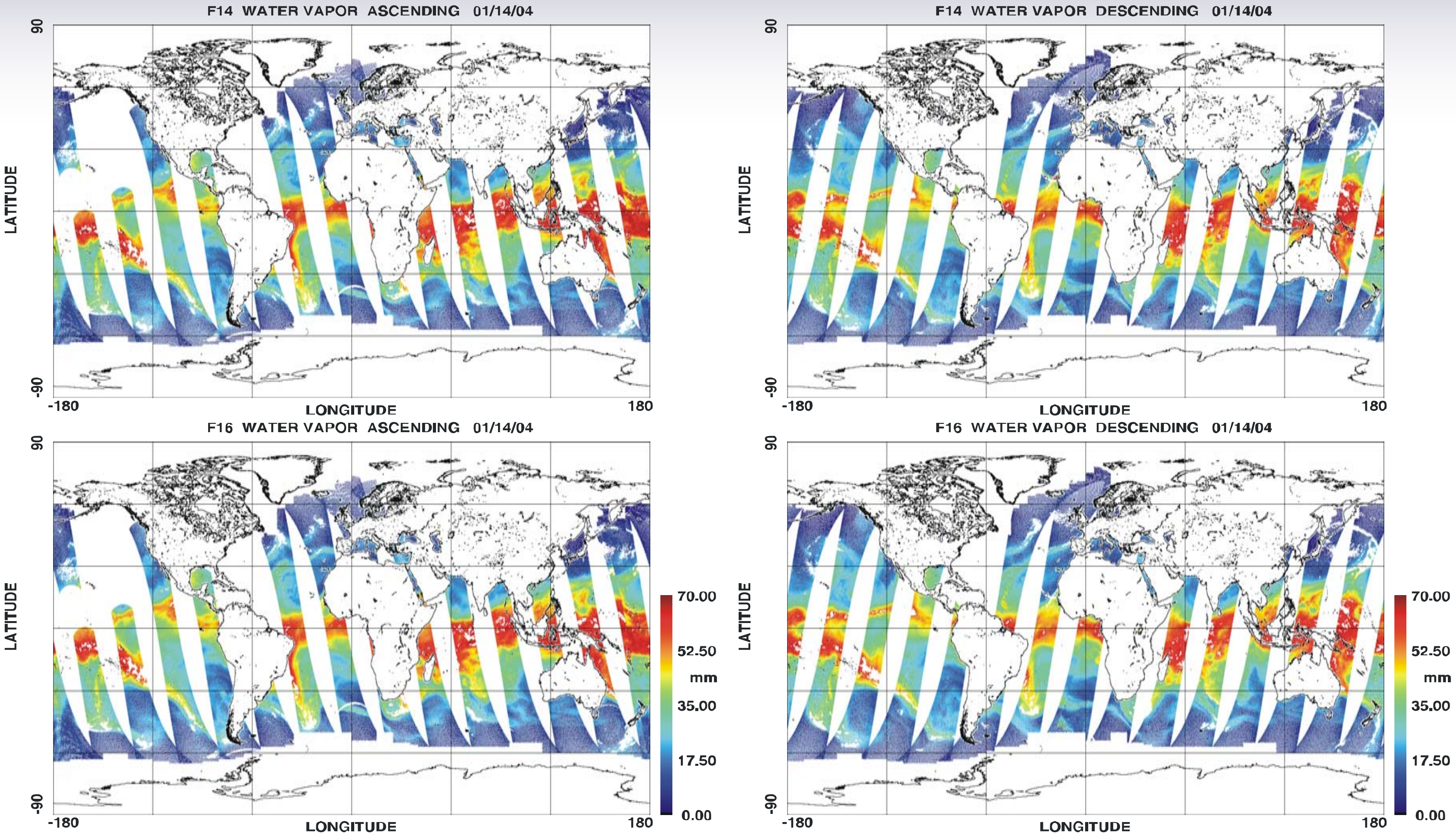

8.9 SSMIS – SSM/I Over Ocean Water Vapor Differences (14 January 2004)

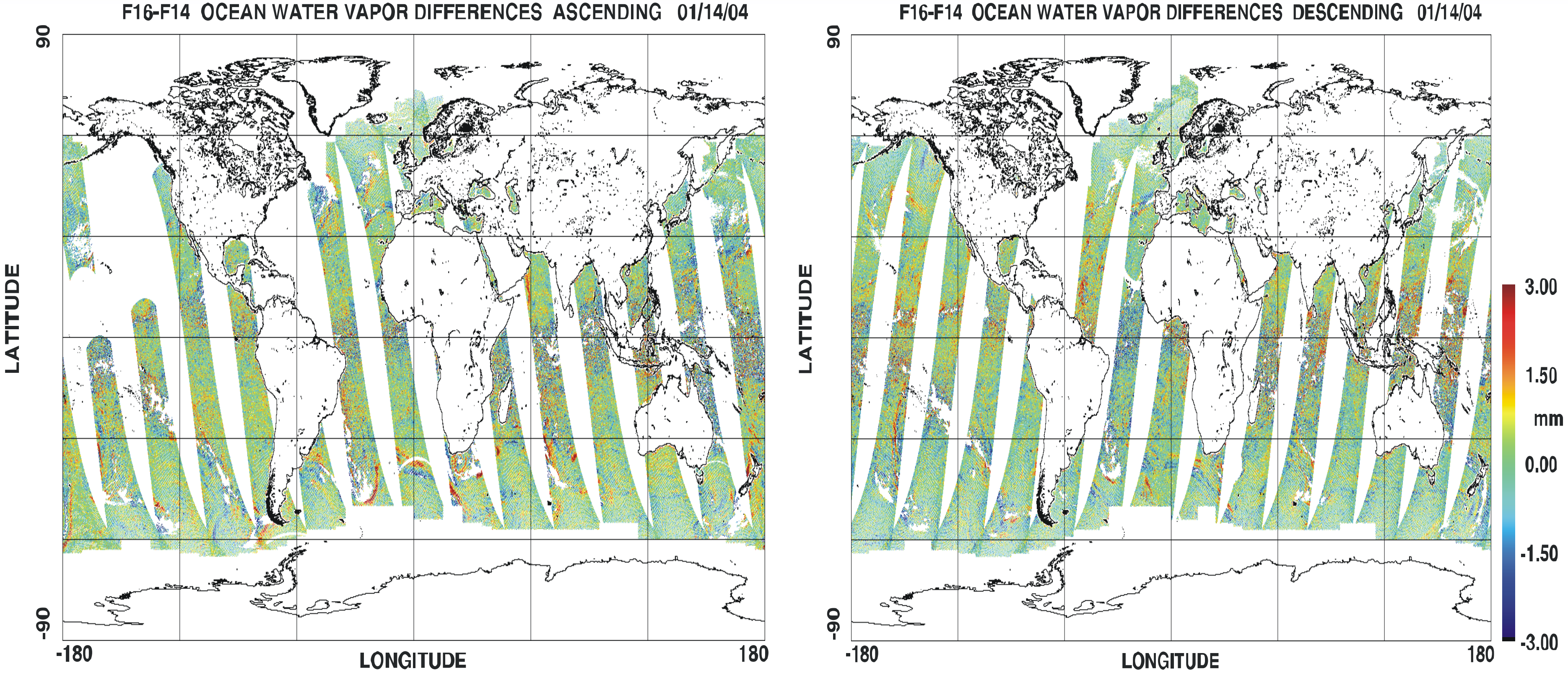

8.9 SSMIS – SSM/I Ocean Surface Wind Speed EDR (23 March 2004)

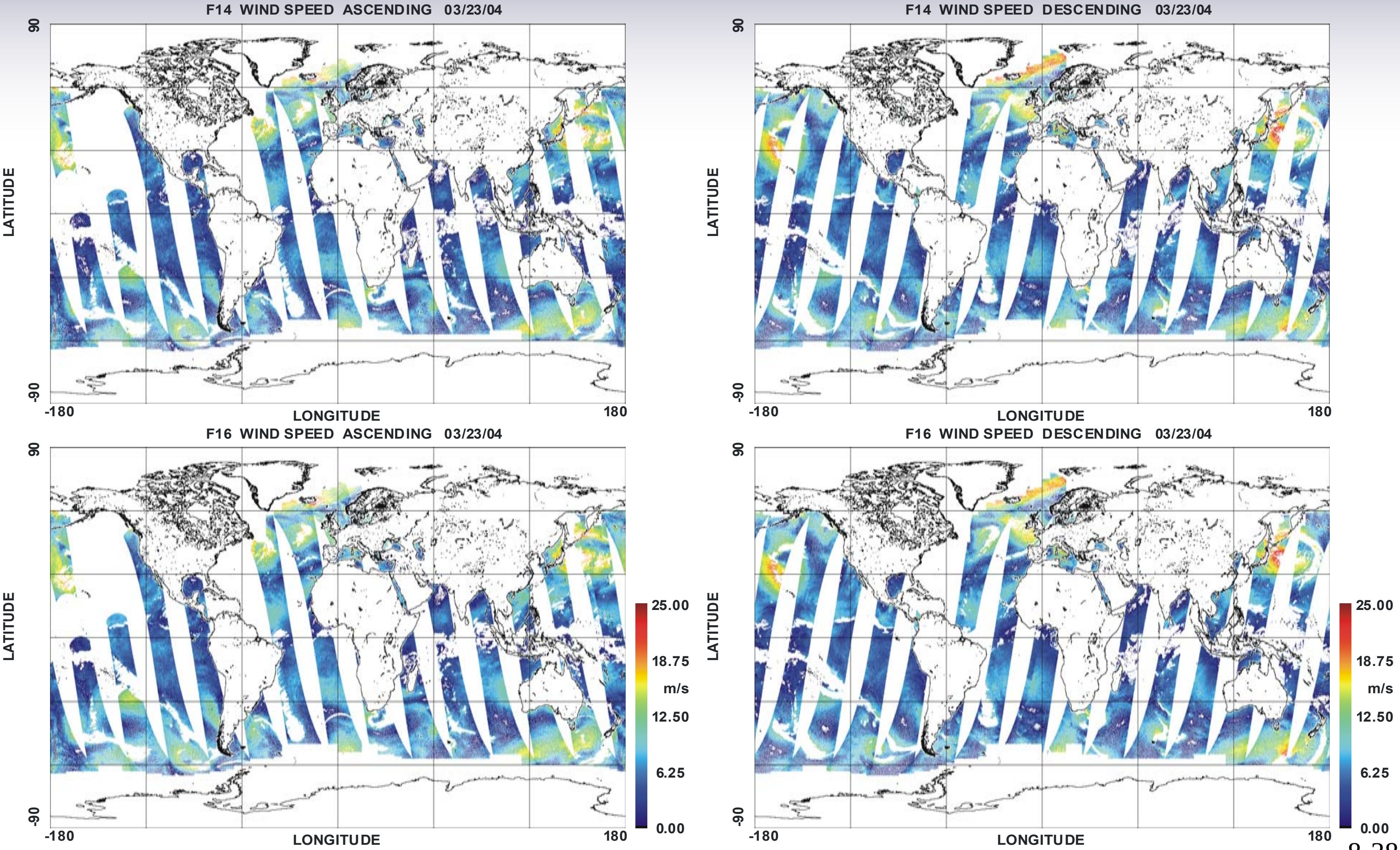
F14 WIND SPEED ASCENDING 03/23/04

F14 WIND SPEED DESCENDING 03/23/04

F16 WIND SPEED ASCENDING 03/23/04

F16 WIND SPEED DESCENDING 03/23/04

8.9 SSMIS – SSM/I Ocean Surface Wind Speed Differences (23 March 2004)

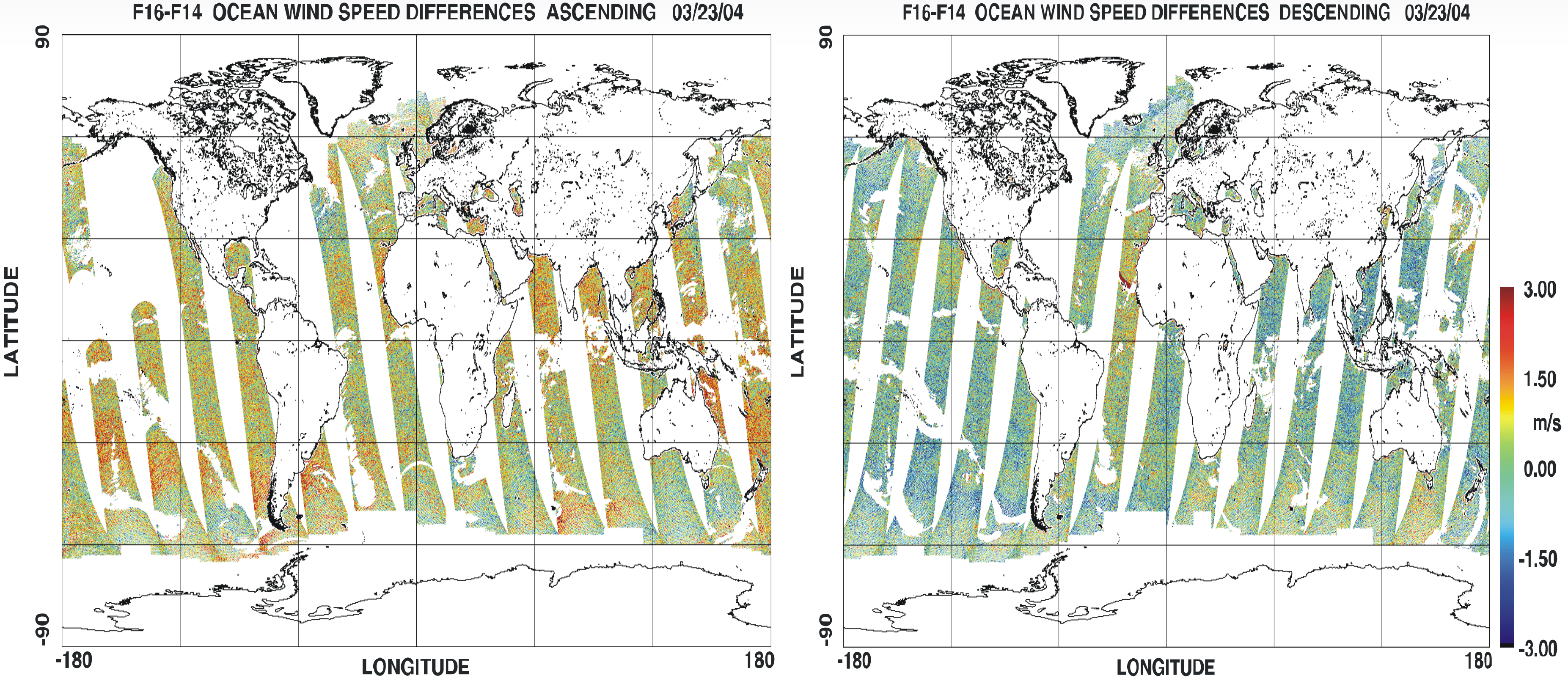

8.9 SSMIS – SSM/I Over Ocean Water Vapor EDR (23 March 2004)

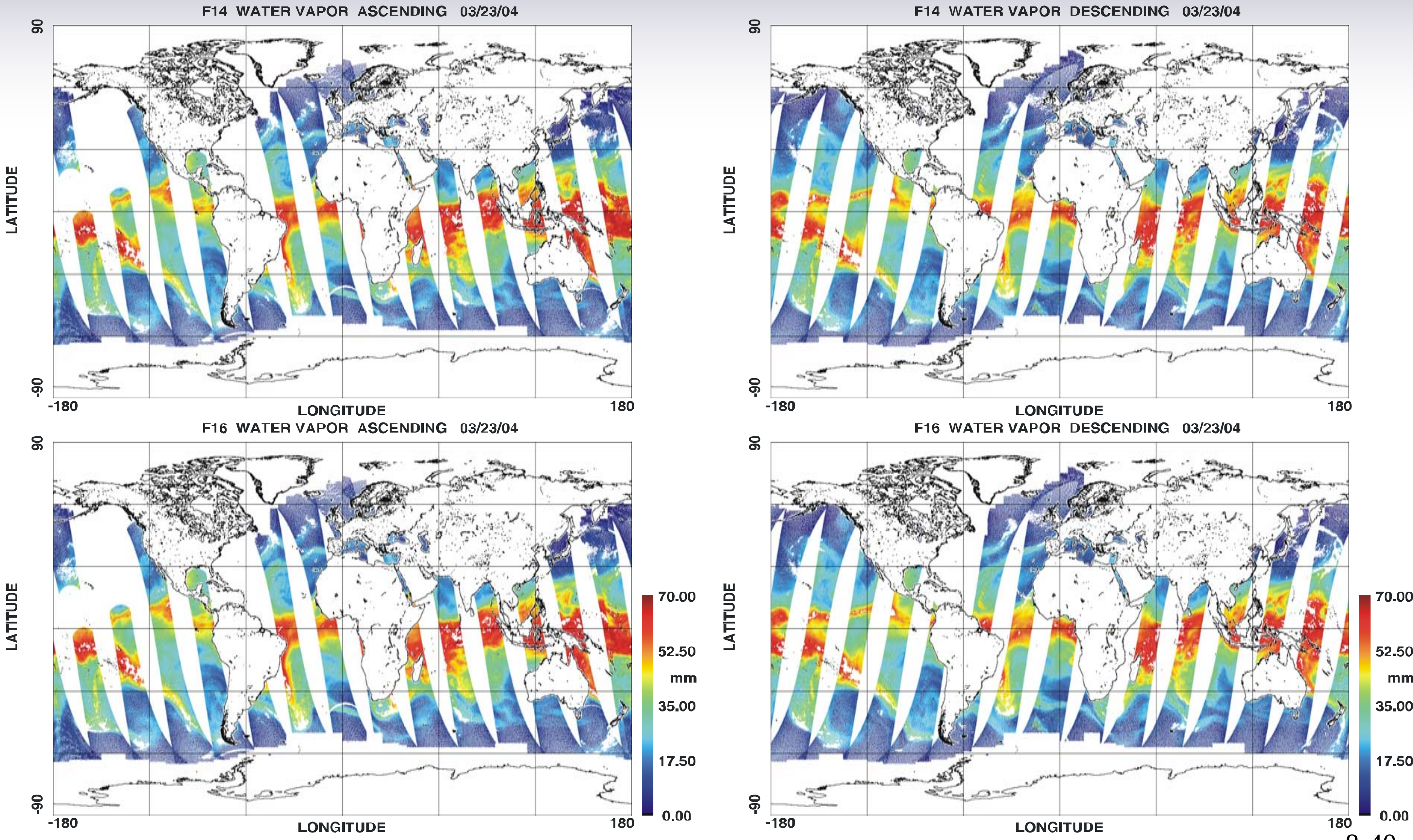

F14 WATER VAPOR ASCENDING 03/23/04

F14 WATER VAPOR DESCENDING 03/23/04

F16 WATER VAPOR ASCENDING 03/23/04

F16 WATER VAPOR DESCENDING 03/23/04

8.9 SSMIS – SSM/I Over Ocean Water Vapor Difference (23 March 2004)

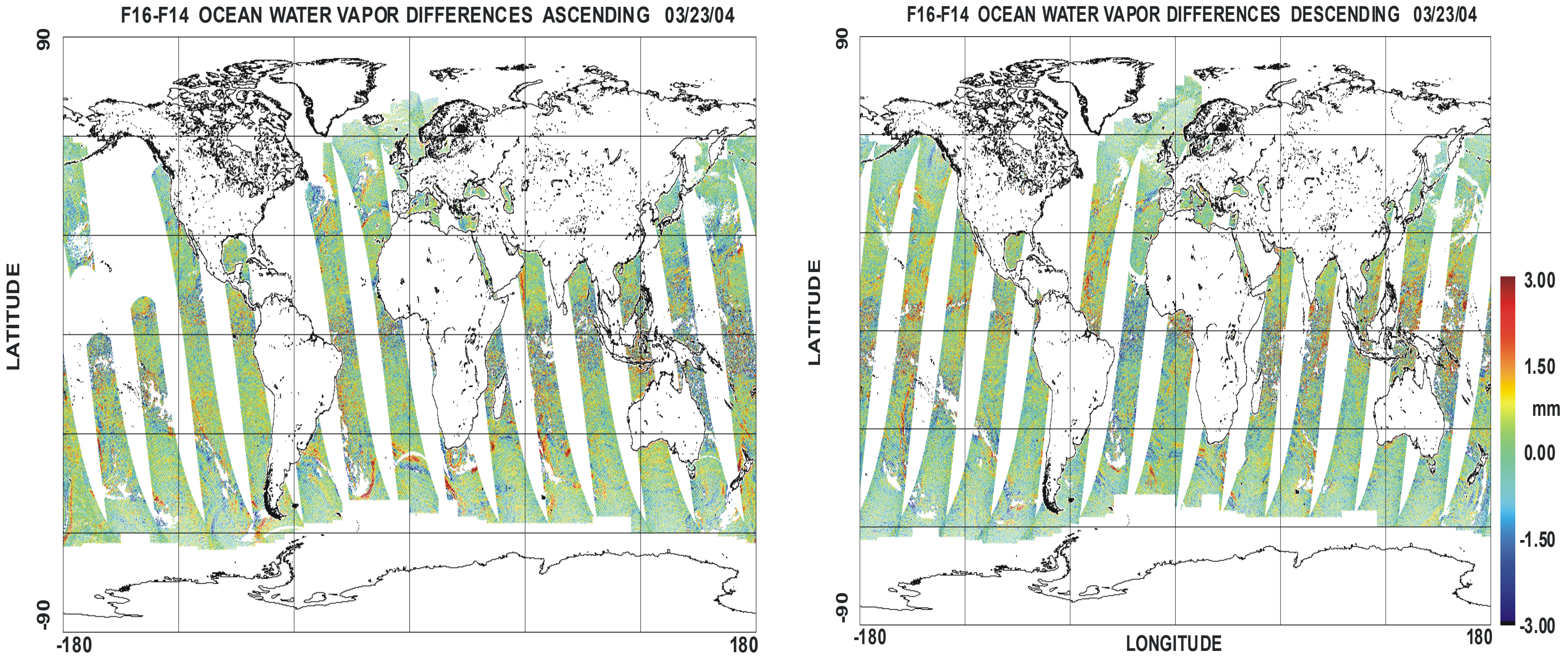

8.10 SSMIS-SSMI Land Surface Type EDR

(06 November 2003)

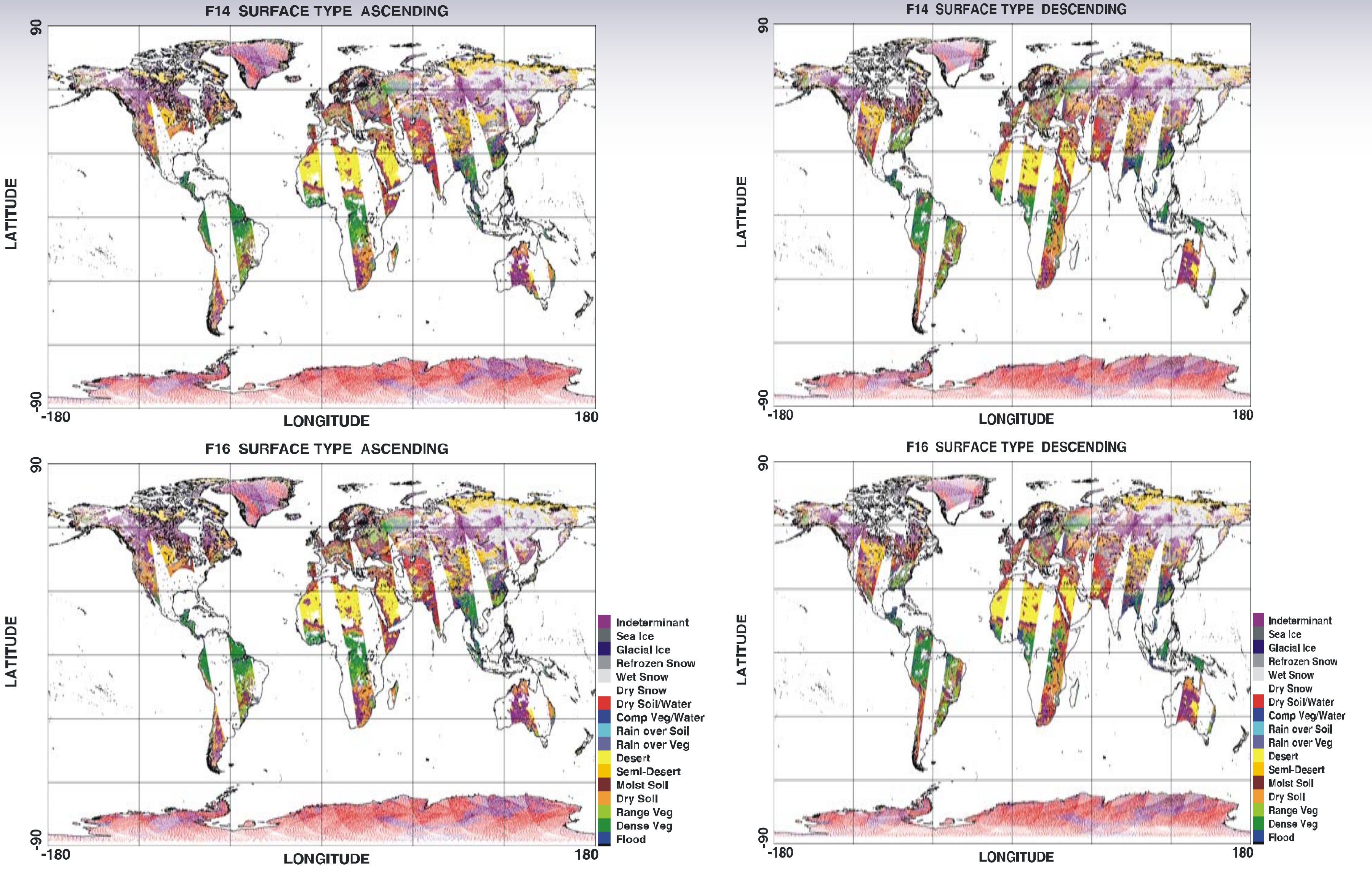

8.10 SSMIS – SSM/I Land Surface Temperatures (06 November 2003)

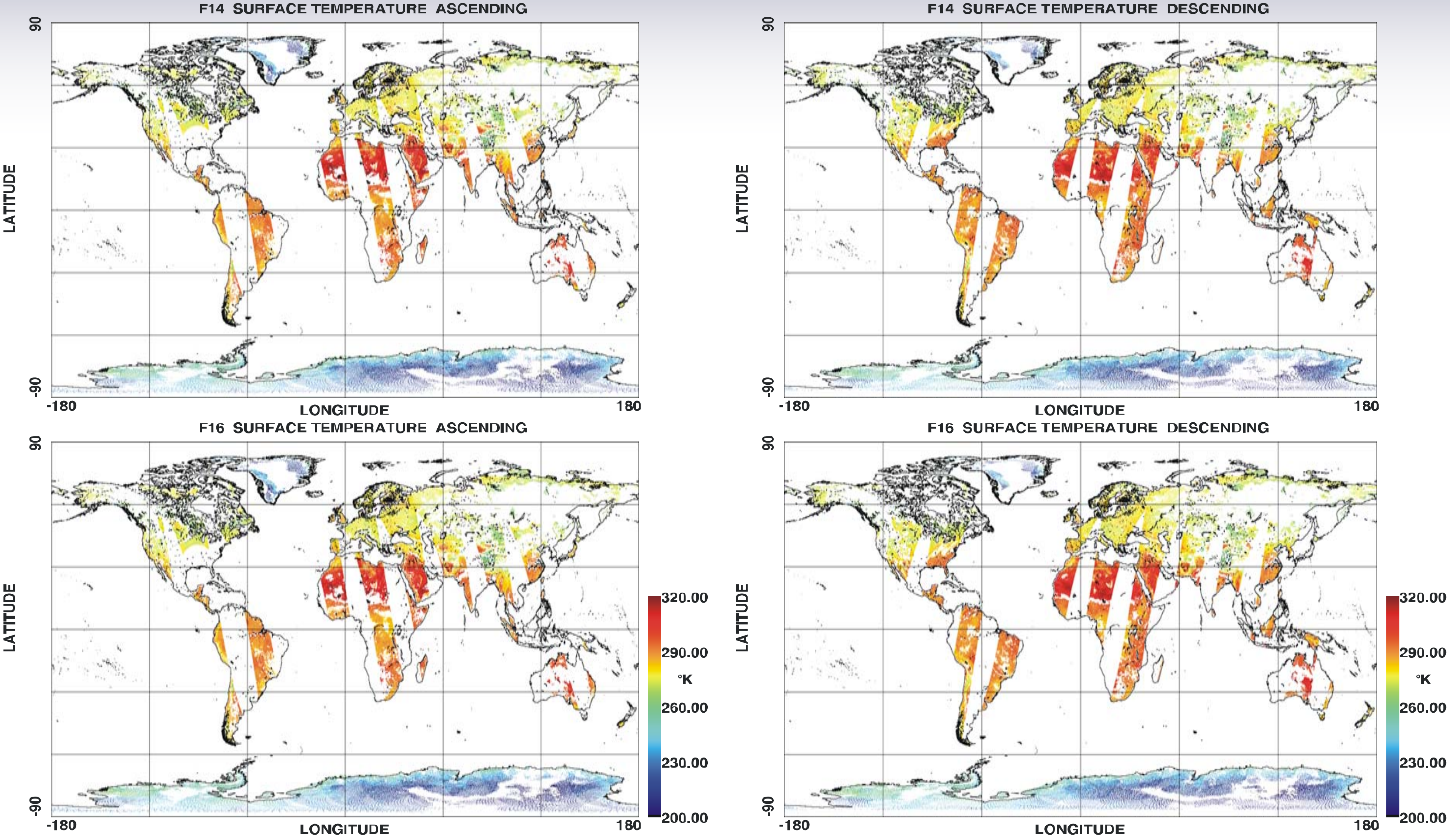

8.10 SSMIS – SSM/I Land Surface Temperature Difference (06 November 2003)

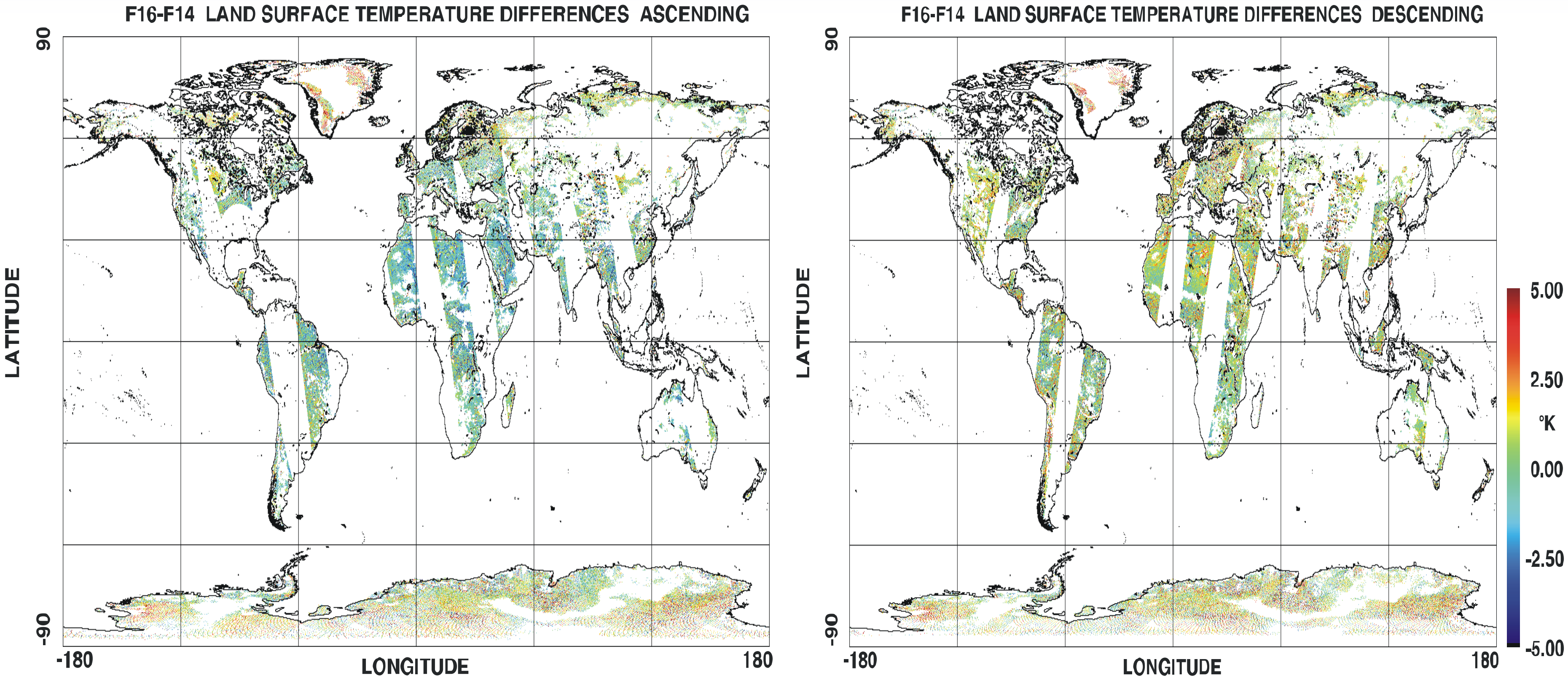

F16-F14 LAND SURFACE TEMPERATURE DIFFERENCES ASCENDING

F16-F14 LAND SURFACE TEMPERATURE DIFFERENCES DESCENDING

8.10 SSMIS – SSM/I Land Surface Temperatures

(14 January 2004)

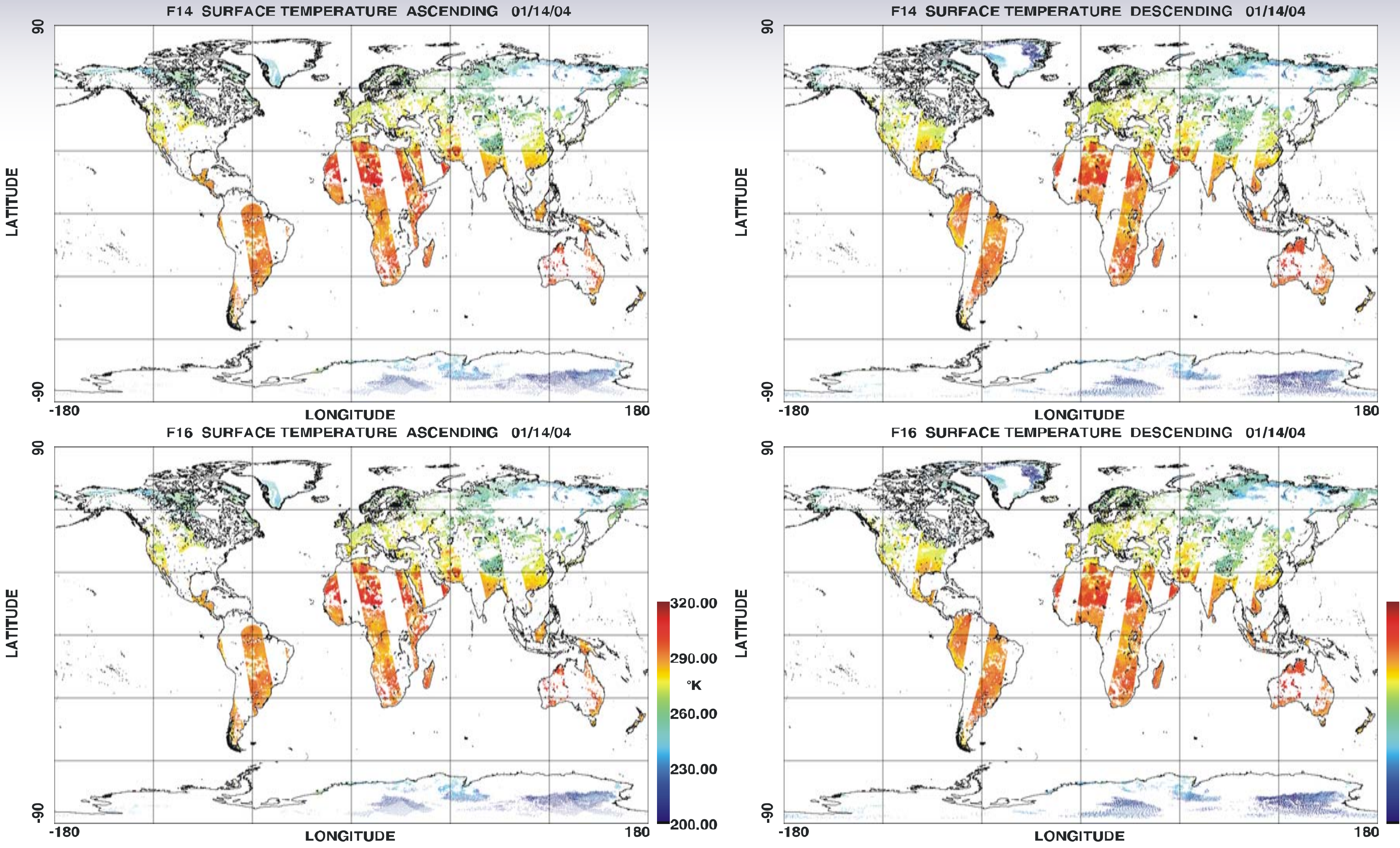

8.10 SSMIS – SSM/I Land Surface Temperature Difference (14 January 2004)

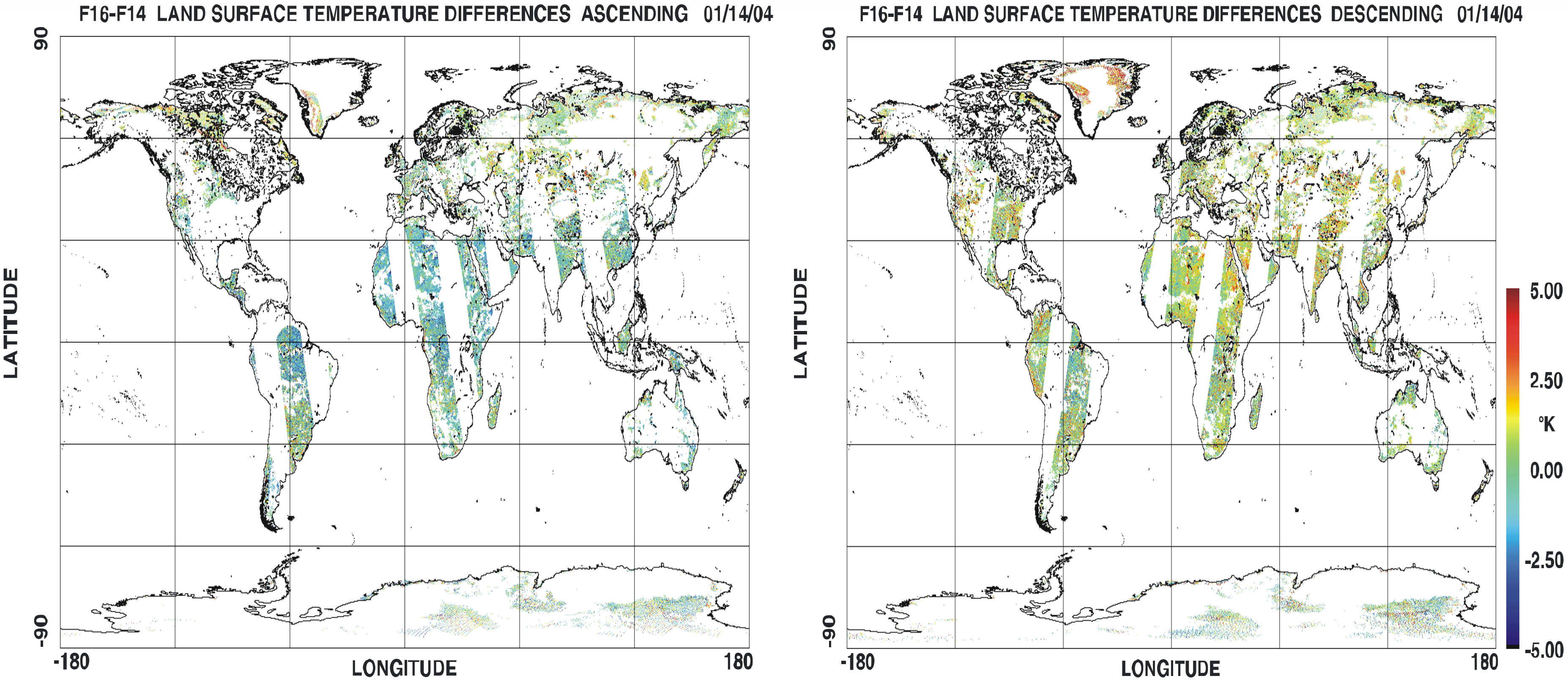

8.10 SSMIS - SSM/I Land EDR Statistics

SSMIS – SSM/I Land EDR's

Surface Temperature (C)

	Mean	Standard Deviation	N
11/06/2003	0.30	2.05	225992
01/14/2004	0.22	2.02	204651
03/23/2004	0.58	2.09	184540

Soil Moisture (API) (mm)

	Mean	Standard Deviation	N
11/06/2003	-0.72	6.44	101574
01/14/2004	-0.66	6.47	50585
03/23/2004	-0.67	6.87	51066

Snow Depth (mm)

	Mean	Standard Deviation	N
11/06/2003	-5.52	27.84	26231
01/14/2004	-7.06	25.90	28090
03/23/2004	-9.60	45.03	21077

Rainfall Rate (mm / Hr)

	Mean	Standard Deviation	N
11/06/2003	0.064	1.37	8474
01/14/2004	0.12	1.51	7071
03/23/2004	0.052	1.60	6421

Land Surface Type EDR (11/06/03)
SSM/I (%)

		1	2	3	4	5	6	7	8	9	10	11	12	13	14	15	16
	1	2.0										0.7					
	2		4.0	0.9													
	3		0.6	3.8													
	4				6.4	0.8											0.9
SSMIS (%)	5				0.7	2.2						0.6					
	6						5.7										
	7							8.4									
	8								1.3								
	9																
	10										1.3						
	11											24.					
	12												5.9				1.5
	13													1.9			0.9
	14																
	15																
	16											1.9	1.0	0.6			21.6

8.11 SSMIS - SSM/I Sea Ice Concentration

(Northern Hemisphere 06 November 2003)

F14 FIRST YEAR ICE CONCENTRATION

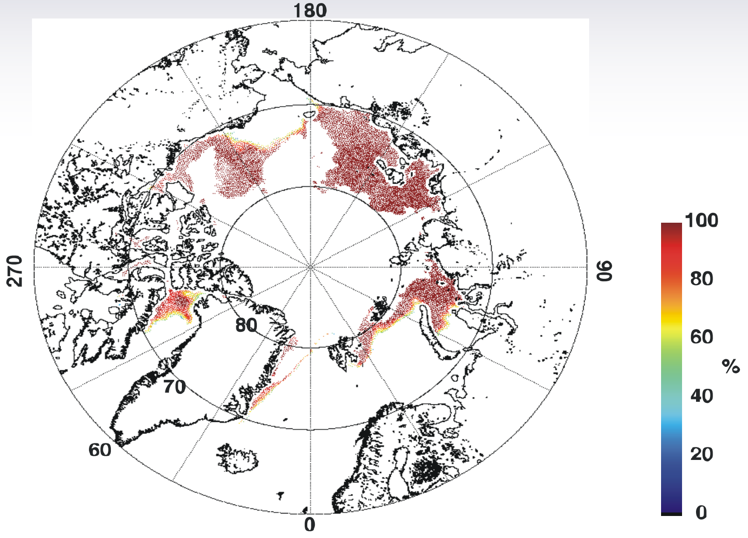

F14 MULTI YEAR ICE CONCENTRATION

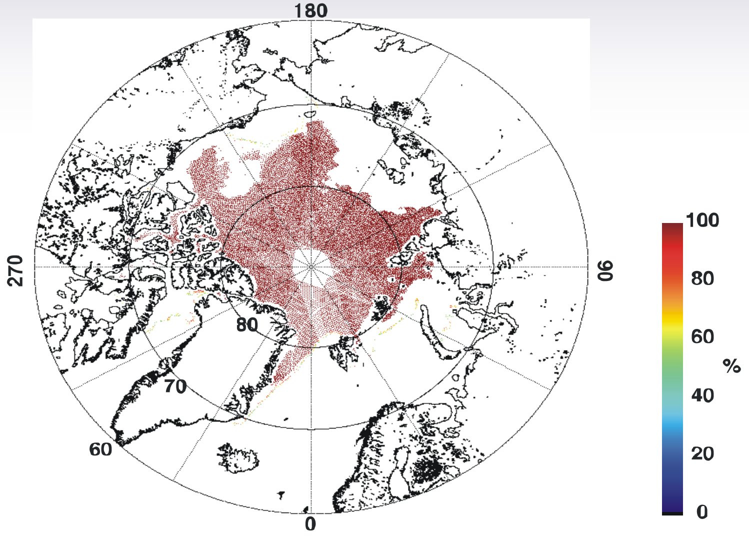

F16 FIRST YEAR ICE CONCENTRATION

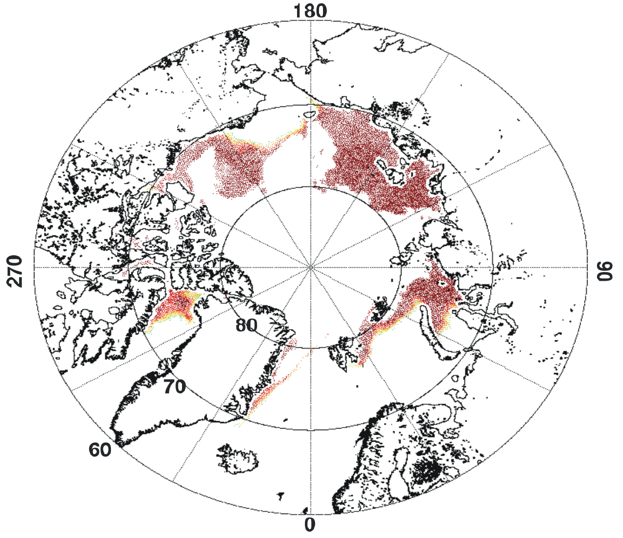

F16 MULTI YEAR ICE CONCENTRATION

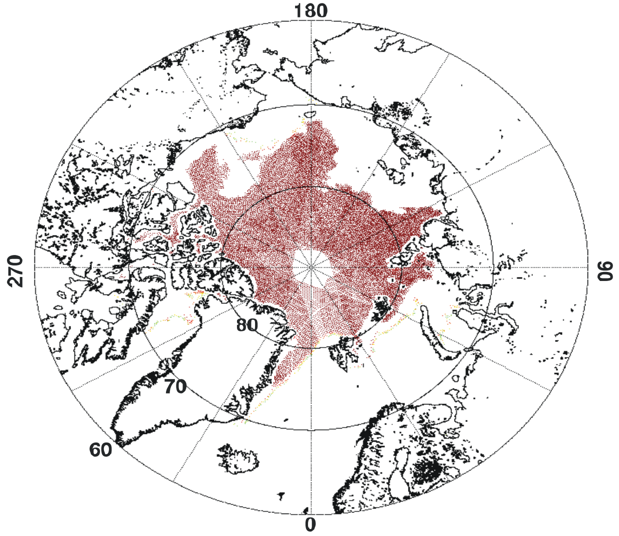

8.11 SSMIS - SSM/I Sea Ice Concentration

(Southern Hemisphere 06 November 2003)

F14 FIRST YEAR ICE CONCENTRATION

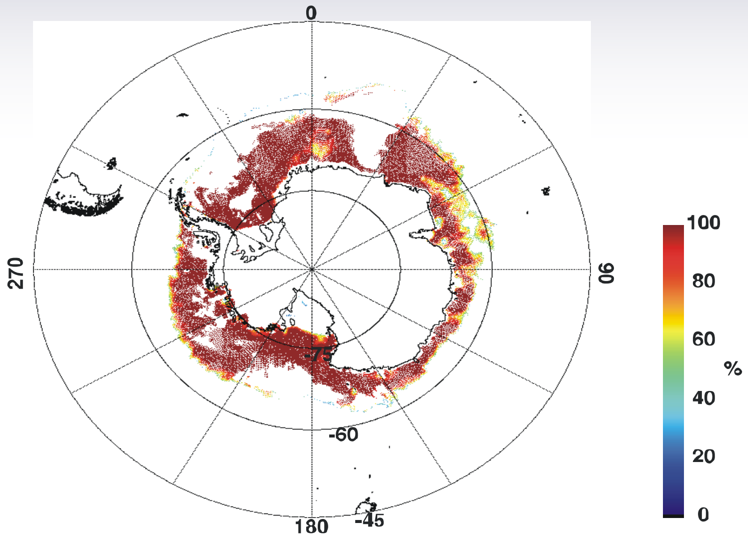

F14 MULTI YEAR ICE CONCENTRATION

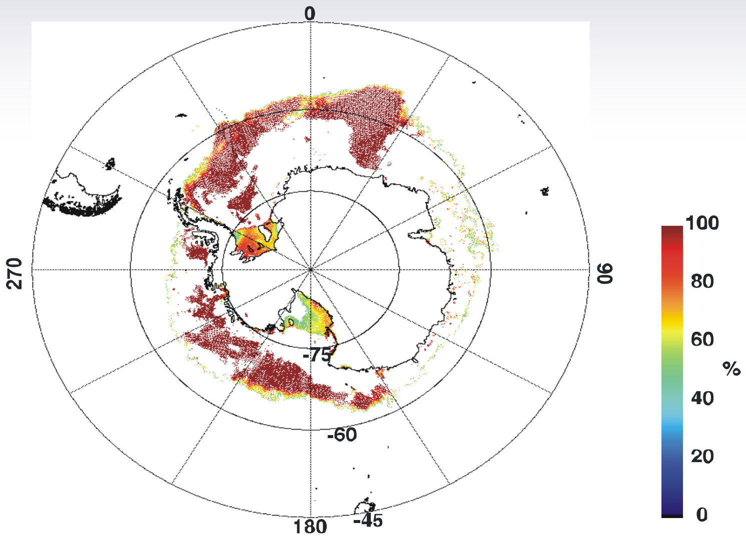

F16 FIRST YEAR ICE CONCENTRATION

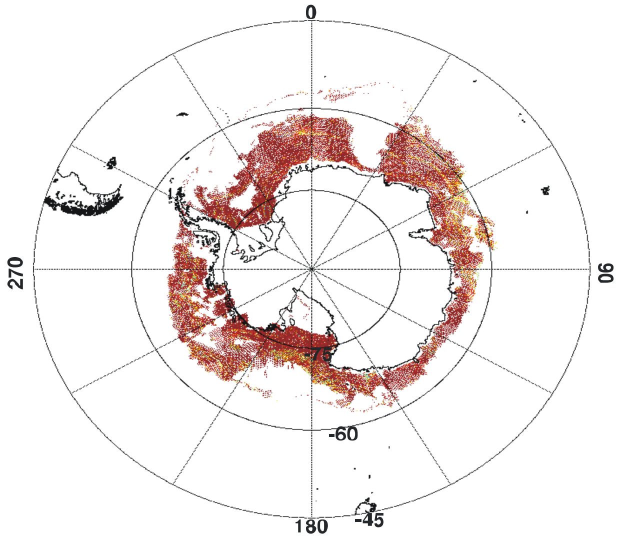

F16 MULTI YEAR ICE CONCENTRATION

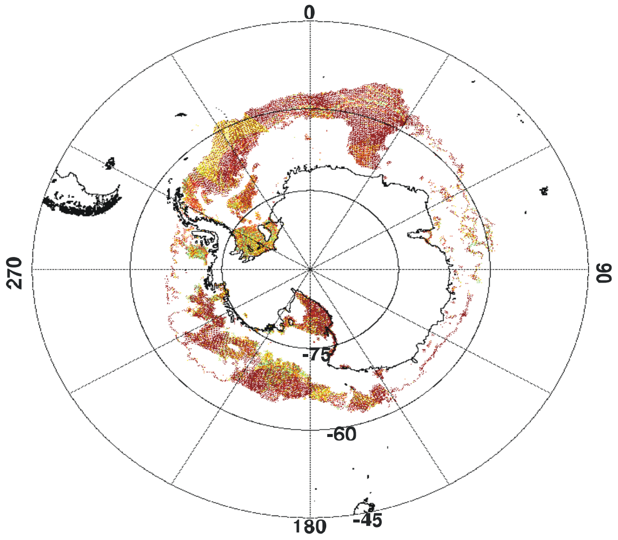

8.11 SSMIS - SSM/I Sea Ice Concentration Difference (06 November 03)

F16-F14 FIRST YEAR ICE CONCENTRATION

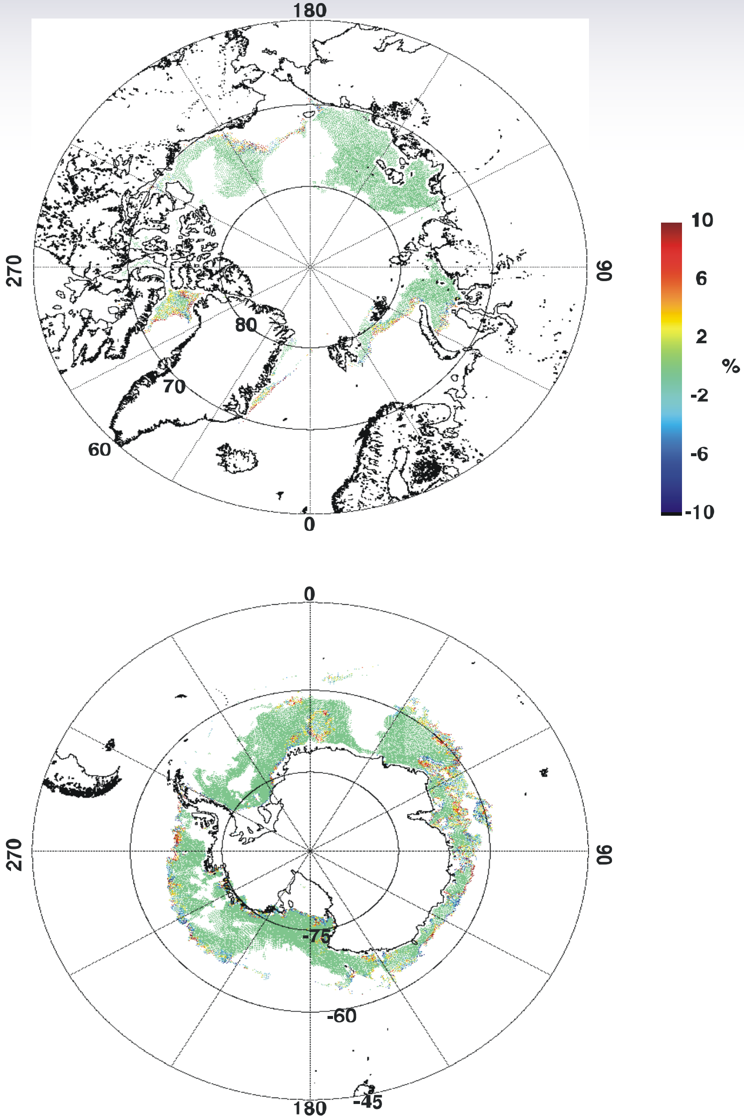

F16-F14 MULTI YEAR ICE CONCENTRATION

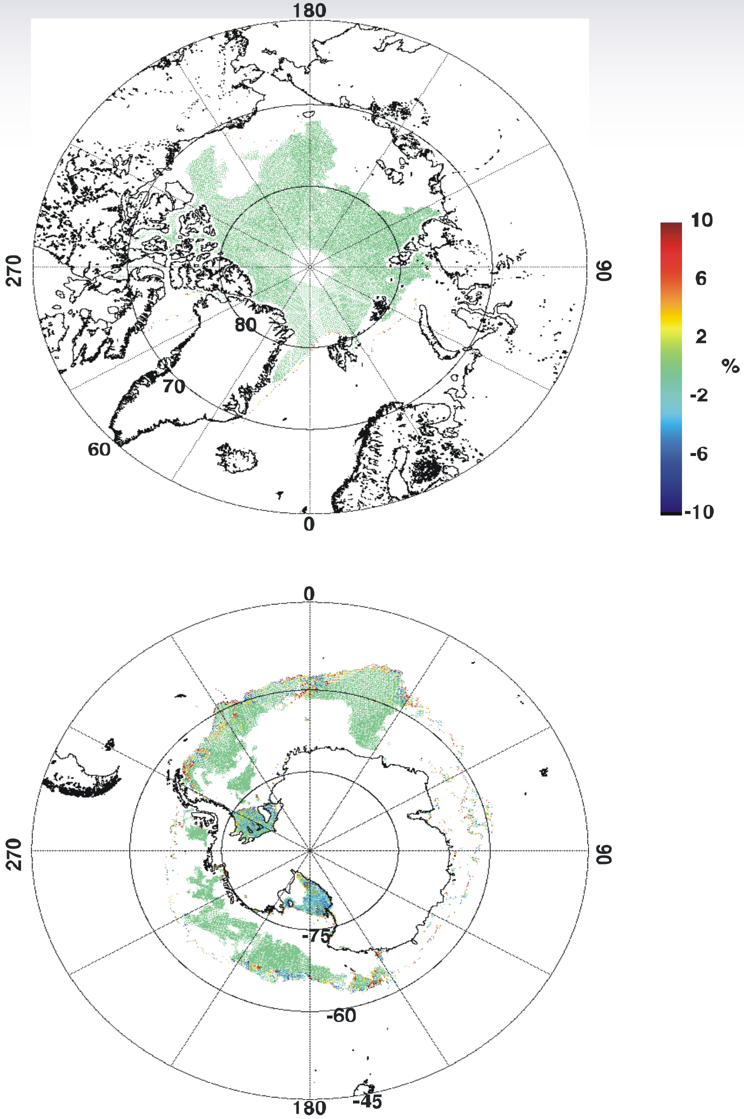

8.11 SSMIS – F-14 SSM/I Ice Edge EDR

(6 November 2003)

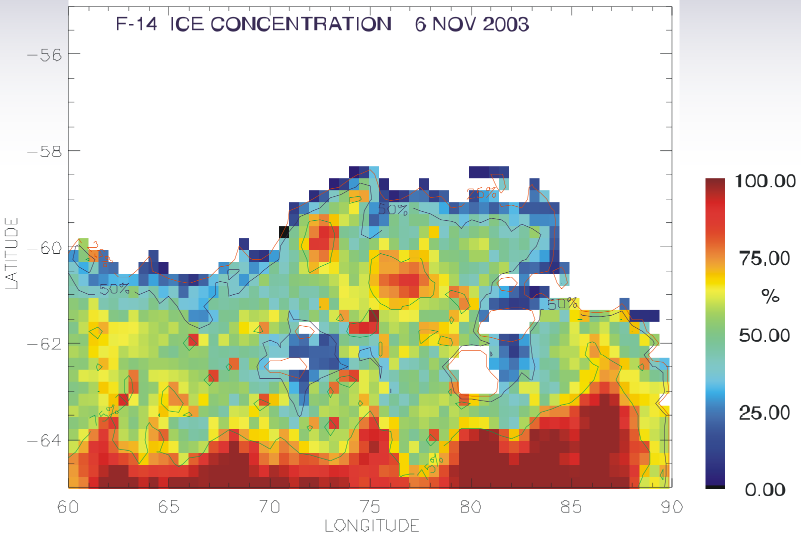

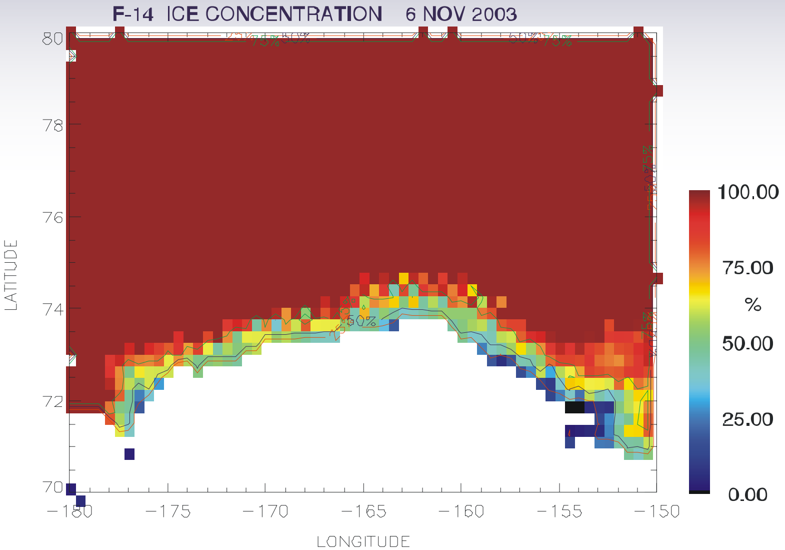

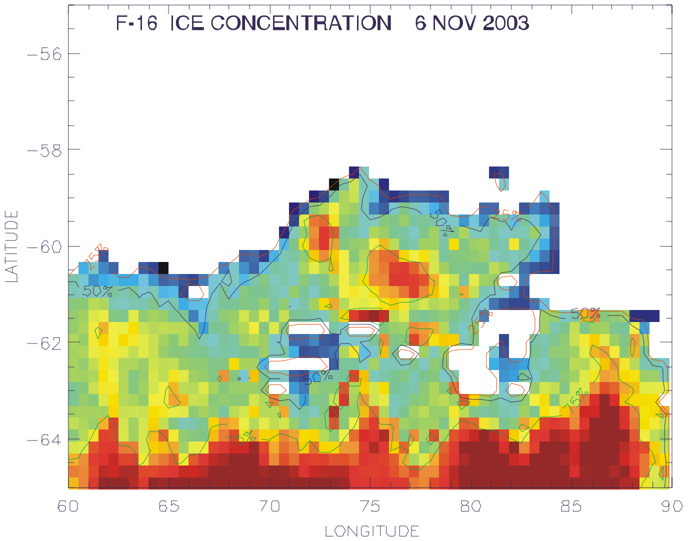

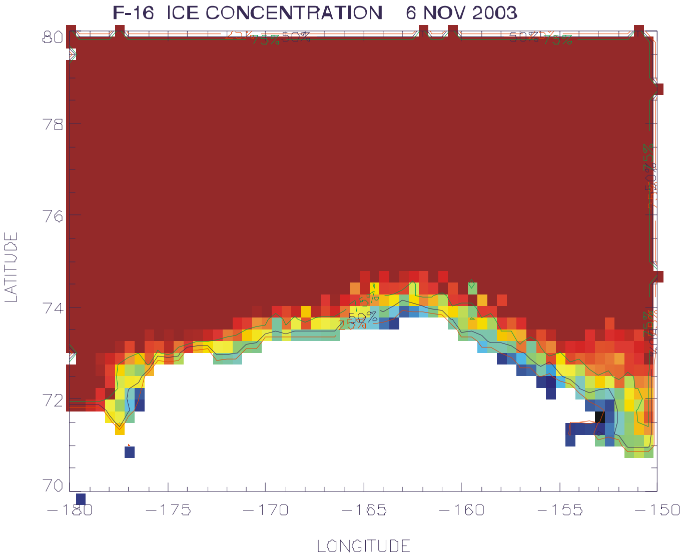

8.12 SSMIS – F-15 SSM/I Coincidence

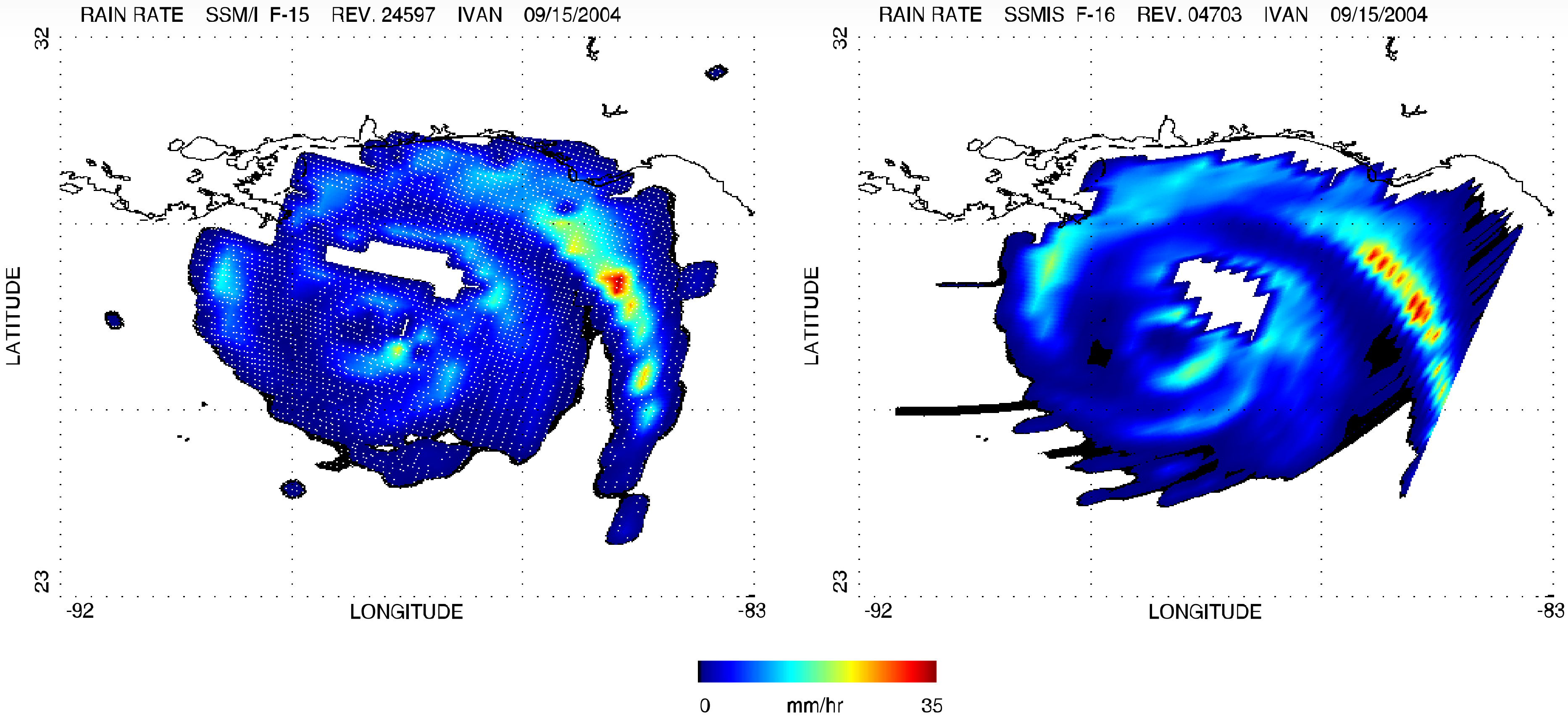

8.13 Hurricane Ivan SSMIS - SSM/I
15 September 2004

SSMIS Ch. 18 (R04703)

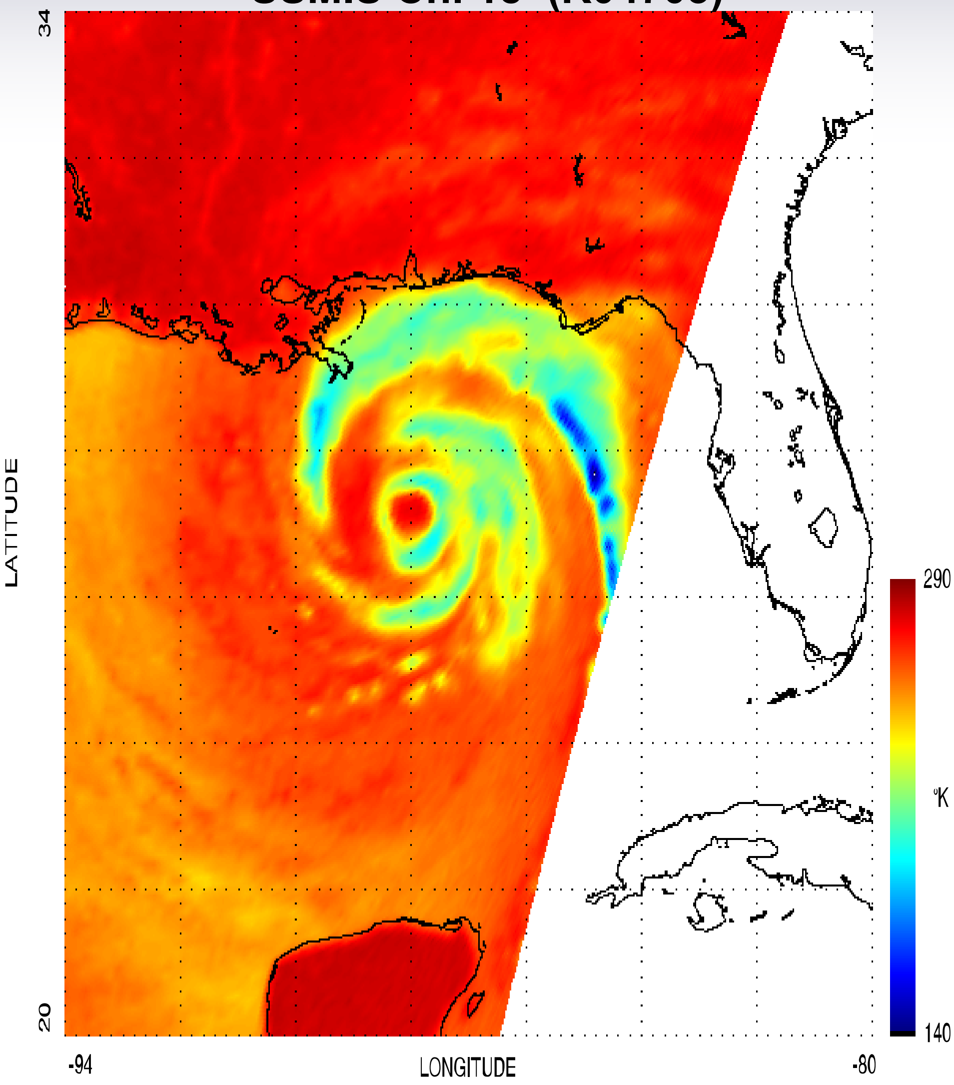

SSM/I 85H (R24597)

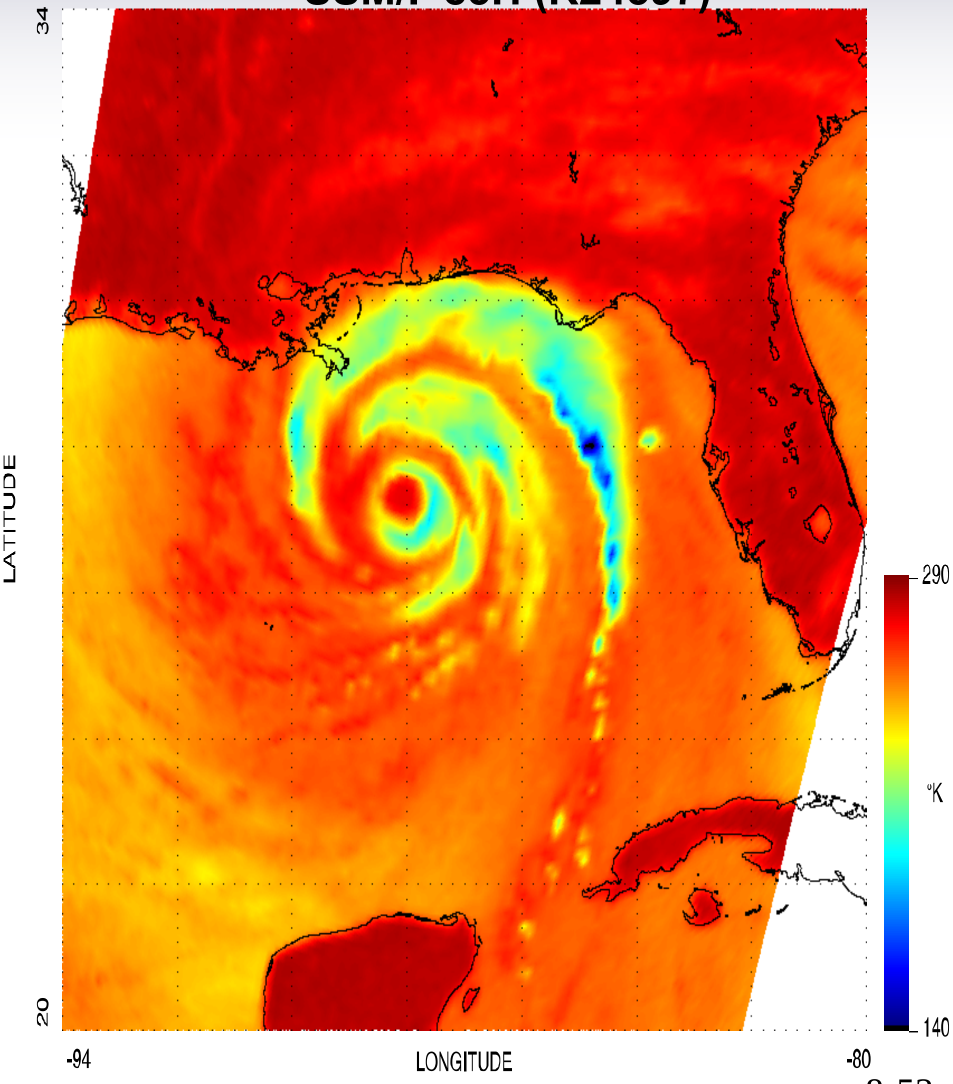

8.13 Hurricane Ivan SSMIS Chs. 8-11 Imagery
15 September 2004

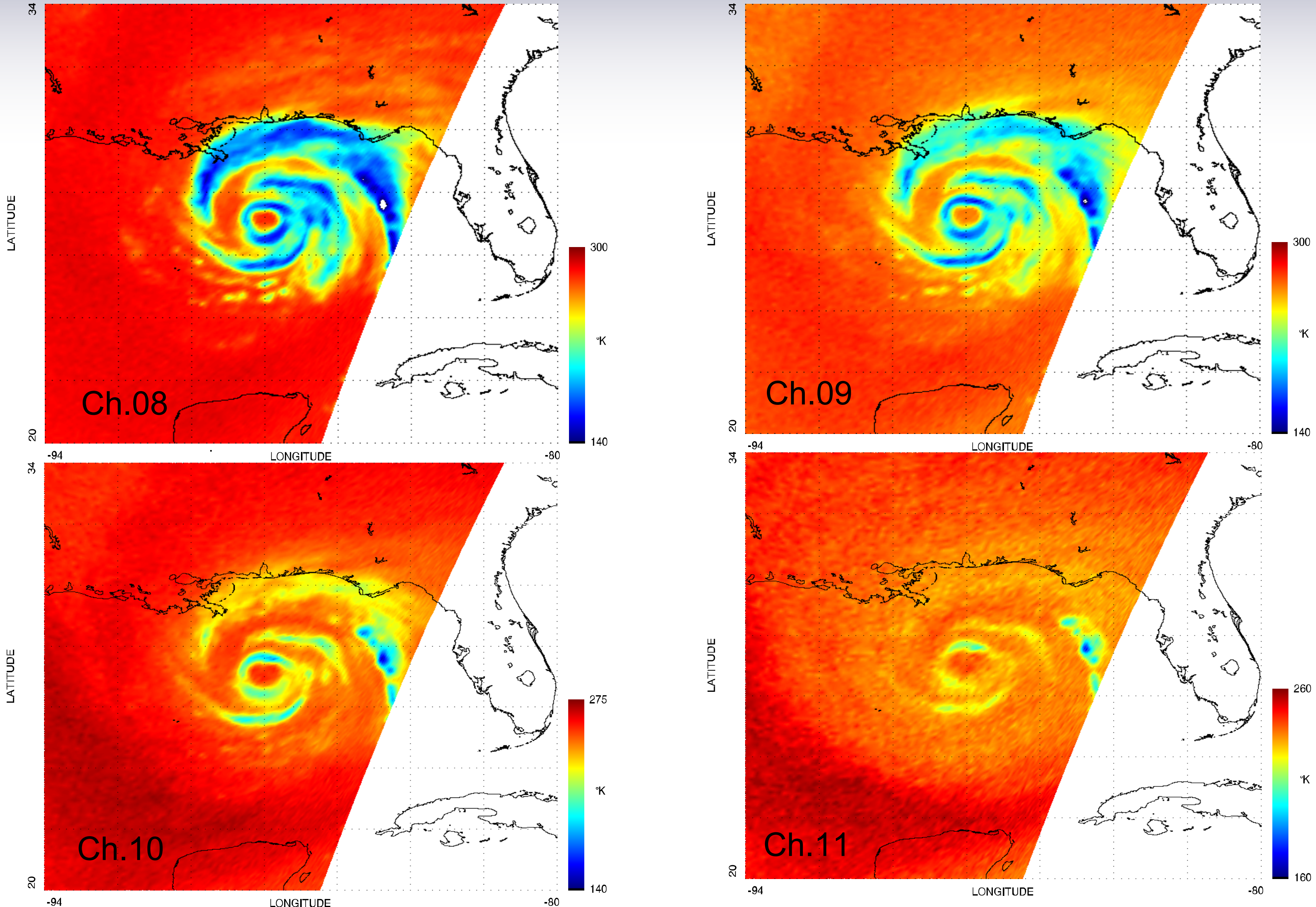

8.13 Dennis (the Menace) 7 July 2005
F-13,F-14,F-15 SSM/I (85H) F-16 SSMIS (91H)

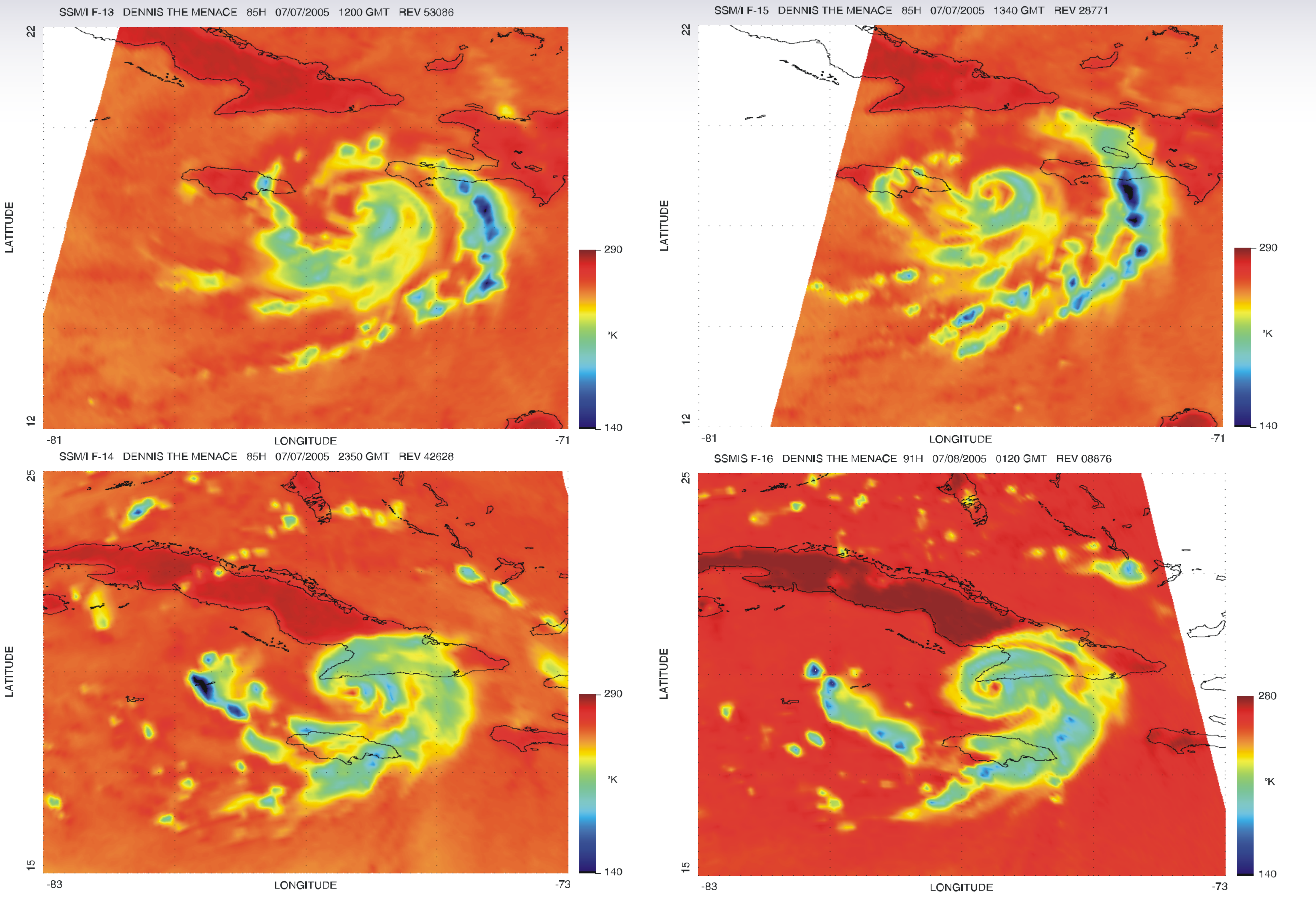

8.13 Dennis (the Menace) 7 July 2005
SSMIS (Chs. 8-11)

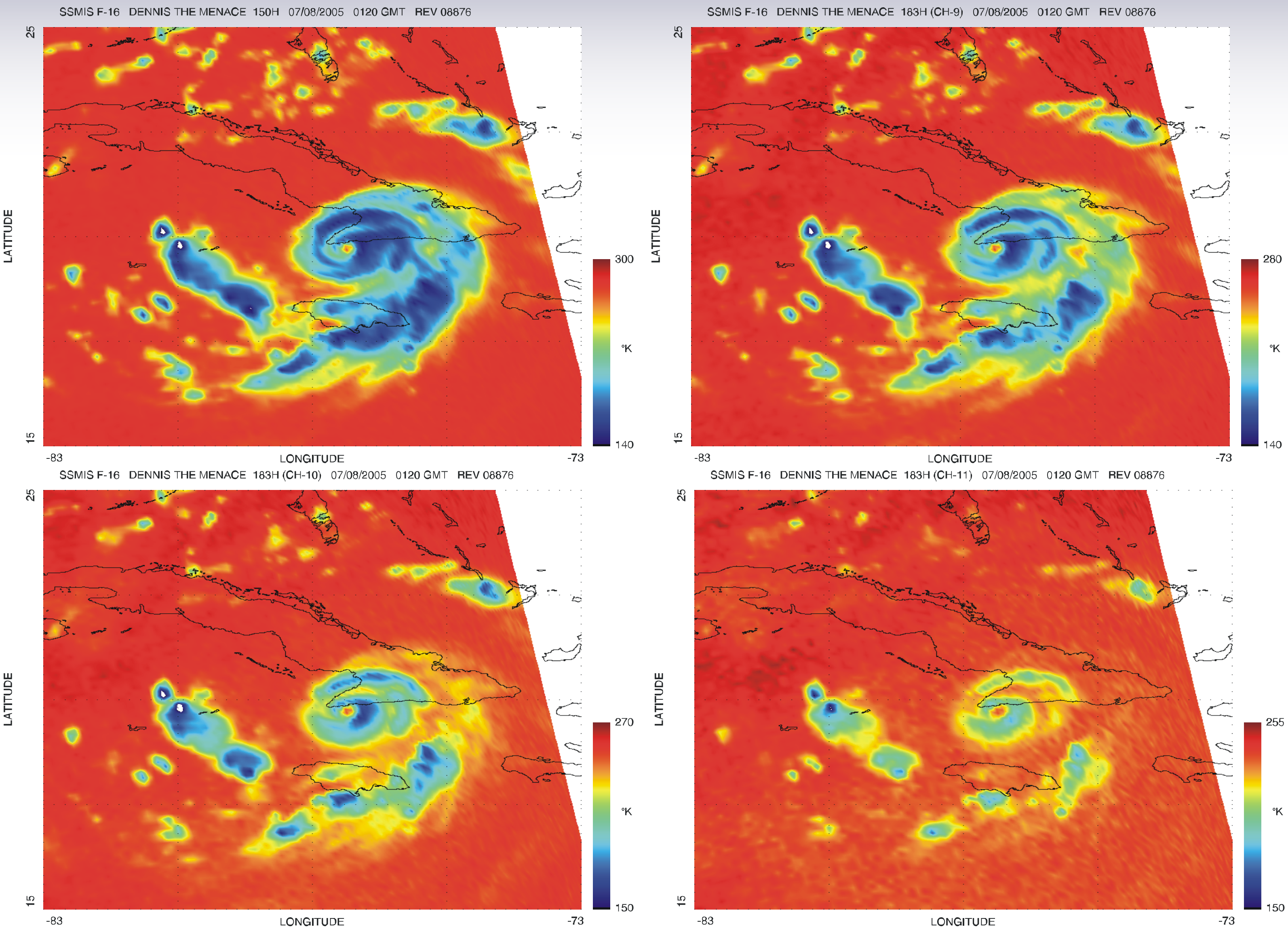
SSMIS F-16   DENNIS THE MENACE 150H   07/08/2005   0120 GMT   REV 08876

SSMIS F-16   DENNIS THE MENACE 183H (CH-9)   07/08/2005   0120 GMT   REV 08876

SSMIS F-16   DENNIS THE MENACE 183H (CH-10)   07/08/2005   0120 GMT   REV 08876

SSMIS F-16   DENNIS THE MENACE 183H (CH-11)   07/08/2005   0120 GMT   REV 08876

8.13 Hurricane Emily SSMIS 17 July 2005

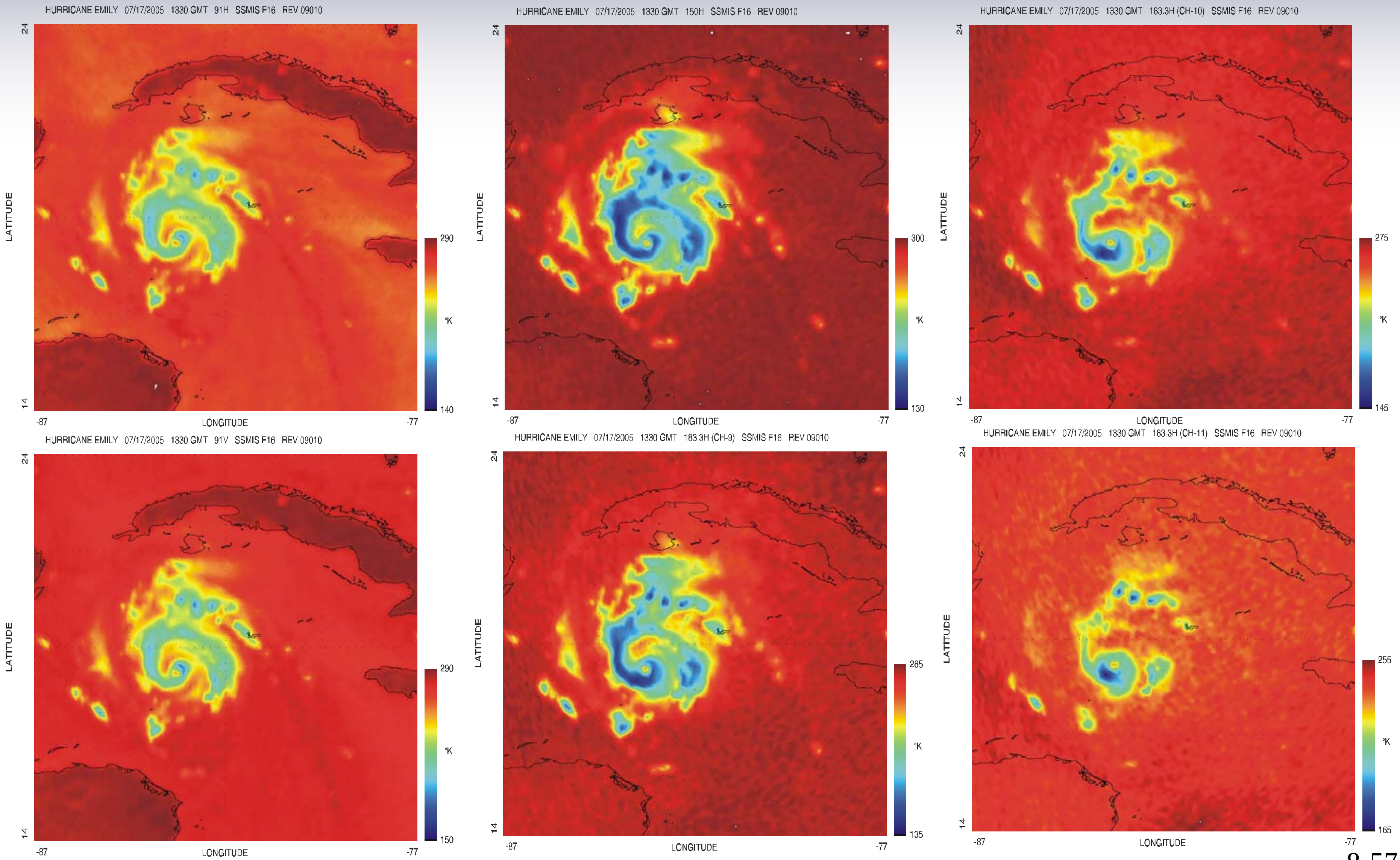

8.13 Hurricane Katrina SSMIS Chs. 8-11
29 August 2005

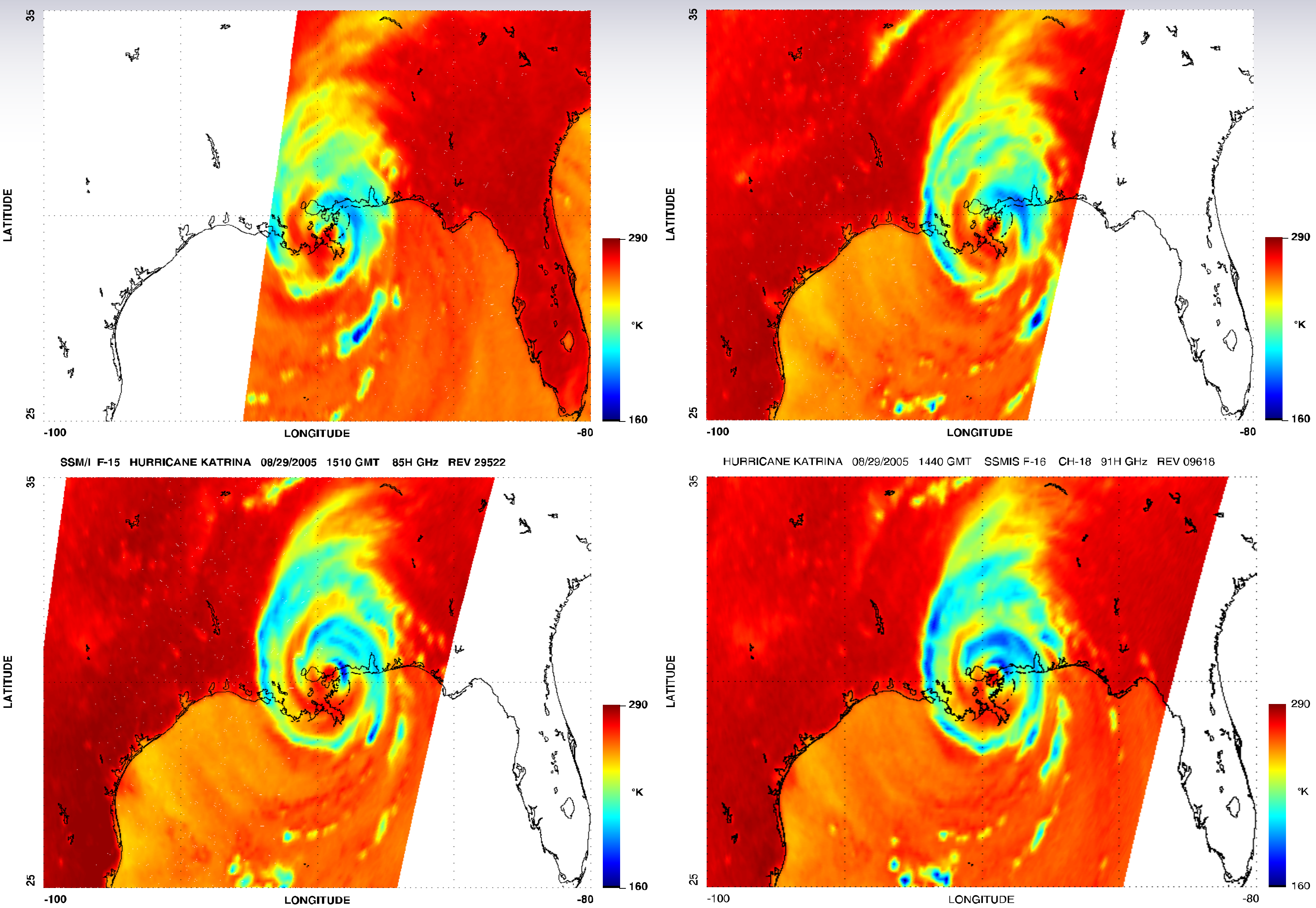

8.13 Hurricane Rita SSMIS Chs. 8-11
24 September 2005

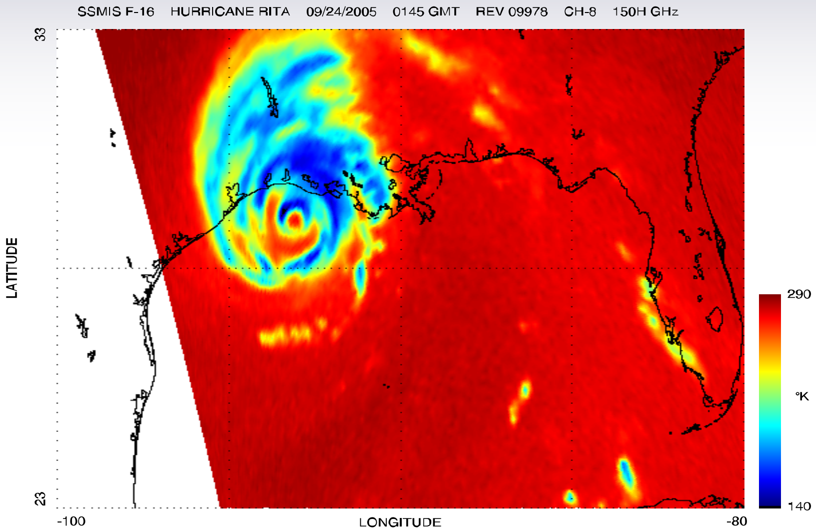
SSMIS F-16 HURRICANE RITA 09/24/2005 0145 GMT REV 09978 CH-8 150H GHz

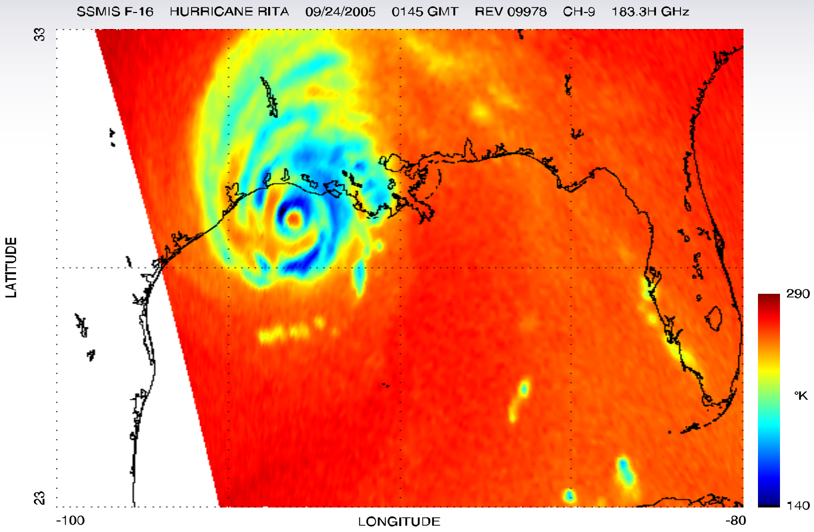
SSMIS F-16 HURRICANE RITA 09/24/2005 0145 GMT REV 09978 CH-9 183.3H GHz

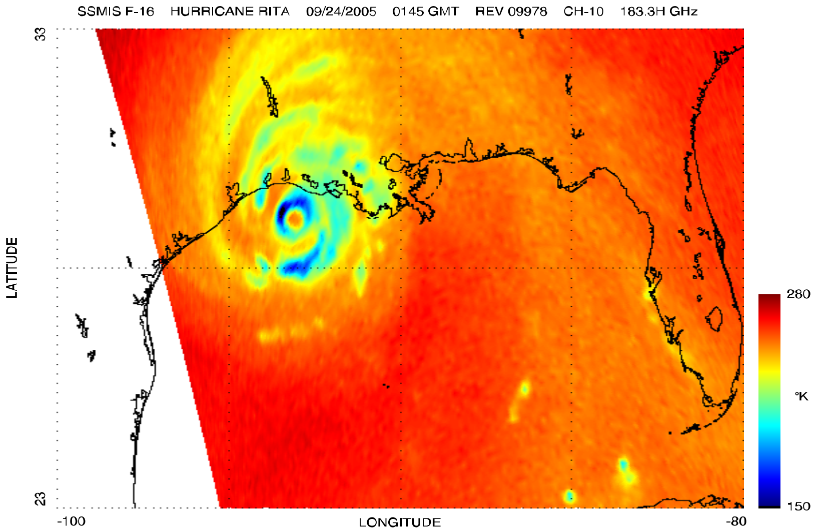
SSMIS F-16 HURRICANE RITA 09/24/2005 0145 GMT REV 09978 CH-10 183.3H GHz

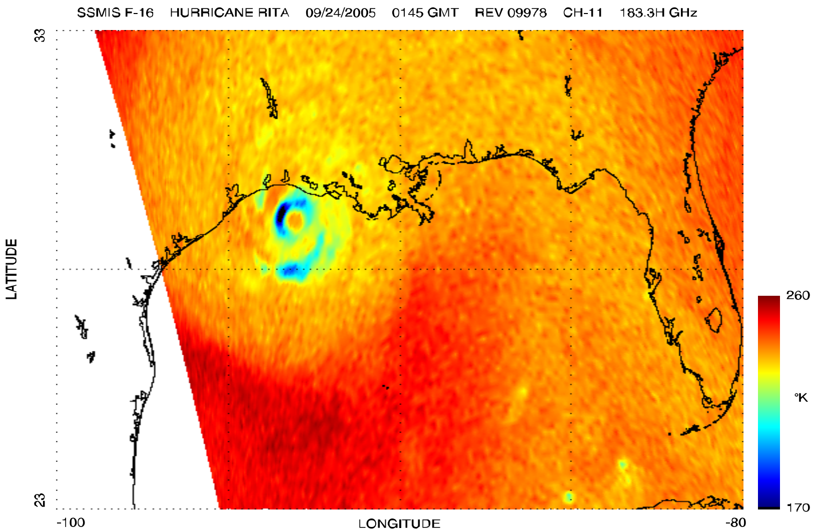
SSMIS F-16 HURRICANE RITA 09/24/2005 0145 GMT REV 09978 CH-11 183.3H GHz

8.14 SSMIS - NOAA/ETL* Precipitable and Cloud Liquid Water EDRs

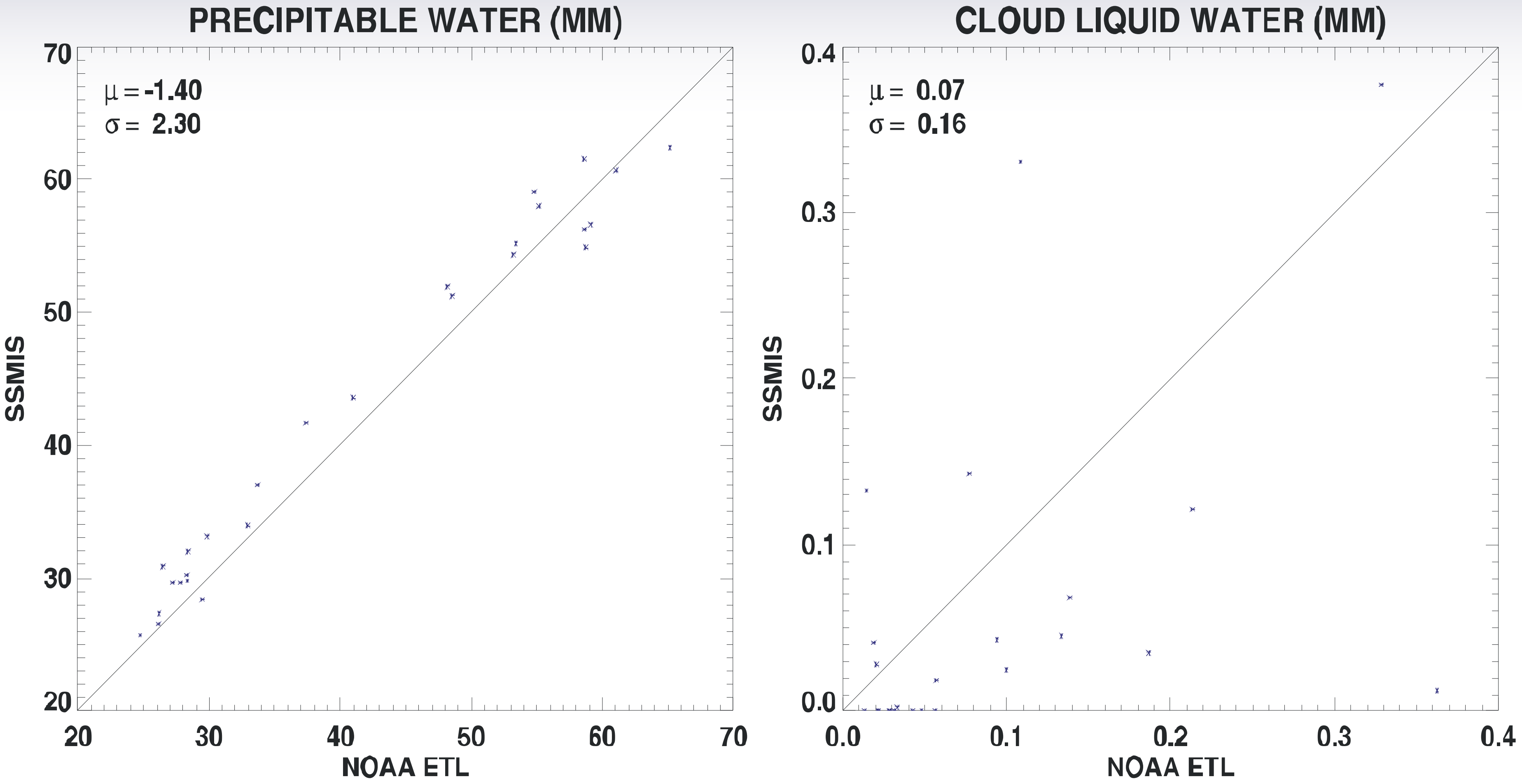

* NOAA/ETL Upward-looking radiometer measurements conducted aboard RV Brown 15 October – 20 November 2003, latitudes –8º to 12º, longitudes –110º , -85º

8.15 SSMIS EDR – FNMOC Buoy Wind Speed (Nov 2003 – Jul 2005)

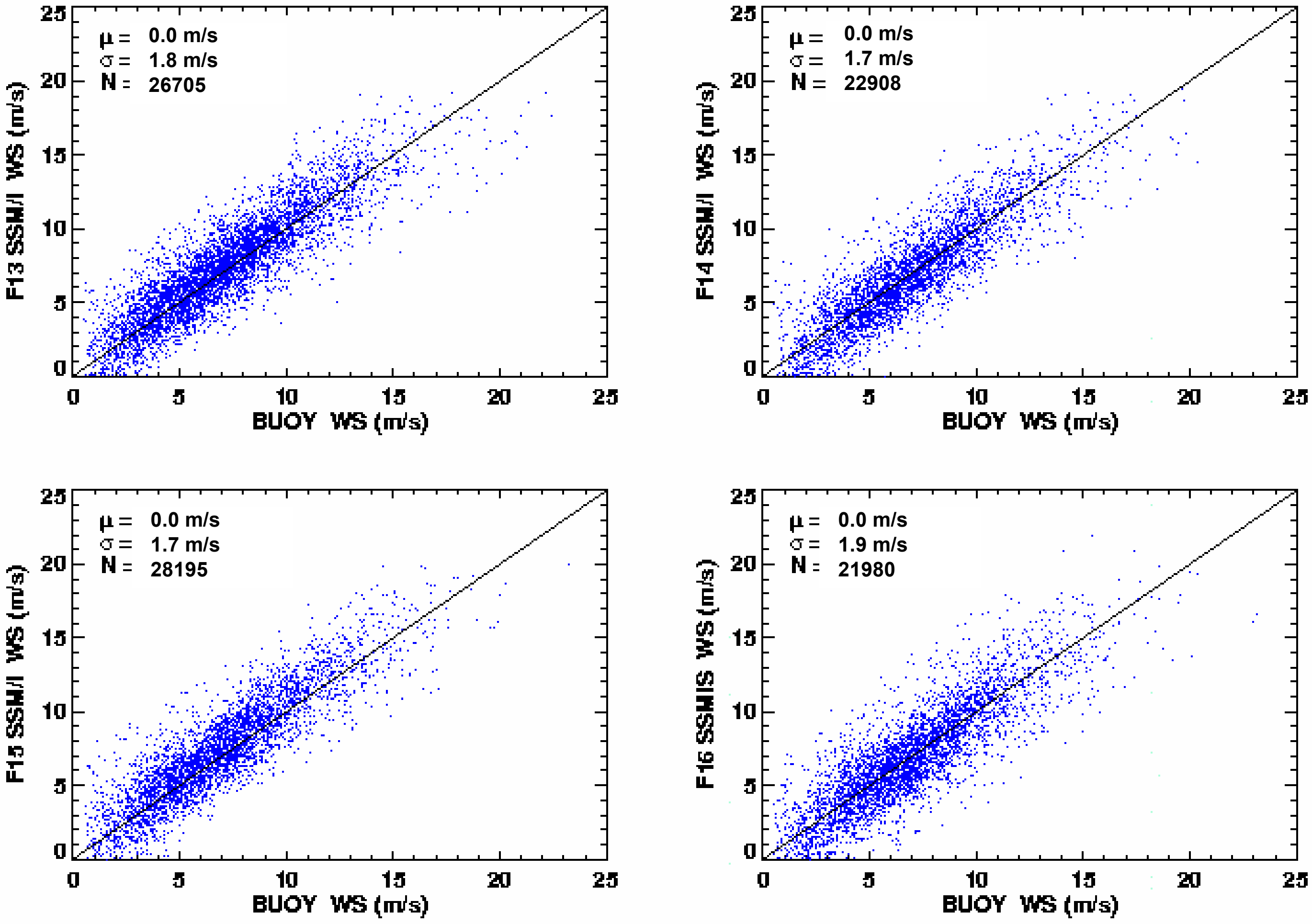

F13, F14, F15 SSM/I & F16 SSMIS OCEAN WIND SPEED EDR PERFORMANCE
(FNMOC BUOY DATA BASE NOV 03 - JUL 05)

8.15 FNMOC ISIS Data Base Ocean Buoy Locations

FNMOC ISIS BUOYS ≥ 100 KM. FROM COASTLINE

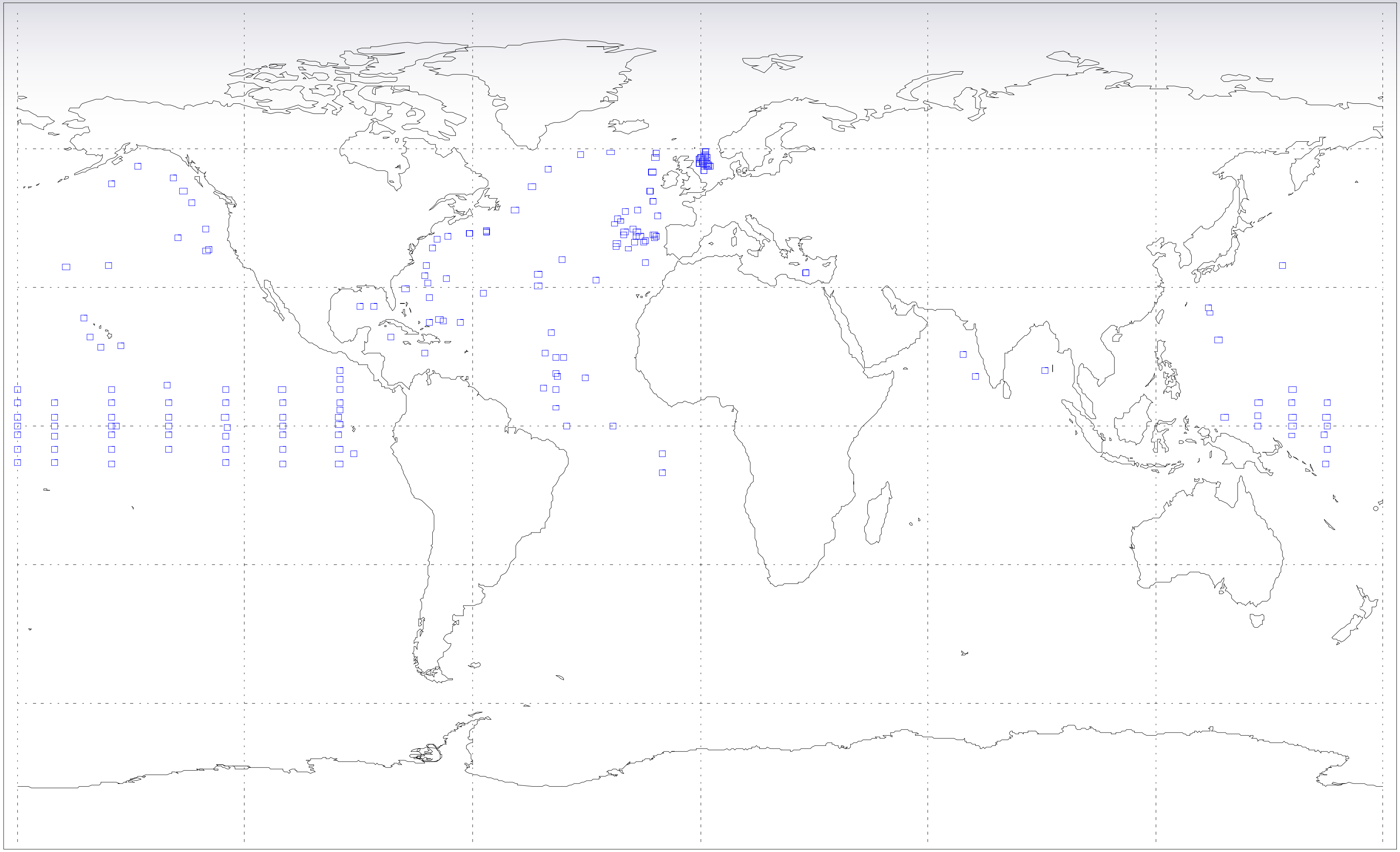

8.16 SSMIS - FNMOC Over Ocean Integrated Water Vapor EDR (Nov 03 - Jul 05)

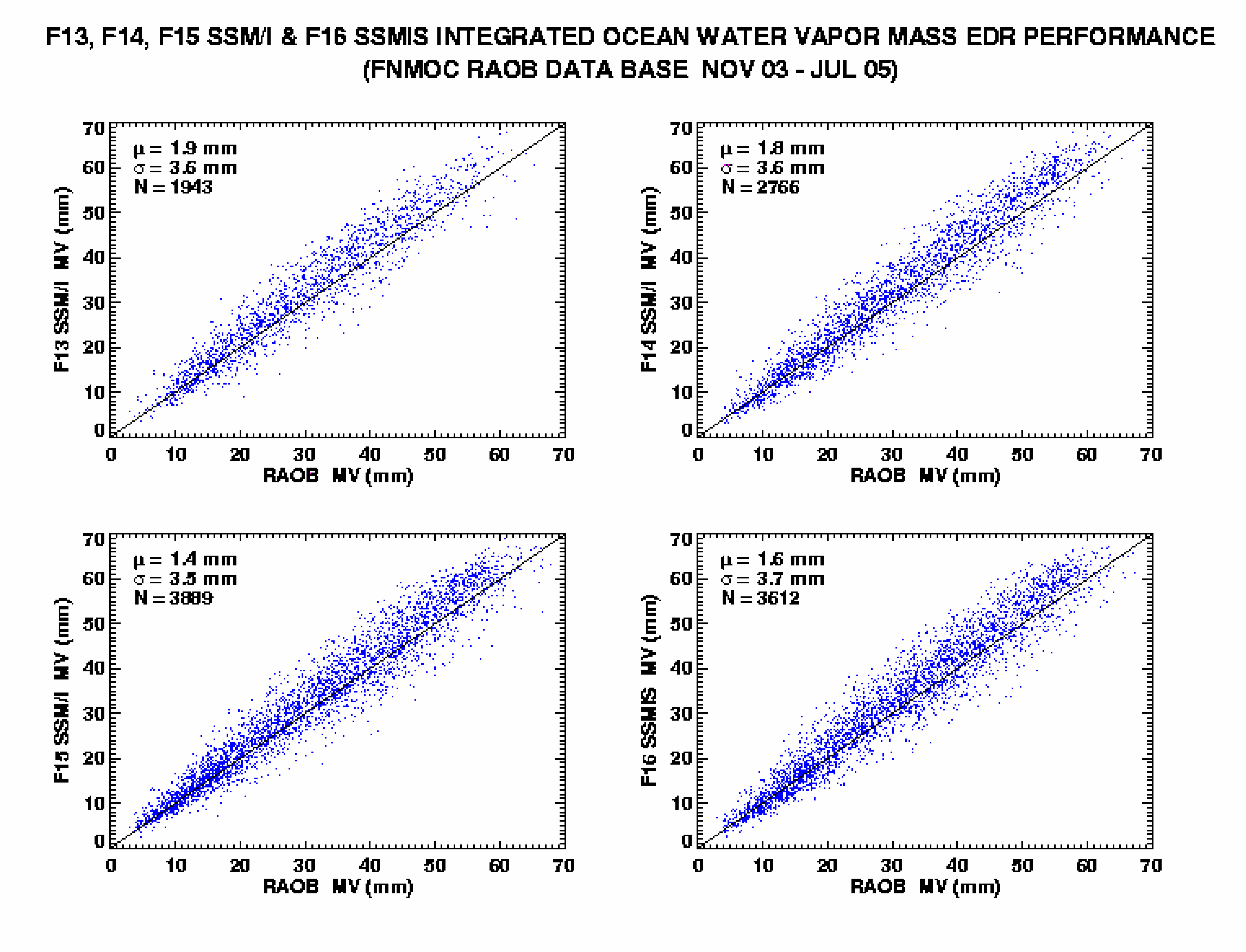

F13, F14, F15 SSM/I & F16 SSMIS INTEGRATED OCEAN WATER VAPOR MASS EDR PERFORMANCE
(FNMOC RAOB DATA BASE NOV 03 - JUL 05)

8.16 FNMOC ISIS Island RAOB Data Base

SELECTED ISLAND RAOB STATIONS

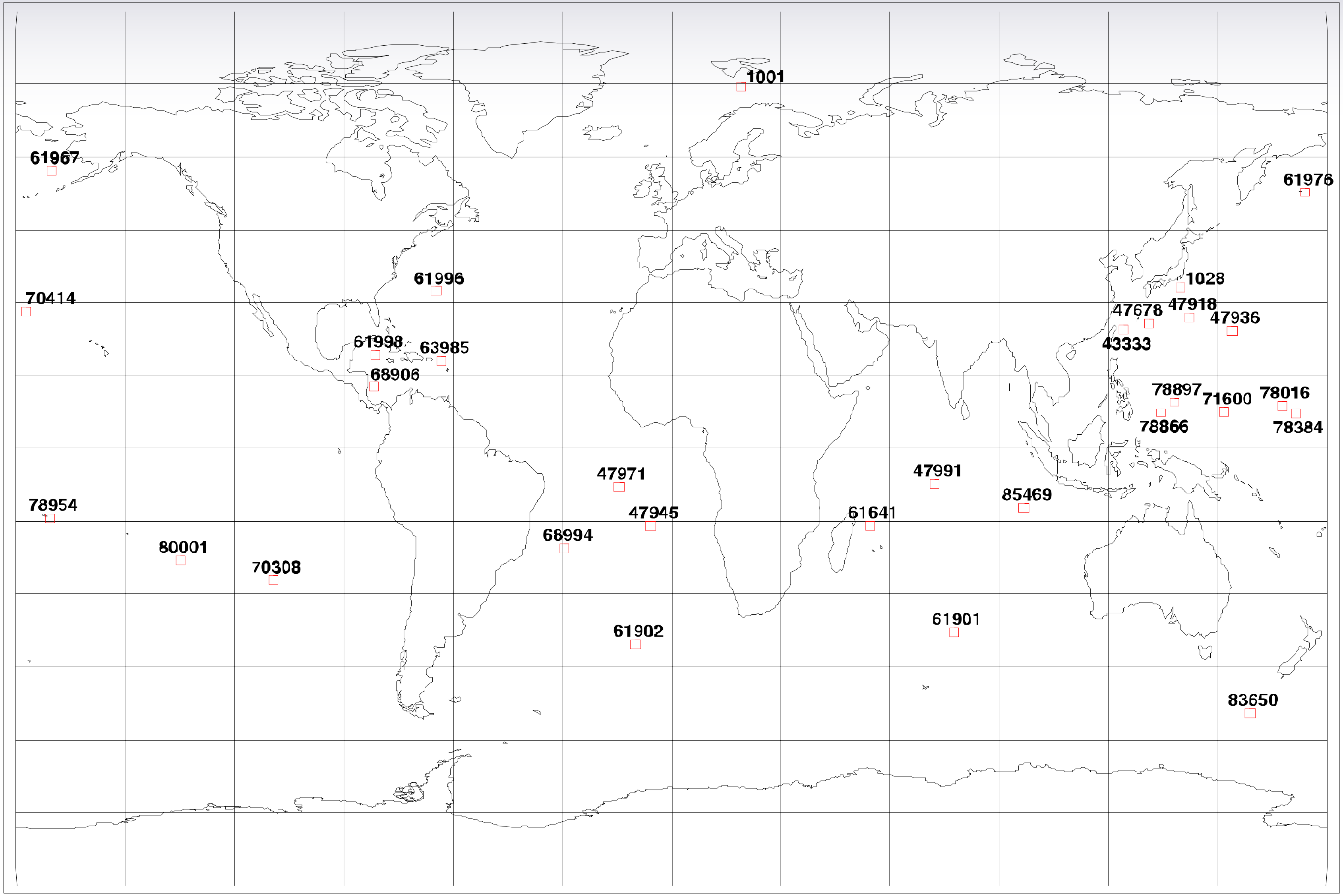

8.17 SSMIS EDR Performance Summary (SSM/I Type EDRs)

- SSMIS EDRs meet global rms accuracy requirement. Based on:

  (1) cross-validation performance with F-14 SSM/I

  (2) RV Brown ship-board NOAA/ETL measurements

  (3) FNMOC buoy wind speed measurements

  (4) FNMOC island RaOb match-ups

- Regional/Seasonal biases observed in difference of SSMIS and SSM/I some EDR imagery. Most notable:

  (1) ocean surface wind speed (~1 m/s)

  (2) land surface temperature (~1 K)

  Believed due to changes in reflector antenna emissions (exit/entry of shadow) and imperfect correction for solar contamination of warm-load calibration target. Similar differences were not observed in total precipitable water (over ocean) and is consistent with frequency dependence of antenna emissions (Chs. 12-14 less affected by emissions than 15-18).

8.17 SSMIS EDR Performance Summary (SSM/I Type EDRs)

Environmental EDR	Scene Spacing (km)	Quantization Intervals	Accuracy Requirement	Accuracy Performance [7]
a) Ocean Surface wind speed [6]	25	1 meter/second	2 m/s	<2.0[8] m/s
b) Rain over land/ocean	25	1mm/hr	5 mm/hr [3]	<5 mm/hr
	12.5	Flag for rain	N/A	
c) Cloud water [1] over ocean	25	0.05 kg/m^2	0.10 kg/m^2	<0.05 kg/m^2
d) Soil Moisture	25	5 percent levels	±10 percent [5]	<10%
e) Ice Concentration (percent area covered)	25	5 percent levels	±10 percent	<10%
f) Ice Age	25	First year/ Multi-year		
g) Ice Edge and Snow Edge	25	Flag		
h) Water Vapor over ocean	25	0.5 kg/m^2	±3 kg/m^2 tropics ±2 kg/m^2 mid-lat ±1, polar	<3 kg/m^2 tropics < 2 kg/m^2 mid-lat <1 kg/m^2 polar
i) Surface Type [2]	25	See below		
j) Snow Water Content	25	0.5 cm	±3 cm [4]	<3 cm
k) Surface Temperature Over Land	25	1 K	±2.5K [4]	<2.5[8] K

1/ Cloud Water (droplets less than 100 micrometers in diameter).

2/ Surface Type parameters: ocean, ice, coastal, and land. The land surface categories will be: Standing water or flooded conditions, dense vegetation (jungle), agricultural/rangeland (some vegetation), arable soil (dry), soil (moist surface), semi-arid surface, desert, and snow.

3/ Goal on a regional basis.

4/ Goal.

5/ Goal. The Antecedent Precipitation Index (API) will be used as a basis for analysis. Accuracy will be verified from curves relating the API to soil moisture.

6/ Error calculation based on a global wind speed distribution (0-20 m/s).

7/ Based on cross-validation with F-14 SSM/I EDRs, and "ground truth" noted in previous chart.

8/ Regional biases (~1 m/s for wind speed; ~1-1.5 K for land temperature. See previous chart).

F16 SSMIS Calibration/Validation Final Report

Section 9.0 Lower-Air Sounding EDR Validation

John Wessel, Al Fote, Steve Swadley, Ye Hong,

Don Boucher, Robert Farley, Bruce Thomas and

Arlene Kishi

THE AEROSPACE CORPORATION

Section 9.0 Lower-Air Sounding EDR Validation Outline

Section 9.1 Foreward

- **This study presents results from SSMIS Lower Air Sounding (LAS) validation efforts applied to data collected mostly between November 2003 and December 2004. It is primarily based on matchup comparisons between collocated SSMIS EDRs and observations by operational radiosondes, ECMWF analysis fields, and results from the Barking Sands lidar campaign. Ground truth measurement accuracy is discussed in the SSMIS Cal/Val Plan and specific examples, taken from the Cal/Val Campaign, are included in the Appendix to the LAS Calibration Final Report. Errors contributed by uncertainty in ECMWF fields and uncertainty in the Barking Sands lidar/radiosonde measurements are unlikely to impact comparison results discussed in this report.**

Foreward (Cont'd)

- Two versions of ground data processing software (GDPS) were employed during F-16 Cal/Val. The first is referred to as revision 4. It was based on prelaunch estimates of instrumental constants, including geolocation and antenna pattern correction parameters, and incorrect identification of instrument polarization. Geolocation, antenna pattern correction, and instrument polarization-related aspects of SDR generation software were improved in revision 5 software. Some EDRs were reprocessed for Cal/Val, using revision 5 corrected SDRs. Although lower air soundings SDRs change up to about 0.5 K when corrected, the effect on retrievals is relatively small. None of the conclusions appear to be impacted by the GDPS changes.

Section 9.2 EDR Requirements

Retrieval accuracy:		Bias (K)	RMS (K)
Temperature			
	1000 mb	<1	8
	850 mb	<1	6
	700 mb	<1	2.5
	500 – 10 mb	<1	2
	7 – 1 mb		5
	0.4		5.5
	0.2-0.03		8 (goal)
Water vapor			
	1000 - 700mb		20% RH
	500 – 300 mb		1.5 g/kg

- SSMIS LAS temperature retrieval requirements vary from level-to-level, starting at 8 K RMS for the 1000 mb altitude level, decreasing to 2K at 500 mb, and then remaining 2K up to 10 mb, which is the highest LAS sounding level. Bias requirements are <1 K for LAS levels. Upper Atmospheric Sounding results are addressed in a separate report.
- The tropopause RMS temperature requirement is 5 K, with a goal of 1 K, and the tropopause pressure goal is +/-20 mb RMS.
- For water vapor, the LAS requirement is 20% RH RMS or 1.5 g/kg, whichever is greater, over ocean surfaces for clear conditions. These values are goals for other surfaces. Bias shall not exceed that determined from an analysis of SSM/T2 data.

Section 9.3 Daily EDR Raob Matchup Summary (2003 Julian Day 322)

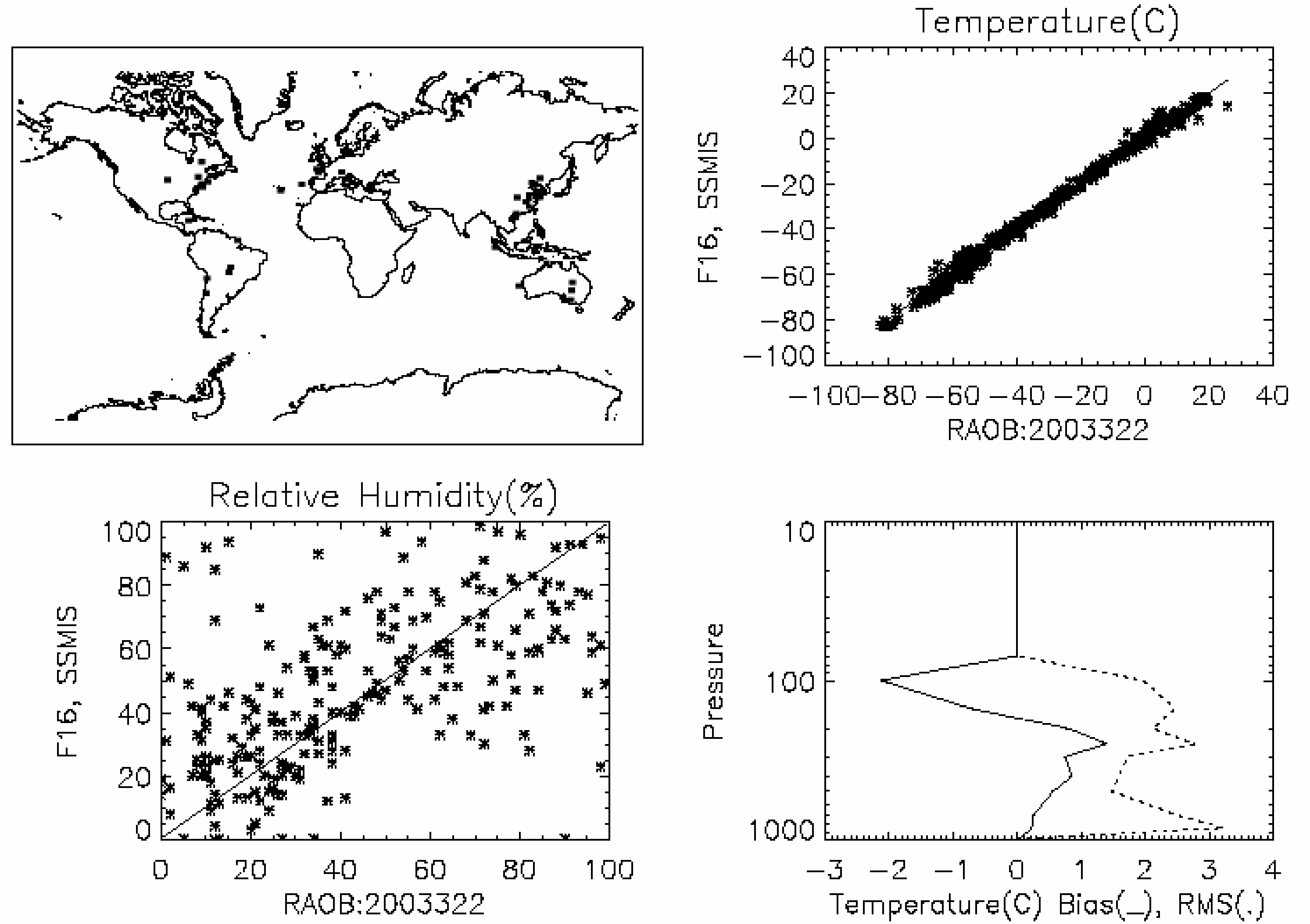

- SSMIS temperature and relative humidity retrieval products were monitored on a daily basis for the first year following launch. The figure above presents a typical example, summarizing matchup data for Julian day 322 of 2003. The panel on the upper left indicates radiosonde stations contributing to the daily matchups. Typically, about 40 percent or less of soundings reported by the global network are accepted by our proprietary quality control software. On this day, about 50 stations provided accepted profiles. The upper right hand panel contains a scatter plot with SSMIS temperature EDRs shown along the vertical axis and corresponding RAOB values on the horizontal axis. RAOB mandatory level parameters are determined by averaging the reported profile over the width of each mandatory pressure level.[1] The panel at lower right presents bias and standard deviation (labeled RMS in this case[2]) for mandatory pressure levels, which are displayed on the vertical axis. In this case, bias requirements are satisfied from the surface to 300 mb, also at 200 and 150 mb. No comparisons are performed above the 100 mb level due to radiosonde altitude limits. Although standard deviations for many levels are less than 2 K, the actual RMS exceeds 2 K for many levels. However, 1000 and 850 mb are well within the large limits allotted to RMS for these levels.

- The relative humidity scatter plot, shown at lower left, is also typical for the Cal/Val period. There is usually some correlation between EDRs and RAOBs, however retrieval skill is typically poor (e.g.. 20-30% RMS RH).

- [1] When more than or other than mandatory levels are reported, the profiles are proportionally averaged across the mandatory level, starting at the mid-point to the level below, ending at the mid-point to the level above. In the case of high resolution temperature profiles, the original profiles are boxcar averaged and then sampled at the mandatory levels.

- [2] Elsewhere in this report, RMS is defined as the square Root of the Sum of Squares (RSS) of bias and standard deviation, which equals the root mean sum of squares of differences between measurement and ground truth.

Section 9.4 Validation of Temperature EDR Retrievals

Separate retrievals used for 3 atmosphere types

Selection involves channel 1 polarization which is V rather than specified H

Switch between D-Matricies based on tropopause height

- **High tropopause (pressure < 120 mb)**
- **Medium altitude tropopause (120 < pressure < 250 mb)**
- **Low tropopause (pressure > 250 mb)**

- **Heavy cloud cover flag: Scatter plot for V and H polarization**

Conclusion:

Await H-polarized sensor before fully evaluating retrieval performance
Matchup data are currently insufficient to evaluate surface altitude correction over land

Typical Validation Site Locations

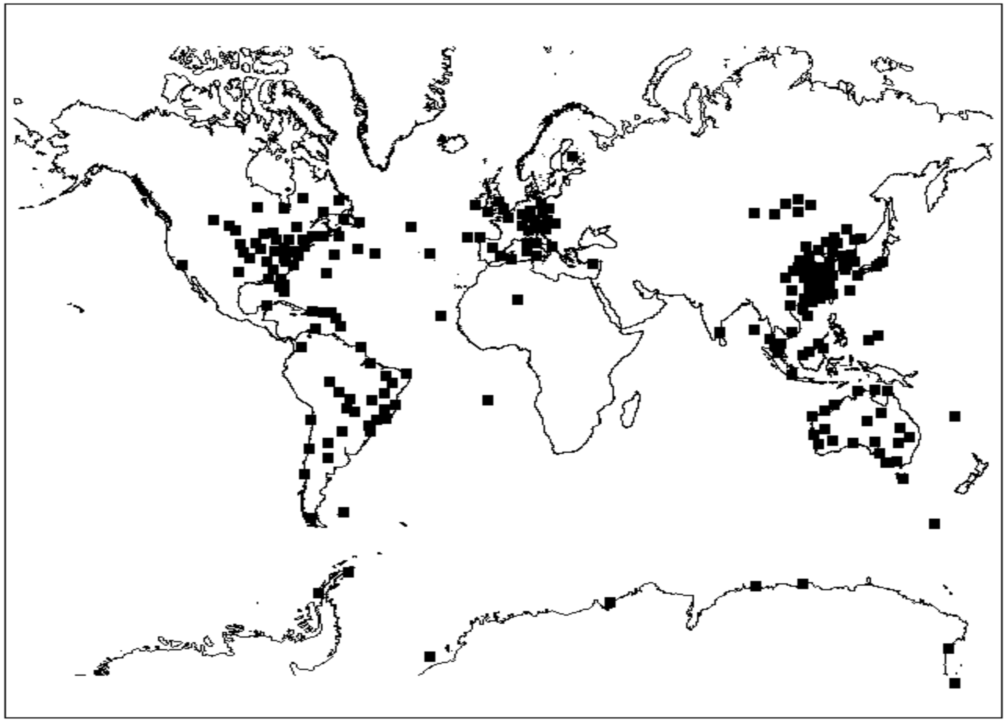

- This is a typical distribution of radiosonde station sites that contribute over an extended period of time to Cal/Val matchup archives. The F-16 orbit combined with synoptic sampling times results in the above distribution. A window of +/-90 minutes and +/-200 km was allowed in order to achieve a reasonable number of useful daily soundings. ECMWF statistics were also compiled at these matchup locations. In that case, there was geographic collocation, however ECMWF analysis field were time-interpolated between the nearest 6 hour runs.

- Contributing sites are concentrated in E. Americas, W. Europe, E. Asia, and Australia. Oceanic and Arctic coverages are sparse.

Winter 2003 R5 Temperature EDRs Versus ECMWF

D-matrix = 1

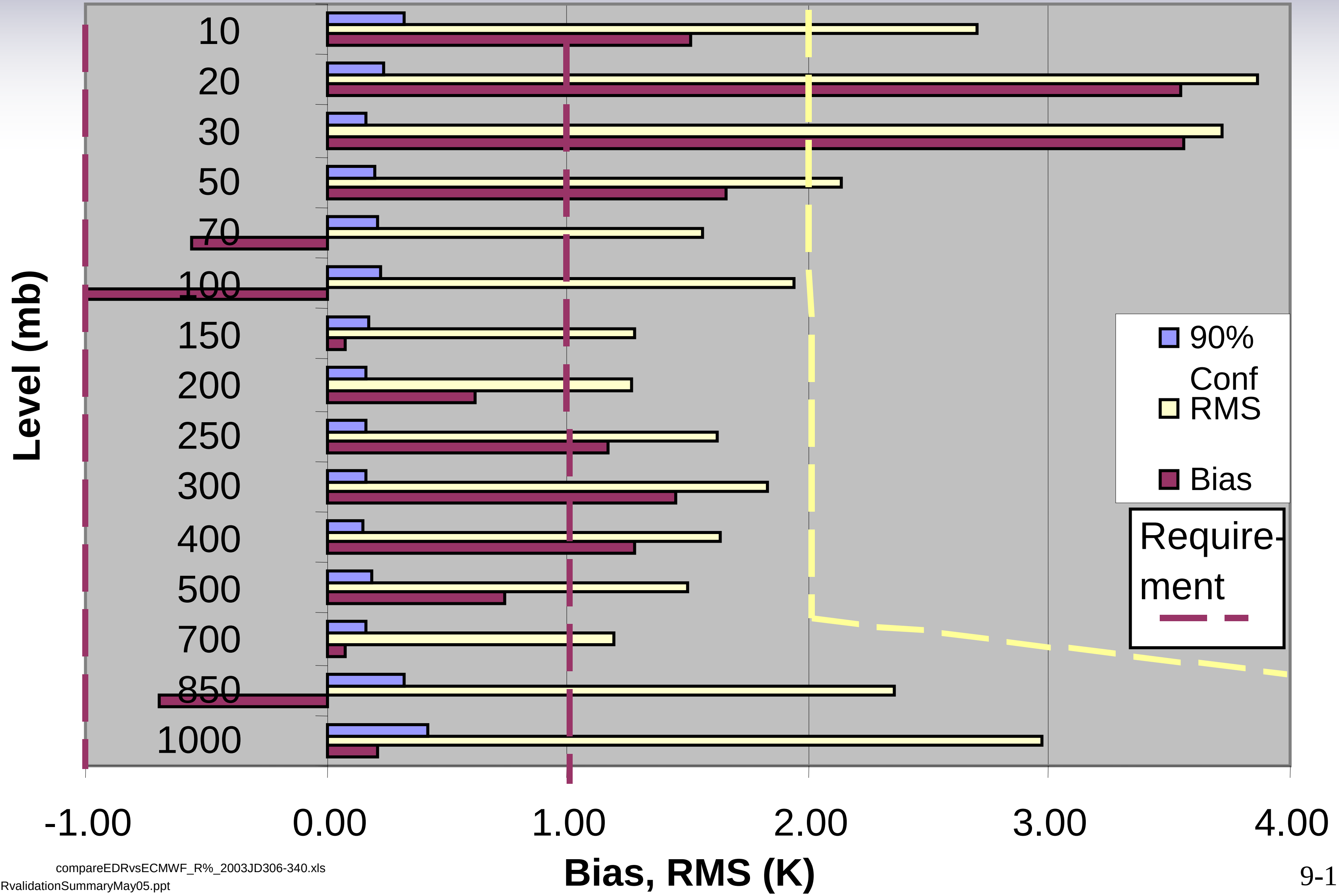

compareEDRvsECMWF_R%_2003JD306-340.xls

EDRvalidationSummaryMay05.ppt

- Retrieval performance was evaluated over extended time periods in order to improve statistical confidence. This figure shows the bias and RMS of SSMIS temperature retrievals as measured against ECMWF profiles for the period November to December 2003.
- SSMIS software invokes three types of temperature retrievals. D-matrix type 1 is used for high (tropical) tropopause, at or above the 120 mb pressure level. Type 2 is used for a mid-altitude tropopause, between 120 and 250 mb, and type 3 retrieval is used if the tropopause is located below the 250 mb pressure level. The chart above applies to high tropopause type 1 D-matrix retrievals. Bias, shown by the maroon bars, exceeds requirements for levels at 400, 300, 250 and 100 mb. The statistical uncertainty in bias (90% confidence level [i]) is given by the blue bars. Therefore, the larger biases are statistically significant. RMS, shown by the cream color bars, meets requirement up to 70 mb, and then exceeds requirements above that. However, ECMWF may have substantial error, for example about +/-1.3 K at 30 mb. Even with this uncertainty, biases at 30 and 20 mb exceeds requirement. For lower altitude levels, additional confirmation is required and it is provided in next two charts.

- **ECMWF analysis fields were time-interpolated to satellite overpass. ECMWF fields provide useful temperature data to 10 mb. Cases of heavy cloud cover were excluded based on analysis of corresponding radiosonde profiles.**

- **[i] Bias is equal to the mean of the differences. The statistical uncertainty in the mean of a limited set of data is estimated using results from Student's t-distribution. The error estimate is equal to the t-distribution factor, t, multiplied by the standard deviation of the data, divided by the square root of n-1, where n is the number of measurements. In our analyses, t was selected for the 90 percent confidence level, for which one expects errors to exceed the error estimate 10 percent of the time, assuming errors are Gaussian distributed. As an example, if the data set were very large, the 68% confidence level error would correspond to 1 standard deviation divided by the square root of n-1. For the 90% confidence level, t=1.64 for a large data set, and t=2 for a small set with n=6.**

- **t accounts for the uncertainty in the estimate of the mean that is used in calculating the standard deviation for a small set of data. The standard deviation gives the normal error estimate (68% confidence) for an individual measurement in a large set of data. It is not equal to the error in the mean, which is vanishingly small for a large set.**

Winter 2003 R5 Temperature EDRs Versus RAOBs

D-matrix = 1

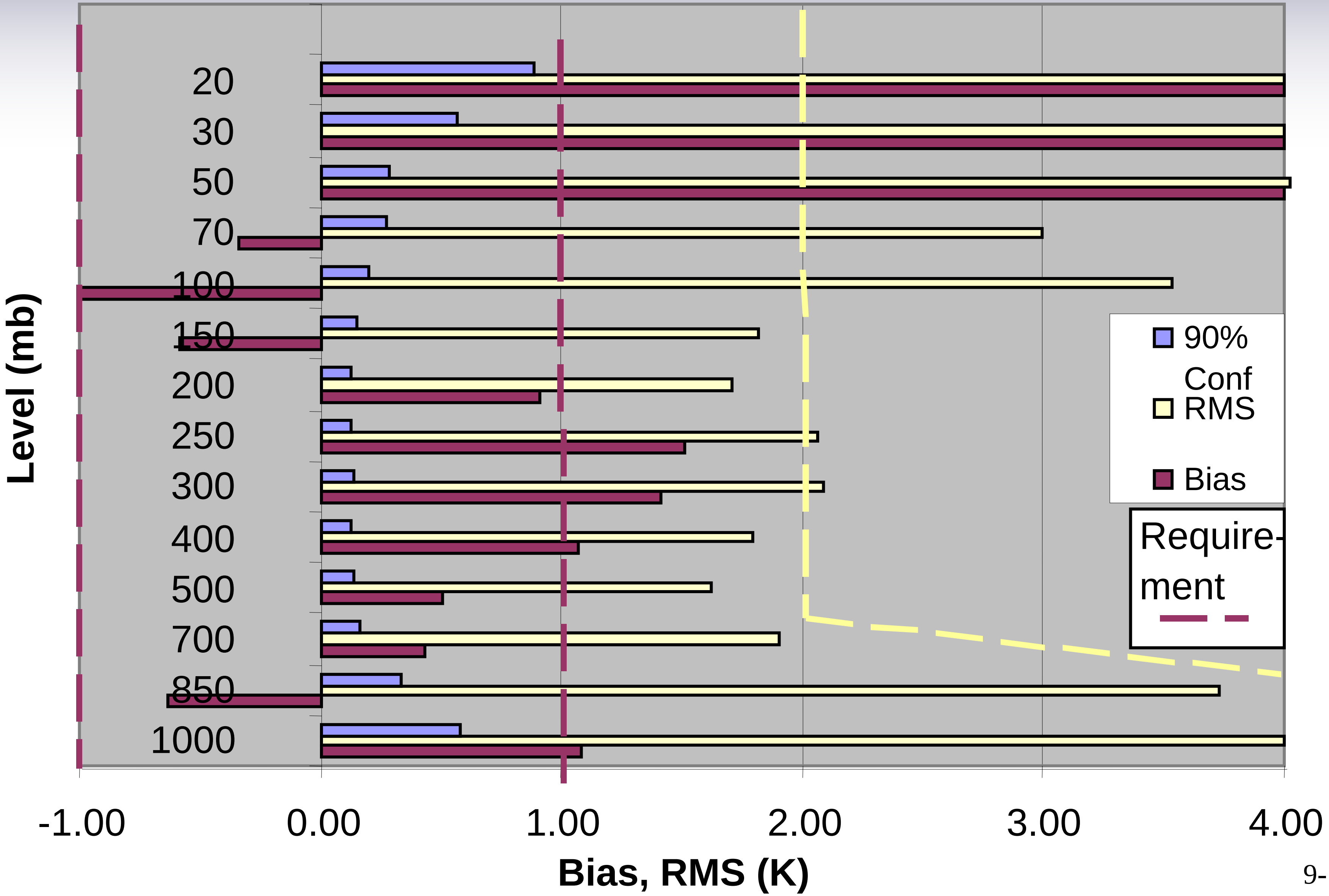

- This chart displays statistics for November-December 2003 comparisons between EDRs and raobs, again for the high tropopause case. Low altitude results are similar to ECMWF comparisons, except for increased standard deviation at 100 and 70 mb. Above 70 mb the measurements are unreliable because many of the raob profiles terminate at lower altitude, in which case temperature is estimated from climatology. The results confirm that retrievals for levels 400, 300, 250, and 100 mb do not meet bias requirements. RMS at 100 and 70 mb is excessive.

January 2004 R5 Temperature EDRs Versus RAOBs

D-matrix = 1

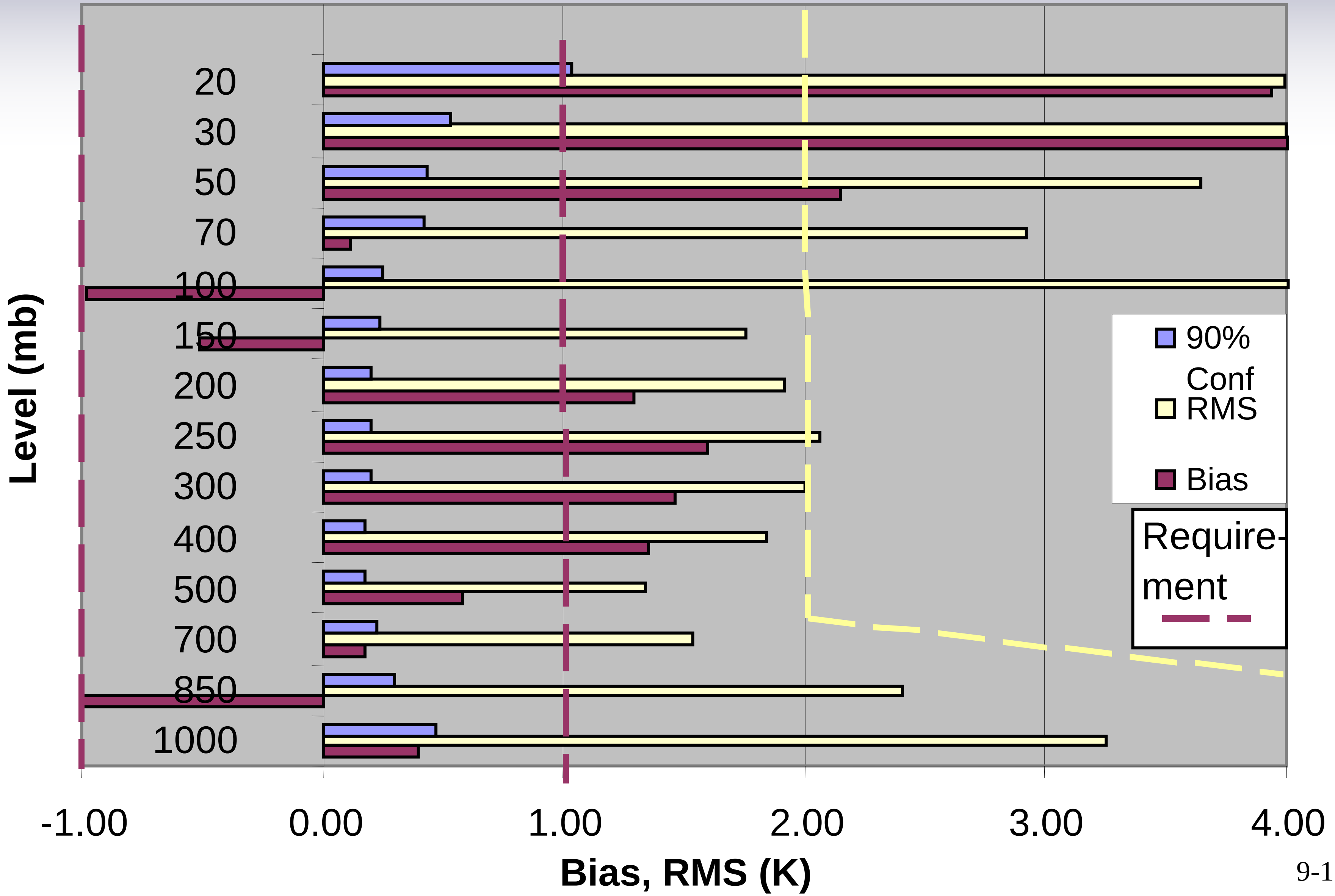

Winter 2003 R5 Temperature EDRs Versus Barking Sands Vaisala RS-90/Lidar Profiles

D-matrix = 1

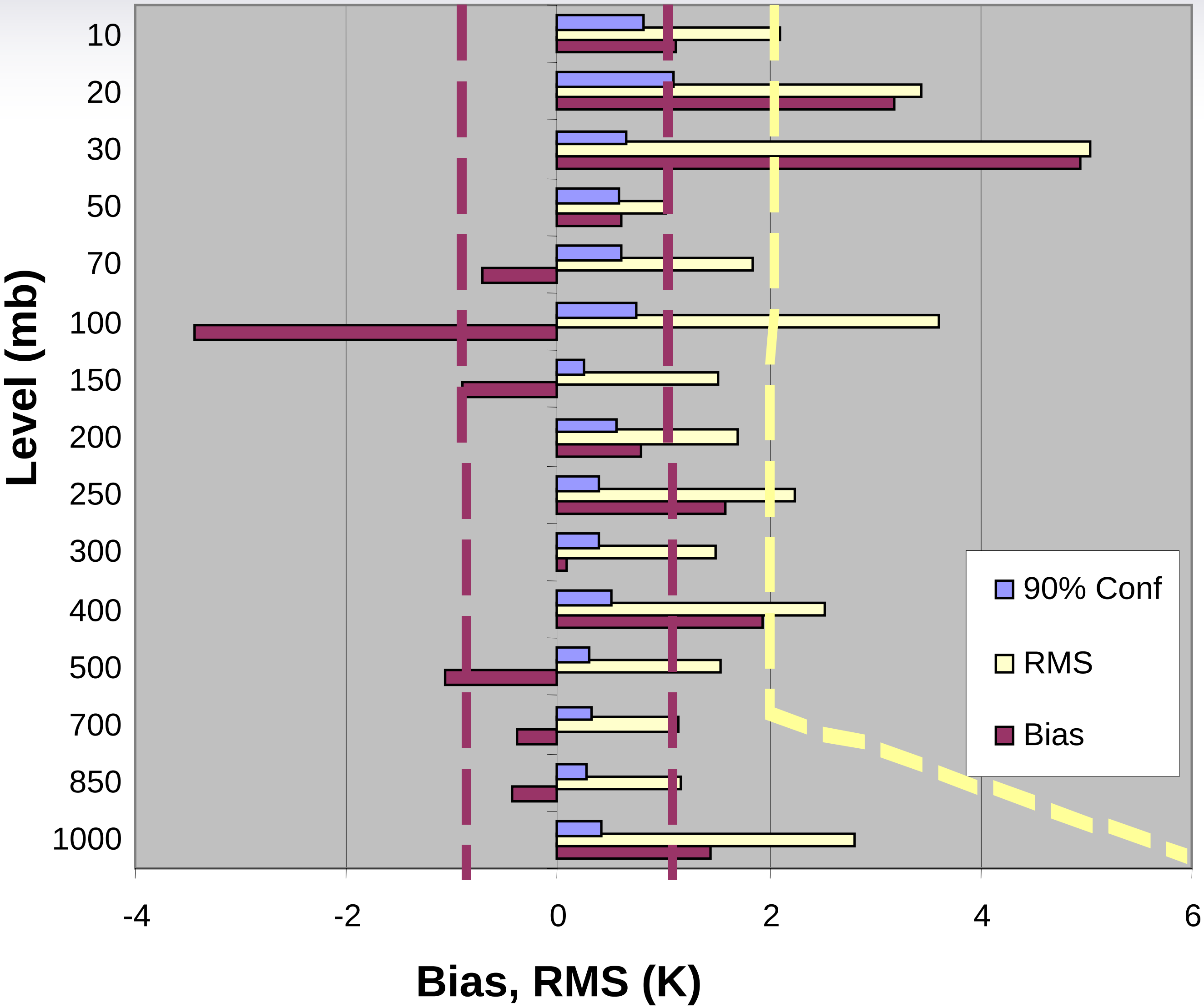

Winter 2003 R5 Temperature EDRs Versus ECMWF

D-matrix = 2

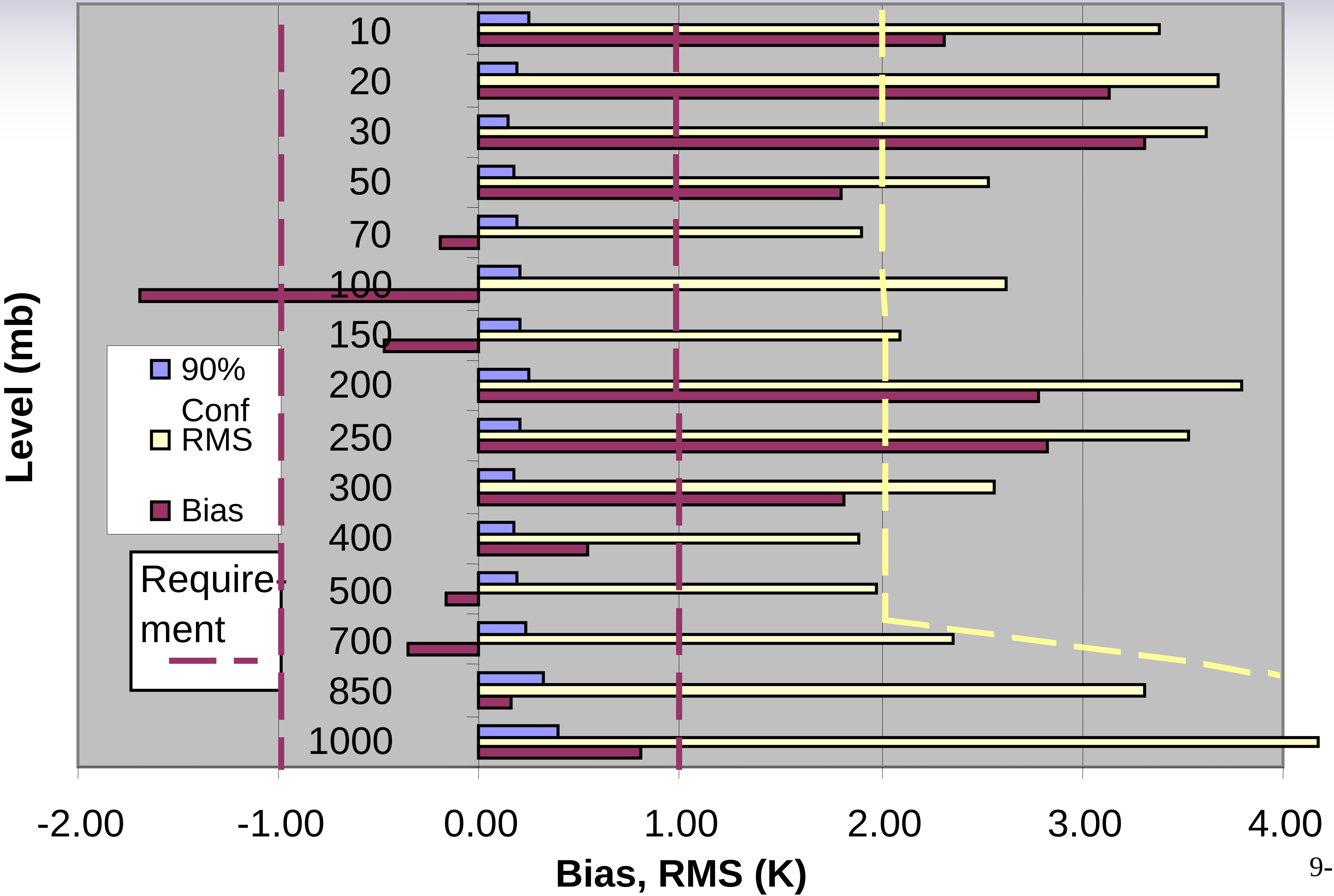

Winter 2003 R5 Temperature EDRs Versus RAOB

D-matrix = 2

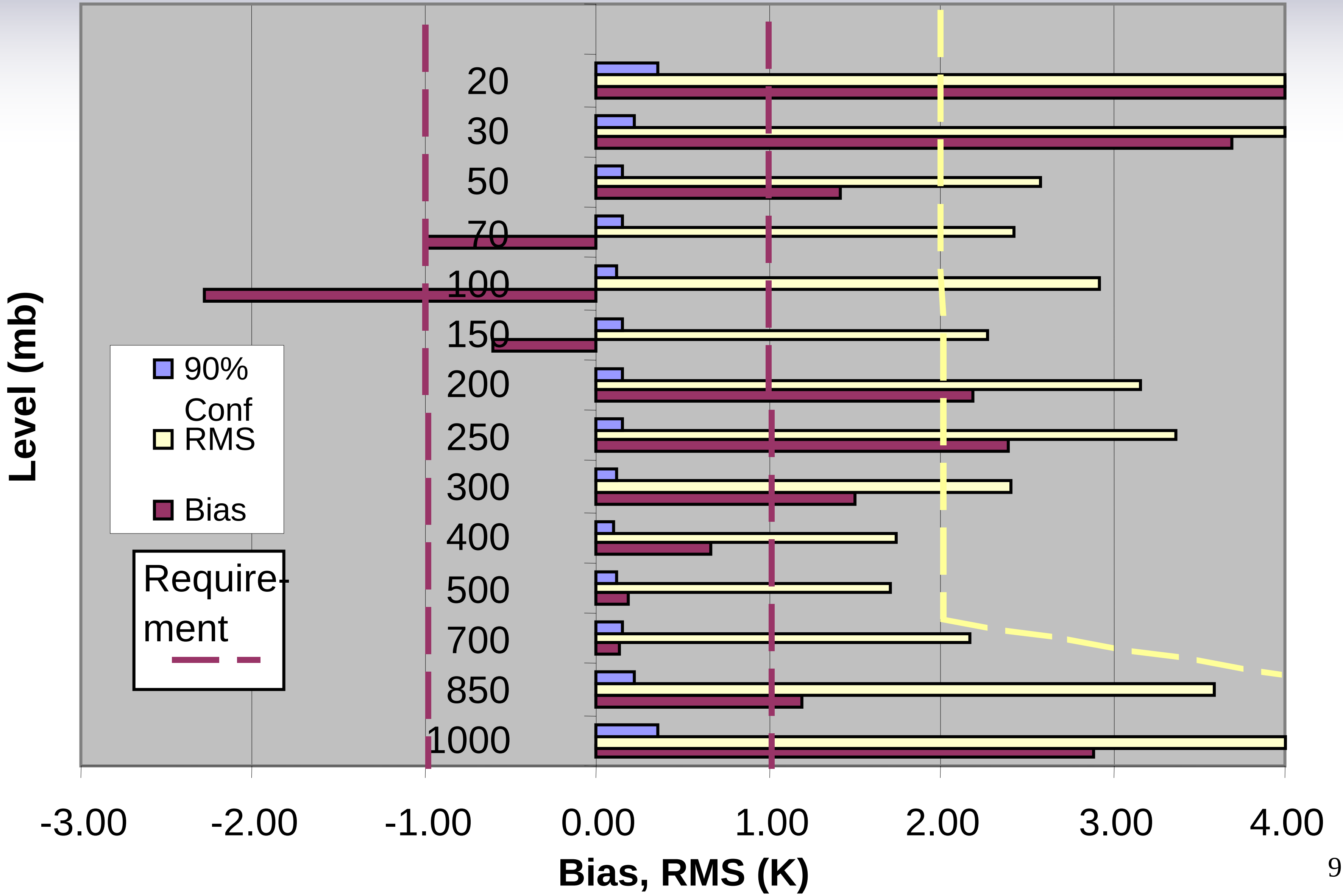

January 2004 R5 Temperature EDRs Versus RAOB

D-matrix = 2

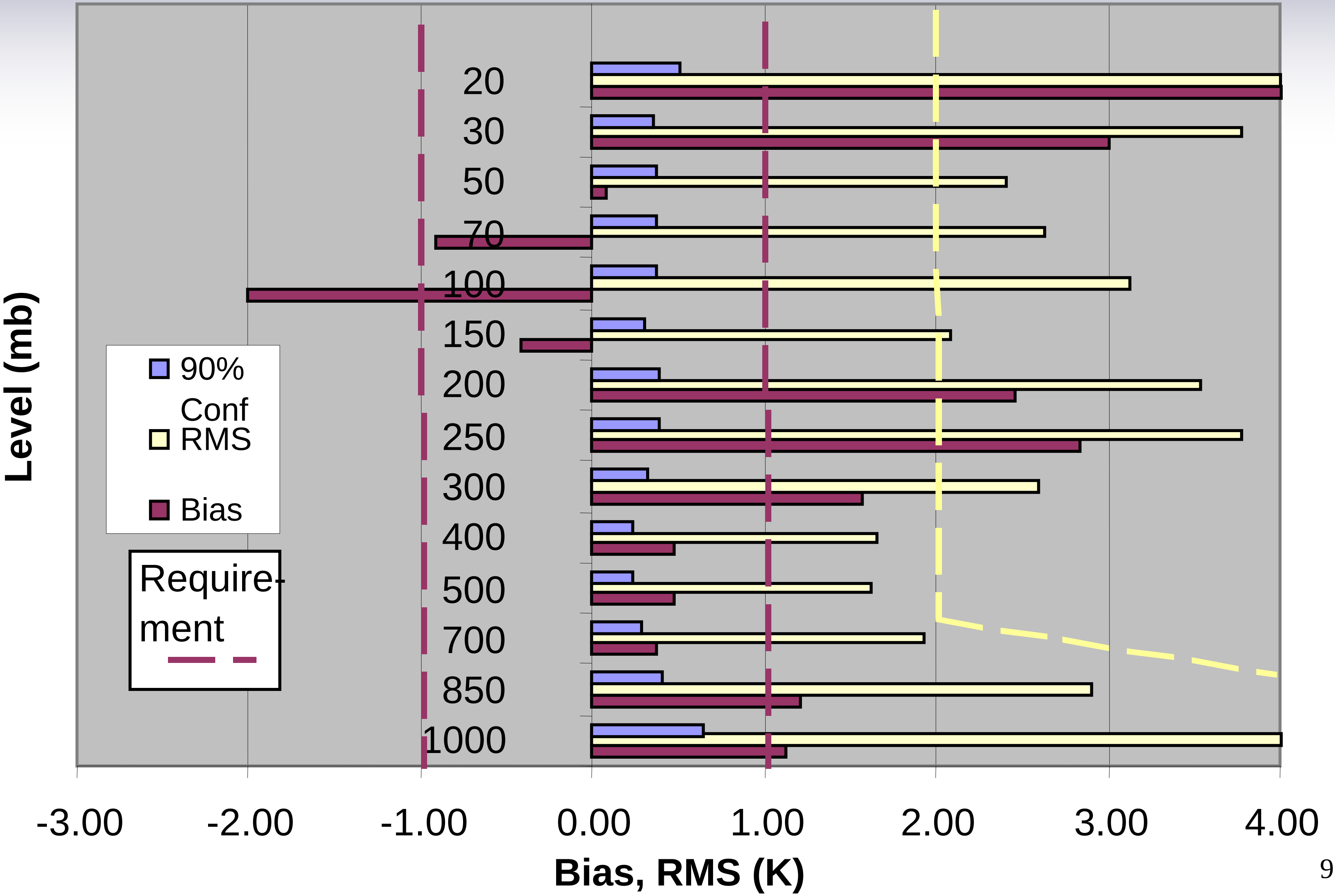

Winter 2003 R5 Temperature EDRs Versus ECMWF

D-matrix = 3

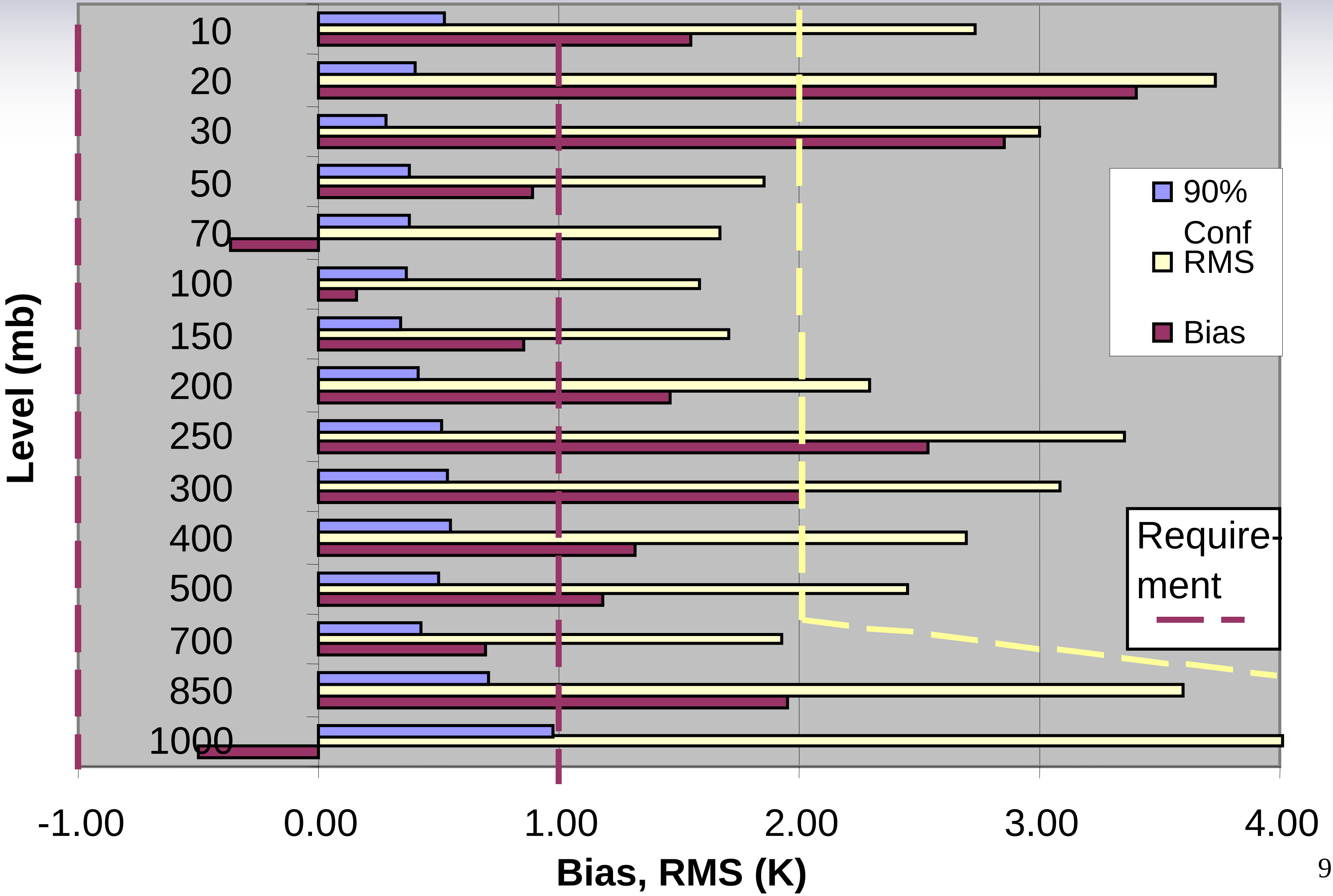

Winter 2003 R5 Temperature EDRs Versus RAOB

D-matrix = 3

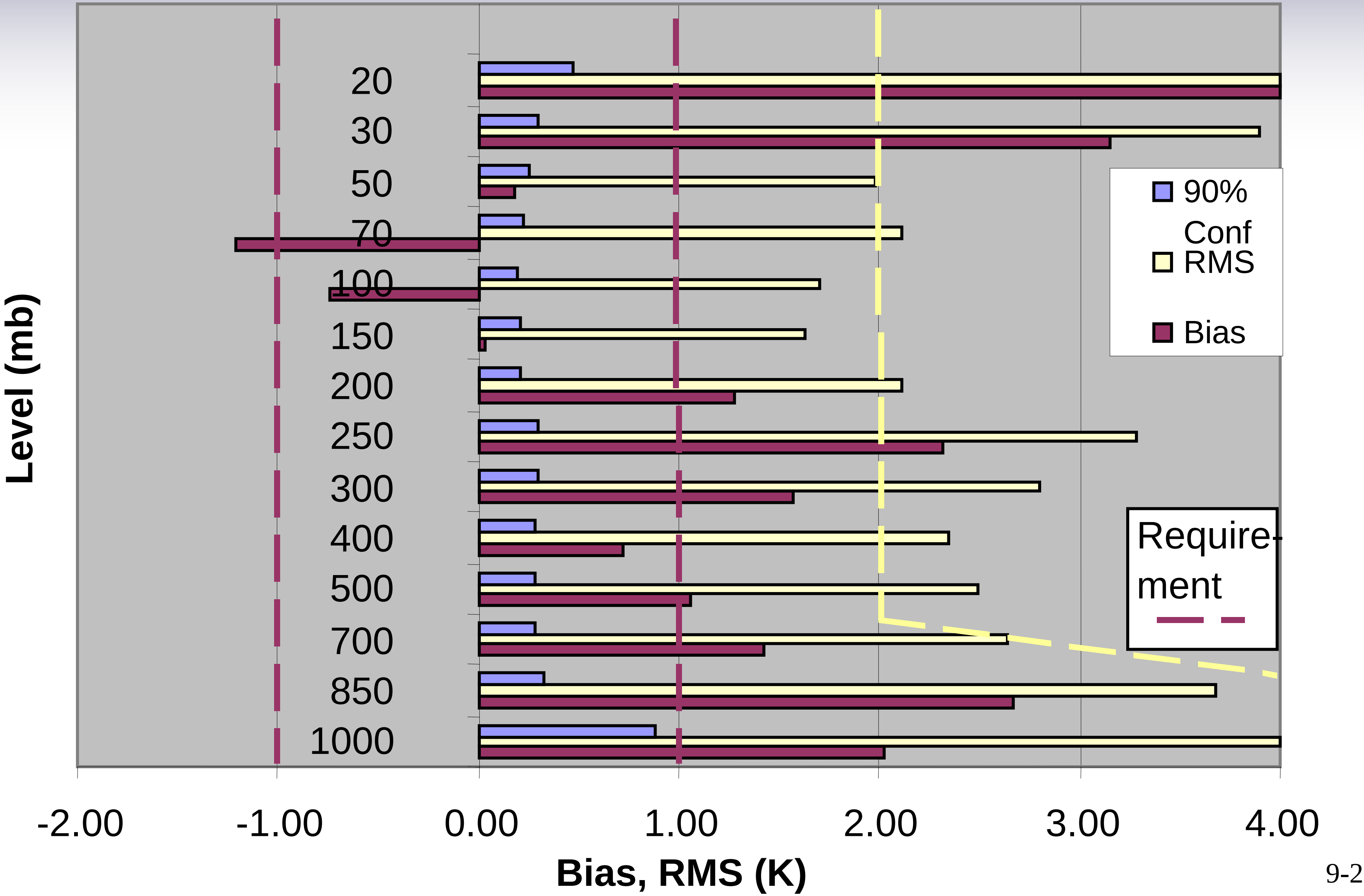

January 2004 R5 RAOB

D-matrix = 3

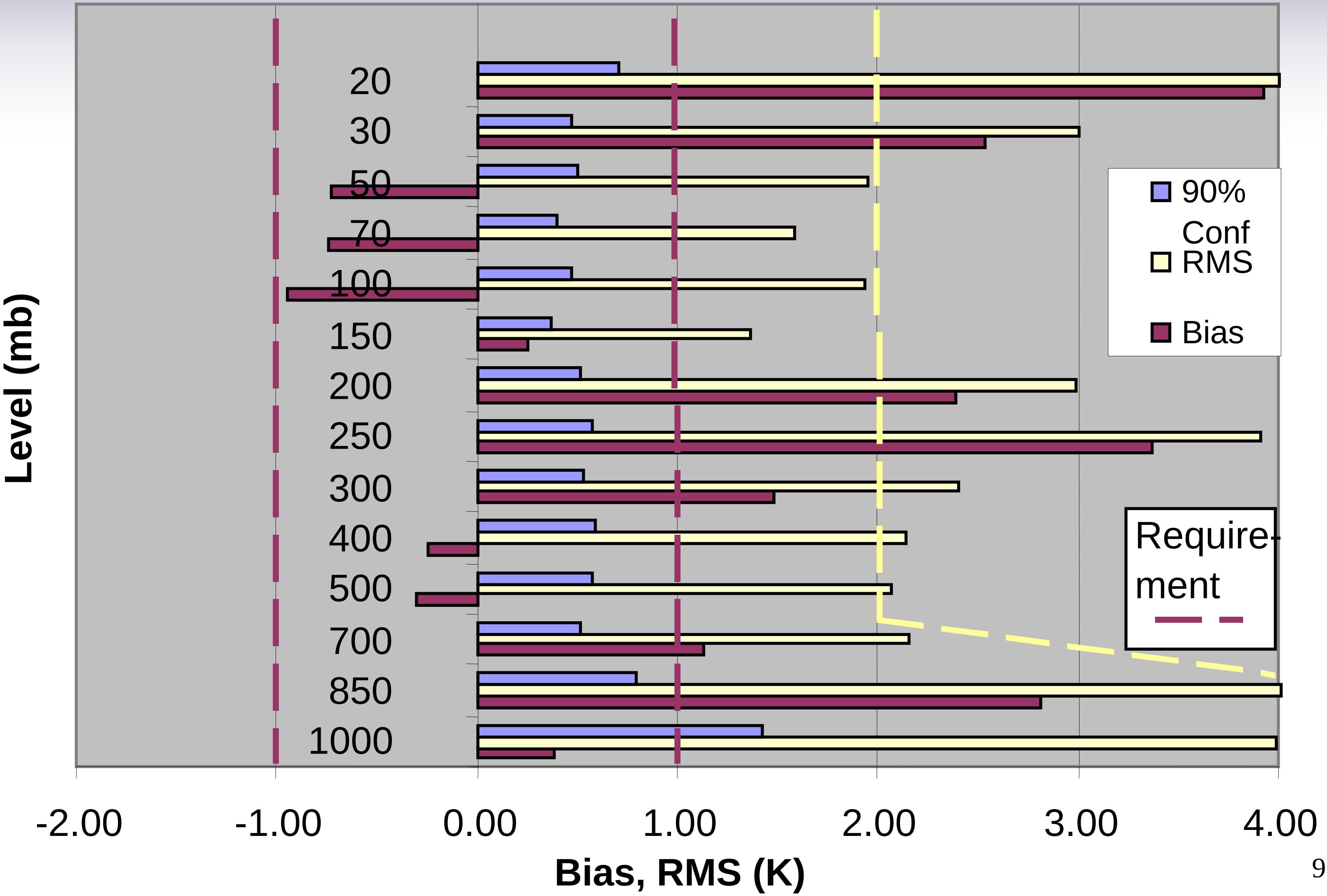

Map of 1000 mb Bias
EDR – ECMWF, Ascending Orbits, 2003 JD 341

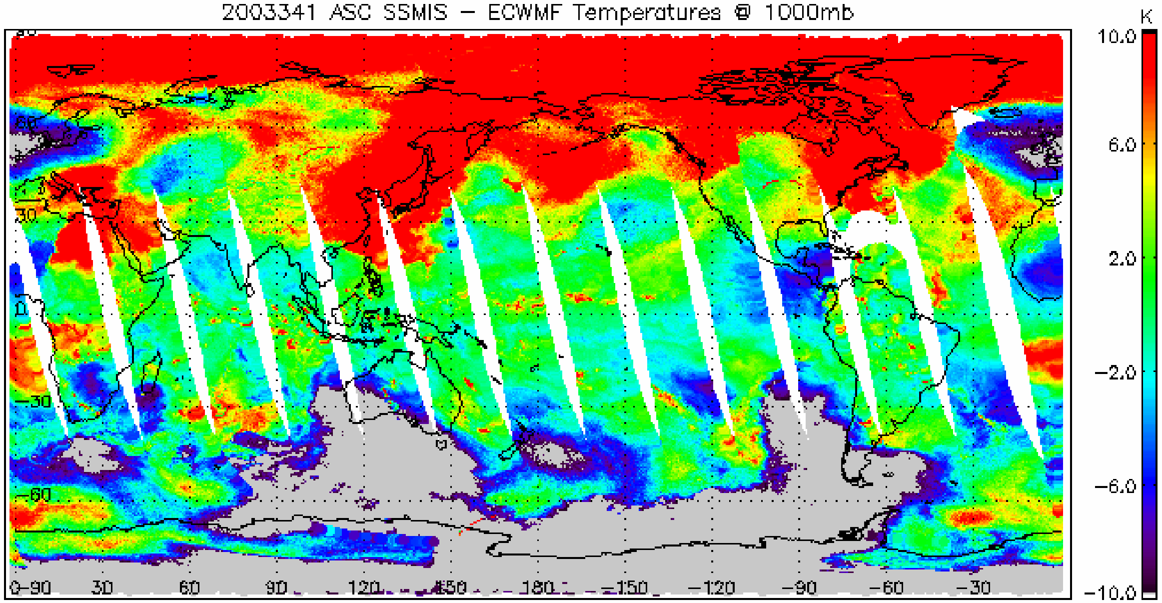

GOES IR Composite 1200 UT

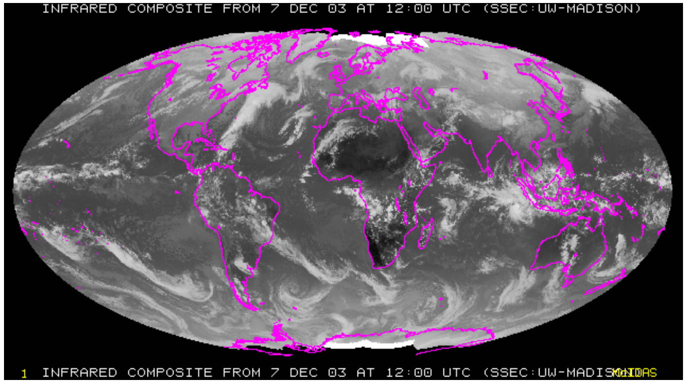

D-Matrix Type

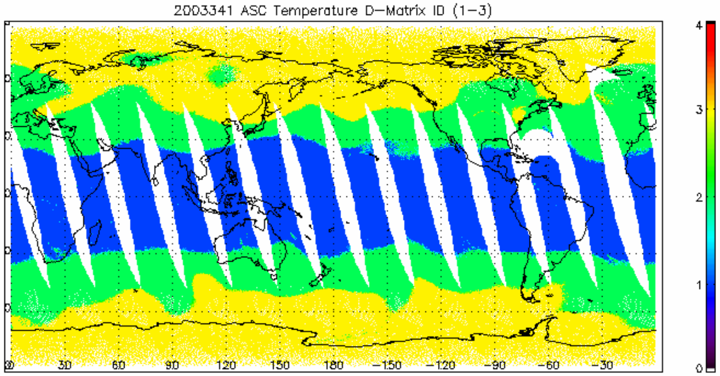

Map of 1000 mb Bias
EDR – ECMWF, Descending Orbits, 2003 JD 341

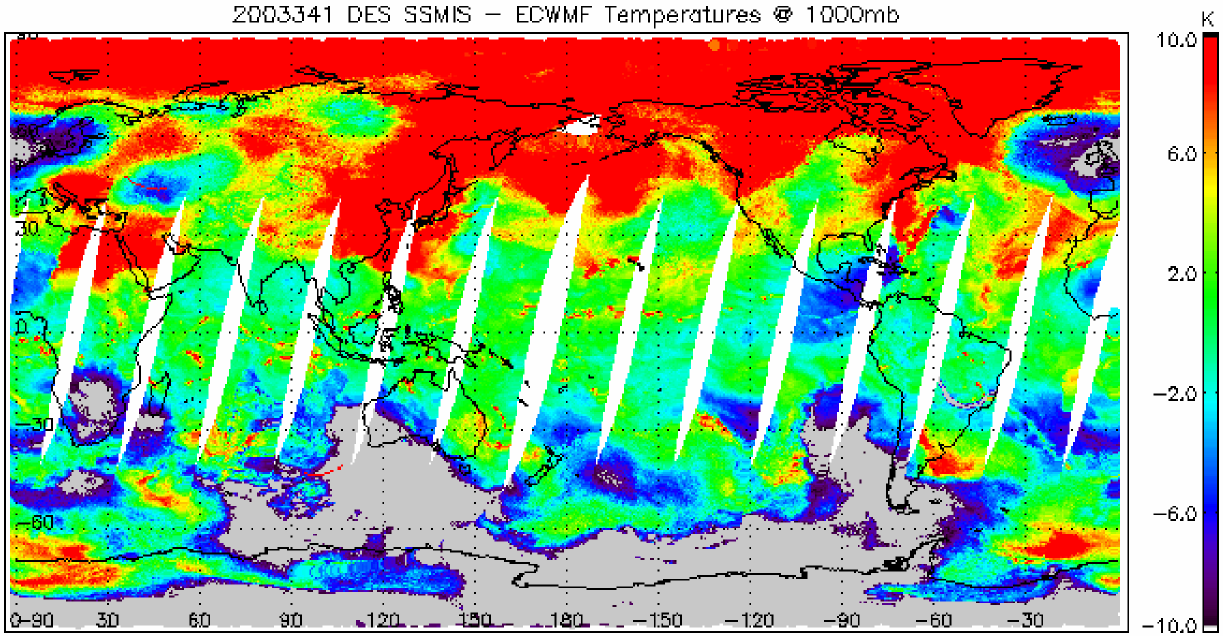

GOES IR Composite 1200 UT

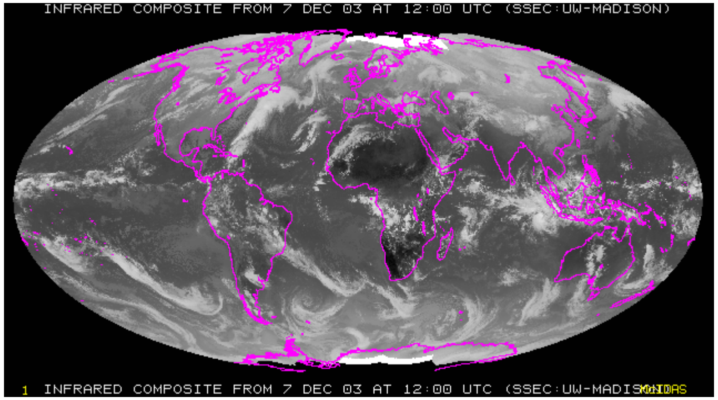

D-Matrix Type

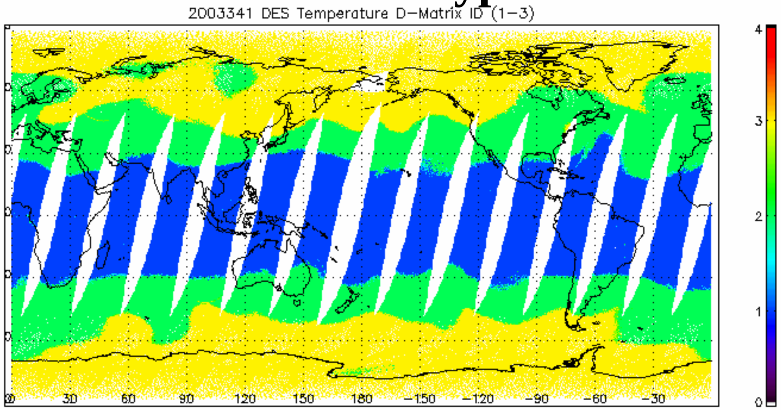

Map of 1000 mb Bias
EDR – ECMWF, Ascending Orbits, 2003 JD 311

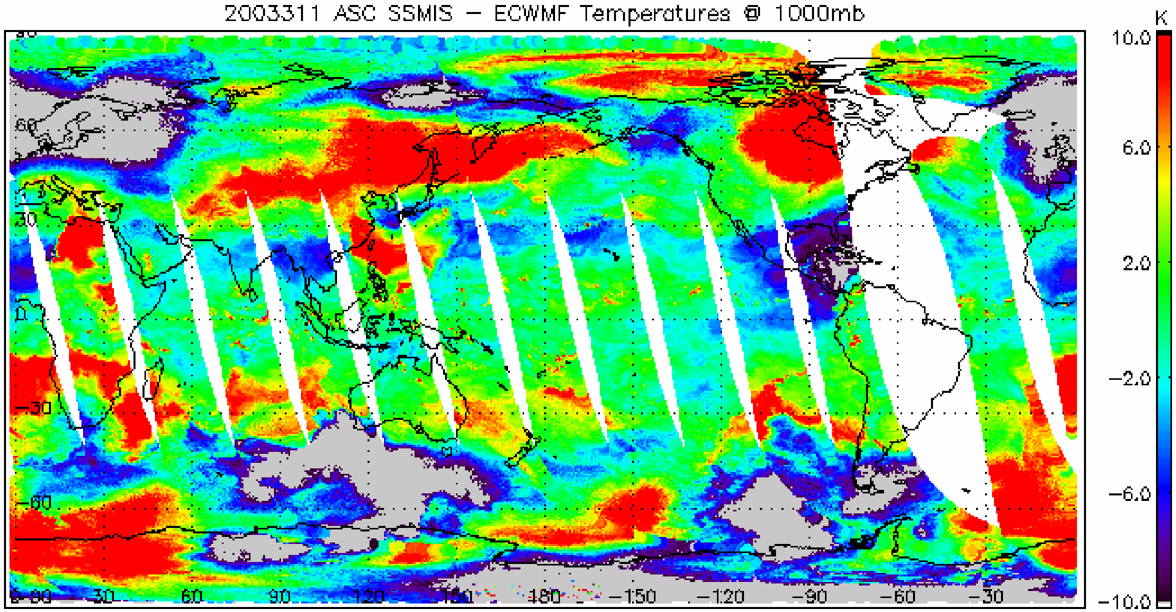

GOES IR Composite 1500 UT

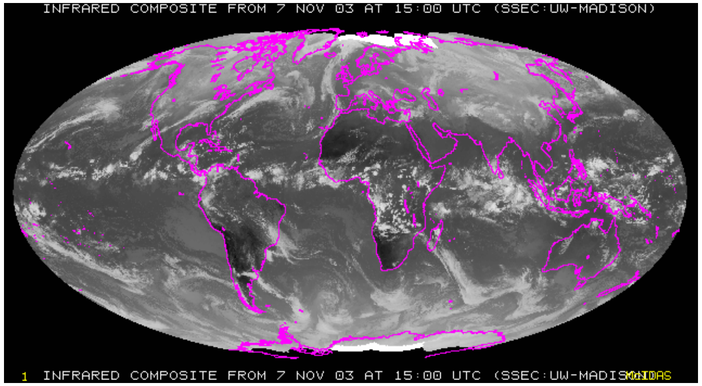

D-Matrix Type

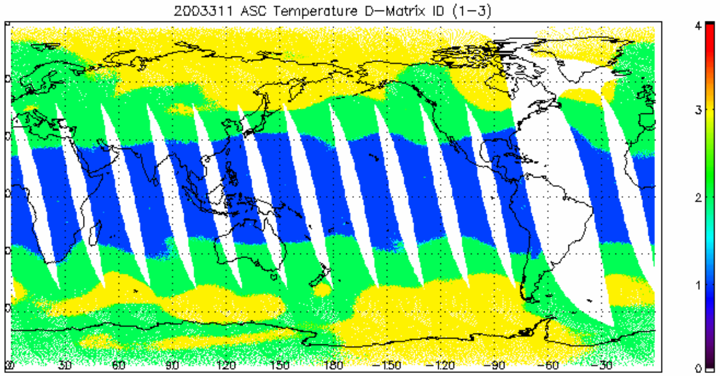

Map of 500 mb Bias
EDR – ECMWF, Ascending Orbits, 2003 JD 311

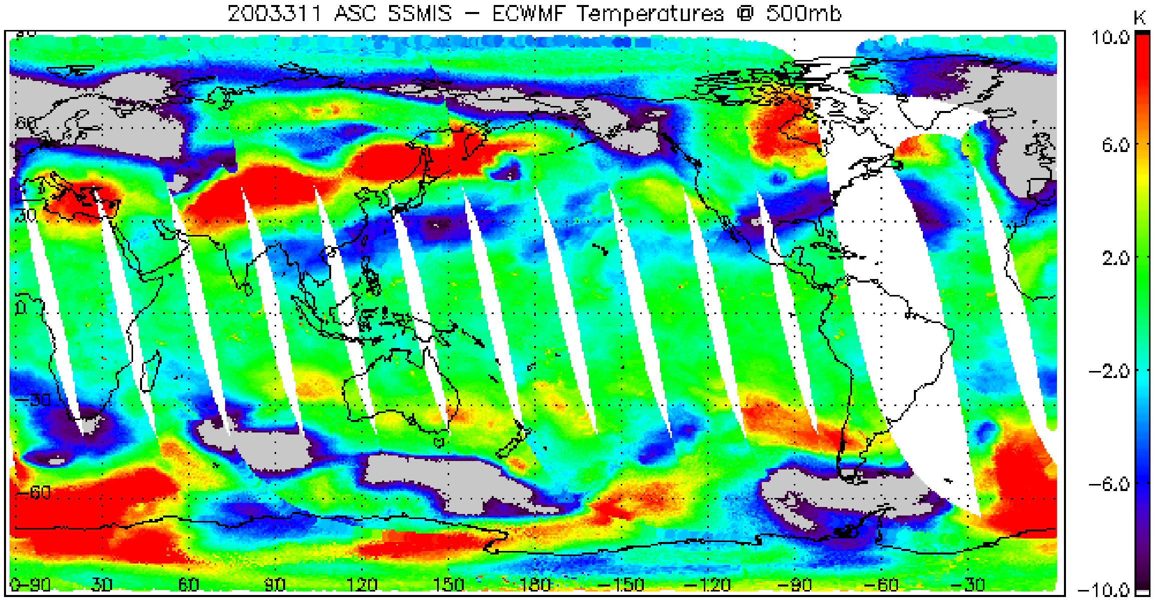

GOES IR Composite 1500 UT

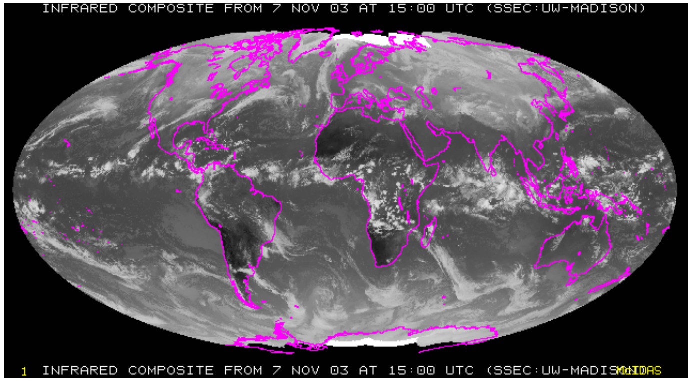

D-Matrix Type

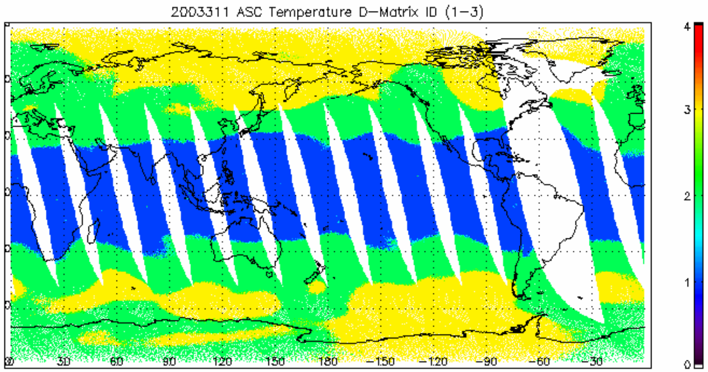

Map of 500 mb Bias
EDR – ECMWF, Ascending Orbits, 15 Feb 2005

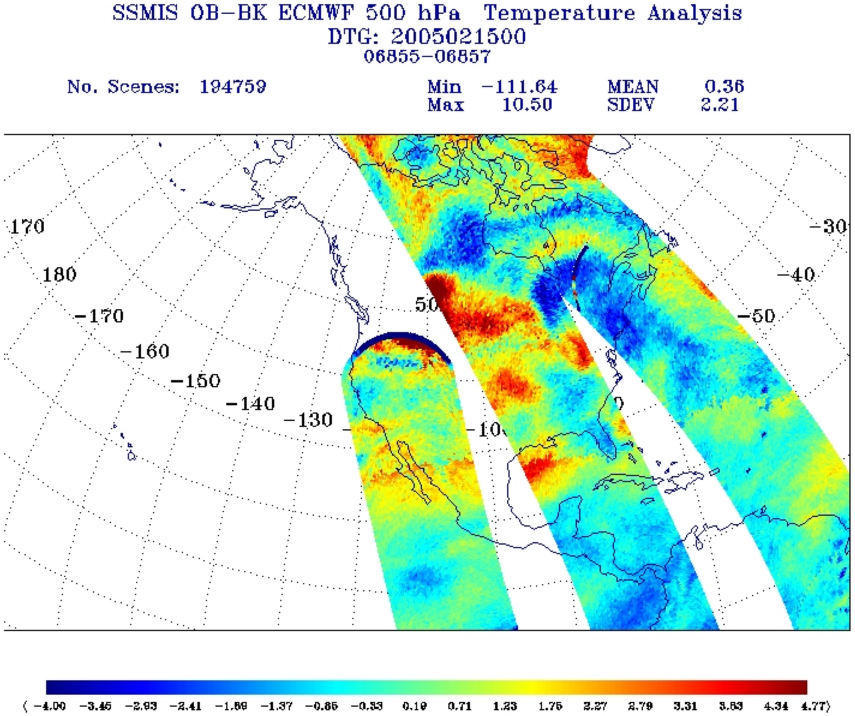

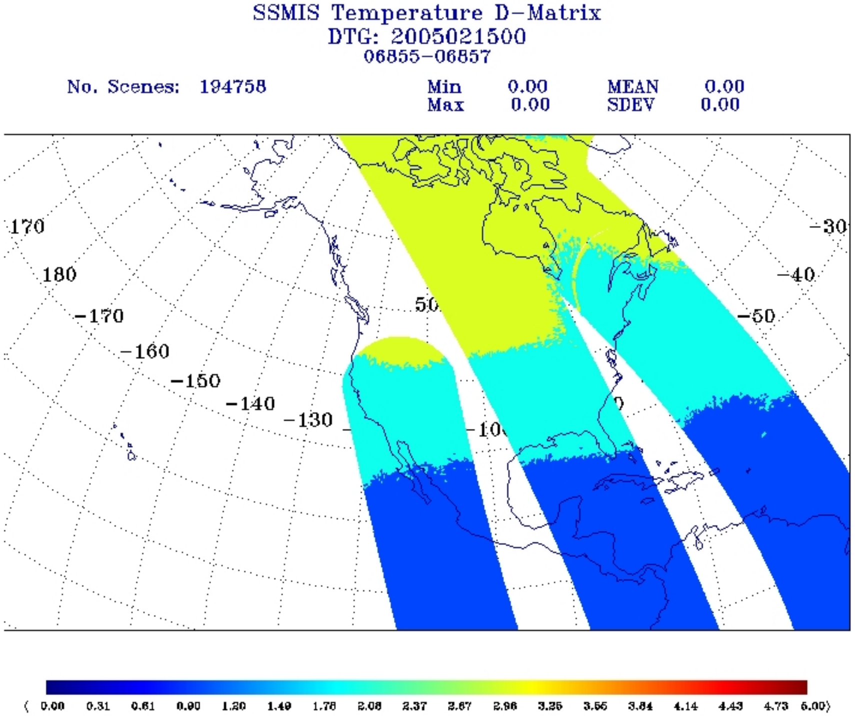

Map of 500 mb Bias
EDR – ECMWF, Descending Orbits, 14 Mar 2005

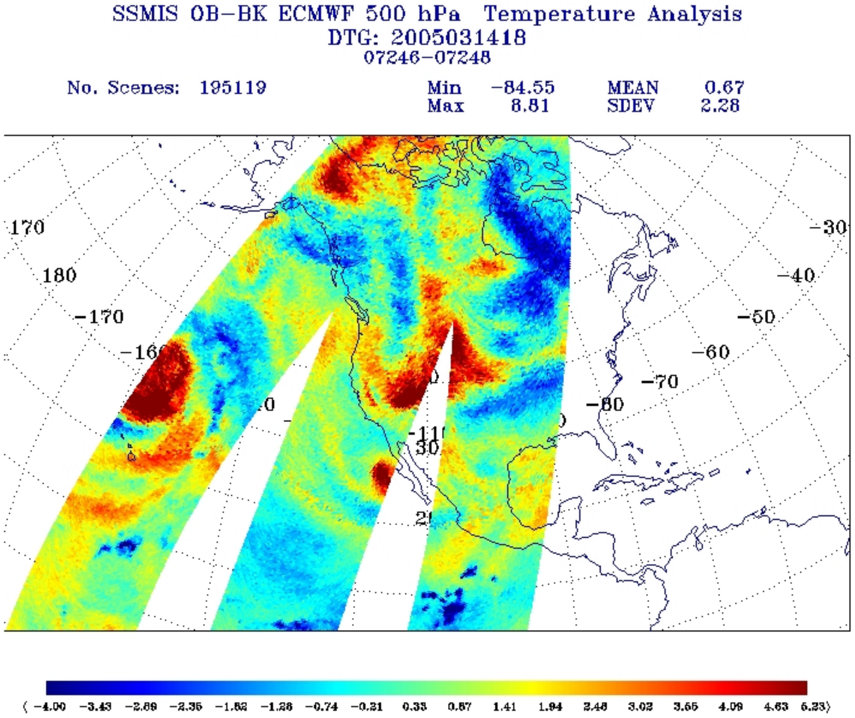

SSMIS OB−BK ECMWF 500 hPa Temperature Analysis
DTG: 2005031418
07246−07248

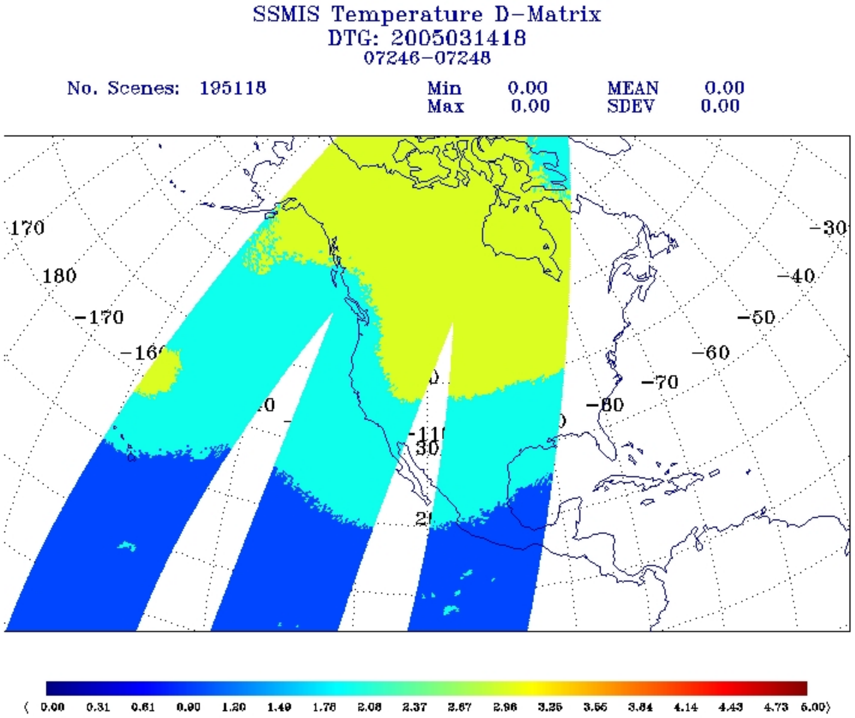

SSMIS Temperature D−Matrix
DTG: 2005031418
07246−07248

Map of 200 mb Bias
EDR – ECMWF, Ascending Orbits, 15 Feb 2005

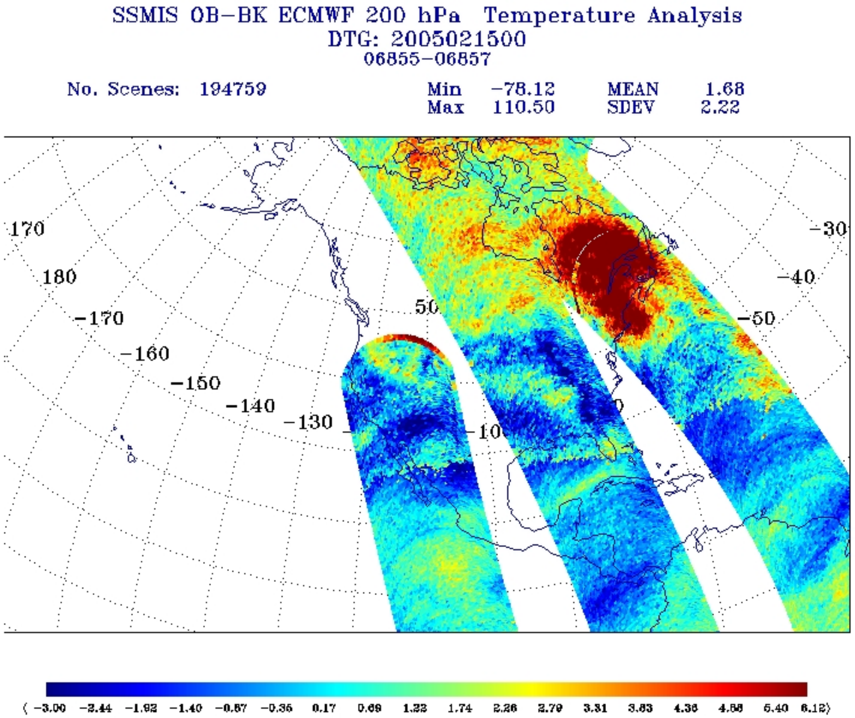
SSMIS OB−BK ECMWF 200 hPa Temperature Analysis
DTG: 2005021500
06855−06857

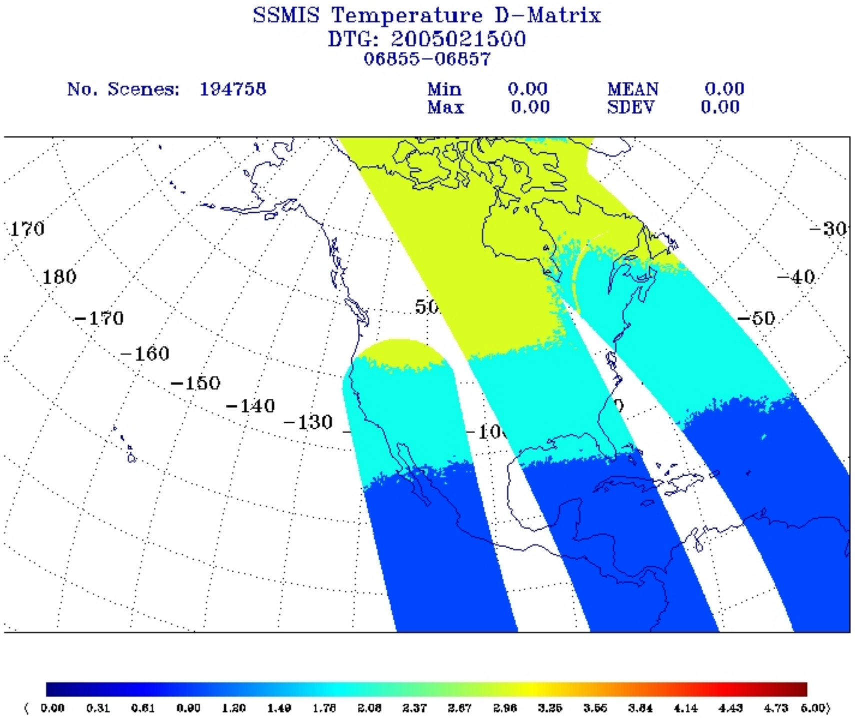
SSMIS Temperature D−Matrix
DTG: 2005021500
06855−06857

Map of 100 mb Bias
EDR – ECMWF, Ascending Orbits, 9 Mar 2005

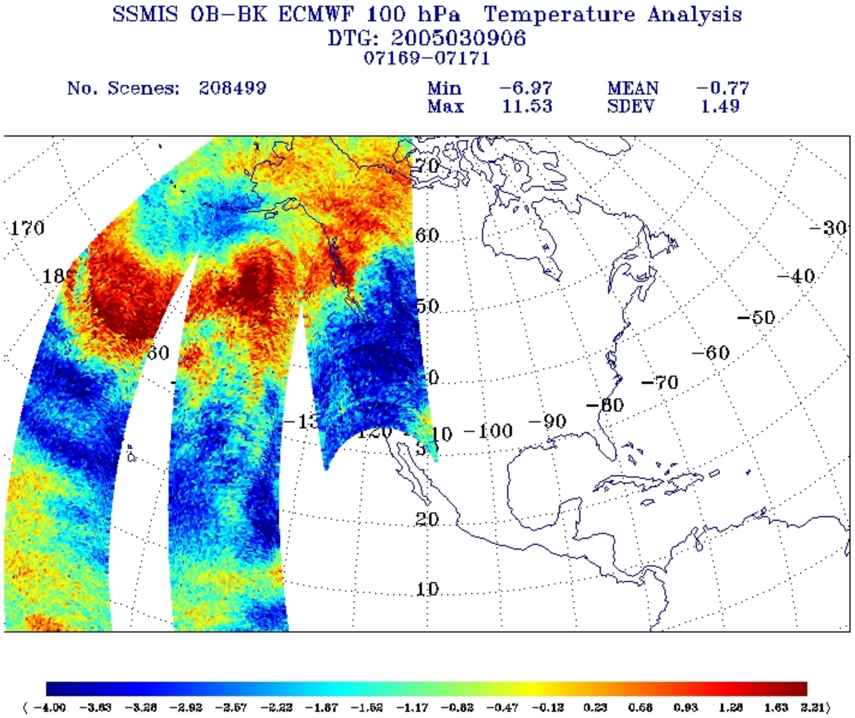

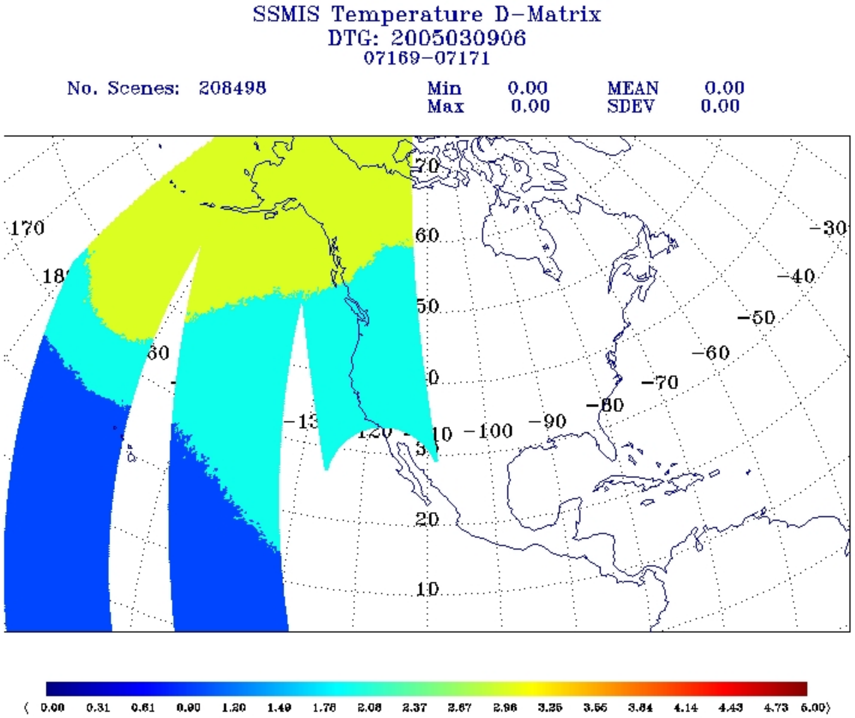

Raob Temperature Map
850 mb 2004 Julian Day 90

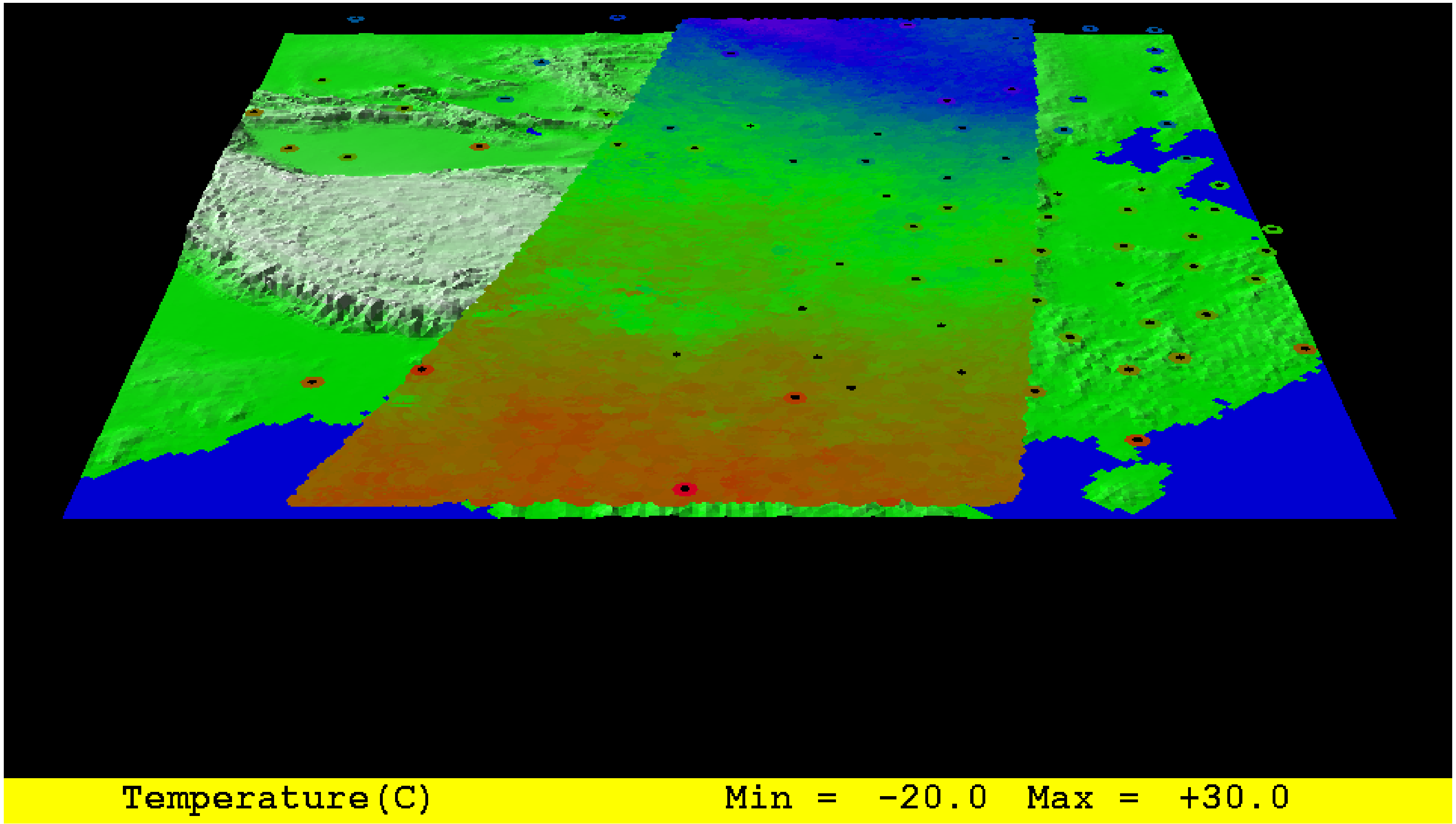

Section 9.5 Validation of Water Vapor EDR Retrievals

25 water vapor D-matricies

Selection involves channel 1 polarization which is V rather than specified H

Type based on

- **Ocean**
  Water vapor content and atmospheric temperature (5)
- **Land**
  High altitude water vapor and atm temp (3) * 5 altitudes
- **Coast**
  Atmosphere D-Matrix temperature type (3)
- **Sea Ice**
  Atmospheric temperature (2)

Limited Validation

- Decision tree for retrieval type involves polarization-dependent SDRs.
- Full evaluation delayed pending results from H-polarized sensor on F-17.

RH and SH EDRs Versus Raobs
Type 1 Temperature D-Matrix Winter 2003 R5 EDRS

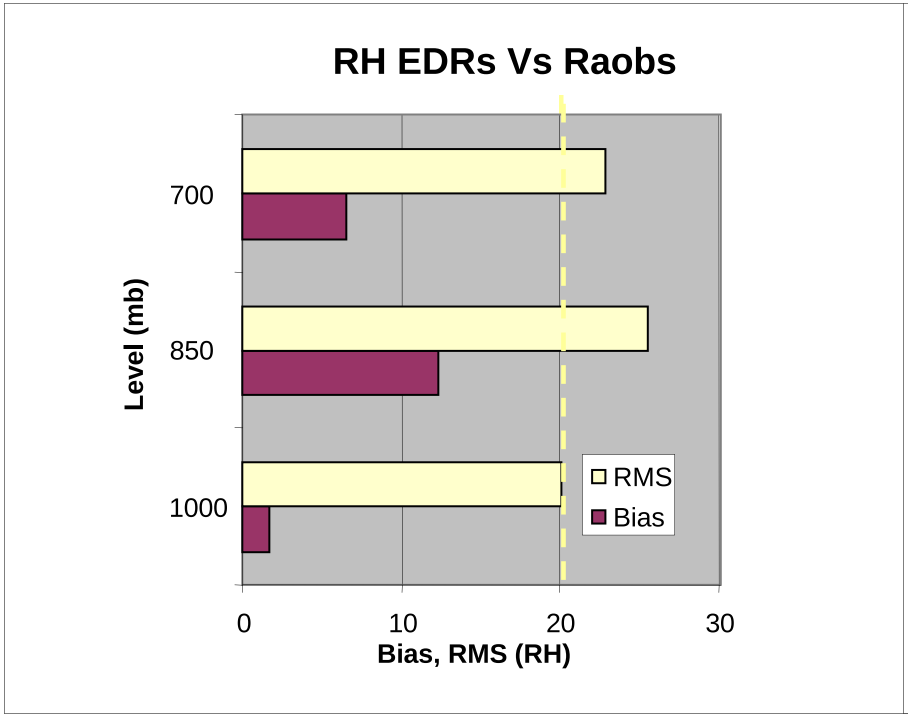

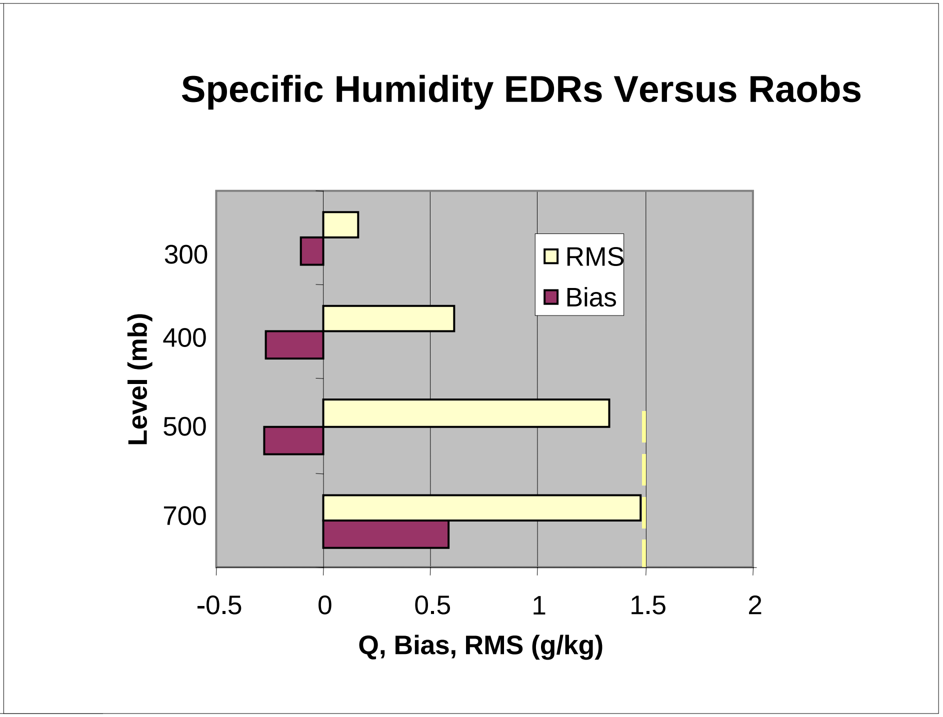

RH and SH EDRs Versus Raobs
Type 1 Temperature D-Matrix Jan 2004 R5 EDRS

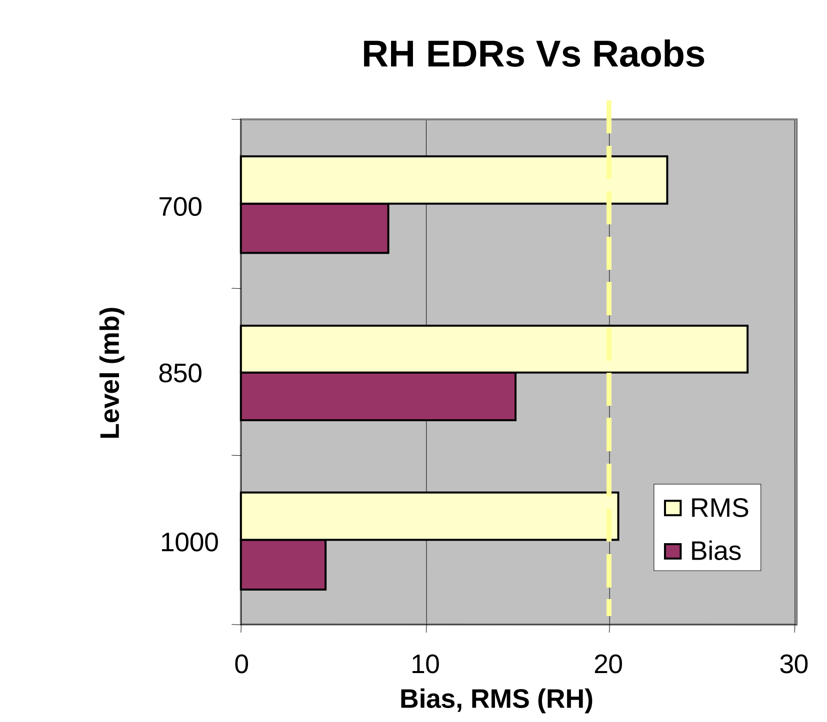

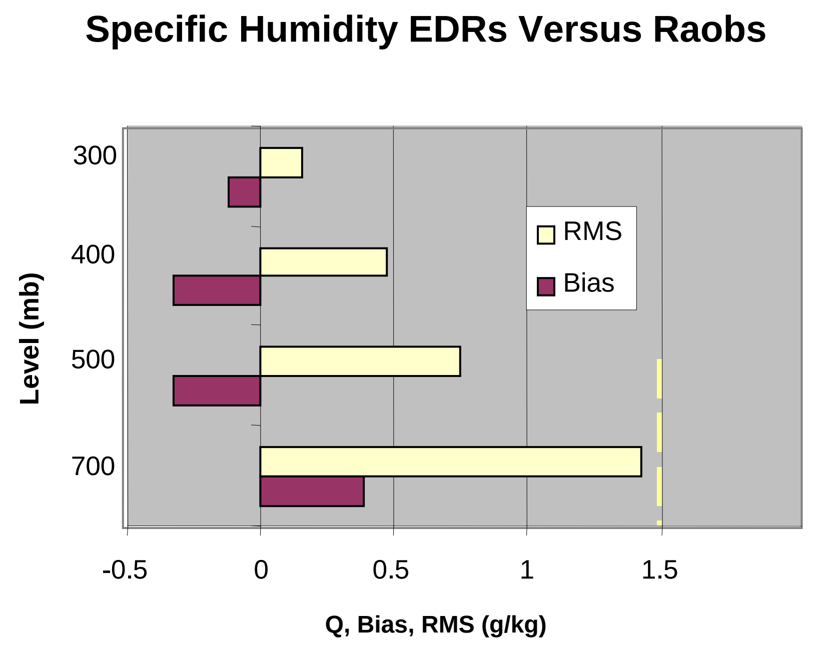

RH and SH EDRs Versus Raobs
Type 2 Temperature D-Matrix
Jan 2004 R5 EDRS

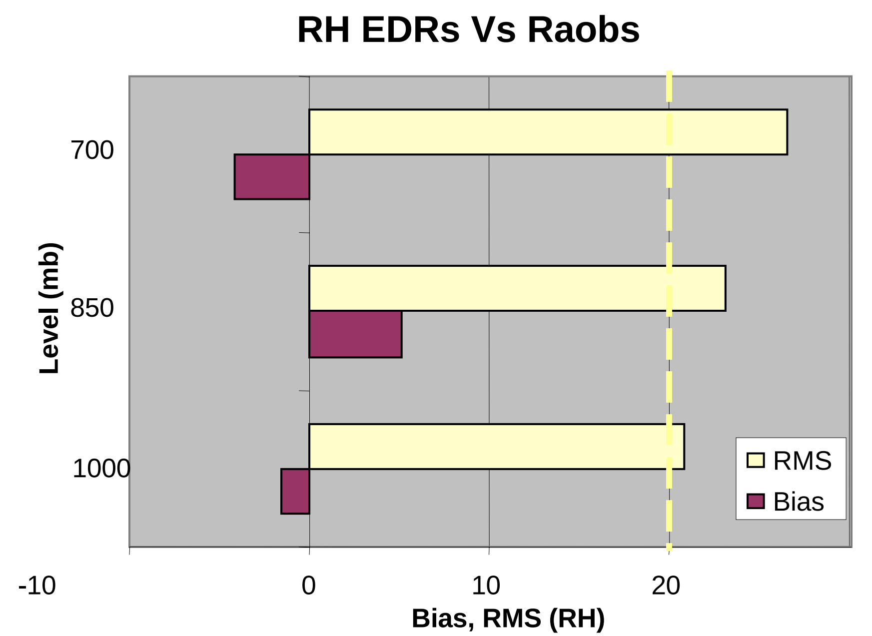

RH EDRs Vs Raobs

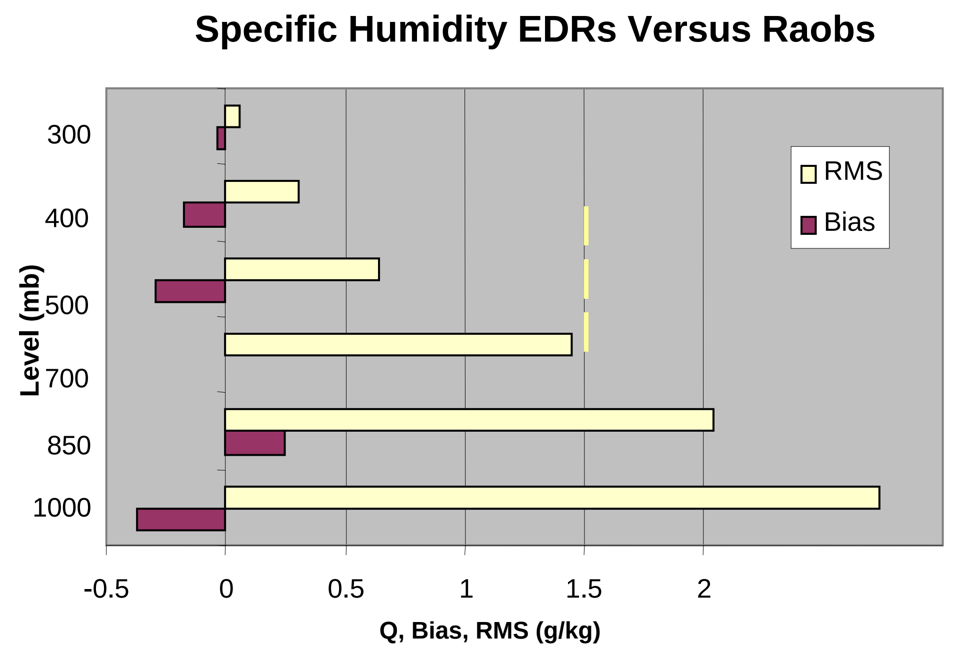

Specific Humidity EDRs Versus Raobs

RH EDRs Versus Lidar
Barking Sands, Winter 2003 R5 EDRs

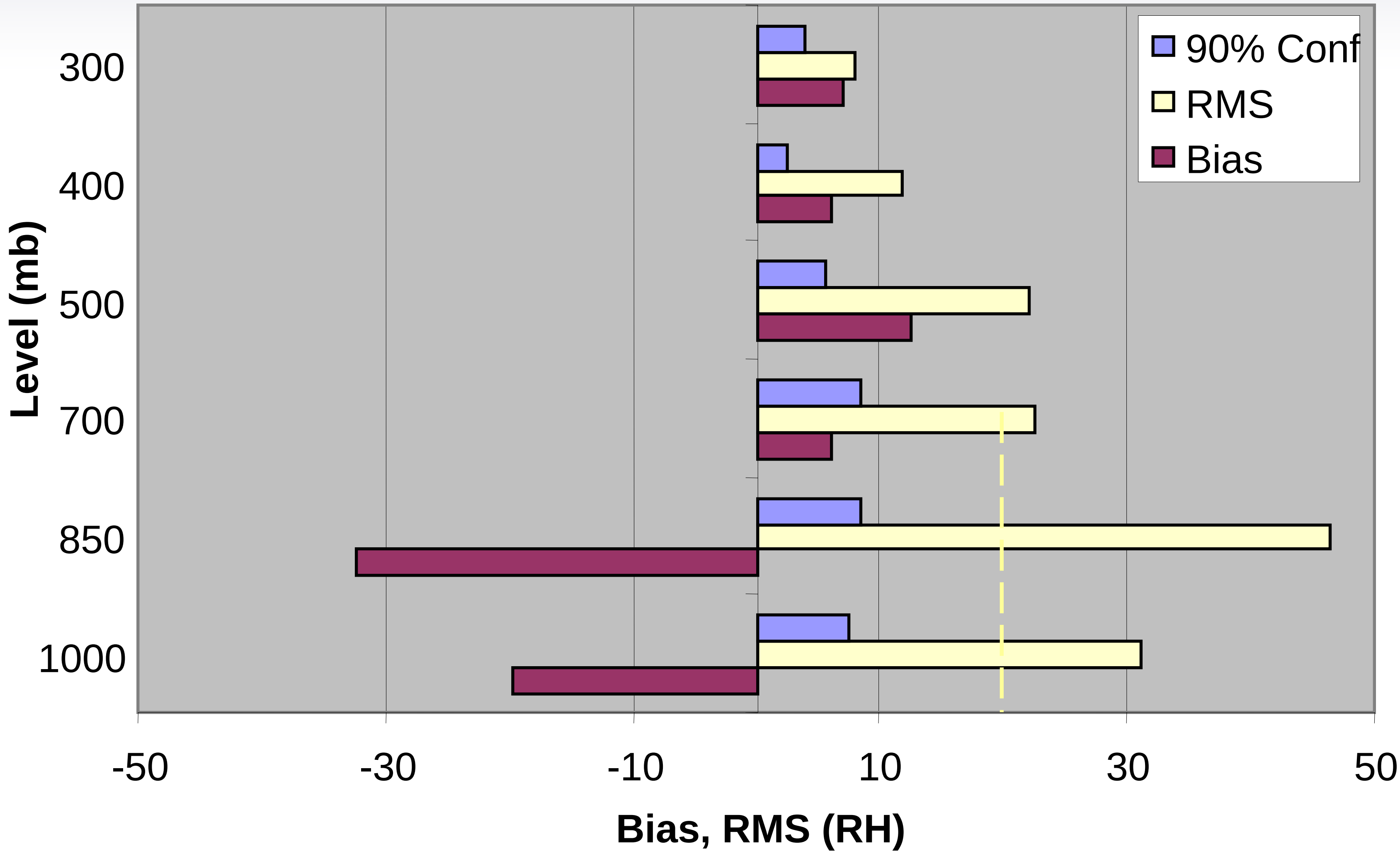

Specific Humidity EDRs Versus Lidar
Barking Sands, 2004 R4 EDRs

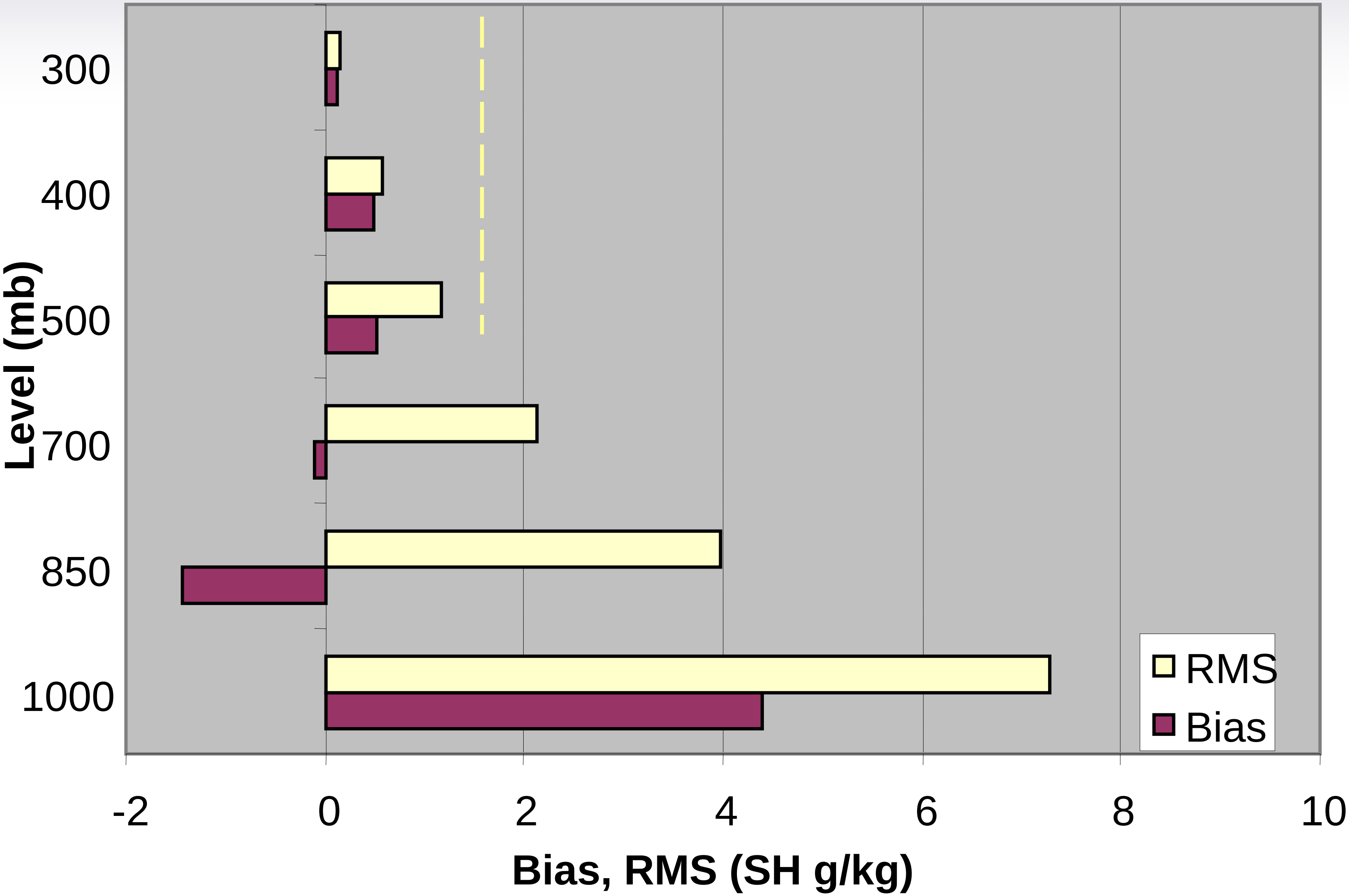

Map of RH EDRs versus Raobs
850 mb 2004 Julian Day 90

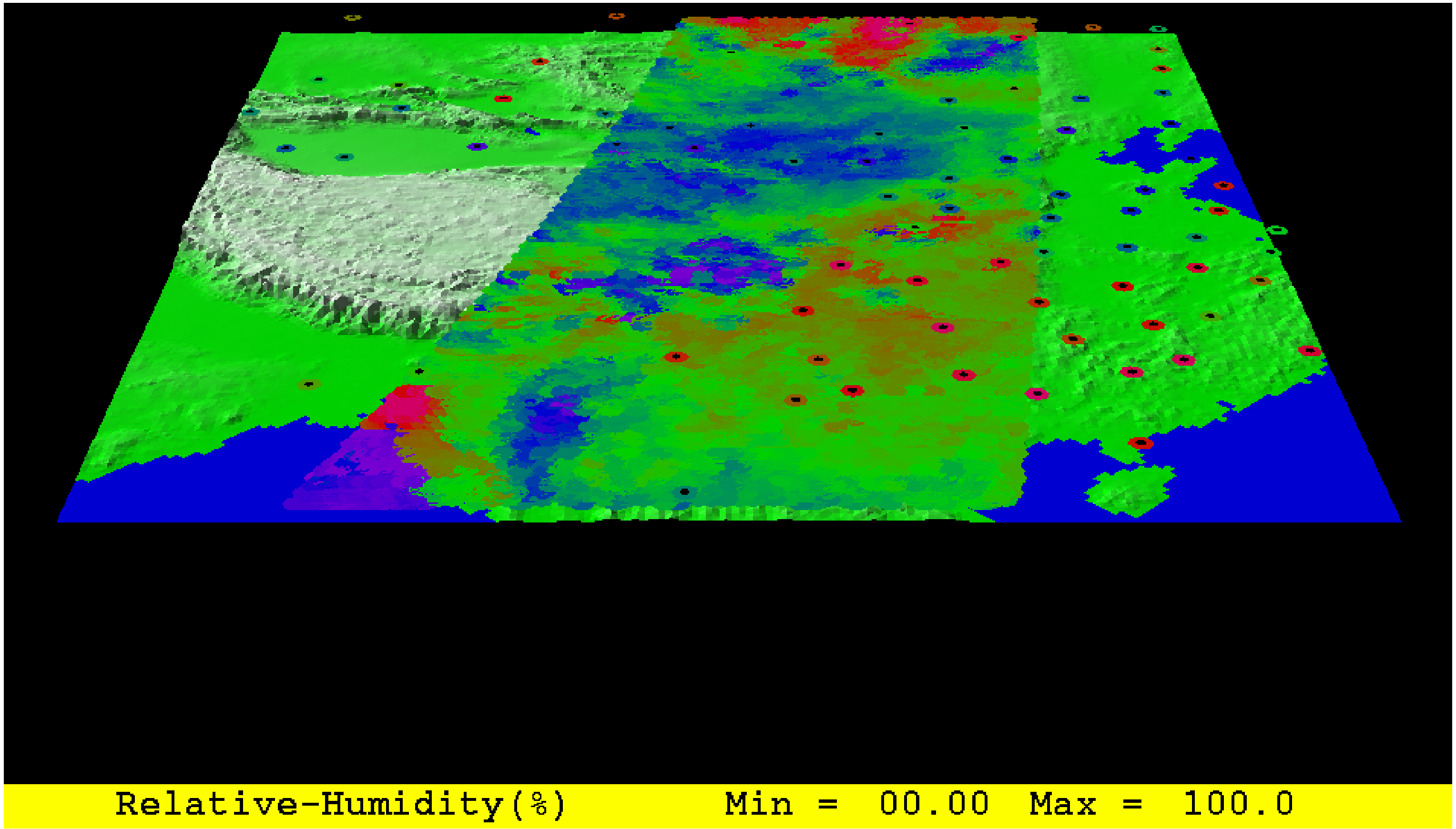

Maps of RH Bias
700 mb EDRs – ECMWF, D-Matrix 1-10, 14 Mar 2005

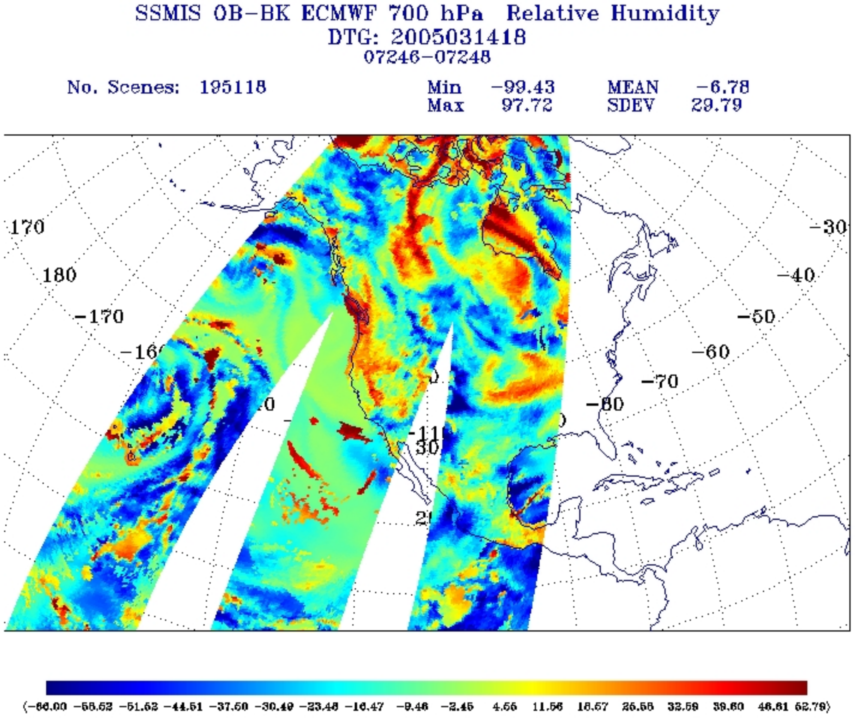

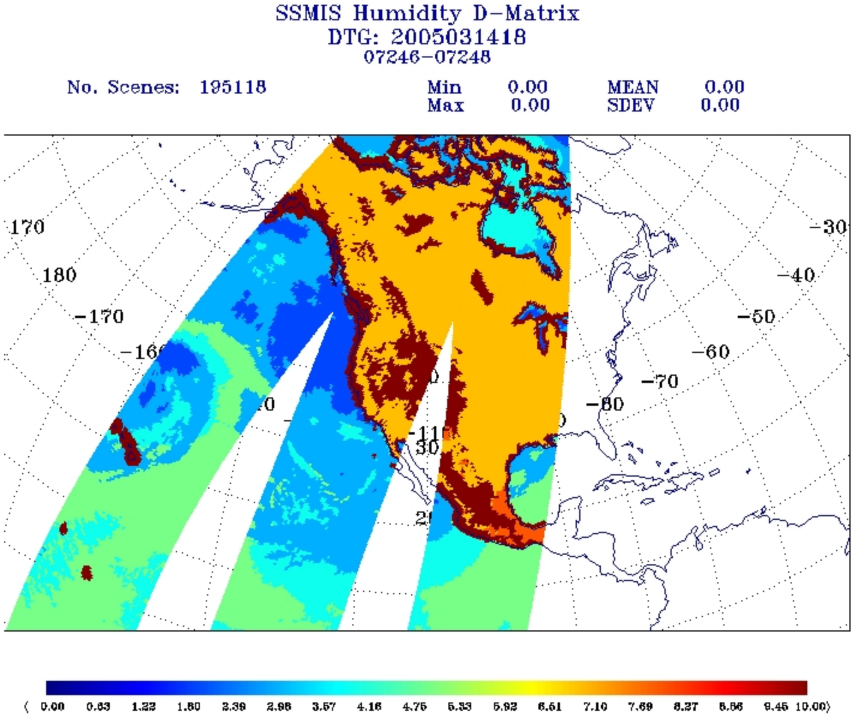

Maps of RH Bias
500 mb EDRs – ECMWF, Various D-Matrix Types

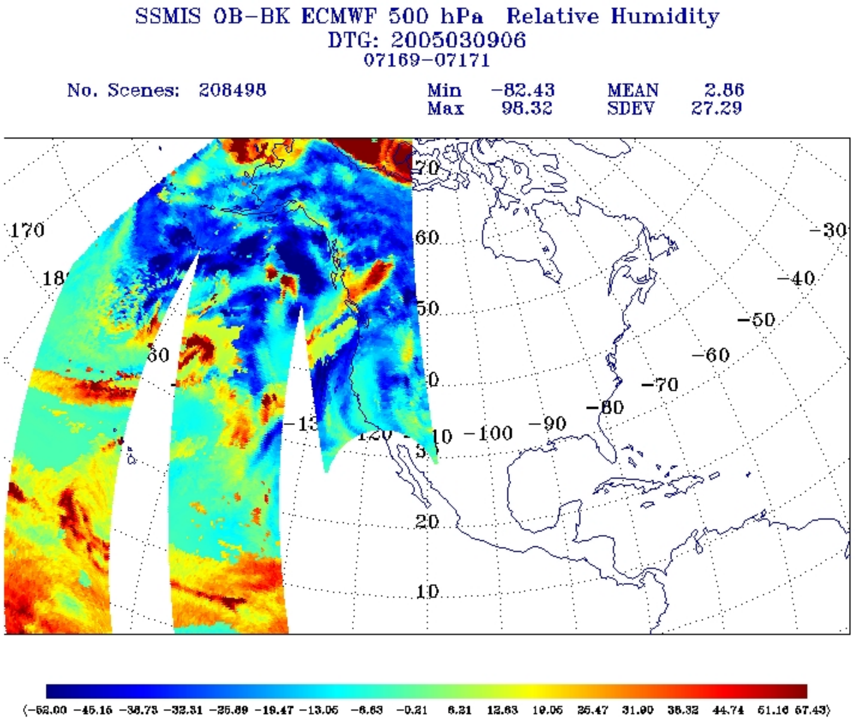

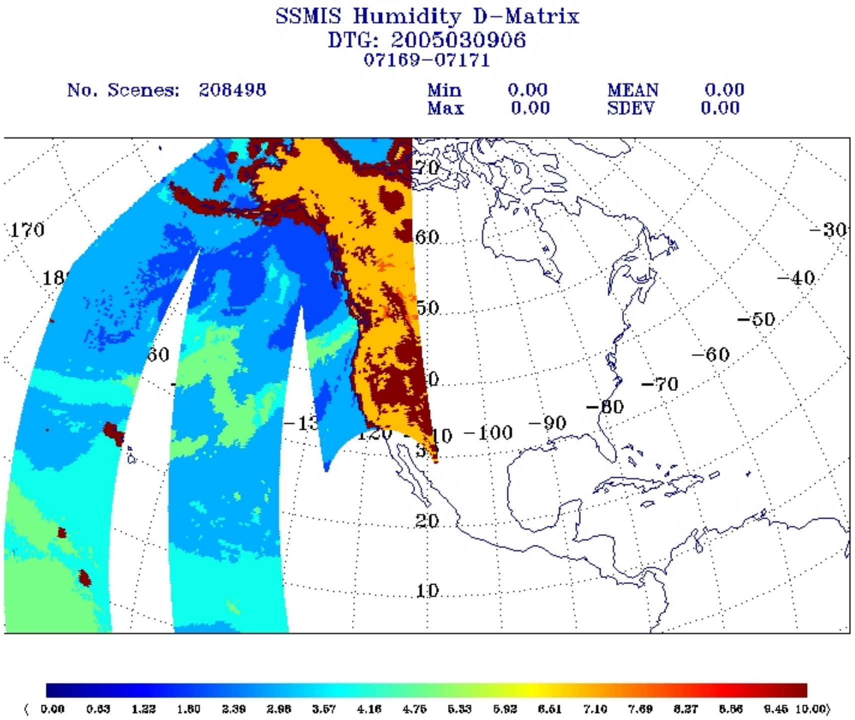

Maps of RH Bias
300 mb EDRs – ECMWF, Various D-Matrix Types

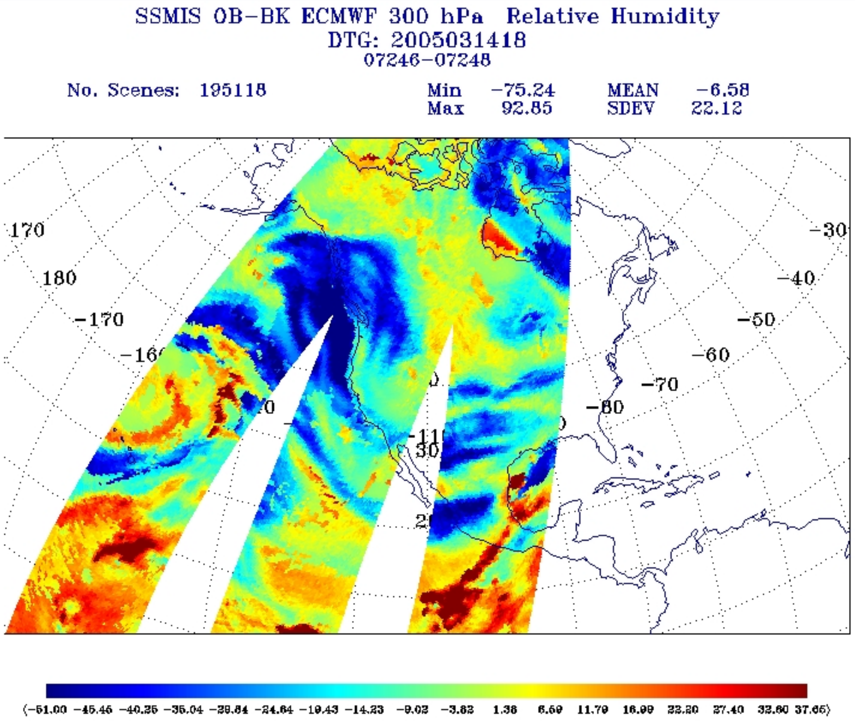

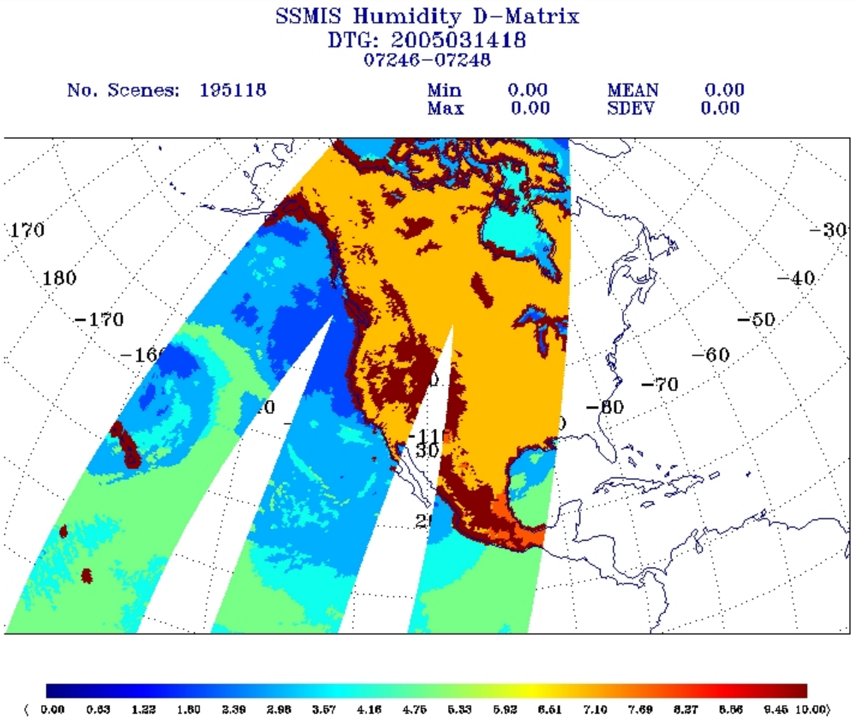

Section 9.6 Tropopause Temperature Retrieval Vs. ECMWF (Rev 5 EDRs Nov. 2003 to Jan. 2004)

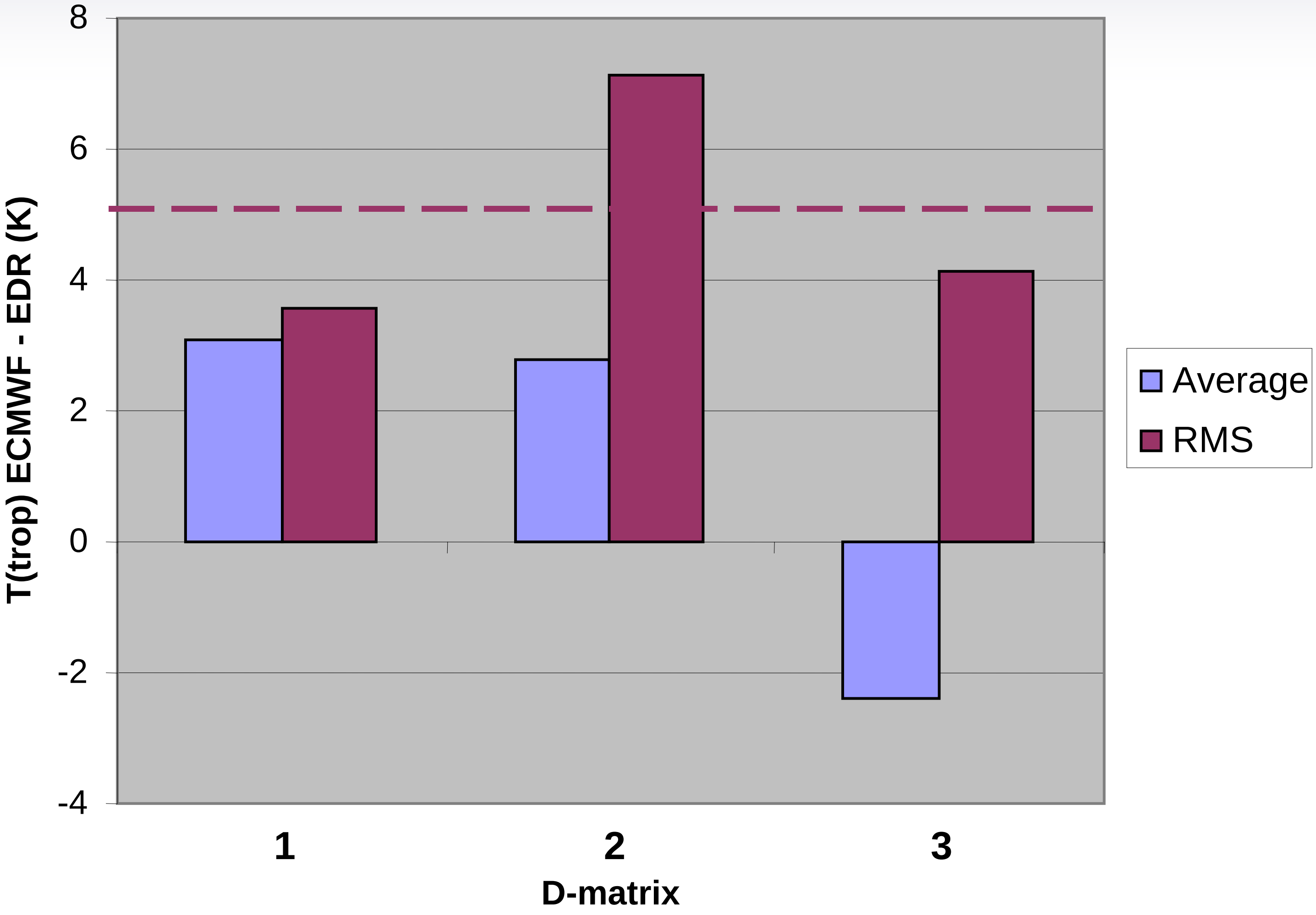

SSMIS Tropopause Temperature Versus ECMWF

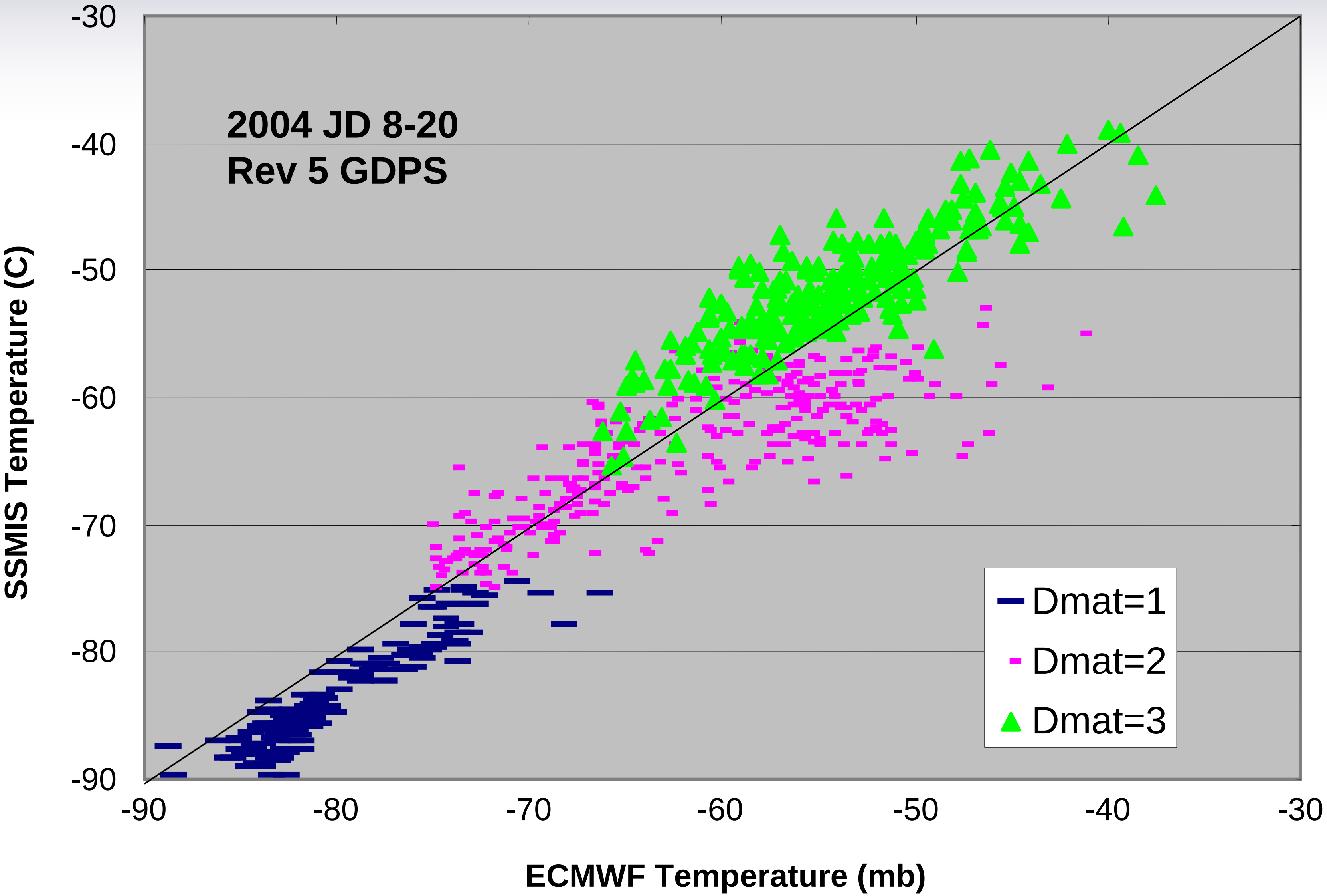

Section 9.7 Tropopause Pressure Retrieval Versus ECMWF (Nov. 2003 to Jan. 2004 Rev 5 EDRs)

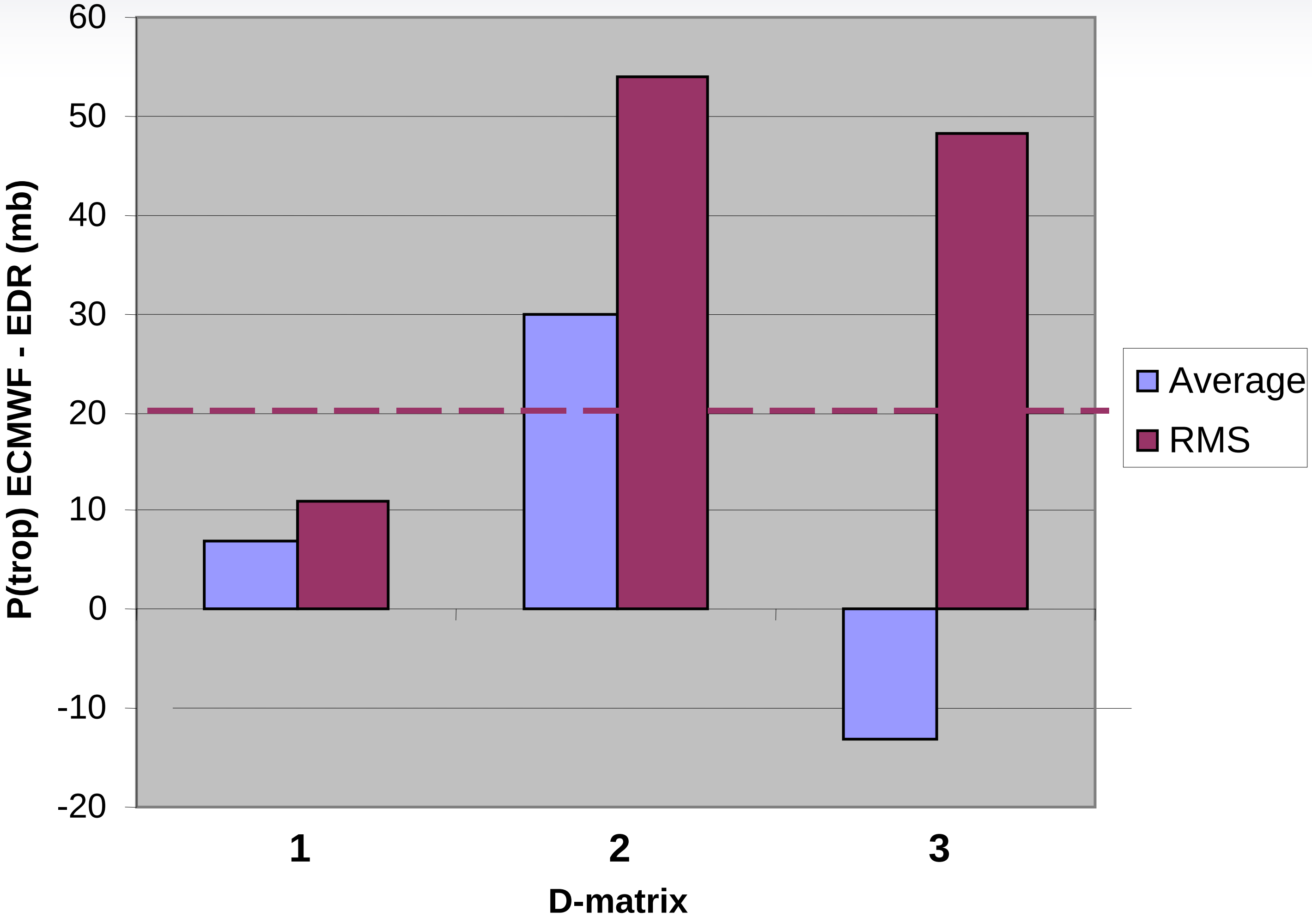

SSMIS Tropopause Pressure Versus ECMWF

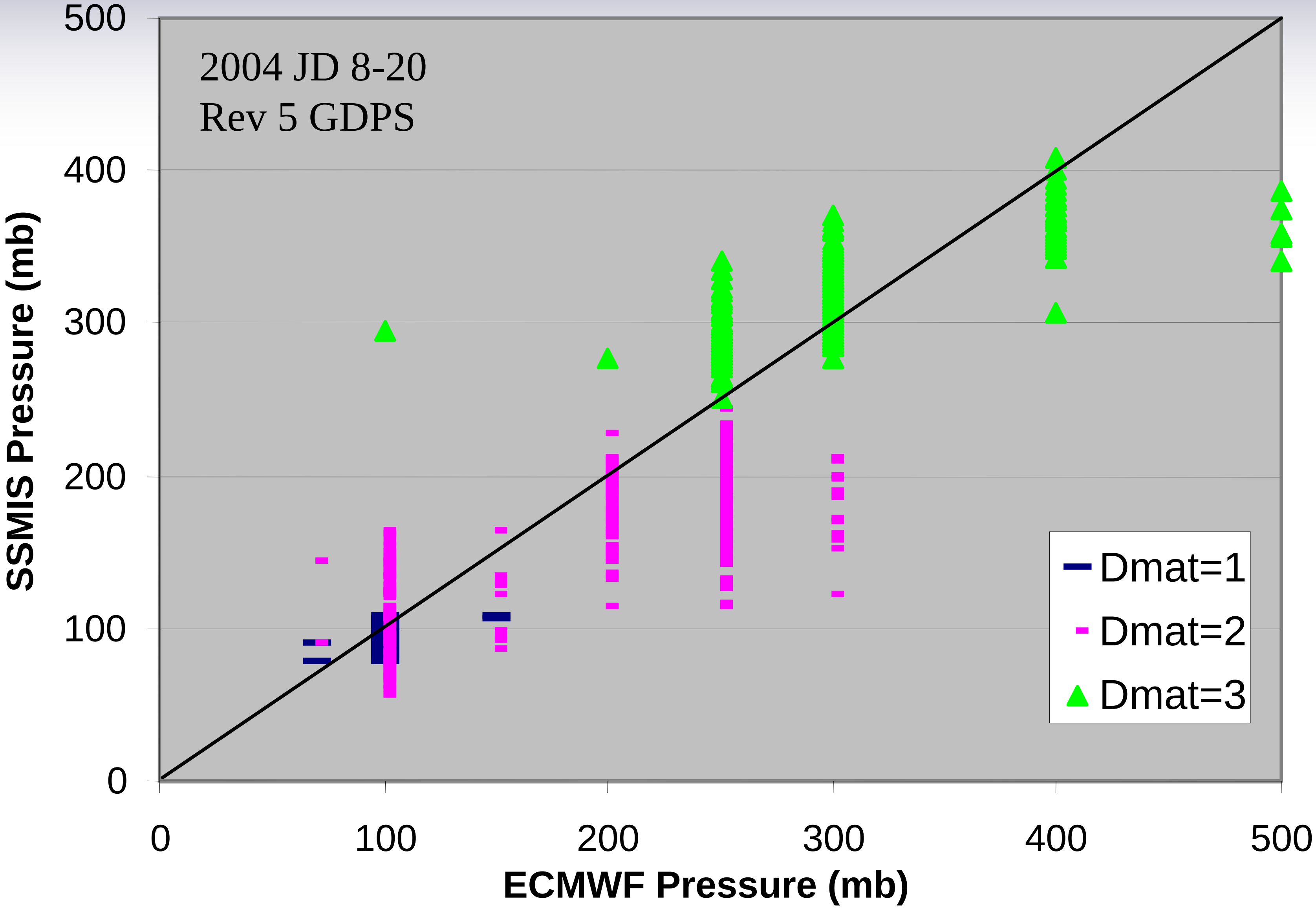

Section 9.8 Geopotential Height Versus ECMWF (Nov. 2003 to Jan. 2004)

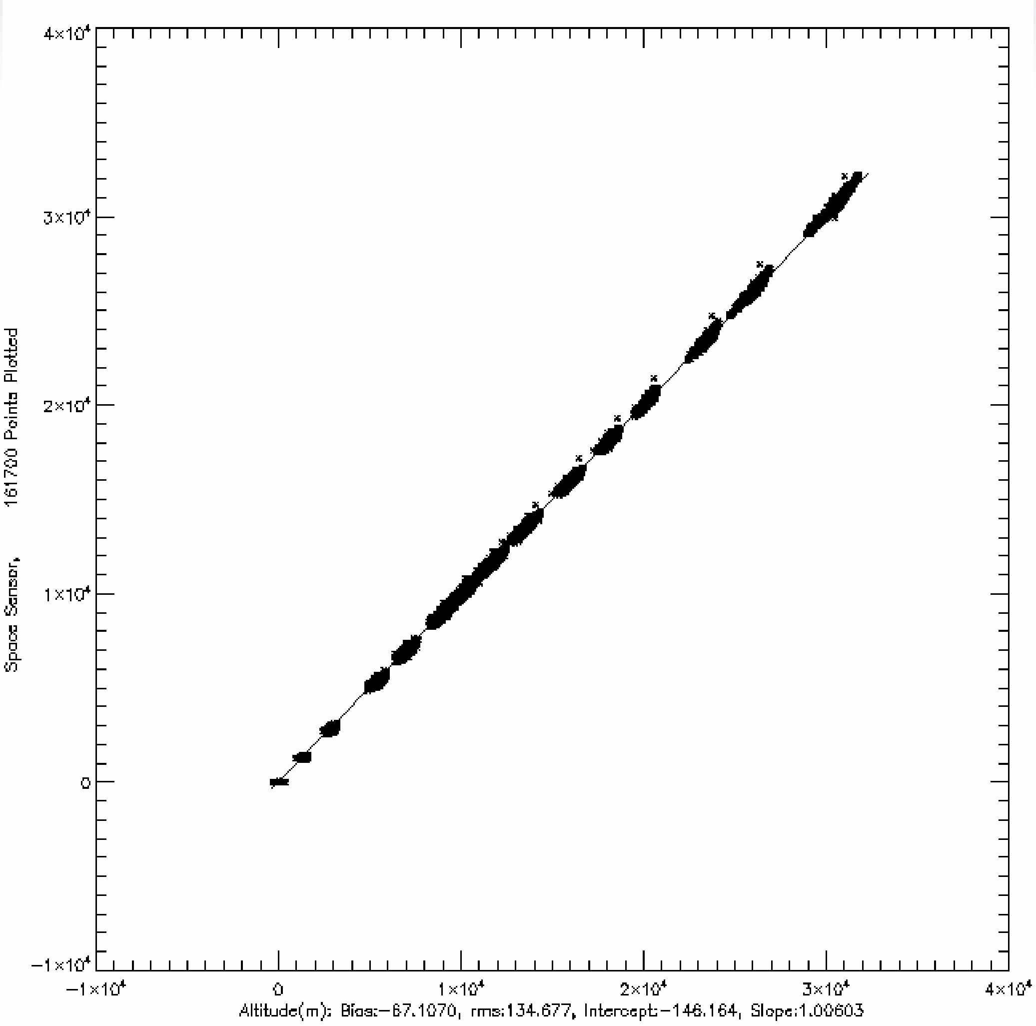

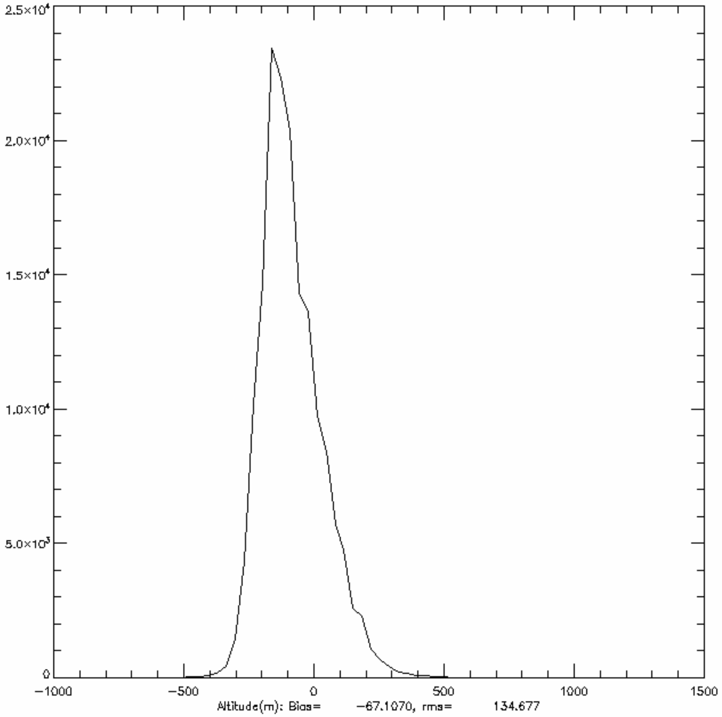

Section 9.9 Summary of SSMIS EDR Retrieval Performance

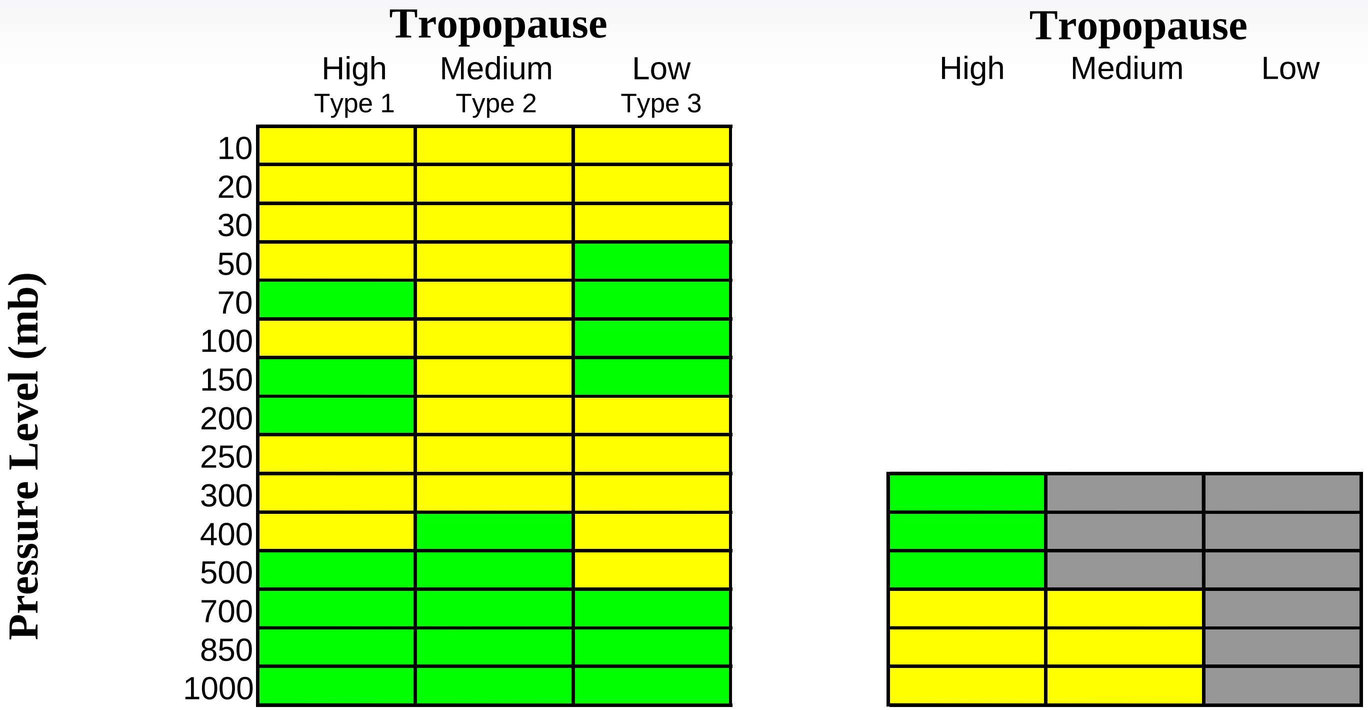

Pressure Level (mb)	Temperature Tropopause High Type 1	 Medium Type 2	 Low Type 3	Water Vapor Tropopause High	 Medium	 Low
10	🟨	🟨	🟨			
20	🟨	🟨	🟨			
30	🟨	🟨	🟨			
50	🟨	🟨	🟩			
70	🟩	🟨	🟩			
100	🟨	🟨	🟩			
150	🟩	🟨	🟩			
200	🟩	🟨	🟨			
250	🟨	🟨	🟨			
300	🟨	🟨	🟨	🟩	▨	▨
400	🟨	🟩	🟨	🟩	▨	▨
500	🟩	🟩	🟨	🟩	▨	▨
700	🟩	🟩	🟩	🟨	🟨	▨
850	🟩	🟩	🟩	🟨	🟨	▨
1000	🟩	🟩	🟩	🟨	🟨	▨

Green: Meets requirements Yellow: Projected to meet T spec with mods, problems expected for RH
Red: Will not meet requirements Gray: Spec probably met, performance poor

Section 9.10 Summary, Recommendations and Conclusions

Ability to Meet Requirements

Low altitude temperature retrievals (1000 - 500 mb) are mostly[1] reasonable

High altitude retrievals require bias adjustment

1000 mb RH may marginally meet requirements

850 and 700 mb RH retrievals fail requirements, may improve by readjustment

High altitude SH meets requirements[2]

Tropopause requirements are not satisfied for medium and low altitude tropopause pressure

Recommendations

Implement modifications to reduce SDR bias

Optimize temperature D-matricies to minimize bias using ECMWF and lidar

Optimize moisture D-matricies

Implement independent cloud screen for comparisons

Conclusion

Most temperature requirements should be satisfied upon implementation of recommendation.

Water vapor and tropopause requirements remain problematic

---

[1] Bias is high for type 3 retrievals (low tropopause) at 850 and 700 mb

[2] High altitude RH exceeds expectations at Barking Sands

Section 9.11
Appendix Monthly Comparisons
ECMWF-R4 EDR

Global Average Temperature Bias
2004 R4 EDRs Versus ECMWF, D-matrix = 1

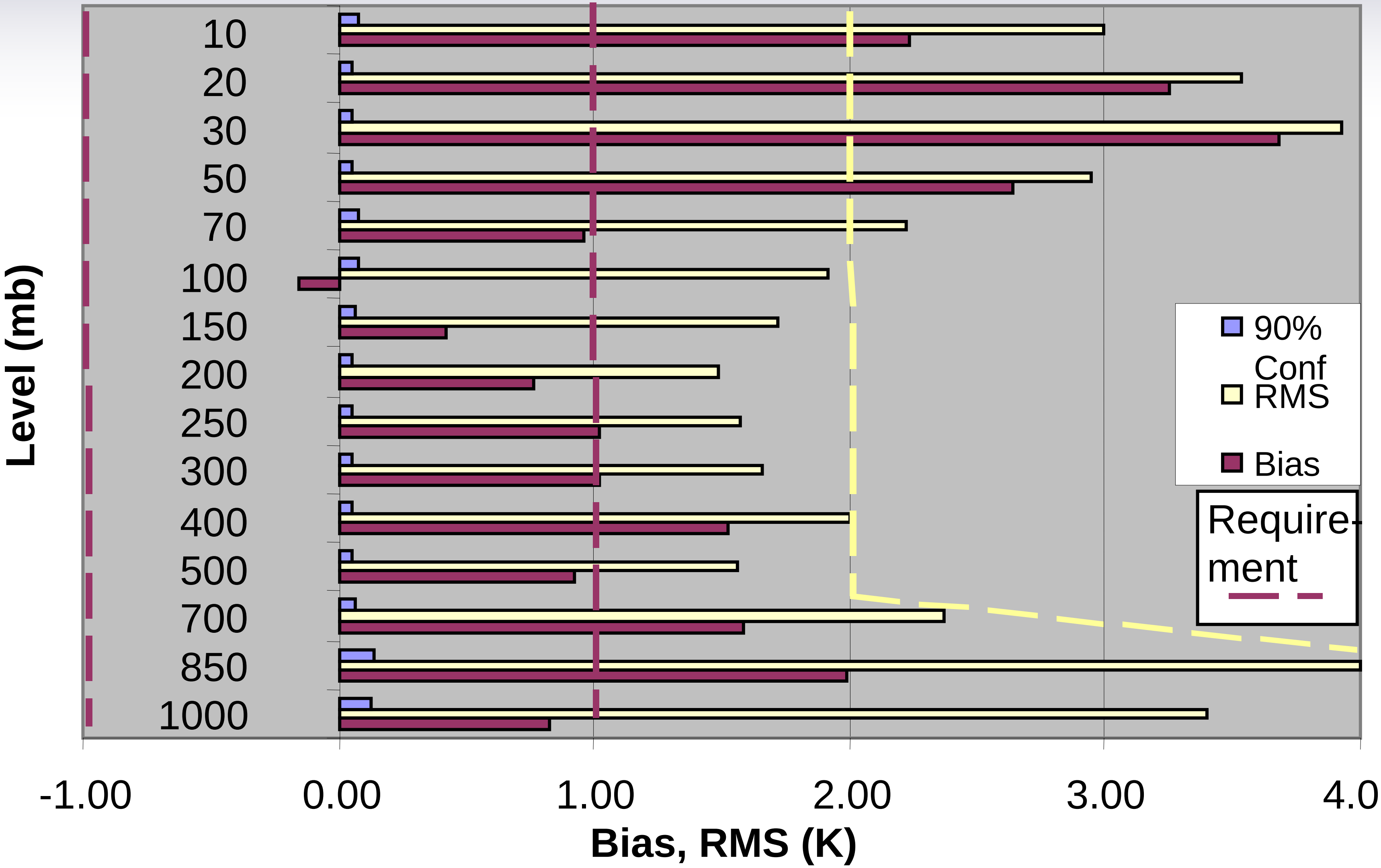

Global Average Temperature Bias
2004 R4 EDRs Versus ECMWF, D-matrix = 2

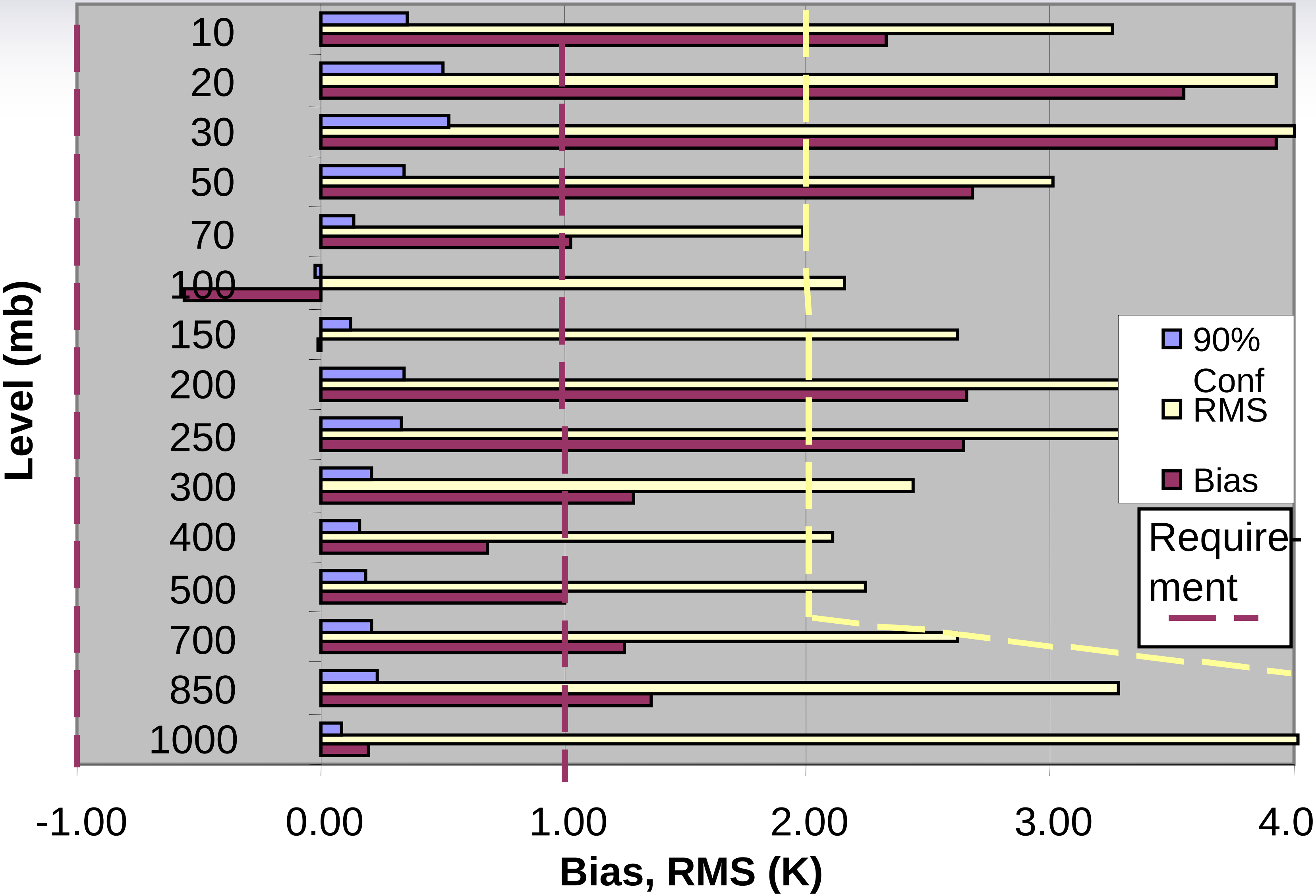

Global Average Temperature Bias
2004 R4 EDRs Versus ECMWF, D-matrix = 3

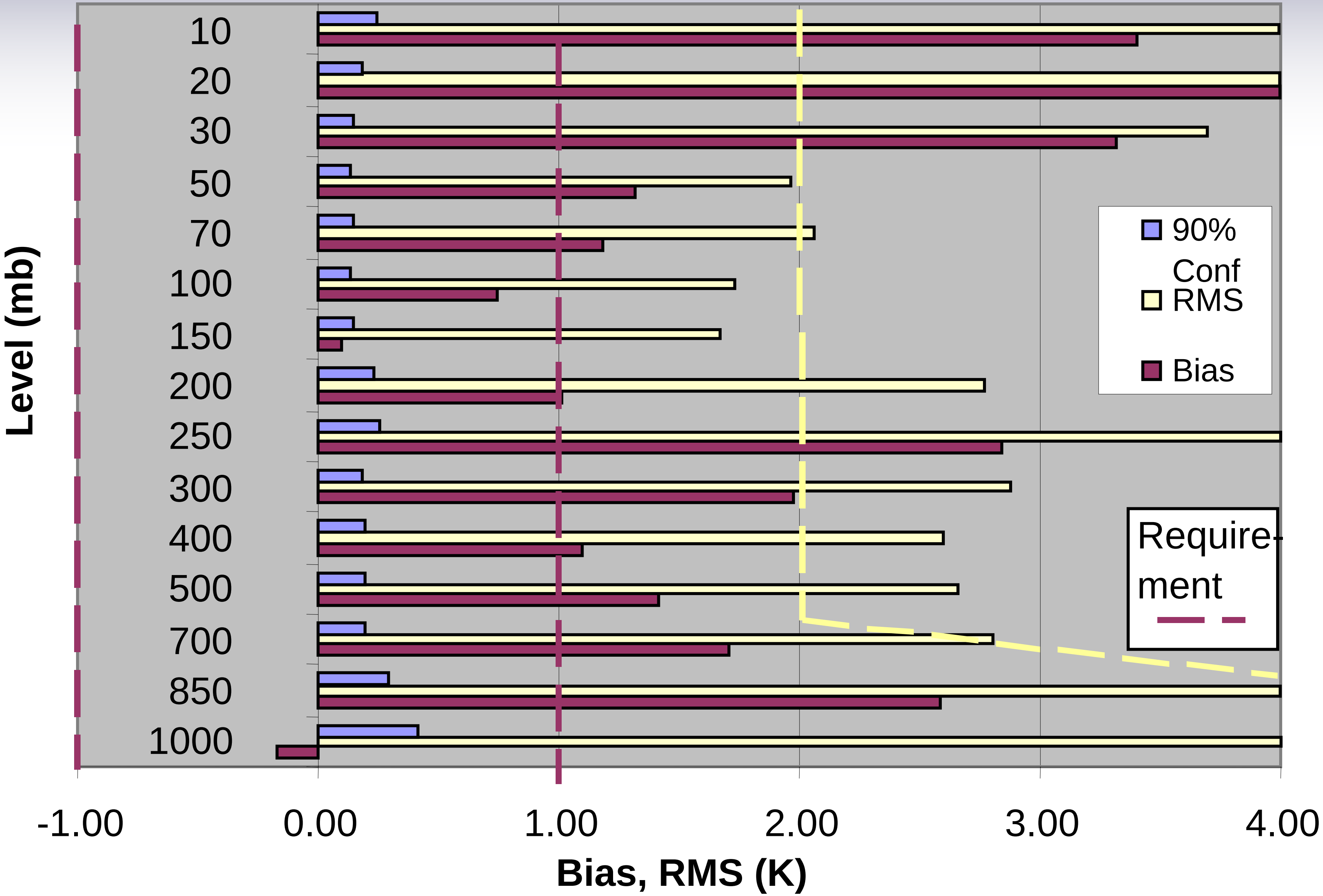

2004 Temperature EDRs Vs ECMWF

Dmat=1 2003 JD 306-335

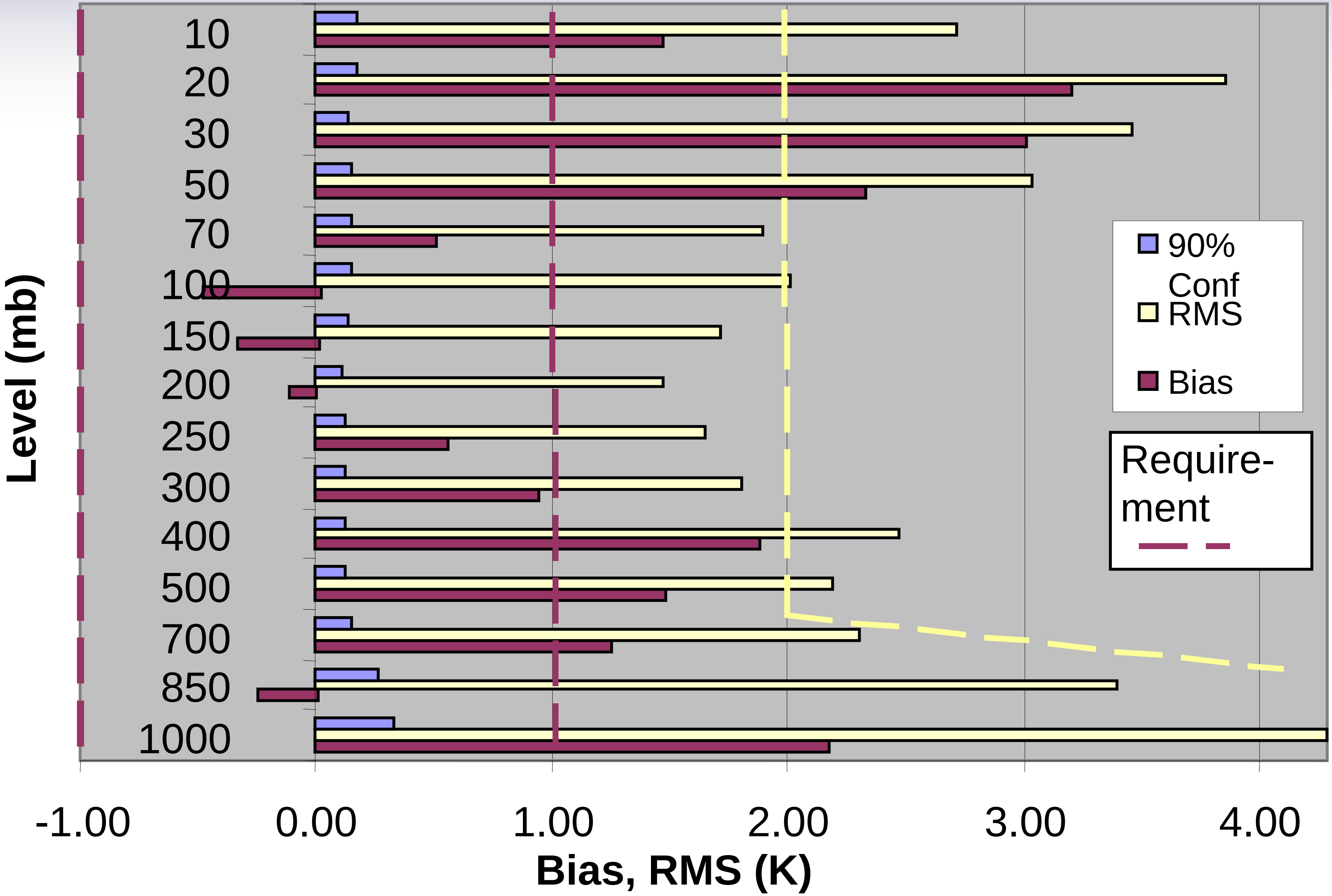

2004 Temperature EDRs Vs ECMWF

Dmat=1 2003 JD 336-365

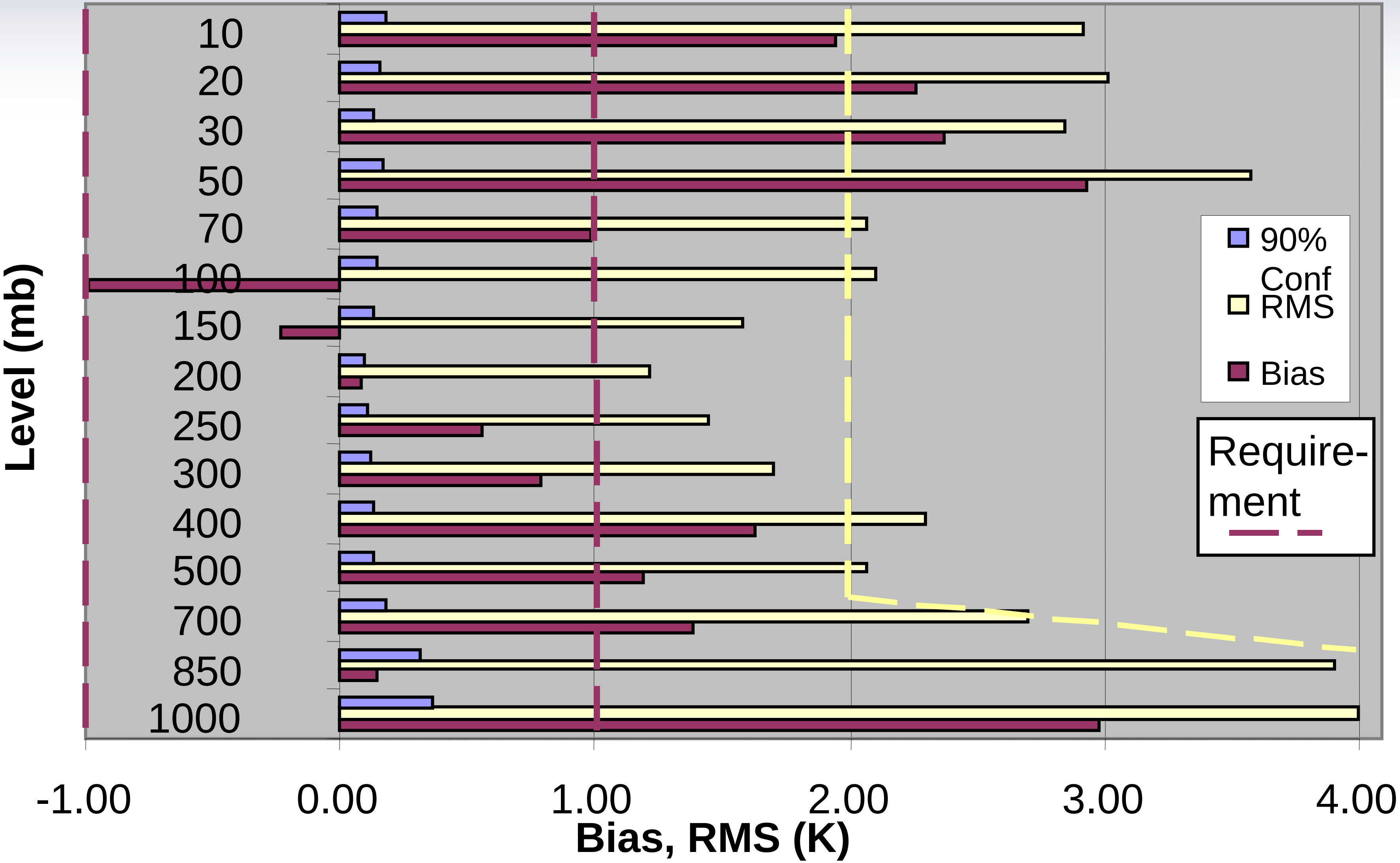

2004 Temperature EDRs Vs ECMWF

Dmat=1 2004 JD 16-45

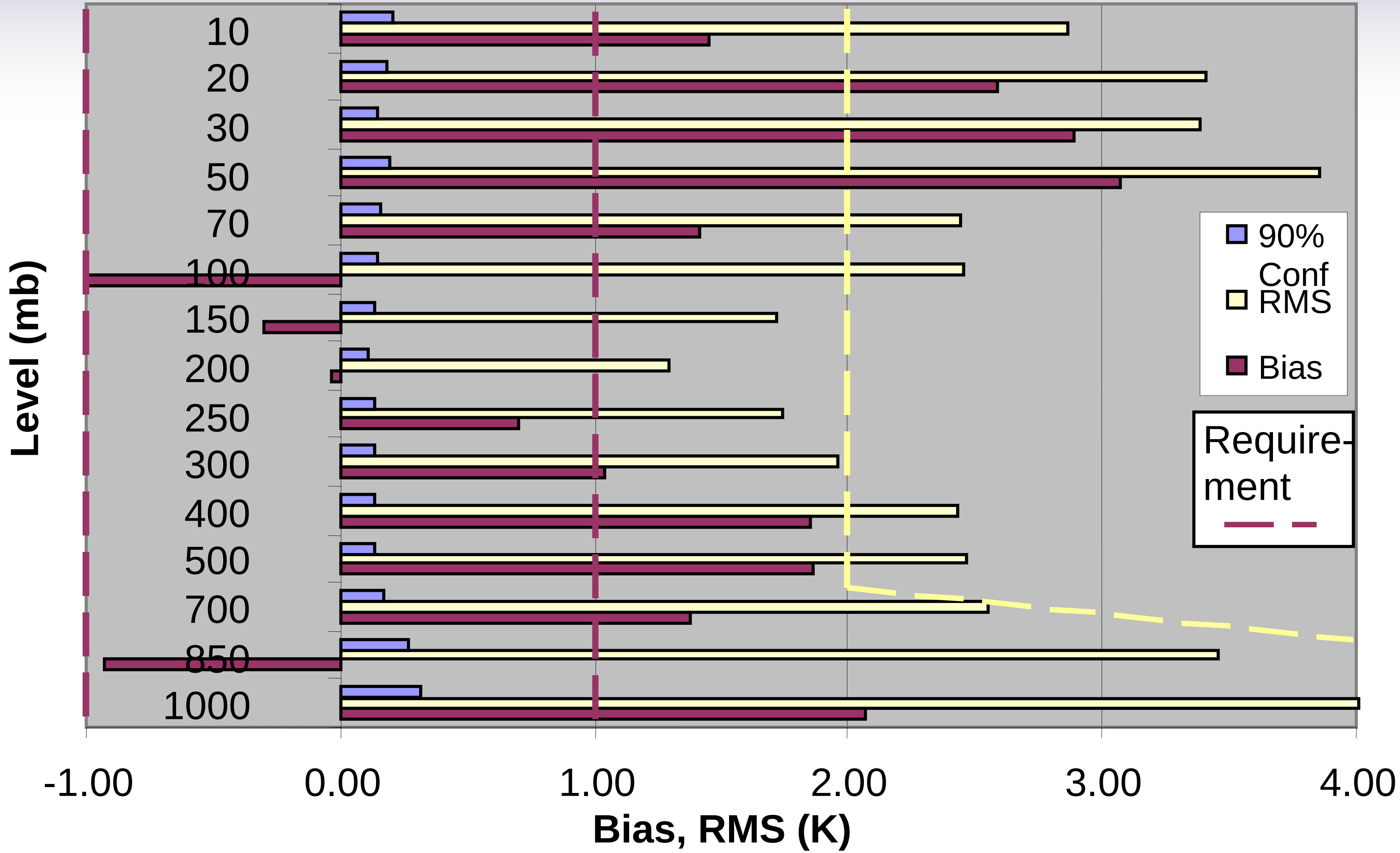

2004 Temperature EDRs Vs ECMWF

Dmat=1 2004 JD 46-75

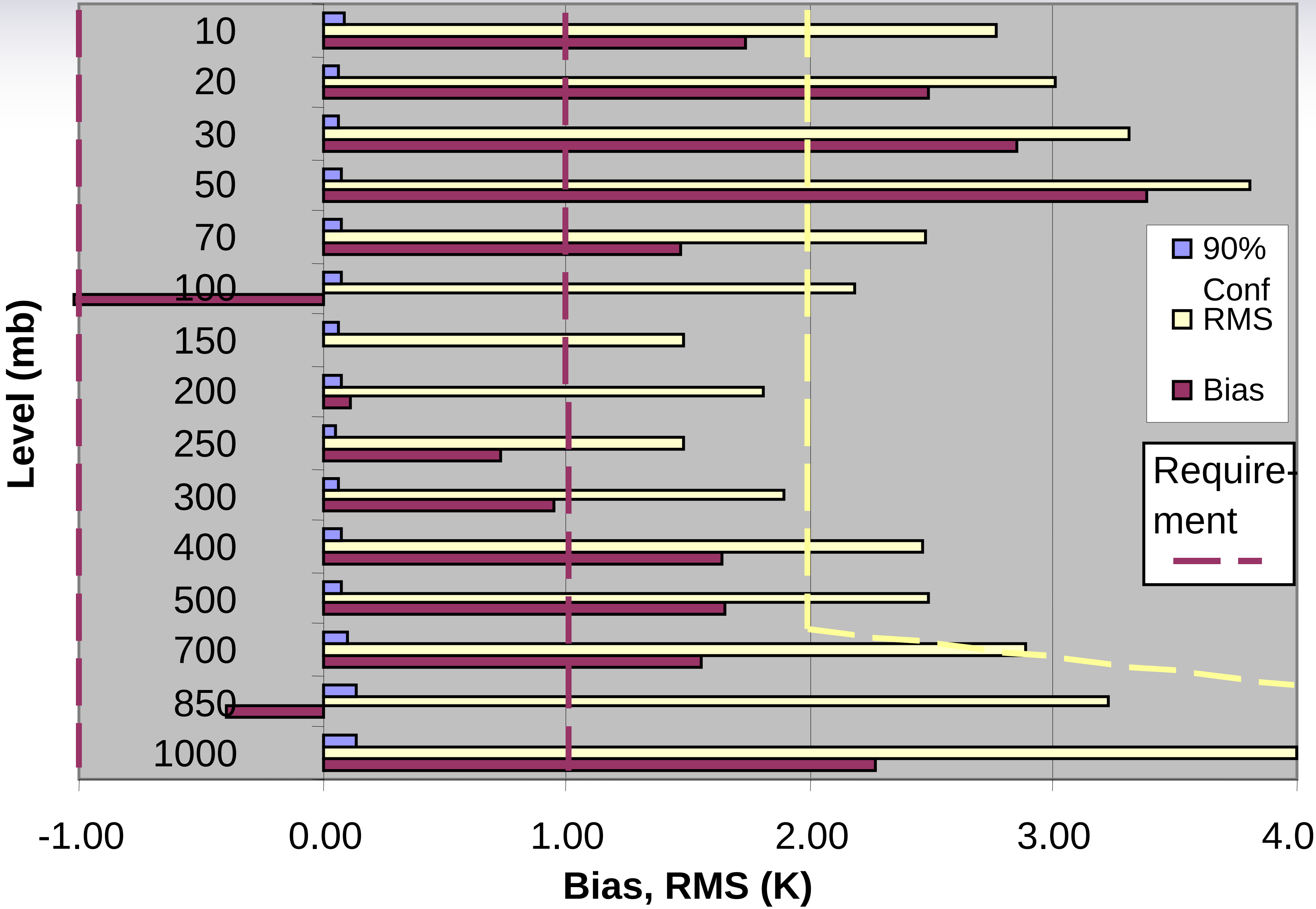

2004 Temperature EDRs Vs ECMWF

Dmat=1 2004 JD 76-105

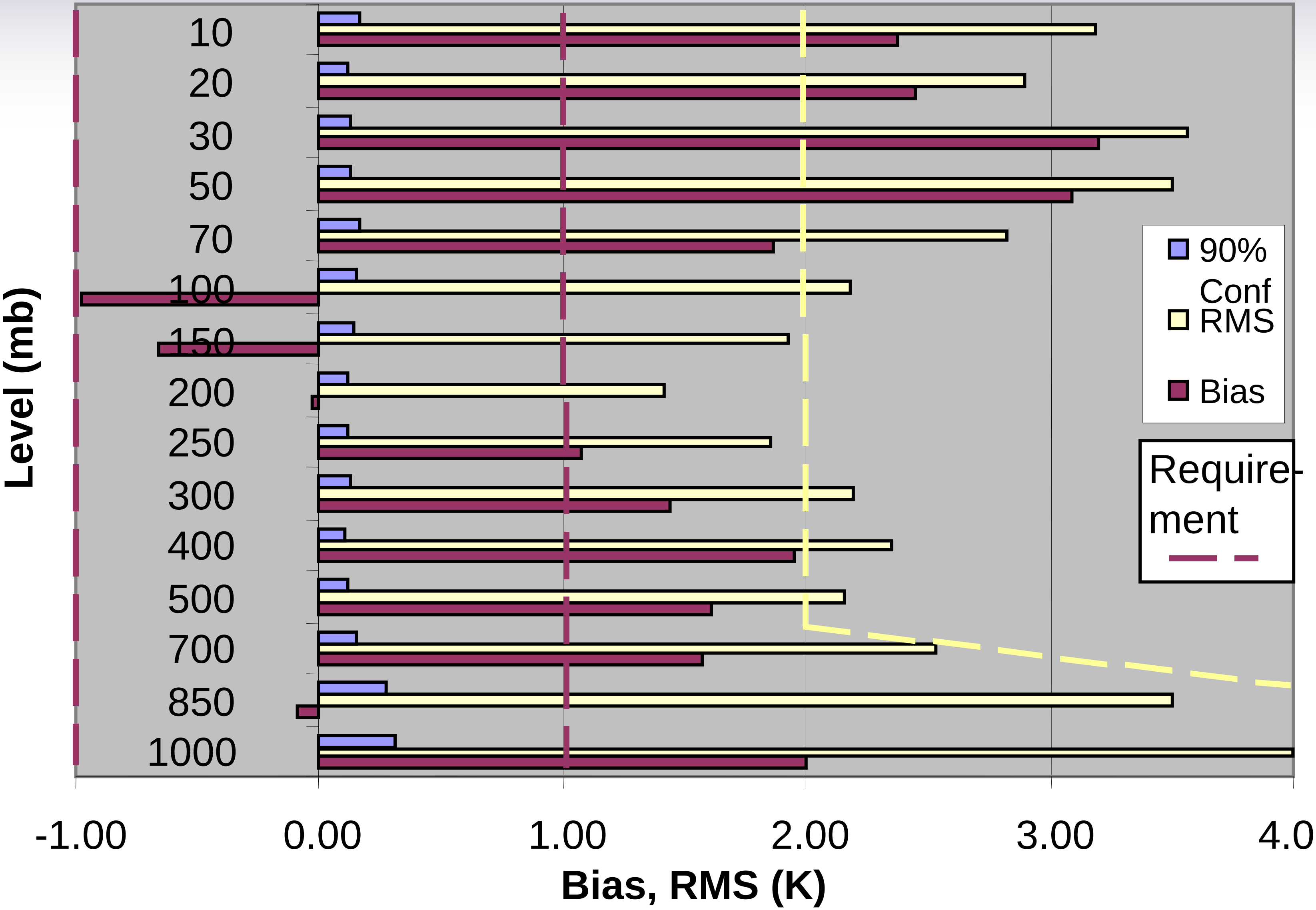

R4

2004 Temperature EDRs Vs ECMWF

Dmat=1 2004 JD 105-135

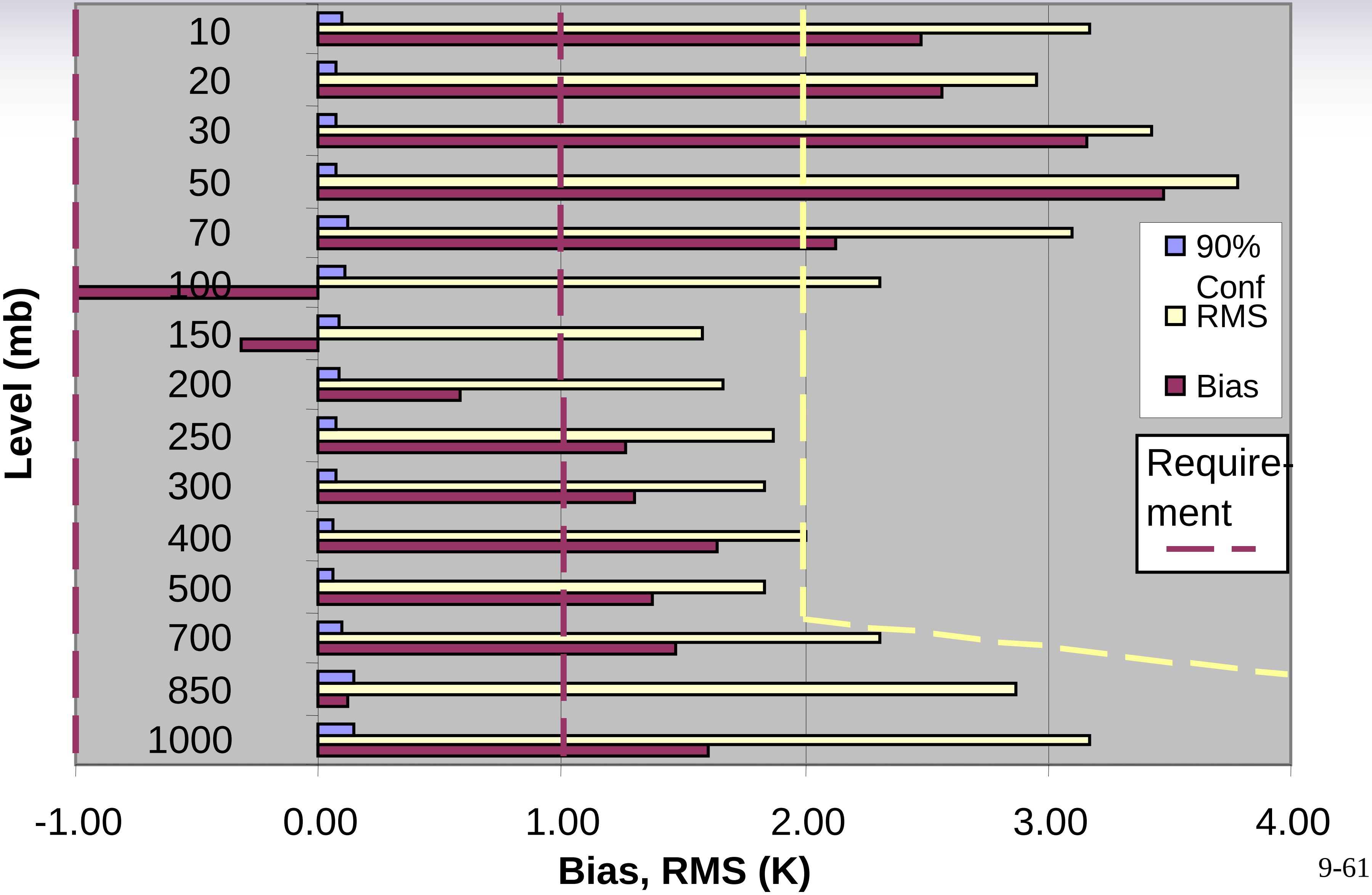

R4

2004 Temperature EDRs Vs ECMWF

Dmat=1 2004 JD 136-165

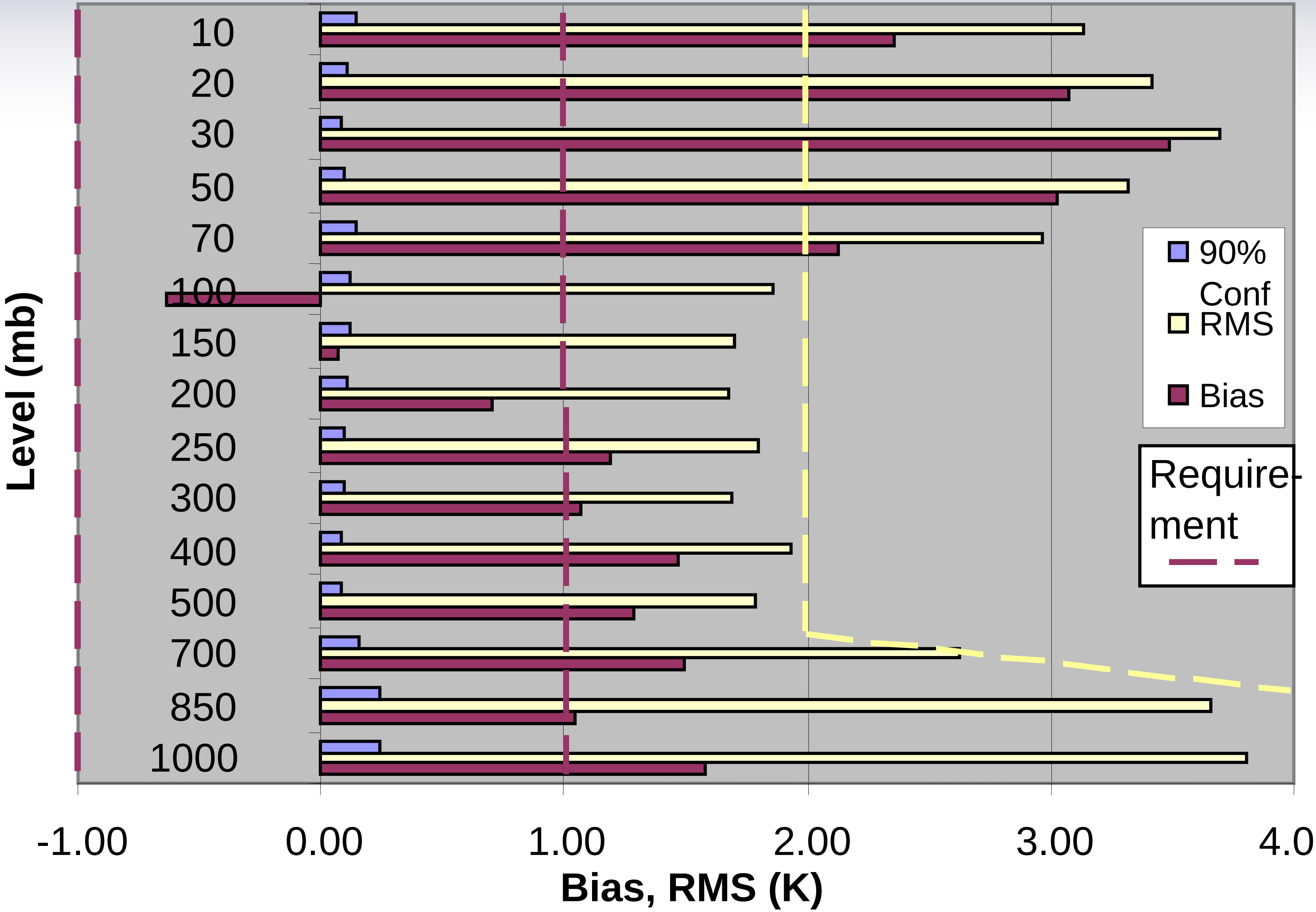

2004 Temperature EDRs Vs ECMWF

Dmat=1 2004 JD 165-195

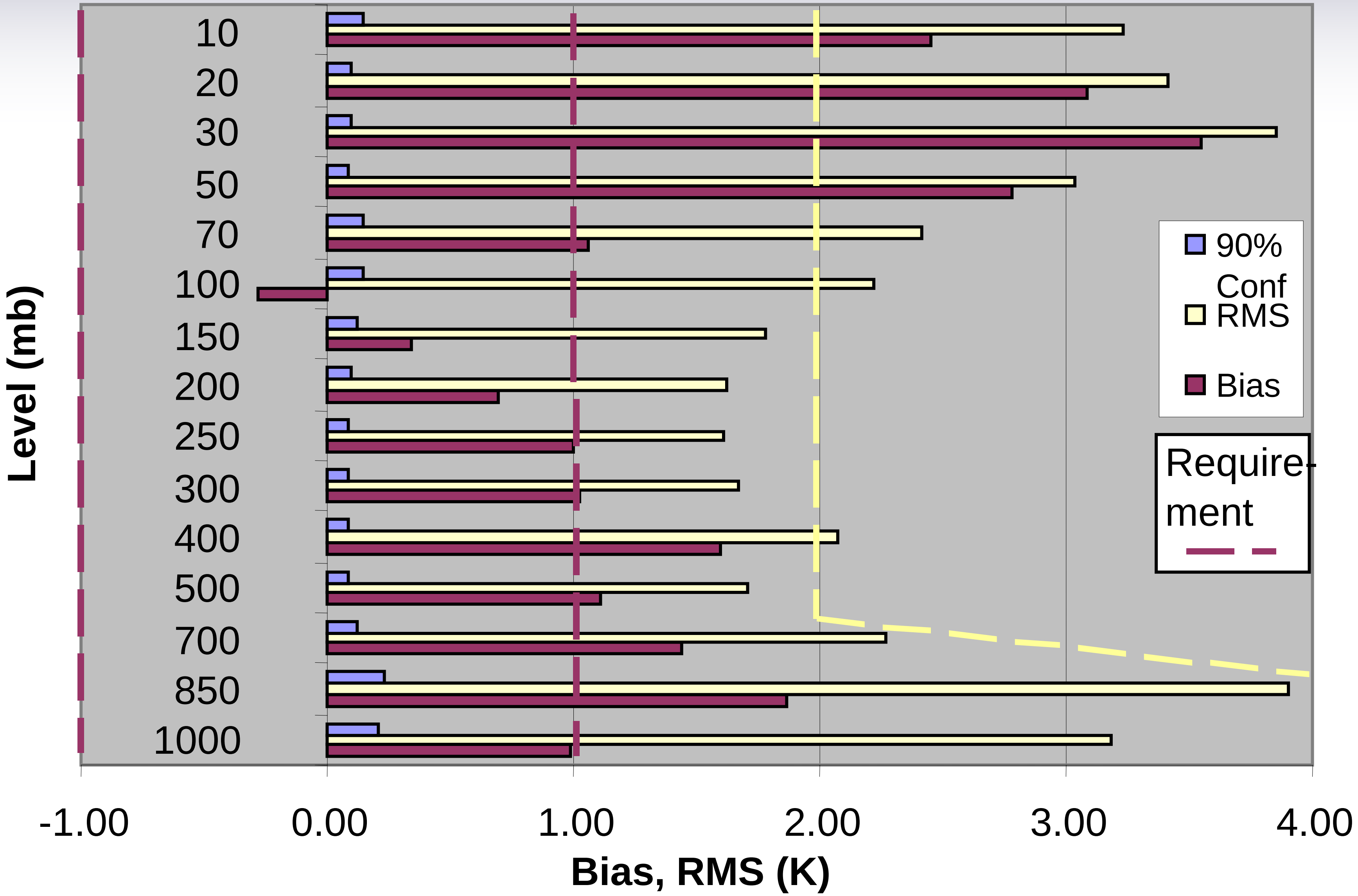

R4

2004 Temperature EDRs Vs ECMWF

Dmat=1 2004 JD 195-225

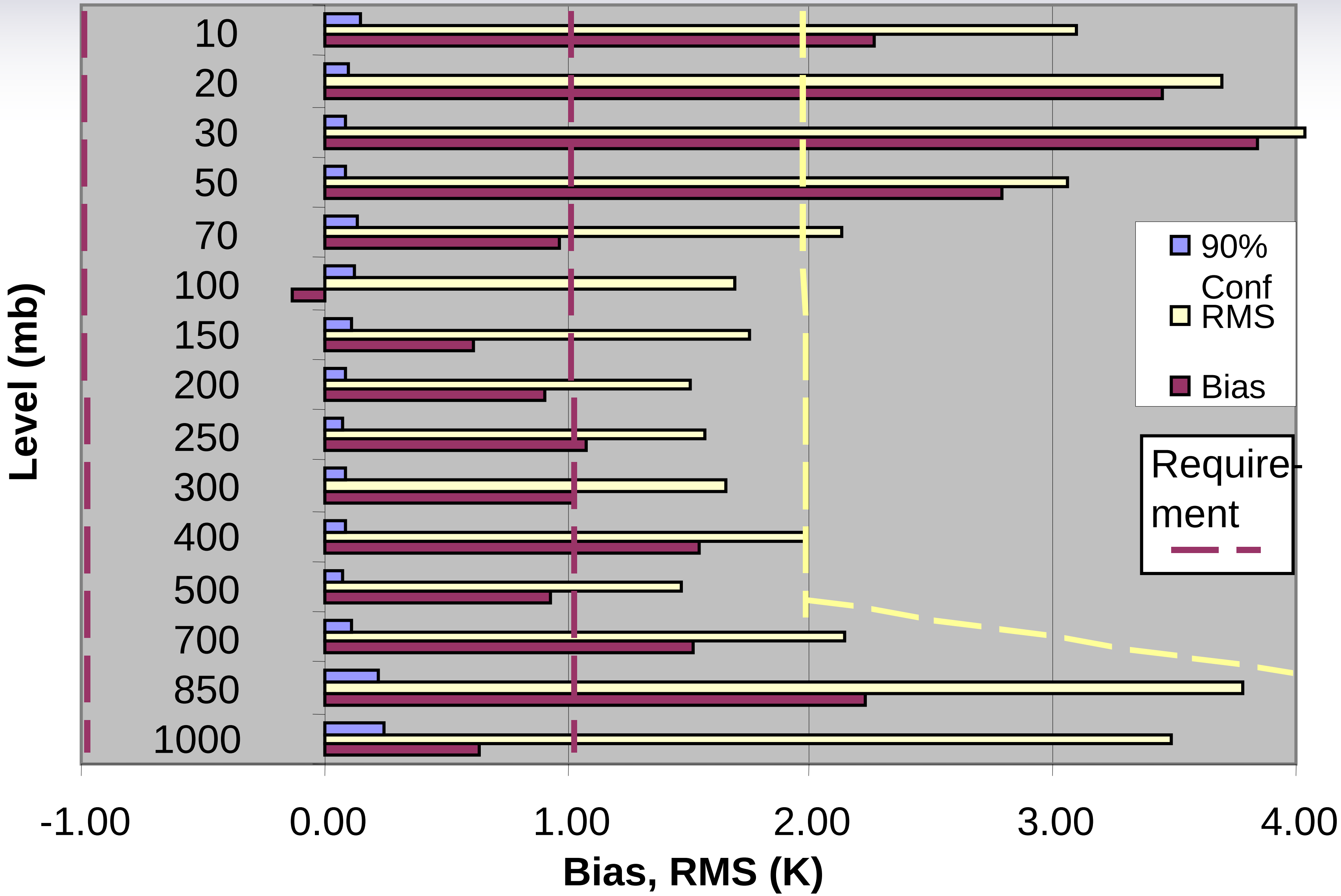

R4

2004 Temperature EDRs Vs ECMWF

Dmat=1 2004 JD 226-255

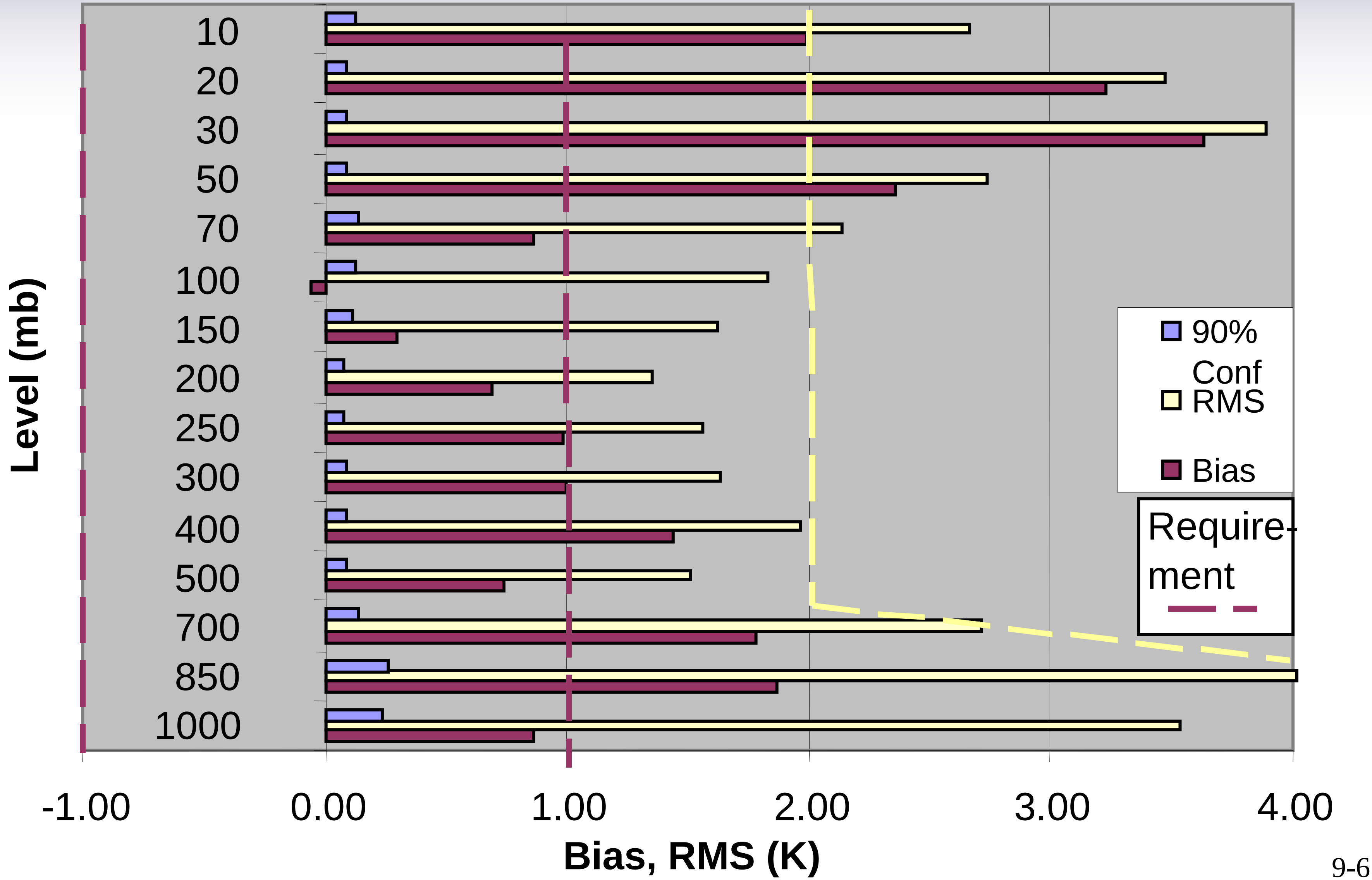

R4

2004 Temperature EDRs Vs ECMWF

Dmat=1 2004 JD 256-285

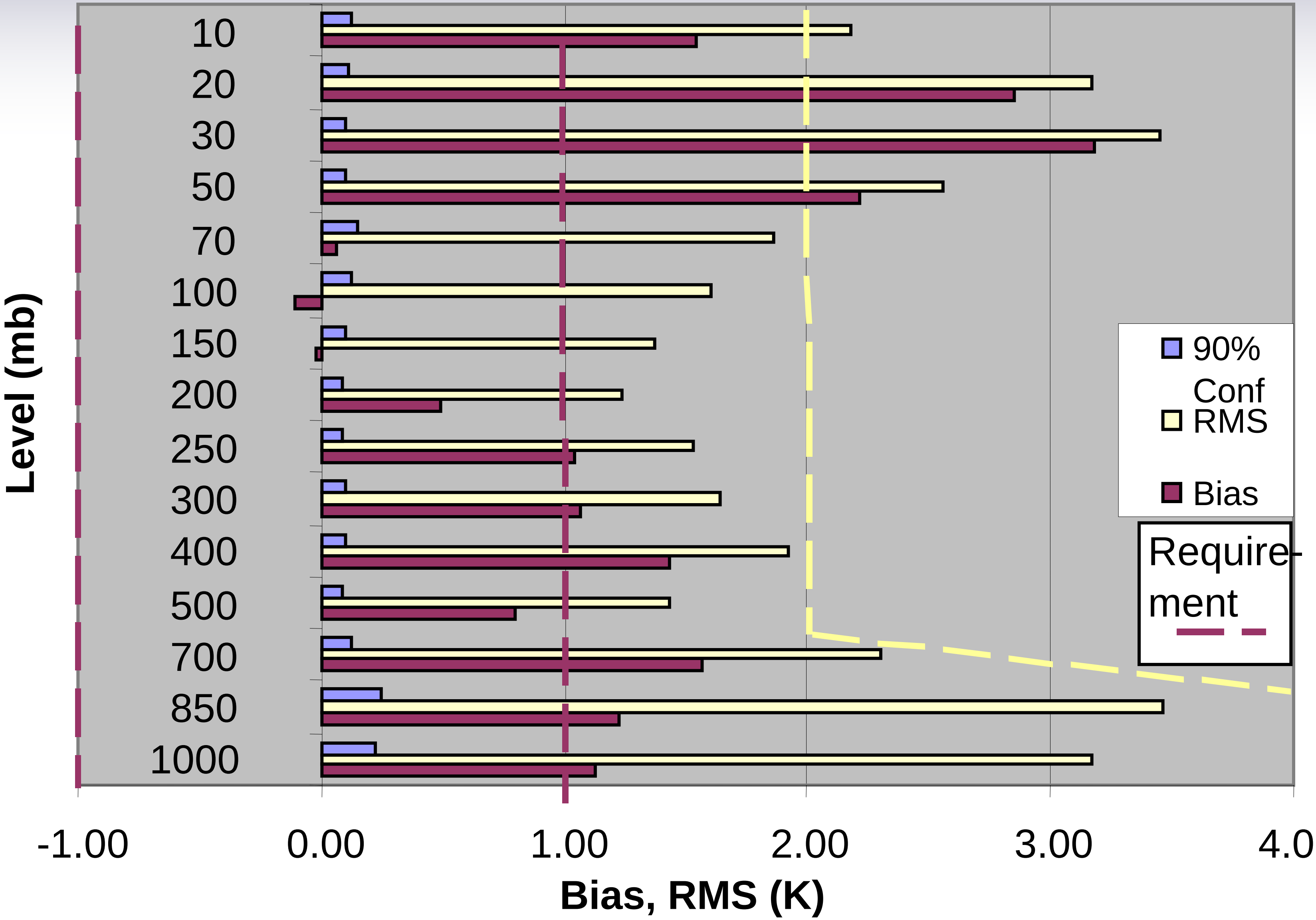

R4

2004 Temperature EDRs Vs ECMWF

Dmat=2 2004 JD 136-165

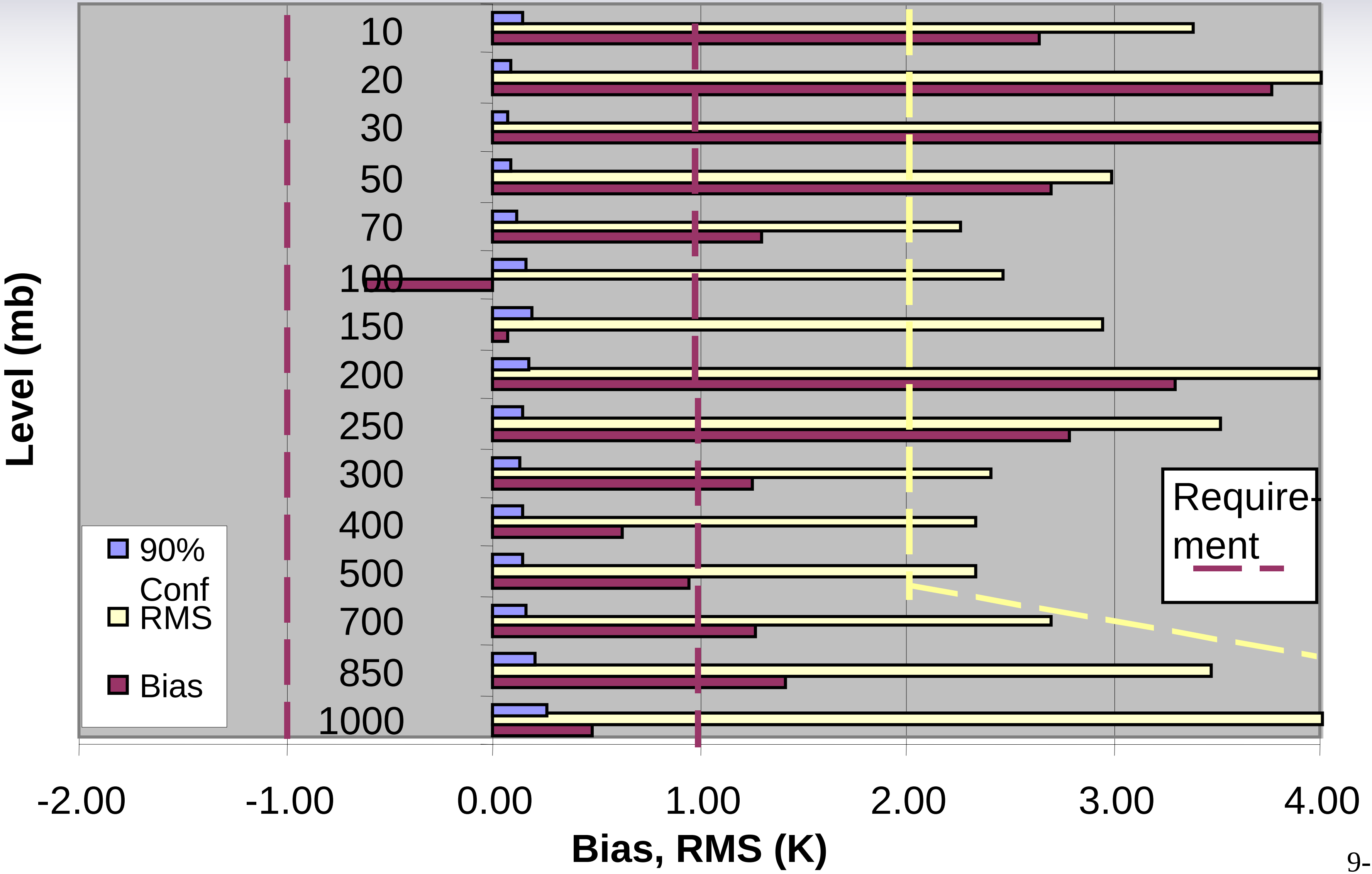

2004 Temperature EDRs Vs ECMWF

Dmat=2 2004 JD 166-195

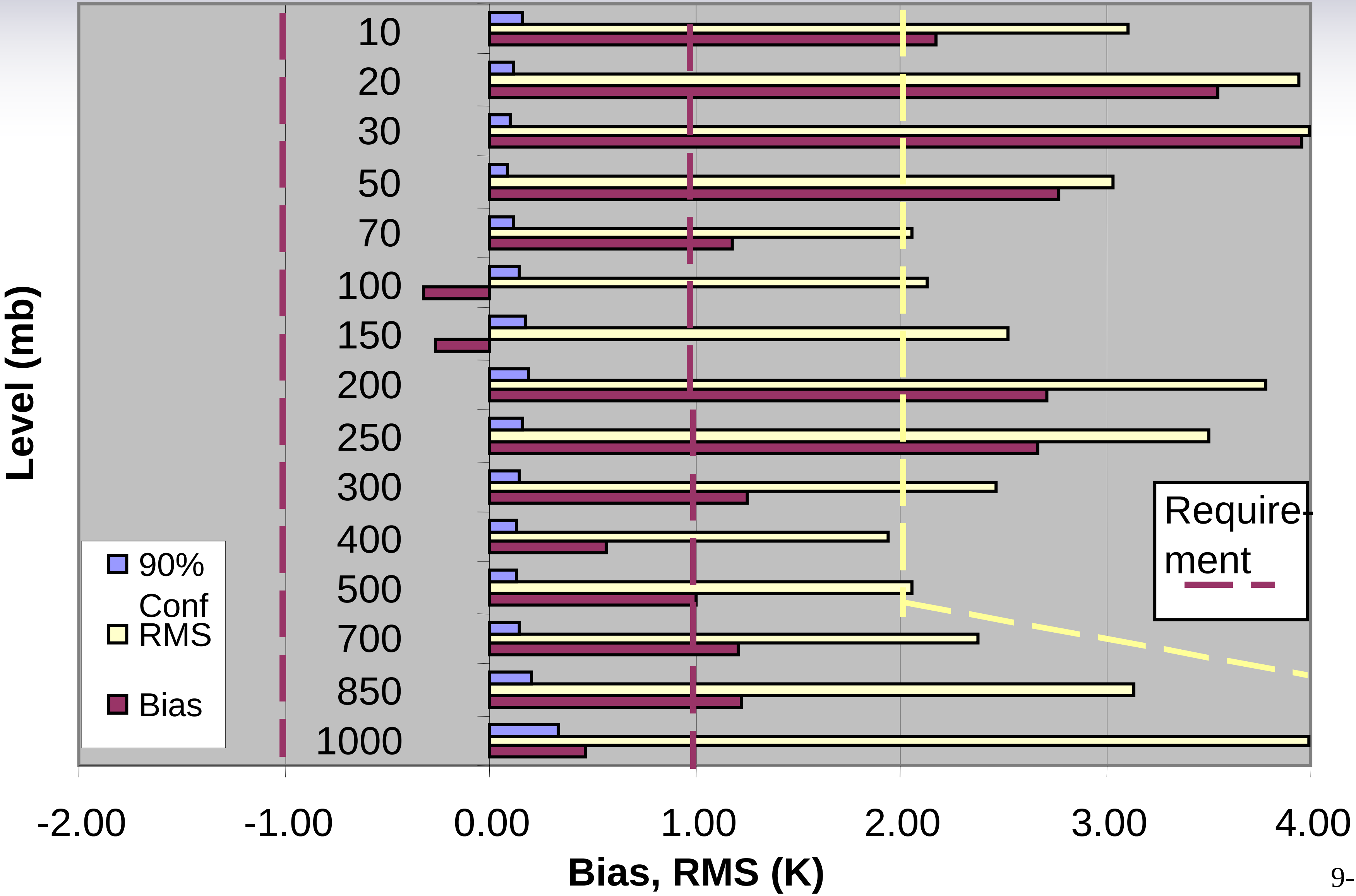

R4

2004 Temperature EDRs Vs ECMWF

Dmat=2 2004 JD 196-225

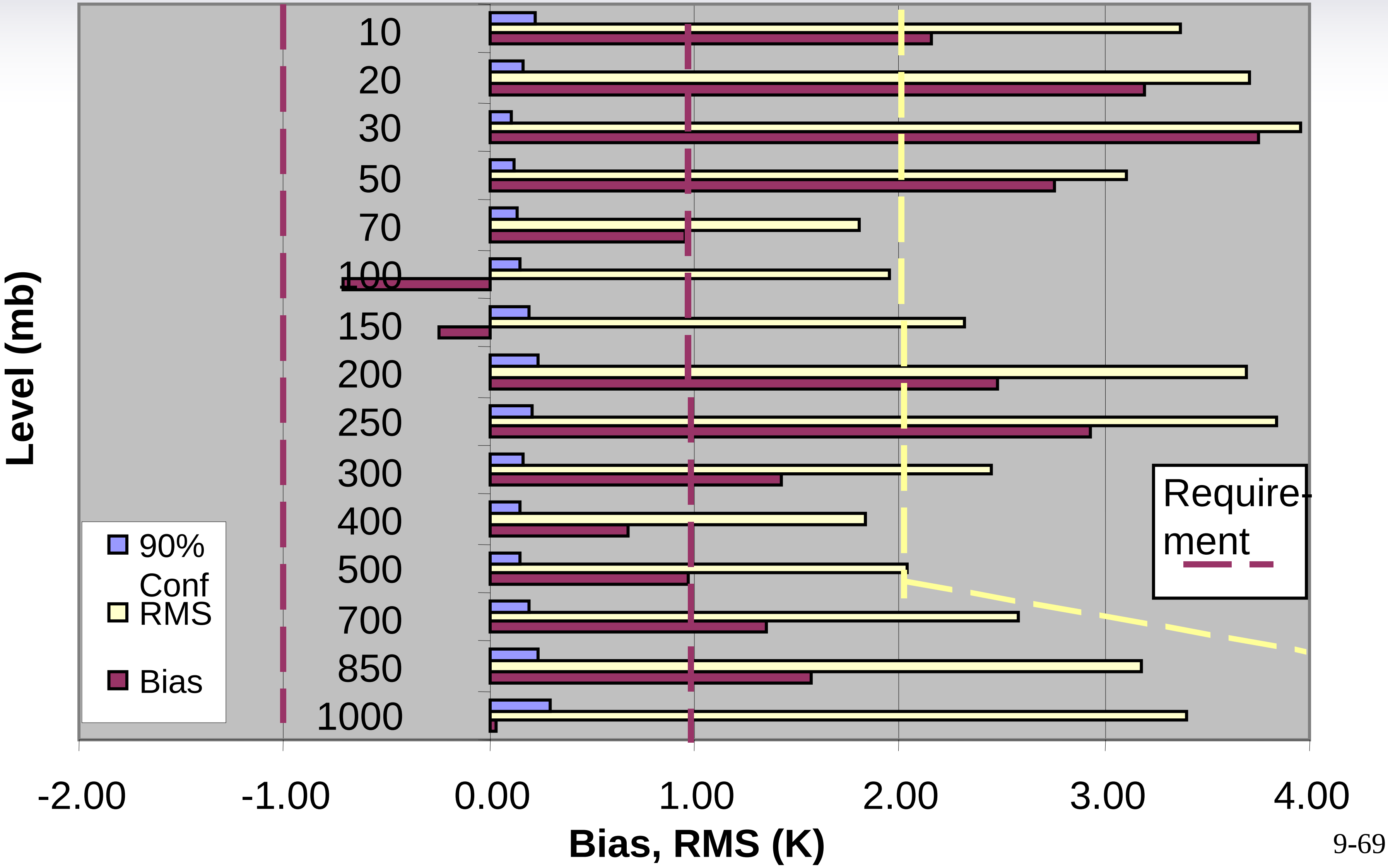

R4

2004 Temperature EDRs Vs ECMWF

Dmat=2 2004 JD 226-255

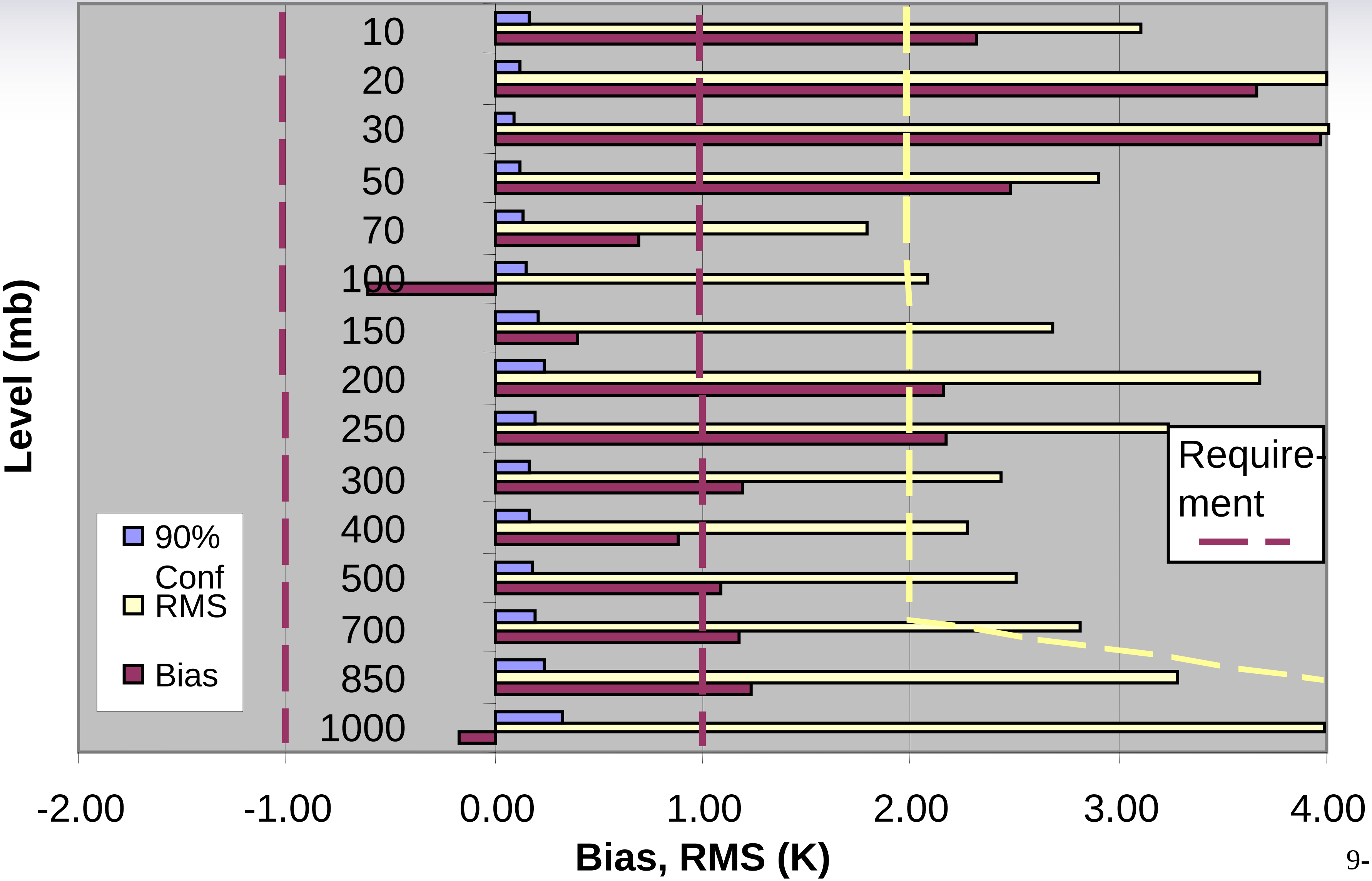

R4

2004 Temperature EDRs Vs ECMWF

Dmat=3 2004 JD 105-135

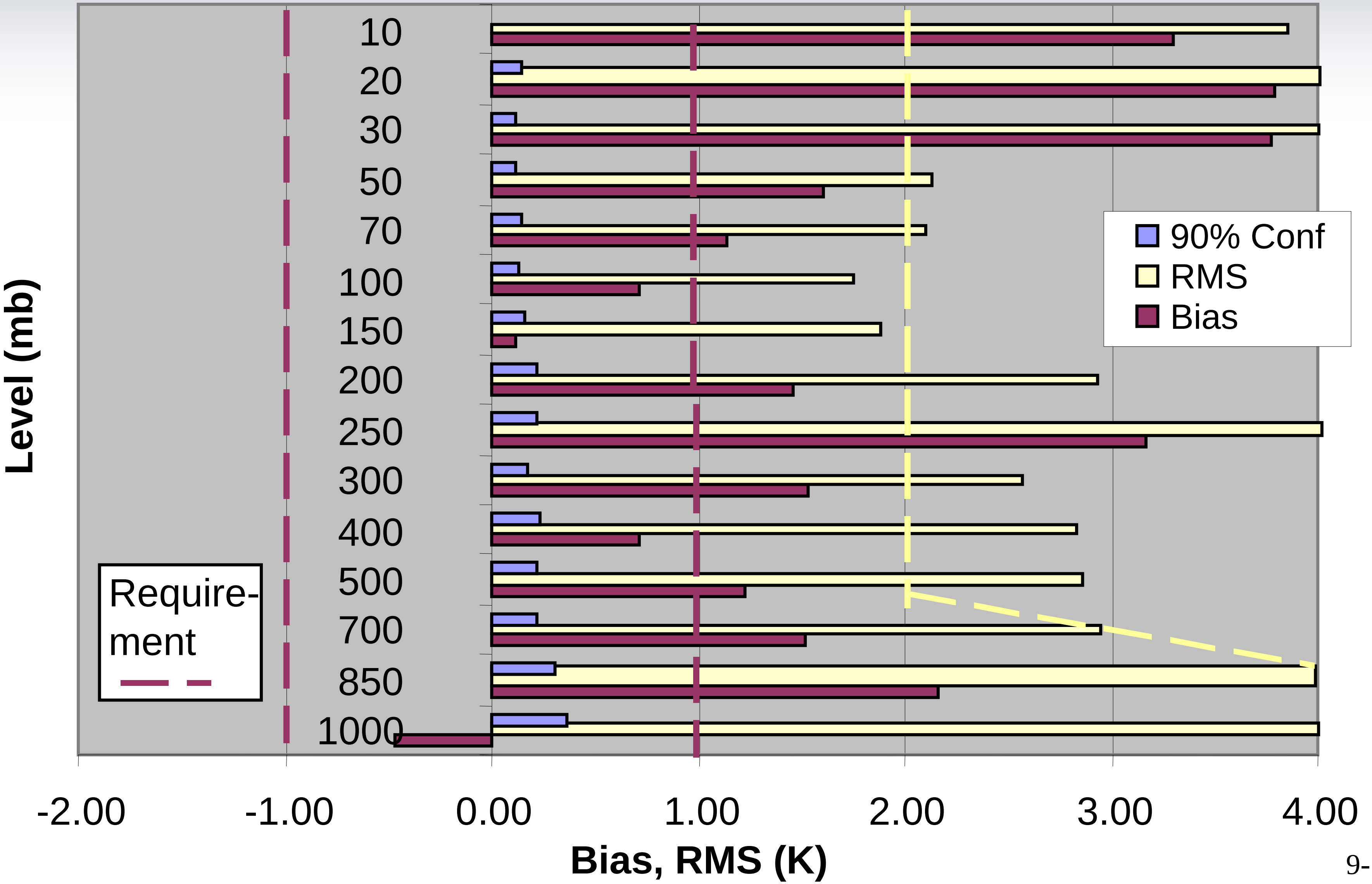

R4

2004 Temperature EDRs Vs ECMWF

Dmat=3 2004 JD 136-165

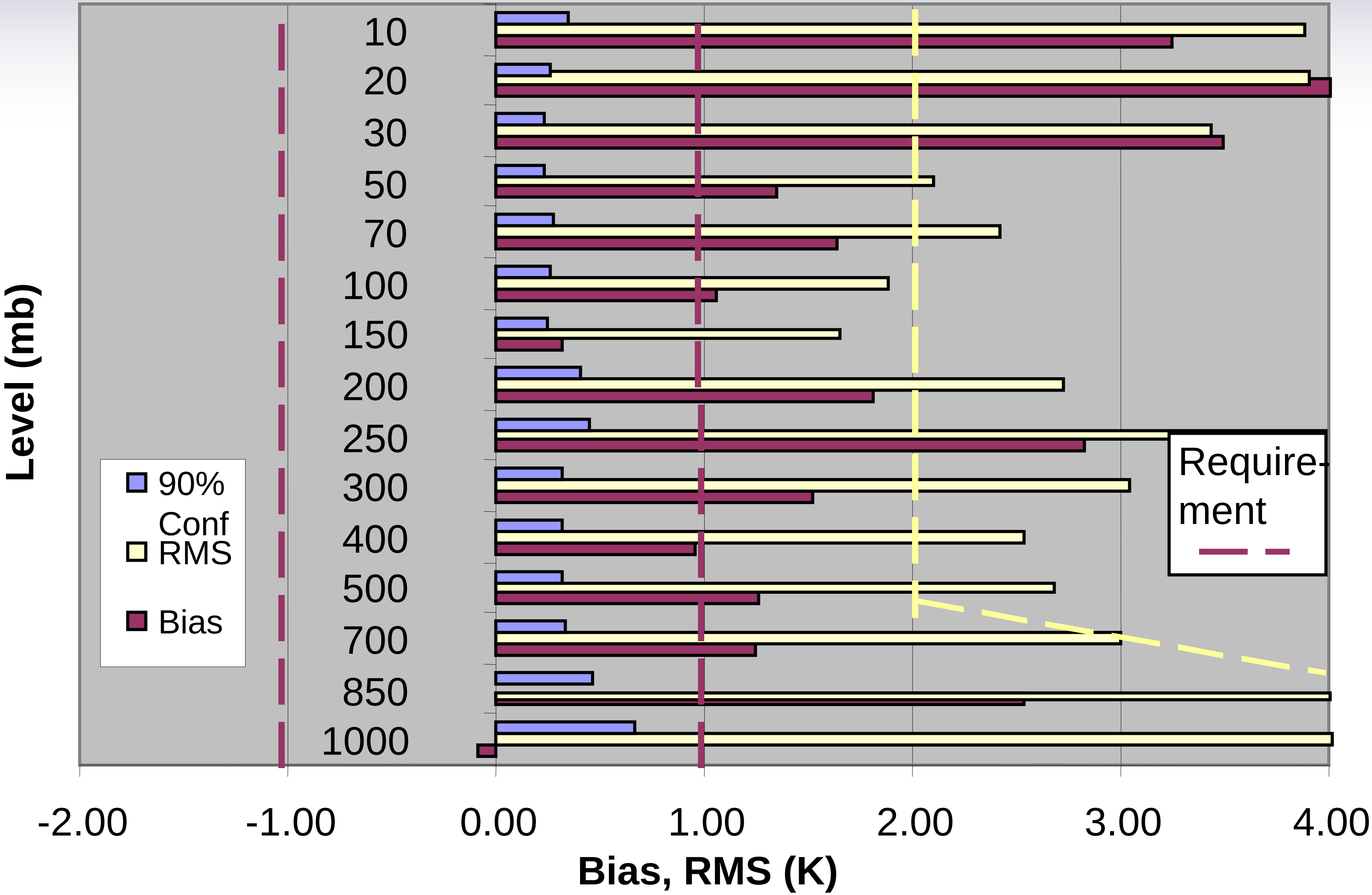

2004 Temperature EDRs Vs ECMWF

Dmat=3 2004 JD 165-195

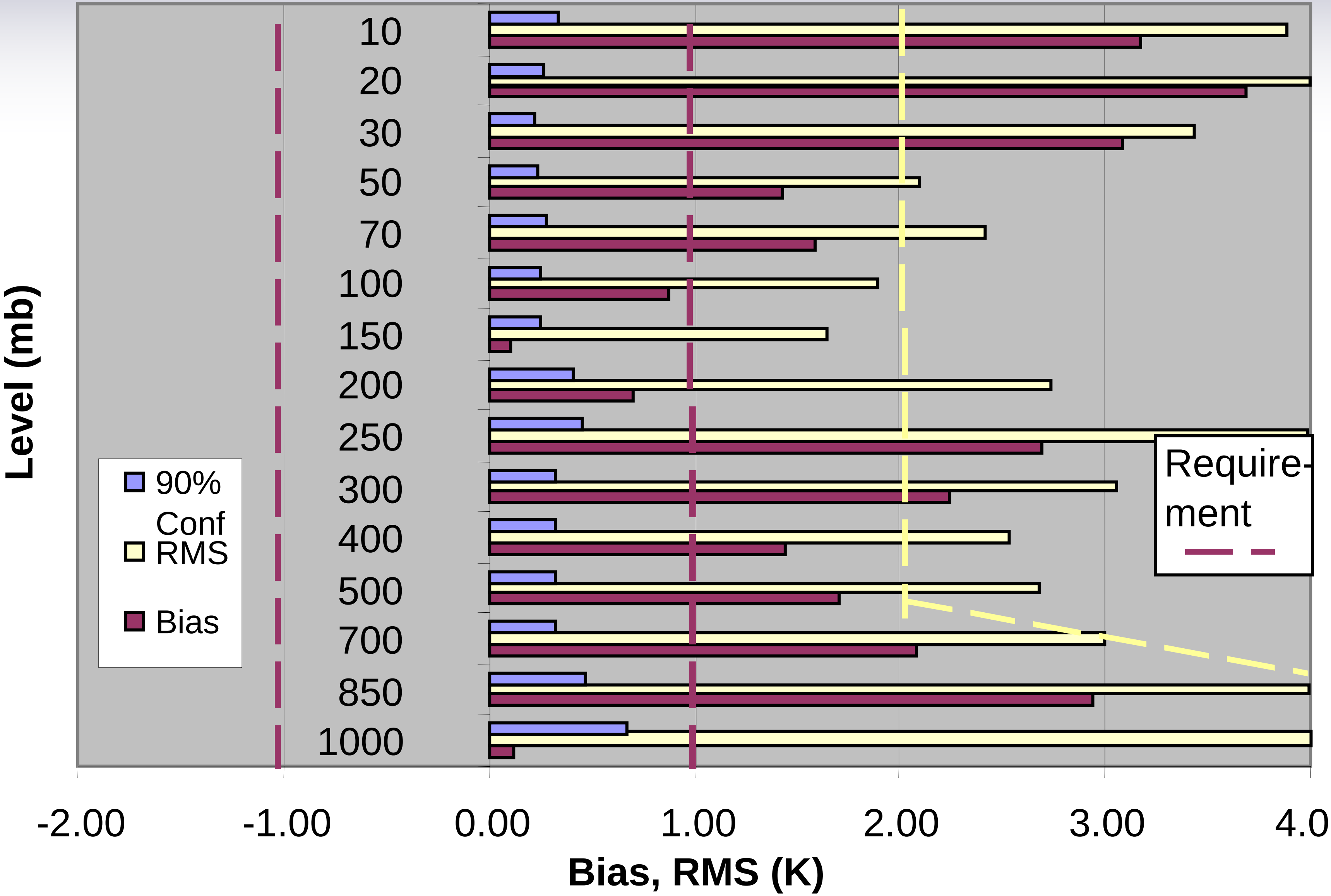

R4

2004 Temperature EDRs Vs ECMWF

Dmat=3 2004 JD 196-225

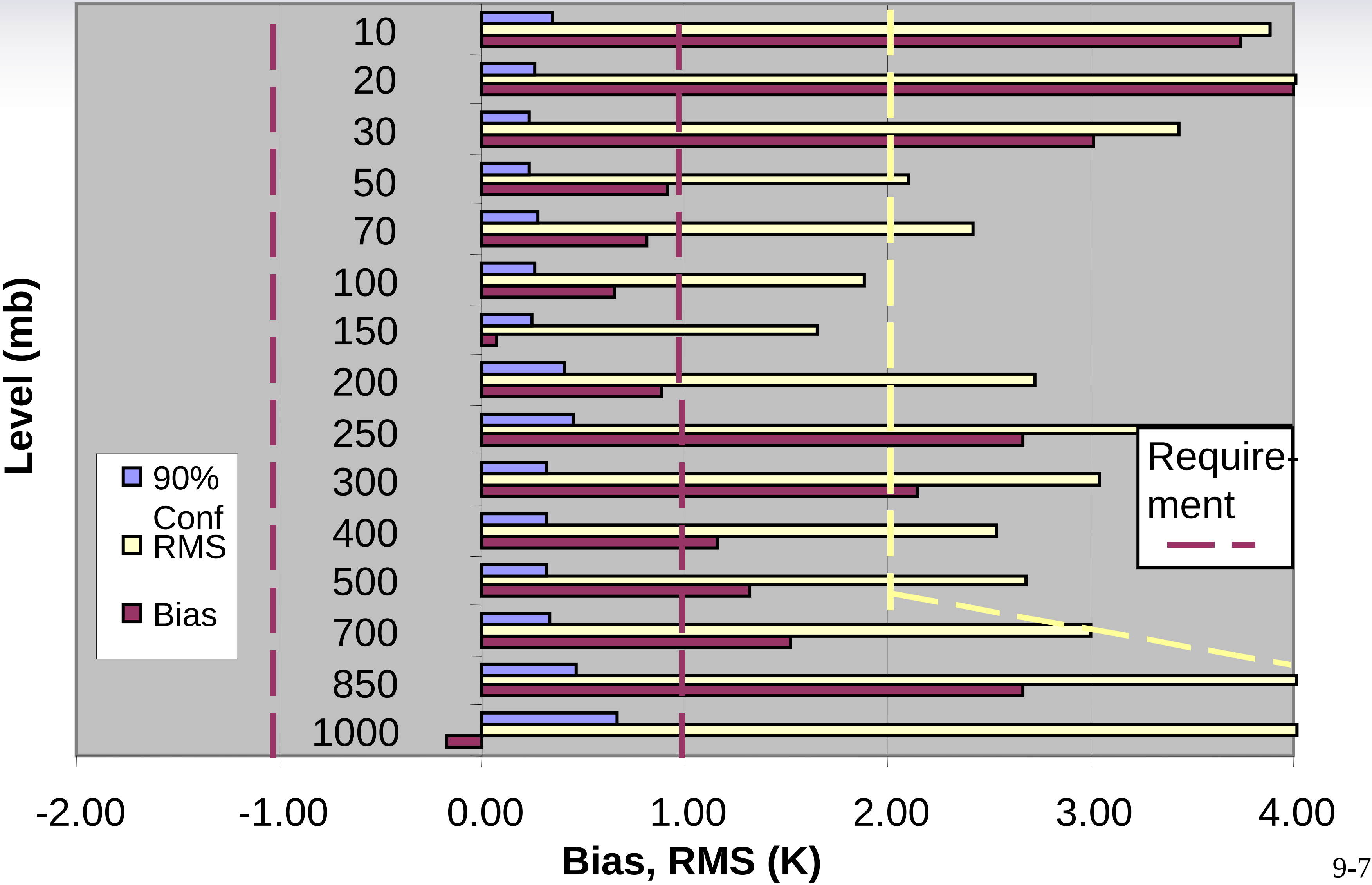

Monthly R4 Temperature Std

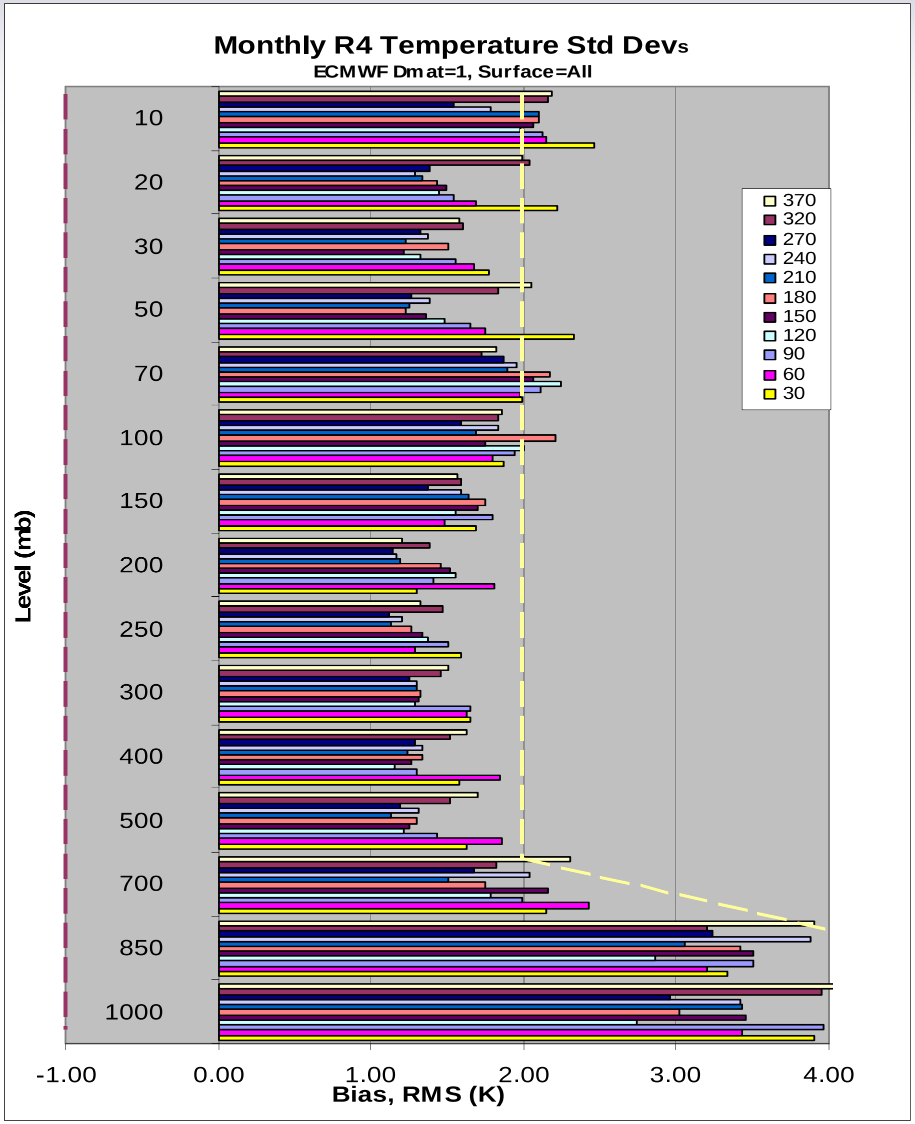

Defense Meteorological Satellite Program
Special Sensor Microwave Imager Sounder (F-16)
Calibration/Validation Final Report

The First Conical Scanning Passive Microwave
Surface and Atmospheric Sounding Imager

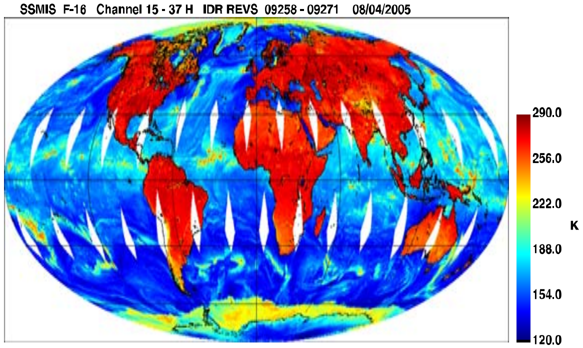

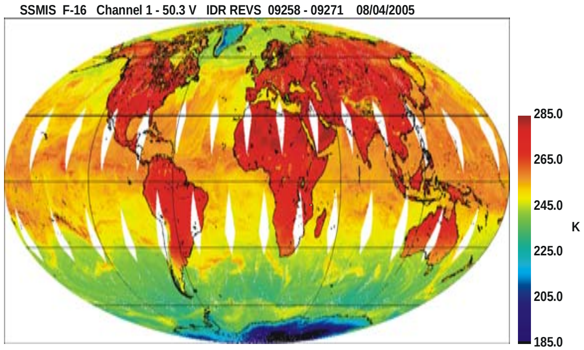

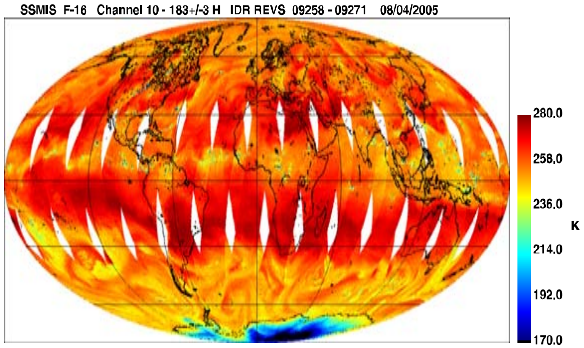

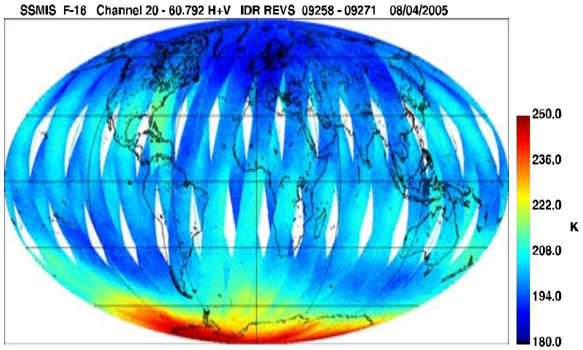

Prepared by

SSMIS Cal/Val Team

30 November 2005

Volume IV

Table of Contents

Volume I

Volume II

Volume III

Volume IV

Volume V

Volume VI

F16 SSMIS Calibration/Validation Final Report

Section 10.0

Upper-Air Sounding

Steve Swadley, Ye Hong, Dana Kerola,

Alex Stogryn and Gene Poe

THE AEROSPACE
CORPORATION

Section 10.0 Upper-Air Sounding (UAS) Outline

- Section 10.1 Objectives
- Section 10.2 Approach
- Section 10.3 Complexities
  - Doppler Shift Corrections
  - UAS Radiative Transfer Models
  - Band Pass Filter Descriptions
  - Polarization Purity
- Section 10.4 Data Acquisition Plan
  - Lidar Observational Campaigns
  - ECMWF NWP Analyses
  - Rocketsonde Observations
- Section 10.5 Analysis Methodology
  - SDR Calibration (OB-RTM)
  - EDR Validation (Retrieval-Lidar)
  - EDR Validation (Retrieval-NWP)
- Section 10.6 Summary

Section 10.1 Objectives

Three Primary Objectives of SSMIS UAS Cal/Val Effort:

- **Verify End-to-End Instrument Radiometric Calibration Accuracy**
- **Verify the Calibration of the Sensor Data Records (SDRs)**
- **Validate UAS Temperature Retrievals (EDRs) Using Independent Measurements of Temperature Profiles.**

If Necessary, Apply New Sensor Calibration Coefficients and Averaging Schemes, Develop New α and β Retrieval Coefficients, and/or Environmental Retrieval Algorithms to Bring the SDR and EDR Products Within Specification

Section 10.2 Approach

- Utilize High-Quality Rayleigh Lidar Temperature Profiles as the Primary Data Source for Both Calibration of SDRs and Validation of EDRs
- Utilize ECMWF NWP Analyses for Broad Geographic Validation of EDRs from 7 to 0.1 hPa
- Utilize Rocketsonde Observations at White Sands Missile Range (WSMR) to Calibrate SDRs and Validate EDRs during Descending Revs

Section 10.2 Approach (2)

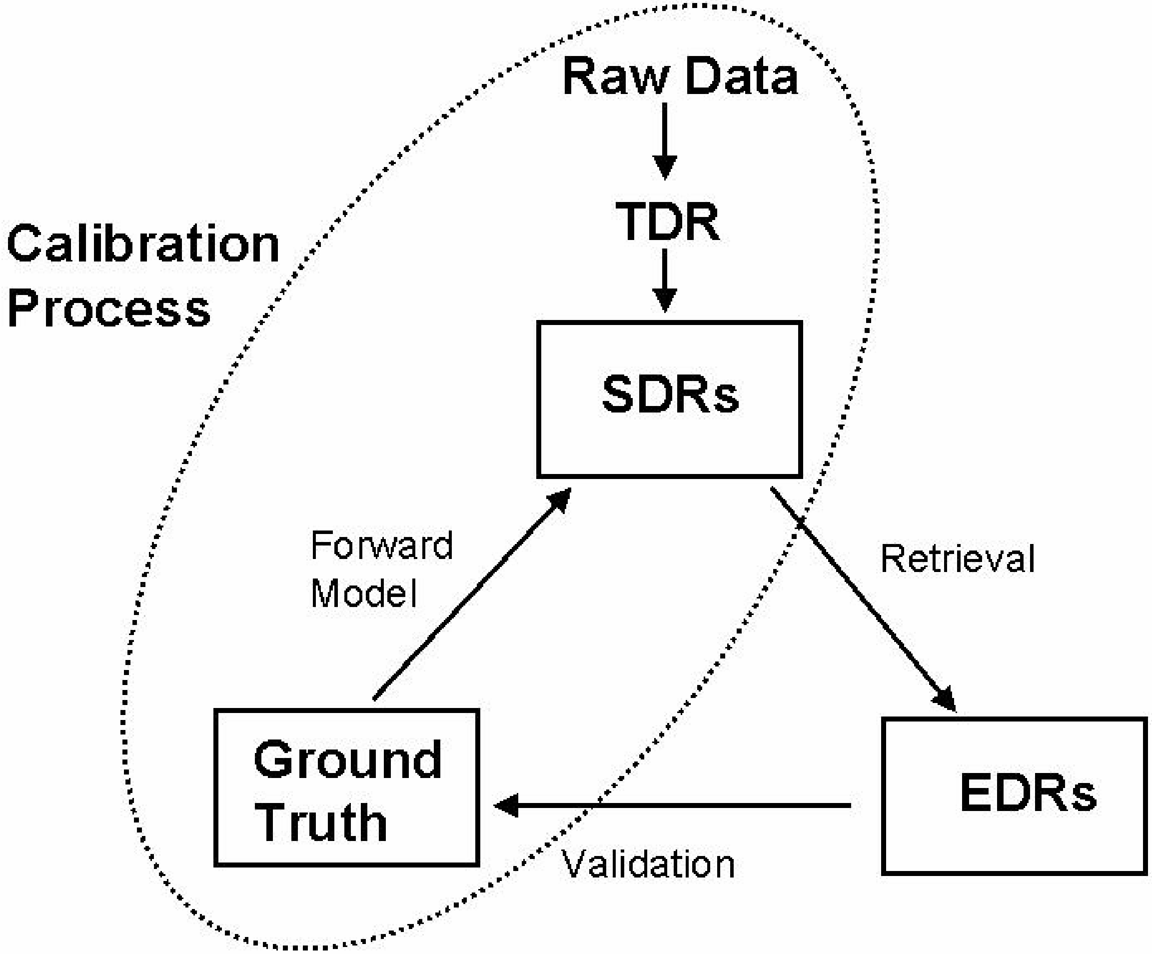

Table 6.2 SSMIS Upper Atmosphere Temperature Retrieval Accuracy Requirements And Predicted Performance.

Section 10.2 Approach (3)

Pre-Launch UAS Temperature Retrieval Accuracy Estimates (NGES)

Upper Atmosphere Temperature Requirements/Goals							
Level [hPa]	Accuracy Requirement [K]	Accuracy Predicted [K]	Worst Case Predicted [K]	MLO Lidar Comparison [K]		TMF Lidar Comparison [K]	
				Bias	RMS	Bias	RMS
7	5.0	1.48	1.49				
5	5.0	1.44	1.45				
2	5.0	2.31	2.37				
1	5.0	3.19	3.17				
0.4	5.0	3.67	3.93				
0.2	7.0	4.26	4.75				
0.1	7.0	5.56	6.03				
0.03	7.0	5.41	6.34				

Do the SSMIS UAS Retrievals Meet These Requirements ?

Section 10.3 Complexities

- Doppler Shift Corrections
- UAS Radiative Transfer Models
- Band Pass Filter Descriptions
- Polarization Purity

Section 10.3 Complexities

Utilizes Narrow Passbands in the 60 GHz Oxygen Line Complex

- **Thermal Emission of O_2 are in the Spin-Rotation Resonance Band**
- **Narrow Bandwidths Required to Attain Desired Vertical Resolution**
- **Observation Frequencies, ν, Chosen to be close to Center of one or several of the Resonances ($\nu - \nu_c \leq 4$ MHz)**
- **Requires Anisotropic Polarized Radiative Transfer to Resolve Zeeman-Splitting due to the Interactions of the Geomagnetic Field and the Permanent Dipole Moment of the O_2 molecule**
- **Double (Ch 19, 20) and Quadruple Sidebands (Ch 21-24)**
- **Doppler Frequency Shifting Due to Satellite Motion can Shift the Frequency Outside the Narrow Passbands**
- **Compensation Required to Account for Satellite Motion as a Function of Scan Position**

SSMIS SN02 UAS Channel Characteristics

Channel Number	Center Frequency [GHz]	1st IF [MHz]	2nd IF [MHz]	Passband Center Frequency [GHz]	Passband Bandwidth [MHz]	Polarization	Measured NEΔT [K] for a 305K Scene
19	63.283248	-285.271	0.	62.997977	1.34	LCP	1.76
19	63.283248	+285.271	0.	63.568519	1.36	LCP	1.76
20	60.792668	-357.892	0.	60.434776	1.34	LCP	1.80
20	60.792668	+357.892	0.	61.150560	1.37	LCP	1.80
21	60.792668	-357.892	-2.	60.432776	1.26	LCP	1.27
21	60.792668	+357.892	-2.	61.148560	1.33	LCP	1.27
21	60.792668	-357.892	+2.	60.436776	1.23	LCP	1.27
21	60.792668	+357.892	+2.	61.152560	1.33	LCP	1.27
22	60.792668	-357.892	-5.5	60.429276	2.62	LCP	0.70
22	60.792668	+357.892	-5.5	61.145060	2.66	LCP	0.70
22	60.792668	-357.892	+5.5	60.440276	2.61	LCP	0.70
22	60.792668	+357.892	+5.5	61.156060	2.67	LCP	0.70
23	60.792668	-357.892	-16.	60.418776	7.01	LCP	0.43
23	60.792668	+357.892	-16.	61.134560	7.40	LCP	0.43
23	60.792668	-357.892	16.	60.450776	7.17	LCP	0.43
23	60.792668	+357.892	16.	61.166560	7.44	LCP	0.43
24	60.792668	-357.892	-50.	60.384776	26.63	LCP	0.44
24	60.792668	+357.892	-50.	61.100560	26.04	LCP	0.44
24	60.792668	-357.892	+50.	60.484776	26.33	LCP	0.44
24	60.792668	+357.892	+50.	61.200560	26.88	LCP	0.44

UAS Line by Line vs. Fast Radiative Transfer Models

Line by Line Transmittance Models

- Line-by-line models provide accurate calculations of the atmospheric transmittances and top of the atmosphere radiances
- Given an atmospheric profile and gaseous constituent concentrations for a given a predefined SSMIS spectral frequency bandwidth
- Assumes local thermodynamic equilibrium (LTE) conditions
- Discrete spectral grid is chosen, depending on how detailed a representation of the line spectrum is desired
- Atmosphere divided into horizontal layers sufficiently thin to be regarded as homogeneous.
- Transmittance Stage - Contributions of all radiating species to the optical depth are summed and these optical depths may themselves be added together to provide the corresponding transmittance.
- Radiance Stage - LTE radiative transfer equation is integrated along the entire viewing path to the satellite.
- Set of spectral radiance values, one for each point on the chosen spectral grid must be convolved with the corresponding channel spectral response function.
- The entire process, layer-by-layer, gas-by-gas, line-by line, and the subsequent channel convolution may be achieved using a line-by-line model. .

General form of Line-by-Line Integrated Opacity

$$\tau_\nu = \sum_{i(layers)} \left[\sum_{j(molecule)} \left(\sum_{k(lines)} \kappa_{\nu k} \right) \right] \times \Delta s_i$$

Δs_i is the path through the atmosphere

$\kappa_{\nu k}$ is the emission coefficent

UAS Line by Line vs. Fast Radiative Transfer Models

Fast RTMs

- Line-by-line approach is not practical for Global applications
- Fast RTMs , such as RTTOV and OPTRAN are very fast and accurate
- Regression relation in which a set of simple profile-dependent predictor functions, based on the layer variables, is governed by a set of channel-dependent coefficients.
- Coefficients are determined by regressing the layer optical depths for a diverse set of atmospheric profiles onto the predictors for the dependent set
- Transmittances are derived by convolving an original set of line-by-line calculations with the spectral response function
- RTTOV is presented with the layer predictors for an independent profile, the transmittance stage for a give instrument channel can proceed very rapidly layer-by-layer through a simple linear combination of predictors and coefficients
- Skill of RTTOV as a fast forward model depends on the appropriate choice of predictors, on the degree to which the predictands are chosen to allow the manipulation of channel-averaged quantities as if they were monochromatic
- The line-by-line models on which RTTOV is based on the Liebe MPM-89/92 model for the SSMIS

UAS Line by Line vs. Fast Radiative Transfer Models

Fast RTMs

- To date a Fast RTM that Includes the Zeeman-Splitting HAS NOT been Developed
- Capability Needs to be Developed for UAS Radiance Assimilation
- Incorporate Geomagnetic into RTM Adjoint (Jacobian)

Doppler Shift Corrections

- Impact of Hardware Doppler Corrections
- Hardware Doppler On Imagery - 2005012505
- Hardware Doppler Off Imagery - 2005012602

Hardware Doppler Shift Corrections ON Switch

DMSP F-16 SSMIS Ch. 19 63.283248±.285271 GHz RCP
DTG: 2005012505
06563-06569

No. Scenes: 743368

Min 3.00
Max 333.22

MEAN 227.01
SDEV 9.43

Doppler On

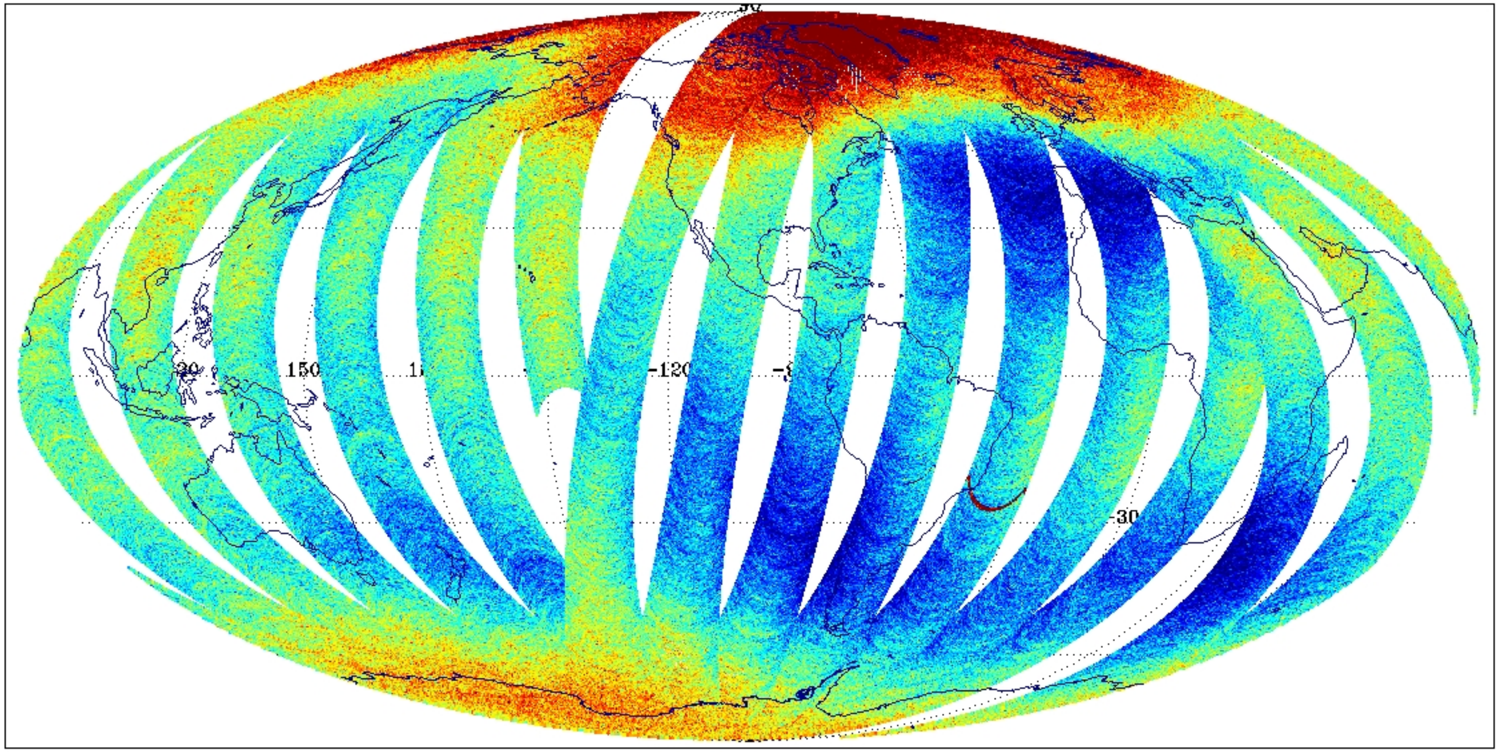

SSMIS Ch 19

Hardware Doppler Shift Corrections ON Switch

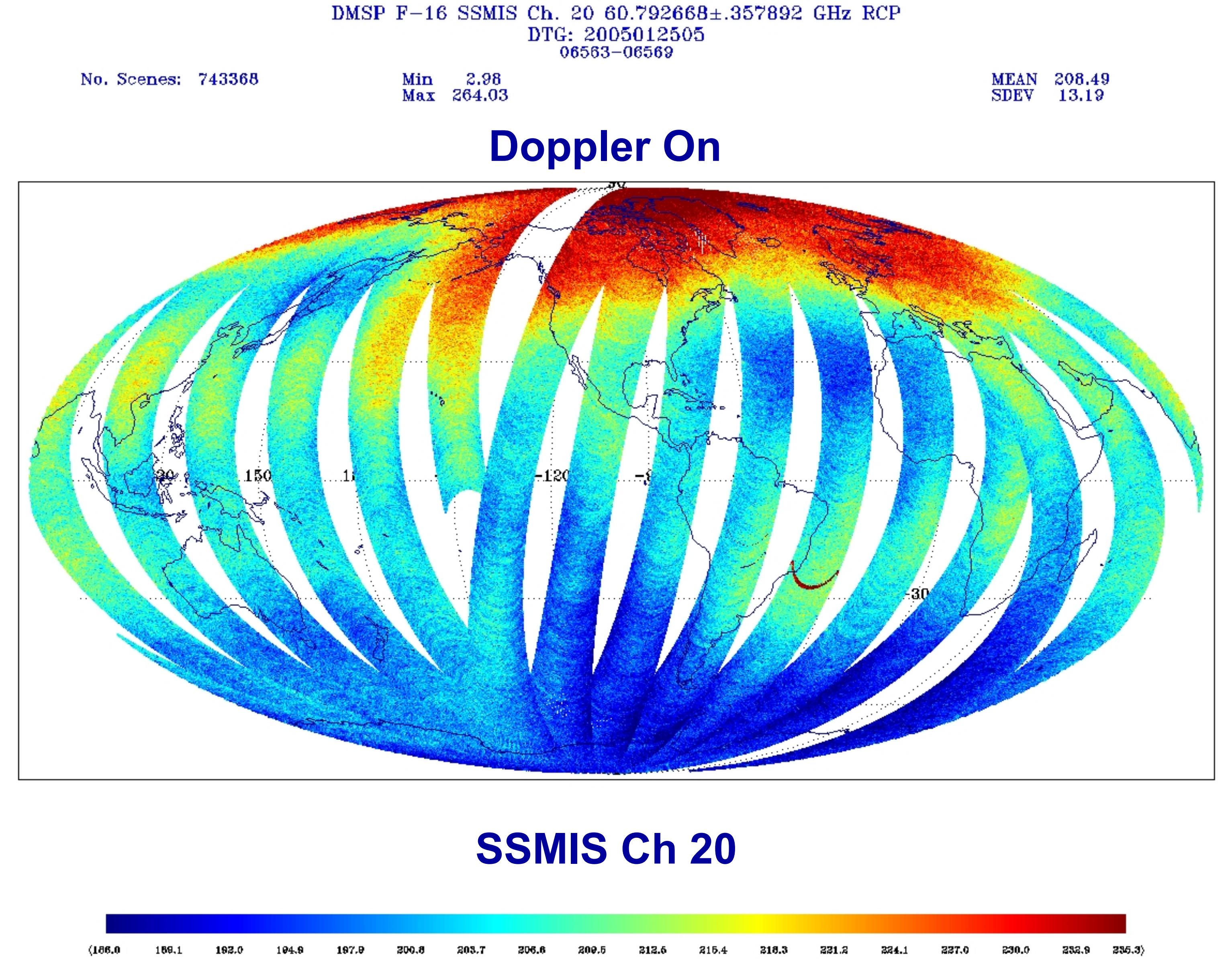

DMSP F-16 SSMIS Ch. 20 60.792668±.357892 GHz RCP
DTG: 2005012505
06563-06569

No. Scenes: 743368

Min 2.98
Max 264.03

MEAN 208.49
SDEV 13.19

Doppler On

SSMIS Ch 20

Hardware Doppler Shift Corrections ON Switch

DMSP F−16 SSMIS Ch. 21 60.792668±.357892±.002 GHz RCP
DTG: 2005012505
06563−06569

No. Scenes: 743368

Min 2.98
Max 289.00

MEAN 247.94
SDEV 7.74

Doppler On

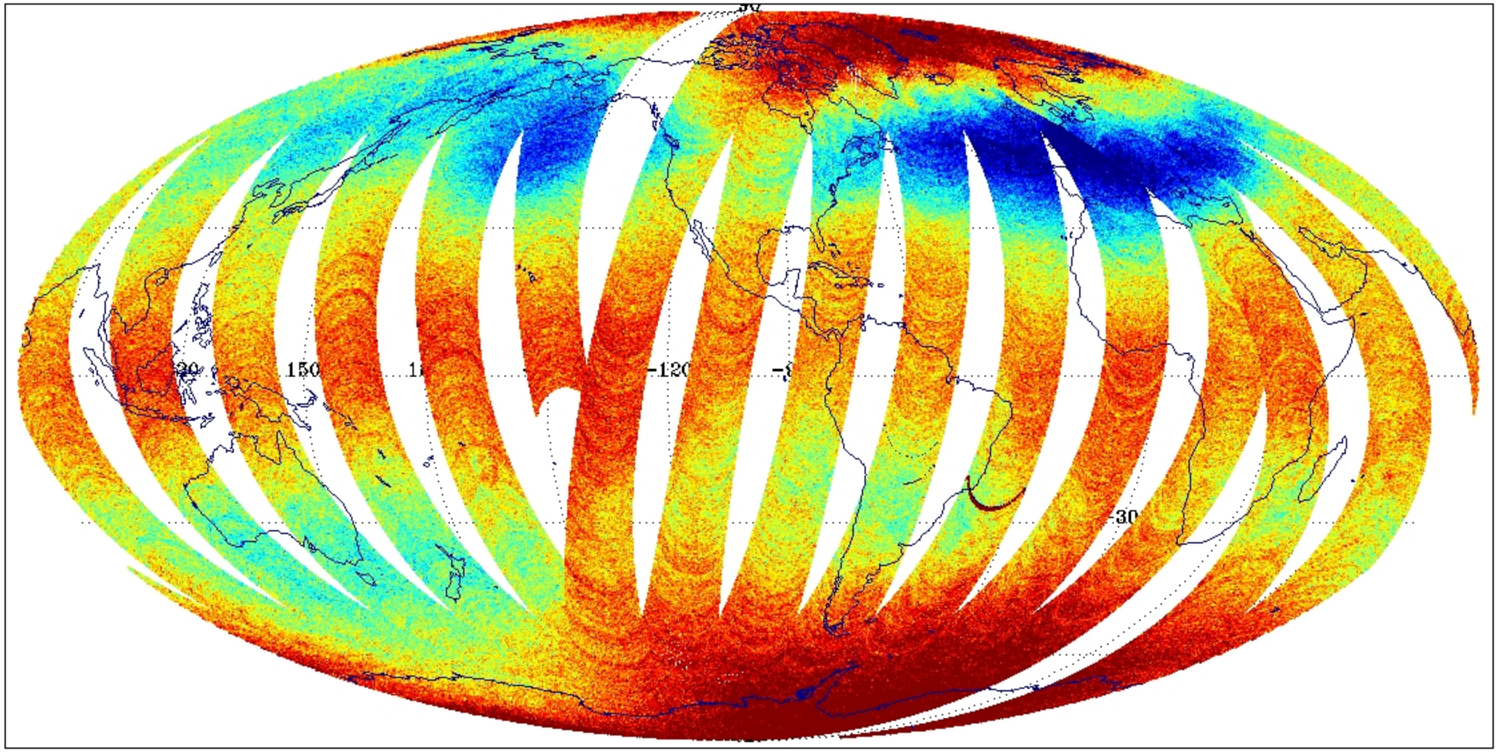

SSMIS Ch 21

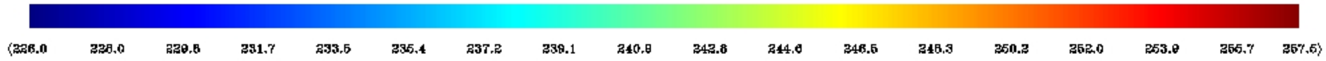

Hardware Doppler Shift Corrections ON Switch

DMSP F−16 SSMIS Ch. 22 60.792668±.357892±.0055 GHz RCP
DTG: 2005012505
06563−06569

No. Scenes: 743368

Min 2.98
Max 320.48

MEAN 252.13
SDEV 9.28

Doppler On

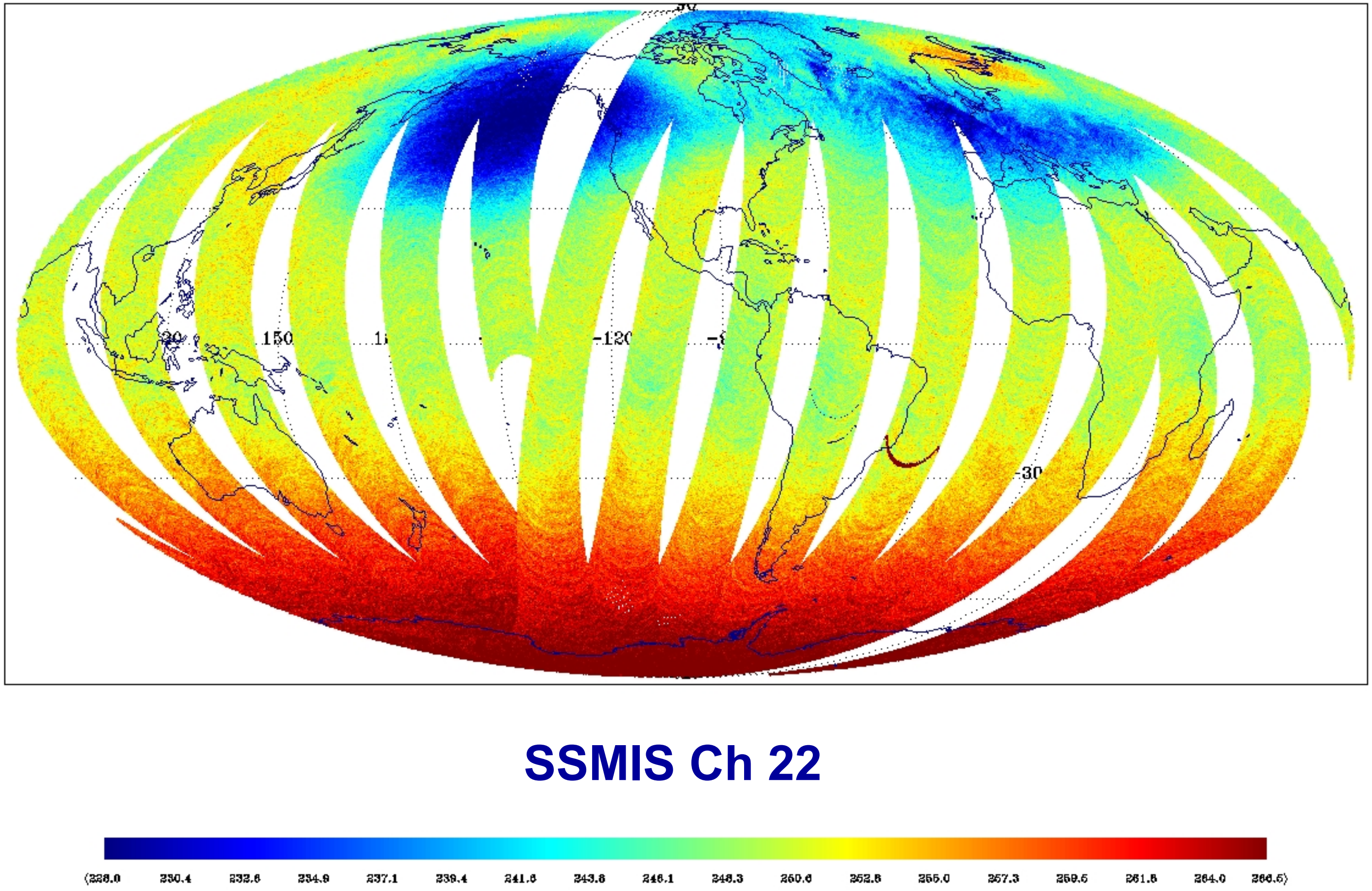

SSMIS Ch 22

Hardware Doppler Shift Corrections ON Switch

DMSP F−16 SSMIS Ch. 23 60.792668±.357892±.016 GHz RCP
DTG: 2005012505
06563−06569

No. Scenes: 743368

Min 2.98
Max 275.78

MEAN 238.32
SDEV 10.07

Doppler On

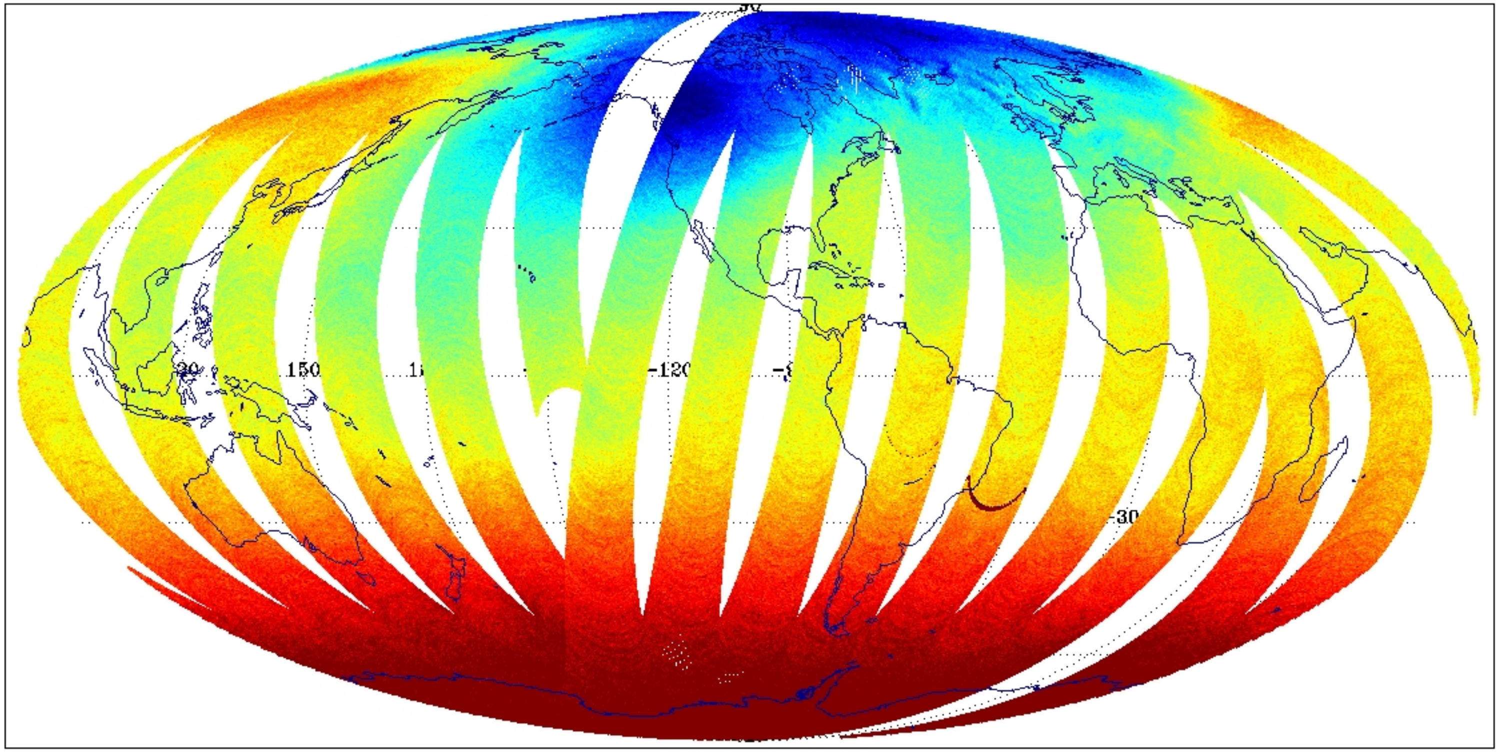

SSMIS Ch 23

Hardware Doppler Shift Corrections in On Mode Dramatically Alter TBs for Channels 19-21, with Bandwidths < 2.0 MHz

Hardware Doppler Shift Corrections were Switched to OFF Mode on January 26, 2005.

Hardware Doppler Shift Corrections Off Switch

DMSP F-16 SSMIS Ch. 19 63.283248±.285271 GHz RCP
DTG: 2005012602
06575–06581

No. Scenes: 710998

Min 3.00
Max 268.43

MEAN 232.53
SDEV 10.29

Doppler Off

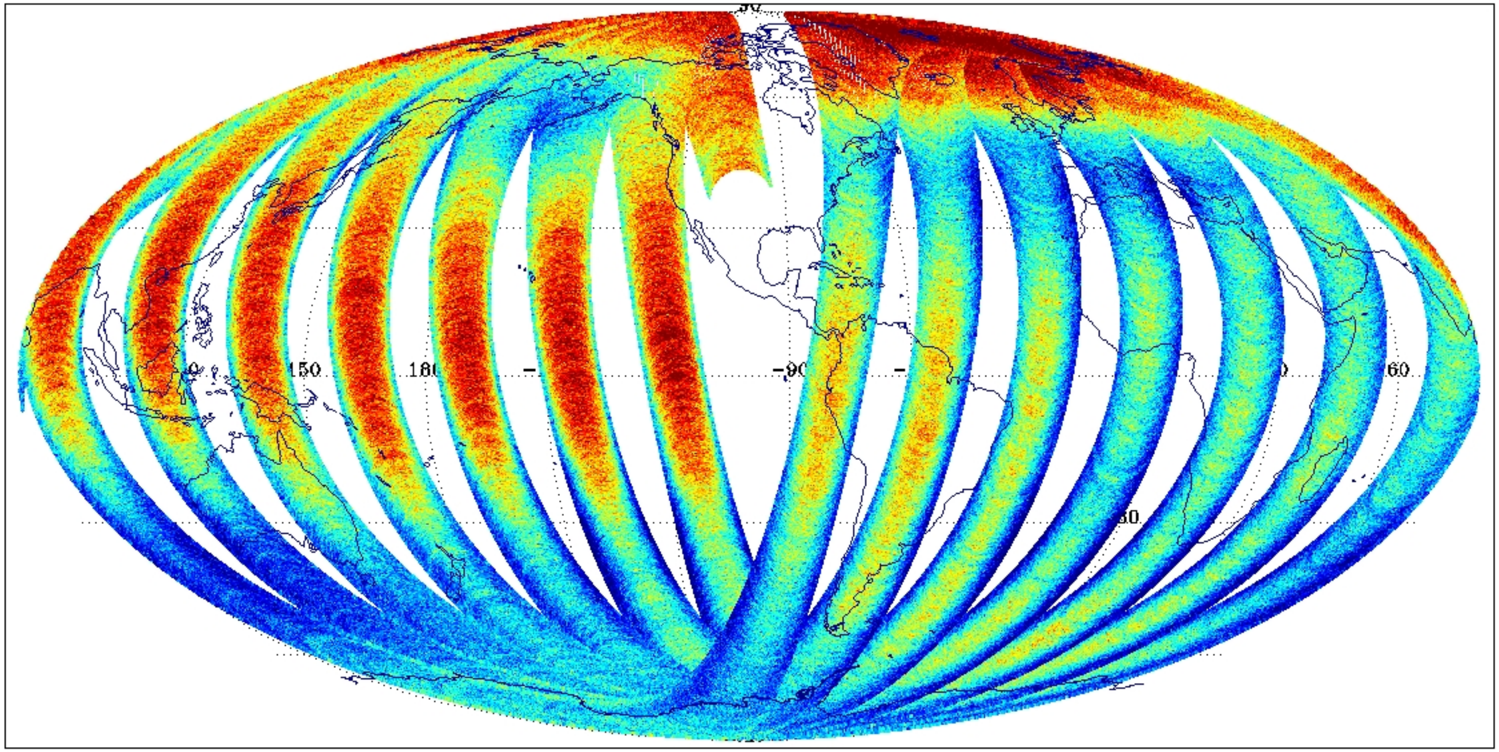

SSMIS Ch 19

Hardware Doppler Shift Corrections Off Switch

DMSP F-16 SSMIS Ch. 20 60.792668±.357892 GHz RCP
DTG: 2005012602
06575-06581

No. Scenes: 710998

Min 2.98
Max 266.94

MEAN 217.16
SDEV 18.07

Doppler Off

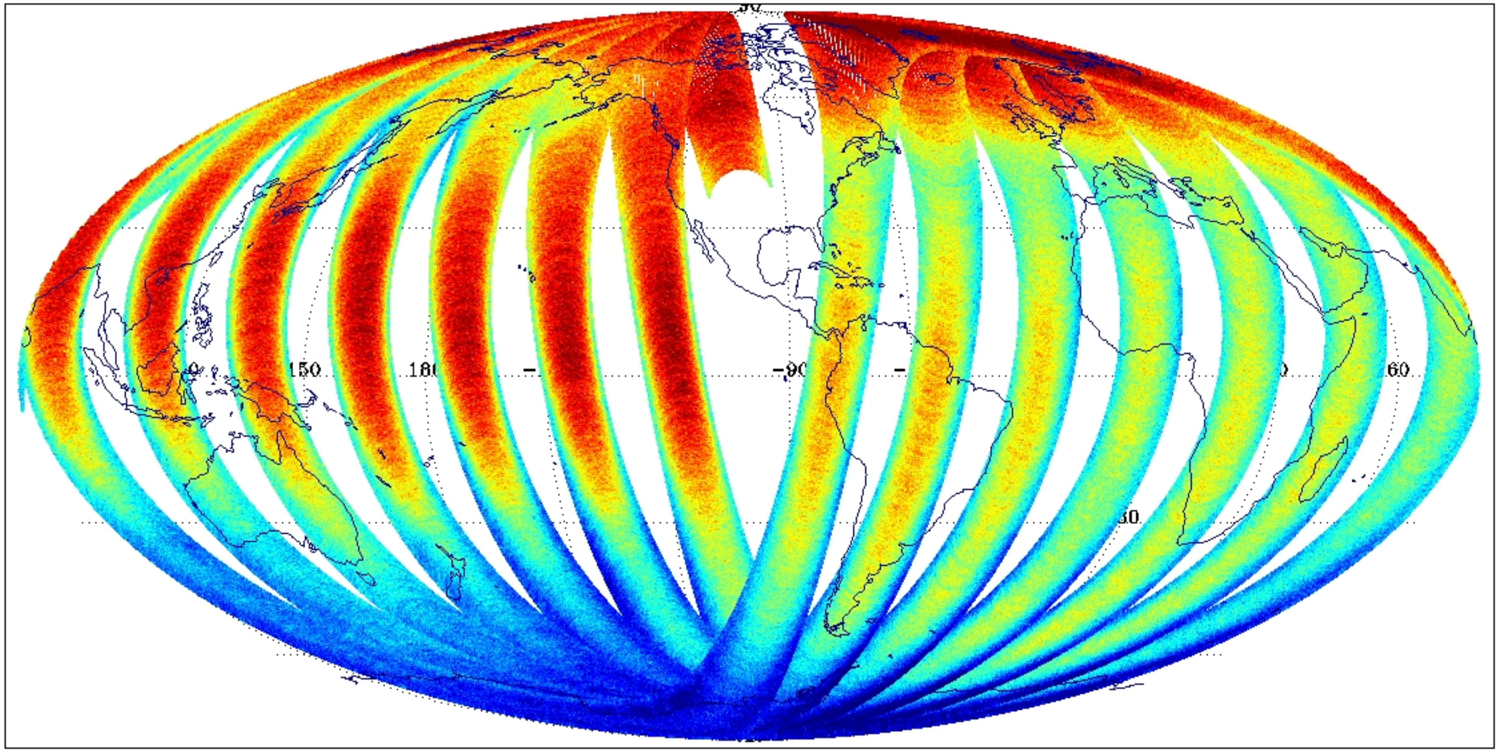

SSMIS Ch 20

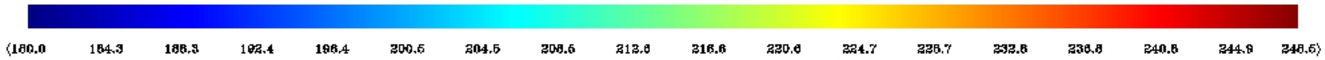

Hardware Doppler Shift Corrections Off Switch

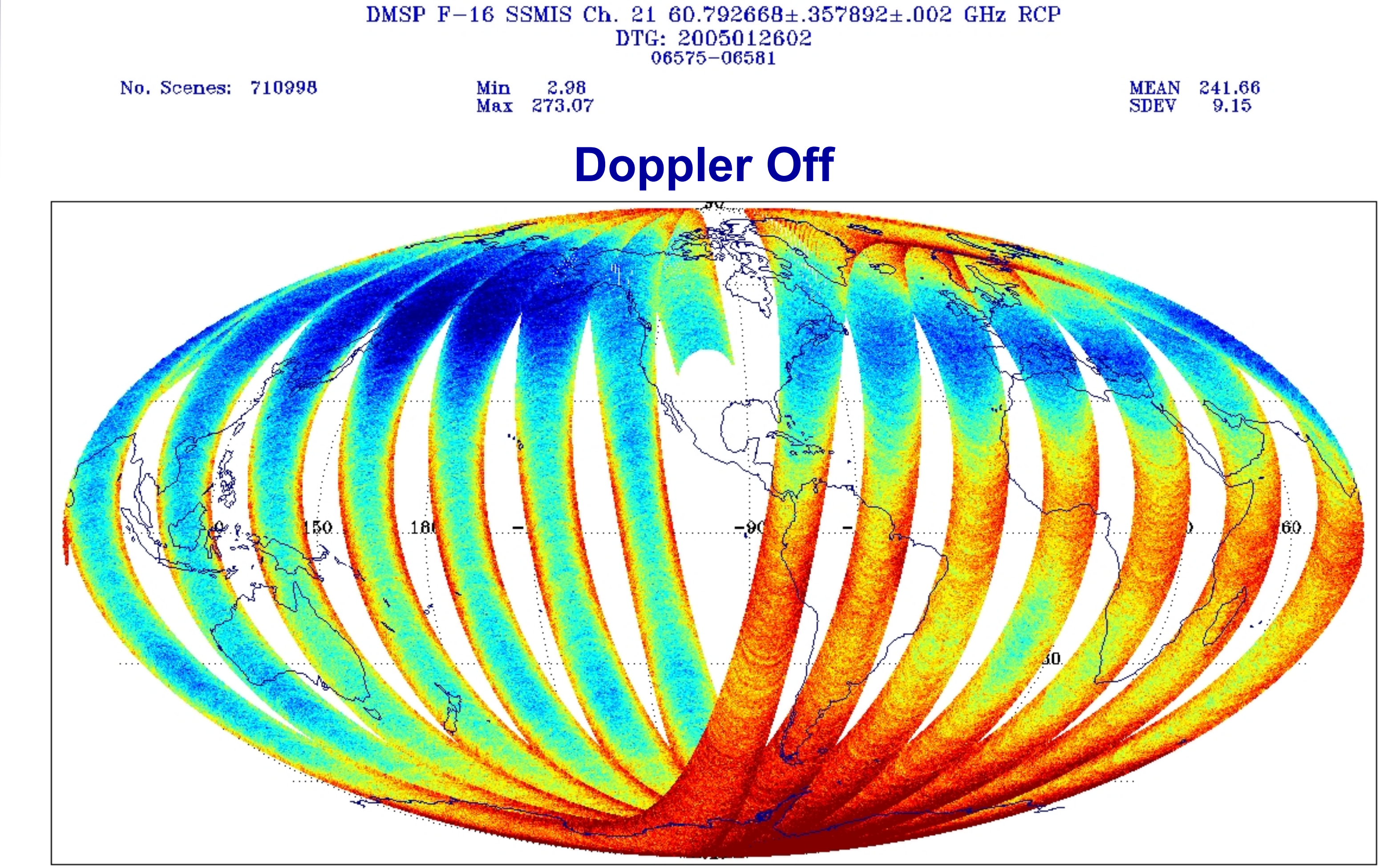

Doppler Off

SSMIS Ch 21

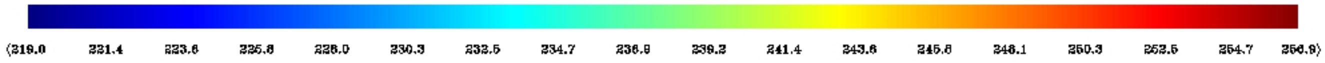

Hardware Doppler Shift Corrections Off Switch

DMSP F-16 SSMIS Ch. 22 60.792668±.357892±.0055 GHz RCP
DTG: 2005012602
06575-06581

No. Scenes: 710998

Min 2.98
Max 276.71

MEAN 252.49
SDEV 8.98

Doppler Off

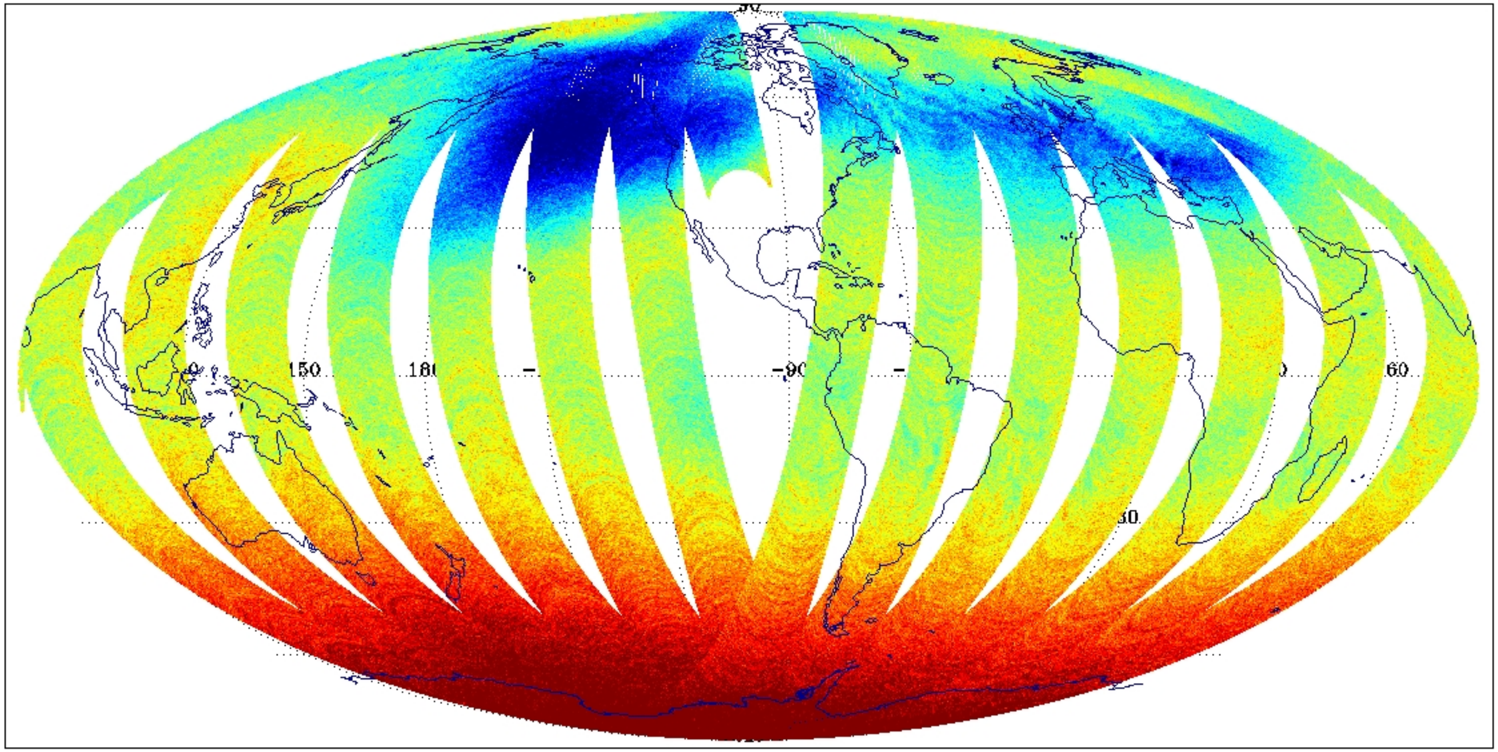

SSMIS Ch 22

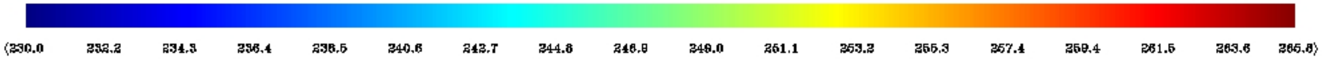

Hardware Doppler Shift Corrections Off Switch

DMSP F-16 SSMIS Ch. 23 60.792668±.357892±.016 GHz RCP
DTG: 2005012602
06575-06581

No. Scenes: 710998

Min 2.98
Max 259.51

MEAN 239.19
SDEV 9.54

Doppler Off

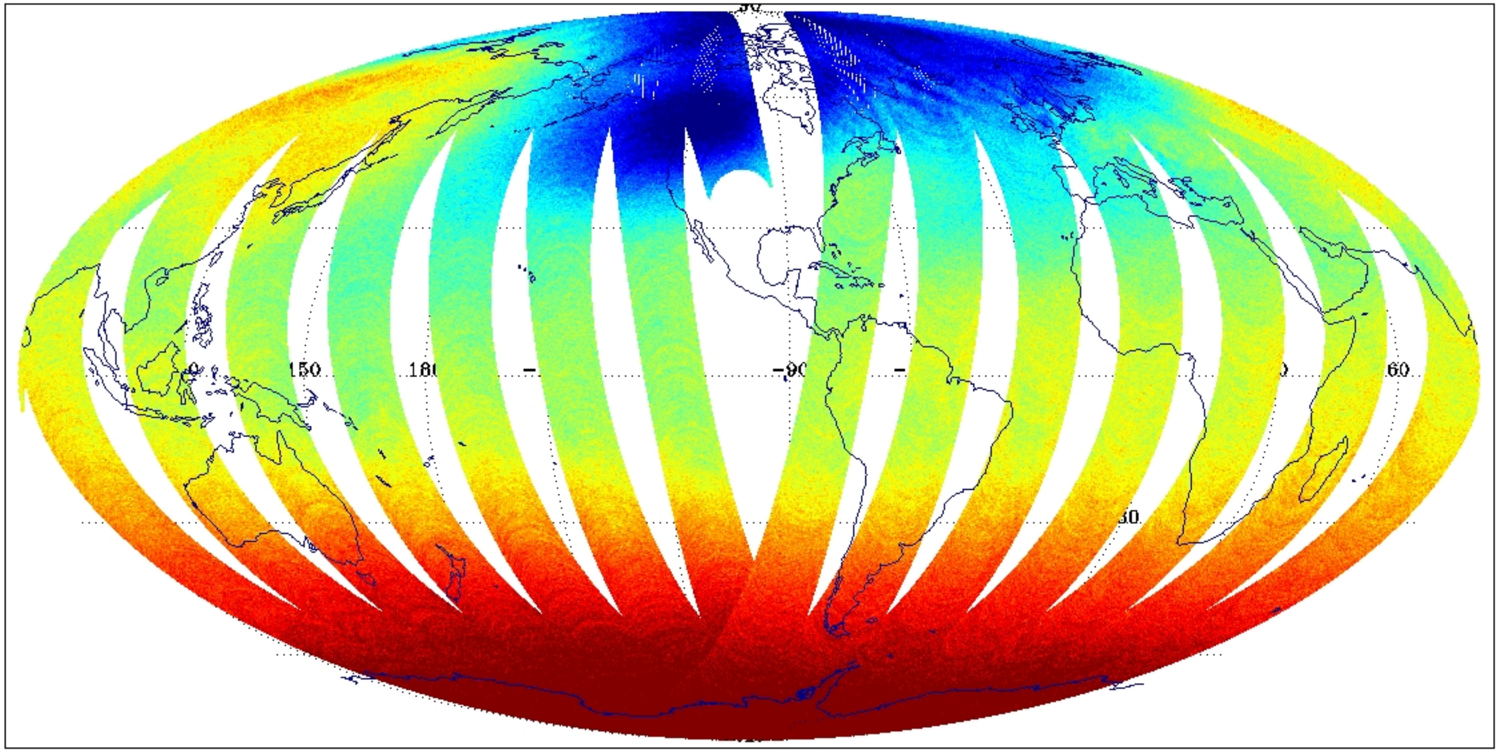

SSMIS Ch 23

Hardware Doppler Shift Corrections Qualitatively Compared in Both On and Off Modes

- TBs for Channels 19-21, with Bandwidths < 2.0 MHz most Effected

SSMIS UAS Channel	Mean Passband Bandwidth [MHz]	Doppler ON Jan. 25, 2005		Doppler OFF Jan. 26, 2005	
		Mean	Std. Dev.	Mean	Std. Dev.
19	1.35	227.0	9.4	232.5	10.5
20	1.36	208.5	13.2	217.2	18.1
21	1.29	247.9	7.7	241.7	9.1
22	2.64	252.1	9.3	252.5	8.4
23	7.25	238.0	10.1	239.2	9.5

- Are these Hardware Doppler Corrections Adequate ?

Doppler Shift Corrections

Dana Kerola and Alex Stogryn

UAS RTM Reconciliations

Hardware

Doppler Compensation

Oscillator frequency Tuning to adjust for Satellite forward Motion Doppler shift as a Function of scan Angle

……………

Involves 1st+2nd down-conversions Of signal thru SAW filters

Software

(Ground-Processing)

SDRP uses "Doppler Compensation Coefficients" to adjust Tb's of lower Air channels

DOPPLER COMPENSATION FOR UAS CHANNELS

- Doppler shifts create a sizeable brightness temperature change in scene data - Therefore corrections have to be made using the on-board Hardware

- The only corrections that could have been made a priori is for the orbital Doppler

- The Doppler shift due to earth rotation appears to be negligible

HARDWARE ---- SOFTWARE

- NG has explored whether on-board down-conversions are adequately performed to account for the frequency dependency of satellite orbital part of Doppler shift across a Channel band-width

Answer: “ YES”

- Incorporated Stogryn derived Doppler shift due to earth rotation
- Model vs. Actual Passband Characterizations
- Polarization Purity ; involves Azimuthal Variation of B-field Orientation and Wave-guide “System Axial Ratio”

Doppler Shift Analysis

1. Doppler Shift:

$$\Delta \mathrm{v} = \frac{\mathrm{v}^{o}}{c} \overline{\mathrm{v}} \cdot \hat{k}$$

$\overline{\mathrm{v}}$ = **Velocity of Emitter Relative to Satellite**

$\hat{k}$ = **Unit Propagation Vector**

2. Decomposition of Velocity:

$$\overline{\mathrm{V}} = -\overline{\mathrm{V}}\, beam + \overline{\mathrm{V}}\, spin$$

$\overline{\mathrm{V}}beam$ = **Velocity of Beam over Emitter (Earth not Rotating)**

$\overline{\mathrm{V}}spin$ = **Velocity of Emitter due to Earth Rotation**

Doppler Shift Analysis

3. Analysis:

$$\bar{r}_e = r_g - (s - \Delta s)\hat{k}$$

$$\bar{\mathrm{v}}_{beam} = \frac{d\,\bar{r}_e}{dt}$$

$$\bar{\mathrm{v}}_{beam} \cdot \hat{k} = \frac{d\,\bar{r}_g}{dt} \cdot \hat{k} - \frac{d}{dt}(s - \Delta s) \qquad \textbf{since} \quad \hat{k} \cdot \frac{d\hat{k}}{dt} = 0$$

$$\bar{\mathrm{v}}_{spin} \cdot \hat{k} = \Omega\,(\hat{z} \times \bar{r}_e) \cdot \hat{k}$$

(Ω = Earth Angular Speed about $\hat{Z}$ Axis)

4. $\Delta \mathrm{v} = (\Delta \mathrm{v})_{orb} + (\Delta \mathrm{v})_{s} + (\Delta \mathrm{v})_{spin}$

Accuracy Criteria

- Based on Spectral Data and Line Widths
  - At a Later Stage, Instrumental Effects (Filter Pass Band Characteristics) will be Included.

1. Spectra
   - Oxygen Molecule Line Centers Known to an Accuracy of ~1-2 KHz
2. Line Widths
   - Pressure Broadening is Dominant Below Height ~70 Km
     - At 70 Km, Width of Individual Zeeman Component ~200 KHz
   - Doppler Broadening due to Thermal Motion of Molecules Dominates above 80 Km
     - Width ~ 50 KHz

Conclusion:

- Doppler Shifts Greater than ~20-30 KHz must be Accounted for in an Accurate Brightness Temperature Calculation

Recommended Equations (Spherical Earth Model)

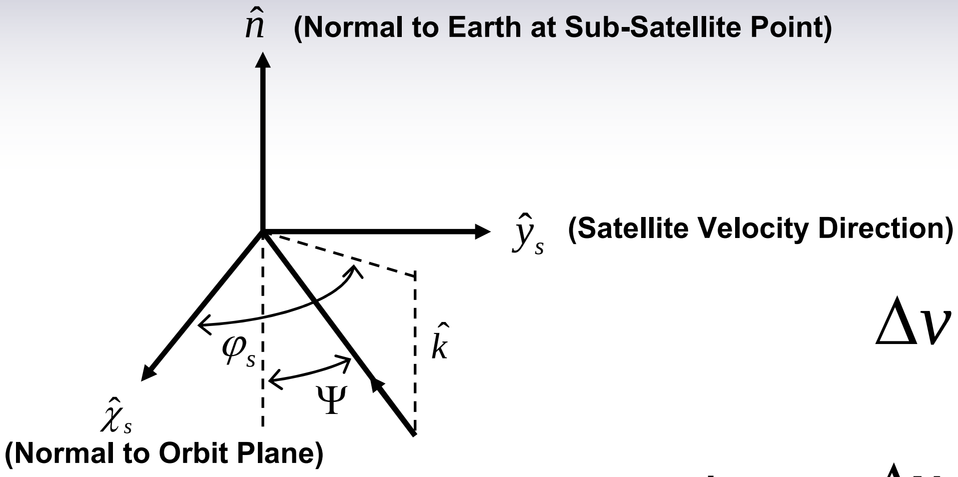
$\hat{n}$ **(Normal to Earth at Sub-Satellite Point)**

$\hat{y}_s$ **(Satellite Velocity Direction)**

$\hat{\chi}_s$ **(Normal to Orbit Plane)**

$$\Delta v = \Delta v_{orb} + \Delta v_{spin}$$

where $$\Delta v_{orb} = \frac{v}{c}\left|\frac{d\bar{r}_s}{dt}\right| \sin\Psi \sin\varphi_s$$

$$\Delta v_{spin} = \frac{v}{c}\Omega R_{orb} \sin \Psi \left\{\sin \varphi_s \cos i_{orb} \mp \cos \varphi_s \sqrt{\sin^2 i_{orb} - \sin^2 \lambda}\right\}$$

R_{orb} = Radius of Satellite Orbit
λ = latitude of Satellite Orbit
i_{orb} = Supplement of Orbit Inclination Angle
– Sign for Ascending Part of Orbit
+ Sign for Descending Part of Orbit

ADD “ACTIVE INGREDIENTS” TO RTM

If you put into Radiative Transfer code: →	You get what SSMIS would see if:
1) FULL DOPPLER	no correction were made for orbital motion + earth spin
2) EARTH SPIN ONLY	“Hardware” Doppler is ON
3) NO DOPPLER	no “Doppler errors” exist

SIMULATED ORBIT T_b CALCULATIONS

Results for sub-satellite latitude near equator, Using orbital simulation code of Barbara Burns in unison with “SSMIS S/N 02- specific” RTM input parameters.

SIMULATED ORBIT T_b RESULTS WITH DOPPLER RTM INGREDIENTS

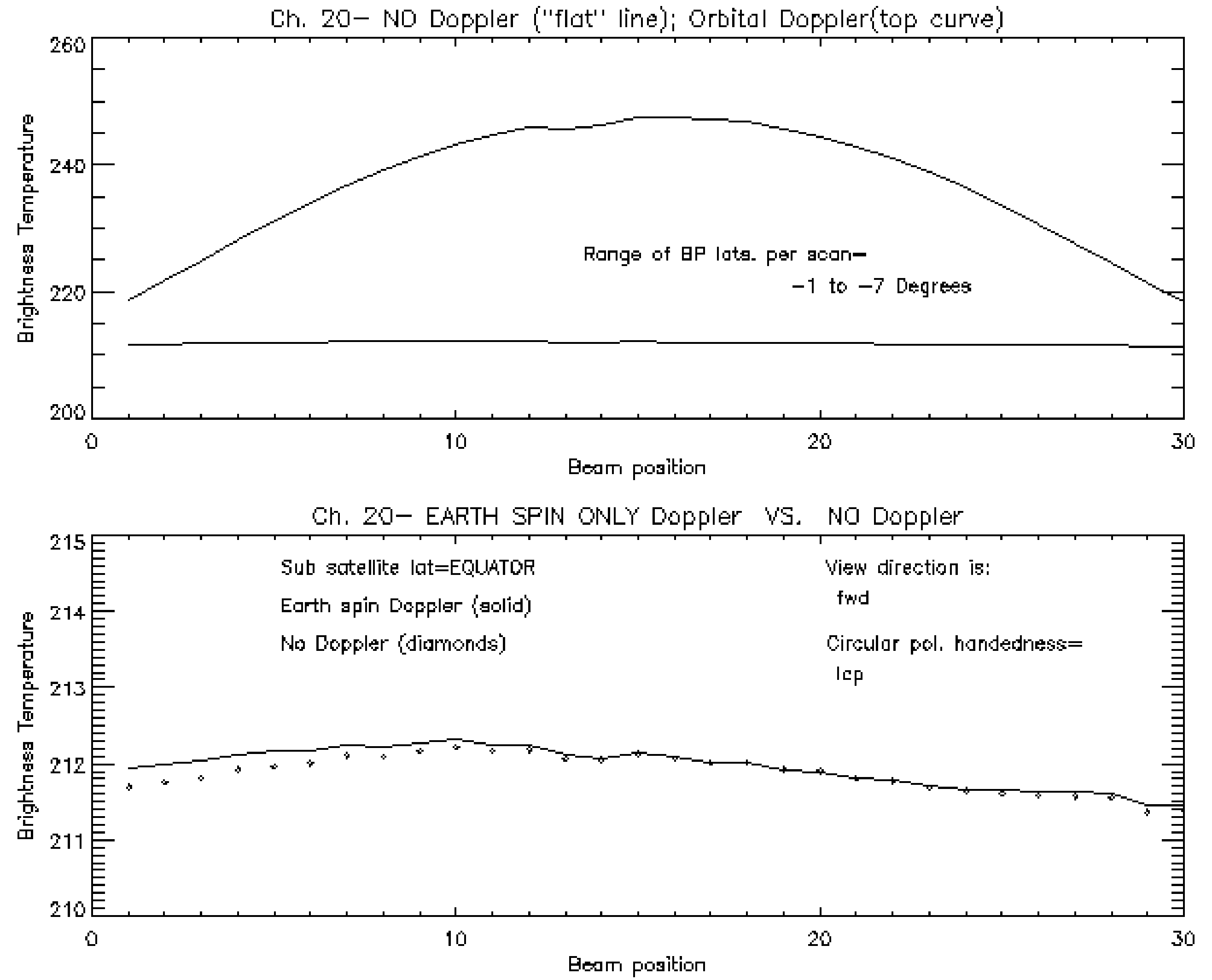

Ch. 20– NO Doppler ("flat" line); Orbital Doppler(top curve)

Ch. 20– EARTH SPIN ONLY Doppler VS. NO Doppler

SSMIS Serial No. 2 Passbands

- **UAS channels 19 thru 24 - We re-examined the calculation (from "research-grade" code) of net transmitted signal across the double (ch. 19 and 20) and quadruple (ch. 21 thru 24) sidebands.**

- **To improve accuracy of T_b determination, a 13th – order polynomial was fit to the "as-measured" , original digitized passband shapes. 20-pt Gaussian quadrature was then performed on the fitted function to determine each channel's "Gain".**

- **Normalization of Gain: We require that the integral of gain over all sidebands be equal to 1.0**

UAS Additional Complexities

- Doppler Shift Corrections
- UAS RTMs (NRL, NGES, Aerospace)
- Band Pass Filter Descriptions
- Polarization Impurity

UAS Radiative Transfer Models

The SSMIS UAS Radiative Transfer Model in the Presence of a Directional Geomagnetic Field, B, means that the atmosphere cannot be considered isotropic but rather, must be treated as an anisotropic medium with polarization-dependent absorption coefficients.

UAS Radiative Transfer Models

Scalar Radiative Transfer Equation

$$T_B(l,\nu)=T_B(0,\nu)\exp(\text{-}\tau_l)+T_B\left[1-\exp(\text{-}\tau_l)\right]$$

Matrix Radiative Transfer Equation

$$T_B(l,\nu)=\exp(\text{-}\mathbf{G}_l)T_B(0,\nu)\exp(\text{-}\mathbf{G}_l^*)+T_B\left[\mathbf{I}-\exp(\text{-}\mathbf{G}_l)\exp(\text{-}\mathbf{G}_l^*)\right]$$

where Tb is now a Coherence Matrix, and τ_ℓ has been replaced with the Complex Propagation Tensor (G_ℓ) , which is a function of the Magnetic Susceptibilty Tensor.

UAS Radiative Transfer Models

The matrix G is defined as

$$\mathbf{G} = -ik\left[\mathbf{I} + \boldsymbol{\chi}'/2\right]$$

where I is the Identity matrix and

$\boldsymbol{\chi}'$ is a 2×2 Susceptibility matrix

$$\boldsymbol{\chi}' = \begin{pmatrix} \chi_{rr}' & \chi_{rh}' \\ \chi_{hr}' & \chi_{hh}' \end{pmatrix}$$

Brightness Temperature Matrix

$$T_B = \begin{pmatrix} T_r & T_{vh} \\ T_{hv} & T_h \end{pmatrix}$$

NRL Line by Line UAS Radiative Transfer Model

- Magnetic Susceptibility Tensor Models Include:
  - Stogryn Model (AS00)
  - Hufford and Liebe (NTIA Report 89-249)
- Both NASA 2000 IGRF Model or NIMA WMM Available
- Uses Geometric Altitude as Vertical Coordinate
- Simulations performed with the both rectangular and actual filter shapes fit to 100 pt. smoothed curve
- Lorentzian Line Shapes
- Trapezoidal Integration over passbands

Northrop-Grumman Line by Line UAS RTM

- Outgrowth of Stogryn's original ATRAN RTM
- Stogryn's (AS00) Magnetic Susceptibility Tensor Model
- Uses Geometric Altitude as Vertical Coordinate
- Gaussian Quadrature using 20 Gauss Points over Passband Frequencies
- Passband Shapes described by 13th order polynomial
- Voigt Line Shapes

Aerospace UAS RTM

- Outgrowth of Rosenkranz and Staelin (1988) RTM
- Stogryn's (AS00) Magnetic Susceptibility Tensor Model
- Uses Geometric Altitude as Vertical Coordinate
- Simulations performed with the both rectangular and actual filter shapes fit to 100 pt. smoothed curve
- Voigt Line Shapes

UAS Additional Complexities

- Doppler Shift Corrections
- UAS RTMs (NRL, NGES, Aerospace)
- Band Pass Filter Descriptions
- Polarization Impurity

Passband Shape Depictions — CH19 (2 side bands)

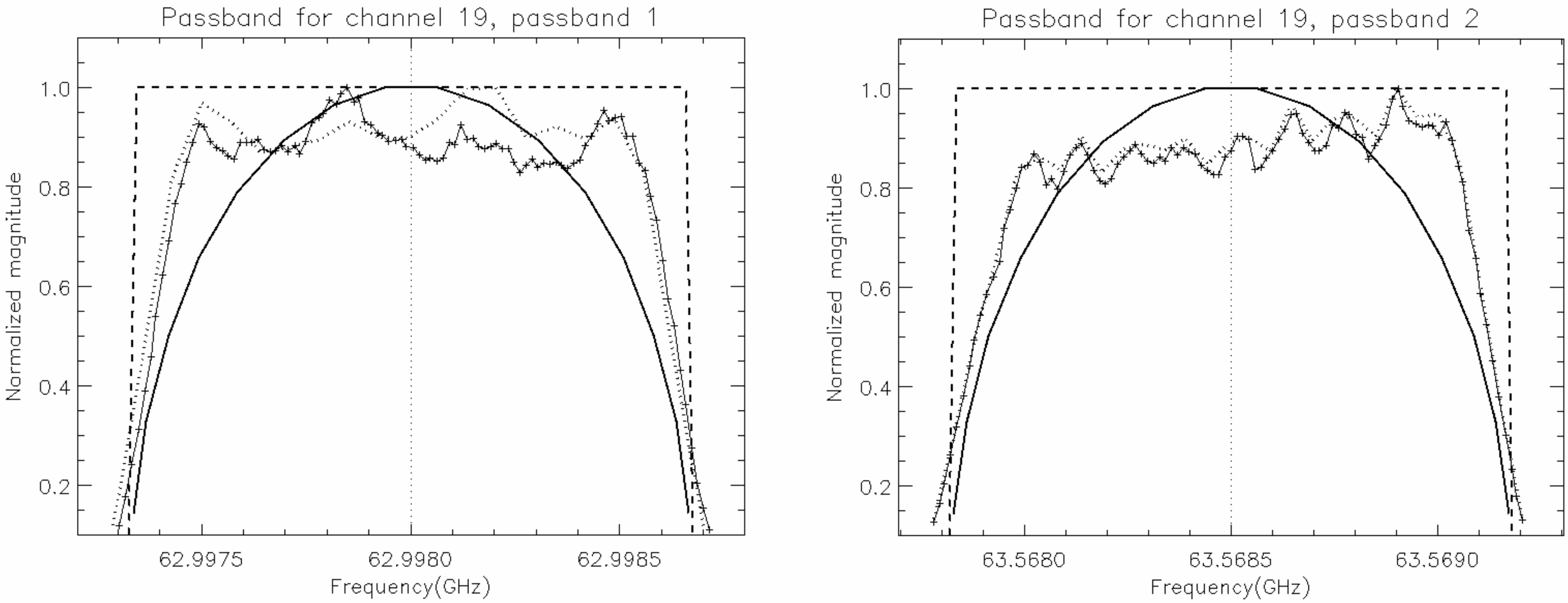

•••••••••• **SN2ffpb, provided by B. Burns (NGES), used for simulations**

—— **SN2recpb, provided by B. Burns (NGES)**

++++++++++ **100 Point Smoothed (NRL, Swadley) used for simulations at NRL and Aerospace**

Passband Shape Depictions — CH20 (2 side bands)

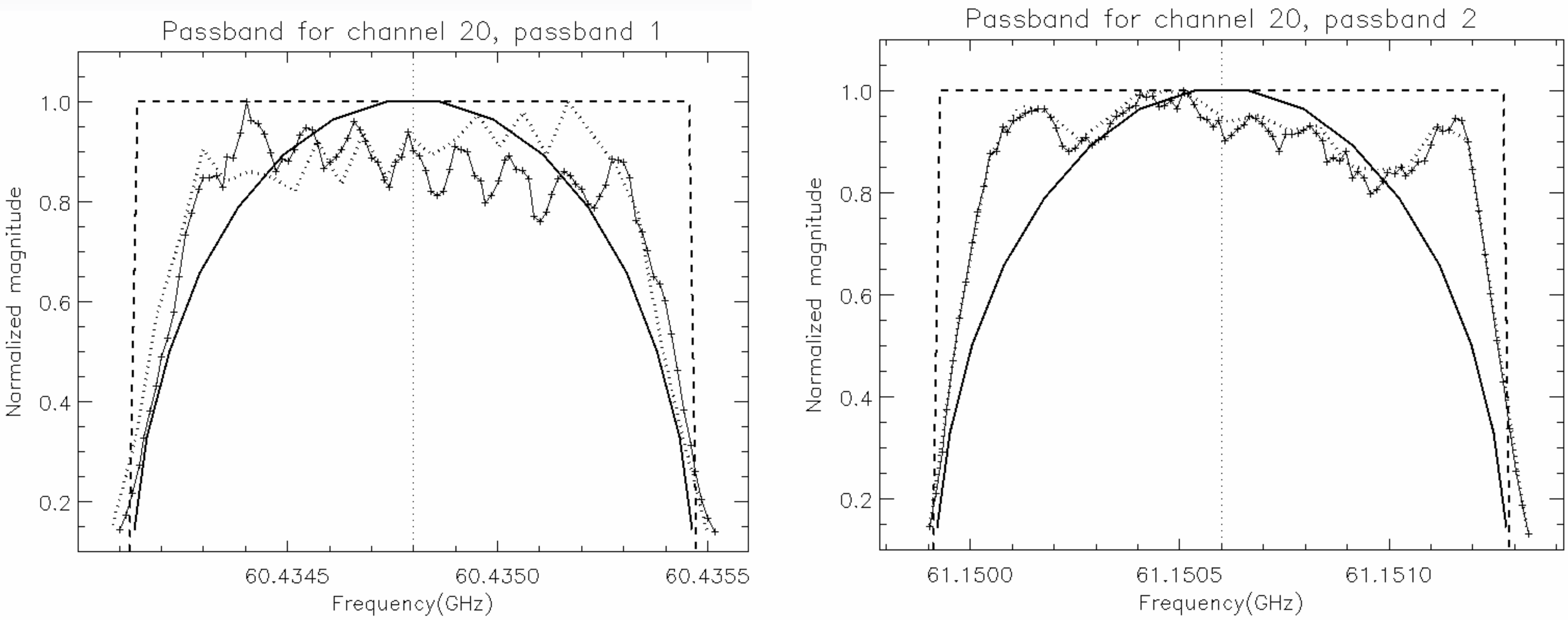

•••••••••• SN2ffpb, provided by B. Burns (NGES), used for simulations

——— SN2recpb, provided by B. Burns (NGES)

++++++++++ 100 Point Smoothed (NRL, Swadley) used for simulations at NRL and Aerospace

Passband Shape Depictions — CH21 (4 side bands)

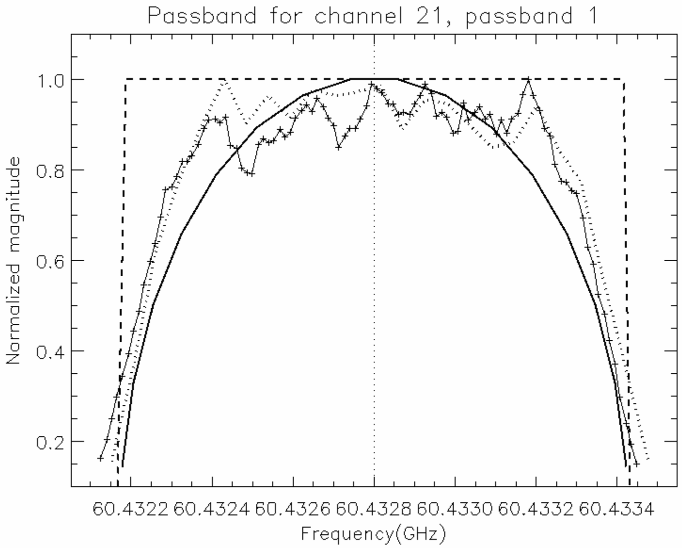

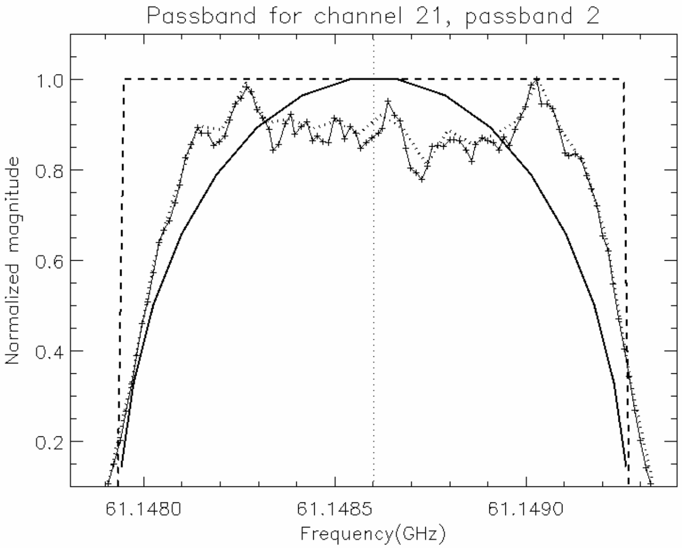

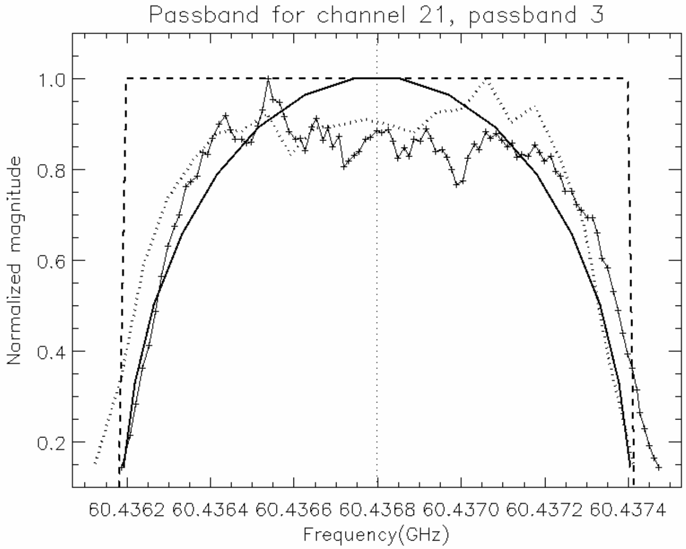

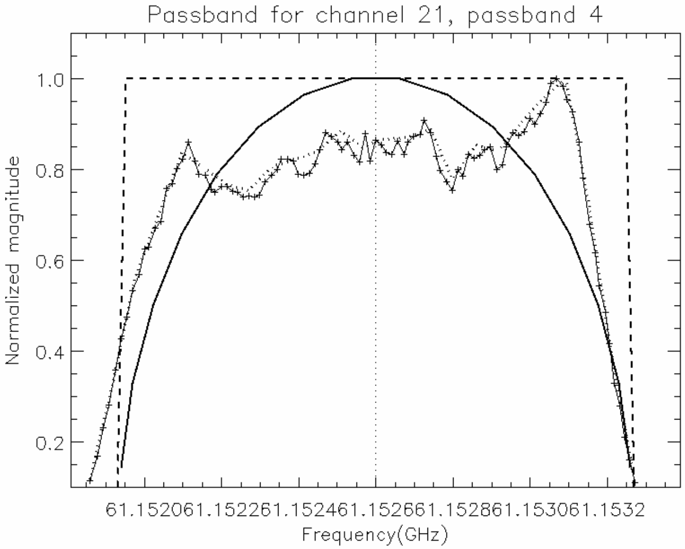

••••••••••••

SN2ffpb, provided by B. Burns (NGES), used for simulations

————

SN2ffpb, provided by B. Burns (NGES)

++++++++++

100 Point Smoothed (NRL, Swadley) used for simulations at NRL and Aerospace

Passband Shape Depictions — CH22 (4 side bands)

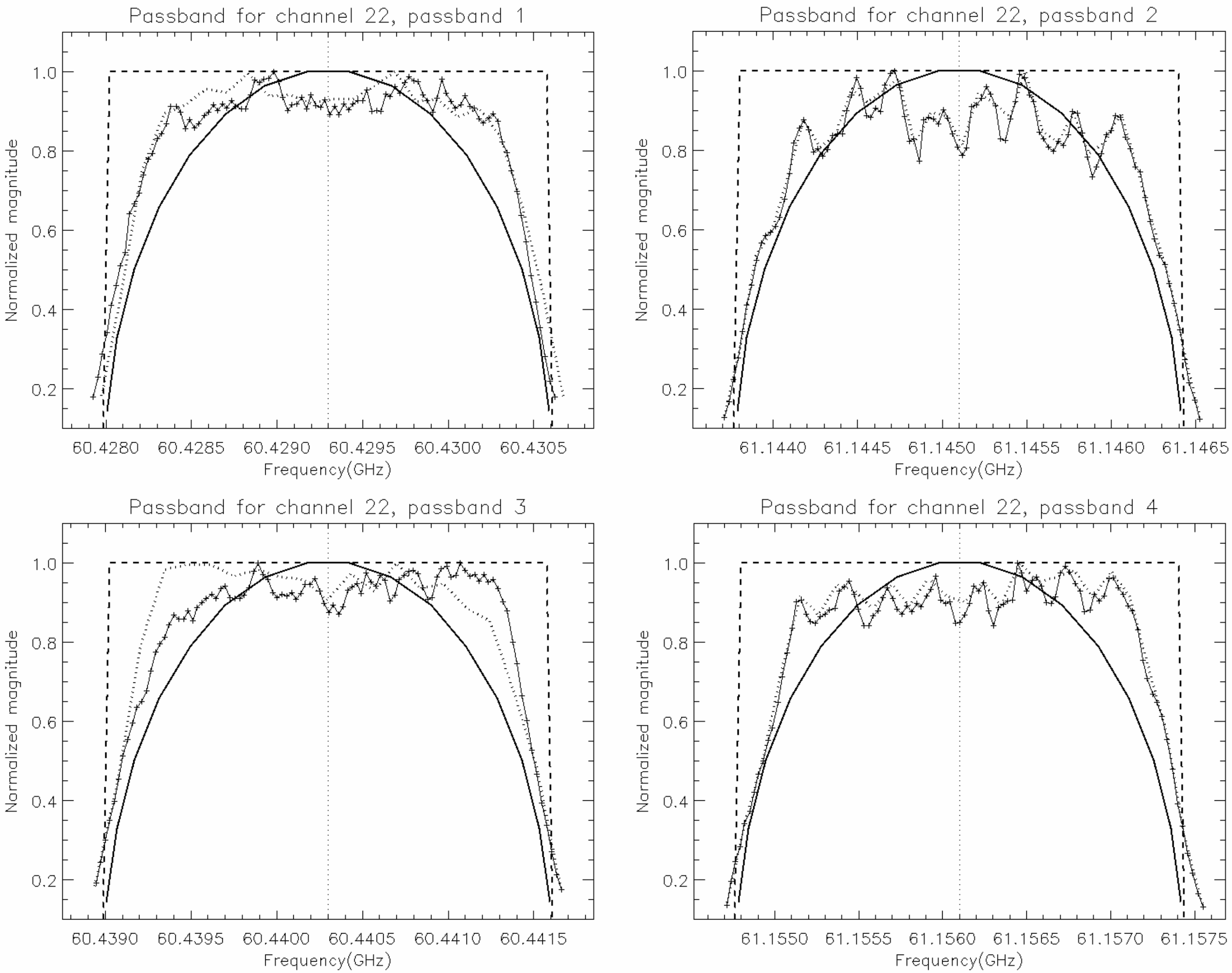

············

SN2ffpb, provided by B. Burns (NGES), used for simulations

———————

SN2ffpb, provided by B. Burns (NGES)

++++++++++

100 Point Smoothed (NRL, Swadley) used for simulations at NRL and Aerospace

Passband Shape Depictions — CH23 (4 side bands)

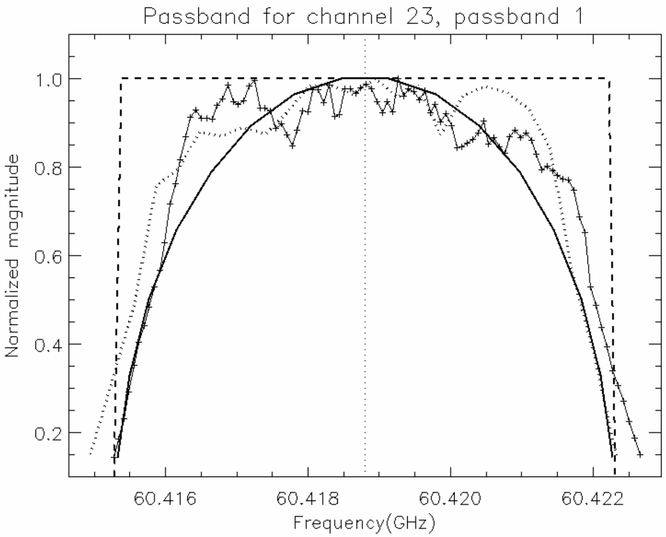
Passband for channel 23, passband 1

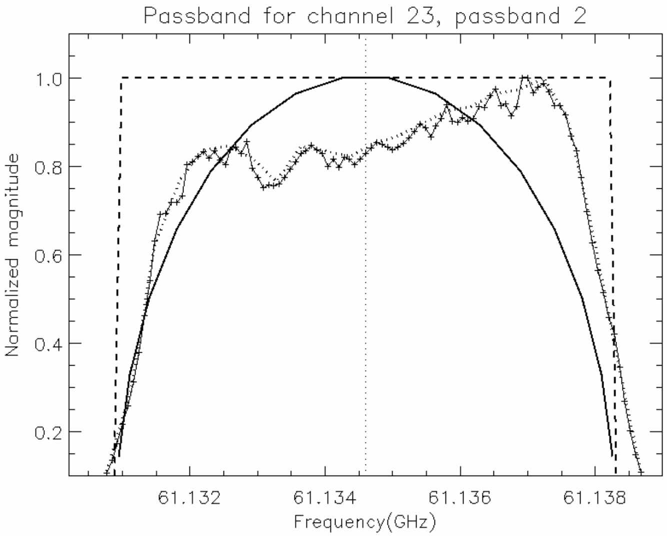
Passband for channel 23, passband 2

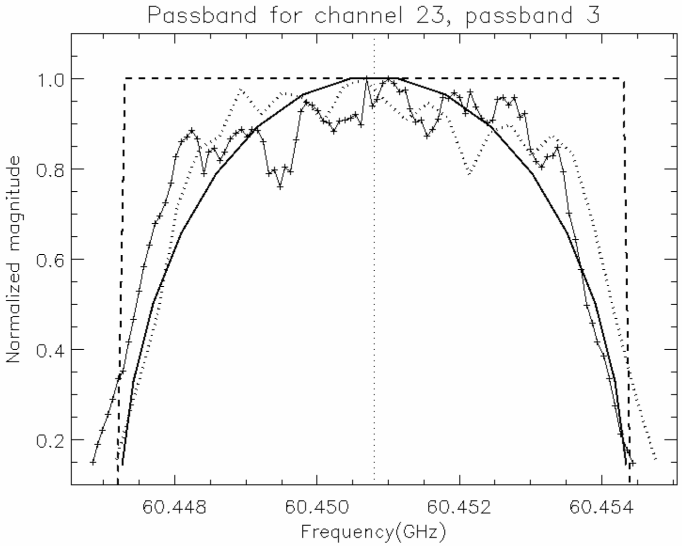
Passband for channel 23, passband 3

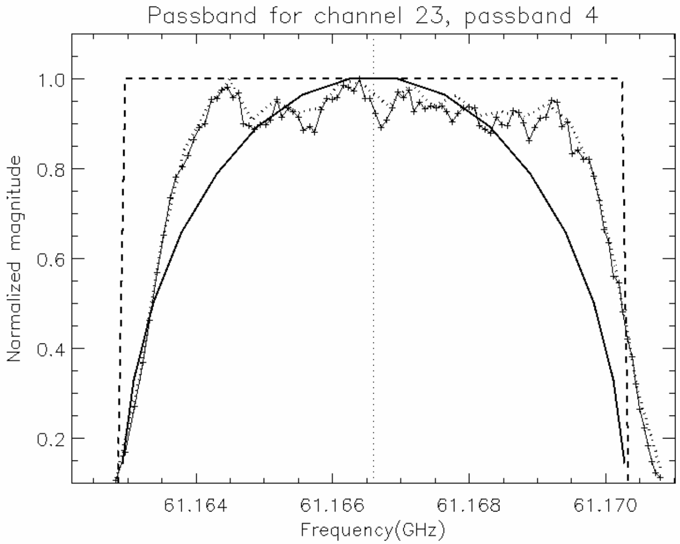
Passband for channel 23, passband 4

…………

SN2ffpb, provided by B. Burns (NGES), used for simulations

————

SN2ffpb, provided by B. Burns (NGES)

++++++++++

100 Point Smoothed (NRL, Swadley) used for simulations at NRL and Aerospace

Passband Shape Depictions — CH24 (4 side bands)

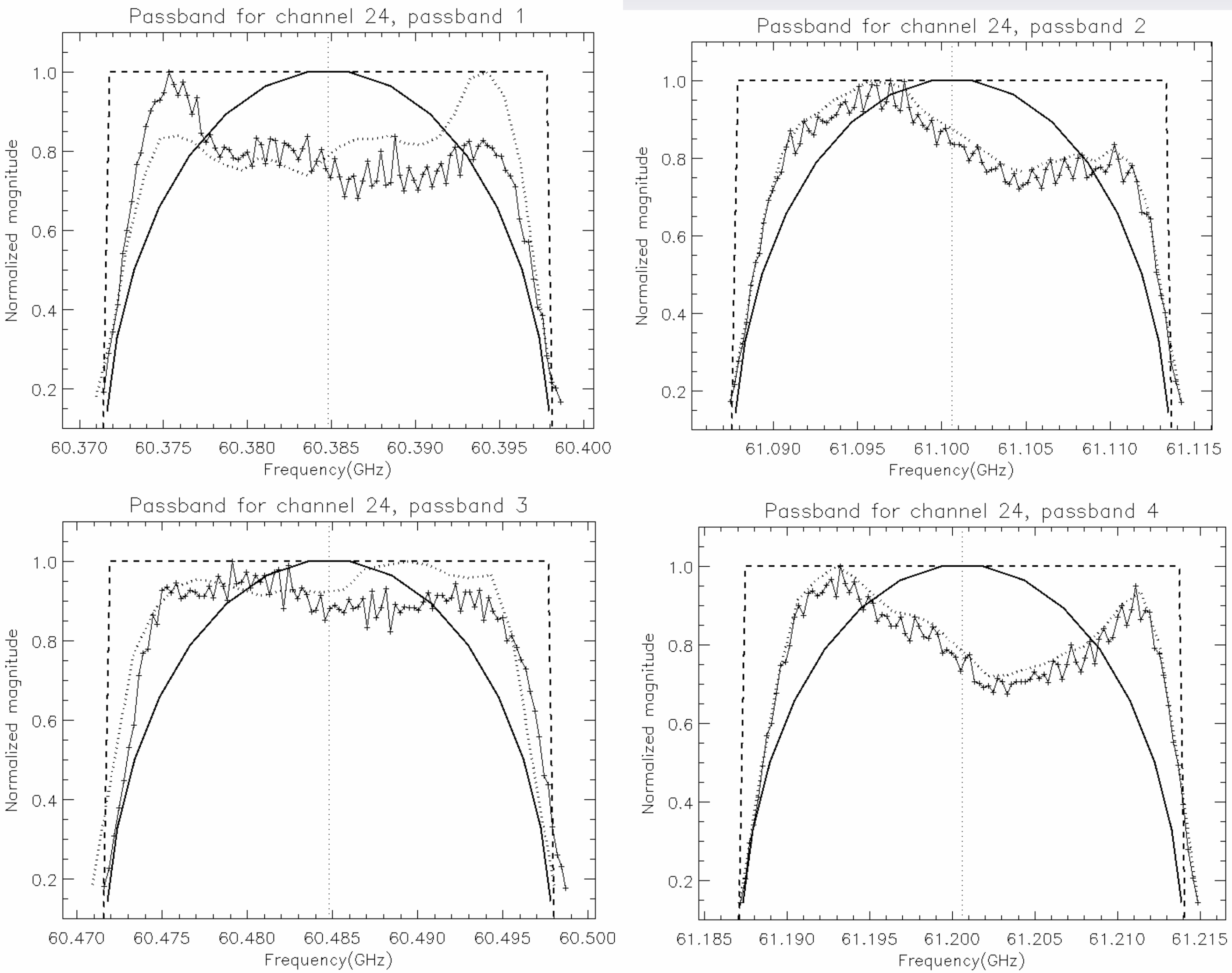

••••••••••••

SN2ffpb, provided by B. Burns (NGES), used for simulations

————————

SN2ffpb, provided by B. Burns (NGES)

++++++++++

100 Point Smoothed (NRL, Swadley) used for simulations at NRL and Aerospace

UAS Additional Complexities

- Doppler Shift Corrections
- UAS RTMs (NRL, NGES, Aerospace)
- Band Pass Filter Descriptions
- Polarization Purity

EFFECTS OF POLARIZATION IMPURITY

- **SSMIS SN2 IDEALLY MEASURES CIRCULARLY POLARIZED ATMOSPHERIC SIGNALS --**

(1) Departures from "pure" Circular Polarization are evident;

(2) Goal in Radiative Transfer Modeling is to do a sensitivity study of simulated orbital - dependent ΔT_b vs. beam position for waveguide "system axial ratios" not equal to 1.

HANDEDNESS OF CIRCULAR POLARIZATION (IEEE vs. physics)

- In terms of the “physics” convention
- Left hand circular polarization (LCP) using right-hand rule is depicted as:

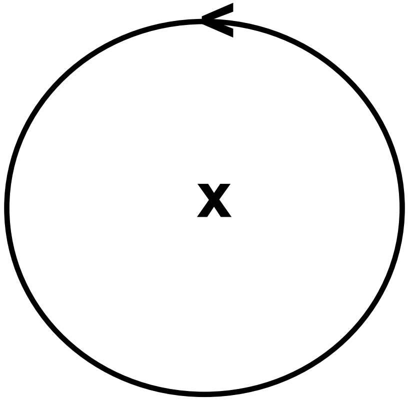

CHANGE IN T_b DUE TO DEPARTURES FROM PURE CIRCULAR POLARIZATION

System Axial Ratio, r

Expressed in terms of dB:

AR=20 log(E_x / E_y)

cf. Don Radovich memo which recommended a maximum value AR=0.5 dB (equivalent to r = 1.06)

Deviations from T_L due to an Axial Ratios different from 1 = Δ

$$\Delta = 0.5\,[(1- rr^*) / (1 + rr^*)](T_{11} - T_{22}) + [1 / (1 + rr^*)]\ \mathrm{Im}\,[(1 + rr^* - 2r^*)\,T_{12}]$$

(Stogryn)

Where, $T_{11}-T_{22} = (\cos^2\Phi_B - \sin^2\Phi_B)T_{v'} + (\sin^2\Phi_B - \cos^2\Phi_B)T_{h'} - (4\sin\Phi_B\cos\Phi_B)\ \mathrm{Re}\ T_{v'h'}$

And, $T_{12} = \sin\Phi_B\cos\Phi_B\,(T_{v'} - T_{h'}) + (\cos^2\Phi_B - \sin^2\Phi_B)\ \mathrm{Re}\ T_{v'h'} + i\ \mathrm{Im}\ T_{v'h'}$

Δ for System Axial Ratios r ; where r is a Real Number

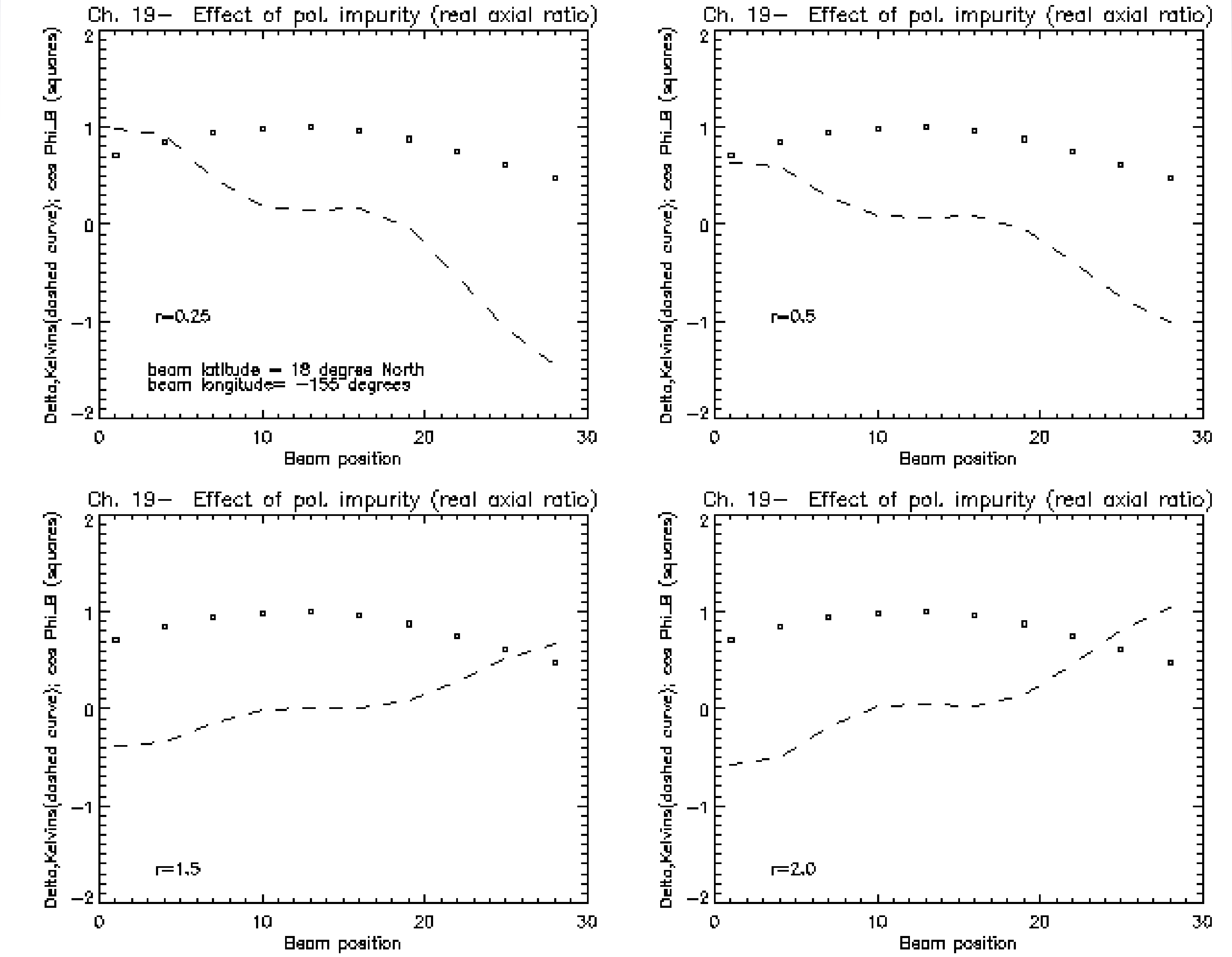

DOWN-CONVERSION THROUGH SAW FILTERS

- **The Doppler shift due to the Orbital Motion of the Satellite is compensated for by tuning the frequency of Local Oscillator as a function of scan angle**

shift to 1st LO @ 56400MHz = 1200 x DOF

shift to 2nd LO @ 4512 MHz = 96 x DOF

shift to 3rd LO @ 6768 MHz = 144 x DOF

where DOF=Doppler Offset Frequency=817.708 Hz

DEVIATION FROM SAW FILTER CENTER

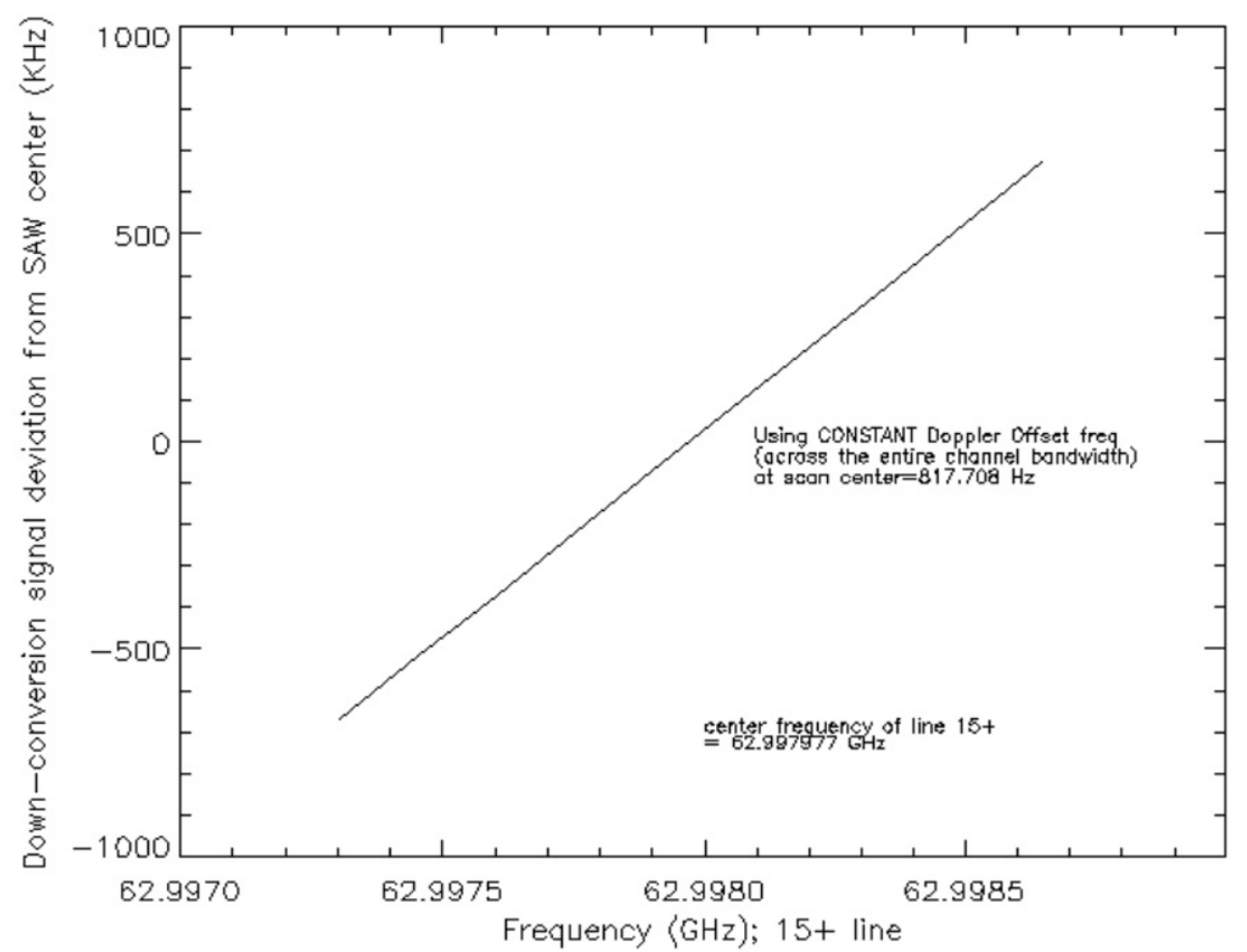

DOF NEEDED TO KEEP SIGNAL AT CENTER FREQUENCY OF SAW

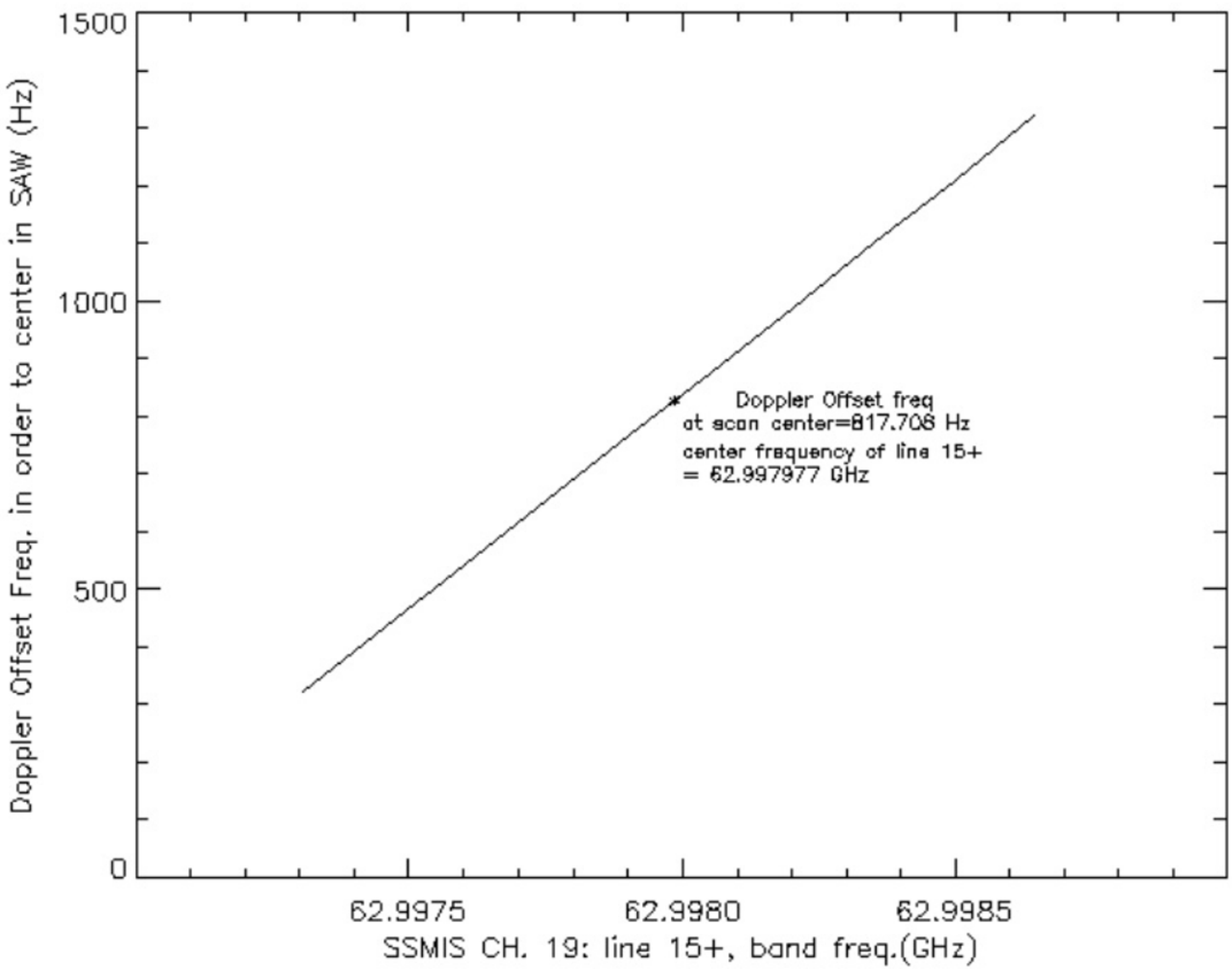

Section 10.4 Data Acquisition Plan

- Lidar Observational Campaigns

- ECMWF MWP Analyses

- Rocketsonde Observations

SSMIS Cal/Val Lidar Coincident Observations Data Base

- JPL Table Mountain Facility (TMF)
  - 101 Merged Profiles Processed

- JPL Mauna Loa Observatory (MLO)
  - 103 Merged Profiles Coincident with SSMIS

- Poker Flat Research Range Lidar Observatory (PFRR)
  - 44 Lidar Profiles Available
  - Climatological Upper Temperature Boundary Condition in Question

SSMIS Cal/Val Lidar Coincident Observations Data Base

- Lidar is Clearly the Best Source of "Ground Truth" Data Above 45 km

- Typical Rayleigh Lidar Accuracies are:

20 - 70 km	< 1.5 K
70 - 80 km	< 1.5 K
80 - 85 km	< 1.5 – 2.0 K
> 85 km	> 5 K

- Limited Geographical Coverage

- Nighttime Only Observations (Ascending Revs for F-16)

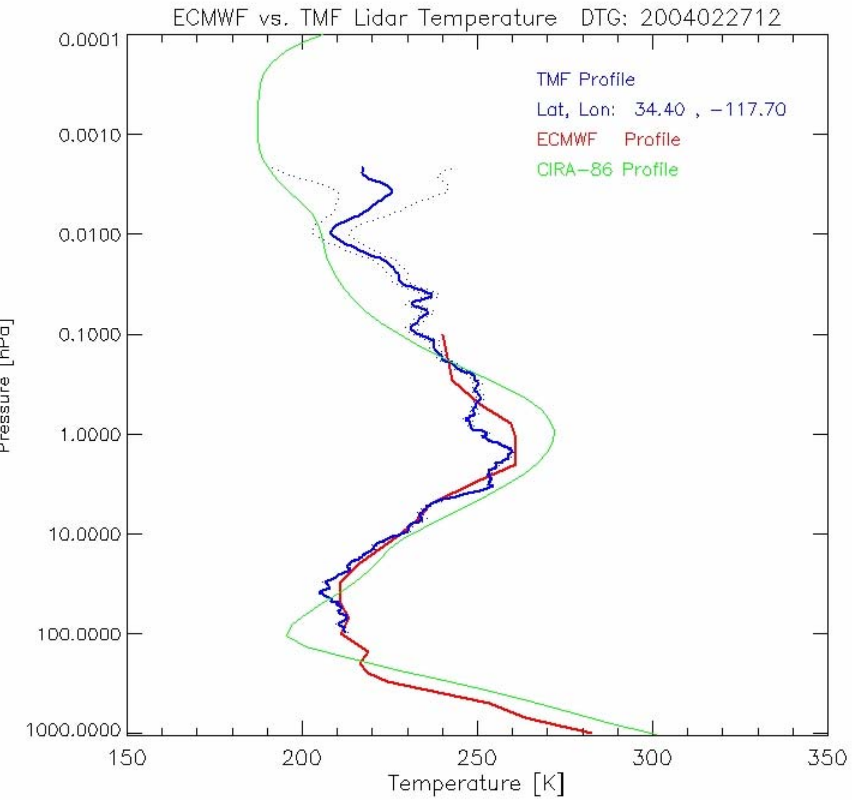

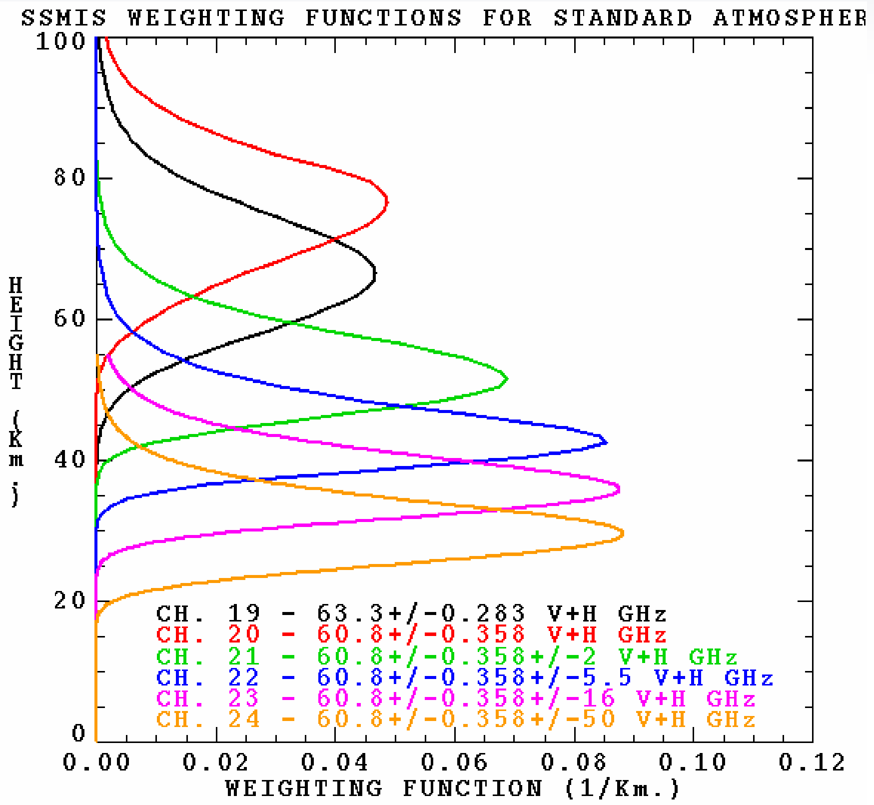

Typical Lidar Vertical Coverage vs. SSMIS Channels

Merged Lidar, ECMWF and COSPAR Climatology Temperature Profile

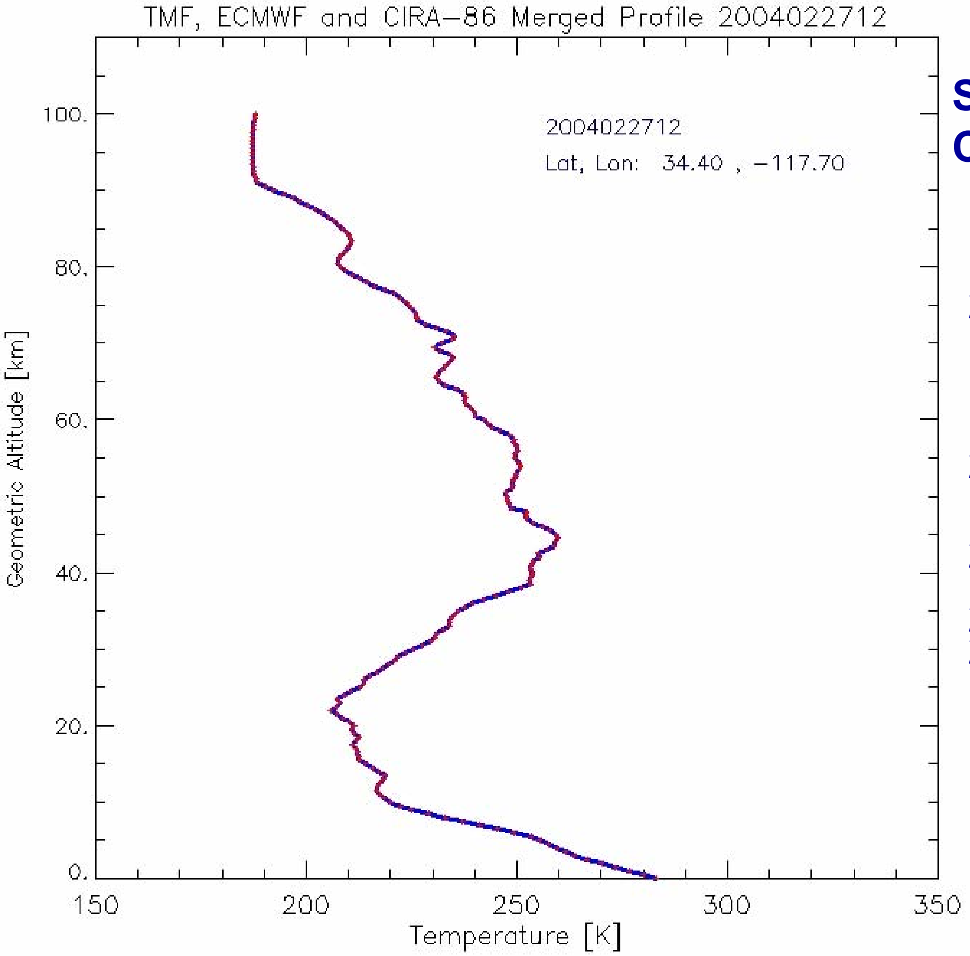

SSMIS Ch. No.

20

19

21

22

23

24

Effect of Vertical Smoothing of Lidar Profile On EDR Validation

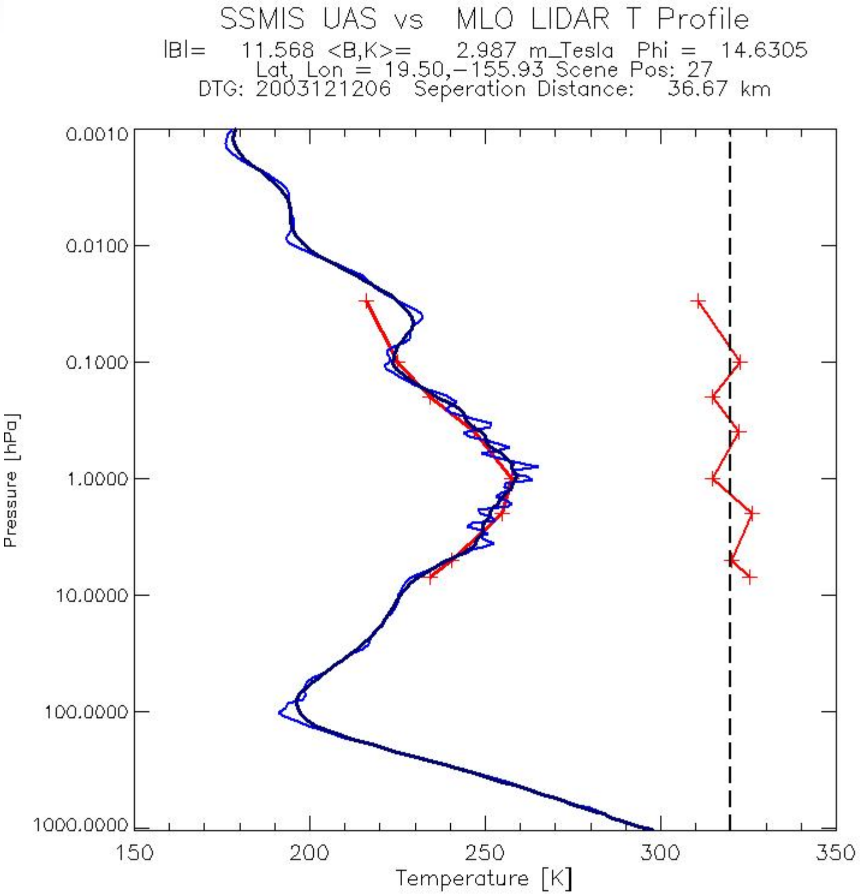

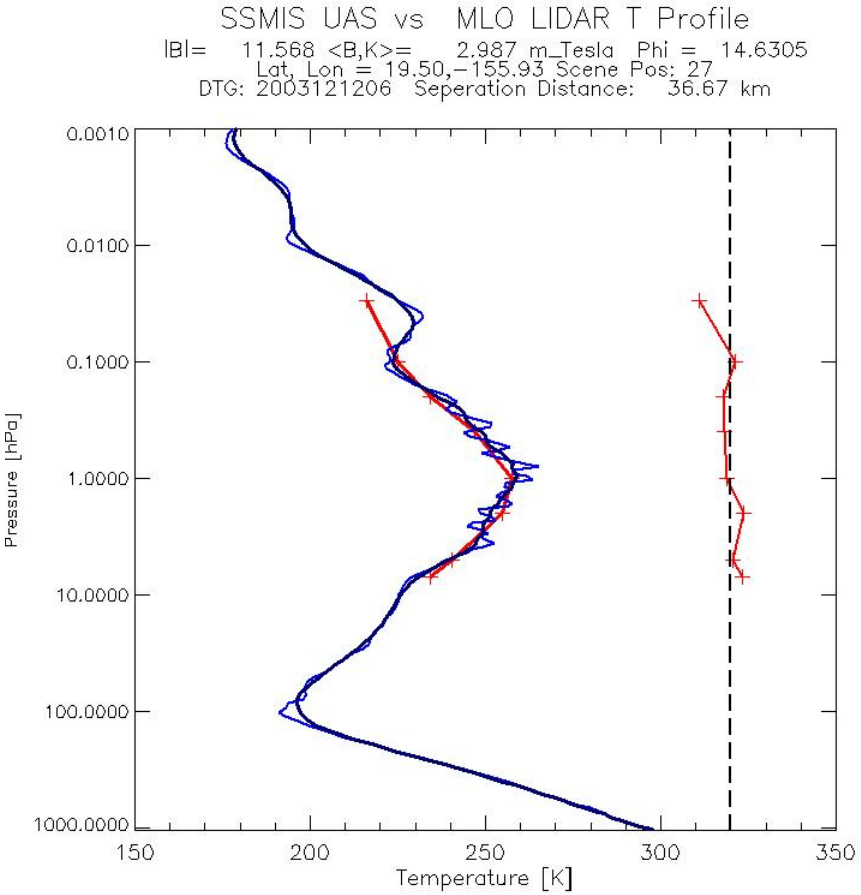

Ensemble TMF and MLO Lidar Statistical Properties

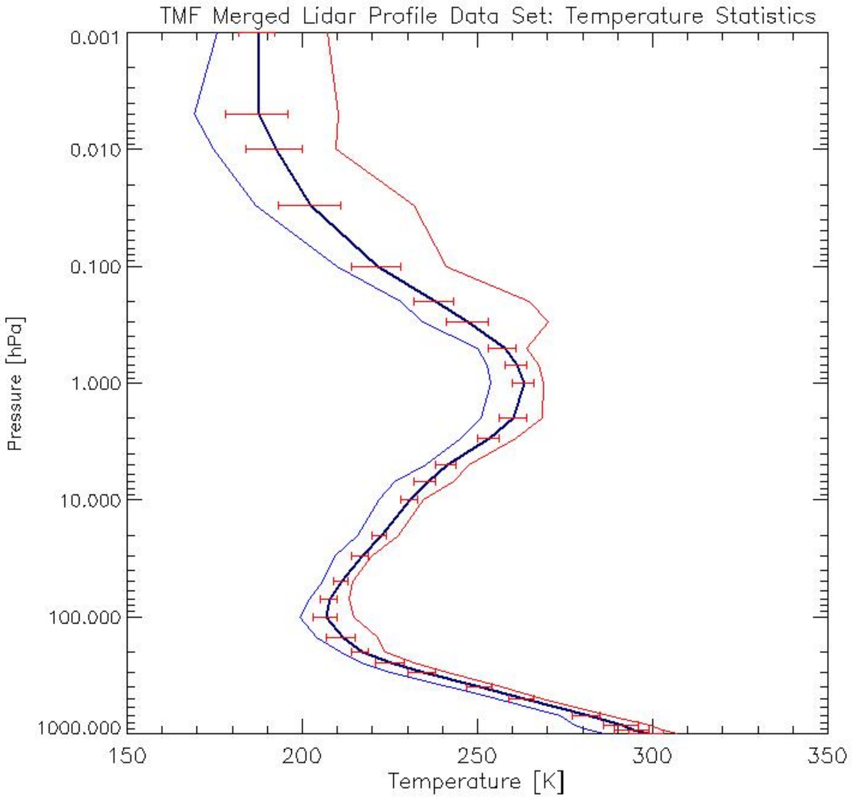

N = 101

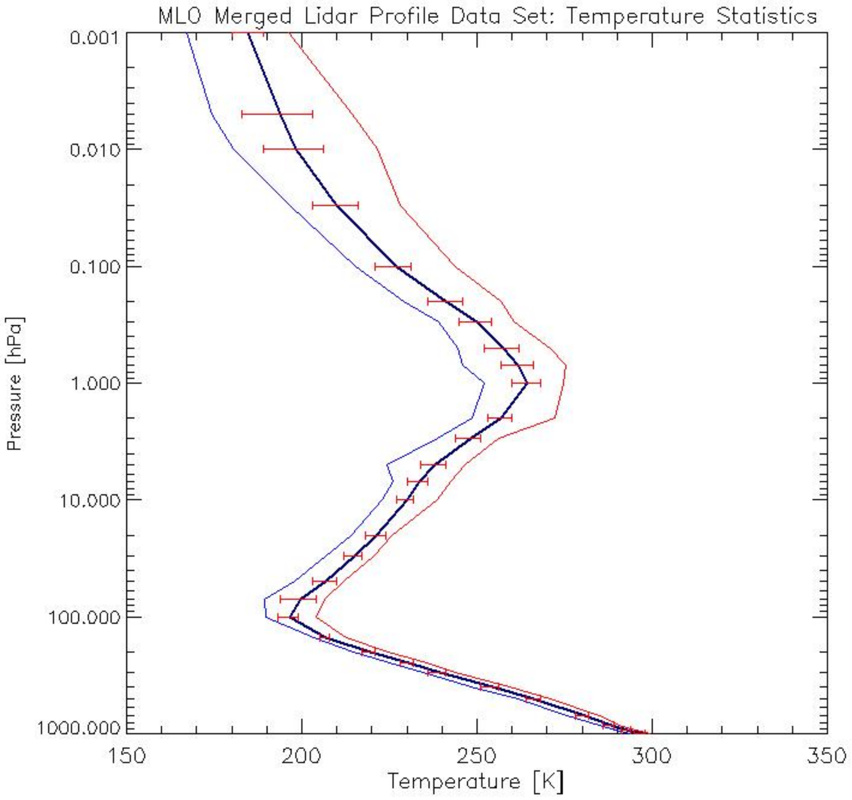

N = 103

Aerospace Mobile Lidar Observations

Robert Farley, John Wessel and Ye Hong

Barking Sands

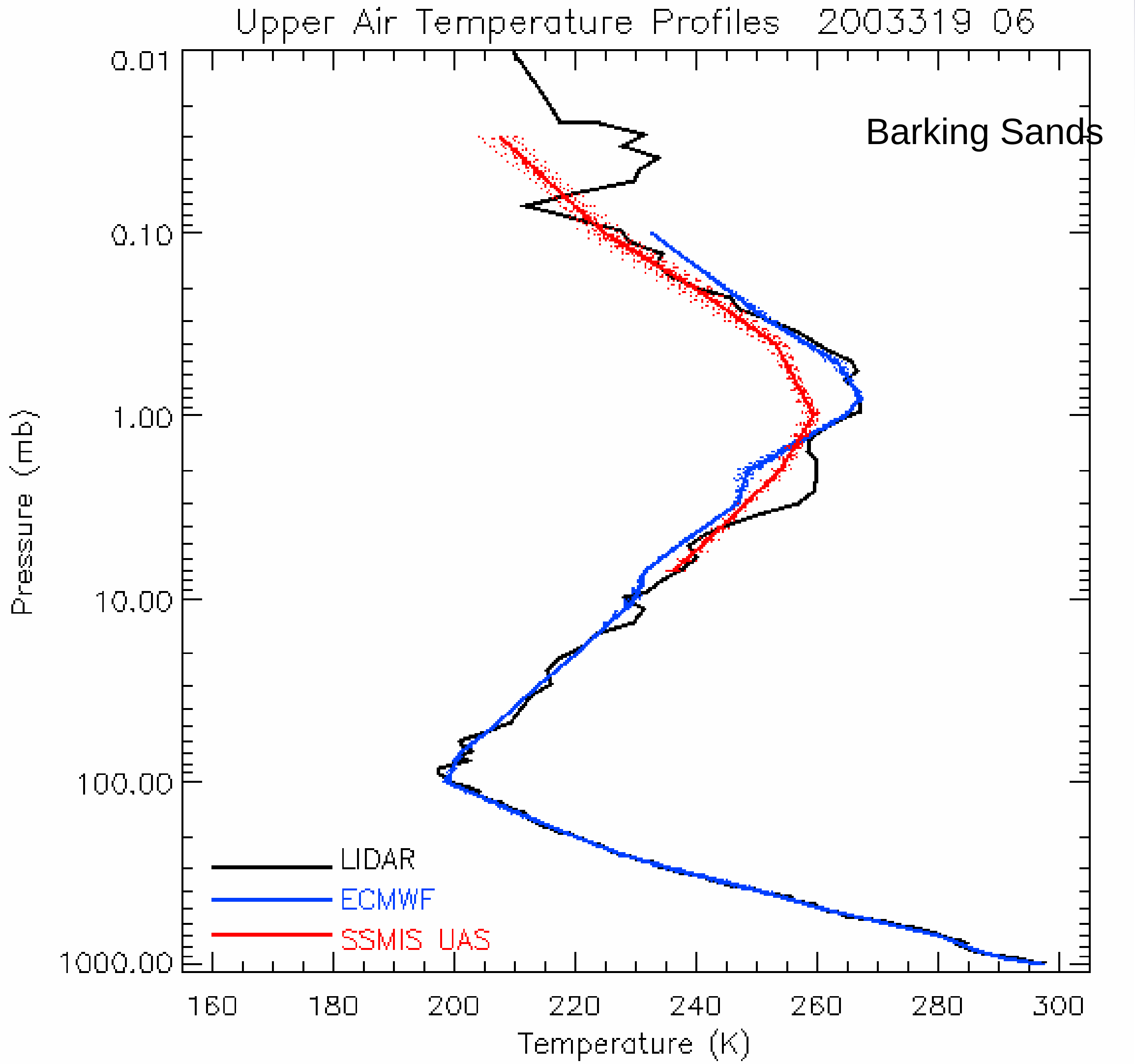

~Height (km)

80

65

50

30

18

0

Collocated SSMIS retrieved UAS profiles

Mean of collocated SSMIS retrieved profiles

Collocated ECMWF profiles

Mean of collocated ECMWF profiles

Aero Lidar profiles

Up to ~90km

Temperature Profiles 2003319 (Nov 15, 2003)

Barking Sands

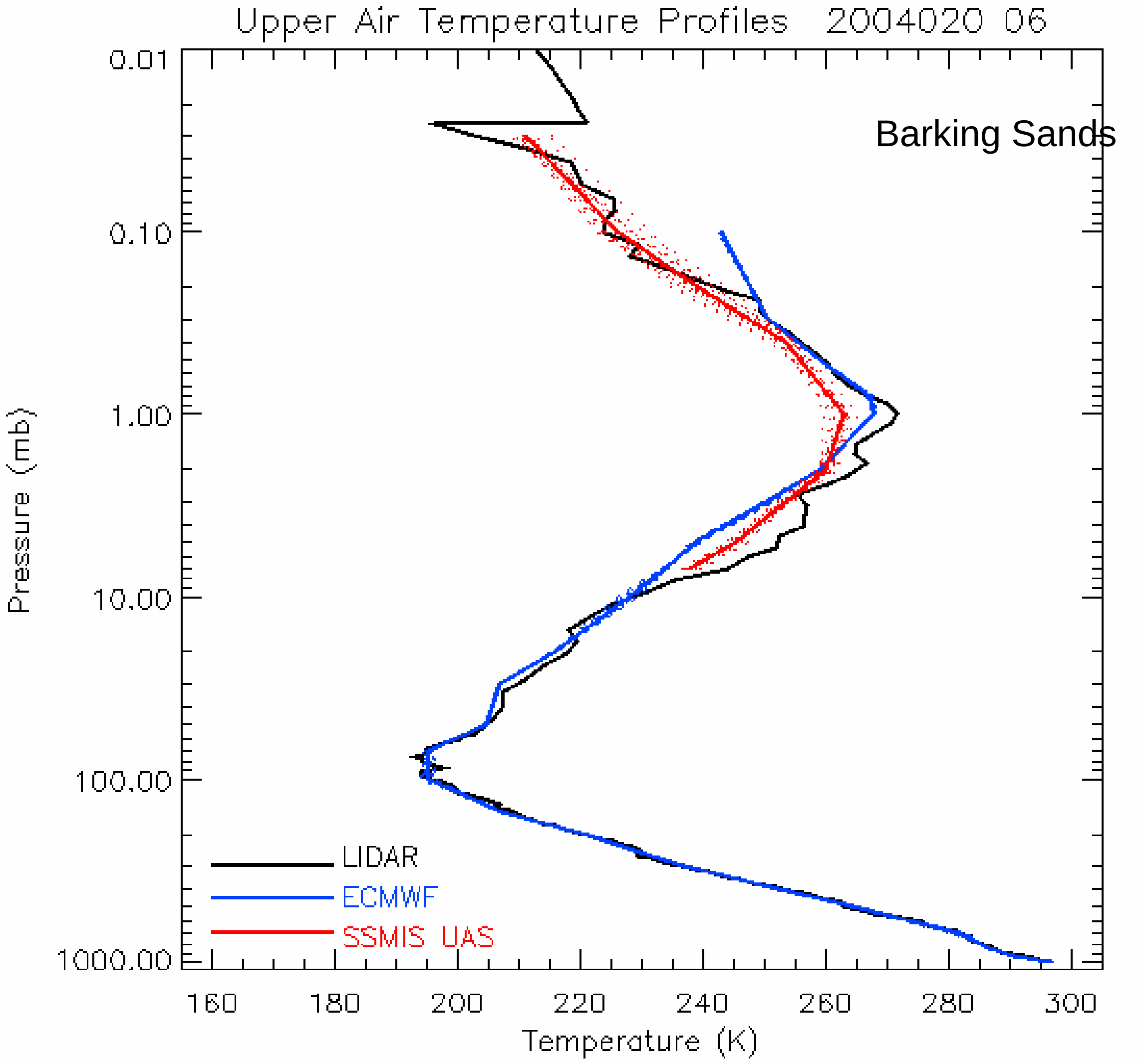

~Height (km)

80

Collocated SSMIS retrieved UAS profiles

65

Mean of collocated SSMIS retrieved profiles

50

Collocated ECMWF profiles

30

Mean of collocated ECMWF profiles

18

Lidar profiles

Up to ~90km

0

Temperature Profiles 2004020 (Jan 20, 2004)

Barking Sands

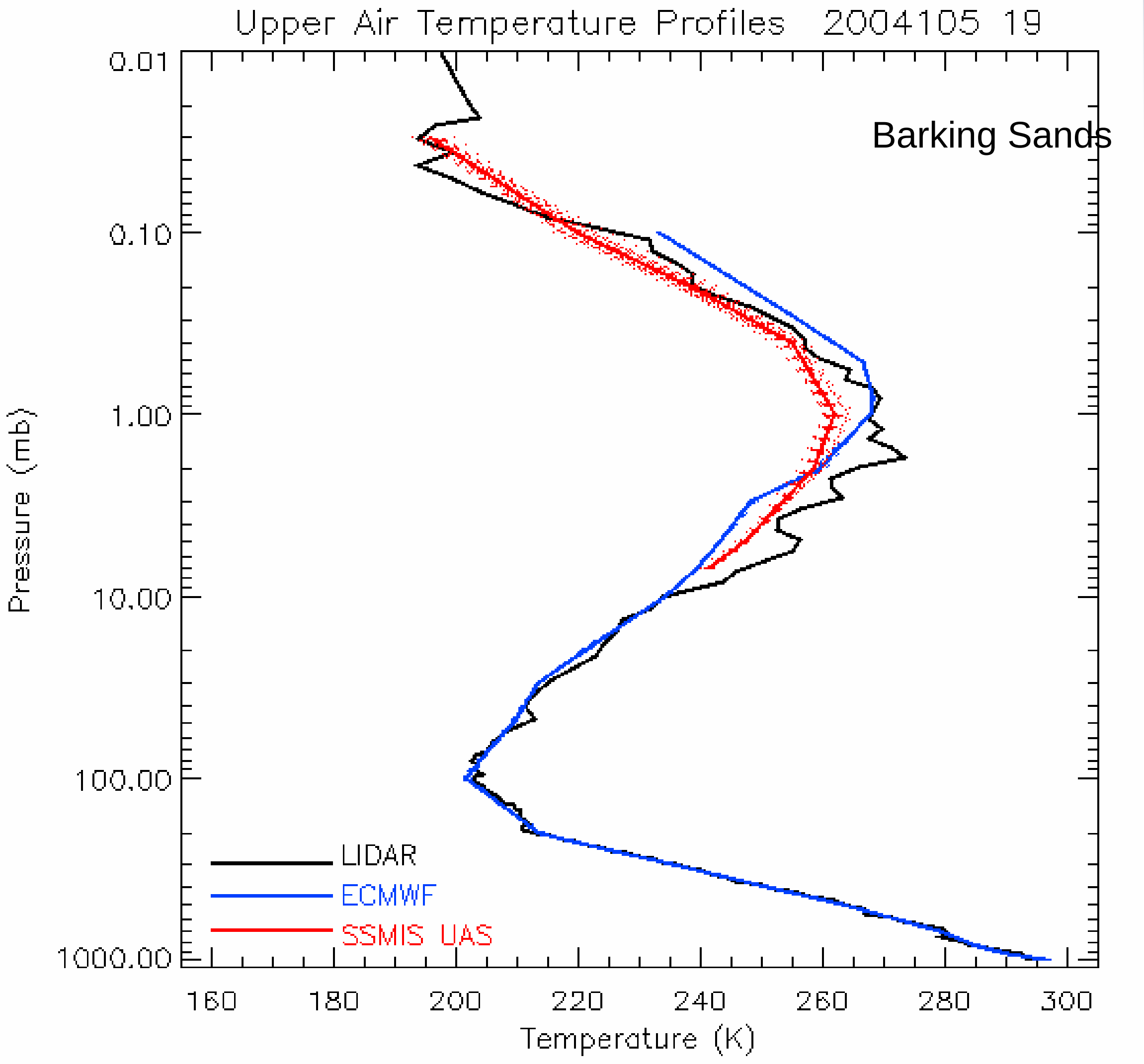

~Height (km)

80

Collocated SSMIS retrieved UAS profiles

65

Mean of collocated SSMIS retrieved profiles

50

Collocated ECMWF profiles

30

Mean of collocated ECMWF profiles

18

Lidar profiles

Up to ~90km

0

Temperature Profiles 2004105 (Apr 14, 2004)

Barking Sands

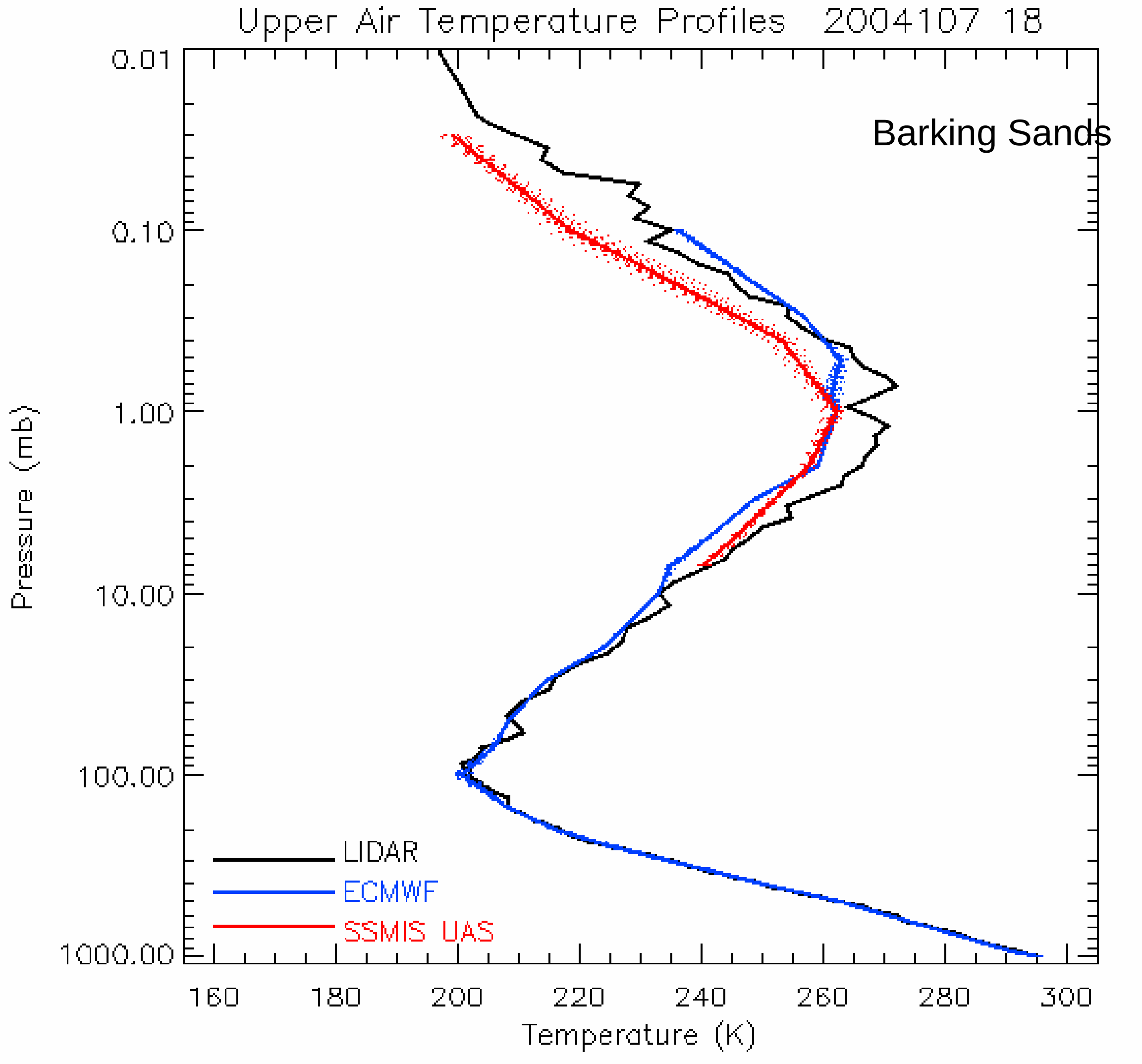

~Height (km)

80

65

50

30

18

0

Collocated SSMIS retrieved UAS profiles

Mean of collocated SSMIS retrieved profiles

Collocated ECMWF profiles

Mean of collocated ECMWF profiles

Lidar profiles

Up to ~90km

Temperature Profiles 2004107 (Apr 16, 2004)

Data Acquisition Plan

- Lidar Observational Campaigns
- ECMWF NWP Analyses
- Rocketsonde Observations

ECMWF Analysis Data Base

- Very Accurate Depiction of the Atmospheric State

- 4-D Variational Analysis System
    - 60 Vertical Levels
    - T-511 (40 km) Horizontal Resolution
- Satellite Radiance Information
    - AMSU-A, HIRS, AIRS, MODIS, AMSU-B, METEOSAT, SSMI, GOES
- Satellite Winds (FTW/AMVs)
    - GEO/MODIS, SSM/I, ERS, QuikScat, Adeos-2, Windsat
- Conventional Observations

- 99.07% of QC Screened Data are Satellite Data

- 91.41% of Assimilated Data are Satellite Data

ECMWF Analysis Data Base

ECMWF Provides the SSMIS Cal/Val Team

- Analyses at 6 hour Intervals
- Parameters required for RTM
- SSMIS Retrieved Parameters
- Surface Parameters
- T, q and Z at 1000 to 0.1 hPa

- Observations Above 35 km Include AMSU-A and AIRS

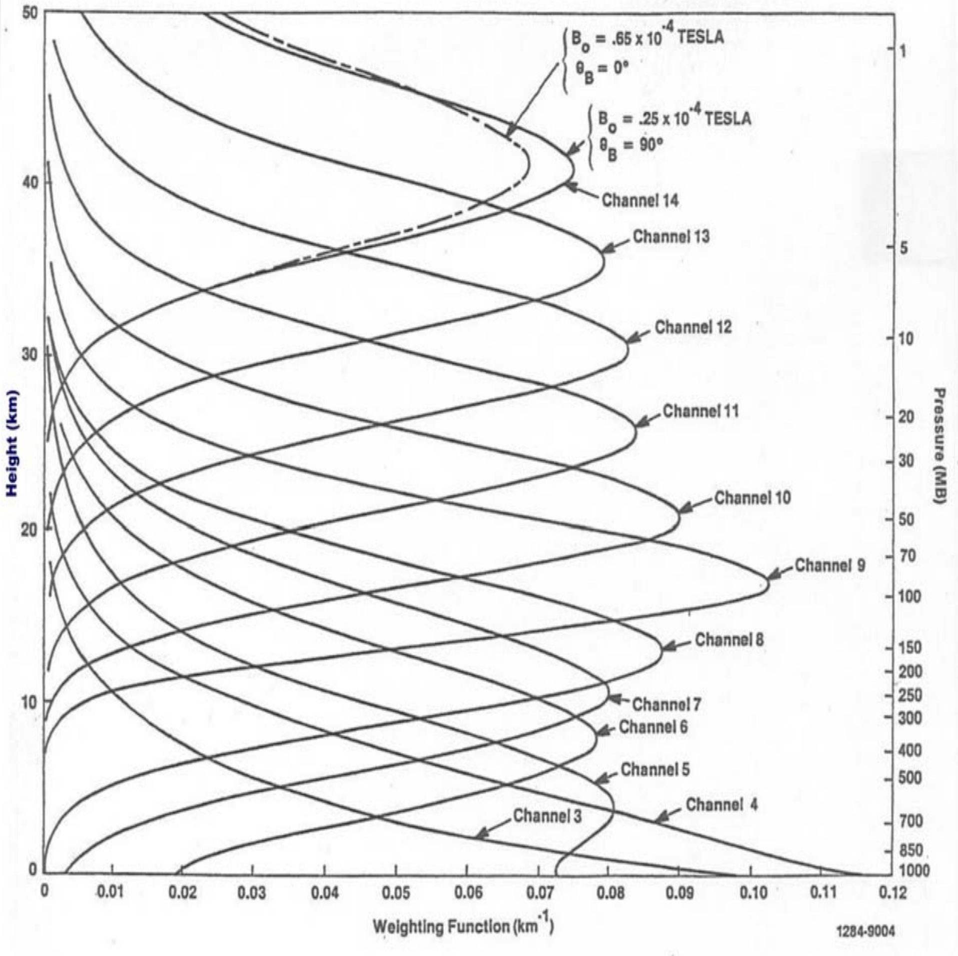

Figure A-5 Channel 3-14 Weighting Functions (Beam Positions 15 and 16, Calm Ocean Background)

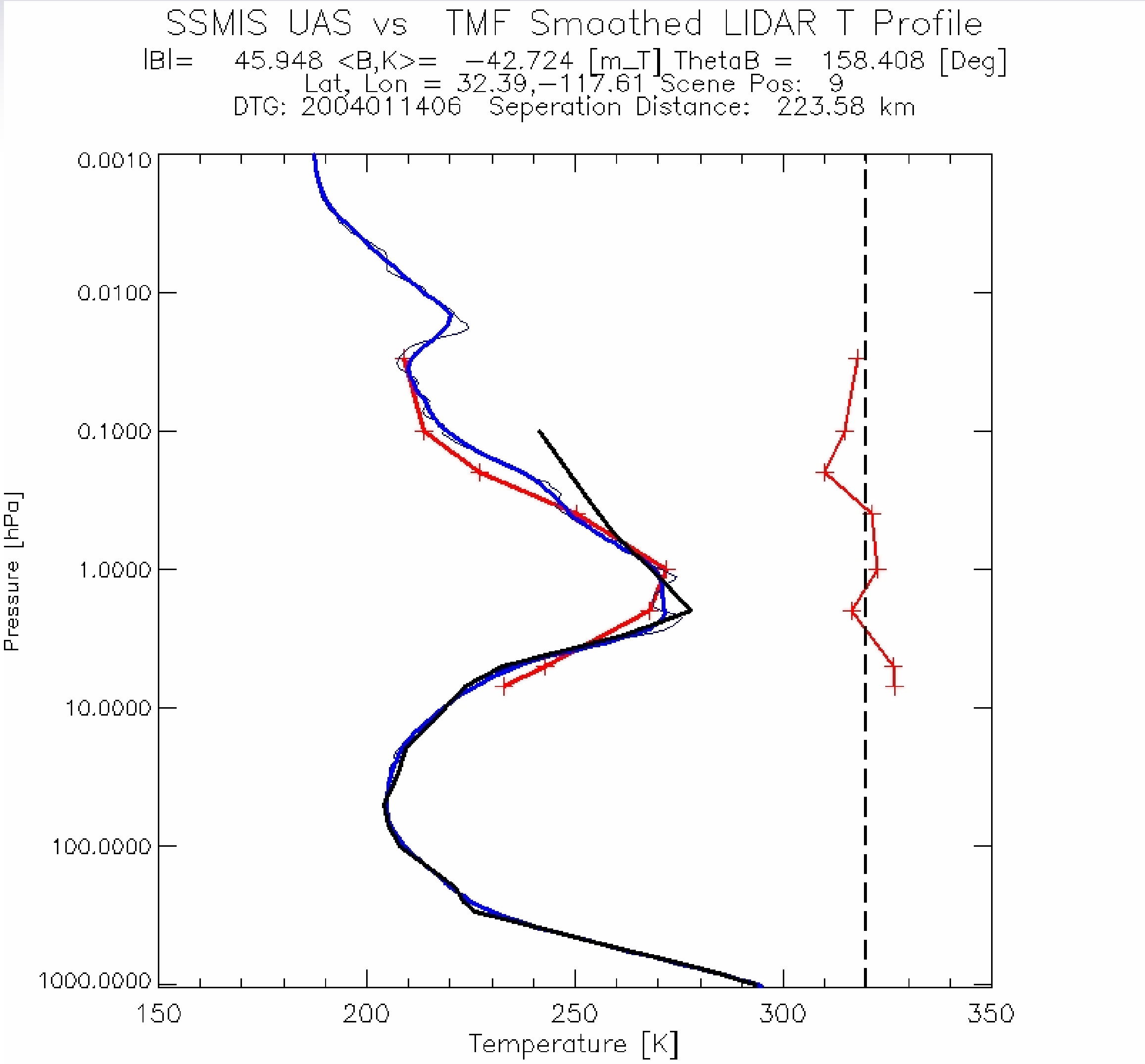
SSMIS UAS vs TMF Smoothed LIDAR T Profile
|B|= 45.948 <B,K>= −42.724 [m_T] ThetaB = 158.408 [Deg]
Lat, Lon = 32.39,−117.61 Scene Pos: 9
DTG: 2004011406 Seperation Distance: 223.58 km
Pressure [hPa]
0.0010
0.0100
0.1000
1.0000
10.0000
100.0000
1000.0000
150
200
250
300
350
Temperature [K]

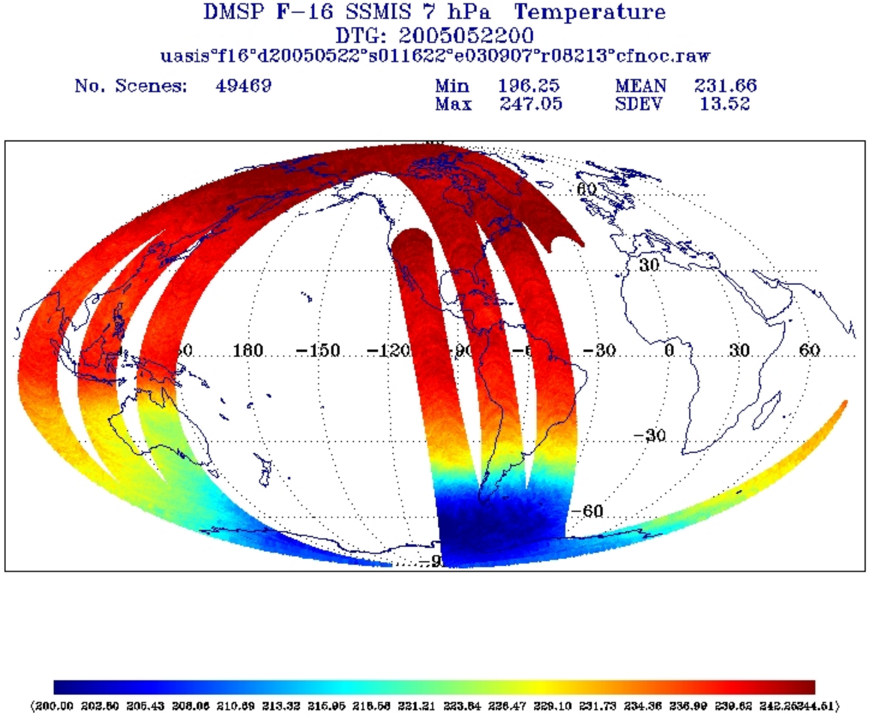

DMSP F−16 SSMIS 7 hPa Temperature
DTG: 2005052200
uasis°f16°d20050522°s011622°e030907°r08213°cfnoc.raw

No. Scenes: 49469 Min 196.25 MEAN 231.66
Max 247.05 SDEV 13.52

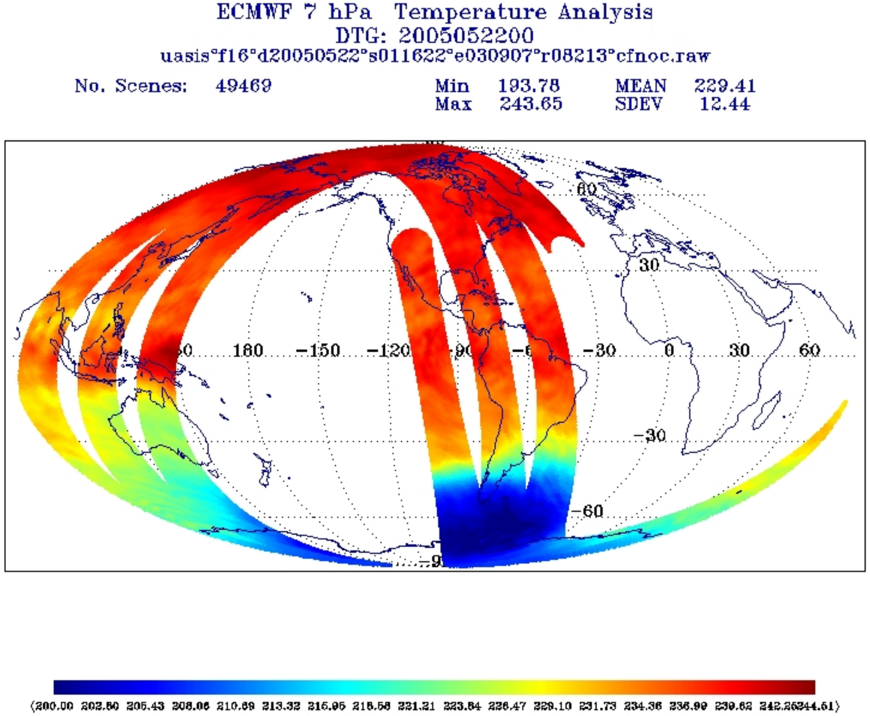

ECMWF 7 hPa Temperature Analysis
DTG: 2005052200
uasis°f16°d20050522°s011622°e030907°r08213°cfnoc.raw

No. Scenes: 49469 Min 193.78 MEAN 229.41
Max 243.65 SDEV 12.44

SSMIS Retrieval vs. ECMWF Analysis at 7.0 hPa

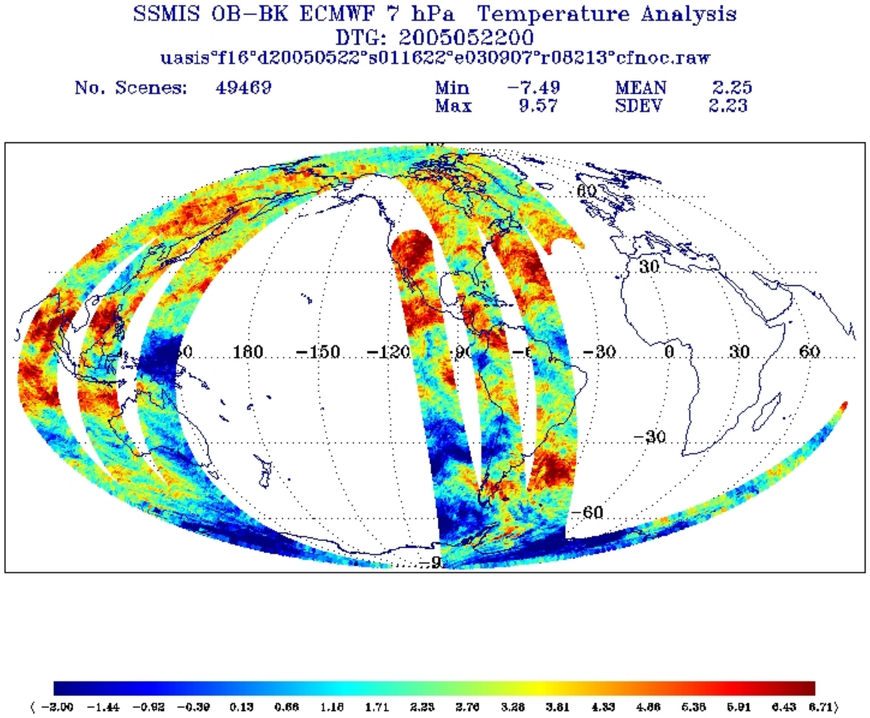

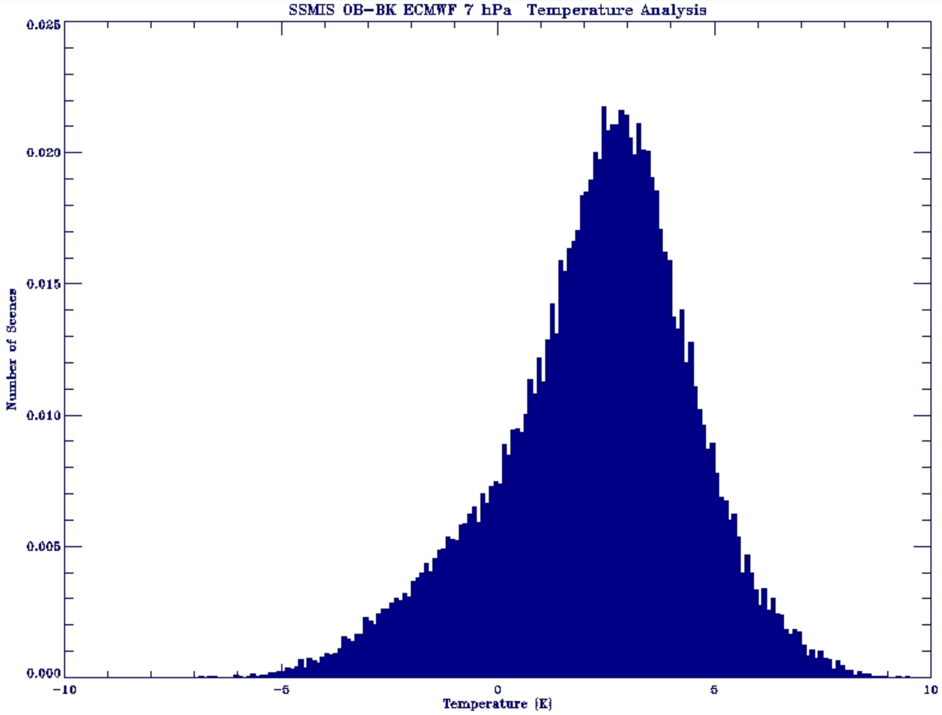

SSMIS Retrieval - ECMWF Analysis at 7.0 hPa

Data Acquisition Plan

- Lidar Observational Campaigns
- ECMWF NWP Analyses
- Rocketsonde Observations

SSMIS Cal/Val Rocketsonde Coincident Observations Data Base

- Rocketsondes are the Only Source of “In Situ Ground Truth” Data Above 45 km

- Typical Rocketsonde Accuracies are:

30 - 70 km	< 1.5 - 2.0 K
70 - 85 km	< 2.5 K
> 85 km	> 3 K

- Limited Geographical Coverage

- Day or Night Coincidence with SSMIS

- WSMR and Cape Canaveral (FSA) have Capability

- To Date NO SSMIS Rocketsondes have been Funded

Section 10.5 Analysis Methodology

- **SDR Calibration (OB-RTM)**
- **EDR Validation (Retrieval-Lidar)**
- **EDR Validation (Retrieval-NWP)**

Analysis Methodology

- **SDR Calibration (OB-RTM)**
- **EDR Validation (Retrieval-Lidar)**
- **EDR Validation (Retrieval-NWP)**

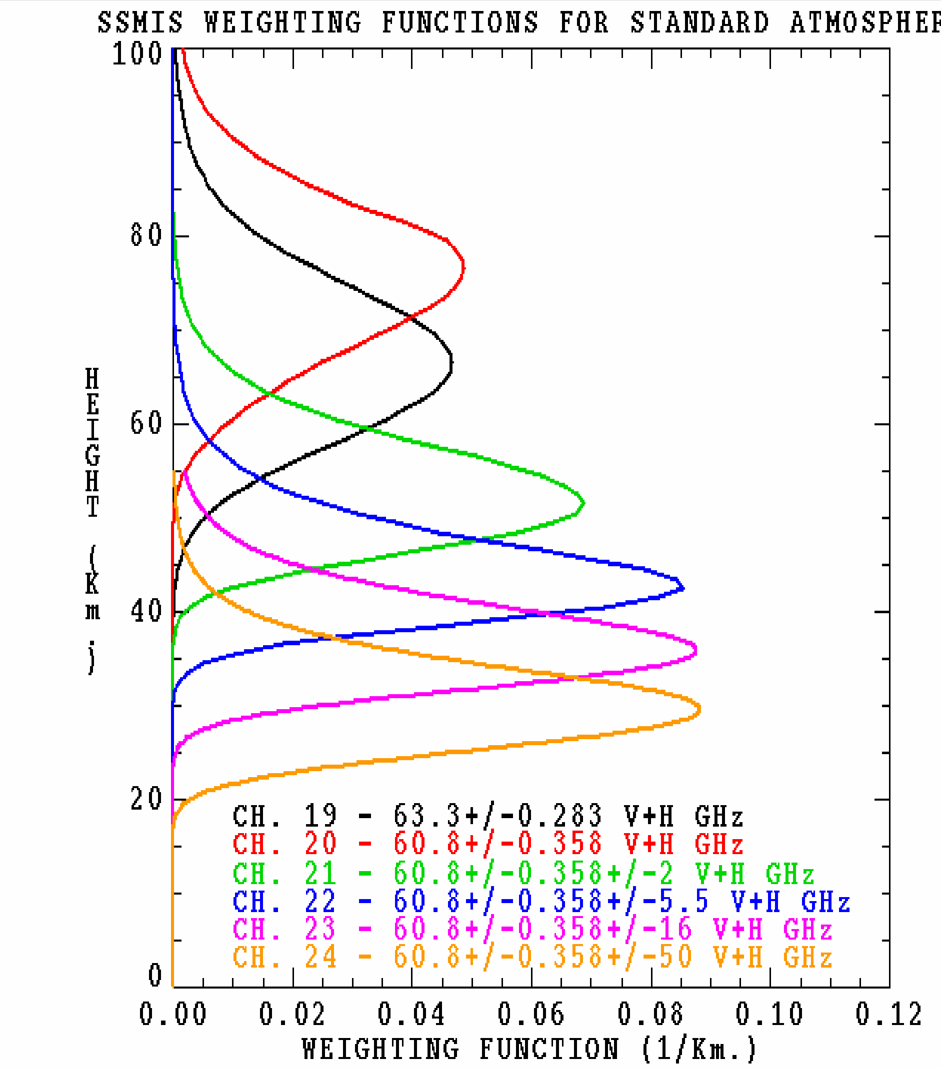

Calibration Averaging Strategies for UAS Channels

- **Original SSMIS GDPS Averaged Previous Eight Scans**
- **Rev4b Employed Symmetric Scan Averaging to Reduce Striping of UAS Channels**
- **Symmetric Scan Averaging uses 32 Scans Surrounding the Current Scan for the UAS channels**

Calibration Equation

Counts to Antenna Temperature

$$T_{Ai} = T_C + \frac{\overline{T_W} - T_C}{\overline{C_W} - \overline{C_C}}\left(C_i - \overline{C_C}\right)$$

T_{Ai} = Antenna Temperature within ith Scan

T_C = Cosmic Background Temperature

T_W = Averaged Warm Load Temp.

C_W = Averaged Warm Load Count

C_C = Averaged Cold Load Count

C_i = Scene Count within ith Scan

Calibration Averaging Strategies for UAS Channels

Original Averaging Scheme

$$\overline{(\xi)} = \frac{1}{8}\sum_{i-8}^{i}(\xi)$$

The Original Averaging Scheme Used Previous Eight Scans to Average T_W, C_W, and C_C, for Calibrating the i^{th} Scan

Symmetric Averaging Scheme

$$\overline{(\zeta)} = \frac{1}{2n+1}\sum_{i-n}^{i+n}\zeta$$

Symmetric Averaging Scheme Uses the Surrounding n Scans to Average T_W, C_W, and C_C, for Calibrating the i^{th} Scan, Where n =32 for the UAS Channels

Original Calibration Averaging

DMSP F−16 SSMIS Ch. 21 60.792668±.357892±.002 GHz RCP
DTG: 2004030907
02015−02021

No. Scenes: 723418

Min 80.00
Max 263.64

MEAN 246.04
SDEV 4.82

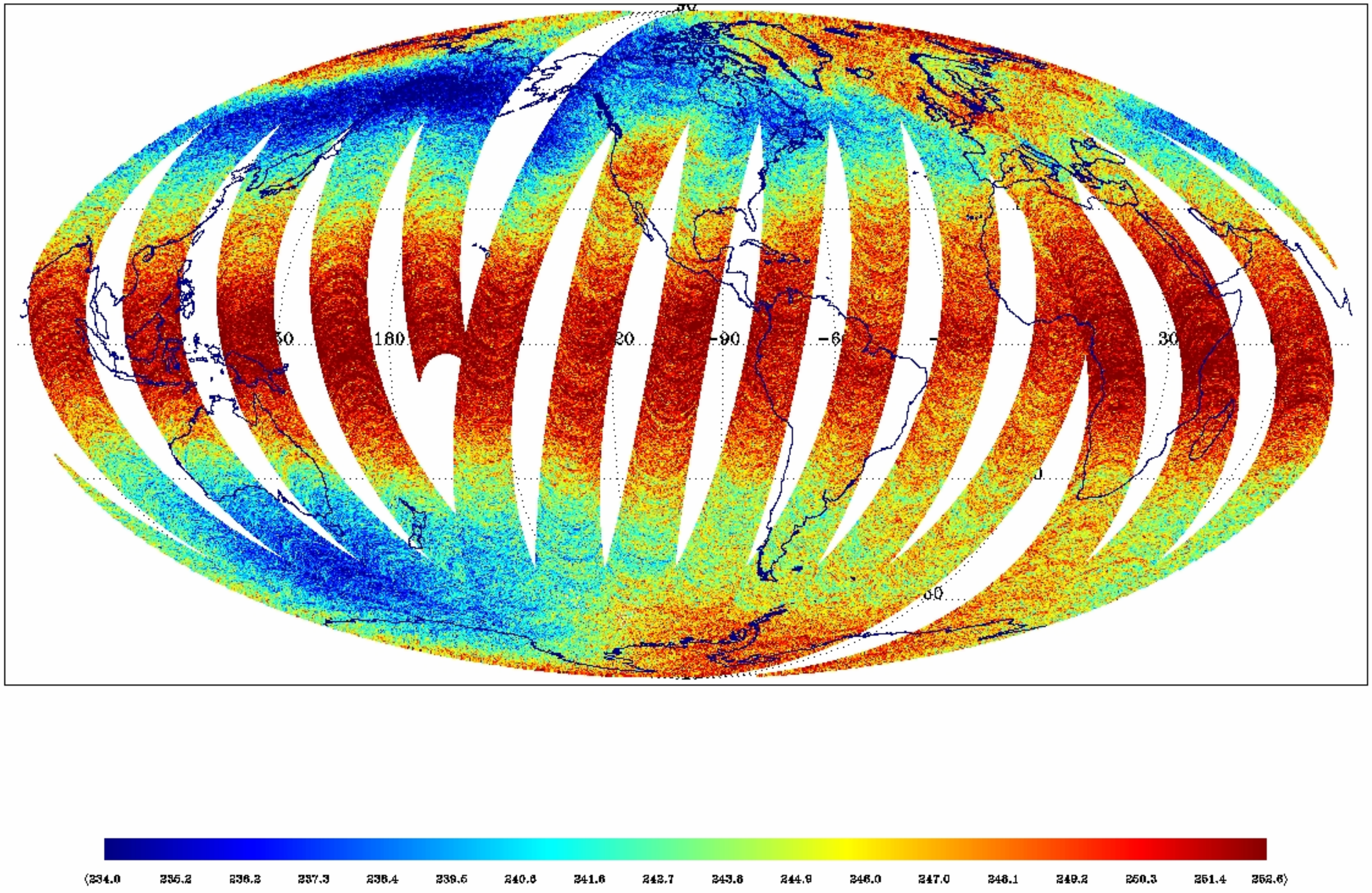

Symmetric Calibration Averaging

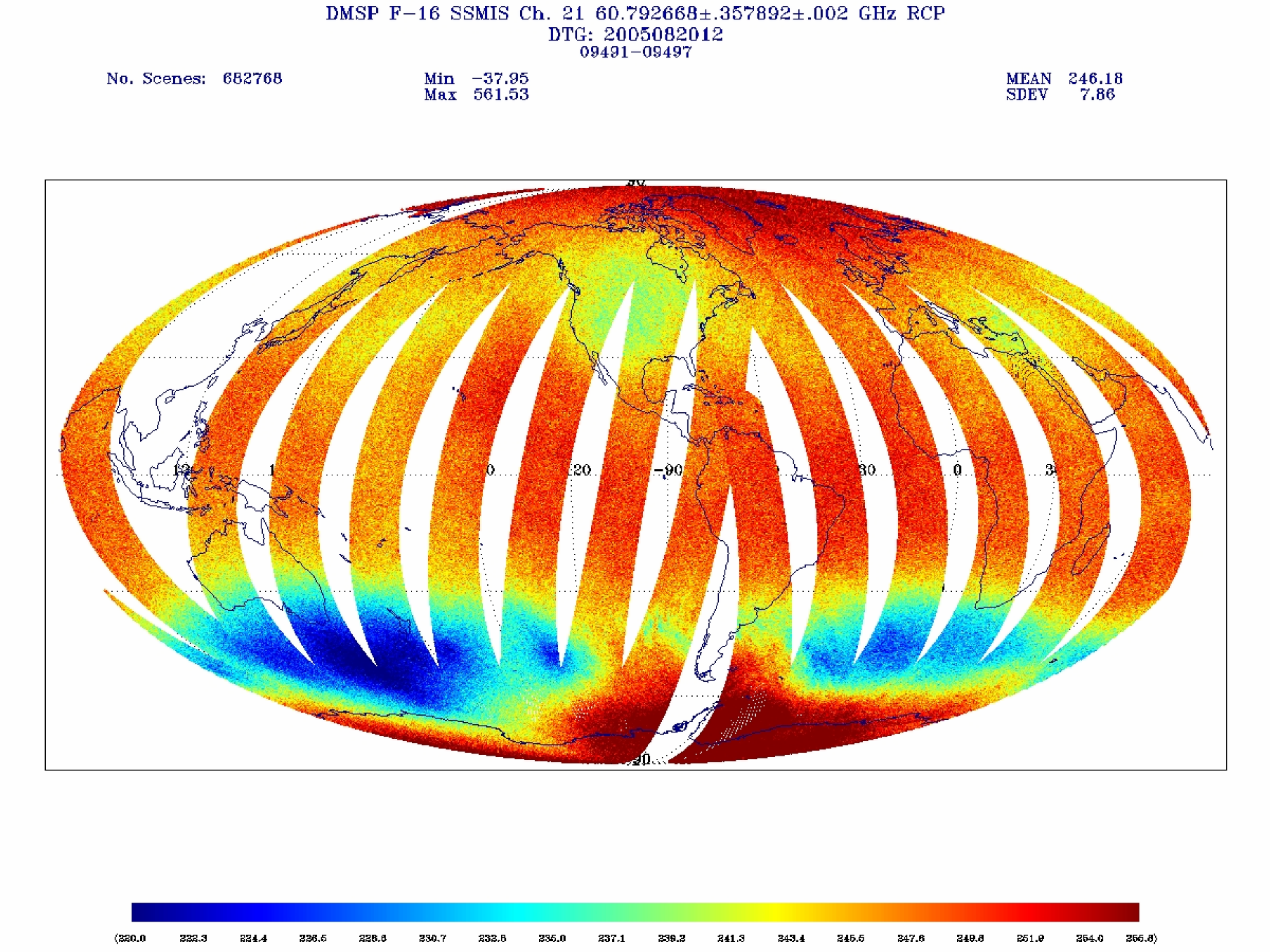

DMSP F−16 SSMIS Ch. 21 60.792668±.357892±.002 GHz RCP
DTG: 2005082012
09491−09497

No. Scenes: 682768

Min −37.95
Max 561.53

MEAN 246.18
SDEV 7.86

Global Patterns of the UAS Channels

- **SSMIS UAS Channel Imagery**
- **SSMIS UAS Geomagnetic Parameters**
- **AMSU-A Channel Comparisons**
- **SSMIS OB vs. ECMWF RTTOV-7 Comparisons**

Global Patterns of the UAS Channels

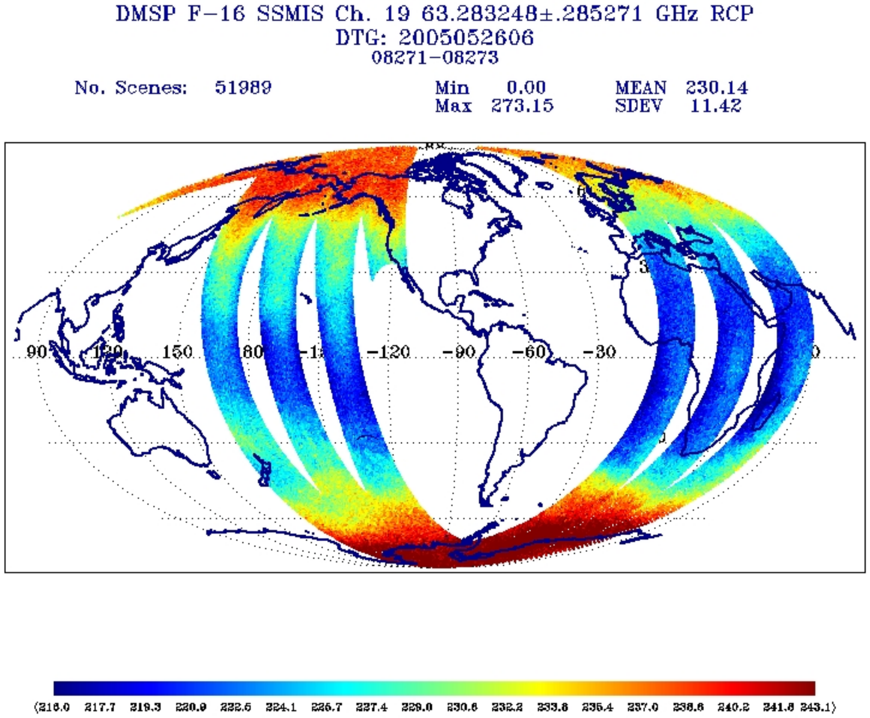

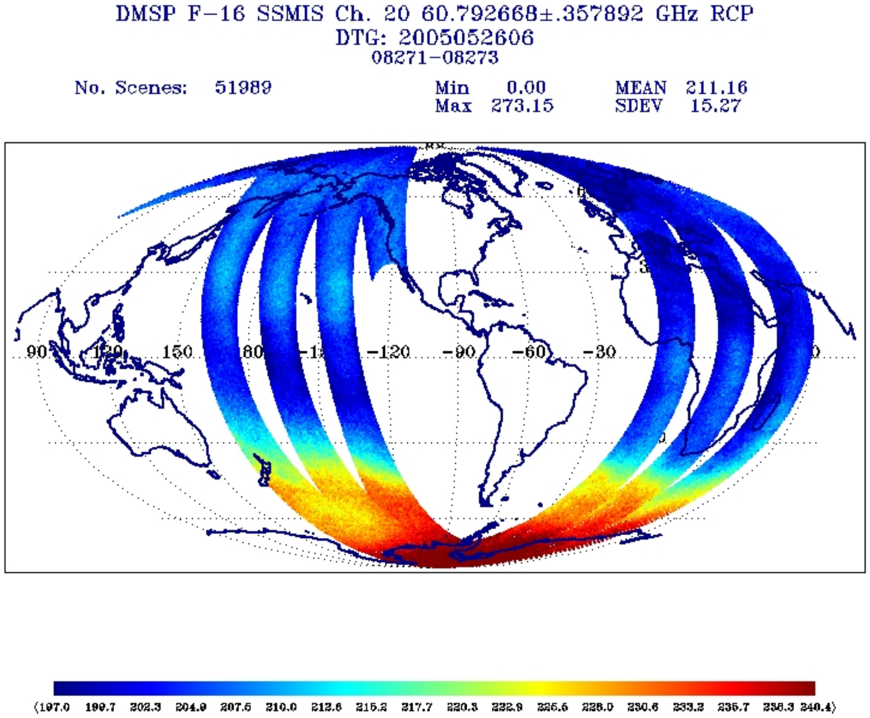

SSMIS Ch 19

SSMIS Ch 20

Global Patterns of the SSMIS UAS Channels

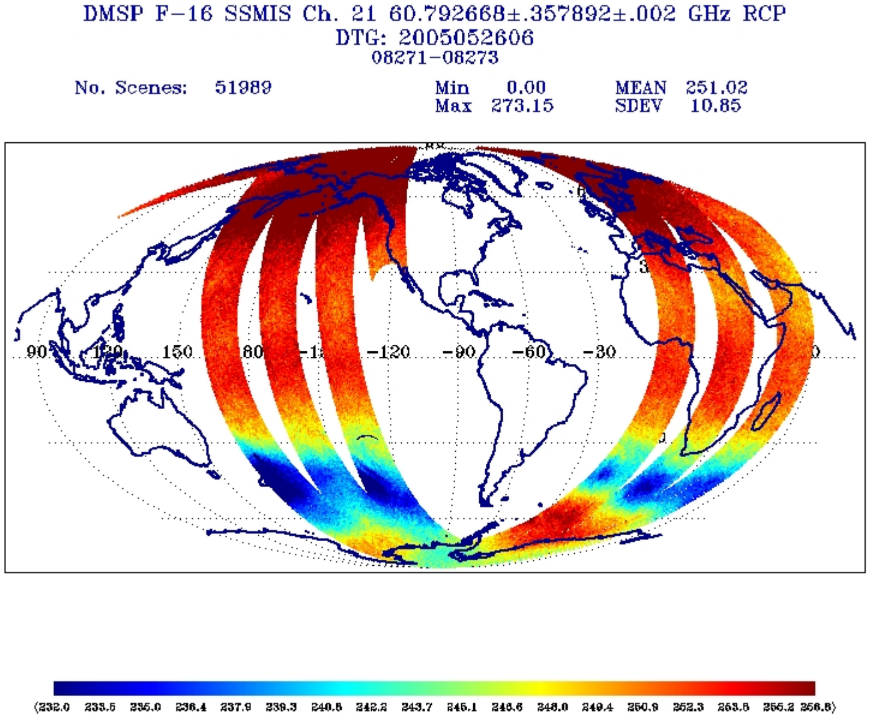

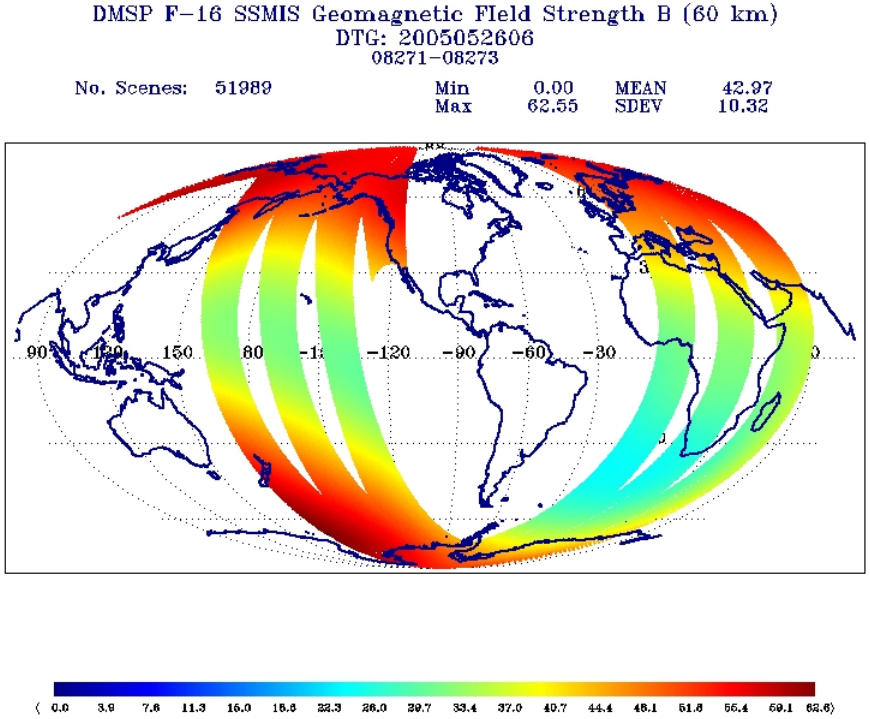

SSMIS Ch 21

Geomagnetic Field |B|

Global Patterns of the UAS Geomagnetic Parameters

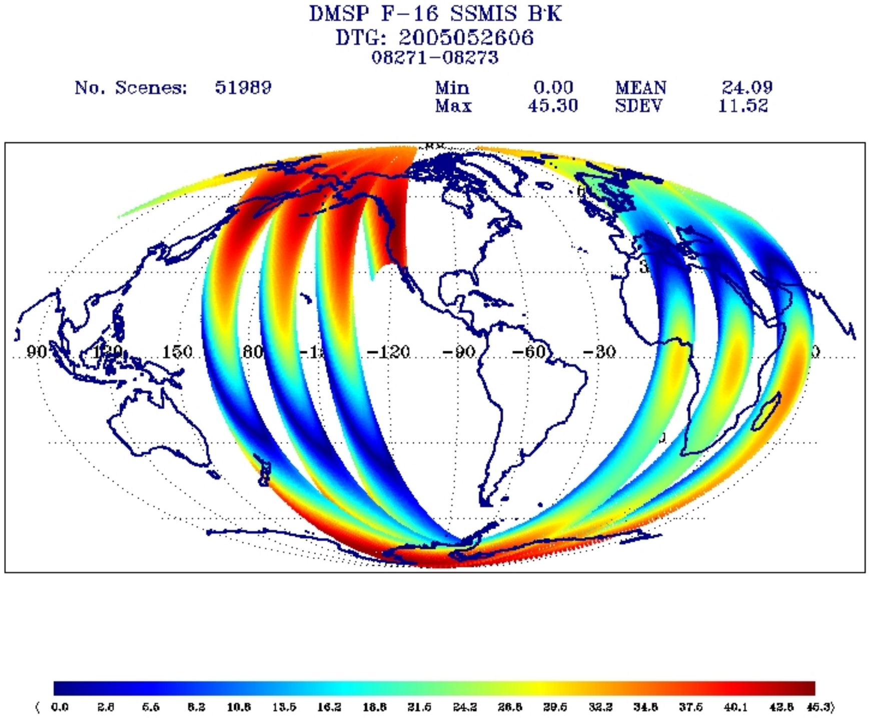

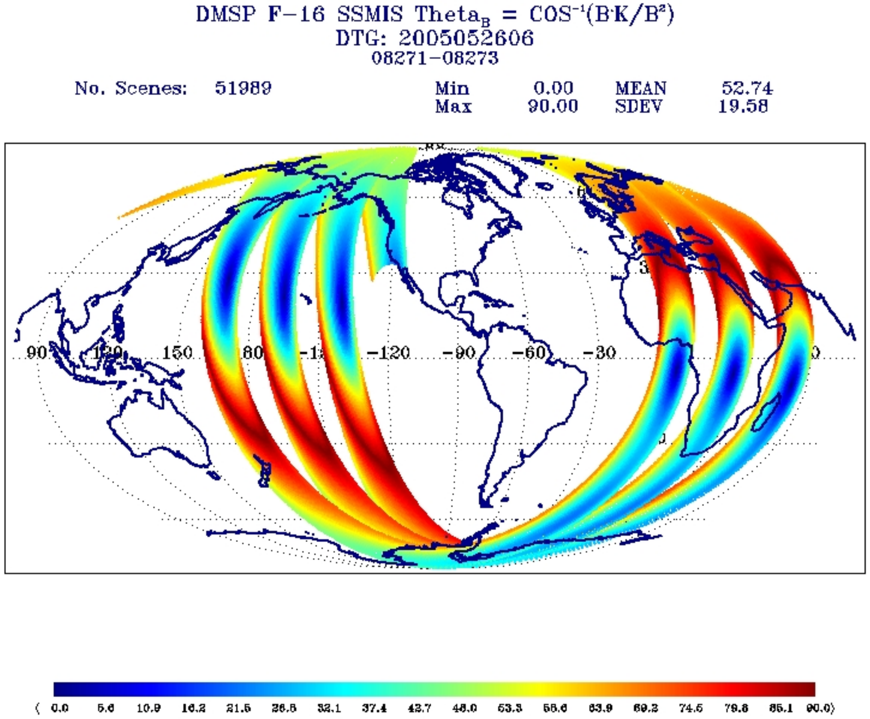

Dot Product of Geomagnetic Field and Propagation Vector B·K

Theta_B = COS^{-1}(B·K /|B|)

Global Patterns of the SSMIS UAS Channels vs. AMSU

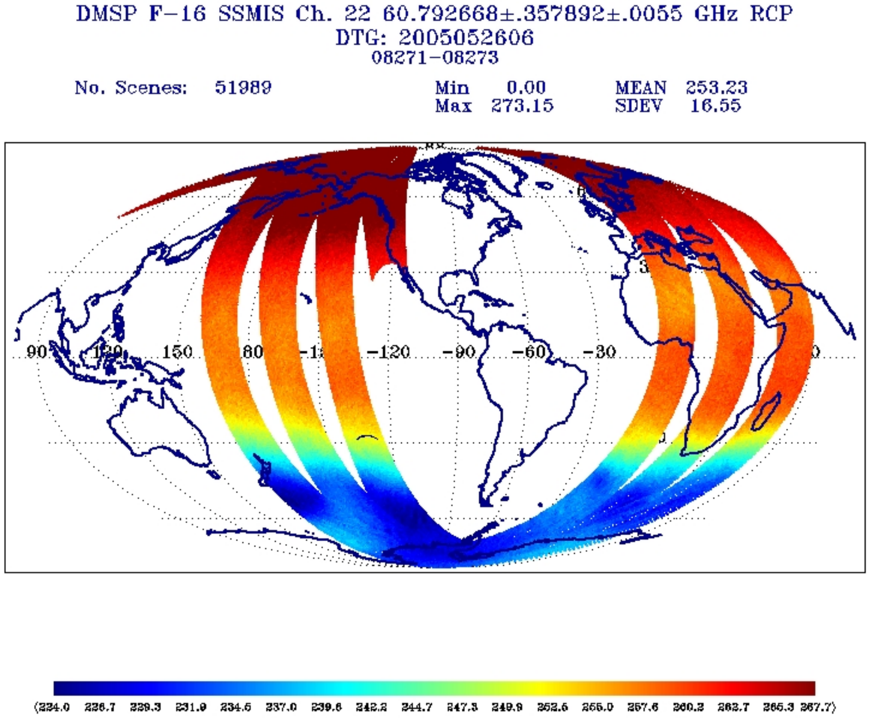

DMSP F-16 SSMIS Ch. 22 60.792668±.357892±.0055 GHz RCP
DTG: 2005052606
08271-08273

No. Scenes: 51989 Min 0.00 MEAN 253.23
Max 273.15 SDEV 16.55

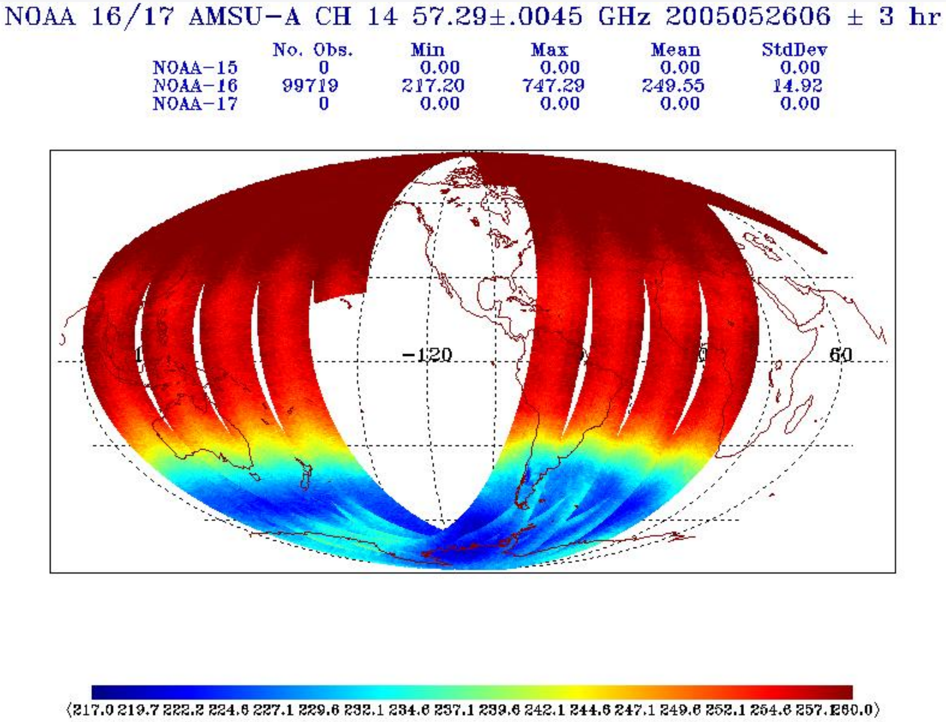

NOAA 16/17 AMSU-A CH 14 57.29±.0045 GHz 2005052606 ± 3 hr

	No. Obs.	Min	Max	Mean	StdDev
NOAA-15	0	0.00	0.00	0.00	0.00
NOAA-16	99719	217.20	747.29	249.55	14.92
NOAA-17	0	0.00	0.00	0.00	0.00

SSMIS Ch 22

AMSU-A Ch 14

Global Patterns of the SSMIS UAS Channels vs. AMSU

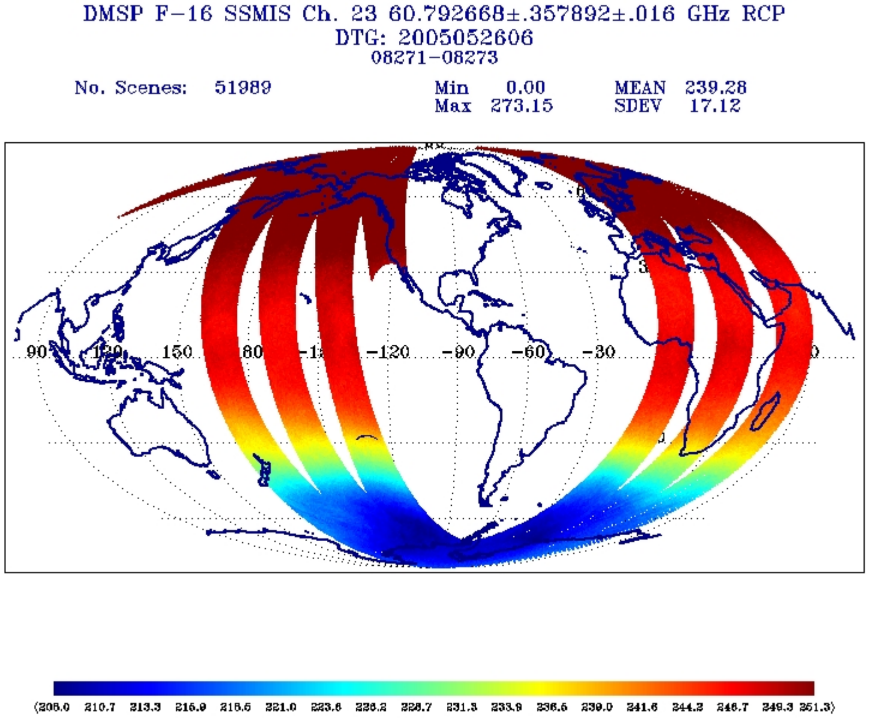

DMSP F-16 SSMIS Ch. 23 60.792668±.357892±.016 GHz RCP
DTG: 2005052606
08271-08273

No. Scenes: 51989
Min 0.00
Max 273.15
MEAN 239.28
SDEV 17.12

SSMIS Ch 23

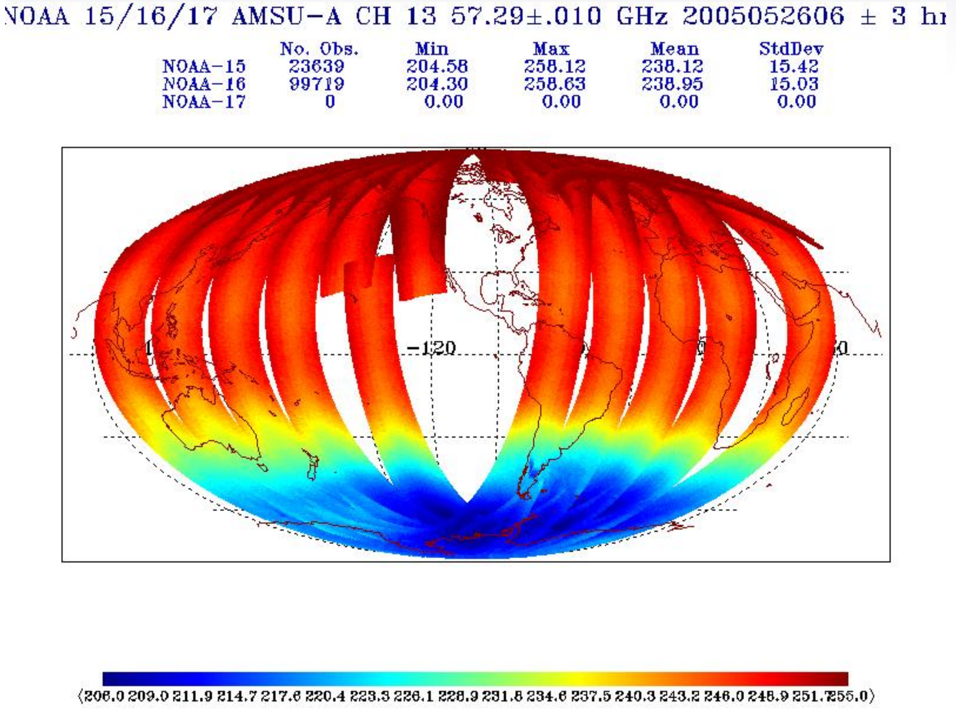

NOAA 15/16/17 AMSU-A CH 13 57.29±.010 GHz 2005052606 ± 3 h

	No. Obs.	Min	Max	Mean	StdDev
NOAA-15	23639	204.58	258.12	238.12	15.42
NOAA-16	99719	204.30	258.63	238.95	15.03
NOAA-17	0	0.00	0.00	0.00	0.00

AMSU-A Ch 13

Global Patterns of the SSMIS UAS Channels vs. AMSU

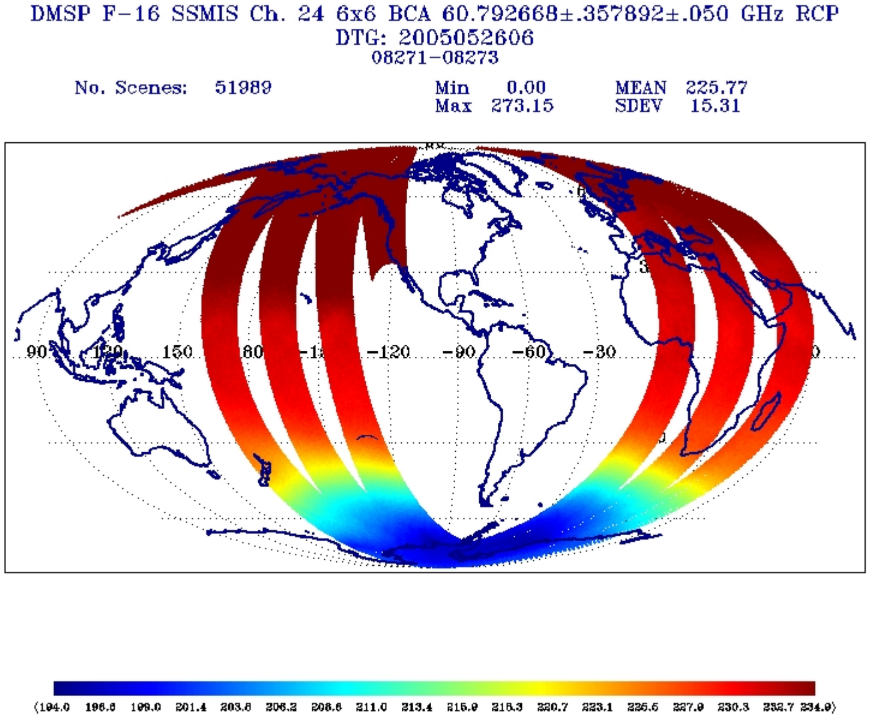

DMSP F-16 SSMIS Ch. 24 6x6 BCA 60.792668±.357892±.050 GHz RCP
DTG: 2005052606
08271-08273

No. Scenes: 51989
Min 0.00
Max 273.15
MEAN 225.77
SDEV 15.31

SSMIS Ch 24

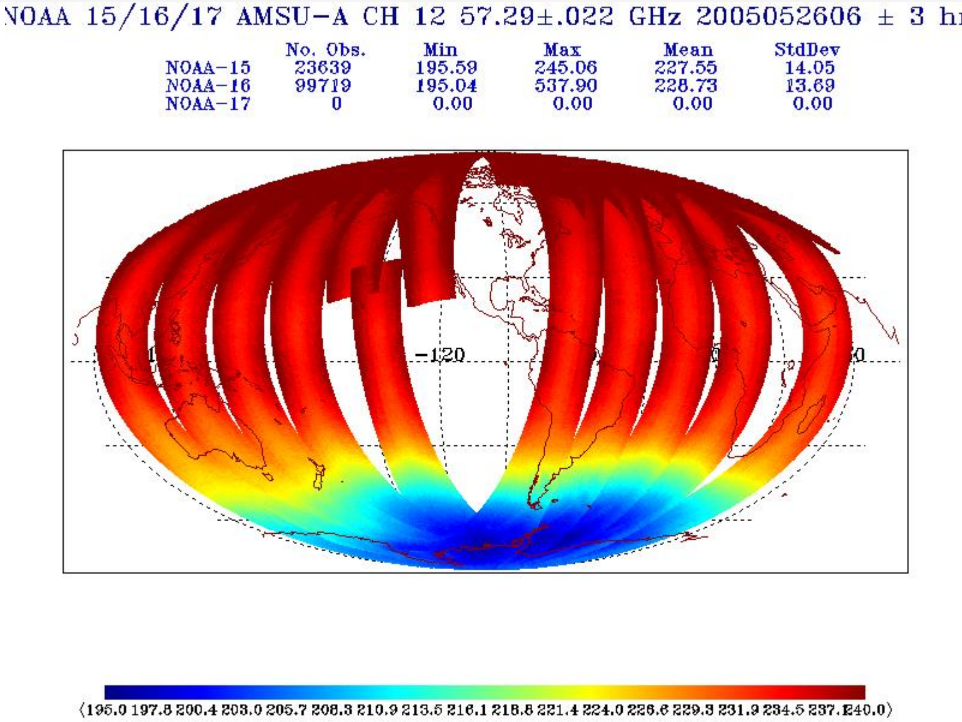

NOAA 15/16/17 AMSU-A CH 12 57.29±.022 GHz 2005052606 ± 3 h

	No. Obs.	Min	Max	Mean	StdDev
NOAA-15	23639	195.59	245.06	227.55	14.05
NOAA-16	99719	195.04	537.90	228.73	13.69
NOAA-17	0	0.00	0.00	0.00	0.00

AMSU-A Ch 12

SSMIS Channel 24 ECMWF RTTOV-7 RTM (BK) and OB-BK

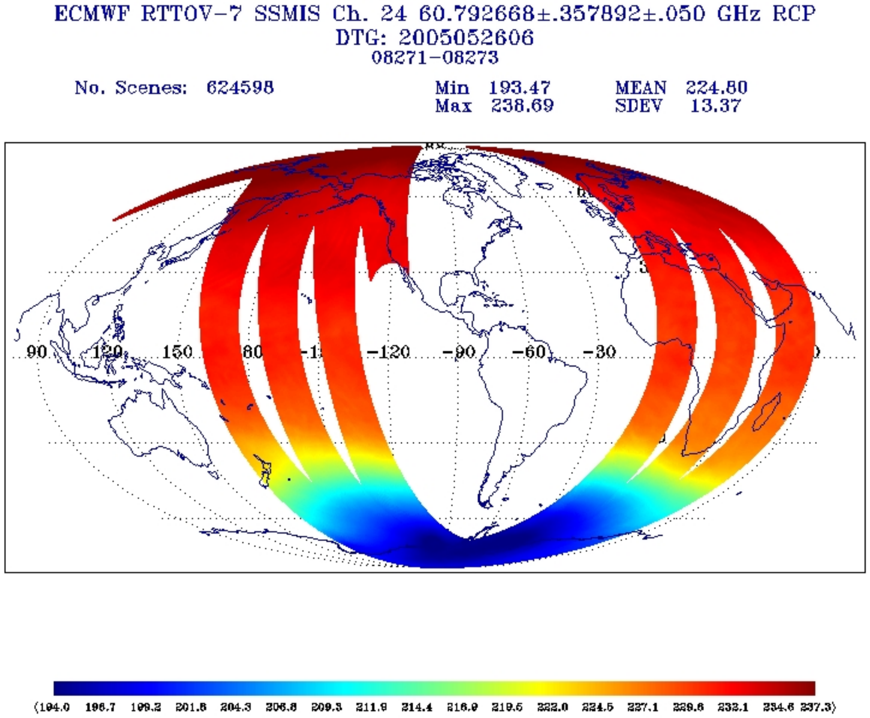

ECMWF RTTOV-7 SSMIS Ch. 24 60.792668±.357892±.050 GHz RCP
DTG: 2005052606
08271–08273

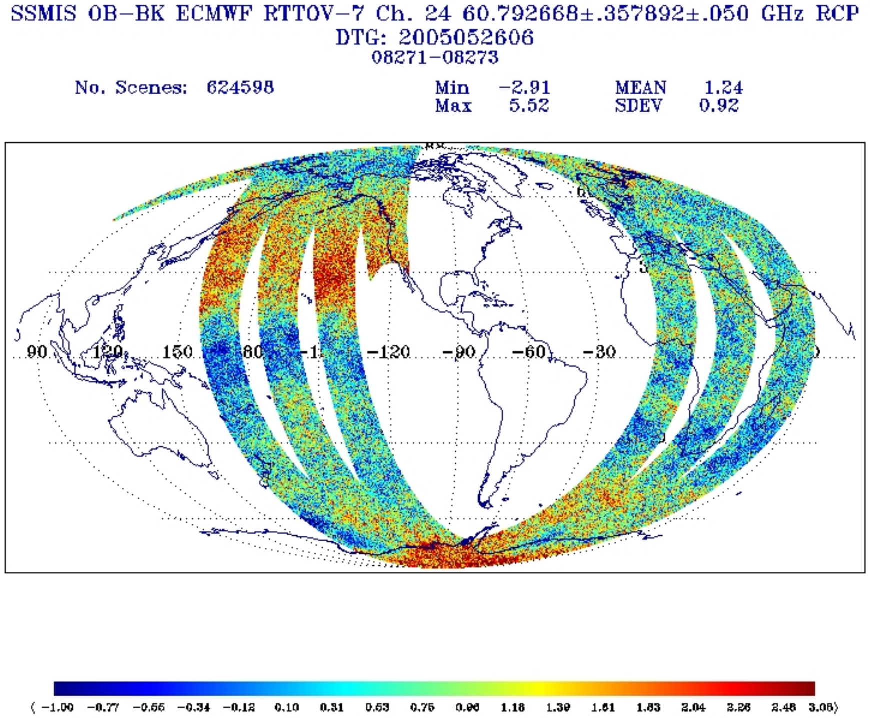

SSMIS OB–BK ECMWF RTTOV–7 Ch. 24 60.792668±.357892±.050 GHz RCP
DTG: 2005052606
08271–08273

SSMIS Ch 24 BK
ECMWF RTTOV-7

SSMIS Ch 24 OB-BK
ECMWF RTTOV-7

SSMIS Channel 23 ECMWF RTTOV-7 RTM (BK) and OB-BK

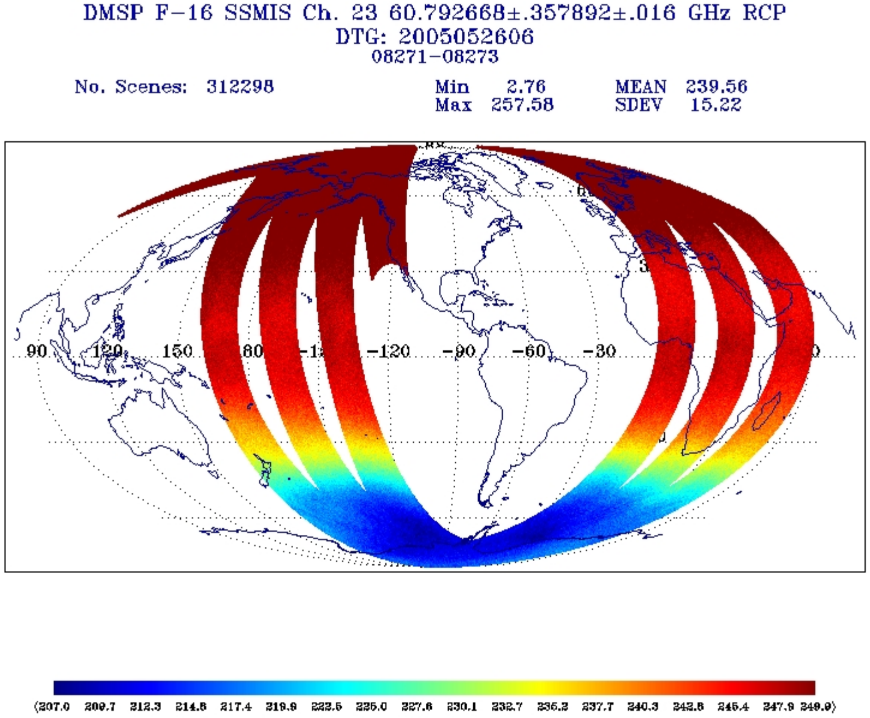

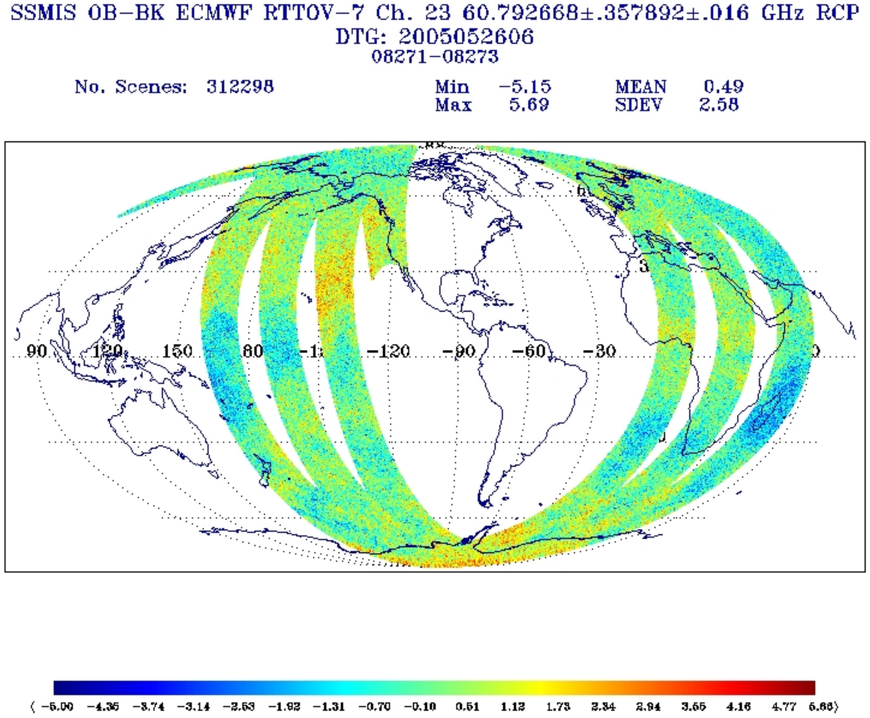

SSMIS Ch 23

SSMIS Ch 23 OB-BK ECMWF RTTOV-7

SSMIS Channel 22 ECMWF RTTOV-7 RTM (BK) and OB-BK

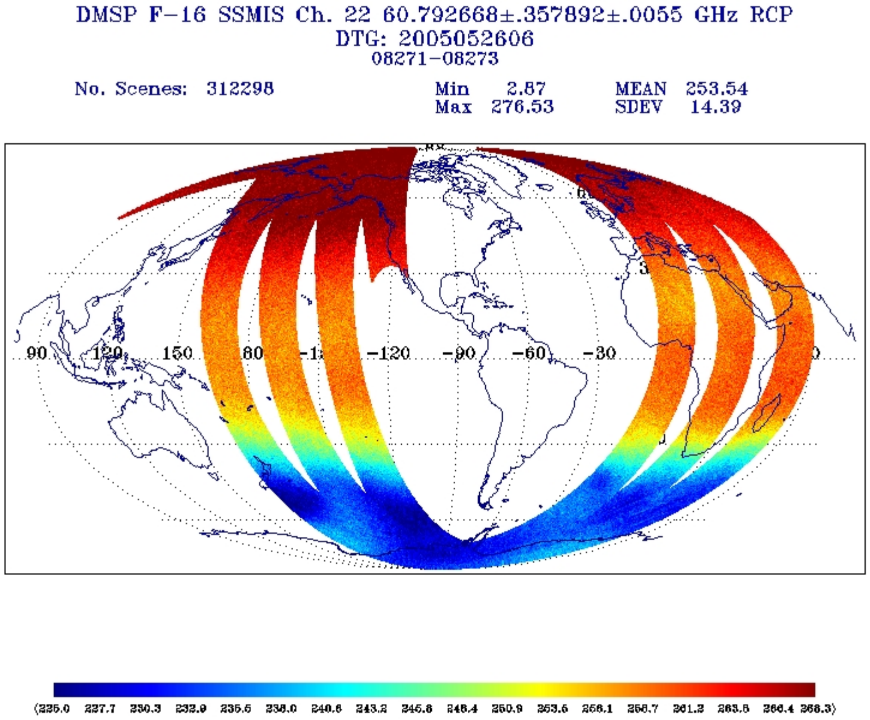

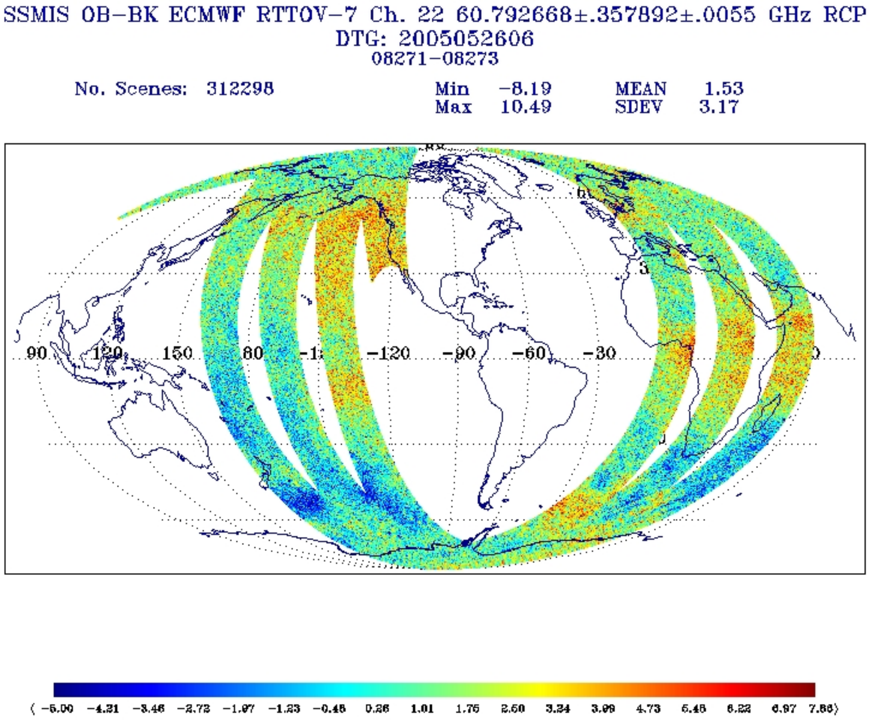

SSMIS Ch 22

SSMIS Ch 22 OB-BK ECMWF RTTOV-7

Upper Atmosphere RTM OB-BK Analysis - LIDAR

- Utilize Merged ECMWF/Lidar/COSPAR Profiles
  - Develop interface utility for both merged Lidar profile and collocated SDR (FORTRAN and IDL)
  - Incorporate FORTRAN utilities into NRL UAS RTM

- Compute TBs for All SSMIS scenes within Matchup Radius
  - Actual filter shapes (100 point NRL data)

- Use SSMIS Observed |B|, - B · k and θ_B for each scene location

- Create SSMIS SDR UAS Channel matchup files for all Lidar Profiles

- Results Indicate a Possible Need to Modify O_2 Absorption

Oxygen Absorption Factor = 1.0

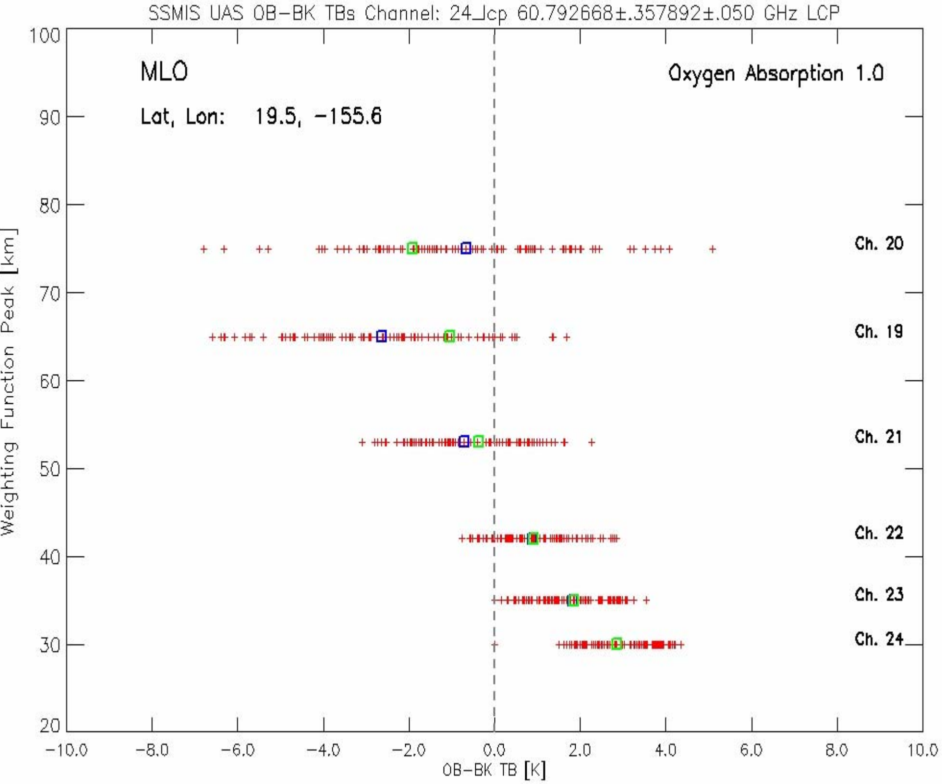

Oxygen Absorption Factor = 1.05

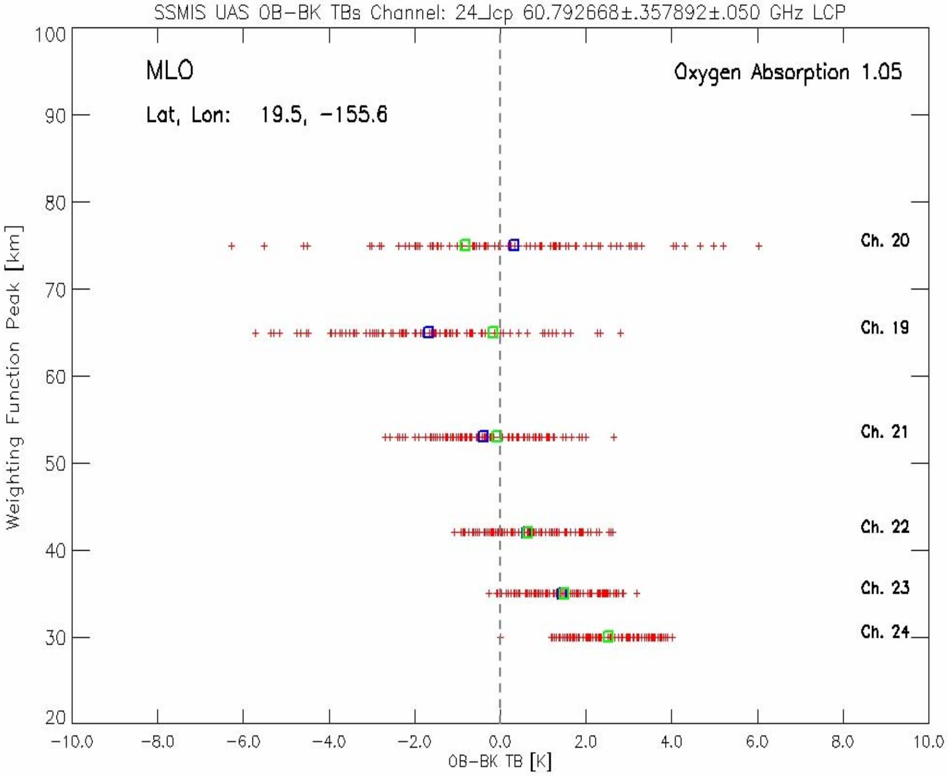

- ☐ **Ensemble Mean OB-BK for LCP**
- ☐ **Ensemble Mean OB-BK for RCP**

OB-RTM with Original O_2 Absorption (Oxygen Absorption Factor = 1.0) shows a Slope in the Bias with respect to Height

Increasing Oxygen Absorption Factor to 1.05 Yields Lower Bias for Channels 19,20 and 21 (Zeeman Effected Channels) LCP

Oxygen Absorption Factor = 1.0

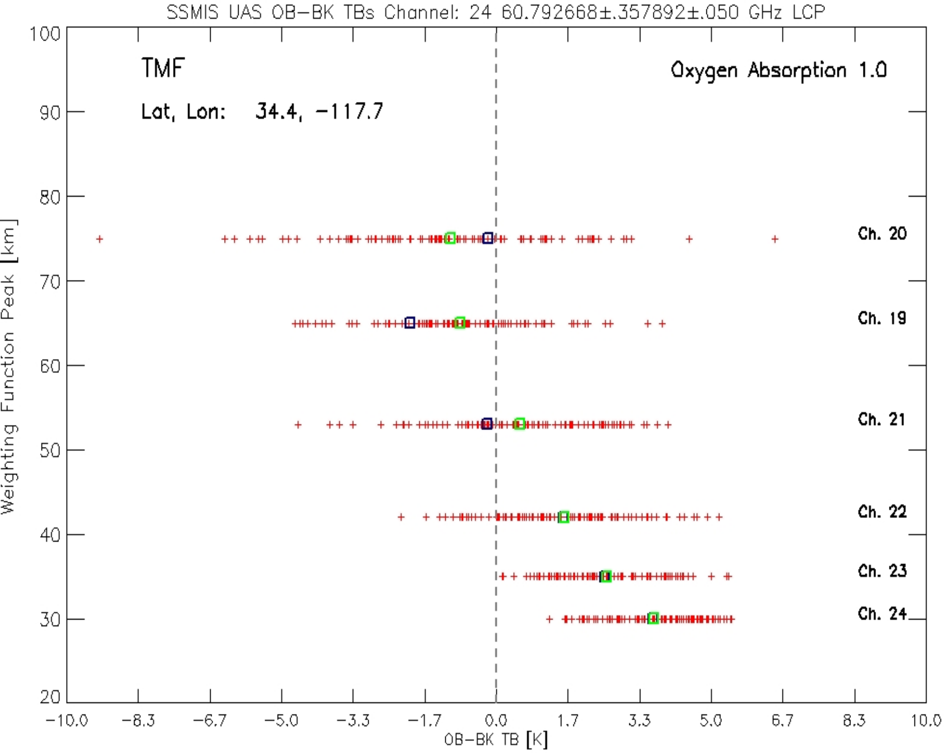

Oxygen Absorption Factor = 1.05

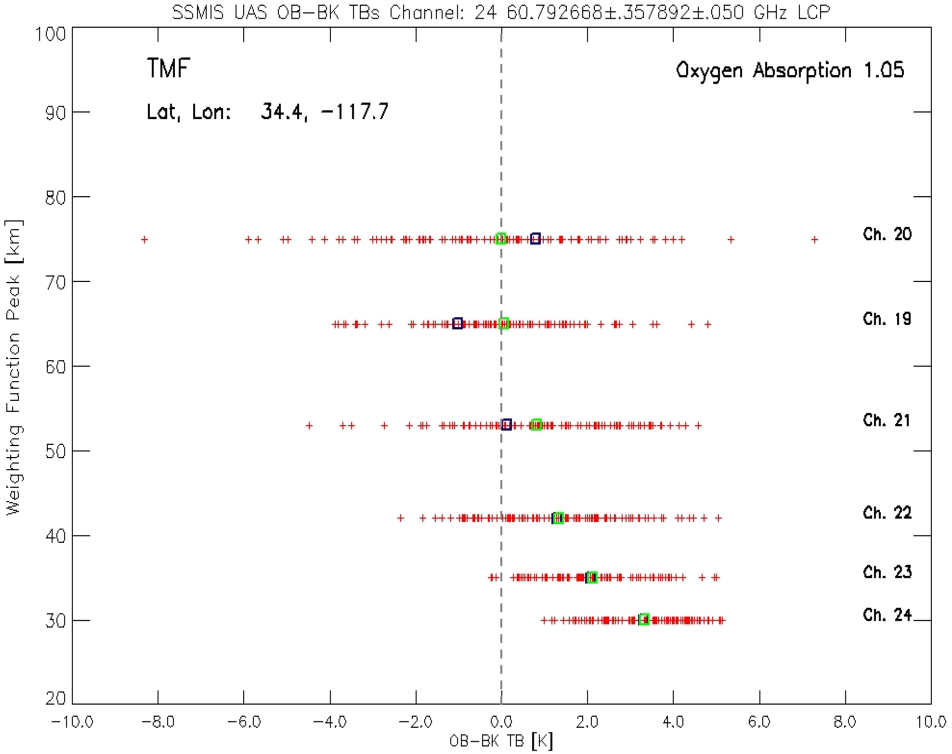

❑ **Ensemble Mean OB-BK for LCP** ❑ **Ensemble Mean OB-BK for RCP**

OB-RTM with Original O_2 Absorption (Oxygen Absorption Factor = 1.0) shows a Slope in the Bias with respect to Height

Increasing Oxygen Absorption Factor to 1.05 Yields Lower Bias for Channels 19,20 and 21 (Zeeman Effected Channels) LCP

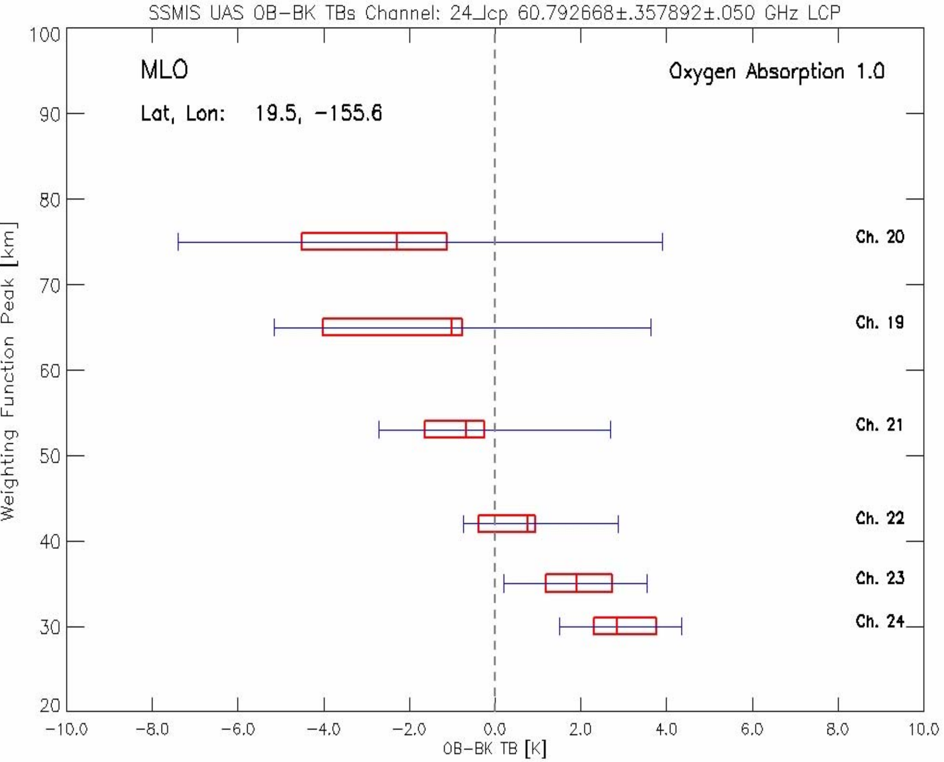

Oxygen Absorption Factor = 1.0
MLO

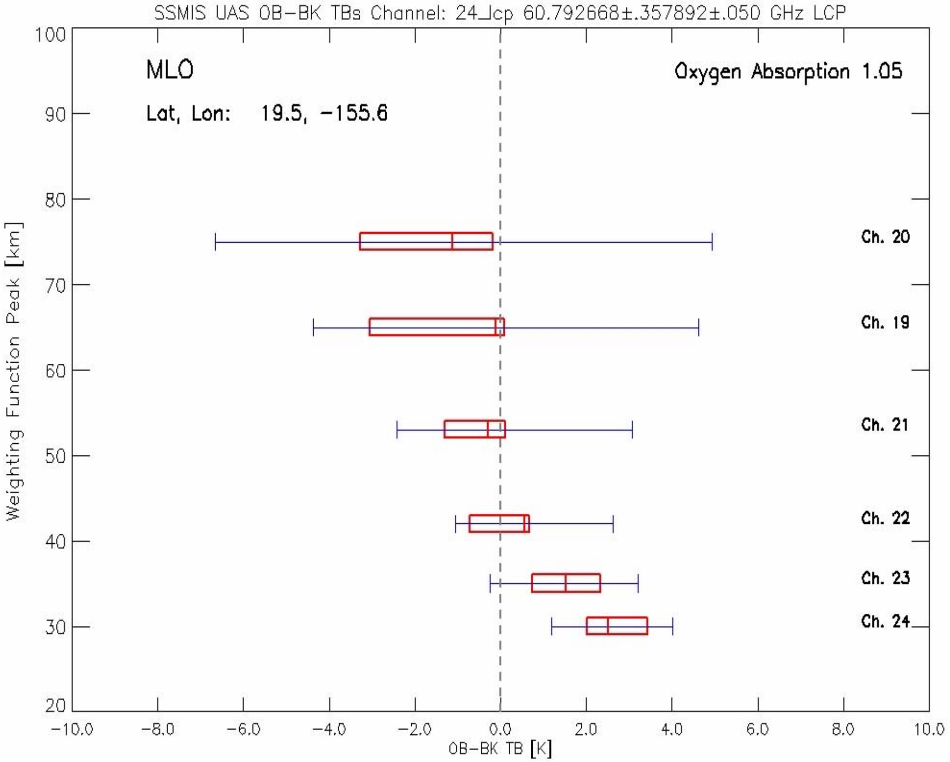

Oxygen Absorption Factor = 1.05
MLO

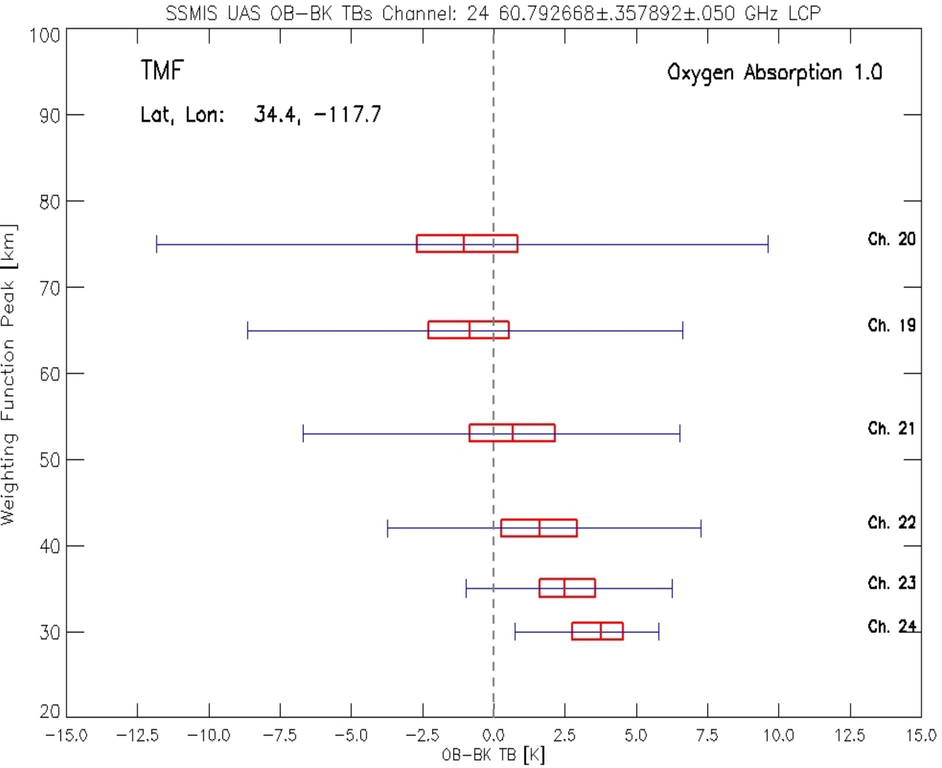

Oxygen Absorption Factor = 1.0
TMF

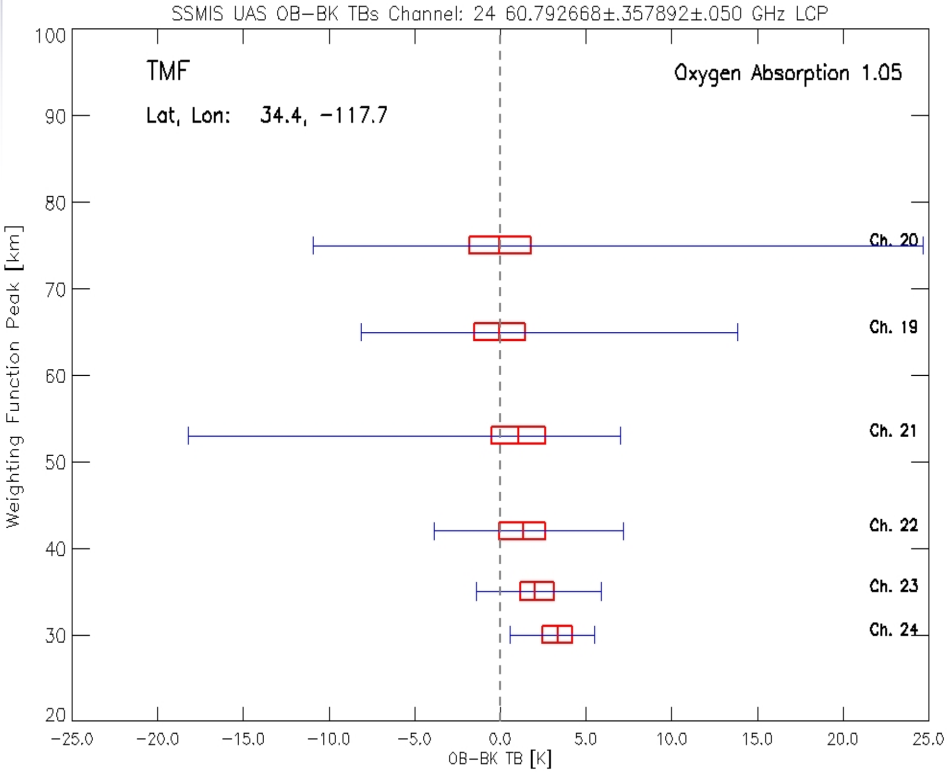

Oxygen Absorption Factor = 1.05
TMF

Upper Atmosphere RTM OB-BK Analysis

- Results for the 103 Coincident MLO Lidar Observations

- $B{\cdot}K$ and θ_B from SDR File for MLO and TMF are computed as

$$B{\cdot}K_{RTM} = -\,SQRT(\,(B{\cdot}K_{SDR})^2\,)$$

$$\theta_B = COS^{-1}\,(\,B{\cdot}K_{RTM}\,/\,|B|\,)$$

+ Observed SSMIS SDRs within Time and Distance Window from Lidar Observation
+ LIDAR Profile RTM Tb using LCP and Geomagnetic Parameters from SDR Scene
+ LIDAR Profile RTM Tb using RCP and Geomagnetic Parameters from SDR Scene

SSMIS OB and RTM BK Temperatures

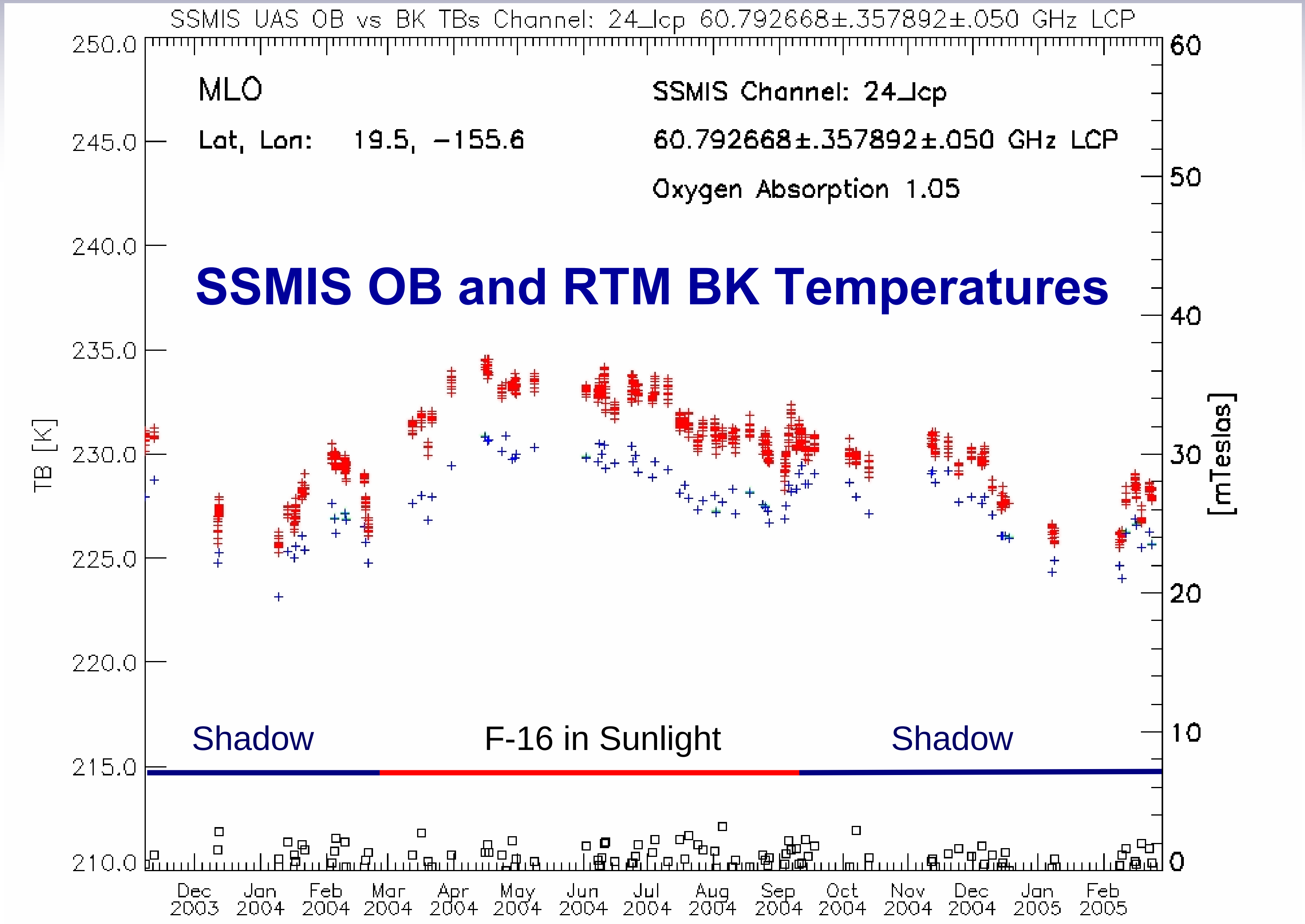

Shadow

F-16 in Sunlight

Shadow

SSMIS OB and RTM BK Temperatures

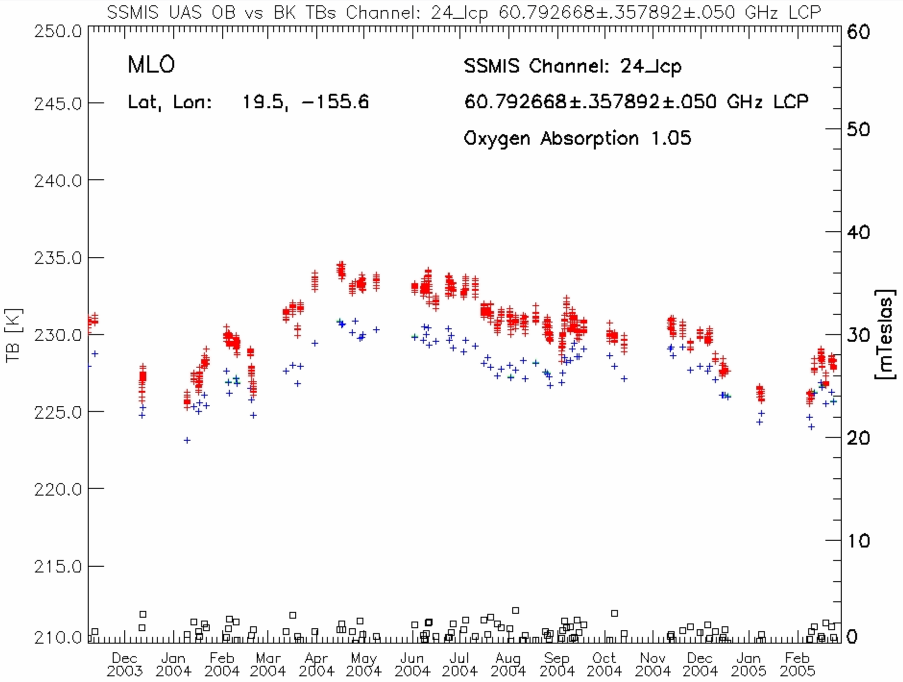

SSMIS Ch 24

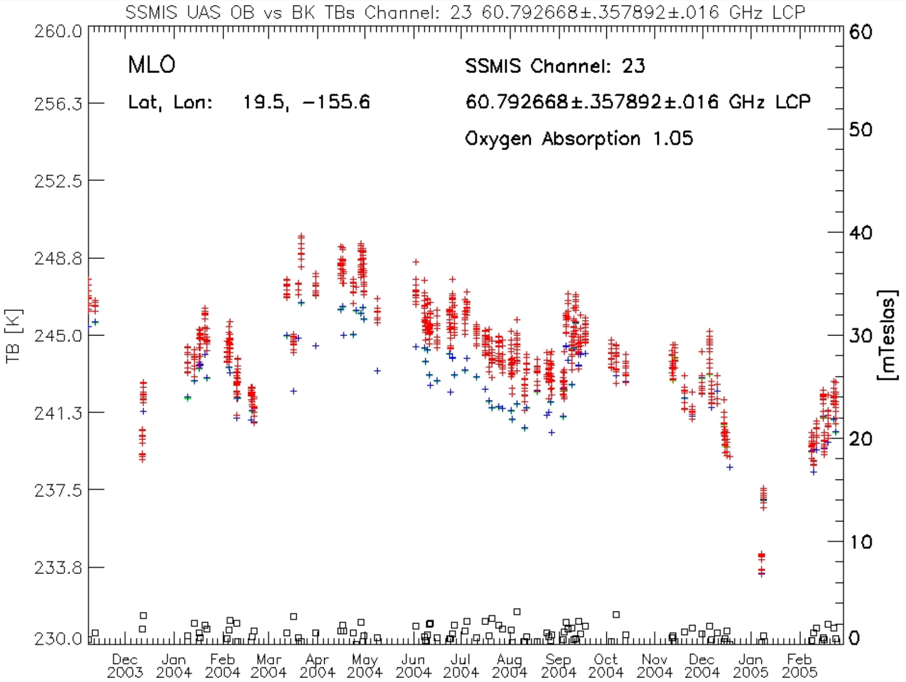

SSMIS Ch 23

SSMIS OB and RTM BK Temperatures

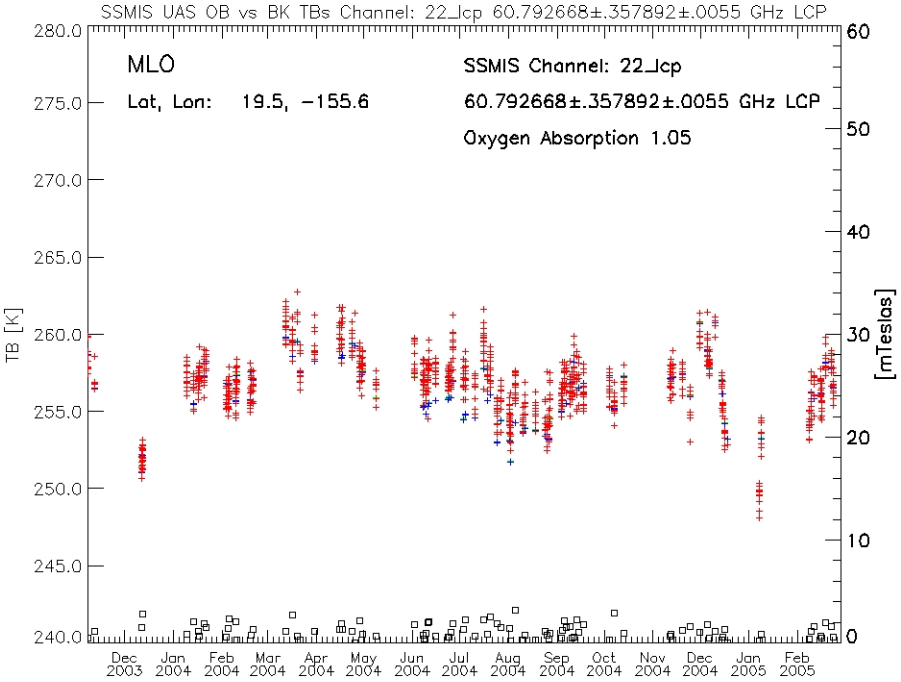

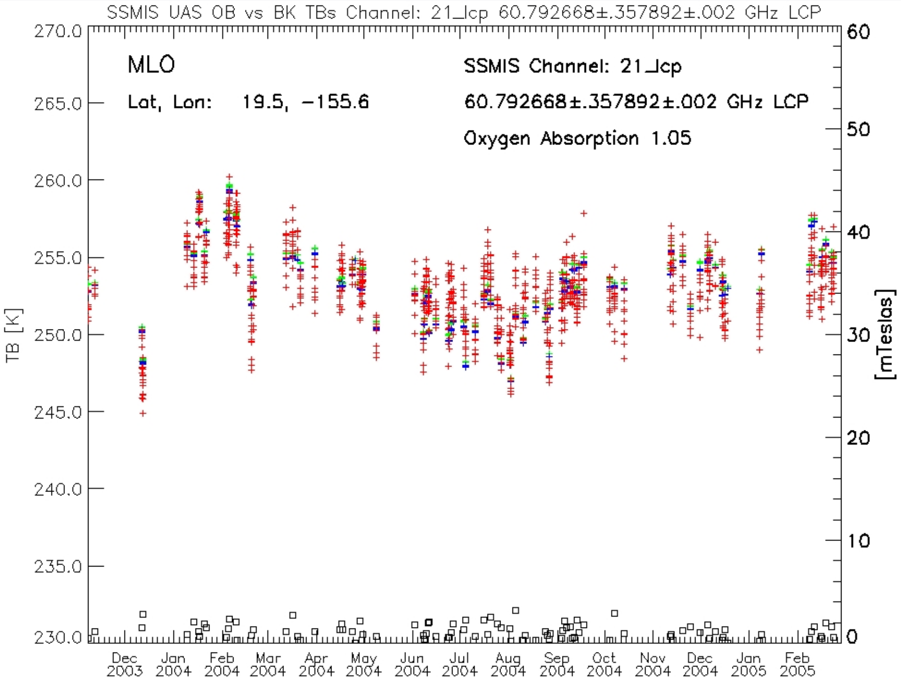

SSMIS Ch 22

SSMIS Ch 21

SSMIS OB and RTM BK Temperatures

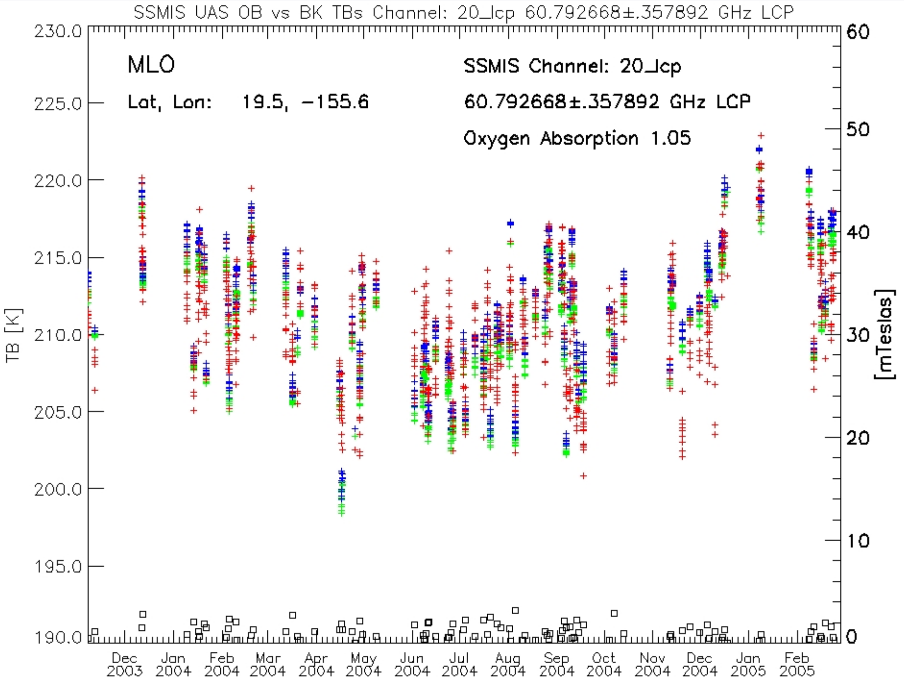

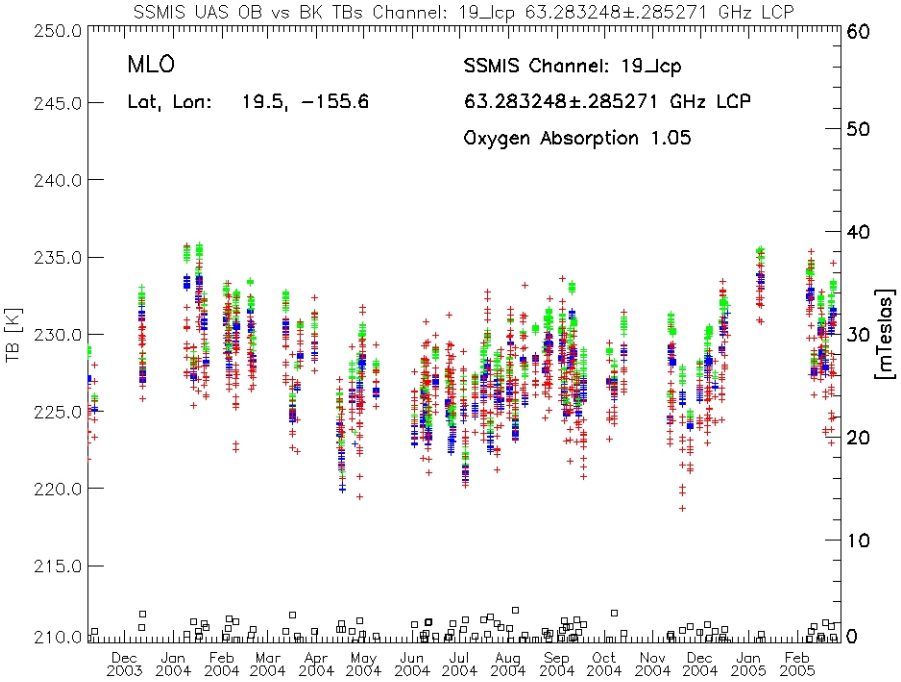

SSMIS Ch 20

SSMIS Ch 19

SSMIS OB - RTM BK Departures

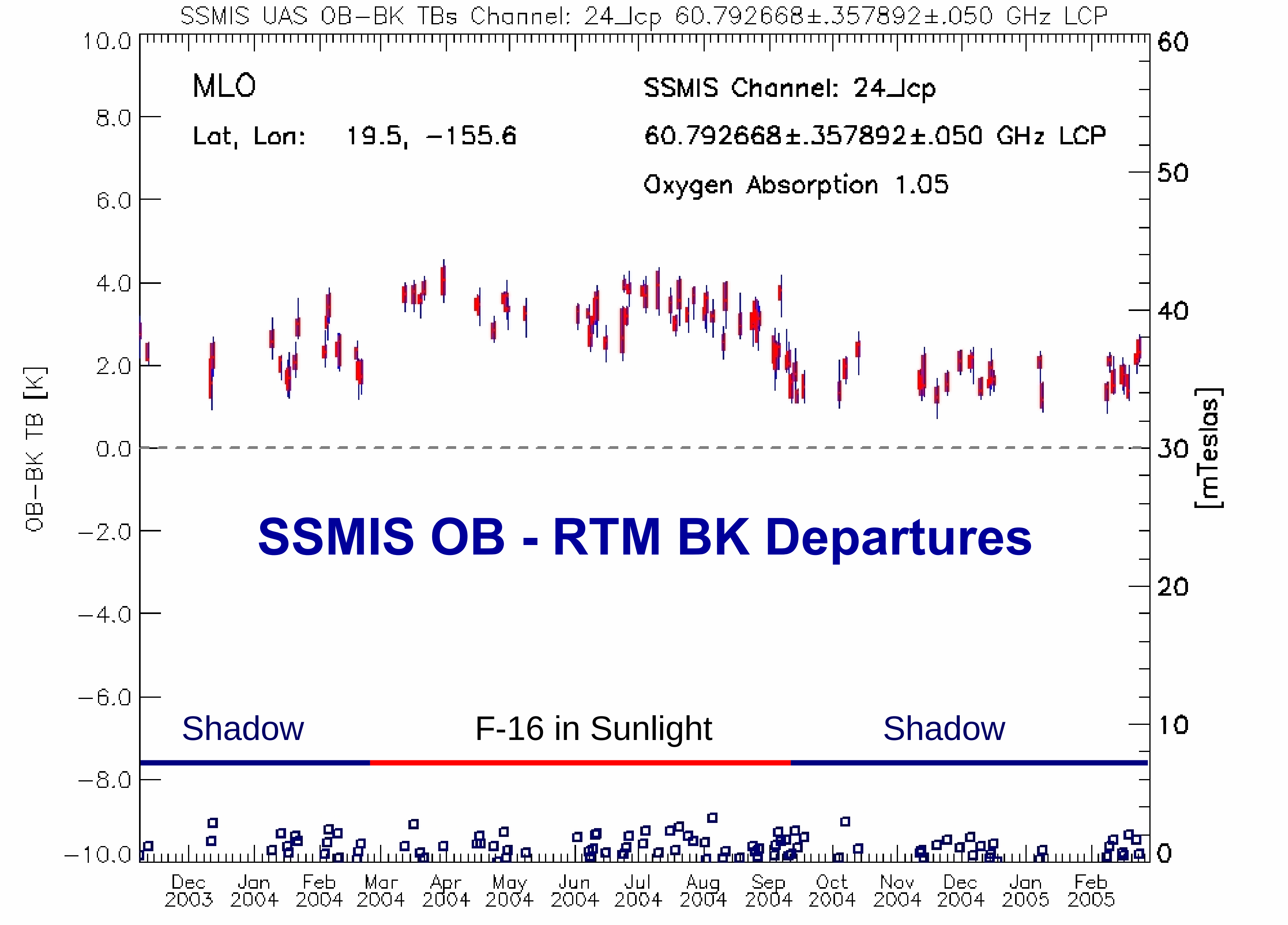

Shadow

F-16 in Sunlight

Shadow

SSMIS OB - RTM BK Departures

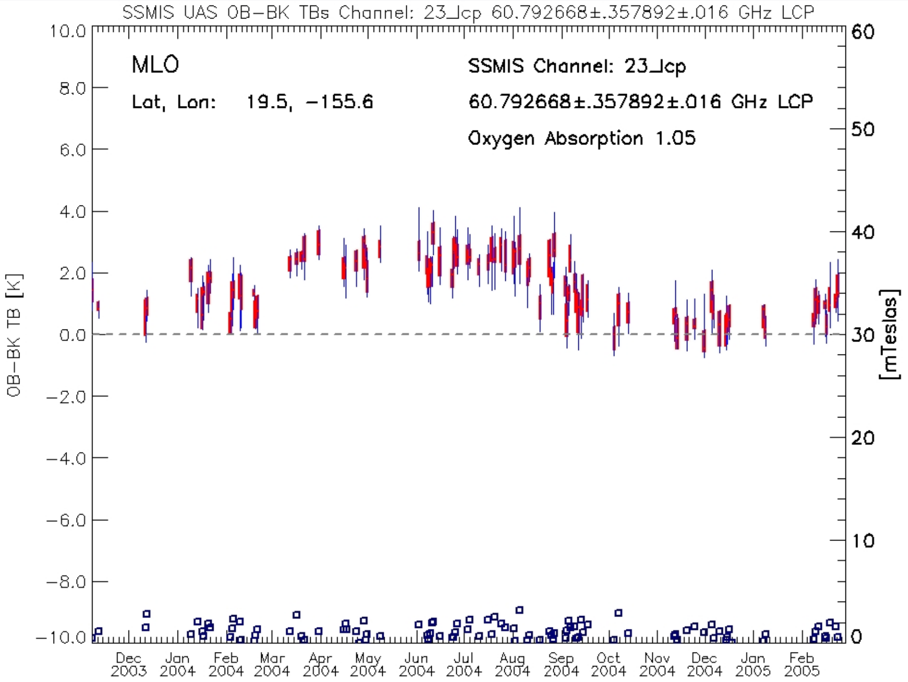

SSMIS Ch 24

SSMIS Ch 23

SSMIS OB - RTM BK Departures

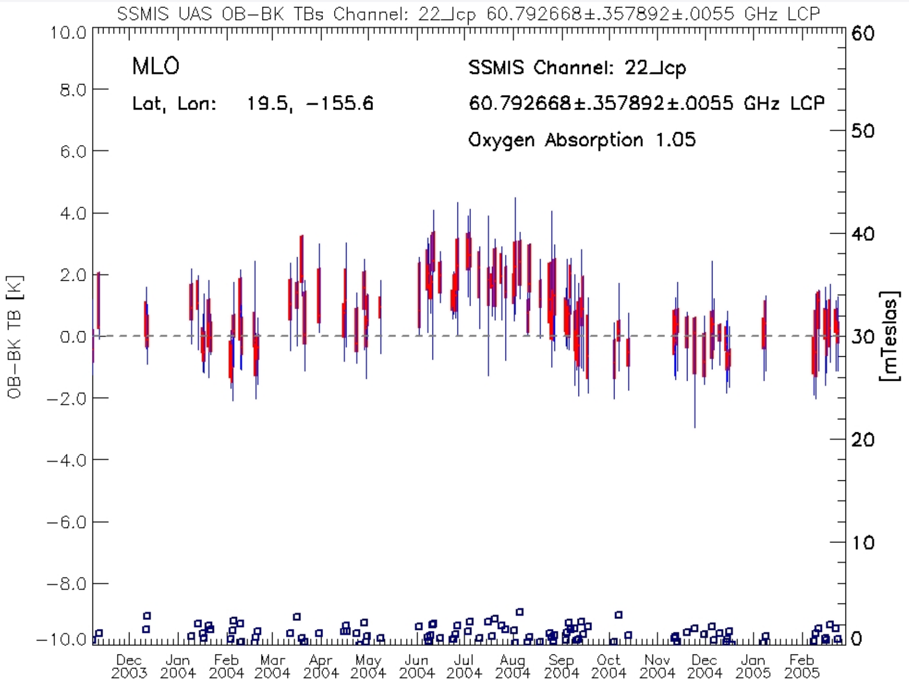

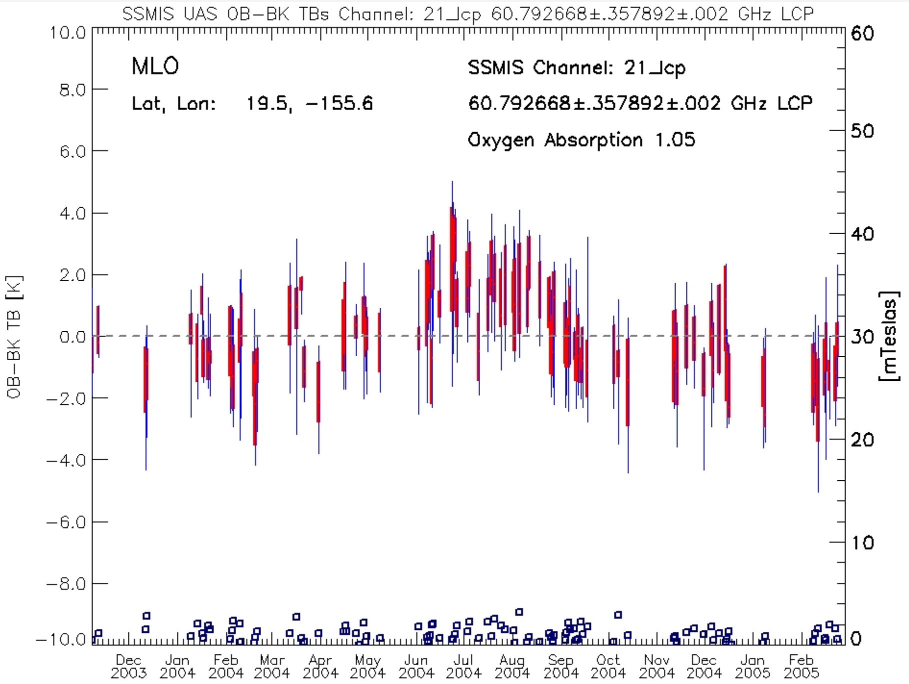

SSMIS Ch 22

SSMIS Ch 21

SSMIS OB - RTM BK Departures

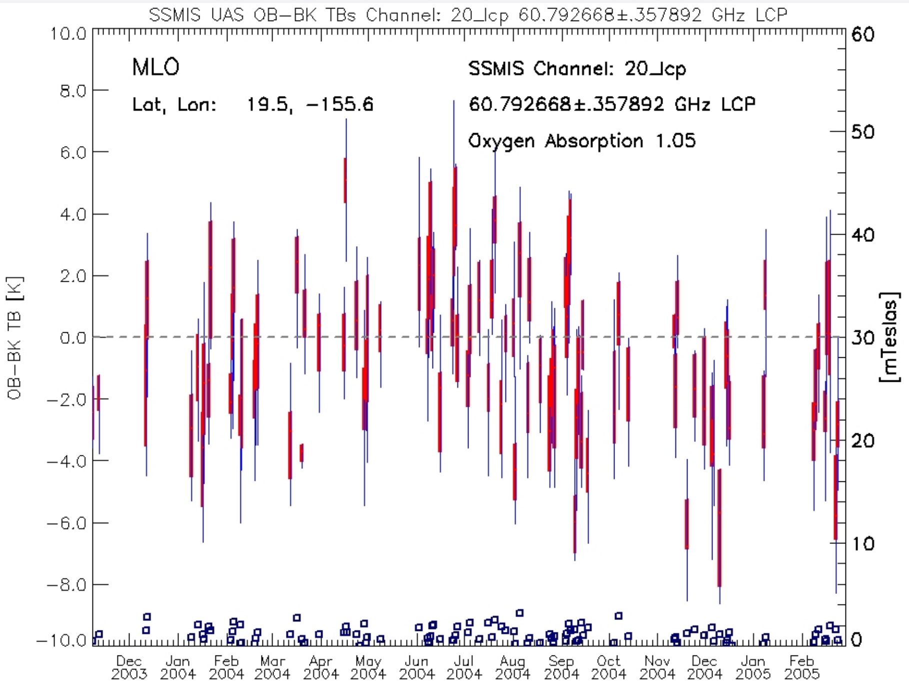

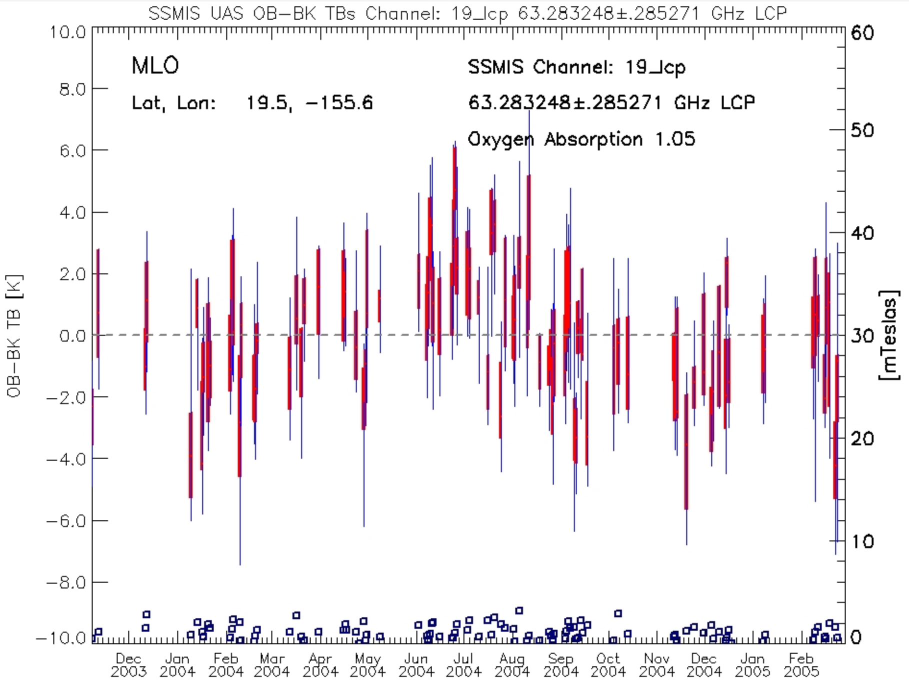

SSMIS Ch 20

SSMIS Ch 19

Upper Atmosphere RTM OB-BK Analysis

- Results for the 101 Coincident TMF Lidar Observations

- $B{\cdot}K$ and ϑ_B from SDR File for MLO and TMF are computed as

$$B{\cdot}K_{RTM} = -\,SQRT(\,(B{\cdot}K_{SDR})^2\,)$$

$$\vartheta_B = COS^{-1}\,(\,B{\cdot}K_{RTM} / |B|\,)$$

+ Observed SSMIS SDRs within Time and Distance Window from Lidar Observation
+ LIDAR Profile RTM Tb using LCP and Geomagnetic Parameters from SDR Scene
+ LIDAR Profile RTM Tb using RCP and Geomagnetic Parameters from SDR Scene

SSMIS OB and RTM BK Temperatures

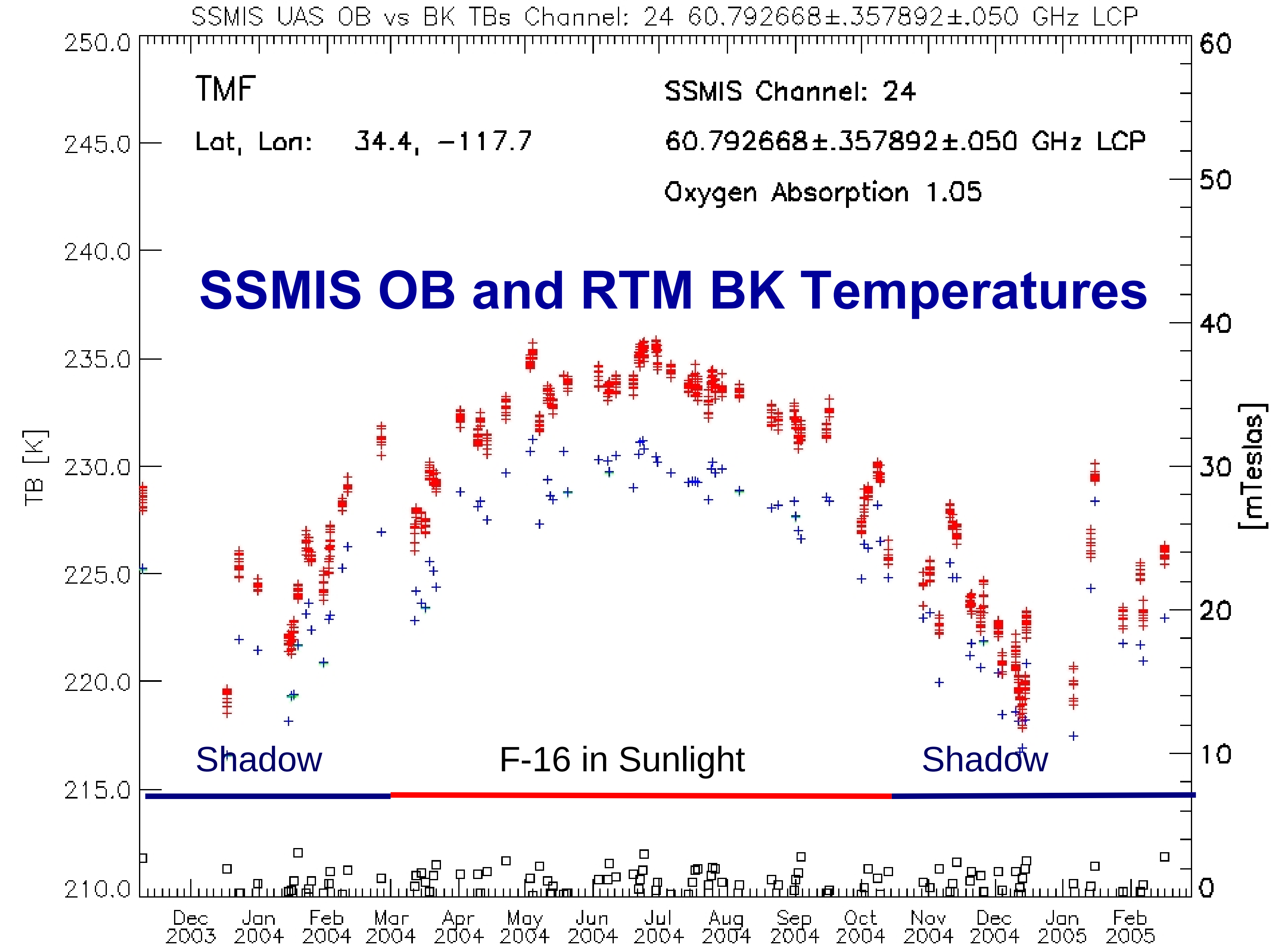

Shadow F-16 in Sunlight Shadow

SSMIS OB and RTM BK Temperatures

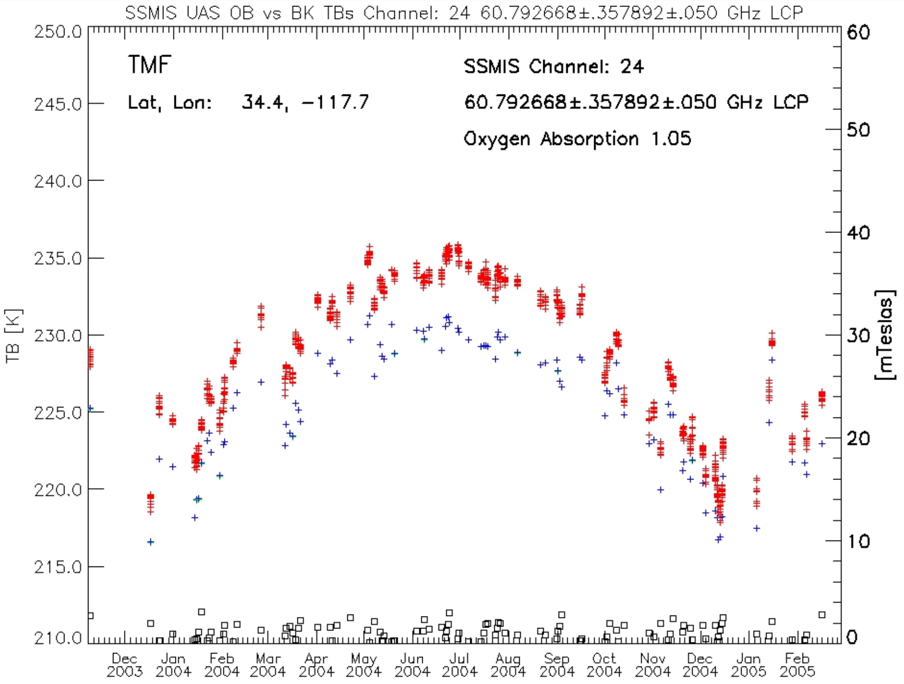

SSMIS Ch 24

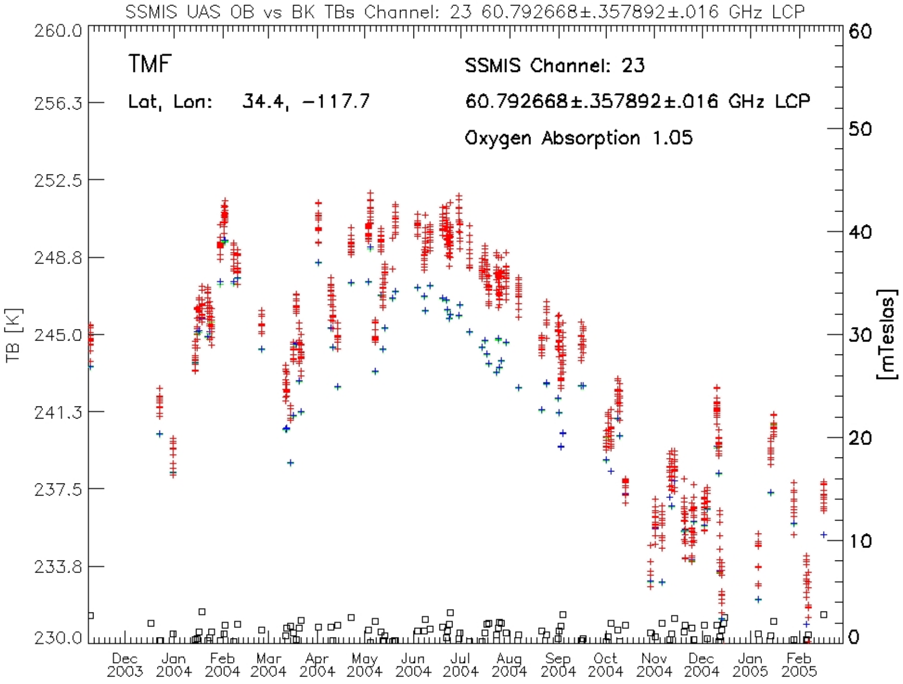

SSMIS Ch 23

SSMIS OB and RTM BK Temperatures

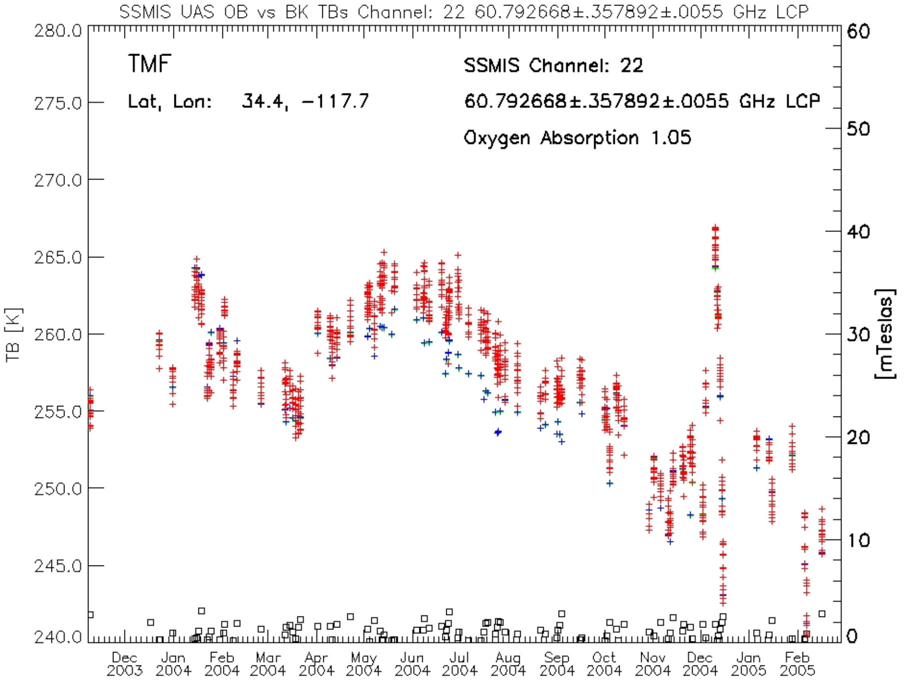

SSMIS Ch 22

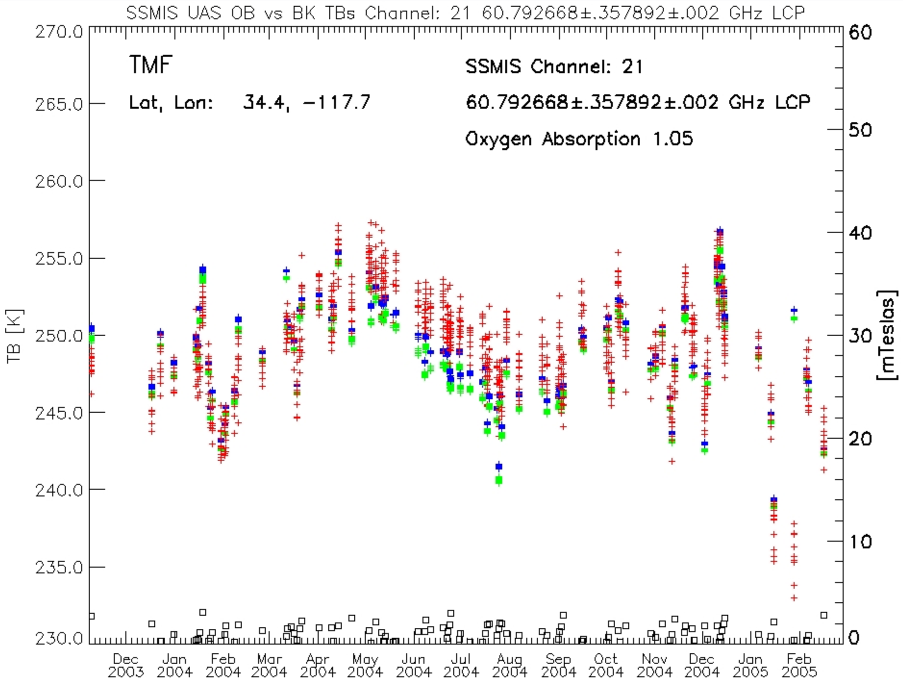

SSMIS Ch 21

SSMIS OB and RTM BK Temperatures

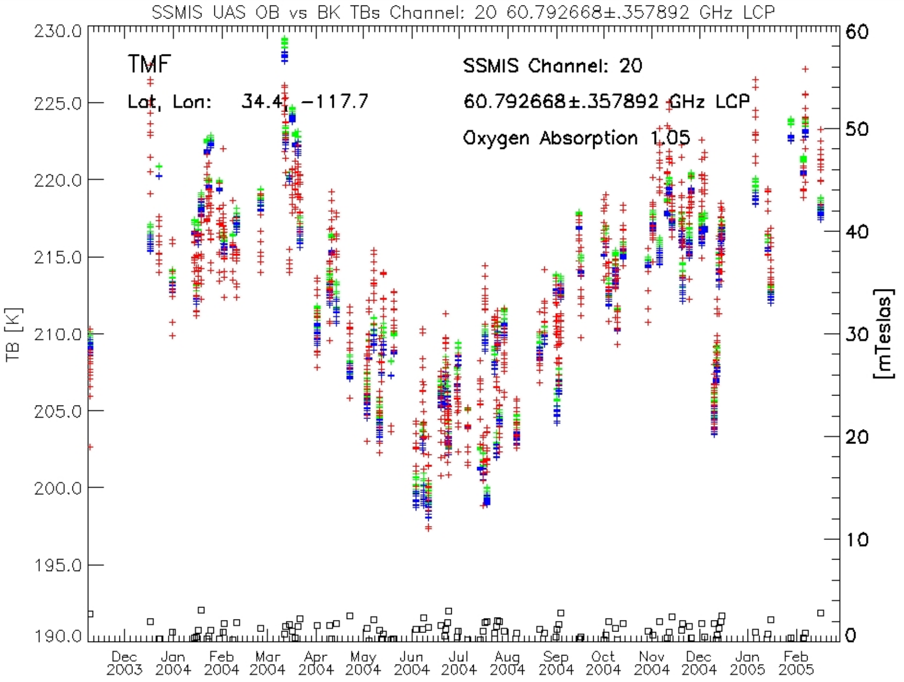

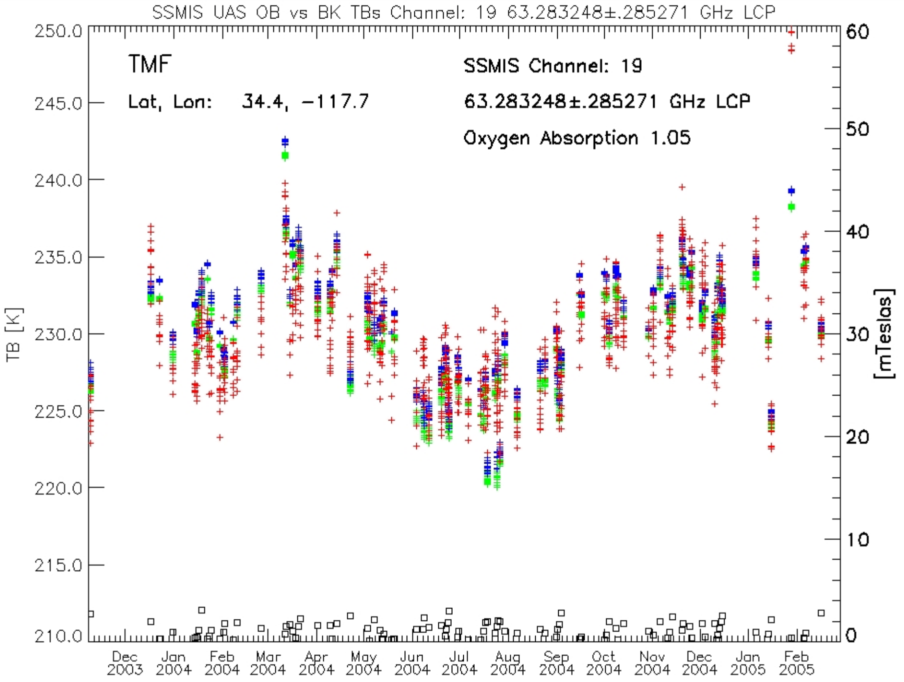

SSMIS Ch 20 **SSMIS Ch 19**

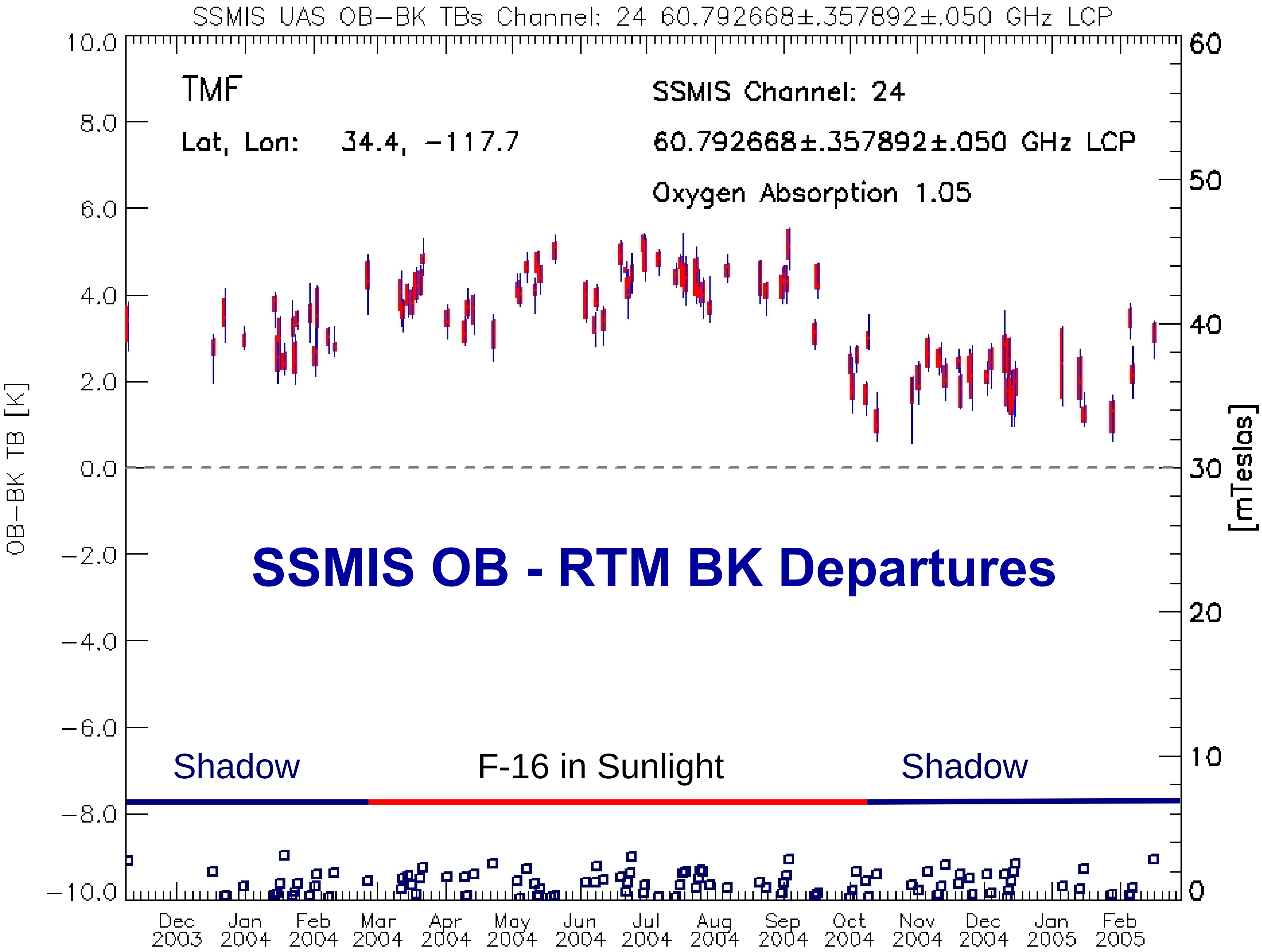

SSMIS OB - RTM BK Departures

Shadow

F-16 in Sunlight

Shadow

SSMIS OB - RTM BK Departures

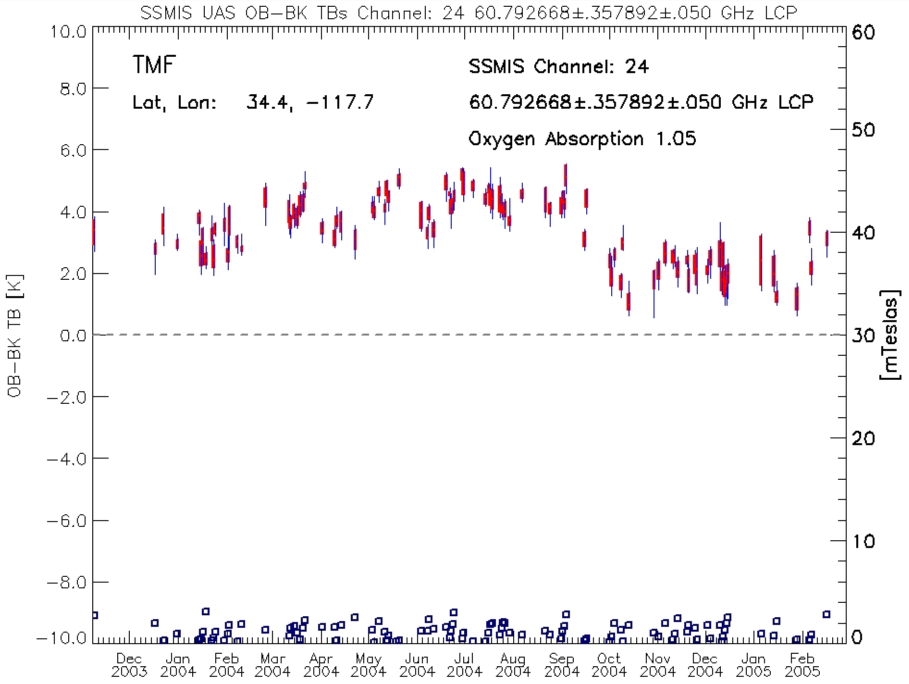

SSMIS Ch 24

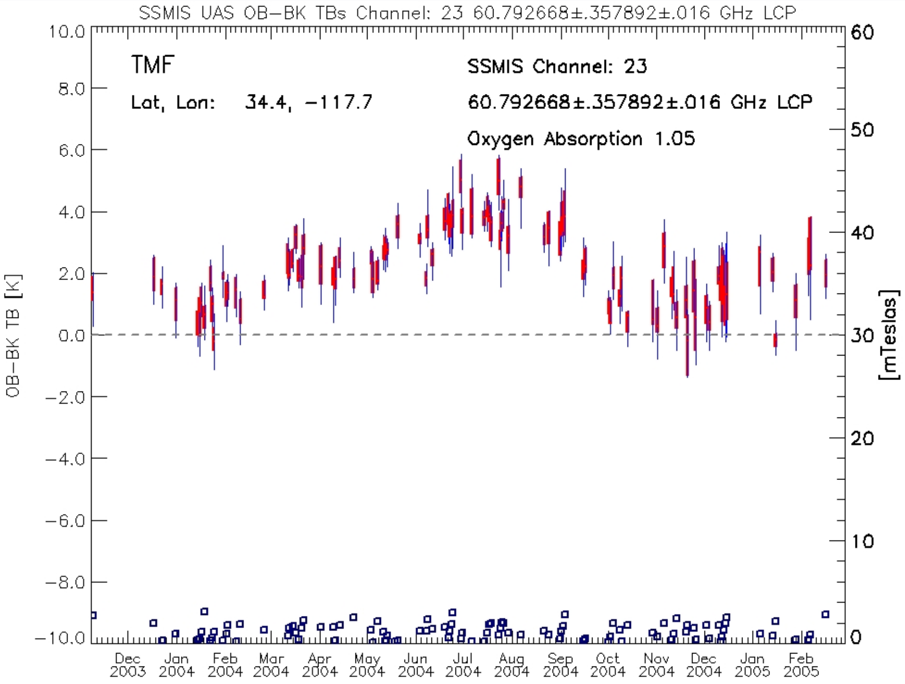

SSMIS Ch 23

SSMIS OB - RTM BK Departures

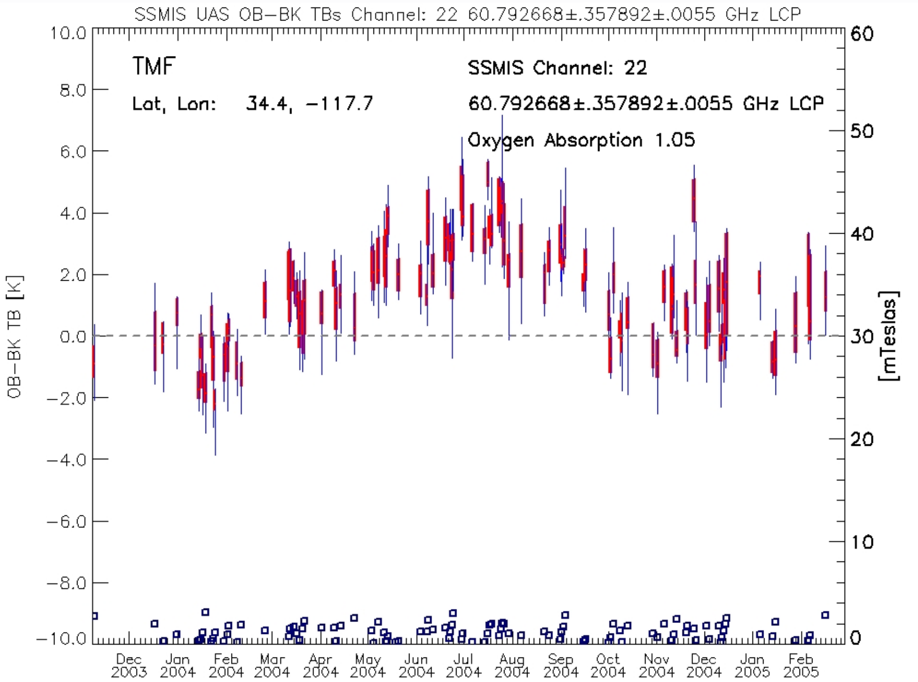

SSMIS Ch 22

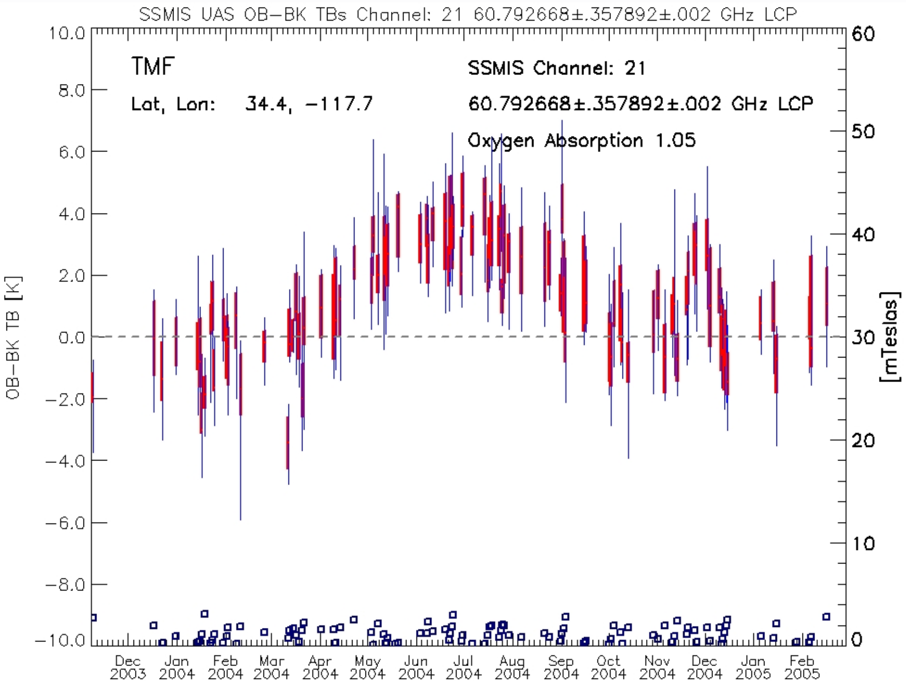

SSMIS Ch 21

SSMIS OB - RTM BK Departures

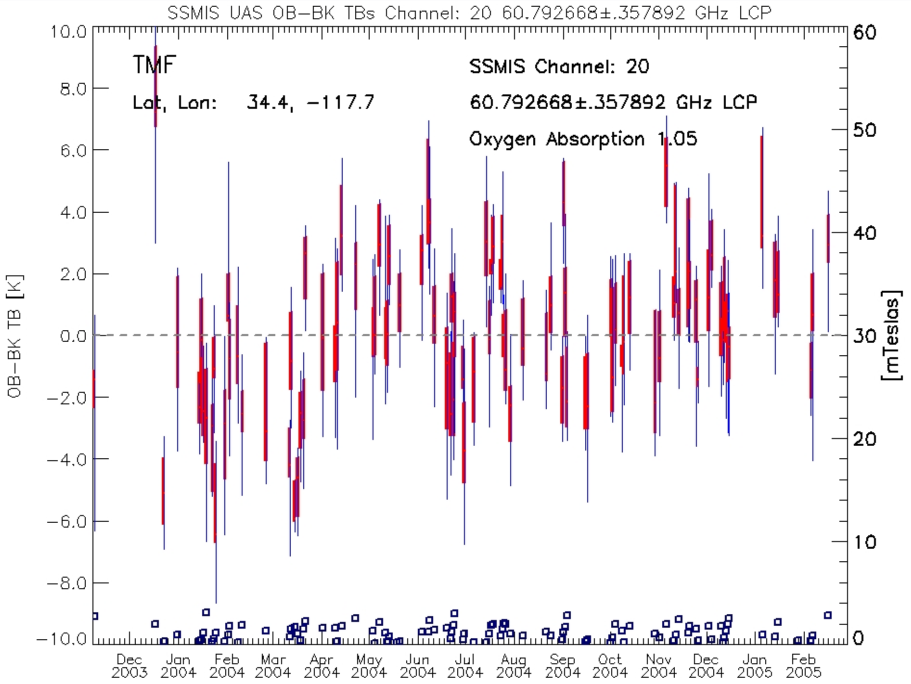

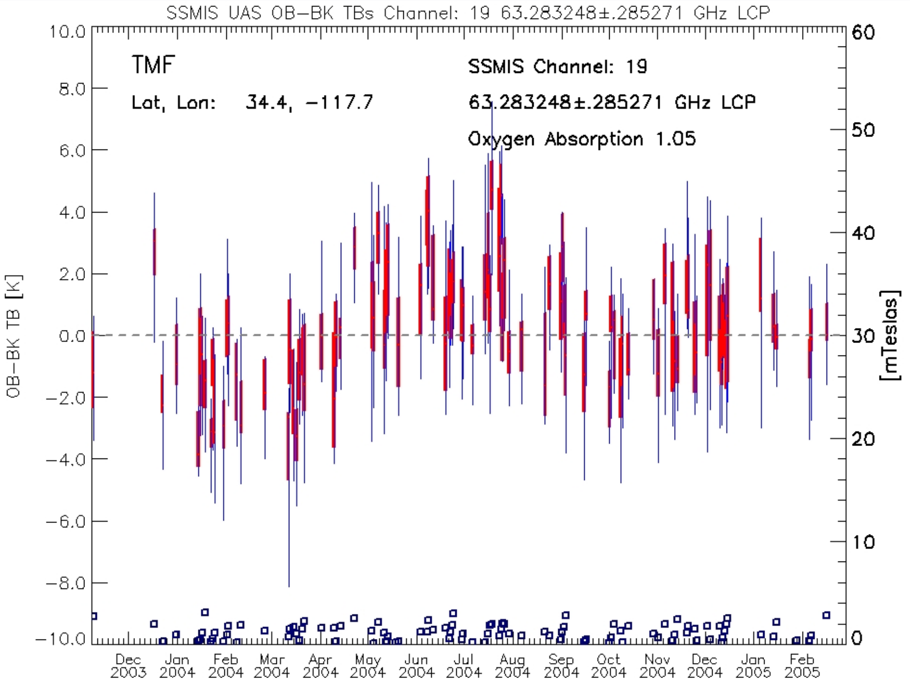

SSMIS Ch 20

SSMIS Ch 19

SSMIS SDR OB – RTM BK Departures Results

- SSMIS Observed Tbs Better Match LCP vs. RCP RTM Results for Polarization

- SSMIS Tracks Seasonal Variation in TBs

- Clearly Exhibit Reflector Emission Bias

Analysis Methodology

- **SDR Calibration (OB-RTM)**
- **EDR Validation (Retrieval-Lidar)**
- **EDR Validation (Retrieval-NWP)**

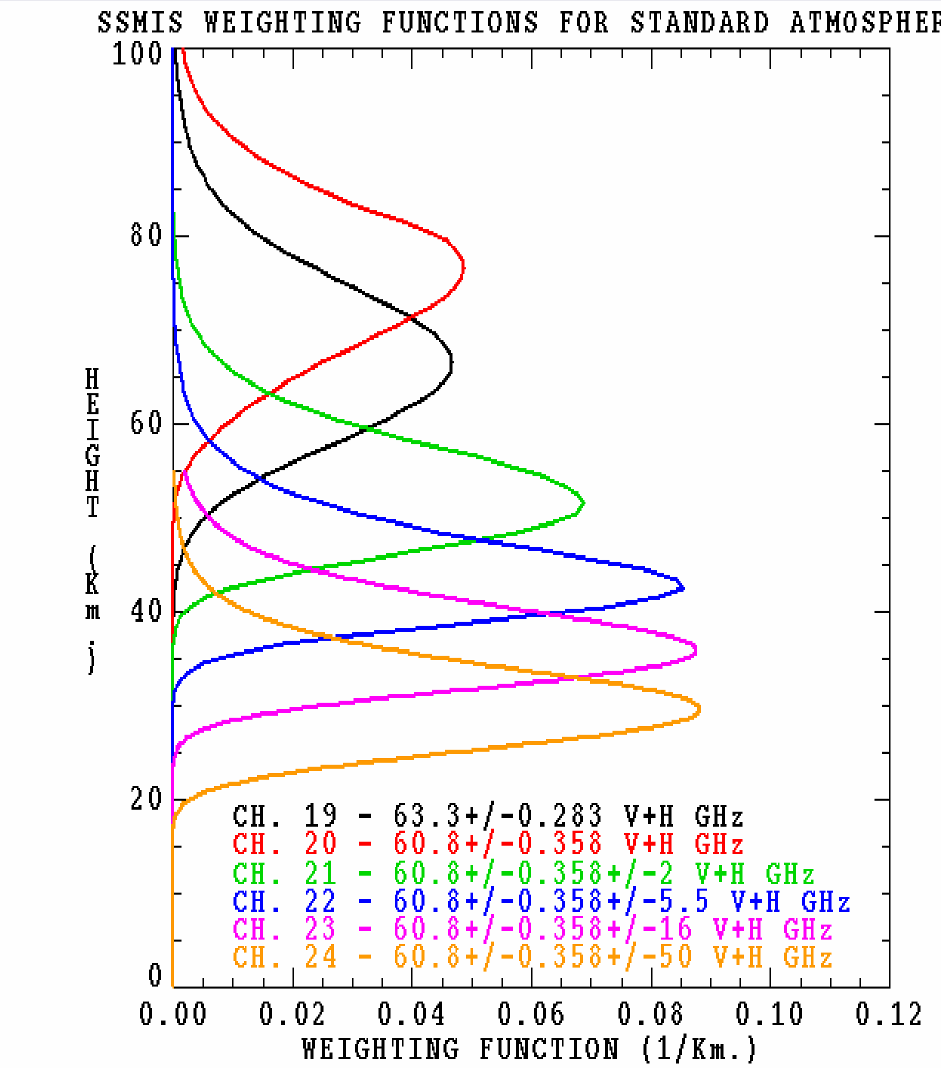

SSMIS UAS Temperature Retrieval Algorithm

Multiple Linear Regression

$$T - \langle T \rangle = \mathbf{D}\left(d - \langle d \rangle\right)$$

T = Retreived Temperature Profile

$\langle T \rangle$ = Expected Value from Apriori Data Base

$\mathbf{D}$ = D-Matrix of Regression Coefficients

$$\mathbf{D} = \mathbf{C}\left(T - \langle T \rangle, d - \langle d \rangle\right)\mathbf{C}^{-1}\left(T - \langle T \rangle, d - \langle d \rangle\right)$$

d = Data Vector, i.e. the Observed TBs (Ch 19-24)

$\mathbf{C}\left(T - \langle T \rangle, d - \langle d \rangle\right)$ = Covariance Matrix

Incorporating Geomagnetic Field Dependence

$\langle d \rangle = \langle d_0 \rangle + \langle d_m \rangle$

$\langle d_0 \rangle$ = Expected TBs from Apriori Data Base and RTM

$\langle d_m \rangle$ = Series Expansion for the Geomagnetic Field Dependence

$$\langle d_m \rangle_{19,\,20,\,21} = \sum_{\alpha=0}^{2} a_{\alpha j} \left(\mathbf{B}_e \cos \theta_{\mathbf{B}} \right)^{2\alpha}$$

$\theta_{\mathbf{B}}$ = Angle between Geomagnetic Field, $\mathbf{B}_e$, and SSMIS line-of-sight, $\vec{k}$

$$a_{\alpha j} = \sum_{l=1}^{4} a_{\alpha jl} \mathbf{L}_l \left(\mathbf{B}_e^2 \right)$$ L is the Lagrange Polynomial

$$\langle d_m \rangle_{22} = a_1 \mathbf{B}_e^2 + a_2 f \mathbf{B}_e^2 + a_3 \left(\mathbf{B}_e \cos \theta_{\mathbf{B}} \right)^2$$

$f = \left\langle \mathbf{B}_e, (v, h) \right\rangle$ Dot product of $\mathbf{B}_e$ and v, h the Orthognal Polarization vectors

$\langle d_m \rangle_{23,\,24} = 0$

Angle Definitions for the UAS Geomagnetic Field Dependence

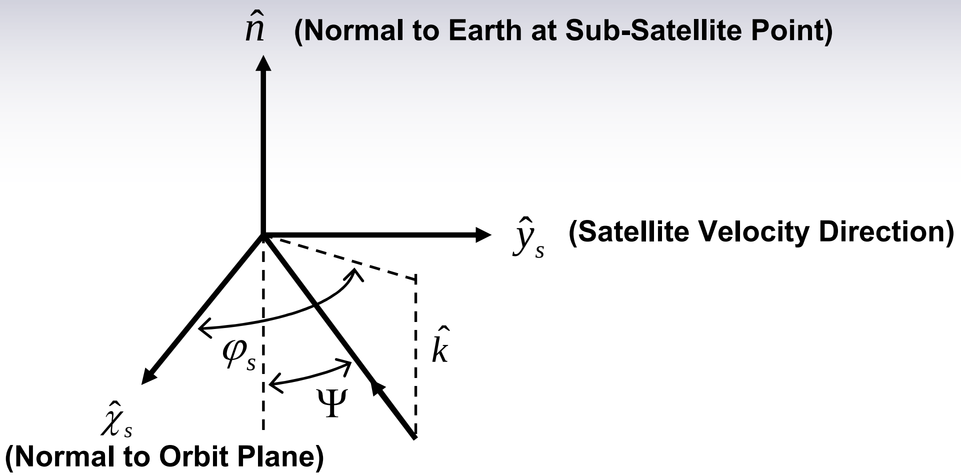

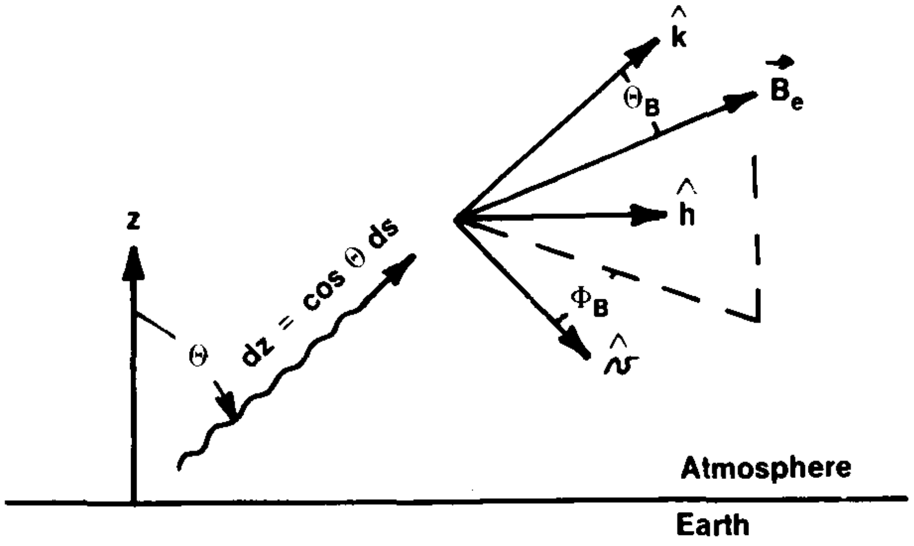

UAS EDR Temperature (SSMIS-Lidar) Analysis

MLO Lidar Observation EDR Comparison Results

- Results for the 103 Coincident Lidar Observations
- 2.5 Degree Separation Window
- SSMIS EDR Temperature Retrieval

SSMIS Retrieved vs. Lidar Temperatures

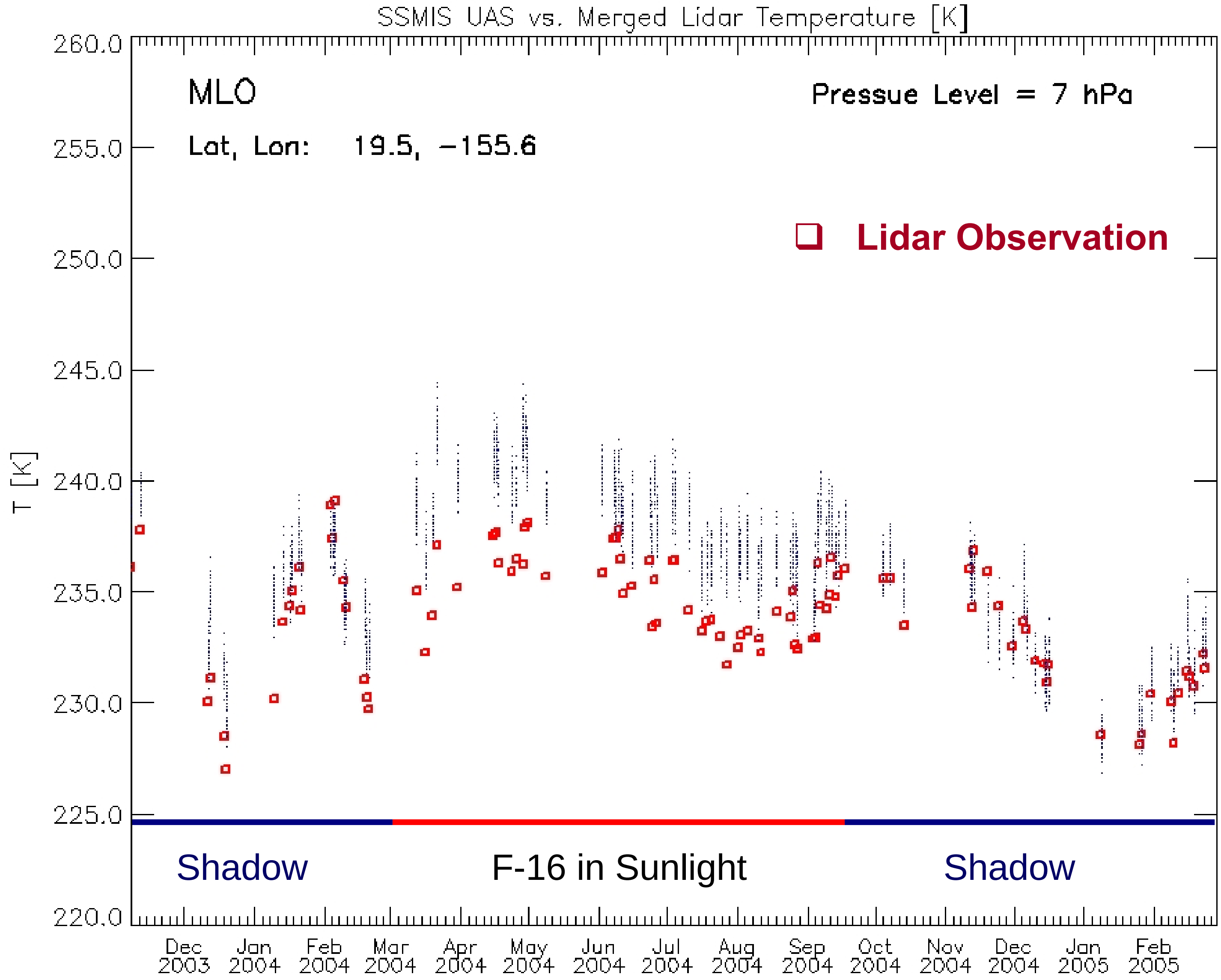

SSMIS Retrieved vs. Lidar Temperatures

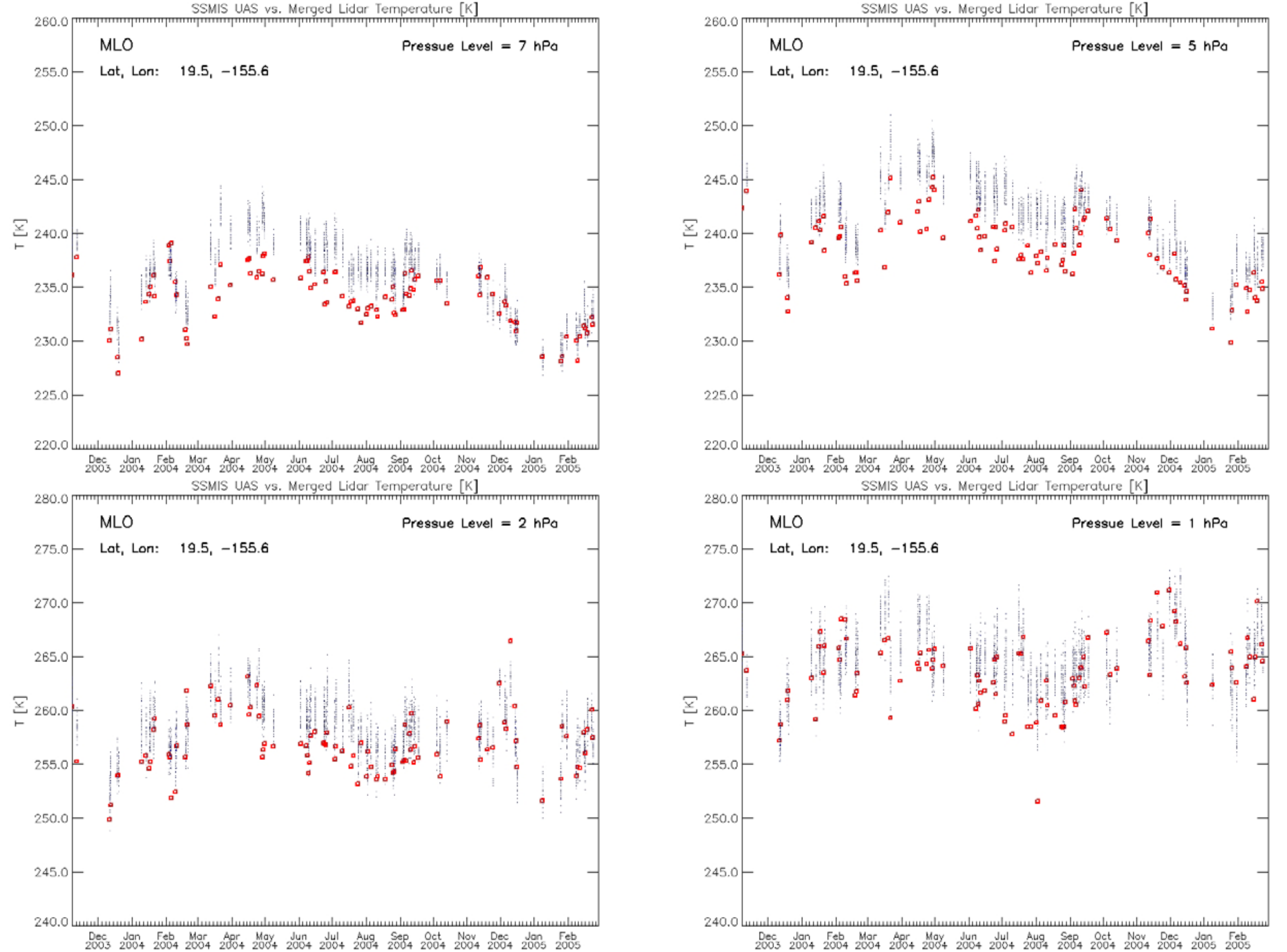

- ❑ **Lidar Observation**

SSMIS Retrieved vs. Lidar Temperatures

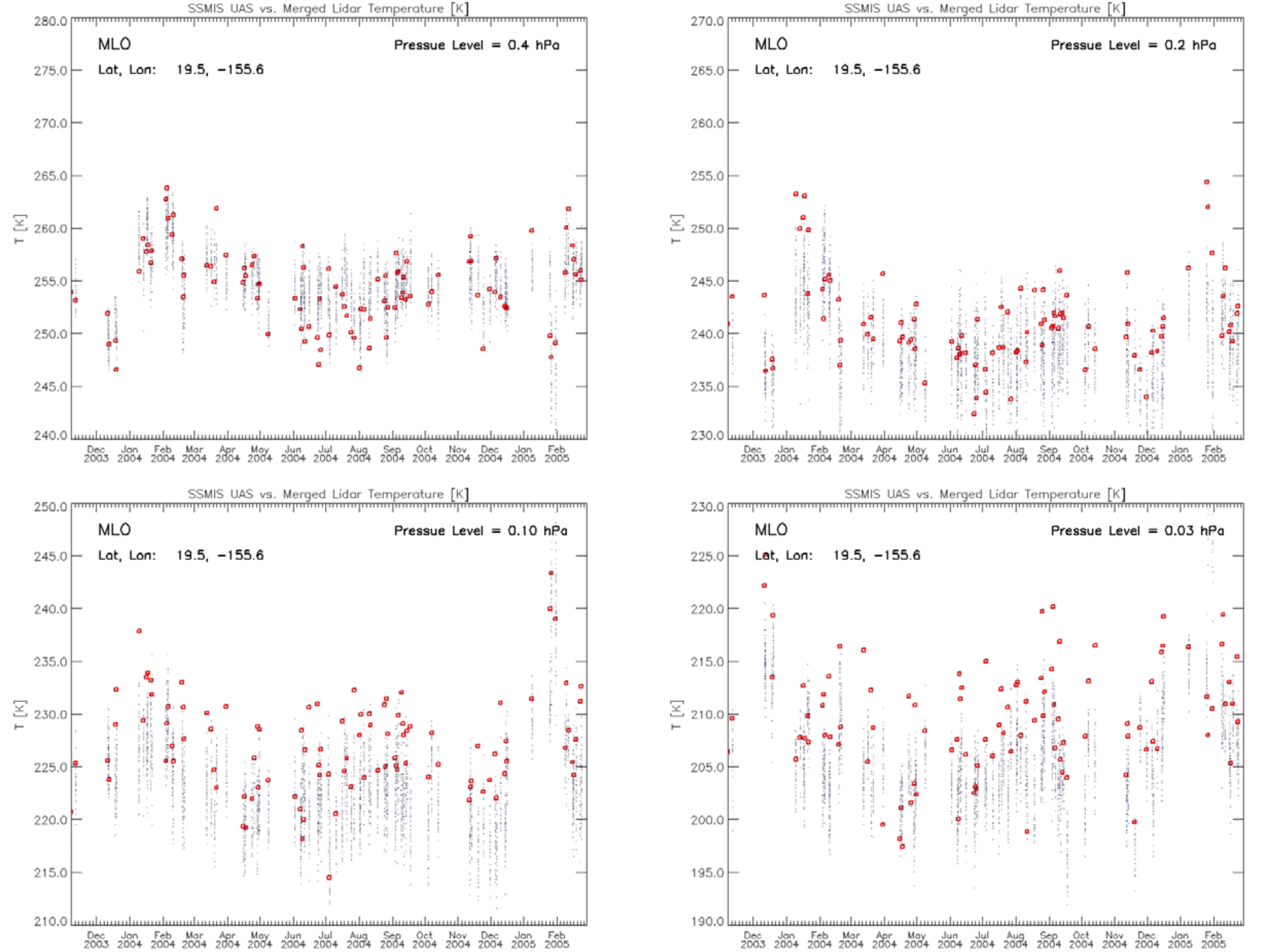

❑ **Lidar Observation**

SSMIS Retrieved-Lidar Temperature

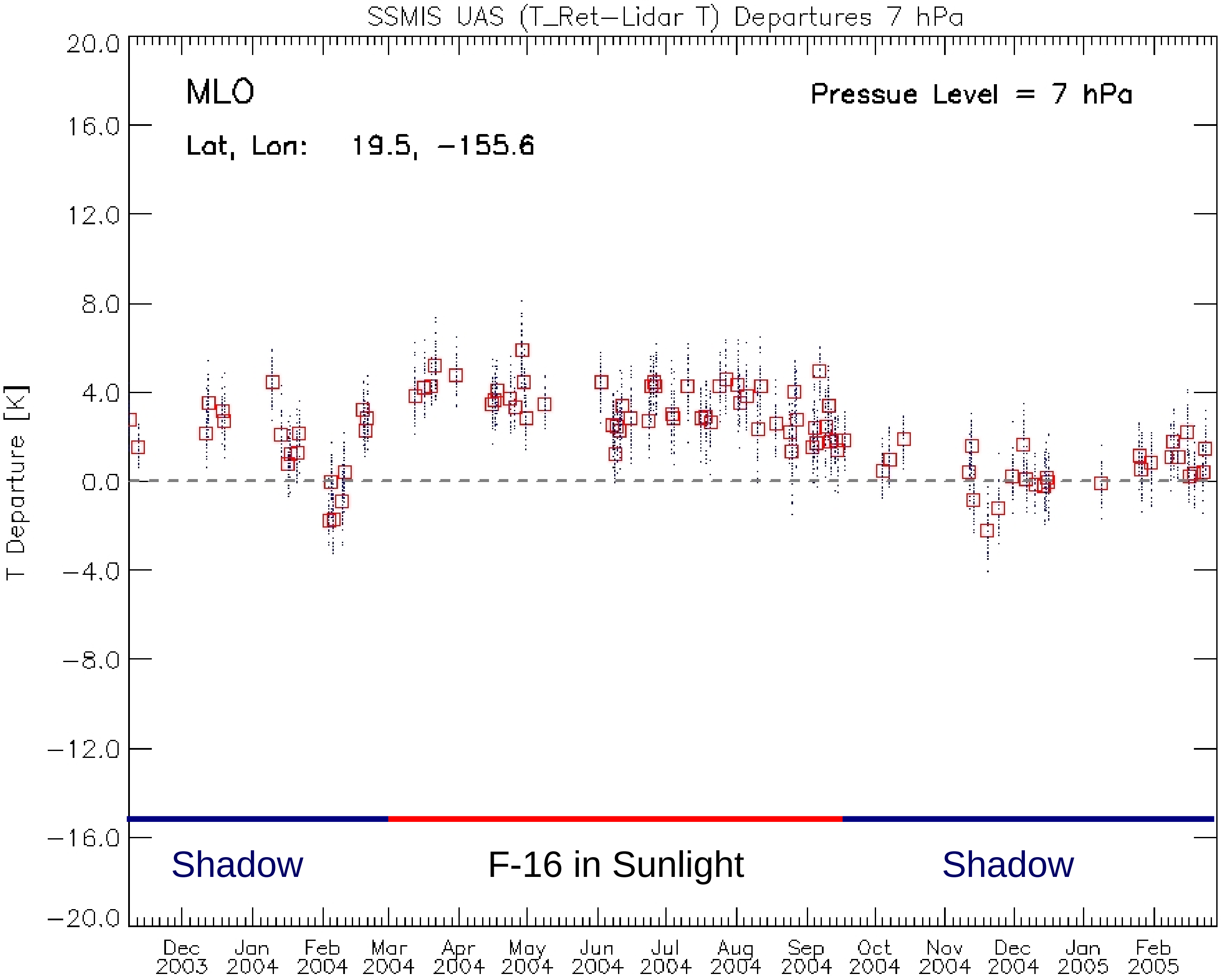

❑ **Mean SSMIS-Lidar T Departure**

SSMIS Retrieved-Lidar Temperature Departures

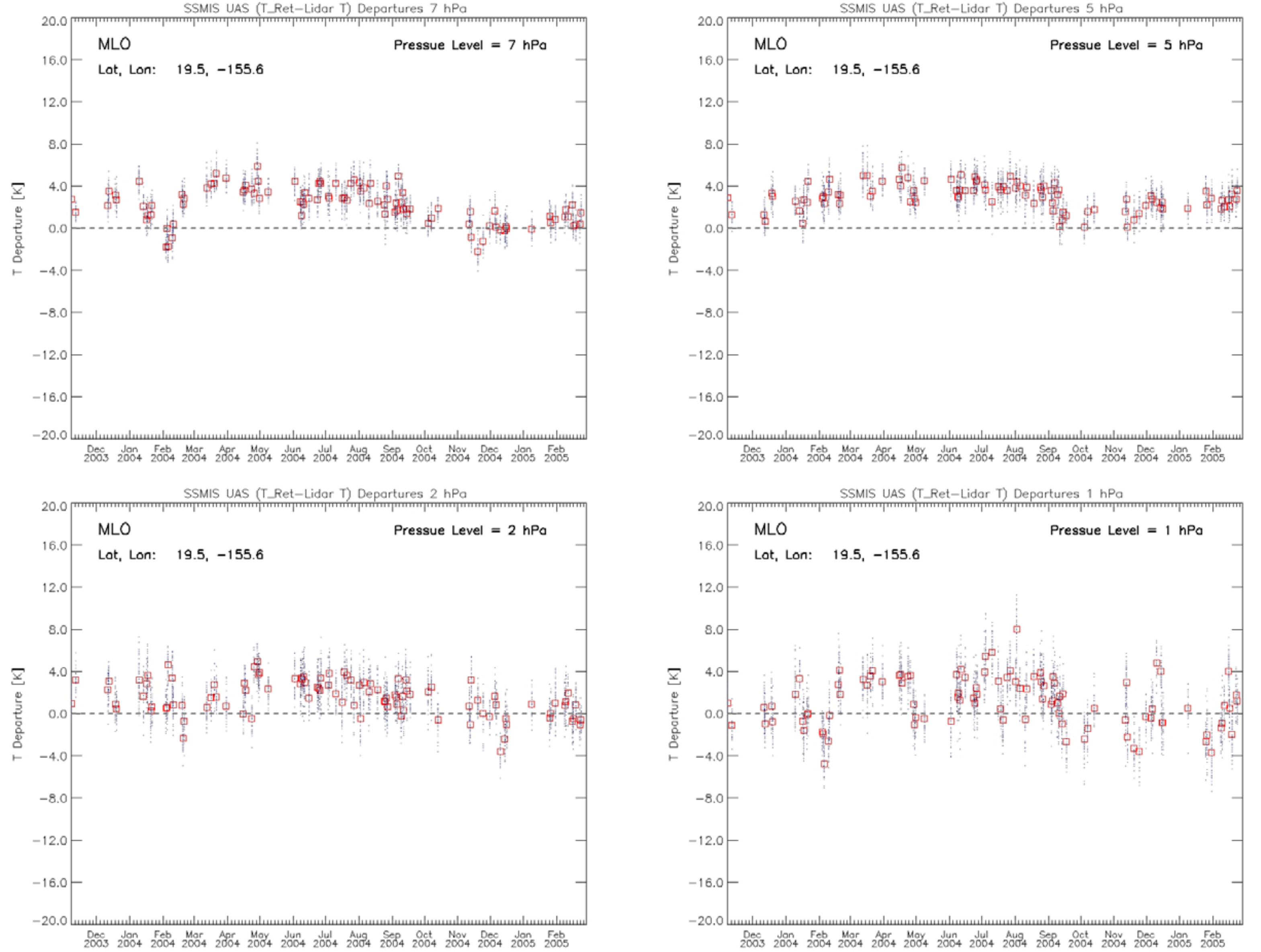

- ❑ **Mean SSMIS-Lidar T Departure**

SSMIS Retrieved-Lidar Temperature Departures

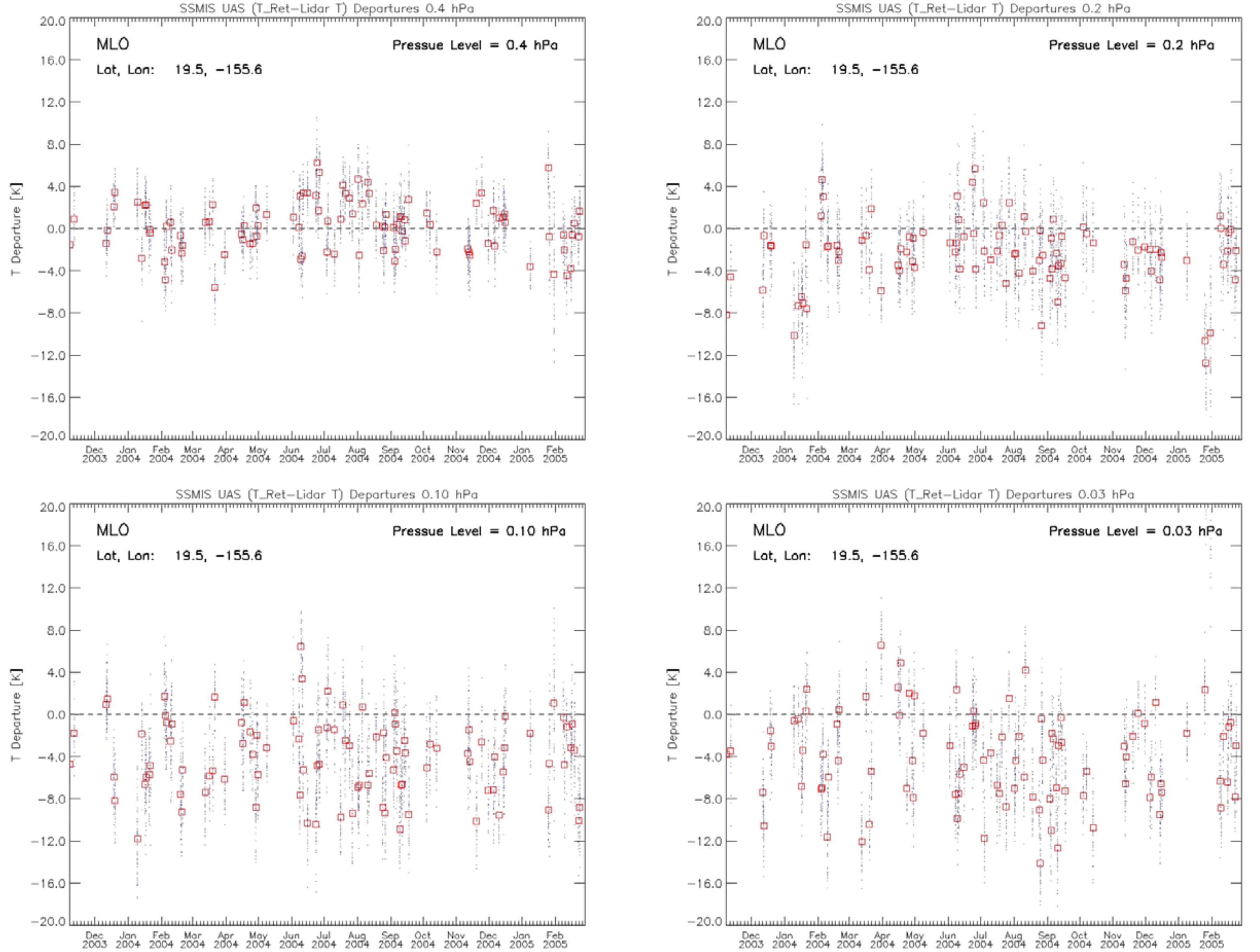

❑ **Mean SSMIS-Lidar T Departure**

Ensemble SSMIS UAS Retrieval-Lidar T Departure Statistics

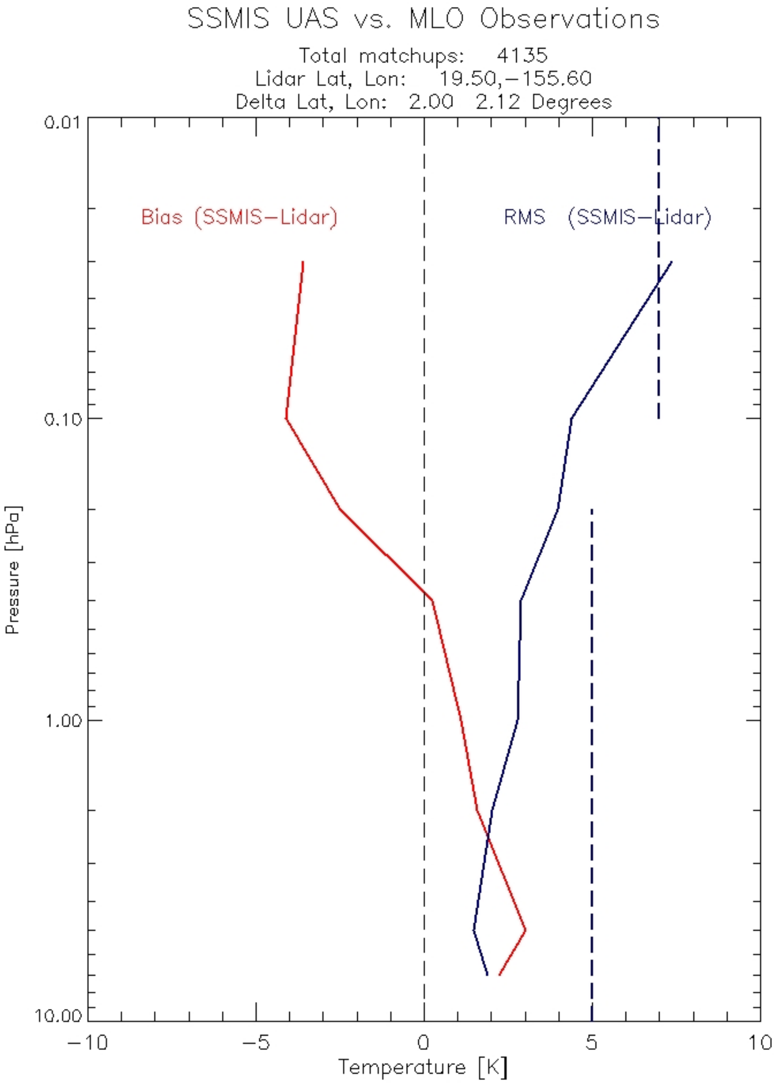

MLO

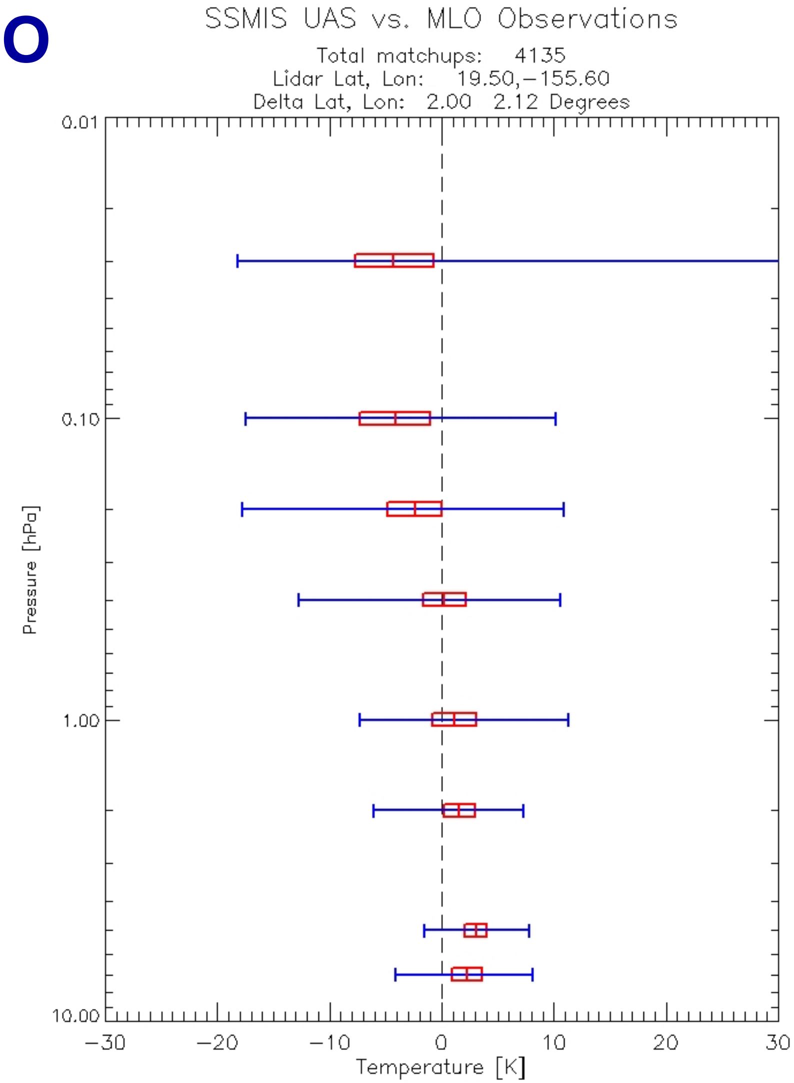

UAS EDR Temperature (SSMIS-Lidar) Analysis

- TMF Lidar Observation EDR Comparison Results
- Results for the 101 Coincident Lidar Observations
- 2.5 Degree Separation Window
- SSMIS EDR Temperature Retrieval

SSMIS Retrieved vs. Lidar Temperatures

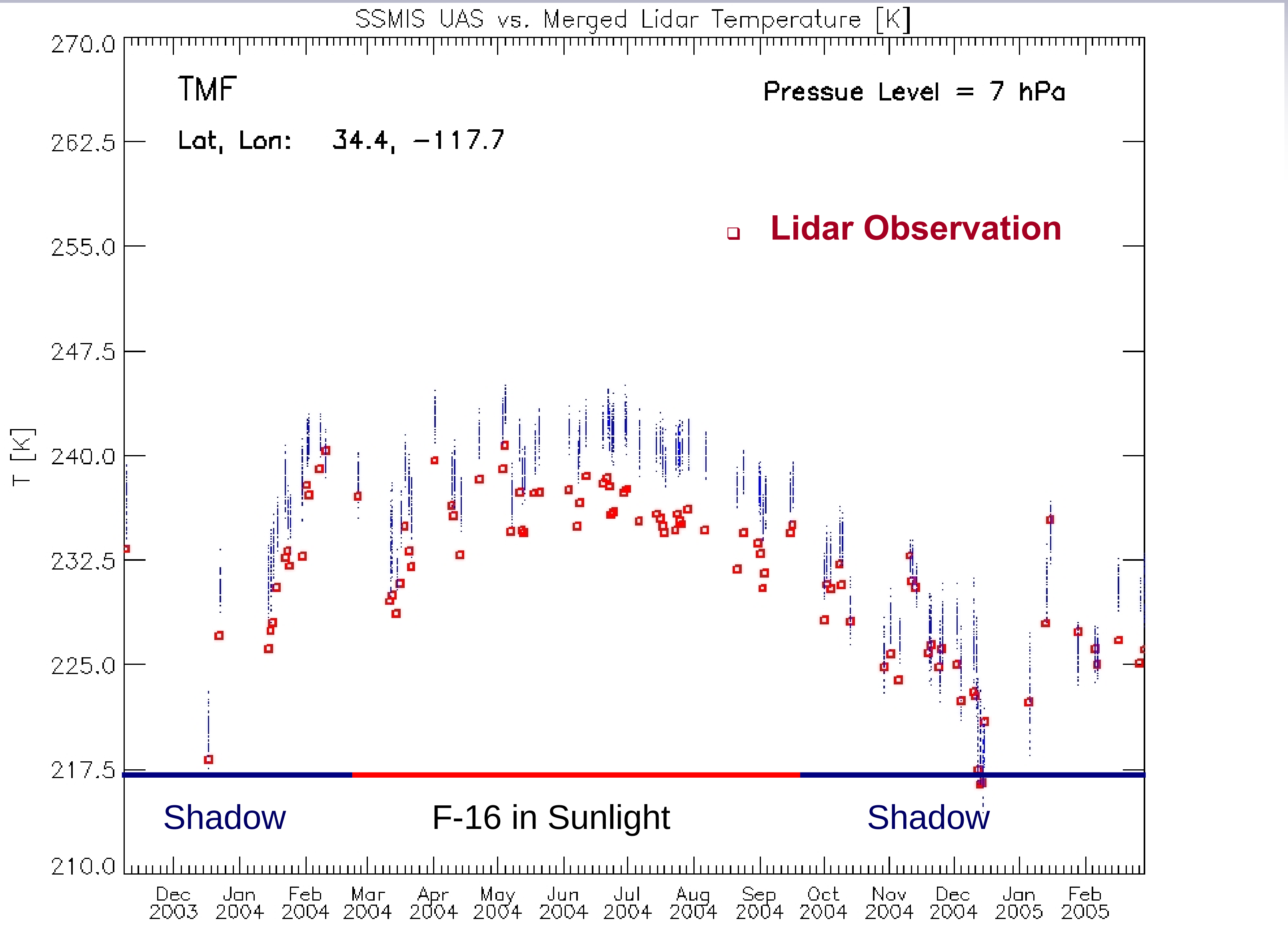

SSMIS Retrieved vs. Lidar Temperatures

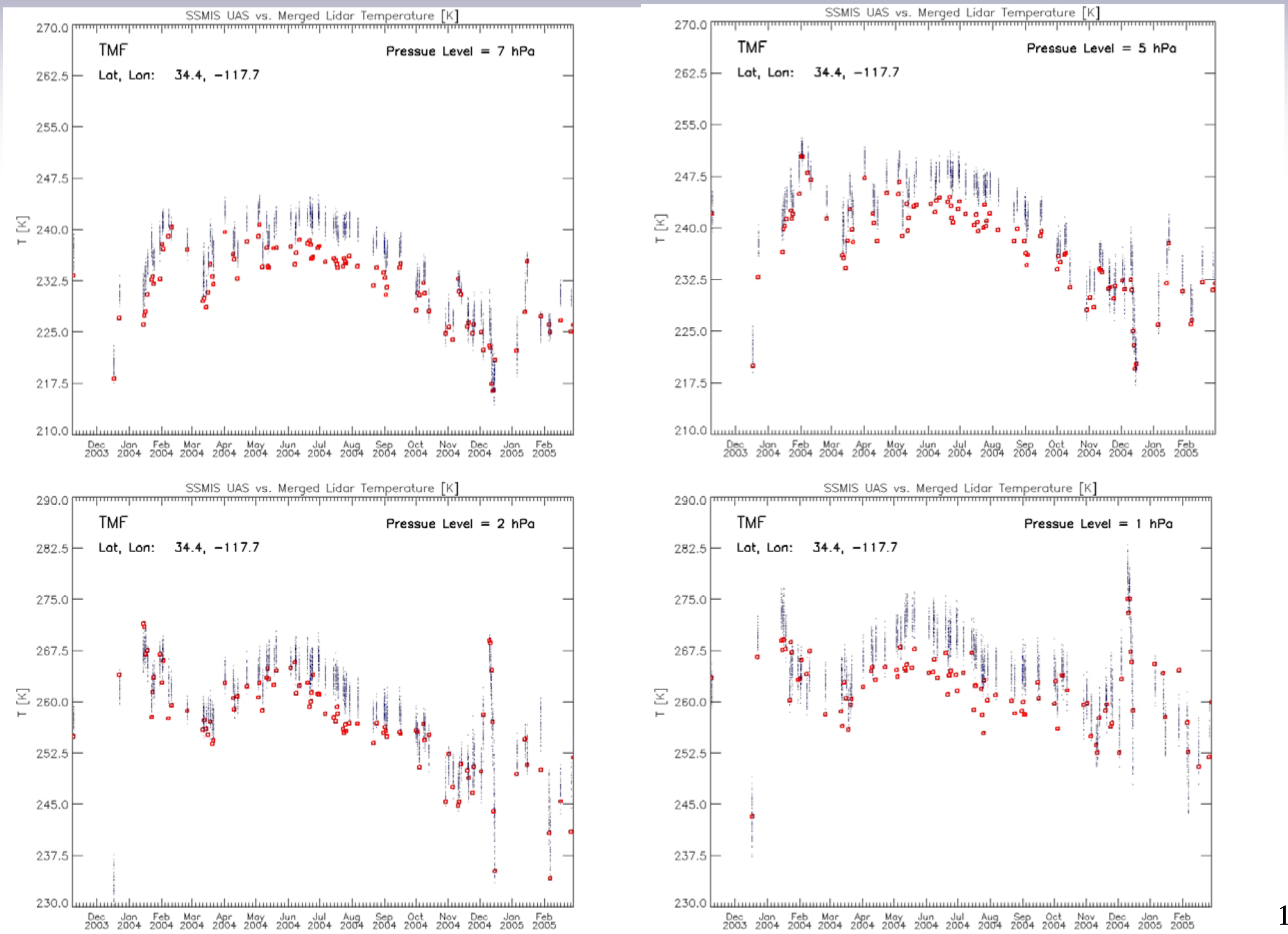

SSMIS Retrieved vs. Lidar Temperatures

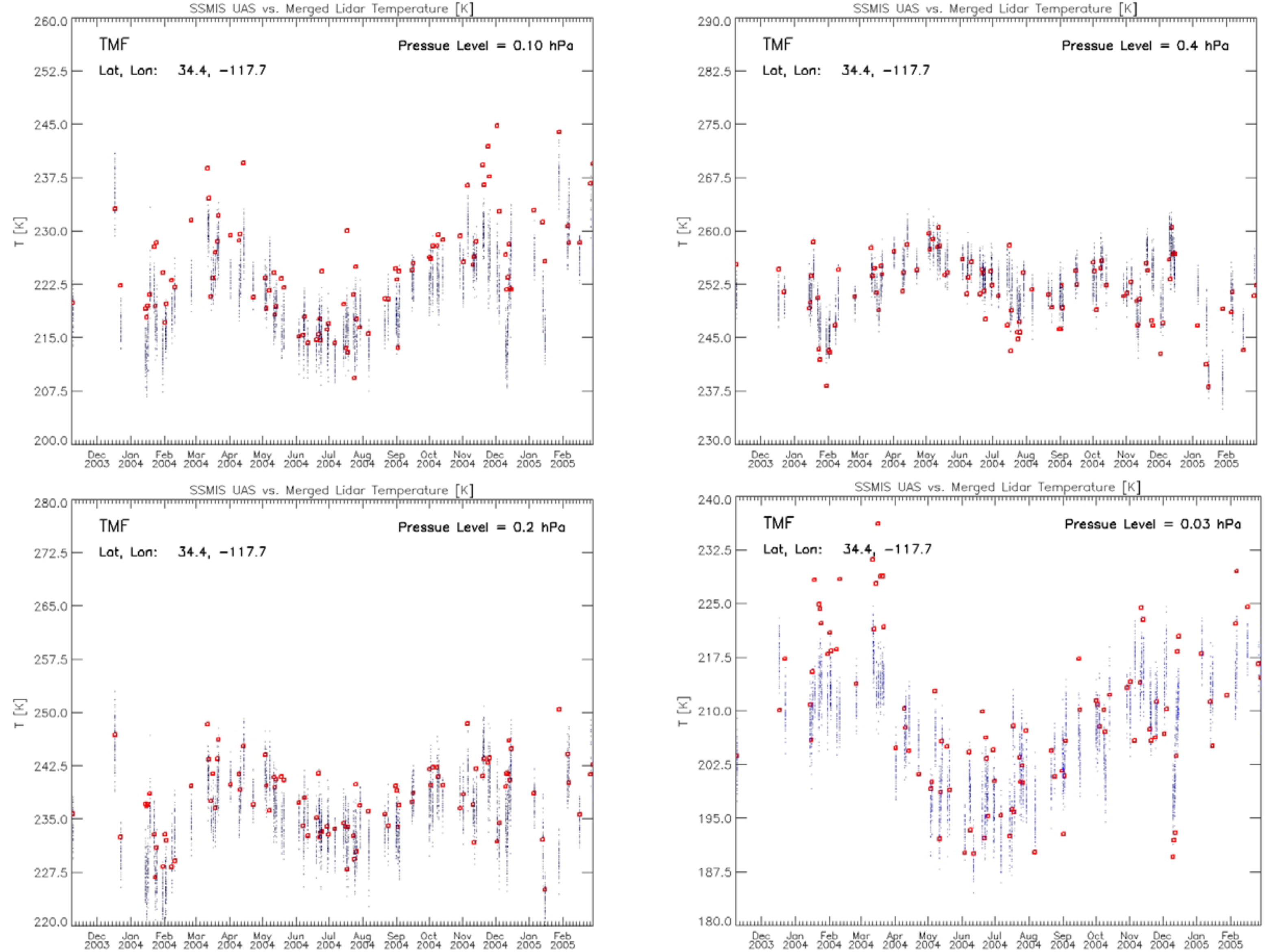

SSMIS Retrieved-Lidar Temperatures

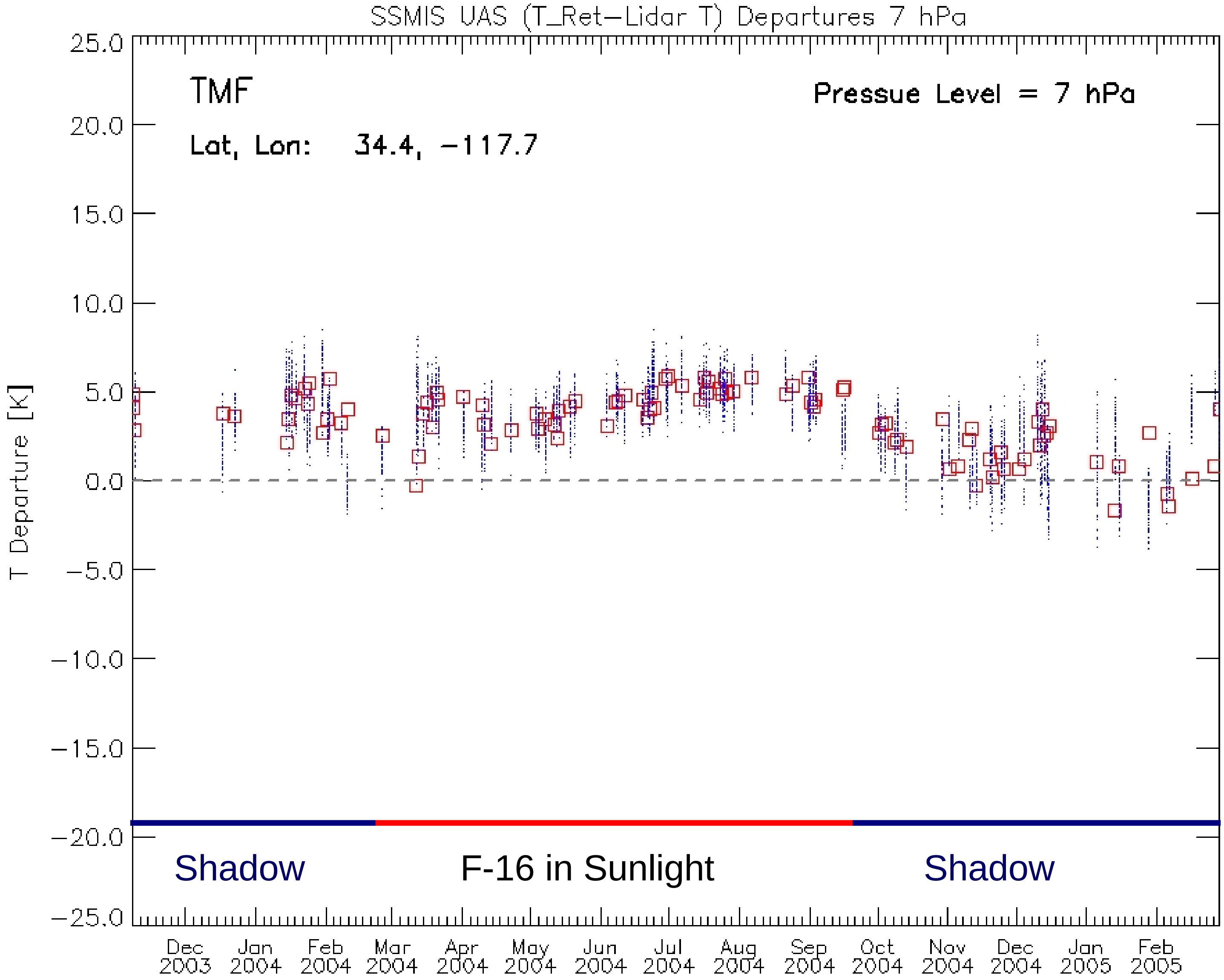

❑ **Mean SSMIS-Lidar T Departure**

SSMIS Retrieved-Lidar Temperature Departures

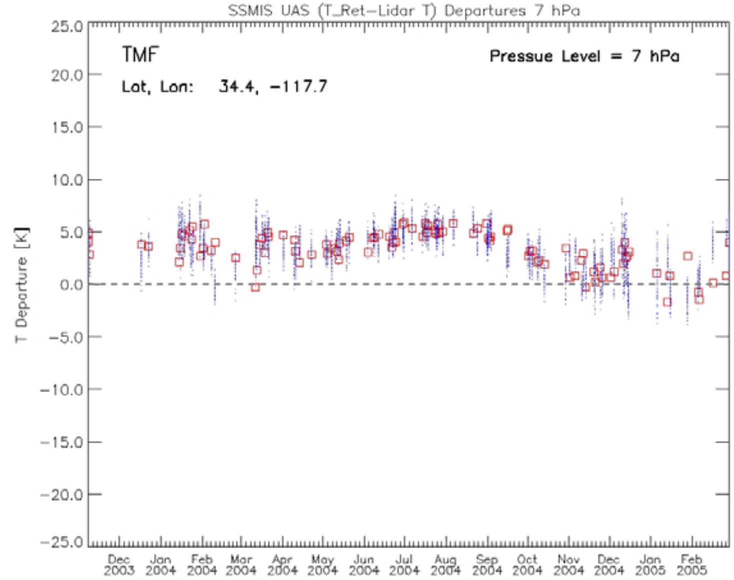

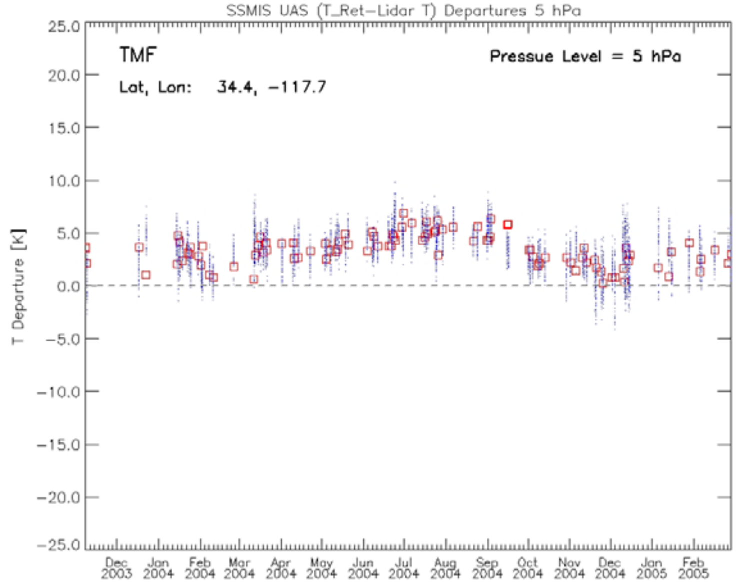

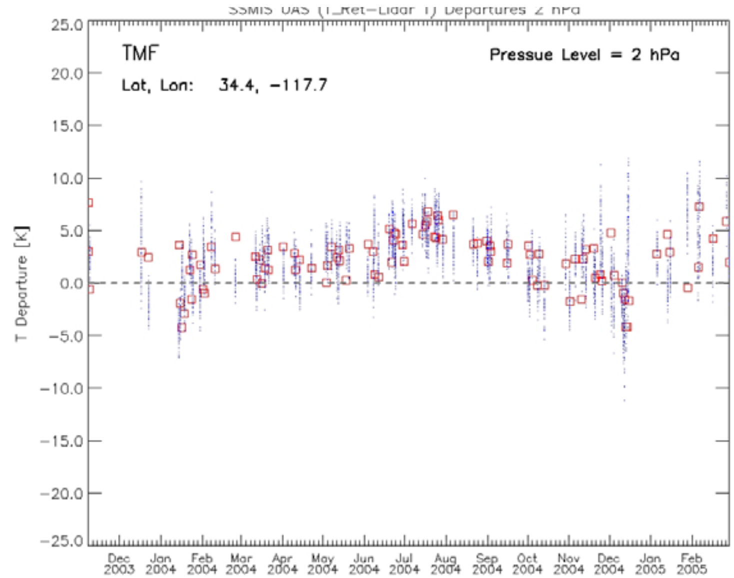

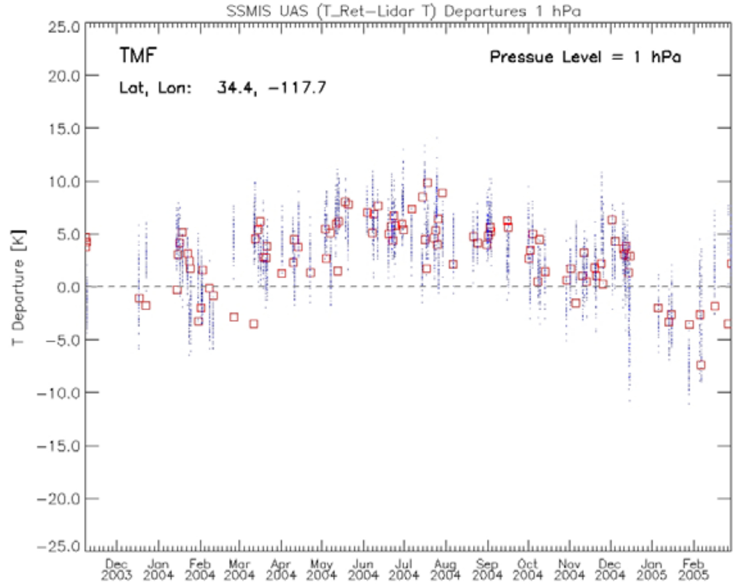

☐ **Mean SSMIS-Lidar T Departure**

SSMIS Retrieved-Lidar Temperature Departures

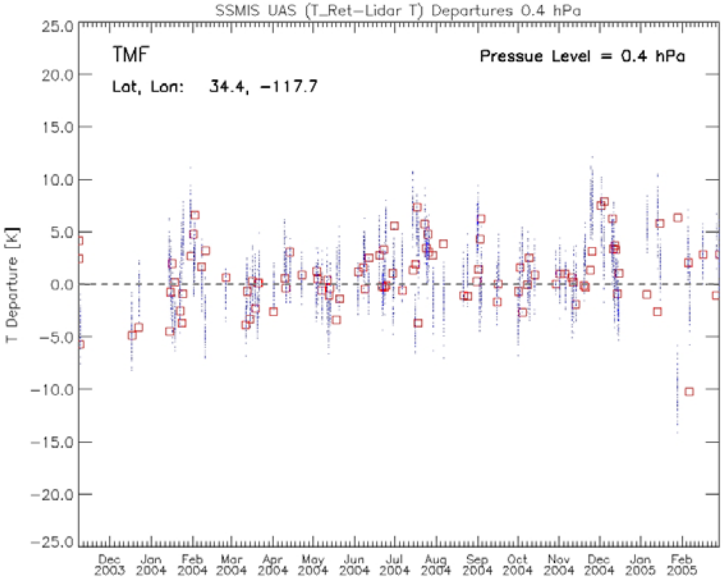

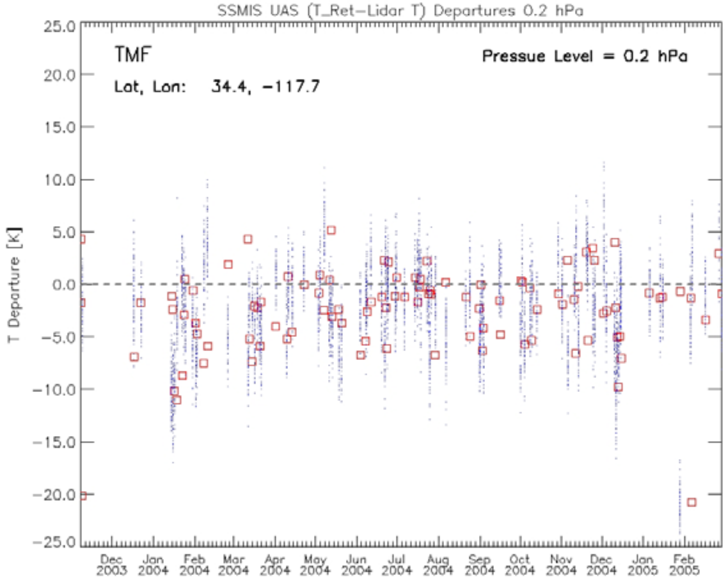

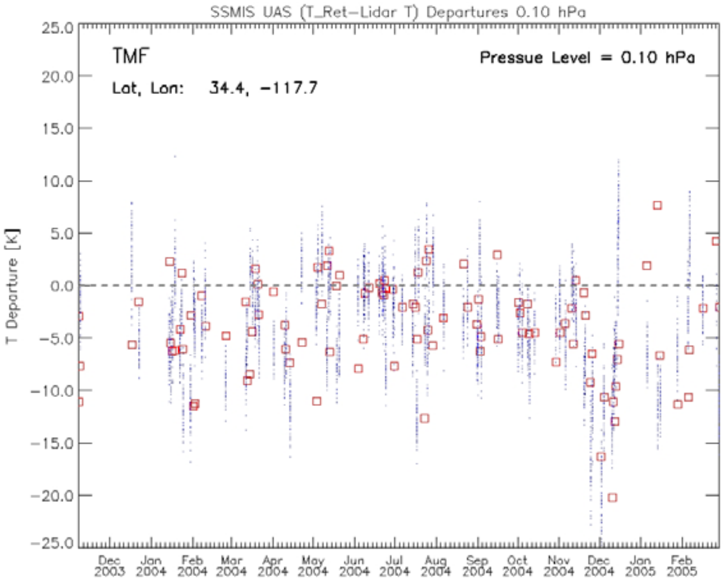

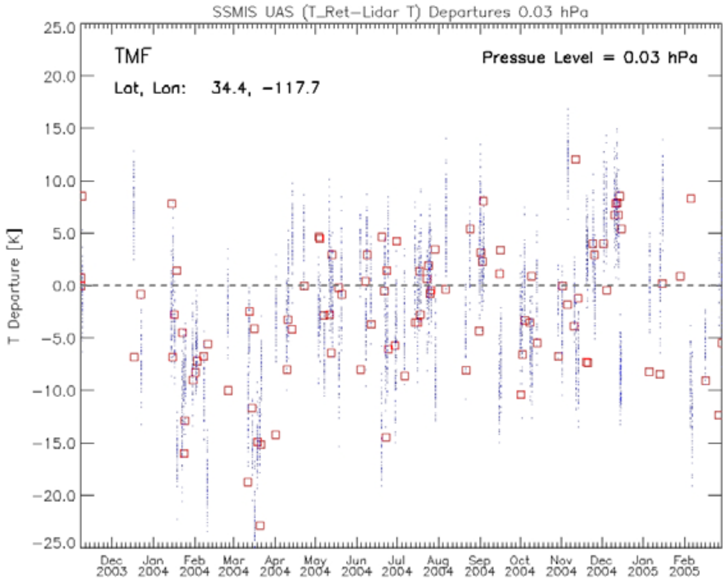

❑ **Mean SSMIS-Lidar T Departure**

Ensemble SSMIS UAS Retrieval-Lidar T Departure Statistics

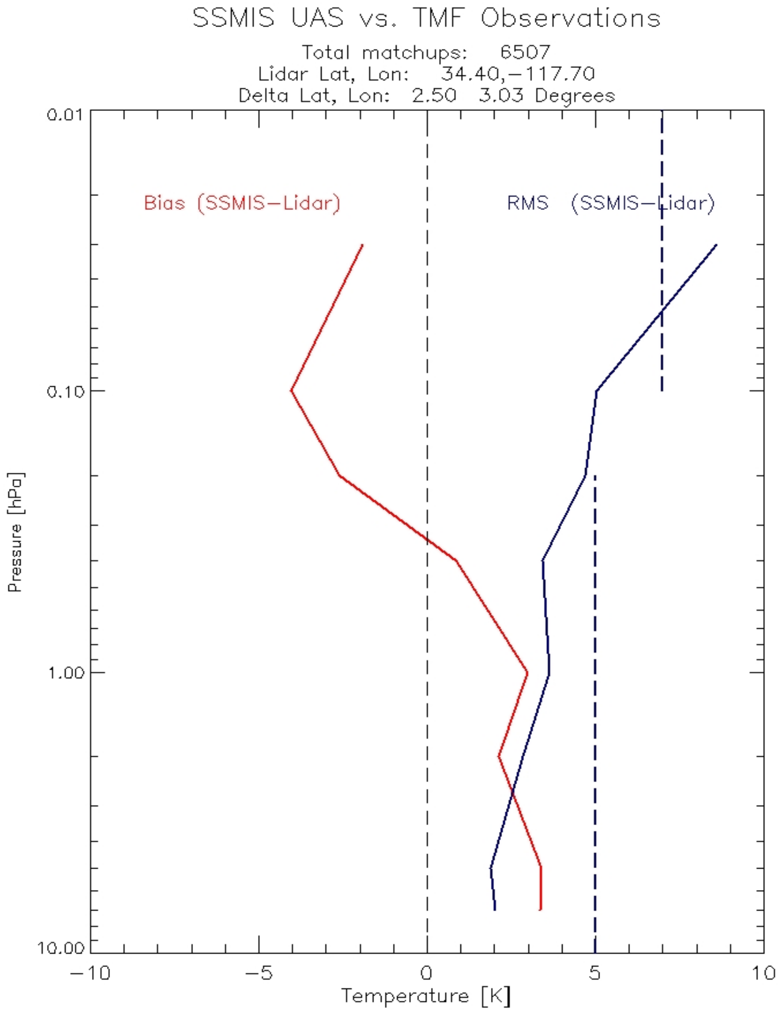

TMF

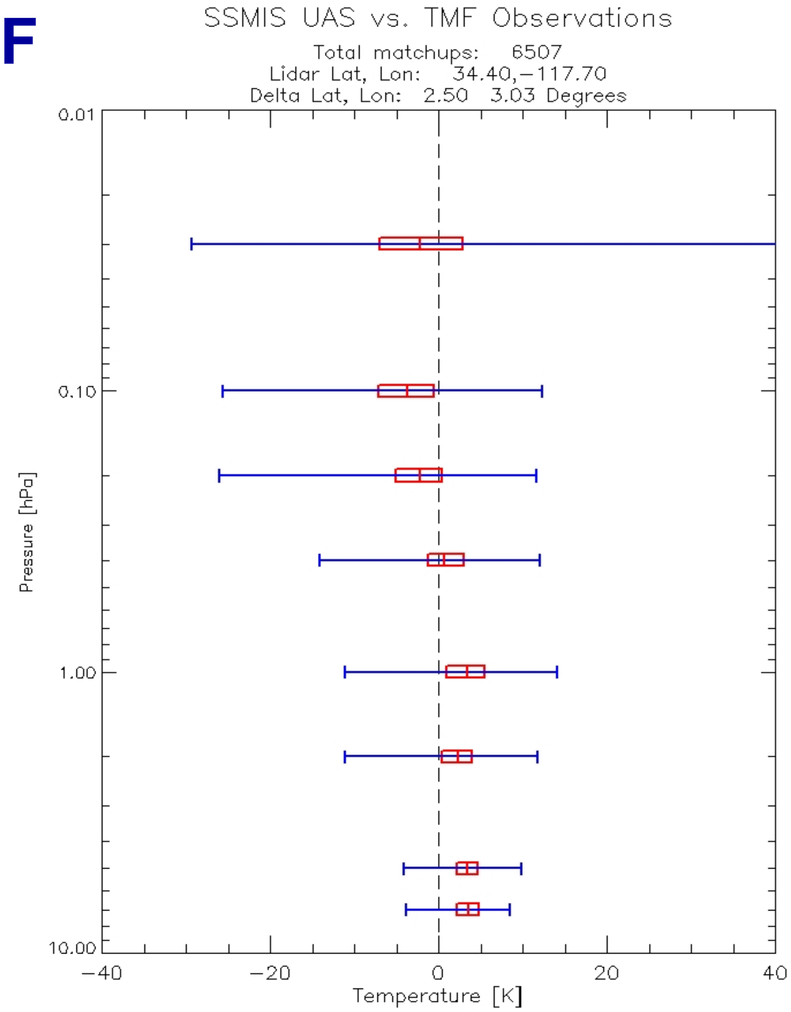

SSMIS Retrieval vs. Lidar Results

- SSMIS Tracks Seasonal Variation in Temperatures
- EDRs Exhibit Reflector Emission Bias

Analysis Methodology

- **SDR Calibration (OB-RTM)**
- **EDR Validation (Retrieval-Lidar)**
- **EDR Validation (Retrieval-NWP)**

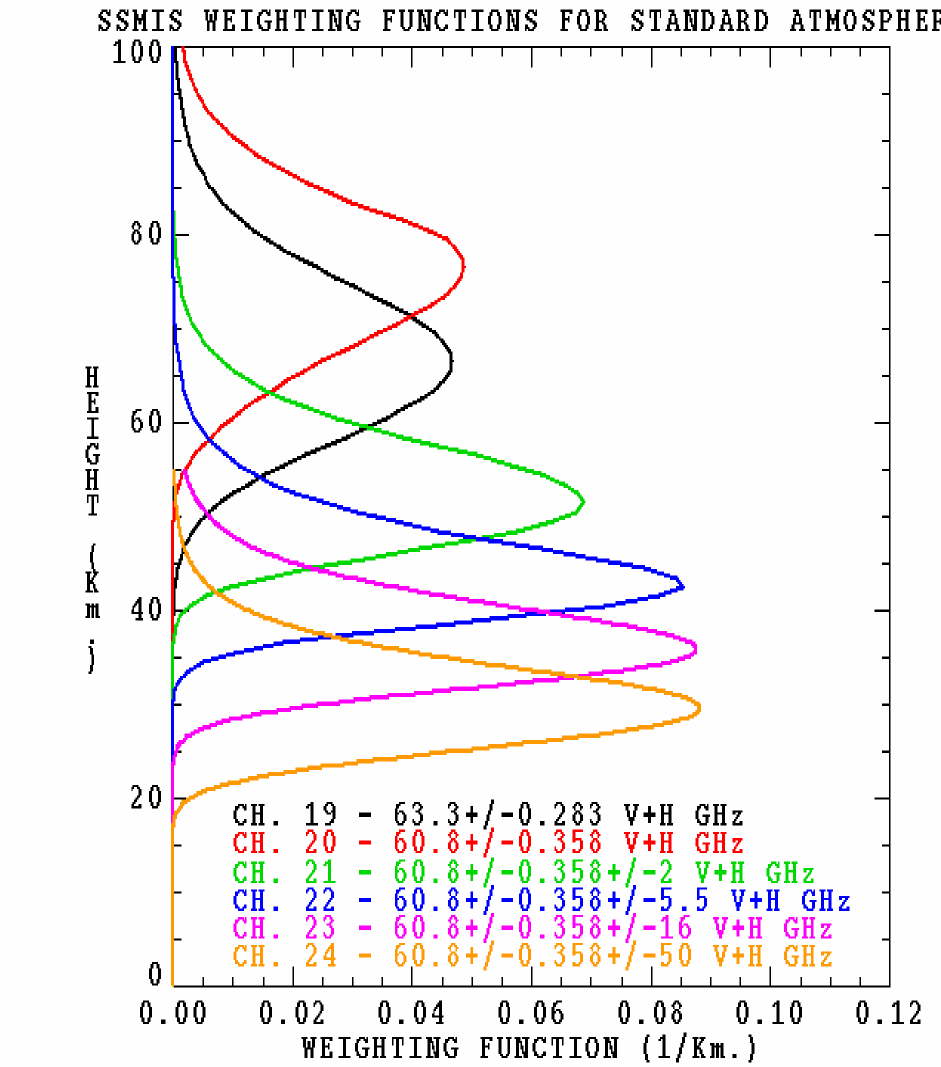

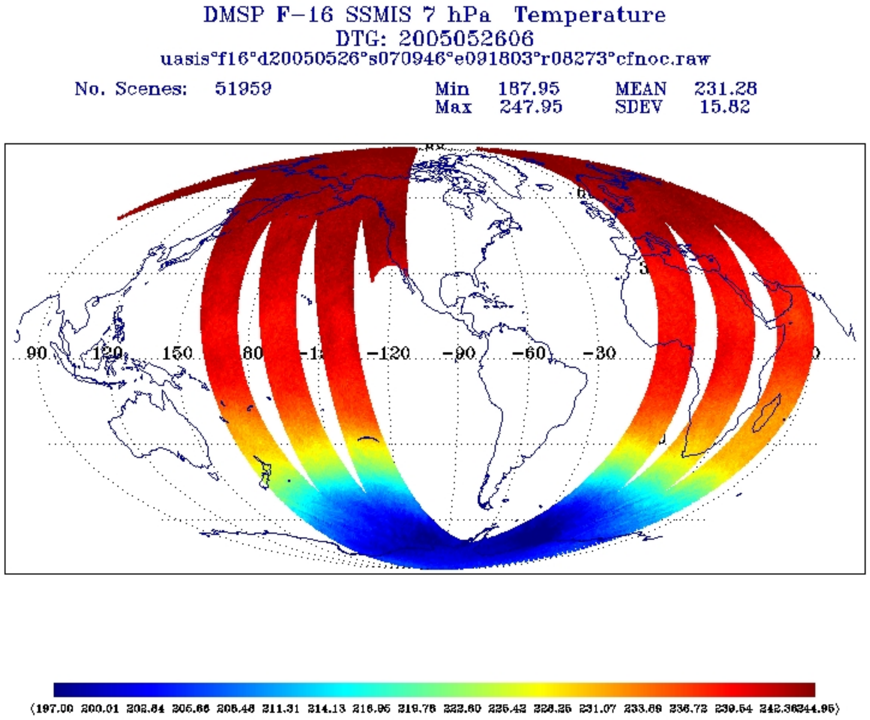

DMSP F−16 SSMIS 7 hPa Temperature
DTG: 2005052606
uasis°f16°d20050526°s070946°e091803°r08273°cfnoc.raw

No. Scenes: 51959
Min 187.95 MEAN 231.28
Max 247.95 SDEV 15.82

SSMIS 7 hPa Temperature

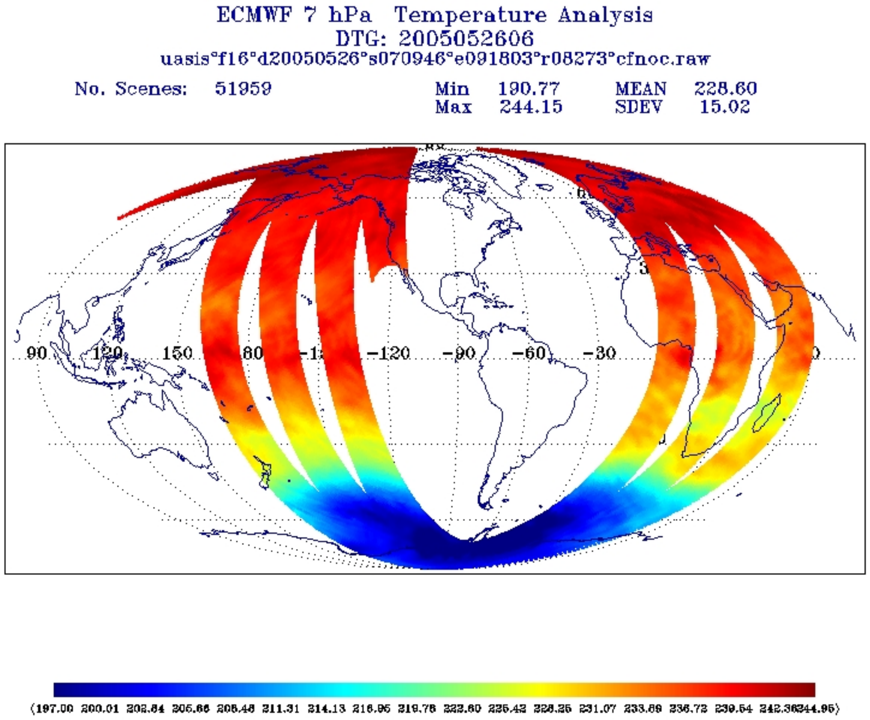

ECMWF 7 hPa Temperature Analysis
DTG: 2005052606
uasis°f16°d20050526°s070946°e091803°r08273°cfnoc.raw

No. Scenes: 51959
Min 190.77 MEAN 228.60
Max 244.15 SDEV 15.02

ECMWF 7 hPa Temperature

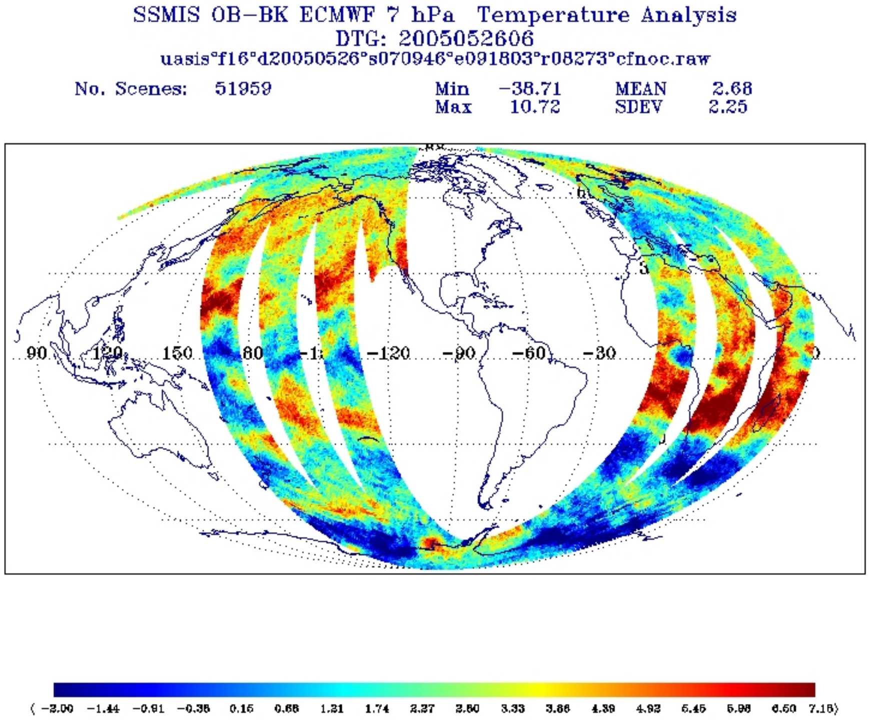

SSMIS - ECMWF 7 hPa Temperature Departure

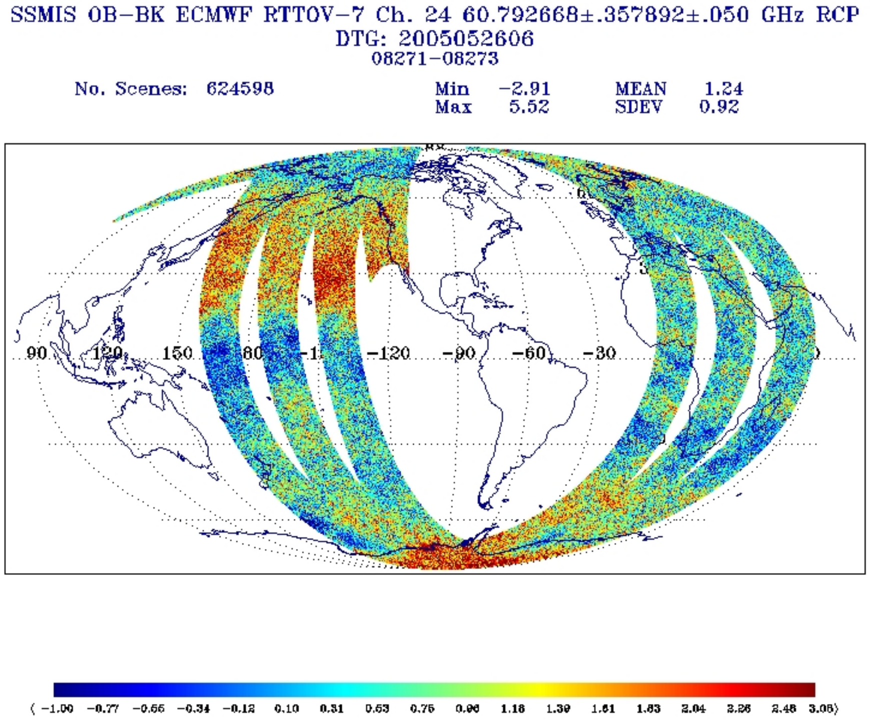

SSMIS Ch 24 – ECMWF RTTOV-7 TB Departure

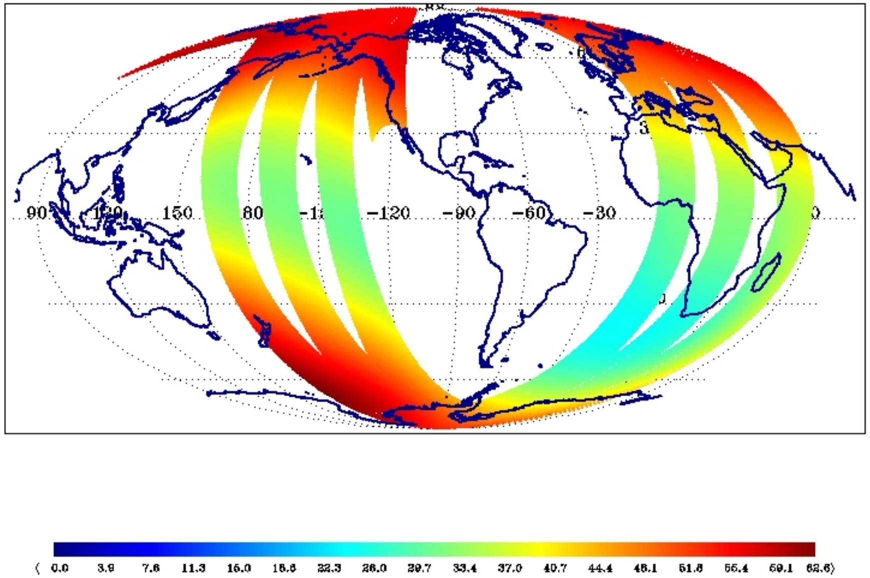

DMSP F−16 SSMIS Geomagnetic FIeld Strength B (60 km)
DTG: 2005052606
08271−08273

No. Scenes: 51989 Min 0.00 MEAN 42.97
Max 62.55 SDEV 10.32

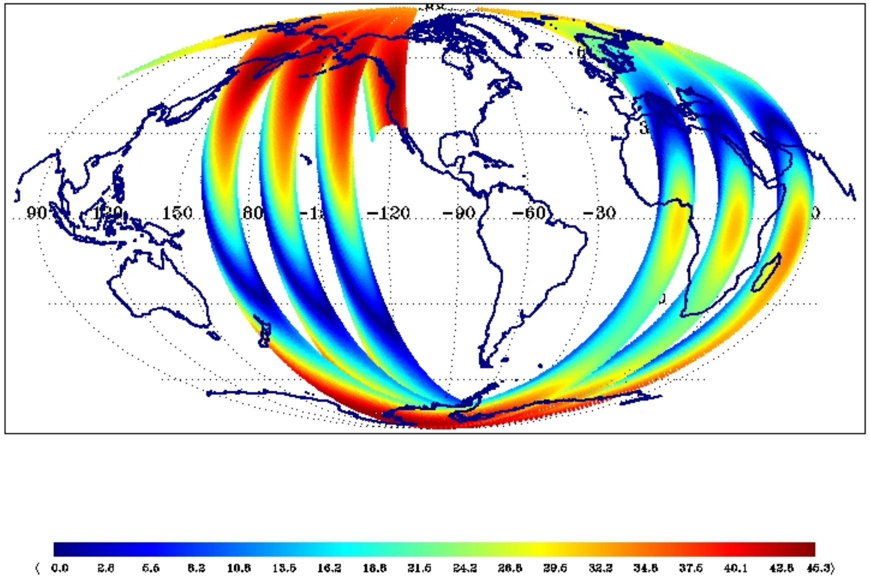

DMSP F−16 SSMIS B·K
DTG: 2005052606
08271−08273

No. Scenes: 51989 Min 0.00 MEAN 24.09
Max 45.30 SDEV 11.52

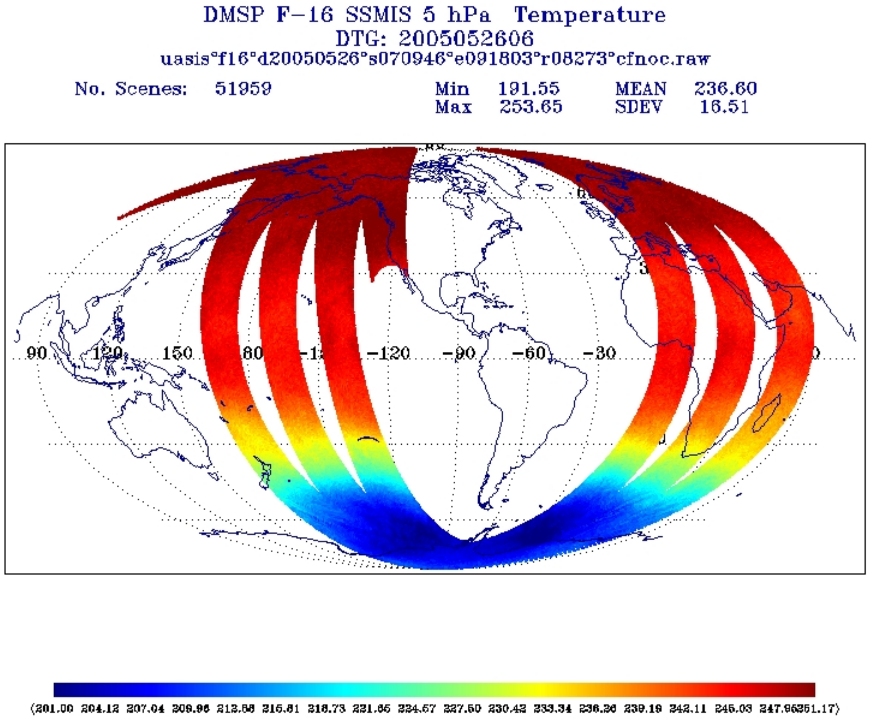

SSMIS 5 hPa Temperature

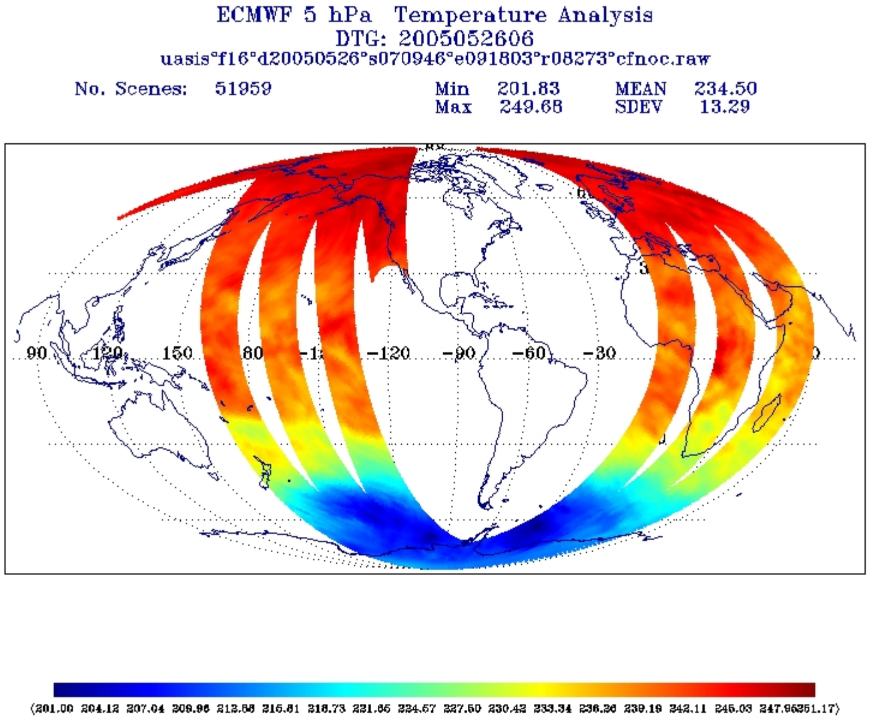

ECMWF 5 hPa Temperature

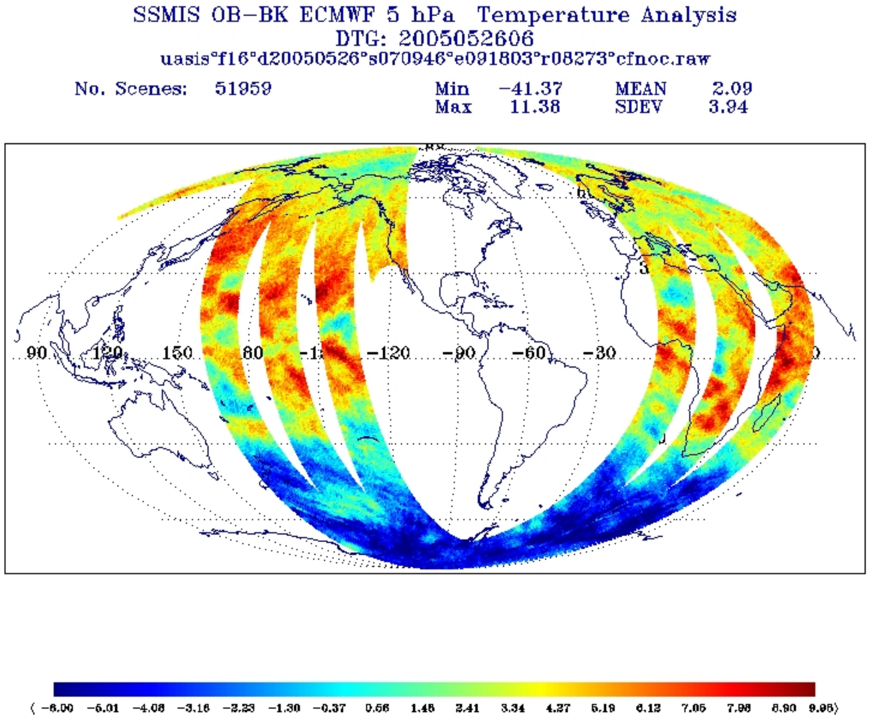

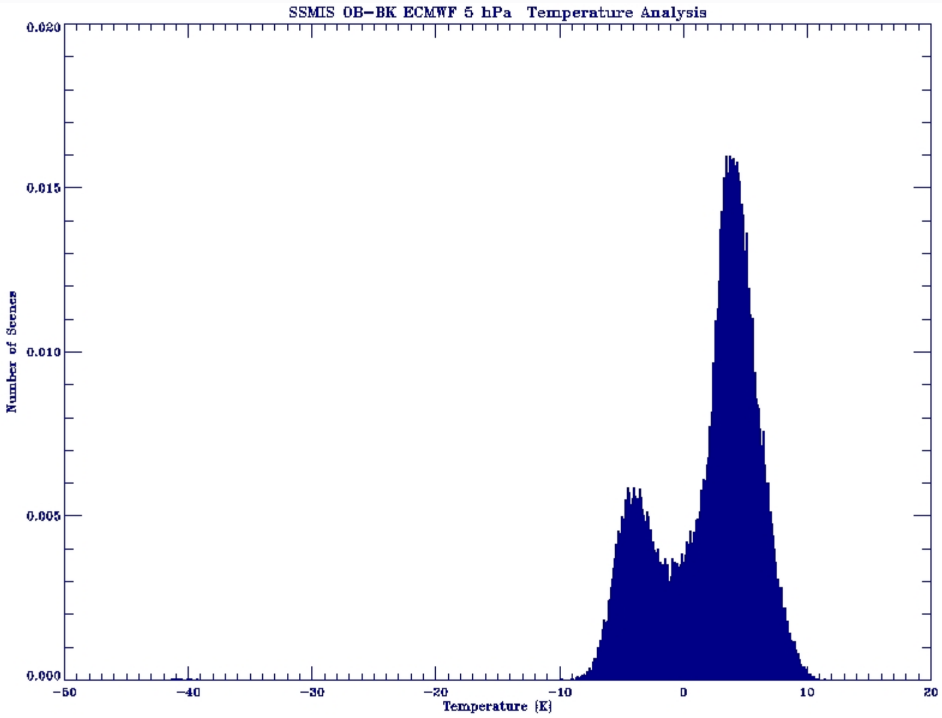

SSMIS - ECMWF 5 hPa Temperature Departure

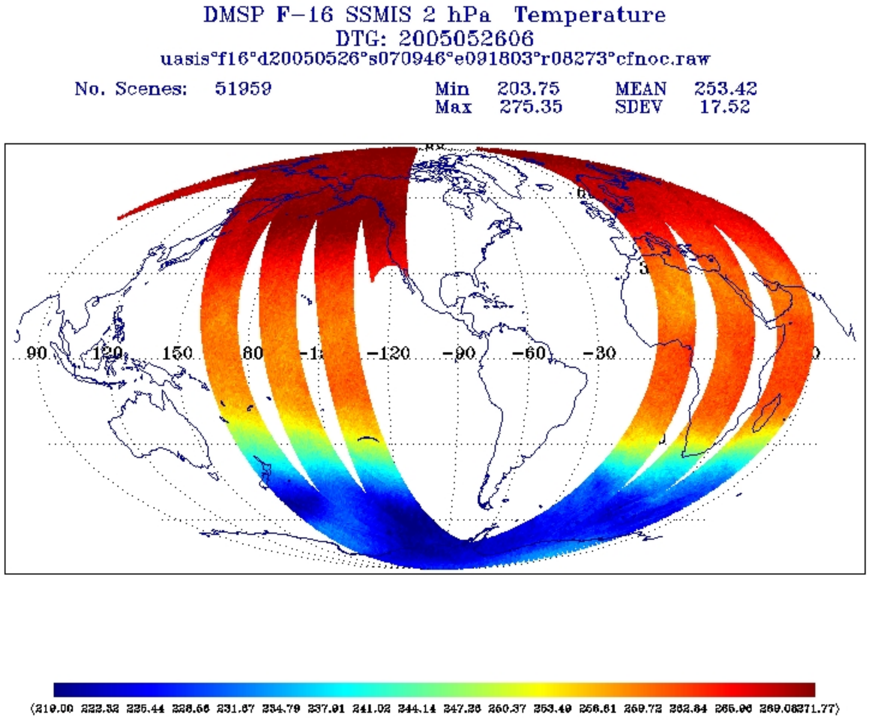

SSMIS 2 hPa Temperature

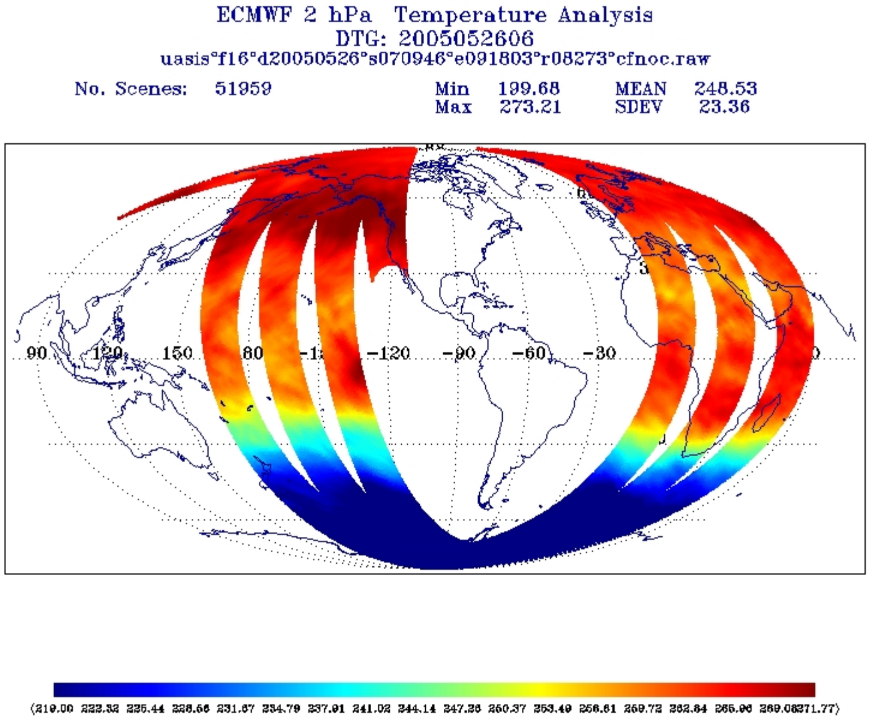

ECMWF 2 hPa Temperature

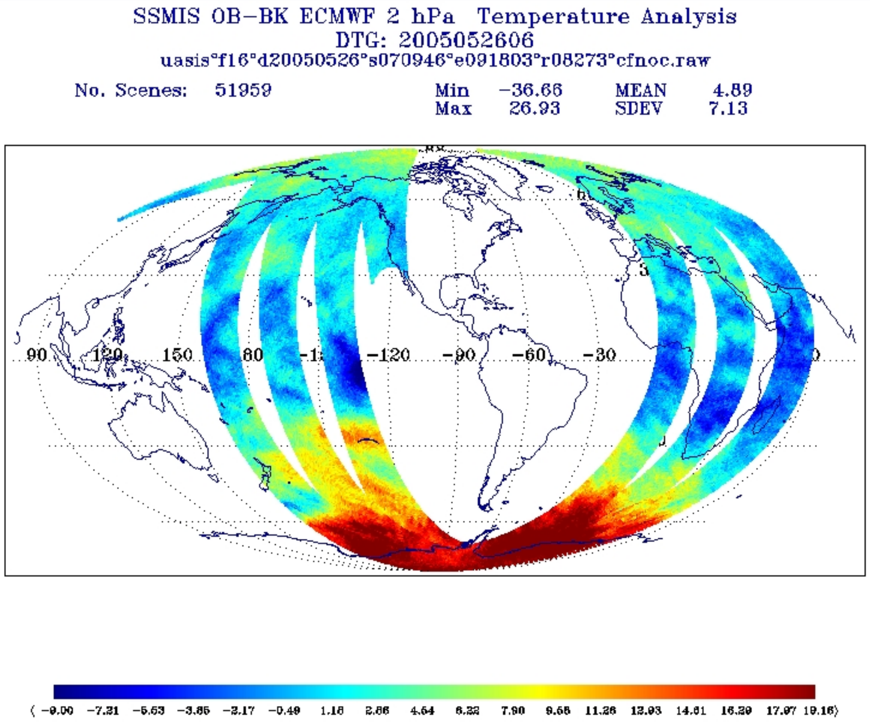

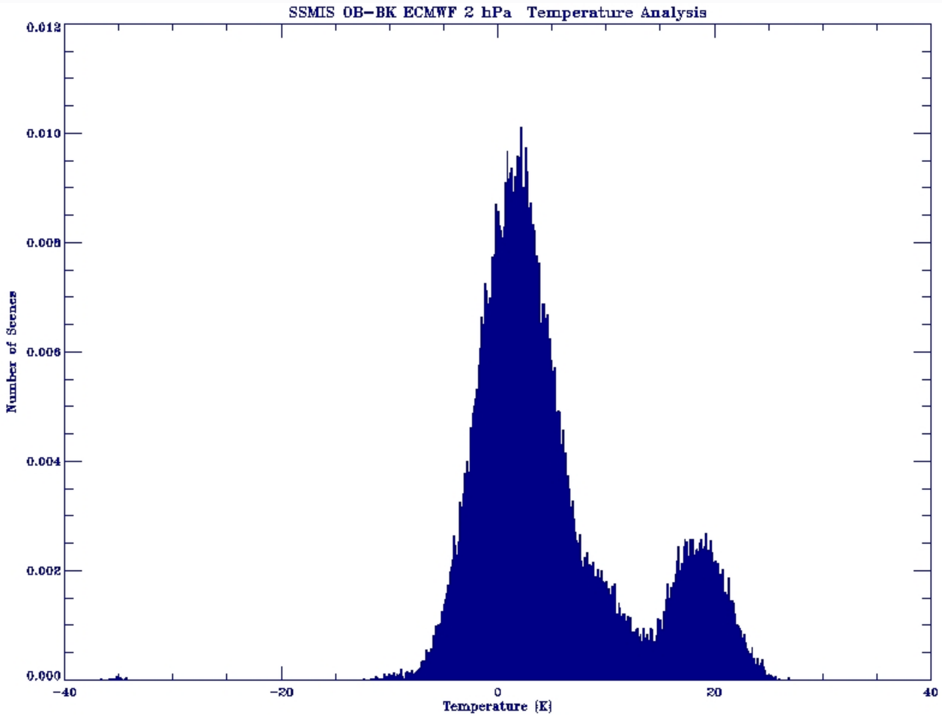

SSMIS - ECMWF 2 hPa Temperature Departure

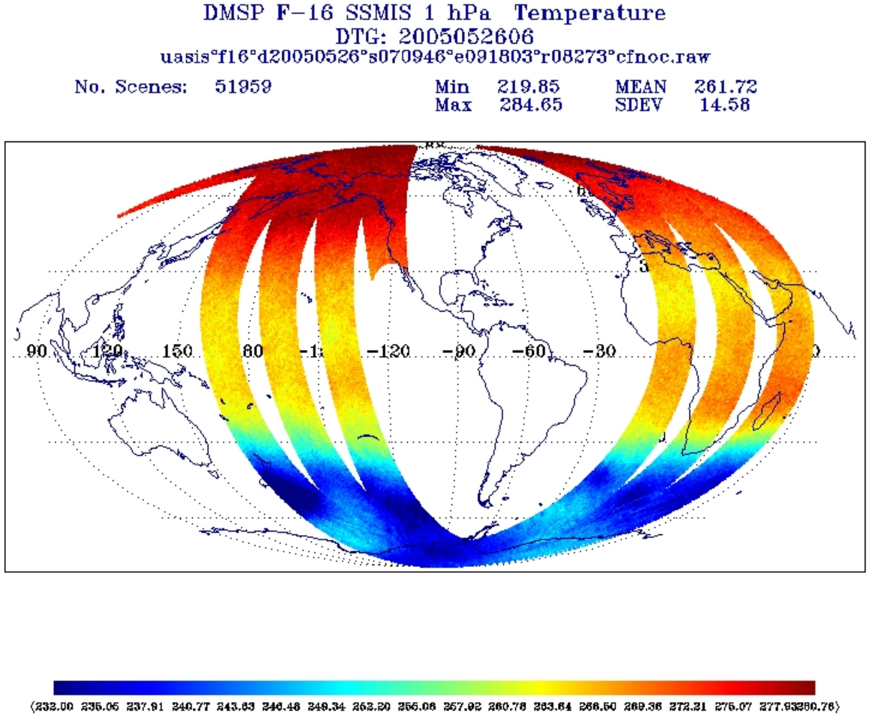

SSMIS 1 hPa Temperature

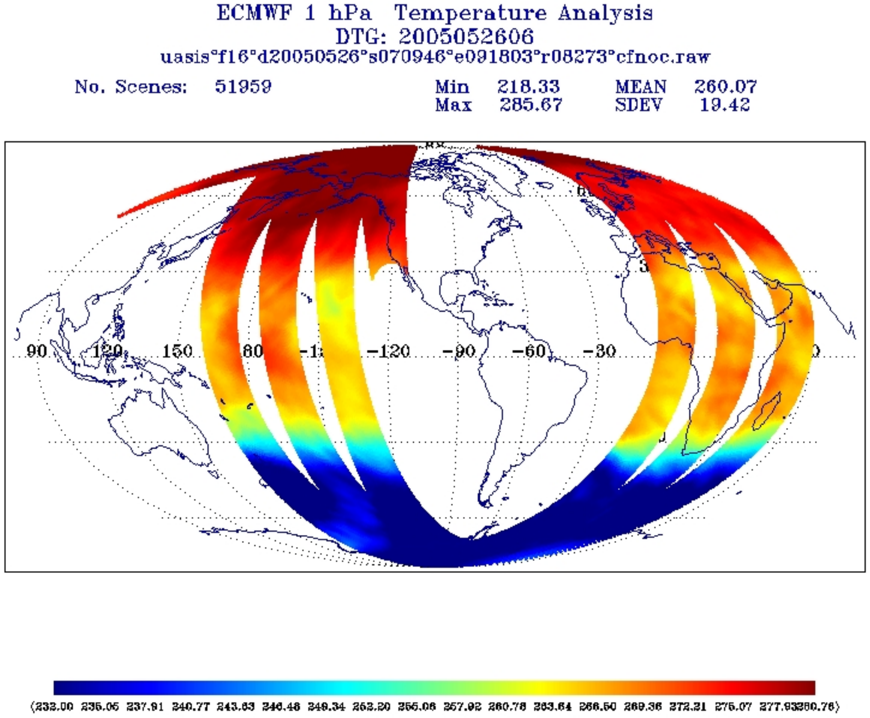

ECMWF 1 hPa Temperature

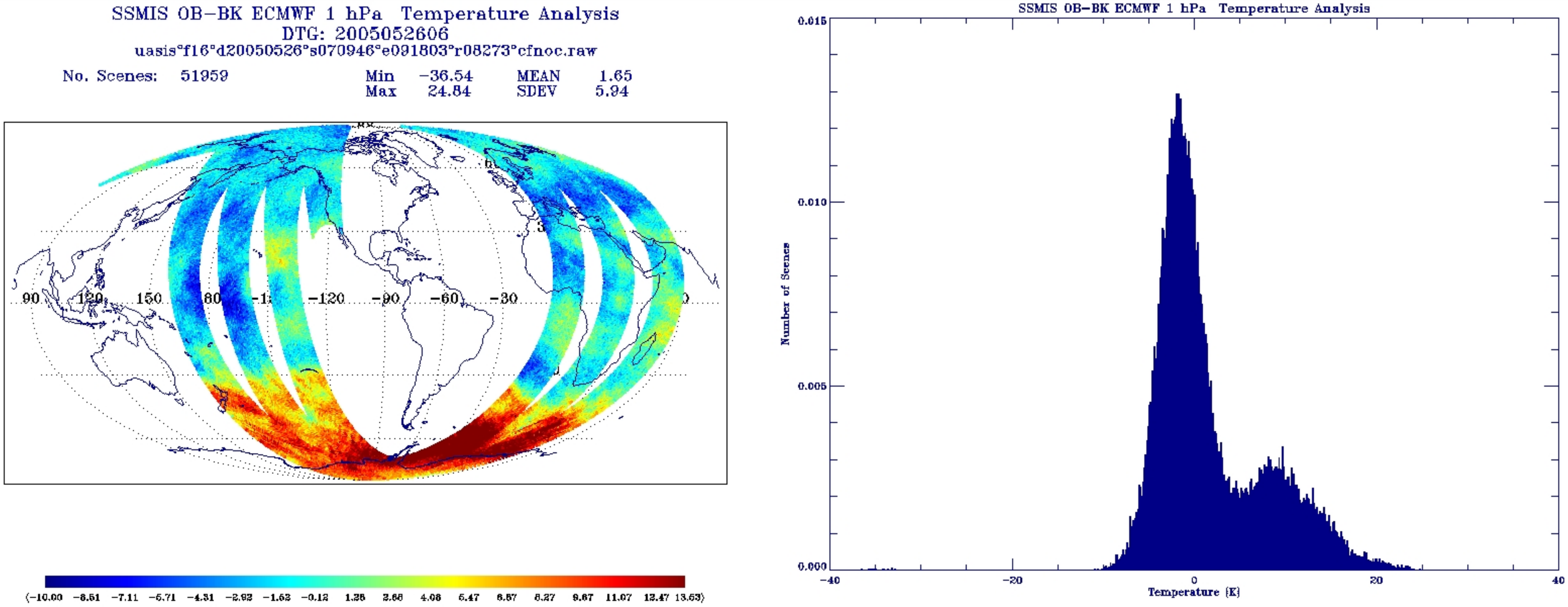

SSMIS - ECMWF 1 hPa Temperature Departure

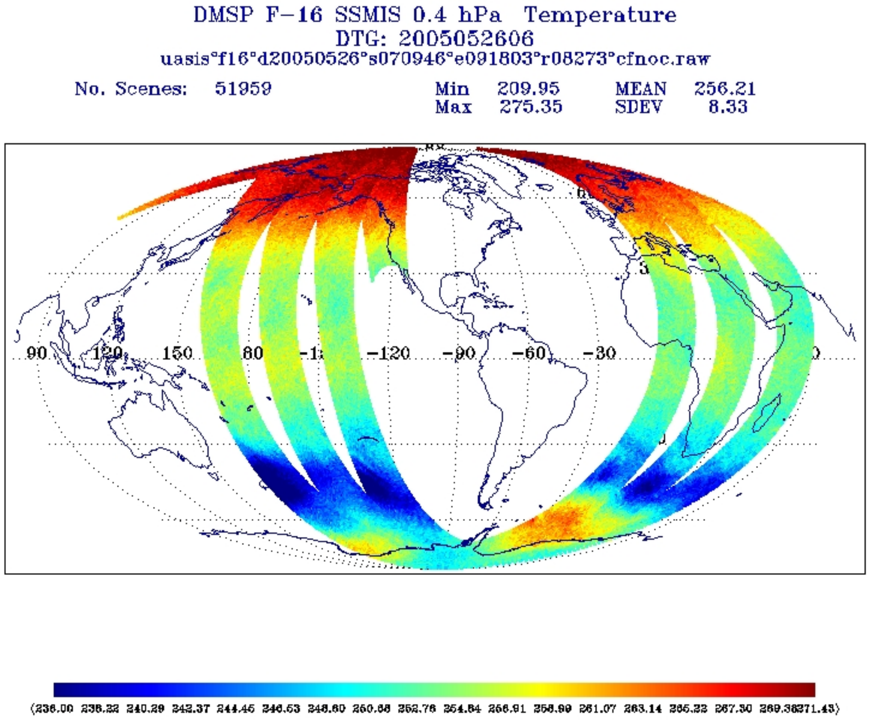

SSMIS 0.4 hPa Temperature

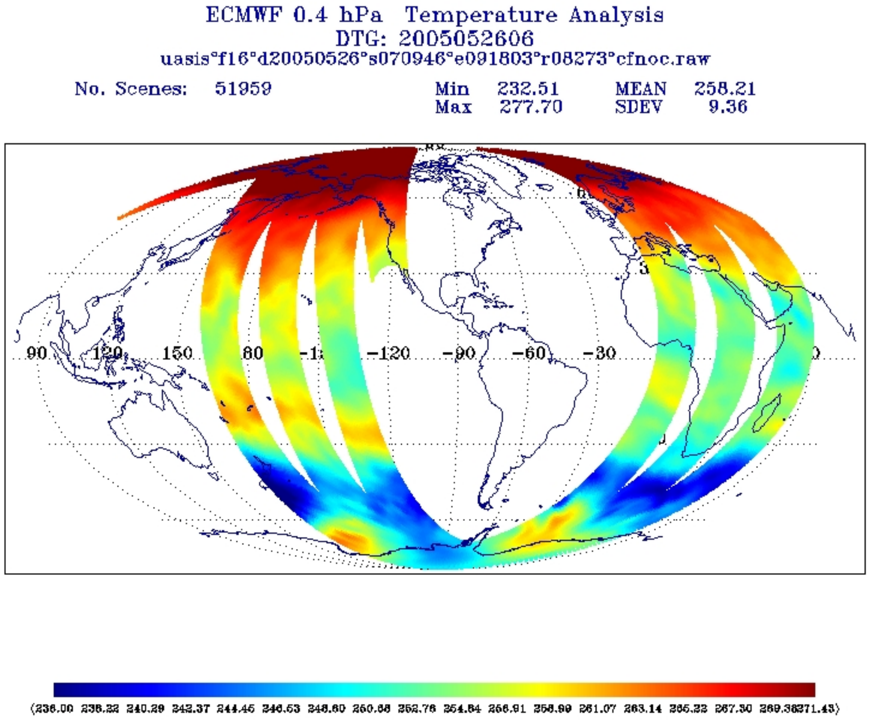

ECMWF 0.4 hPa Temperature

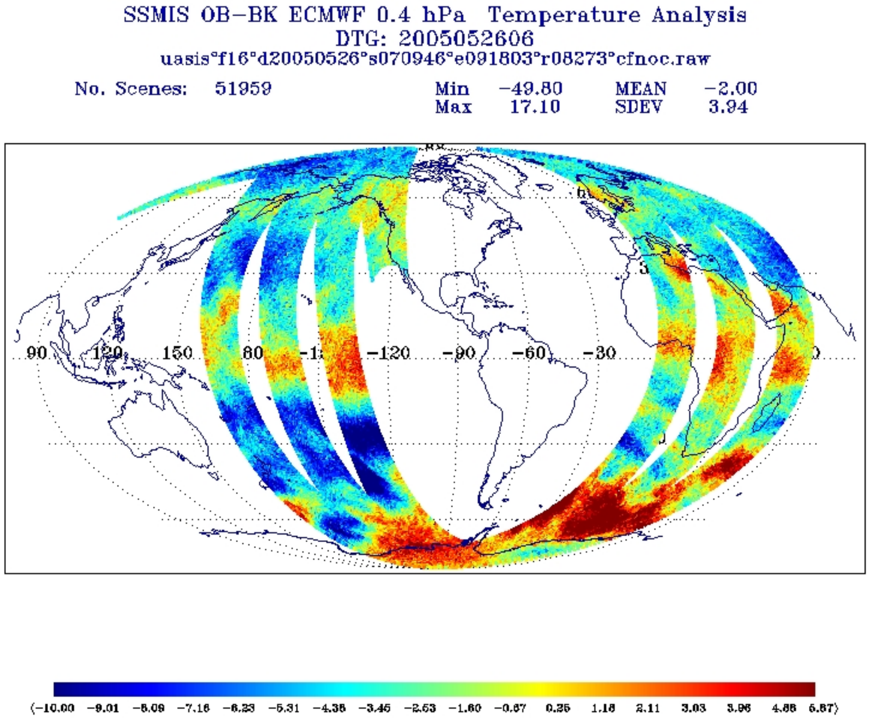

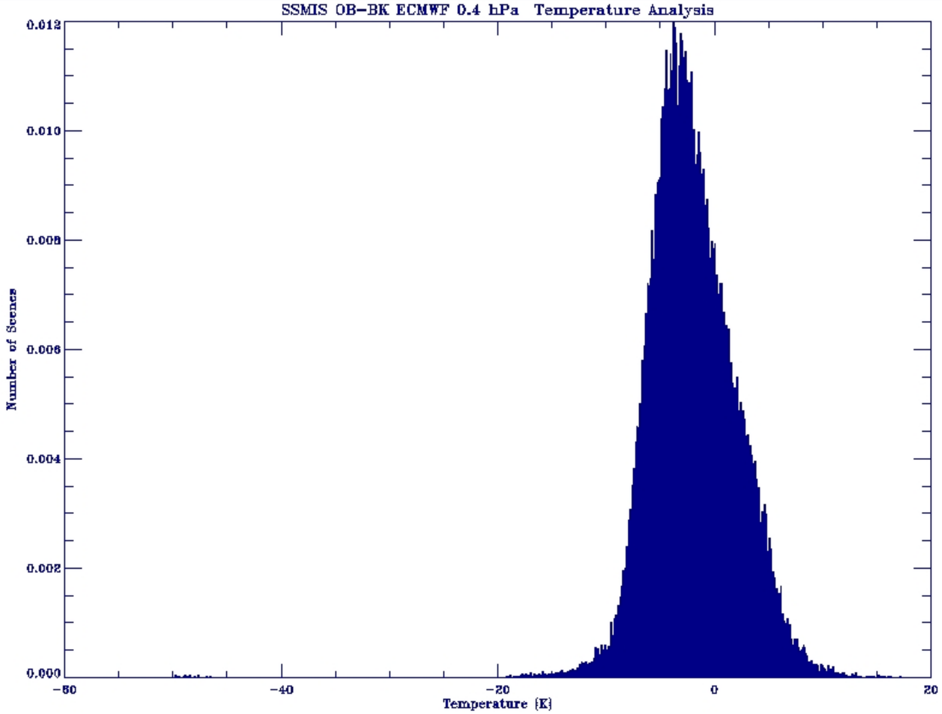

SSMIS - ECMWF 0.4 hPa Temperature Departure

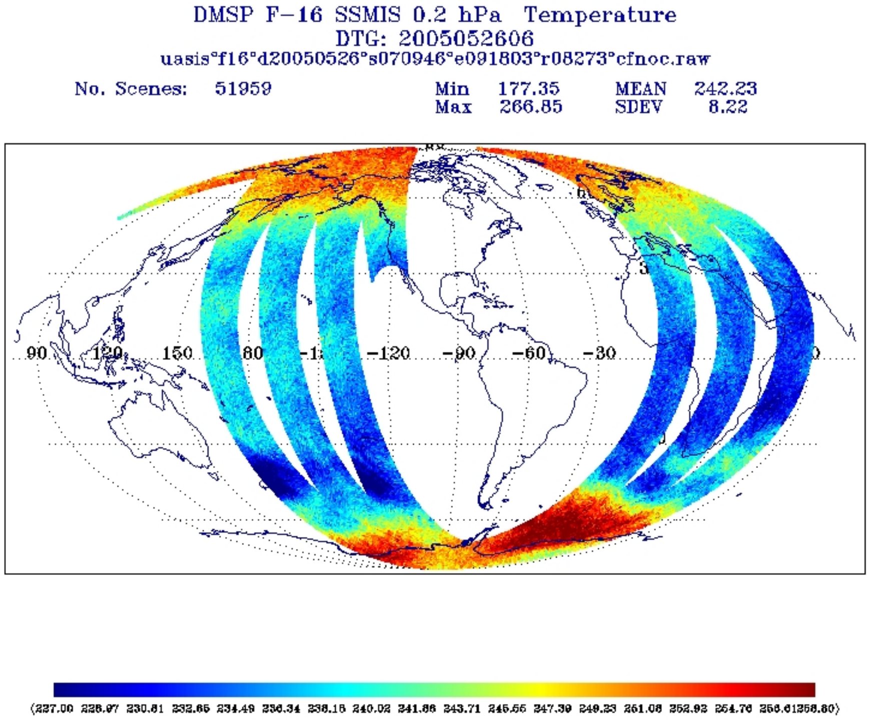

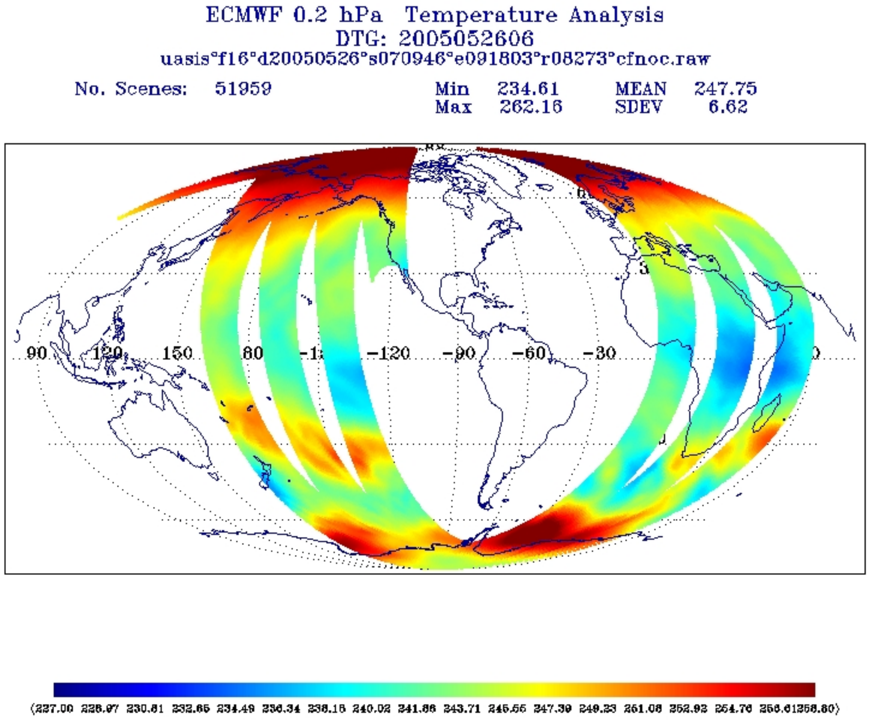

SSMIS 0.2 hPa Temperature

ECMWF 0.2 hPa Temperature

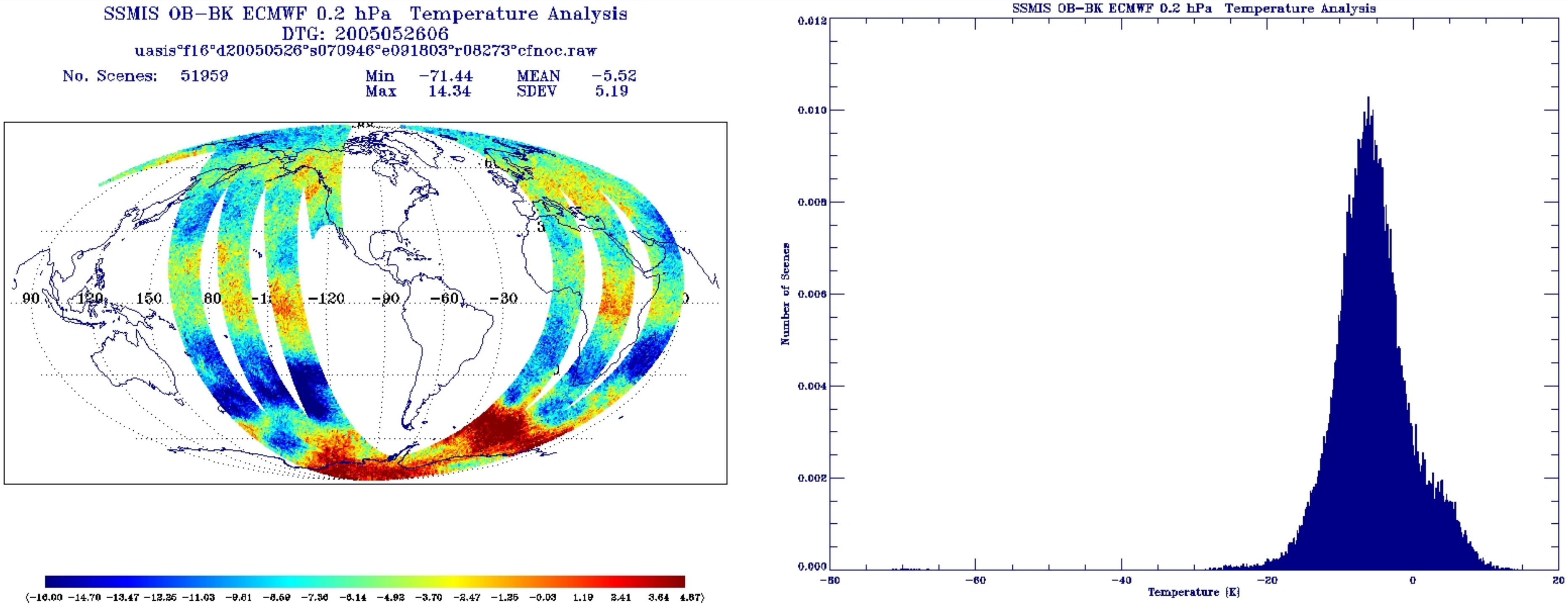

SSMIS - ECMWF 0.2 hPa Temperature Departure

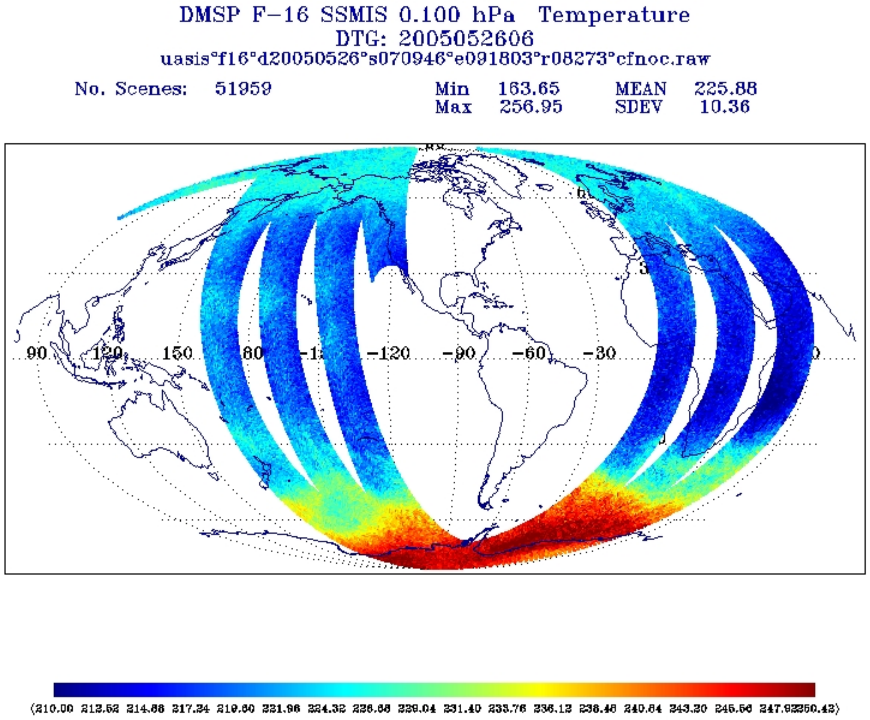

SSMIS 0.1 hPa Temperature

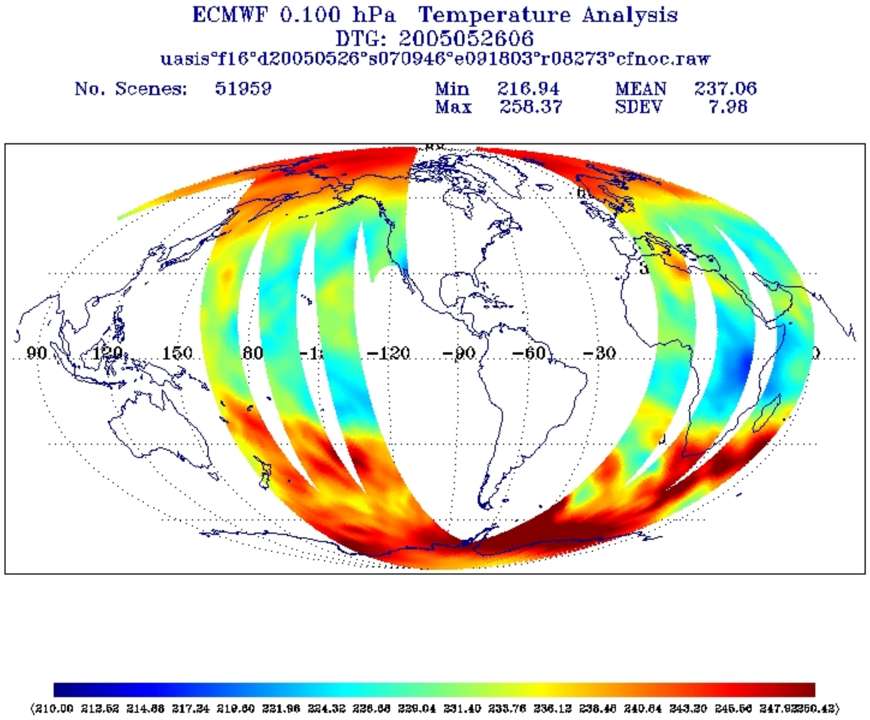

ECMWF 0.1 hPa Temperature

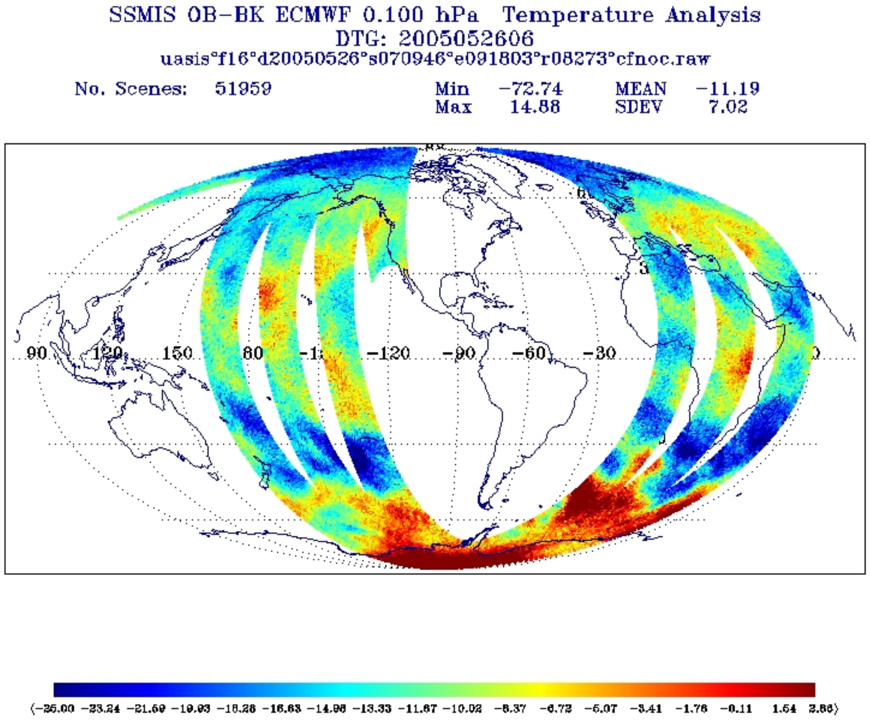

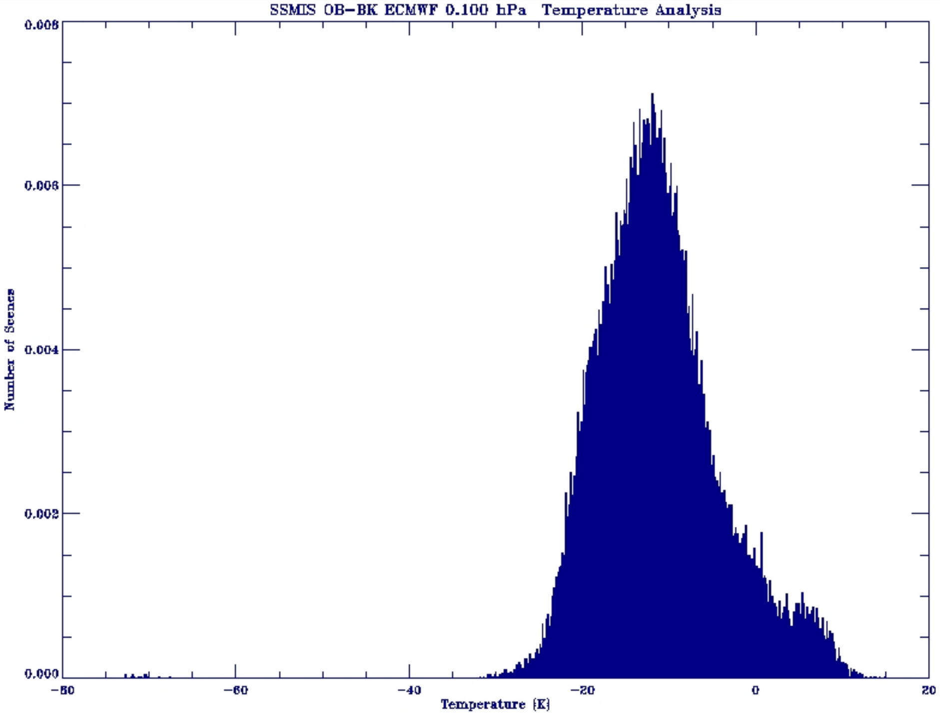

SSMIS - ECMWF 0.1 hPa Temperature Departure

SSMIS EDR vs. ECMWF Analysis Results

- ECMWF Appears to have Warm Bias at Levels Above 1.0 hPa

- ECMWF Bias also evident in Lidar vs. ECMWF

Status and Future Work

Section 10.6 Summary

Three Primary Objectives of SSMIS UAS Cal/Val Effort:

- **End-to-End Instrument Radiometric Calibration Accuracy**
- **Verify the Calibration of the Sensor Data Records (SDRs)**
- **Validate UAS Temperature Retrievals (EDRs) Using Independent Measurements of Temperature Profiles.**

If Necessary, Apply New Sensor Calibration Coefficients and Averaging Schemes, Develop New α and β Retrieval Coefficients, and/or Environmental Retrieval Algorithms to Bring the SDR and EDR Products Within Specification

End-to-End Instrument Radiometric Calibration Accuracy

- Hardware Doppler Shift Correction Appears Adequate

- Symmetric Averaging Required for UAS Channels

- Greater Geographic and Temporal Distribution of Independent Correlative Observations Necessary

- Further Understanding of Warm Load Intrusions and Reflector Emissions Necessary

Verify the Calibration of the Sensor Data Records (SDRs)

- SDR versus RTM Comparison Indicate Presence of the SSMIS Calibration Anomalies Described in Appendix 1.

- UAS RTMs O_2 Absorption Models may also need Adjustment

- SDR Data Produced by GDPS Outputs only $|B|$ and $|B{\cdot}k_{SDR}|^2$

  whereas,

$$B{\cdot}K_{RTM} = -\,\mathrm{SQRT}(\,(B{\cdot}k_{SDR})^2\,)$$

$$\theta_B = \mathrm{COS}^{-1}\,(\,B{\cdot}k_{RTM}\,/\,|B|\,)$$

are required for RTM analysis

Validate UAS Temperature Retrievals (EDRs) Using Independent Measurements of Temperature Profiles

- SSMIS UAS Temperature Retrievals Meet RMS Specification at both TMF and MLO

- EDR Biases need to be Greatly Improved

- SSMIS UAS have Warm Bias below 0.4 hPA compared to Lidar

- SSMIS UAS have Cold Bias above 0.4 hPa compared to Lidar

- Wider Geographic Distribution of Lidar Profiles Needed

Ensemble SSMIS-Lidar T Departure Statistics

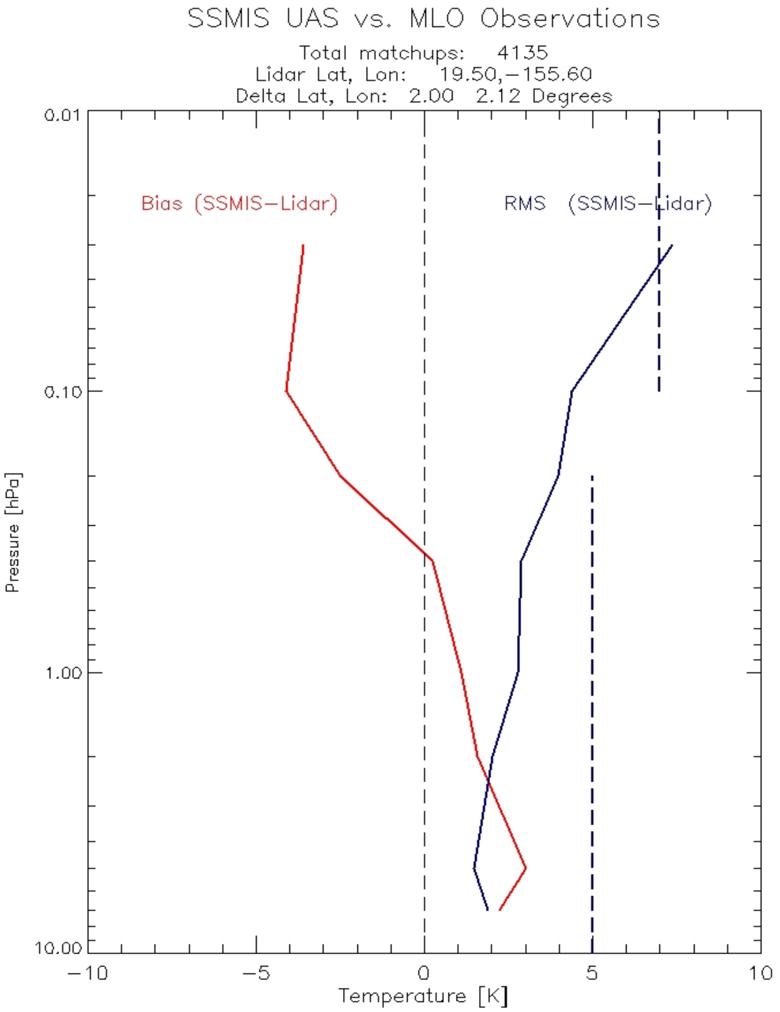

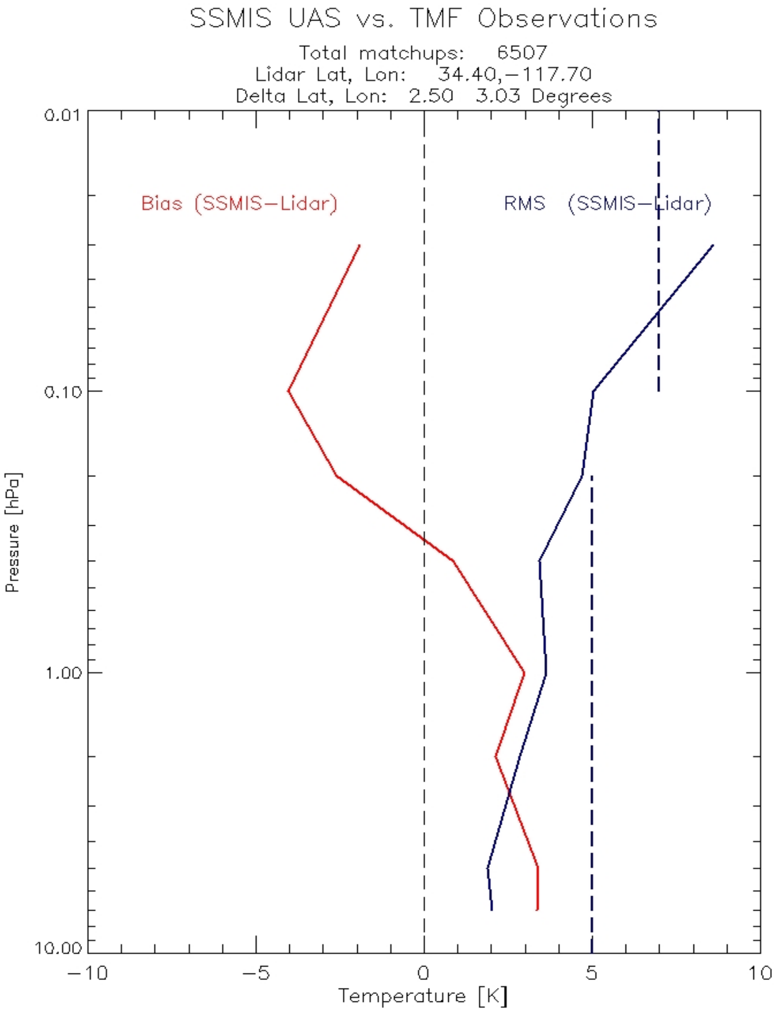

Upper Atmosphere Temperature Requirements/Goals

Level [hPa]	Accuracy Requirement [K]	Accuracy Predicted [K]	Worst Case Predicted [K]	MLO Lidar Comparison [K]		TMF Lidar Comparison [K]	
				Bias	RMS	Bias	RMS
7	5.0	1.48	1.49	2.1	1.9	3.3	2.0
5	5.0	1.44	1.45	3.2	1.5	3.3	1.9
2	5.0	2.31	2.37	1.4	2.1	2.1	3.0
1	5.0	3.19	3.17	1.2	2.9	2.8	3.6
0.4	5.0	3.67	3.93	0.2	2.9	1.2	3.2
0.2	7.0	4.26	4.75	-2.5	3.8	-2.8	4.5
0.1	7.0	5.56	6.03	-4.0	4.2	-4.1	5.0
0.03	7.0	5.41	6.34	-3.5	7.5	-1.8	8.6

Recommendation for Future Work

- Retain the Symmetric Averaging Schemes for UAS Channels

- Develop New α and β Retrieval Coefficients to Bring EDR Products Within Specification (Bias)

- Apply Polarization Impurity Corrections in Manner Similar to Cross-Polarization Corrections

Recommendations for Future Work

- Continue Monitoring UAS SDR and EDR data versus Lidar

- Test Validity of Extrapolating the Liebe, Rosenkranz and Hufford (1992) Experimental O_2 Absorption Data from measurements made above 7.6 hPa and 280K to the Mesosphere ($p < 5$ hPa and T approaching 220 K)

- Current UAS RTM Treats Individual Zeeman Component Contributions and then Sums

- Investigate Importance of Quantum Interference Between O_2 Absorption Lines for the Multiple Zeeman Lines

- Develop Fast RTM with Zeeman/Geomagnatic Effects included

- ECMWF Model Top Extending to 0.01 hPa by end of 2005 may Provide Additional Global Correlative Data

Defense Meteorological Satellite Program
Special Sensor Microwave Imager Sounder (F-16)
Calibration/Validation Final Report

The First Conical Scanning Passive Microwave Surface and Atmospheric Sounding Imager

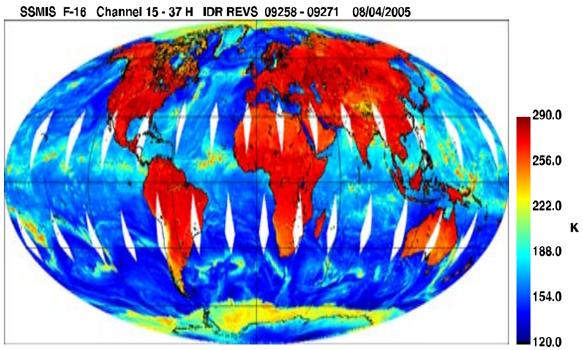
SSMIS F-16 Channel 15 - 37 H IDR REVS 09258 - 09271 08/04/2005

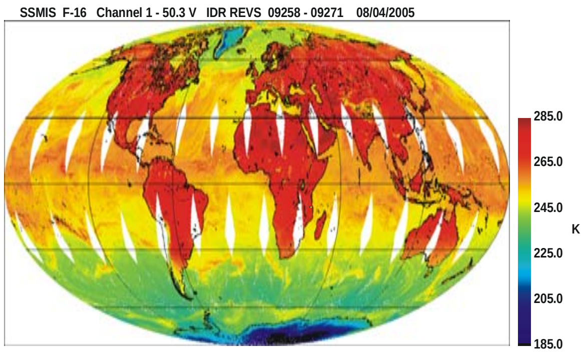
SSMIS F-16 Channel 1 - 50.3 V IDR REVS 09258 - 09271 08/04/2005

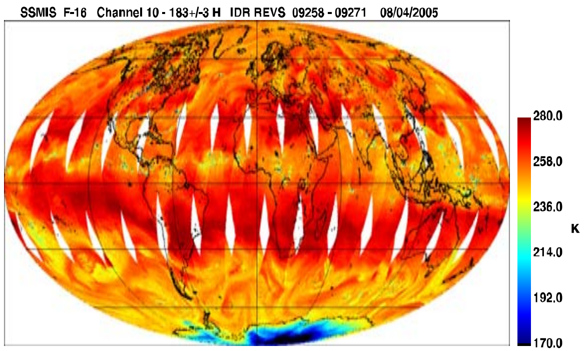
SSMIS F-16 Channel 10 - 183+/-3 H IDR REVS 09258 - 09271 08/04/2005

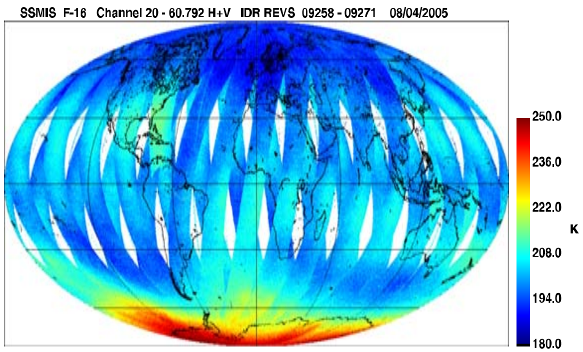
SSMIS F-16 Channel 20 - 60.792 H+V IDR REVS 09258 - 09271 08/04/2005

Prepared by

SSMIS Cal/Val Team

30 November 2005

Volume V

Table of Contents

F16 SSMIS Calibration/Validation Final Report

Section 11 Calibration Anomalies I

David Kunkee, Steve Swadley, Gene Poe, Ye Hong, Michael Werner, James Wang, Michael Meshishnek

THE AEROSPACE CORPORATION

Section 11 Radiometric Calibration Anomalies I: Sensor Phenomenology

11.1 SSMIS Warm Load Assembly

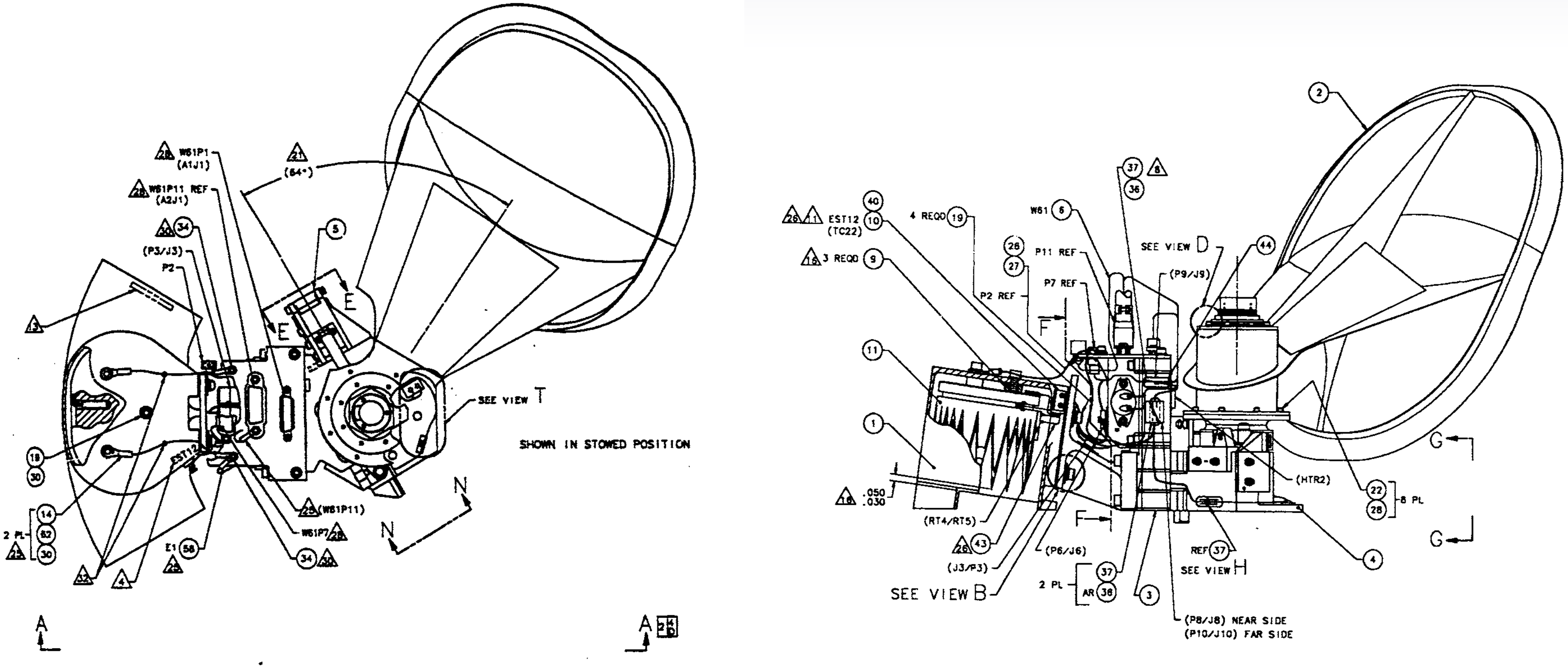

The SSMIS Calibration assembly is shown in the stowed configuration. When it is deployed, the Cold Sky Reflector (CSR) will rotate ~180 degrees CW with respect to Warm Load.

11.2 Definition of Warm Load and Cold Sky Reflector Solar Reference Angles

Page 11-5 shows an elevation and plan view of the SSMIS Warm Load (WL). On the left hand side the angle θ in the orbital reference frame is called the solar azimuth angle, however, in the WL reference frame it is the elevation of the sun above the SSMIS canister top. Likewise on the right hand side ϕ in the orbital reference frame is called the elevation angle, but in the WL reference frame it is called the azimuth angle due its relationship with the WL. We will use the WL reference frame in referring to these angles. These angles are calculated by the DGS simulation shown on page 11-6. The Orange line represents the WL azimuth vector (ϕ_{WL} = 0°) translated to the spin axis of the SSMIS. Similarly, the blue line represents the Cold Sky Reflector (CSR) azimuth vector (ϕ_{CSR} = 0°) also translated to the spin axis. For the CSR, zero azimuth is the direction opposite of the cold sky viewing direction. The violet represents the normal vector of the CSR reflecting surface also translated to the SSMIS spin axis at the canister top. The yellow line which appears on pages 11- 8 and 11- 9, is the direction of the Sun. This vector can not be seen on pages 11- 5 or 11- 6 because the view of the vehicle on these pages is from the Sun. The elevation angle with respect to the CSR and WL is the same as the Sun elevation in Yellow in the panel on the left hand side of the DGS simulation.

Definition of Warm Load Sun Angle

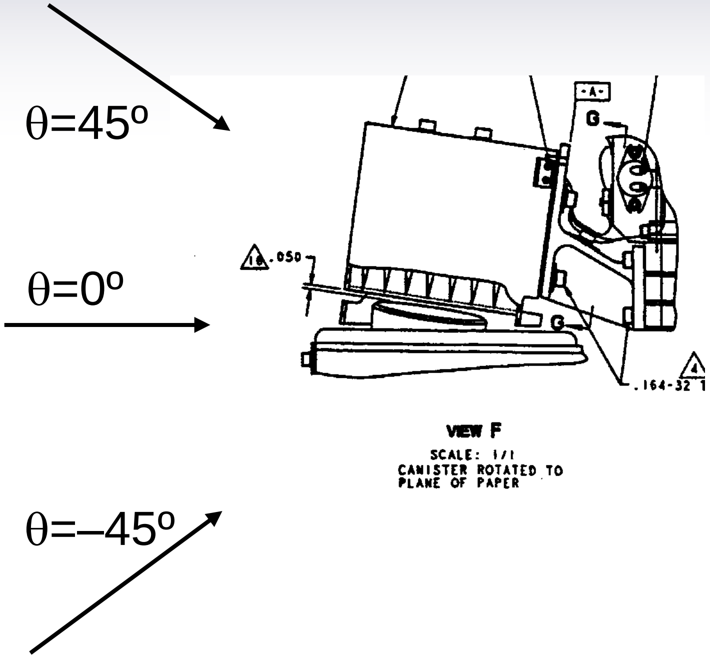

θ_{WL}

Orbital Ref: Azimuth Angle
WL Ref: Elevation Angle

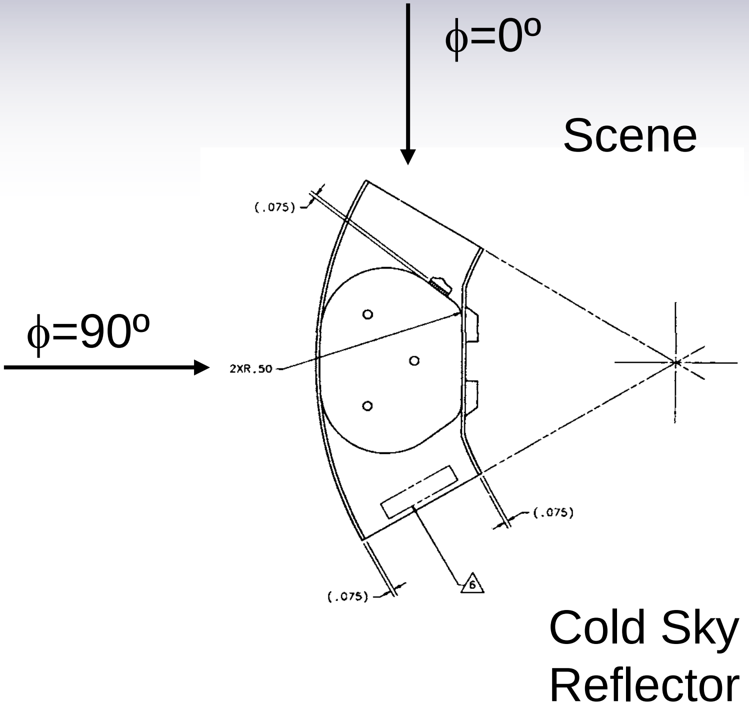

ϕ_{WL}

Orbital Ref: Polar Angle
WL Ref: Azimuth Angle

DGS Simulation of the SSMIS Calibration Assembly

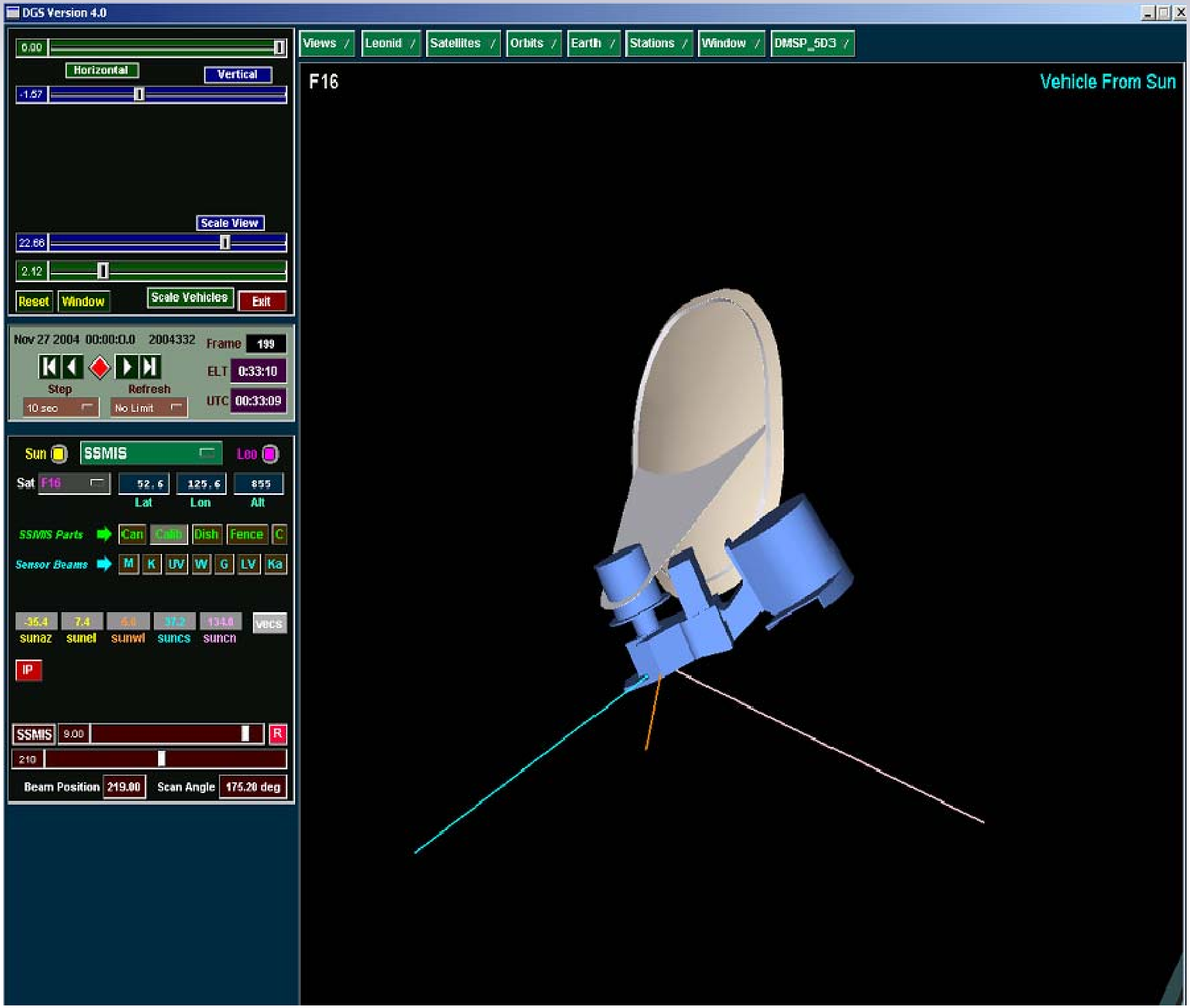

Nov 27 2004 00:00:0.0 2004332

Frame 199

ELT 0:33:10

UTC 00:33:09

Step 10 sec

Refresh No Limit

SSMIS

Sat F16

52.6 Lat

125.6 Lon

855 Alt

-35.4 sunaz

7.4 sunel

sunwl

suncs

suncn

Beam Position 219.00

Scan Angle 175.20 deg

DGS Simulation of the SSMIS Calibration Assembly

8.00

-1.57

22.66

2.12

Nov 27 2004 00:00:0.0 2004332

Frame 199

ELT 0:33:10

UTC 00:33:09

Step 10 sec

Refresh No Limit

SSMIS

Sat F16

52.6 Lat

125.6 Lon

855 Alt

-35.4 sunaz

7.4 sunel

6.6 sunwl

37.2 suncs

134.0 suncn

SSMIS 9.00

210

Beam Position 219.00

Scan Angle 175.20 deg

DGS Simulation of the SSMIS Calibration Assembly

-1.83
-1.67
104.3
-73.0
78.9
17.77
1.00

Nov 27 2004 00:00:0.0 2004332

Frame 199

ELT 0:33:10

UTC 00:33:09

Step 10 sec

Refresh No Limit

SSMIS

Sat F16

Lat	Lon	Alt
52.6	125.6	855

sunaz	sunel	sunwl	suncs	suncn
-35.4	7.4	5.6	37.2	134.0

SSMIS 9.00

210

Beam Position 219.00

Scan Angle 176.20 deg

DGS Simulation of the SSMIS Calibration Assembly

-1.83

-1.57

104.3

-73.0

76.9

17.77

1.00

Nov 27 2004 00:00:0.0 2004332

Frame 199

ELT 0:33:10

UTC 00:33:09

Step 10 sec

Refresh No Limit

SSMIS

Sat F16

Lat	Lon	Alt
52.6	125.6	855

sunaz	sunel	sunwl	suncs	suncn
-35.4	7.4	6.6	37.2	134.0

SSMIS 9.00

210

Beam Position 219.00

Scan Angle 175.20 deg

11.3 Definition of Warm Load Solar Intrusion Regions

Early orbit data collected soon after the F16 SSMIS spin up in October 2003 was used for early analysis of the solar warm load intrusion. The EO2 mode data was acquired from F16 revs 136 – 145 as shown on page 11-11. The solar angle (Yellow on page 11-6 through 11-9) is estimated by the graph on page 11- 12 as a function of seconds from the beginning of the orbit. Simulations appearing on pages 11-13 and 11-14 show the graphically first two significant solar intrusions on the SSMIS WL for the October F-16 orbital season. Page 11-13 shows the direct illumination of the SSMIS WL tines, shown in red, when the Sun elevation angle is ~ 5° – 6° below the top of the canister. Page 11-14 shows the strong reflected interaction which occurs with Sun elevation angle near 15° – 20° for the associated Sun azimuth in the October season. The graphic simulation assumes highly reflecting surfaces and limits the interactions to 4 reflections. The two strong regions of interaction (1) and (2) lead to changes in the observed brightness temperature of the WL as shown on Pages 11-15 and 11-16 for several beam positions where the K$_A$-band feedhorn (Channel 15) is viewing the WL. Note that each of the traces on the graph are offset by 5 K to allow comparison of the measurements at each BP as a function of time from beginning of orbit. It can easily be seen that each BP is affected at a slightly different time. This is due to the localized nature of the WL solar heating and changes in the direct (1) and specular reflection from the top deck (2) as time progresses and the sun angle on the WL changes.

Early Orbit Mode 2 Data from S/N02 (2003)

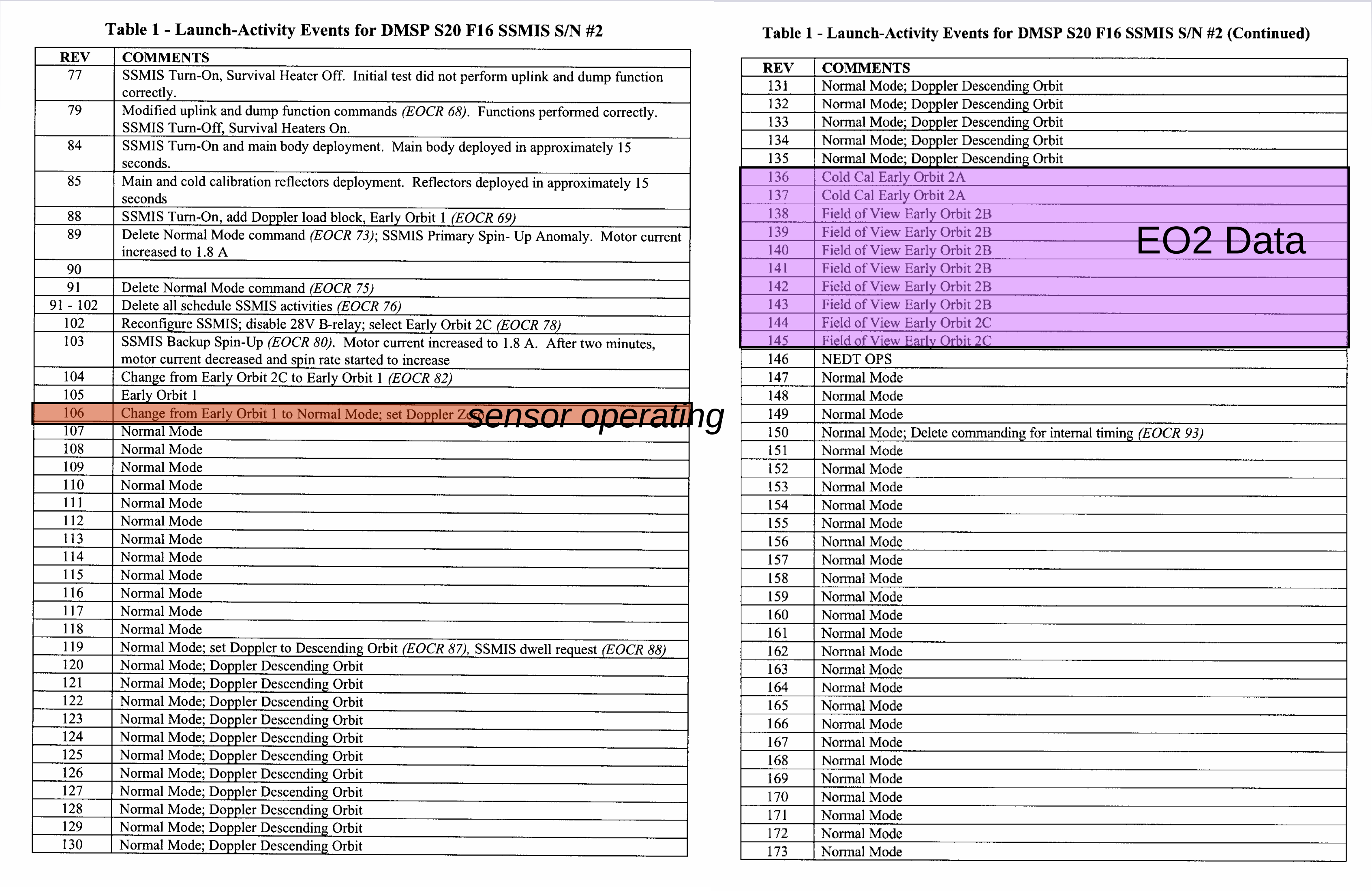

Table 1 - Launch-Activity Events for DMSP S20 F16 SSMIS S/N #2

REV	COMMENTS
77	SSMIS Turn-On, Survival Heater Off. Initial test did not perform uplink and dump function correctly.
79	Modified uplink and dump function commands *(EOCR 68)*. Functions performed correctly. SSMIS Turn-Off, Survival Heaters On.
84	SSMIS Turn-On and main body deployment. Main body deployed in approximately 15 seconds.
85	Main and cold calibration reflectors deployment. Reflectors deployed in approximately 15 seconds
88	SSMIS Turn-On, add Doppler load block, Early Orbit 1 *(EOCR 69)*
89	Delete Normal Mode command *(EOCR 73)*; SSMIS Primary Spin- Up Anomaly. Motor current increased to 1.8 A
90	
91	Delete Normal Mode command *(EOCR 75)*
91 - 102	Delete all schedule SSMIS activities *(EOCR 76)*
102	Reconfigure SSMIS; disable 28V B-relay; select Early Orbit 2C *(EOCR 78)*
103	SSMIS Backup Spin-Up *(EOCR 80)*. Motor current increased to 1.8 A. After two minutes, motor current decreased and spin rate started to increase
104	Change from Early Orbit 2C to Early Orbit 1 *(EOCR 82)*
105	Early Orbit 1
106	Change from Early Orbit 1 to Normal Mode; set Doppler Zero
107	Normal Mode
108	Normal Mode
109	Normal Mode
110	Normal Mode
111	Normal Mode
112	Normal Mode
113	Normal Mode
114	Normal Mode
115	Normal Mode
116	Normal Mode
117	Normal Mode
118	Normal Mode
119	Normal Mode; set Doppler to Descending Orbit *(EOCR 87)*, SSMIS dwell request *(EOCR 88)*
120	Normal Mode; Doppler Descending Orbit
121	Normal Mode; Doppler Descending Orbit
122	Normal Mode; Doppler Descending Orbit
123	Normal Mode; Doppler Descending Orbit
124	Normal Mode; Doppler Descending Orbit
125	Normal Mode; Doppler Descending Orbit
126	Normal Mode; Doppler Descending Orbit
127	Normal Mode; Doppler Descending Orbit
128	Normal Mode; Doppler Descending Orbit
129	Normal Mode; Doppler Descending Orbit
130	Normal Mode; Doppler Descending Orbit

sensor operating

Table 1 - Launch-Activity Events for DMSP S20 F16 SSMIS S/N #2 (Continued)

REV	COMMENTS
131	Normal Mode; Doppler Descending Orbit
132	Normal Mode; Doppler Descending Orbit
133	Normal Mode; Doppler Descending Orbit
134	Normal Mode; Doppler Descending Orbit
135	Normal Mode; Doppler Descending Orbit
136	Cold Cal Early Orbit 2A
137	Cold Cal Early Orbit 2A
138	Field of View Early Orbit 2B
139	Field of View Early Orbit 2B
140	Field of View Early Orbit 2B
141	Field of View Early Orbit 2B
142	Field of View Early Orbit 2B
143	Field of View Early Orbit 2B
144	Field of View Early Orbit 2C
145	Field of View Early Orbit 2C
146	NEDT OPS
147	Normal Mode
148	Normal Mode
149	Normal Mode
150	Normal Mode; Delete commanding for internal timing *(EOCR 93)*
151	Normal Mode
152	Normal Mode
153	Normal Mode
154	Normal Mode
155	Normal Mode
156	Normal Mode
157	Normal Mode
158	Normal Mode
159	Normal Mode
160	Normal Mode
161	Normal Mode
162	Normal Mode
163	Normal Mode
164	Normal Mode
165	Normal Mode
166	Normal Mode
167	Normal Mode
168	Normal Mode
169	Normal Mode
170	Normal Mode
171	Normal Mode
172	Normal Mode
173	Normal Mode

EO2 Data

Sun Angle in Warm Load Reference Frame

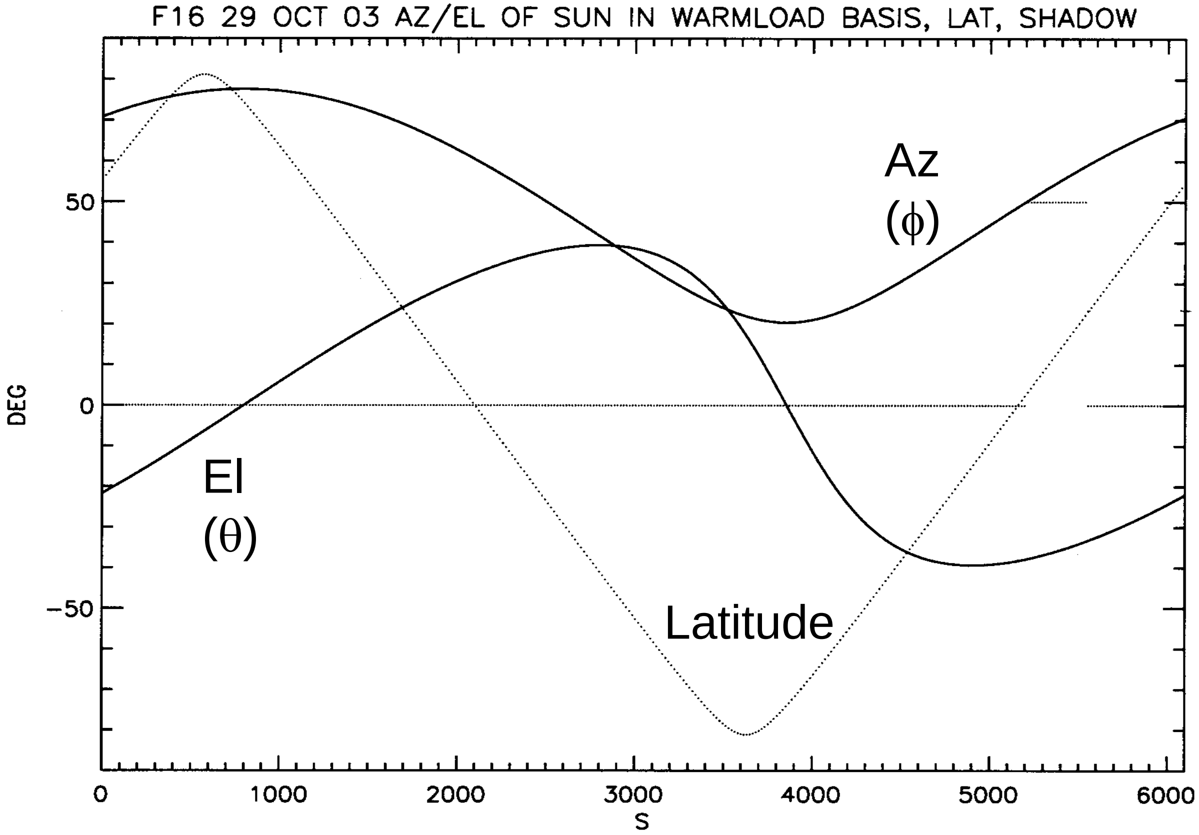

Sun-Induced Warm Load Gradients: Region 1 Direct Illumination

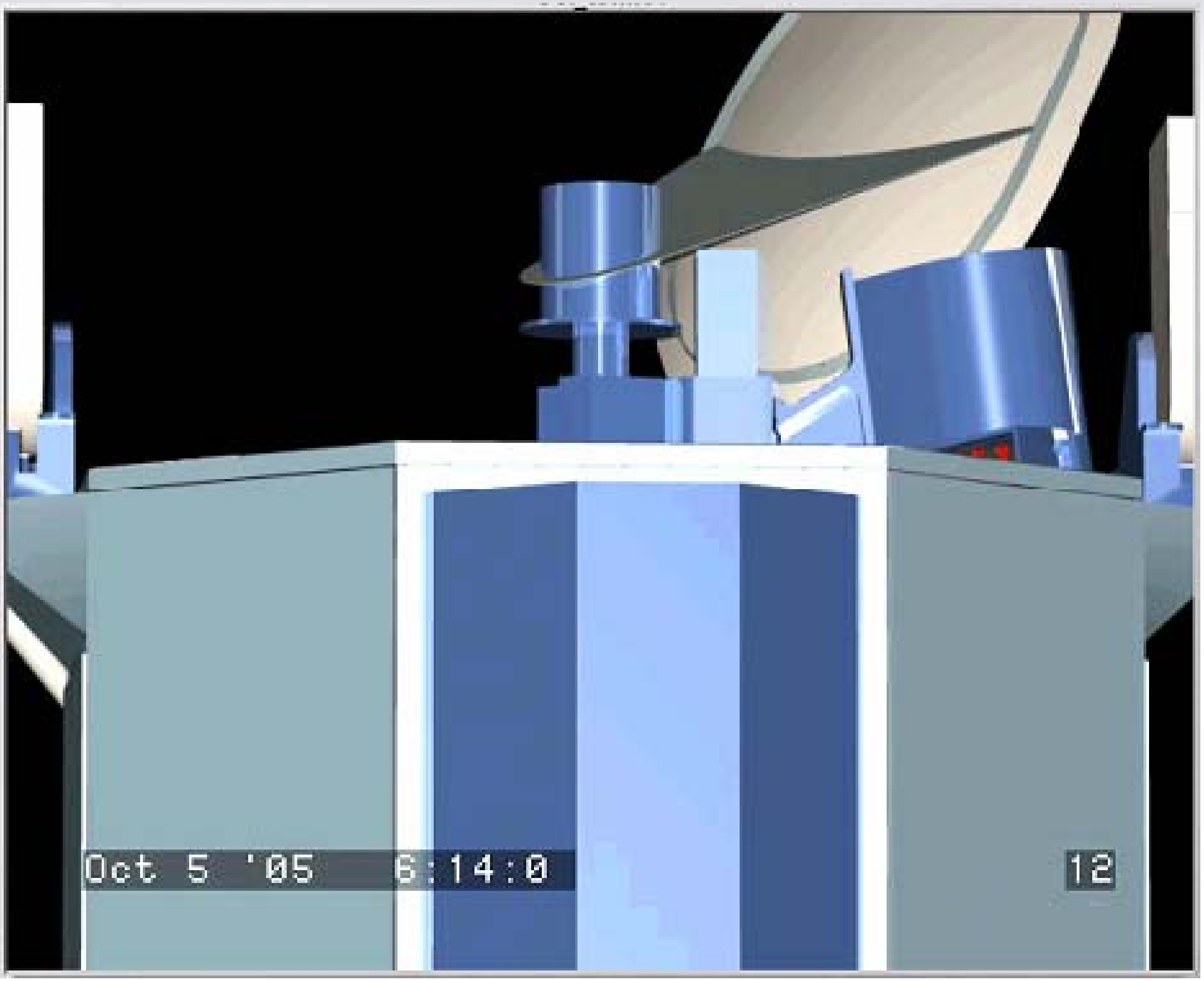

Sun-Induced Warm Load Gradients: Region 2
Reflected Illumination

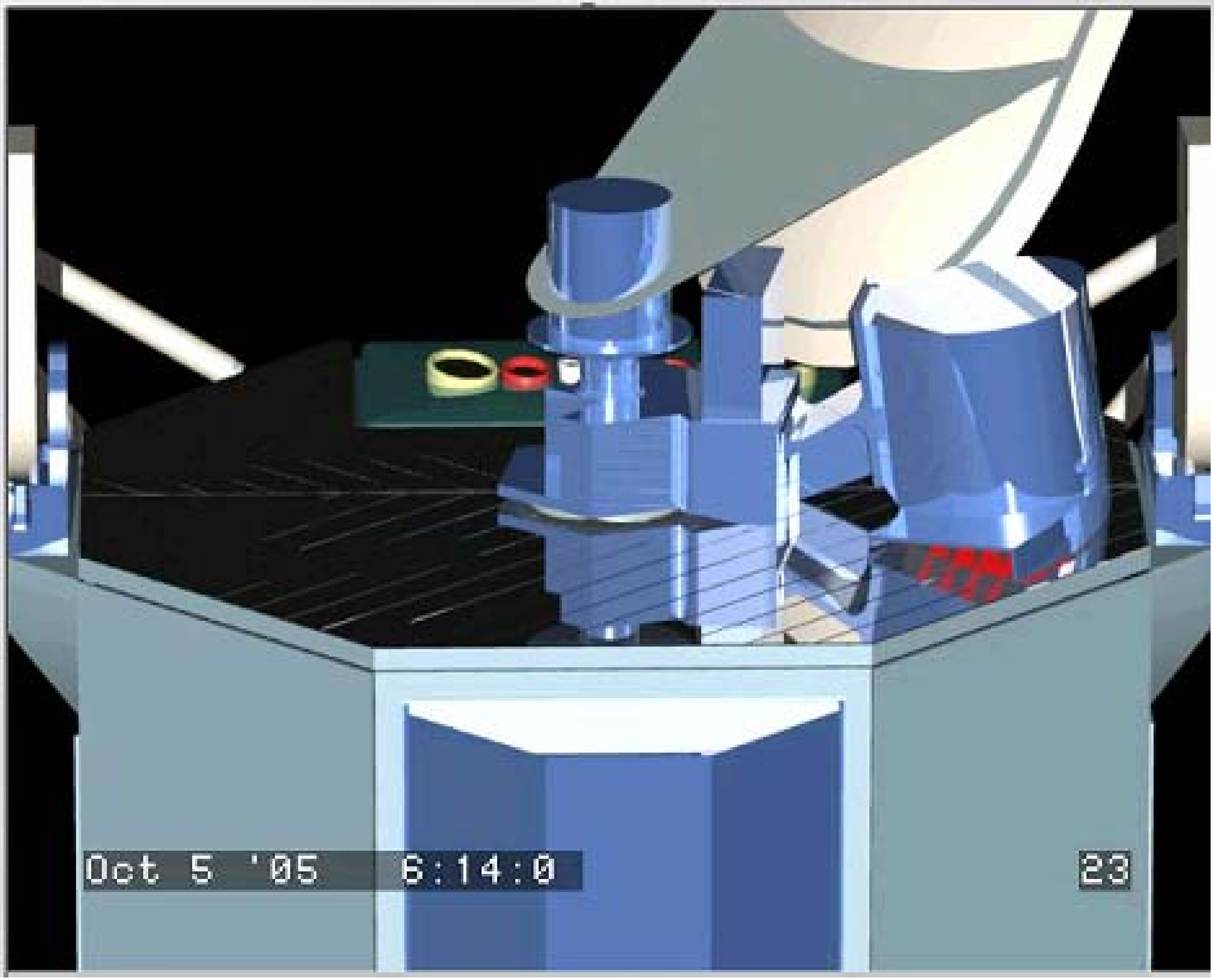

Sun Glint on Warm Load Shown in EO data: Ch 15

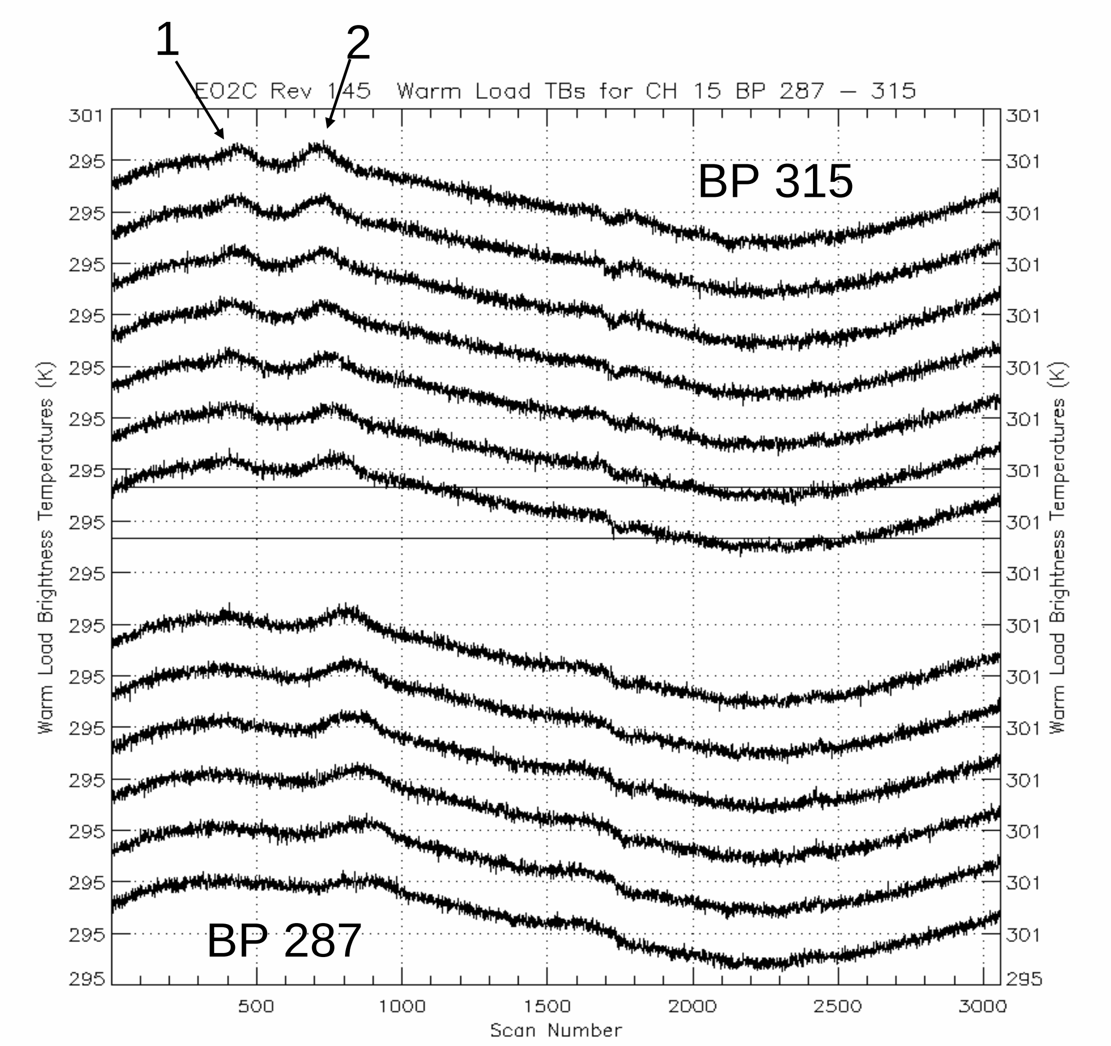

Sun Glint on Warm Load Shown in EO data: Ch 15

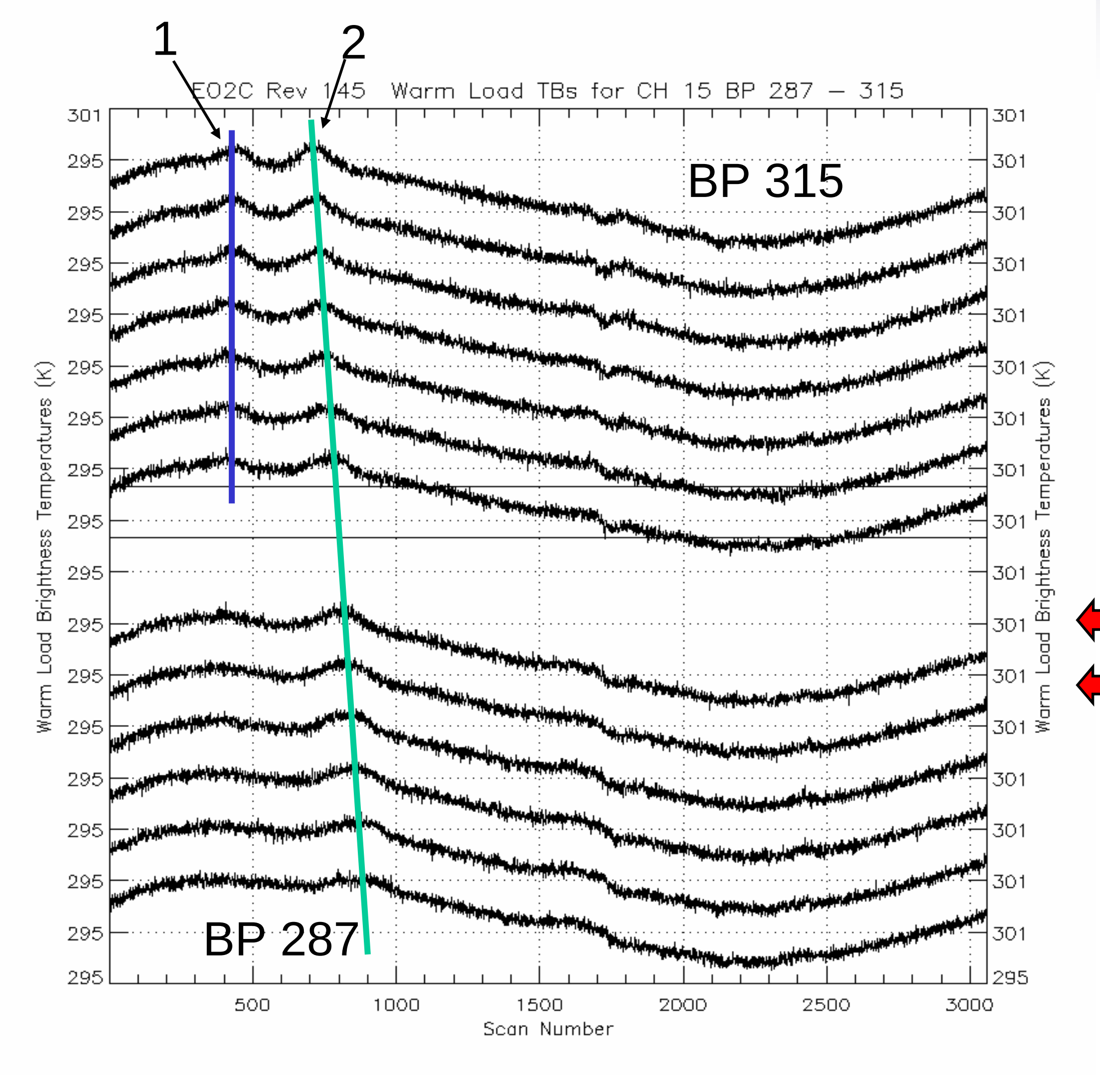

1

i) Before #2 in time sequence

ii) Not seen for BP>~303

iii) All BP affected at the same time

2

i) After #1 in time sequence

ii) Broadens for higher BP

iii) Later for lower BP

Warm Load Calibration uses BP 296 – 299 Hence “Region 1” will not appear in calibrated data ca. Oct 28

Sun Glint on Warm Load Shown in EO data: Ch 15

Page 11-18 shows additional periods of WL solar heating later in the orbital period. There is another point where the Sun again reflects onto the portion of the WL surface that is observed by the K_A-band feedhorn (and other feeds). The interaction is shown graphically by the model on page 11-19. A red color (WL tines) is visible under the lip of the WL shroud. The Sun is illuminating the active region of the WL directly above the feedhorn path under the WL (a fixed radial distance from the spin axis). Page 11-20 shows the areas of WL - Sun interaction as a function of S/C latitude and warm load temperature. The WL temperature is measured by Platinum Resistance Transducers (PRT) mounted on the back of the WL that do not track changes in the effective radiometric brightness temperature due to direct or indirect (reflected) solar heating of the WL. These changes can be seen in the image of Channel 15 EO2C data shown on page 11-21. Raw counts have been scaled to represent approximate brightness temperature of the WL surface as the K_A-band feed scans underneath the WL. Solar intrusions (1) and (2) can be seen by the red streaks near scan 700 and 1000 respectively. The third interaction is more difficult to observe in the image, however, between scans 1700 and 1800 there is a small increase in brightness temperature that can be seen near the bottom of the vertical range of the image near BP 284. The areas identified by (1), (2) and (3) represent transient changes from the slowly varying channel gain characteristics and WL temperature over the SSMIS orbit. An additional region (4) can also identified in Channel 15 WL graph on page 11- 23, however, it is very weak. A better indication of the additional region (4) can be seen in EO2B Channel 1 data shown on a similar graph on page 11- 24.

Sun Glint on Warm Load Shown in EO data: Ch 15

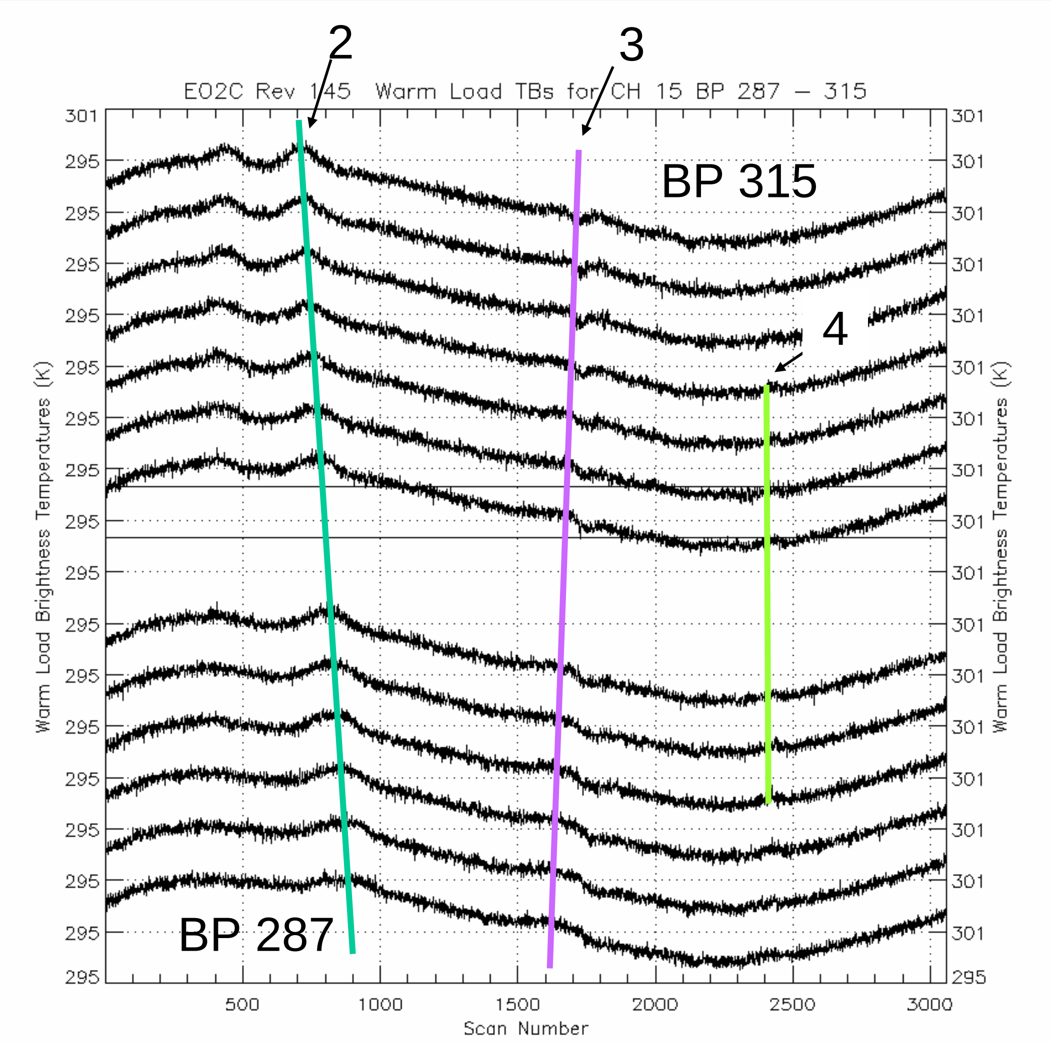

2

i) After #1 in time sequence

ii) Broadens for higher BP

iii) Later for lower BP

3

i) Characteristics similar to #2

ii) Same θ lower ϕ

iii) Later for higher BP;
different time lag

Warm Load Calibration
uses BP 296 – 299

4

i) Appears at negative

ii) WL sun elevation angles

iii) Similar to Region 1

Sun-Induced Warm Load Gradients: Region 3 Reflected Illumination

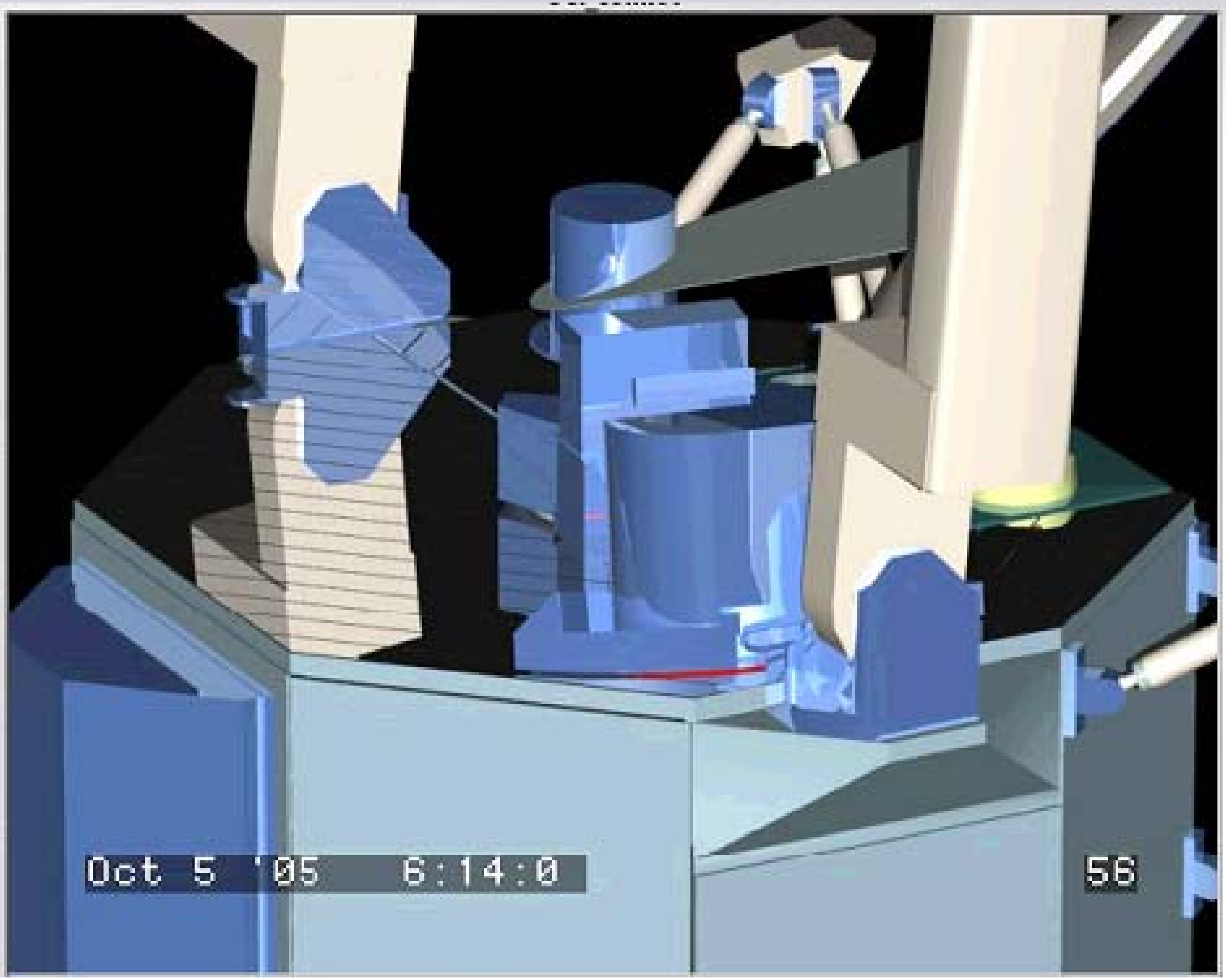

Latitude vs. Scan Number for Rev 145

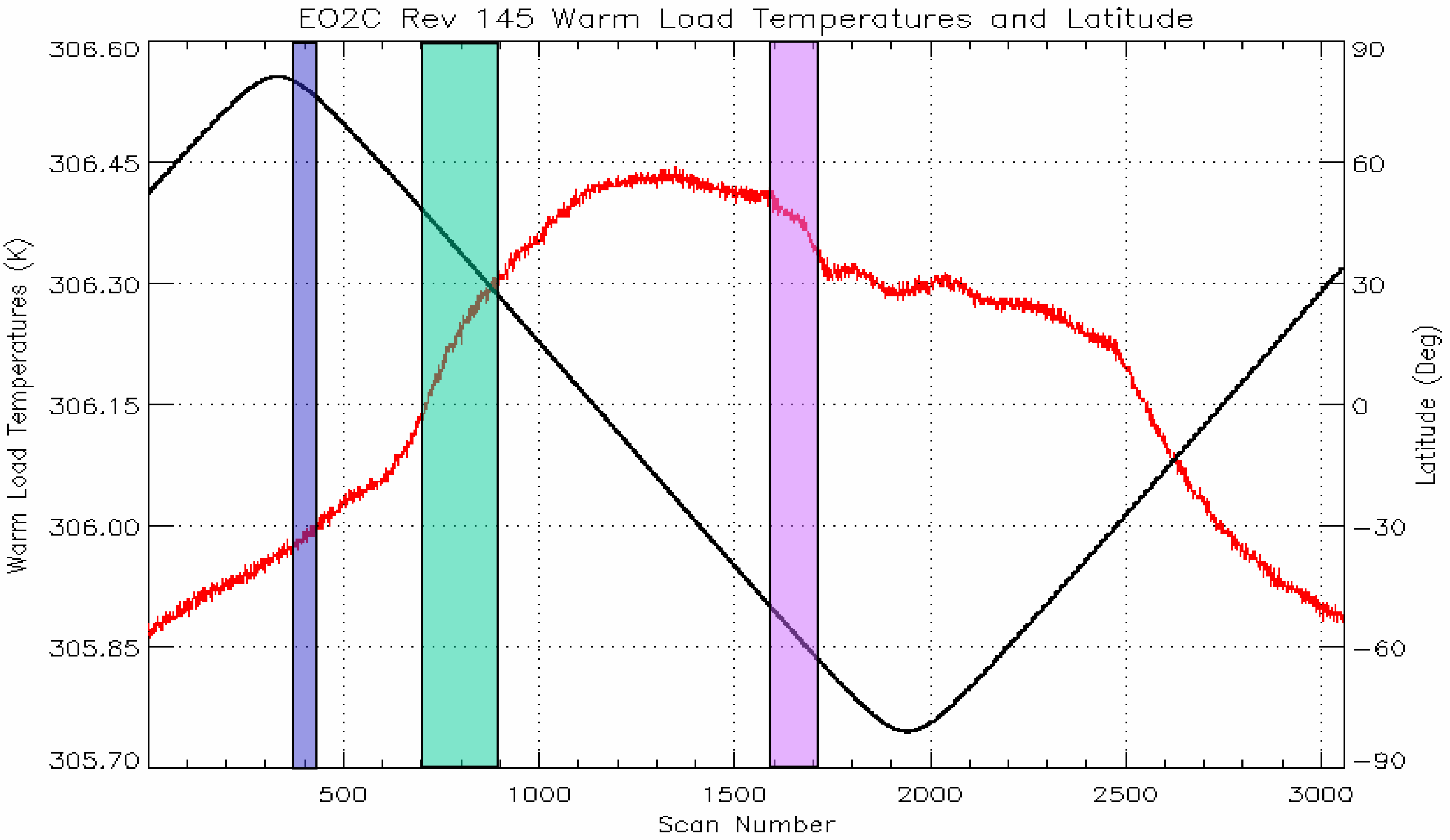

Sun Glint on Warm Load Shown in EO data: Ch 15

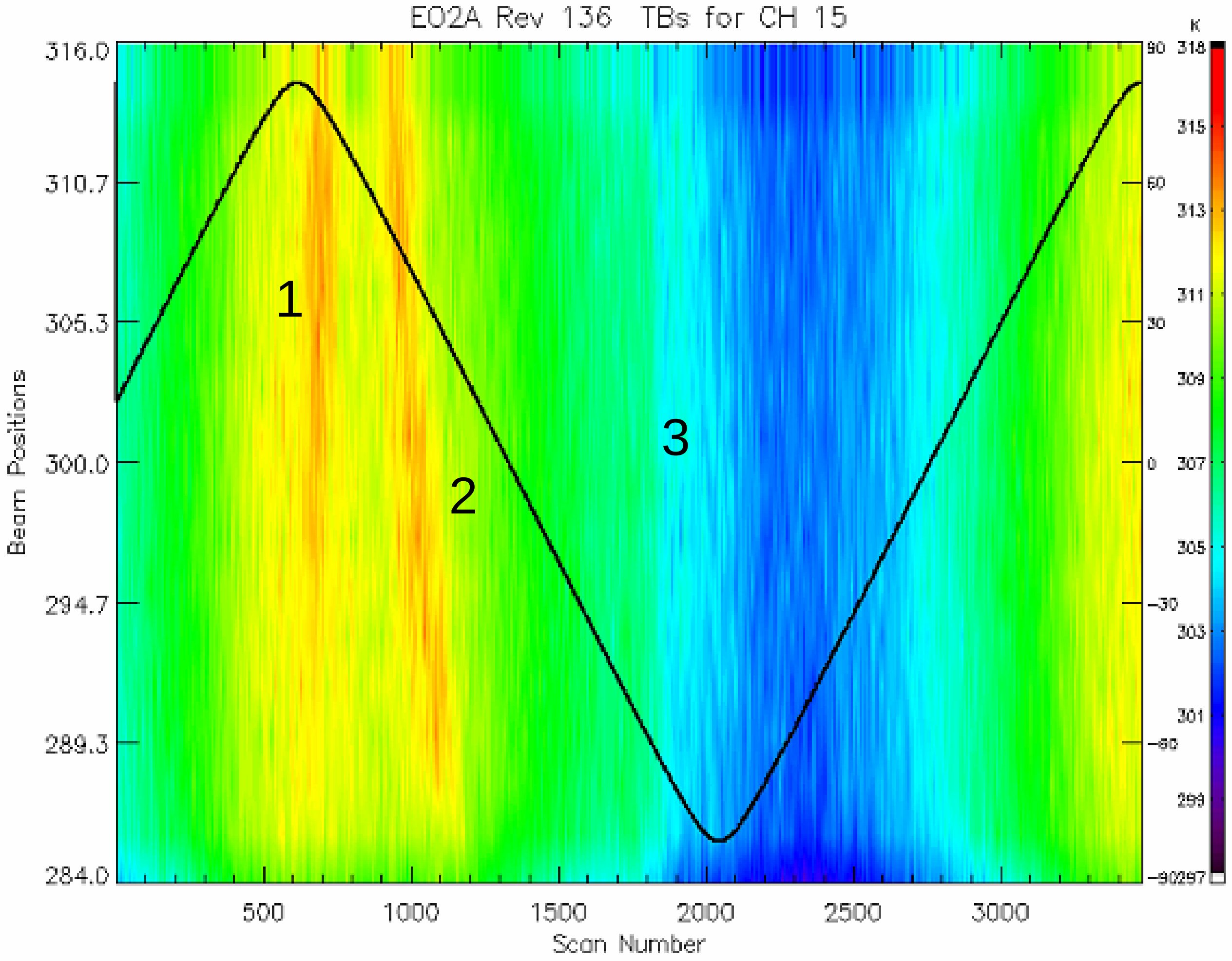

Sun Glint on Warm Load Shown in EO data: Ch 15

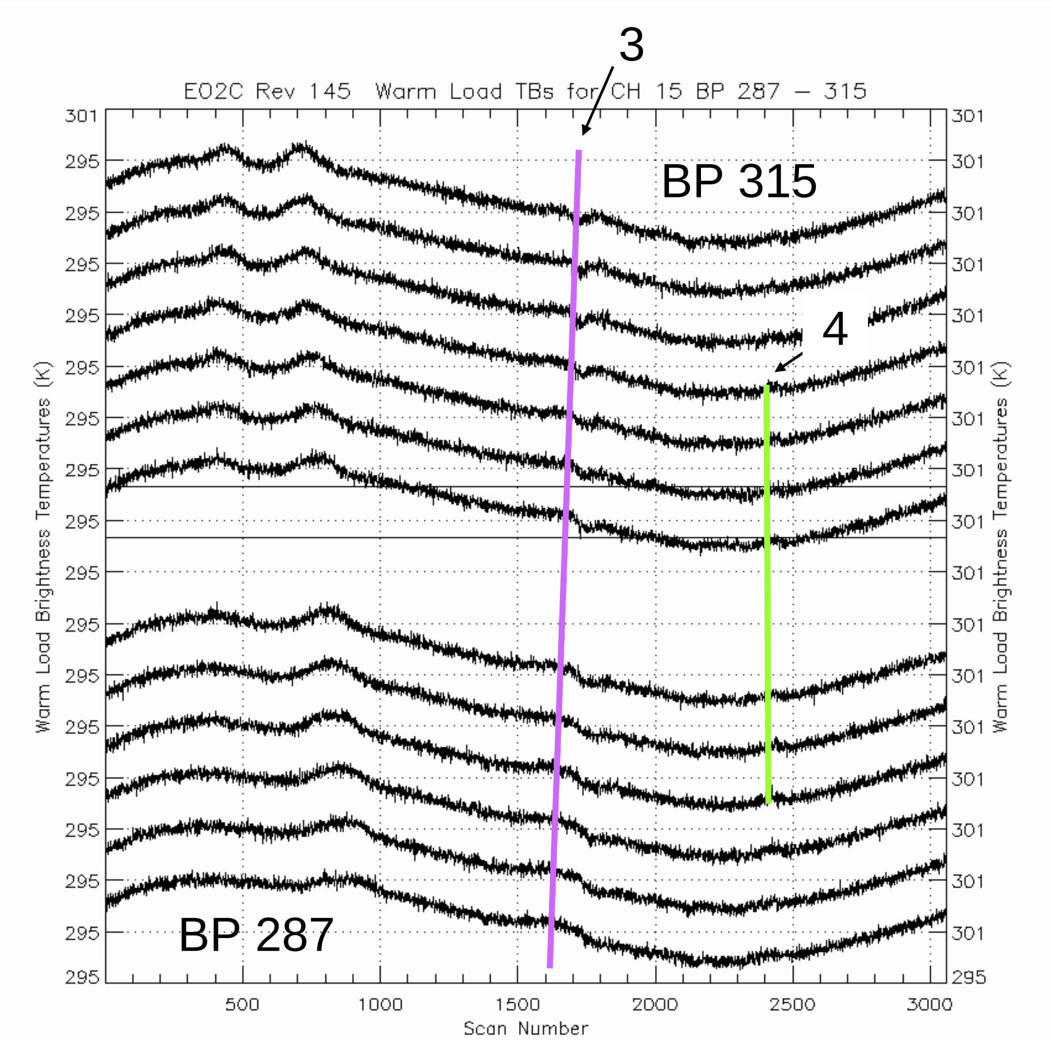

3
i) Characteristics similar to #2
ii) Same θ lower ϕ
iii) Later for higher BP;
different time lag

4 (Weak in Channel 15)
i) Appears at negative
ii) WL sun elevation angles
iii) Direct illumination

Warm Load Calibration
uses BP 296 – 299

Sun Glint on Warm Load Shown in EO data: Ch 1

Page 11-24 displays Channel 1 WL observations showing all 4 regions of WL anomalies from solar intrusion. Region 4 is shown graphically by the SSMIS ray-tracing model on page 11- 25. For this case, no red is visible from the WL for the azimuthal orientation (BP) of SSMIS that is shown. This is shown by the DGS simulation on page 11- 26. The SSMIS is modeled with the same orbital parameters but with the SSMIS at BP 240 where the WL tines are visible. The 4 WL anomalous regions are mapped and identified as a function of time on page 11-27 and an image of the scaled Channel 1 radiometric counts from the WL region is shown on page 11-28. Region 3 is observed by the dark blue streak below the "3" in the white box. Likewise region 4 is the black area below the "4" also in the white box. The table on page 11- 29 summarizes the 4 regions of Sun-interaction with the WL and lists the relative levels of the error introduced into the SSMIS calibration for Channel 15 by the anomaly.

Sun Glint on Warm Load Shown in EO data: Ch 1

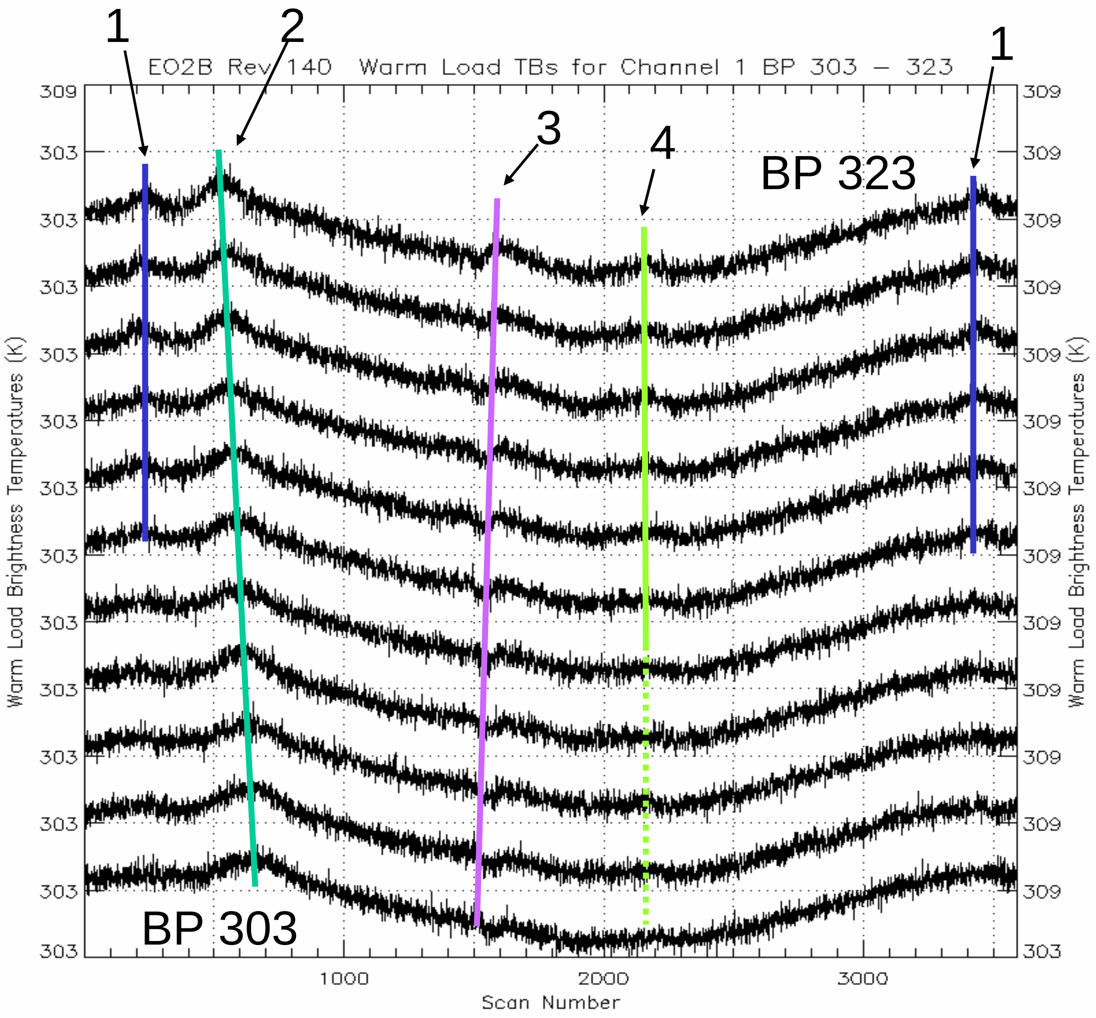

Anomalies at 1, 2 & 3 have similar characteristics as seen in Ch15 data And with similar WL solar illumination angles. Region 4 is stronger for Channel 1

4:

i) Appears at negative

ii) WL sun elevation angles

iii) Direct illumination

SSMIS Hot Calibration utilizes BP 308 – 311:

Region “2” and “3” WL anomalies may be the largest

Sun-Induced Warm Load Gradients: Region 4 Direct Illumination (at selected BP)

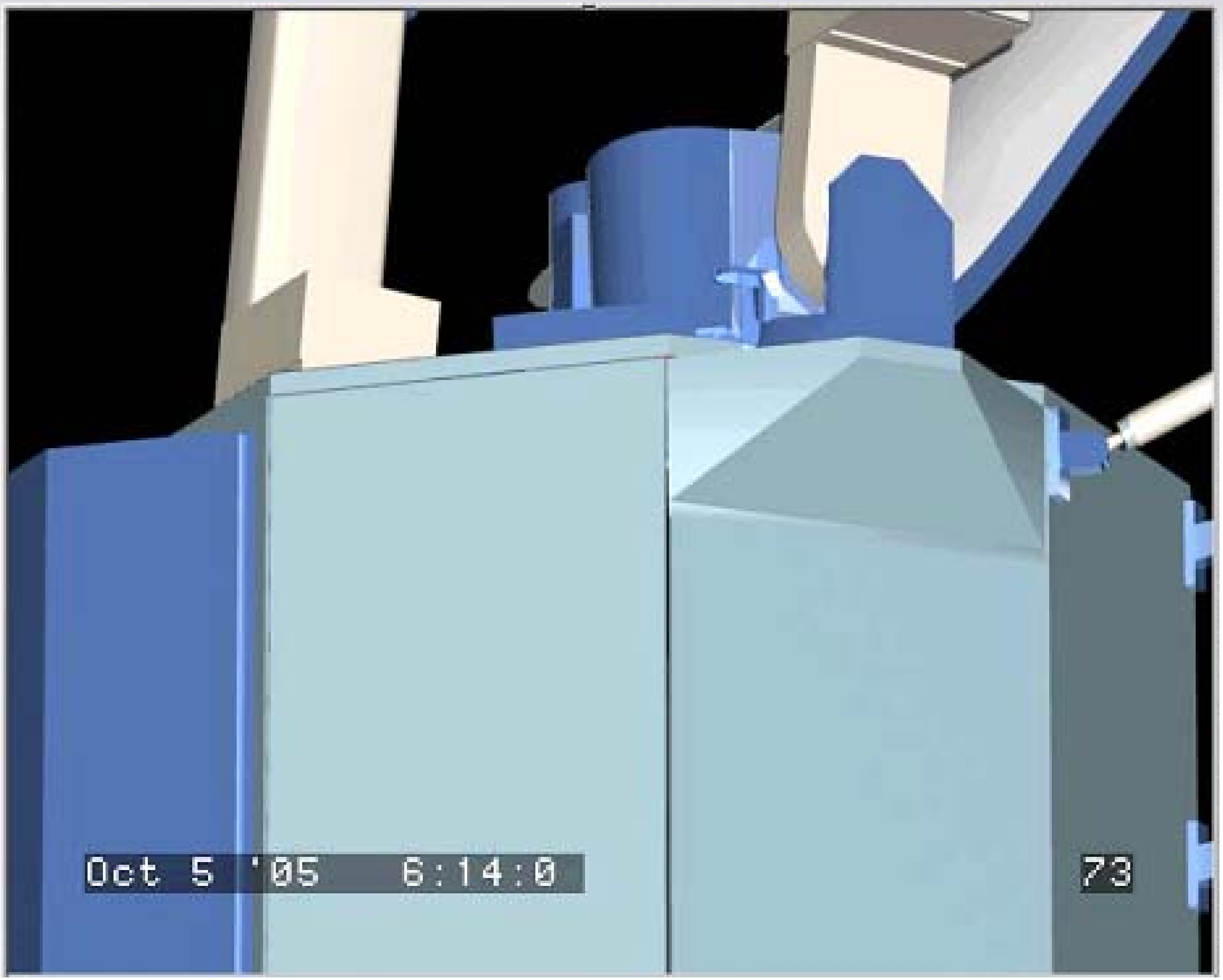

DGS Simulation of Region 4

1.11
0.00
5.00
4.67

Oct 29 2003 00:00:0.0

Frame 435

ELT 1:12:30

UTC 01:12:30

Step: 10 sec

Refresh: No Limit

SSMIS

Sat: F16

Lat -47.2

Lon -69.0

Alt 063

sunaz 28.4

sunel -16.3

sunwl 43.4

suncs 101.0

suncn 71.3

SSMIS 9.00

310

Beam Position 319.00

Scan Angle 255.20 deg

Latitude vs. Scan Number for Rev 140: Ch 1

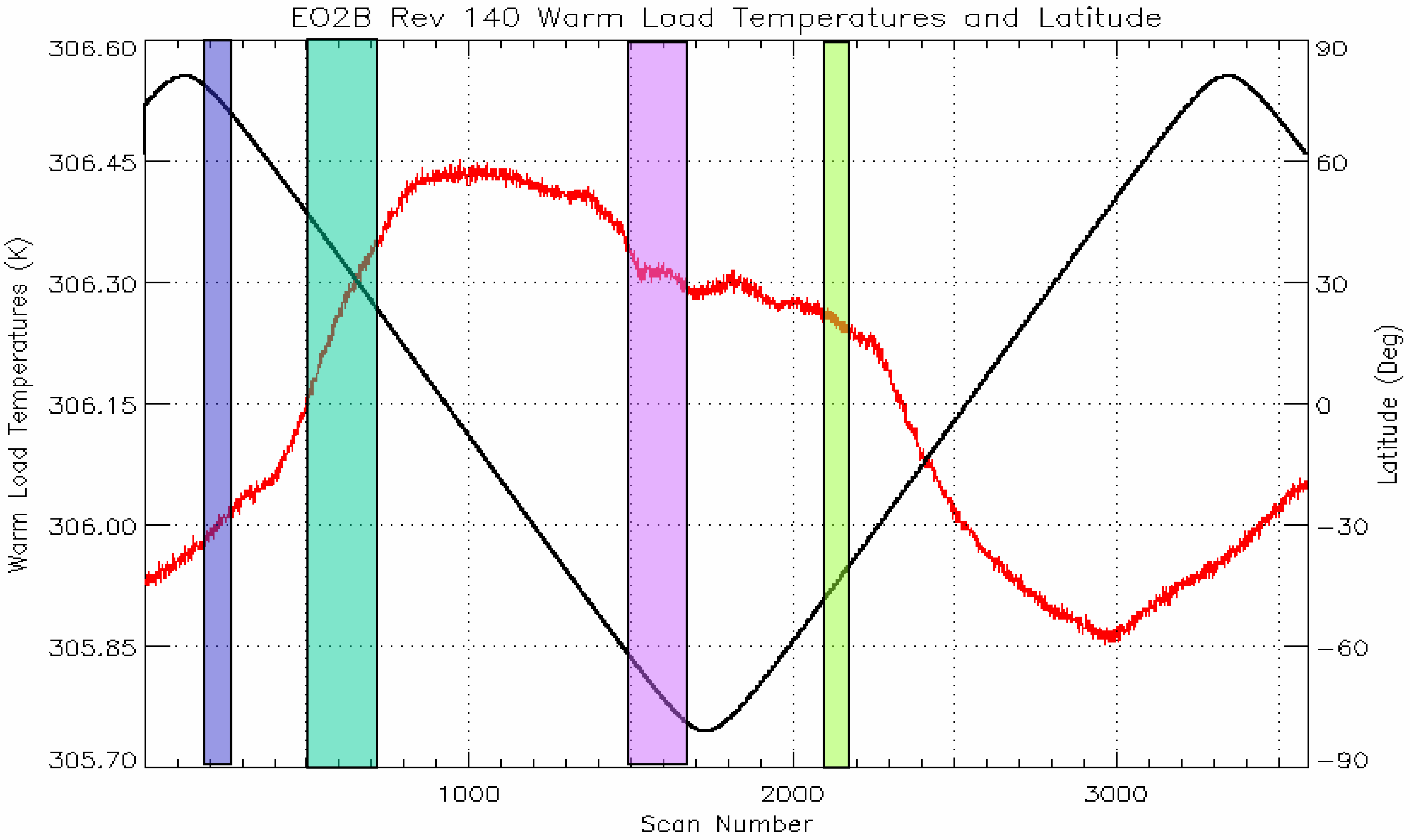

Sun Glint on Warm Load Shown in EO data: Ch 1

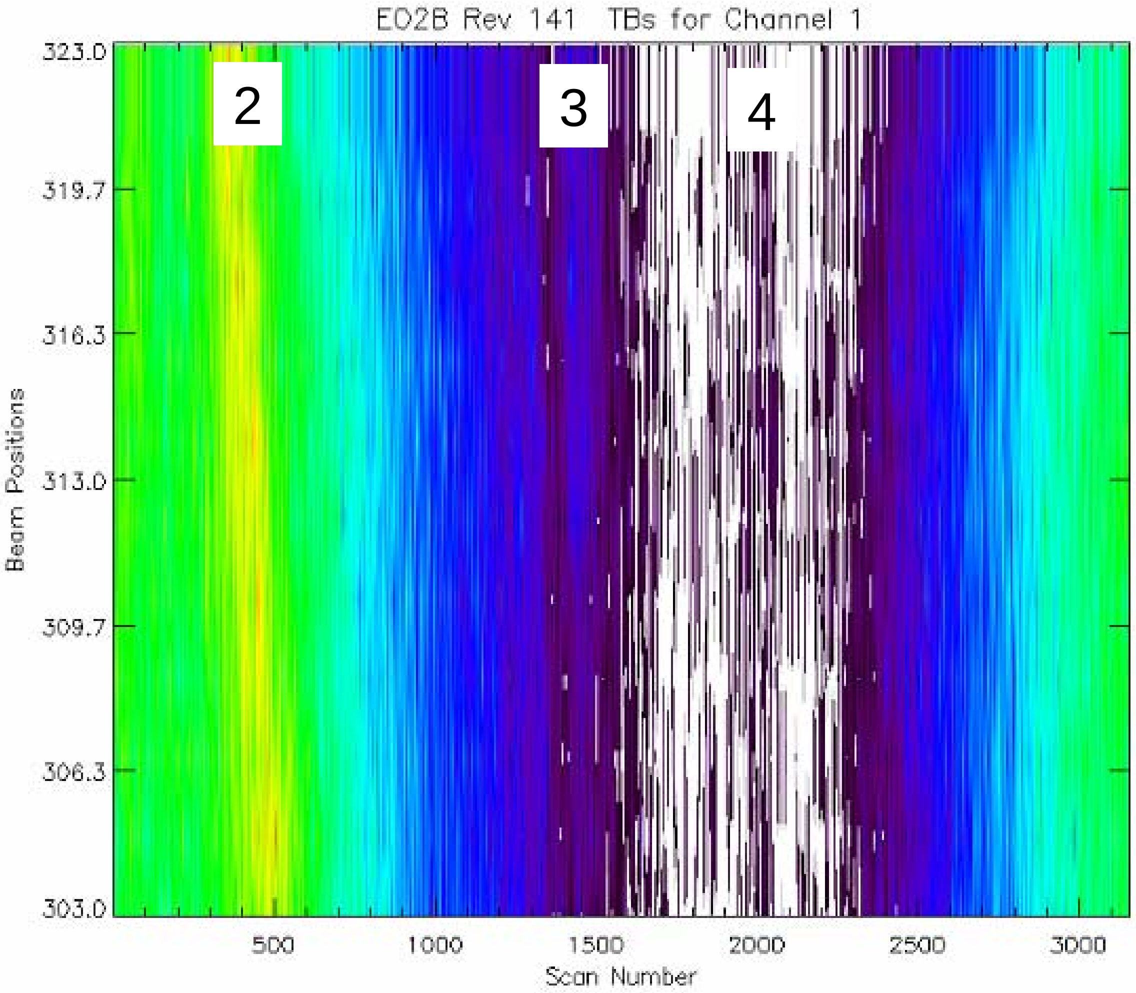

Solar Angle vs. Channel 15 EO Warm Load Anomalies

Region	Latitude	WL El	WL Az	ΔT_B(K)	Notes
1	75 Desc	-5	75	2	
2 BP 315	47 Desc	15	72	3	Along scan
2 BP 287	30 Desc	22	69	2	Along scan
3 BP 287	-60 Desc	39	33	<1	Under lip
3 BP 315	-54 Desc	40	35	<1	Under lip
4	-67 Asc	-5	20	<1	Very weak

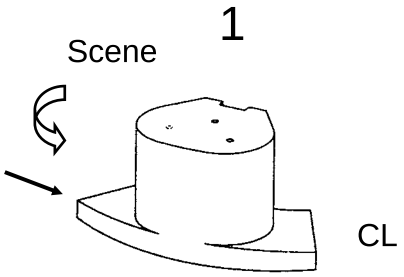

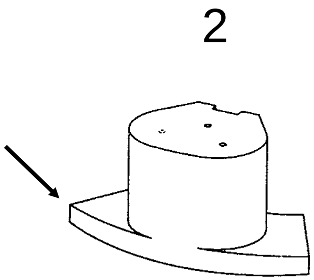

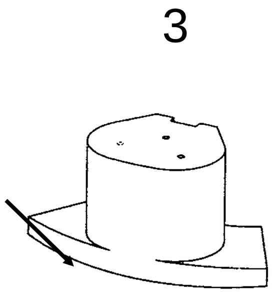

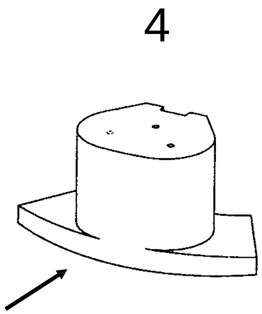

11.4 Effect of Warm Load Solar Intrusions on SSMIS Calibration in Normal Mode

The effect of transient changes in the effective radiometric brightness temperature of the SSMIS warm load on the sensor calibration can be seen in Channel 4 data. Page 11-31 shows plots of the scaled radiometric counts from Channel 4 with the 4 WL anomaly regions identified. The graph on page 11-32 identifies the four regions against the orbit timeline and spacecraft latitude. Page 11-33 shows the image of effective relative radiometric brightness of the WL as a function of time and position. Recall the BP used for calibrating Channel 4 are BP 308 – 311 as identified on page 11-31. The scaled calibration counts for Channel 4 (BP 308 – 311) and Channel 17 are compared on page 11-34 and 11-35 showing some differences in the impact of solar intrusions on a per-channel basis, however, there is general consistency regarding the locations where anomalies occur for each channel. Page 11-36 uses the time and/or S/C latitude position information to determine the angle that the sun is illuminating the WL. The solar illumination data can be used to determine when an anomaly may exist, to flag data for possible errors or used in an algorithm to correct for errors introduced by the solar illumination. Note that on page 11-32, the largest anomaly appears to be on the order of 1.5 K for region 2 and less than 1 K for the other 3 regions in general. However, Region 3 exhibits an interesting double mode behavior. It is interesting that its unique shape can be explained by the DGS simulation. At the point in the orbit shown on page 11-40, the Magnetometer boom on the F-16 S/C is passing between the Sun and the SSMIS WL temporarily blocking the sun. This causes the impact of the anomaly in Region 3 to recede for a short while during the most direct period of interaction.

Sun Glint on Warm Load Shown in EO Data: Ch 4

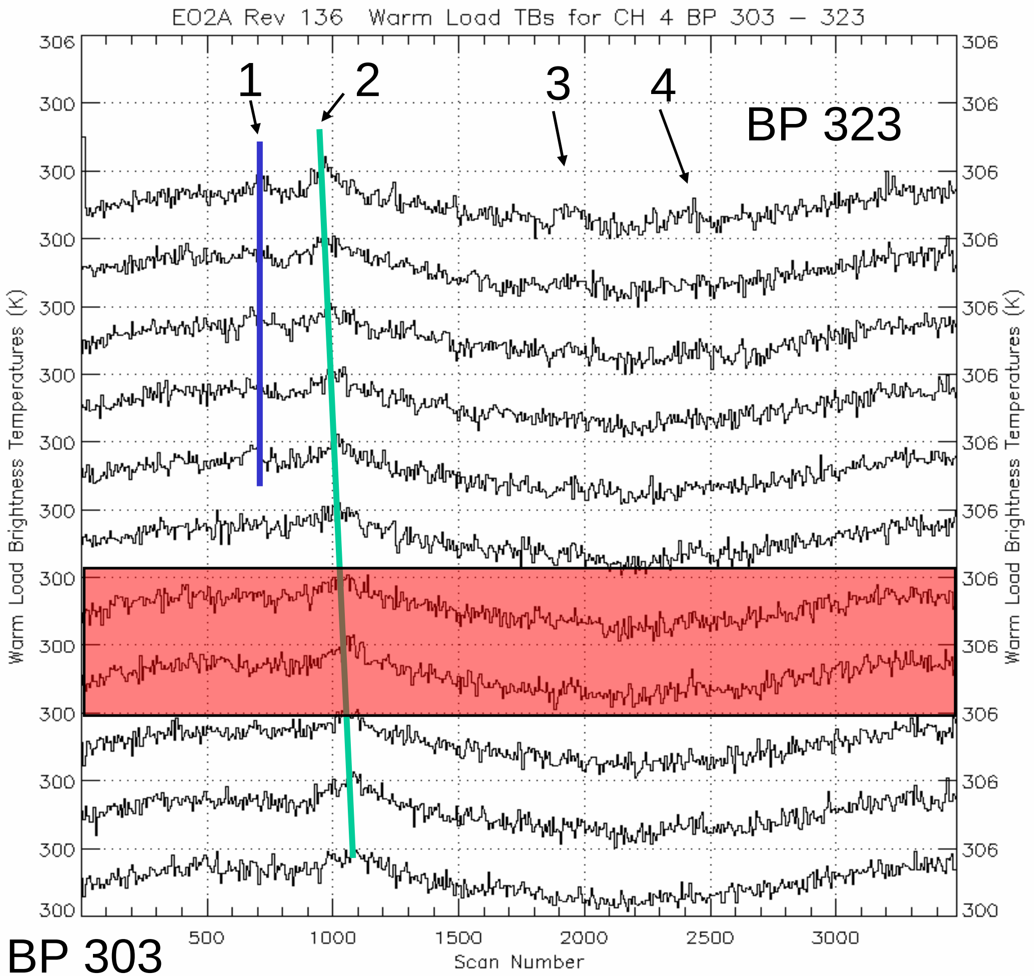

BP 323

BP 303

SSMIS Calibration utilizes BP 308 - 311

Latitude vs. Scan Number for Rev 136

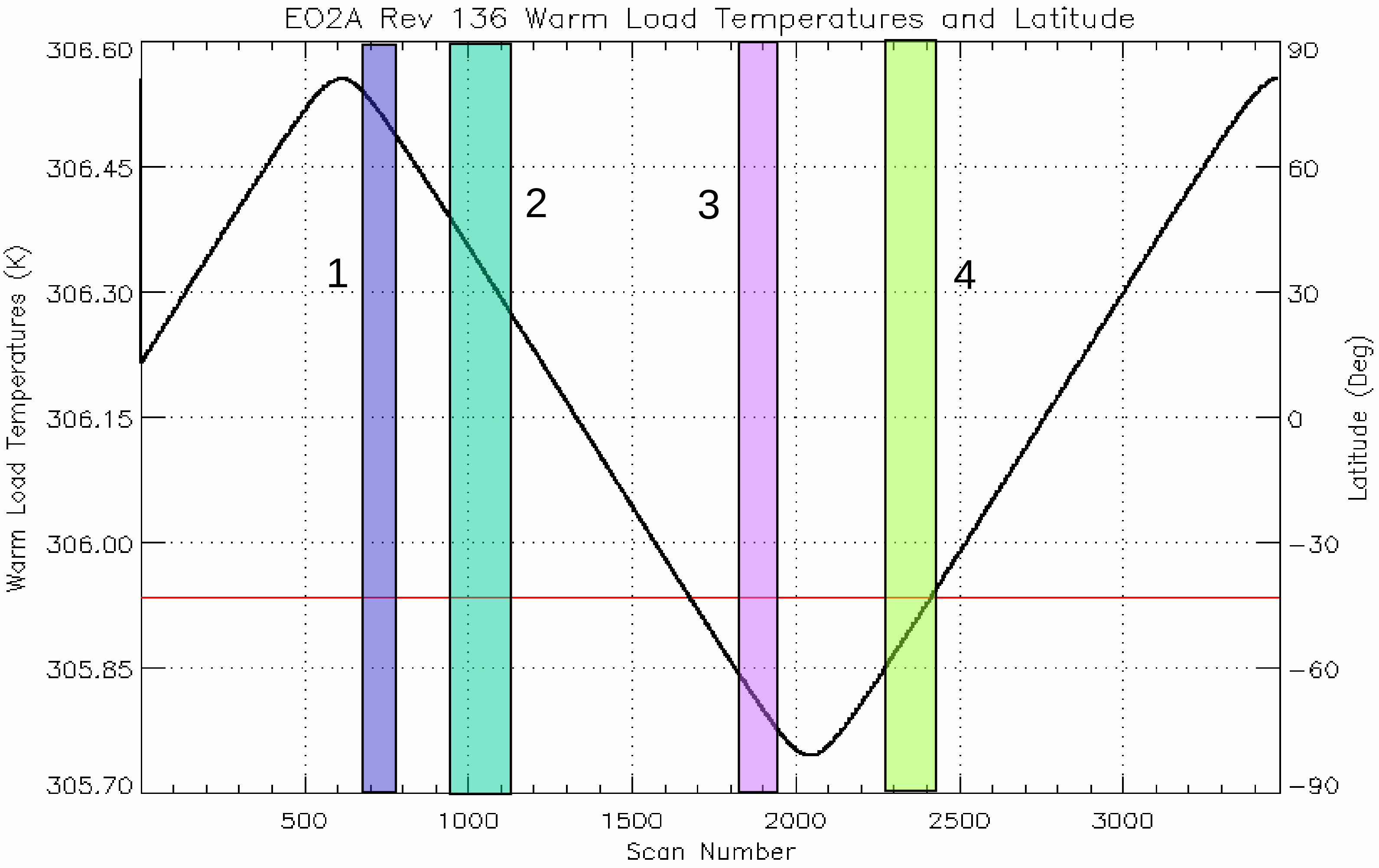

Sun Glint on Warm Load Shown in EO data: Ch 4

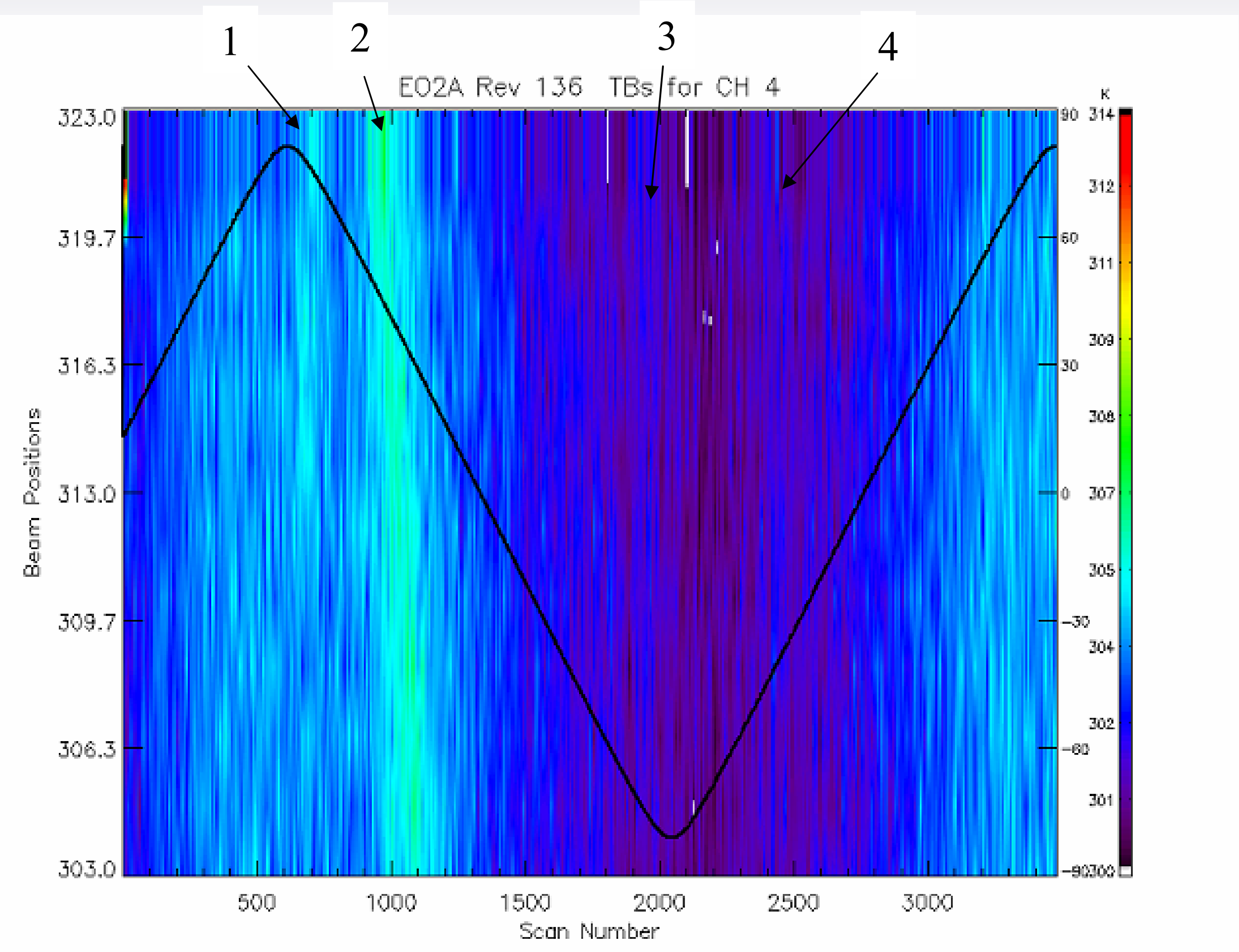

Sun Glint on Warm Load Shown in Normal Mode: Ch 4

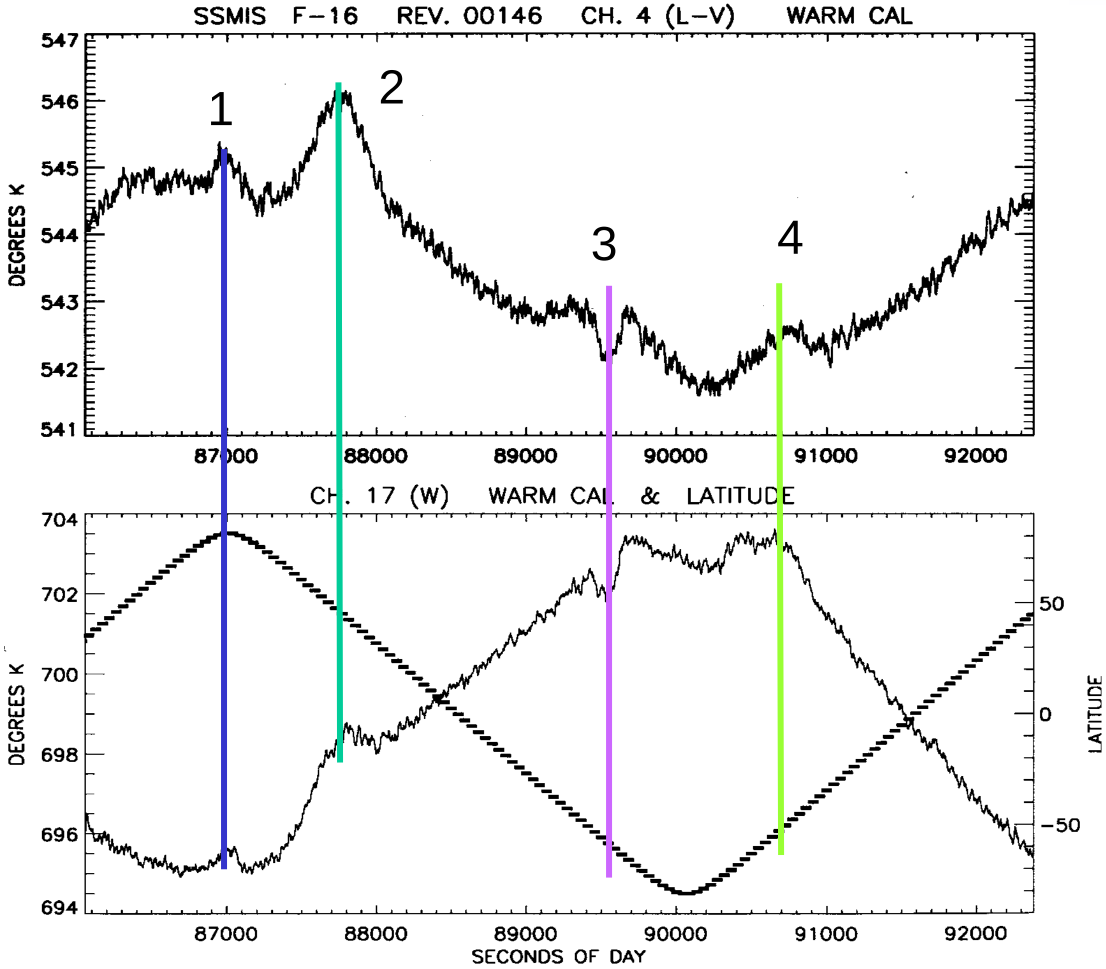

1: ~80° descending

2: ~47° descending

3: ~-60° descending

4: ~-50° ascending

Sun Glint on Warm Load Shown in Normal Mode: Ch 4

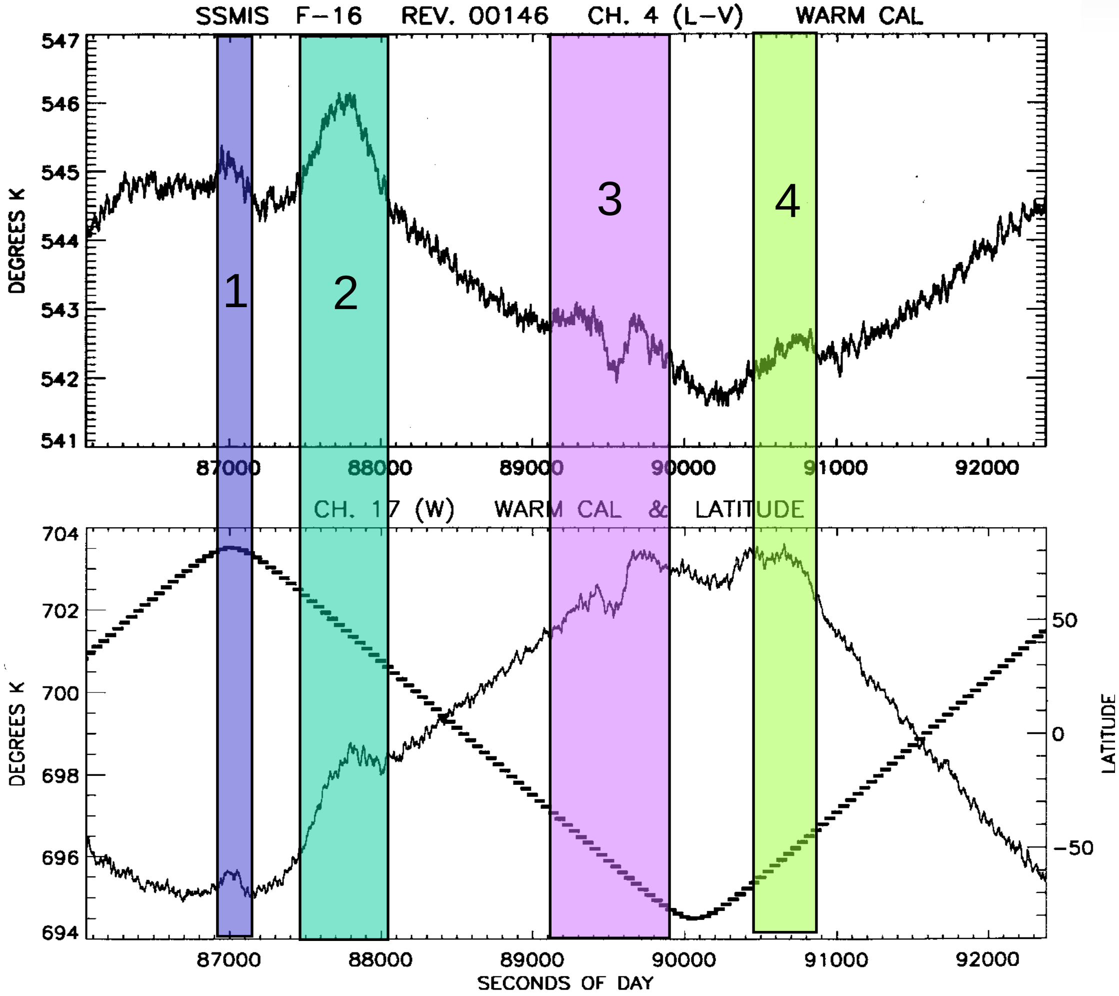

1: ~80° desc

2: ~47° desc

3: ~-60° desc

4: ~-50° asc

SSMIS WL Solar Angle: 29-Oct-2003;

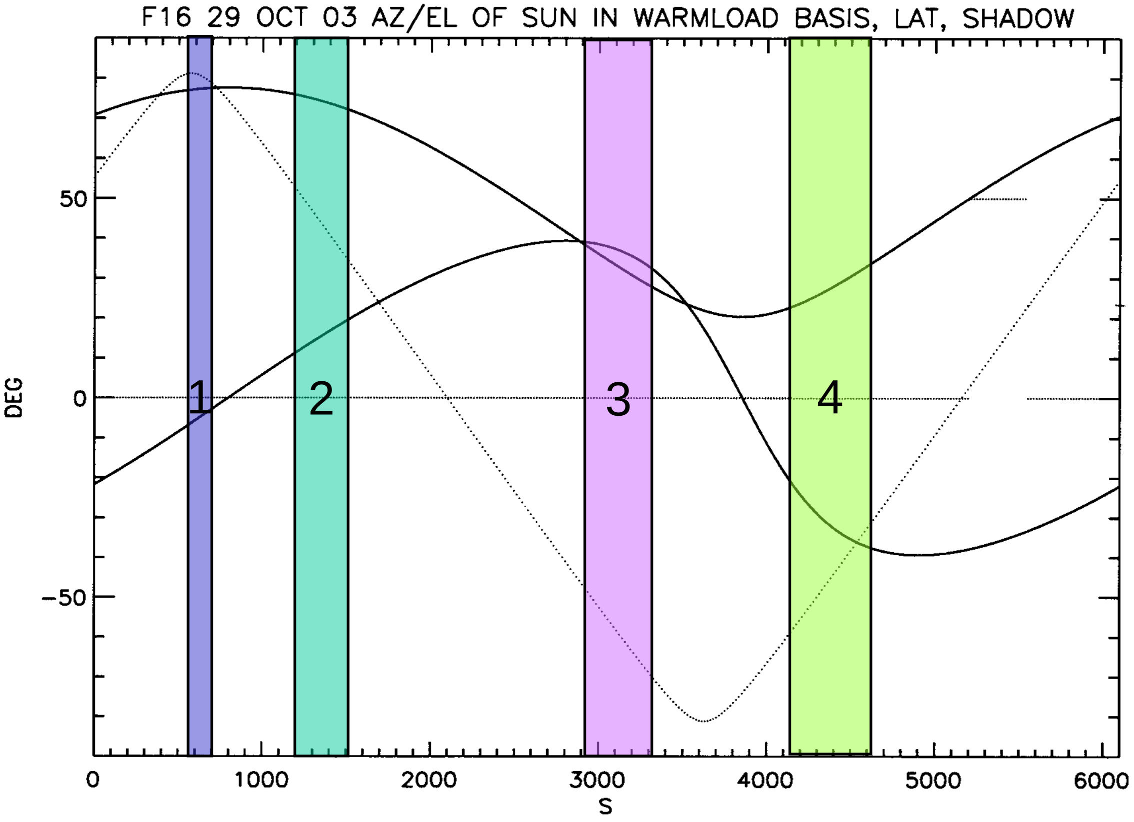

11.5 DGS Simulation of F-16 Vehicle in Warm Load Intrusion Regions

The following pages 11-38 to 11-44 show the DGS F-16 and SSMIS model in the Warm Load Intrusion Regions for October 28, 2003, the period of Early Orbit data collection. Page 11-40 shows the role of the F-16 Magnetometer mast in blocking the sun at the middle of the Region 3 intrusion in turn causing the anomaly to have a smaller overall impact on the sensor calibration. Note that Region 4 shown on page 11-44 with a close-up of the SSMIS sensor shown earlier on page 11-26 indicates the sun is illuminating the reflective surface of the Cold Sky Reflector (CSR) as well as the Warm Load. This may also lead to errors in the SSMIS Cold Calibration as well as the Warm calibration due to errors attributable to emission from the reflector antenna surface as described later in Section 11.7.

DGS Simulation: Region 1, 28-Oct-2003; 80 N Descending

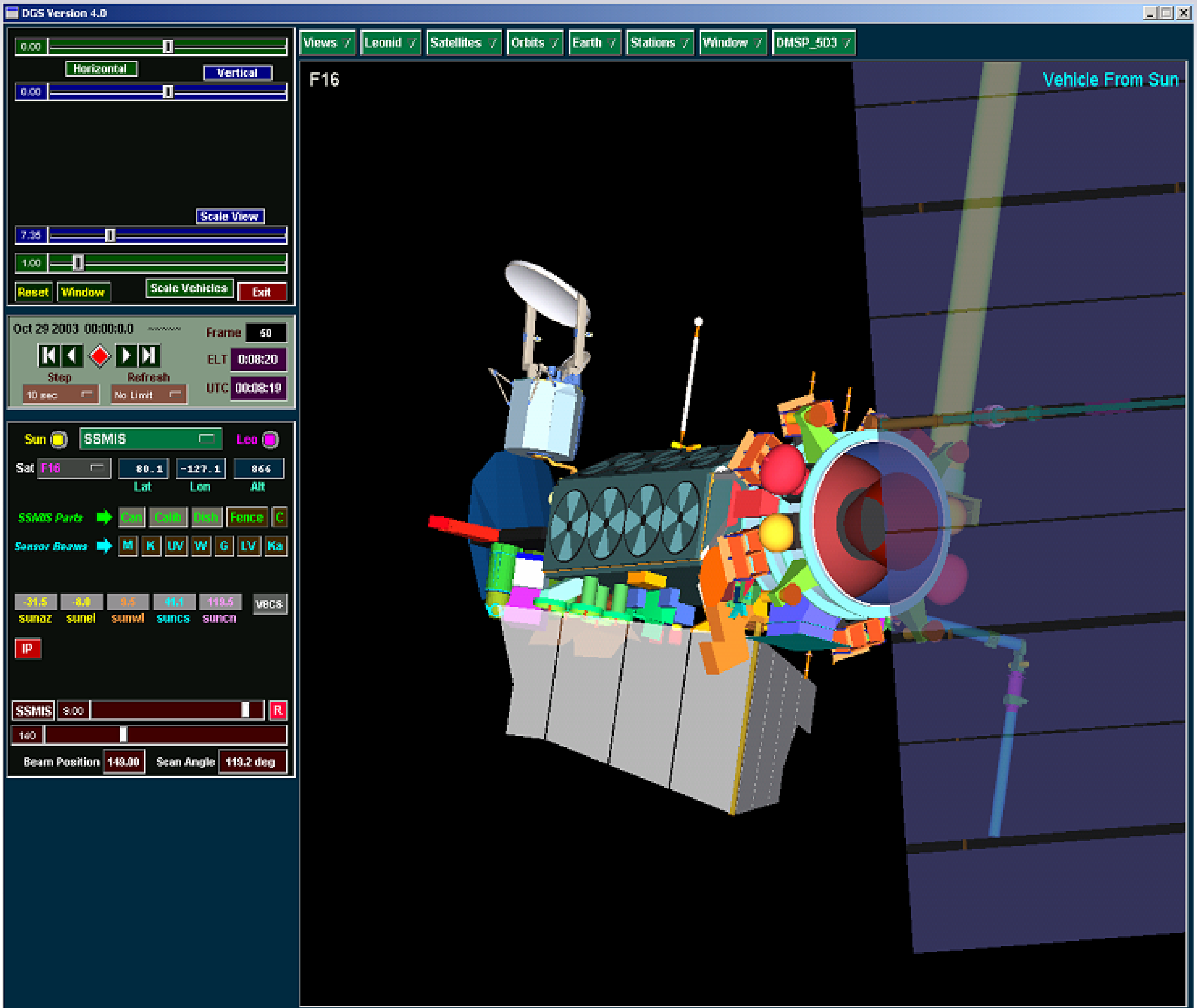

0.00

0.00

7.26

1.00

Oct 29 2003 00:00:0.0

Frame 50

ELT 0:08:20

UTC 00:08:19

Step 10 sec

Refresh No Limit

SSMIS

Sat F16

80.1 Lat

-127.1 Lon

866 Alt

-31.5 sunaz

-8.0 sunel

9.5 sunwl

41.1 suncs

119.5 suncn

SSMIS 9.00

140

Beam Position 149.00

Scan Angle 119.2 deg

DGS Simulation: Region 2, 28-Oct-2003; 46 N descending

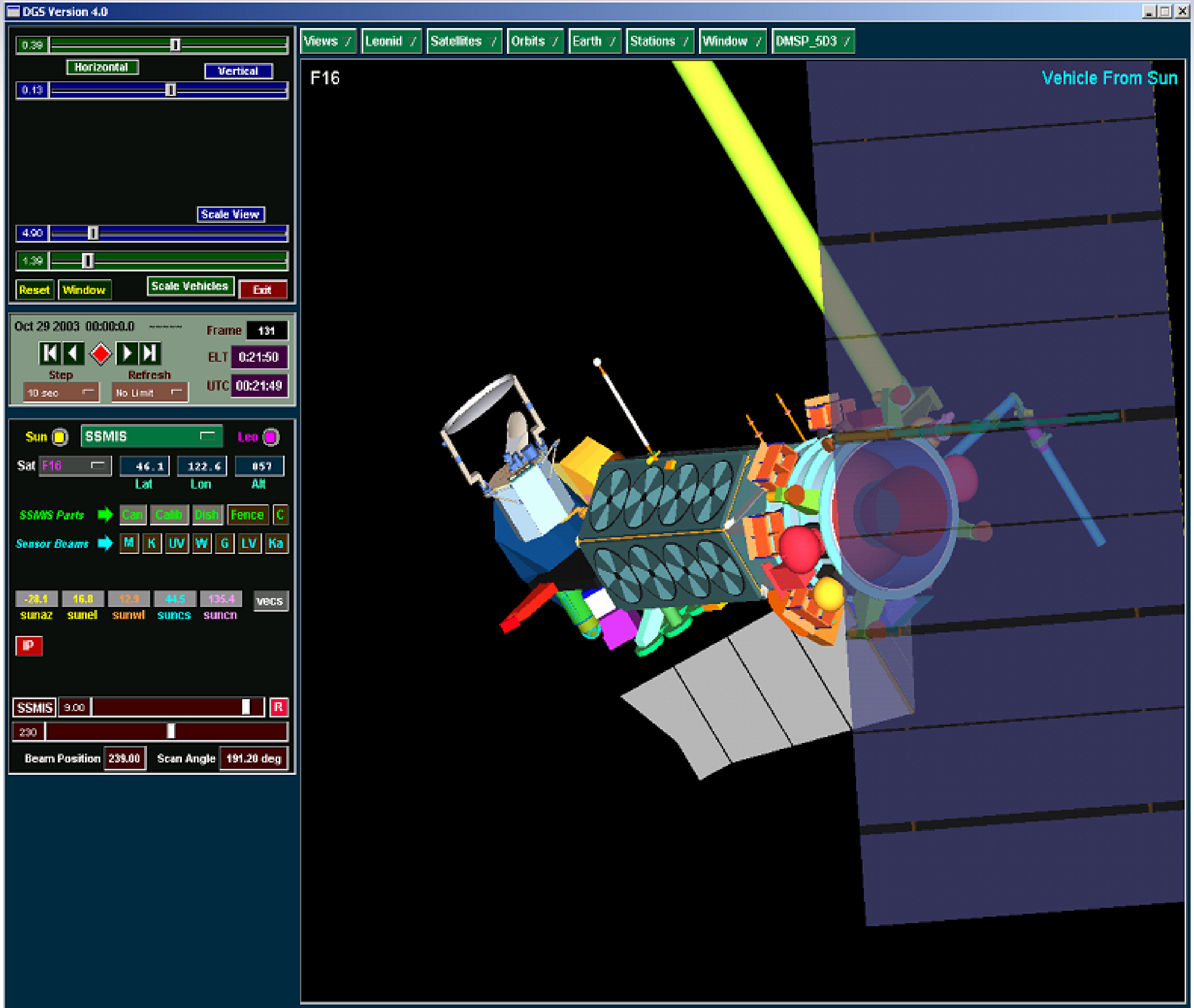

0.39

0.13

4.90

1.39

Oct 29 2003 00:00:0.0 --------

Frame 131

ELT 0:21:50

UTC 00:21:49

Step 10 sec

Refresh No Limit

SSMIS

Sat F16

46.1 Lat

122.6 Lon

857 Alt

-28.1	16.8	12.9	44.5	135.4
sunaz	sunel	sunwl	suncs	suncn

SSMIS 9.00

230

Beam Position 239.00

Scan Angle 191.20 deg

DGS Simulation Region 3; 28-Oct-2003; 40 S descending

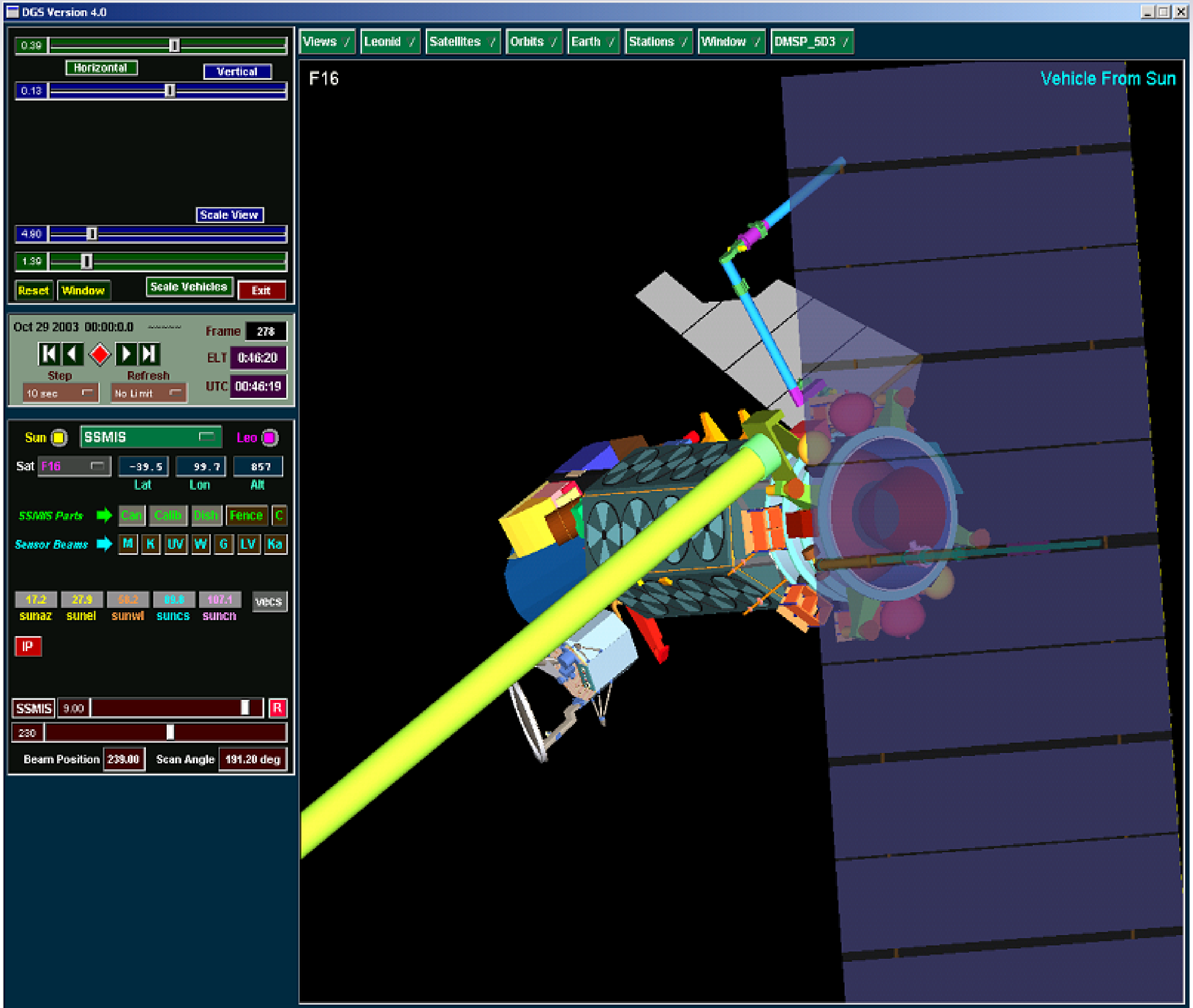

Oct 29 2003 00:00:0.0

Frame 278

ELT 0:46:20

UTC 00:46:19

Step 10 sec

Refresh No Limit

SSMIS

Sat F16

-39.5 Lat

99.7 Lon

857 Alt

17.2 sunaz

27.9 sunel

50.2 sunwl

89.8 suncs

107.1 sunch

SSMIS 9.00

230

Beam Position 239.00

Scan Angle 191.20 deg

DGS Simulation Region 3; 28-Oct-2003; 50 S descending

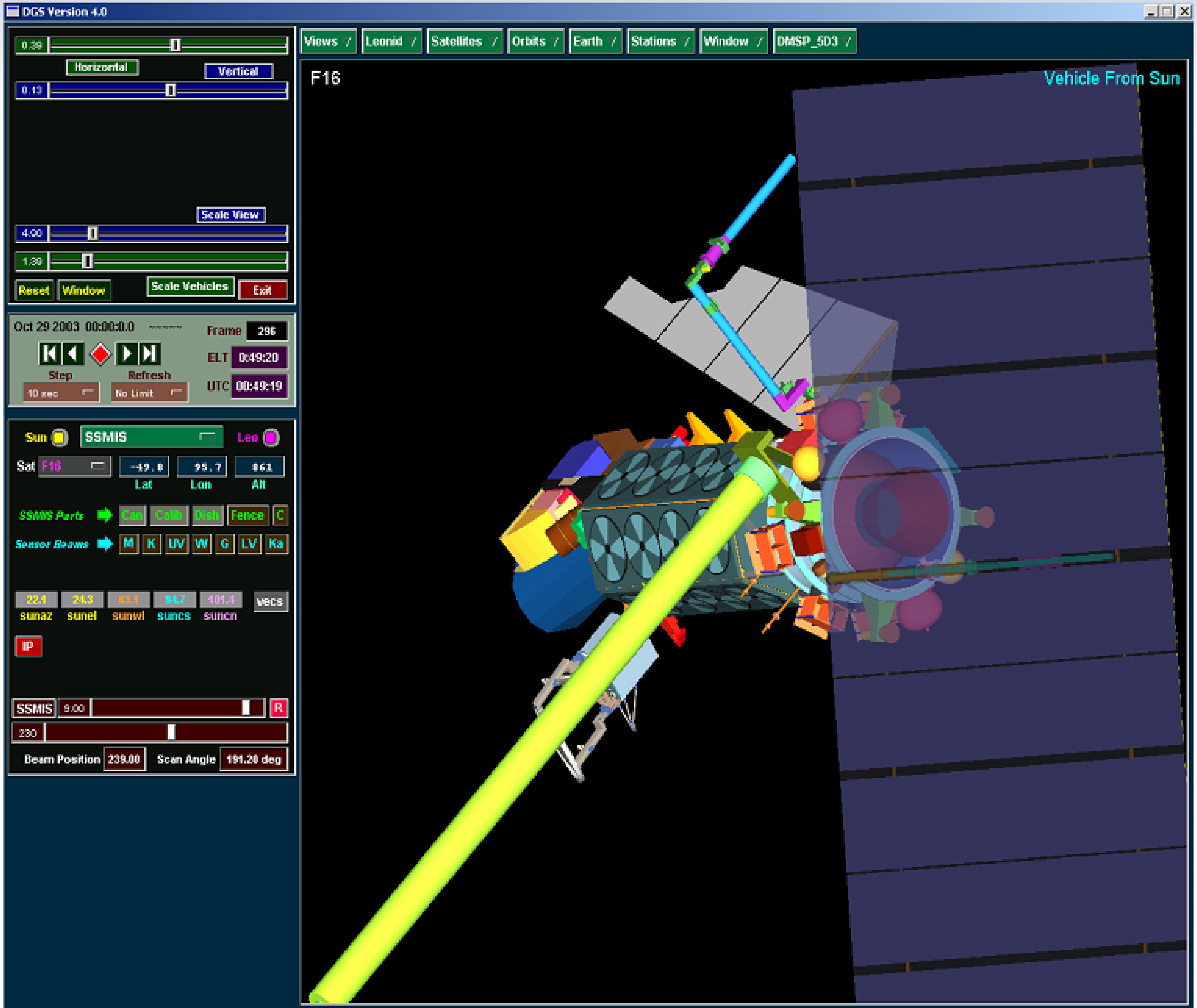

Oct 29 2003 00:00:0.0

Frame 296

ELT 0:49:20

UTC 00:49:19

Step 10 sec

Refresh No Limit

SSMIS

Sat F16

Lat -49.8

Lon 95.7

Alt 861

sunaz 22.1

sunel 24.3

sunwl 63.1

suncs 94.7

suncn 101.4

Beam Position 239.00

Scan Angle 191.20 deg

DGS Simulation Region 3; 28-Oct-2003; 74 S Ascending

0.00

0.00

7.35

1.00

Oct 29 2003 00:00:0.0

Frame 340

ELT 0:56:40

UTC 00:56:40

Step 10 sec

Refresh No Limit

SSMIS

Sat F16

-73.9 Lat

71.9 Lon

869 Alt

30.0

12.7

71.0

102.6 suncs

88.3

SSMIS 9.00

240

Beam Position 249.00

Scan Angle 199.20 deg

DGS Simulation: Region 4, 28-Oct-2003; 62 S Ascending

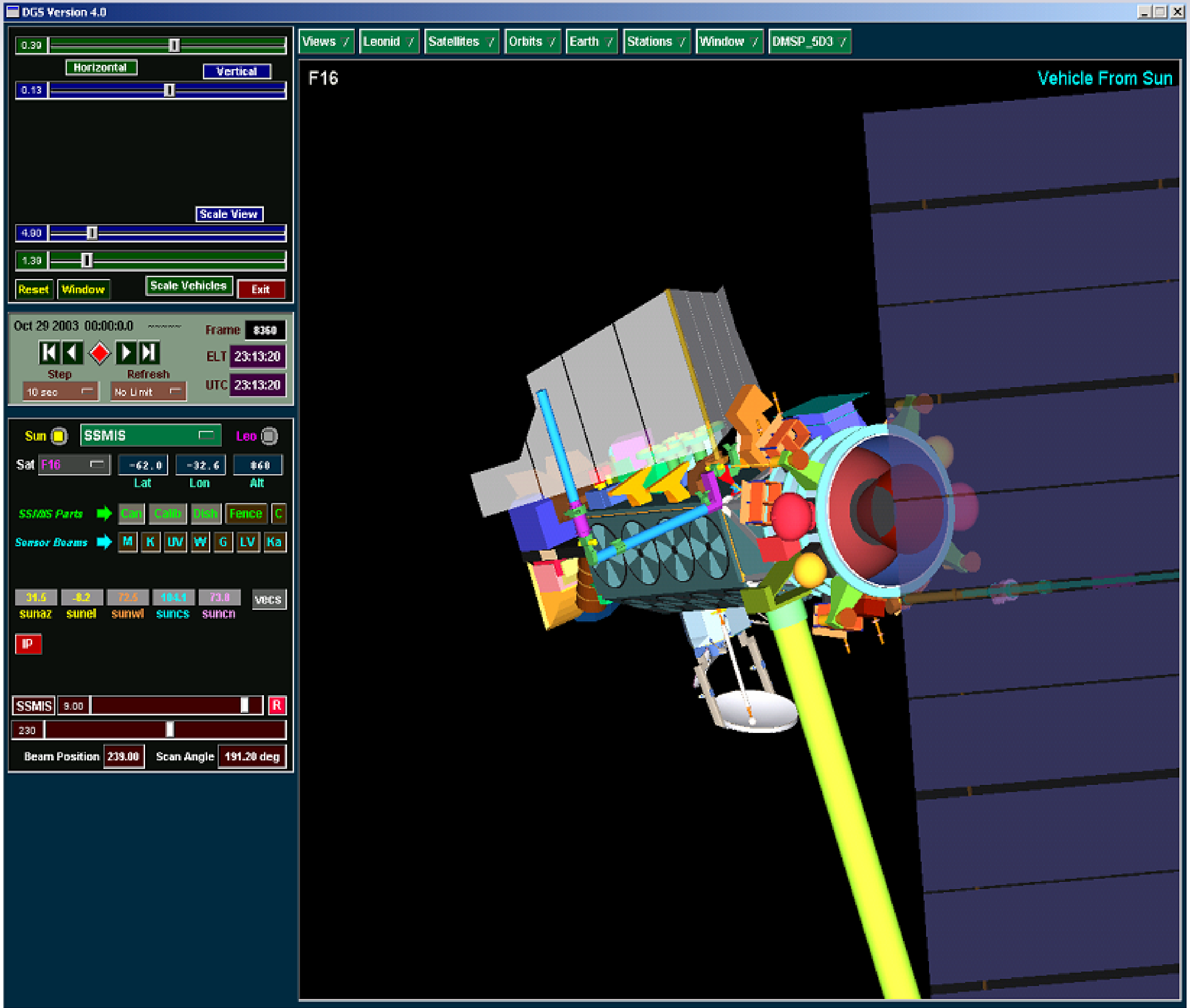

DGS Version 4.0

Oct 29 2003 00:00:0.0

Frame 8360

ELT 23:13:20

UTC 23:13:20

Step 10 sec

Refresh No Limit

Sat F16

Lat -62.0

Lon -32.6

Alt 860

sunaz 31.5

sunel -8.2

sunwl 72.5

suncs 104.1

suncn 73.8

SSMIS 9.00

230

Beam Position 239.00

Scan Angle 191.20 deg

DGS Simulation: Region 4, 28-Oct-2003; 50 S Ascending

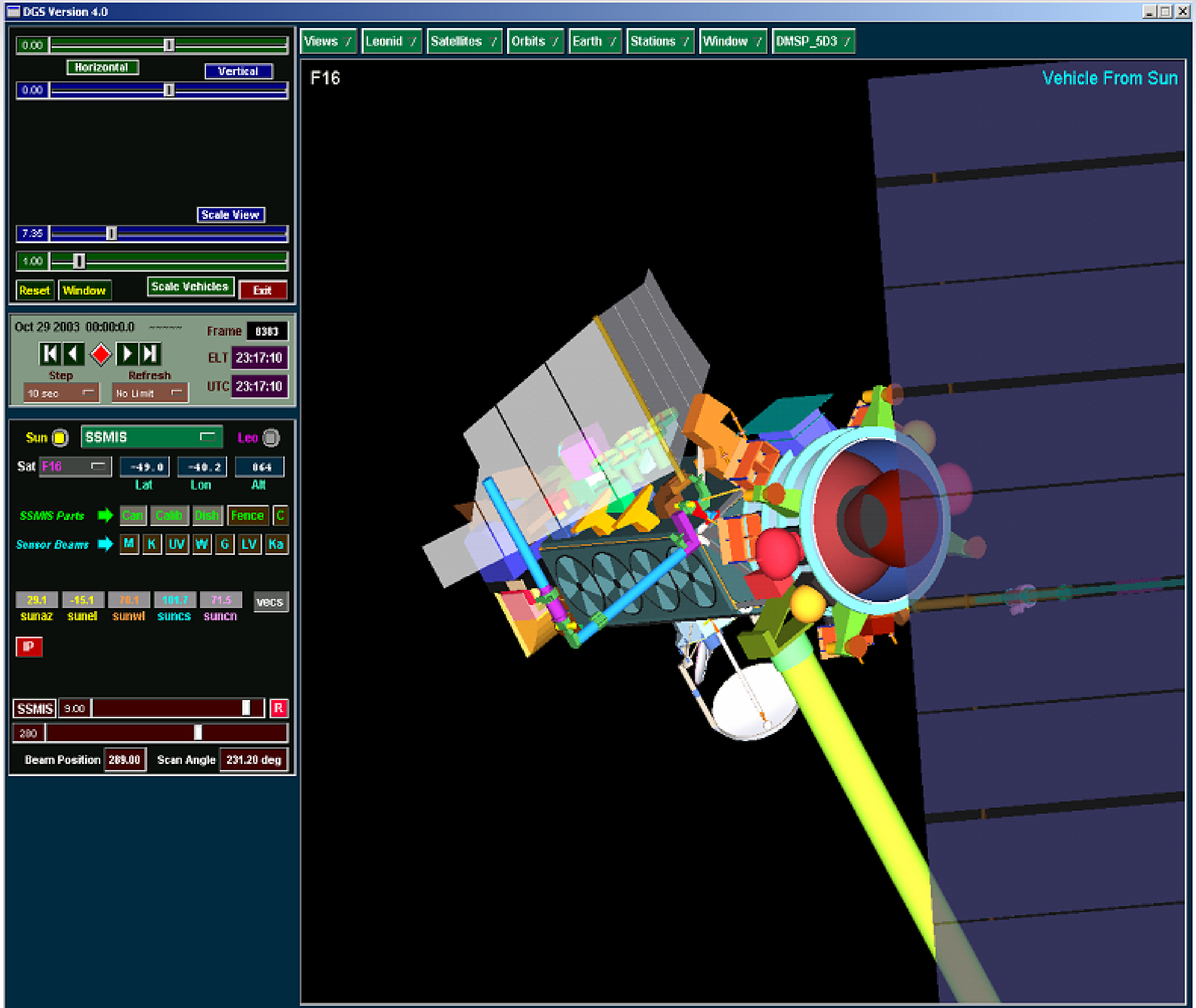

Oct 29 2003 00:00:0.0

Frame 0383

ELT 23:17:10

UTC 23:17:10

Step 10 sec

Refresh No Limit

SSMIS

Sat F16

Lat -49.0

Lon -40.2

Alt 064

sunaz 29.1

sunel -15.1

sunwl 70.1

suncs 101.7

suncn 71.5

SSMIS 9.00

280

Beam Position 289.00

Scan Angle 231.20 deg

11.6 Summary of the Initial SSMIS Warm Load Solar Intrusion Analysis

The previous pages in this Section described the initial investigation of residual calibration errors attributable to solar heating and thermal gradients on the SSMIS warm load. In general four regions where these errors are large (~< 1K) were identified. Two of the Regions are characterized by direct illumination of the warm load tines (1) and (4) and will be addressed in Section 12 of this report as the Direct #1 (D1) and Direct #2 (D2) WL anomalies. The other 2 Regions (2) and (3) are the result of reflected sunlight from the top of the SSMIS canister and will be called the Reflected #1 (R1) and Reflected #2 (R2) WL anomalies. For the F-16 orbit, (2) and (3) have larger impacts to the SSMIS Calibration than (1) or (4) in general. As shown in the graph on page 11-36, and the multiple ray tracing examples on pages 11-13, 14, 19, 25 and 26, the WL anomalies are defined by the solar angle of illumination of the Warm Load throughout the orbit. The angle of the sun with respect to the warm load and CSR was defined in Section 11.2 and will be used in SSMIS data processing to flag data with a high possibly of increased calibration error and is applied in algorithms to correct the residual calibration error caused by the WL gradients as described in the following Section .

11.7 Warm Load Anomaly Analysis: Phase 2

11.7A Early Orbit Mode 2 Data Collection in 2005

The Early Orbit (EO) analysis described in Section 11.7 was designed to support development of correction schemes for the warm load anomalies. The EO Warm Load imaging used with ECMWF backgrounds, sensor telemetry, DGS and the ray trace physical model can all be used together to determine the best way forward to minimize the impact of WL solar anomalies. The EO analyses was also designed to elucidate the effect of Doppler correction on brightness temperatures. The EO 2005 experiment was designed to collect 2 days of EO2A, and 1 day each of EO2B and EO2C. This was to be followed by a week of Normal mode data with Doppler correction off and then repeat the EO2A, B and C periods with the Doppler off in Phase B and then return to Normal mode with Doppler on. However, the instrument experienced difficulties midway through phase B after entering the EO2A mode. At this point the EO2 collect was discontinued and the instrument returned to its nominal configuration operating the normal mode with the Doppler correction on.

Early Orbit Mode 2 Data from S/N02 (2005)

Phase A Doppler On

Date	REV	Mode
2005018	6472	EO2A
	6473	EO2A
2005019	6474	EO2A
	6475	EO2A
	6476	EO2A
	6477	EO2A
	6478	EO2A
	6479	EO2A
	6480	EO2A
	6481	EO2A
	6482	EO2A
	6483	EO2A
	6484	EO2A
	6485	EO2A
	6486	EO2A
	6487	EO2A
2005020	6488	EO2A
	6489	EO2A
	6490	EO2A
	6491	EO2A
	6492	EO2A
	6493	EO2A
	6494	EO2A
	6495	EO2A

Date	REV	Mode
2005020	6496	No Synch
	6497	No Synch
	6498	No Synch
	6499	No Synch
	6500	EO2B
	6501	EO2B
2005021	6502	EO2B
	6503	EO2B
	6504	EO2B
	6505	EO2B
	6506	EO2B
	6507	EO2B
	6508	EO2B
	6509	EO2B
	6510	EO2B
	6511	EO2B
	6512	EO2B
	6513	EO2B
	6514	EO2C
	6515	EO2C
	6516	EO2C (?)
2005022	6517	EO2C
	6518	EO2C
	6519	EO2C

Date	REV	Mode
2005022	6520	EO2C
	6521	EO2C
	6522	EO2C
	6523	EO2C
	6524	EO2C
	6525	EO2C
	6526	EO2C
	6527	EO2C
	6528	EO2C
	6529	EO2C
	6530	EO2C (?)
2005023	6531	EO2C
2005024	--	EO2C
	6556	EO2C/Nor
	6557	Normal
	6558	Normal
2005025	--	Normal
2005026	--	Normal
2005027	--	Normal
2005028	--	Normal
2005029	--	Normal
2005030	--	Normal
2005031	--	Normal
2005031	6655	EO2A

Date	REV	Mode
2005031	6656	EO2A
	6657	EO2A
2005032	6658	EO2A
	6659	EO2A
	6660	EO2A
	6661	EO2A
	6662	EO2A
	6663	EO2A
	6664	EO2A
	6665	No Synch
	6666	No Synch
	6667	No Synch
	6668	No Synch
	6669	No Synch
	6670	No Synch
	6671	No Synch
2005033	--	No Synch
2005034	--	No Synch
2005035	--	No Synch

🟩 Phase B: Doppler Off

EO experiment ended after synch word was lost during EO2A mode in Phase B

11.7B DGS and Ray Tracing Simulation Summary of the Four Warm Load Anomaly Regions

The following series of graphics show SSMIS (DGS and Ray Tracing) and the F-16 vehicle (DGS only) in orbit during the period of the 2005 EO2 data collection period (January 18, 2005). This series of charts illustrates the four general regions of the WL anomaly for this EO2 data collection period. Region 1 (Direct Illumination #1) is shown on pages 11 - 50, 51 and 52. This is characterized by occurrences in the Northern Hemisphere when the solar elevation angle is slightly below the canister top deck and the solar azimuth angle is low (ϕ ~-10° to +15°).

Region 1: DGS Simulation January 18, 2005 07:58 Z

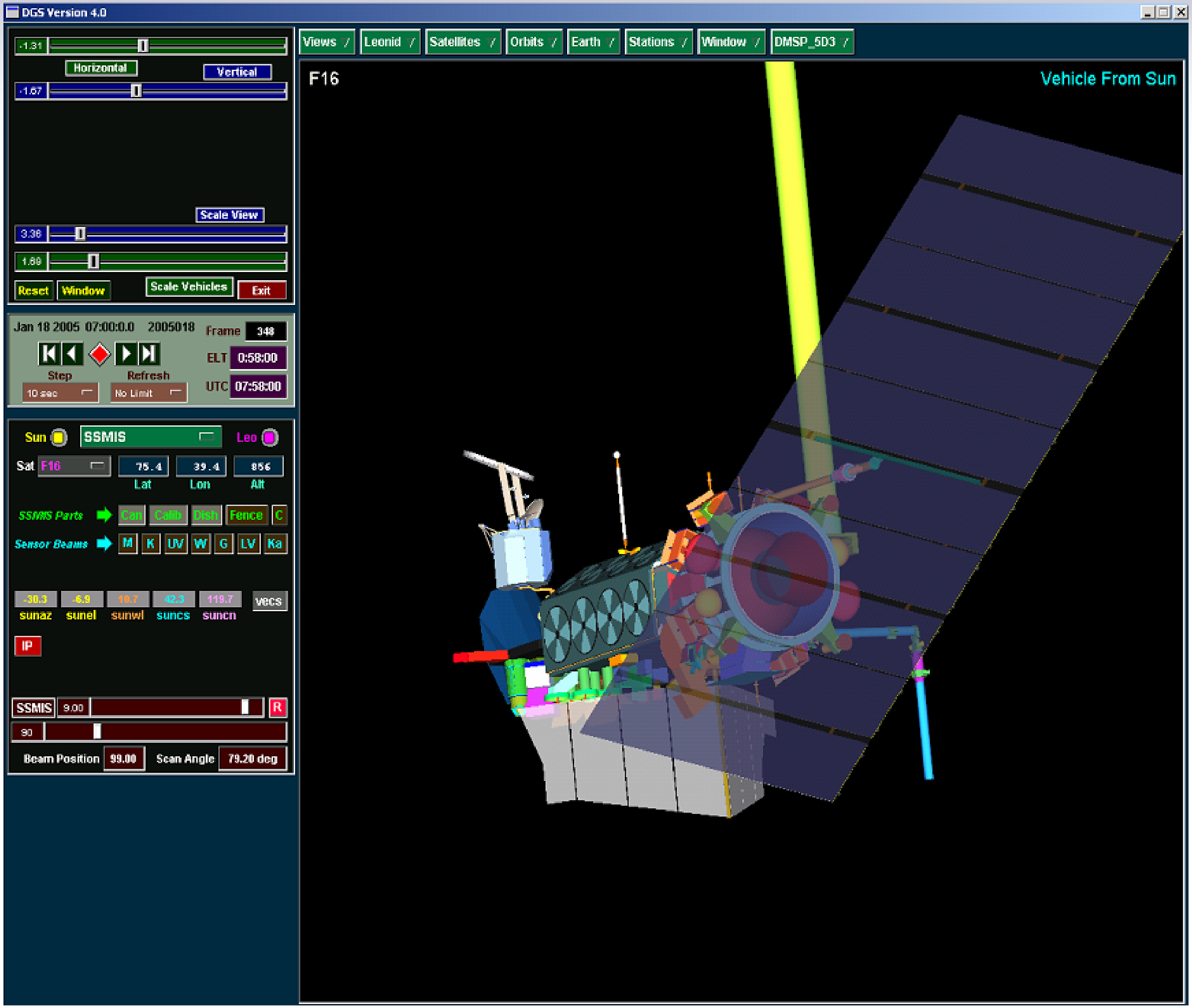

DGS Version 4.0

-1.31

-1.67

3.36

1.69

Jan 18 2005 07:00:0.0 2005018

Frame 348

ELT 0:58:00

UTC 07:58:00

Step 10 sec

Refresh No Limit

SSMIS

Sat F16

Lat 75.4

Lon 39.4

Alt 856

sunaz -30.3

sunel -6.9

sunwl 10.7

suncs 42.3

suncn 119.7

SSMIS 9.00

90

Beam Position 99.00

Scan Angle 79.20 deg

F16

Vehicle From Sun

Region 1: DGS Simulation January 18, 2005 07:58 Z

3.94

-1.31

10.83

1.69

Jan 18 2005 07:00:0.0 2005018

Frame 348

ELT 0:58:00

UTC 07:58:00

Step 10 sec

Refresh No Limit

Sat F16

75.4 Lat

39.4 Lon

856 Alt

-30.3 sunaz

-6.9 sunel

10.7 sunwl

42.3 suncs

119.7 suncn

SSMIS 9.00

40

Beam Position 49.00

Scan Angle 39.20 deg

Region 1: Ray Trace Simulation January 18, 2005 07:58 Z

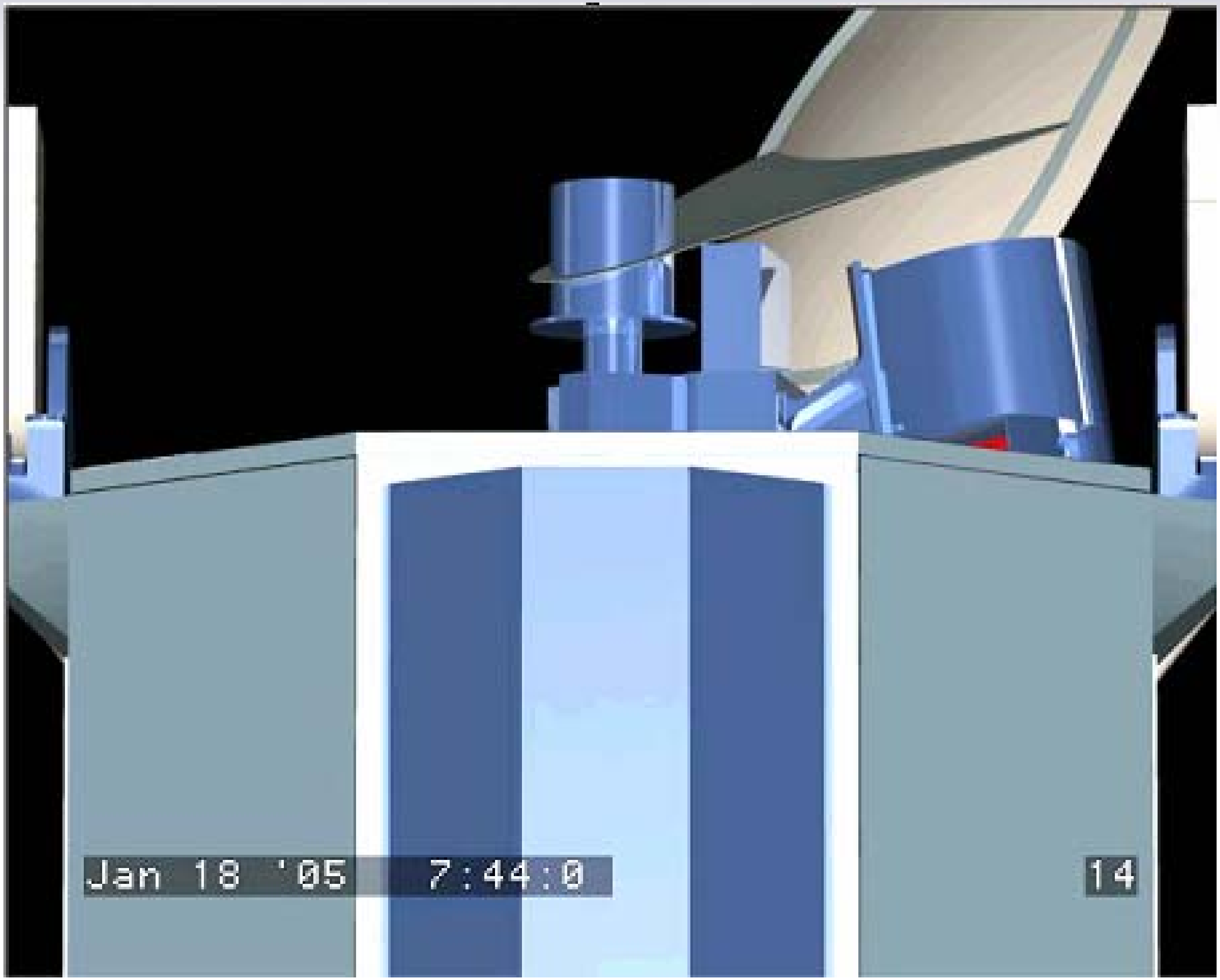

Region 2 (Reflected #1)

Pages 11- 54 and 11- 55 show the DGS Simulation of F-16 with SSMIS in the center of the Warm Load “Region 2” Anomaly. The red tines of the warm load can not be seen because DGS does not have the ability to show reflected images. This is why the ray tracing model, shown on page 11 - 56 for this region is included. Region 2 typically causes the largest calibration bias of any SSMIS Warm Load anomaly regions and is characterized by solar illumination elevation angle θ > 0° and ~<25° - 30° with solar azimuth angles, ϕ > 0° and ~< 45°.

Region 2: DGS Simulation January 18, 2005 08:09 Z

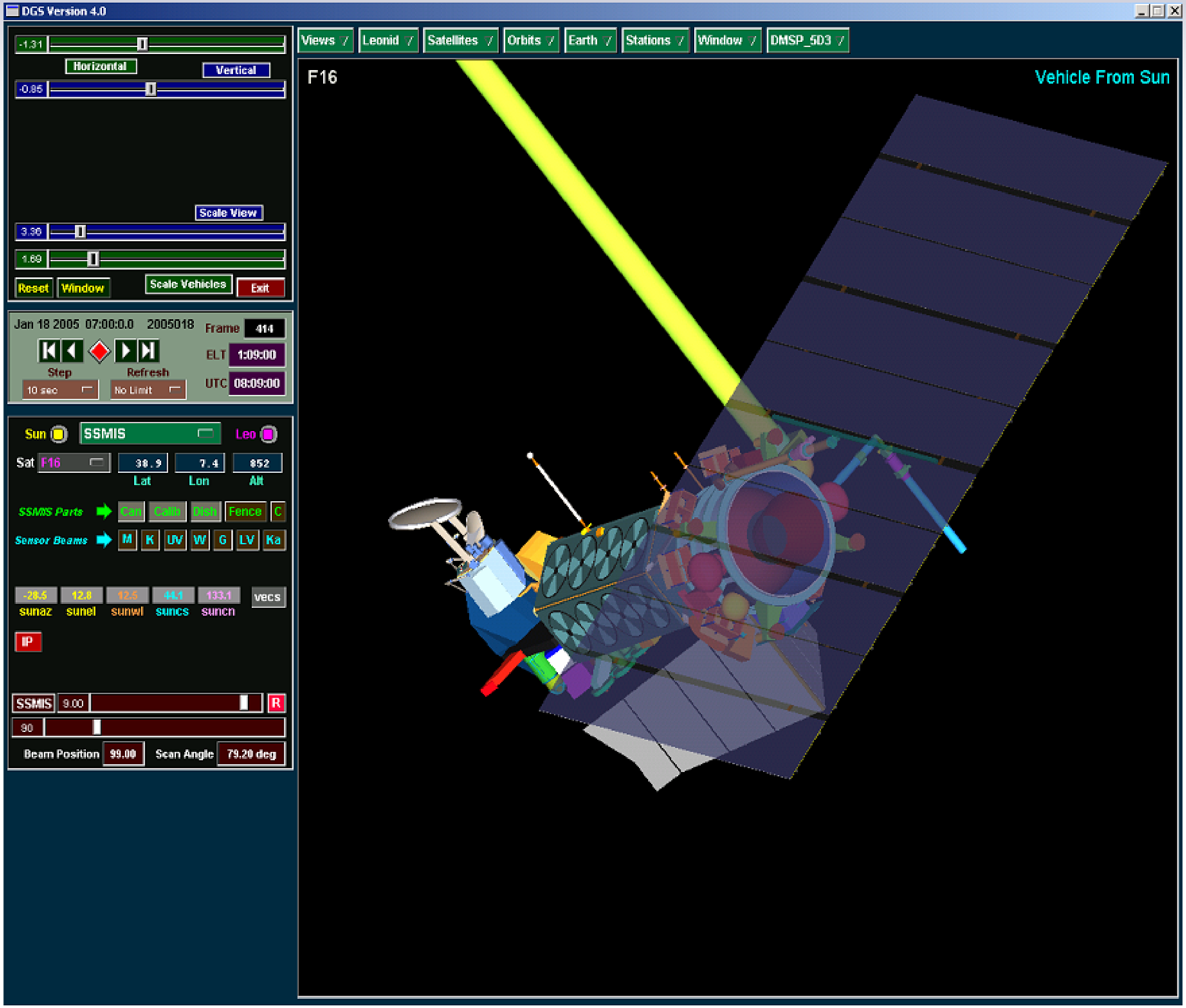

DGS Version 4.0

F16

Vehicle From Sun

Jan 18 2005 07:00:0.0 2005018

Frame 414

ELT 1:09:00

UTC 08:09:00

Step 10 sec

Refresh No Limit

Sat F16

Lat 38.9

Lon 7.4

Alt 852

sunaz -28.5

sunel 12.8

sunwl 12.5

suncs 44.1

suncn 133.1

SSMIS 9.00

90

Beam Position 99.00

Scan Angle 79.20 deg

Region 2: DGS Simulation January 18, 2005 08:09 Z

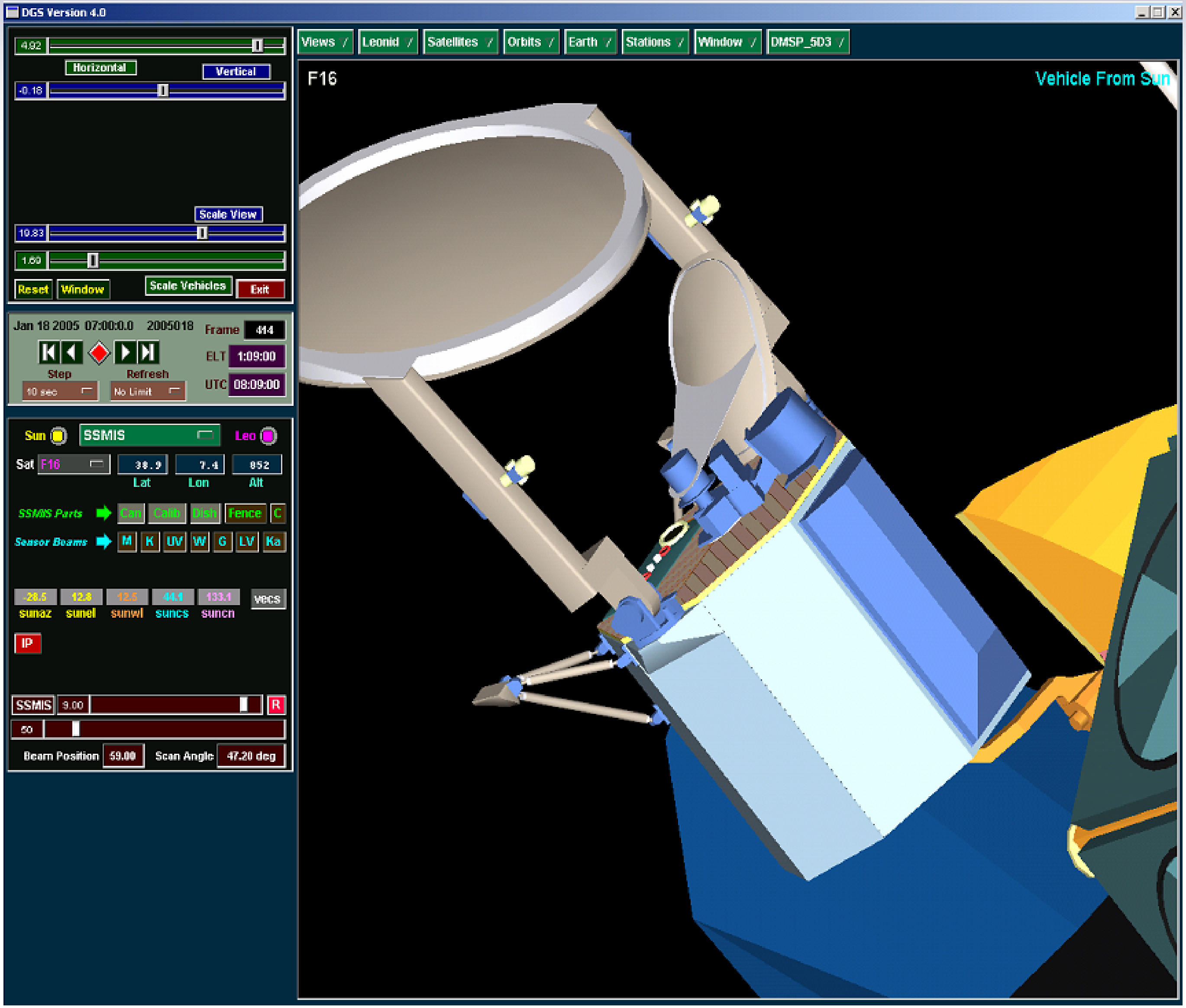

4.92

-0.18

19.83

1.69

Jan 18 2005 07:00:0.0 2005018

Frame 414

ELT 1:09:00

UTC 08:09:00

Step 10 sec

Refresh No Limit

Sun SSMIS Leo

Sat F16

Lat	Lon	Alt
38.9	7.4	852

sunaz	sunel	sunwl	suncs	suncn
-28.5	12.8	12.5	44.1	133.1

SSMIS 9.00

50

Beam Position 59.00

Scan Angle 47.20 deg

Region 2: Ray Trace Simulation January 18, 2005 08:09 Z

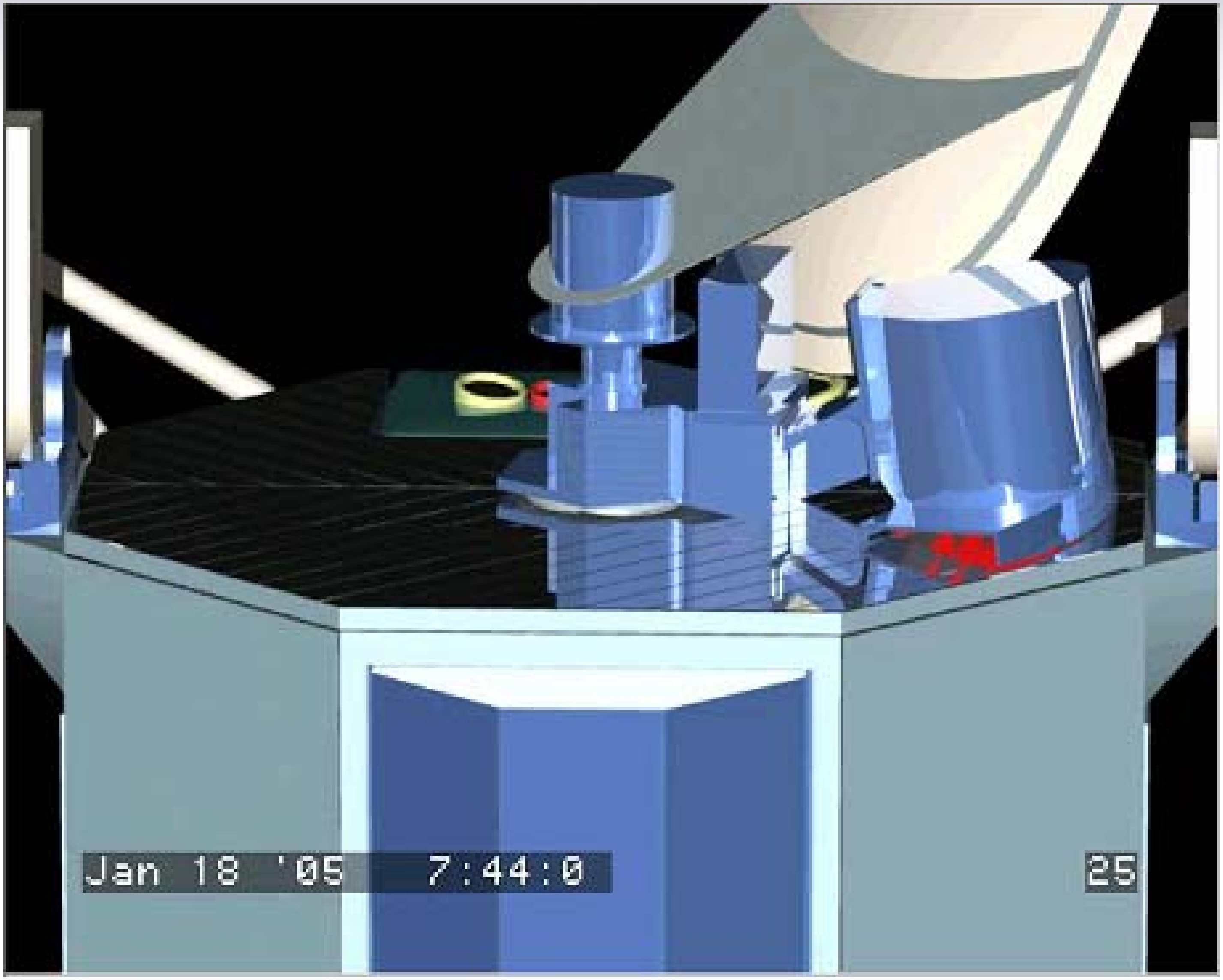

Region 3 (Reflected #2)

Pages 11- 58 and 11- 59 show the DGS Simulation of F-16 with SSMIS in the center of the Warm Load “Region 3” Anomaly. Similar to Region 2, the red tines of the warm load can not be seen in this region because DGS does not have the ability to show reflected images. This is why the ray tracing model, shown on page 11- 60 for this region is included. Region 3 typically causes the second largest calibration bias of the SSMIS Warm Load anomaly regions and is characterized by solar illumination elevation angle $\theta > 0°$ and ~<25° - 30° with solar azimuth angles, $\phi > 40°$ and < 90°. Many times, the magnetometer mast of the F-16 spacecraft blocks the sun from illuminating the Warm load near the peak of the Region 3 anomaly. The results in a “double peaked” characteristic gain anomaly which is prevalent in Normal Mode data from January 15 (three days before the 2005 EO2 data collection period). The characteristic double peak of the Region 3 anomaly can be seen most clearly in the Channel 17 gain series plot on page 11- 84 from January 15, 2005.

Region 3: DGS Simulation January 18, 2005 08:42 Z

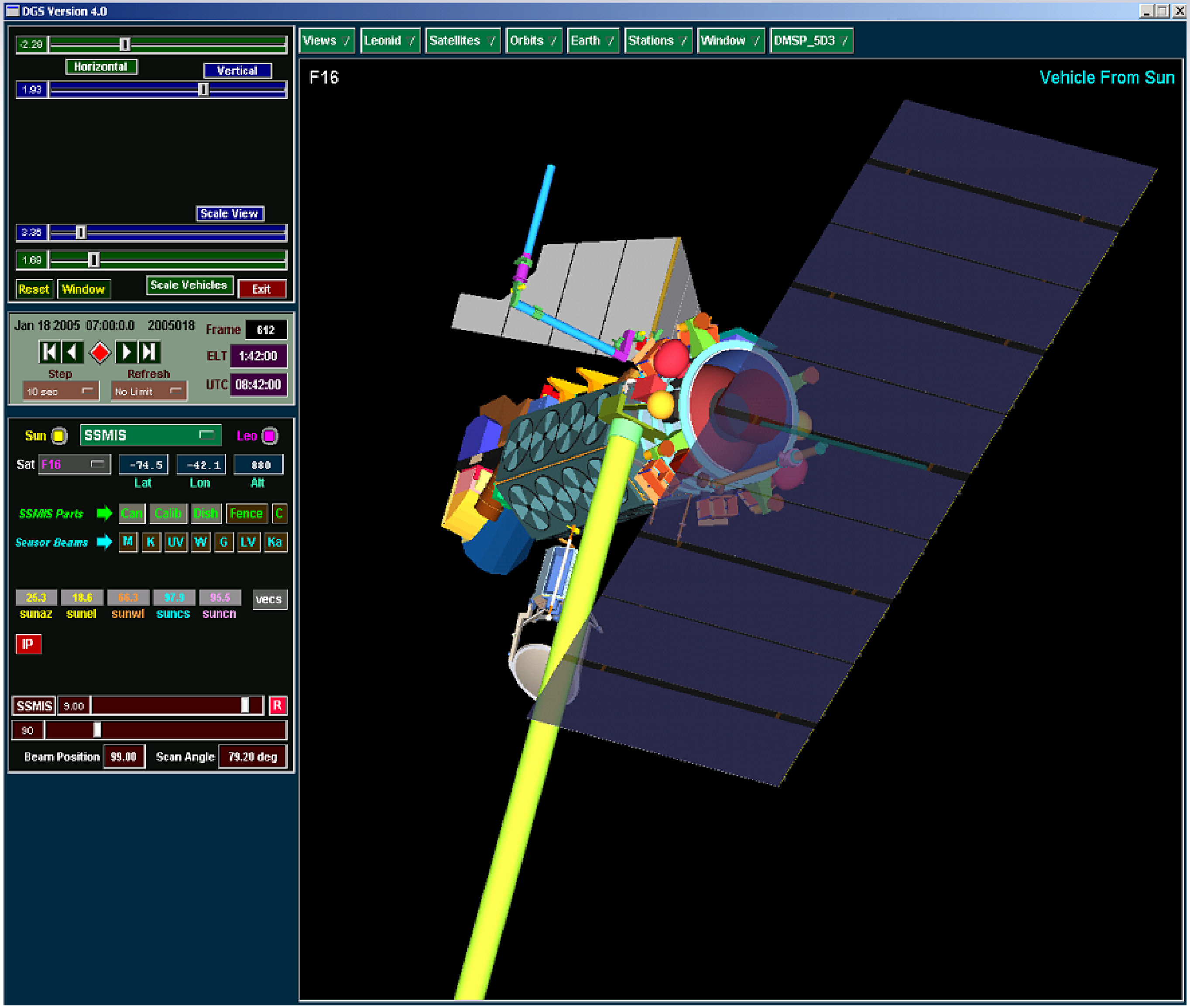

DGS Version 4.0

-2.29

1.93

3.38

1.69

Jan 18 2005 07:00:0.0 2005018

Frame 612

ELT 1:42:00

UTC 08:42:00

Step 10 sec

Refresh No Limit

SSMIS

Sat F16

Lat -74.5

Lon -42.1

Alt 880

sunaz 25.3

sunel 18.6

sunwl 66.3

suncs 97.9

suncn 95.6

SSMIS 9.00

90

Beam Position 99.00

Scan Angle 79.20 deg

F16

Vehicle From Sun

Region 3: DGS Simulation January 18, 2005 08:42 Z

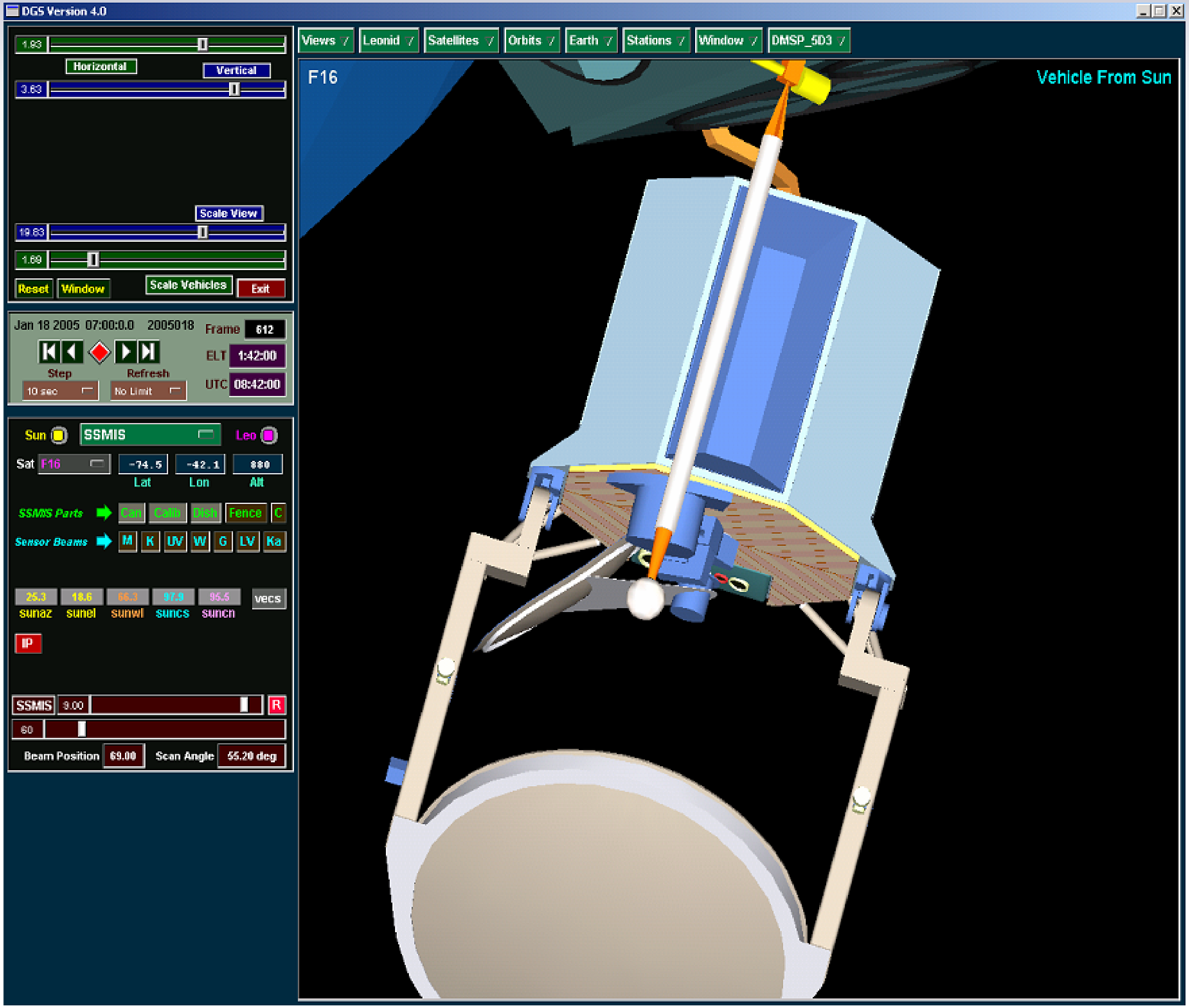

1.93
3.63
19.83
1.69

Jan 18 2005 07:00:0.0 2005018

Frame 612

ELT 1:42:00

UTC 08:42:00

Step 10 sec

Refresh No Limit

SSMIS

Sat F16

Lat -74.5

Lon -42.1

Alt 880

sunaz 25.3

sunel 18.6

sunwl 66.3

suncs 97.9

suncn 95.5

SSMIS 9.00

60

Beam Position 69.00

Scan Angle 55.20 deg

Region 3: Ray Trace Simulation January 18, 2005 08:42 Z

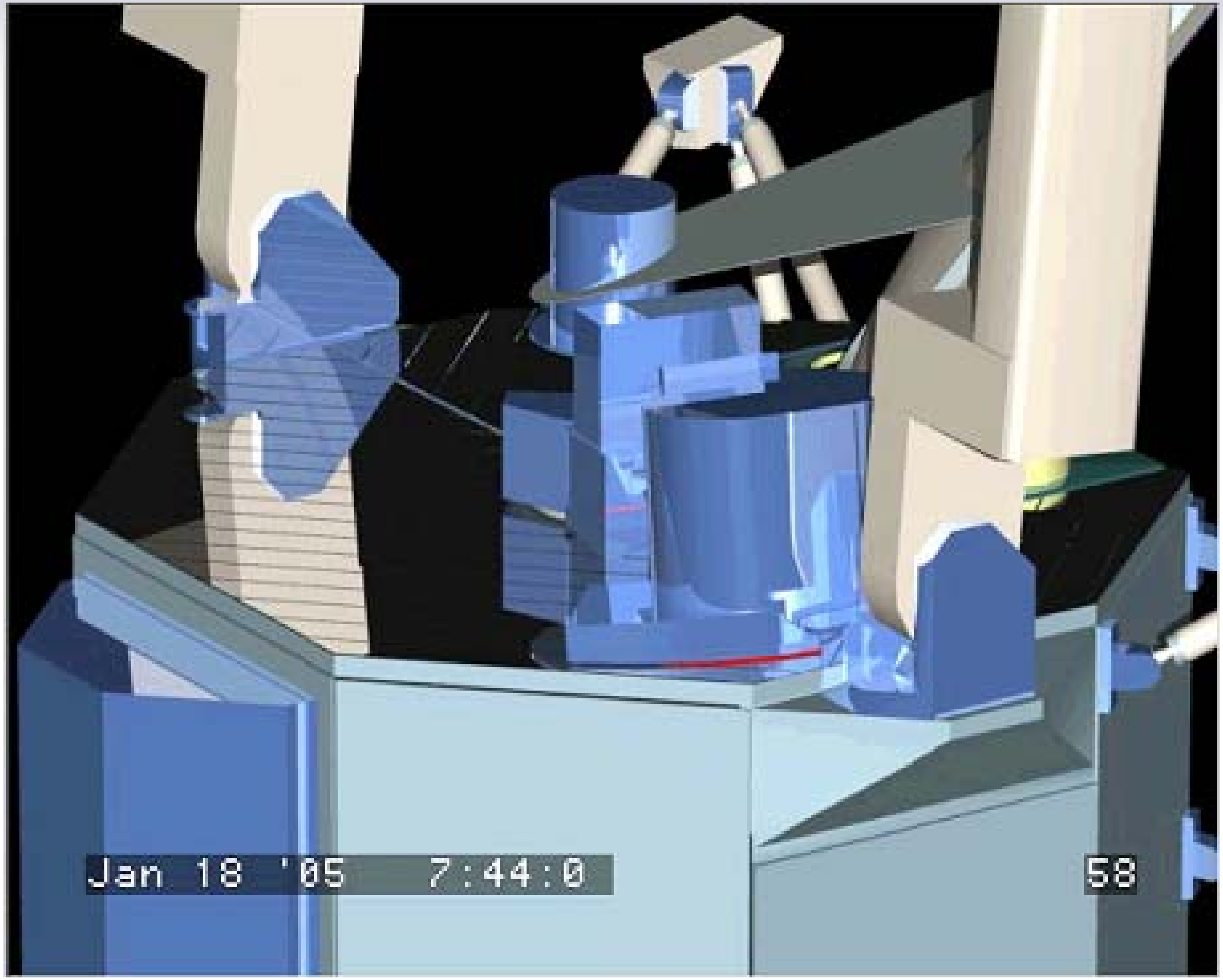

Region 4 (Direct #2)

Pages 11- 62 and 11- 63 show the DGS Simulation of F-16 with SSMIS in the center of the Warm Load "Region 4" Anomaly (Direct Illumination #2), therefore, the red tines of the warm load can be seen in the DGS graphic on page 11- 62 and 11- 63. An example of the the ray tracing model for this region is shown on page 11- 64, however, due to the canister azimuth position shown, the Warm Load tine are not seen. The Region 4 Warm Load anomaly is not always seen in the characteristic gain time series plots due to blockage of the sun by the spacecraft or the solar array for some orbital seasons. However, for the January 15 data shown in this Section, the Region 4 anomaly is quite strong. Region 4 is characterized by solar illumination elevation angle $\theta < 0°$ with solar azimuth angles, $\phi \sim > 0°$ and $< 40°$. When the spacecraft is in Region 4, many times the Cold Sky Reflector (CSR) reflecting surface is also illuminated by the sun causing additional and sometimes offsetting calibration biases. Occurrences of "dual calibration biases" and uncertainty regarding blockage of the sun from eclipse from the S/C or Earth, adds significant difficulty to designing an approach to correct the SSMIS calibration in Region 4.

Region 4: DGS Simulation January 18, 2005 08:57 Z

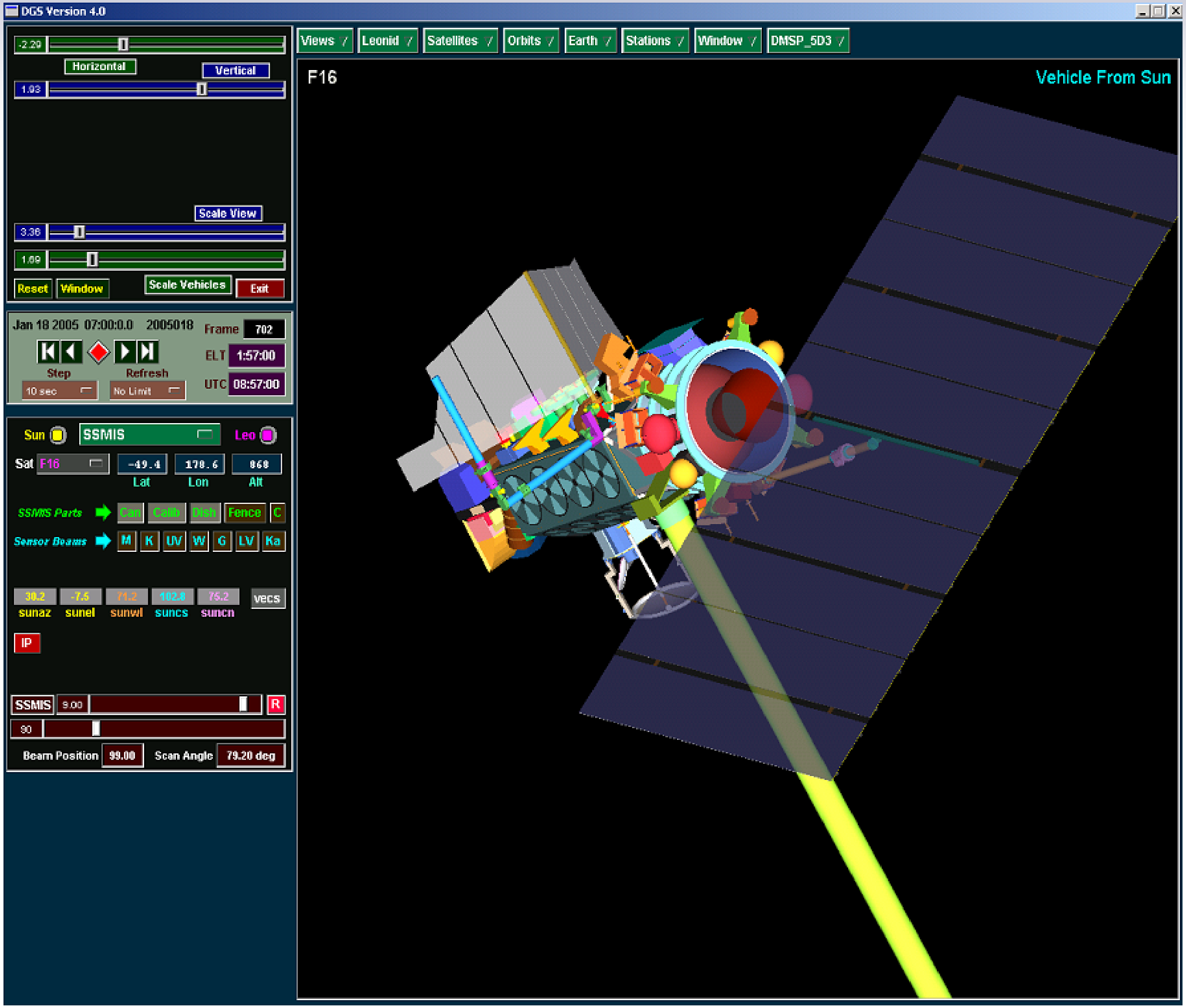

DGS Version 4.0

-2.29

1.93

3.36

1.09

Jan 18 2005 07:00:0.0 2005018

Frame 702

ELT 1:57:00

UTC 08:57:00

Step 10 sec

Refresh No Limit

SSMIS

Sat F16

Lat -49.4

Lon 178.6

Alt 868

sunaz 30.2

sunel -7.5

sunwl 71.2

suncs 102.8

suncn 75.2

SSMIS 9.00

90

Beam Position 99.00

Scan Angle 79.20 deg

F16

Vehicle From Sun

Region 4: DGS Simulation January 18, 2005 08:57 Z

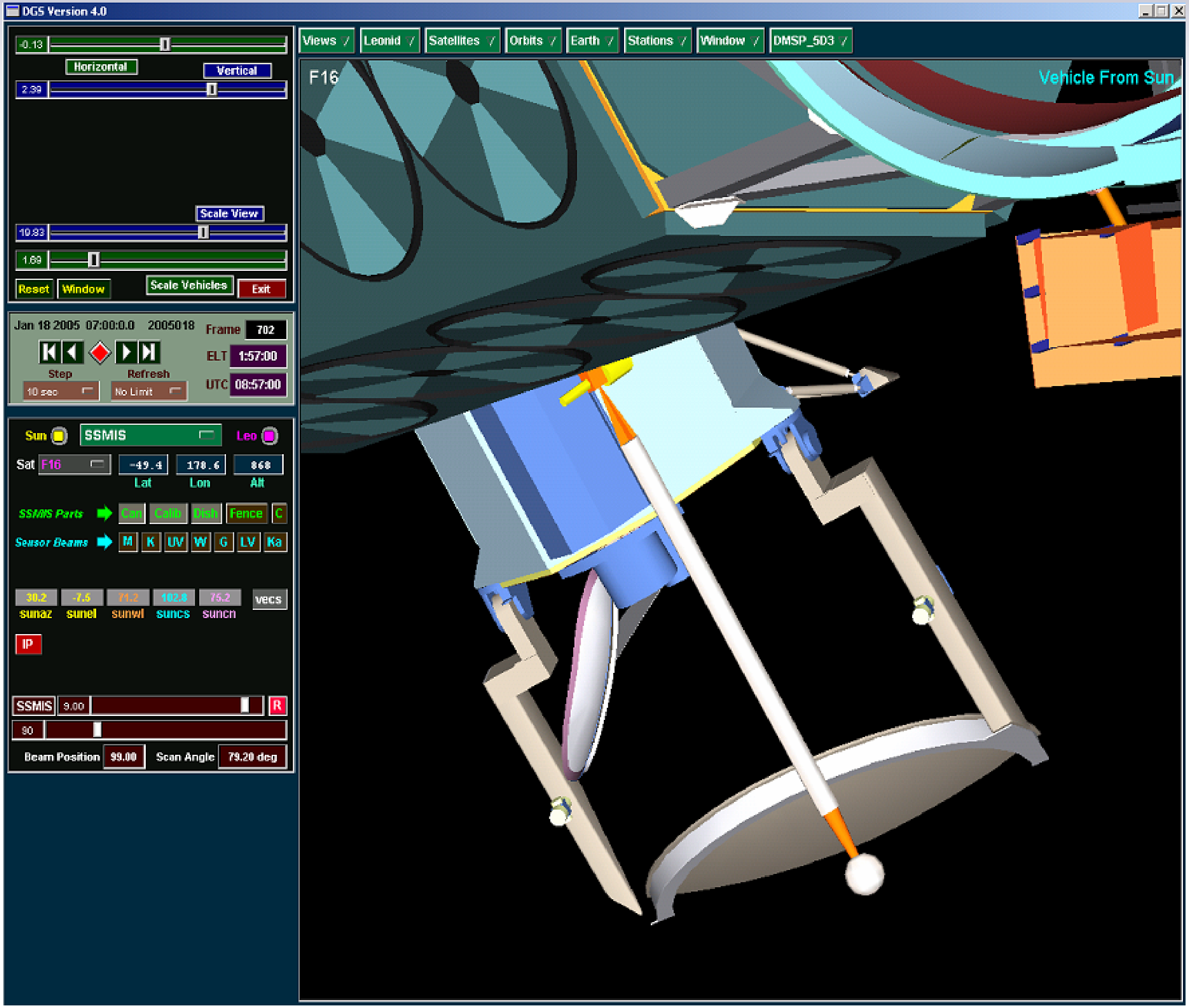
DGS Version 4.0

Jan 18 2005 07:00:0.0 2005018

Frame 702

ELT 1:57:00

UTC 08:57:00

Step 10 sec

Refresh No Limit

Sat F16

Lat -49.4

Lon 170.6

Alt 868

sunaz 30.2

sunel -7.5

sunwl 71.2

suncs 102.8

suncn 75.2

SSMIS 9.00

Beam Position 99.00

Scan Angle 79.20 deg

Region 4: Ray Trace Simulation January 18, 2005 08:57 Z

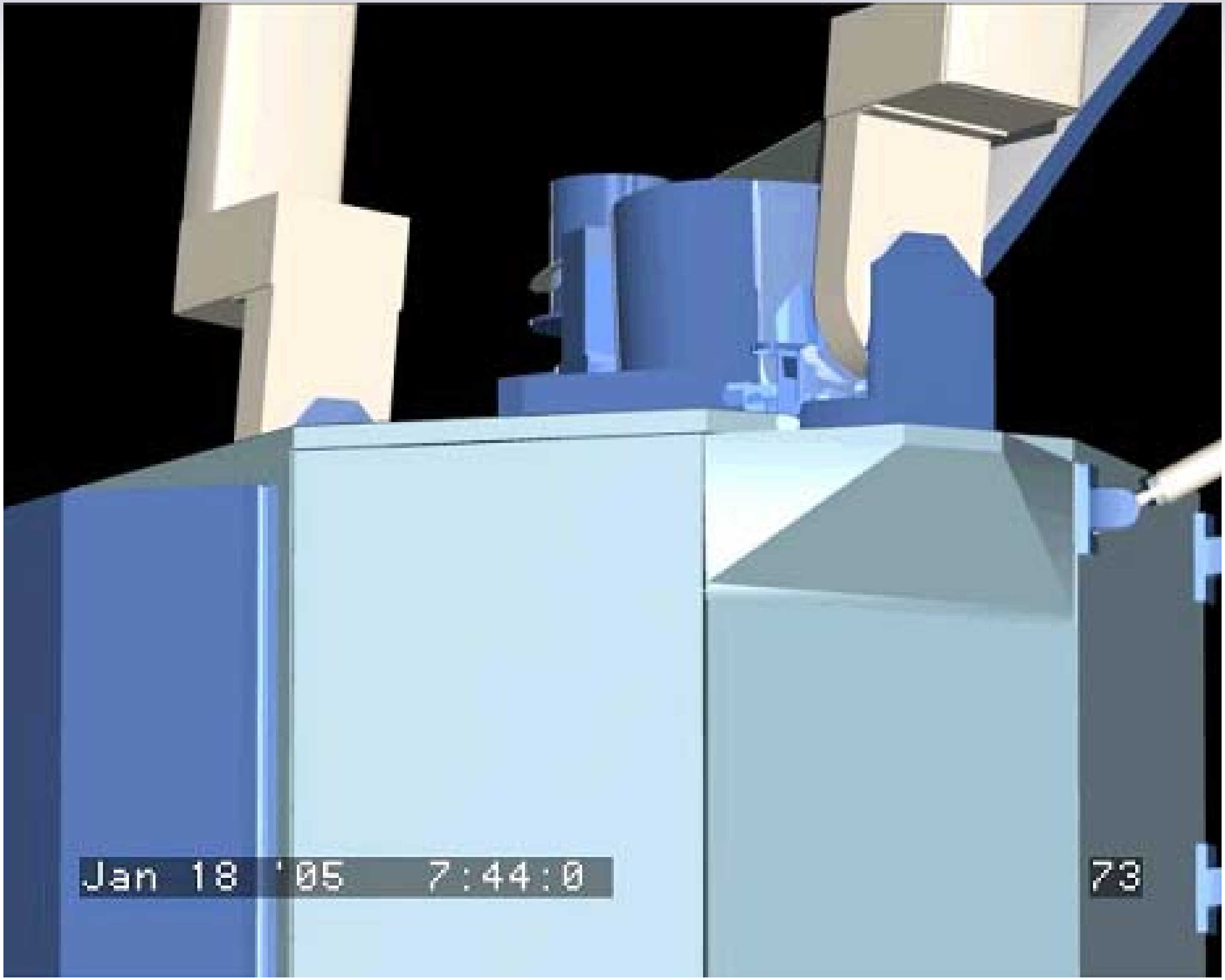

11.7C Time-averaged Warm Load Images from EO2A Data from Each Feedhorn

The following images of the Warm Load (WL) surface have been derived by averaging 19 revs of EO2A data. For every channel that is included in this Section, a WL image derived from a single orbit appears first followed by the WL image created by averaging 19 revs. Improvement in the image detail is quite apparent in all cases. Each image pair is preceded by the time-series plot of the channel gains derived from the Normal mode calibration in orbits just three days prior to the EO2 collection period. The structure of the 4 WL anomalies can be clearly seen in most images but particularly for channels where the gain variations are smaller such as Channel 4 and 16. Note that the WL anomalies appear as transient "bumps" on the slowly varying gain values for each Channel as shown by the red line plot on pages 11-66, 69, 72, 75, 78, 81, and 84. The same variation exists in the WL because a fixed "calibration" is applied to scale the raw radiometric counts to pseudo T_B's. These images allow improved analysis and understanding of the solar interactions for all 4 WL anomaly Regions.

Channel 4 Time Series Gain Plot

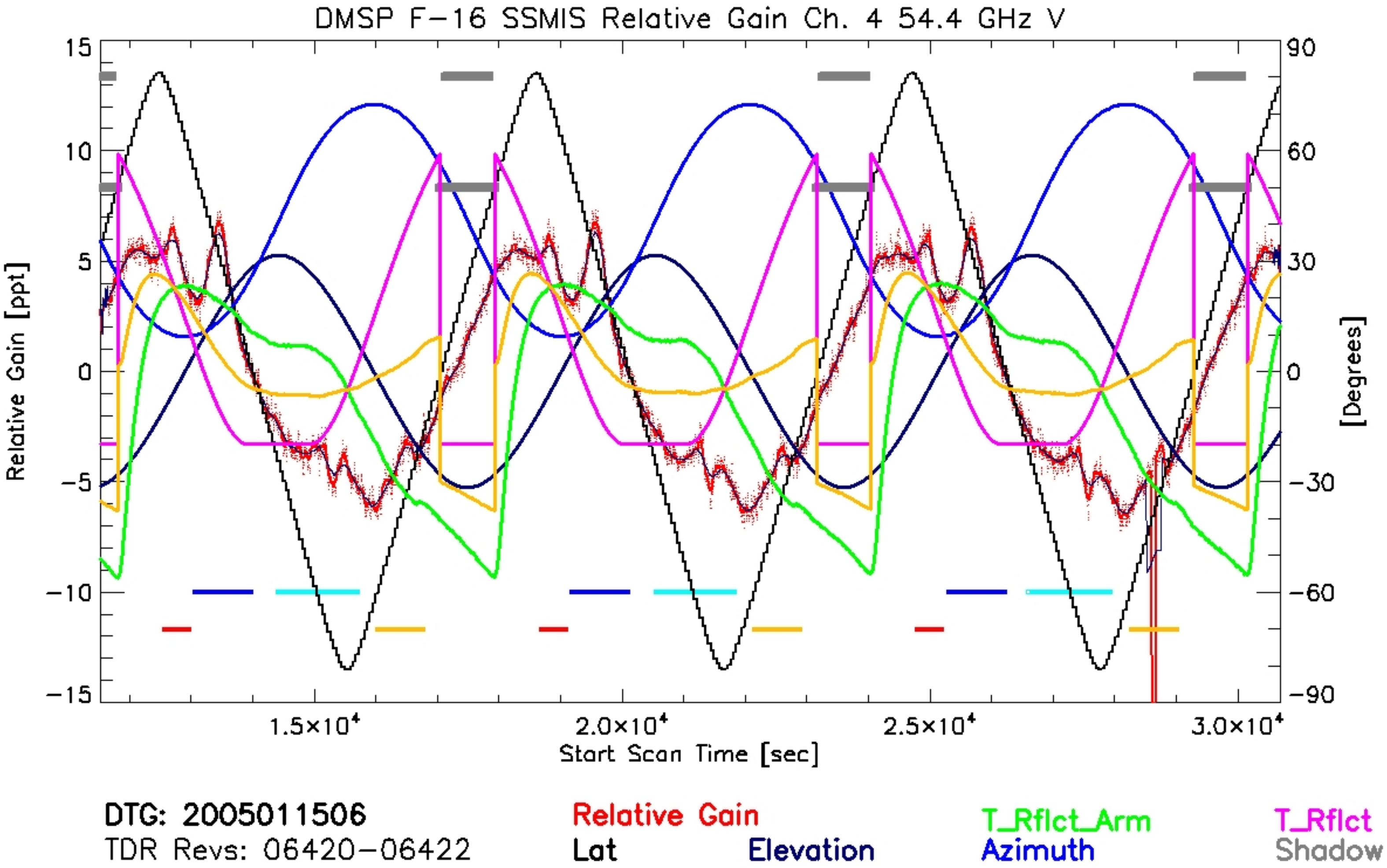

Channel 4 Warm Load Image (rev 6472)

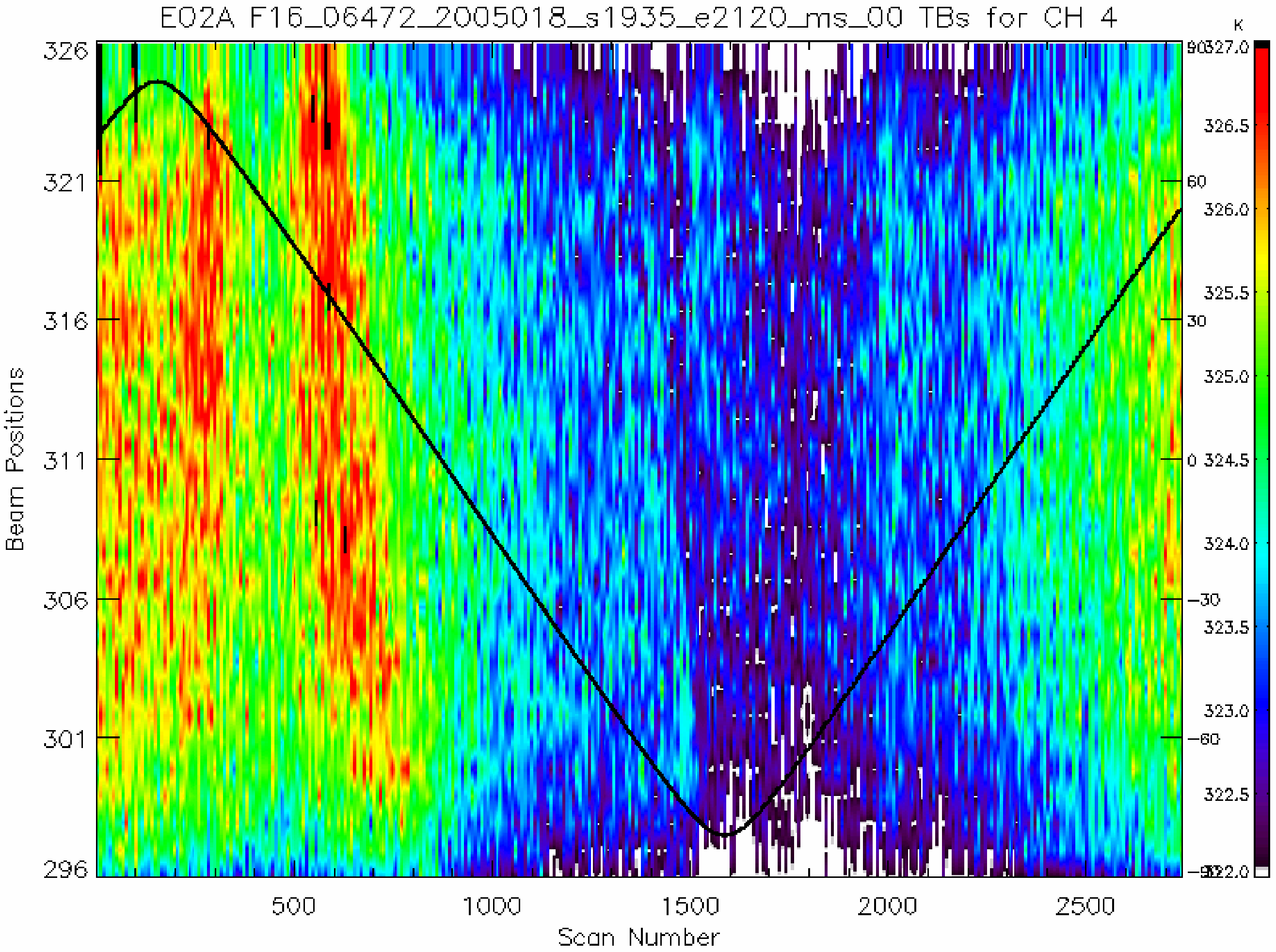

Channel 4 Warm Load Image (revs 6472 - 6494)

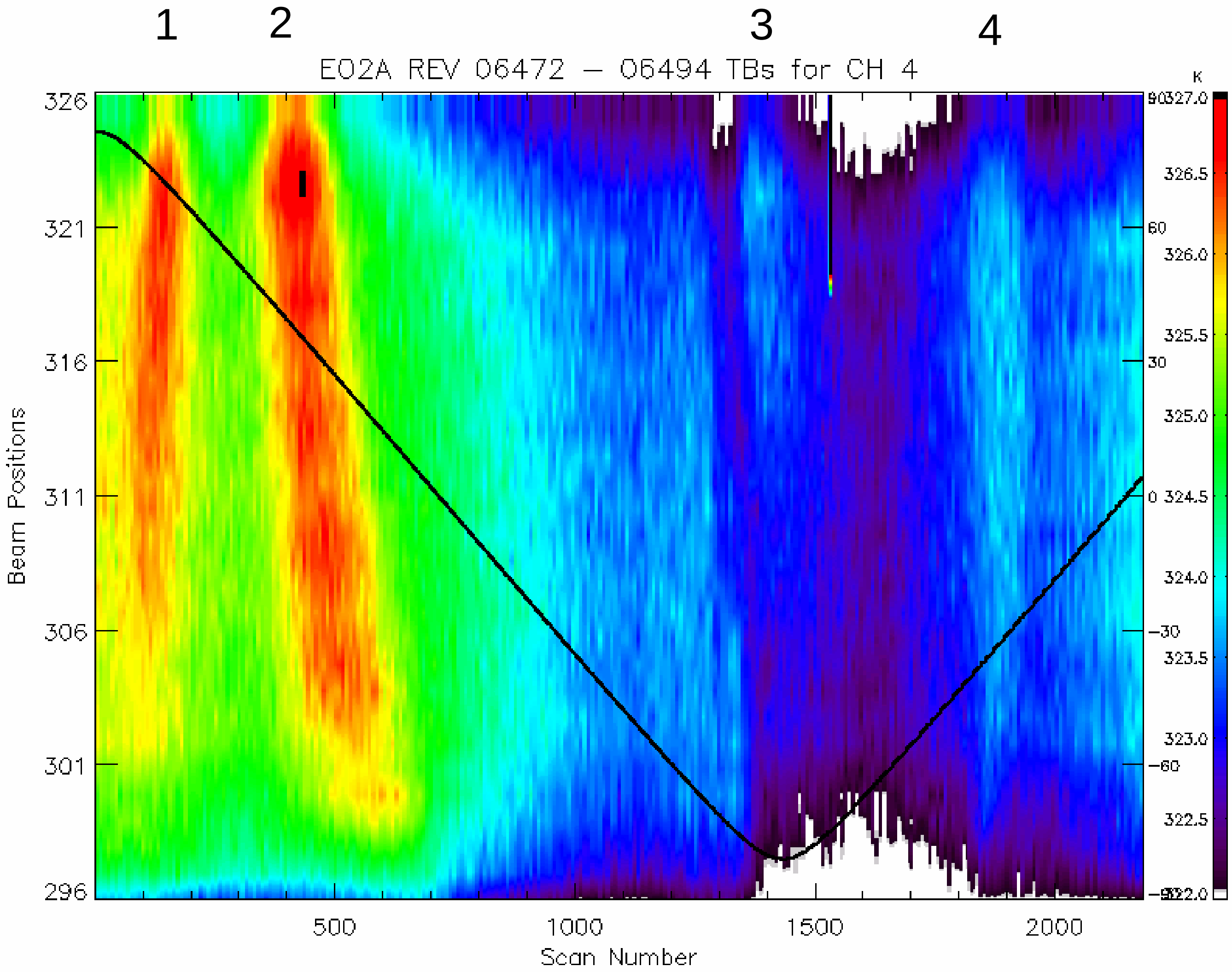

Channel 22 Time Series Gain Plot

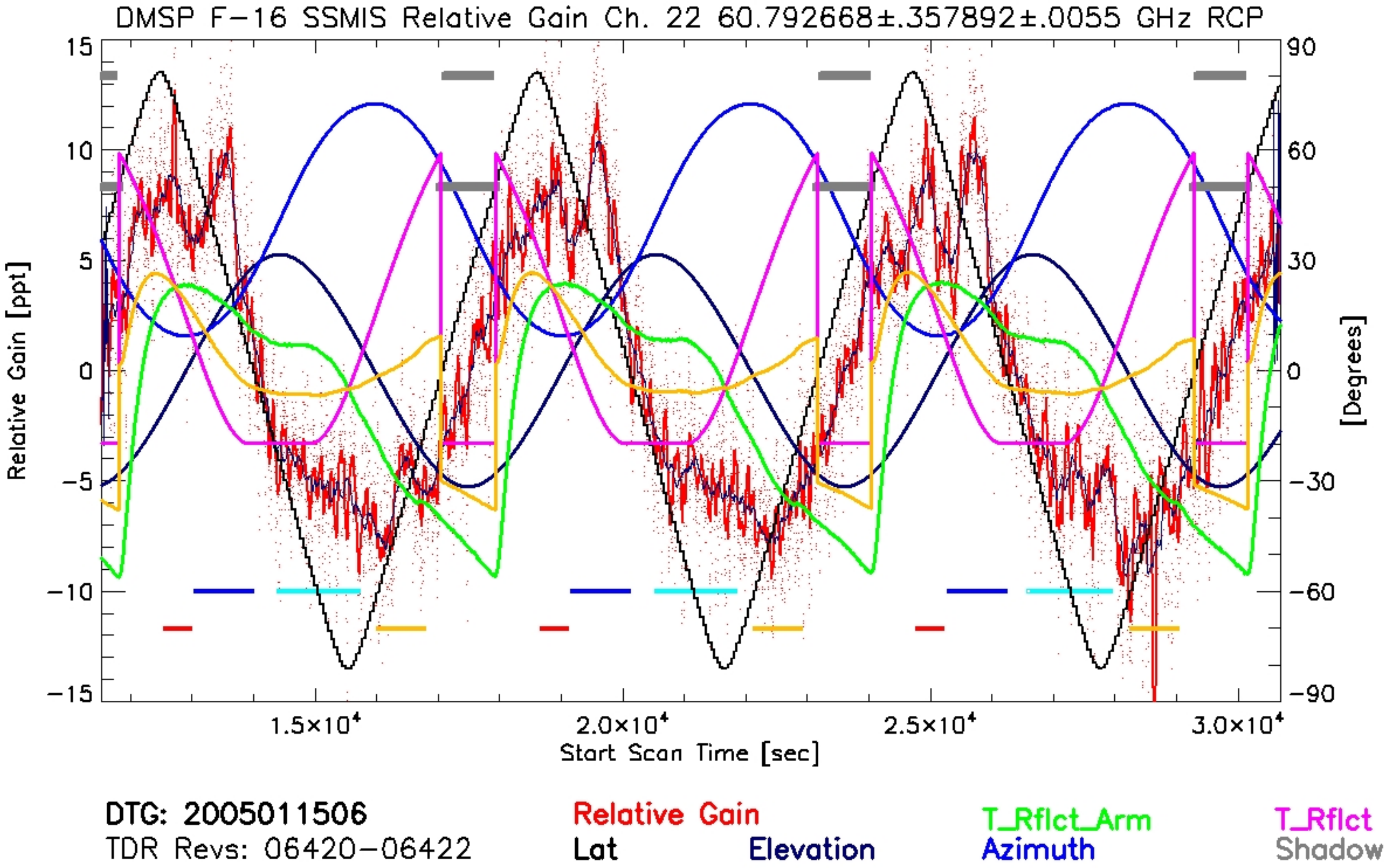

Channel 22 Warm Load Image (rev 6472)

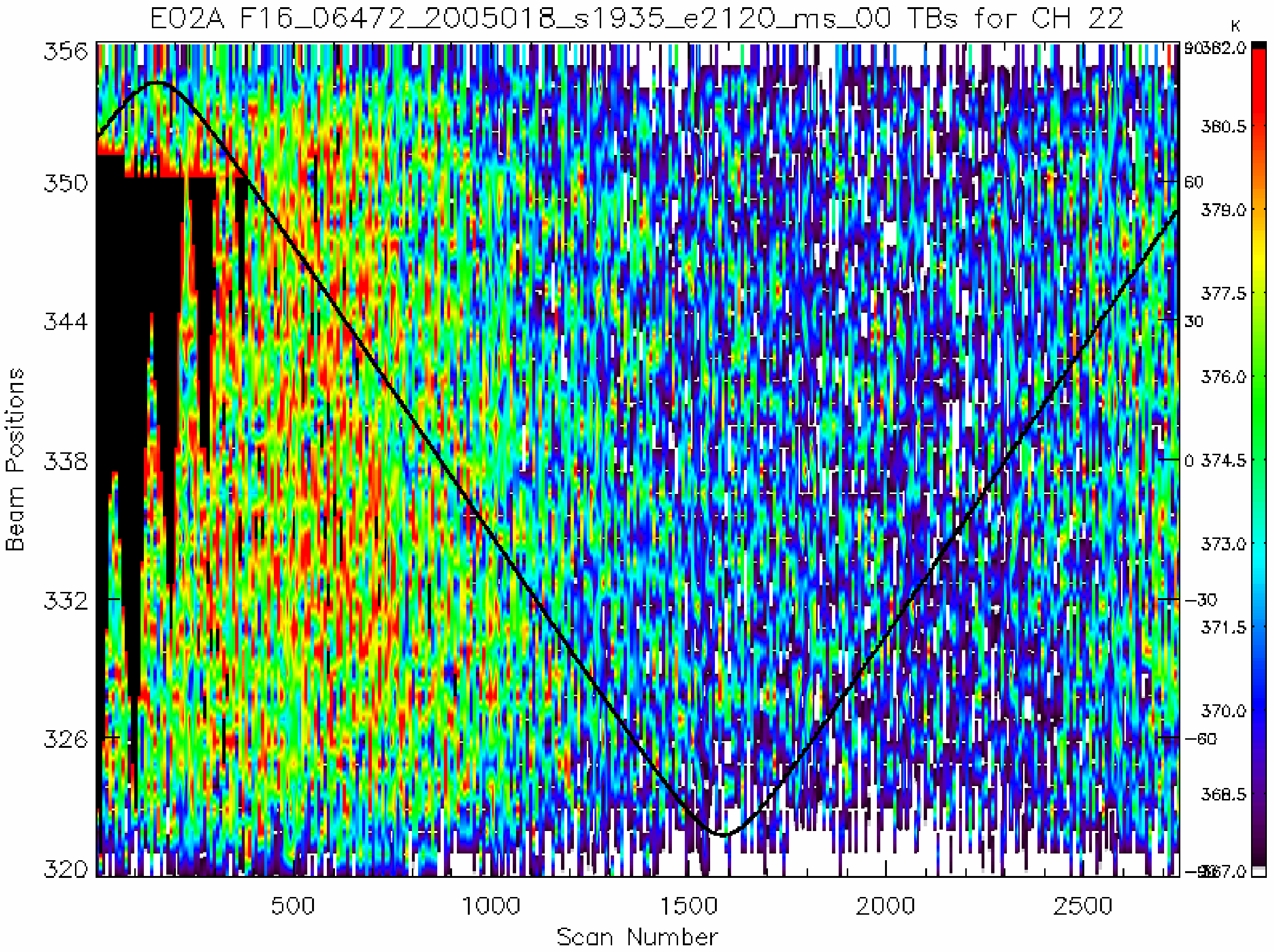

Channel 22 Warm Load Image (revs 6472 - 6494)

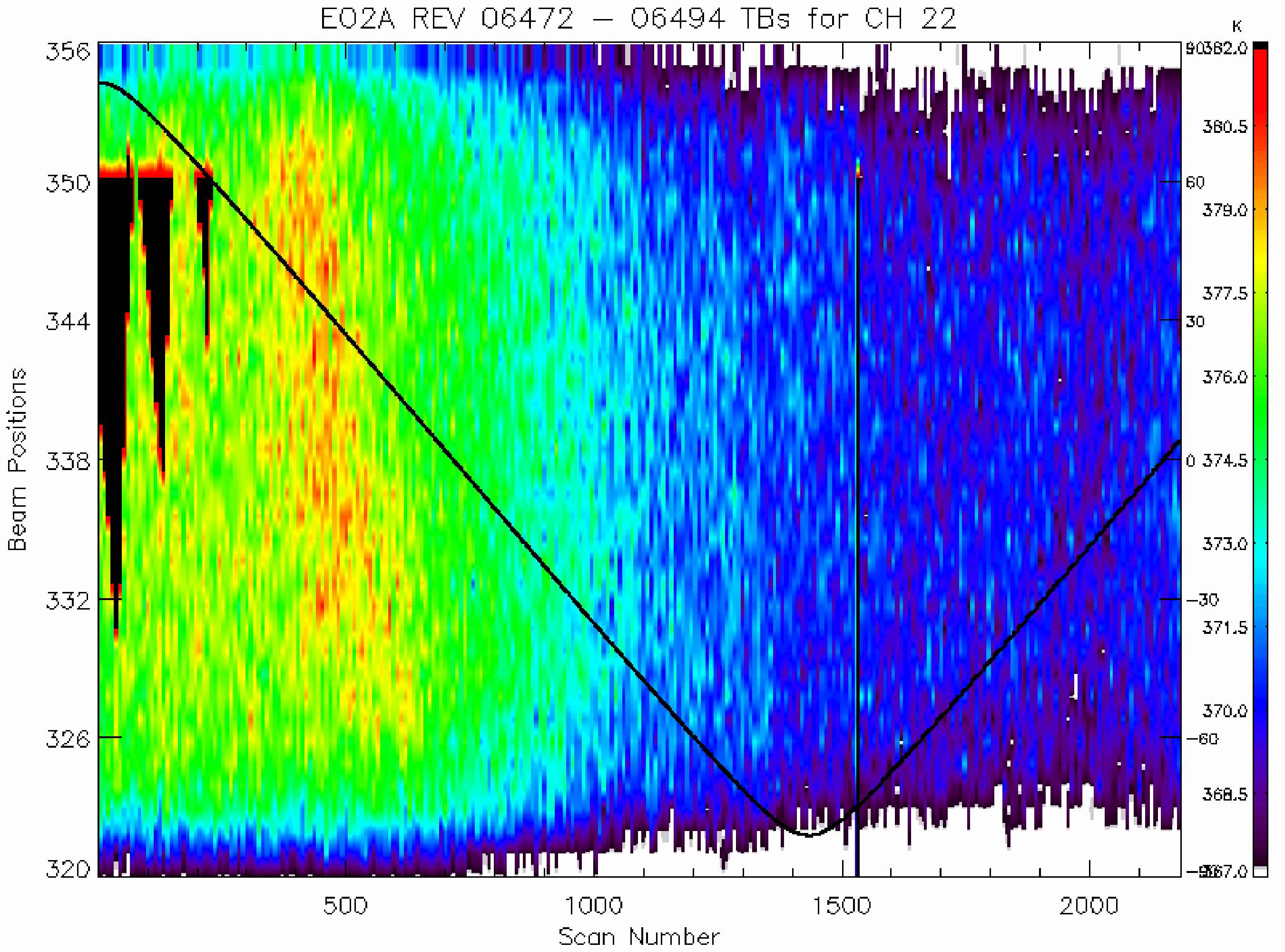

Channel 8 Time Series Gain Plot

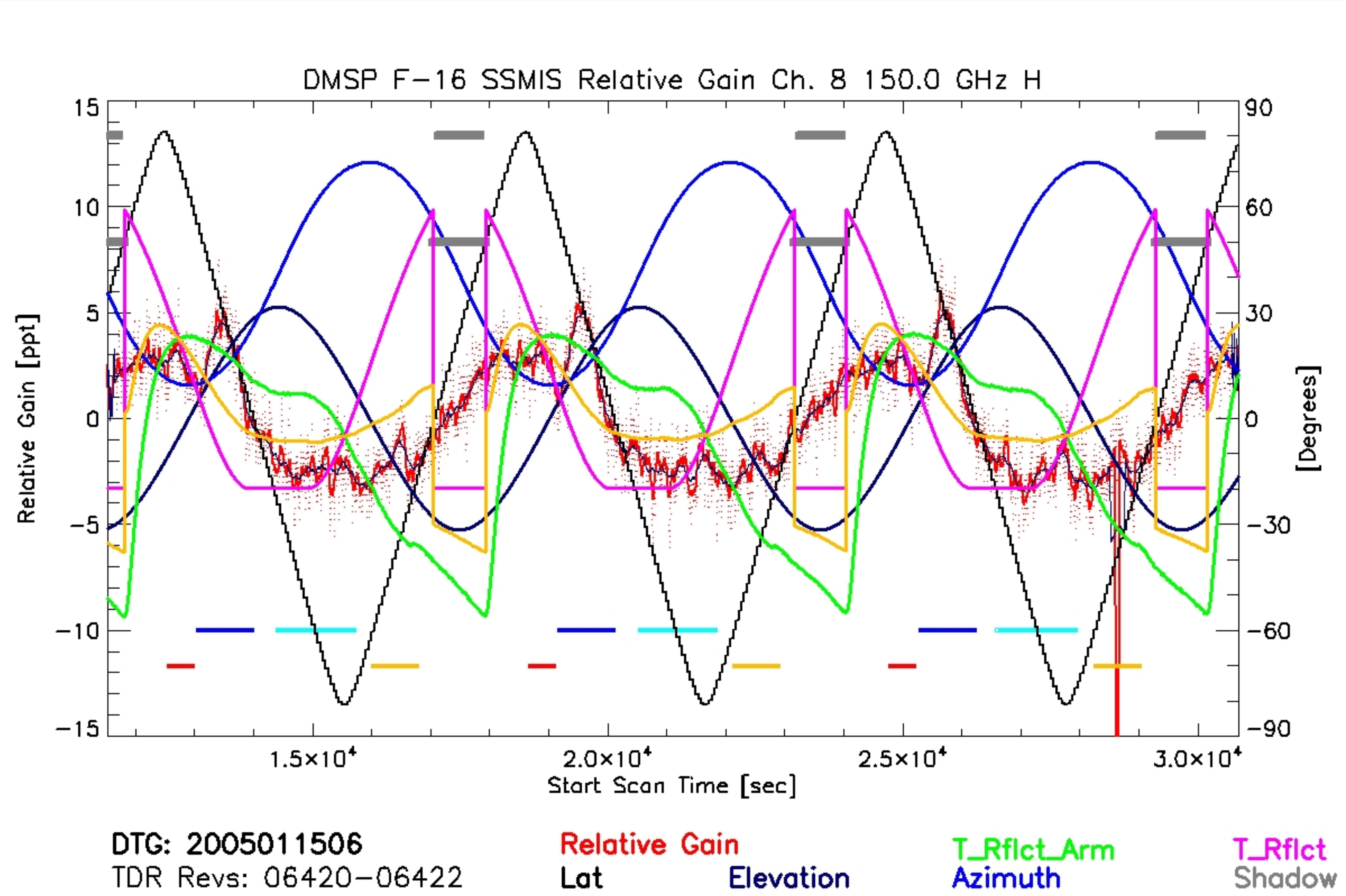

Channel 8 Warm Load Image (rev 6472)

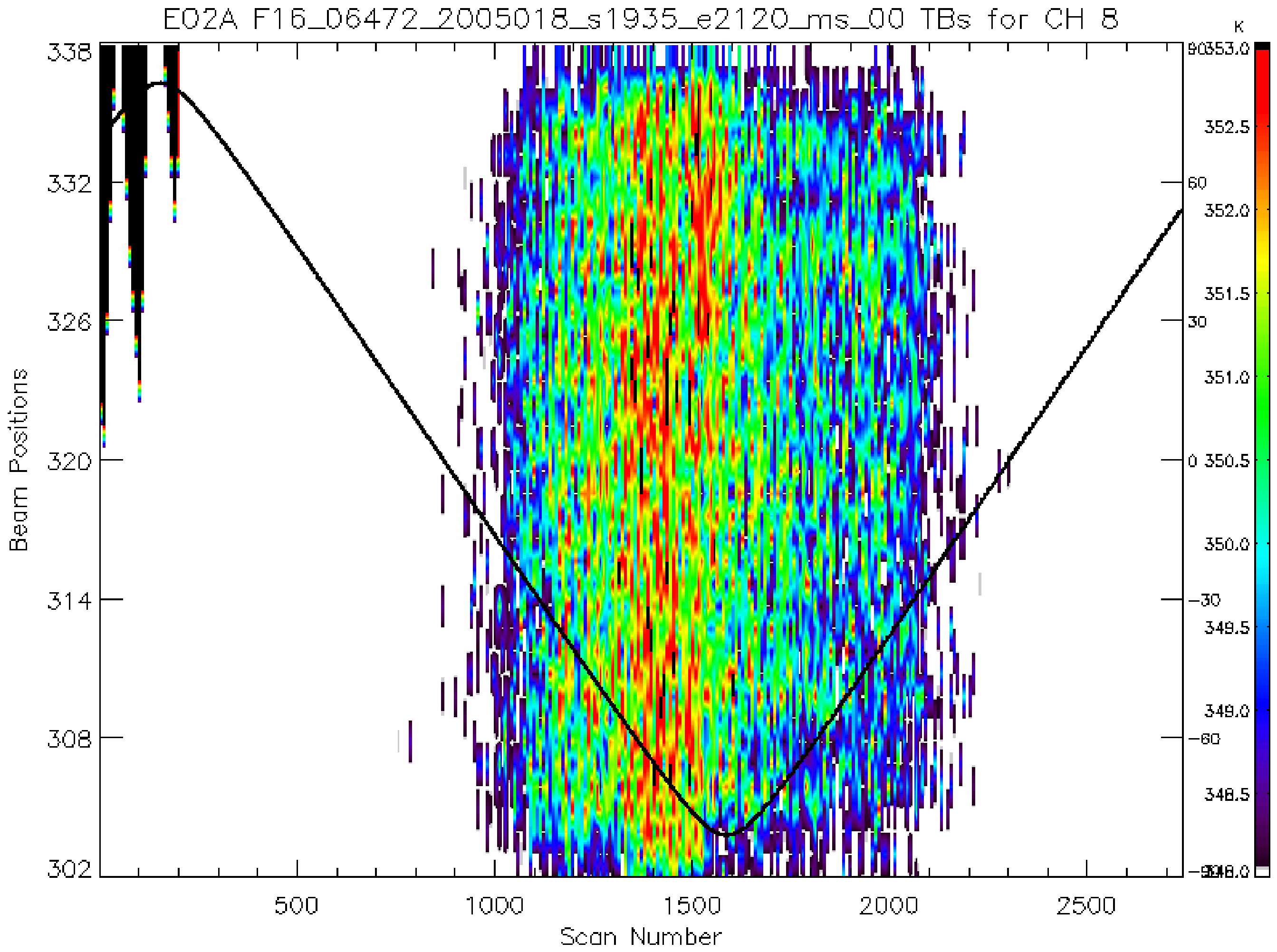

Channel 8 Warm Load Image (revs 6472 - 6494)

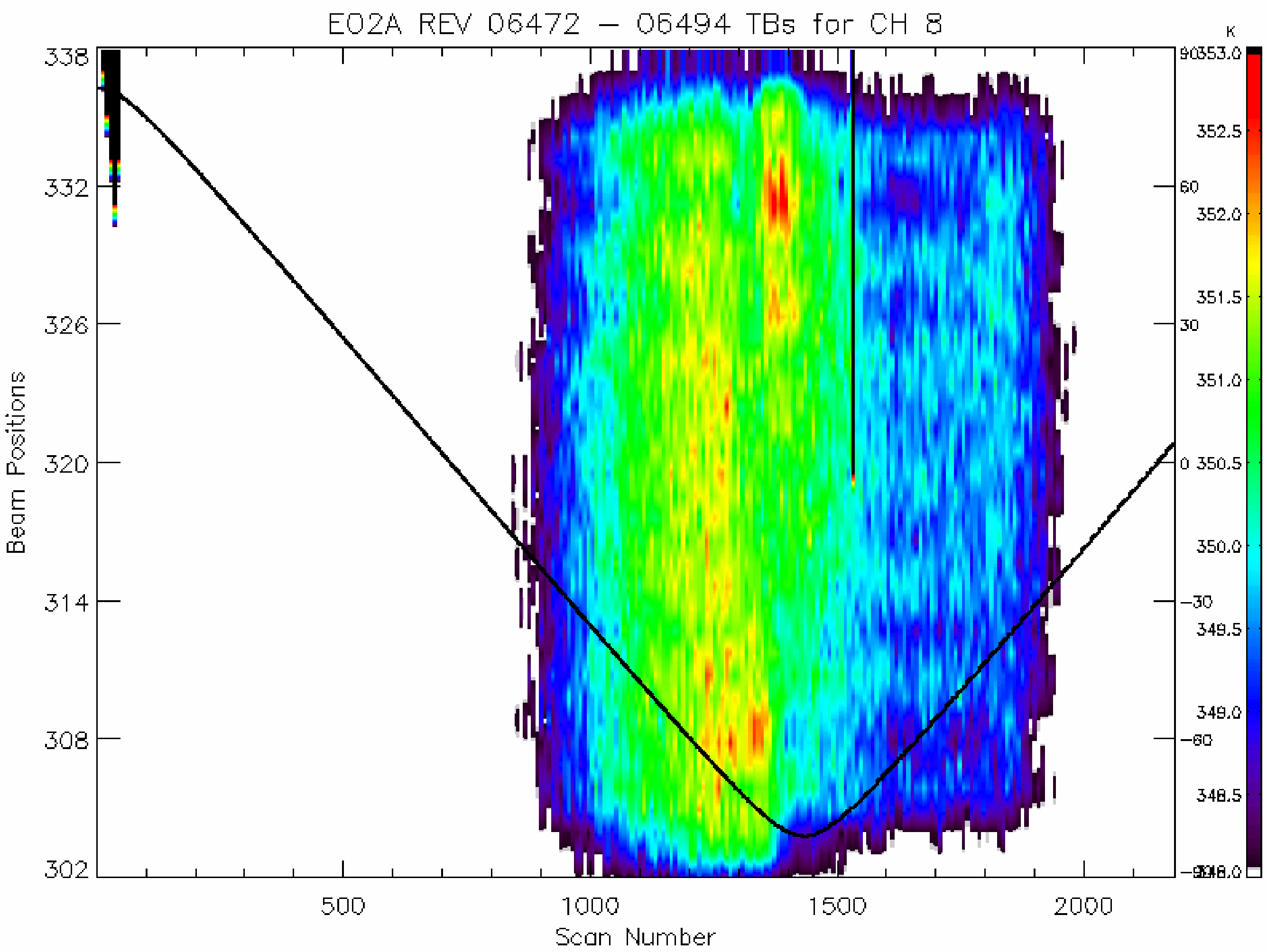

Channel 14 Time Series Gain Plot

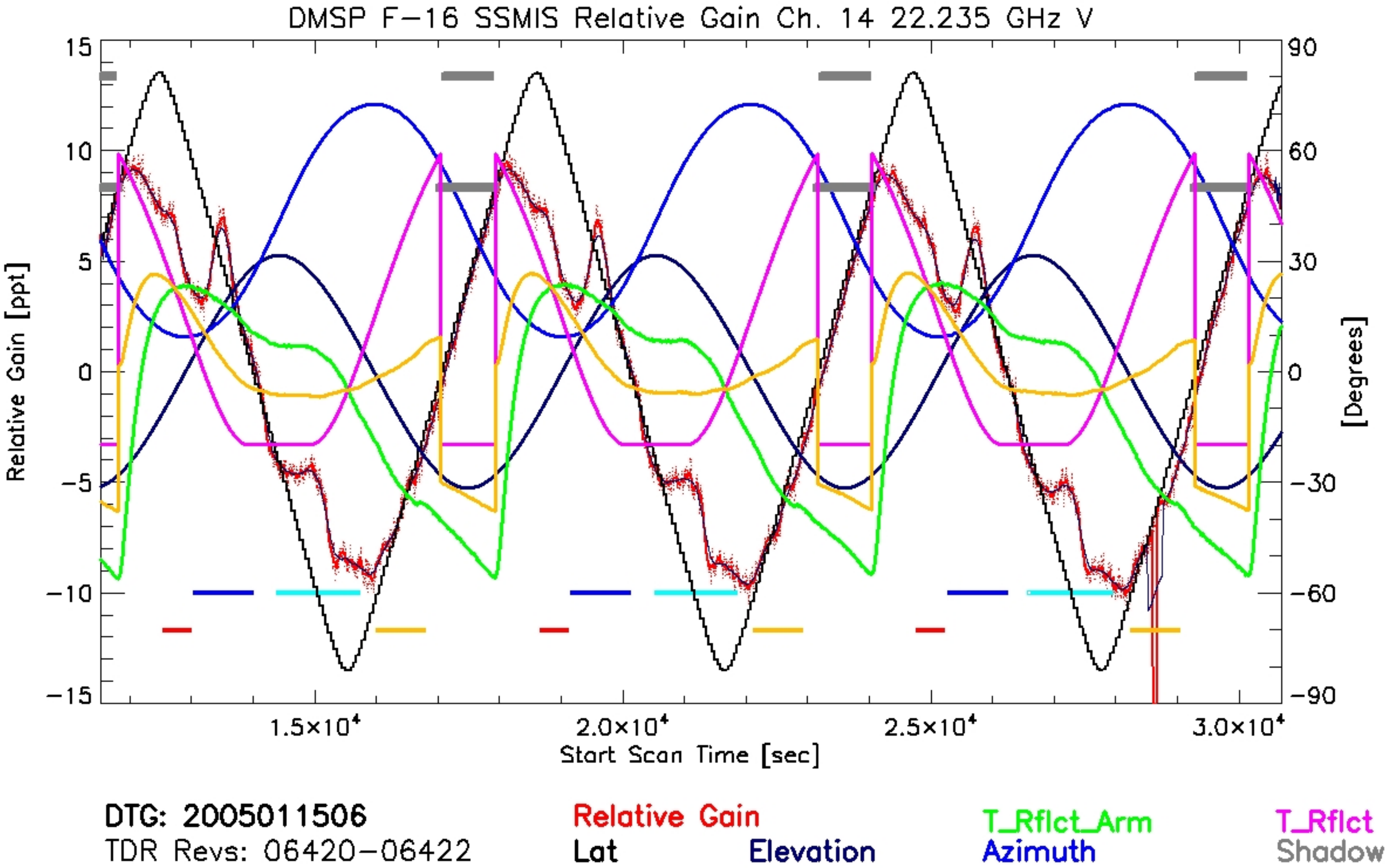

Channel 14 Warm Load Image (rev 6472)

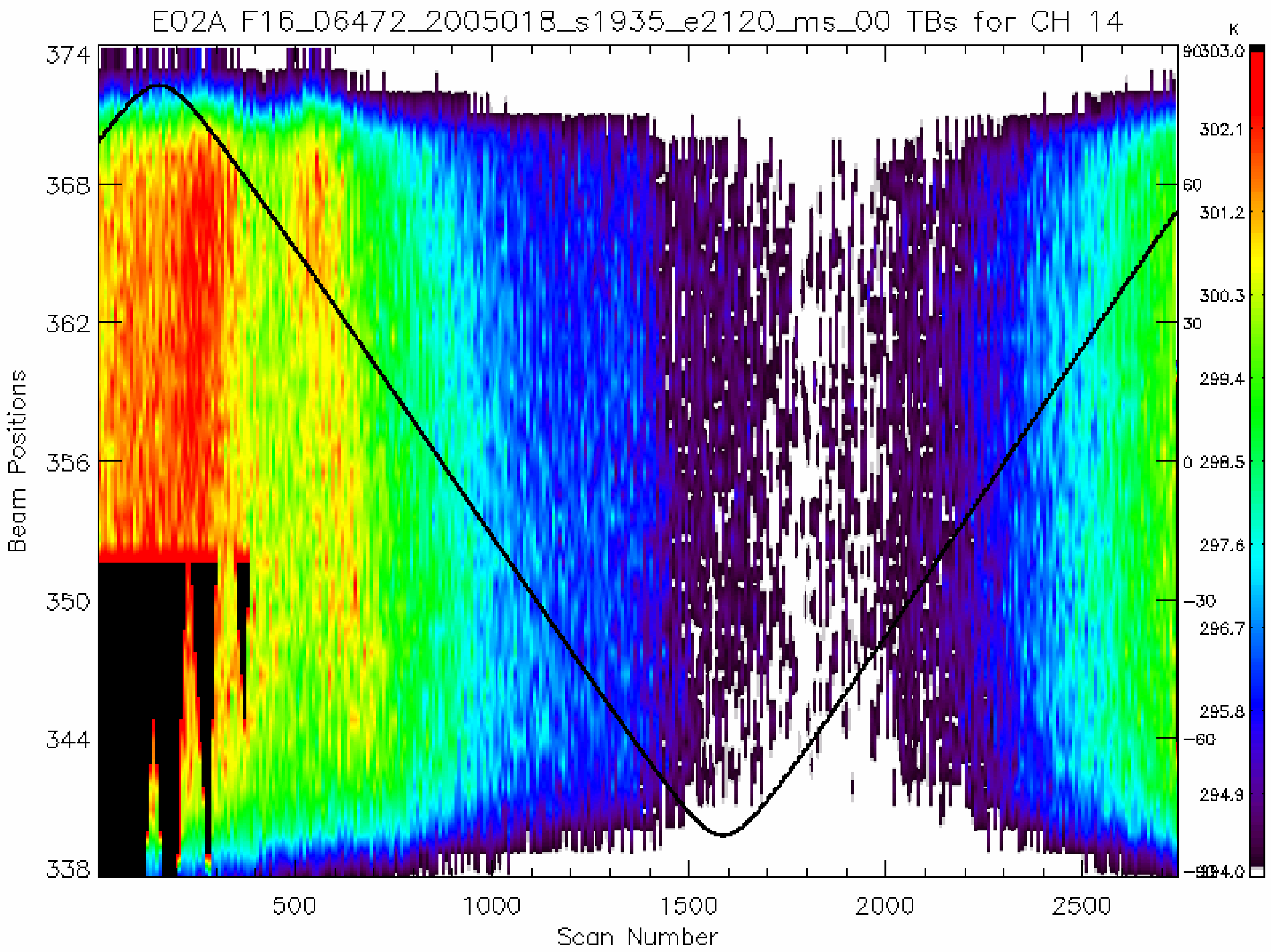

Channel 14 Warm Load Image (revs 6472 - 6494)

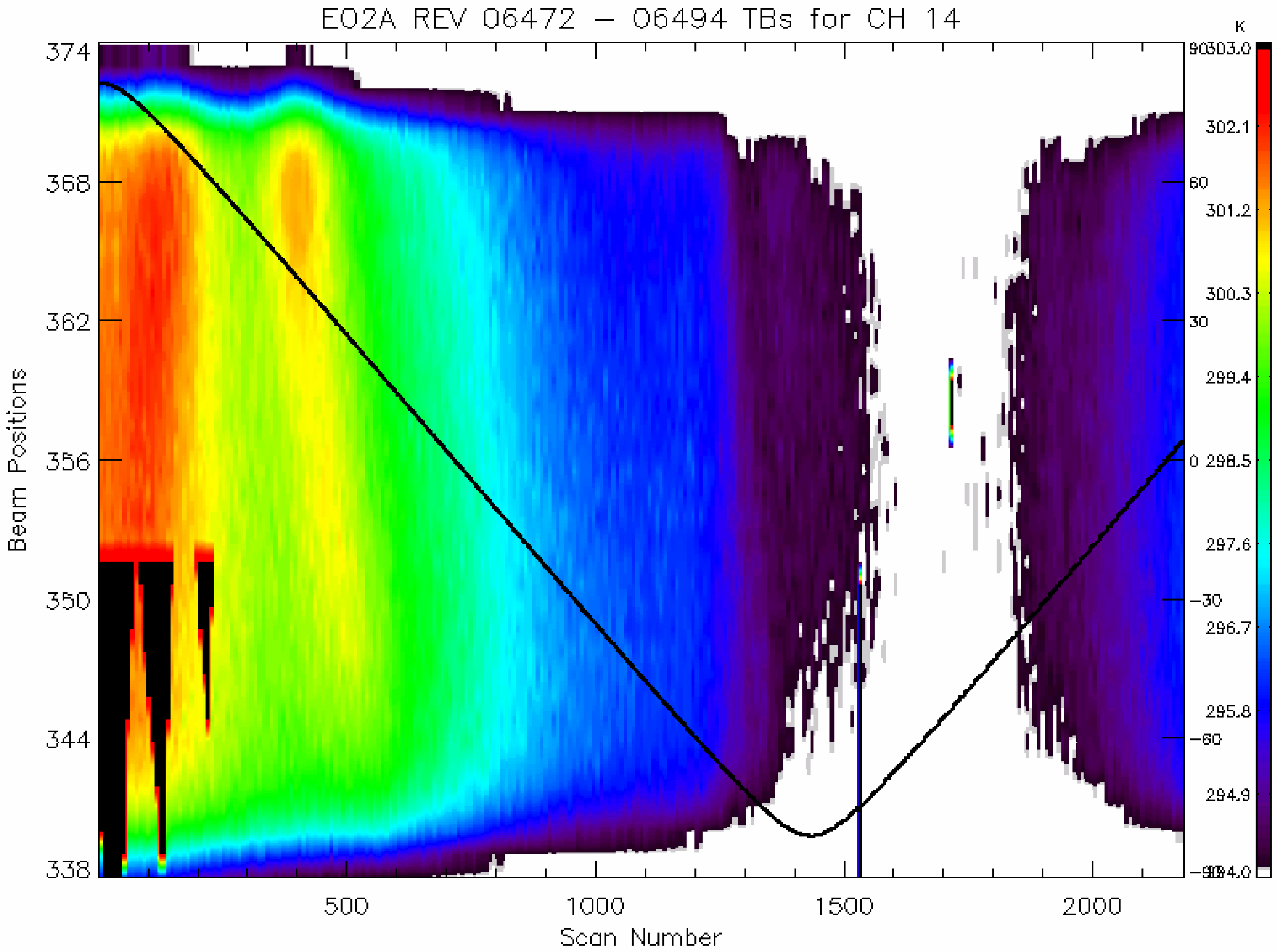

Channel 15 Time Series Gain Plot

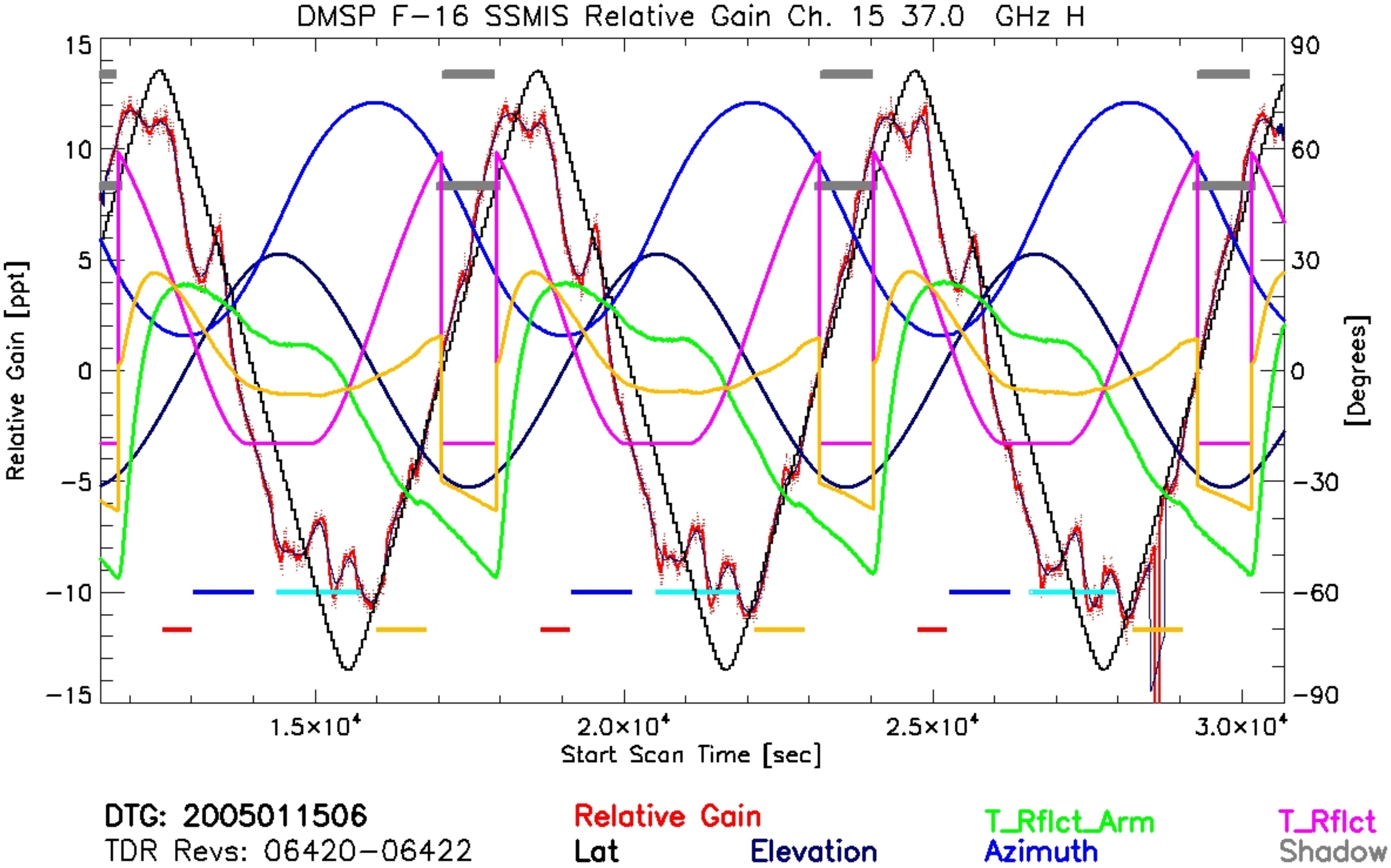

Channel 15 Warm Load Image (rev 6472)

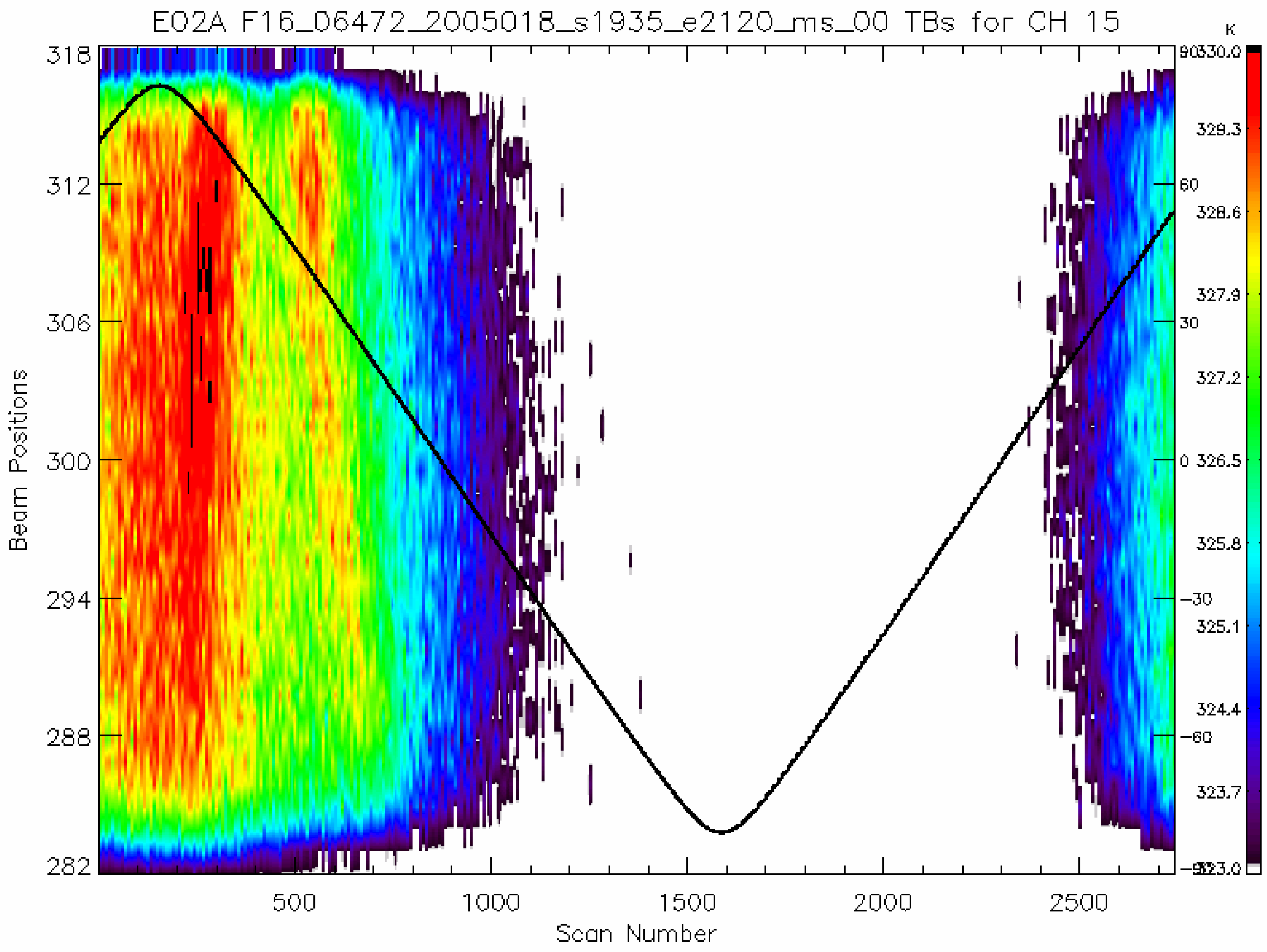

Channel 15 Warm Load Image (revs 6472 - 6494)

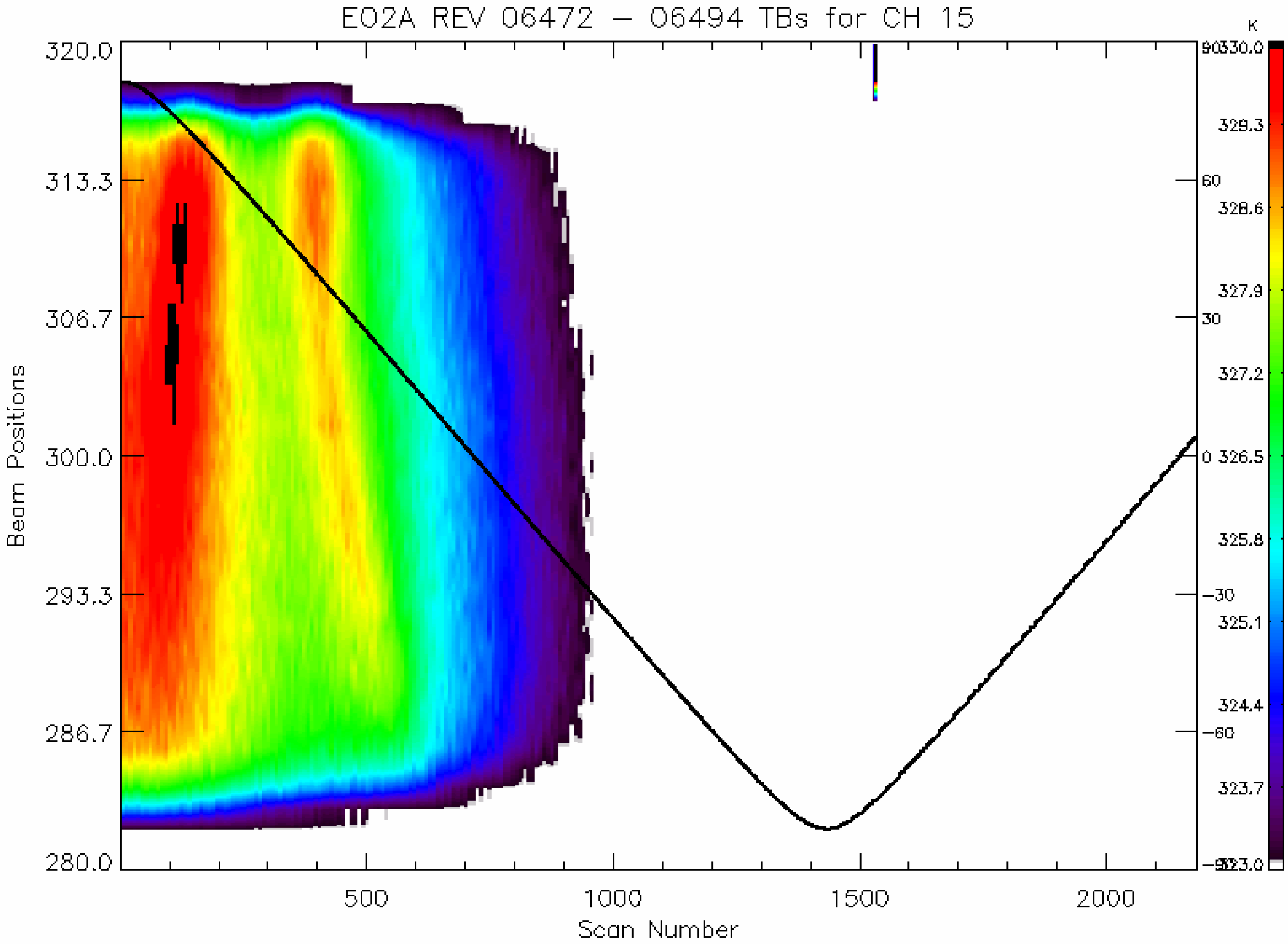

Channel 16 Time Series Gain Plot

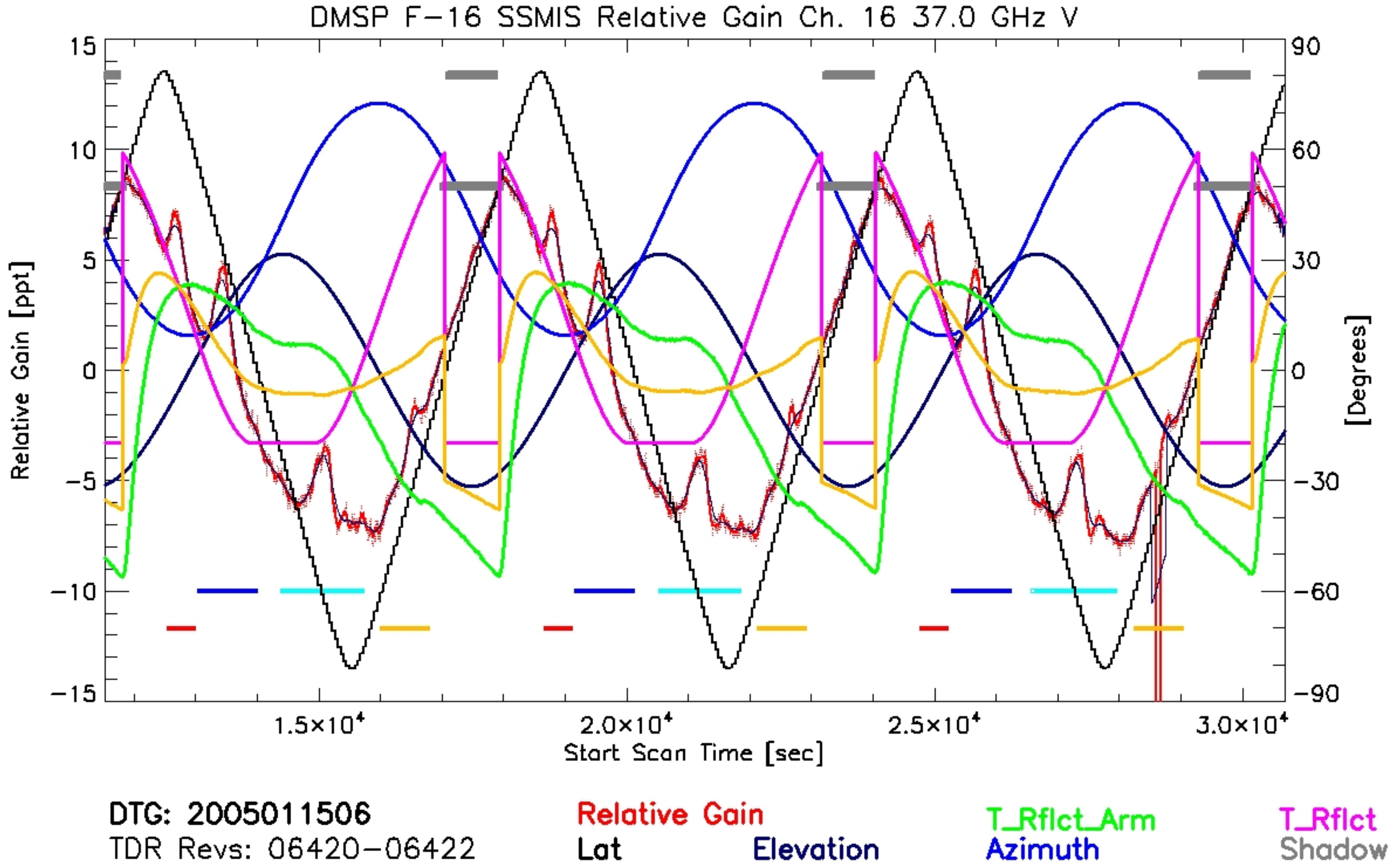

Channel 16 Warm Load Image (rev 6472)

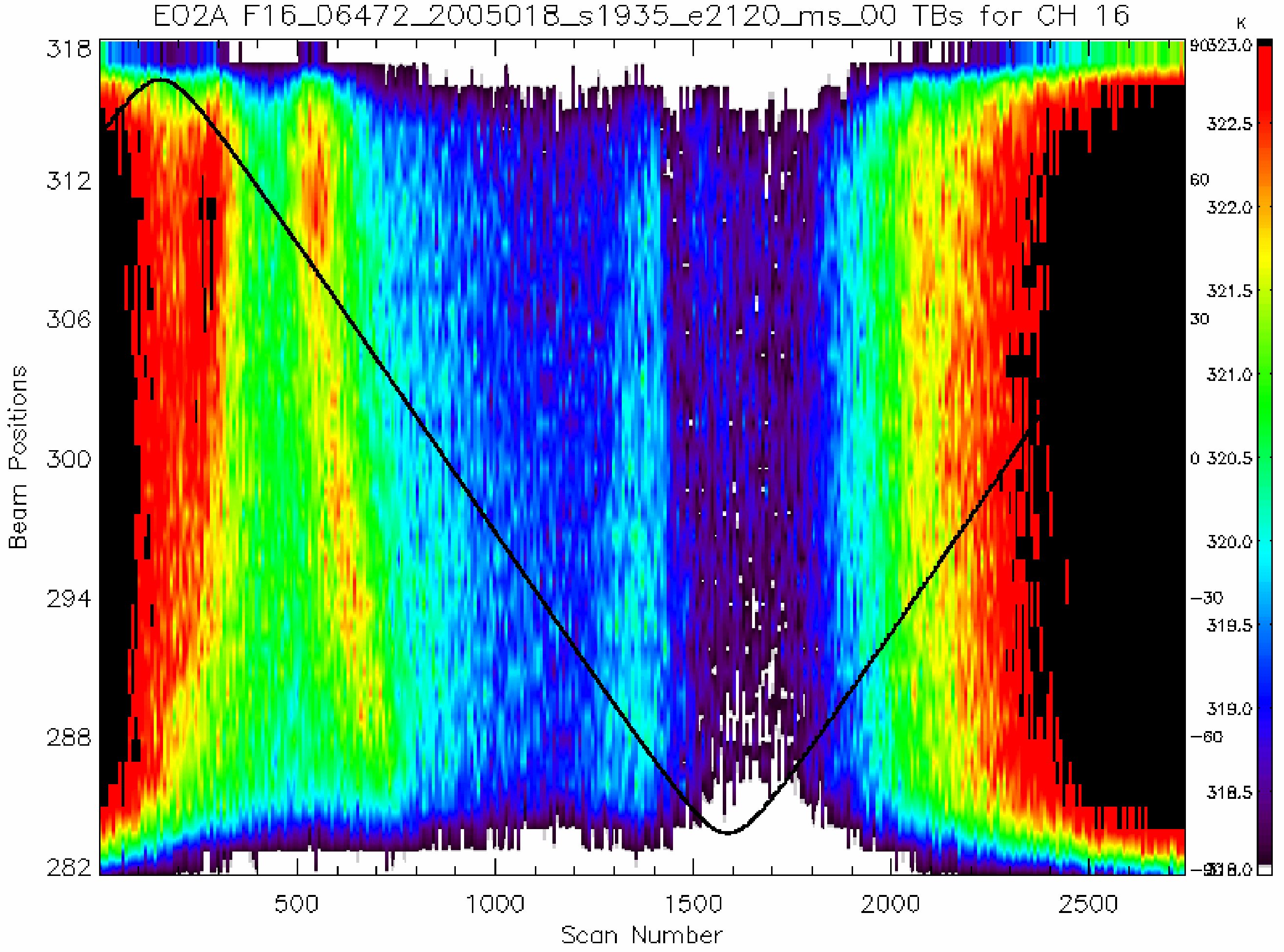

Channel 16 Warm Load Image (revs 6472 - 6494)

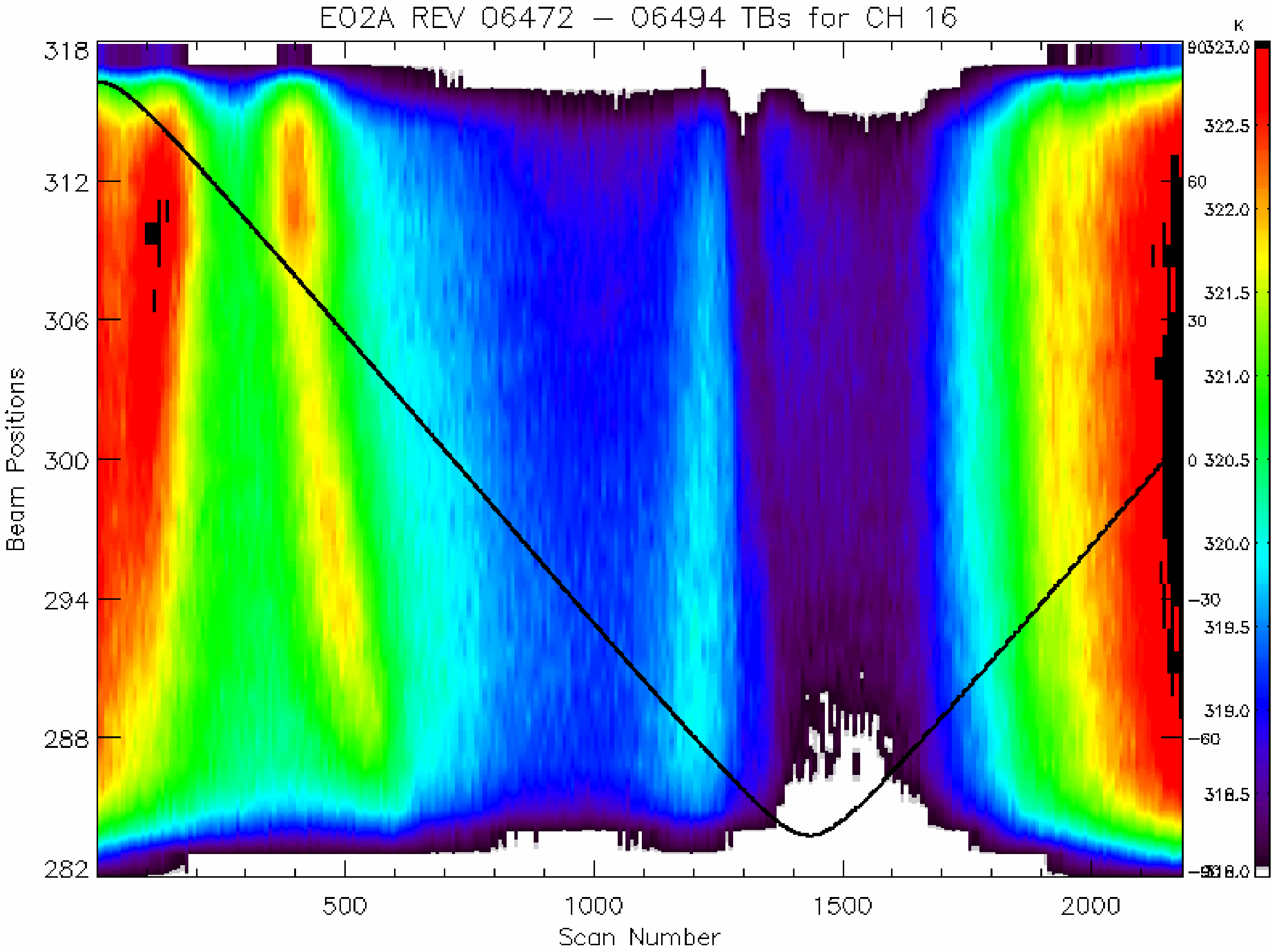

Channel 17 Time Series Gain Plot

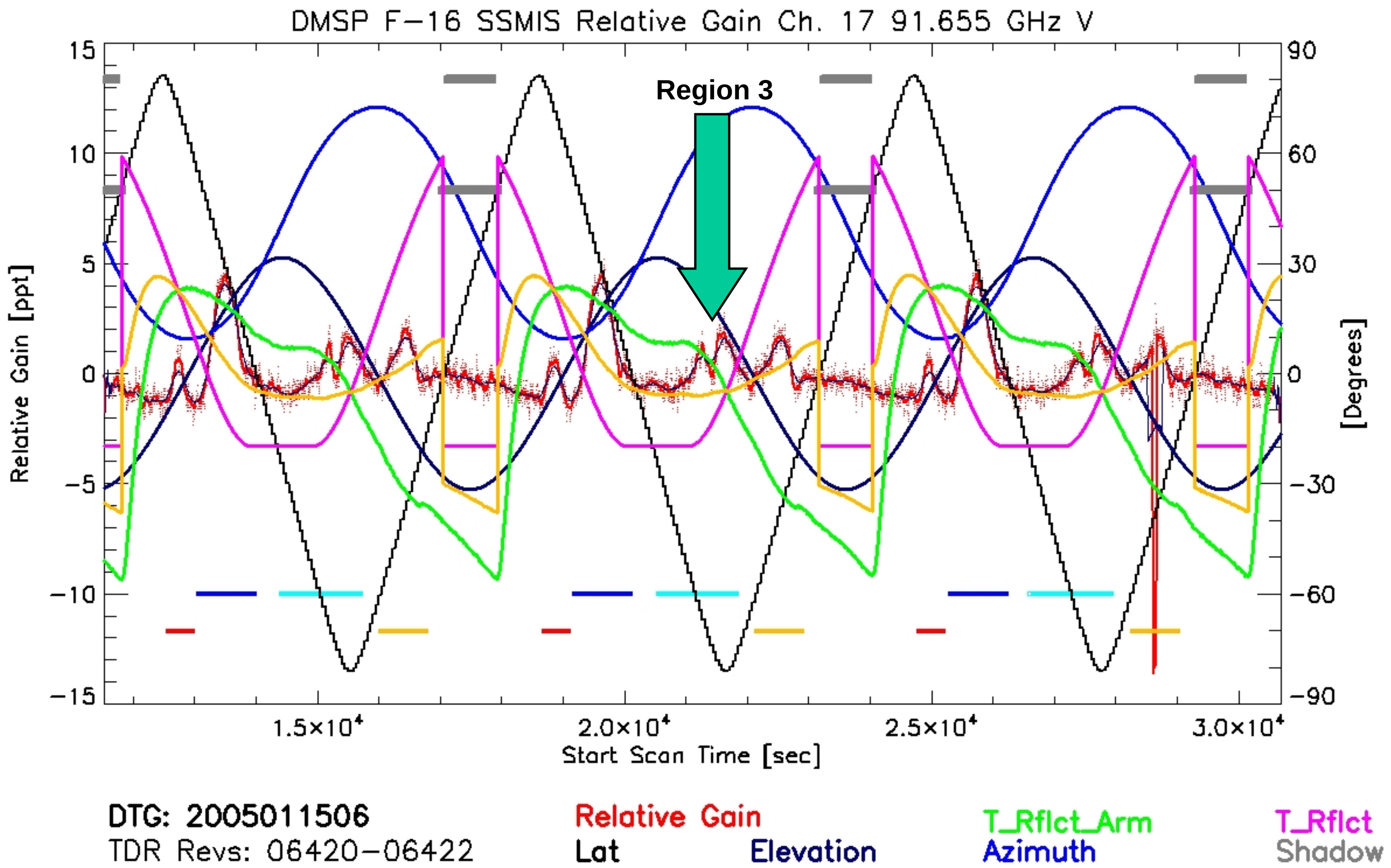

Channel 17 Warm Load Image (rev 6472)

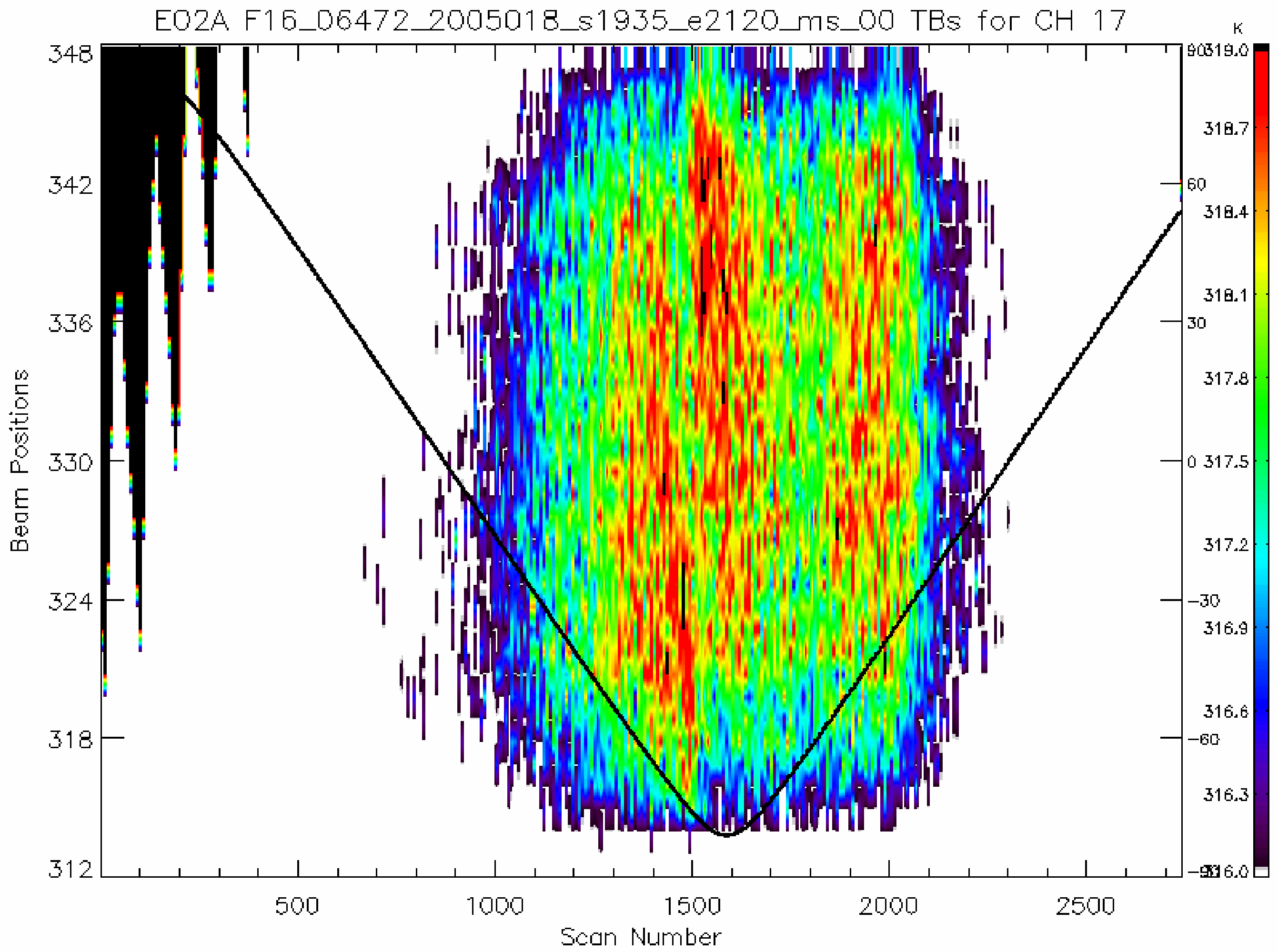

Channel 17 Warm Load Image (revs 6472 - 6494)

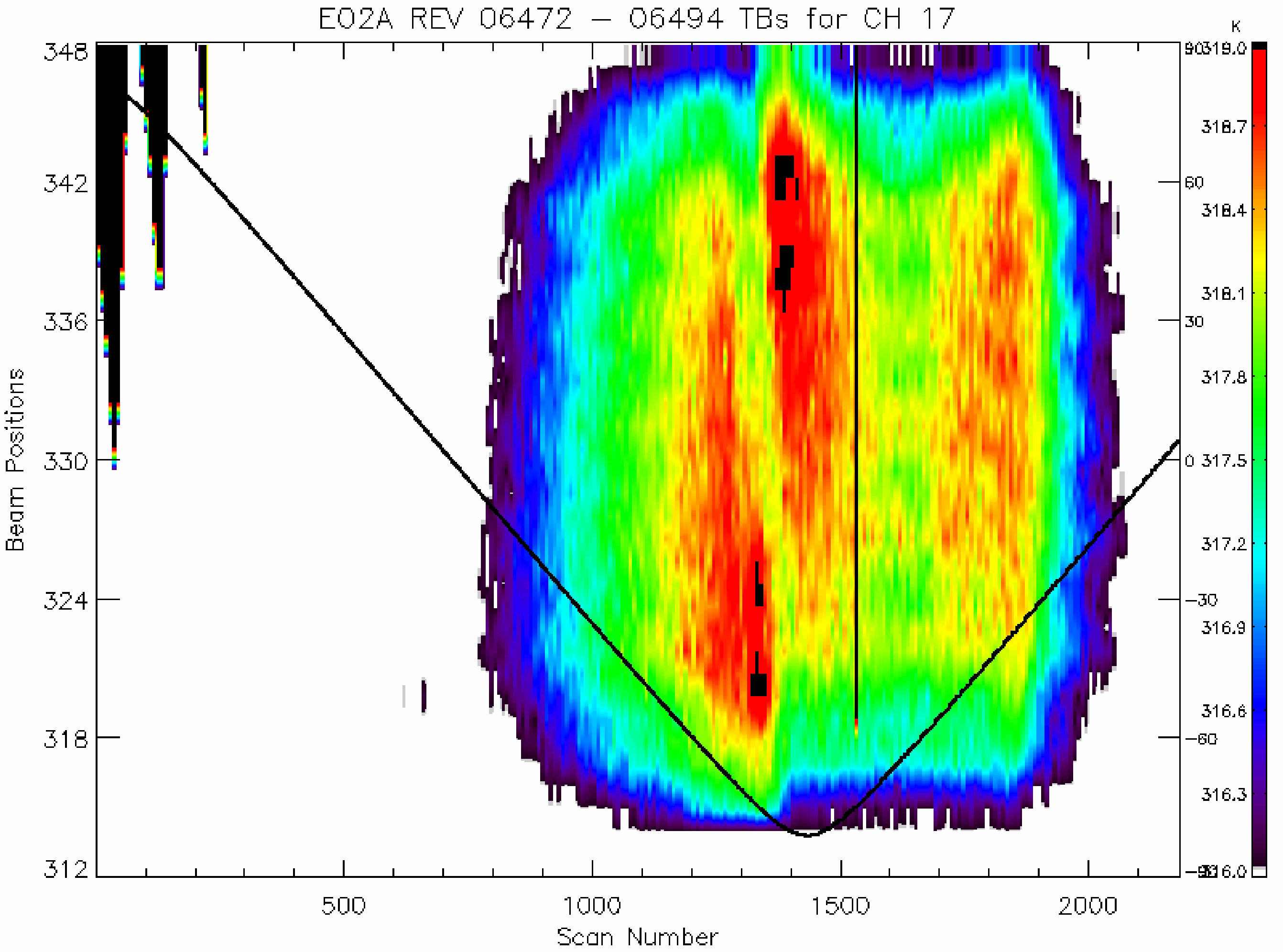

11.7D Warm Load Anomaly Corrections

The DGS tool was designed to include imaging processing. This capability, shown on page 11-88, allows a tabulated output showing the number of pixels representing the WL surface (red) that are illuminated by the sun. This could help to design a correction algorithm based on the level of sun exposure determined by DGS for the specific orbit or time of year. In general however, a gating process that identifies the period that the WL errors may exist that is based on the solar angle with respect to the WL will have to be implemented (see Section 12 page 26). Correct gating and flagging of the affected regions is critical for establishing a reliable WL correction. Key to this is the "tie" point of corrections between Region 2 and 3 (Reflected #1 and #2). In fact the ray tracing model is shown for the midway point between these regions in February (lowest maximum solar elevation, page 11-89) and June (largest maximum solar elevation, page 11-91). The resulting red visible under the WL for the ray tracing model in February (solar elevation of 26 degrees, page 11-89) indicates that errors still exist in this region where it is critical to establish an anomaly free tie point also confirming the joined nature of Region 2 (dark blue line) and 3 (light blue line) at the bottom of the graph on page 11-90. It is also clear looking at the Ch 17 gain plots on page 11-90 that this area is not free of the solar intrusion. Because this area is critical for establishing a smooth and uniform gain correction, it is suggested that an empirical relationship be derived between the amount of visible red tines in the ray trace model in order to design an (empirical) correction at the maximum solar elevation point when Regions 2 and 3 are joined. This would allow the corrected gain to always have a tie point between the two largest and lengthy WL anomalies.

Image Processing capability of DGS

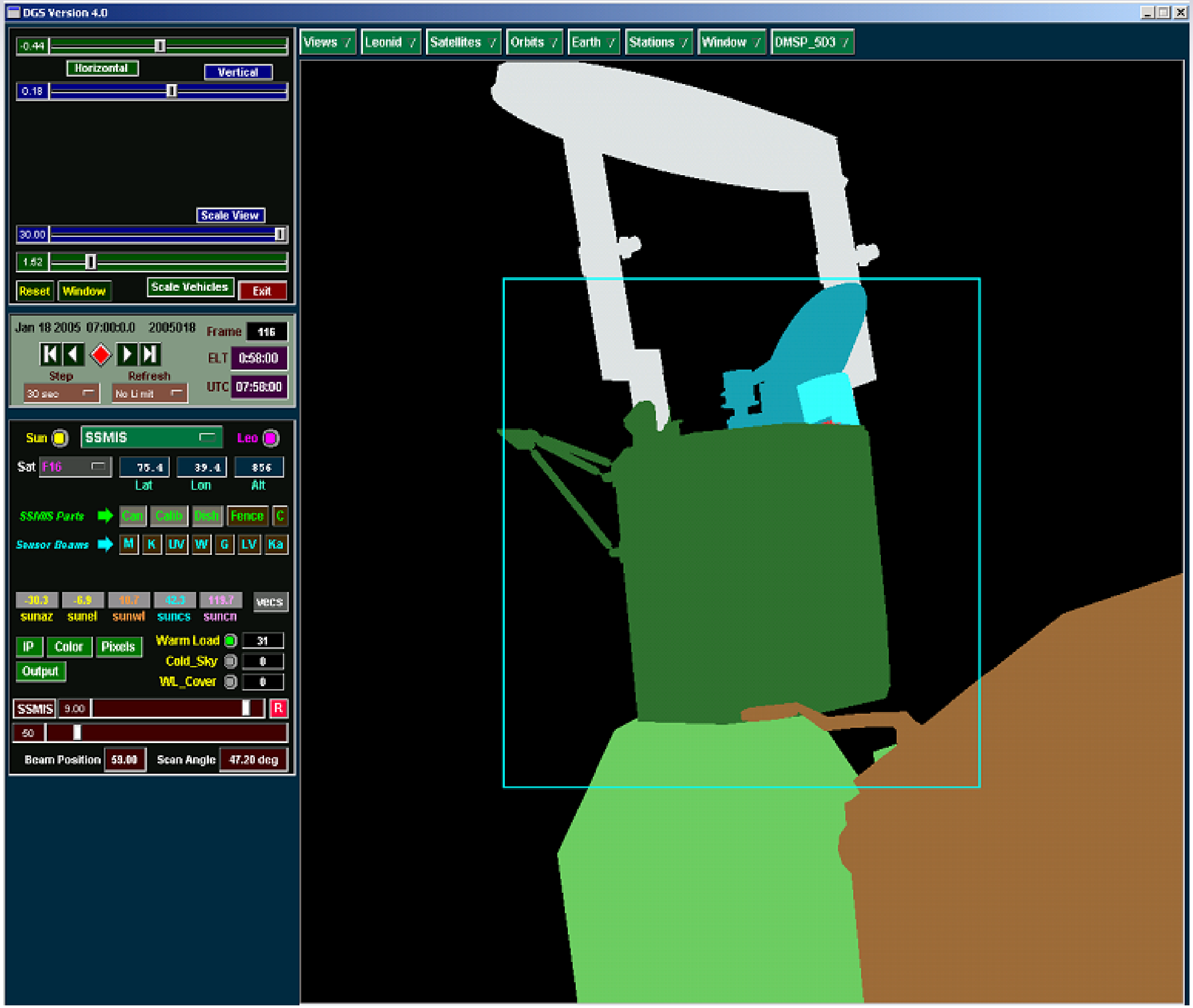

DGS Version 4.0

Jan 18 2005 07:00:0.0 2005018

Frame 116

ELT 0:58:00

UTC 07:58:00

Step 30 sec

Refresh No Limit

Sat F16

Lat 75.4

Lon 39.4

Alt 856

sunaz -30.3

sunel -6.9

sunwl 10.7

suncs 42.3

suncn 119.7

Warm Load 31

Cold_Sky 0

WL_Cover 0

Beam Position 59.00

Scan Angle 47.20 deg

SSMIS Ray Trace Model; High Sun Elevation February 11, 2004

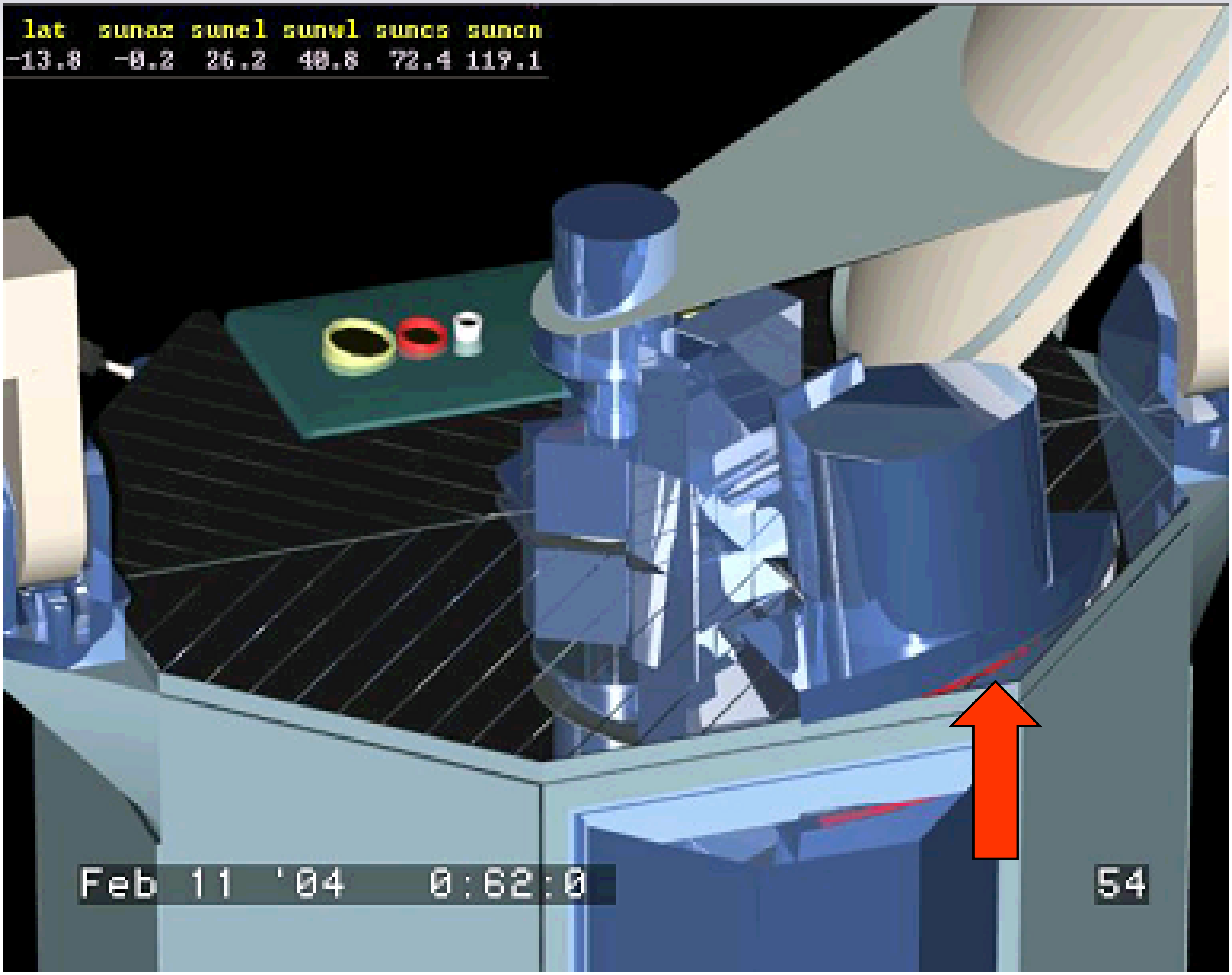

lat	sunaz	sunel	sunwl	suncs	suncn
-13.8	-0.2	26.2	40.8	72.4	119.1

Channel 17 Time Series Gain Showing Warm Load Anomaly Regions (February 2004)

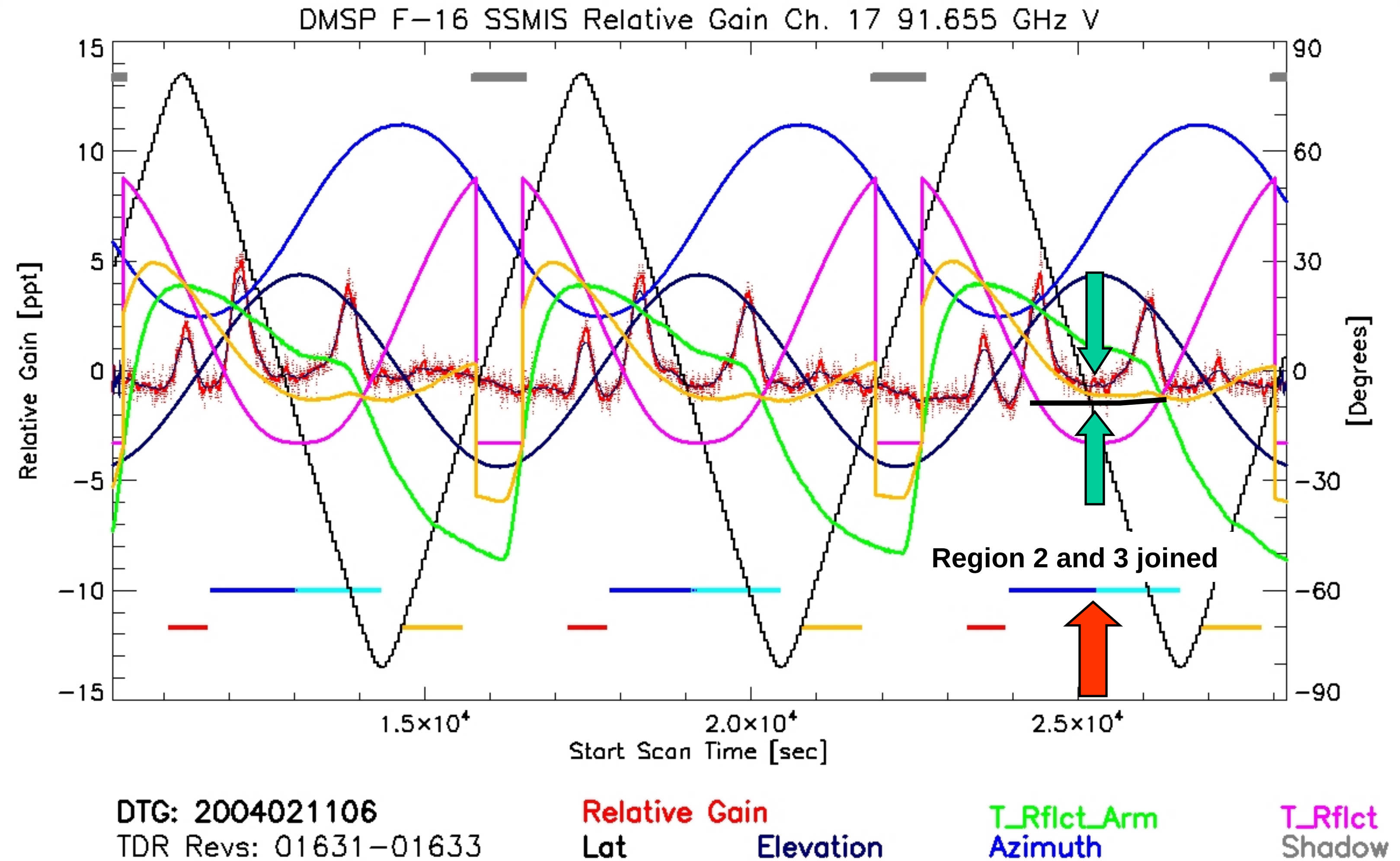

SSMIS Ray Trace Model; High Sun Elevation
June 21, 2004

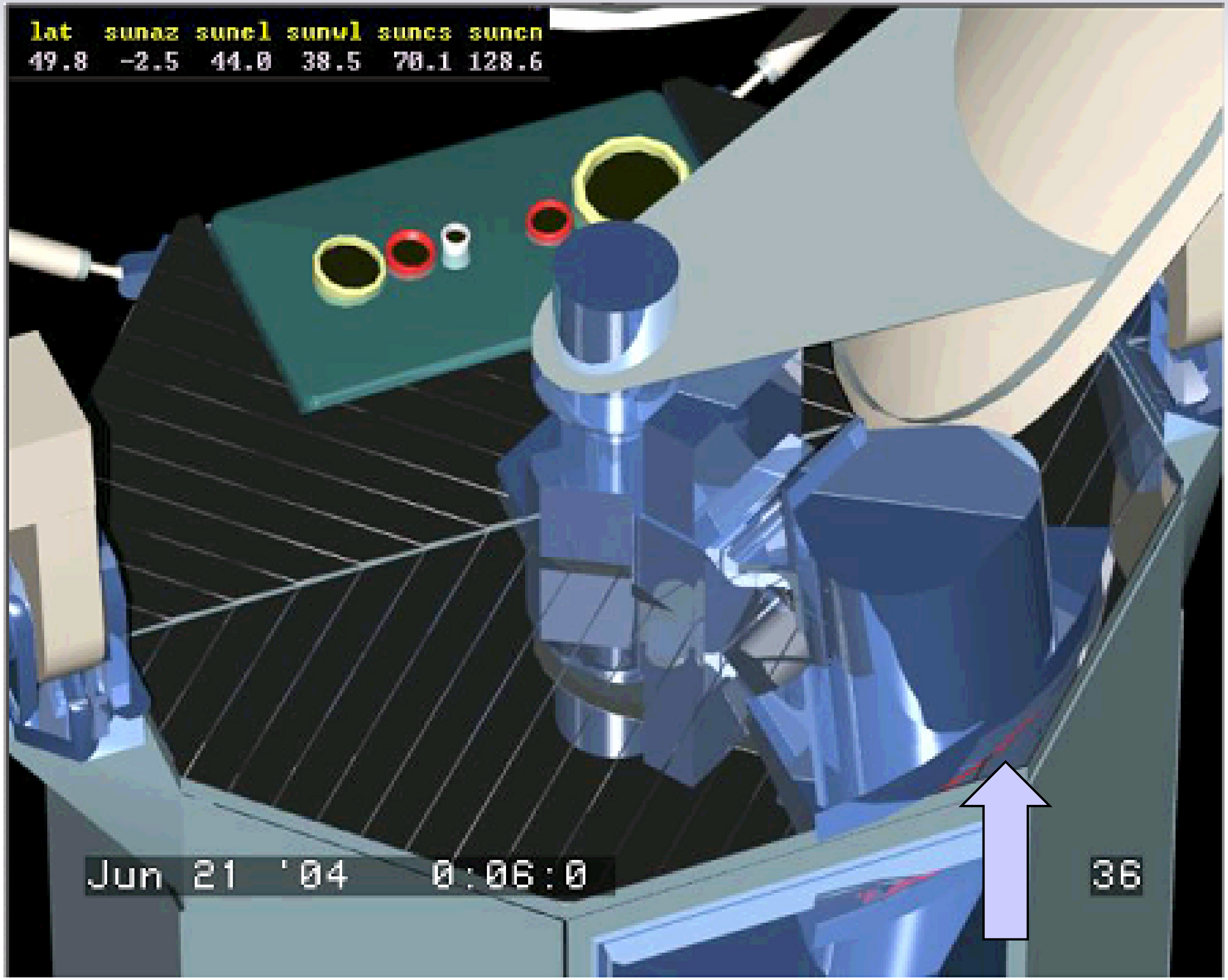

Channel 17 Time Series Gain Showing Warm Load Anomaly Regions (June 2004)

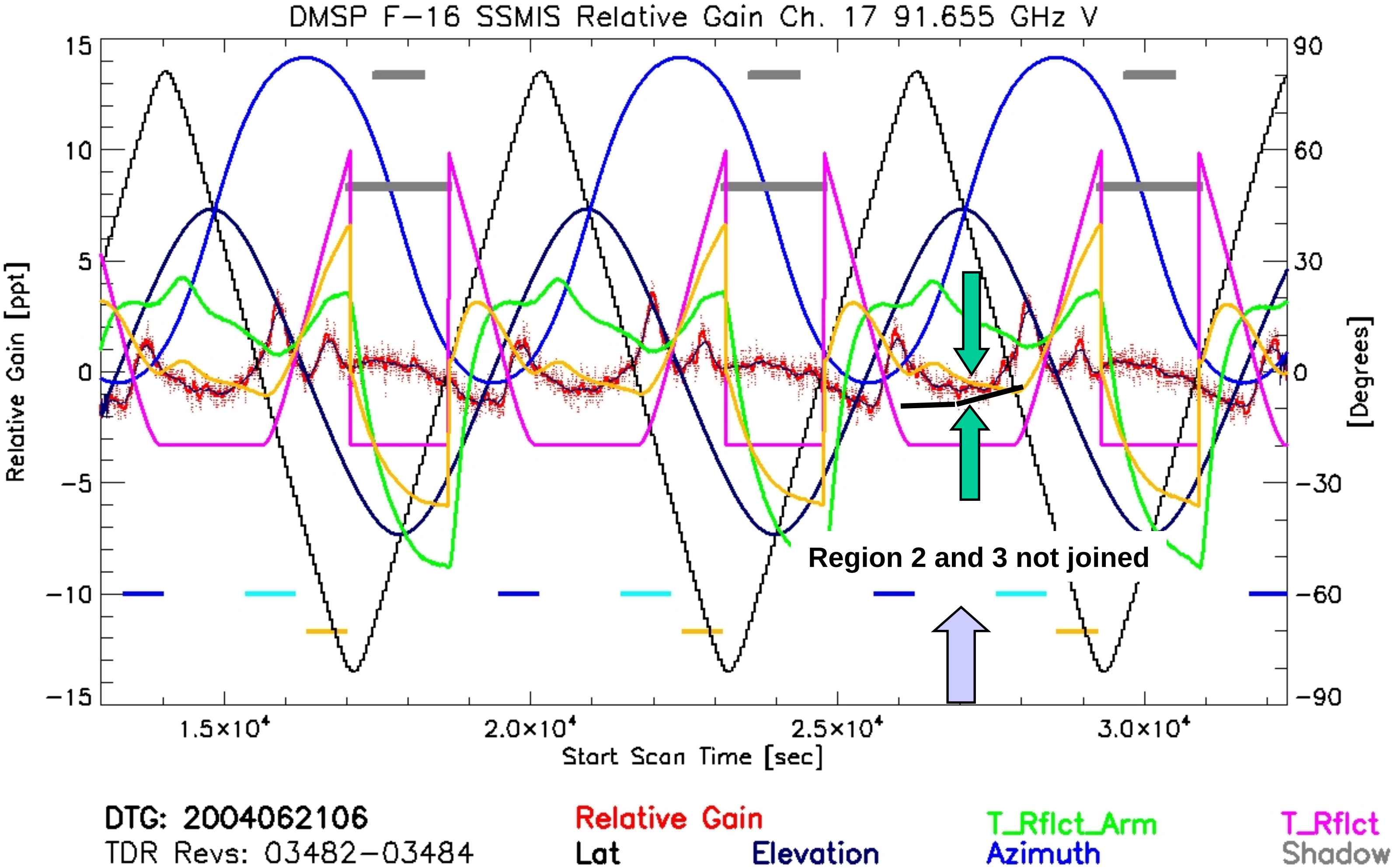

SSMIS Ray Trace Model; High Sun Elevation
March 1, 2004

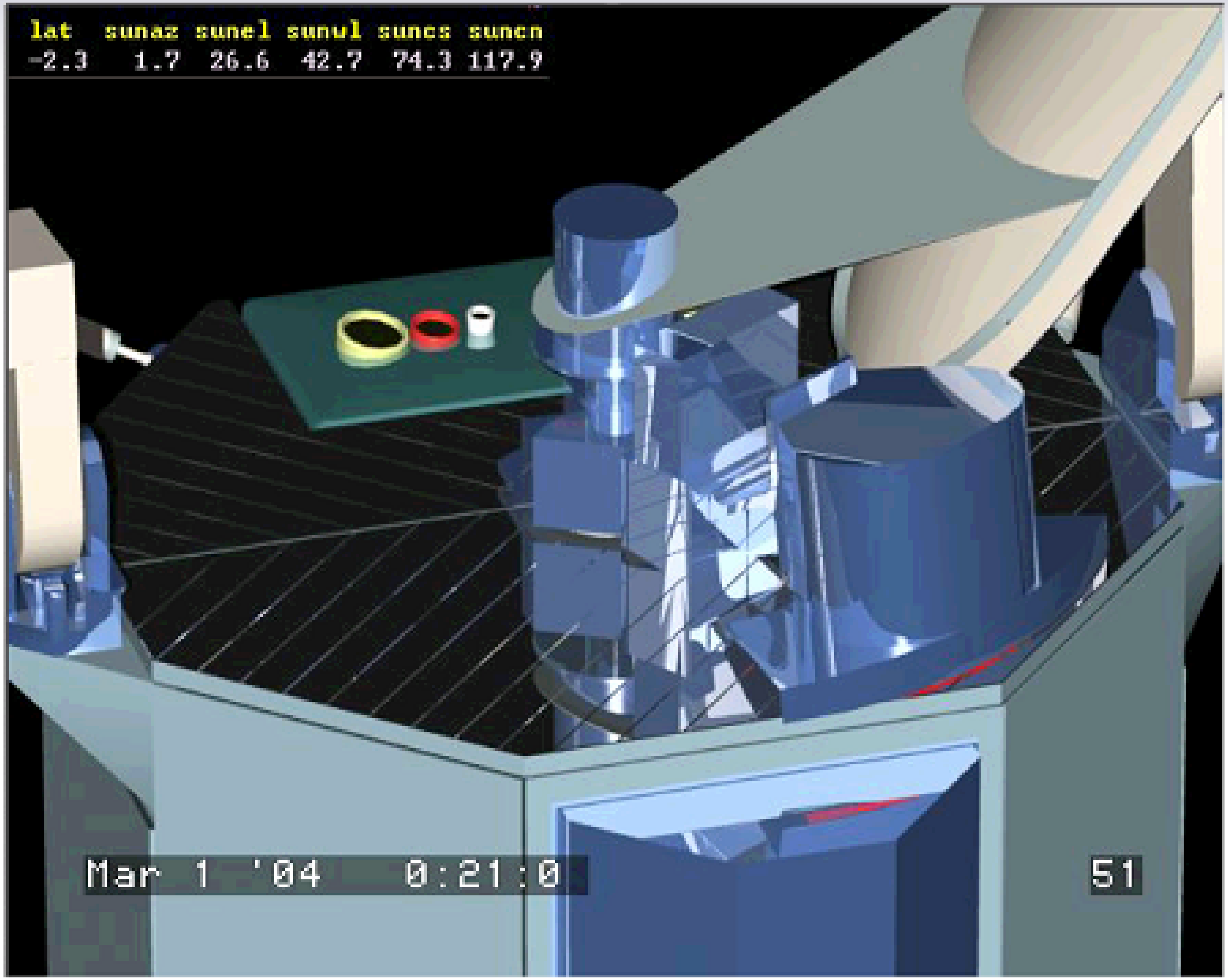

lat	sunaz	sunel	sunwl	suncs	suncn
-2.3	1.7	26.6	42.7	74.3	117.9

Channel 17 Time Series Gain Showing Warm Load Anomaly Regions (March 2004)

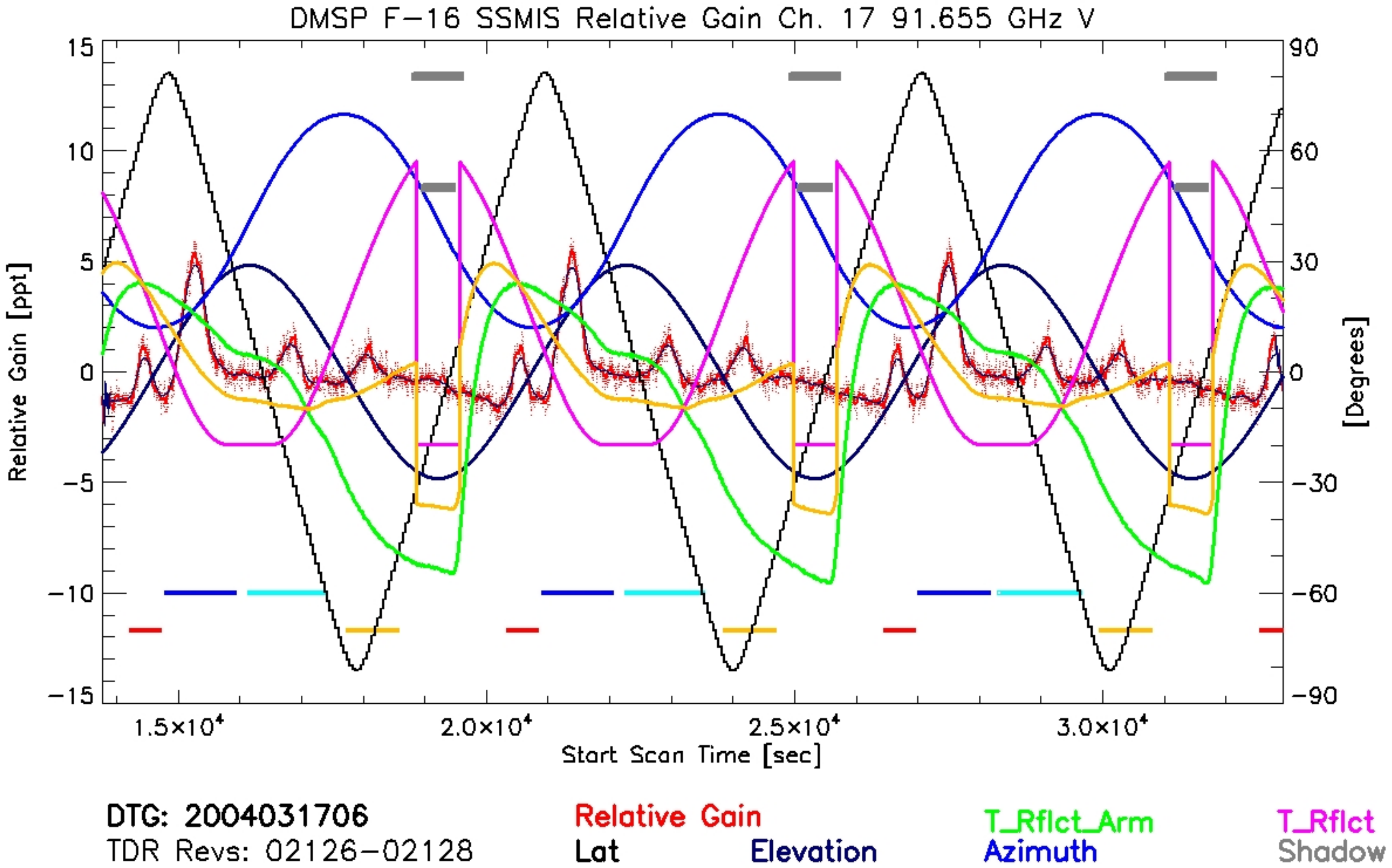

SSMIS Ray Trace Model; High Sun Elevation
August 5, 2004

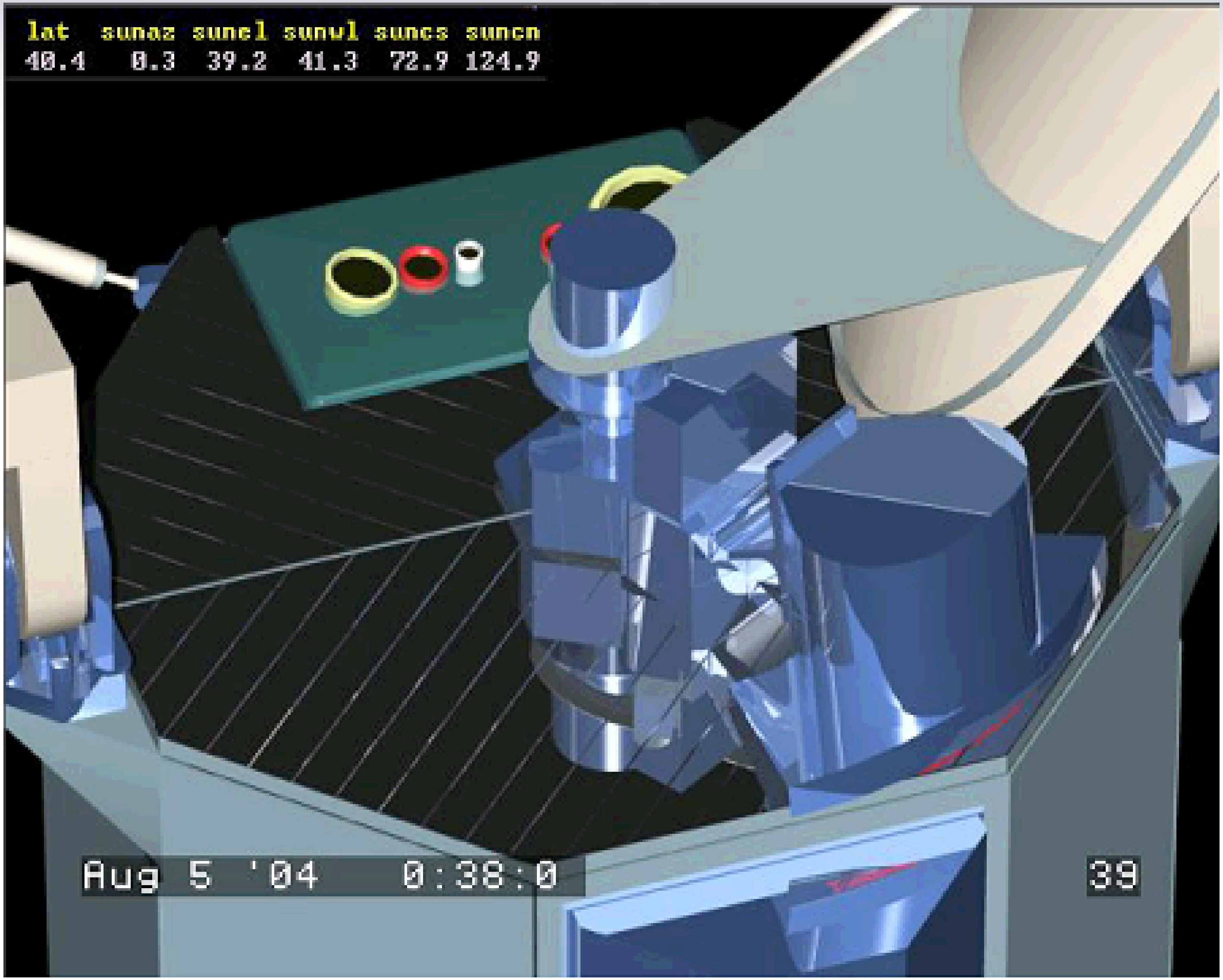

Channel 17 Time Series Gain Showing Warm Load Anomaly Regions (August 2004)

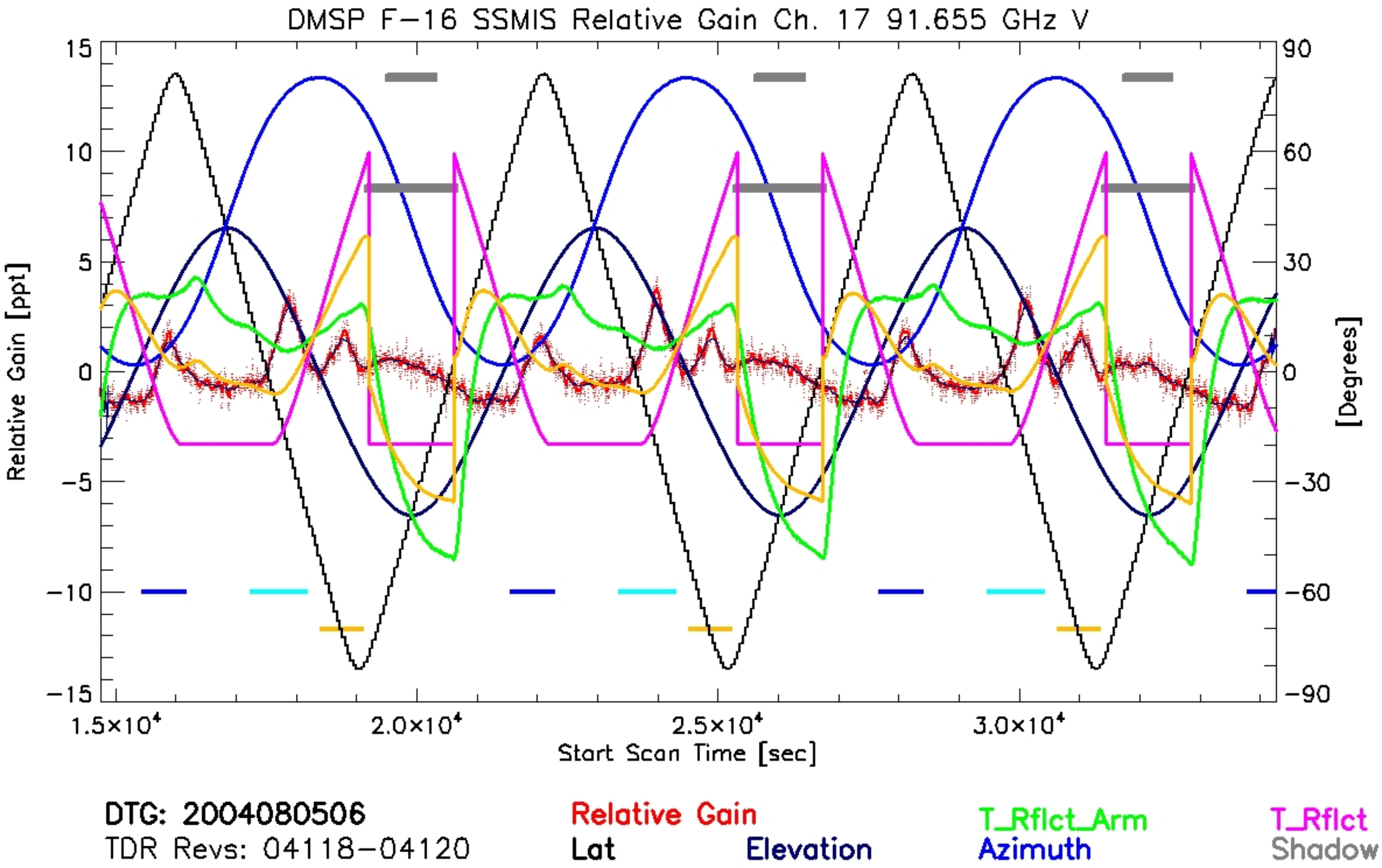

11.7E Summary of EO2 2005 Analysis for Correction of WL Anomalies

The DGS and Ray Tracing simulation tools developed for SSMIS have helped to identify and characterize the Warm Load solar intrusion regions. This process has been aided by collections of Early Orbit data in 2003 and 2005. The 2005 EO collection was more extensive allowing detailed images of the WL anomalies to be created which help to characterize the solar intrusion and determine the best approach for correcting the residual calibration errors caused by the anomalies. The strongest anomaly is typically from Region 2 (Reflected #1) and therefore, the ray tracing tool is necessary for characterizing these cases. Several algorithms have been conceptualized for correcting residual calibration errors caused by the WL anomalies, however, the most difficult part appears to be treatment of the area between Region 2 and 3. The ray tracing SSMIS simulation indicates that during seasons of the orbit where the maximum solar elevation angle does not rise above ~ 30° there is no period between Region 2 and 3 that can be uses as an error-free tie point for a calibration correction scheme. However, the WL error is much smaller at the maximum solar elevation point in any season even if a residual exists. This may allow an empirical correction at this point to establish a calibration "tie" point at a critical time for maintaining small residual calibration errors overall. The current algorithm for correcting WL anomalies needs improvement before the corrected values can be used operationally.

11.8 Introduction to the SSMIS Reflector Emission Anomaly

Page 11-99 shows the SSMIS calibration system comprising the warm calibration load, the cold sky reflector (cold calibration target), and the main reflector which for conically scanning radiometers, is not part of the radiometric calibration. Therefore corrections attributable to the main reflector must be accounted for in the conversion from Temperature Data Records (TDRs) to Sensor Data Records (SDRs). Indeed, spillover and main beam sidelobes account for the largest post-calibration corrections required in computing the SDRs. However, until SSMIS was flown, antenna emission was generally not considered a significant contributor to the calibration error – even for conically scanning radiometers – and was not corrected. Detailed comparisons with background data and testing of designed-for-flight hardware have shown that antenna emission for SSMIS is almost certainly the cause of significant residual biases that are most noticeable using ECMWF background observations as the sensor transitions from solar eclipse into sunlight in the F16 ascending node. A full description of these comparisons appears in Section 12 beginning on page 12-42. Page 11-100 describes the main reflector geometry. There were no specific requirements on reflector emissivity or purity of the surface construction. Page 11-101 and 11-102 are photographs of the main reflector S/N02 which is mounted on SSMIS S/N01 prior to launch. The photographs show a uniform surface with no noticeable defects. Note that the bright strip across the main reflector appearing on page 11-102 is due to a reflection of the photoflash from the side of the SSMIS canister onto the antenna.

The remaining parts of Section 11 describe the phenomenology of the antenna emission residual calibration anomaly using DGS and a sample background observation (11.9), report on the emissivity tests performed on the SSMIS Mass Model Cold Sky Reflector (MMCSR) designed to confirm the root cause of the anomaly (11.10), and then a summary and status is provided indicating the way forward for resolution of the root cause(11.11).

Antenna/Calibration Subsystem

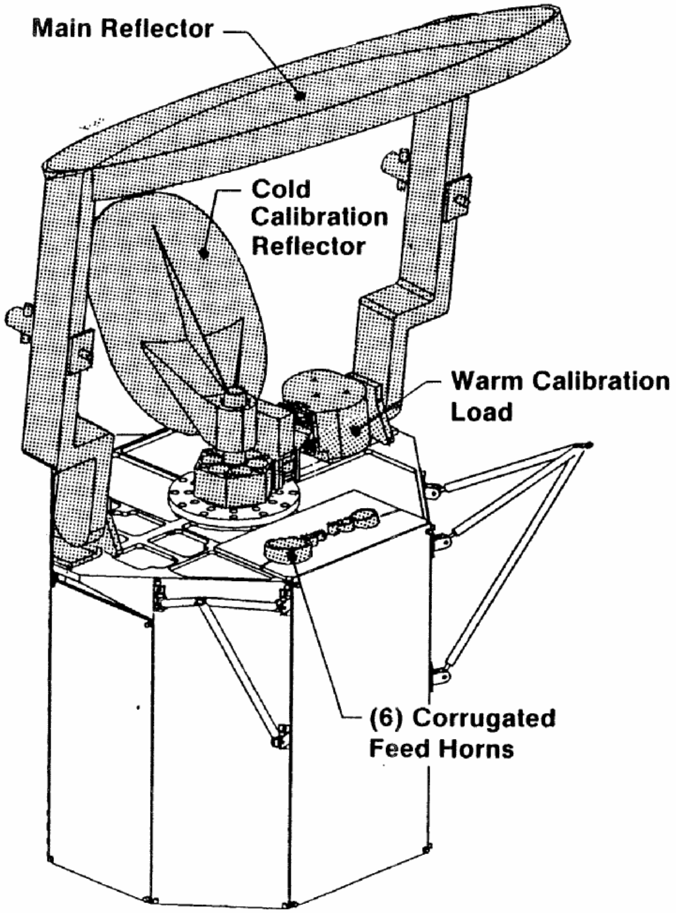

Main Reflector

- Offset Paraboloidal Reflector
- Graphite Epoxy Composite
- Reflector And Feed Horns Rotate Together Providing Equal Incidence Scan

Feed Horns

- Six Corrugated Feed Horns
- Polarization Diversity Provides Multi-Channel Capability

Inflight Calibration Assembly

- Remains Stationary To Allow Feed Horns To Rotate Under Cold Calibration Reflector And Warm Load To Provide A Two Point Calibration On Each Scan

Reflector Configuration

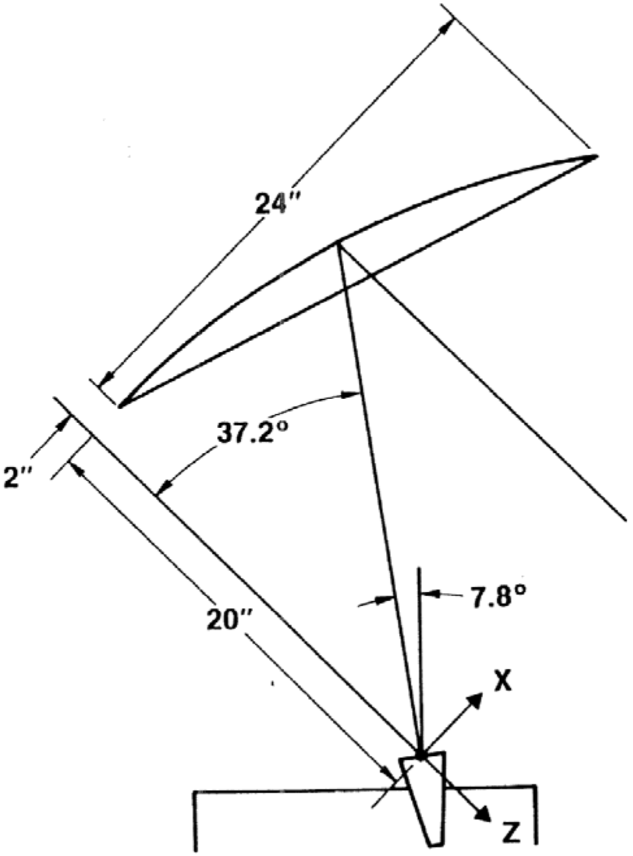

Reflector Equations

$$Z = \frac{X^2 + Y^2}{80} - 20$$

(Paraboloid)

$$Y = \pm\sqrt{144 - (x-14)^2}$$

$$2.0 \leq x \leq 26$$

(Circular Aperture)

Notes:

RMS Surface Deviation Of 0.0010 For: R = 0” to 8”RMS
Surface Deviation Of 0.0015 For: R = 8” to 12”

S/N002 Main Reflector

Photo Was Taken On 25 April 2005 Courtesy Northrop Grumman Corp.

S/N002 Main Reflector was integrated with S/N01 SSMIS Sensor in early 1995

From late 1995 through mid-1997 S/N01 sensor was used as "Pathfinder" for SSMIS program

In early 1998 S/N01 Sensor was refurbished into a flight unit

S/N01 Main Reflector on DMSP F16

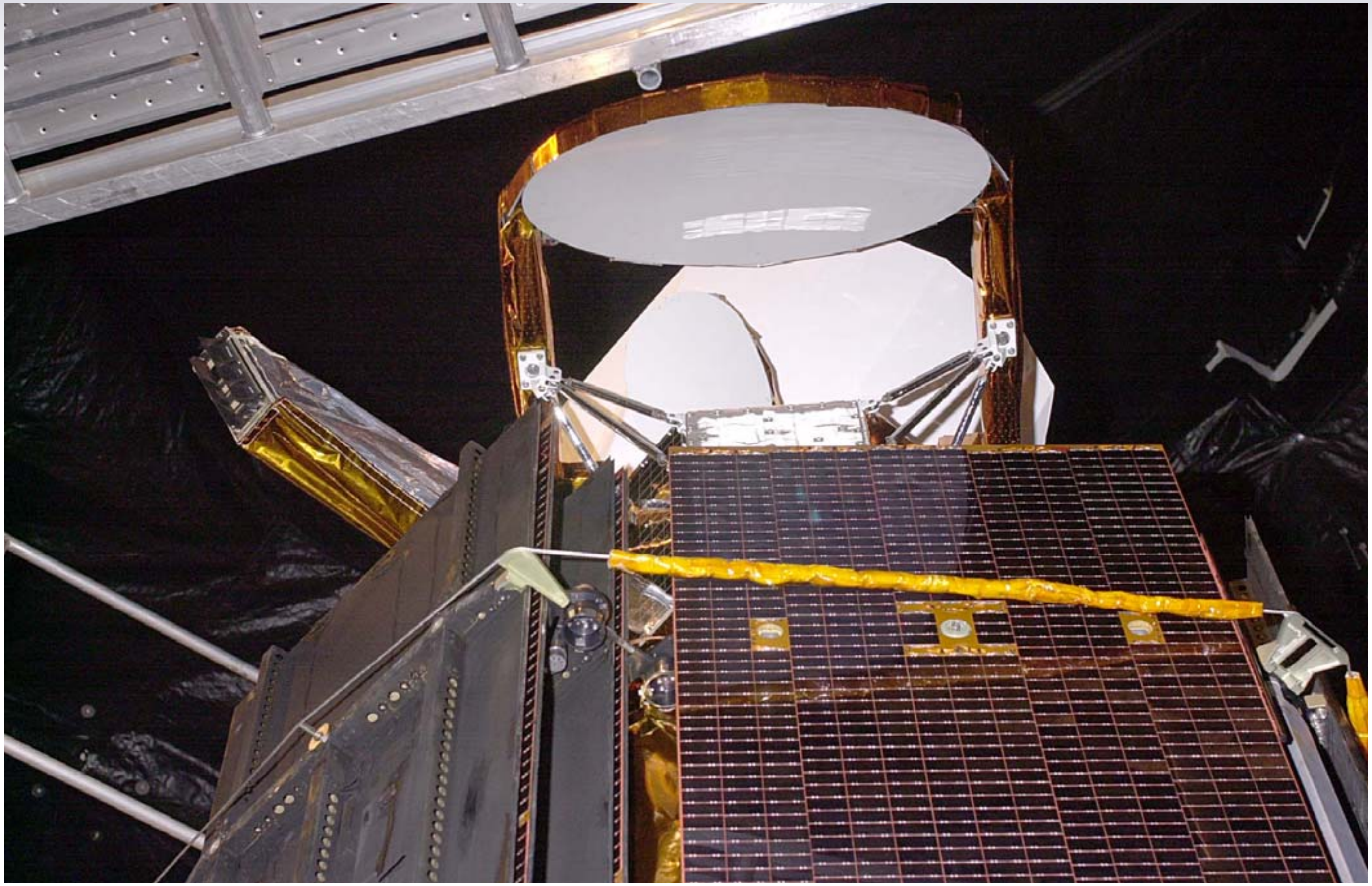

S/N02 SSMIS Sensor on F16 DMSP Spacecraft on Launch Pad at VAFB

11.9 Residual Calibration Errors Due To Antenna Emission

Pages 11-104, 11-105, and 11-106 show the DGS model of DMSP F-16 as it emerges from solar eclipse in the ascending node in March 2004. Note the arrow showing the location of the DGS sun indicator that shows yellow when the sun is illuminating the spacecraft (11-105 and 106) and the simulation is showing the spacecraft view from the sun. The sequence shows the location of the SSMIS main reflector as emerging from "behind" the spacecraft as it is crossing the equator for this season. Page 11-107 shows the difference between SSMIS observations (SDR) and the ECMWF forecast applied to RTTOVS 7 to simulate the SSMIS T_Bs. Note the conical scan geometry appearing as a "step" in the biases near ~10° N latitude as indicated by the arrow. This is exactly the position of SSMIS observing location as the main reflector is illuminated by the sun coming out of eclipse. Note that the SSMIS is looking forward of the spacecraft and the DGS model shows the location of the ground-track rather than the SSMIS viewing location. Section 12 (beginning on page 12-42) shows a detailed series of comparisons for many orbital seasons that reinforces the conclusion that solar illumination and subsequent temperature change of the SSMIS reflecting surface coupled with higher-than-expected RF emission from the main reflector surface (~2 – 3% at 50 GHz) is responsible for the sudden change in bias with respect to the background observations shown on page (11-107) . Note that channel 3 was chosen on page 11-107 due to it's smoothly varying characteristic brightness temperature over the globe with virtually no contributions from surface emission. Therefore, sudden changes in sensor biases are easily discerned from errors in background brightness temperature estimation in general.

DGS Simulation March 2004 11.2°S

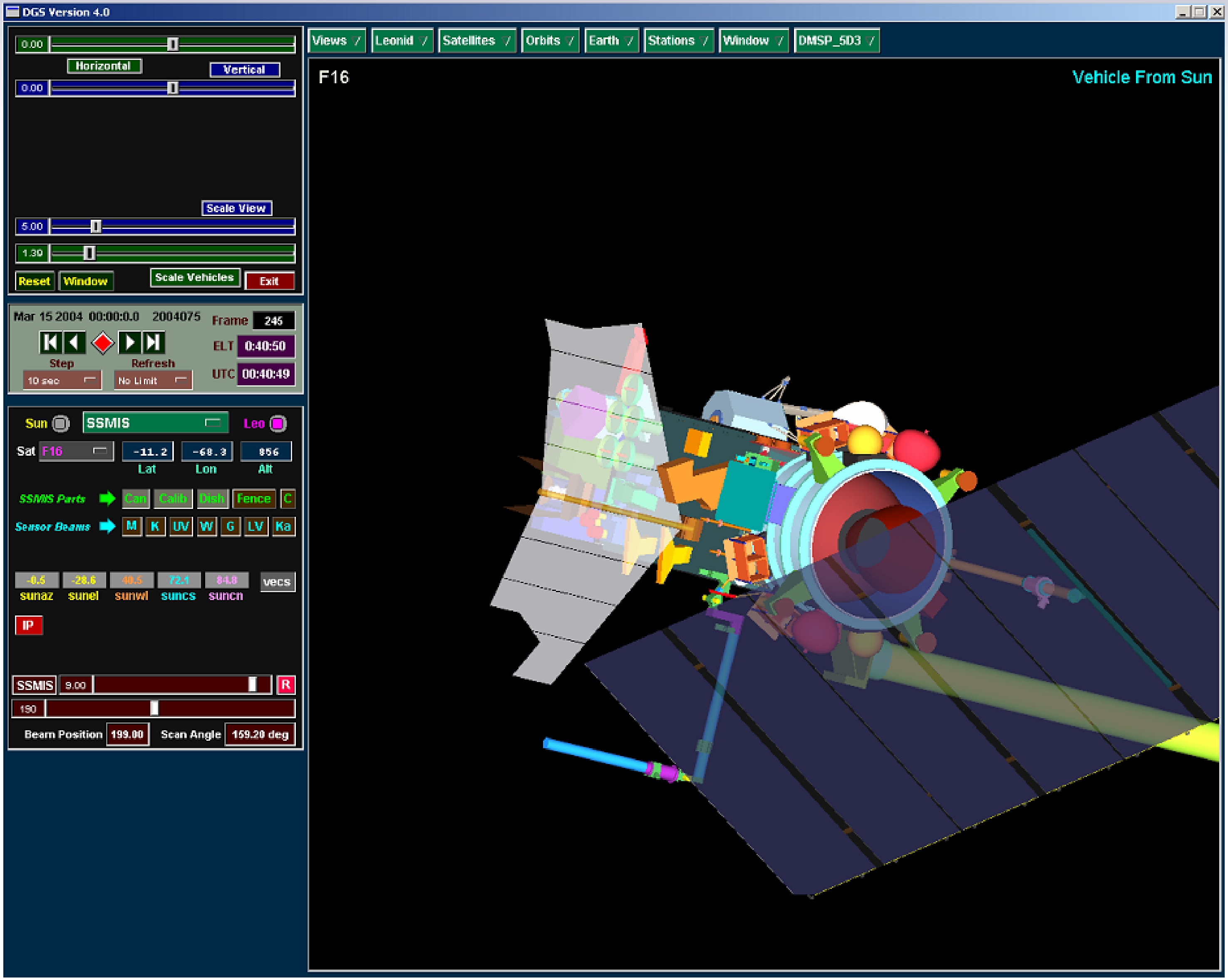

0.00
0.00
5.00
1.30

Mar 15 2004 00:00:0.0 2004075
Frame 245
ELT 0:40:50
UTC 00:40:49
Step 10 sec
Refresh No Limit

SSMIS
Sat F16
Lat -11.2
Lon -68.3
Alt 856

sunaz -0.5
sunel -28.6
sunwl 40.5
suncs 72.1
suncn 84.8

SSMIS 9.00
190
Beam Position 199.00
Scan Angle 159.20 deg

DGS Simulation March 2004 2.4°S

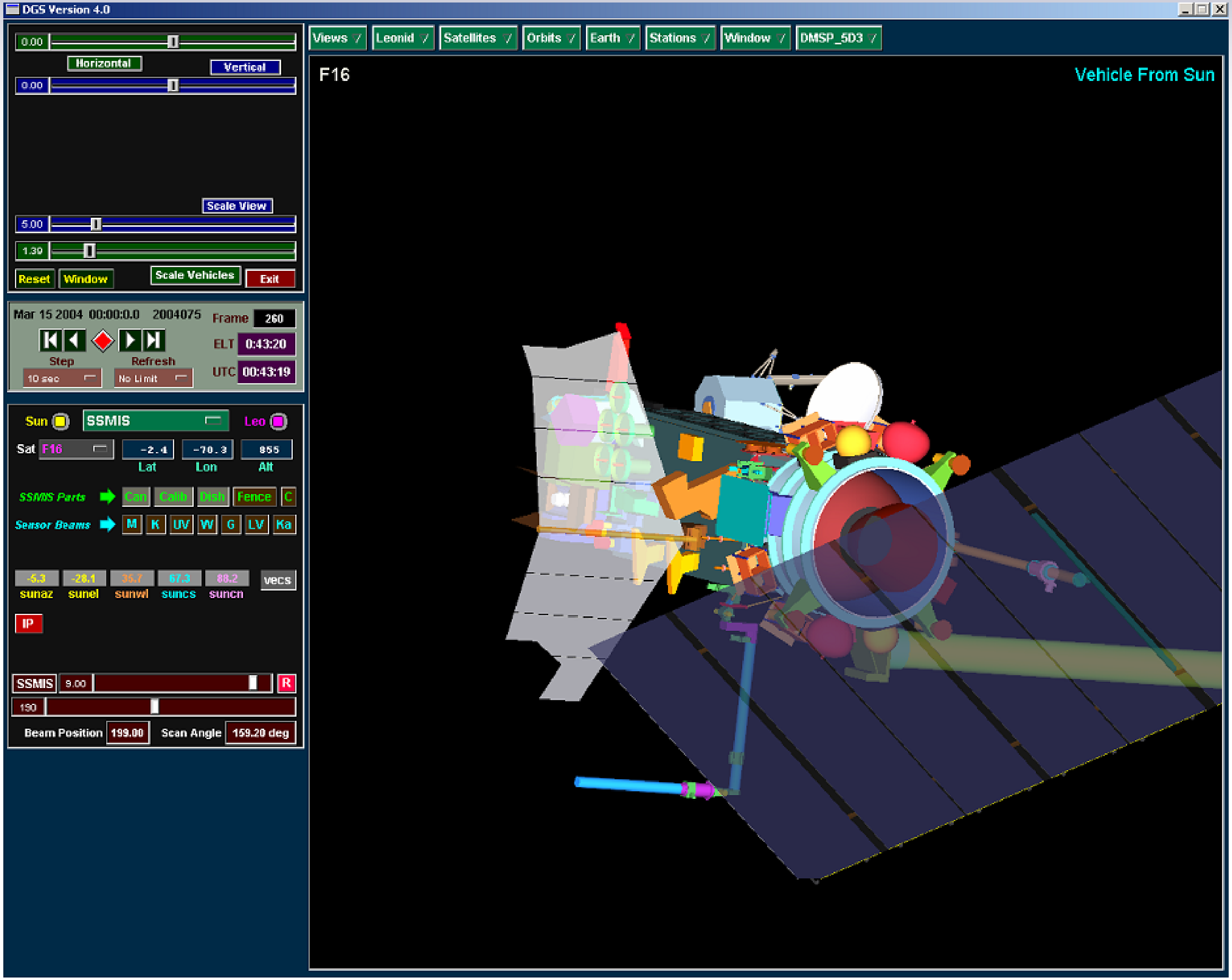

0.00

0.00

5.00

1.39

Mar 15 2004 00:00:0.0 2004075

Frame 260

ELT 0:43:20

UTC 00:43:19

Step 10 sec

Refresh No Limit

SSMIS

Sat F16

Lat	Lon	Alt
-2.4	-70.3	855

sunaz	sunel	sunwl	suncs	suncn
-5.3	-28.1	35.7	67.3	88.2

SSMIS 9.00

190

Beam Position 199.00

Scan Angle 159.20 deg

DGS Simulation March 2004 6.9°N

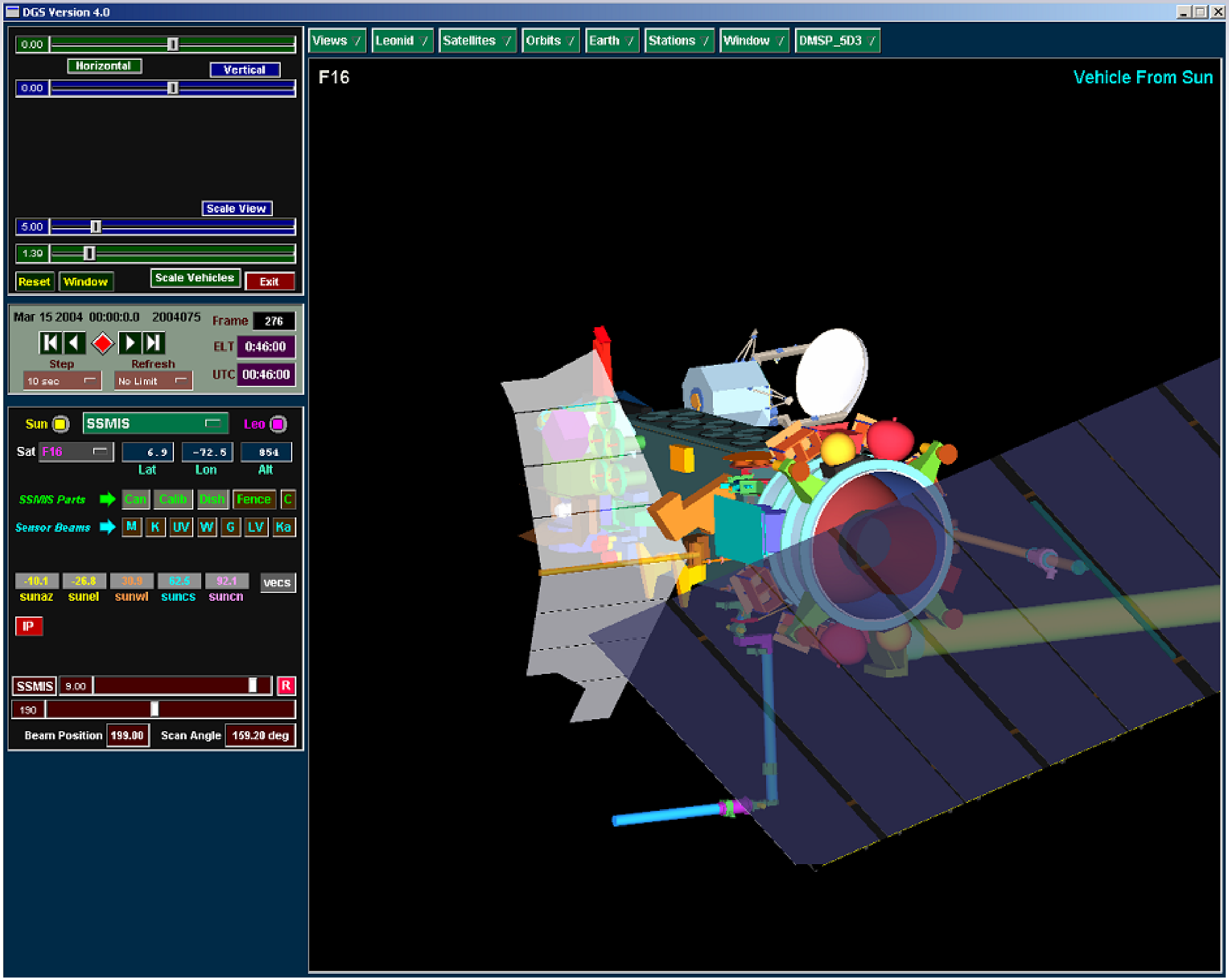

0.00

0.00

5.00

1.30

Mar 15 2004 00:00:0.0 2004075

Frame 276

ELT 0:46:00

UTC 00:46:00

Step 10 sec

Refresh No Limit

SSMIS

Sat F16

Lat 6.9

Lon -72.5

Alt 854

sunaz	sunel	sunwl	suncs	suncn
-10.1	-26.8	30.9	62.5	92.1

SSMIS 9.00

190

Beam Position 199.00

Scan Angle 159.20 deg

SSMIS Observation vs. Background T_B at 53.6 GHz

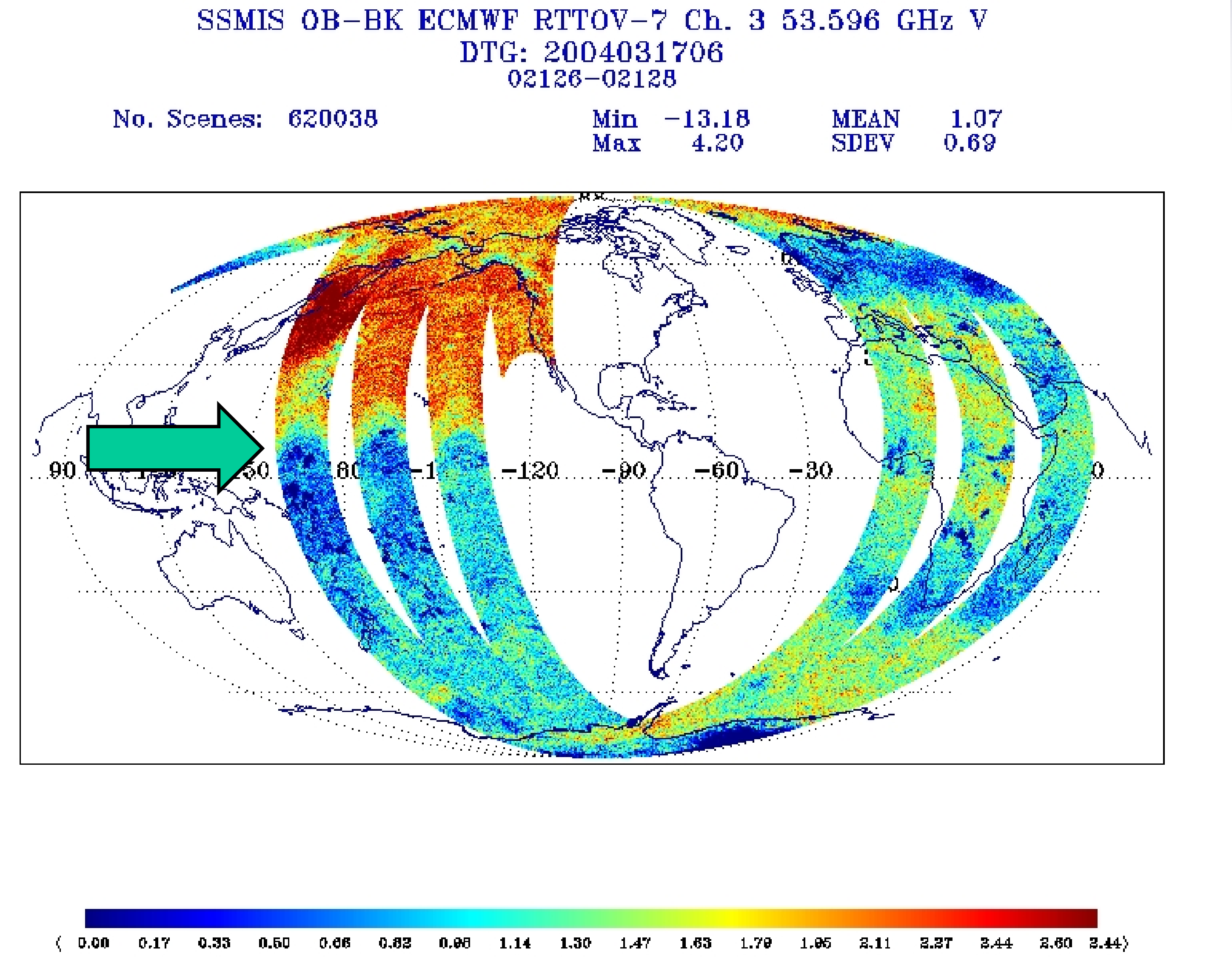

11.10 Emissivity Investigation Using the SSMIS Mass Model Cold Sky Reflector

Page 11-109 shows a “fishbone” analysis chart for resolving the root cause of the apparent high emissivity of the SSMIS main reflector. Starting by addressing the “wrong surface” thread, a routine investigation concerning the SSMIS main reflector’s Vapor Deposited Aluminum (VDA) and Silicon Dioxide Coatings with Northrop Grumman turned up no apparent defects in the surface construction. Although coupons of the antenna coatings were not available Northrop provided Aerospace with their Mass Model Cold Sky Reflector (MMCSR) in order to begin a more detailed investigation. The MMCSR is a flight-heritage CSR that was damaged during the development of a SSMIS Flight Unit (FU). The CSR’s surface coating was sampled for Secondary Ion Mass Spectroscopy (SIMS) testing to determine the structure of the reflecting surface. Page 11-110 shows the pedigree of the SSMIS main reflectors. The MMCSR was received by NG in 1993 the same year as the other coated main and CSR reflector combinations. Page 11-111 shows the “as-designed” reflector coatings. The CSR and Main reflector are designed with the same surface coating. Page 11-112 shows the results of the Aerospace SIMS test of the MMCSR. Note that the “as-designed” surface structure appears on the right hand side of the graph and the green arrows indicate the expected delineation between surface layers according to the “as-designed” structure. The SIMS test indicates the surface on the MMCSR is not representative of the “as-designed” structure. The key aspect appears to be the level of Aluminum concentration in the outer layer of Silicon Oxide coating. The SIMS tests shows this concentration to be ~3% (left end of blue trace). The level of Al “contamination in the outer layer strongly influences the level of emissivity as modeled by NRL (See Page 11-116).

Way Forward for SSMIS

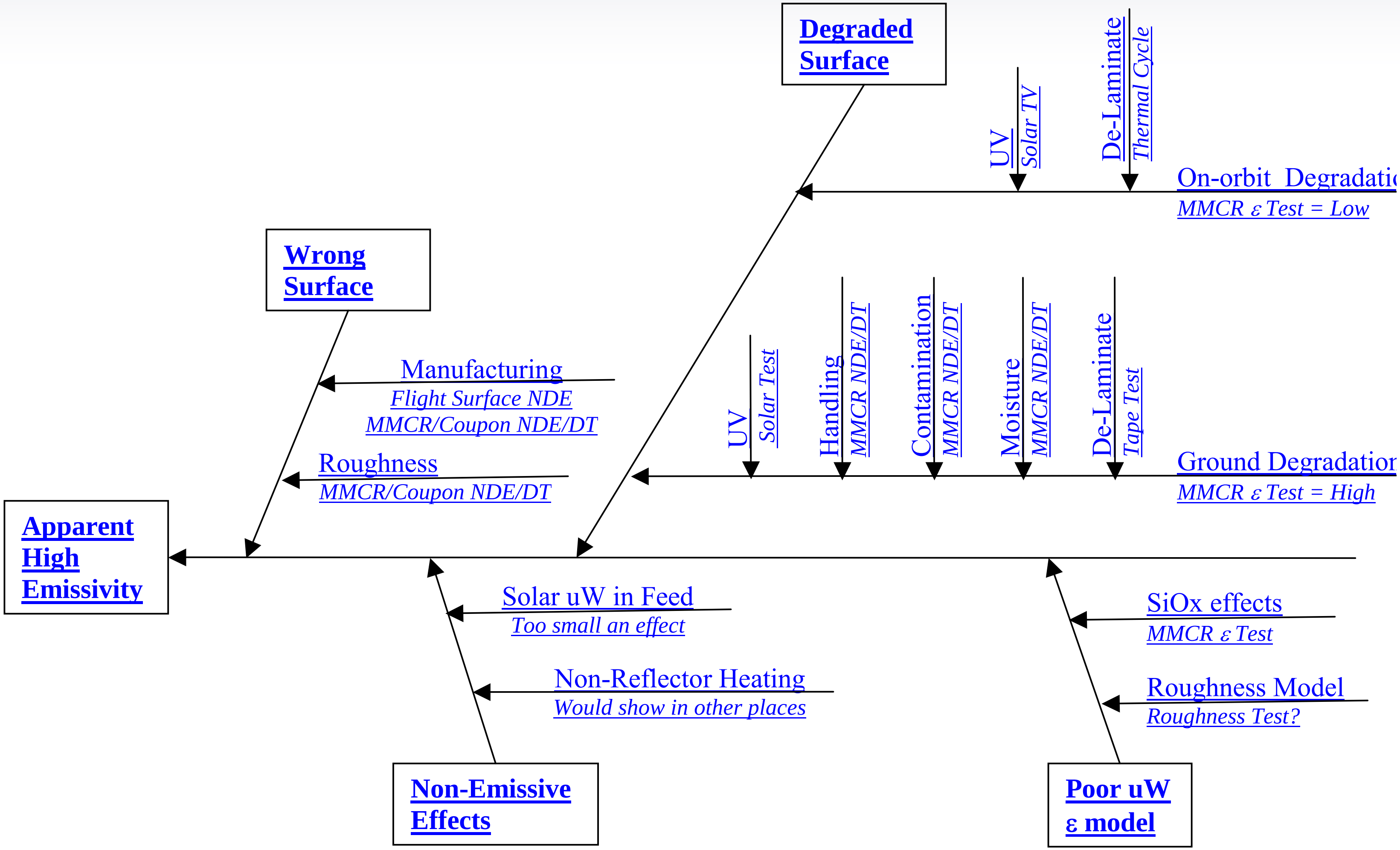

Degraded Surface

On-orbit Degradati

MMCR ε Test = Low

UV

Solar TV

De-Laminate

Thermal Cycle

Ground Degradatio

MMCR ε Test = High

UV

Solar Test

Handling

MMCR NDE/DT

Contamination

MMCR NDE/DT

Moisture

MMCR NDE/DT

De-Laminate

Tape Test

Wrong Surface

Manufacturing

Flight Surface NDE

MMCR/Coupon NDE/DT

Roughness

MMCR/Coupon NDE/DT

Apparent High Emissivity

Non-Emissive Effects

Solar uW in Feed

Too small an effect

Non-Reflector Heating

Would show in other places

Poor uW ε model

SiOx effects

MMCR ε Test

Roughness Model

Roughness Test?

Status of SSMIS Main Reflectors

- **Mass Model, rcvd 12 Dec'92 – On Mass Model Instrument, at NG-Azusa**
- **S/N001, rcvd 15 Dec'93 – On S/N05 Instrument at NG-Azusa**
- **S/N002, rcvd 18 Jan'93 – On S/N01 Instrument, at NG-Azusa**
- **S/N003, rcvd 15 Jun'93 – On S/N02 Instrument in orbit since Jan'03**
- **S/N004, rcvd 21 May'93 – On S/N04 Instrument at NG-Azusa**
- **S/N005, rcvd 15 Jun'93 – On S/N03 Instrument on F17 Spacecraft at LM-Sunnyvale**
- **S/N006, rcvd 7 Nov'00 – Spare reflector in long-term storage**

Reflector Construction

Offset Paraboloidal Reflector

- 24.0 Inch Projected Aperture
- 20.0 Inch Focal Length
- 0.02 Inch Shell Thickness, Graphite Fiber Laminate
- 0.06 Inch Structure Thickness, Graphite Fiber Laminate

Coating Layers

1. BR-127 Epoxy Primer with 5% Cabosil (Inner-most layer)
2. Chromium 600 Angstroms
3. Aluminum 6,000 Angstroms
4. Silicon Oxide (SiOx) 5,000 Angstroms
5. Aluminum 6,000 Angstroms
6. Silicon Oxide (SiOx) 22,000 Angstroms

Coating Process

- Coating layers shall be applied under the control of a supplier-generated and customer approved “Reflector Coating Specification” with in-process witness samples supplied with each reflector

Secondary Ion Mass Spectrometry (SIMS) Testing Of SSMIS CSR

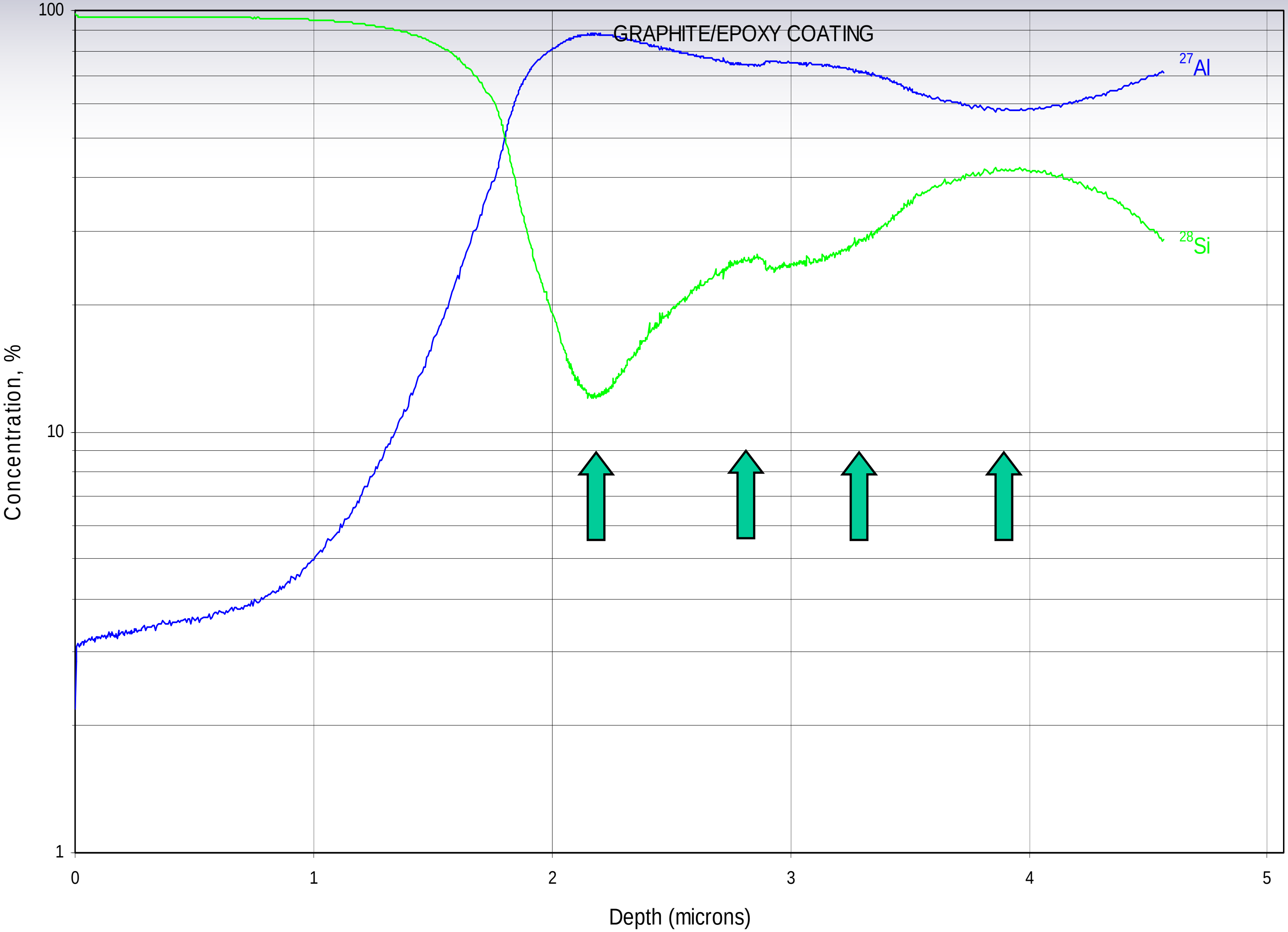

22000Å SiO_X

6000Å Al

5000Å SiO_X

6000Å VDA

600Å Cr

Epoxy Primer

Emissivity Tests at NASA Goddard Spaceflight Center

To investigate the microwave emissivity of the SSMIS reflector surface coatings and cause of the residual errors shown on page 11-107, the MMCSR was shipped to NASA Goddard Spaceflight Center (GSFC) in order to measure the RF emissivity of the MMCSR with the Conical-Scanning Microwave Imaging Radiometer (CoSMIR) instrument. The CoSMIR is an airborne radiometer that was used in the SSMIS Cal/Val to under-fly SSMIS and played an important role in identifying the SSMIS polarization error in Channels 1-5 (See Section 6). In May 2005, the CoSMIR was available for laboratory testing. A series of experiments were designed to measure the emissivity of the CSR using CoSMIR. The experiments are described on page 11-114 and were carried and refined over the summer of 2005 and provided a good estimate of the microwave emissivity of the MMCSR. The CoSMIR measured the brightness temperature of a stabilized room-temperature calibration target using the CSR to reflect the target scene into the radiometers view. The CSR was then heated from room temperature (~25° C) to ~85° C and differences in the observed brightness temperature were recorded (page 11-115). Small changes in observed scene temperature indicate the CSR is highly reflective and does not generate residual biases. The experiments were carried out several times and consistent results indicated an emissivity that although higher than expected for an uncoated pure Aluminum surface, was far lower than needed to explain the level of residual error observed on-orbit (page 11-107). The Laboratory measurements showed ~1% emissivity but the orbit errors suggest that ~7% emissivity is needed to explain the biases. Results are summarized on Page 11-116 and compared to an NRL model of the emissivity of a reflector with surface coating having the profile as a function of depth as shown by the Aerospace SIMS test.

Absolute Emissivity Measurement Set-up (H-pol)

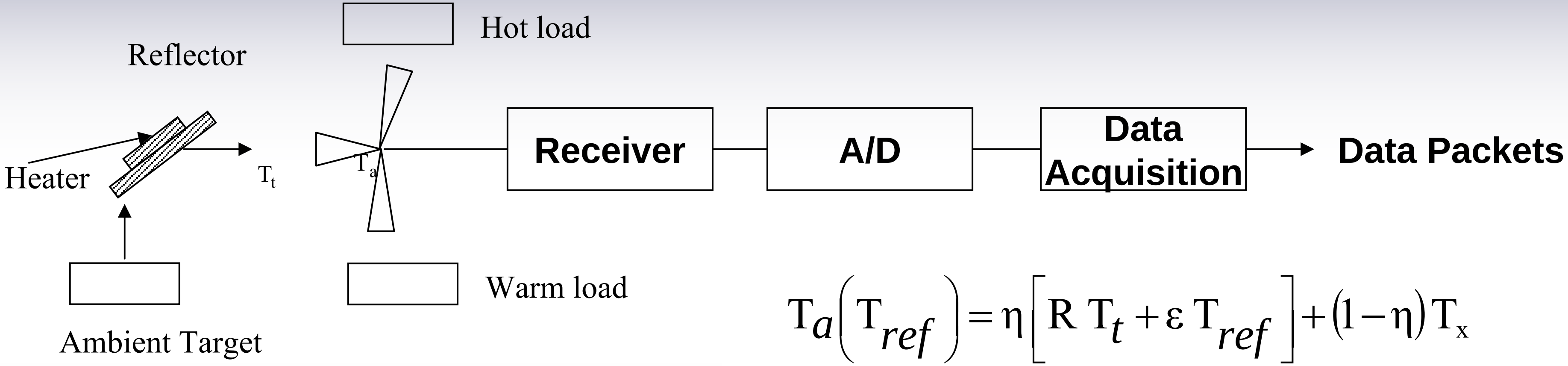

Hot load

Reflector

Heater

T_t

T_a

Receiver

A/D

Data Acquisition

Data Packets

Warm load

Ambient Target

$$T_a\left(T_{ref}\right) = \eta\left[R\,T_t + \varepsilon\,T_{ref}\right] + (1-\eta)\,T_x$$

η = Beam-fill fraction on reflector (> 0.9)

R = Reflector reflectivity

ε = Reflector emissivity

T_{ref} = Reflector temperature

T_x = Effective room temperature

T_t = Target temperature

$$\frac{\partial T_a}{\partial T_{ref}} = \eta\,\varepsilon_{ref} \approx \varepsilon_{ref}$$

Results of Emissivity Measurements at 183 GHz (H-pol)

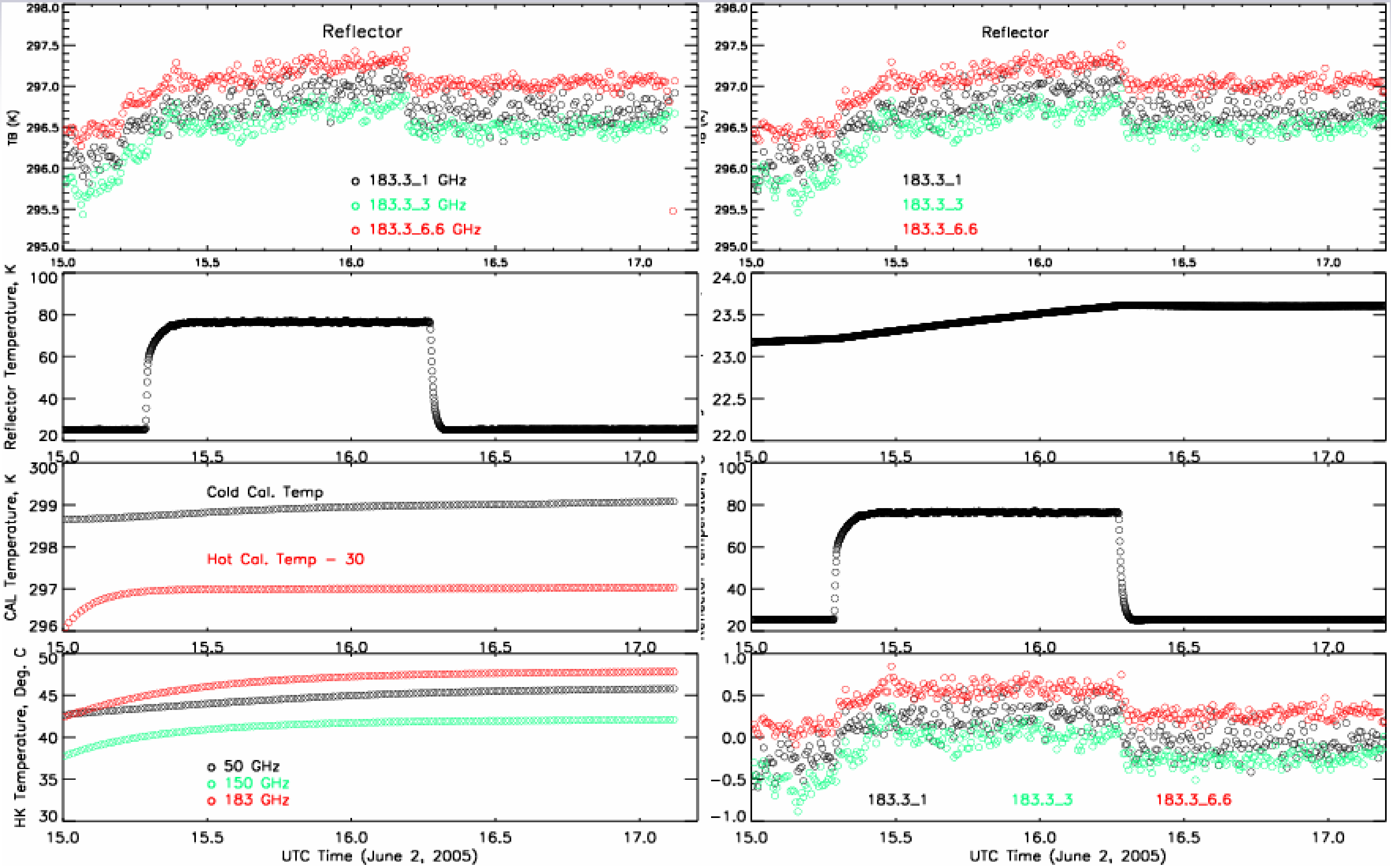

Comparison of CoSMIR Emissivity Measurements and Modeled Emissivity of CSR

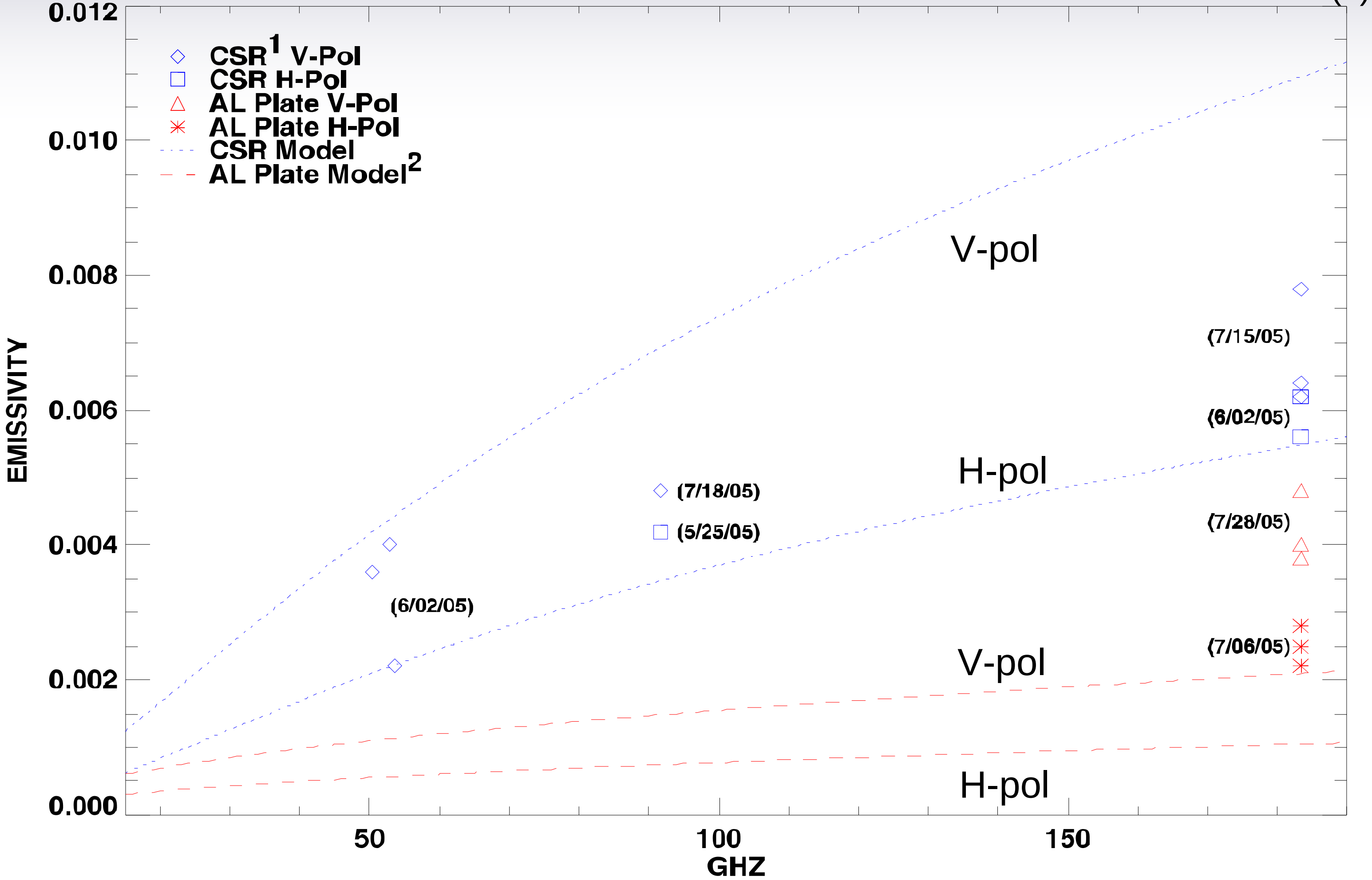

CoSMIR Observations of SSMIS CSR Emissivity and Model Comparison (3)

1. CSR: Cold Sky Reflector Mass Model
2. Al Plate Model: Flat Aluminum Plate (Smooth)
3. Model: NRL RF Model using Aerospace SIMS Al Profile with SiO_X Coating

11.11 Summary and Status of Antenna Emission Root Cause Investigation

Because the estimates of reflector emissivity based on laboratory measurements (CSR) and on-orbit observations disagree by a factor of 7 – 10, the root cause of the on-orbit antenna emissivity is still uncertain. Generally, the way forward requires testing to determine the likelihood of pre- or post-launch degradation of the reflector surfaces as indicated by the upper right hand corner of the "fishbone" diagram highlighted on page 11-118. There is also the possibility, although very remote, that the residual calibration bias shown on page 11-107 is not due to another phenomenon. However, antenna emission due to contamination by Aluminum in the top layer of Silicon Oxide on the reflector coating remains, the most likely conclusion. Possible explanations for the laboratory vs. on-orbit discrepancy include manufacturing variability or error with reflector S/N03 (on-orbit), pre-launch surface contamination, damage caused by humidity during development or during the extended period prior to launch while on the pad, etc. The next steps in the analysis involve exposing the CSR to a simulated space environment (primarily Ultra-Violet radiation) followed by a retest of microwave emissivity to determine if it is likely the surface characteristics will degrade post-launch in a manner that may be consistent with observations from F-16.

Way Forward for SSMIS

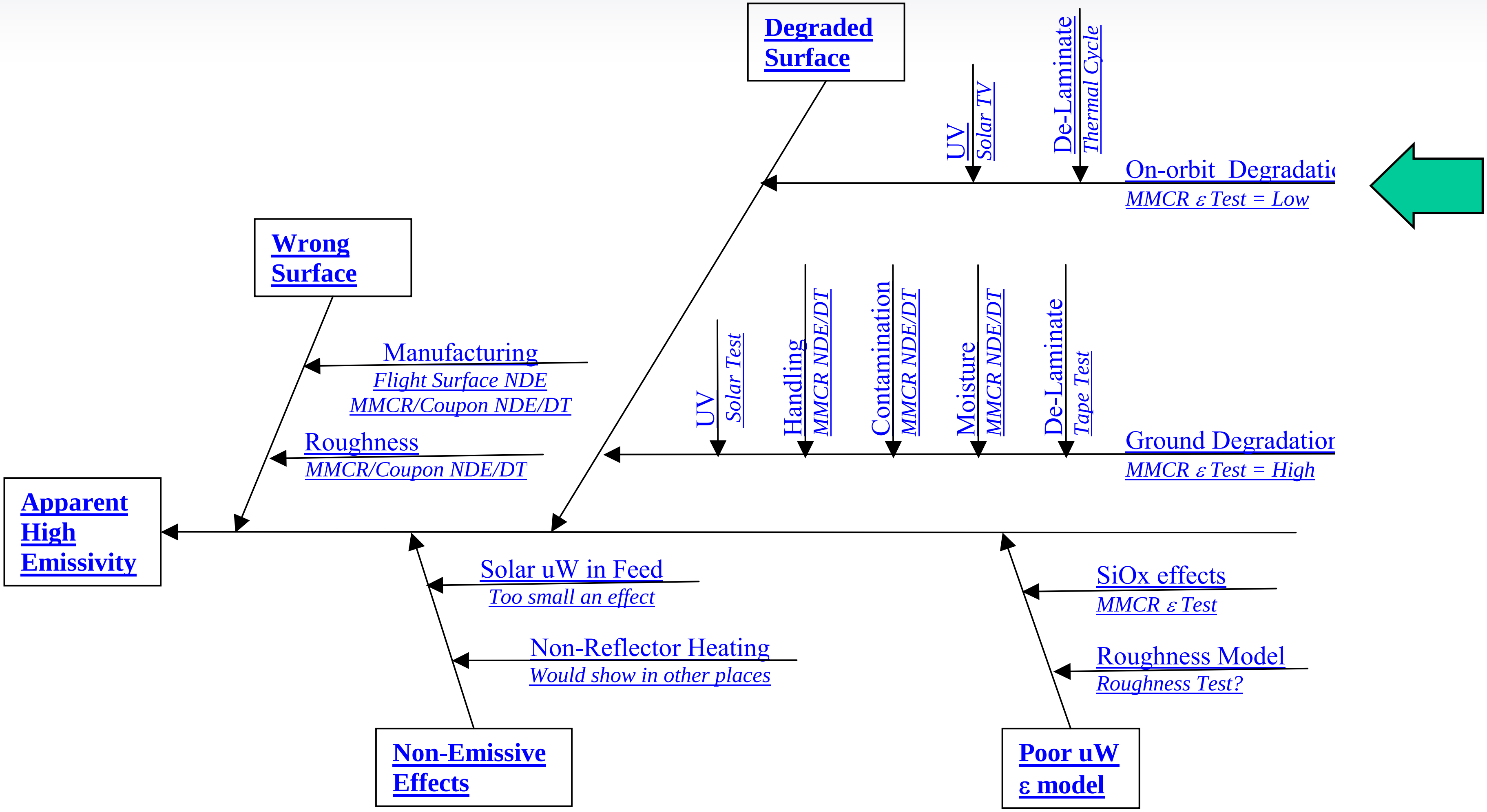

Apparent High Emissivity

Wrong Surface

Manufacturing
Flight Surface NDE
MMCR/Coupon NDE/DT

Roughness
MMCR/Coupon NDE/DT

Degraded Surface

UV
Solar TV

De-Laminate
Thermal Cycle

On-orbit Degradati
MMCR ε Test = Low

UV
Solar Test

Handling
MMCR NDE/DT

Contamination
MMCR NDE/DT

Moisture
MMCR NDE/DT

De-Laminate
Tape Test

Ground Degradatio
MMCR ε Test = High

Non-Emissive Effects

Solar uW in Feed
Too small an effect

Non-Reflector Heating
Would show in other places

Poor uW ε model

SiOx effects
MMCR ε Test

Roughness Model
Roughness Test?

Defense Meteorological Satellite Program
Special Sensor Microwave Imager Sounder (F-16)
Calibration/Validation Final Report

The First Conical Scanning Passive Microwave Surface and Atmospheric Sounding Imager

SSMIS F-16 Channel 15 - 37 H IDR REVS 09258 - 09271 08/04/2005

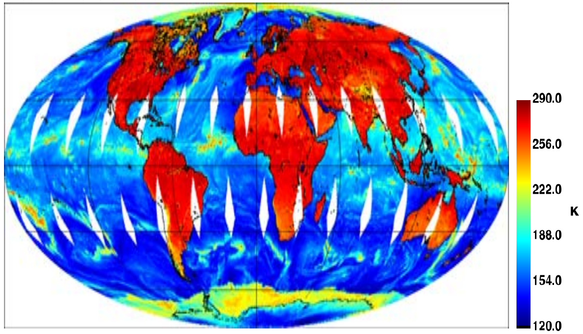

SSMIS F-16 Channel 1 - 50.3 V IDR REVS 09258 - 09271 08/04/2005

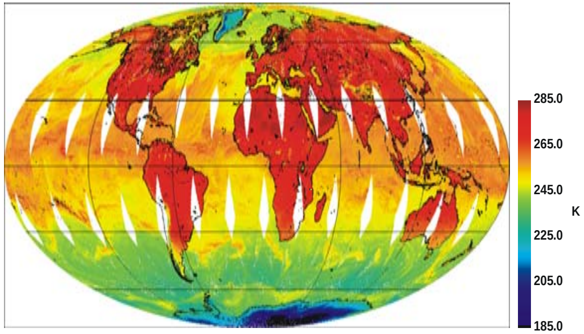

SSMIS F-16 Channel 10 - 183+/-3 H IDR REVS 09258 - 09271 08/04/2005

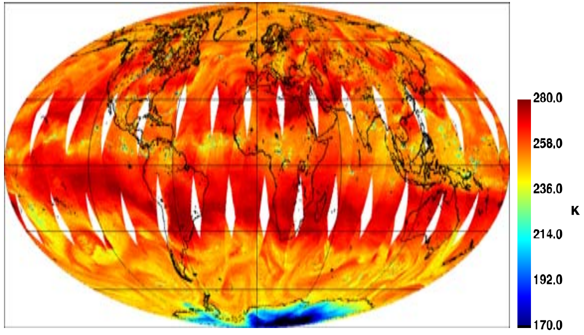

SSMIS F-16 Channel 20 - 60.792 H+V IDR REVS 09258 - 09271 08/04/2005

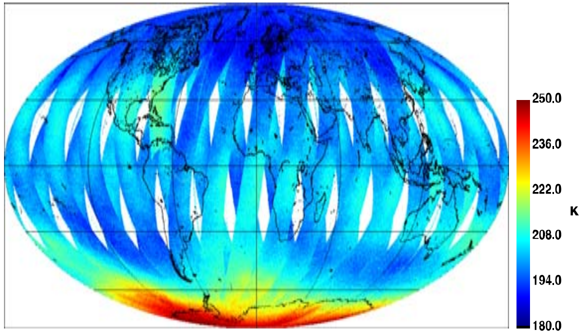

Prepared by

SSMIS Cal/Val Team

30 November 2005

Volume VI

Table of Contents

F16 SSMIS Calibration/Validation Final Report

Section 12.0 Calibration Anaomalies II

Steve Swadley, David Kunkee, Gene Poe and Ye Hong

THE AEROSPACE CORPORATION

Radiometric Calibration Anomalies

- Warm Load Intrusions
- Reflector Emissions due to Solar Heating
- Lunar Intrusions into Cold Sky View
- Spurious Spikes and Non-Gaussian Noise
- Plans to Address Anomaly and Future Efforts

Radiometric Calibration Anomalies

- SSMIS Radiometric Anomalies Were Difficult to Detect from Global Radiosonde Network without Previous Knowledge of Calibration Anomaly Patterns

- Calibration Anomalies and Subsequent Biases are Related to Proximity to Warm Load Intrusions and Reflector Emissions

- Geographic Locations of Calibration Anomalies Dramatically Change Throughout the Year

- Comparison of SSMIS Observed TBs (OB) with RTM Simulations using ECMWF NWP Analyses (BK) Provided SSMIS Cal/Val Team an Invaluable Tool in Describing the Time Evolution of the Calibration Anomaly Patterns

- Utilizing ECMWF OB-BK Patterns in Conjunction With the DGS Software System Allowed Quantification of the Physical Phenomena Causing the Calibration Anomalies

Radiometric Calibration Anomalies

DGS

Simulation tool: Recent software modifications added substantial capability to DGS. Allowed Cal/Val Team to analyze the SSMIS calibration anomalies and Field of View (FOV) intrusions

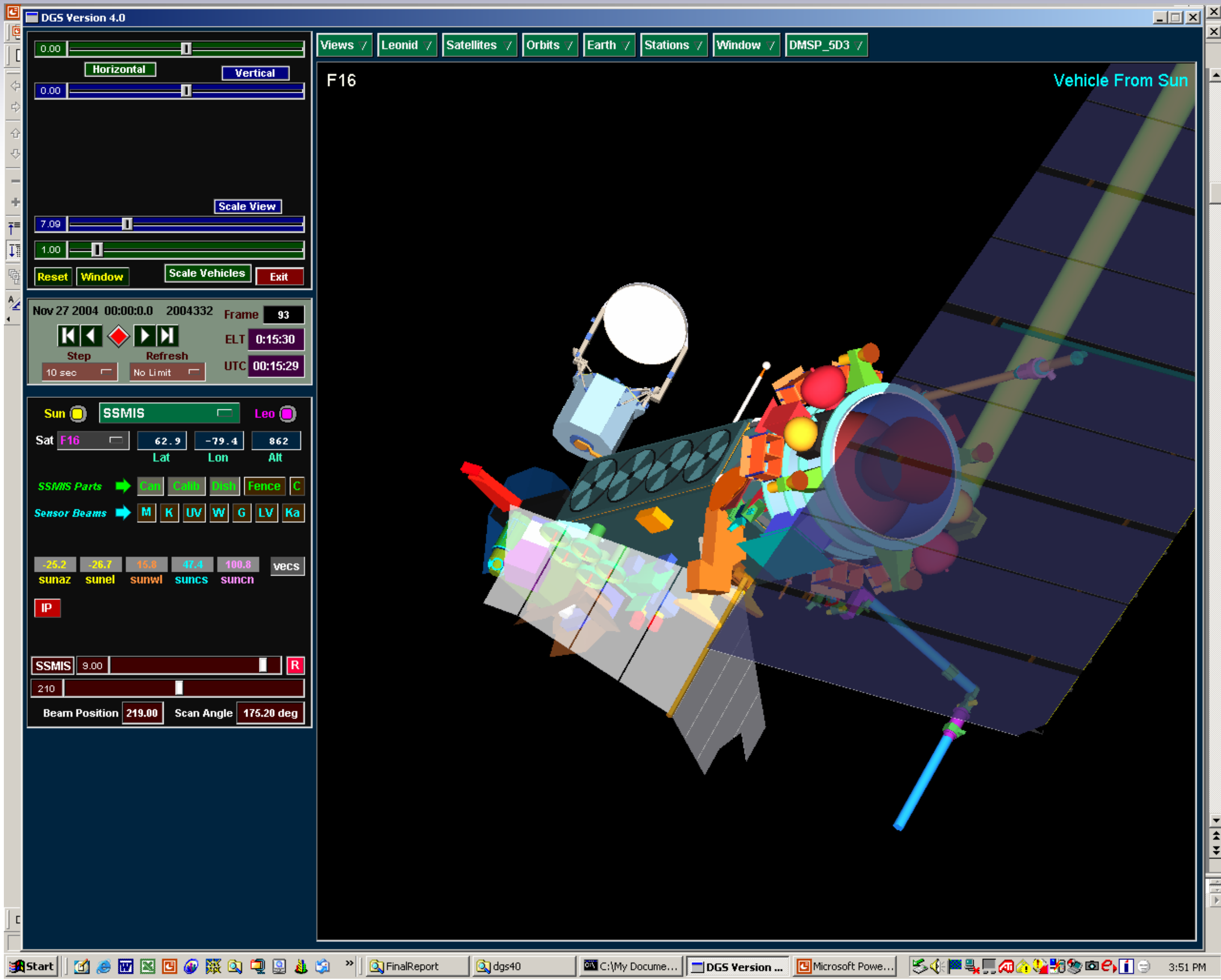

Nov 27 2004 00:00:0.0 2004332

Frame 93

ELT 0:15:30

UTC 00:15:29

Step 10 sec

Refresh No Limit

SSMIS

Sat F16

62.9 Lat

-79.4 Lon

862 Alt

-25.2 sunaz

-26.7 sunel

15.8 sunwl

47.4 suncs

100.8 suncn

SSMIS 9.00

210

Beam Position 219.00

Scan Angle 175.20 deg

Radiometric Calibration Anomalies

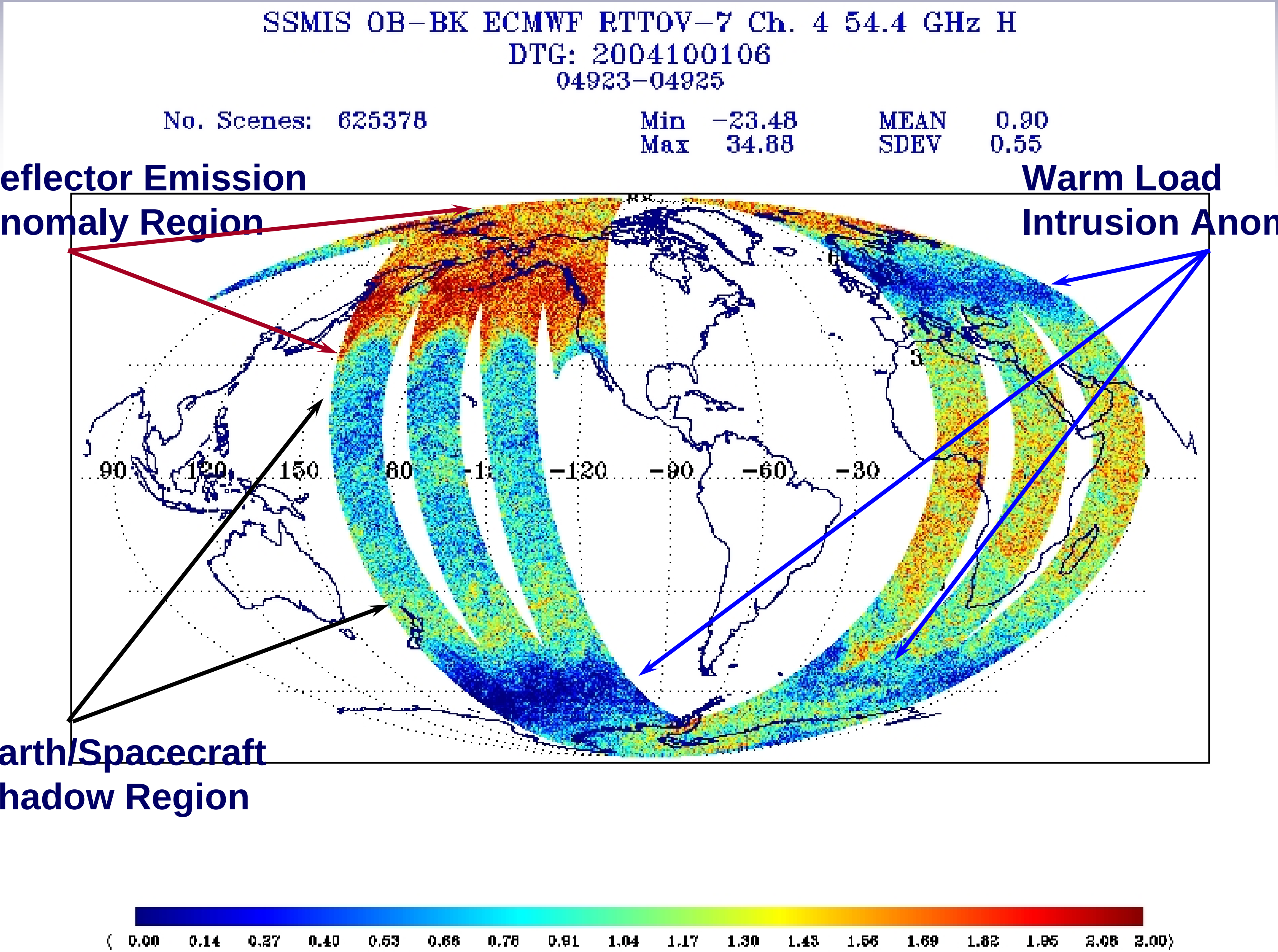

Reflector Emission Anomaly Region

Warm Load Intrusion Anomalies

Earth/Spacecraft Shadow Region

Radiometric Calibration Anomalies

02/11/2004

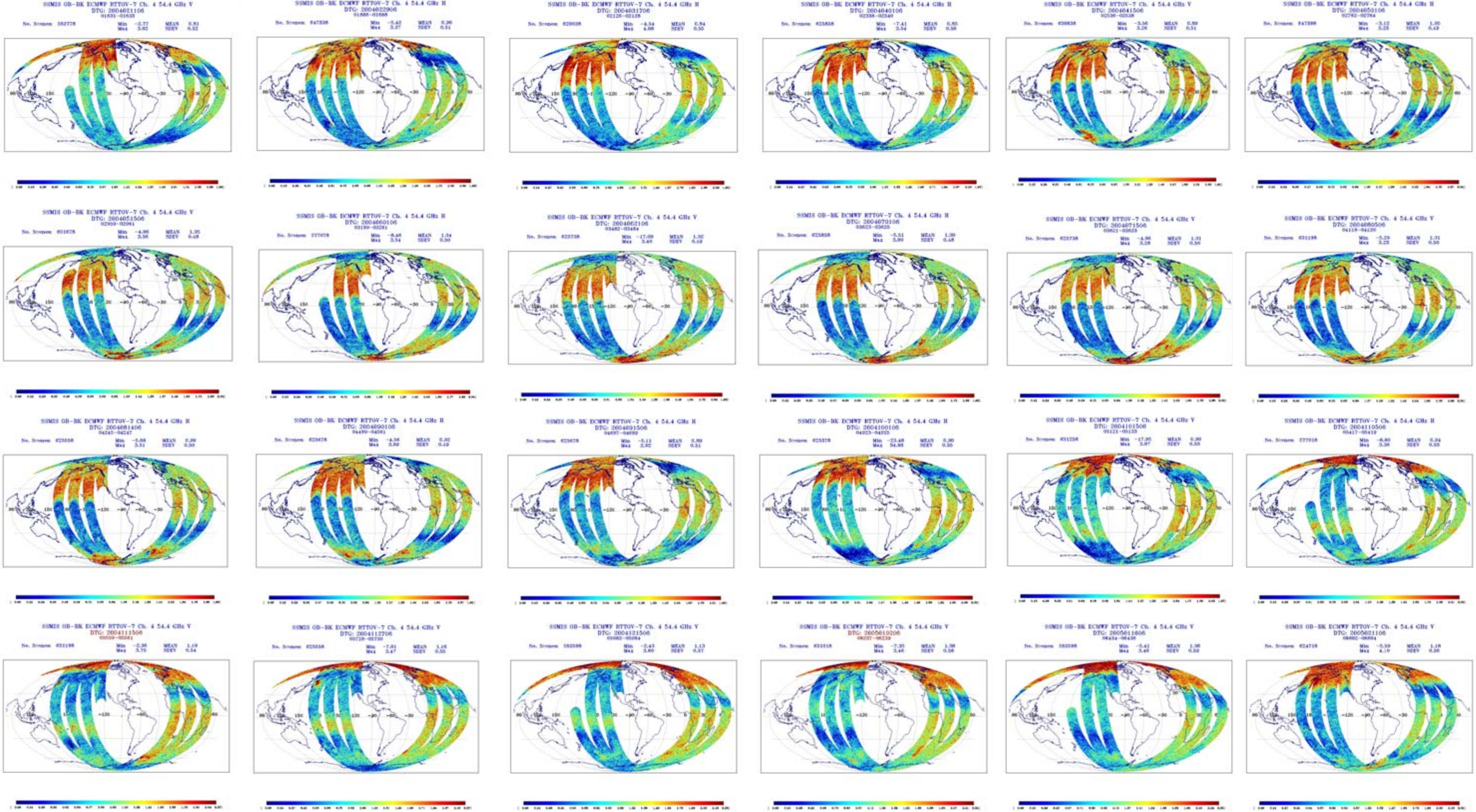

02/11/2005

SSMIS OB-BK Departures Channel 4 54.4 GHz
Yearly Cycle at ~2 Week Intervals 02/11/2004 – 02/11/05

Radiometric Calibration Anomalies

Warm Load Intrusions

- Description of Problem
- General Definitions of Anomalous Regions
- Early Orbit Mode Warm Load Imaging
- DGS Examples
- Analysis of Impact
- Plans and Implementation of Resolution in GPS

Radiometric Calibration Anomalies

- **Description of Problem**
  - **Caused by Short Term Heating of the Warm Load Tines**
  - **Solar Reflection Off the Canister Top into Warm Load**
    - **Occurs at distinct combinations of Solar Elevation and Azimuth Angles and Interactions with SSMIS Canister Top**
  - **Direct Solar Illumination of the Warm Load Tines**
  - **Radiometer "Sees" Rapid Heating of Warm Load Tines before Warm Load Thermistors can Register Temperature Change**

Radiometric Calibration Anomalies

Description of Problem

- Positive Anomalies in Gain Plots
  - Relative Gain G/G_{AVG} Time Series
  - $G = (C_W – C_c) / (T_W – T_c)$
- Results in a Cooler Scene Temperature

$$T_s = (C_s – C_c) / G$$

$$= (C_s – C_c) (T_W – T_c) / (C_W – C_c)$$

Where, C is Counts, T is Temperature, and subscripts C, W, and S are Cold-Space, Warm Load, Scene, respectively.

- Negative Anomalies in the Scan Averaged OB-BK Plots

Radiometric Calibration Anomalies

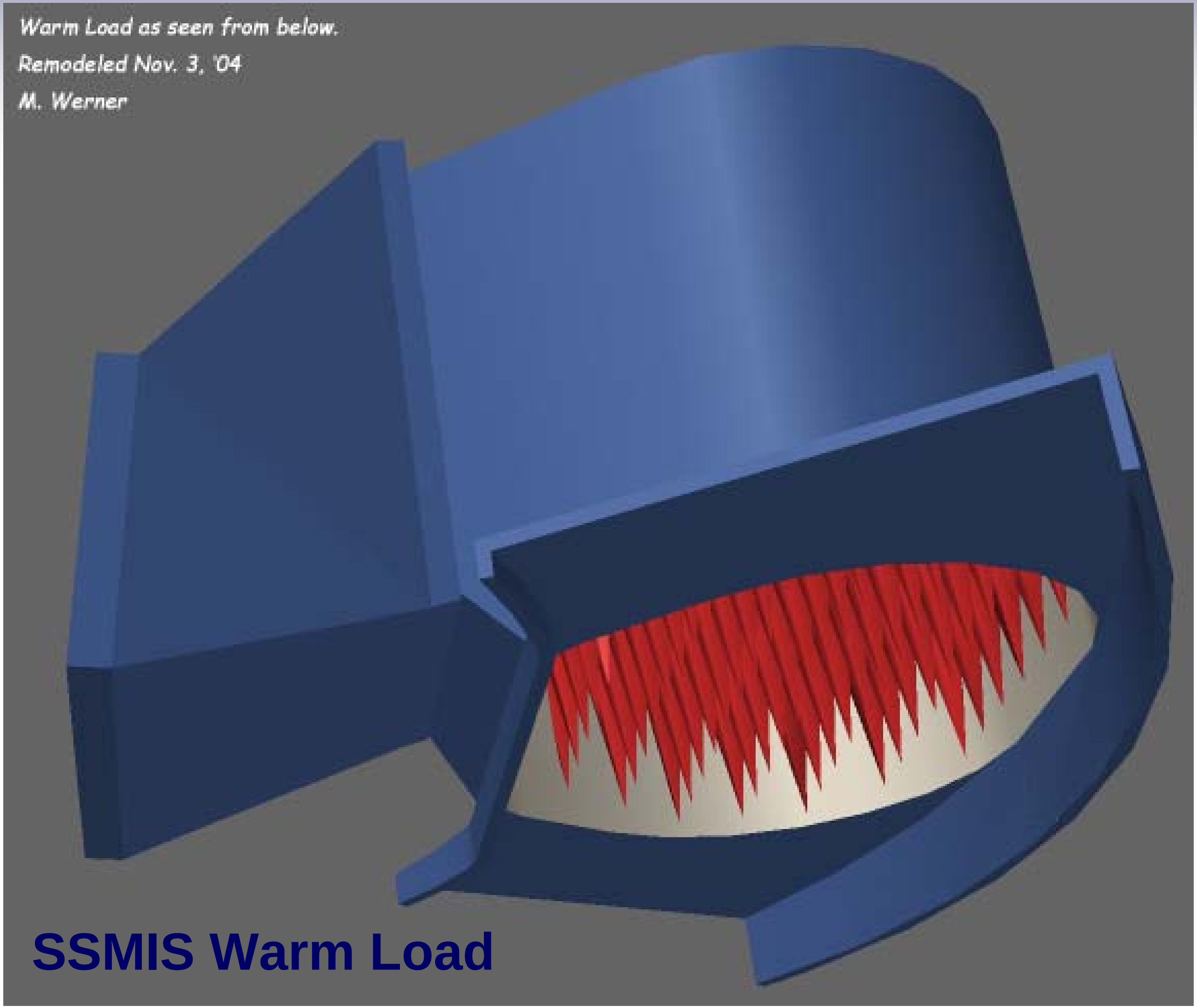

SSMIS Warm Load

Radiometric Calibration Anomalies

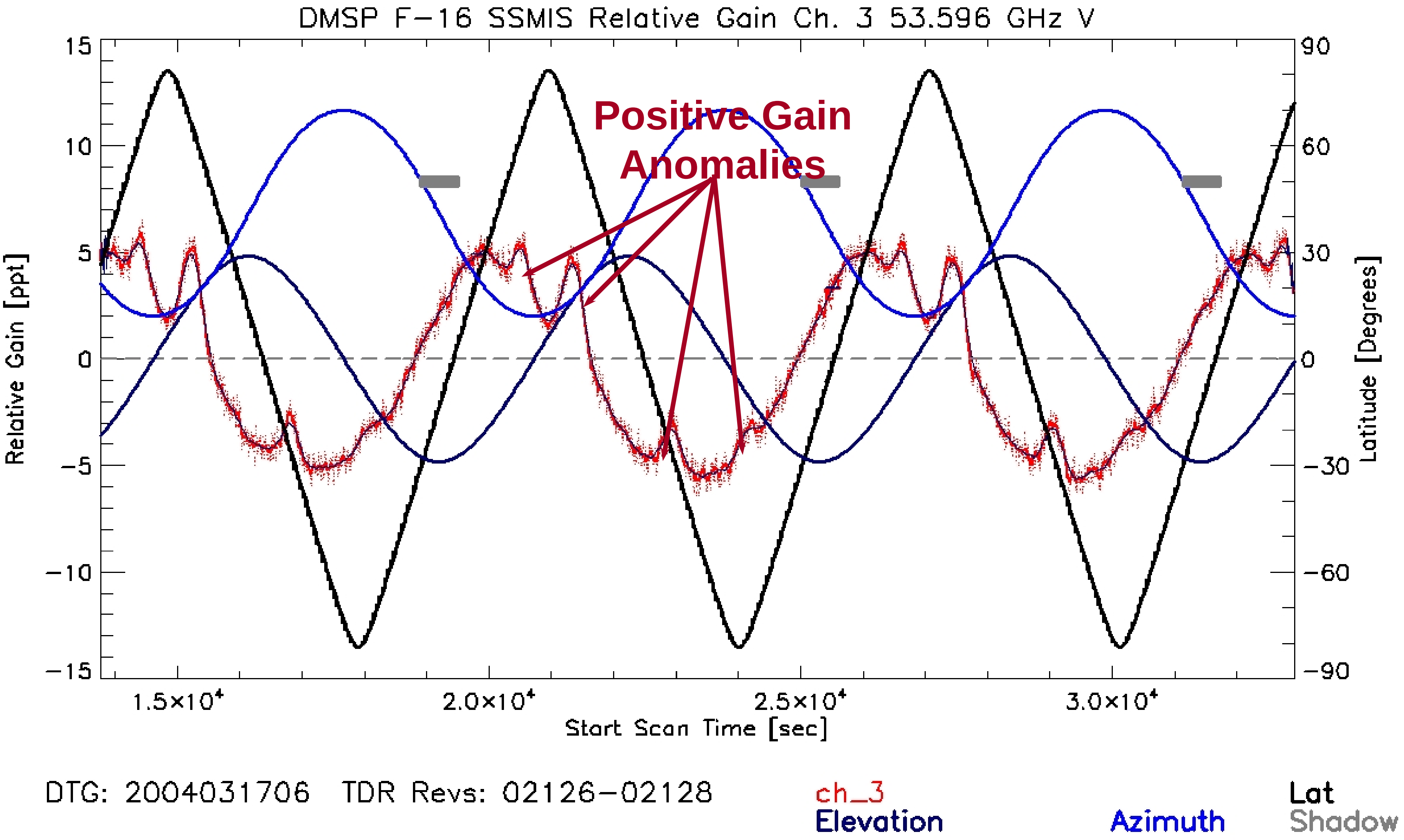

Positive Gain Anomalies

Radiometric Calibration Anomalies

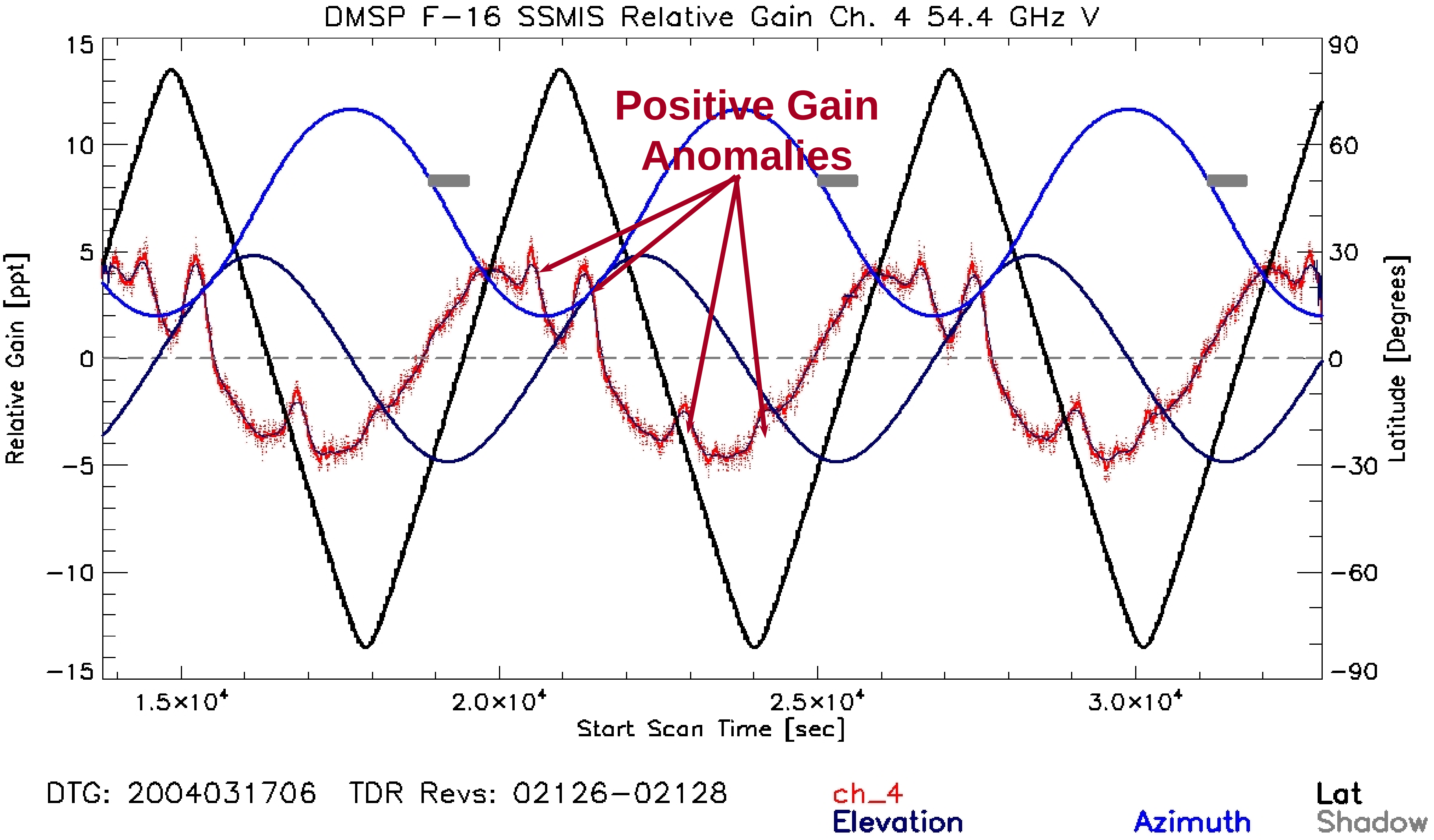

Positive Gain Anomalies

Radiometric Calibration Anomalies

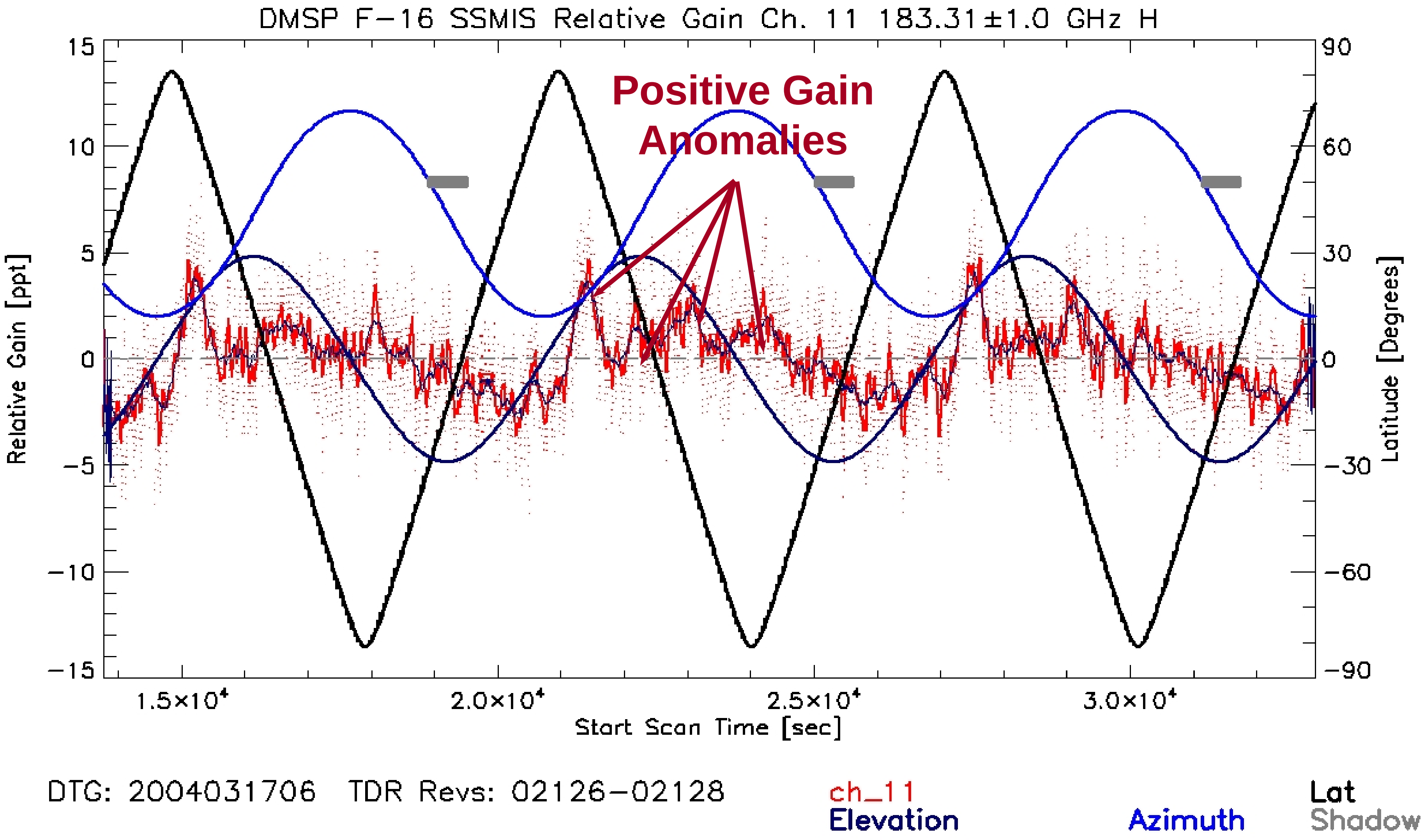

Positive Gain Anomalies

Radiometric Calibration Anomalies

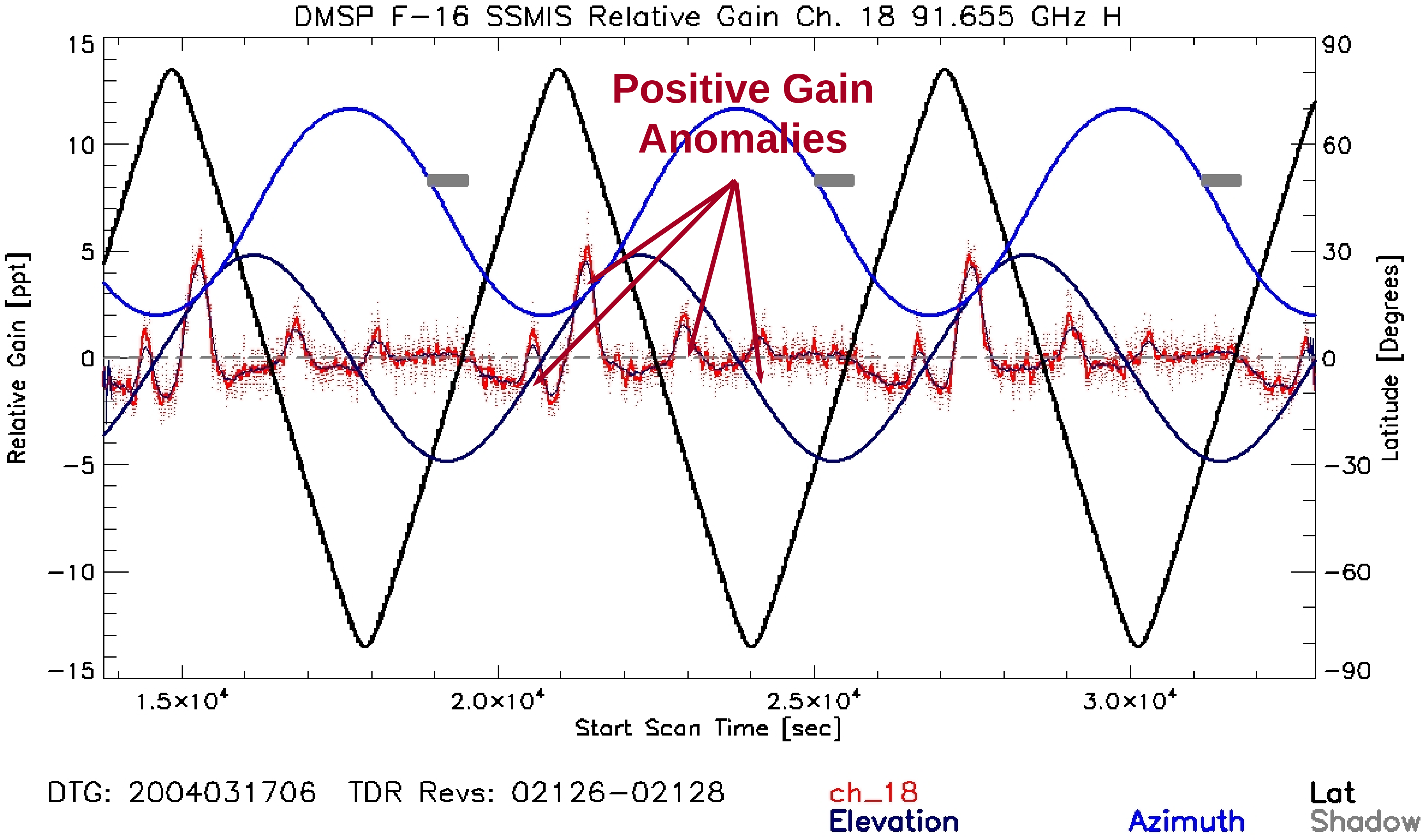

Positive Gain Anomalies

Radiometric Calibration Anomalies

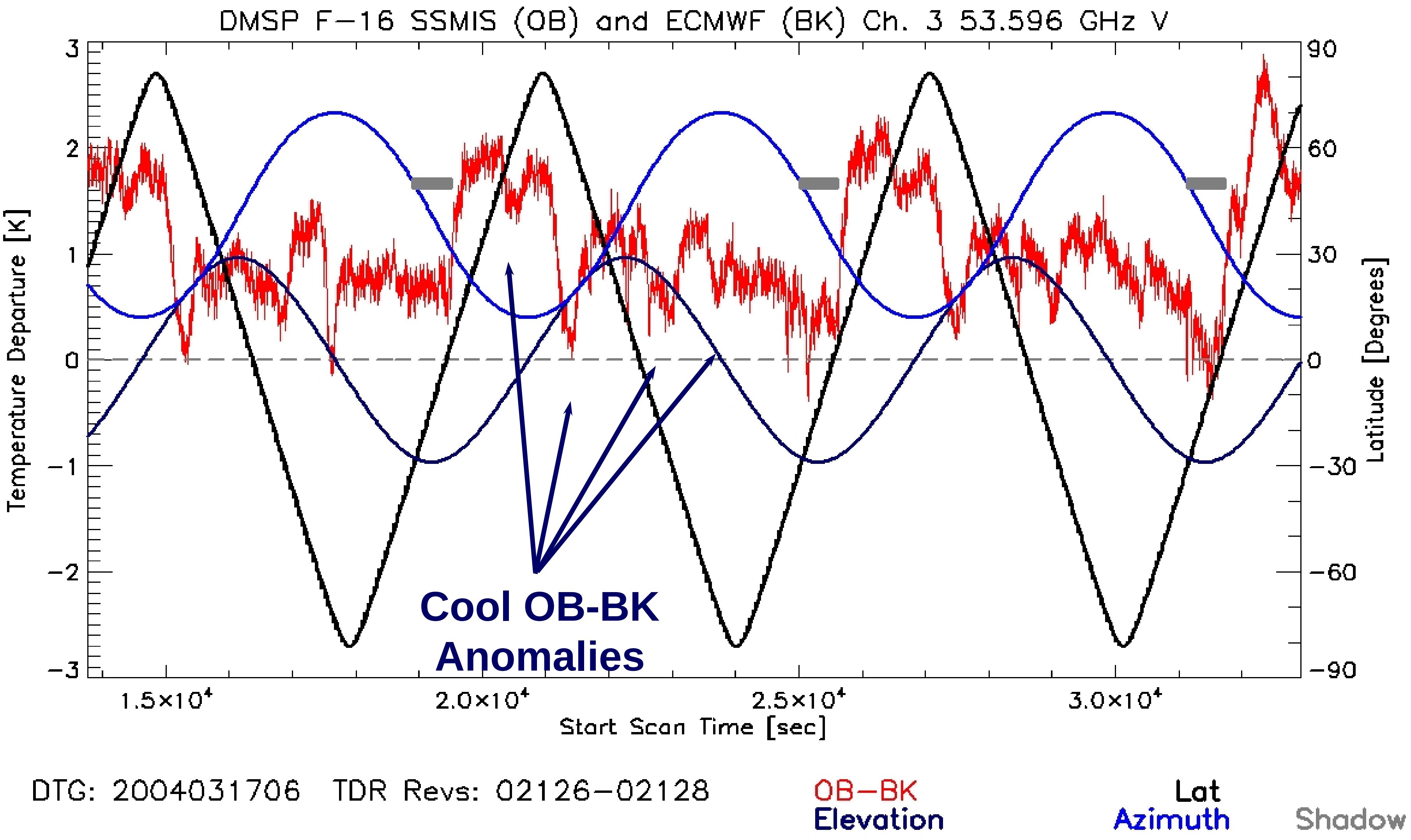

Cool OB-BK Anomalies

Radiometric Calibration Anomalies

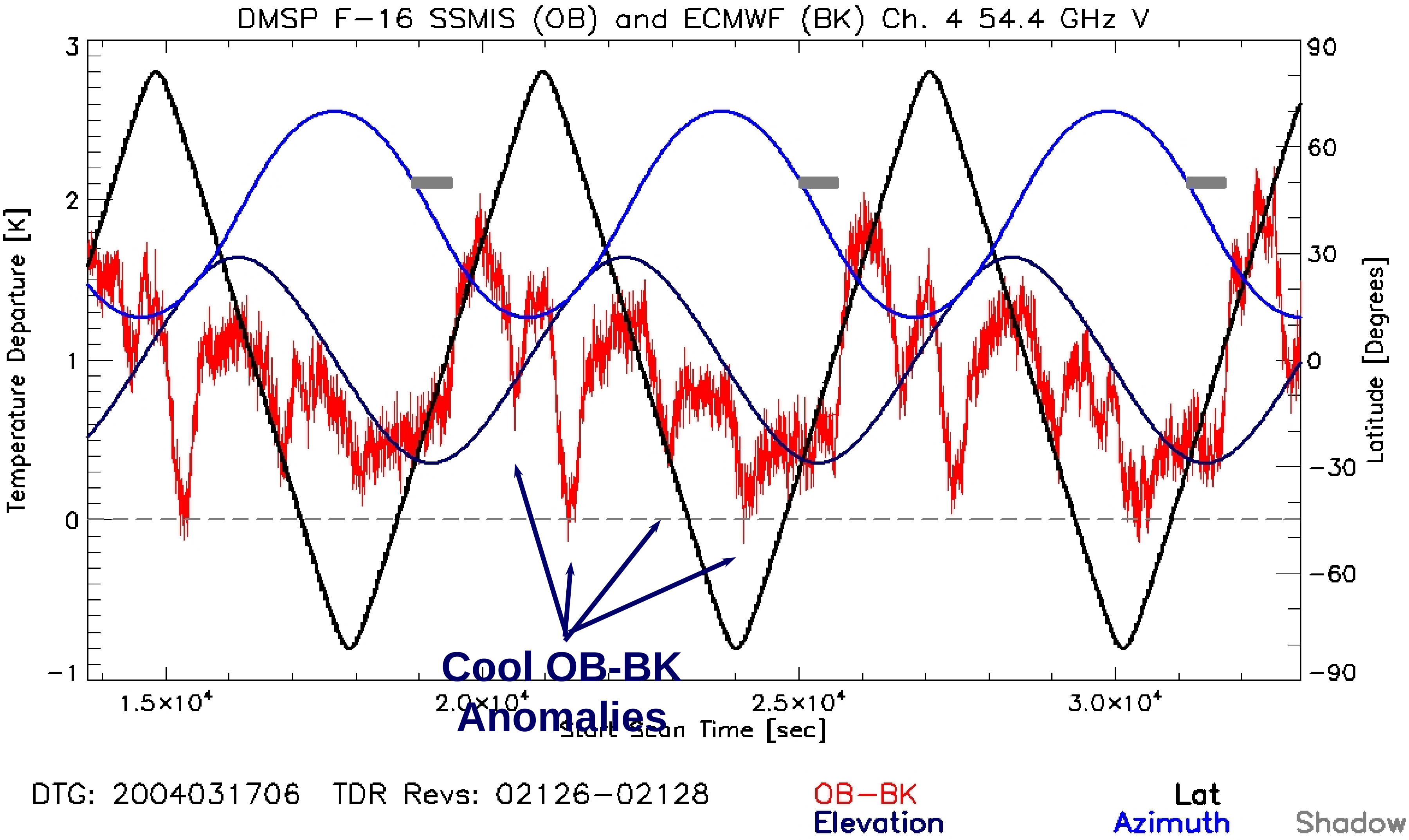

Cool OB-BK Anomalies

Radiometric Calibration Anomalies

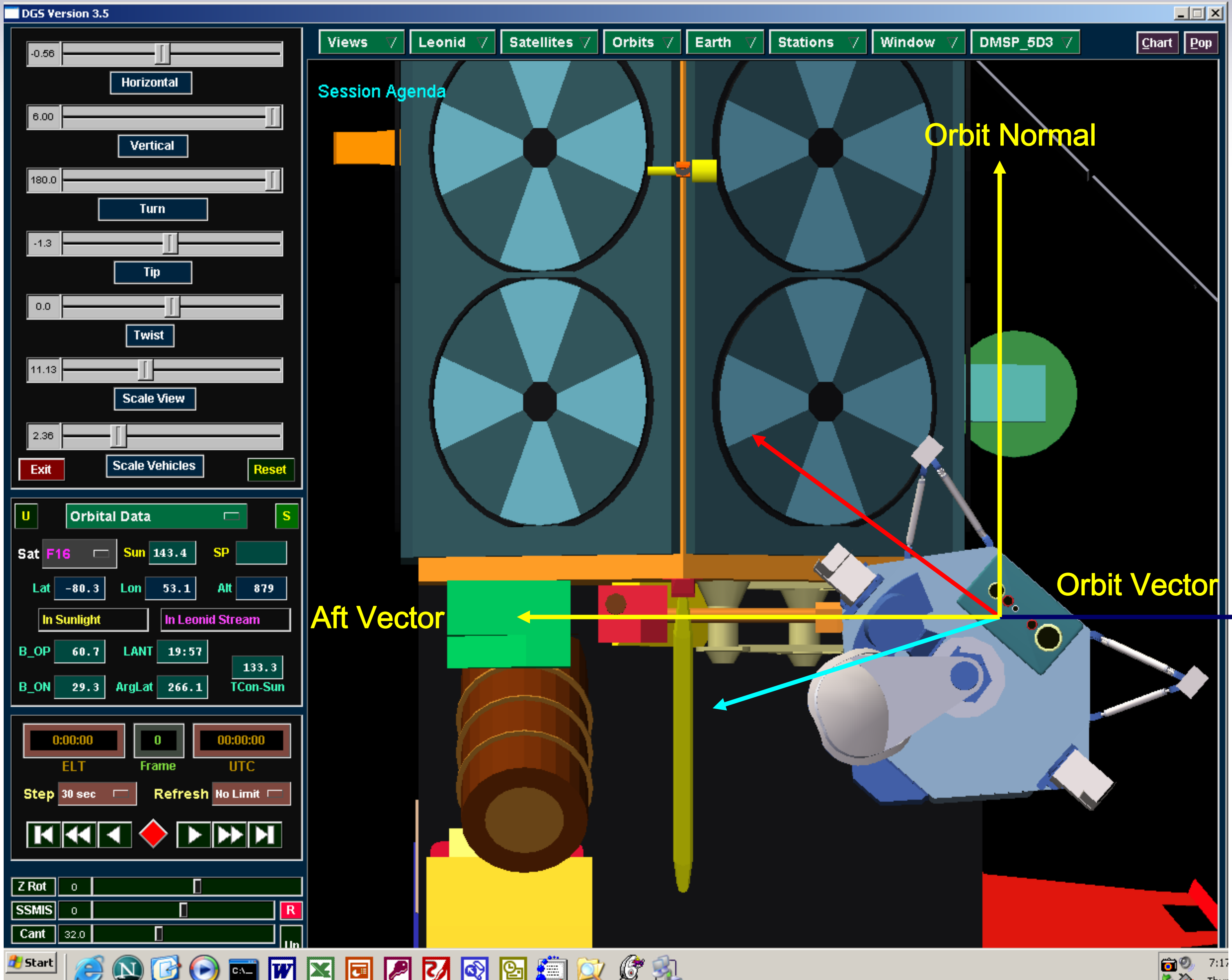

DGS Version 3.5

Horizontal -0.56
Vertical 6.00
Turn 180.0
Tip -1.3
Twist 0.0
Scale View 11.13
Scale Vehicles 2.36

Orbital Data
Sat F16
Sun 143.4
SP
Lat -80.3
Lon 53.1
Alt 879
In Sunlight
In Leonid Stream
B_OP 60.7
LANT 19:57
TCon-Sun 133.3
B_ON 29.3
ArgLat 266.1

ELT 0:00:00
Frame 0
UTC 00:00:00
Step 30 sec
Refresh No Limit

Z Rot 0
SSMIS 0
Cant 32.0

Radiometric Calibration Anomalies

Warm Load and Cold-Space Reflector Spacecraft Geometries

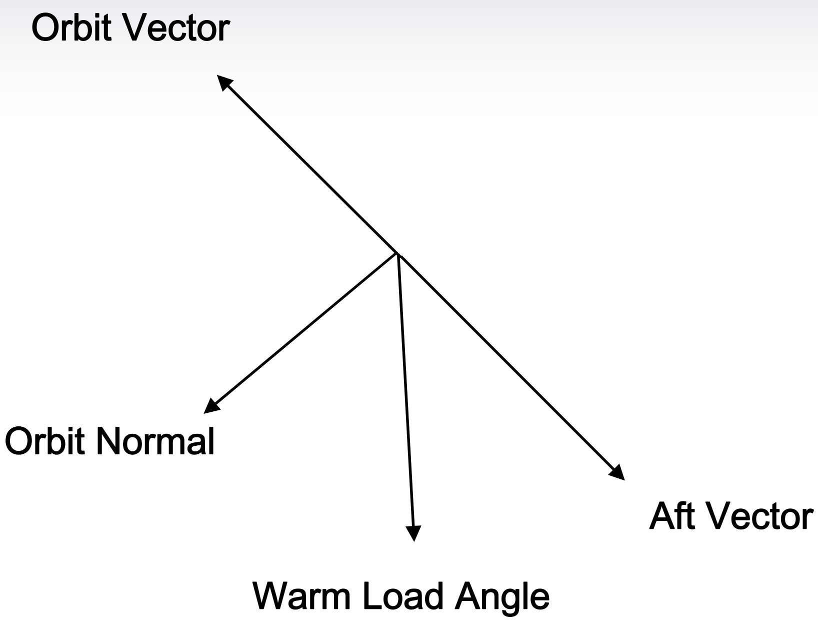

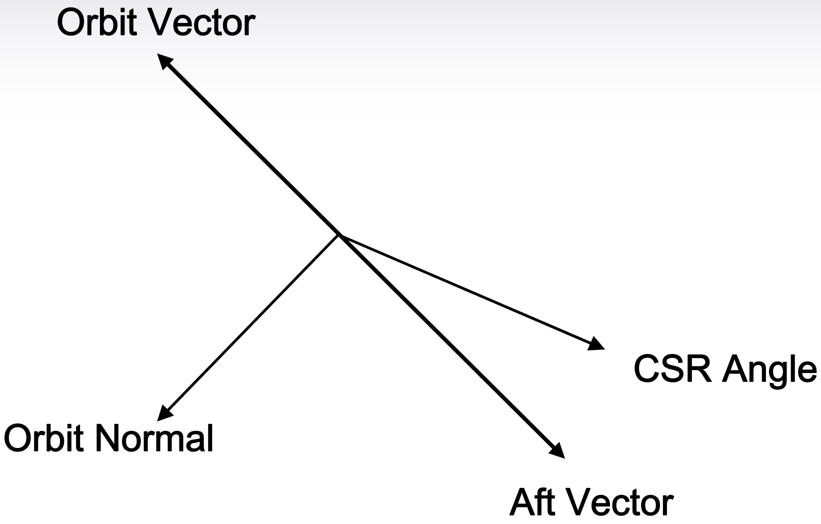

Warm Load Position
49.2º From Orbit Normal

Cold Space Reflector Position
112.9º From Orbit Normal

Radiometric Calibration Anomalies

General Definitions of Anomalous Regions

- Two Reflection Intrusion Regions per Orbit

  - Reflection 1
    - Elevation Angles Between 4° and 28°
    - Azimuth Angles < 45 °
    - Elevation Angle Increasing

  - Reflection 2
    - Elevation Angles Between 8° and 35°
    - Azimuth Angles > 35 °
    - Elevation Angle Decreasing

Radiometric Calibration Anomalies

Reflection 1

DGS Version 4.0

Aug 4 2005 00:00:0.0 2005216

Frame 4662

ELT 12:57:00

UTC 12:57:00

Step 10 sec

Refresh No Limit

Sat F16

75.7	71.7	864
Lat	Lon	Alt

-37.1	18.0	3.9	35.5	142.7
sunaz	sunel	sunwl	suncs	suncn

SSMIS 8.50

190

Beam Position 198.50

Scan Angle 158.80 deg

F16

Vehicle From Sun

Highly Reflective SSMIS Canister Top

Warm Load

Radiometric Calibration Anomalies

Reflection 2

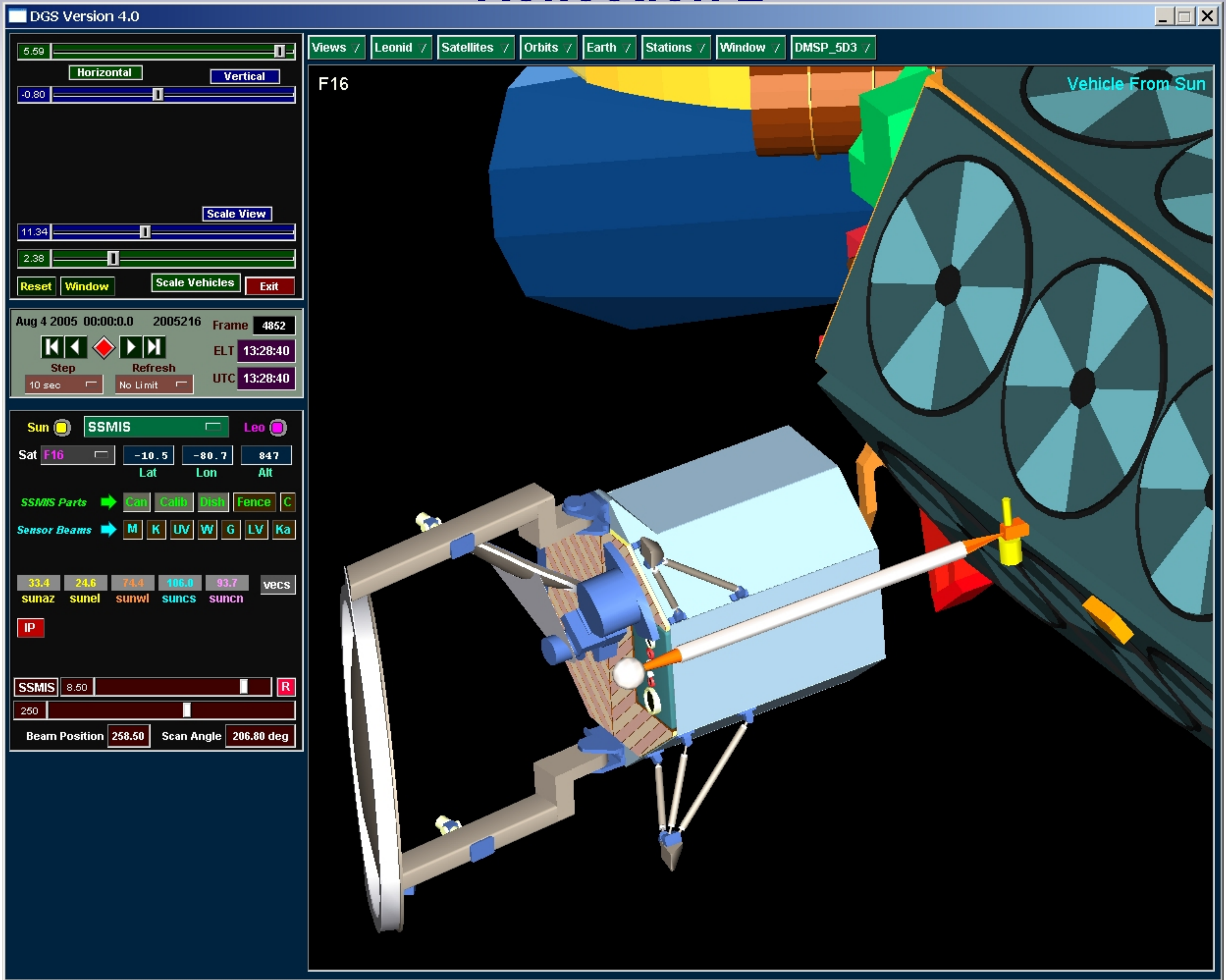

5.59

-0.80

11.34

2.38

Aug 4 2005 00:00:0.0 2005216

Frame 4852

ELT 13:28:40

UTC 13:28:40

Step 10 sec

Refresh No Limit

Sun SSMIS Leo

Sat F16

-10.5	-80.7	847
Lat	Lon	Alt

33.4	24.6	74.4	106.0	93.7
sunaz	sunel	sunwl	suncs	suncn

SSMIS 8.50

250

Beam Position 258.50

Scan Angle 206.80 deg

F16

Vehicle From Sun

Radiometric Calibration Anomalies

General Definitions of Anomalous Regions

- One or two Direct Intrusion Regions per Orbit
  - Number Depends on Solar Geometry
  - Direct Intrusion 1
    - Elevation Angles < 2° and > -18°
    - Azimuth Angles > 5° and < 45°
  - Direct Intrusion 2
    - Elevation Angles < 0° and > -28°
    - Azimuth Angles > 45°

Radiometric Calibration Anomalies

Direct 1

1.31

-1.52

25.50

1.00

Feb 18 2005 00:00:0.0 2005049

Frame 429

ELT 1:11:30

UTC 01:11:29

Step 10 sec

Refresh No Limit

SSMIS

Sat F16

Lat 73.3

Lon -106.4

Alt 861

sunaz -26.9

sunel -10.6

sunwl 14.1

suncs 45.7

suncn 114.7

SSMIS 2.75

70

Beam Position 72.75

Scan Angle 58.20 deg

Radiometric Calibration Anomalies

Direct 2


DGS Version 4.0

2.45

0.44

16.61

1.90

Aug 4 2005 00:00:0.0 2005216

Frame 4350

ELT 12:05:00

UTC 12:05:00

Step 10 sec

Refresh No Limit

Sat F16

Lat -72.8

Lon -88.1

Alt 870

sunaz 37.9

sunel -15.9

sunwl 78.9

suncs 110.5

suncn 64.1

SSMIS 8.50

80

Beam Position 88.50

Scan Angle 70.80 deg

Radiometric Calibration Anomalies

Warm Load Basis Solar Angle Definitions

- **Elevation Angle defined with respect to Canister Top**
  - **> 0 Above Canister Top**
  - **< 0 Below Canister Top**

- **Azimuth Angle defined with respect to Warm Load Angle**
  - **90° when Solar Angle = Warm Load Angle**
  - **0° when Solar Angle Normal to Warm Load Angle**
  - **DGS Azimuth Angle = Azimuth Angle – 49.2 °**

Radiometric Calibration Anomalies

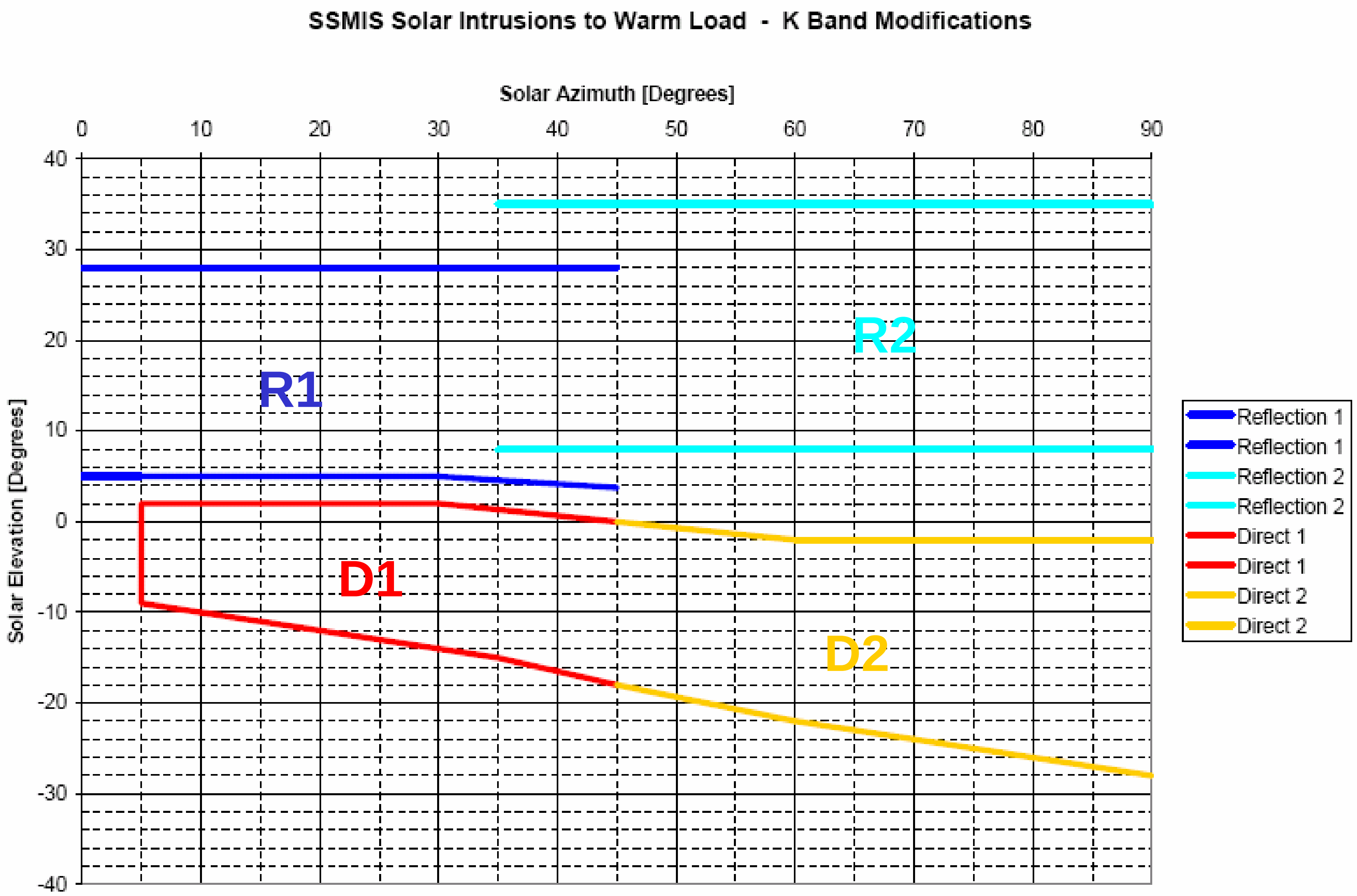

Radiometric Calibration Anomalies

Intrusion Detection Algorithm Based upon Solar Geometry

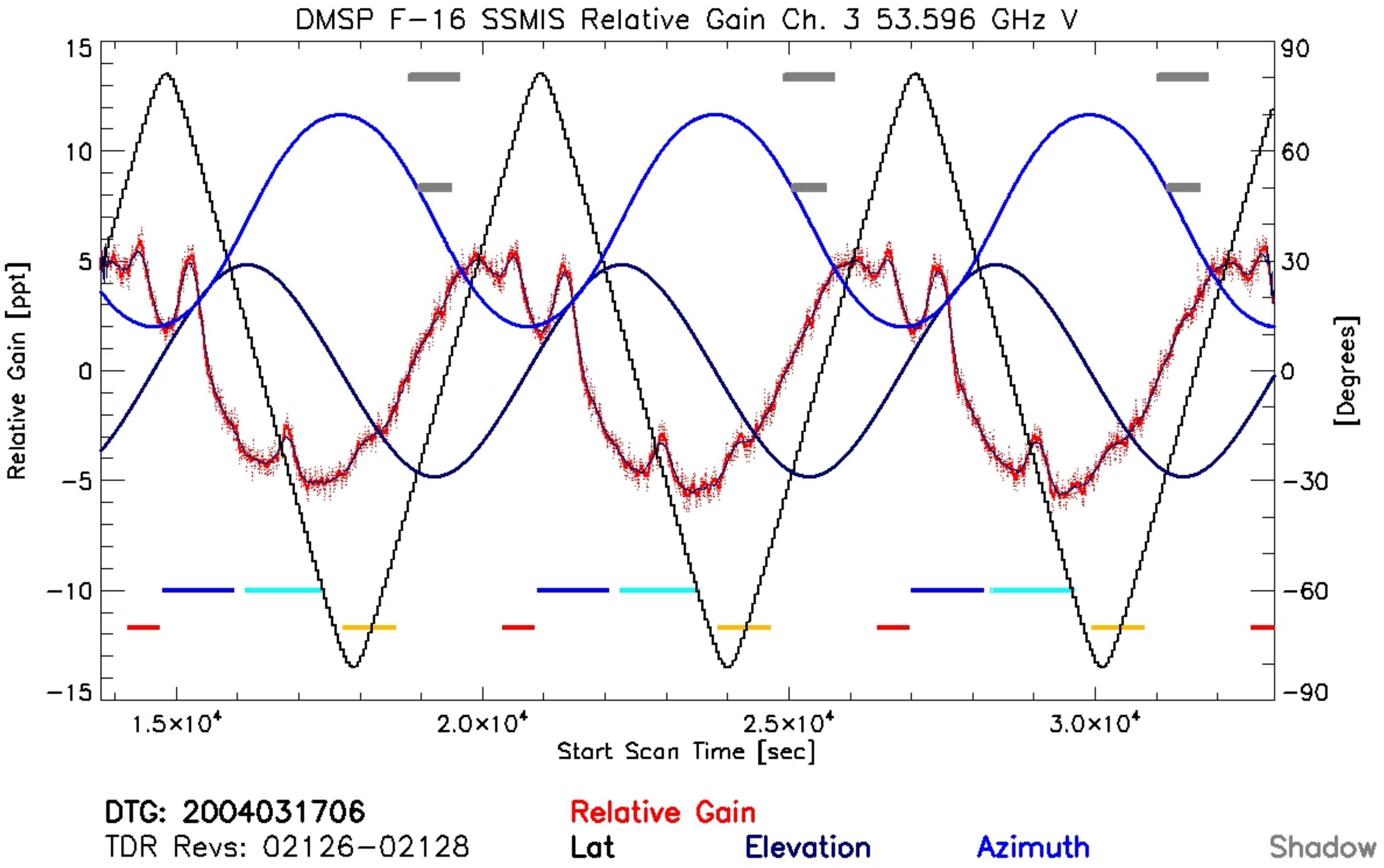

R1

R2

D1

D2

Radiometric Calibration Anomalies

Intrusion Detection Algorithm Based upon Solar Geometry

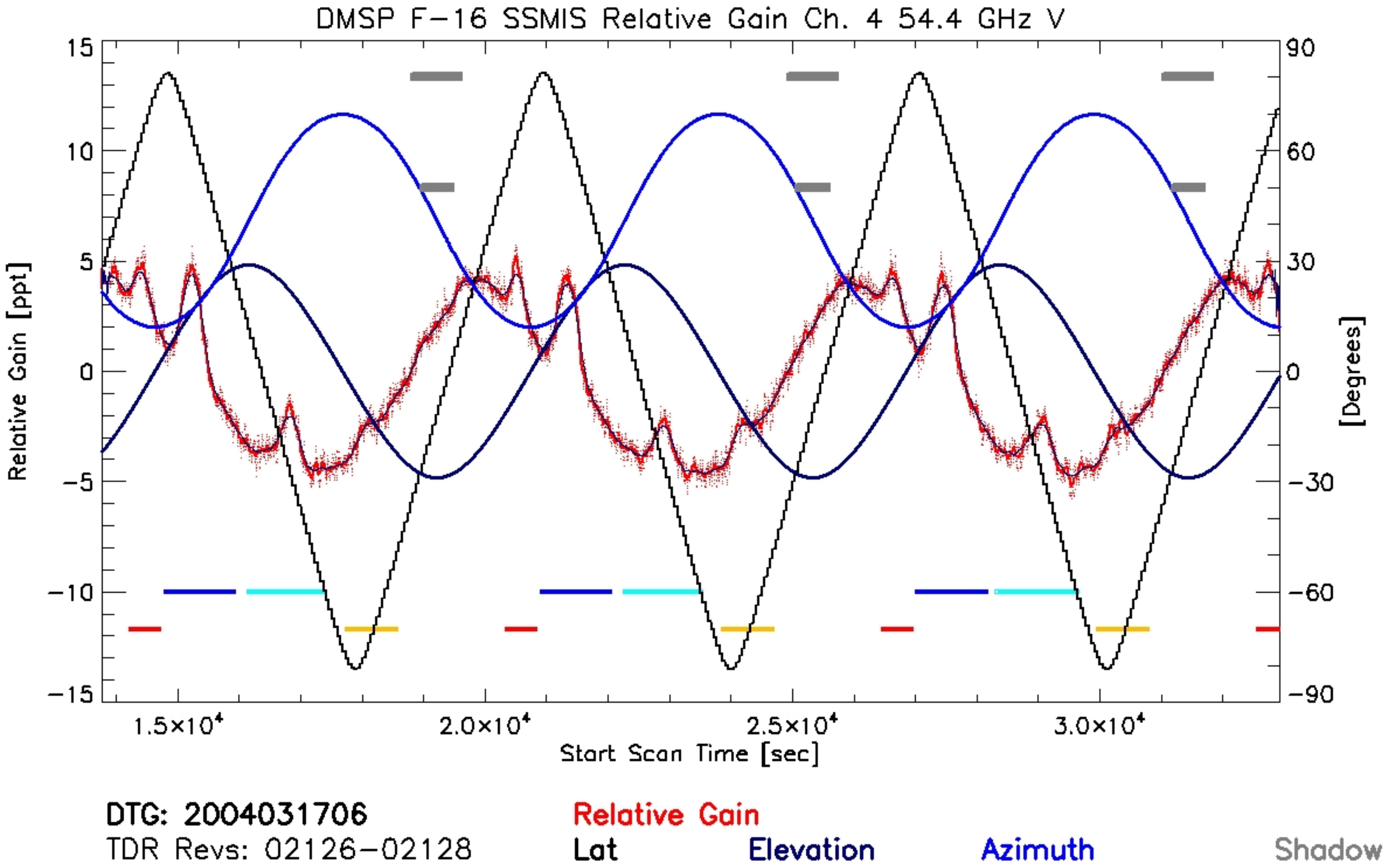

R1
R2
D1
D2

Radiometric Calibration Anomalies

Intrusion Detection Algorithm Based upon Solar Geometry

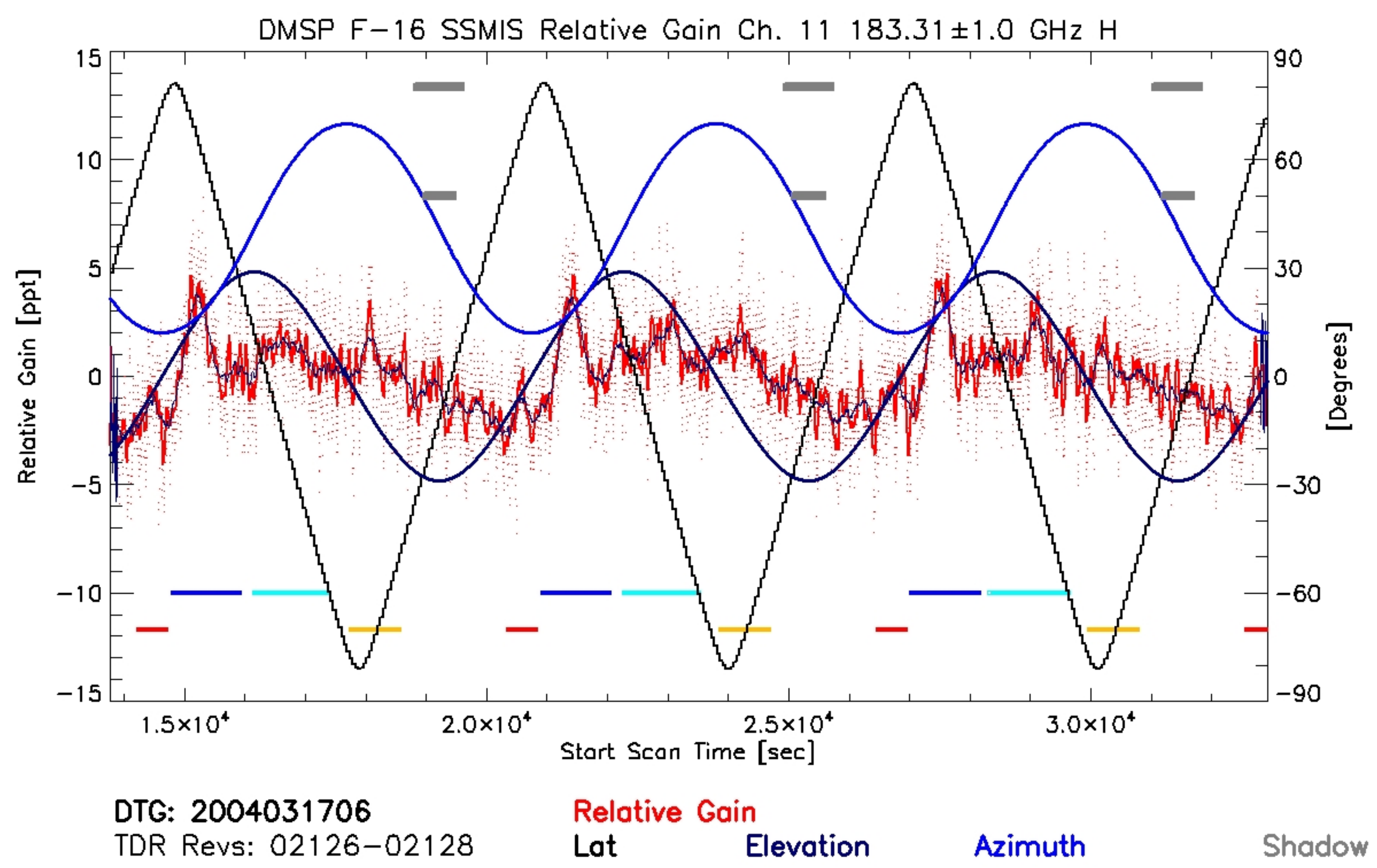

R1
R2
D1
D2

Radiometric Calibration Anomalies

Intrusion Detection Algorithm Based upon Solar Geometry

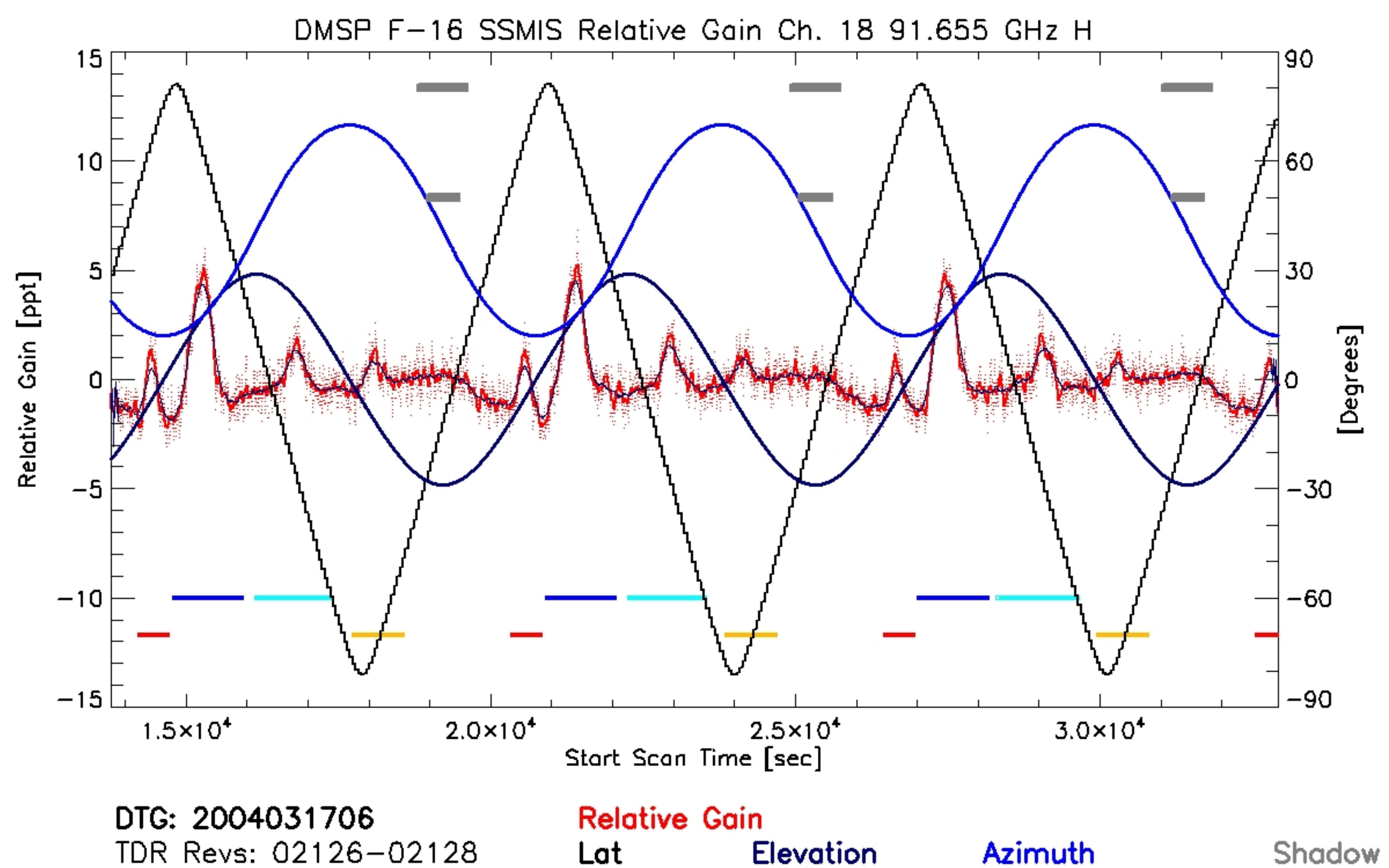

R1

R2

D1

D2

Radiometric Calibration Anomalies

Intrusion Detection Algorithm Based upon Solar Geometry

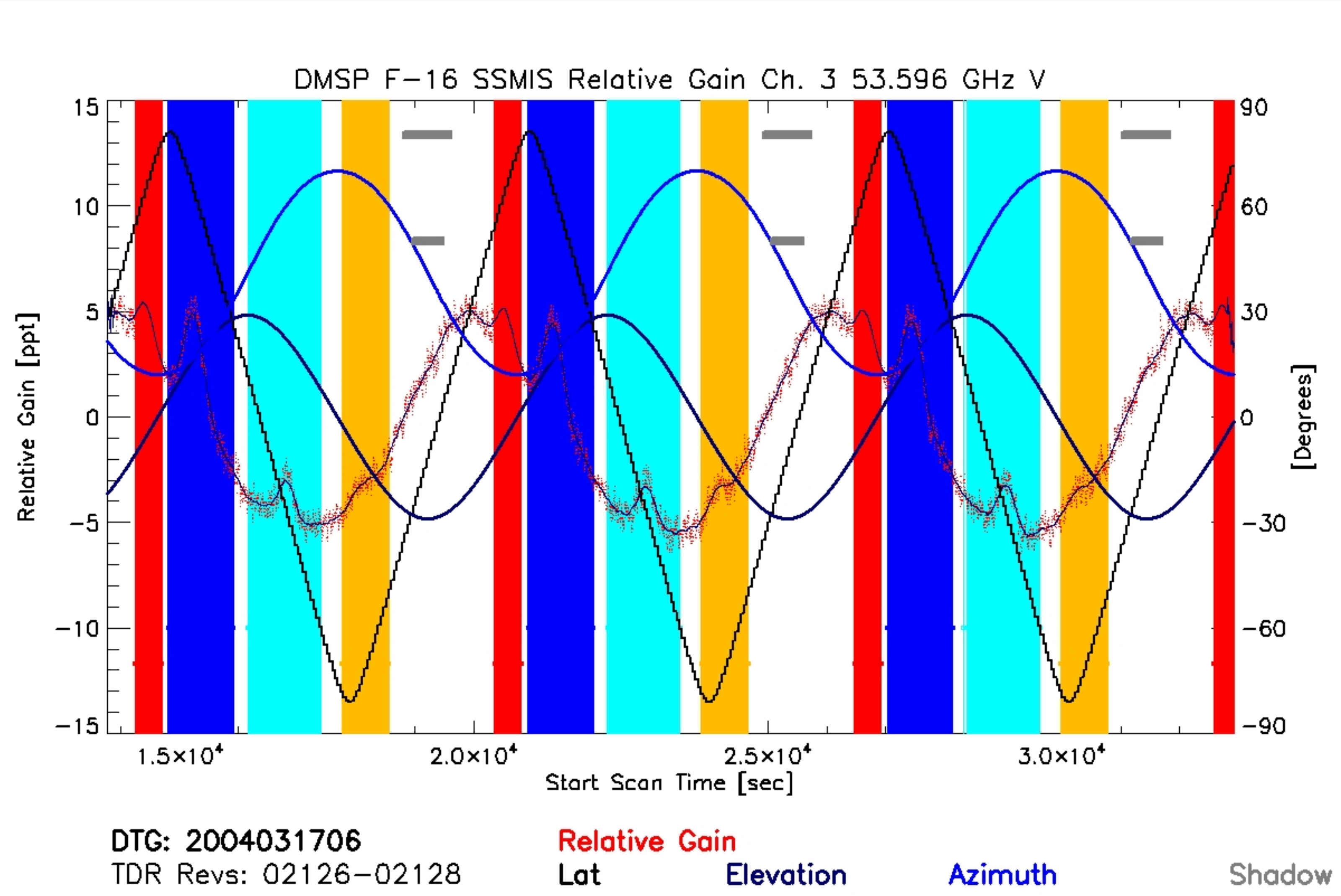

R1
R2
D1
D2

Radiometric Calibration Anomalies

Intrusion Detection Algorithm Based upon Solar Geometry

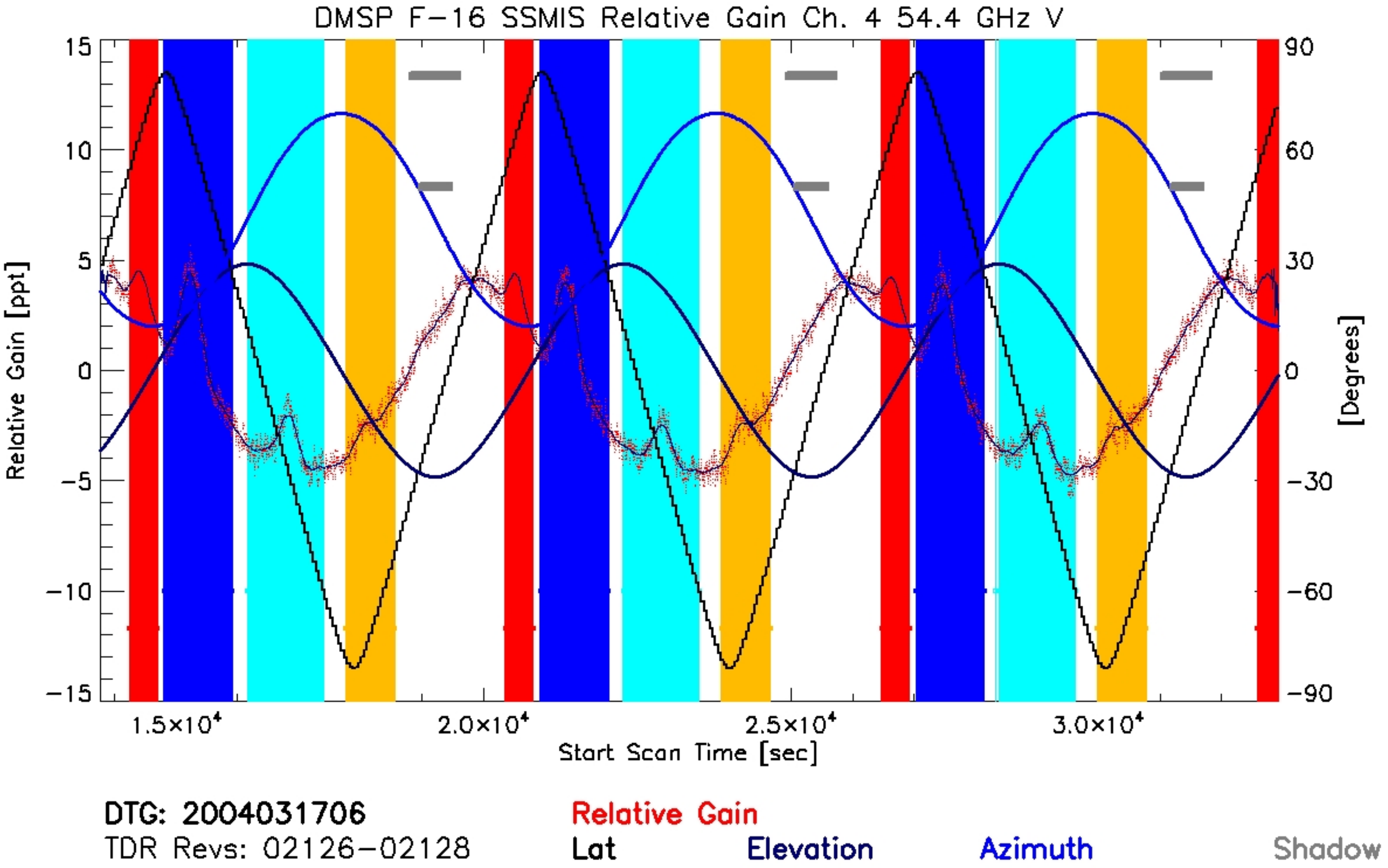

R1
R2
D1
D2

Radiometric Calibration Anomalies

Intrusion Detection Algorithm Based upon Solar Geometry

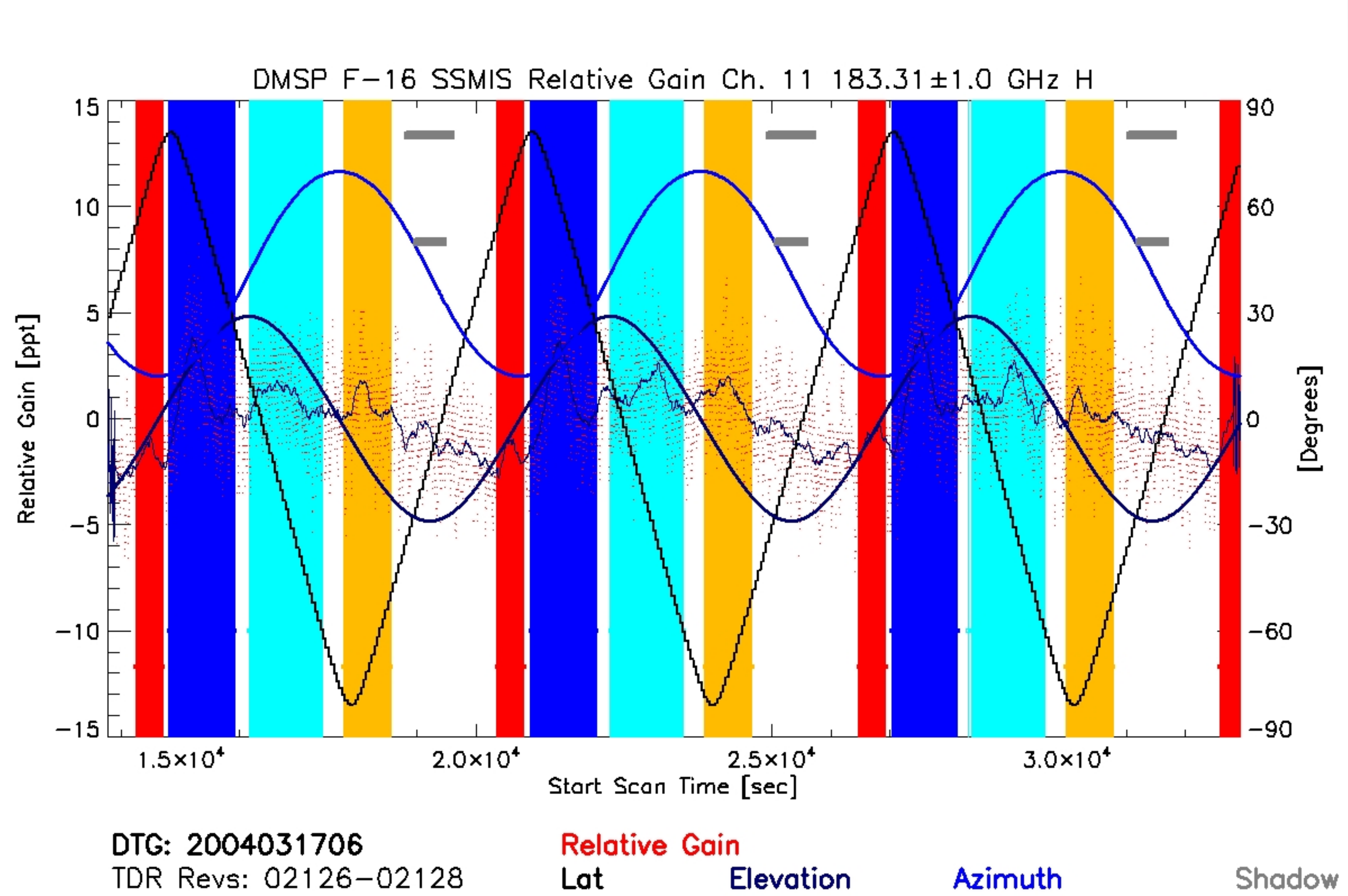

R1
R2
D1
D2

Radiometric Calibration Anomalies

Intrusion Detection Algorithm Based upon Solar Geometry

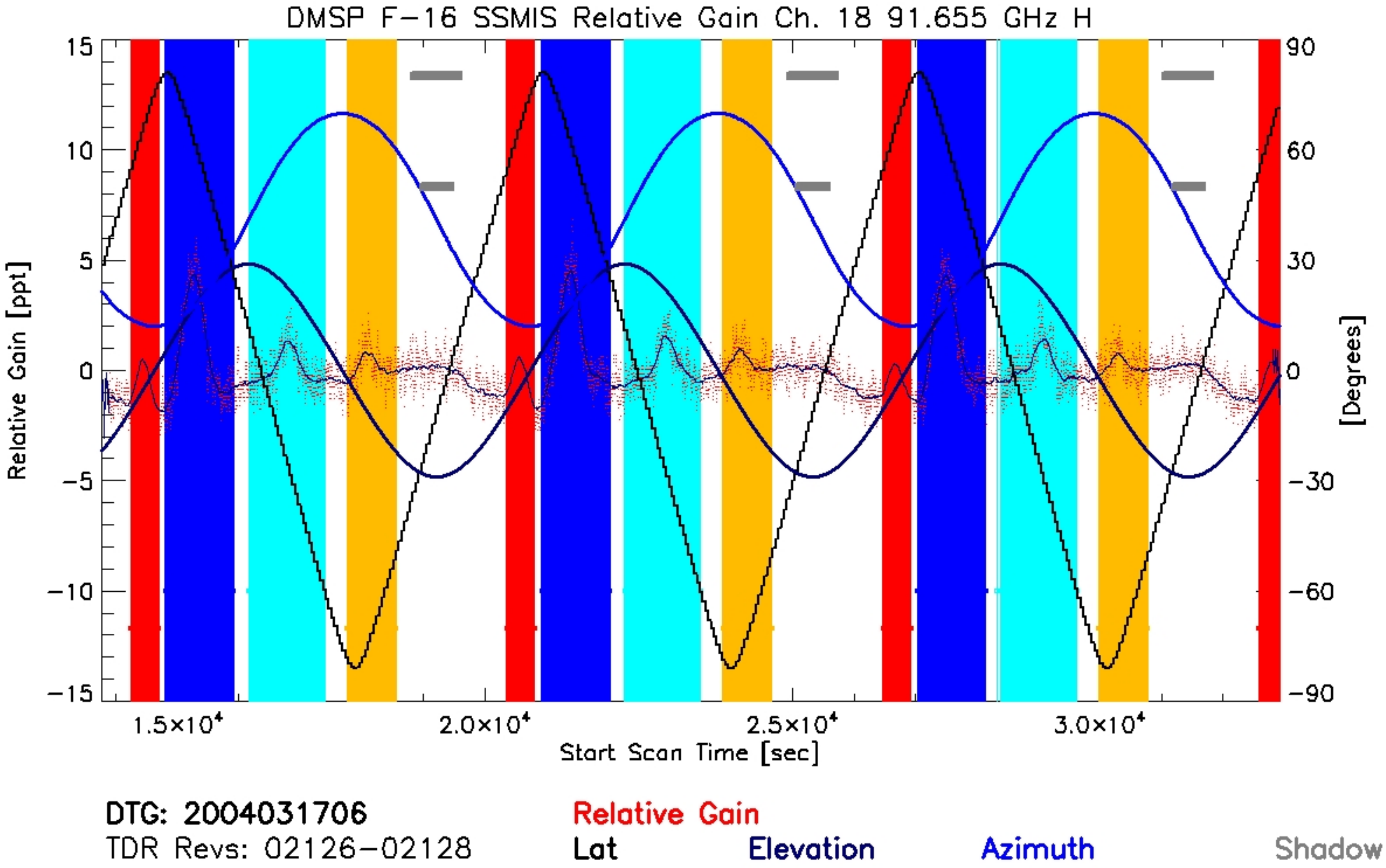

R1
R2
D1
D2

Radiometric Calibration Anomalies

Early Orbit Mode Warm Load Imaging

Kunkee and Hong

Radiometric Calibration Anomalies

DGS

Simulation tool:

Recent software modifications added substantial capability to DGS.

Allowed Cal/Val Team to analyze the SSMIS calibration anomalies and Field of View (FOV) intrusions

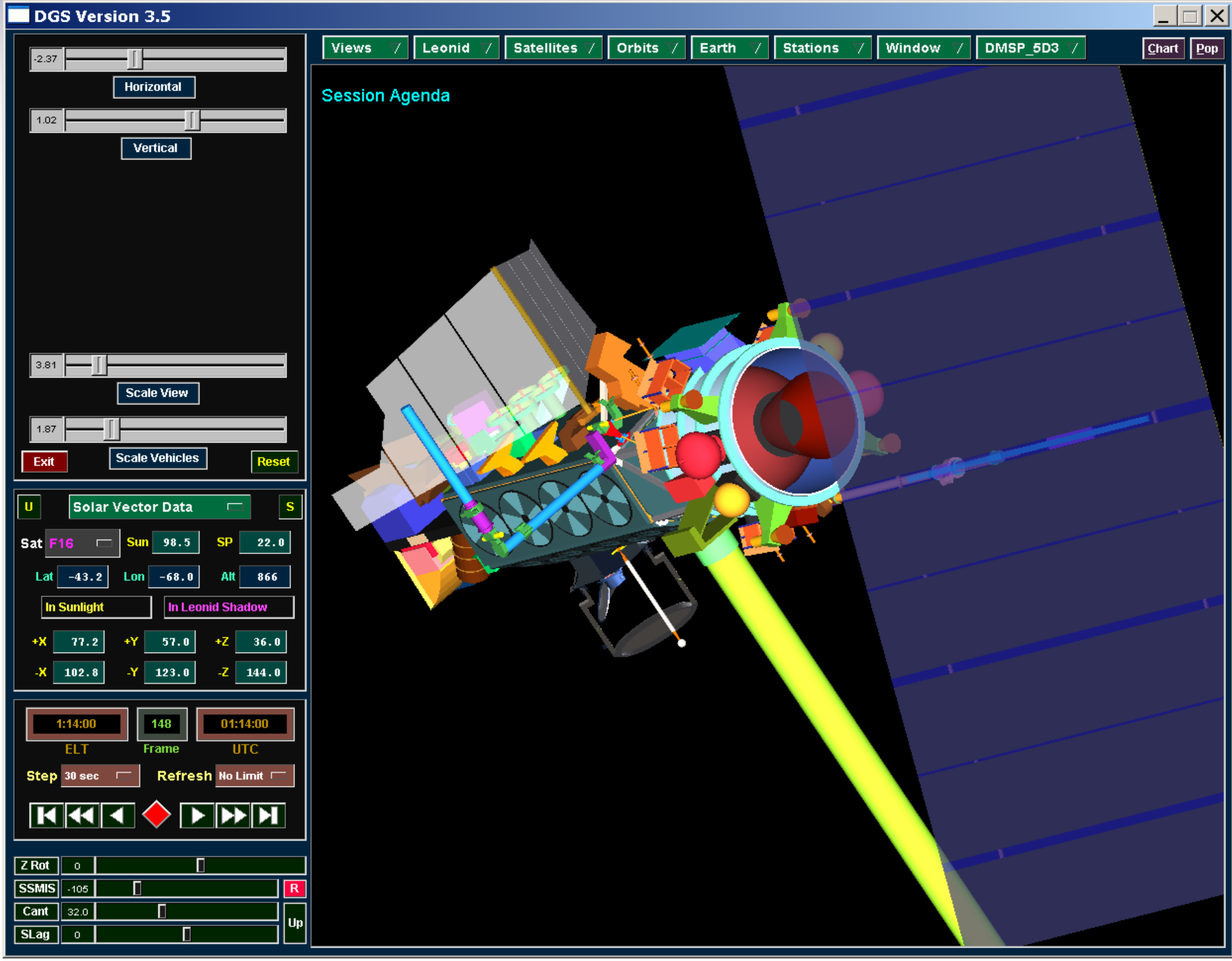

Horizontal -2.37

Vertical 1.02

Scale View 3.81

Scale Vehicles 1.87

Sat F16 Sun 98.5 SP 22.0

Lat -43.2 Lon -68.0 Alt 866

In Sunlight

In Leonid Shadow

+X 77.2 +Y 57.0 +Z 36.0

-X 102.8 -Y 123.0 -Z 144.0

ELT 1:14:00 Frame 148 UTC 01:14:00

Step 30 sec Refresh No Limit

Z Rot 0

SSMIS -105

Cant 32.0

SLag 0

Radiometric Calibration Anomalies

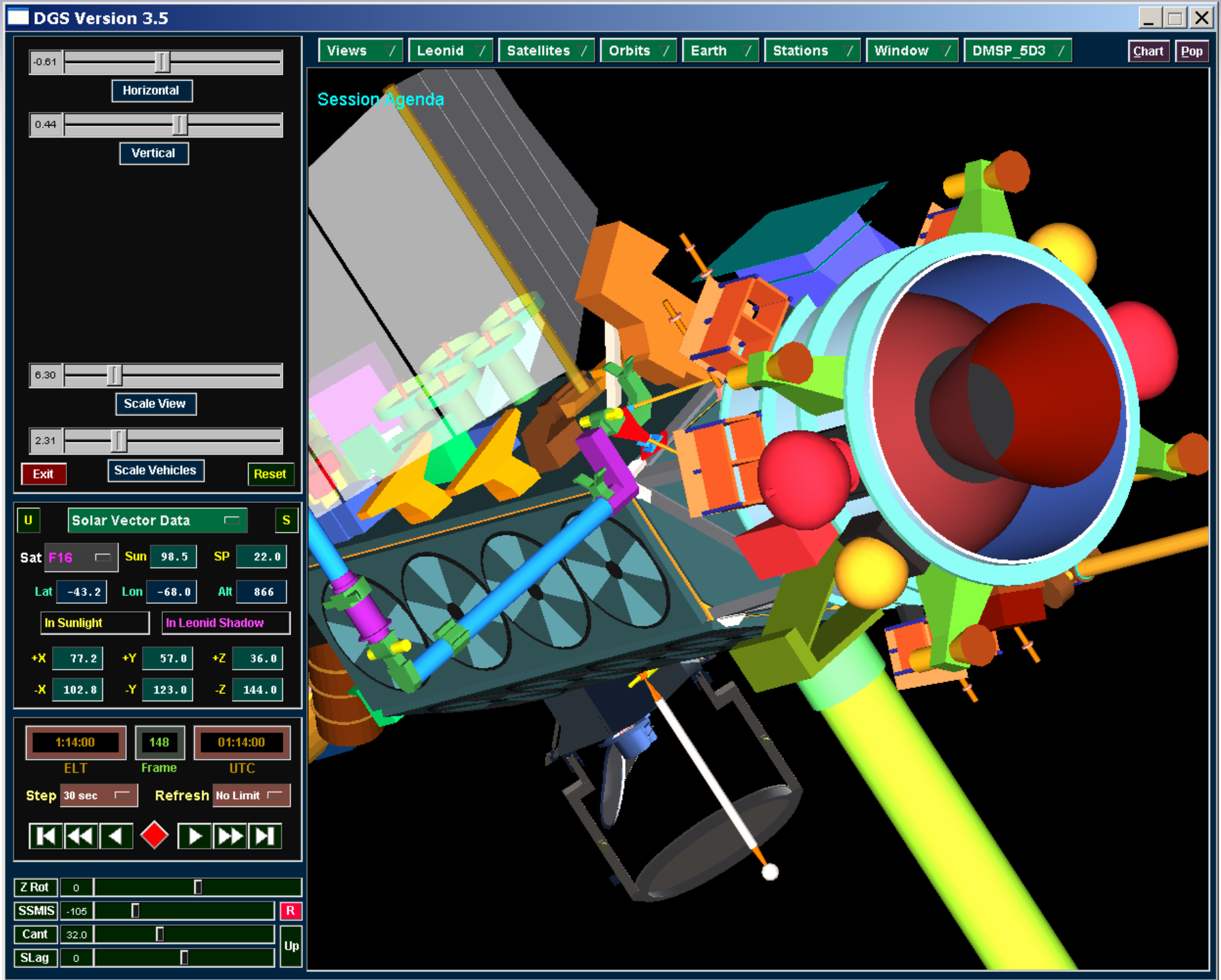
DGS Version 3.5

Horizontal -0.61

Vertical 0.44

Scale View 6.30

Scale Vehicles 2.31

Solar Vector Data

Sat F16 Sun 98.5 SP 22.0

Lat -43.2 Lon -68.0 Alt 866

In Sunlight

In Leonid Shadow

+X 77.2 +Y 57.0 +Z 36.0

-X 102.8 -Y 123.0 -Z 144.0

ELT 1:14:00

Frame 148

UTC 01:14:00

Step 30 sec

Refresh No Limit

Z Rot 0

SSMIS -105

Cant 32.0

SLag 0

Session Agenda

Radiometric Calibration Anomalies

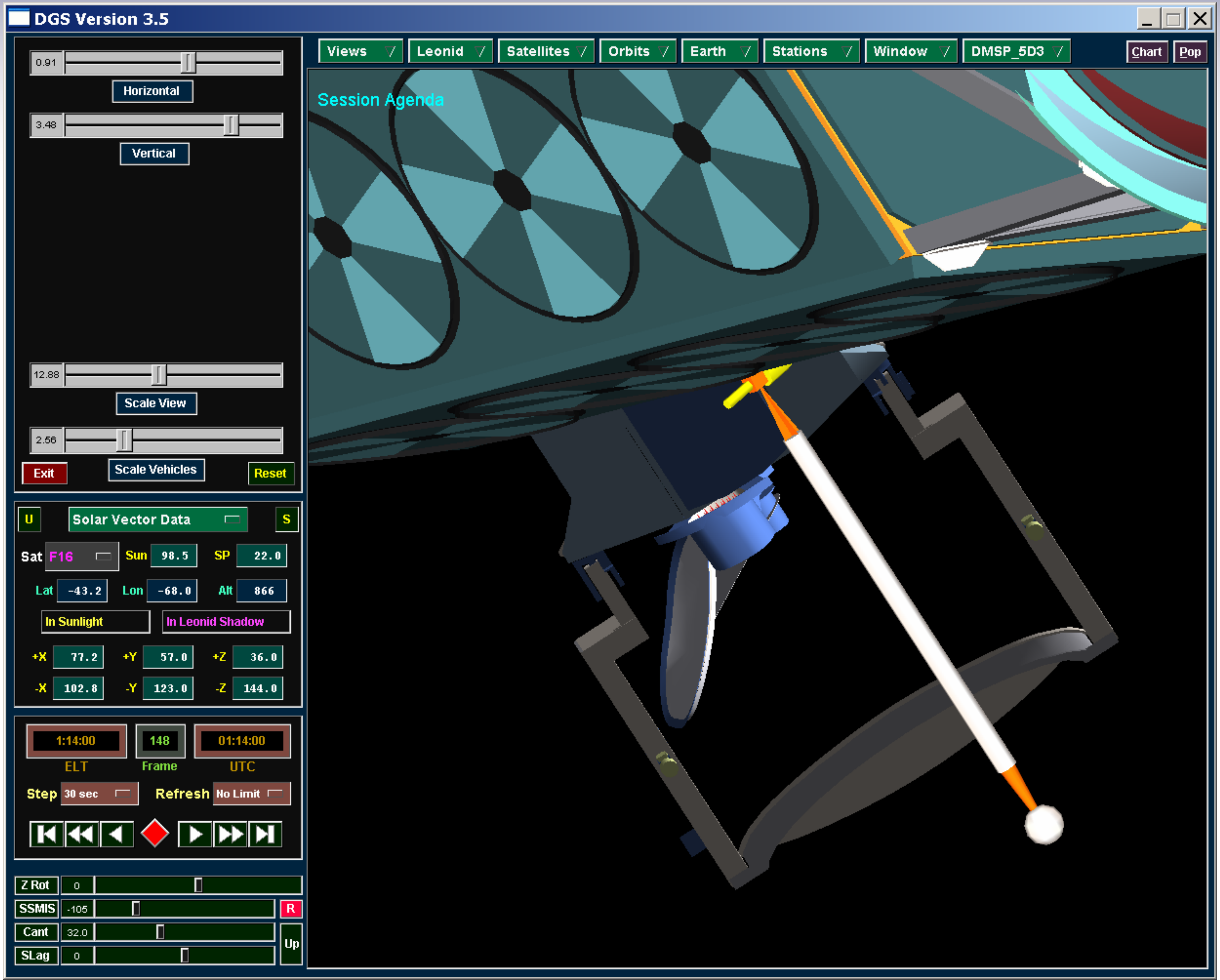

Horizontal 0.91

Vertical 3.48

Scale View 12.88

Scale Vehicles 2.56

Sat F16 Sun 98.5 SP 22.0

Lat -43.2 Lon -68.0 Alt 866

In Sunlight In Leonid Shadow

+X 77.2 +Y 57.0 +Z 36.0

-X 102.8 -Y 123.0 -Z 144.0

ELT 1:14:00 Frame 148 UTC 01:14:00

Step 30 sec Refresh No Limit

Z Rot 0

SSMIS -105

Cant 32.0

SLag 0

Radiometric Calibration Anomalies

Horizontal 5.36

Vertical -2.31

Scale View 7.03

Scale Vehicles 3.83

Sat F16
Sun 98.5
SP 22.0
Lat 77.2
Lon 136.8
Alt 862

In Sunlight
In Leonid Stream

+X 81.3
+Y 124.6
+Z 36.0
-X 98.7
-Y 55.4
-Z 144.0

ELT 1:54:30
Frame 229
UTC 01:54:29

Step 30 sec
Refresh No Limit

Z Rot 0
SSMIS 180
Cant 32.0
SLag 0

Radiometric Calibration Anomalies

Analysis of Impact

- Solar Intrusions to Warm Load Occur 3-4 Times per Orbit
- Scene Temperature Drops up to 1.5 K at Anomaly Peak
- Single Intrusion Duration can Last 350-450 Scans
- Locations can be Predicted and Gated Out
- Reflection Intrusions have Largest Impact
- Depending Upon Solar Geometry,
  40% of Total Scans can be effected

Radiometric Calibration Anomalies

Plans and Implementation of Resolution in GDPS

- Using Fourier Filtering Based Smoother (NGES)
  - Interpolate Nominal Gain to Remove Solar Intrsuions
  - Provide Modified Gains with Flags
  - SDR Data will Provide Gain “Corrected” TBs

- TDR data to remain unchanged

Radiometric Calibration Anomalies

Reflector Emissions

- Description of Problem
- Thermal Modeling of Reflector Surface
- Development of Correction Algorithm
- Characterization of Reflector Surface Coatings
- Analysis of Impact
- Resolution Plans

Radiometric Calibration Anomalies

Description of the Problem

- Reflector “Looks” Directly into Sun Twice Each Orbit
  - Primary Effect as Spacecraft Emerges from Earth and/or Spacecraft Shadow
  - Secondary Effect as Spacecraft Enters the Earth and/or Spacecraft Shadow
- Reflector undergoes Large Thermal Cycle each Orbit
- Reflector Arm Temperature is Only Telemetry Data Providing Insight to Actual Reflector Surface Temperature

Radiometric Calibration Anomalies

Description of the Problem

- **Ideal SiOx/Al Reflector Surface Emissivity, $\in_R$**

Frequency (GHz)	$\in_R$
19.35	0.00051
37.0	0.00071
60.0	0.00090
91.65	0.00111
183.0	0.00157

These $\in_R$ values would result in scene Temperatures Not effected by Reflector Emission

Radiometric Calibration Anomalies

Description of the Problem

- Consider a Reflector Surface of Graphite Epoxy

Frequency (GHz)	$\in_R$ (GrEp)
19.35	0.012
37.0	0.016
60.0	0.020
91.65	0.025
183.0	0.035

These $\in_R$ values would result in scene Temperatures Strongly effected by Reflector Emission

Radiometric Calibration Anomalies

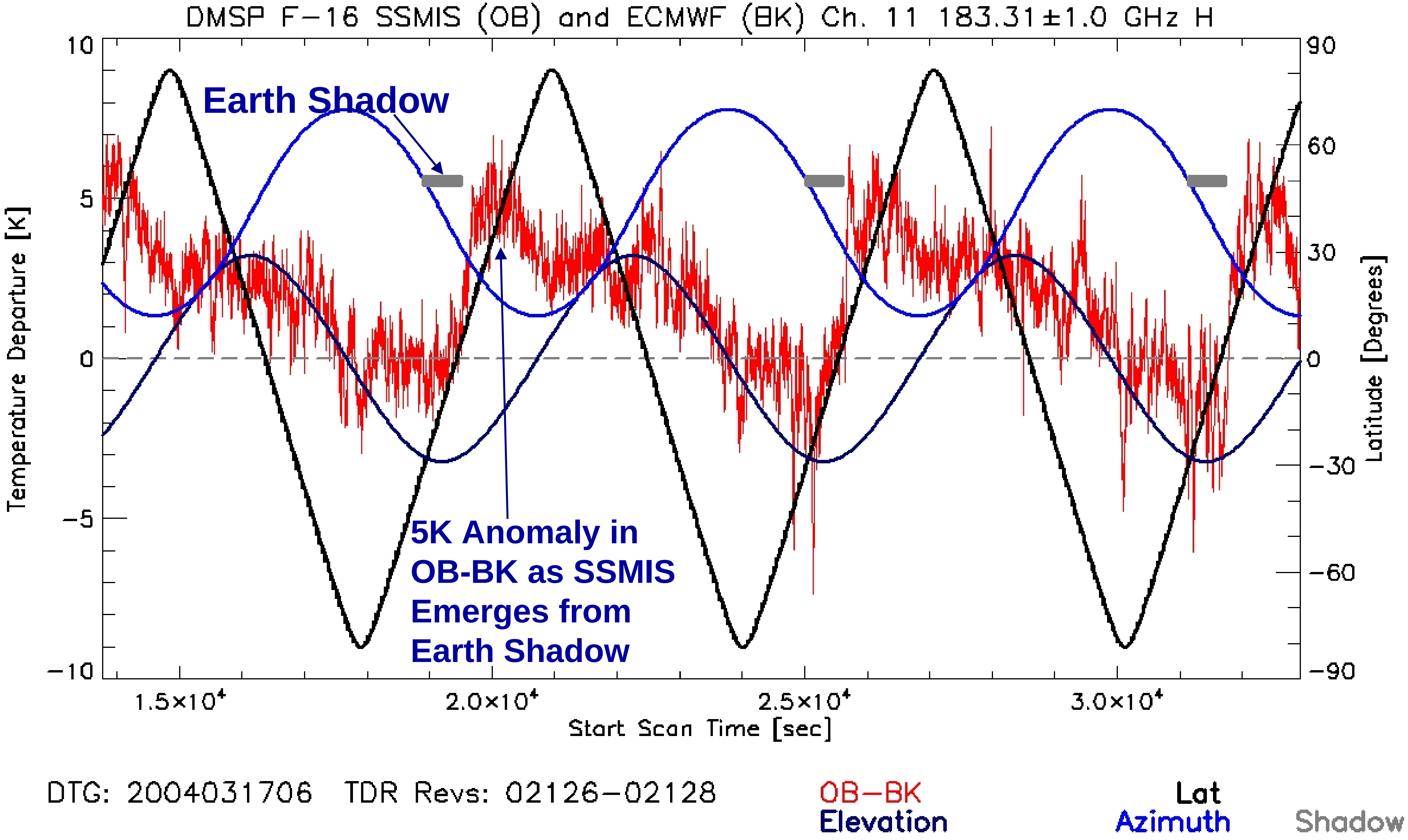

Earth Shadow

5K Anomaly in OB-BK as SSMIS Emerges from Earth Shadow

Radiometric Calibration Anomalies

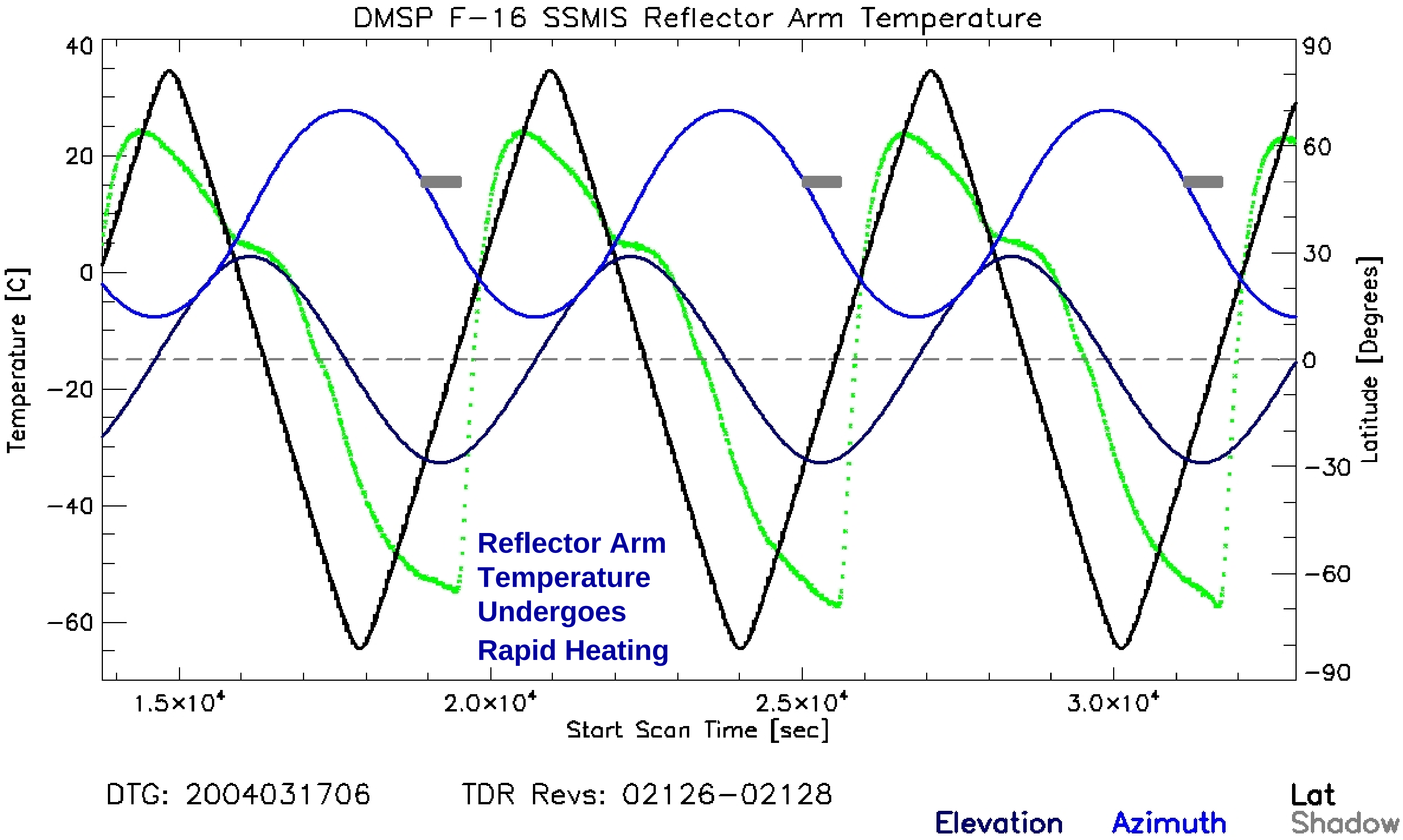

Reflector Arm Temperature Undergoes Rapid Heating

Radiometric Calibration Anomalies

Normalized Reflector Arm Temperature

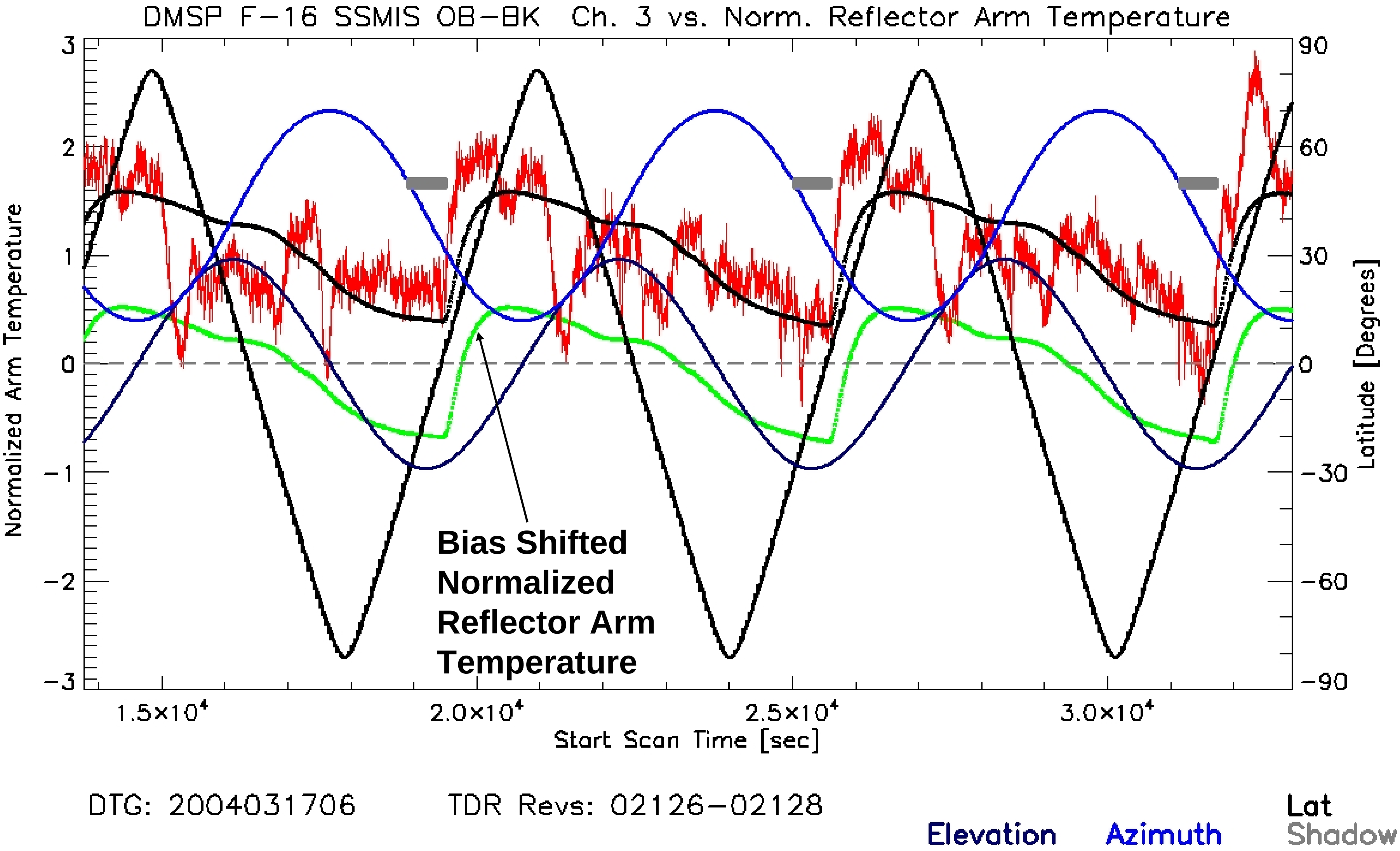

Bias Shifted Normalized Reflector Arm Temperature

Radiometric Calibration Anomalies

Normalized Reflector Arm Temperature

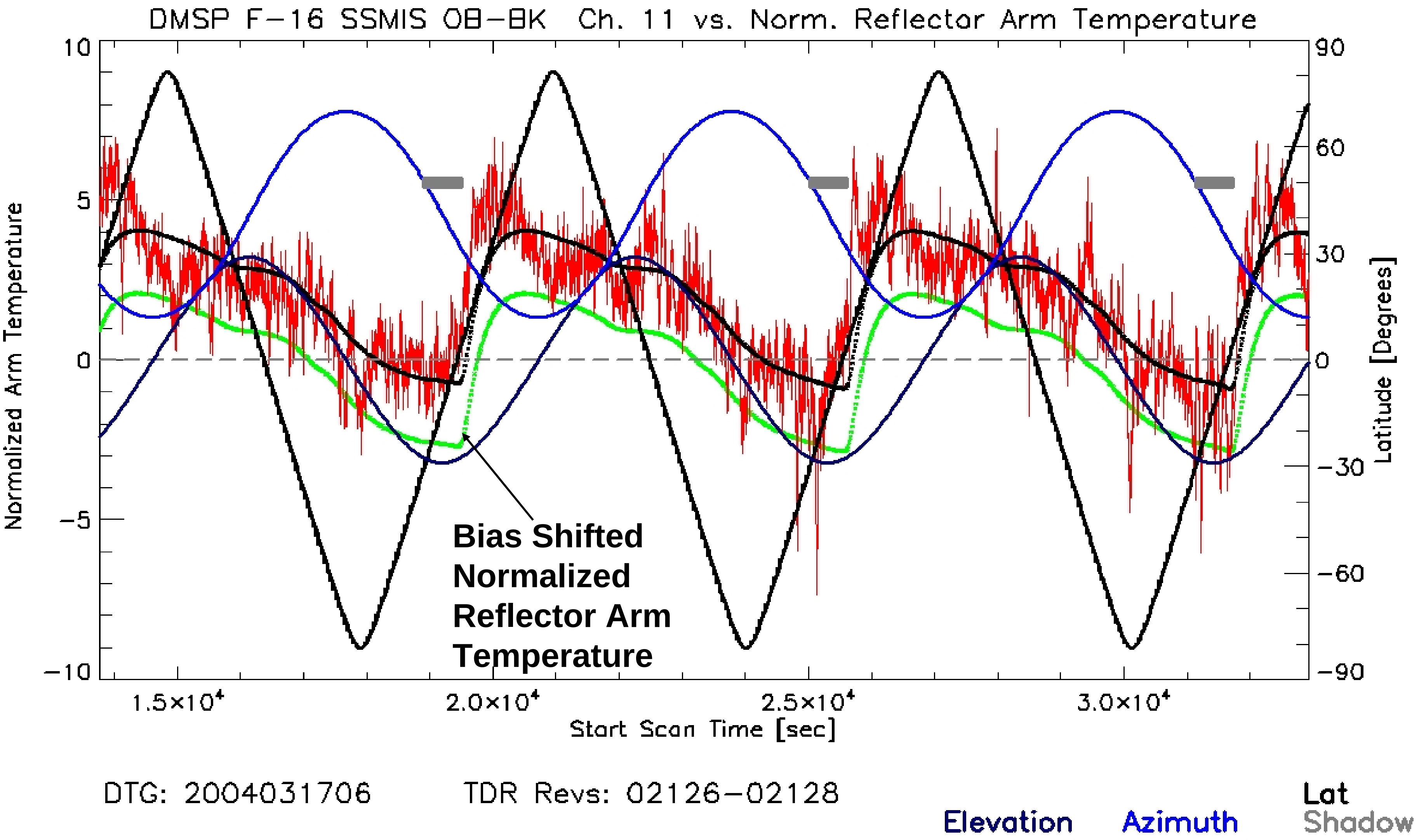

Bias Shifted Normalized Reflector Arm Temperature

Radiometric Calibration Anomalies

Thermal Modeling of Reflector Surface Temperature

- Reflector Arm Temperature Thermal Cycle is correlated to Reflector Face Thermal Cycle, but Underestimates Magnitude of Heating

- Reflector Arm Temperature does not Respond as Fast as the Reflector Face to Solar Heating

- OB-BK Plots Show Faster Response to Solar Heating then to Reflector Arm Temperature

- Developed Simplified Thermal Model based upon Solar Flux, Outgoing Longwave Radiation from Top of Atmosphere, and Shadowing from the Earth and cylindrical Spacecraft Body

- Fully developed Thermal Model of Reflector Surface (Aerospace)

Radiometric Calibration Anomalies

Reflector Temperature Model Using Constant Mean Global OLR

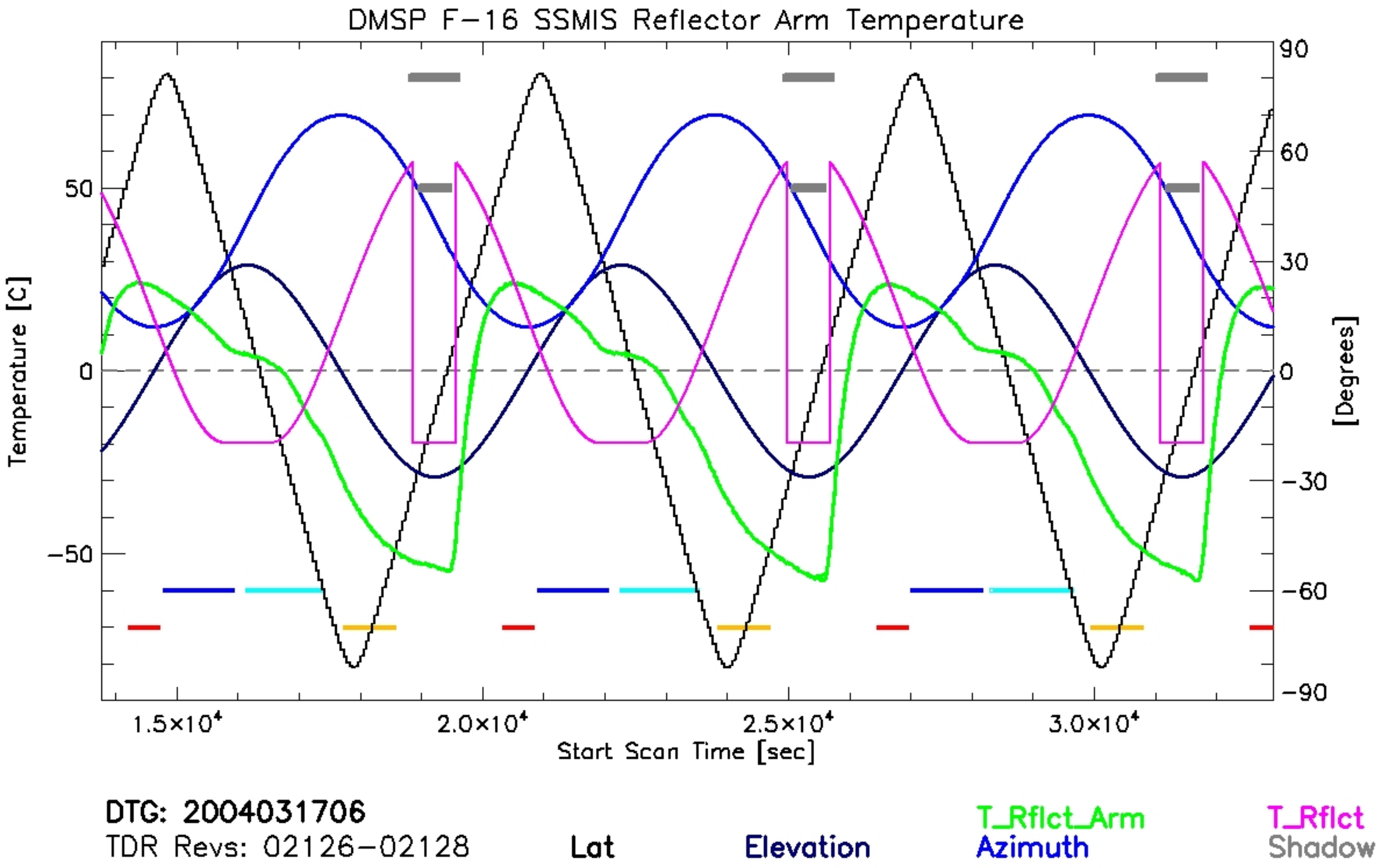

Radiometric Calibration Anomalies

Reflector Temperature Model Using Monthly Mean OLR

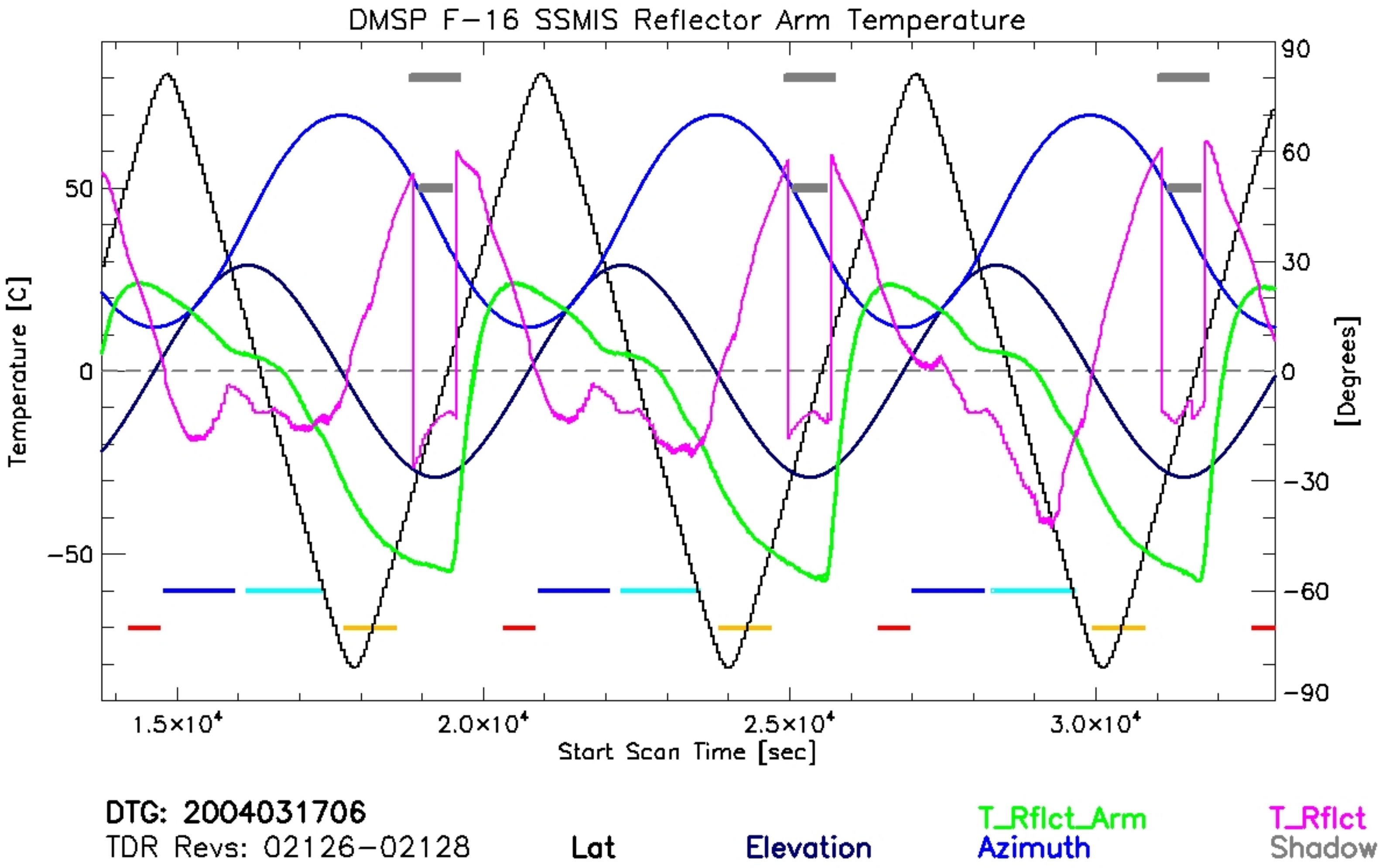

Radiometric Calibration Anomalies

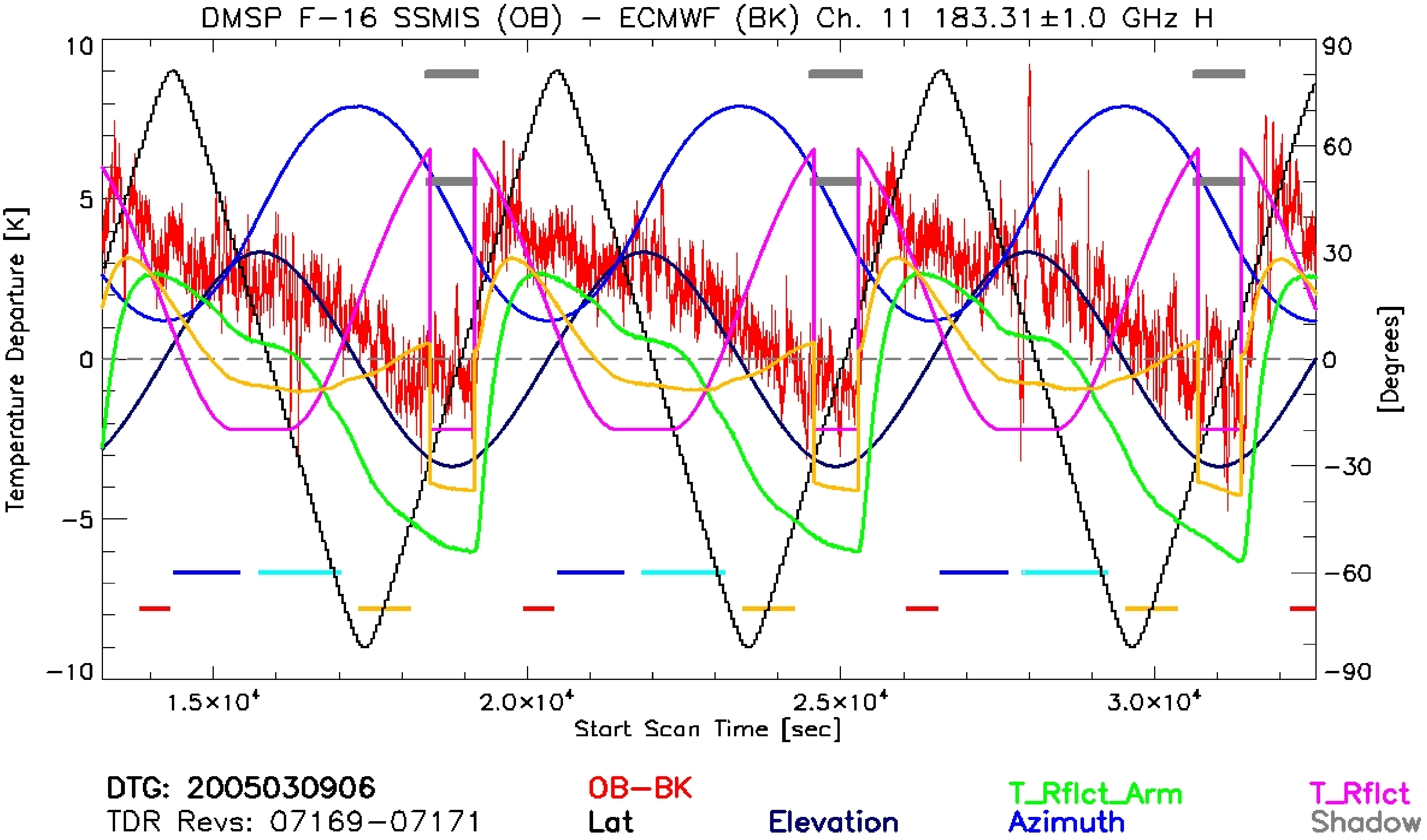

Radiometric Calibration Anomalies

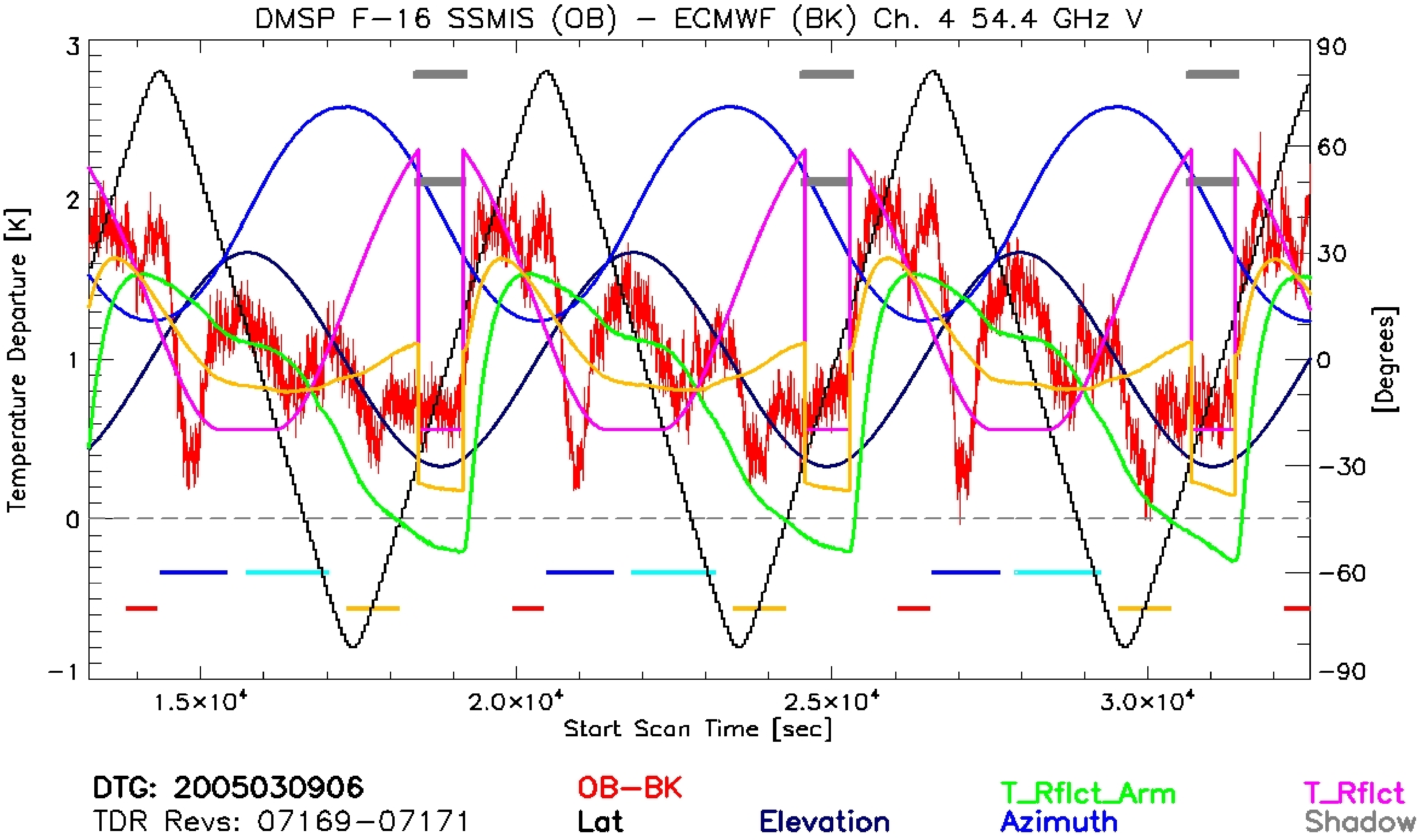

Radiometric Calibration Anomalies

Development of Correction Algorithm

$$T_{Apparent} = (1 - \in_R)\, T_{Scene} + \in_R\, T_{Reflector}$$

$$= T_{Scene} + \in_R\, (T_{Reflector} - T_{Scene})$$

Need Accurate Measurement of $T_{Reflector}$ and $\in_R$

Use T_{BK} as the T_{scene}

Use Mean of $T_{Reflector\_Model}$ T and $T_{Reflector\_Arm}$ as surrogate $T_{Reflector}$

Use the $\in_R\, (T_{Reflector} - T_{Scene})$ Term as a correction to the SSMIS OB

Radiometric Calibration Anomalies

Using the Mean of the $T_{\text{Reflector Arm}}$ and the $T_{\text{Reflector Model}}$

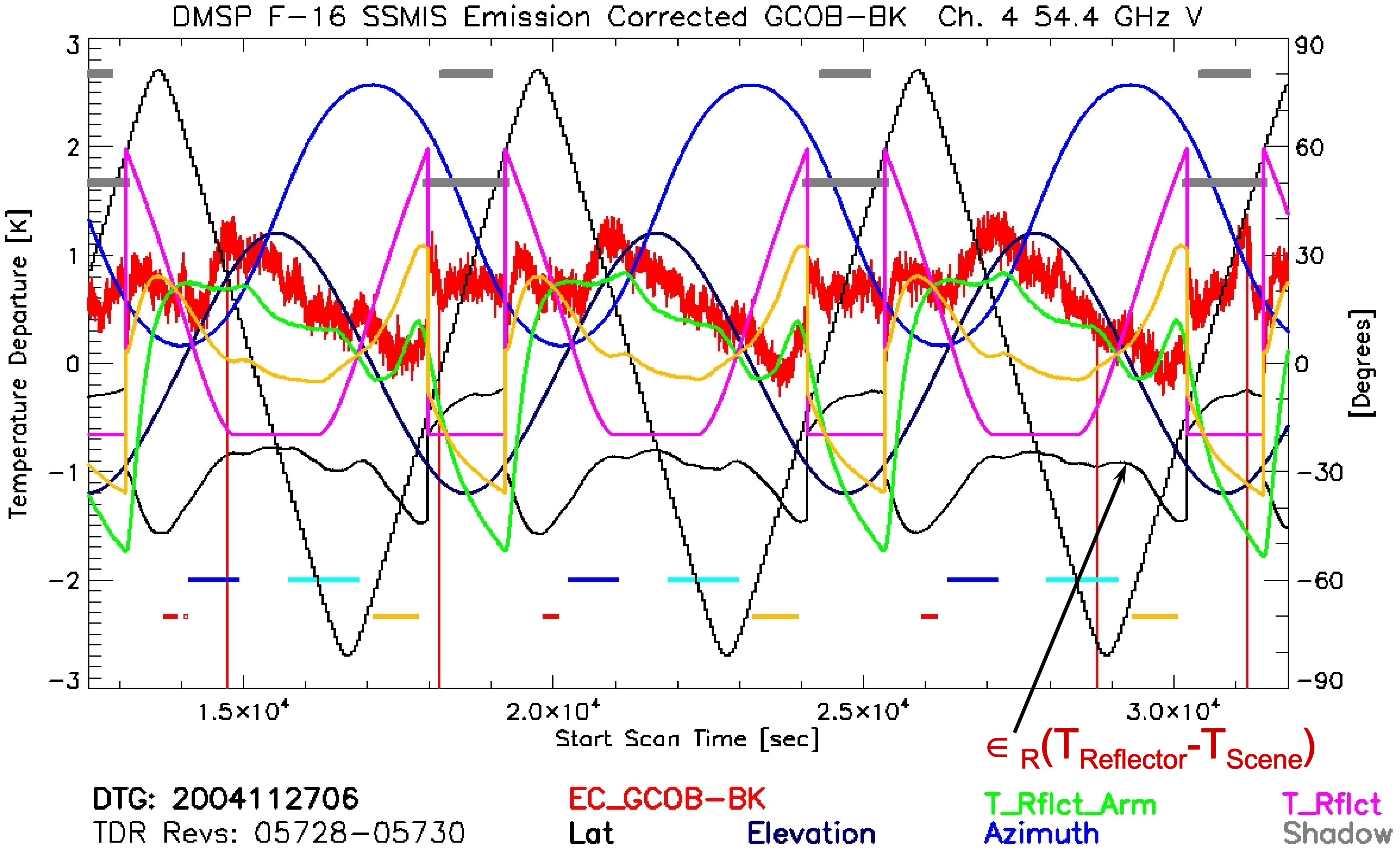

$\in_R(T_{Reflector}-T_{Scene})$

Radiometric Calibration Anomalies

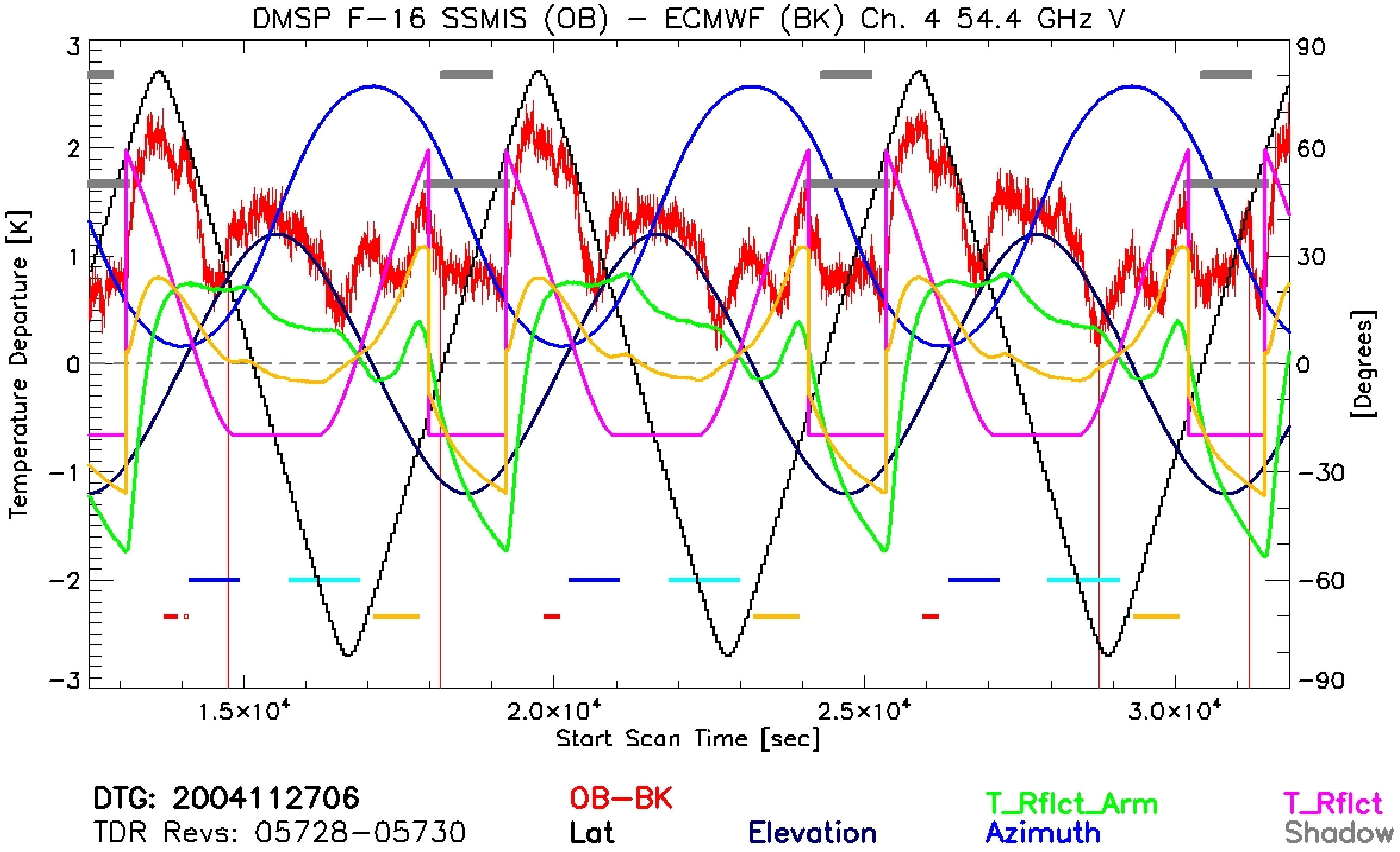

Radiometric Calibration Anomalies

Antenna Emission Effect seen in the EDRs

- Signal Evident in Temperature Retrievals
- Signal Difficult to Detect in Moisture Retreivals
- Strong Signal in Geopotential Height Fields

Radiometric Calibration Anomalies

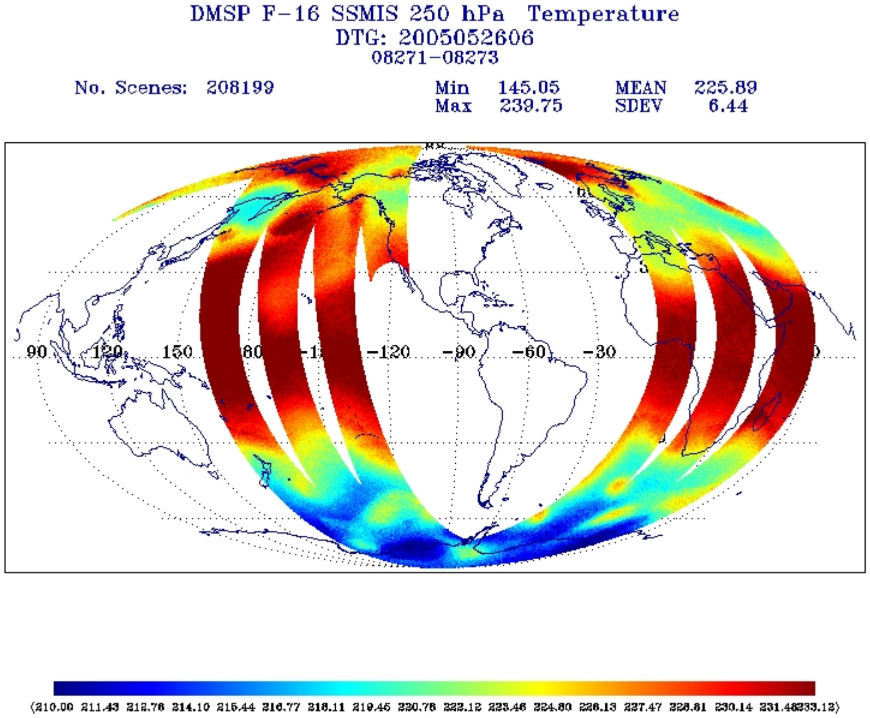

SSMIS 250 hPa T

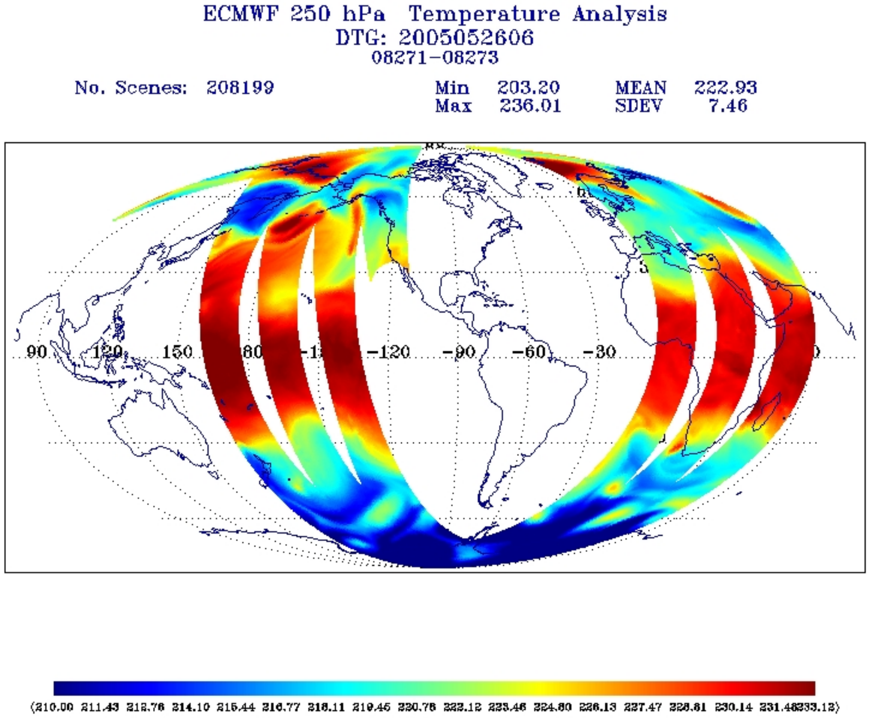

ECMWF 250 hPa T

Radiometric Calibration Anomalies

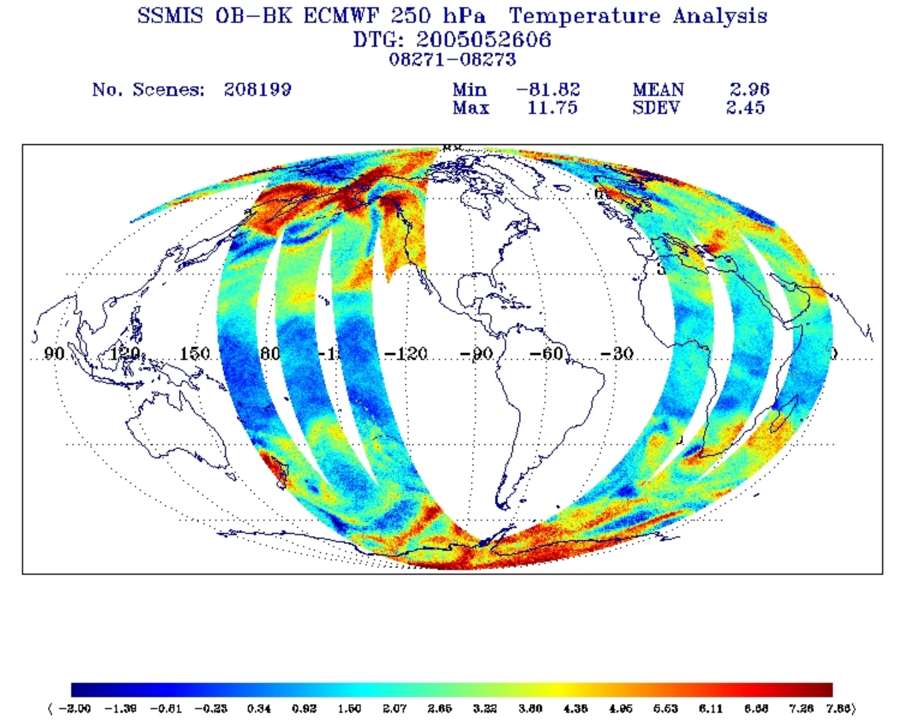

SSMIS – ECMWF 250 hPa Temperature Departure

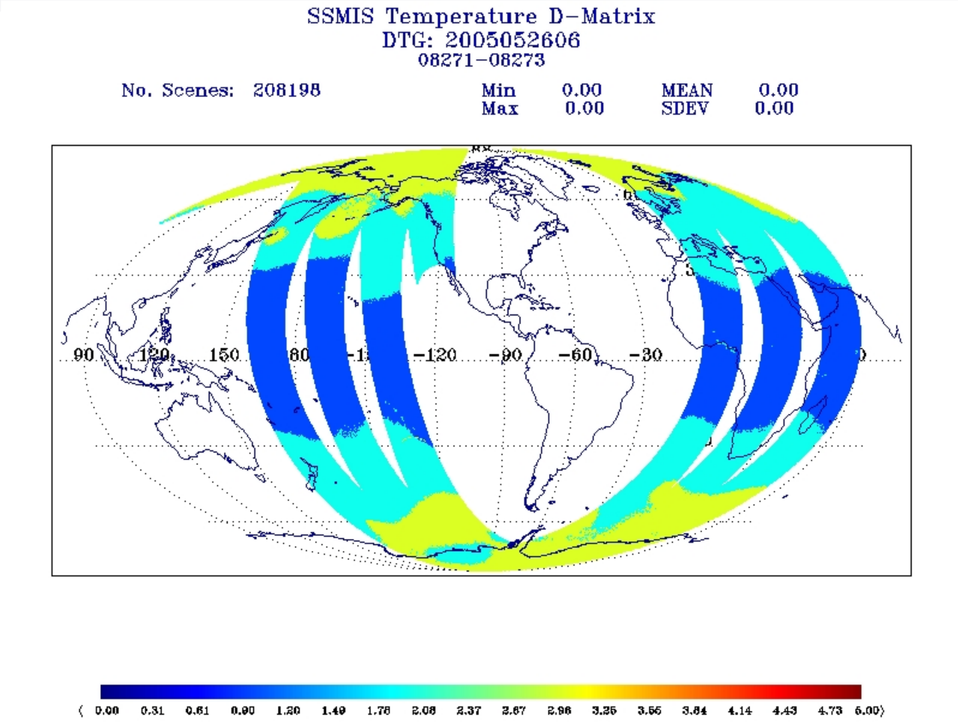

SSMIS Temperature D-Matrix

Radiometric Calibration Anomalies

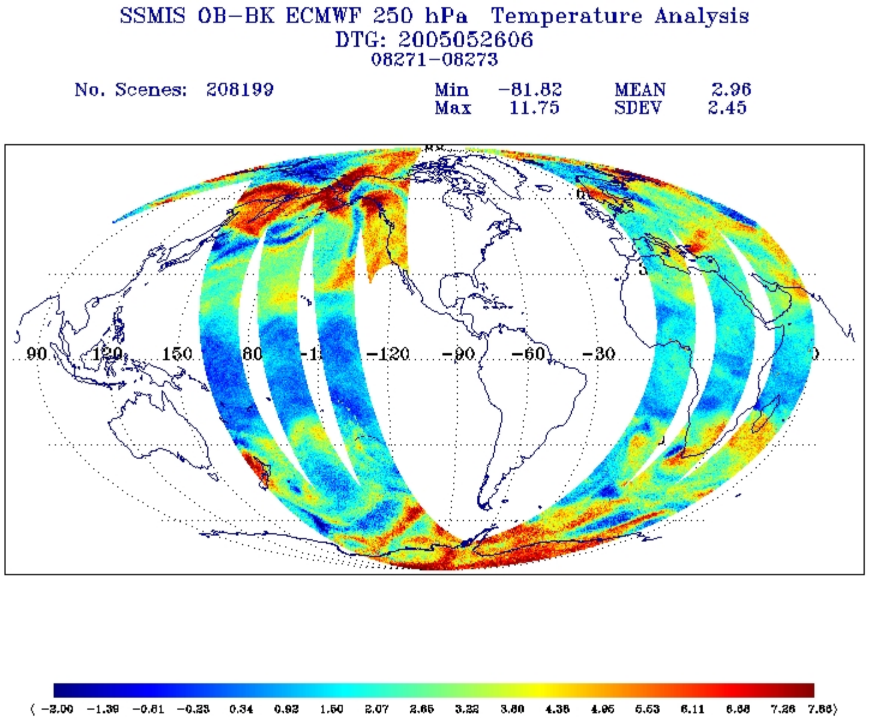

SSMIS – ECMWF 250 hPa
Temperature Departure

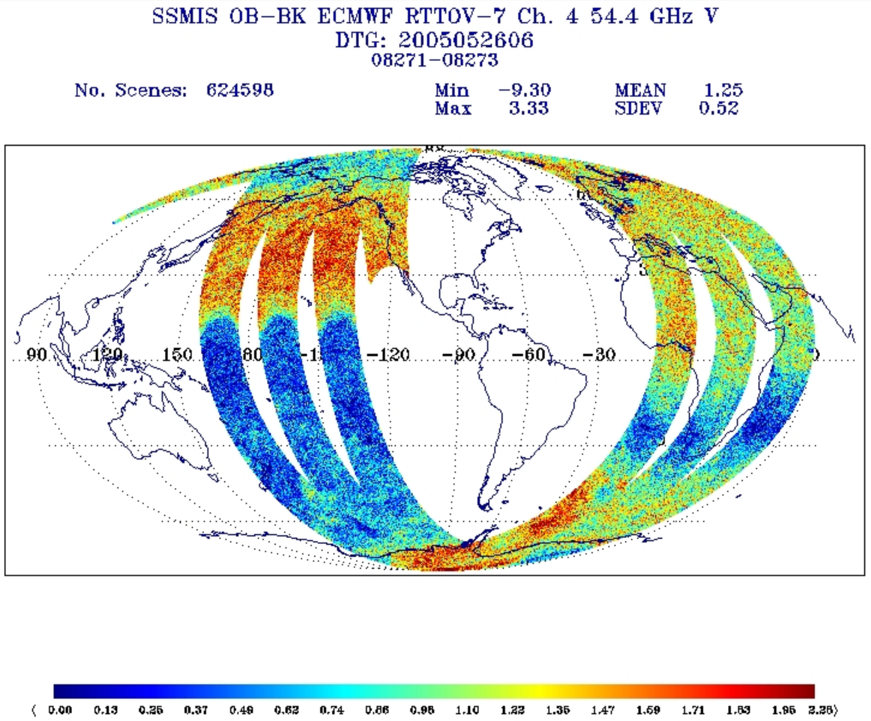

SSMIS – ECMWF RTTOV-7
Ch. 4 Departure

Radiometric Calibration Anomalies

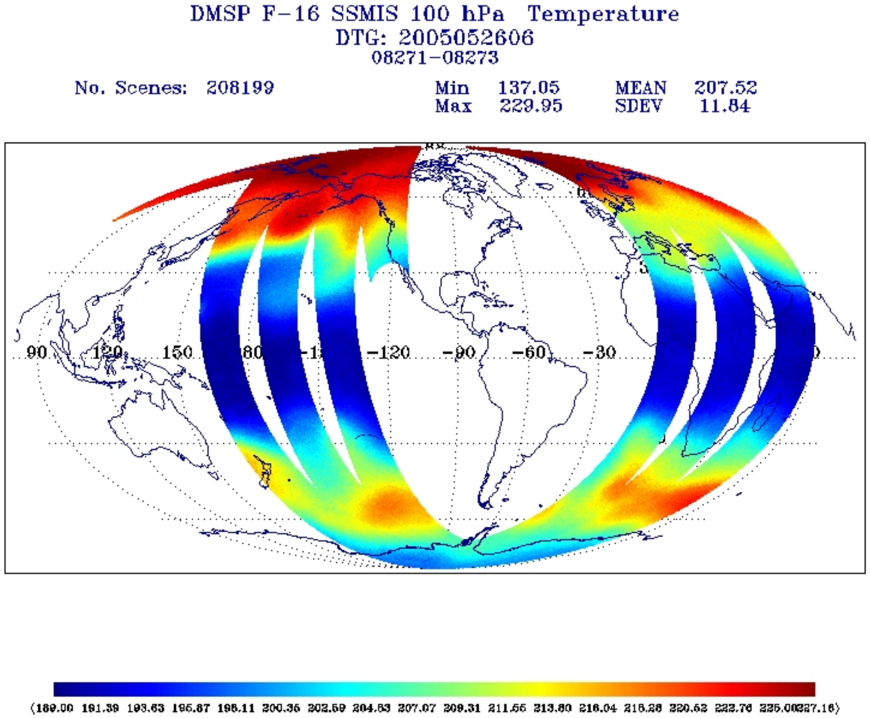

SSMIS 100 hPa T

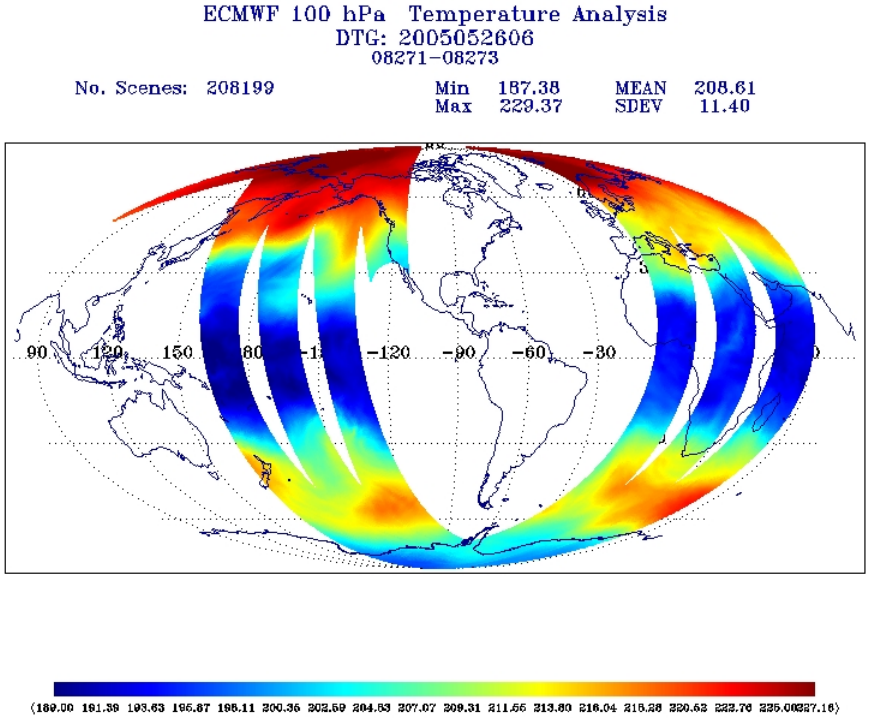

ECMWF 100 hPa T

Radiometric Calibration Anomalies

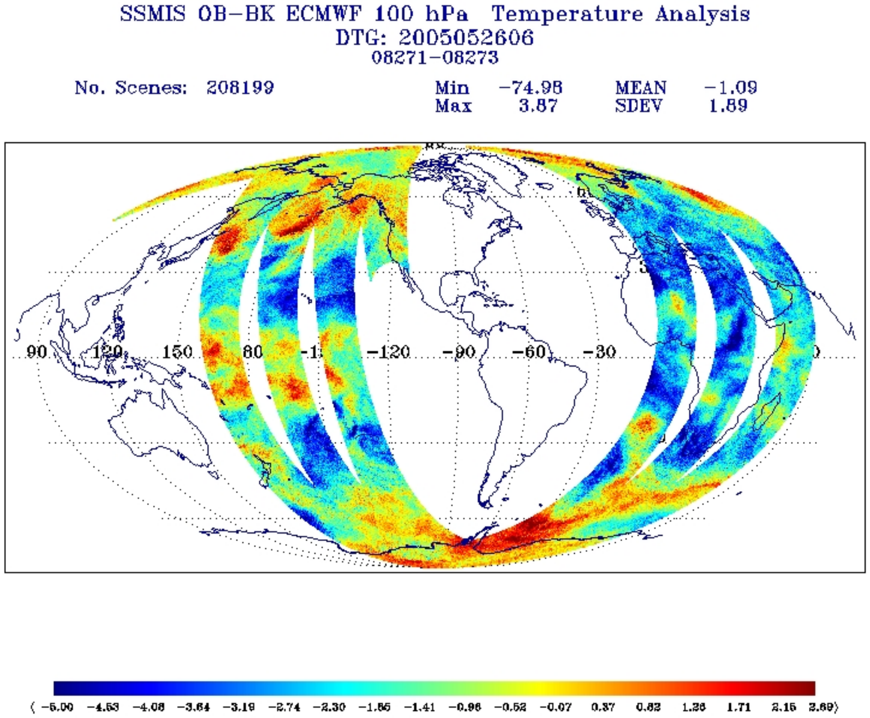

SSMIS – ECMWF 100 hPa Temperature Departure

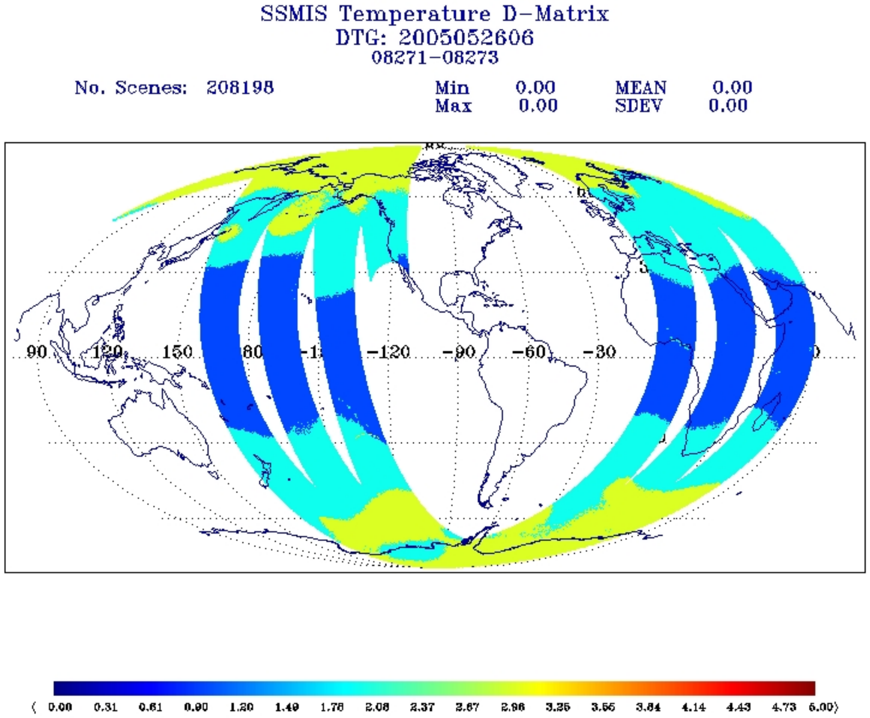

SSMIS Temperature D-Matrix

Radiometric Calibration Anomalies

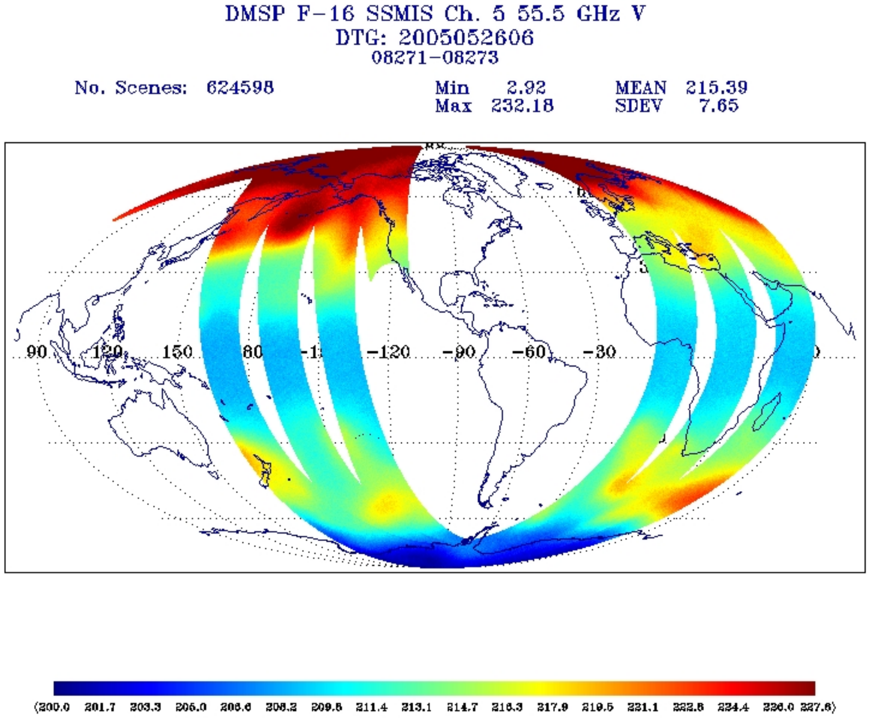

SSMIS
Ch. 5 Temperature

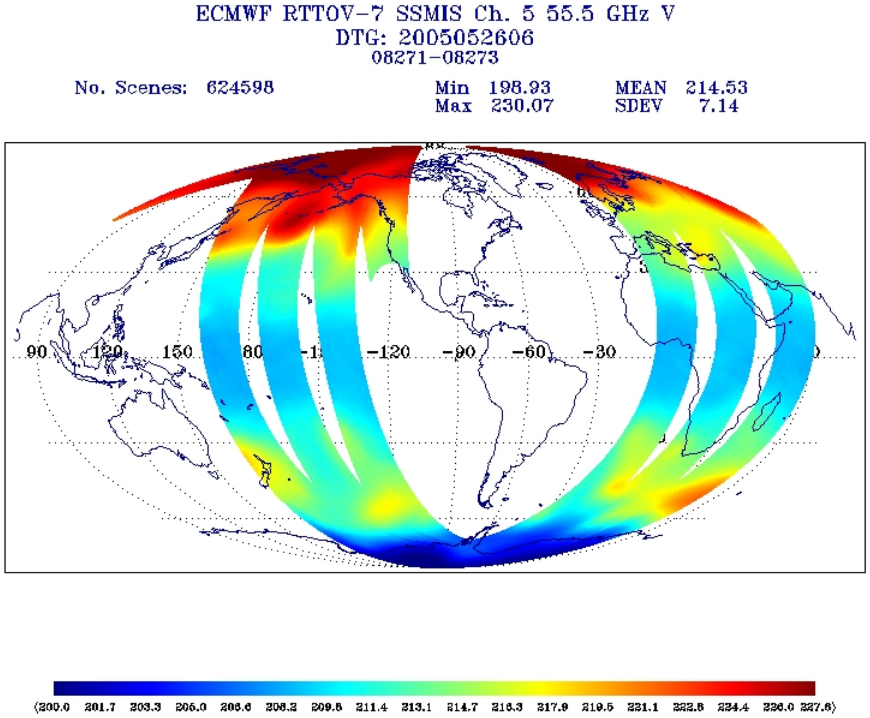

ECMWF RTTOV-7
Ch. 5 Temperature

Radiometric Calibration Anomalies

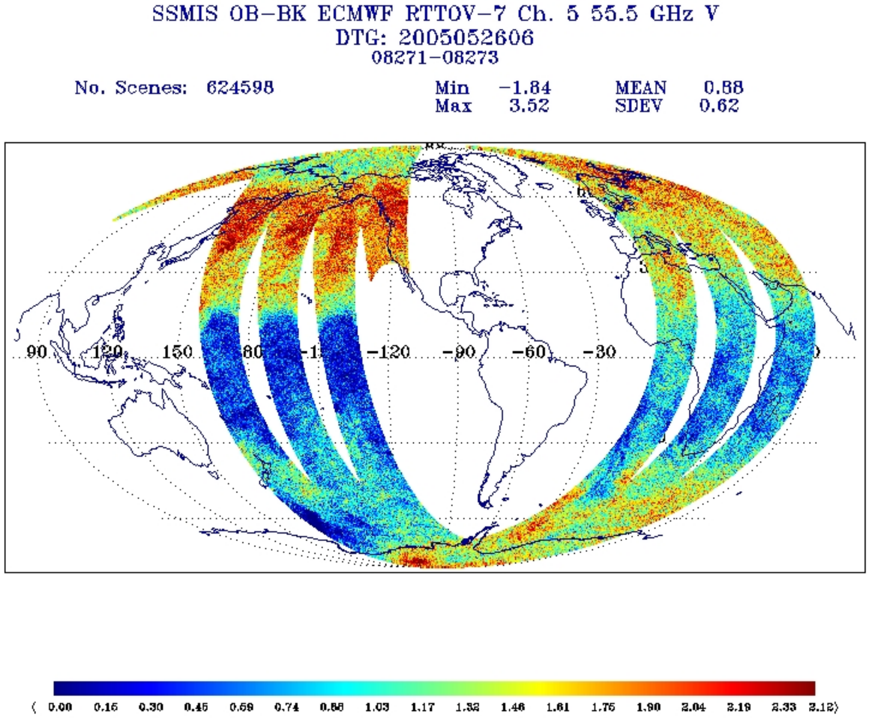

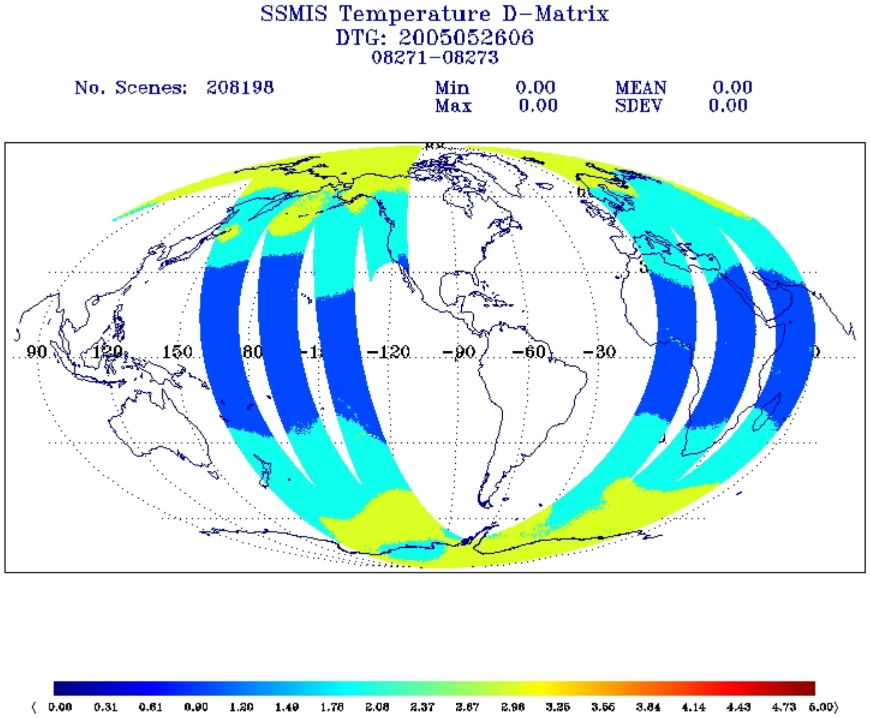

SSMIS – ECMWF RTTOV-7
Ch. 5 Departure

SSMIS Temperature D-Matrix

Radiometric Calibration Anomalies

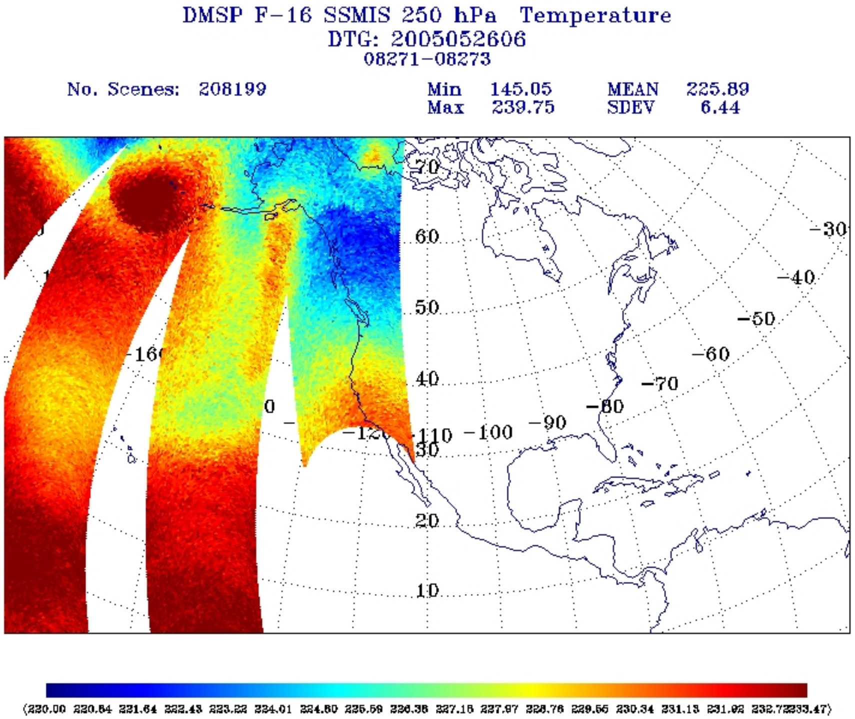

SSMIS 250 hPa T

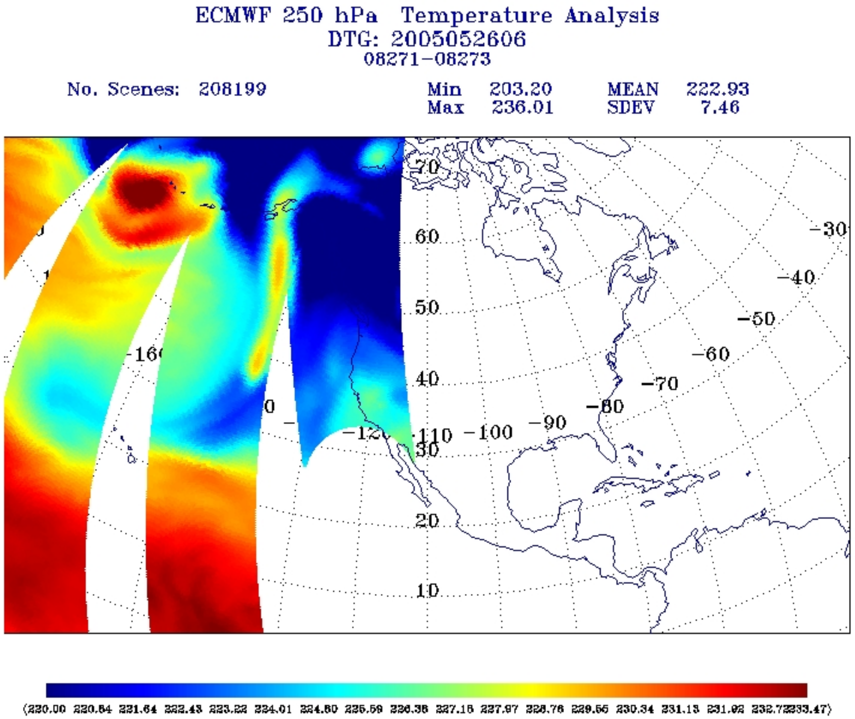

ECMWF 250 hPa T

Radiometric Calibration Anomalies

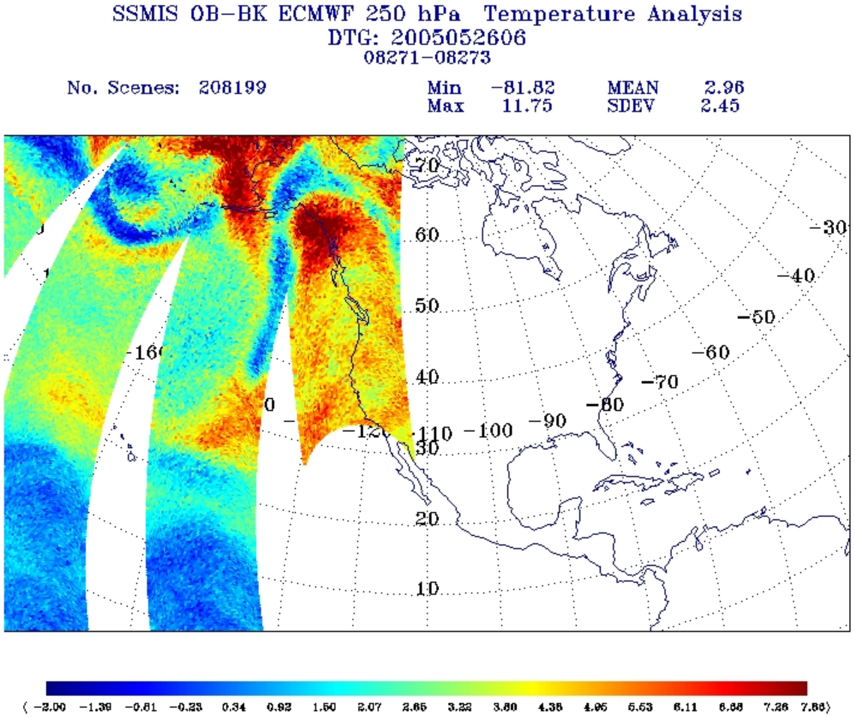

SSMIS – ECMWF 250 hPa Temperature Departure

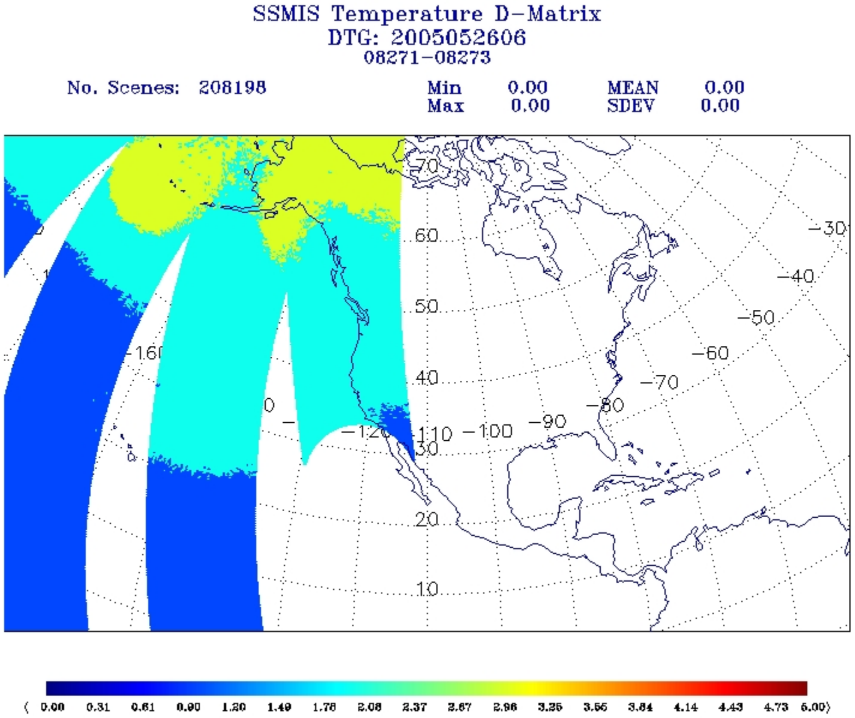

SSMIS Temperature D-Matrix

Radiometric Calibration Anomalies

SSMIS Cal/Val SSMIS LAS T and RH vs. ECMWF Analyses

- **SSMIS Retrieval – ECMWF Analyses (OB-BK)**

- **Both Warm Load and Reflector Anomalies Effect Sounding EDRs**

- **However, the Calibration Anomalies are Not the Dominant Signature in the SSMIS Retrieval – ECMWF Patterns**

- **OB-BK Transition patterns Correlated with D-Matrix**

- **Temperature Retrieval OB-BK Transition Patterns Show Correlation with D-Matrix Transitions**

Radiometric Calibration Anomalies

- **Lunar Intrusions to Cold-Space FOV**
  - **Analysis and Examples of Occurrences**
  - **Development and Identification of Correction Algorithm**

Radiometric Calibration Anomalies

LUNAR ENCROACHMENT DETECTION SCHEME

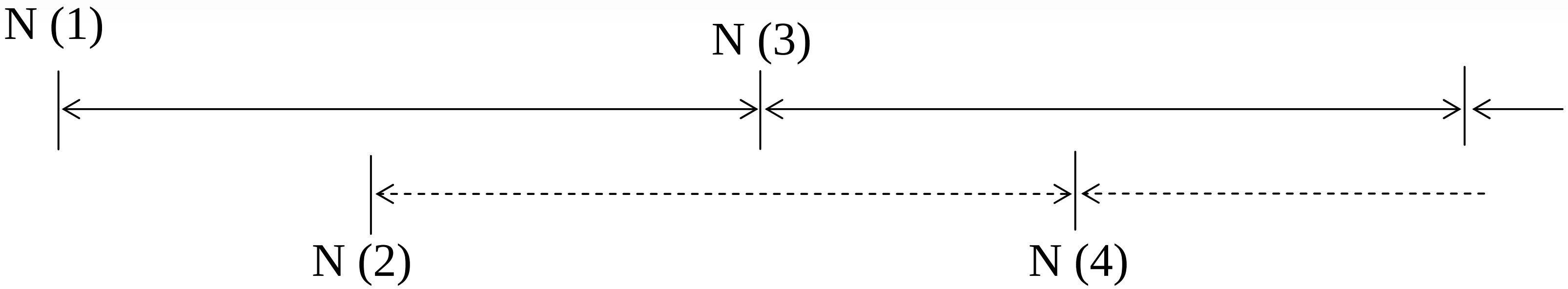

$$BASE = \frac{\underline{COLD\ CAL\ (1) + COLD\ CAL\ (3)}}{2}$$

<u>LUNAR ENCROACHMENT</u>

COLDCAL > BASE + <u>THRESHOLD</u>
NUMBER TO EXCEED <u>8</u>
NO EFFECT ON WARM CAL
ONLY TESTED CHANNEL 4 AND CHANNEL 17

Radiometric Calibration Anomalies

Table showing Lunar Incursions into the SSMIS Cold Sky FOV SSMIS Launch to 10/2004

Date	Seconds of Day	First Rev.	Last Rev.
11/5/2003	31486	249	255
11/17/2003	49626	422	427
12/5/2003	14696	671	676
12/17/2003	8307	839	845
1/3/2004	78121	1091	1096
1/15/2004	53485	1256	1260
2/2/2004	42852	1509	1514
2/13/2004	61920	1667	1671
3/3/2004	87687	1926	1931
3/13/2004	57962	2076	2082
4/1/2004	58216	2345	2350
4/11/2004	60021	2486	2492
5/1/2004	53193	2767	2773
5/11/2004	12328	2902	2908
5/31/2004	48021	3190	3198
6/10/2004	7155	3325	3331
6/30/2004	18580	3610	3615
7/10/2004	20332	3751	3758
7/30/2004	38952	4022	4027
8/9/2004	9222	4173	4179
8/27/2004	47149	4433	4438
9/8/2004	60101	4591	4598
9/25/2004	55557	4844	4850

Radiometric Calibration Anomalies

Example of Lunar incursion on Sept 8, 2004

Channels 4, 10, 16, 17, and 23 shown

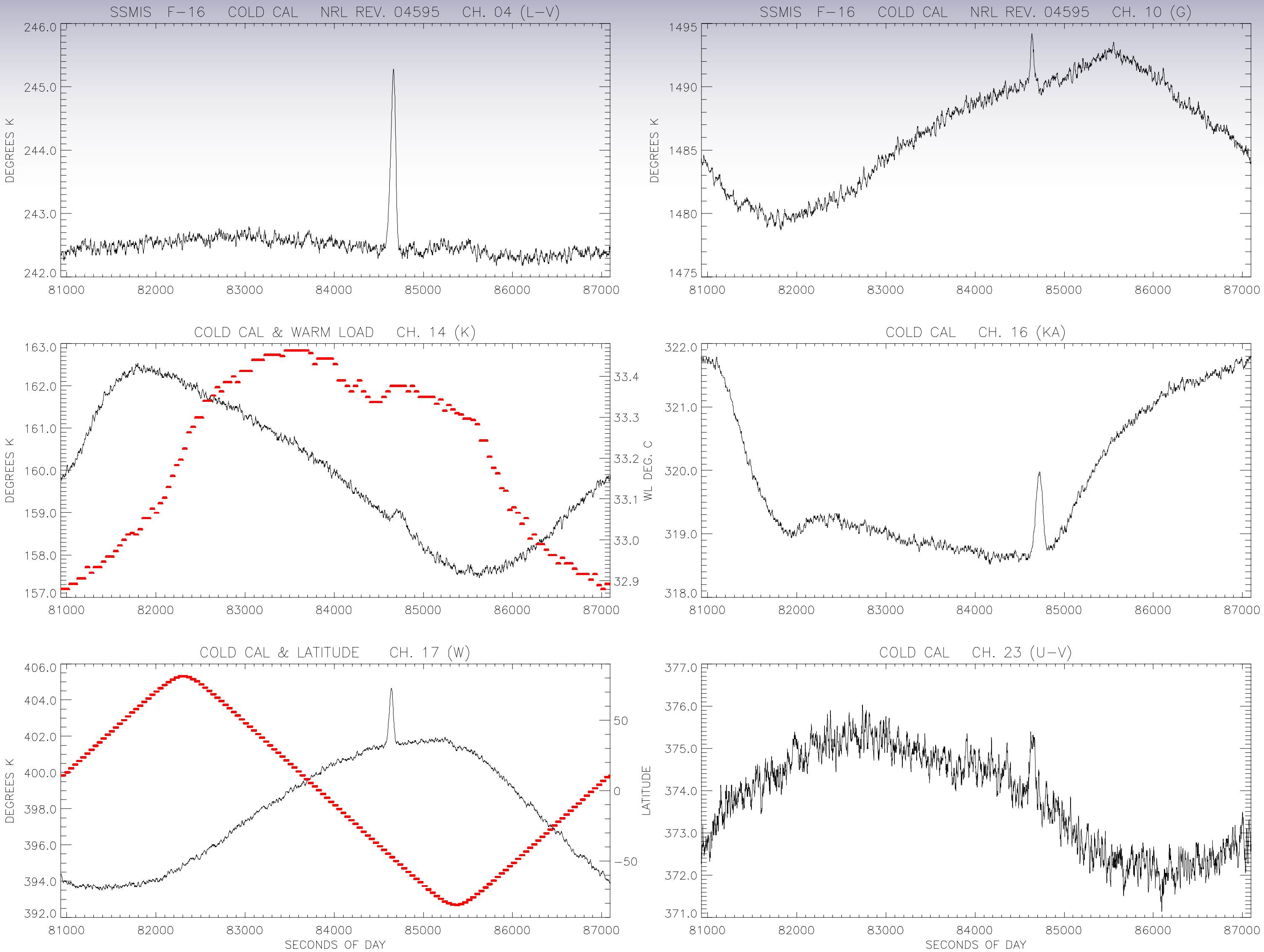

Radiometric Calibration Anomalies

- **Spurious Spikes and Non-Gaussian Noise**

  - **Description of Problem**
  - **Example and Hypothesis of Noise: S/C Charging**

Radiometric Calibration Anomalies

Example of calibration noise anomalies that are found to occur simultaneously in all channels

Currently this phenomenon has been detected 100s of times in SSMIS normal mode operation

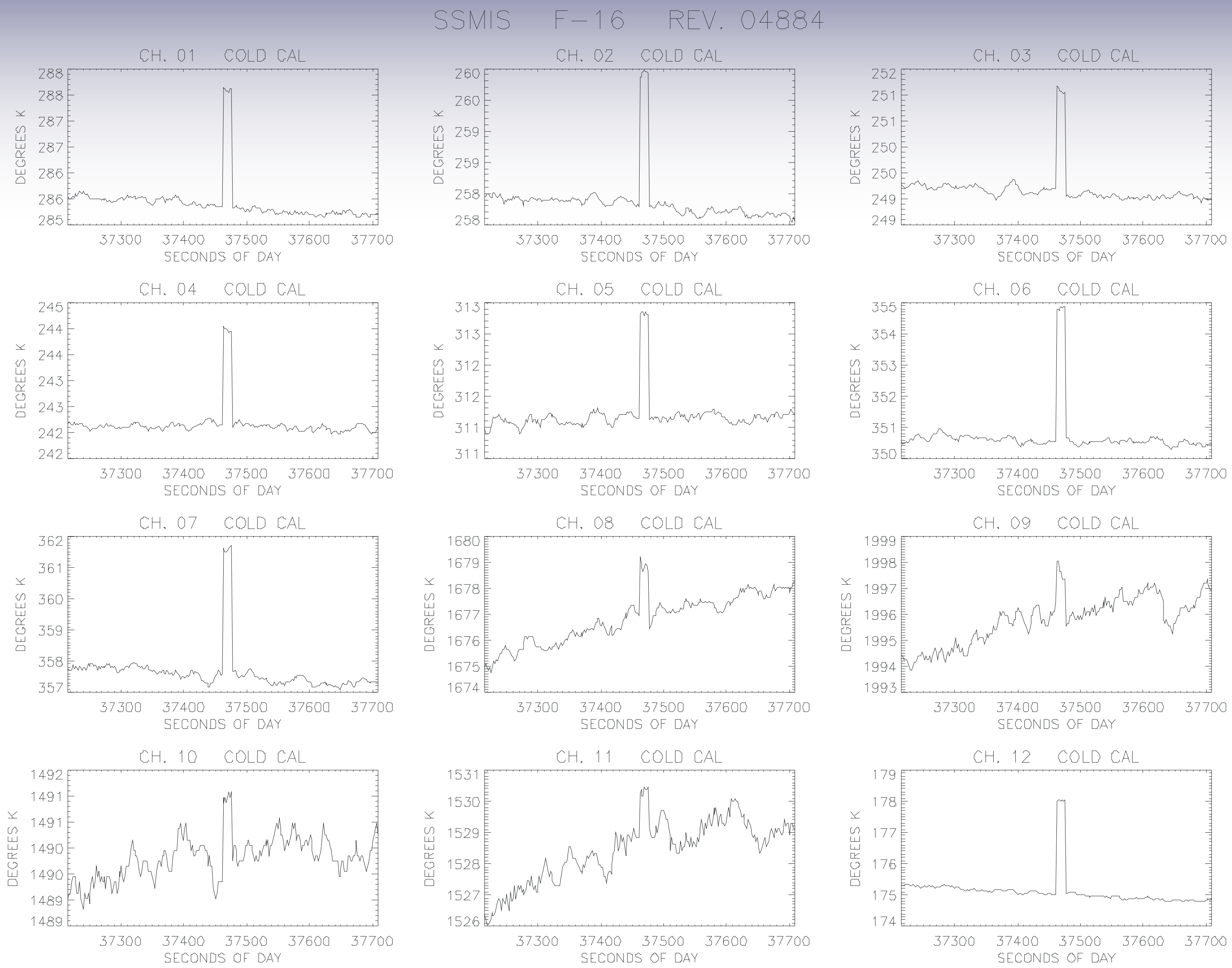

Radiometric Calibration Anomalies

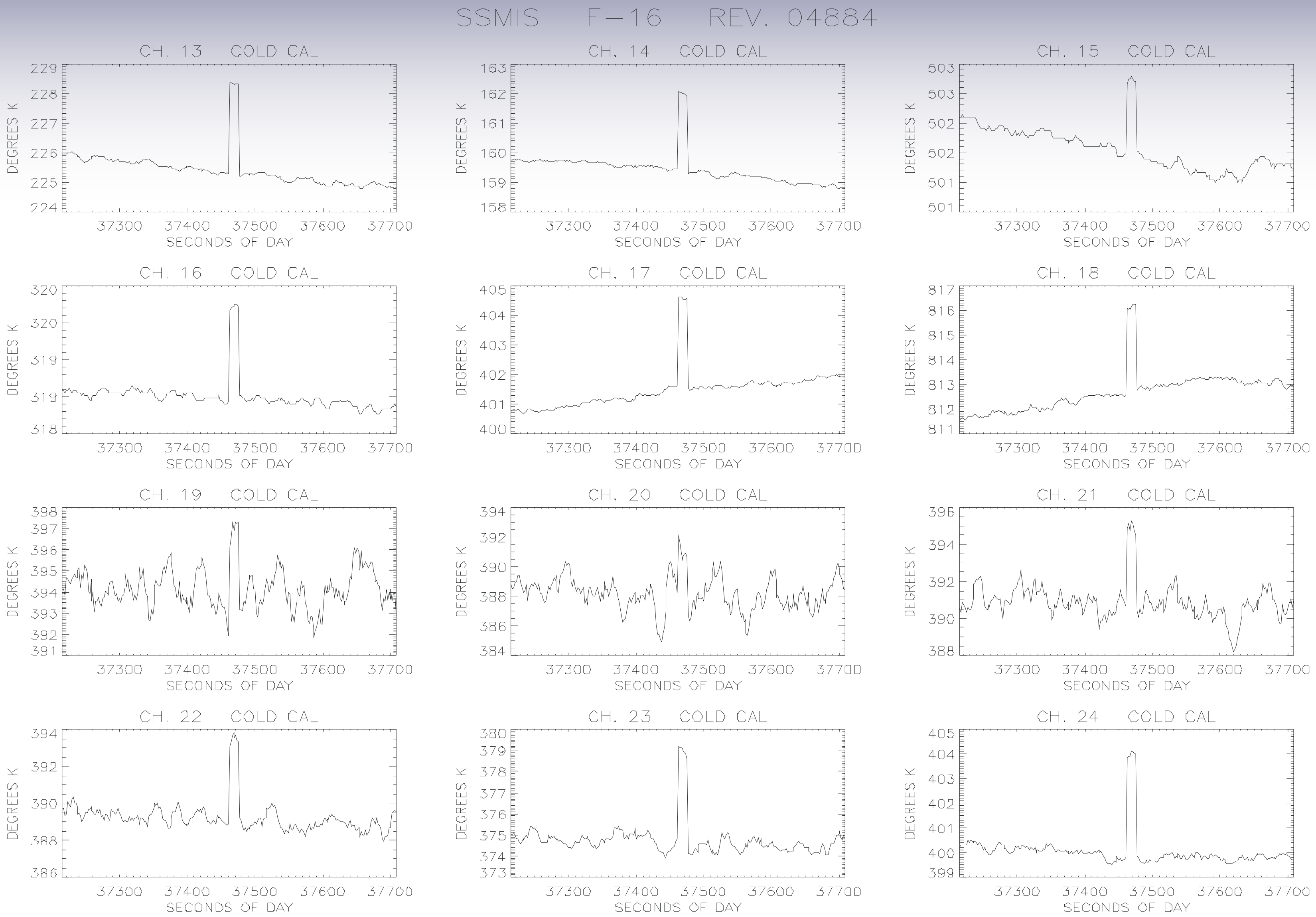

Radiometric Calibration Anomalies

Plans to Address Anomaly

- Gain Filtering
- Thermal Modeling of Reflector Temperature
- Regression Based Bias Corrections

Radiometric Calibration Anomalies

Sources of Bias in Scan Averaged OB-BK

- Errors and Biases in the NWP background fields
- Errors in Forward Model
  - Surface Emissivity Errors
  - Low Water Vapor Continuum Uncertainty
  - O_2 Absorption at Low Pressures and Temperatures
- Residual contamination of the observations from clouds or precipitation
- Within Scan Variations
- SSMIS Calibration Anomalies
- Inaccurate specification of SSMIS spectral response filters

Radiometric Calibration Anomalies

Regression Based Bias Corrections

Can the Scan Averaged OB-BK Bias be Modeled based upon Physical Mechanisms Identified as Sources of the OB-BK Anomalies ?

- Physically Mechanism Terms (Predictors) Include:
  - Reflector Arm Temperature
  - Time Derivative of the Reflector Arm Temperature
  - Direct Solar Intrusion Location Functions
  - Reflected Solar Intrusion Location Functions
  - Reflector Temperature Model Including Mean OLR Effects

So that, Predicted Bias for Channel, k

$$\delta_k = \left(\sum_{i=0}^{N} a_i P_i \right)_k \quad \text{, where } P_i \text{ are the predictors}$$

Radiometric Calibration Anomalies

Regression Based Bias Correction Predictors

Reflection 1 Warm Load Intrusion Location:	R_1
Reflection 2 Warm Load Intrusion Location:	R_2
Direct Warm Load Intrusion Locations:	D
Observed Reflector Arm Temperature:	T_{Arm}
Modeled Reflector Temperature:	T_{Rflct}
Time Derivative of Reflector Arm Temperature:	dT_{Arm} /dt

Radiometric Calibration Anomalies

Uncorrected OB-BK ____ Bias Corrected OB-BK ____ Bias Correction ____

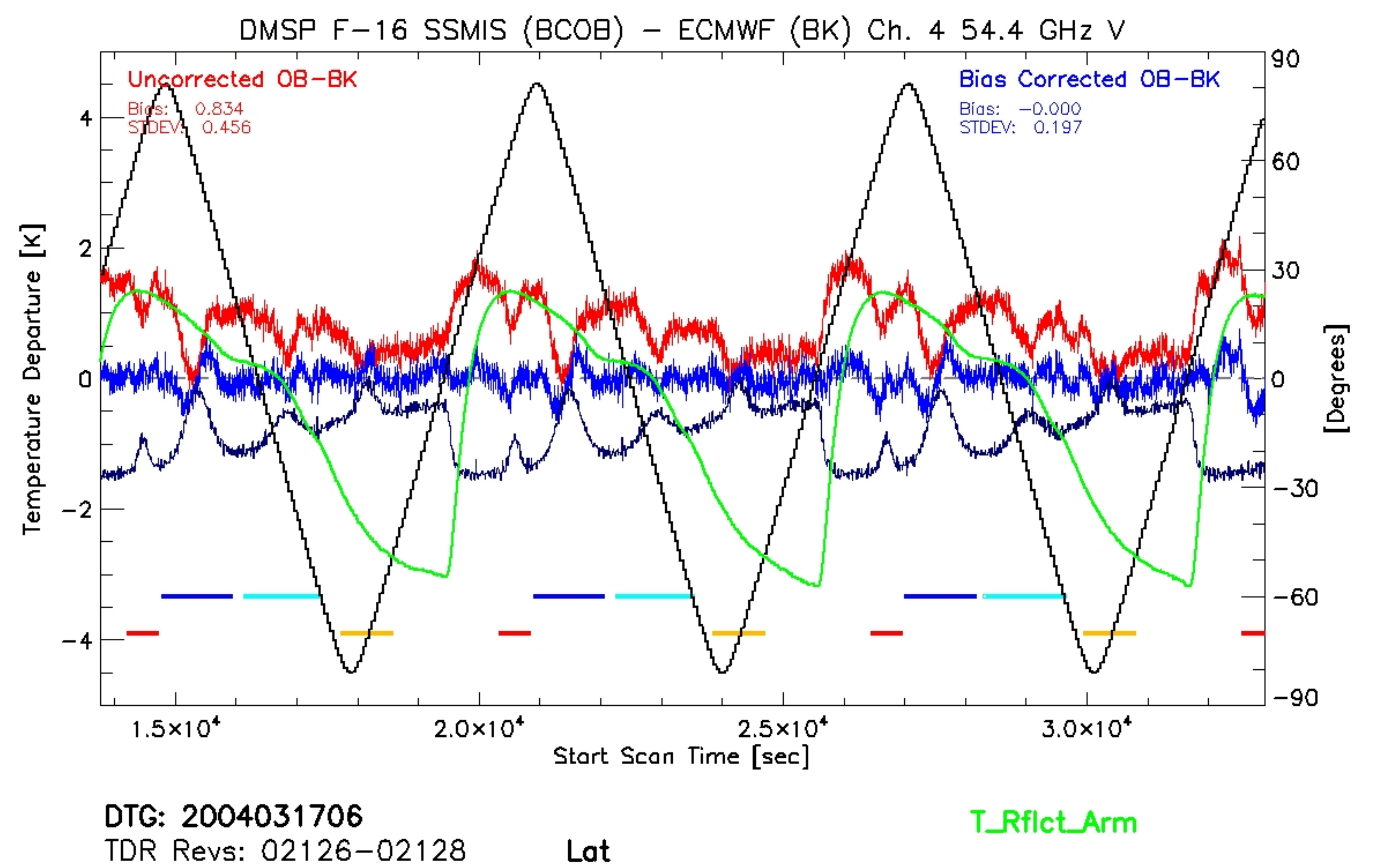

Radiometric Calibration Anomalies

Term by Term Bias Contributions

R_1

R_2

D

T_{Arm}

T_{Rflct}

dT_{Arm} /dt

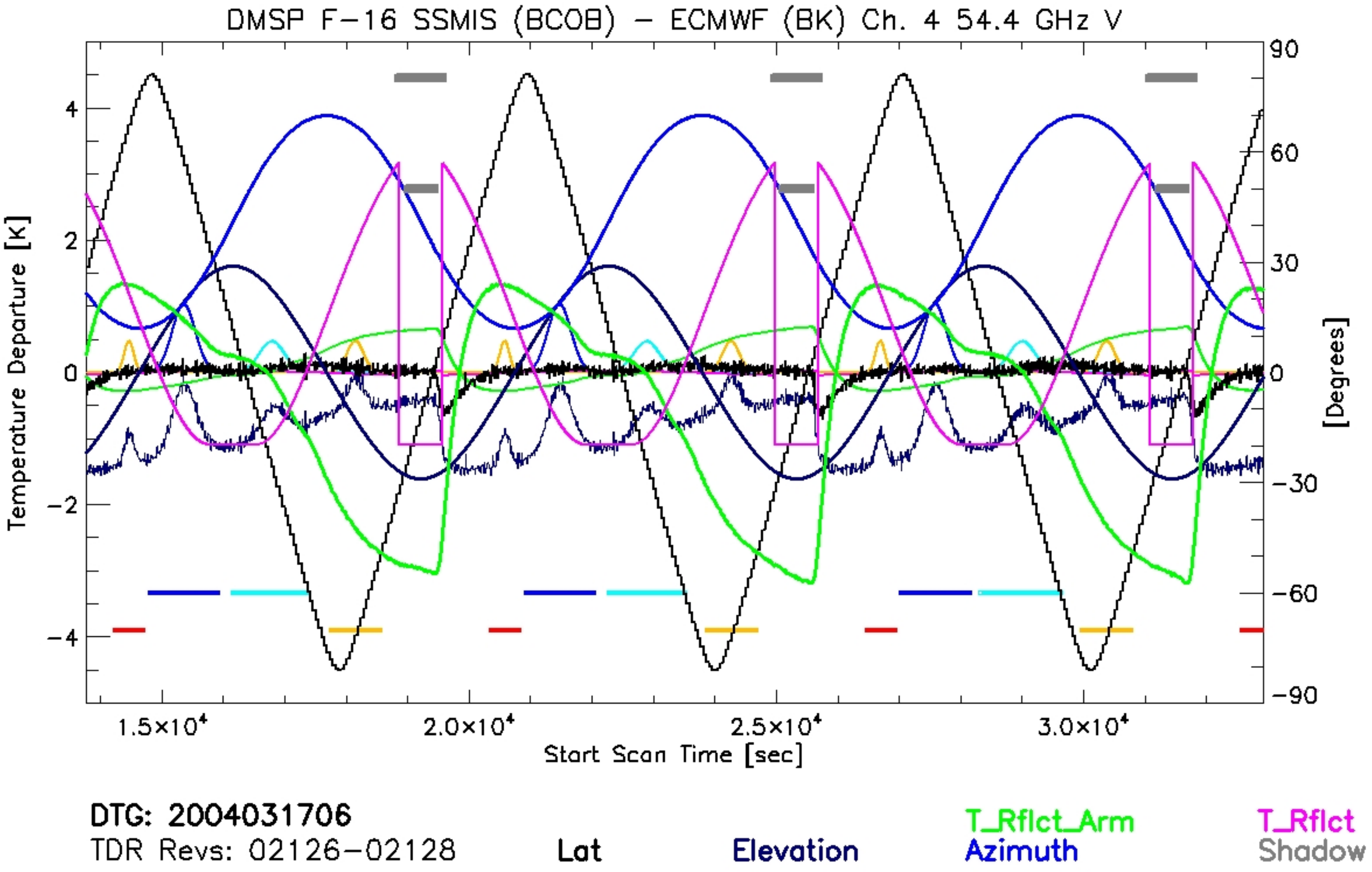

Radiometric Calibration Anomalies

Uncorrected OB-BK ____ Bias Corrected OB-BK ____ Bias Correction ____

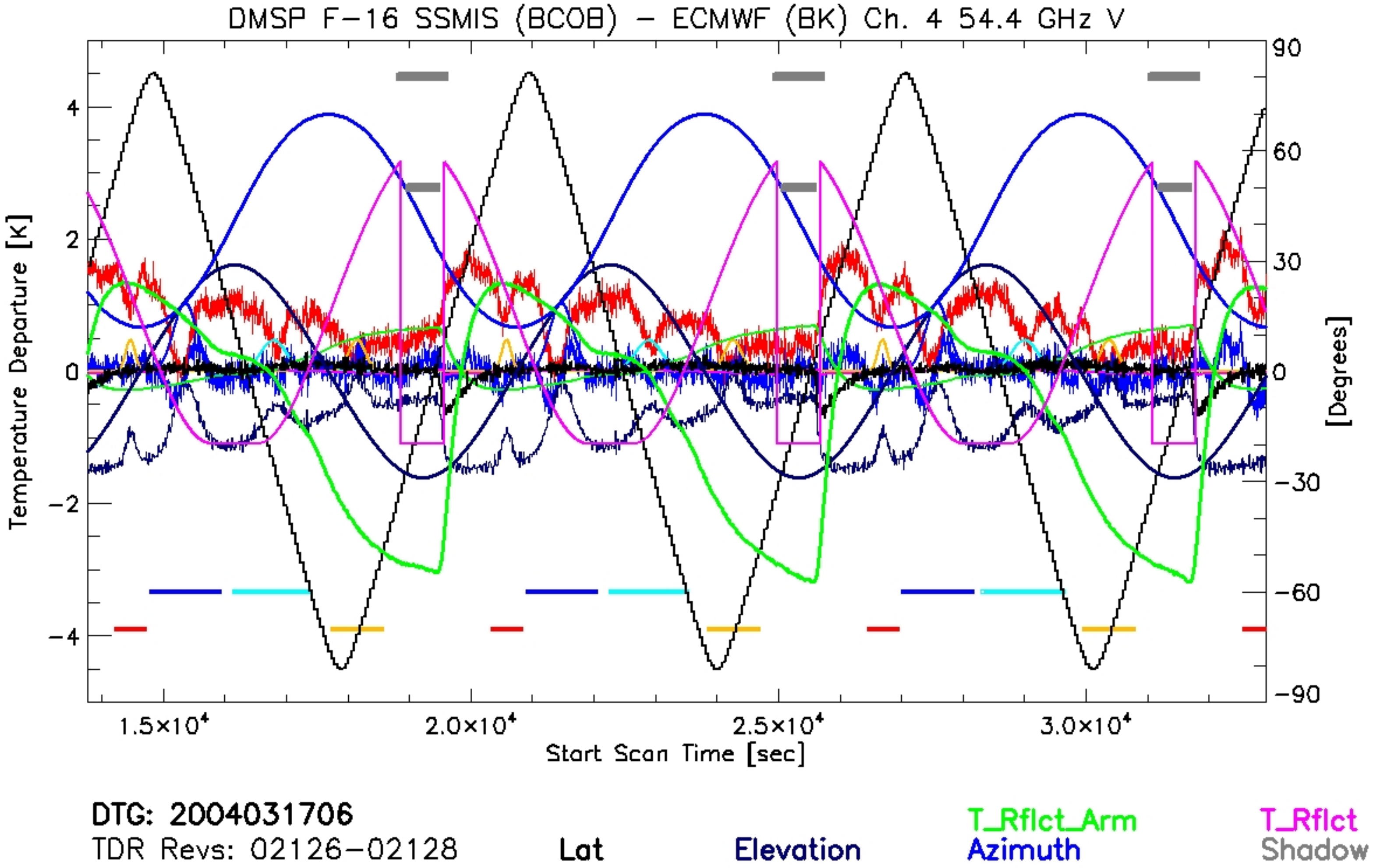

Radiometric Calibration Anomalies

Uncorrected OB-BK ____ Bias Corrected OB-BK ____ Bias Correction ____

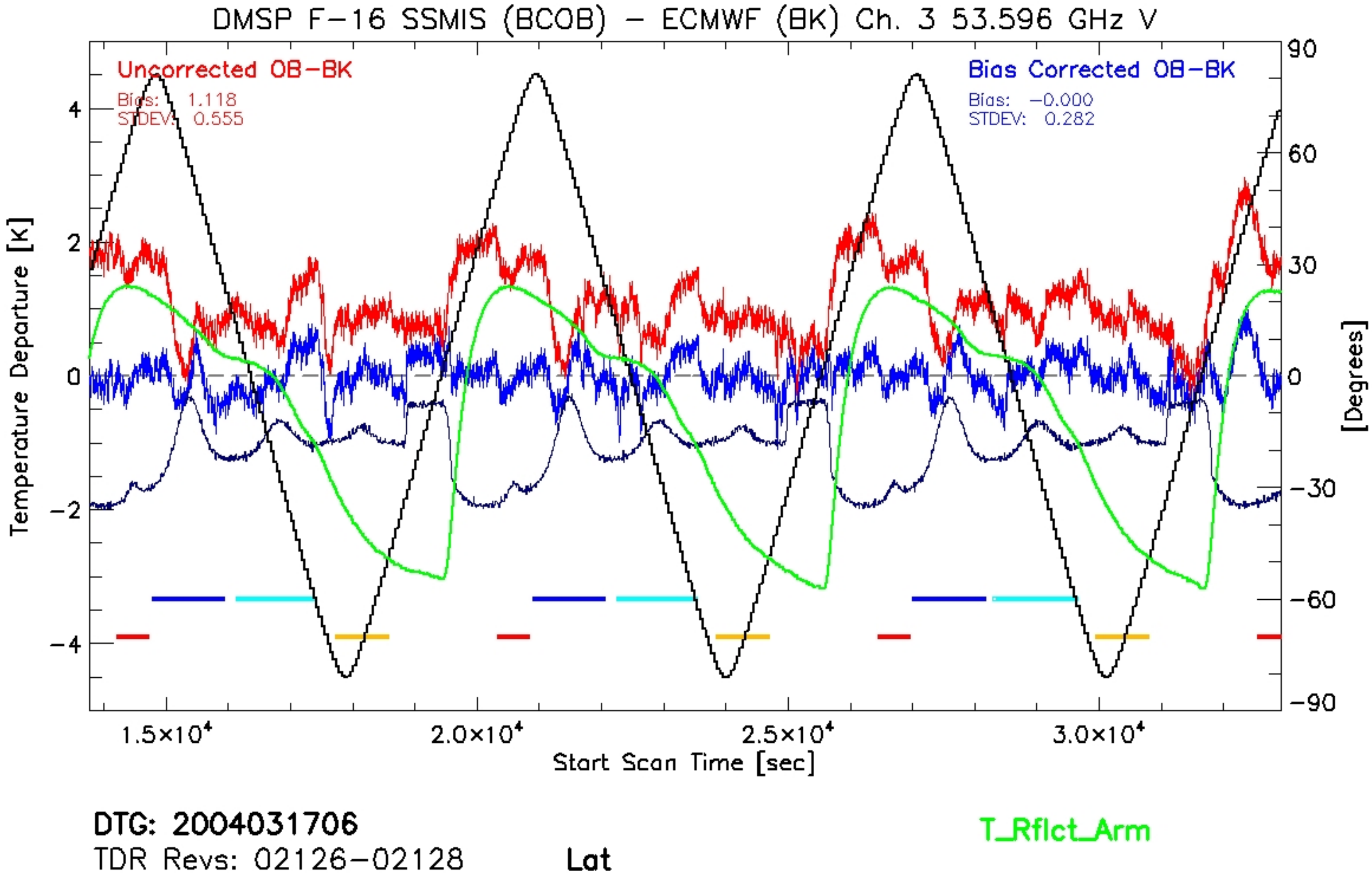

Radiometric Calibration Anomalies

Uncorrected OB-BK ____ Bias Corrected OB-BK ____ Bias Correction ____

R_1

R_2

D

T_{Arm}

T_{Rflct}

dT_{Arm} /dt

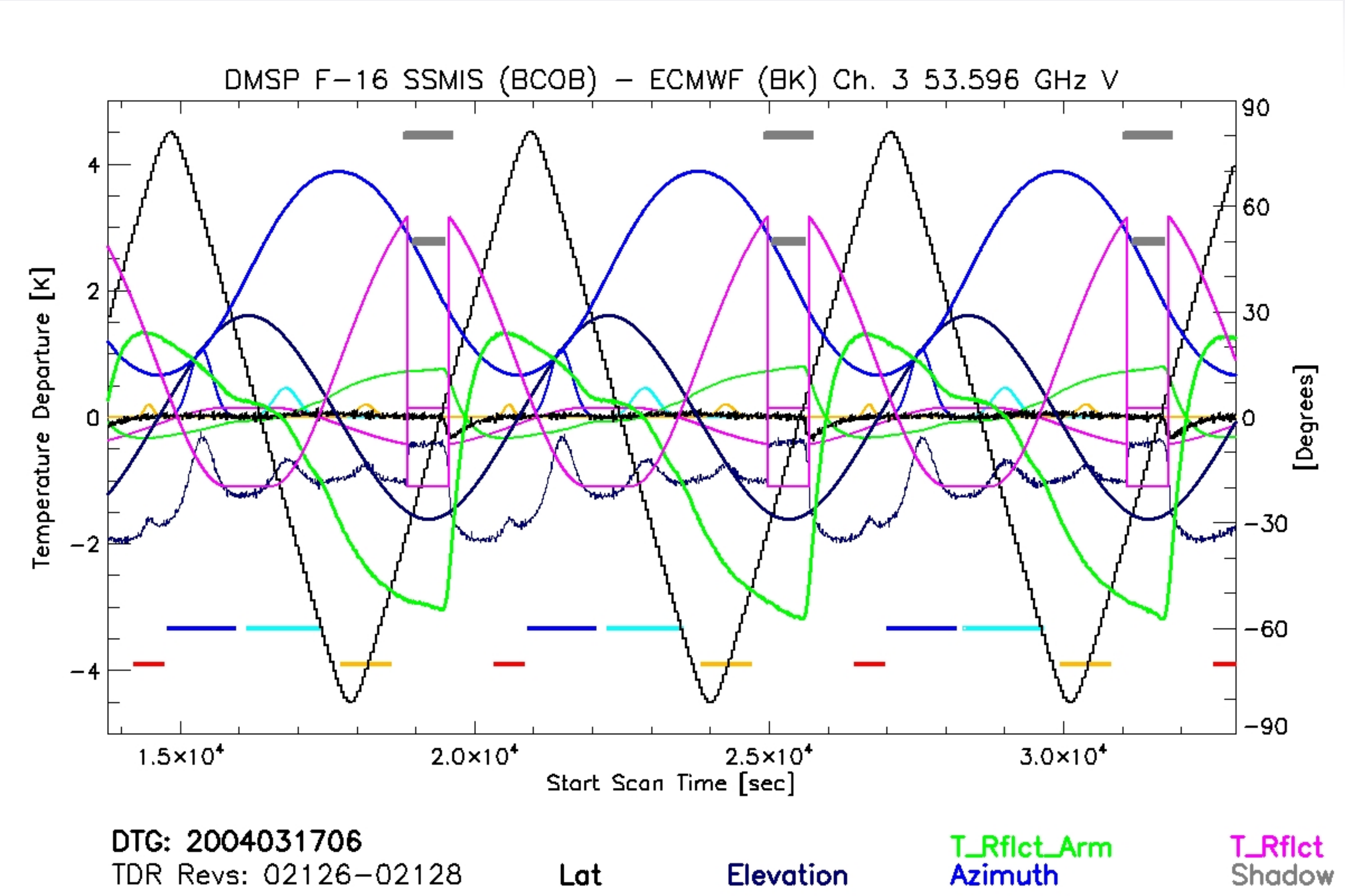

Radiometric Calibration Anomalies

Uncorrected OB-BK ____ Bias Corrected OB-BK ____ Bias Correction ____

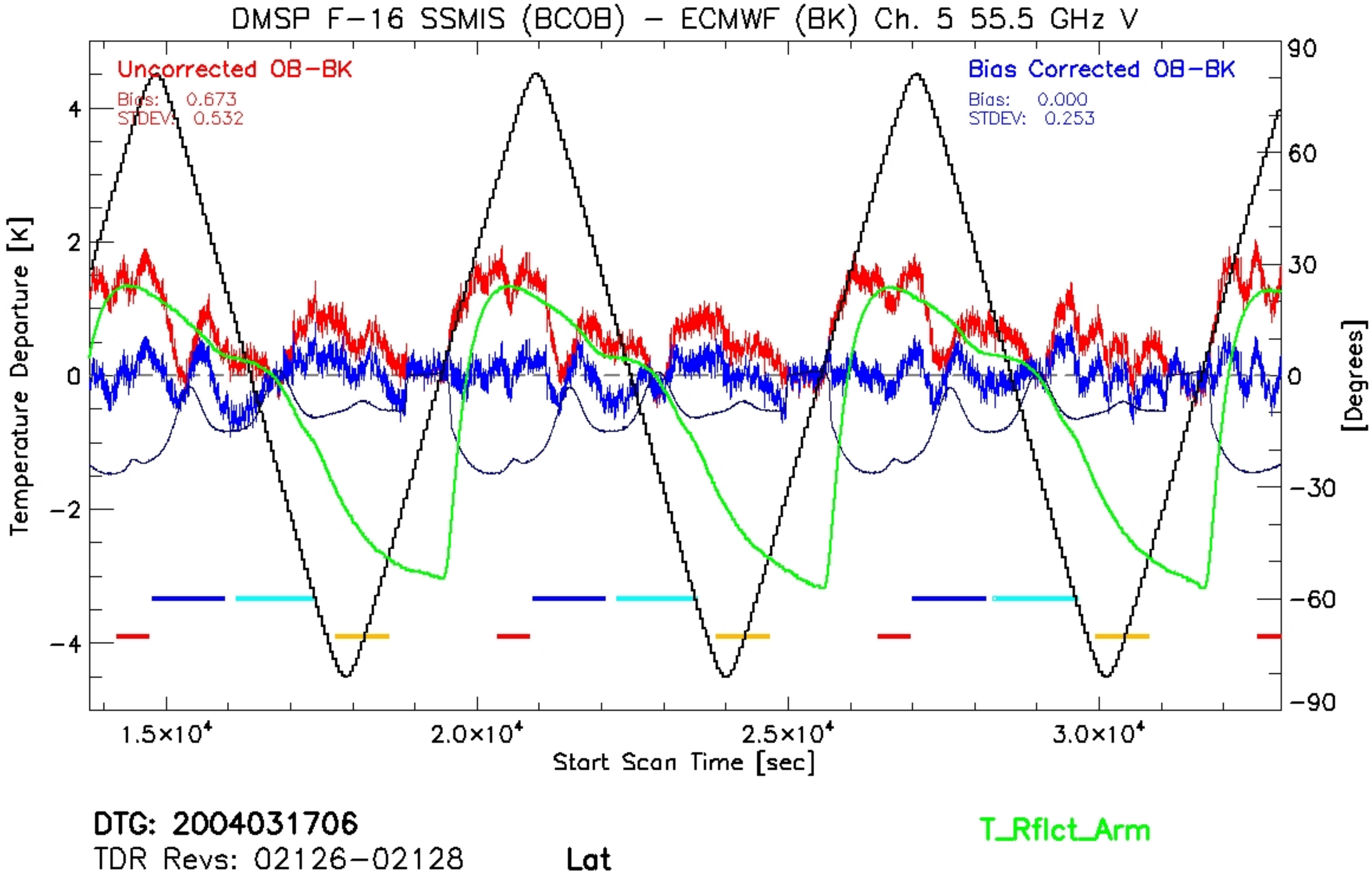

Radiometric Calibration Anomalies

Uncorrected OB-BK ____ Bias Corrected OB-BK ____ Bias Correction ____

R_1

R_2

D

T_{Arm}

T_{Rflct}

dT_{Arm} /dt

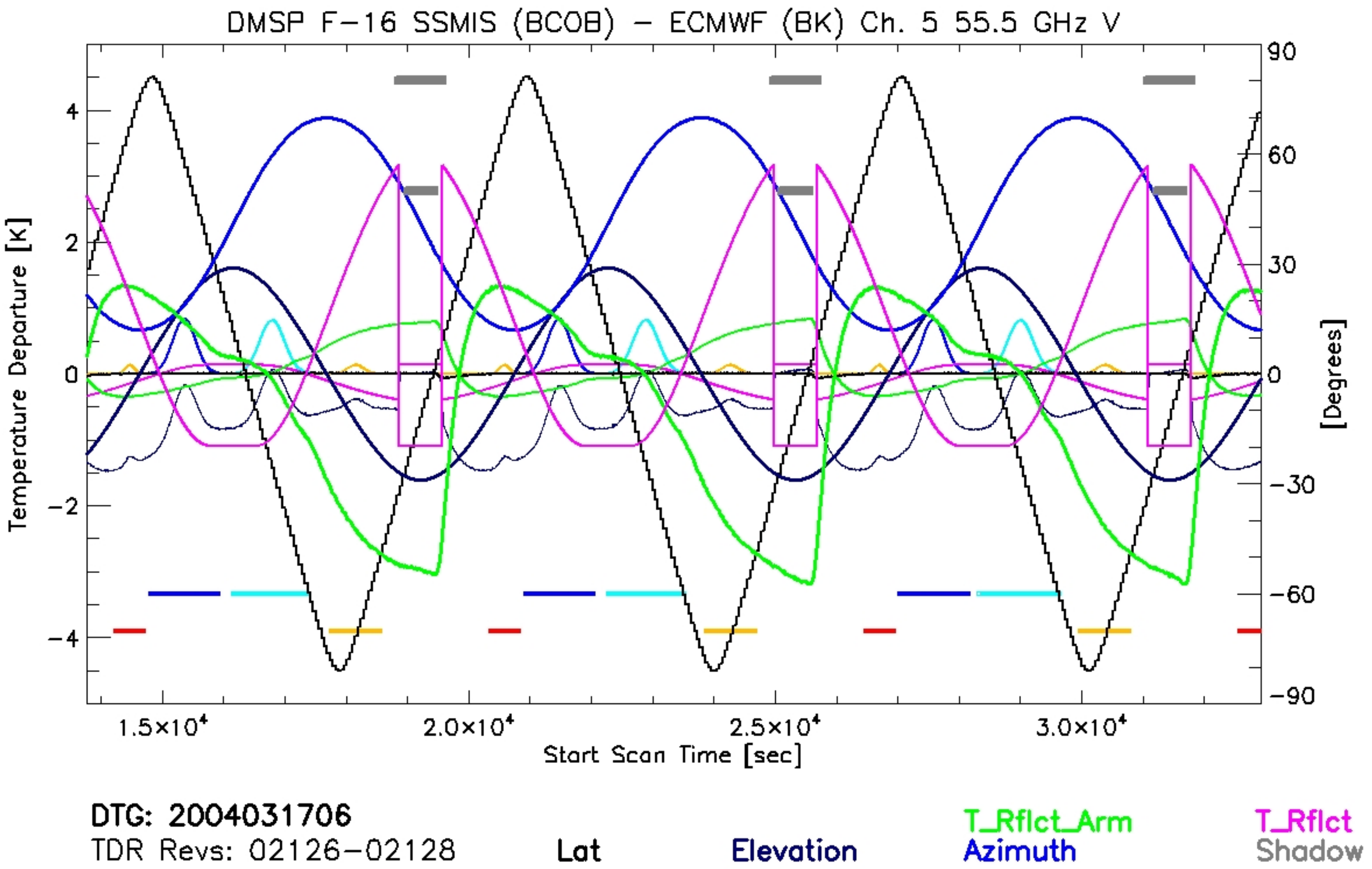

Radiometric Calibration Anomalies

Uncorrected OB-BK ____ Bias Corrected OB-BK ____ Bias Correction ____

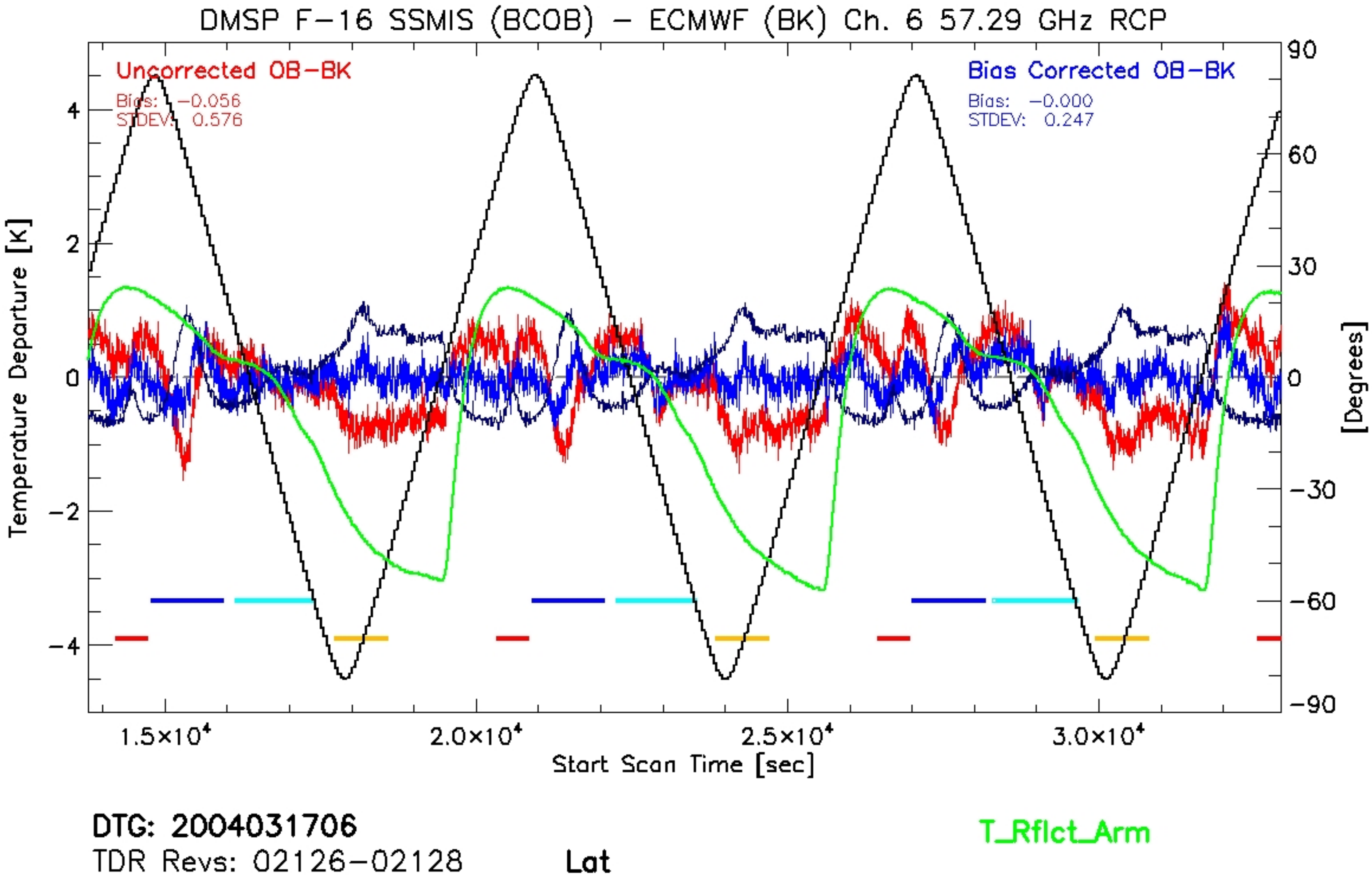

Radiometric Calibration Anomalies

Uncorrected OB-BK ____ Bias Corrected OB-BK ____ Bias Correction ____

R_1

R_2

D

T_{Arm}

T_{Rflct}

dT_{Arm}/dt

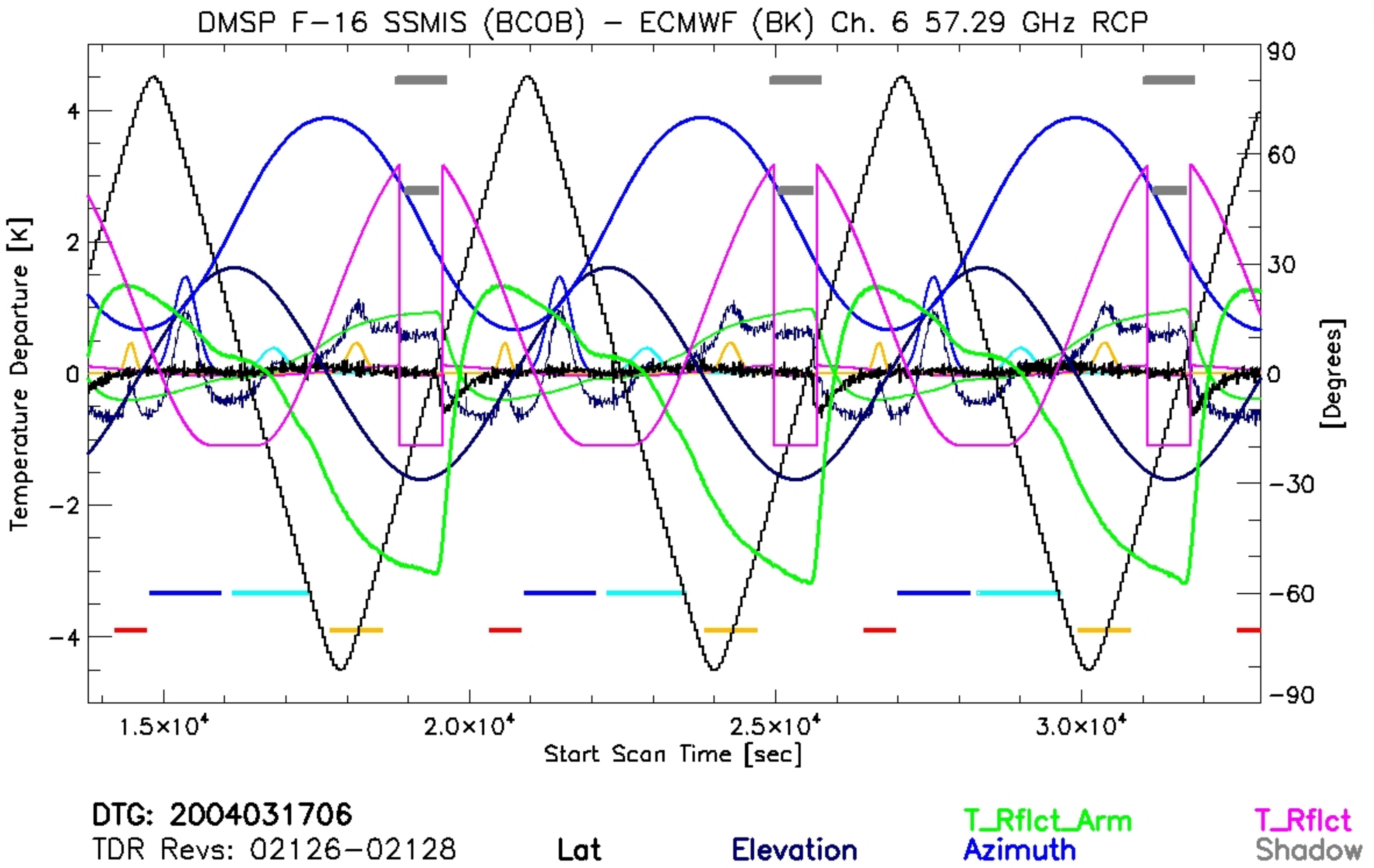

Radiometric Calibration Anomalies

Uncorrected OB-BK ____ Bias Corrected OB-BK ____ Bias Correction ____

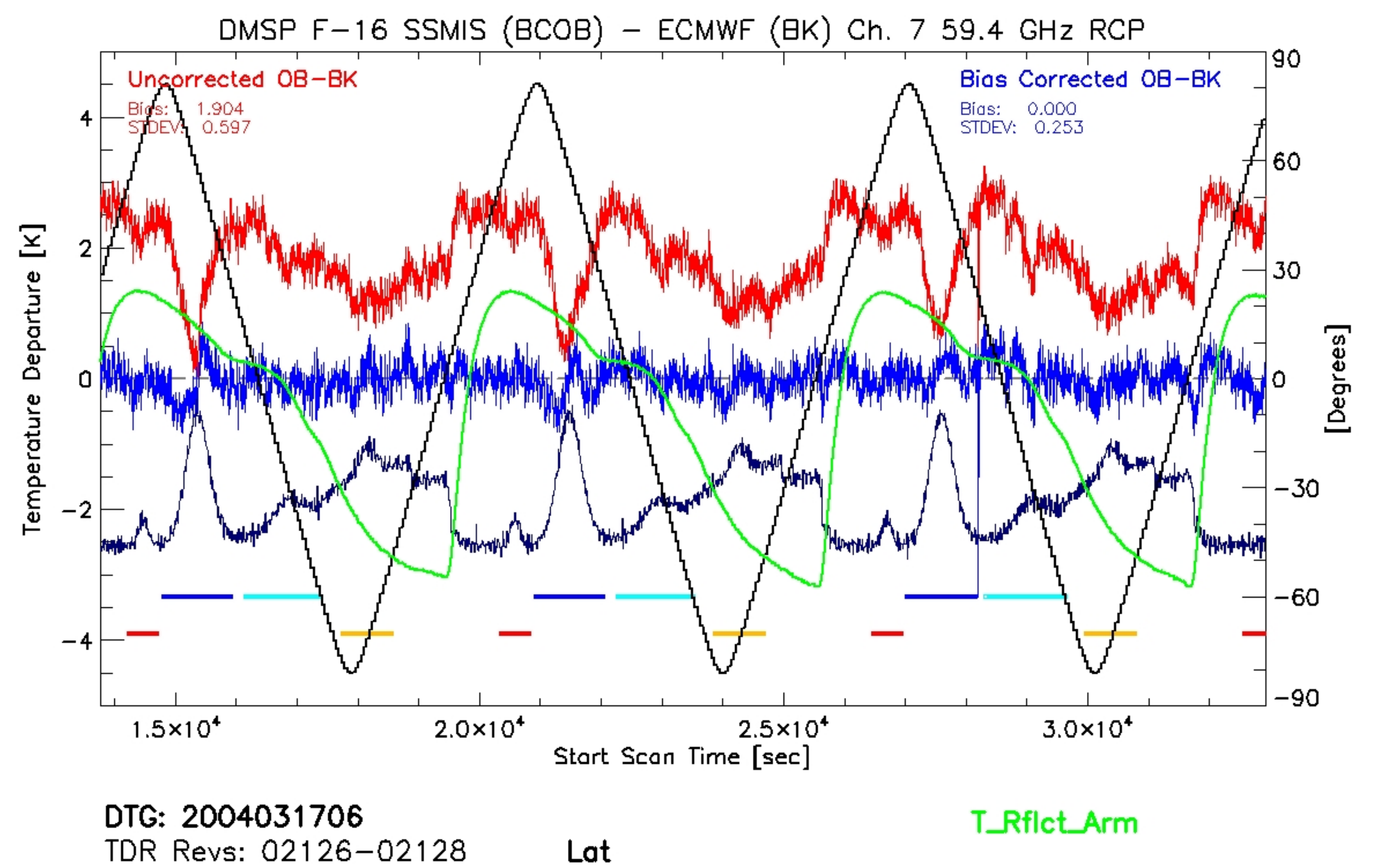

Radiometric Calibration Anomalies

Uncorrected OB-BK ____ Bias Corrected OB-BK ____ Bias Correction ____

R_1

R_2

D

T_{Arm}

T_{Rflct}

dT_{Arm}
/dt

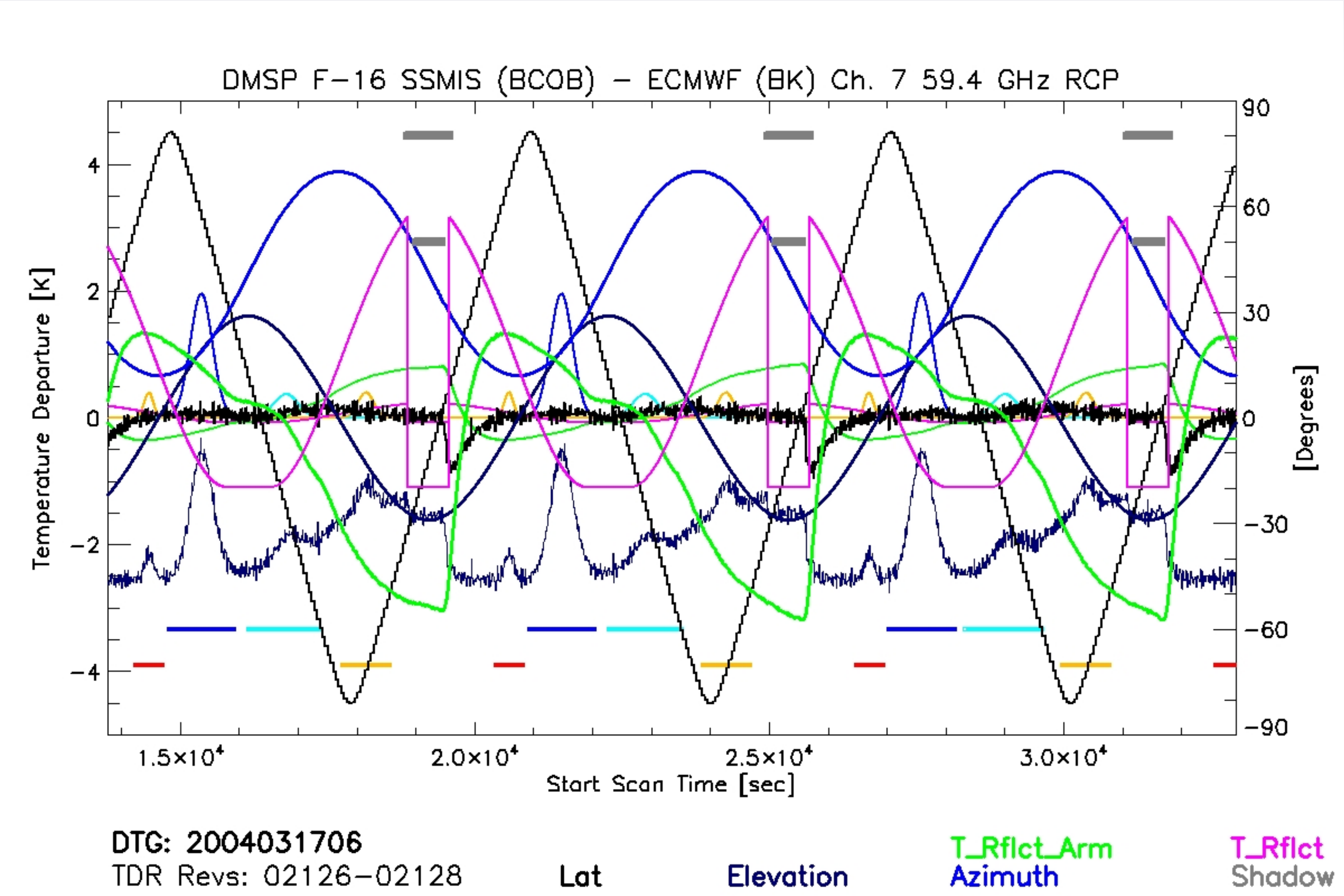

Radiometric Calibration Anomalies

Uncorrected OB-BK ____ Bias Corrected OB-BK ____ Bias Correction ____

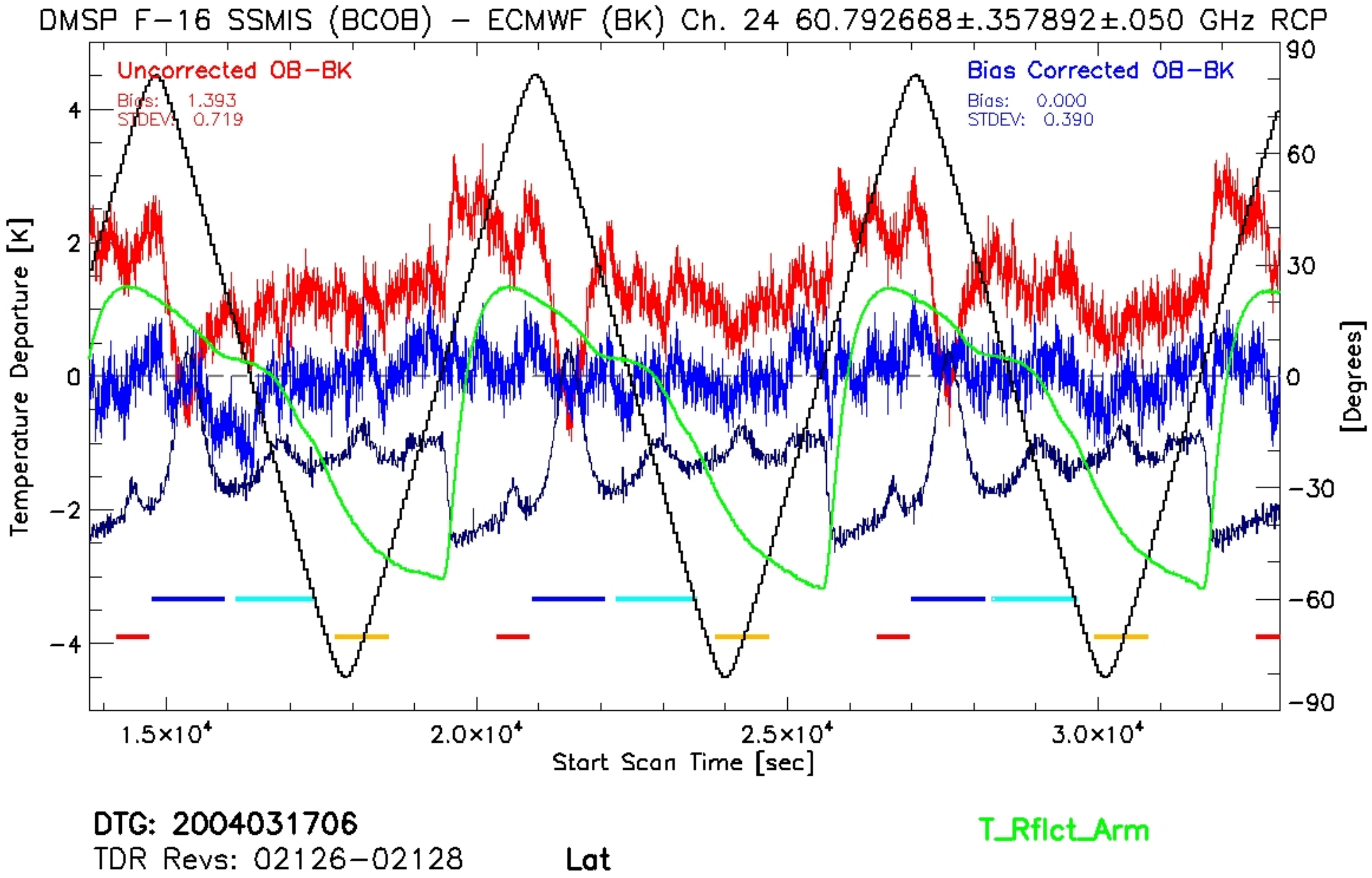

Radiometric Calibration Anomalies

Uncorrected OB-BK ____ Bias Corrected OB-BK ____ Bias Correction ____

R_1

R_2

D

T_{Arm}

T_{Rflct}

dT_{Arm}/dt

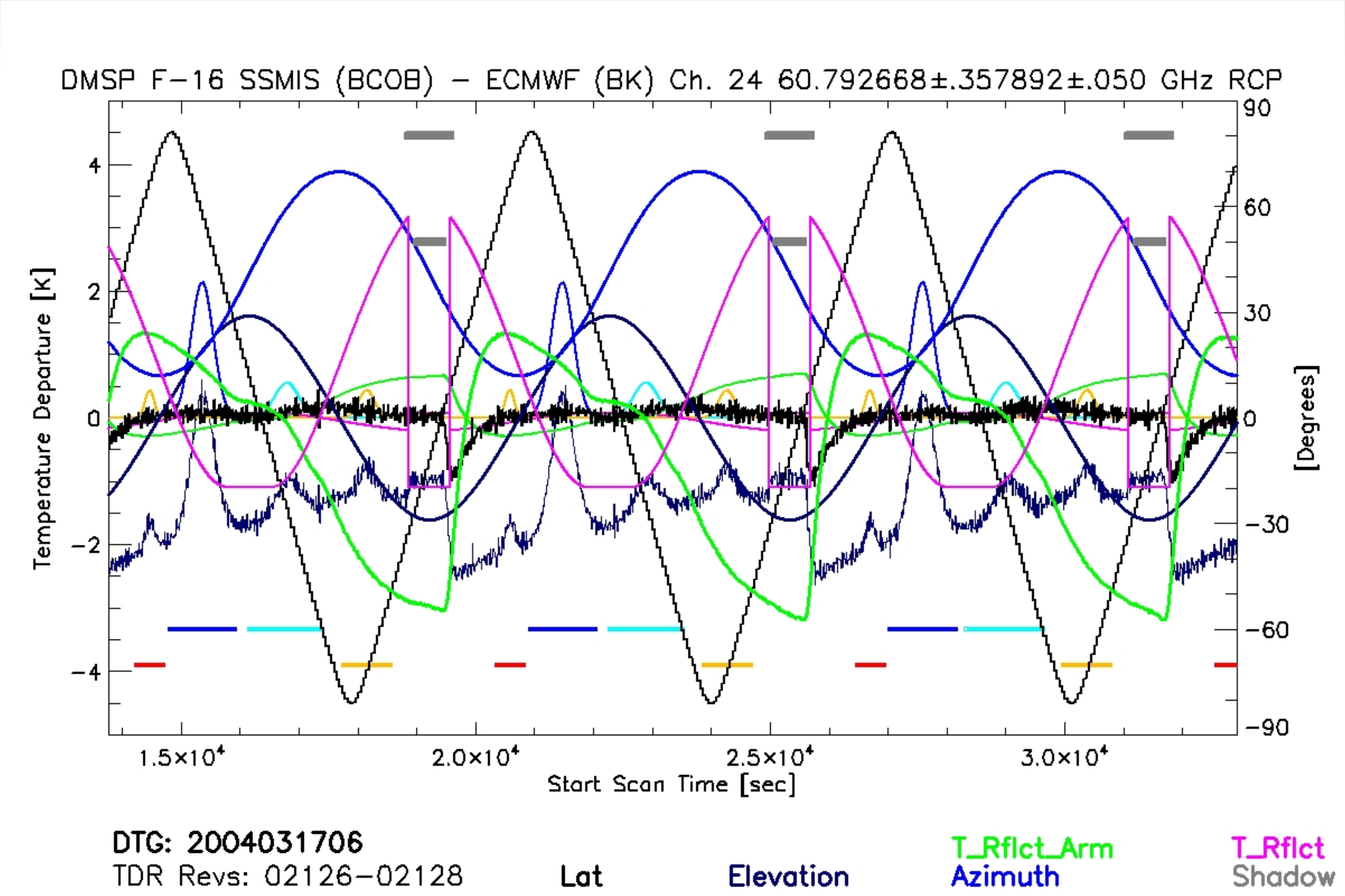

Radiometric Calibration Anomalies

Uncorrected OB-BK ____ Bias Corrected OB-BK ____ Bias Correction ____

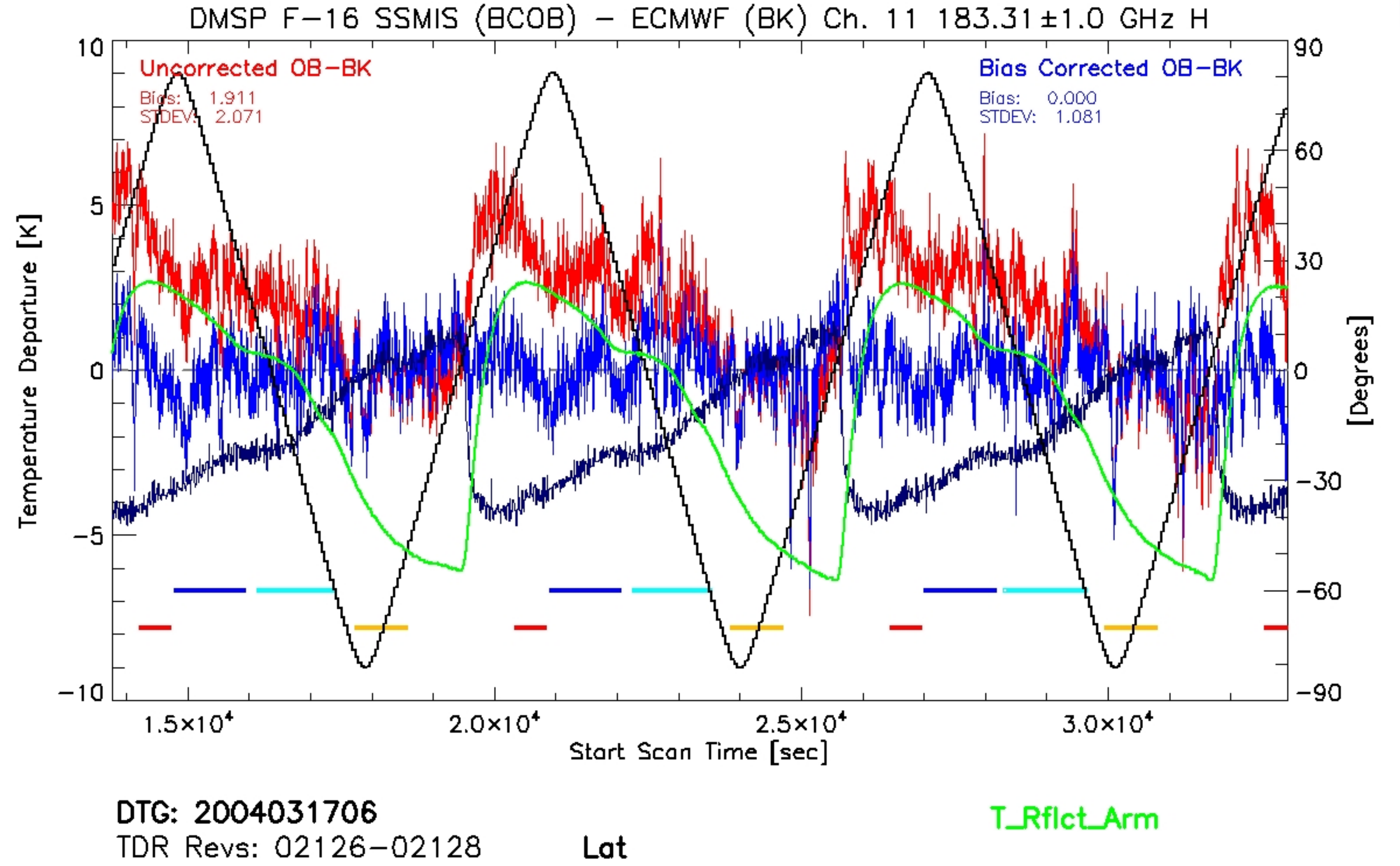

Radiometric Calibration Anomalies

Uncorrected OB-BK ____ Bias Corrected OB-BK ____ Bias Correction ____

R_1

R_2

D

T_{Arm}

T_{Rflct}

dT_{Arm}/dt

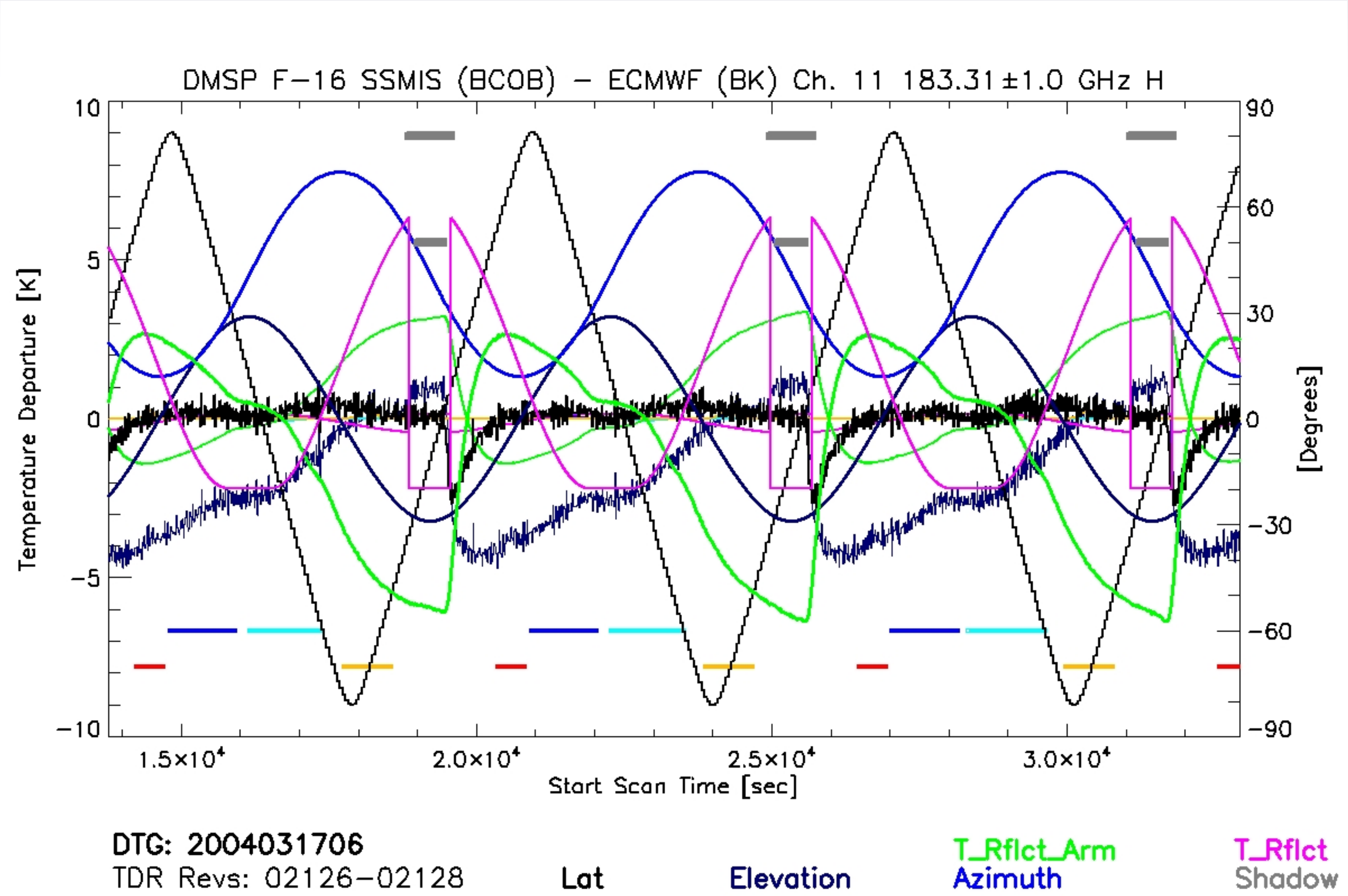

Radiometric Calibration Anomalies

Scan Averaged Regression Based Bias Corrections

- Apply Scan Averaged Bias Corrections to each Scan of the TDR Data
- Sample Before and After Geographic Patterns
- OB-BK versus BCOB-BK Histograms

Radiometric Calibration Anomalies

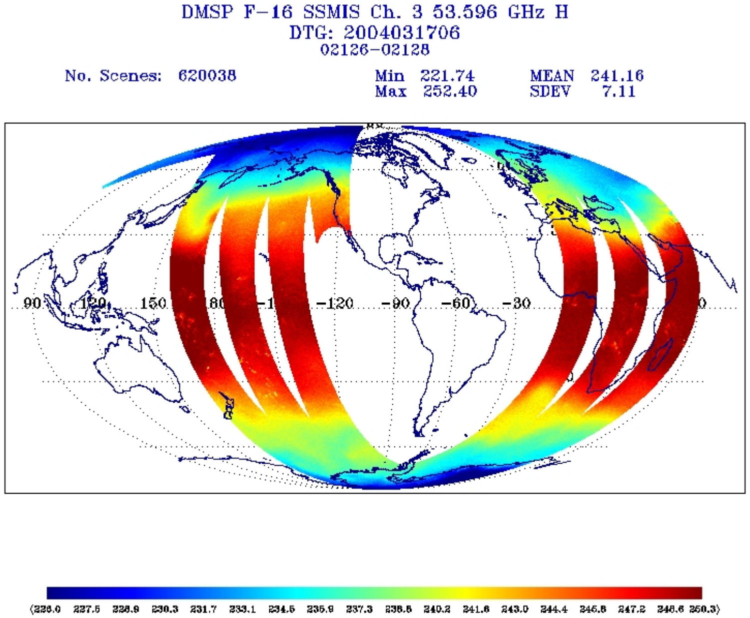

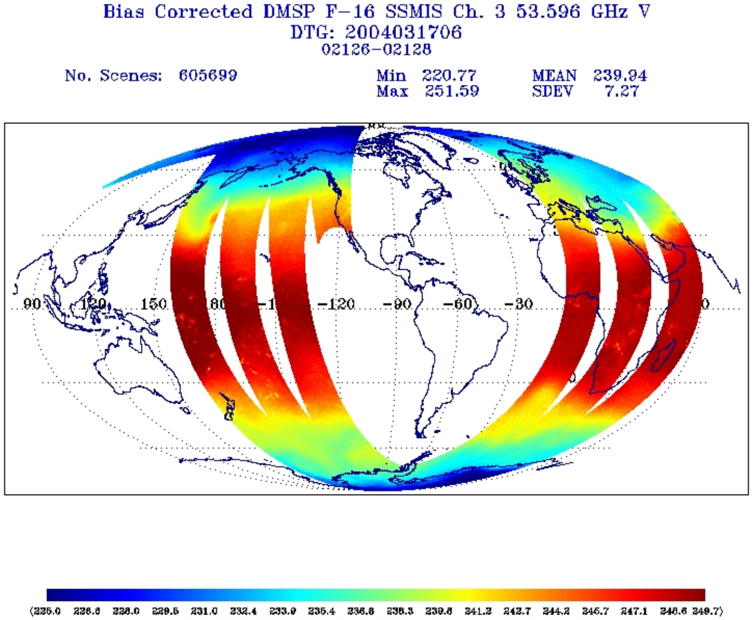

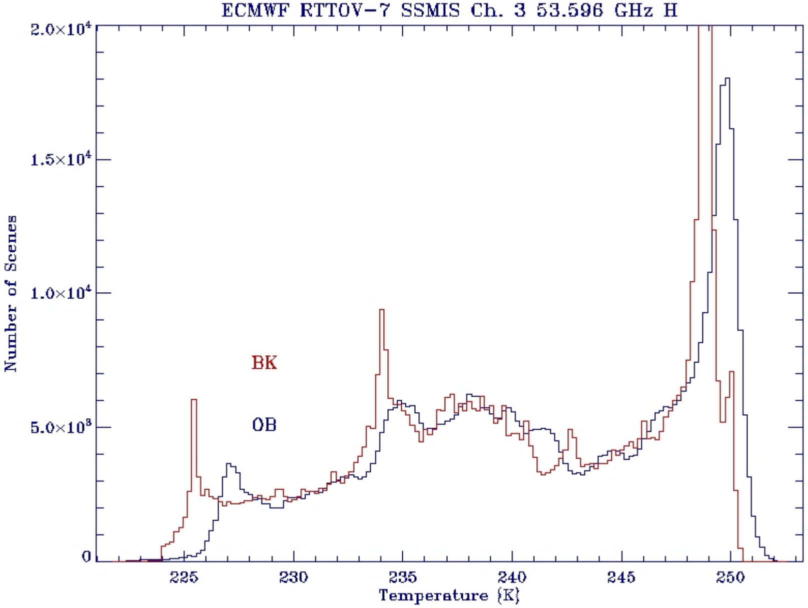

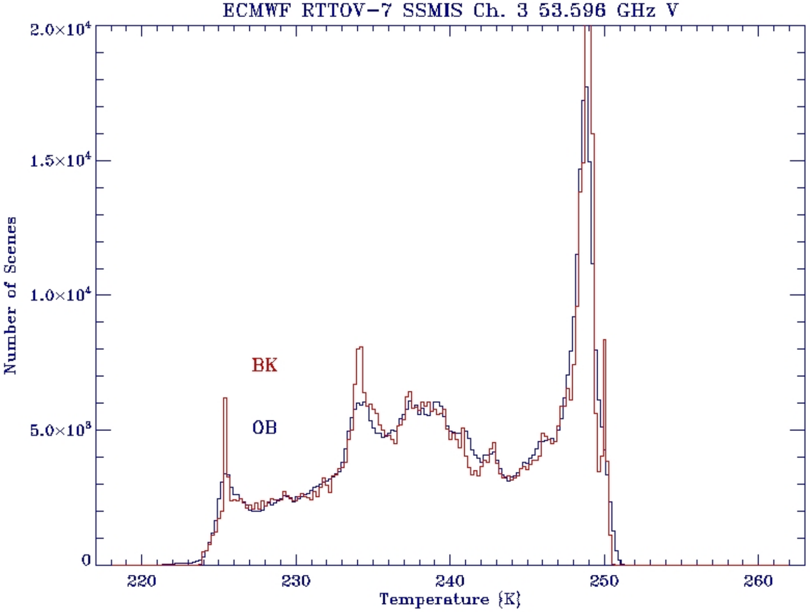

Radiometric Calibration Anomalies

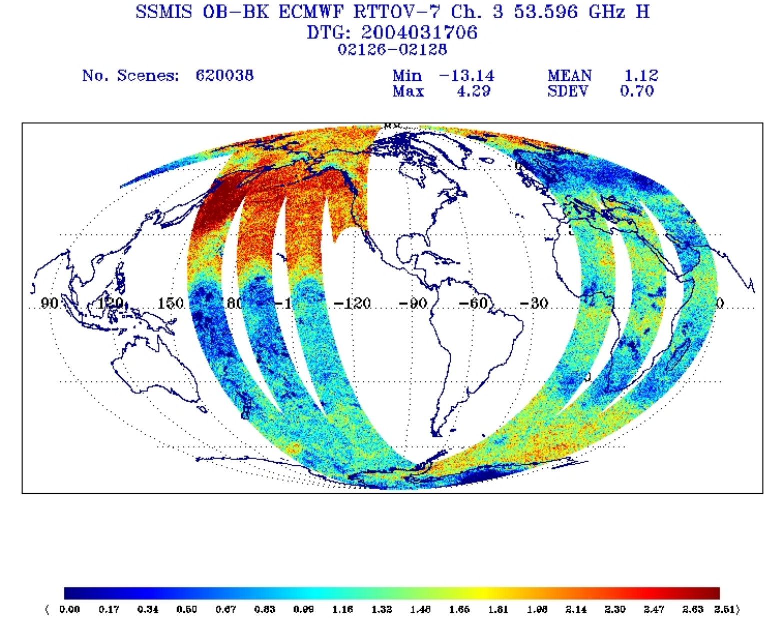

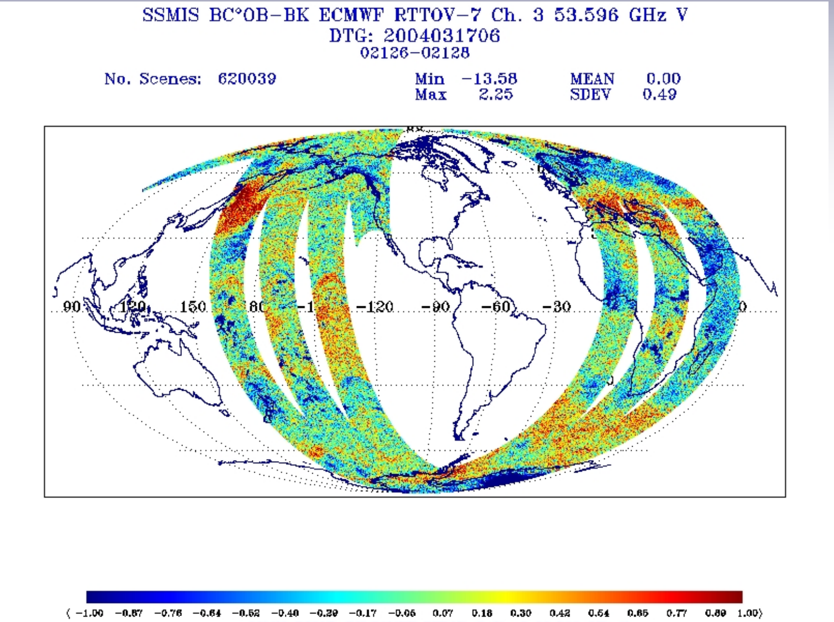

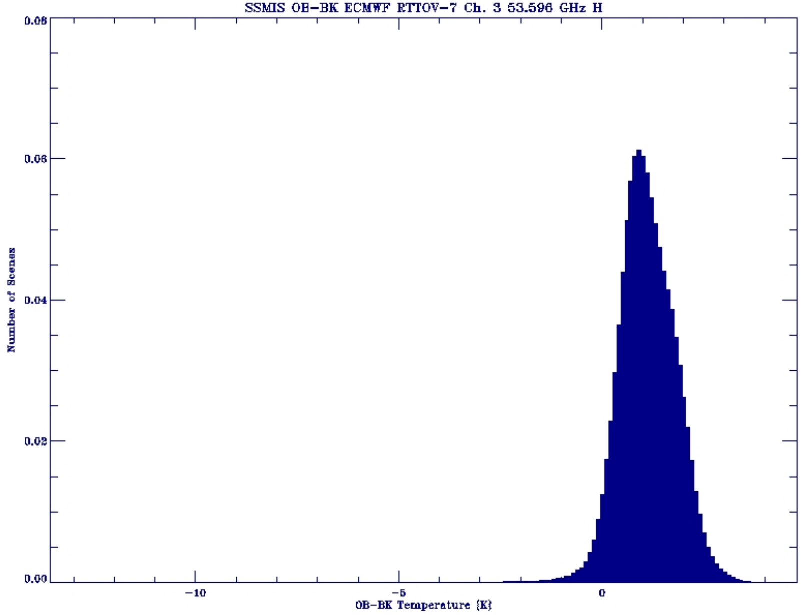

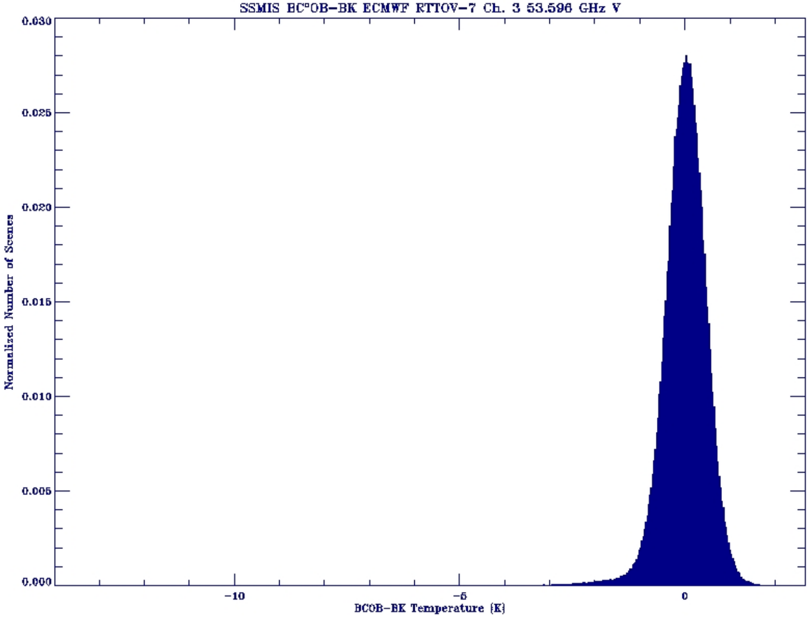

Radiometric Calibration Anomalies

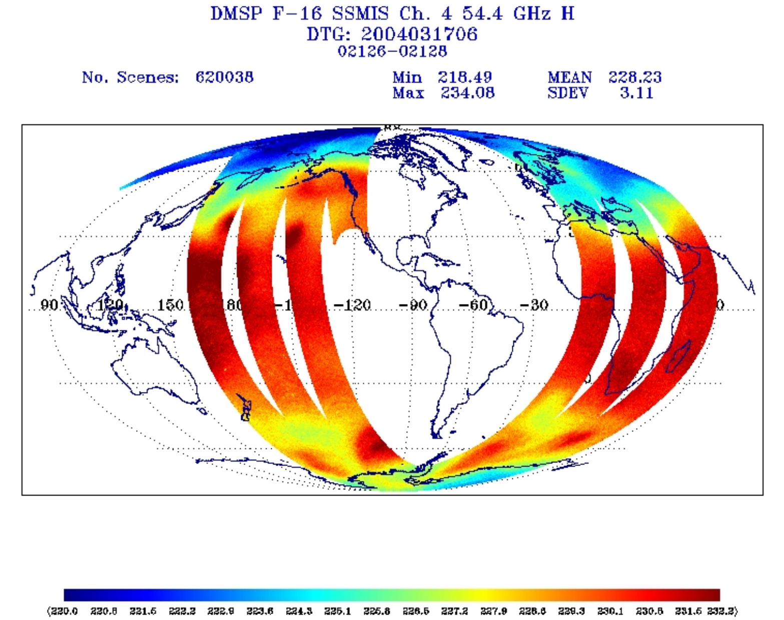

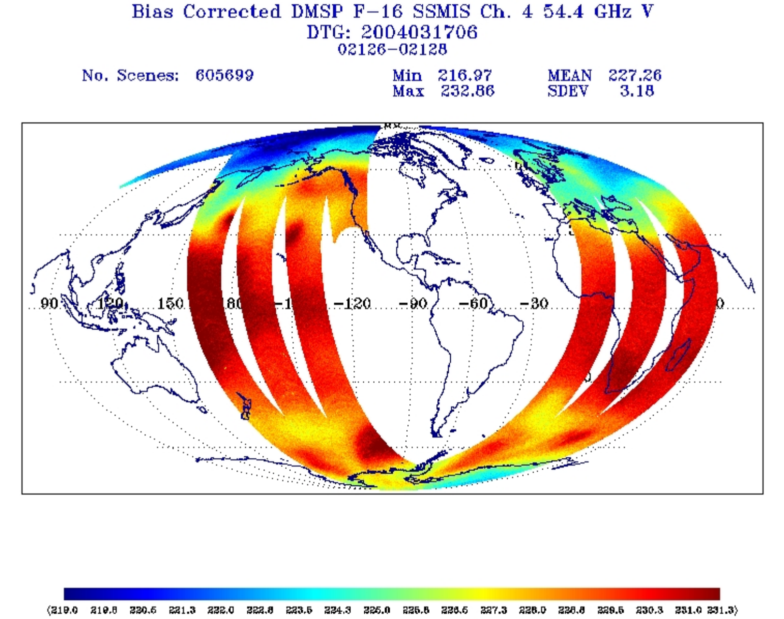

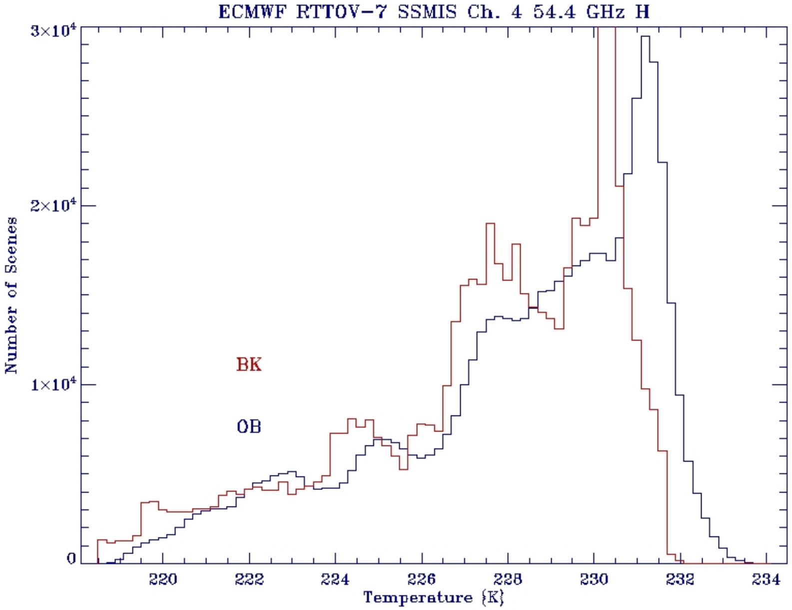

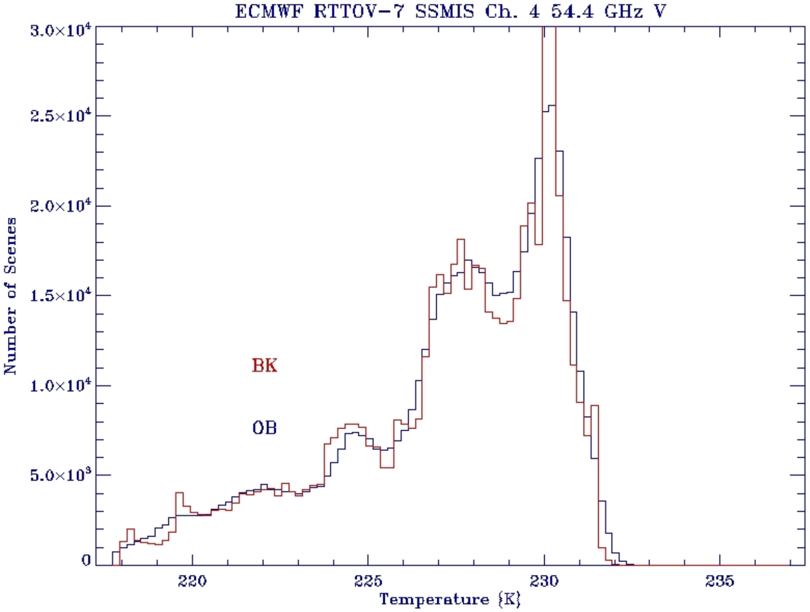

Radiometric Calibration Anomalies

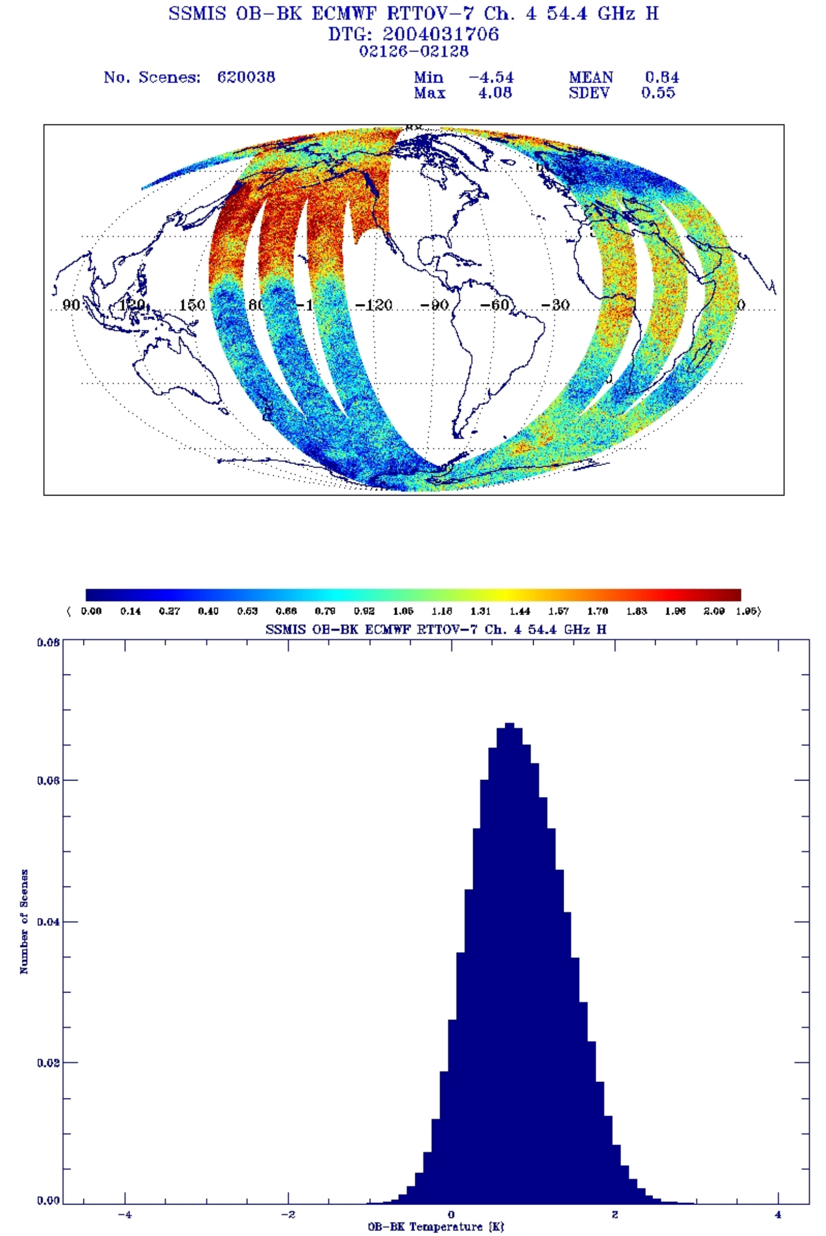

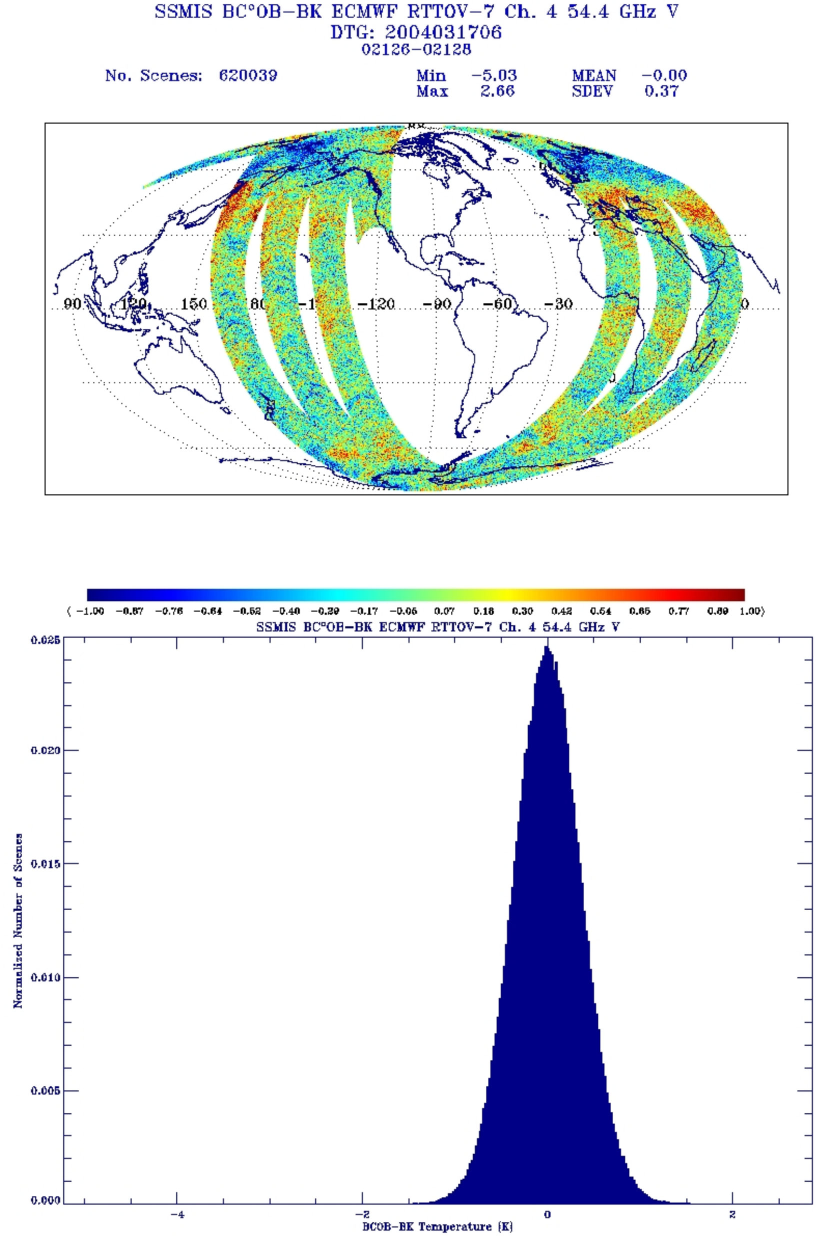

Radiometric Calibration Anomalies

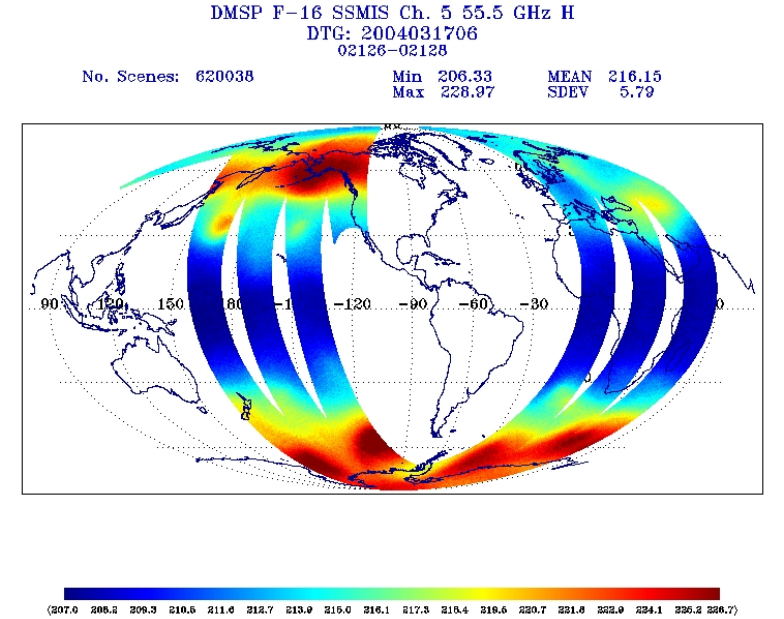

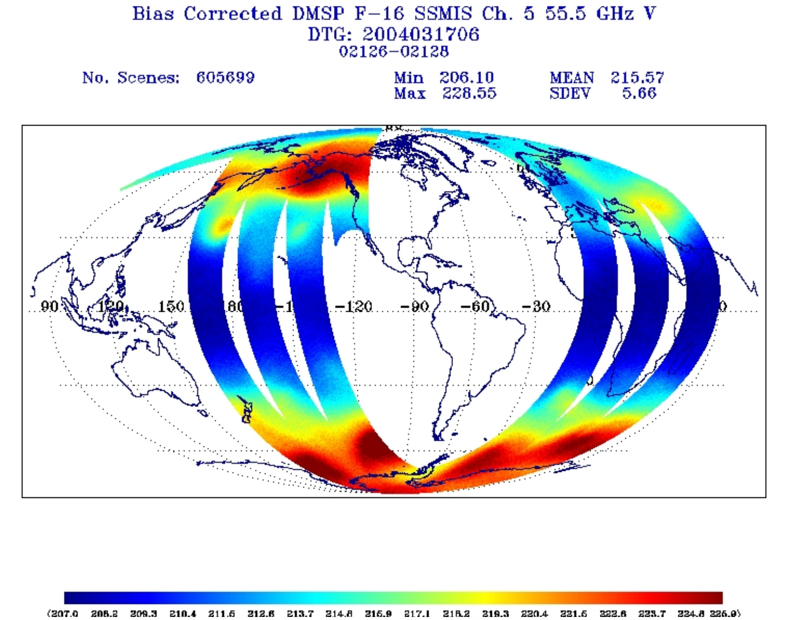

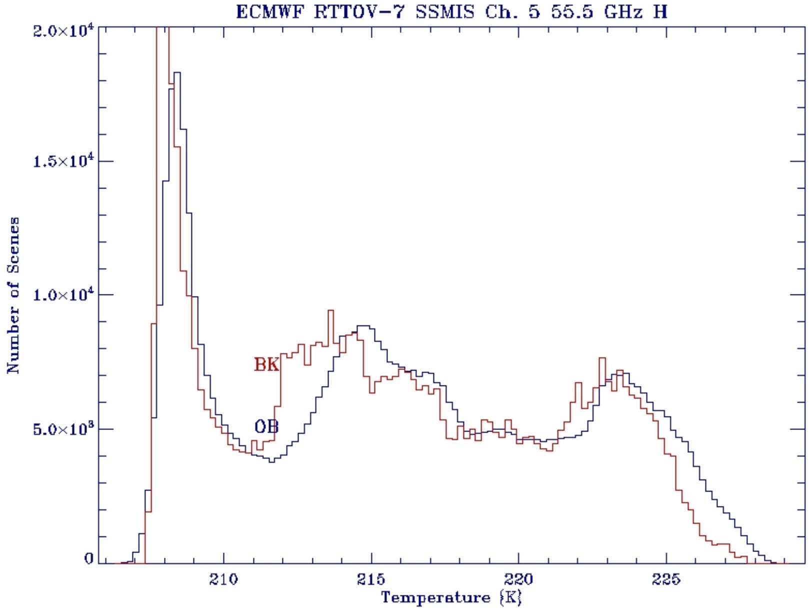

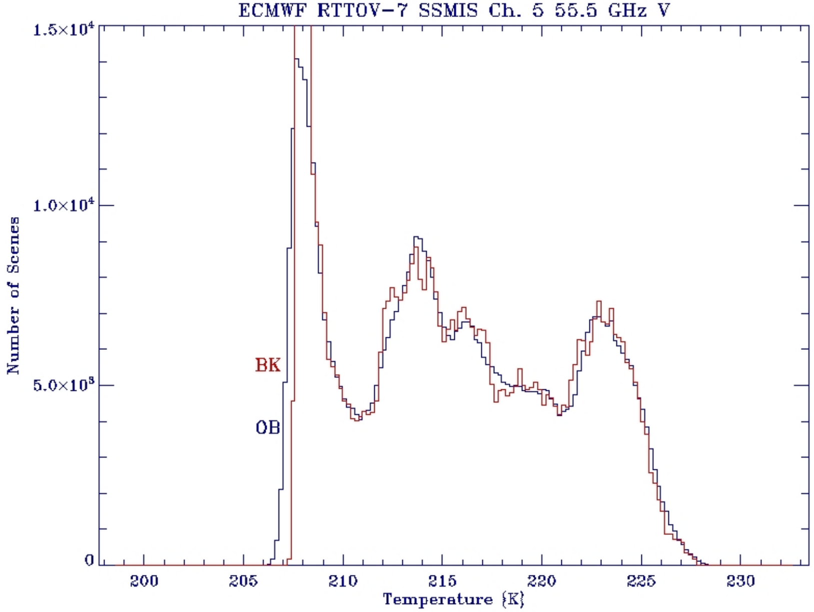

Radiometric Calibration Anomalies

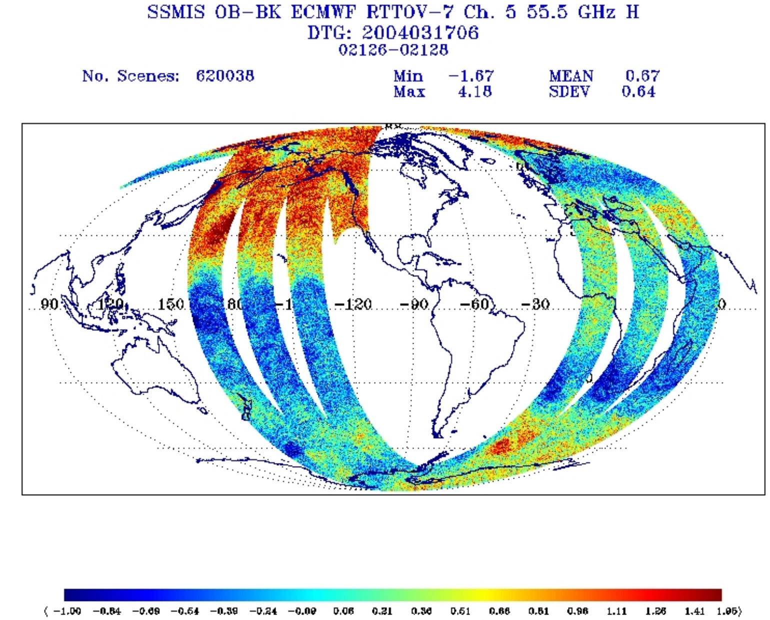

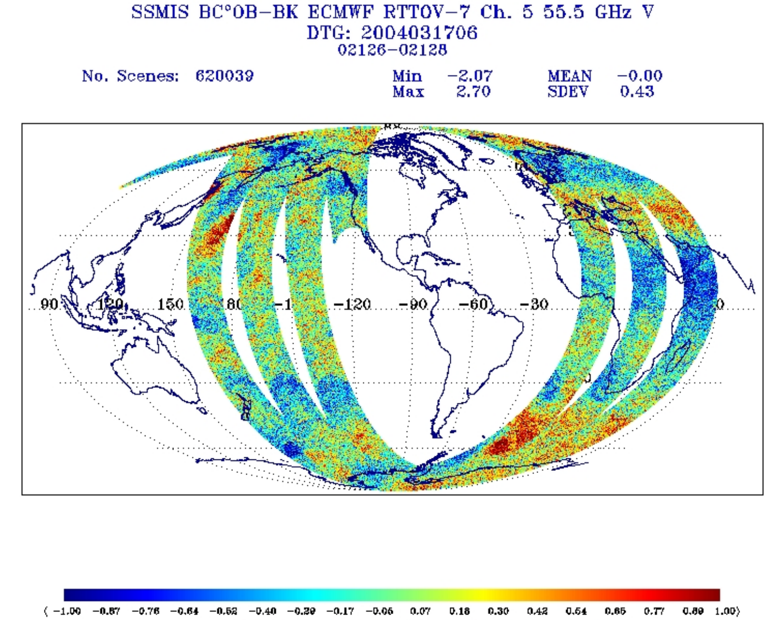

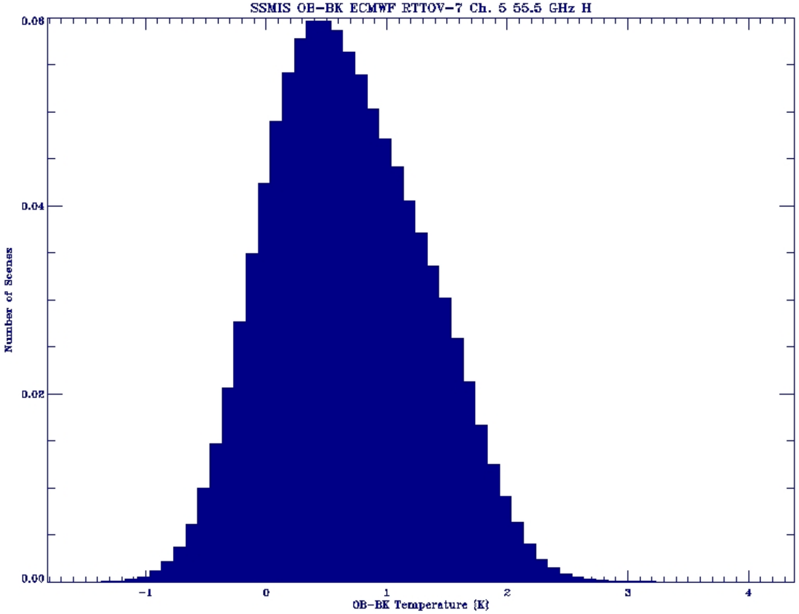

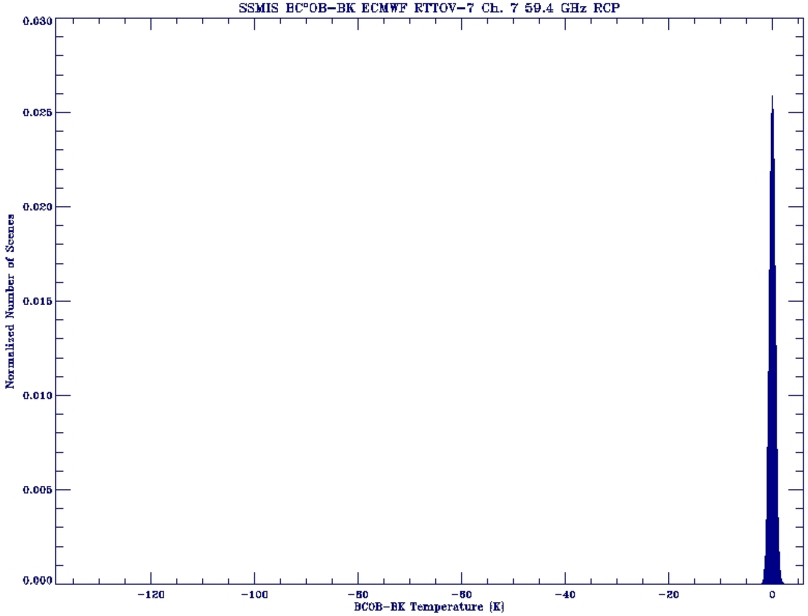

Radiometric Calibration Anomalies

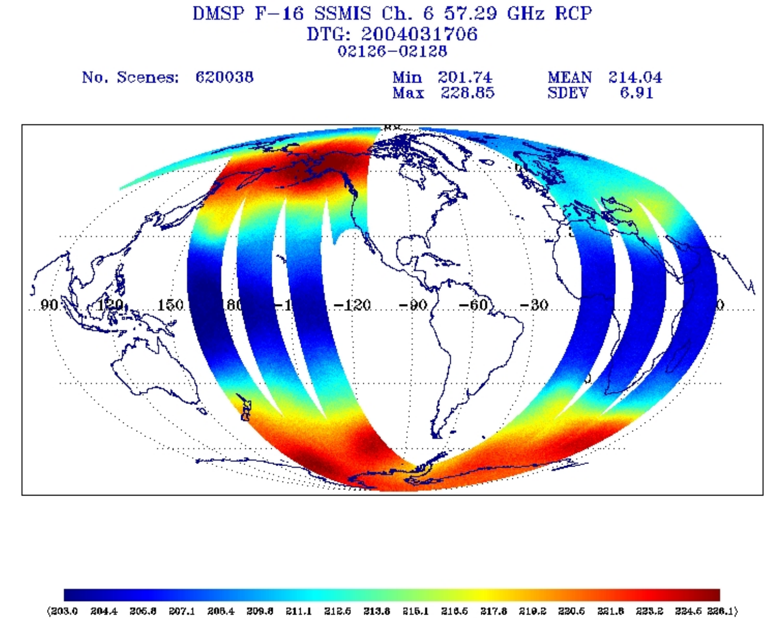

DMSP F-16 SSMIS Ch. 6 57.29 GHz RCP
DTG: 2004031706
02126-02128

No. Scenes: 620038
Min 201.74 MEAN 214.04
Max 228.85 SDEV 6.91

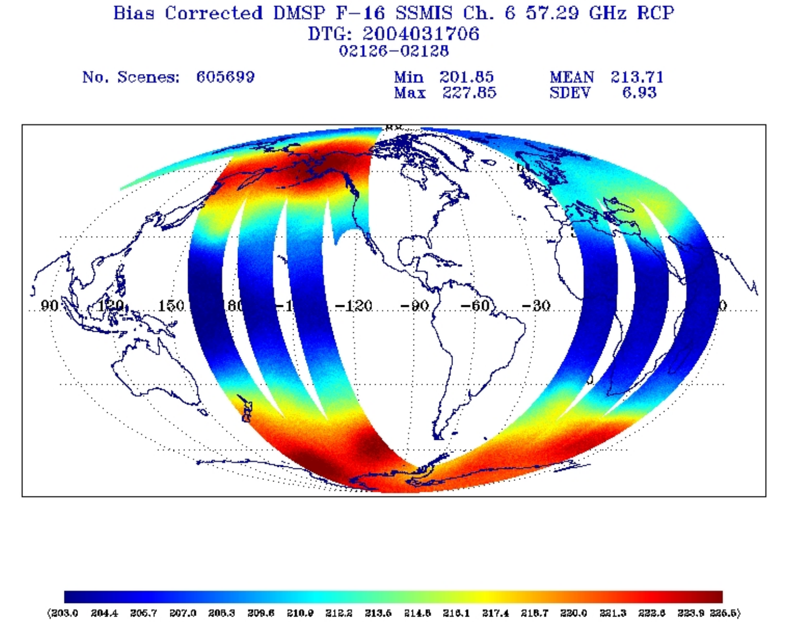

Bias Corrected DMSP F-16 SSMIS Ch. 6 57.29 GHz RCP
DTG: 2004031706
02126-02128

No. Scenes: 605699
Min 201.85 MEAN 213.71
Max 227.85 SDEV 6.93

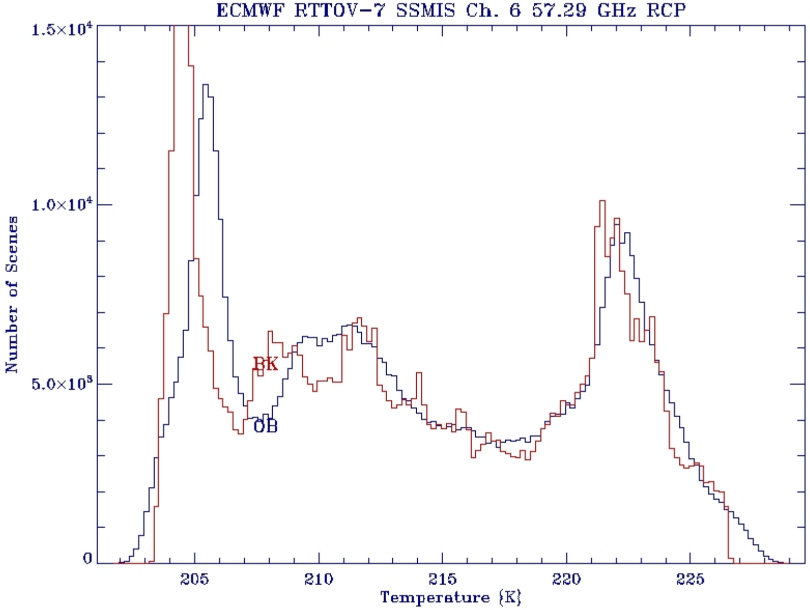

ECMWF RTTOV-7 SSMIS Ch. 6 57.29 GHz RCP

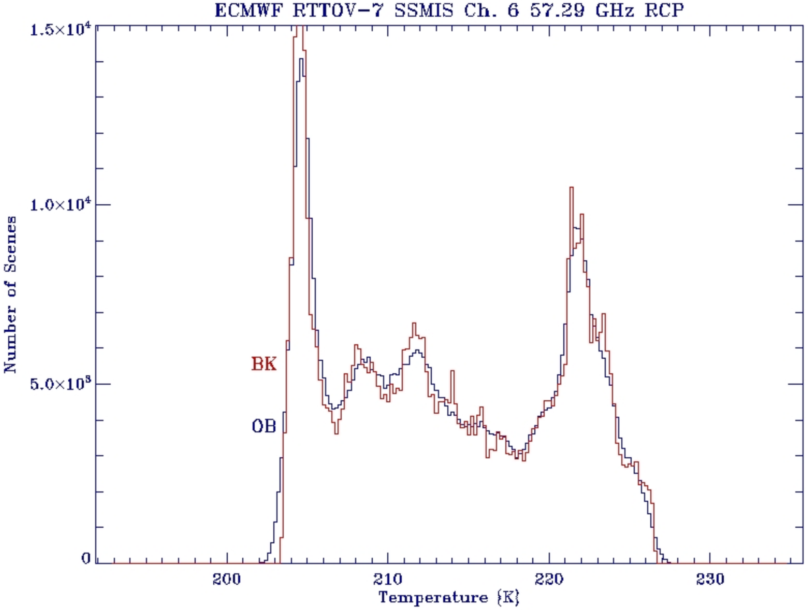

ECMWF RTTOV-7 SSMIS Ch. 6 57.29 GHz RCP

Radiometric Calibration Anomalies

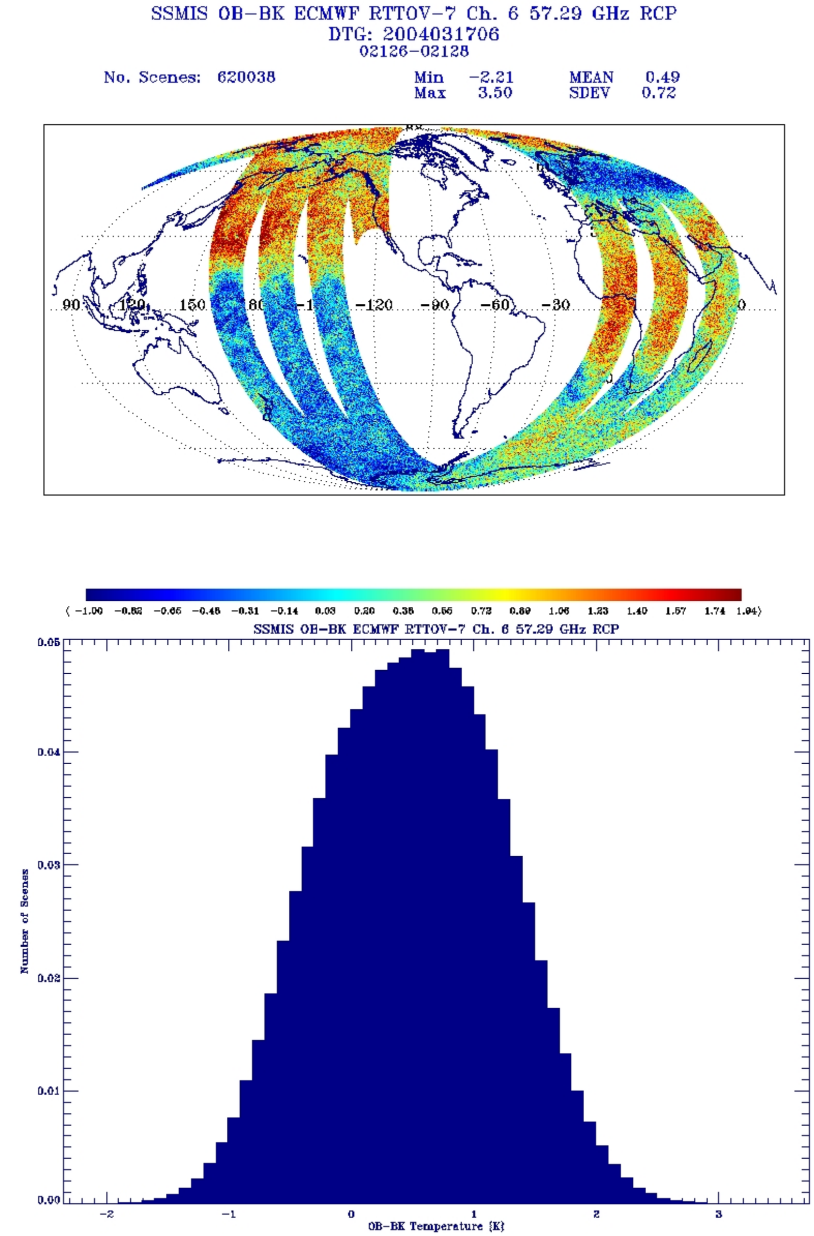

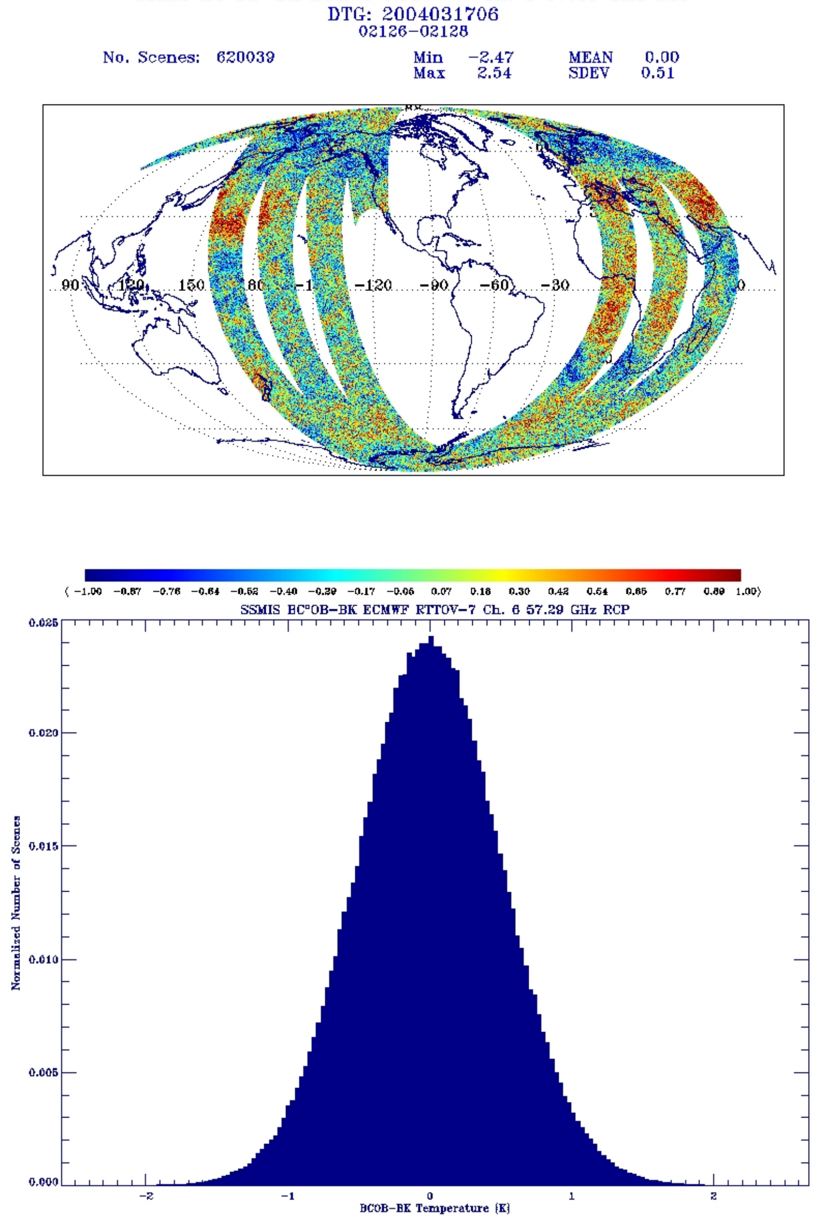

Radiometric Calibration Anomalies

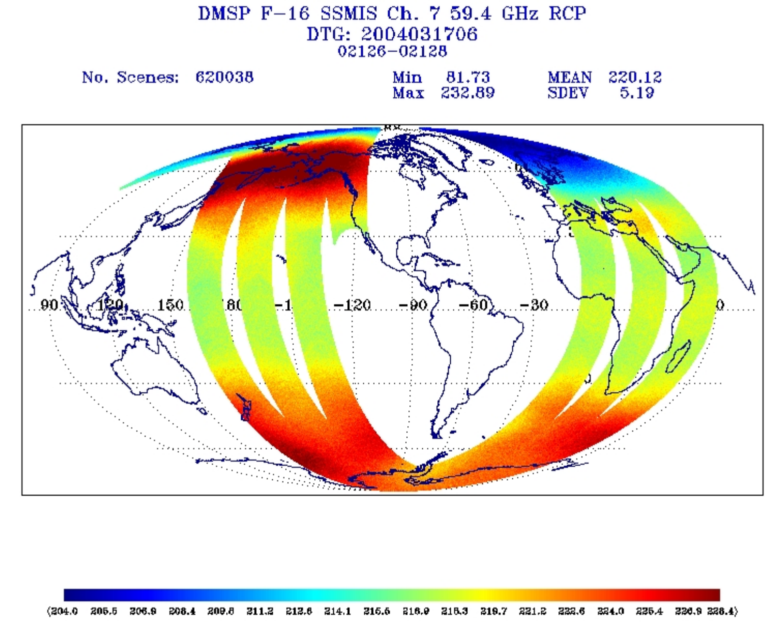

DMSP F-16 SSMIS Ch. 7 59.4 GHz RCP
DTG: 2004031706
02126-02128

No. Scenes: 620038 Min 81.73 Max 232.89 MEAN 220.12 SDEV 5.19

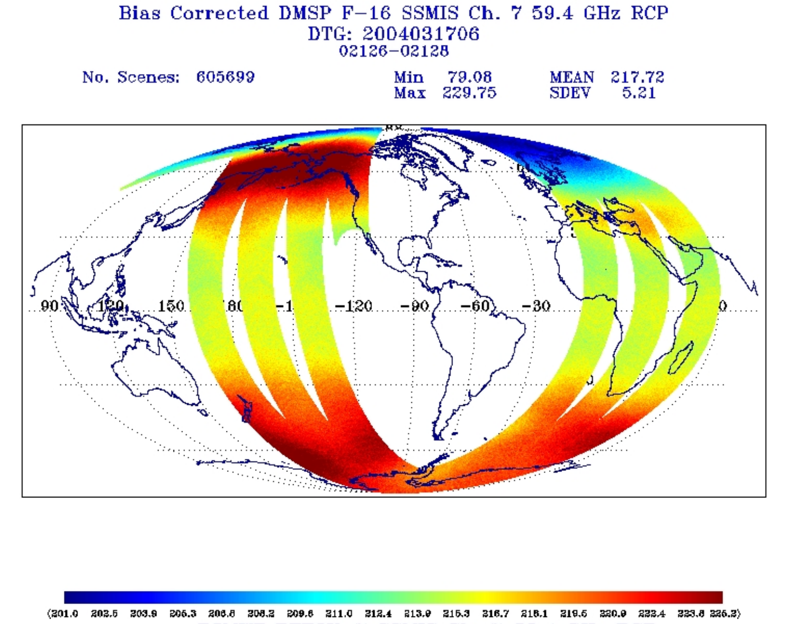

Bias Corrected DMSP F-16 SSMIS Ch. 7 59.4 GHz RCP
DTG: 2004031706
02126-02128

No. Scenes: 605699 Min 79.08 Max 229.75 MEAN 217.72 SDEV 5.21

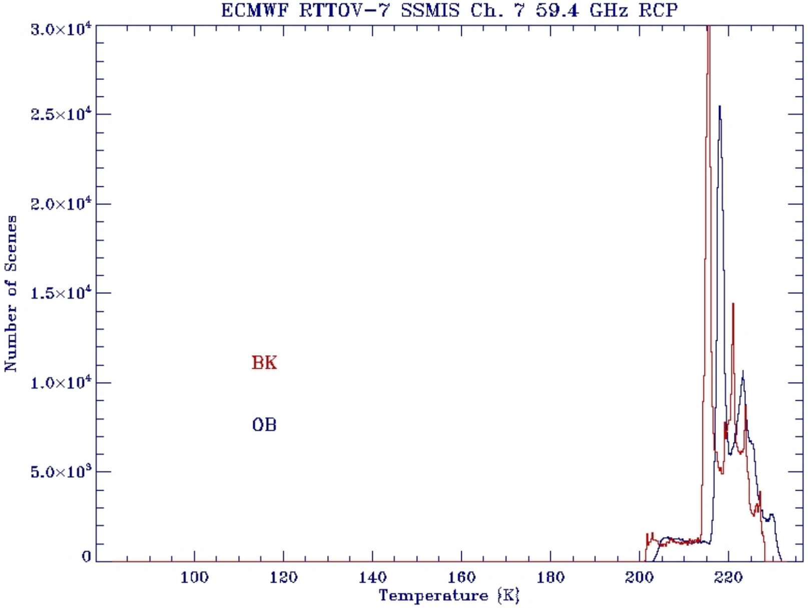

ECMWF RTTOV-7 SSMIS Ch. 7 59.4 GHz RCP

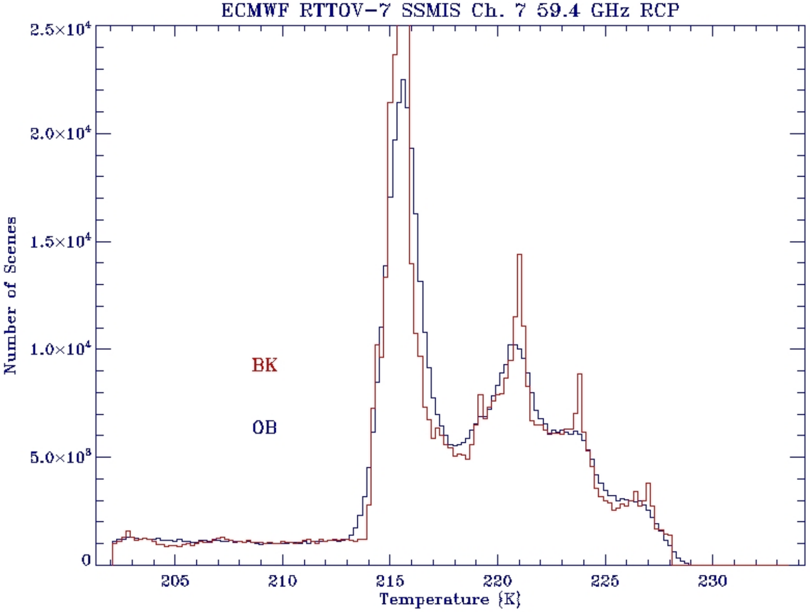

ECMWF RTTOV-7 SSMIS Ch. 7 59.4 GHz RCP

Radiometric Calibration Anomalies

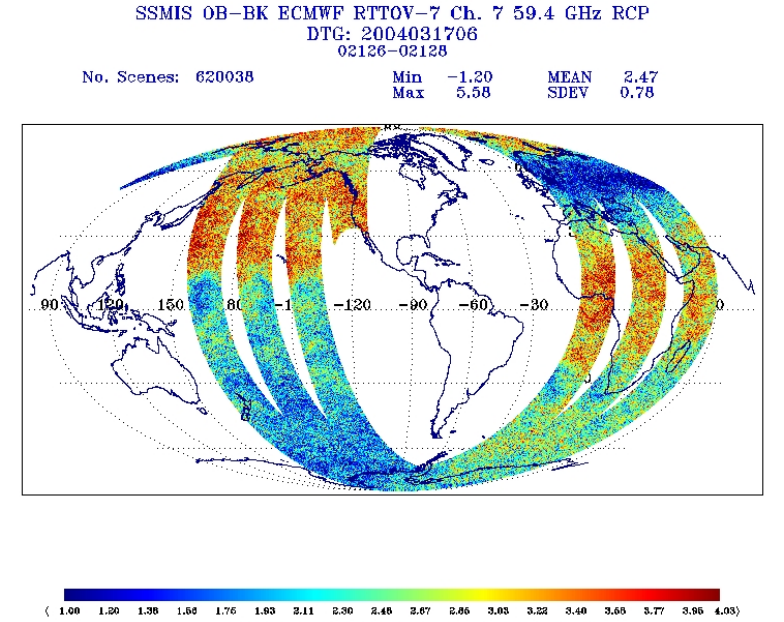

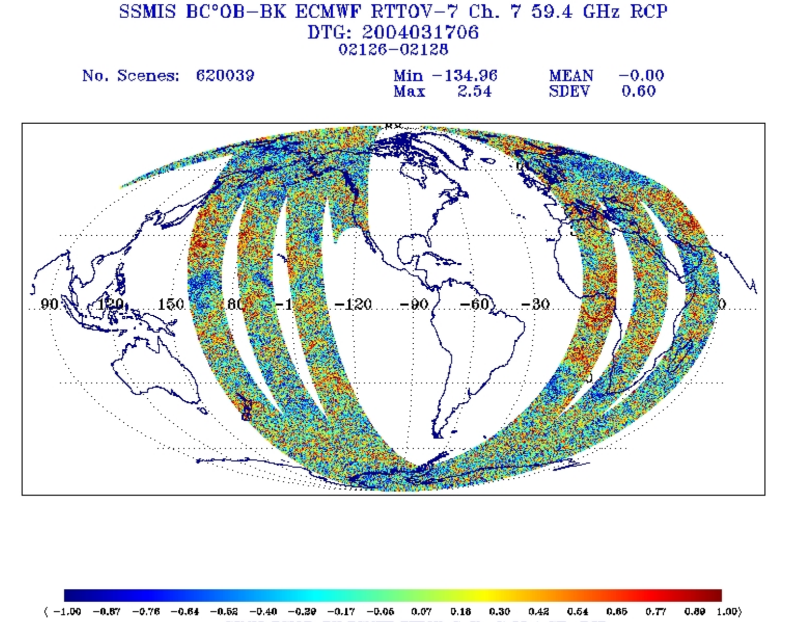

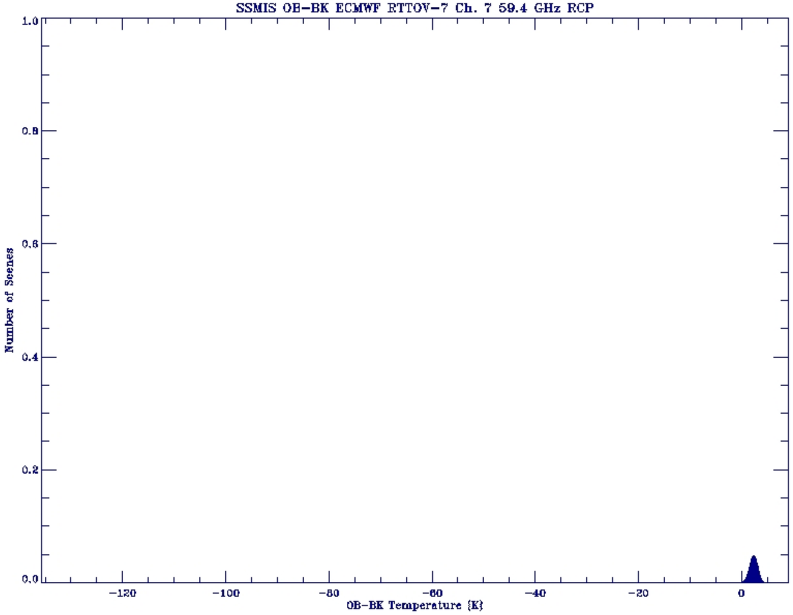

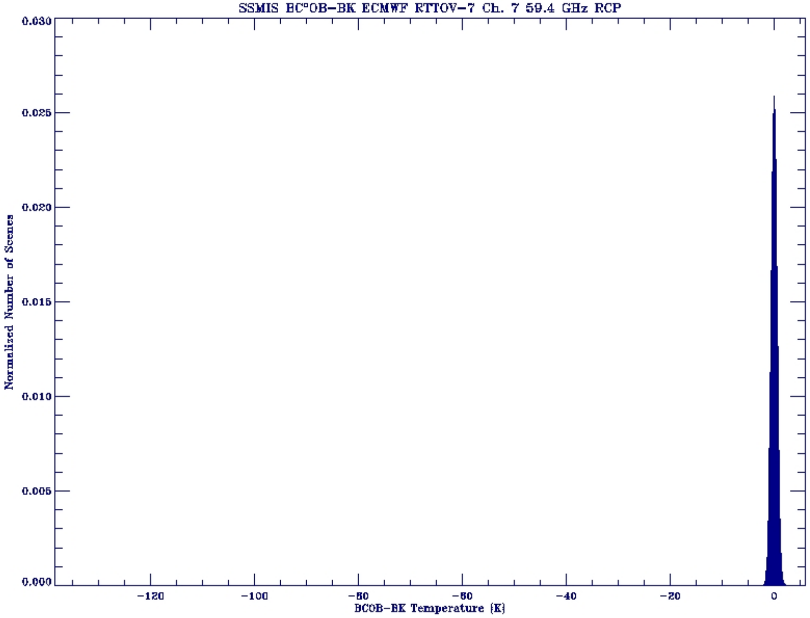

Radiometric Calibration Anomalies

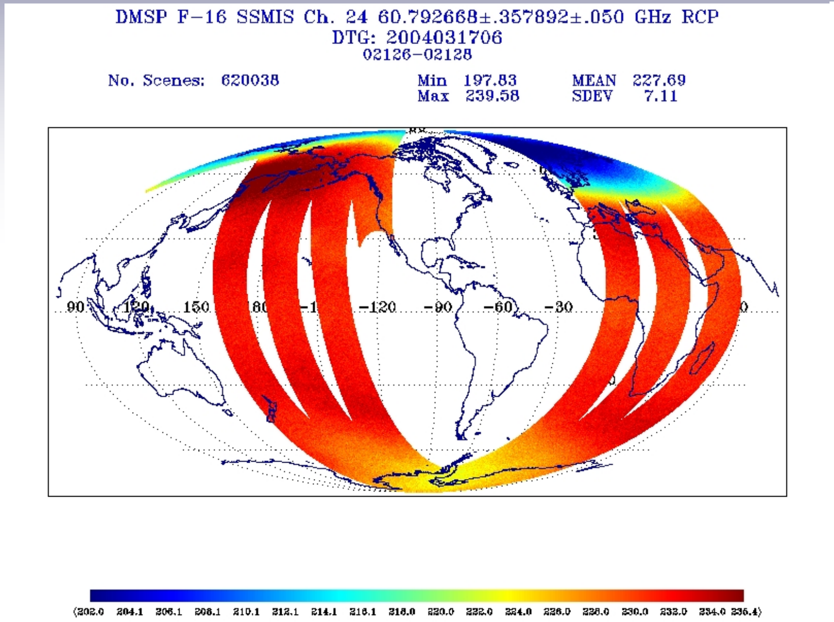

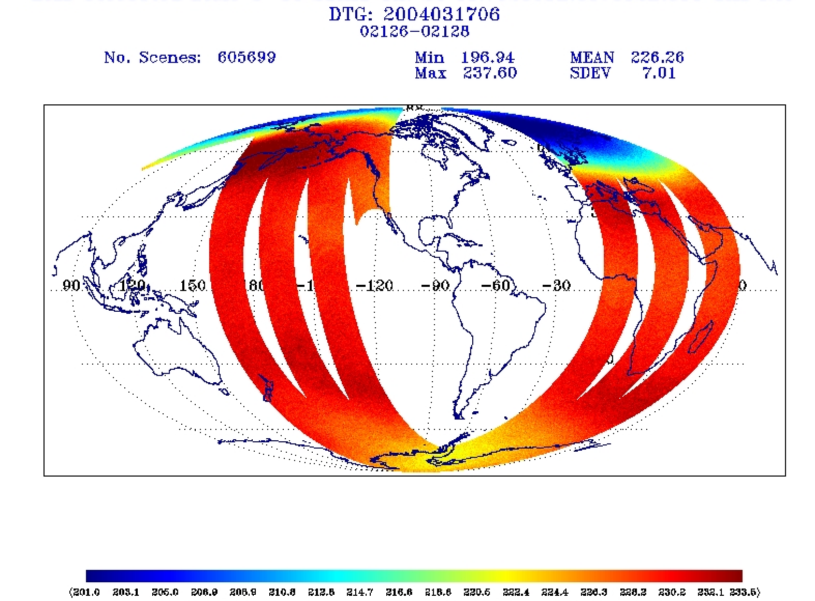

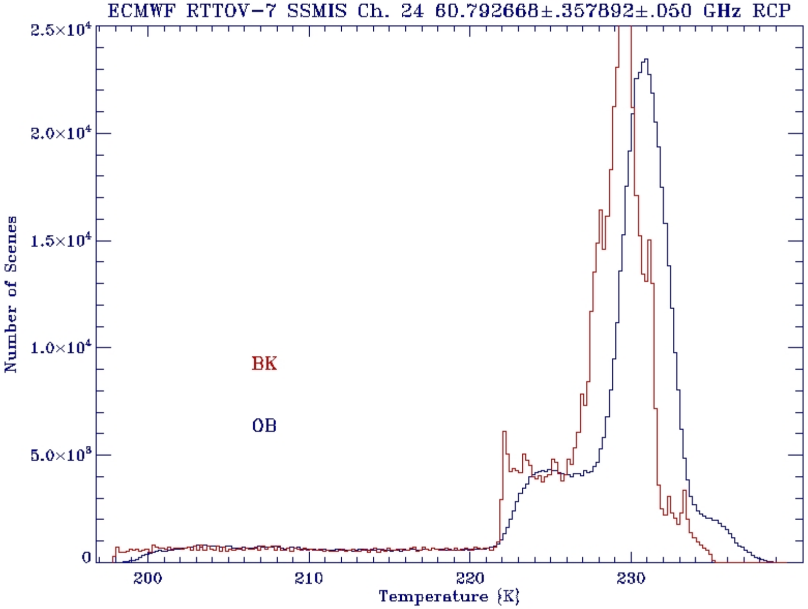

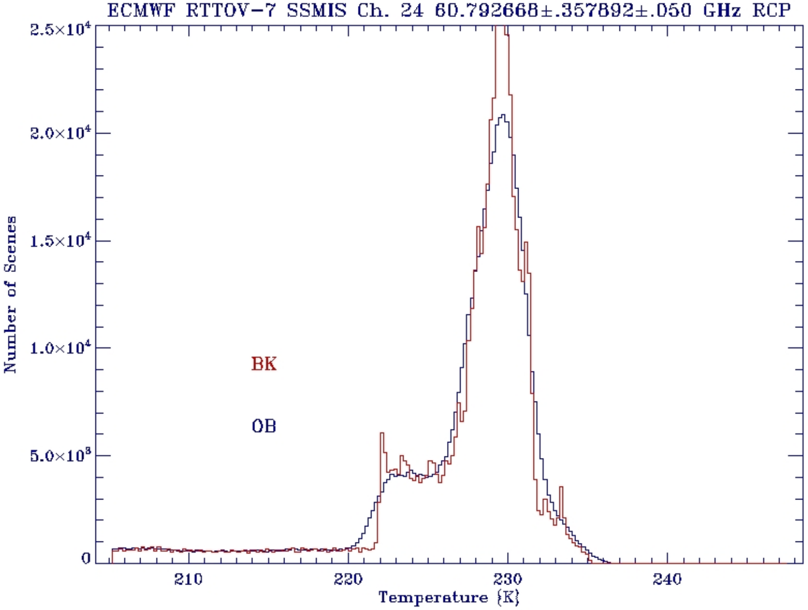

Radiometric Calibration Anomalies

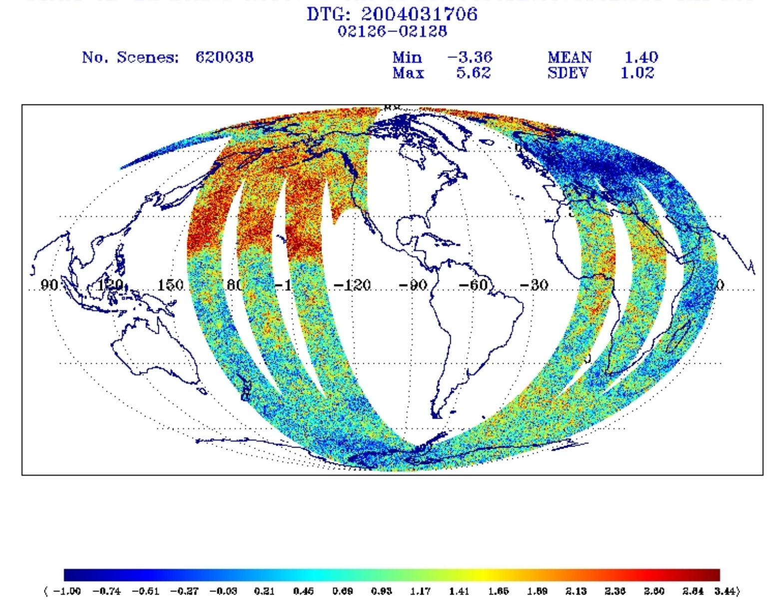

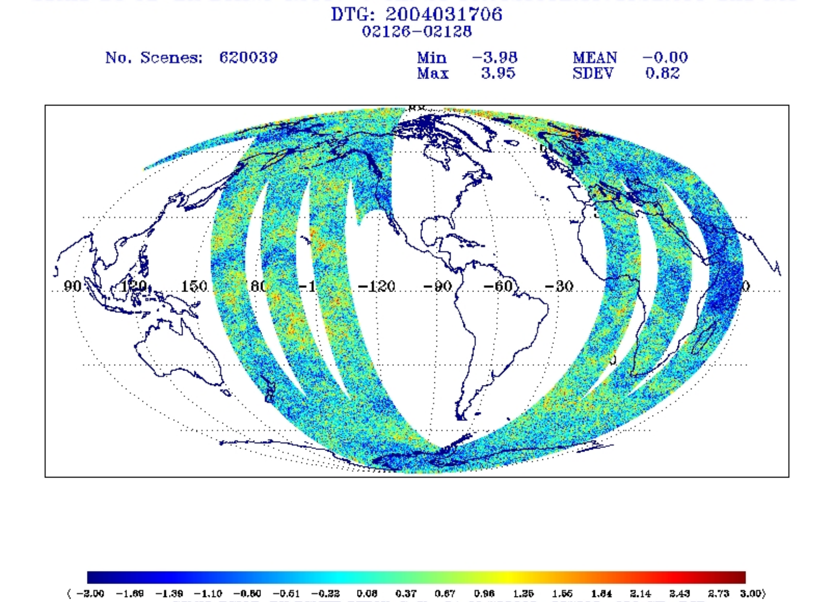

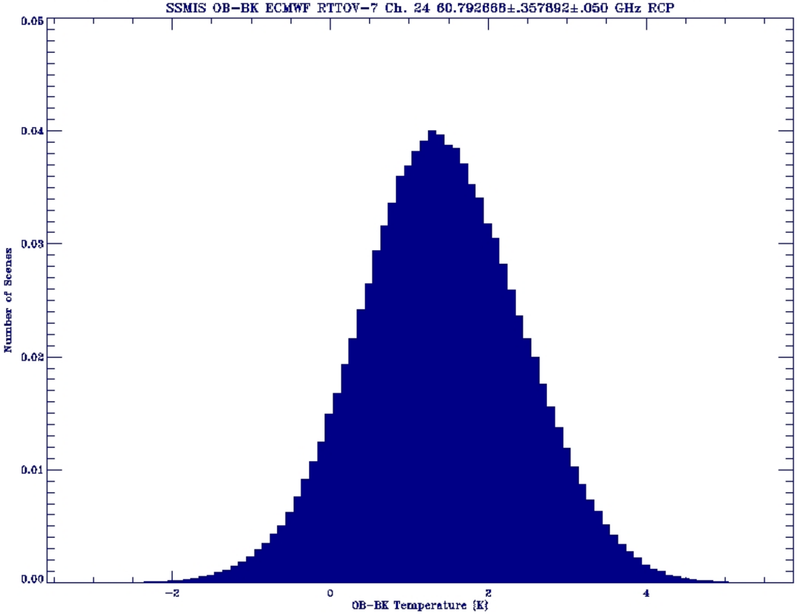

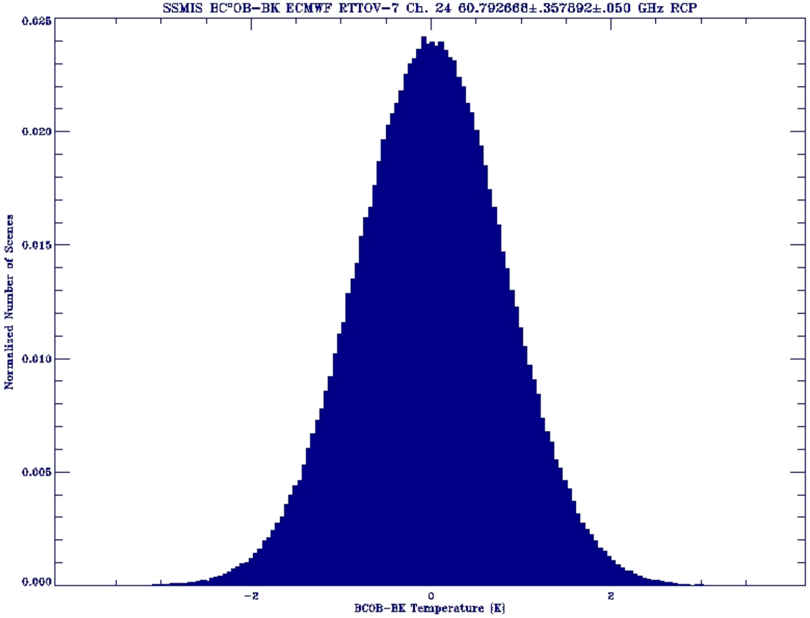

Radiometric Calibration Anomalies

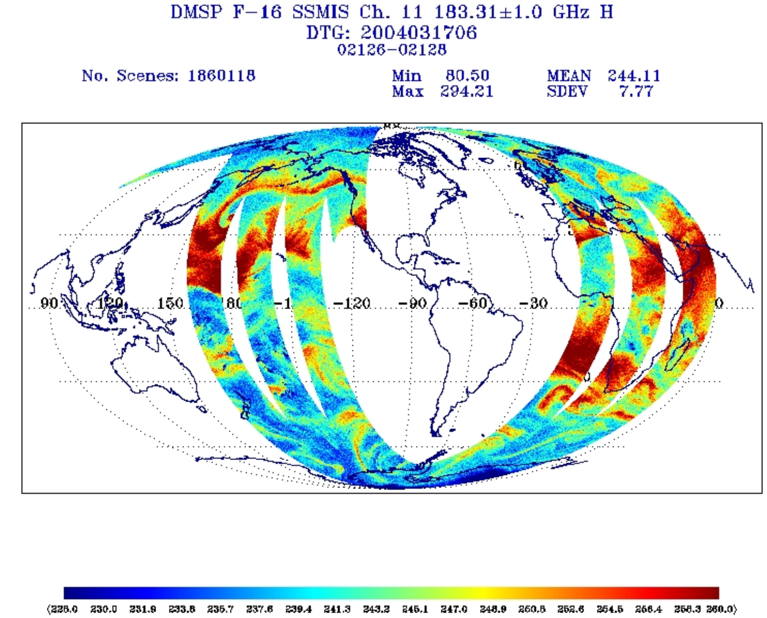

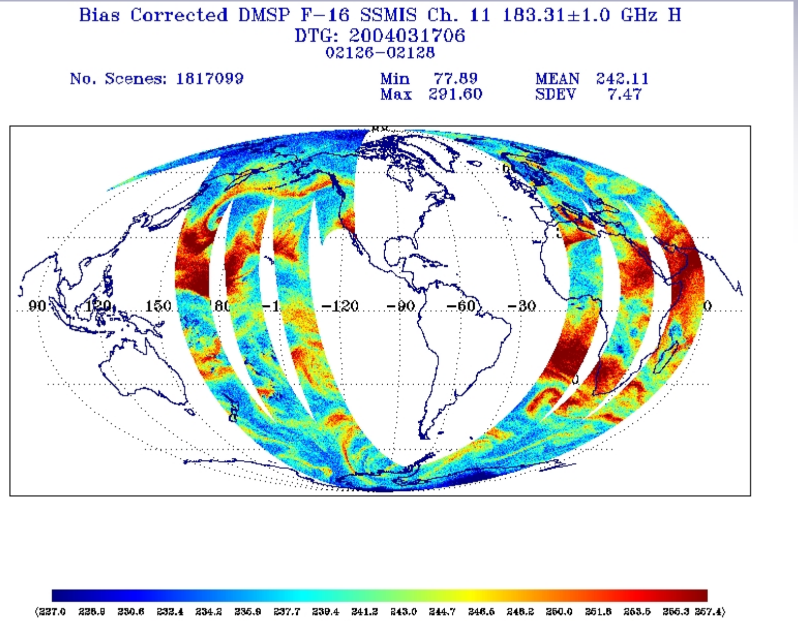

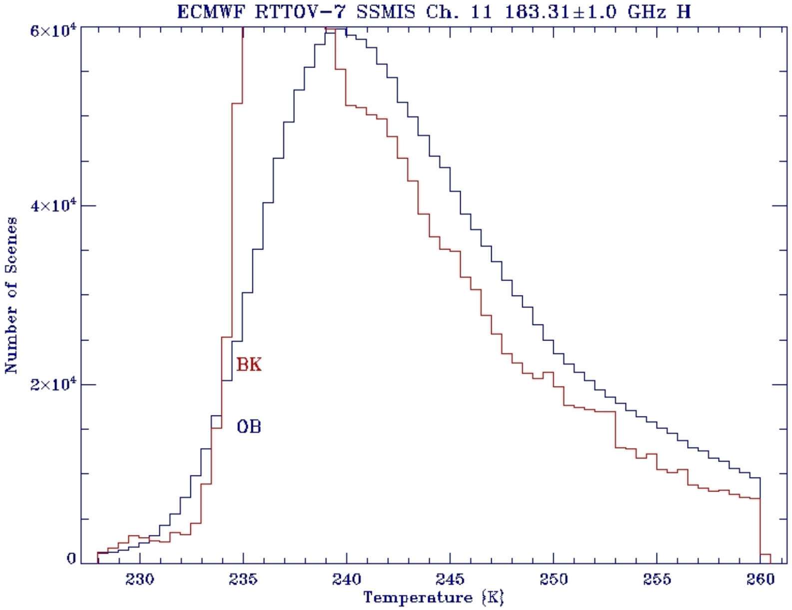

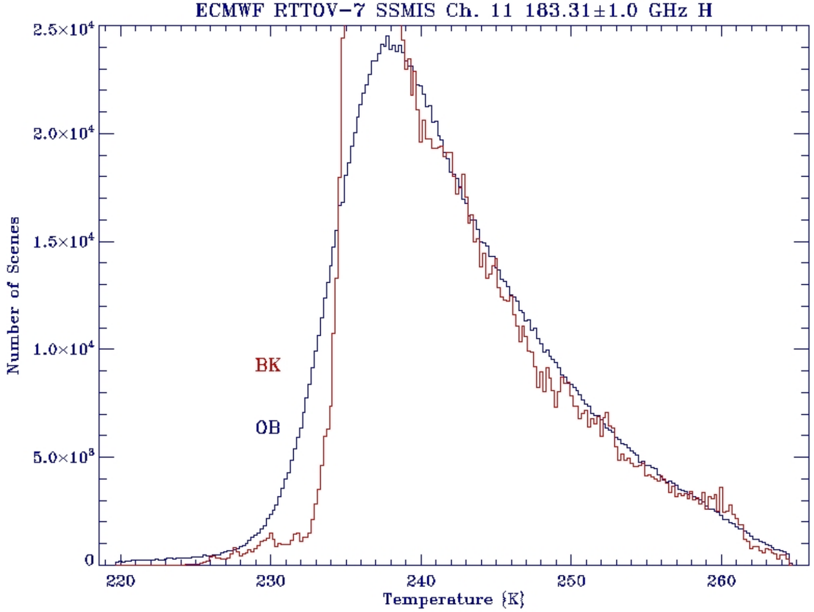

Radiometric Calibration Anomalies

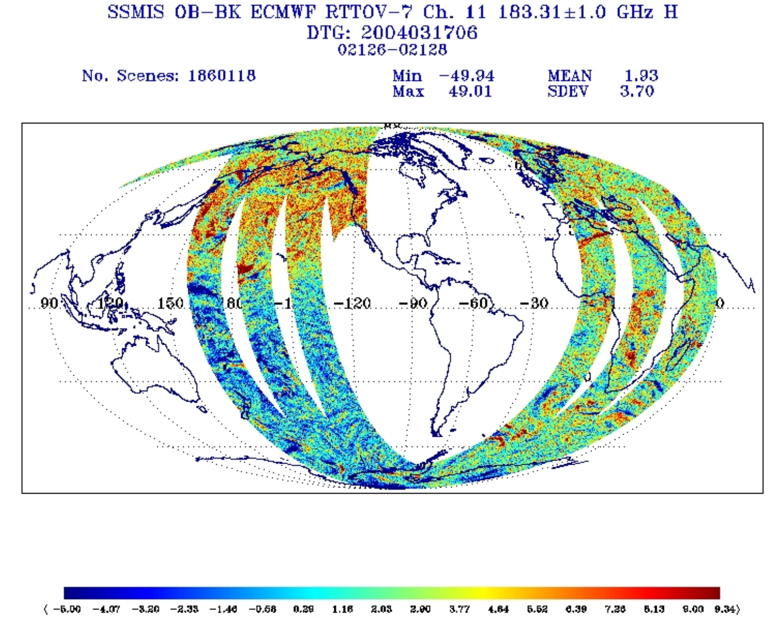
SSMIS OB−BK ECMWF RTTOV−7 Ch. 11 183.31±1.0 GHz H
DTG: 2004031706
02126−02128

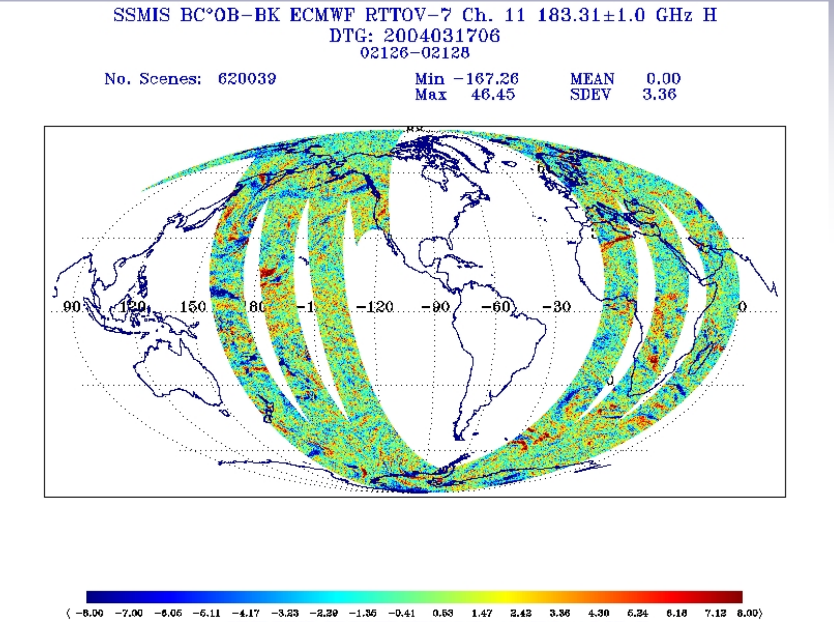
SSMIS BC°OB−BK ECMWF RTTOV−7 Ch. 11 183.31±1.0 GHz H
DTG: 2004031706
02126−02128

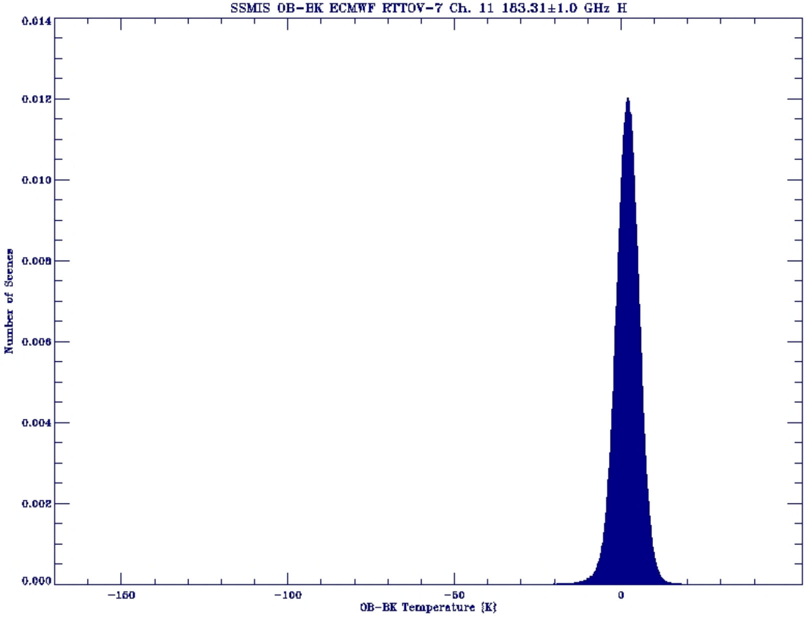
SSMIS OB−BK ECMWF RTTOV−7 Ch. 11 183.31±1.0 GHz H

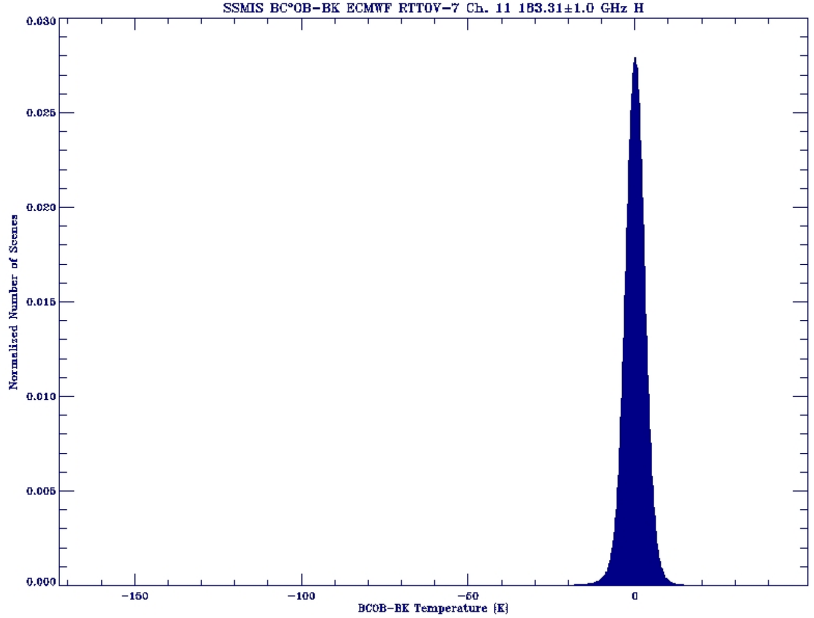
SSMIS BC°OB−BK ECMWF RTTOV−7 Ch. 11 183.31±1.0 GHz H

Radiometric Calibration Anomalies

Plans to Address Anomaly and Future Efforts

Warm Load Intrusion Anomaly

- **NG has implemented a Fourier Filter based Warm Load Intrusion Detection and Correction Algorithm in GDPS**

- **NG's Algorithm Still Needs Rigorous Testing and OB-BK Monitoring**

- **Does it Adequately Remove Scan Averaged OB-BK Anomalies ?**

- **Can a Gaussian Filter Based Algorithm do a Better Job ?**

- **For radiance Assimilation, Is it Better to Remove Warm Load Intrusion Anomaly as a Pre-Processor or Treated Separately with Regression Based Bias Correction ?**

Radiometric Calibration Anomalies

Plans to Address Anomaly and Future Efforts

Reflector Emission Anomaly

- What is the Reflector Emissivity at SSMIS Frequencies?

- Do the Cold Space Reflector Emissivity measurements correspond to the SSMIS F-16 Reflector Emissivities in space ?

- Could the F-16 Reflector Surface have been Damaged by Out-gassing of trapped H_2O within Coating layers ?

- Will Moving the Reflector Arm Temperature Thermistor to the Back Of the Reflector Provide an Adequate Estimate of the Reflector Surface Temperature

- Would Re-Coating the Remaining Reflector Surfaces with SiO_2 Provide the Best Answer ?

Radiometric Calibration Anomalies

Plans to Address Anomaly and Future Efforts

Reflector Emission Anomaly

- Develop an Computationally Fast and Accurate Reflector Surface Temperature Model to aid in the Bias Correction

- Utilize this Model in the Emission Correction Term

$$\in_R \ (T_{Reflector} - T_{Scene})$$

- Utilize this Model in the Regression Based Bias Corrections Required for Radiance Assimilation Efforts